

IAEA-TECDOC-1474

Natural circulation in water cooled nuclear power plants

*Phenomena, models, and methodology for
system reliability assessments*



IAEA

International Atomic Energy Agency

November 2005

IAEA-TECDOC-1474

Natural circulation in water cooled nuclear power plants

*Phenomena, models, and methodology for
system reliability assessments*



IAEA

International Atomic Energy Agency

November 2005

The originating Section of this publication in the IAEA was:

Nuclear Power Technology Development Section
International Atomic Energy Agency
Wagramer Strasse 5
P.O. Box 100
A-1400 Vienna, Austria

NATURAL CIRCULATION IN WATER COOLED NUCLEAR POWER PLANTS:
PHENOMENA, MODELS, AND METHODOLOGY FOR
SYSTEM RELIABILITY ASSESSMENTS

IAEA, VIENNA, 2005
IAEA-TECDOC-1474
ISBN 92-0-110605-X
ISSN 1011-4289

© IAEA, 2005

Printed by the IAEA in Austria
November 2005

FOREWORD

In recent years it has been recognized that the application of passive safety systems (i.e. those whose operation takes advantage of natural forces such as convection and gravity), can contribute to simplification and potentially to improved economics of new nuclear power plant designs. Further, the IAEA Conference on The Safety of Nuclear Power: Strategy for the Future which was convened in 1991 noted that for new plants “the use of passive safety features is a desirable method of achieving simplification and increasing the reliability of the performance of essential safety functions, and should be used wherever appropriate”. Considering the weak driving forces of passive systems based on natural circulation, careful design and analysis methods must be employed to assure that the systems perform their intended functions.

To support the development of advanced water cooled reactor designs with passive systems, investigations of natural circulation are an ongoing activity in several IAEA Member States. Some new designs also utilize natural circulation as a means to remove core power during normal operation. In response to the motivating factors discussed above, and to foster international collaboration on the enabling technology of passive systems that utilize natural circulation, an IAEA Coordinated Research Project (CRP) on Natural Circulation Phenomena, Modelling and Reliability of Passive Systems that Utilize Natural Circulation was started in early 2004. Building on the shared expertise within the CRP, this publication presents extensive information on natural circulation phenomena, models, predictive tools and experiments that currently support design and analyses of natural circulation systems and highlights areas where additional research is needed. Therefore, this publication serves both to provide a description of the present state of knowledge on natural circulation in water cooled nuclear power plants and to guide the planning and conduct of the CRP in order to focus the CRP activities on advancing the state of knowledge. With the benefit of the results of the CRP, this publication will be updated in the future to produce a report on the state of the art of natural circulation in water cooled nuclear power plants.

This publication also contains material from an intensive IAEA training course on Natural Circulation in Water Cooled Reactors for research scientists and engineers involved in the design, testing or analysis of natural circulation systems.

The IAEA appreciates the contributions of the following persons in drafting this TECDOC:

N. Aksan and B. Smith from the Paul Scherrer Institute, Switzerland; D. Araneo, B. Bousbia-Salah, A.L. Costa, F. D’Auria, A. Del Nevo and B. Neykov from the University of Pisa, Italy; N. Muellner from the University of Vienna, Austria; M. Marques from CEA, France; A.K. Nayak, D. Saha and P.K. Vijayan from the Bhabha Atomic Research Centre, India.

The IAEA officers responsible for this publication were J. Reyes and J. Cleveland of the Division of Nuclear Power.

EDITORIAL NOTE

The papers in these proceedings are reproduced as submitted by the authors and have not undergone rigorous editorial review by the IAEA.

The views expressed do not necessarily reflect those of the IAEA, the governments of the nominating Member States or the nominating organizations.

The use of particular designations of countries or territories does not imply any judgement by the publisher, the IAEA, as to the legal status of such countries or territories, of their authorities and institutions or of the delimitation of their boundaries.

The mention of names of specific companies or products (whether or not indicated as registered) does not imply any intention to infringe proprietary rights, nor should it be construed as an endorsement or recommendation on the part of the IAEA.

The authors are responsible for having obtained the necessary permission for the IAEA to reproduce, translate or use material from sources already protected by copyrights.

CONTENTS

1.	INTRODUCTION	1
1.1.	Overview of requirements and goals for future nuclear plants	2
1.2.	Examples of natural circulation systems for advanced designs	6
1.2.1.	AP1000 passive safety systems	6
1.2.2.	SWR1000 passive safety systems	8
1.2.3.	ESBWR passive safety systems	10
1.2.4.	Natural circulation core cooling	11
2.	ADVANTAGES AND CHALLENGES OF NATURAL CIRCULATION SYSTEMS IN ADVANCED DESIGNS	12
2.1.	Some advantages	12
2.2.	Some disadvantages	12
2.3.	Need for natural circulation system data and analysis methods	13
2.3.1.	Local and integral system phenomena	13
2.3.2.	Benchmark data	13
2.3.3.	Predictive tools	13
2.3.4.	Reliability analysis methods	13
3.	LOCAL TRANSPORT PHENOMENA AND MODELS	14
3.1.	Reactor core phenomena	14
3.2.	Interconnecting piping	14
3.3.	Heat sinks (steam generators)	14
3.4.	Passive residual heat removal system	16
3.5.	Containment shell (external air or water cooling)	16
3.6.	Containment cooling condensers/heat exchangers	16
3.7.	Large cooling pools (for heat exchangers, spargers and as a source of coolant)	17
4.	INTEGRAL SYSTEM PHENOMENA AND MODELS	18
4.1.	Working principles of a natural circulation loop	18
4.2.	Governing equations for single and two-phase natural circulation flow	19
4.2.1.	Governing equations for single-phase natural circulation flow	19
4.2.2.	Governing equations for two-phase natural circulation flow	20
4.3.	Instabilities in natural circulation systems	21
4.3.1.	Analysis tools for thermal hydraulic instabilities	22
5.	NATURAL CIRCULATION EXPERIMENTS	26
5.1.	Integral system experiment scaling methodology	26
5.2.	Integral system test facilities for studies of natural circulation	26
5.2.1.	Argentina, CNEA, CAPCN-Rig experimental facility	28
5.2.2.	India, BARC, ITL and PCL test facilities	29
5.2.3.	Japan, JAERI, large scale test facility (LSTF)	30
5.2.4.	Switzerland, PSI, PANDA test facility	31
5.2.5.	United States of America, OSU, APEX-1000 and MASLWR test facilities	31
5.2.6.	United States of America, Purdue, PUMA test facility	33
5.2.7.	Euratom's NACUSP project	33

6.	ADVANCED COMPUTATION AND RELIABILITY ASSESSMENT METHODS	35
6.1.	Advanced computation methods	35
6.2.	Reliability assessment methodology	37
6.2.1.	Identification and quantification of the sources of uncertainties in NC systems	38
6.2.2.	Reliability evaluations of passive systems that utilize NC	38
6.2.3.	Integration of NC system reliability in probabilistic safety analysis	38
	REFERENCES.....	39
ANNEXES		
ANNEX 1	Overview of global developments of advanced nuclear power plants..... <i>J. Cleveland</i>	41
ANNEX 2	Overview on some aspects of safety requirements and considerations for future nuclear reactors	75
	<i>N. Aksan</i>	
ANNEX 3	Natural circulation systems: Advantages & challenges	89
	<i>P.K. Vijayan, A.K. Nayak</i>	
ANNEX 4	Applications of natural circulation systems: Advantages and challenges II..	101
	<i>N. Aksan</i>	
ANNEX 5	Local phenomena associated with natural circulation.....	115
	<i>D. Saha</i>	
ANNEX 6	Governing equations in two-phase fluid natural circulation flows	155
	<i>J. N. Reyes, Jr.</i>	
ANNEX 7	Introduction to instabilities in natural circulation systems.....	173
	<i>P.K. Vijayan, A.K. Nayak</i>	
ANNEX 8	Insights into natural circulation stability.....	203
	<i>F. D'Auria, A. Del Nevo, N. Muellner</i>	
ANNEX 9	Stability analysis of NC based systems: Pressure tube type BWR and steam generators	231
	<i>P.K. Vijayan, A.K. Nayak</i>	
ANNEX 10	The boiling water reactor stability	281
	<i>F. D'Auria, A.L. Costa, A. Bousbia-Salah</i>	
ANNEX 11	Integral system experiment scaling methodology	321
	<i>J.N. Reyes, Jr.</i>	
ANNEX 12	AP600 and AP1000 passive safety system design and testing in APEX.....	357
	<i>J.N. Reyes, Jr.</i>	
ANNEX 13	Experimental validation and database of simple loop facilities	383
	<i>P.K. Vijayan, A.K. Nayak</i>	
ANNEX 14	Overview on PANDA test facility and ISP-42 PANDA tests data base.....	415
	<i>N. Aksan</i>	
ANNEX 15	Flow stagnation and thermal stratification in single and two-phase natural circulation loops.....	433
	<i>J.N. Reyes, Jr.</i>	
ANNEX 16	Examples of natural circulation in PHWR.....	461
	<i>D. Saha</i>	
ANNEX 17	Selected examples of natural circulation for small break LOCA and some severe accident conditions	471
	<i>N. Aksan</i>	

ANNEX 18	Use of natural circulation flow map.....	487
	<i>F. D'Auria, D. Araneo, B. Neykov</i>	
ANNEX 19	Coupled 3D neutron kinetics and thermal-hydraulics techniques and relevance for the design of natural circulation systems	497
	<i>F. D'Auria, A. Bousbia-Salah</i>	
ANNEX 20	Computational fluid dynamics for natural circulation flows	535
	<i>B. Smith</i>	
ANNEX 21	The CSNI separate effects test and integral test facility matrices for validation of best-estimate thermal hydraulic computer codes.....	553
	<i>N. Aksan</i>	
ANNEX 22	Reliability of passive safety systems that utilize natural circulation	581
	<i>M. Marques</i>	
CONTRIBUTORS TO DRAFTING AND REVIEW		637

1. INTRODUCTION

New generations of nuclear power plants are being developed, building upon the background of nuclear power's success and applying lessons learned from the experience of operating plants. Annex 1 provides an overview of global development of advanced nuclear power plants. Some new reactor designs rely on active systems of proven high reliability to meet safety requirements. Other designs rely on passive systems [1] to meet safety requirements, while others rely on combinations of the two. The use of passive safety systems was addressed in the IAEA Conference on "The Safety of Nuclear Power: Strategy for the Future" [2]. This subject has been co-operatively reviewed by experts from several IAEA Member States with their common views presented in a paper entitled "Balancing passive and active systems for evolutionary water cooled reactors" in Ref. [3]. The experts note that a designer's first consideration is to satisfy the required safety function with sufficient reliability. However, the designer must also consider other aspects such as the impact on plant operation, design simplicity and costs.

The use of passive safety systems such as accumulators, condensation and evaporative heat exchangers, and gravity driven safety injection systems eliminate the costs associated with the installation, maintenance and operation of active safety systems that require multiple pumps with independent and redundant electric power supplies. As a result, passive safety systems are being considered for numerous reactor concepts and may potentially find applications in the Generation-IV reactor concepts, as identified by the Generation IV International Forum (GIF). Another motivation for the use of passive safety systems is the potential for enhanced safety through increased safety system reliability.

As part of the IAEA's overall effort to foster international collaborations that strive to improve the economics and safety of future water cooled nuclear power plants, a 4-year IAEA Coordinated Research Project (CRP) was started in early 2004. This CRP, entitled Natural Circulation Phenomena, Modelling and Reliability of Passive Safety Systems that Utilize Natural Circulation, provides an international coordination of work currently underway at the national level in several IAEA Member States. This CRP has been organized within the framework of the IAEA Department of Nuclear Energy's Technical Working Groups for Advanced Technologies for Light Water Reactors and Heavy Water Reactors (the TWG-LWR and the TWG-HWR).

The CRP benefits from earlier IAEA activities that include developing databases on physical processes of significant importance to water cooled reactor operations and safety [4], [5], technical information exchange meetings on recent technology advances [6], [7], [8], [9], [10], [11], [12], and Status Reports on advanced water cooled reactors [13], [14]. In the area of thermal hydraulic phenomena in advanced water cooled reactors, recent IAEA activities have assimilated data internationally on heat transfer coefficients and pressure drop [4]; and have shared information on natural circulation data and analytical methods [6], and on experimental tests and qualification of analytical methods [7].

The aim of this publication is to document the present knowledge in the following areas as a starting point for the CRP's efforts:

- Advantages and Challenges of Natural Circulation Systems in Advanced Designs
- Local Transport Phenomena and Models
- Integral System Phenomena and Models
- Natural Circulation Experiments
- Advanced Computation Methods
- Reliability Assessment Methodology

The following sections provide a brief introduction to the requirements and technology goals for advanced reactors and serve to illustrate several passive safety systems that use natural circulation. This background information will be of value in understanding the remaining chapters.

1.1. Overview of requirements and goals for future nuclear plants

Europe, the USA and other countries, and the IAEA have established some basic goals and requirements for future nuclear power plants. In Europe, the major utilities have worked together to propose a common set of nuclear safety requirements known as the European Utility Requirements (EUR). The goal is to establish a common set of utility requirements in Europe to allow the development of competitive, standardized designs that would be licensable in the respective countries. Similarly, the U.S. Department of Energy has launched a major international research initiative, named Generation IV (Gen-IV), to develop and demonstrate new and improved reactor technologies. A set of goals have been established as part of the Generation-IV effort. User requirements documents have also been prepared in Japan, the Republic of Korea and China.

To provide some examples of requirements and goals for future plants, this section provides a brief overview of the EUR, the Gen-IV goals, and the basic principles for future nuclear energy systems that have been established by IAEA's International Project on Innovative Nuclear Reactors (INPRO).

A short overview of the EUR is provided in Annex 2. Top-tier requirements have been developed for the following:

- Plant Characteristics
- Operational Targets
- Standardization
- Economic Objectives
- Core Damage Prevention
- Accident Mitigation
- Release Rates

Table 1 provides a list of some examples of EUR requirements related to plant safety.

The Gen-IV goals serve as a basis for developing criteria to assess and compare systems, are challenging and stimulate the search for innovative nuclear systems and serve to motivate and guide in research and development. Table 2 presents these goals.

There are six nuclear power systems being developed by members of GIF. Two systems employ a thermal neutron spectrum with coolants and temperatures that enable electricity production with high efficiency: the supercritical water reactor (SCWR) and the very high temperature reactor (VHTR). Three employ a fast neutron spectrum to enable more effective management of nuclear materials through recycling of most components in the discharged fuel: the gas cooled fast reactor (GFR), the lead cooled fast reactor (LFR), and the sodium cooled fast reactor (SFR). One, the molten salt reactor (MSR) employs a circulating liquid fuel mixture that offers considerable flexibility for recycling nuclear materials.

Table 1. Some EUR safety requirements

1.1	Application of as low as reasonably achievable (ALARA) principle
1.2	Design to be forgiving and characterized by simplicity and transparency with the use, where appropriate, of passive safety features.
1.3	Safety classification based on: design basis conditions (DBC) and design extension conditions (DEC).
1.4	Safety systems performing DBC functions and certain DEC functions are required to have a degree of redundancy, diversity (e.g. passive versus active), independence, functional isolation and segregation to ensure prevention from common cause failure
1.5	Design shall ensure autonomy that for DBCs and complex sequences, a safe shutdown state can be reached, as a goal within 24 hours from accident start and in any case within 72 hours. For DEC a safe shutdown state should be reached within 1 week as a goal and before 30 days in any case.
1.6	EUR requires in addition the consideration of other engineering criteria, such as prevention of common cause failures, diversity, independence and segregation
1.7	External hazards like earthquake, extreme weather, floods, aircraft crash, adjacent installations, electromagnetic interference, sabotage and internal hazards like fire, noxious substances, failure of pressure parts, disruption of rotary equipment, dropped loads and electromagnetic interference must be addressed
1.8	Requirements on the systems are set in terms of operational performance to ensure the reactivity control, heat removal and radioactivity confinement. Reactivity coefficients acceptable values, stable operation and reliability of the shutdown systems are all EUR requirements
1.9	For the core heat removal, temperature, pressure, flow and inventory control are required besides depressurization capability and pressure boundary integrity. For the latter, the use of the leak before break (LBB) methodology is foreseen
1.10	In the very long term after an accident, provisions for the connection of mobile equipment are required.
1.11	Important provisions required by EUR to demonstrate the in vessel corium cooling and avoidance of base mat perforation by the use of automatic depressurization system and the core spreading area that allows for solidification of the crust
1.12	Under DECs, a classical environmental qualification is not required; rather, equipment survival must be demonstrated.

Table 2. Goals for Generation IV nuclear systems

Sustainability–1.	Generation IV nuclear energy systems will provide sustainable energy generation that meets clean air objectives and promotes long term availability of systems and effective fuel utilization for worldwide energy production.
Sustainability–2.	Generation IV nuclear energy systems will minimize and manage their nuclear waste and notably reduce the long term stewardship burden, thereby improving protection for the public health and the environment.
Safety and Reliability–1.	Generation IV nuclear energy systems operations will excel in safety and reliability.
Safety and Reliability–2.	Generation IV nuclear energy systems will have a very low likelihood and degree of reactor core damage.
Safety and Reliability–3.	Generation IV nuclear energy systems will eliminate the need for offsite emergency response.
Economics–1.	Generation IV nuclear energy systems will have a clear life cycle cost advantage over other energy sources.
Economics–2.	Generation IV nuclear energy systems will have a level of financial risk comparable to other energy projects.
Proliferation Resistance and Physical Protection–1	Generation IV nuclear energy systems will increase the assurance that they are a very unattractive and the least desirable route for diversion or theft of weapons-usable materials, and provide increased physical protection against acts of terrorism.

In an international activity involving 21 IAEA Member States and the European Commission, the IAEA’s INPRO project has prepared guidance for the evaluation of innovative nuclear reactors and fuel cycles by establishing basic principles¹ and user requirements for innovative nuclear energy systems in the areas of economics, safety, environment, waste management, proliferation resistance and infrastructure [15]. The INPRO basic principles are presented below and user requirements are presented in Appendix 1 of Annex 1:

Economics

- Energy and related products and services from Innovative Nuclear Energy Systems shall be affordable and available.

Safety of nuclear installations

- Installations of an Innovative Nuclear Energy System shall incorporate enhanced defence-in-depth as a part of their fundamental safety approach and ensure that the levels of protection in defence-in-depth shall be more independent from each other than in existing installations.

¹ In the context of INPRO, a basic principle is a statement of a general rule providing guidance for the development of an innovative nuclear energy system. A user requirement is a condition that should be met to achieve users’ acceptance of an innovative nuclear energy system.

- Installations of an INS shall excel in safety and reliability by incorporating into their designs, when appropriate, increased emphasis on inherently safe characteristics and passive systems as a part of their fundamental safety approach.
- Installations of an INS shall ensure that the risk from radiation exposures to workers, the public and the environment during construction/commissioning, operation, and decommissioning, are comparable to the risk from other industrial facilities used for similar purposes.
- The development of INS shall include associated research, development and demonstration work to bring the knowledge of plant characteristics and the capability of analytical methods used for design and safety assessment to at least the same confidence level as for existing plants.

Environment

- (Acceptability of expected adverse environmental effects) The expected (best estimate) adverse environmental effects of the innovative nuclear energy system shall be well within the performance envelope of current nuclear energy systems delivering similar energy products.
- (Fitness for purpose) The INS shall be capable of contributing to the energy needs in the 21st century while making efficient use of non-renewable resources

Waste management

- (Waste minimization) Generation of radioactive waste in an INS shall be kept to the minimum practicable.
- (Protection of human health and the environment) Radioactive waste in an INS shall be managed in such a way as to secure an acceptable level of protection for human health and the environment, regardless of the time or place at which impacts may occur.
- (Burden on future generations) Radioactive waste in an INS shall be managed in such a way that it will not impose undue burdens on future generations.
- (Waste optimization) Interactions and relationships among all waste generation and management steps shall be accounted for in the design of the INS, such that overall operational and long term safety is optimized.

Proliferation resistance

- Proliferation resistance features and measures shall be implemented throughout the full life cycle for innovative nuclear energy systems to help ensure that INSs will continue to be an unattractive means to acquire fissile material for a nuclear weapons programme.
- Both intrinsic features and extrinsic measures are essential, and neither shall be considered sufficient by itself.

Infrastructure

- Regional and international arrangements shall provide options that enable any country that so wishes to adopt INS for the supply of energy and related products without making an excessive investment in national infrastructure.

It is important to note that some advanced nuclear power plant designs incorporate the use of systems based on natural circulation to achieve plant safety and economic goals described above. The next section introduces some of the design concepts for natural circulation systems.

1.2. Examples of natural circulation systems for advanced designs

Various organizations are involved in the development of advanced reactors, including governments, industries, utilities, universities, national laboratories, and research institutes. Global trends in advanced reactor designs and technology development are periodically summarized in status reports, symposia and seminar proceedings prepared by the IAEA [13], [14], [16], [17], [18] to provide all interested IAEA Member States with balanced and objective information on advances in nuclear plant technology.

Advanced designs comprise two basic categories. The first category consists of evolutionary designs and encompasses direct descendants from predecessors (existing plant designs) that feature improvements and modifications based on feedback of experience and adoption of new technological achievements, and possibly also introduction of some innovative features, e.g. by incorporating passive safety systems. Evolutionary designs are characterized by requiring at most engineering and confirmatory testing prior to commercial deployment. The second category consists of designs that deviate more significantly from existing designs, and that consequently need substantially more testing and verification, probably including also construction of a demonstration plant and/or prototype plant, prior to large-scale commercial deployment. These are generally called innovative designs. Often a step increase in development cost arises from the need to build a prototype reactor or a demonstration plant as part of the development programme.

Annex 1 provides a discussion of the advanced water cooled reactors currently being developed worldwide. This section provides examples of natural circulation systems being incorporated into advanced water cooled reactor designs. More detailed information can be found in Annex 3, Annex 4, Annex 12 and Reference [13].

Natural circulation can be used as a means of cooling the core under normal operation (see the example in Section 1.2.3). Also, several advanced water cooled reactors incorporate passive safety systems based on natural circulation. Before delving into the details, it is useful to define what is meant by a passive safety system. A passive safety system provides cooling to the core or the containment using processes such as natural convection heat transfer, vapour condensation, liquid evaporation, pressure driven coolant injection, or gravity driven coolant injection. It does not rely on external mechanical and/or electrical power, signals or forces such as electric pumps following its initiation. For example, to obtain final Design Approval from the U.S. Nuclear Regulatory Commission in the United States, a passively safe nuclear plant designer must demonstrate that under worst-case accident conditions the plant can be passively cooled without external power or operator actions for a minimum of 3 days [19]. A useful list of terminology related to passive safety is provided in IAEA-TECDOC-626 [1].

1.2.1. AP1000 passive safety systems

1.2.1.1. AP1000 passive residual heat removal systems (PRHR)

This section describes the PRHR implemented in the Westinghouse AP1000 design. The PRHR consists of a C-Tube type heat exchanger in the water-filled In-containment Refueling Water Storage Tank (IRWST) as shown in the schematic given in Figure 1. The PRHR provides primary coolant heat removal via a natural circulation loop. Hot water rises through the PRHR inlet line attached to one of the hot legs. The hot water enters the tubesheet in the top header of the PRHR heat exchanger at full system pressure and temperature. The IRWST is filled with cold boric acid water and is open to containment. Heat removal from the PRHR heat exchanger occurs by boiling on the outside surface of the tubes. The cold primary coolant returns to the primary loop via the PRHR outlet line that is connected to the steam generator lower head.

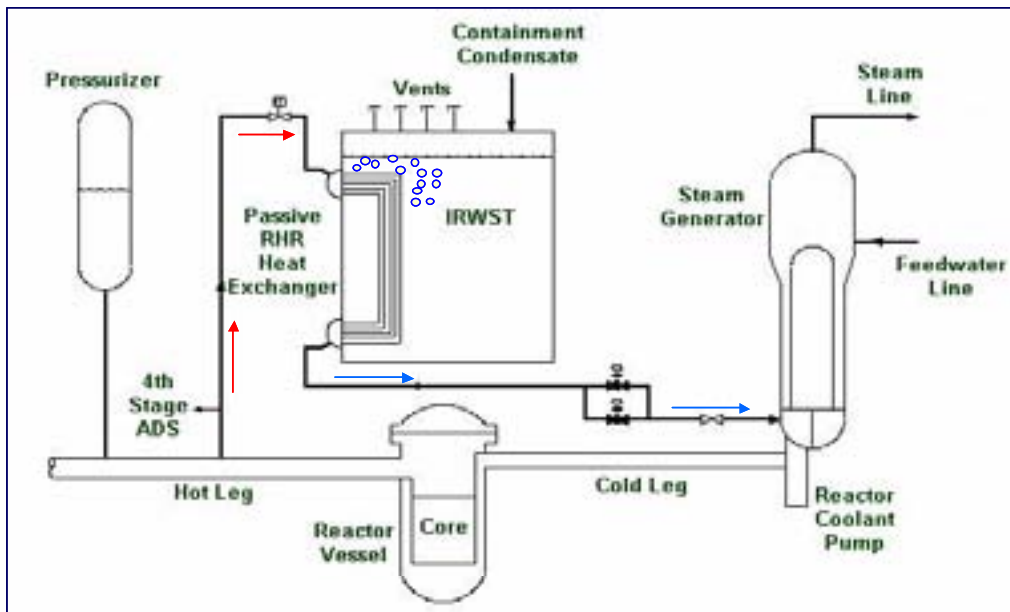


FIG. 1. AP1000 passive residual heat removal systems (PRHR).

1.2.1.2. AP1000 core make-up tank (CMT)

This section describes the CMTs incorporated into the AP1000 design. The Core Make-up Tanks effectively replace the high-pressure safety injection systems in conventional PWRs. A schematic is shown in Figure 2. Each CMT consists of a large volume stainless steel tank with an inlet line that connects one of the cold legs to the top of the CMT and an outlet line that connects the bottom of the CMT to the Direct Vessel Injection (DVI) line. The DVI line is connected to the reactor vessel downcomer. Each CMT is filled with cold borated water. The CMT inlet valve is normally open and hence the CMT is normally at primary system pressure. The CMT outlet valve is normally closed, preventing natural circulation during normal operation. When the outlet valve is open, a natural circulation path is established. Cold borated water flows to the reactor vessel and hot primary fluid flows upward into the top of the CMT.

1.2.1.3. AP1000 containment sump recirculation

Figure 2 also shows the containment sump recirculation loop. After the lower containment sump and the IRWST liquid levels are equalized, the sump valves are opened to establish a natural circulation path. Primary coolant is boiled in the reactor core by decay heat. This low-density mixture flows upward through the core and steam and liquid is vented out of the Automatic Depressurization System 4 (ADS-4) lines into containment. Cooler water from the containment sump is drawn in through the sump screens into the sump lines that connect to the DVI lines.

1.2.1.4. AP1000 passive containment cooling system (PCCS)

Figure 3 presents a schematic of the AP600/AP1000 containment. It consists of a large steel vessel that houses the Nuclear Steam Supply System (NSSS) and all of the passive safety injection systems. The steel containment vessel resides inside of a concrete structure with ducts that allows cool outside air to come in contact with the outside surface of the containment vessel. When steam is vented into containment via a primary system break or ADS-4 valve actuation, it rises to the containment dome where it is condensed into liquid. The energy of the steam is transferred to the air on the outside of containment via conduction through the containment wall and natural convection to the air. As the air is heated, it rises through the ducts creating a natural circulation flow path that draws cool air in from the inlet duct and vents hot air out the top of the concrete structure. The condensate inside containment

is directed back into the IRWST and the containment sump where it becomes a source of cool water in the sump recirculation process. Early in a LOCA transient, cold water is sprayed by gravity draining onto the containment vessel head to enhance containment cooling. A large tank of water, located at the top of the containment structure, serves as the source of water for this operation.

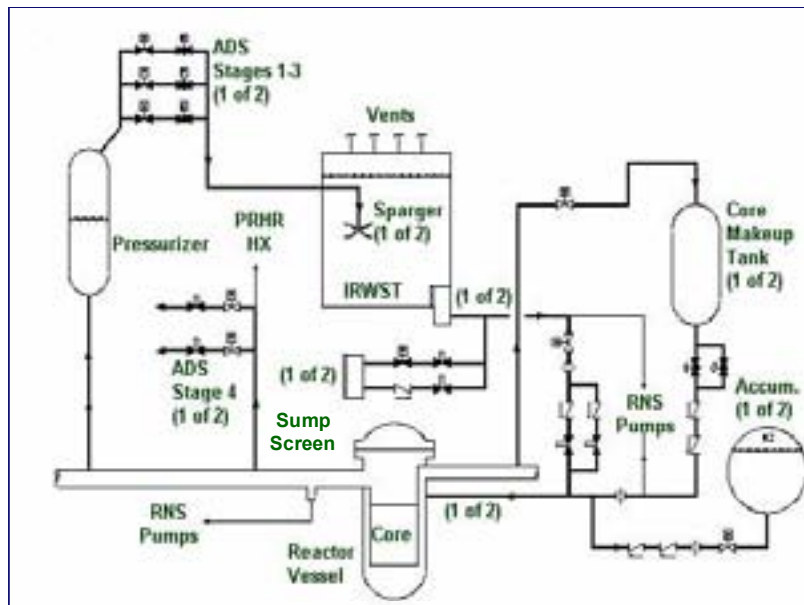


FIG. 2. Schematic of the AP1000 passive safety systems including the CMTs and sump recirculation system.

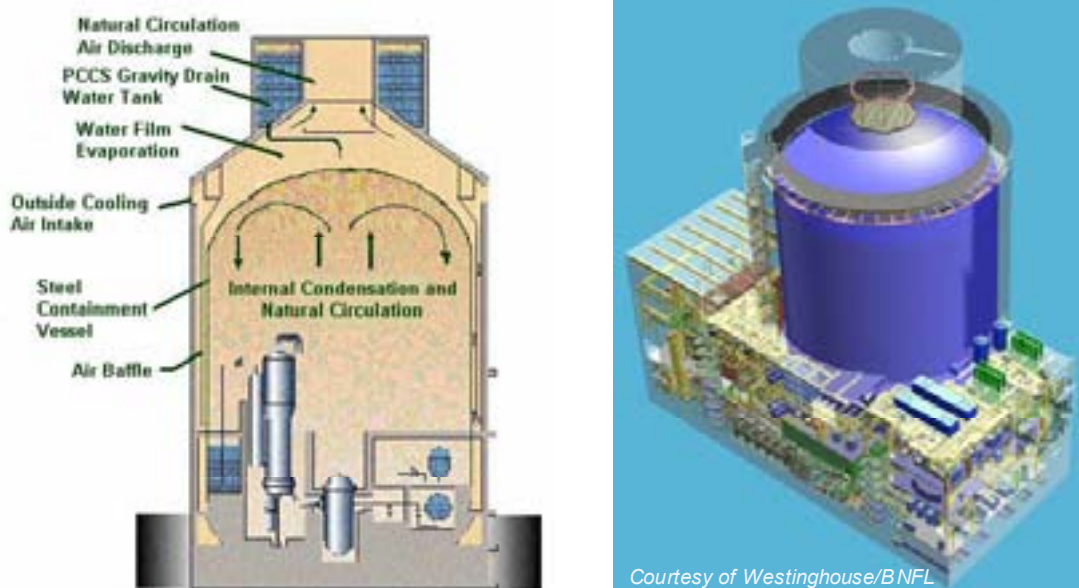


FIG. 3. AP1000 containment and passive containment cooling system (PCCS).

1.2.2. SWR1000 passive safety systems

The cooling of the containment atmosphere by containment condensers installed near the roof is also proposed for the SWR1000 reactor design. The SWR1000 has a containment-cooling condenser (CCC) with its secondary system connected to an external pool, as in Figure 5. In the event of failure

of the active residual heat removal systems, four CCCs are designed to remove residual heat from the containment to the dryer-separator storage pool located above the containment. The CCCs are actuated by rising temperatures in the containment. They use natural circulation both on the primary and on the secondary sides. The CCC is a simple heat exchanger mounted about 1 m above the water level of the core reflooding pool. If the temperature in the drywell atmosphere increases over that in the dryer-separator storage pool, the water inside the heat exchanger tubes heats up. It flows to the outlet line due to the slope of the exchanger tubes. The outlet line ends at a higher elevation level than the inlet line; consequently the lifting forces are increased for the whole system. Depending on the heat transfer rate and cooling water temperature, secondary-side flow can be single-phase, intermittent, or two-phase. In the hypothetical case of a core melt accident, a hydrogen-steam mixture would also be possible. Given nitrogen, steam and mixture thereof, primary flow is downwards due to the densities of pure gases and a nitrogen-steam mixture increase with decreasing temperature. This results in the expected downward flow. Condensed steam drops into the core flooding pool. However, the opposite is true for a hydrogen-steam mixture, as the density of this mixture decreases with decreasing temperature, resulting in an upward flow through the heat exchanger tube bundle. But this does not pose any problem for the SWR1000 because both directions of flow on the primary side are equivalent.

The SWR-1000 implements a passive emergency condenser as shown in Figure 4. The reactor vessel (RV) is connected, via a feed line and a back line, to a tube heat exchanger that resides in a very large pool of water at ambient temperature. The feed line, tube bundle and back line, form a loop that acts as a manometer. Hence the liquid elevation in the loop equals the liquid elevation in the reactor vessel. During normal operating conditions, the feed line is partially filled with liquid because the reactor liquid level is high. The high liquid level prevents vapour from the vessel head to enter the tube bundle. This is shown on the left side of Figure 4.

Accidents that cause the liquid level in the vessel to drop will cause a corresponding drop in the liquid level in the loop. This is shown on the right side of Figure 4. If the level RV drops such that the feed line clears, vapour from the RV head will enter the tube bundle and condense. Steam condensation creates a low-pressure region inside the heat exchanger tubes, drawing in additional steam. The condensate returns to the RV via the back line. The condensate also fills the loop-seal portion of the back line to prevent counter-current flow in the back line.

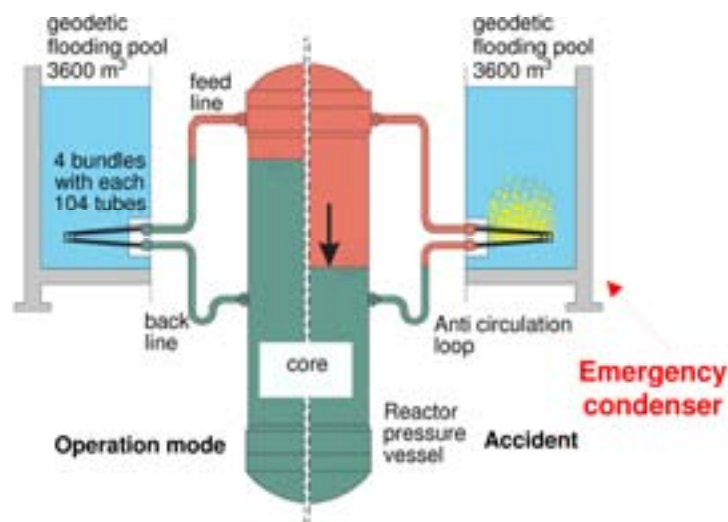


FIG. 4. SWR-1000 emergency condenser.

1.2.3. ESBWR passive safety systems

The PCCS is the preferred means of decay heat removal following a LOCA for ESBWR (Figures 5 and 6). The system is a unique ESBWR engineered safety feature (similar to the SBWR PCCS). Containment heat removal is provided by the PCC system, consisting of four low-pressure loops, which is a safety related system [20], [21]. Each loop consists of a heat exchanger, which opens to the containment, a condensate drain line that returns the PCCS condensate to a PCCS condensate tank, which is connected to the RPV via its own nozzle, and a vent discharge line submerged in the suppression pool. The four heat exchangers, similar to the ICs, are located in cooling pools external to the containment. Once PCCS operation is initiated following RPV depressurization, the condensate return line to the vessel is opened permanently. The PCCS uses natural convection to passively provide long term containment cooling capability. The PCCS pool is sized to remove post-LOCA decay heat at least 72 hours without requiring the addition of pool inventory.

The PCCS heat exchangers are extensions of containment. The lines entering and leaving the PCCS from the drywell do not have containment isolation valves. No sensing, control, logic or power operated devices are required for the PCCS to initiate. Flow through the PCCS loop is driven by the pressure difference created between the containment drywell and the suppression pool that exists following a LOCA and the pressure drop through the PCCS tubes. The PCCS condensate is returned to the RPV under the force of gravity.

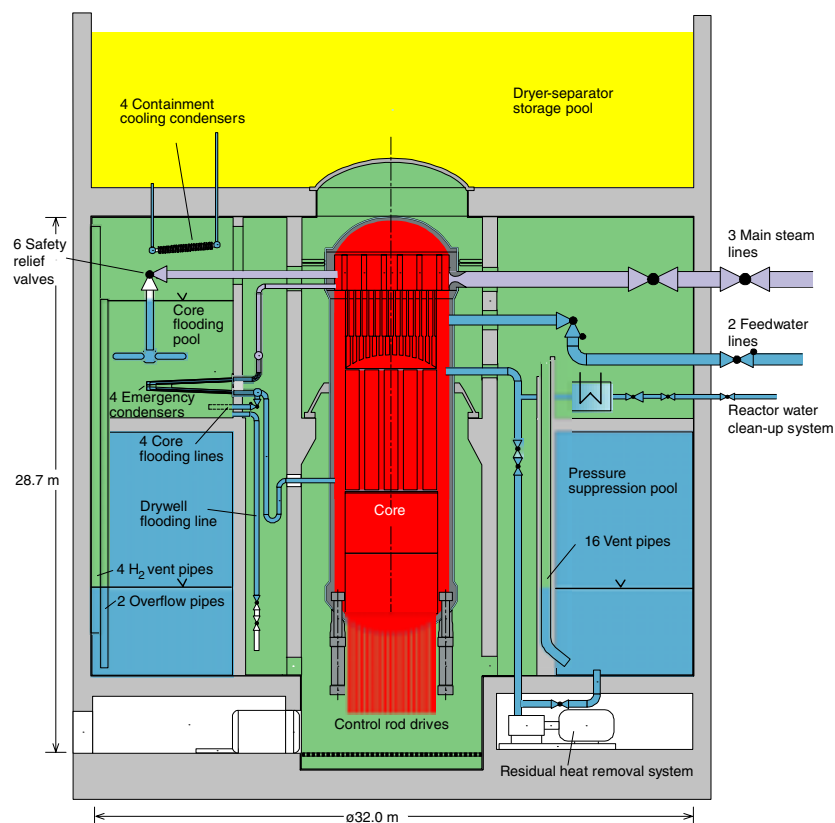


FIG. 5. Conceptual arrangement of the SWR1000 containment and passive safety cooling systems.

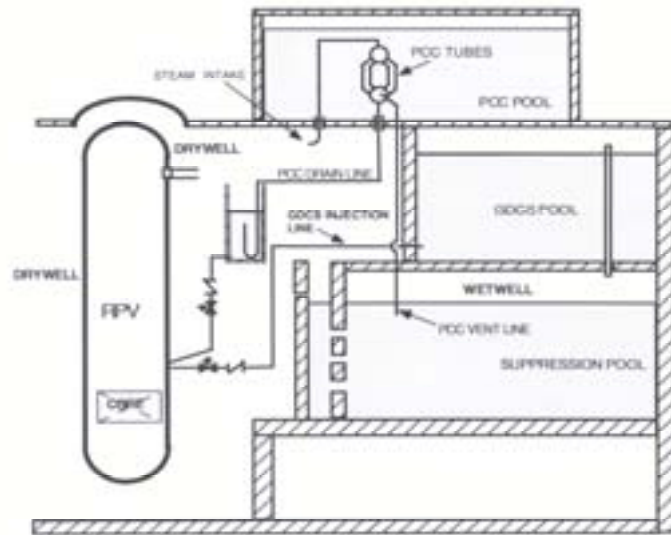


FIG. 6. The ESBWR passive containment cooling system condenses containment steam and vents the non-condensable to the suppression pool.

1.2.4. Natural circulation core cooling

Several advanced reactor designs use natural circulation for core cooling during normal operation. These systems operate at full reactor power using natural circulation to drive fluid flow through the core. They tend to be small integral reactors like the Multi-Application Small Light Water Reactor (MASLWR) described in Annex 11 or the CAREM and SMART reactors described in Reference [13]. Figure 7 presents a schematic that illustrates the salient features. Natural circulation arises because of the fluid density difference between the heat source (core) and the elevated heat sink (helical coil heat exchanger).

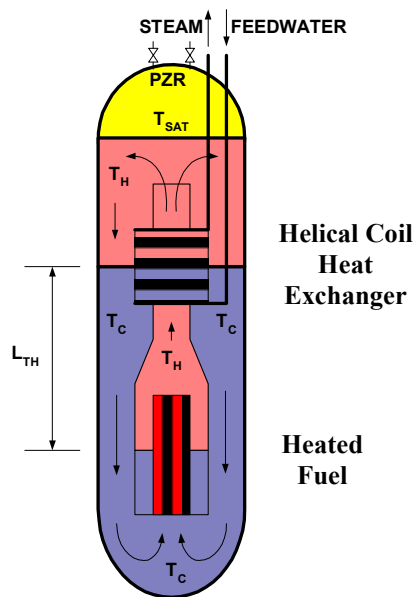


FIG. 7. Single-phase natural circulation flow within an integral reactor.

2. ADVANTAGES AND CHALLENGES OF NATURAL CIRCULATION SYSTEMS IN ADVANCED DESIGNS

Table 3 highlights some of the advantages and disadvantages of natural circulation systems in advanced designs. Annex 2 and Annex 3 provide more detailed comparisons.

Table 3. Some advantages and disadvantages of natural circulation systems

Advantages	Disadvantages
Reduced Cost through Simplicity	Low Driving Head
Pumps Eliminated	Lower Maximum Power per Channel
Possibility of Improved Core Flow Distribution	Potential Instabilities
Better Two-Phase Characteristics as a Function of Power	Low Critical Heat Flux
Large Thermal Inertia	Specific Start up Procedures Required

2.1. Some advantages

The primary advantage of a natural circulation system is simplicity. The elimination of active power supplies and pumps can greatly simplify the construction, operation and maintenance of the system. Furthermore, elimination of the pumps and connecting piping also eliminates accident scenarios associated with loss of pump flow, pump seal rupture accidents and loop seal manometer effects during Small Break Loss-of-Coolant-Accidents (SBLOCAs).

Another advantage is that the flow distribution in parallel channel cores is much more uniform in a natural circulation system. In addition, the two-phase fluid flow characteristics as a function of power are also better in a natural circulation system. That is, the flow increases with power, whereas in a forced circulation two-phase fluid system, the flow decreases with an increase in power.

Because of the low head requirements, natural circulation reactor systems tend to have large volumes and relatively low power densities compared to forced flow systems of the same power rating. As a result, the thermal response of natural circulation systems is slow, giving operators ample time to respond to plant upsets.

2.2. Some disadvantages

The primary disadvantage of a natural circulation system is that the driving head is low. To increase the flow rate at a fixed power would require either an increase in the loop height or a decrease in the loop resistance, either of which might increase plant costs.

In general, the mass flux through a natural circulation cooled core is low. As a result, the allowable maximum channel power is lower leading to a larger core volume compared to a forced circulation system of the same rating. Furthermore, large core volumes can result in zonal control problems and stability. While instability is common to both forced and natural circulation systems, the latter is inherently less stable than forced circulation systems. This is attributable to the nonlinear nature of the natural circulation phenomenon, where any change in the driving force affects the flow which in turn affects the driving force that may lead to an oscillatory behavior.

The low mass flux also has an impact on the critical heat flux in BWRs. Since flow in natural circulation reactors is lower, they tend to use the maximum allowable exit quality to minimize their size. In the process, their CHF value tends to be significantly lower than that of forced circulation BWRS. This calls for several measures to increase the CHF.

Natural circulation reactors are to be started up from stagnant low pressure and low temperature condition. During the pressure and power raising process, passing through an unstable zone shall be avoided as instability can cause premature CHF occurrence. Under the circumstances, it is essential to

specify a start up procedure that avoids the instability. Selection of the pressure at which to initiate boiling and appropriate procedures for raising pressure and power is central to the specification of a start up procedure. In addition, it may become essential to control the inlet subcooling as a function of power. For a cold start up (first start up) an external source for pressurization may be required. For these reasons, the selection of a start up procedure for a natural circulation reactor is not always an easy task.

2.3. Need for natural circulation system data and analysis methods

Based on the foregoing discussion, it is apparent that implementing natural circulation as a central mechanism for nuclear core heat removal, either directly or through the use of passive safety systems, will require a thorough understanding of both local and integral system natural circulation phenomena, validated benchmark data, accurate predictive tools, and comprehensive reliability analysis methods.

2.3.1. Local and integral system phenomena

There are three important reasons for identifying the local and integral system phenomena that can impact the natural circulation behavior of a passive safety system or nuclear plant design. First, some local and integral system phenomena may have the potential of adversely affecting the reliability of passive safety systems. Second, some model development may be needed to accurately model these phenomena using predictive tools. Last, it is important to assure that all of the important phenomena are faithfully simulated in the test facilities that will be used to assess the safety and operation of an advanced plant design.

2.3.2. Benchmark data

A predictive tool, such as a computer code, must be assessed against applicable experimental data before it can be used in the design or analysis of a reactor system. The uncertainty in the code's predictions of key safety parameters must be established and its ability to model system operation during normal and transient conditions must be demonstrated. This is typically required to obtain final design approval and plant certification. Although numerous natural circulation experiments have been conducted, finding a database that directly relates to new design may be difficult. It is more likely that a new, properly scaled, test facility will need to be designed and operated to obtain a sufficiently broad range of data so that the code is fully exercised and assessed.

2.3.3. Predictive tools

Analysis of single-phase fluid natural circulation systems under steady-state conditions is relatively straightforward for water cooled reactors. However, the tools for analysing complex two-phase fluid natural circulation systems may not be readily available for some designs, particularly when considering operational stability. For example, assessing the stability of a two-phase fluid natural circulation system under transient conditions may require using a coupled neutron kinetics and thermal hydraulics computer code. Some model development may be required to address the features of a particular design.

2.3.4. Reliability analysis methods

The reliability of passive systems that utilize natural circulation may be influenced by a variety of phenomena. This includes the effect of non-condensable gases on heat transfer, thermal stratification, mass stratification, pool heat transfer, moisture carryover, and others. It is important that all the phenomena that can impact the reliability of a natural circulation based passive system be identified and addressed in the design. Furthermore, a method that is both auditable and traceable is needed to assess the reliability of such passive safety systems.

The present knowledge in each of these areas is considered in the sections that follow.

3. LOCAL TRANSPORT PHENOMENA AND MODELS

This chapter describes some of the local transport phenomena encountered in the natural circulation systems of an advanced water cooled reactor. Generally speaking, local transport phenomena govern the mass, momentum, and energy transfers within, and at the boundaries of, the components and subsystems that comprise the integral system. The types of mathematical models used to describe local transport phenomena consist of local conservation equations and correlations that have been validated by experiment.

Some typical passive safety systems and key components are listed in Table 4 and the phenomena occurring in each are briefly explained. A comprehensive coverage of related thermal hydraulic relationships and models is provided in Annex 5.

Additional information on thermal hydraulic phenomena of interest in advanced reactors can be found in OECD/CSNI Report No. 132 on integral test facility, computer code validation matrix [22]. It includes both local transport and integral system transport phenomena of importance to advanced reactors.

3.1. Reactor core phenomena

Three categories of local transport phenomena in the core can impact natural circulation behavior in the system. The first category is core heat transfer since it is the mechanism that provides the buoyant fluid that drives natural circulation flow. The second is the core pressure drop, which tends to be the largest source of flow resistance in the natural circulation loop. The last category is core flow stability, which is of particular importance to boiling water reactors having a large numbers of parallel channels. Parallel channel flow stability in BWRs is addressed in Annex 10 and will be discussed in the next chapter of this report.

The ability of the fluid to remove core heat depends on numerous factors such as the fuel geometry (rod bundle fuel, annular fuel, square array, triangular array, surface area), the fluid properties (thermal conductivity, specific heat, density, viscosity), the flow properties (fluid velocity, flow distribution), the fuel materials (conductivity, specific heat, stored energy) and the fuel decay heat. Numerous convective heat transfer correlations have been developed over the years. These are summarized in Annex 5.

3.2. Interconnecting piping

The pressure drop in the interconnecting piping will impact the loop natural circulation flow rates. If two-phase fluid is present, the pressure drop will be strongly influenced by the two-phase fluid flow regime and density. Some advanced designs implement a tall vertical chimney (i.e. riser) at the exit of the core. The static pressure in the chimney decreases with increasing height. As the fluid travels upward through the chimney, it is possible for hot single-phase liquid to reach its saturation pressure and flash to vapor. This phenomenon may affect the flow rate (e.g. geysering) and possibly impact system stability.

3.3. Heat sinks (steam generators)

The primary means of core heat removal during normal operation is either by vapor generation in the core (direct cycle BWR) or by heat transfer to a steam generator. Two categories of local transport phenomena in the steam generator can impact natural circulation behavior in the system. The first phenomenon is steam generator heat transfer since it is the mechanism that provides the negatively buoyant fluid that helps drive natural circulation flow. The second phenomenon is the steam generator pressure drop, which tends to be the second largest source of flow resistance in the natural circulation loop.

Table 4. Local transport phenomena in a variety of NPP natural circulation systems

Component	Phenomena
Reactor Core (Heat Source)	Fuel Heat Transfer
	<ul style="list-style-type: none"> • Fuel/Cladding Conduction (geometry specific)
	<ul style="list-style-type: none"> • Gap Conductance (fuel specific)
	<ul style="list-style-type: none"> • Stored Energy Release
	<ul style="list-style-type: none"> • Cladding Convective Heat Transfer <ul style="list-style-type: none"> ○ Single-Phase Forced, Mixed or Natural Convection ○ Two-Phase Subcooled, Nucleate or Film Boiling ○ Critical Heat Flux (DNB or Dryout)
	<ul style="list-style-type: none"> • Decay Heat
	Pressure Drop (Single and Two-Phase Fluid)
	<ul style="list-style-type: none"> • Friction, Static, and Acceleration Pressure Drops • Void Fraction
	Parallel Channel Flow Stability
	Interconnecting Piping
<ul style="list-style-type: none"> • Friction, Static, and Acceleration Pressure Drops • Void Fraction 	
<ul style="list-style-type: none"> • Single-Phase Fluid Flashing 	
Heat Sinks (Steam Generators)	Convective Heat Transfer in Horizontal or Vertical Tubes
	Pressure Drop
Passive Residual Heat Removal Heat Exchanger	Natural Circulation Flow Rate
	Tube Bundle Internal and External Convective Heat Transfer
	Tube Wall Conduction Heat Transfer
	Tube Bundle Pressure Drop
Containment Shell (External Air or Water Cooling)	Internal Wall Heat Transfer
	<ul style="list-style-type: none"> • Non-condensable Gas Mass Fraction • Vapour Condensation Rates • Condensate Film • Natural Convection Flow Rates and Patterns • Containment Shell Heat Capacitance
	Wall Heat Conductance
	External Heat Transfer
	<ul style="list-style-type: none"> • Natural Convection Heat Transfer • Natural Convection Flow Patterns
Containment Cooling Condensers/Heat Exchangers	Tube Heat Transfer
	<ul style="list-style-type: none"> • Non-condensable Gas Mass Fraction • Vapour Condensation Rates
	Counter-Current Flow Limitations
	Entrainment/De-entrainment
	Flow Resistance
Large Cooling Pools (For Heat Exchangers, Spargers and as a Source of Coolant)	Thermal Stratification/Fluid Mixing
	Vortex Formation
	Direct Contact Condensation

The ability of the steam generator to remove core heat depends on numerous factors such as the steam generator tube bundle geometry and orientation (vertical or horizontal), the fluid properties (thermal conductivity, specific heat, density, viscosity, void fraction), the flow properties (fluid velocity, flow distribution), and the tube bundle materials (conductivity, specific heat, stored energy). It is important to note that the integral reactors implement helical coil steam generators that permit boiling inside the tubes. This presents the potential for some steam side instabilities. Several convective heat transfer correlations applicable to steam generators are summarized in Annex 5.

3.4. Passive residual heat removal system

As described in Section 1.1.1, some advanced designs implement a passive residual heat removal (PRHR) system for the purpose of removing core decay heat subsequent to reactor scram. Several thermal hydraulic phenomena can impact the performance of the PRHR system. The internal convection heat transfer coefficient is governed by the natural circulation flow rate through the tubes. The natural circulation flow rate is strongly impacted by the tube and tube sheet pressure drops. Typical operation is under single-phase fluid conditions inside the tubes. Heat conduction through the tube walls may also have an impact on heat transfer, particularly if tube fouling occurs.

Convection heat transfer on the outside surface of the tubes is typically two-phase nucleate boiling which is a very efficient means of heat removal. Heat transfer correlations for heat exchanger tubes are provided in Annex 5.

3.5. Containment shell (external air or water cooling)

Some advanced reactor designs (e.g. AP600, AP1000, MASLWR) provide either air-cooling or water-cooling to the exterior surface of the containment shell. In so doing, the containment shell serves as the ultimate heat sink during a LOCA. The important local transport phenomena include heat transfer from vapor to the inside surface of the containment shell, thermal conduction through the containment wall and heat transfer from the exterior surface of the containment shell to the ambient air or liquid.

The capability of the containment shell to act as a heat exchanger is impacted by the amount of non-condensable gas present inside the containment free space. Non-condensable gases can effectively act as insulation resulting in reduced heat transfer and vapor condensation rates. The containment geometry and internal surface area are also important because they can affect the condensate film thickness, which in turn impacts heat transfer. The natural convection flow rates and flow patterns of the vapor inside containment will also impact heat transfer from the vapor to the containment shell.

Containment shell heat capacitance plays an important role during the initial part of a LOCA because a significant amount of energy is transferred from the vapor to the containment structure during its initial heating. The transport of heat through the containment wall is impacted by the wall conductance.

Heat transfer from the exterior surface of the containment shell is dictated by the natural convection heat transfer coefficient and natural convection flow patterns at the exterior surface.

3.6. Containment cooling condensers/heat exchangers

Section 1.2.5 describes the passive containment cooling system for the SWR-1000 and ESBWR. Several local transport phenomena can impact PCCS tube heat transfer, including the presence of non-condensable gases, the vapor condensation rate, counter-current flow limitations, entrainment and de-entrainment and flow resistance. Models for each of these phenomena are needed to model PCCS behavior.

3.7. Large cooling pools (for heat exchangers, spargers and as a source of coolant)

Several advanced designs use large pools of water as heat sinks for passive heat exchangers that provide either core or containment cooling via natural circulation. These large pools also serve as pressure suppression pools that condense steam by direct contact condensation. A variety of phenomena can impact their function as serving as a heat sink or suppression pool.

Natural convection flow patterns and thermal stratification of the liquid in the tank will impact the heat exchanger heat transfer rate. Steam condensation chugging (condensation pressure waves), liquid subcooling and sparger geometry can impact the pool's function of pressure suppression. Heat and mass transfer at the upper interface (e.g. vaporization) may have a minor impact.

Some cooling pools also serve as gravity drain tanks for coolant injection into the primary system or for containment cooling. The phenomenon of vortex formation at the drain location can impact the draining rate.

The local transport phenomena identified in this section are representative of many of the advanced designs that implement natural circulation systems. The paper included as Annex 5 to this report provides a description of additional local transport phenomena and models.

4. INTEGRAL SYSTEM PHENOMENA AND MODELS

This chapter describes some of the integral system phenomena encountered in the natural circulation systems of an advanced water cooled reactor. Integral system behavior can be rather complex because it arises through the synergy of the many local transport phenomena occurring in components and subsystems. The predictive tools used to describe integral system phenomena typically consist of systems analysis computer codes. This chapter has three main sections. The first section provides a brief overview of the working principles of a natural circulation loop. The second section presents the governing equations for single and two-phase natural circulation flow. The third section briefly examines the issue of natural circulation stability. The detailed description of each of these topics can be found in Annex 6 through Annex 10.

4.1. Working principles of a natural circulation loop

Natural circulation in a fluid filled closed loop is established by locating a heat sink in the loop at an elevation that is higher than the heat source. A simple rectangular loop is illustrated in Figure 8.

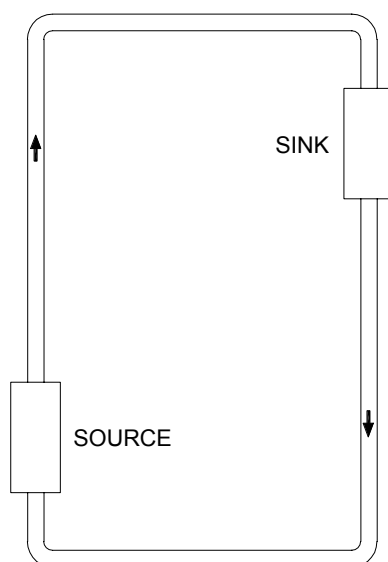


FIG. 8. A Rectangular closed natural circulation loop.

The fluid in contact with the heat source is being heated so that its density is decreasing. The fluid in contact with the heat sink is being cooled so that its density is increasing. Hence, a fluid density difference is established in the loop. This density difference, acted upon by gravity over the difference in elevation between the source and the sink, produces a buoyancy force that drives the fluid through the loop. This behavior is known as natural circulation.

Fluid density differences can be created by changes in temperature or by changes in phase (i.e. vapor/liquid), as is the case for two-phase fluids. The flow rate through the loop is limited by the sum of the resistances in the components and interconnecting piping. Because of its simplicity, natural circulation loops are widely used in energy conversion systems.

The following section presents the governing equations for single and two-phase fluid natural circulation loops.

4.2. Governing equations for single and two-phase natural circulation flow

Annex 6, Annex 7 and Annex 11 of this report provide useful descriptions of the governing equations for single-phase and two-phase natural circulation. This chapter summarizes the results of those formulations for the loops shown in Figures 8 and 9.

4.2.1. Governing equations for single-phase natural circulation flow

As shown in this figure, the loop being considered consists of the core, which serves as a heat source, the riser, the annular downcomer region between the riser and the reactor vessel, and the helical steam generator coil that serves as the heat sink. A simple sketch is presented in Figure 9. As shown in this figure, the primary loop is divided into a hot fluid side having an average temperature T_H and a cold fluid side having an average temperature T_C .

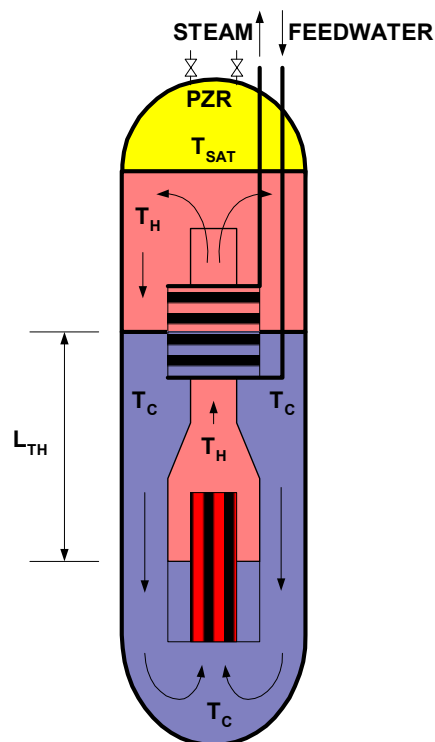


FIG. 9. Hot and cold regions of single-phase natural circulation flow within an integral reactor.

Mass, momentum and energy control volume balance equations can be written for each component. For purposes of the single-phase natural circulation flow analysis, the following assumptions were made:

1. The flow was one-dimensional along the loop axis, therefore fluid properties were uniform at every cross-section.
2. The Boussinesq approximation was applicable.
3. The fluid was incompressible.
4. T_C is constant
5. Form losses, primarily in the core and steam generator regions, dominate the loop resistance.

By implementing the Boussinesq approximation, all of the fluid densities in the loop were assumed equal to an average fluid density except for those that comprise the buoyancy term. T_M is a mixed mean temperature for the system.

The fact that the components of the loop remain liquid filled during the natural circulation mode of operation coupled with the third assumption eliminates the time dependence in the component mass conservation equation. Applying these assumptions to the component balance equations and integrating the momentum and energy equations over the entire loop, yielded the following momentum and energy balance equations for fluid transport around the loop:

Loop Momentum Balance Equation:

$$\sum_{i=1}^N \left(\frac{l_i}{a_i} \right) \cdot \frac{d\dot{m}}{dt} = \beta g \rho (T_H - T_C) L_{th} - \frac{\dot{m}^2}{\rho_l a_c^2} \sum_{i=1}^N \left[\frac{1}{2} \left(\frac{fl}{d_h} + K \right)_i \left(\frac{a_c}{a_i} \right)^2 \right] \quad (1)$$

Loop Energy Balance Equation:

$$C_{vl} M_{sys} \frac{d(T_M - T_C)}{dt} = \dot{m} C_{pl} (T_H - T_C) - \dot{q}_{SG} - \dot{q}_{loss} \quad (2)$$

Under steady-state conditions, these equations yield the following simple solution for the fluid velocity through the core.

$$u_{co} = \left(\frac{\beta \dot{q}_{co} L_{th} g}{\rho_l a_c C_{pl} \Pi_{Fl}} \right)^{1/3} \quad (3)$$

where the dimensionless loop resistance term is given by:

$$\Pi_{Fl} = \sum_{i=1}^N \left\{ \frac{1}{2} \left(\frac{fl}{d_h} + K \right)_i \left(\frac{a_c}{a_i} \right)^2 \right\} \quad (4)$$

Annex 11 provides the details and nomenclature for each of the terms in the equations shown above.

4.2.2. **Governing equations for two-phase natural circulation flow**

Figure 10 depicts the loop geometry considered for this analysis. The loop is divided into two regions; a two-phase region with a fluid density ρ_{TP} and a single-phase region with a fluid density ρ_l . The simplifying assumptions are as follows:

- Constant core inlet enthalpy,
- Uniform fluid properties at every cross-section,
- Homogeneous flow in the two phase region,
- Chemical Equilibrium – no chemical reactions,
- Thermal Equilibrium – both phases at the same temperature,
- The sum of convective accelerations due to vaporization and condensation are negligible,
- Viscous effects included in determination of form losses only,
- Form losses, primarily in the core and steam generator regions, dominate the loop resistance.

The assumptions listed above were applied to the mass, momentum, and energy equations for each component in the loop to obtain the conservation equations. The equations were then integrated over their respective single-phase and two-phase regions to obtain the following loop balance equations.

Loop Momentum Balance Equation:

$$\sum_{i=1}^N \left(\frac{l_i}{a_i} \right) \cdot \frac{d\dot{m}}{dt} = g(\rho_l - \rho_{TP})L_{th} - \frac{\dot{m}^2}{\rho_l a_c^2} \left\{ \sum_{SP} \left[\frac{1}{2} \left(\frac{fl}{d_h} + K \right)_i \left(\frac{a_c}{a_i} \right)^2 \right] + \frac{\rho_l}{\rho_{TP}} \sum_{TP} \left[\frac{1}{2} \left(\frac{fl}{d_h} + K \right)_i \left(\frac{a_c}{a_i} \right)^2 \right] \right\} \quad (5)$$

Loop Energy Balance Equation:

$$M_{sys} \frac{d(e_M - e_l)}{dt} = \dot{m}(h_{TP} - h_l) - \dot{q}_{SG} - \dot{q}_{loss} \quad (6)$$

For two-phase flow conditions, the equilibrium vapor quality and the mixture density are defined as follows:

Equilibrium Vapor Quality at Core Exit:

$$x_e = \frac{h_{TP} - h_f}{h_{fg}} \quad (7)$$

Homogeneous Two-Phase Fluid Mixture Density:

$$\rho_{TP} = \frac{\rho_f}{1 + x_e \left(\frac{\rho_f - \rho_g}{\rho_g} \right)} \quad (8)$$

Unlike single-phase natural circulation, a simple analytical expression for the velocity at the core inlet cannot be readily obtained from the steady-state solution. This is due to the fact that the two-phase mixture density is dependent on core flow rate. The resulting steady-state expression for the velocity is a cubic equation as described in Annex 11.

4.3. Instabilities in natural circulation systems

Thermal-hydraulic instabilities represent a very important class of integral system phenomena. It is particularly important to BWR operations because core power is tightly coupled to the core void fraction, which is strongly dependent on the flow. In general, a thermal-hydraulic instability is any periodic time oscillation of flow, flow-pattern, temperature, fluid density, pressure or core power in a thermal hydraulic system. Such oscillations may arise in multiple parameters simultaneously, may be in-phase or out-of-phase with each other, and may be present at multiple locations in the system (e.g., parallel channels). It is important to note that fuel surfaces may experience temperature excursions as result of thermal-hydraulic instabilities. This section lists the types of thermal hydraulic instabilities that can arise in natural circulation loops. Annexes 7 through 10 provide excellent descriptions of the different types of instabilities and the methods used for their analysis.

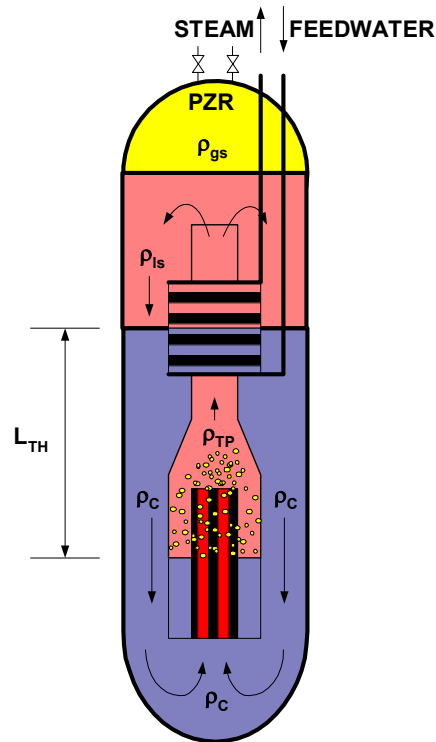


FIG. 10. Regions of single-phase and two-phase natural circulation within an integral reactor.

Thermal-hydraulic instabilities can be classified using a variety of methods (Annexes 7, 8 and 10). Two broad classes of thermal-hydraulic instabilities are generally acknowledged; *static instabilities* and *dynamic instabilities*. Static instabilities are explainable in terms of steady state laws, whereas dynamic instabilities require the use of time dependent conservation equations. Table 5, taken from Annex 8, provides a classification and brief description of thermal-hydraulic instabilities in terms of these two broad classes.

4.3.1. Analysis tools for thermal hydraulic instabilities

Two classes of computer codes have been developed to evaluate the stability of BWRs and other boiling channel systems. They are *Frequency Domain Codes* and *Time Domain Codes*. Frequency domain codes are used for linear stability analyses of BWRs or other boiling systems. Examples of frequency domain codes are presented in Table 6. Time domain codes are used to simulate the transient behavior of plant systems. These codes have the capability of analyzing the non-linear behaviors of BWRs. Examples of time domain codes are presented in Table 7.

As seen in these tables, a variety of neutron kinetics models, ranging from point kinetics (P-K) to three-dimensional models (3-D), are used in the codes. These neutron kinetics models are coupled to a variety of thermal hydraulic analysis models ranging from three-equation homogeneous equilibrium models, HEM (3), to non-equilibrium two-fluid models, TFM (6). Descriptions of these codes are provided in Annexes 9 and 10.

Table 5. Classification of thermal hydraulic instabilities (Annex 8)

Class	Type	Mechanism	Characteristic
<i>Static Instabilities</i>			
Fundamental (or pure) static instabilities	Flow excursion or Ledinegg instabilities	$\left. \frac{\partial \Delta p}{\partial G} \right _{\text{int}} \leq \left. \frac{\partial \Delta p}{\partial G} \right _{\text{ext}}$	Flow undergoes sudden, large amplitude excursion to a new, stable operating condition.
	Boiling crisis	Ineffective removal of heat from heated surface	Wall temperature excursion and flow oscillation
Fundamental relaxation instability	Flow pattern transition instability	Bubbly flow has less void but higher ΔP than that of annular flow	Cyclic flow pattern transitions and flow rate variations
Compound relaxation instability	Bumping, geysering, or chugging	Periodic adjustment of metastable condition, usually due to lack of nucleation sites	Period process of superheat and violent evaporation with possible expulsion and refilling
<i>Dynamic Instabilities</i>			
Fundamental (or pure) dynamic instabilities	Acoustic oscillations	Resonance of pressure waves	High frequencies (10-100Hz) related to the time required for pressure wave propagation in system
	Density wave oscillations	Delay and feedback effects in relationship between flow rate, density, and pressure drop	Low frequencies (1Hz) related to transit time of a continuity wave
Compound dynamic instabilities	Thermal oscillations	Interaction of variable heat transfer coefficient with flow dynamics	Occurs in film boiling
	BWR instability	Interaction of void reactivity coupling with flow dynamics and heat transfer	Strong only for small fuel time constant and under low pressures
	Parallel channel instability	Interaction among small number of parallel channels	Various modes of flow redistribution
Compound dynamic instability as secondary phenomena	Pressure drop oscillations	Flow excursion initiates dynamic interaction between channel and compressible volume	Very low frequency periodic process (0.1Hz)

Table 6. Commonly used linear stability analysis codes (frequency domain codes)

Name of code	Thermal-Hydraulics Model		Neutron Kinetics Model	Reference Annex 9 and 10
	Channels	TPFM (Eq)		
NUFREQ NP	Multiple	DFM (4)	Simplified 3-D	Peng (1985)
LAPUR5	1-7	HEM (3)	P-K ¹ & M-P-K ²	Otaudy (1989)
STAIF	10	DFM (5)	1-D	Zerreßen (1987)
FABLE	24	HEM (3)	P-K ¹	Chan (1989)
ODYSY	Multiple	DFM (5)	1-D	D'Auria (1997)
MATSTAB	All	DFM (4)	3-D	Hänggi (1999)
HIBLE	1-20	SFM (3)	P-K	Hitachi, Japan
K2	Multiple	DFM (3)	P-K	Toshiba, Japan

¹ P-K: point kinetics; ² M-P-K: modal point kinetics; TPFM: two-phase flow model; DFM: Drift Flux Model; SFM: Slip Flow Model; TFM: Two-Fluid Model

Table 7. Commonly used nonlinear stability analysis codes (time domain codes)

Name of code	Thermal-Hydraulics Model		Neutron Kinetics Model	Reference Annex 9 and 10
	Channels	TPFM (Eq)		
RAMONA-5	All	DFM (4 or 7)	3-D	RAMONA-5 catalogue
RELAP5/MOD 3.2	Multiple	TFM (6)	P-K	RELAP5 (1995)
RETRAN-3D	4	Slip Eq (5)	1-D	Paulsen (1991)
TRACG	Multiple	TFM (6)	3-D	Takeuchi (1994)
ATHLET	Multiple	TFM (6)	P-K or 1-D	Lerchl (2000)
CATHARE	Multiple	TFM(6)	P-K	Barre (1993)
CATHENA	Multiple	TFM(6)	P-K	Hanna (1998)
DYNAS-2	Multiple	DFM (5)	3-D	Nuclear Fuel Industries Ltd., Japan
DYNOBOSS	Parallel	DFM (4)	P-K	Instituto de Estudos Avançados (Brazil), RPI (USA)
BWR EPA	3	DFM (4)	P-K	NRC and BNL, USA
PANTHER		DFM	3-D	Nuclear Electric, United Kingdom
QUABOX/CUBBOX-HYCA		DFM	3-D	Gesellschaft für Anlagen- und Reaktorsicherheit (GRS) mbH, (Germany)
SABRE	Parallel	HEM	P-K	Pennsylvania Power & Light, USA
SIMULATE-3K Code (Version 2.0)	Multiple	HEM	3-D	Studsvik, Sweden-USA
EUREKA-RELAP5	Multiple	TFM (5)	3-D	Japan Institute of Nuclear Safety (JINS), Japan
STANDY		DFM	3-D	TEPCo and Hitachi Ltd., Japan, for the full 3D version
TOSDYN-2	Parallel	DFM (5)	3-D	Toshiba Corp., Japan
TRAB	1-3	DFM (4)	1-D	Valtion Teknillinen Tutkimuskeskus, Finland

¹ P-K : point kinetics; ² M-P-K : modal point kinetics; TPFM: two-phase flow model; DFM: Drift Flux Model; SFM: Slip Flow Model; TFM: Two-Fluid Model

5. NATURAL CIRCULATION EXPERIMENTS

The advantages of using natural circulation as a means of core heat removal has prompted the worldwide development of separate effects and integral system test facilities. The data from these facilities has been used to identify a wide range of thermal hydraulic phenomena important to natural circulation systems and has also served to assess the predictive capabilities of a variety of thermal hydraulic analysis codes. This chapter provides a brief overview of international natural circulation experiments and briefly describes one process for designing such facilities. Detailed information on these two topics is presented in seven full papers identified as Annex 11 through Annex 17.

5.1. Integral system experiment scaling methodology

Because of the expense of conducting full-scale integral system tests, much of the thermal hydraulic testing for advanced reactor designs is conducted in “reduced-scale” integral system test facilities. The design of such facilities requires performing a thorough thermal hydraulic scaling analysis. The general objective of a scaling analysis is to obtain the physical dimensions and operating conditions of a reduced scale test facility capable of simulating the important flow and heat transfer behavior of the system under investigation. To develop a properly scaled test facility, the following objectives must be met for each operational mode of interest. First, the thermal hydraulic processes that should be modeled must be identified. Second, the similarity criteria that should be preserved between the test facility and the full-scale prototype must be obtained. Third, because all of the similarity criteria cannot be simultaneously preserved in a reduced scale facility, priorities for preserving the similarity criteria must be established. Fourth, based on satisfying the most important similarity criteria, the specifications for the test facility design are established. Fifth, biases due to scaling distortions can then be quantified. Lastly, the critical attributes of the test facility that must be preserved to meet Quality Assurance requirements must be identified.

The flow chart shown in Figure 11 depicts the general scaling methodology that has been used for the design of the AP600, AP1000 and MASLWR integral system test facilities. A comprehensive discussion of the approach is given in Annex 11.

5.2. Integral system test facilities for studies of natural circulation

This section presents a brief description of several integral system test facilities that are investigating natural circulation phenomena in advanced water cooled nuclear power plants. Most of the organizations responsible for the facilities described herein are currently participating in the IAEA Co-ordinated Research Project (CRP) on natural circulation phenomena, modelling and reliability of passive systems that utilize natural circulation. These facilities are representative of the broad spectrum of ongoing work in the area of natural circulation and passive safety system testing. It is not an all-inclusive list of the worldwide testing effort. Refer to the appendices of Annex 21 for a more comprehensive listing of international test facilities.

It should also be noted that a significant amount of natural circulation and passive safety system data has been obtained in simple loop experiments and separate effects tests capable of providing detailed information under well-known and carefully controlled system conditions. The simple loop experiments of the Bhabha Atomic Research Centre (BARC) described in Annex 13 are an excellent example. Valuable advanced BWR separate effects tests are being conducted by the Forschungszentrum (FRZ) Institute of Safety Research using their NOKO and TOPFLOW experiments located in Rossendorf, Germany. Similarly, useful WWER-1000/V-392 component testing has been conducted using the Gidropress SPOT and HA-2 facilities in Obninsk, Russia.

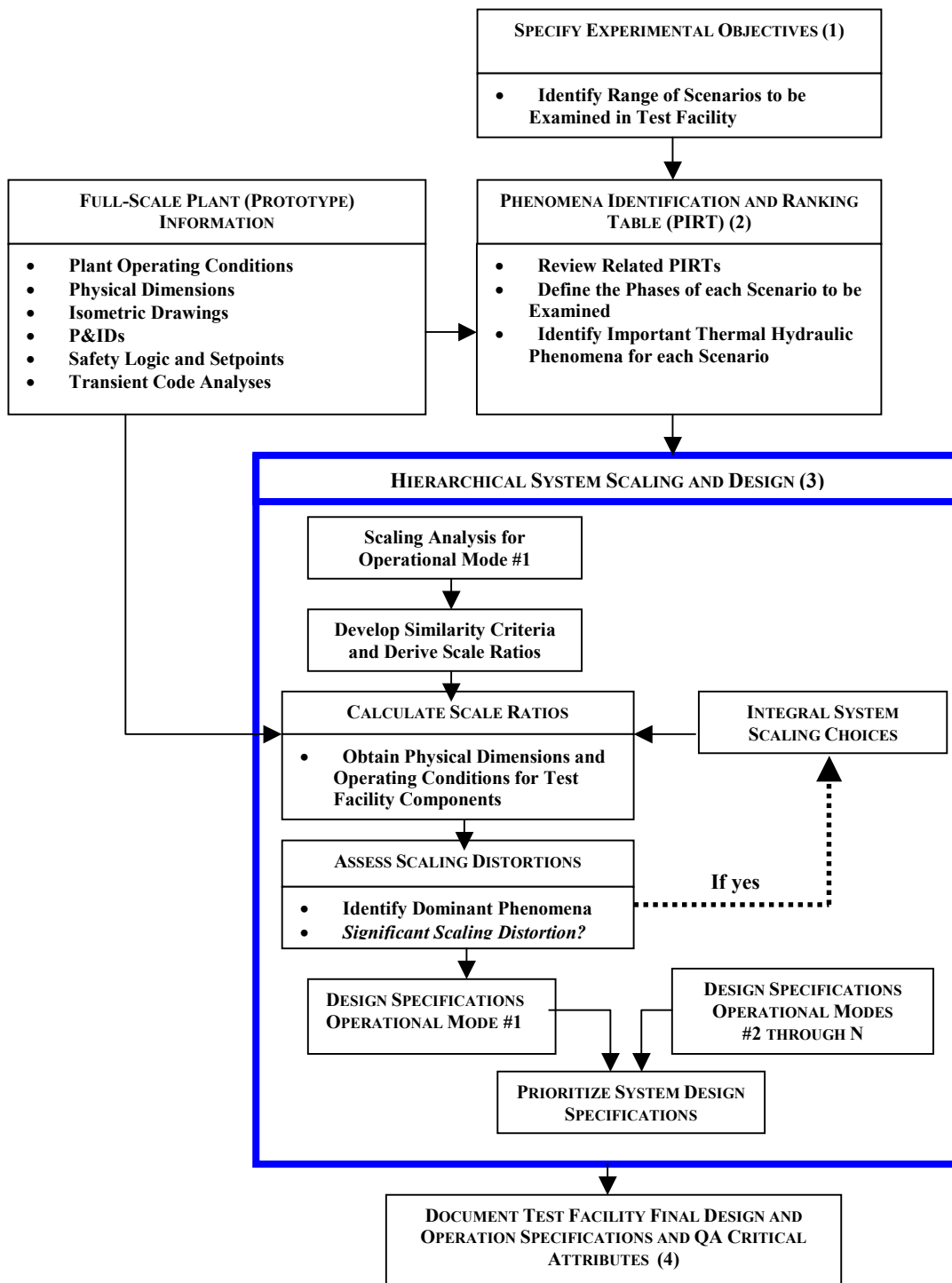


FIG. 11. General scaling methodology.

Brief descriptions of the following integral system test facilities are provided in this section:

- Argentina, CNEA, CAPCN
- India, BARC, IITL and PLC
- Japan, JAERI, LSTF
- Switzerland, PSI, PANDA
- United States of America, OSU, APEX-1000 and MASLWR
- United State of America, Purdue, PUMA

In addition to the test facilities from organizations participating in the IAEA CRP on natural circulation phenomena, a brief overview of the NACUSP Project [23], [24] with its four test facilities (DESIRE, CLOTAIRE, CIRCUS, PANDA) is also provided.

5.2.1. Argentina, CNEA, CAPCN-Rig experimental facility

The CAPCN experimental facility is located at the Pilcaniyeu Technological Center in Patagonia, Argentina, approximately 70 km from the city of Bariloche. The facility is operated by the Centro Atómico de Bariloche-CNEA and the Balseiro Institute. CAPCN was designed to simulate most of the dynamic phenomena of the CAREM reactor coolant system near nominal operations. It has been used to study the dynamics of CAREM by means of power imbalances, with and without active control, and to provide experimental data to assess the codes to be used for CAREM modelling. Several thermo-hydraulic phenomena have been investigated, including two-phase natural circulation, self-pressurization, condensation and stratification in the dome, void fraction generation (flashing) and collapse in the riser, and heat transfer in the steam generator and to surrounding structures.

The test facility is full height relative to CAREM and has a volume scale factor of 1:280. It can operate at full pressure, 12 MPa, and at a maximum power of 300 kW. Figure 12 presents a process and instrumentation diagram of the CAPCN test facility.

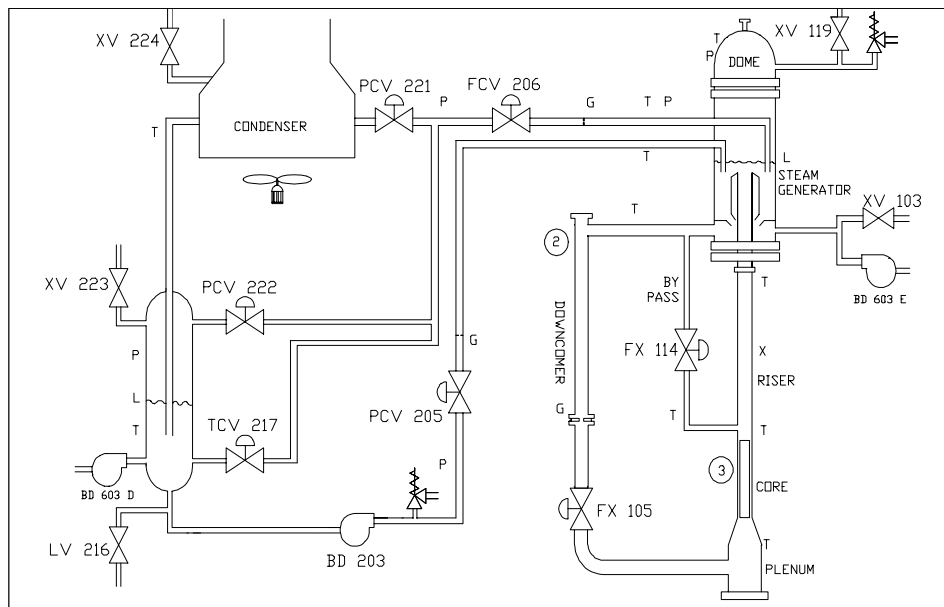


FIG. 12. Schematic of CNEA's CAPCN test facility to simulate CAREM.

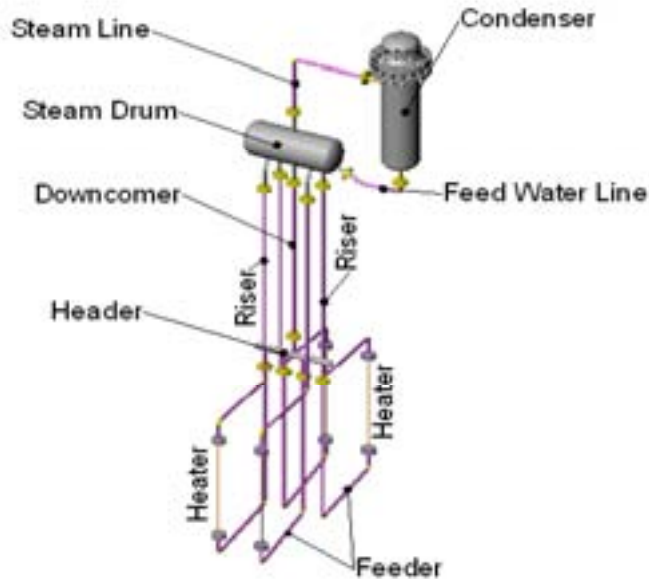


FIG. 14. Schematic of BARC Parallel Channel Loop (PCL)

5.2.3. Japan, JAERI, large scale test facility (LSTF)

The Japan Atomic Energy Research Institute (JAERI) has performed numerous integral system tests using different configurations of its large scale test facility (LSTF). The LSTF has been configured to simulate the Tsuruga-2, a four loop PWR that produces 1100 MW(e). The LSTF is a full height (~30 m) test facility with a volumetric scaling factor of 1:48. It operates at full pressure (16 MPa) and has a 10 MW electrically heated core consisting of 1008 heater rods. It has approximately 2500 instruments. Figure 15 presents a schematic of the LSTF. Three loops in the plant are simulated by one loop in the test facility.

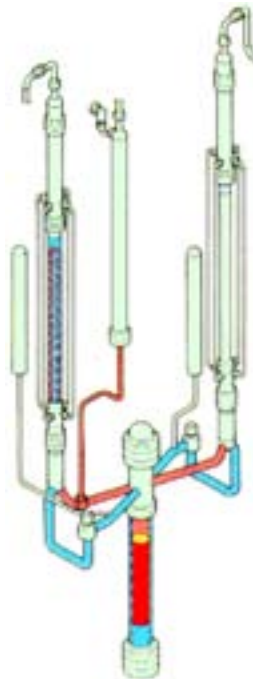


FIG. 15. Schematic of JAERI's large scale test facility (LSTF).

JAERI has conducted 14 steady-state natural circulation tests in LSTF with step changes in primary side mass inventory at a fixed steam generator pressure (~0.1 MPa) and core power. These test provide useful data on single-phase and two-phase natural circulation for use in RELAP5 validation and potential modification.

The LSTF will also be used to simulate natural circulation in a reduced moderator water reactor (RMWR). The RMWR is a natural circulation cooled BWR with a void coefficient one order smaller than the current BWR and hence a weak coupling between the thermal hydraulics and the neutron kinetic. The LSTF will be used to investigate RMWR stability during start up and steady state conditions.

5.2.4. Switzerland, PSI, PANDA test facility

PANDA is a large scale test facility that has been used for a variety of thermal hydraulic test programs at the Paul Scherrer Institute in Switzerland. It basically consists of six cylindrical pressure vessels, connecting piping and four pools open to the atmosphere. Figure 16 shows the PANDA configuration for simulating the full-height ESBWR. The height of the reactor pressure vessel is 20 m and the installed power is 1.5 MW generated by a bundle of heater rods having a length of 1.3 m. The vessel is 1.25 m in diameter and the riser section above the core simulator is approximately 10 m tall. The diameter of the riser is about 1 m. PANDA is designed for 10 bar and 200°C maximum operating conditions.

A detailed description of the PANDA test facility and its test programs is provided in Annex 14.

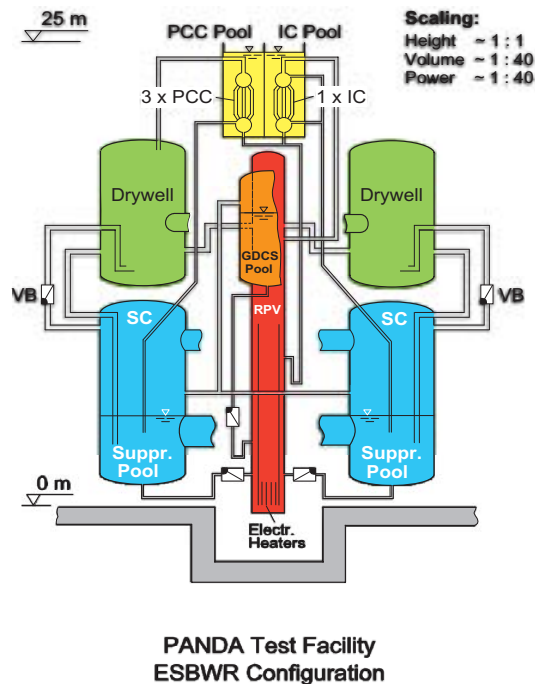


FIG. 16. Schematic of the PANDA integral test facility to simulate the ESBWR.

5.2.5. United States of America, OSU, APEX-1000 and MASLWR test facilities

The advanced plant experiment (APEX-1000) is a low-pressure integral system test facility used for certification testing for the Westinghouse Electric AP1000. The test facility was scaled, built and operated by Oregon State University in Corvallis, Oregon in the United States. As shown in Figure 17, the APEX-1000 includes a complete 2x4 primary loop with all of the AP1000 passive safety systems and safety actuation logic. The reactor vessel houses a core consisting of a 1 MW electrically heated rod bundle and a complete set of prototypic upper plenum internals. The APEX-1000 Passive Safety systems include 2 core makeup tanks (CMTs), 2 accumulators, a passive residual heat removal

(PRHR) heat exchanger, an in-containment refueling water storage tank (IRWST), and a 4-Stage automatic de-pressurization system (ADS).

The facility is one-fourth scale in height and operates at a pressurizer pressure of 25.5 bars and a steam generator shell side pressure of 20 bars. It has been used to conduct a wide range of hot and cold leg loss-of-coolant-accidents, main steam line breaks, inadvertent opening of the ADS, double-ended direct vessel injection (DVI) line breaks, station blackout and long term natural circulation.

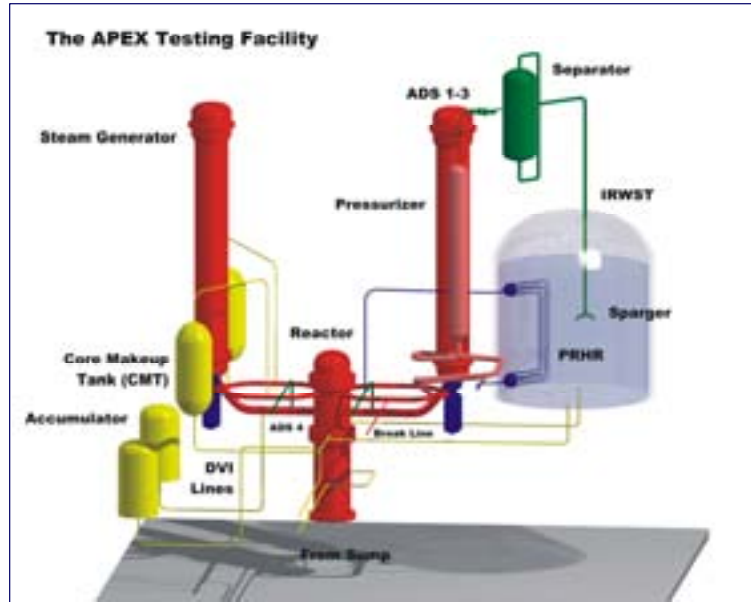


FIG. 17. Schematic of the APEX-1000 integral system test facility to simulate the AP1000.

OSU has also developed an integral system test facility to examine natural circulation phenomena of importance to integral reactors such as those proposed for IRIS, CAREM and SMART. The OSU multi-application small light water reactor (MASLWR) test facility simulates the MASLWR integral reactor design developed by Idaho National Laboratory, OSU and NEXANT-Bechtel. Figure 18 presents a schematic of the MASLWR test facility.

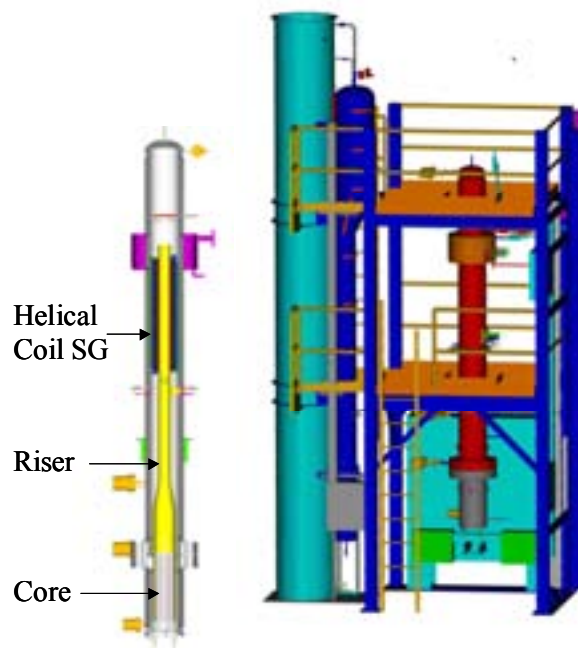


FIG. 18. Schematic of the MASLWR test facility to simulate integral type LWRs.

The MASLWR loop is one-third length scale and has a volumetric scale factor of 1:254. It includes a 14-tube helical coil steam generator, an internal pressurizer, and a reactor vessel with an electrically heated core bundle consisting of 60 heater rods. It operates at full pressure (120 bars) and temperature (590°K) with a total core power of 700 kW. The helical coil steam generator has an internal tube pressure of 14 bars. The MASLWR test facility includes a passively cooled high-pressure containment with a scaled active heat transfer area and volume, an exterior cooling pool, a Steam Vent Valve System and an Automatic Depressurization System.

Studies being conducted include primary loop flow stability for single and two phase natural circulation, helical coil heat transfer, assessment of containment performance during ADS and Steam Vent Valve blowdown and benchmarks of the RELAP5 system code and the GOTHIC containment code against test data.

5.2.6. United States of America, Purdue, PUMA test facility

The Purdue multi-dimensional integral test assembly (PUMA) is operated by Purdue University in West Lafayette, Indiana, USA. PUMA is a low-pressure test facility that has been used to simulate a variety of advanced SBWR thermal hydraulic phenomena. It is a 1:400 volume scale test facility with a multi-channel core. Current studies are aimed at gaining a greater understanding of BWR instabilities at low pressure and low flow. This includes investigations of start up transients with simulated void reactivity feedback, condensation induced geysering, and flashing induced loop oscillations. PUMA experiments will be used to develop a database to benchmark NRC's TRACE computer code. Figure 18 presents a schematic of the PUMA test vessel. PUMA also includes SBWR passive safety systems.

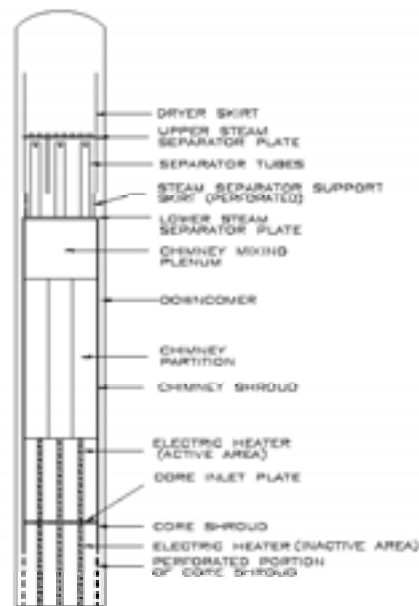


FIG. 19. Schematic of the PUMA test facility to simulate advanced BWRs.

5.2.7. Euratom's NACUSP Project

Four integral system test facilities are part of an important project to investigate stability issues in current and future BWRs. This project, called the natural circulation and stability performance (NACUSP) [23] of boiling water reactors, is part of the 5th Euratom framework programme of the European Commission. One of the NACUSP test facilities, PANDA, was already described in Section 5.2.4 as PSI is also a member of the current CRP on natural circulation. The remaining three facilities, DESIRE, CLOTAIRE, and CIRCUS are briefly described in the paragraphs that follow.

5.2.7.1. *DESIRE test facility*

DESIRE [24] is a reduced scale integral system test facility located at the Interfaculty Reactor Institute (IRI) at the Delft University of Technology in the Netherlands. The facility simulates the Dodewaard natural-circulation BWR. The working fluid is Freon-12 and it was designed to investigate natural-circulation and stability characteristics at nominal system pressures. The primary loop of the facility consists of an electrically heated 6×6 fuel bundle, riser, downcomer and downcomer loops. Separation of liquid and vapour occurs at the free surface at the top of the riser. A riser-exit restriction has been added in order to enable the simulation of thermal-hydraulic instabilities. The height of the riser and core section of the facility is approximately 2.5 m, which is about half the size of the dimensions of the Dodewaard reactor.

5.2.7.2. *CLOTAIRE test facility*

The CLOTAIRE facility [23] is an integral system test facility operated by the Commissariat à l’Energie Atomique (CEA) in Cadarache, France. It has been designed to simulate steam-water at a pressure of 73 bar using Freon-114 as the working fluid. The boiler section of the loop consists of a 7 m tall, electrically heated bundle (184 tubes) inserted in a semi-cylindrical pressure vessel having a 0.6 m diameter. A pressure vessel on top of the boiler section will serve as a riser. It will implement bi-optical probes for local void-fraction and velocity measurements. The pressure at the outlet of the mock-up will be fixed at 0.9 MPa, the riser height will be 3 m, and the liquid freon level will be approximately 10.5 m. A base set of tests will be performed to cover the operating point of the ESBWR reactor. The CLOTAIRE-facility will provide unique full-scale data.

5.2.7.3. *CIRCUS test facility*

The CIRCUS test facility [23] is a low-pressure scaled model of the Dodewaard BWR located at the Interfaculty Reactor Institute (IRI) at the Delft University of Technology in the Netherlands. It was designed and built to study the thermal–hydraulic stability of a natural-circulation BWR at low-pressure conditions typical for start-up. The pressure in the facility can be varied between 1 and 5 bar. The height of the core and riser section is approximately 5 m, which is equivalent to the height of the core and riser in the Dodewaard reactor. Portions of the CIRCUS facility are transparent, enabling direct visualisation of the flow and the use of advanced diagnostics, such as a gamma densitometer for void-fraction measurements, and a Laser Doppler Anemometer for local velocity measurements. The core is comprised of four electrically heated fuel channel simulators, four bypass channels, and one common riser section. The facility can be modified to study the effect of parallel risers and the inlet friction and inlet subcooling can be varied.

6. ADVANCED COMPUTATION AND RELIABILITY ASSESSMENT METHODS

This chapter presents a brief overview of the advanced computation and reliability methods being used for the analysis of natural circulation systems and passive safety system that use natural circulation. Annexes 18 through 20 provide detailed information regarding these assessment methods. They also provide useful examples demonstrating their application to water cooled nuclear power plants.

6.1. Advanced computation methods

A variety of computation methods have been developed to predict thermal hydraulic phenomena related to natural circulation. Analytical approaches to predict single-phase and two-phase natural circulation flow rates in simple loops are presented in comparison with experimental data in Annex 13. Another, novel approach to characterizing natural circulation flow behaviour in reactor systems is the Natural Circulation Flow Map described in Annex 18.

Modelling more complex natural circulation phenomena requires using detailed systems analysis codes. The transport equations implemented in typical thermal hydraulic system analysis codes are described in Annex 6. Figure 20 presents a summary of the many different formulations used in thermal hydraulic safety analysis codes. They range from very simple 3-equation homogeneous equilibrium models to advanced full non-equilibrium models using 6 balance equations. New codes, such as NRC's TRACE code are also under development.

As demonstrated in Annex 9 and Annex 19, neutron kinetics can have a large impact on the stability of two-phase natural circulation flows, particularly during BWR operations. Tables 6 and 7 of this report lists the computer codes used for linear and non-linear stability analysis. These codes have neutron kinetics models ranging from point kinetics to full 3-D kinetics.

Computational fluid dynamic (CFD) codes can also serve as valuable tools for the analysis of natural circulation flows. CFD codes are particularly well suited for analysing single-phase fluid flow inside complex geometries. Annex 20 provides an excellent overview of the use of CFD codes in nuclear power plant applications. Some examples include thermal fluid stratification in the cold legs as a result of safety injection and plume formation in the downcomer. Both phenomena are important to the study of pressurized thermal shock in nuclear power plants.

Lastly, regardless of the method used to predict the various natural circulation thermal hydraulic phenomena, it is important that the predictive tool be assessed against experimental data. Annex 21 describes internationally agreed upon separate effects test (SET) and integral test facility (ITF) matrices for the validation of realistic thermal hydraulic system computer codes. These matrices were established by sub-groups of the task group on thermal hydraulic system behaviour as requested by the OECD/NEA committee on the safety of nuclear installations (CSNI) principal working group 2 on coolant system behaviour. These valuable SET and ITF matrices are included as appendices to Annex 21.

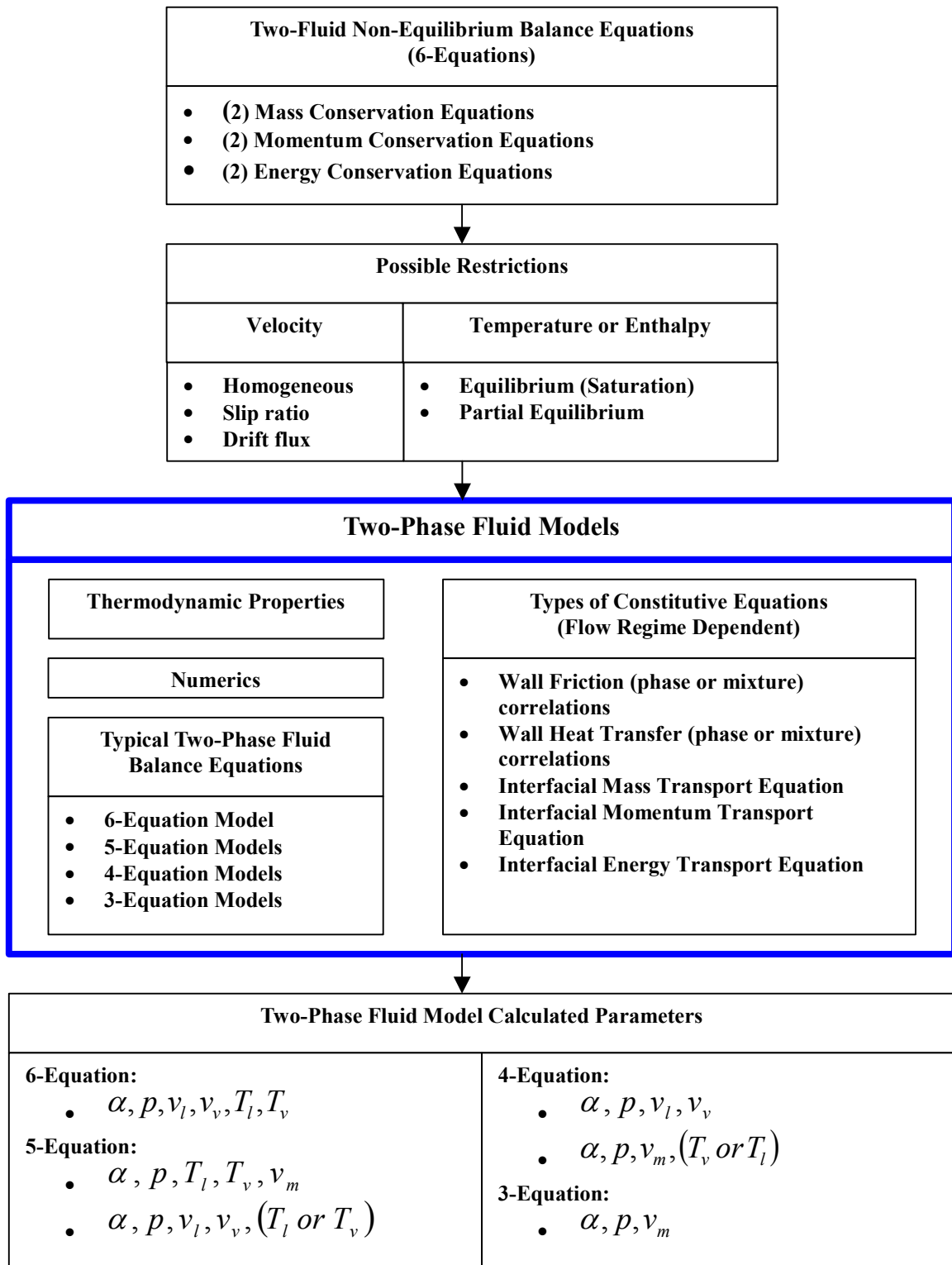


FIG. 20. Types of two-phase flow models used in nuclear reactor safety analyses.

6.2. Reliability assessment methodology

Several organizations are actively involved in developing reliability assessment methods for advanced reactor systems that implement natural circulation core cooling or passive safety systems. In particular, the European Commission's 5th framework programme included a project on reliability methods for passive safety functions (RMPS), a project on testing and modelling passive safety systems for BWR containment cooling, and a project to improve the understanding of natural circulation and stability of BWRs. A roadmap of this reliability methodology is shown in Figure 21 and briefly explained in the following paragraphs. A detailed explanation is given in Annex 22 of this report.

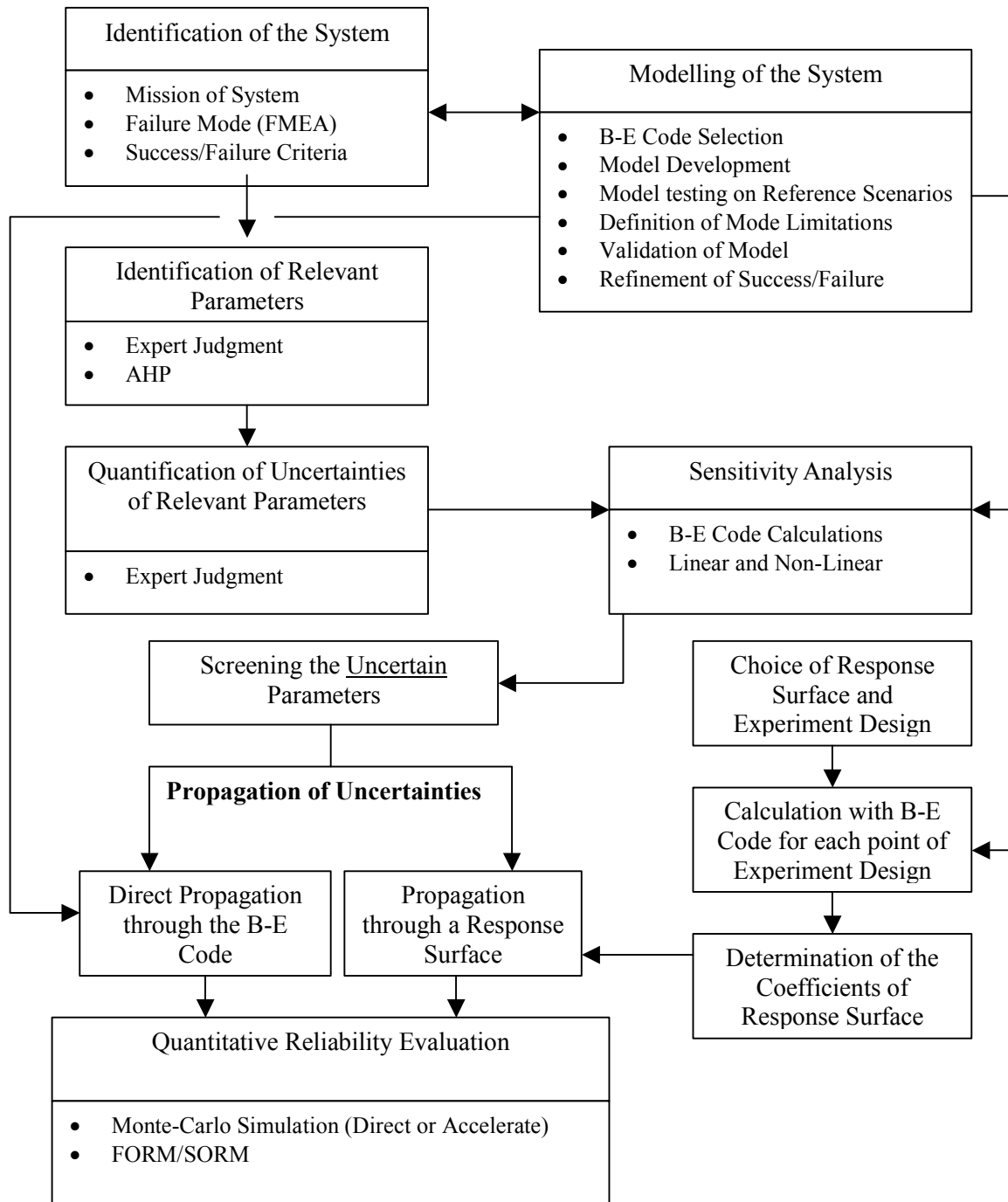


FIG. 21. Roadmap for RMPS reliability assessment methodology.

The reliability assessment methodology can be categorized into the following three parts:

- Identification and Quantification of the sources of uncertainties in NC systems
- Reliability evaluations of passive systems that utilize NC, and
- Integration of NC system reliability in Probabilistic Safety Analysis

6.2.1. Identification and quantification of the sources of uncertainties in NC systems

The methodology shown in Figure 21 is applied to a specific accident scenario to which a particular passive safety system would respond. Having specified the scenario of interest, the first step, identification of the system, requires fully characterizing the system under investigation. That is, specifying the goals of the system, the methods by which it can fail, and providing a definition of system failure, (i.e. success/failure criteria). Modelling the system is also required. This is done using best-estimate (B-E) computer codes. The numerous sources of uncertainties present in the modelling process should be documented. This includes approximations in modelling the physical process and system geometry and uncertainties in the input variables such as initial and boundary conditions.

Identifying the thermal hydraulic phenomena and parameters most important to the system being investigated is an important part of the methodology. This can be done using an expert panel having a good understanding of the system functions, B-E code calculations and a method for developing a relative ranking of the phenomena. The ranking technique implemented in the RMPS project was the Analytical Hierarchy Process (AHP) as described in Annex 22.

Having identified and ranked the important thermal hydraulic parameters, the next step is to quantify their uncertainties. This requires expert judgement to identify the range of uncertainty and to select an appropriate probability density function for a given set of variables. The methodology then incorporates a sensitivity analysis to guide improvements to the state of knowledge in order to reduce the output uncertainties most effectively.

6.2.2. Reliability evaluations of passive systems that utilize NC

The second part of the methodology requires evaluating the uncertainty in the physical response of the T-H code using a confidence interval or a probability density function. The RMPS study found that methods giving an uncertainty range of the system performance are not very useful for reliability estimation. Therefore using a probability density function was the approach that was implemented.

The probability density function of the system performance can be directly used for reliability estimation once a failure criterion is given. For the evaluation of the probability density function, the existing methods are generally based on Monte-Carlo simulations. Monte-Carlo simulations require a large number of calculations. As a result, these calculations can be prohibitively long. To avoid this problem, two approaches are possible: the variance reduction techniques in Monte-Carlo methods or the use of response surfaces. It is also possible to use approximate methods such as First and Second Order Reliability Methods (FORM/SORM).

6.2.3. Integration of NC system reliability in probabilistic safety analysis

The third and final part of the methodology involves integrating the passive system reliability model into the whole plant probabilistic safety analysis (PSA) model. There is a number of different ways this could be done. It could be done directly in the event tree of the relevant accident sequence as a single basic event, or a separate fault tree could be developed. In the RMPS study, the reliability of the physical process was represented as a single basic event using the results from the thermal-hydraulic modelling calculations.

Part of the RMPS study involved applying the methodology to a simplified PSA carried out for a fictitious reactor equipped with two types of safety passive systems. For this test case, an Event Tree (ET) representation of the accident scenario was chosen. The failures analyses performed on this

reactor allowed the characterisation of the technical failures and the ranges of variation of the uncertain parameters that influence the physical process. The majority of the sequences that comprise this event tree were analysed by deterministic evaluations using envelope values of the uncertain parameters. For some sequences where the definition of envelope cases was impossible, basic events corresponding to the failure of the physical process were added and uncertainty analyses were performed to evaluate the corresponding probability of failure.

It was determined that the RMPS reliability assessment methodology can be used for the probabilistic evaluation of the influence of a passive system on an accident scenario. It could also be used to support studies that assess the feasibility of replacing an active system by a passive system for specific situations.

REFERENCES

- [1] INTERNATIONAL ATOMIC ENERGY AGENCY, Safety Related Terms for Advanced Nuclear Power Plants, IAEA-TECDOC-626, Vienna (1991).
- [2] INTERNATIONAL ATOMIC ENERGY AGENCY, The Safety of Nuclear Power: Strategy for the Future, (Proc. of a Conf., Vienna), IAEA, Vienna (1991).
- [3] INTERNATIONAL ATOMIC ENERGY AGENCY, Evolutionary Water cooled Reactors: Strategic Issues, Technologies and Economic Viability, IAEA-TECDOC-1117, Vienna (1999).
- [4] INTERNATIONAL ATOMIC ENERGY AGENCY, Thermo-hydraulic Relationships for Advanced Water Cooled Reactors, IAEA-TECDOC-1203, Vienna (2001).
- [5] INTERNATIONAL ATOMIC ENERGY AGENCY, Thermo-physical Properties of Materials for Water Cooled Reactors, IAEA-TECDOC-949, Vienna (1997).
- [6] INTERNATIONAL ATOMIC ENERGY AGENCY, Natural Circulation Data and Methods for Advanced Nuclear Power Plant Design, IAEA-TECDOC-1281, Vienna (2002).
- [7] INTERNATIONAL ATOMIC ENERGY AGENCY, Experimental Tests and Qualification of Analytical Methods to Address Thermo-hydraulic Phenomena in Advanced Water Cooled Reactors, IAEA-TECDOC-1149, Vienna 2000).
- [8] INTERNATIONAL ATOMIC ENERGY AGENCY, Improving Economics and Safety of Water Cooled Reactors: Proven Means and New Approaches, IAEA-TECDOC-1290, Vienna 2002).
- [9] INTERNATIONAL ATOMIC ENERGY AGENCY, Performance of Operating and Advanced LWR Designs, IAEA-TECDOC-1245, Vienna (2001).
- [10] INTERNATIONAL ATOMIC ENERGY AGENCY, Technologies for Improving Current and Future Light Water Reactor Operations and Maintenance: Development on the Basis of Experience, IAEA-TECDOC-1175, Vienna (2000).
- [11] INTERNATIONAL ATOMIC ENERGY AGENCY, Fuel Cycle Options for LWRs and HWRs, IAEA-TECDOC-1122, Vienna, (1999).
- [12] INTERNATIONAL ATOMIC ENERGY AGENCY, Technical Feasibility and Reliability of Passive Safety Systems for Nuclear Power Plants, IAEA-TECDOC-920, Vienna (1996).
- [13] INTERNATIONAL ATOMIC ENERGY AGENCY, Status of Advanced Light Water Cooled Reactor Designs: 2004. IAEA-TECDOC-1391, Vienna (2004).
- [14] INTERNATIONAL ATOMIC ENERGY AGENCY, HWRs – Status and Projected Development, Technical Reports Series No. 407, IAEA, Vienna (2002).
- [15] INTERNATIONAL ATOMIC ENERGY AGENCY, Methodology for the Assessment of Innovative Nuclear Reactors and Fuel Cycles: Report of Phase 1B (first part) of the International Project on Innovative Nuclear Reactors and Fuel Cycles (INPRO), IAEA-TECDOC-1434, Vienna (2005).
- [16] INTERNATIONAL ATOMIC ENERGY AGENCY, Status of Liquid Metal Cooled Fast Reactor Technology, IAEA-TECDOC-1083, Vienna (1999).

- [17] INTERNATIONAL ATOMIC ENERGY AGENCY, Review of National Accelerator Driven System Programmes for Partitioning and Transmutation, IAEA-TECDOC-1365, Vienna (2003).
- [18] INTERNATIONAL ATOMIC ENERGY AGENCY, Current Status and Future Development of Modular High Temperature Gas Cooled Reactor Technology, IAEA-TECDOC-1198, Vienna (2001).
- [19] Title 10, Energy, Code of Federal Regulations, Part 50, Office of Federal Register, National Archives and Records Administration, Available through Superintendent of Documents, U.S. Government Printing Office, Washington, D.C. 20402 (2004).
- [20] LUMINI, E., UPTON, H., MASONI, P., BILLIG, P., “ESBWR Passive heat exchanger design and performance – Reducing plant development costs”, Proceedings of the SFEN/ENS International Conference, TOPNUX 96 (1996).
- [21] CHALLBERG, R.C., CHEUNG, Y.K., KHORANA, S.S., UPTON, H.A., “ESBWR Evolution of passive features”, Proceedings of the 6th International Conference on Nuclear Engineering (ICONE-6), San Diego, California, USA, May 10–15 (1998).
- [22] OECD/NUCLEAR ENERGY AGENCY/COMMITTEE ON THE SAFETY OF NUCLEAR INSTALLATIONS, “CSNI Integral Test Facility Validation Matrix for the Assessment of Thermal-hydraulic Codes for LWR LOCA and Transients”, OCDE/GD(97)12 (CSNI Report 132/Revision 1), Paris (1997).
- [23] DE KRUIJF, W.J.M., et. al, Planned experimental studies on natural-circulation and stability performance of boiling water reactors in four experimental facilities and first results (NACUSP), Nuclear Engineering and Design, Volume 221, Issues 1–3 , April 2003, p. 241–250.
- [24] DE KRUIJF, W.J.M., SENGSTAG, T., DE HAAS, D.W., and VAN DER HAGEN, T.H.J.J., “Experimental thermohydraulic stability map of a Freon-12 boiling water reactor facility with high exit friction,” Nuclear Engineering and Design, Volume 229, Issue 1, April 2004, p. 75–80.

ANNEX 1

OVERVIEW OF GLOBAL DEVELOPMENT OF ADVANCED NUCLEAR POWER PLANTS

J. Cleveland

International Atomic Energy Agency, Vienna

Abstract

Nuclear power has proven its viability as an energy source in many countries. Nuclear power technology is mature, and has achieved tremendous progress in the last decades. Like any other progressing technology, it continues to pursue improvements. The accumulated experience, which now exceeds 11,000 reactor-years of operation, is being used to develop advanced nuclear power plant designs. This development is proceeding for all reactor lines — water cooled reactors, gas cooled reactors, and liquid metal cooled reactors so that nuclear power can play an important and increasing role in global energy supply in the future. Improved economic competitiveness and a very high level of safety are common goals for advanced designs. To achieve economic competitiveness for new plants, proven means for achieving cost efficiency are being applied and new approaches are being pursued. There is also considerable potential for nuclear energy to expand beyond production of electricity to other applications such as sea-water desalination and hydrogen production.

1. CURRENT STATUS OF NUCLEAR POWER

In the past 50 years, nuclear power has grown from a new scientific development to become a major part of the energy mix in many countries. At the end of 2003, there were 439 nuclear power plants operating in 30 IAEA Member States with a total worldwide installed nuclear capacity of 361.1 GW(e)¹. In addition, 29 units were under construction. During 2003 nuclear power plants produced a total of 2524 billion kW·h of electricity, which was 16.1% of the world's total electricity production [1].

The future contribution of nuclear power to meeting global energy demand is difficult to predict. Some countries have policies to phase out nuclear power while other countries see advantages in nuclear power to provide energy security. Countries planning to increase their nuclear capacity include China, India, Japan, the Republic of Korea and Finland.

Based on information provided by its Member States, the IAEA's projects that nuclear power will provide about 17–19% of the world's electricity in 2010; 15 to 17% of the world's electricity by 2020, and 13 to 14% by 2030 [1]. Although the IAEA estimates that the percentage of the world's electricity produced by nuclear power will decrease in the long term, it estimates that the actual amount of nuclear generated electricity will increase. Compared to 2003's nuclear electricity production of 2524 billion kW·h, the IAEA estimates that nuclear power will produce between 3147 and 3241 billion kW·h annually by 2010, between 3378 and 4032 billion kW·h annually by 2020, and between 3379 and 4702 billion kW·h annually by the year 2030 [1].

Of course these estimates will change with time, and longer term estimates are even more uncertain depending on economic growth and environmental constraints. Several important factors will influence nuclear energy's future contribution, including:

- The degree of global commitment to greenhouse gas reduction;
- Continued vigilance in safe operation of nuclear plants and fuel cycle facilities;
- Continued vigilance in safeguards;
- Technological maturity, economic competitiveness; and financing arrangements for new nuclear plants;
- Implementation of nuclear waste disposal;
- Public perception, information and education.

Clearly the nuclear community should focus on insuring success in each of these areas.

¹ The data are available from IAEA's Power Reactor Information System (PRIS). The totals include the nuclear capacity and nuclear electricity generation in Taiwan, China.

2. GOALS OF NUCLEAR POWER DEVELOPMENT

2.1. Economic competitiveness

Economic competitiveness with other energy sources is an obvious goal of new plant development. Many of the world's electricity markets are moving towards greater competition. Both private sector and state-owned electricity generating organizations carefully examine the costs of their operations, and focus on supply technologies that are low cost and low risk.

Capital costs for nuclear plants generally account for 45–75% of the total nuclear electricity generation costs, compared to 25–60% for coal plants and 15–40% for gas plants. This high capital cost presents a significant challenge to the addition of new nuclear power capacity. Until recently, nuclear power's advantage in having a small share of its generating costs in fuel costs could offset the disadvantage of its high capital costs. Moreover, in protected markets, investment costs could be recovered over several decades through regulated rates. Now, with increased competition in the electric power industry, short-term profitability has become a criterion for successful generation along with long-term economic viability. With deregulation, owners are not guaranteed cost recovery through regulated rates, and, with privatization, investors seek appropriately rewarded risk, which often translates into seeking small capital investments and high returns, and the minimization of their economic risks. If nuclear plants are to form a significant part of the future generating mix in competitive electricity markets, capital cost reduction through simplified designs must be an important focus. Reductions in operating, maintenance and fuel costs should also be pursued².

Design organizations are challenged to develop advanced nuclear power plants with lower capital costs and shorter construction times (e.g. by simplification, standardization, modularization, etc.) and sizes suitable for various grid capacities and owner investment capabilities. This includes large sizes for some markets and small and medium sizes for others.

To meet the competitiveness challenge, construction delays must be avoided, regulatory procedures and requirements must be stable, plant design must be well in hand before the start of construction, and construction and operations management personnel need to have high levels of competence. It is important to fully implement proven means of cost reduction, and to examine, develop and implement new approaches to reduce costs. To achieve the largest reductions in capital cost, both proven means and new approaches should be applied. These proven means and new approaches are discussed in more detail in Section 3.

Studies on projected costs of generating electricity provide results that depend strongly on the assumptions used. Due to the range of market conditions and generating costs in various countries, and the wide variety of assumptions used to forecast such costs, no single technology can be declared optimal in all countries. Importantly, in addition to economics, a country's national policy issues, such as diversity and security of its energy supply as well as environmental policies, may affect the decision on whether or not to construct nuclear power plants.

It is also important to note that the different generating options also have different cost sensitivities. Because of high capital costs and long construction periods, nuclear power generation costs, and, to a somewhat lesser extent, coal power generation costs, are highly sensitive to discount rates. Generating costs for coal-fired plants vary with coal prices and with the level of pollution abatement required.

²Although the economic competitiveness of fossil fuelled plants may be reduced in the future due to, for example, rising fuel costs and, in some countries, the introduction of taxes on CO₂ emissions, the nuclear power industry should not have a reduced incentive for cost reduction. Importantly, technologies for fossil fuelled plants also progress and one area of current development involves “clean” new plants with carbon capture.

Generating costs for gas fired power plants are highly sensitive to gas prices, which account for a large proportion of total costs³.

In examinations of economic competitiveness, the external costs of various energy options should also be addressed. In idealized markets all costs associated with a technology would be internalised as part of its economic cost, and decisions based solely on economic costs would automatically properly reflect all social considerations. Nuclear energy is largely ahead of other energy technologies in internalising its external costs. The costs of waste disposal, decommissioning and meeting safety requirements are in most countries already included in the price of nuclear electricity. Progress towards a more level playing field where external costs of other energy technologies are more consistently internalised as part of their economic costs would thus result in more balanced assessments of energy options. As indicated by the results of the ExternE studies in Europe [3], external costs for fossil-fired plants operated to current standards are well above external costs of NPPs, also operated to current standards.

2.2. Achieving very high safety levels

In the course of nuclear power development in the latter part of the twentieth century, there have been significant developments in technology for reactor safety. These include:

- Advances in the application of PSA;
- Introduction of more rigorous quality assurance programmes for plant design, licensing, construction and operation;
- Increased attention to the effect of internal and external hazards — in particular the seismic design and qualification of buildings;
- Major advances in fracture mechanics and non-destructive testing and inspection;
- Increased emphasis on the man-machine interface including improved control room design, and plant design for ease of maintenance;
- Rapid progress in the field of control and instrumentation — in particular, the introduction of micro-processors into the reactor protection system; and
- Increased emphasis on prevention and mitigation of severe accidents.

New nuclear plant designs are being developed to meet stringent safety requirements. While there are differences in safety requirements among countries developing new designs, the stringent requirements are generally reflected in the IAEA's **Safety Standards Series** [see for example 4, 5, 6], which consists of the following categories:

Safety Fundamentals present basic objectives, concepts and principles of safety and protection in the development and application of nuclear energy for peaceful purposes;

Safety Requirements establish the requirements that must be met to ensure safety. These requirements, which are expressed as 'shall' statements, are governed by the objectives and principles presented in the Safety Fundamentals; and

Safety Guides recommend actions, conditions or procedures for meeting safety requirements. Recommendations in Safety Guides are expressed as 'should' statements, with the implication that it is necessary to take the measures recommended or equivalent alternative measures to comply with the requirements.

The IAEA's safety standards are not legally binding on Member States but may be adopted by them, at their own discretion, for use in their national regulations.

³ In this context it is important to note that liberalized markets do not necessarily favour less capital-intensive energy conversion systems and penalize capital intensive projects. Under conditions of low power prices and increasing prices for fossil fuel, the capital investment payback times for nuclear plants can be shorter than those for coal fired plants and CCGT plants [2].

Technical aspects of safety including principles are discussed in Reference [4] for siting, design and construction, commissioning, operation and maintenance, and radioactive waste management and decommissioning.

In 2000 the IAEA published the report “Safety of Nuclear Power Plants: Design” [5] which establishes nuclear plant safety design requirements applicable to safety functions and associated structures, systems and components, as well as to procedures important to nuclear plant safety. It recognizes that technology and scientific knowledge will continue to develop, and that nuclear safety is not a static entity; however, these requirements reflect the current consensus. They are expressed as ‘shall’ statements, and are governed by the objectives and principles in the Safety Fundamentals report. The Design Requirements report avoids statements regarding the measures that ‘should’ be taken to comply with the requirements. Rather, Safety Guides are published from time to time by the IAEA to recommend measures for meeting the requirements, with the implication that either these measures, or equivalent alternative measures, ‘should’ be taken to comply with the requirements.

The new nuclear power plant designs currently under development incorporate various technical features to meet very stringent safety requirements [5]. Specifically, safety objectives for future plants include reducing the likelihood of accidents as well as mitigating their consequences in the extremely unlikely event that they occur. The objectives include the practical elimination of accident sequences that could lead to large early radioactive release, whereas severe accidents that could imply late containment failure are to be considered in the design process so that their consequences would necessitate only protective measures limited in area and in time [7], [8].

Discussions of the safety of future plants often involve different types of probabilistic safety criteria (PSC). PSC can be defined as *limits*, not to be exceeded, or as *targets*, *goals* or *objectives* (to strive for, but without the implication of unacceptability if the criteria are not met). PSC can be related to the core damage frequency (CDF), which is predicted by performing a level 1 PSA. Another type of PSC can be related to the large early release frequency (LERF) that would follow from severe core damage together with a major early failure of the containment. Use of LERF in PSC carries the implication that a late failure of the containment may be averted by accident management procedures, or mitigated by emergency response (e.g. evacuation of the public in the vicinity of the plant).

Discussions of PSC *targets* for CDF and large off-site-release have been provided for more than a decade in INSAG publications [9–12]. In 1988, INSAG-3 stated “The target for existing nuclear power plants is a likelihood of occurrence of severe core damage that is below about 10^{-4} events per plant operating year. Implementation of all safety principles at future plants should lead to the achievement of an improved goal of not more than about 10^{-5} such events per plant operating year. Severe accident management and mitigation measures should reduce by a factor of at least ten the probability of large off-site releases requiring short term off-site response.” The more stringent safety target for future plants was confirmed by INSAG-5 in 1992 with the statement that [evolutionary] light and heavy water nuclear plants “should meet the long term target of a level of safety ten times higher than that of existing plants”.

In 1996 INSAG-10 noted that prevention of accidents remains the highest priority among the safety provisions for future plants and that probabilities for severe core damage below 10^{-5} per plant year ought to be achievable. INSAG-10 noted that values that are much smaller than this would, it is generally assumed, be difficult to validate by methods and with operating experience currently available. INSAG-10, therefore, considers improved mitigation to be an essential complementary means to ensure public safety. INSAG-10 also stated the need to demonstrate that for accidents without core melt there will be no necessity for protective measures (evacuation or sheltering) for people living in the vicinity of the plant, and for severe accidents that are considered in the design, that only protective measures that are very limited in area and time would be needed (including restrictions in food consumption). In 1999, INSAG-12 (Revision 1 of INSAG-3), confirmed that the target frequency for CDF for existing nuclear power plants is below about 10^{-4} with severe accident management and mitigation measures reducing by a factor of at least 10 the probability of large off-site releases requiring short term off-site response. INSAG-12 continued by noting that for future

plants, improved accident prevention (e.g. reduced common mode failures, reduced complexity, increased inspectability and maintainability, extended use of passive features, optimized human-machine interface, extended use of information technology) could lead to achievement of an improved CDF goal of not more than 10^{-5} per reactor-year. With regard to off-site release for future plants, INSAG-12 stated that an objective for future plants is “the practical elimination of accident sequences that could lead to large early radioactive releases, whereas severe accidents that could imply a late containment failure would be considered in the design process with realistic assumptions and best estimate analyses so that their consequences would necessitate only protective measures limited in area and in time”.

From the IAEA’s Safety Standards Series and INSAG publications, a number of safety goals for future nuclear plants can be identified:

- A reduction in core damage frequency (CDF) relative to current plants;
- Consideration of selected severe accidents in the design of the plants;
- Ensuring that releases to the environment in the event of a severe accident are kept as low as practicable with the aim of providing a technical basis for simplification of emergency planning;
- Reduction of the operator burden during an accident by an improved man-machine interface;
- The adoption of digital instrumentation and control; and
- The introduction of passive components and systems.

Technological advances are being incorporated into advanced designs to meet the stringent safety goals and objectives. Design features both to improve prevention of severe accidents involving core damage, as well as for mitigating their consequences are being incorporated. Considerable development has been carried out worldwide on new systems for heat removal during accidents. Progress has been made in containment design and in instrumentation and control systems.

To further reduce the probability of accidents and to mitigate their consequences, designers of new plants are adopting various technical measures. Examples are:

- Larger water inventories (large pressurizers, large steam generators), lower power densities, negative reactivity coefficients to increase margins and grace periods thereby reducing system challenges;
- Redundant and diverse safety systems with proven high reliability with improved physical separation between systems;
- Passive cooling and condensing systems; and
- Stronger containments large enough to withstand the pressure and temperatures from design basis accidents without fast acting pressure reduction systems, and with support systems to assure their integrity during severe accidents (for example, to control hydrogen concentrations). In some designs there is an outer second containment that provides protection against external events, and allows for detection and filtration of activity that potentially would leak from the inner containment.

Some new designs rely on well-proven and highly reliable active safety systems to remove decay heat from the primary system and to remove heat from the containment building during accidents. Other new designs incorporate safety systems that rely on passive means using, for example, gravity, natural circulation, and compressed gas as driving forces to transfer heat from the reactor system or the containment to either evaporating water pools or to structures cooled by air convection. Considerable development and testing of passive safety systems has been and is being carried out in several countries. In other designs a coupling of active safety systems and passive safety systems is adopted. For each of the aforementioned approaches, the main requirement is that the proposed safety systems fulfill the necessary functions with appropriate reliability.

2.3. Proliferation-resistance

The potential linkage between peaceful use of nuclear energy and the proliferation of nuclear weapons has been a continuing societal concern. To ensure the absence of un-declared nuclear material and activities or diversion of nuclear material for weapons purposes, an international non-proliferation regime has been developed. This regime consists of the following components:

- An international institutional framework for non-proliferation based on the Non-Proliferation Treaty and comprehensive IAEA safeguards agreements and protocols;
- International verification measures (the IAEA Safeguards system plus regional and bilateral agreements) to provide credible assurance of the non-diversion of nuclear material and of the absence of undeclared nuclear material and activities;
- Export controls on nuclear materials, specified facilities, equipment and other materials, including dual-use technologies and materials; and
- National physical protection measures and material accounting and controls measures, as well as IAEA recommendations on physical protection.

It is desirable that IAEA safeguards have a minimal impact on plant operations while ensuring efficient acquisition of safeguards data. With these goals in mind, as designs of nuclear plants and IAEA safeguards techniques have developed, guidelines for plant design measures have been identified by the IAEA [13], which, if taken into account in the plant design phase, would help to ensure efficient acquisition of safeguards data and minimize the impact of the safeguards activities on plant operations. These guidelines⁴ are based on IAEA experience in implementing safeguards, as well as on developments in safeguards technology.

Proliferation resistance is defined [14] as *that characteristic of a nuclear energy system that impedes the diversion or undeclared production of nuclear material, or misuse of technology, by States intent on acquiring nuclear weapons or other nuclear explosive devices*. The degree of proliferation resistance results from a combination of, *inter alia*, technical design features, operational modalities, institutional arrangements and safeguards measures. These can be classified as *intrinsic proliferation resistant features* and *extrinsic proliferation resistant features*. Specifically:

1. *Intrinsic proliferation resistant features* are those features that result from technical design of nuclear energy systems, including those that facilitate the implementation of extrinsic measures; and
2. *Extrinsic proliferation resistance measures* are those measures that result from States' decisions and undertakings related to nuclear energy systems.

Safeguards is an extrinsic measure comprising legal agreements between the party having authority over the nuclear energy system and a verification or control authority, binding obligations on both parties and verification using, *inter alia*, on-site inspections.

Four general types of intrinsic proliferation resistant features of nuclear energy systems (i.e. nuclear plants and fuel cycle facilities) have been identified in [14] and are, in summary:

1. Technical features that reduce the attractiveness for nuclear weapons programmes of nuclear material during production, use, transport, storage and disposal;
2. Technical features that prevent or inhibit the diversion of nuclear material;
3. Technical features that prevent or inhibit the undeclared production of direct-use material; and
4. Technical features that facilitate verification, including continuity of knowledge. These features include those described in [13].

⁴ These guidelines address, for example, design of the spent fuel pool area to facilitate viewing of the spent fuel assemblies; provisions that facilitate the verification of fuel transfers out of the spent fuel pool; provision of appropriate back-up for power supply outages to avoid interruption of power to safeguards equipment; provision of access to appropriate penetrations in the containment building for data transfer lines serving remote safeguards equipment; and other design measures.

Approaches for introducing proliferation resistant features into nuclear energy systems include, but are not limited to, the following:

- a. Reliance on the once-through fuel cycle** would reduce fissile material diversion opportunities that might be associated with fuel reprocessing and recycling.
- b. Establishment of energy parks with both nuclear power plants and fuel cycle facilities** would avoid the need to transport fissile material between sites.
- c. Establishment of a closed fuel cycle with reprocessing that returns minor actinides with plutonium to the reactor for consumption**, could avoid the separation of minor actinides from fissile material so that the material is not weapons useable.
- d. Operating reactors with long operating cycles (e.g. several years) without refuelling or fuel shuffling** could assure that fissile material in the core is not accessible as long as the reactor vessel is not opened. Some new design concepts include the measure that the reactor be returned to the supplier country for refuelling.
- e. Incorporating features to increase the difficulty of extracting fissile material from fresh or spent fuel.**
- f. Incorporating features that greatly reduce the fraction of plutonium in spent fuel** would require that a very large volume of spent fuel would need to be processed to extract sufficient plutonium for a nuclear weapon.
- g. Reducing the fuel stored at a site** would reduce the amount of material that could potentially be diverted from that site.
- h. Reducing the fissile material produced in the reactor** could reduce the weapons-useable material in spent fuel.

It is important to note that some approaches are mutually incompatible in the sense that one approach may not allow, or may be detrimental to, another approach.

Also, there are drawbacks associated with some of the above approaches. For example, the once-through fuel cycle does not allow nuclear energy to become a long term sustainable source of energy. Operating reactors with long fuel cycles of several years requires higher fuel enrichment and the parasitic absorption of neutrons by fission products reduces the fuel utilization efficiency. Features that greatly increase the difficulty of extracting fissile material from spent fuel can create a cost penalty on fuel reprocessing.

2.4. Sustainable energy supply

To assure that the long term potential of nuclear energy can be fully exploited, the nuclear community must not only meet the economic challenge. It must also meet the challenges of achieving acceptance of nuclear power in international discussions on climate change as a technology compatible with sustainable energy development, and achieving improved public understanding in all areas. Clearly nuclear power can put the world's large uranium resource to productive use, can reduce harmful emissions associated with burning fossil fuels, and can expand electricity supplies. To be a truly sustainable energy supply, in addition to being economically competitive, nuclear power must implement a long-term solution to disposal of high-level radioactive waste, continue to achieve the highest level of safety for nuclear plants and for fuel cycle facilities, and assure strong vigilance in security and safeguards of nuclear material.

In the longer term, recycling the fissile content of spent fuel and breeding additional fissile material from the world's resources of U^{238} and Th^{232} can extend the energy resource available from uranium for centuries. This long-term energy strategy will be supported by fast breeder reactors. Also, thermal reactors with high conversion ratios are being developed with goals of assuring a long term energy supply as well as reducing spent fuel accumulation.

3. MEANS FOR REDUCING COSTS OF NEW PLANTS

3.1. Proven means for reducing plant costs

There is a set of proven means for reducing costs during any construction project, including nuclear projects [15], [16], [17], [18]. These means can be generally grouped and listed as follows:

1. Capturing economies of scale;
2. Streamlining construction methods;
3. Shortening construction period;
4. Standardization, and construction in series;
5. Multiple unit construction;
6. Simplifying plant design, improving plant arrangement, and use of modeling;
7. Efficient procurement and contracting;
8. Cost and quality control;
9. Efficient project management; and
10. Working closely and cooperating with relevant regulatory authorities.

The larger the construction project, and the greater the financing burden, as is the case for nuclear power plants, the more important these approaches become.

The best combination of approaches depends on market conditions. In some countries, such as the Republic of Korea and Japan, **economies of scale** are being pursued for new, large⁵ evolutionary LWRs.

However, for some market conditions, and especially for some developing countries, large size plants are not an appropriate match for the grid capacity, the incremental increase in demand or for the potential owner's financial investment capability. For such conditions, small and medium size reactors (SMRs) offer an alternative choice. SMRs have the potential to capture **economies of series production**, if several units are constructed.

Reducing the construction period is important because of the interest and financing charges that accrue during this period without countervailing revenue. One way to reduce the schedule is to reduce on-site and tailor-made construction and emphasize instead the manufacture of modular units or systems. Addressing licensing issues before start of construction is also a key means of achieving a short construction period. Other measures involve improved construction techniques as well as efficient management of construction and commissioning activities. Approaches that have resulted in recent good experience include extensive use of integrated design tools (known as Computer Aided Design; Computer Aided Design and Drafting; and Computer Aided Engineering). These tools facilitate the modularization process, planning and sequencing of construction activities and provide support to procurement planning.

Significant improvements can be made in plant **design** and layout, and use of computer technology and modelling. Several simplifications have been made in the last decade including computer control, process information display, and other areas. Careful planning can result in improvements in plant arrangement and system accessibility, and in design features to facilitate decommissioning.

Standardization and construction in series offer significant cost savings by spreading fixed costs over several units built, and from productivity gains in equipment manufacturing, field engineering, and building construction. First-of-a-kind reactor designs or plant components require detailed safety cases and licensing procedures, resulting in major expenditures before any revenue is realized. Standardization of a series is therefore a vitally important component of capital cost reduction.

⁵ The IAEA differentiates nuclear plants of various power levels by classifying them as:

Large size designs: 700 MW(e) and larger
Medium size designs: 300–700 MW(e)
Small size designs: below 300 MW(e)

Standardization and construction in series offer reduced average licensing times and costs over the series. A detailed account of the lessons from the standardized plant design and construction programme in France is provided in Ref. [19]. Experience is being established within Japan's ABWR activities and the Republic of Korea's KSNP and KSNP + activities.

Closely related is the cost-saving practice of **multiple unit construction** at a single site. The average cost for identical units on the same site can be about 15% or more lower than the cost of a single unit, with savings coming mostly in siting and licensing costs, site labour and common facilities. A good example of multiple unit construction are the 58 PWRs that are operating in France, which have been built as multiple units at 19 sites.

Many of the benefits of technology advances would be lost without some accompanying **regulatory reform** to accommodate change. These include greater regulatory certainty, more prioritization of regulatory requirements, streamlining of regulation to match streamlined engineering and designs, and more flexibility to accommodate technological innovation.

In developing countries, **furthering self-reliance**, and **enhancing local participation** in major projects are goals pursued by governments for a variety of policy reasons. Cost savings in any of several areas — materials and construction costs, foreign exchange costs, labor costs — may result. Reducing the costs of technology transfer and relevant training are areas of emphasis for developing countries. In China, it is considered very important that favourable conditions for technology transfer and personnel training are provided with the help of industrialized countries so that a considerable portion of the work in fabricating the plant equipment and in plant construction can be done by organizations in the developing country. Because of the low cost of manpower, some materials and products can be made cheaper, with due assurance of quality. Experience in China is that the construction cost of the Qinshan-II plant (2 × 600 MW(e) units, the first unit achieving commercial operation in April, 2002) indicates that the cost of this plant is less than that for imported large-size plants because of localization of design and provision of a large amount of the equipment by domestic organizations.

Reference [15] provides further examples of recent and present activities to incorporate the proven means discussed above. These and other traditional proven approaches should help to achieve cost competitiveness for new nuclear power plants. However, the nuclear community must continue to move forward in identifying and implementing new approaches for further reducing the costs of new nuclear plants.

3.2. New approaches for reducing plant costs

Reference [15] discusses new approaches to reduce capital cost that should be developed and implemented in order to gain the greatest possible cost reductions. In summary, these are:

- Modularization, factory fabrication, and series production;
- Development of highly reliable components and systems, including “*smart*” (instrumented and monitored) components and methods for detecting incipient failures — o improve system reliability so that dependence on costly redundancy and diversity practices could be reduced. Development is also required to correlate signals from the “*smart*” components with reliability, and criteria must be developed for when to do maintenance and replacement;
- Further development of passive safety systems where the safety function can be met more cheaply than with active systems. This would include development of reliability models for passive systems;
- Development of computer based advanced technologies for design, procurement, manufacture, construction and maintenance with a focus on coordination of activities to reduce costs and schedules;
- Further development of Probabilistic Safety Analysis (PSA) methods and data bases to support plant simplification and to support examination of potential risk-informed regulatory requirements for new plants leading to more economical designs with very high safety levels. PSA assessments

must (a) be capable of assessing the total risk including full power, low power, shutdown, fires and external events; (b) be capable of accounting for safety culture and human factors; (c) accurately account for ageing effects; and (d) include capability to quantify uncertainties. The challenge will be to establish PSA methods, including understanding of uncertainties in predicted results, to demonstrate that sufficient defense-in-depth, and sufficient balance among the various levels of defense-in-depth, can be achieved through simpler and cheaper technical solutions;

- Improvement of the technology base for eliminating over-design (i.e. improved understanding of thermo-hydraulic phenomena, more accurate data bases of thermo-hydraulic relationships and thermo-physical properties, better neutronic and thermo-hydraulic codes, and further code validation). The focus could be on removing the need to incorporate excessively large margins into the design simply for the purpose of allowing for limitations of calculational methodology and uncertain data;
- Reduction of number of components and materials requiring nuclear grade standards;
- Design for higher temperature (higher thermal efficiency);
- Design for multiple applications (e.g. co-generation of electricity and heat; sea-water desalination); and
- Achieving international consensus regarding commonly acceptable safety requirements that would facilitate development of standardized designs which can be built in many countries without requiring significant re-design efforts.

4. DEVELOPMENT OF ADVANCED NUCLEAR PLANT DESIGNS

New generations of nuclear power plants are being developed, building upon the background of nuclear power's success and applying lessons learned from the experience of operating plants. Various organizations are involved in this development, including governments, industries, utilities, universities, national laboratories, and research institutes. Global trends in advanced reactor designs and technology development are periodically summarized in status reports, symposia and seminar proceedings prepared by the IAEA [20], [21], [22], [23], [24], [25] to provide all interested IAEA Member States with balanced and objective information on advances in nuclear plant technology.

Advanced designs comprise two basic categories. The first category is called evolutionary designs and encompasses direct descendants from predecessors (existing plant designs) that feature improvements and modifications based on feedback of experience and adoption of new technological achievements, and possibly also introduction of some innovative features, e.g. by incorporating passive safety systems. Evolutionary designs are characterized by requiring at most engineering and confirmatory testing prior to commercial deployment. The second category consists of designs that deviate more significantly from existing designs, and that consequently need substantially more testing and verification, probably including also construction of a demonstration plant and/or prototype plant, prior to large-scale commercial deployment. These are generally called innovative designs. Often a step increase in development cost arises from the need to build a prototype reactor or a demonstration plant as part of the development programme (see Figure 1).

In the near term most new nuclear plants will likely be evolutionary designs building on today's successful proven systems while incorporating technology advances and often pursuing economies of scale. In the longer term, development and demonstration of new, innovative designs, including their promised short construction and start-up times and low capital costs, could help to promote a new era of nuclear power.

Several innovative designs are in the small-to-medium size range and would be constructed with factory built structures and components, including complete modular units for fast on-site installation. Such smaller and easier to finance systems would be particularly attractive for countries with small electricity grids or remote locations. They could also be used for district heating, sea-water desalination, hydrogen production, and other non-electric applications.

Advanced nuclear plant designs presently under development comprise the following basic reactor types:

- Water cooled reactors, utilizing water as coolant and moderator. These are comprised of light water reactors (LWRs), which use light water as both the coolant and the moderator, and heavy water reactors (HWRs), which use heavy water as moderator and either light or heavy water as coolant;
- Gas cooled reactors, using helium as coolant and graphite as moderator; and
- Fast reactors, using liquid metal (e.g. sodium) or gas (helium) as coolant.

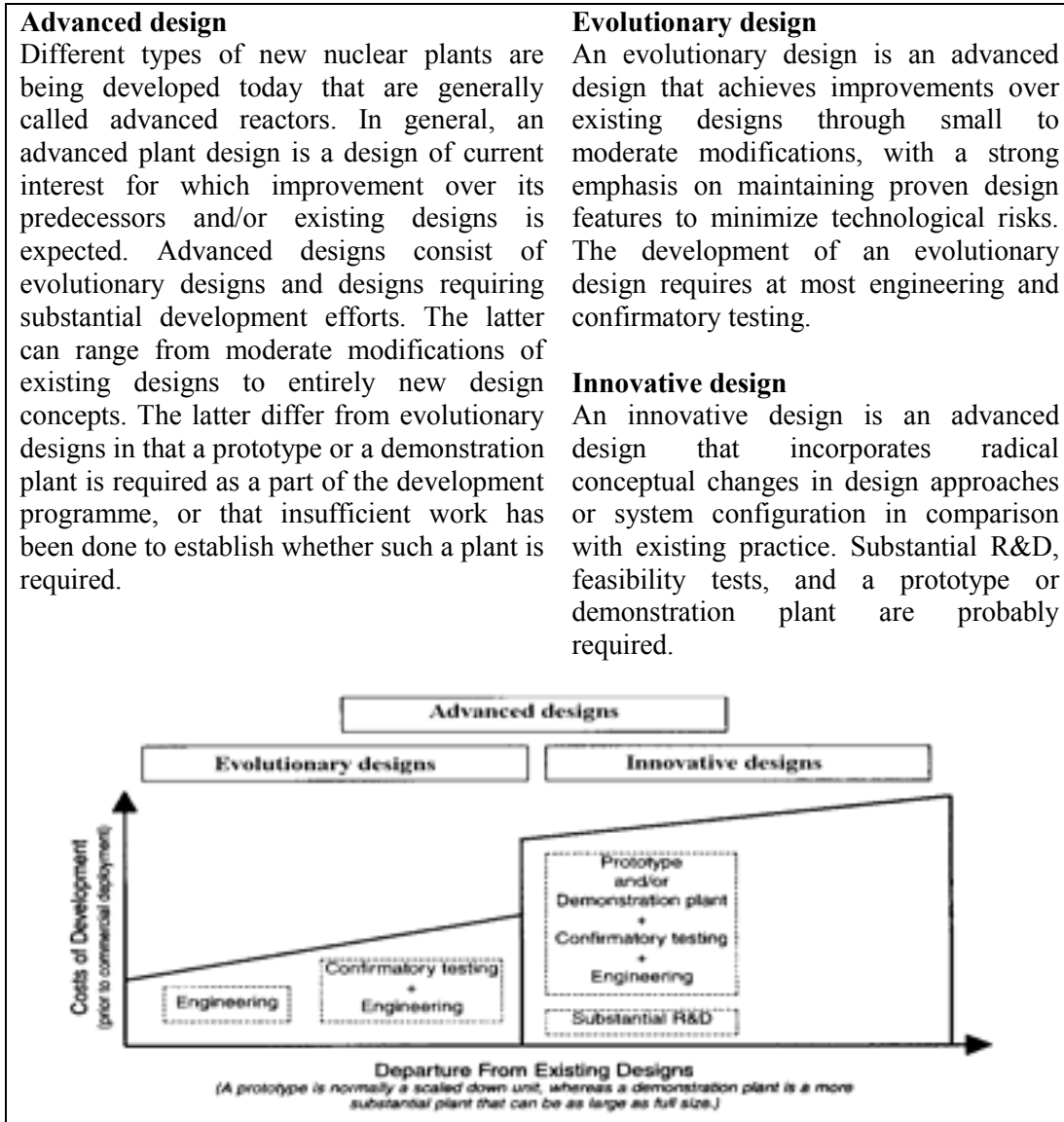


FIG. 1. Efforts and development costs for advanced designs versus departure from existing designs (terms are excerpted from Ref. [26]).

4.1. Light water reactors

LWRs comprise 80.5% of the total number of nuclear units in operation worldwide. This is reflected in the considerable activities which are underway to develop advanced LWR designs, as is indicated in Annex 1 which lists various advanced LWR designs together with the design organizations and the status of the development.

4.1.1. *Overview of evolutionary LWR development*

In France and Germany, Framatome ANP has completed the basic design for the large-size European Pressurized Water Reactor (EPR) in 1998, which meets European utility requirements. The EPR's higher power level relative to the latest series of PWRs operating in France (the N4 series) and Germany (the Konvoi series) has been selected to capture economies of scale. In December 2003, Teollisuuden Voima Oy (TVO) of Finland signed a turnkey contract with Framatome ANP and Siemens AG for an EPR for the Olkiluoto site. Commercial operation is planned for mid-2009. Also, Electricite de France is planning to construct an EPR at Flamanville (Unit 3). Framatome has received design approval for the EPR from the French Safety Authority in October 2004. Start of construction is projected for 2007 with grid connection in 2012.

In Germany, Framatome ANP with international partners from Finland, the Netherlands, Switzerland and France is developing the basic design of the SWR-1000, an advanced BWR with passive safety features. In 2002 Framatome submitted the SWR-1000 for a pre-application phase for Design Certification by the U.S. NRC.

In Japan, benefits of standardization and construction in series are being realized with the ABWR units. The first two ABWRs in Japan, the 1360 MW(e) Kashiwazaki-Kariwa 6 and 7 units, have been in commercial operation since 1996 and 1997 respectively. The ABWR, Hamaoka Unit 5, began commercial operation in January 2005, and an ABWR is under construction at Shika Unit No. 2. Deployment programmes are underway for 8 more ABWRs. Two ABWRs are under construction in Taiwan, China.

Expectations in Japan are that future ABWRs will achieve a significant reduction in generation cost relative to the first ABWRs. The means for achieving this cost reduction include standardization, design changes and improvement of project management, with all areas building on the experience of the ABWRs currently in operation. In addition, a development programme was started in 1991 for ABWR-II, aiming to further improve and evolve the ABWR, with the goal of significant reduction in power generation costs relative to a standardized ABWR. The power level of ABWR-II has been increased relative to the ABWR, and benefits of economies-of-scale are expected. Commissioning of the first ABWR-II is foreseen in the late 2010s. Also in Japan, the basic design of a large advanced PWR has been completed by Mitsubishi Heavy Industries and Westinghouse for the Japan Atomic Power Company's Tsuruga-3 and -4 units, and a larger version, the APWR⁺ is in the design stage.

In the Republic of Korea, the benefits of standardization and construction in series are being realized with the Korean Standard Nuclear Plants (KSNPs). The first two KSNPs, Ulchin 3 and 4 began commercial operation in 1998 and 1999. Yonggwang 5 and 6 began commercial operation in 2002. The Ulchin 5 KSNP began commercial operation in 2004, and the Ulchin 6 KSNP was connected to the grid in January 2005. The accumulated experience is now being used by Korea Hydro and Nuclear Power (KHNP) to develop the improved KSNP⁺. The first units of KSNP⁺ are planned for Shin-Kori Units 1 and 2 with commercial operation planned for 2010 and 2011, respectively. In addition, the development of the Korean Next Generation Reactor, now named the Advanced Power Reactor 1400 (APR-1400), was started in 1992, building on the experience of the KSNPs. The higher power level of the APR-1400 relative to the KSNP and the KSNP⁺ has been selected to capture economies of scale. Recent development of the APR-1400 focused on improving availability and reducing costs. In March 2001, KHNP started the Shin-kori 3,4 project for the APR1400, with completion scheduled for 2012 and 2013.

In the USA, designs for a large sized advanced PWR (the Combustion Engineering System 80+) and a large sized BWR (General Electric's ABWR) were certified in May 1997. Westinghouse's mid-size AP-600 design with passive safety systems was certified in December 1999. Westinghouse is developing the AP-1000 applying the passive safety technology developed for the AP-600 with the goal of reducing the capital costs through economies-of-scale. Westinghouse received Final Design Approval for the AP-1000 from the U.S.NRC in September 2004 and Design Certification is expected in 2005. An adaptation of the AP-1000, called the EP-1000, is being designed by Westinghouse and Genesi (Italy) applying the passive safety technology to meet European Utility Requirements and licensing requirements in Europe. A Westinghouse led international team is developing the modular, integral IRIS design in the small to medium-size range, with a core design capable of operating on a 4-year fuel cycle⁶. The IRIS design is in pre-application review during which the NRC will provide feedback on necessary testing and an assessment of the risk-informed regulation approach. Design Certification for IRIS is targeted for 2008–2010. General Electric is designing a large ESBWR applying economies-of-scale together with modular passive safety systems. The design draws on technology features from General Electric's ABWR and from their earlier mid-size simplified BWR with passive systems. The ESBWR is in the pre-application review phase with the U.S.NRC.

The U.S. DOE's Nuclear Power 2010 programme is conducting cooperative projects with industry to obtain U.S. NRC approval of three sites for new nuclear plants under the Early Site Permit (ESP) process, and to develop application preparation guidance for the combined Construction and Operating License (COL) and to resolve generic COL regulatory issues. The COL process is a "one-step" process by which safety concerns are resolved prior to start of construction, and NRC issues a license for construction and operation of a new plant.

In the Russian Federation, efforts continue on evolutionary versions of the currently operating WWER-1000 (V-320) plants. This includes the WWER-1000 (V-392) design, of which two units are planned at the Novovoronezh site, and WWER-1000 units under construction in China, India and the Islamic Republic of Iran. Development of a larger WWER-1500 design has been initiated.

In China, the China National Nuclear Corporation (CNNC) has developed the AC-600 design, and is currently developing the CNP-1000 for electricity production. CNNC is also developing the QS-600 e/w, which is based on the design of the Qinshan Phase II, for electricity production and sea-water desalination. China is pursuing self-reliance both in designing the plant to meet Chinese safety requirements, and in fostering local equipment manufacture with the objective of reducing construction and operation costs. Experience gained and lessons learned from the design, construction and operation of the Qinshan and Daya Bay NPPs are being incorporated.

4.1.2. Overview of innovative LWR development

A trend in the design of small and medium sized light water reactors has been simplified designs with long core life and modular design for factory production of standardized components and systems. Several small sized PWR designs are of the integral reactor type in which the steam generator is housed in the same vessel as the reactor core. This approach eliminates primary system piping. The Argentinian CAREM reactor (prototype design 27 MW(e)) is cooled by natural circulation, and has passive safety systems. Designers of CAREM are planning a prototype (27 MW(e)) plant prior to commercial deployment. The SMART design that has been developed in the Republic of Korea is an integral PWR and, like CAREM, uses no soluble boron. A decision has been made to build a 1/5th scale, 65 MW(th), SMART pilot plant with operation planned in 2008. The Japan Atomic Energy Research Institute is developing the small passively safe integral PSRD-100 system for electricity

⁶ IRIS is considered to be an evolutionary LWR in the context of Figure 1. IRIS has innovative features and the integral design represents a radical change in system configuration from existing loop reactors. However Westinghouse states that while it is innovative engineering, it relies on proven LWR technology and thus it only requires engineering and confirmatory testing. A prototype or demonstration plant is not required, but a first of a kind will be, since no other IRIS-type integral reactors have been built.

and/or heat supply and sea-water desalination, and Mitsubishi together with other organizations is developing the IMR design for electricity production.

In Russia, development is on-going at OKBM for both the VBER-300 integral design with the steam generator system inside the reactor pressure vessel and for the KLT-40, a floating small NPP design for electricity and heat; at RDIPE for the VK-300 BWR design for electricity and district heating; and at Atomenergoprojekt / Hidropress on a mid-size WWER-640 with passive safety systems.

In Japan the Toshiba Corporation and the Tokyo Institute of Technology are developing a long operating cycle, natural circulation simplified LSBWR with passive safety systems. The LSBWR's power level is in the small size range with a target 15-year core life. Hitachi Ltd. is also developing the mid-size Hitachi Simplified BWR (HSBWR), the mid-size Advanced BWR (HABWR), and the small-size SSBWR with passive safety systems and a 20-year core life.

Also in Japan, with the goals of ensuring sustainable energy supplies by achieving a high conversion (conversion ratio equal to or beyond 1.0) of fertile isotopes to fissile isotopes and reducing spent fuel accumulation, Hitachi Ltd. is also developing the large-size, reduced moderation RBWR and JAERI is developing the large-size RMWR.

A prototype or a demonstration plant will most likely be required for thermodynamically supercritical water cooled systems, which have been selected for development by the Generation-IV International Forum (see the summary discussion of the Generation-IV International Forum (GIF) in Section 5). In a supercritical system the reactor operates above the critical point of water (22.4 MPa and 374°C) resulting in higher thermal efficiency than current LWRs. Thermal efficiencies of 40–45% are projected with simplified plant designs. Core design options include both thermal neutron spectrum cores and fast neutron spectrum cores for high conversion. The large-size SCPR concept being developed by Toshiba Hitachi and the University of Tokyo is an example thermodynamically supercritical LWR. In Europe, the HP-LWR project has been funded by the European Commission to assess the merit and economic feasibility of an LWR operating thermodynamically in the supercritical regime. Activities on super-critical water cooled system concepts are also on-going at universities and research centers in the USA and in the Russian Federation.

Appendix 1 presents summary information on advanced LWR designs and their status of development.

4.2. Heavy water reactors

HWRs account for about 8% of the nuclear power reactors that are currently operating. Two types of commercial pressurized heavy water cooled reactors have been developed, the pressure tube and the pressure vessel versions. HWRs with power ratings from a few hundred MW(e) up to approximately 900 MW(e) are available. The heavy water moderation yields a good neutron economy and has made it possible to utilize natural uranium as fuel. Both the pressure tube and pressure vessel designs use on-load refuelling.

In Canada, the approach taken by AECL in development of next generation CANDU plants (the ACR-700) is to essentially retain the present evolutionary CANDU reactor characteristics and power levels (e.g. the CANDU-6 and CANDU-9 with net electric power levels around 650 MW(e) and 900 MW(e) respectively) and to improve economics through plant optimization and simplification. The ACR-700 design uses slightly enriched uranium and light water coolant. It is currently undergoing a pre-application licensing review by the US Nuclear Regulatory Commission. Following that review, AECL intends to seek a Design Certification in 2005. The ACR-700 is simultaneously undergoing a licensing review in Canada, and an ACR-1000 plant is being designed.

Also, in Canada in the framework of GIF, AECL is developing an innovative design, the CANDU-X, which would use supercritical light-water coolant to achieve high thermodynamic efficiency.

In India, a continuing process of evolution of HWR design has been carried out since the Rajasthan 1 and 2 projects. In 2000 construction began on two 540 MW(e) units at Tarapur which incorporate feedback from the indigenously designed 220 MW(e) units⁷.

India is also developing the advanced heavy water reactor (AHWR), a heavy water moderated, boiling light water cooled, vertical pressure tube type reactor, optimized for utilization of thorium for power generation, with passive safety systems.

Reference [20] provides a detailed discussion of the status and projected development of HWRs.

4.3. Gas cooled reactors

Gas cooled reactors have been in operation for many years. In the United Kingdom (UK), the nuclear electricity is mostly generated by CO₂-cooled Magnox and advanced gas cooled reactors (AGRs). Development of high temperature reactors (HTGRs) with helium as coolant, and graphite as moderator, has also been going on for a long period of time. Prototype and demonstration plants with the Rankine steam cycle for electric power generation have been built and operated.

The inert He coolant and the coated fuel particle design enable HTGRs to operate at temperatures considerably above those in water-cooled reactors. Development is also conducted for high temperature heat applications. Currently two helium cooled test reactors are in operation. The High-Temperature Engineering Test Reactor (HTTR) at the Japan Atomic Energy Research Institute (JAERI) in Japan and the HTR-10 at the Institute of Nuclear Energy Technology (INET) in China.

Presently, a considerable effort is devoted to the gas-turbine direct cycle, pebble bed small-size modular HTR (PBMR) that promises high thermal efficiency and low power generation cost. Eskom, South Africa's Industrial Development Corporation, and BNFL (United Kingdom) are jointly developing such a system. Also, the Ministry of the Russian Federation for Atomic Energy, the Experimental Design Bureau for Machine Building (OKBM), General Atomics, Framatome and Fuji Electric are jointly developing a small gas turbine modular helium reactor (GT-MHR) for electricity production and the consumption of weapons grade plutonium.

A helium cooled very high temperature reactor (VHTR) with a focus on hydrogen production is being developed within the framework of GIF (see Section 5).

4.4. Fast reactors

Liquid metal cooled fast reactors (LMFRs) have been under development for many years in a number of countries, primarily as breeders. The successful design, construction and operation of several sodium cooled reactor plants, such as the small size prototype fast reactor in the United Kingdom, the prototype Phénix fast reactor in France, the BN-350 in Kazakhstan (part of its thermal energy was used for sea-water desalination), both the demonstration BN-600 in the Russian Federation, and the Monju in Japan, as well as the commercial size Superphénix in France, have provided an extensive experience base of more than 200 reactor-years for further improvements. In addition, this is a considerable base of experience with lead-bismuth (eutectic) cooled propulsion (submarine) reactors built and operated in the former USSR.

Fast reactors use fast neutrons for sustaining the fission process, and they can actually produce fuel, as well as consuming it. Plutonium breeding allows fast reactors to extract sixty-to-seventy times more energy from uranium than thermal reactors do. Their capability to produce more fissile material than they consume may become indispensable in the longer term if the deployment of nuclear power is increased substantially. Fast reactors may also contribute to reducing plutonium stockpiles, and to the

⁷ The most recent plants in this series, the 220 MWe Kaiga-1 and the Rajasthan-3 and -4 units, were connected to the grid in the year 2000.

reduction of the required isolation time for high-level radioactive waste by utilizing transuranic radioisotopes and transmuting some of the most cumbersome long-lived fission products.

Examples of current LMFR activities include: the construction in China of the small size Chinese Experimental Fast Reactor (CEFR) with first criticality scheduled for 2006; the development of the small-size KALIMER design in the Republic of Korea; the successful operation of the Indian Fast Breeder Test Reactor (FBTR) and its utilization for fast reactor R&D, especially fuel irradiation and materials research; the development of the medium size Prototype FBR (PFBR) in India for which construction has started in 2004; efforts in Japan aimed at restarting MONJU, and the Japan Nuclear Cycle Development Institute's "Feasibility Study on a Commercialised Fast Reactor Cycle System"; efforts in Russia to complete the BN-800 reactor at Beloyarsk by 2010, and design studies of advanced fast reactors (sodium cooled, lead cooled, and lead-bismuth eutectic cooled) having improved economics and enhanced safety.

In France, the Phénix plant has restarted in 2003 with the main mission of conducting experiments on long lived radioactive nuclide incineration and transmutation.

Development activities for a gas (helium) cooled fast reactor (GFR) with an integrated fuel cycle with full actinide recycle and for lead alloy and sodium cooled systems are being conducted within GIF.

Co operative international research is underway in several countries on fast neutron spectrum hybrid systems (e.g. accelerator driven systems (ADS)). The potential advantages of ADS systems are low waste production, high transmutation capability, enhanced safety characteristics and better long-term utilization of resources (e.g. with thorium fuels). ADS activities include development of the HYPER concept by the Republic of Korea; design studies in Japan on a lead-bismuth eutectic cooled concept and R&D at JAERI in the fields of sub-critical core design, spallation target technology, accelerator development and minor actinide fuel development; and research on basic physical processes in Russia and in eight countries in the European Union, and in the Advanced Accelerator Applications programme of the USA (recently merged with the Advanced Fuel Cycles initiative).

5. INTERNATIONAL INITIATIVES FOR INNOVATIVE PLANTS

Many countries believe that nuclear energy must remain or become an integral part of their energy mix to meet energy supply needs. To help achieve this goal, there are two major international efforts, the Generation IV International Forum and the IAEA's International Project on Innovative Nuclear Reactors and Fuel Cycles (INPRO).

Concerns over energy resource availability, climate change, air quality, and energy security suggest an important role for nuclear power in future energy supplies. While the current Generation II (commercial power reactors) and Generation III ([currently available] advanced LWRs) nuclear power plant designs provide an economically, technically, and publicly acceptable electricity supply in many markets, further advances in nuclear energy system design can broaden the opportunities for the use of nuclear energy.

To explore these opportunities, the U.S. Department of Energy's Office of Nuclear Energy, Science and Technology has engaged governments, industry, and the research community worldwide in a wide-ranging discussion on the development of next-generation nuclear energy systems known as "Generation IV". This has resulted in the formation of the Generation-IV International Forum (GIF), a group whose member countries are interested in jointly defining the future of nuclear energy research and development. Members are Argentina, Brazil, Canada, Euratom, France, Japan, the Republic of Korea, South Africa, Switzerland, the United Kingdom and the United States of America. The IAEA and the OECD/NEA have permanent observer status in the GIF Policy Group, which governs the project's overall framework and policies. In short, "Generation IV" refers to the development and demonstration of one or more Generation IV nuclear energy systems that offer advantages in the areas of economics, safety and reliability, sustainability, and could be deployed commercially by 2030.

As stated in [27] the purpose of the GIF and the Vision for Generation IV is “The development of concepts for one or more Generation IV nuclear energy systems that can be licensed, constructed, and operated in a manner that will provide a competitively priced and reliable supply of energy to the country where such systems are deployed, while satisfactorily addressing nuclear safety, waste, proliferation and public perception concerns.” Following evaluations of many concepts, six systems have been selected by the GIF Policy Group for future bilateral and multilateral cooperation, and a Technology Roadmap has been prepared to guide the research and development [28]. The six selected systems are:

- Gas cooled fast reactor systems,
- Lead alloy liquid metal-cooled reactor systems,
- Molten salt reactor systems,
- Sodium liquid metal cooled reactor systems,
- Supercritical water cooled reactor systems,
- Very high temperature gas reactor systems.

The IAEA’s International Project on Innovative Nuclear Reactors and Fuel Cycles (INPRO) is based on an IAEA General Conference resolution in September 2000 inviting all interested Member States, both technology suppliers and technology users, to consider jointly international and national actions required to achieve desired innovations in nuclear reactors and fuel cycles. Additional endorsement came in a UN General Assembly resolution in December 2001 that emphasized “the unique role that the Agency can play in developing user requirements and in addressing safeguards, safety and environmental questions for innovative reactors and their fuel cycles” and stressed “the need for international collaboration in the development of innovative nuclear technology”.

The overall objectives of INPRO are (a) to help to ensure that nuclear energy is available to contribute to fulfilling energy needs in the 21st century in a sustainable manner; (b) to bring together all interested Member States, both technology holders and technology users, to consider jointly the international and national actions required to achieve desired innovations in nuclear reactors and fuel cycles; and (c) to create a process that involves all relevant stakeholders that will have an impact on, draw from, and complement the activities of existing institutions, as well as ongoing initiatives at the national and international level. The INPRO time horizon is 50 years into the future. As of December 2003, members of INPRO include Argentina, Armenia, Brazil, Bulgaria, Canada, Chile, China, Czech Republic, France, Germany, India, Indonesia, Morocco, the Netherlands, Pakistan, the Republic of Korea, the Russian Federation, South Africa, Spain, Switzerland, Turkey, and the European Commission. In its first Phase, INPRO has prepared basic principles and user requirements⁸ for innovative energy systems in the areas of economics, safety, environment, waste management, proliferation resistance and infrastructure. These are presented in Appendix 2. INPRO has published guidelines for the evaluation of innovative nuclear reactors and fuel cycles addressing economics, sustainability and environment, safety of nuclear installations, waste management, proliferation resistance as well as cross-cutting issues [14].

6. NON-ELECTRIC APPLICATIONS OF NUCLEAR ENERGY

As has been discussed in the preceding sections, nuclear energy is playing an important role in electricity generation, producing about 16% of the world’s electricity. However, only about one-fifth of the world’s energy consumption is used for electricity generation [29]. Most of the world’s energy consumption is for heat and transportation. There is currently some use of nuclear energy for providing heat, and interest in the future use of nuclear energy in the heat market is growing. Nuclear energy has considerable potential to penetrate into the energy sectors now served by fossil fuels.

⁸ In the context of INPRO, a basic principle is a statement of a general rule providing guidance for the development of an innovative nuclear energy system. A user requirement is a condition that should be met to achieve users’ acceptance of an innovative nuclear energy system.

For heat applications of nuclear energy, the temperature requirements vary greatly. As shown in Figure 2 from [30], for heat applications the temperatures range from around 100°C for hot water and steam for district heating and seawater desalination, to up to 1000°C for heat for the production of hydrogen by high temperature thermo-chemical processes. Although various forms of nuclear heat application are technically feasible and pursued between these temperature ranges, the major applications are directed to the lower end using water cooled reactors [31] and to the higher end using high temperature gas cooled reactors [30], [32], [33]. Figure 2 also shows the temperatures produced by the various reactor types⁹ and the temperatures necessary for different non-electric applications.

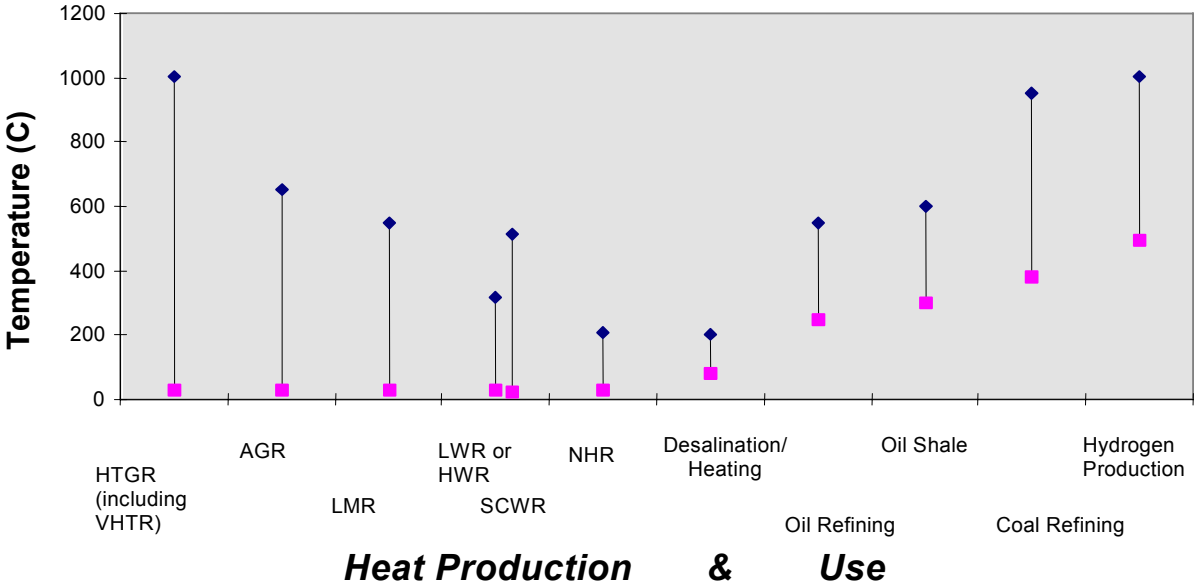


FIG. 2. Temperatures of heat produced by different reactor types and temperatures of heat used for different non-electric applications of nuclear energy. See text for an explanation of terms.

Low temperature heat applications include district heating, seawater desalination and a large variety of agricultural and industrial processes. Seawater desalination requires temperatures up to about 130°C, district heating up to about 170°C and low temperature industrial processes up to about 250°C. Applications involving use of high temperature nuclear heat are not well proven and remain in the laboratory or in small-scale demonstration phase. For large-scale deployment significant research and development is still required.

6.1. Nuclear energy for hydrogen production

Hydrogen as an energy carrier is receiving increasing attention in OECD countries, notably in the US and the European Union. Ref. [35] examines the wide range of activities required to realize hydrogen’s potential in solving US energy security, diversity, and environmental needs. Ref. [36] provides a vision outlining the research, deployment and non-technical actions that would be necessary to move from today’s fossil-based energy economy to a future sustainable hydrogen-oriented economy with fuel cell energy converters.

⁹ It should be noted that reactor and fuel technology development could increase the achievable temperatures. For example, super-critical water cooled reactors would provide temperatures up to about 500°C; a lead or lead-bismuth cooled fast reactor system possibly may achieve core outlet temperatures ranging up to 800°C with advanced materials; and a graphite moderated, helium cooled, very high temperature reactor system would supply heat with core outlet temperature above 1000°C [34].

Nuclear energy can be used for hydrogen production by using nuclear produced electricity for water electrolysis or by using nuclear heat from high or very high temperature reactors for indirect thermo-chemical water-splitting cycles. Production of hydrogen by nuclear electricity and/or high temperature nuclear heat would open the application of nuclear energy for the transportation sector and reduce the reliance of the transportation sector on fossil fuel with the associated price volatility, finite supply and greenhouse gas emissions. Using electricity in electrolyzers to produce hydrogen would allow a near-term option for distributed hydrogen generation at the point of delivery to the customer, such as at a fuelling station. Although the efficiency of hydrogen production by electrolyzers is lower than with high temperature thermo-chemical processes, such distributed production could play an initiating role, because of the lower capital investment and especially until large networks for hydrogen distribution become common. In the longer term, production of hydrogen at central nuclear stations with high or very high temperature reactors connected to extensive distribution networks may become cost efficient, with distributed production continuing to meet some needs.

Some experience for high temperature applications of nuclear energy is available on the laboratory scale and from component tests for earlier development programmes for HTGR applications. Significant research and development is still required before large scale deployment such as steam reforming of methane and thermo-chemical cycles for production of hydrogen.

Programmes are on-going in Japan and China with the goal of demonstrating the use of heat from HTGRs for high temperature applications [37] and [38]. In the USA, construction of an advanced reactor for hydrogen production is under consideration.

6.2. District heating

District heating networks generally have installed capacities in the range of 600 to 1200 MW(th) in large cities, decreasing to approximately 10 to 50 MW(th) in towns and small communities. For heat applications with nuclear plants, there are basically two options: Co-generation of electricity and heat, and dedicated nuclear heating reactors. Co-generation has been widely applied and experienced. In the co-generation mode, electricity will usually constitute the main product. Large size reactors, therefore, have to be integrated into the electrical grid system and optimized for base load electricity production. For reactors in the small to medium-size range, and in particular for small and very small reactors, the share of process heat generation could be larger, and heat could even be the predominant product.

Experience with nuclear district heating has been gained in Bulgaria, China, Germany, Hungary, the Russian Federation, Slovakia, Sweden, Switzerland and the Ukraine. A listing of operating nuclear heating plants is provided in [30]. Obviously, a potential market for the application of nuclear energy for district heating appears mainly in climatic zones with relatively long and cold winters. In Western Europe, for example Finland, Sweden, and Denmark are countries where district heating is widely used.

In the district heating field, the Russian Federation is reflecting its accumulated extensive experience in the improved design concept of a local district heating source and heat supply system. Restarting of the construction work of the site of Voronez and Tomsk is expected, both using AST-500 reactors. Some other cogeneration plants for district heating are also foreseen for replacing existing plants that are approaching the end of their design lifetime.

6.3. Seawater desalination

Application of nuclear heat for seawater desalination is another field with some operational experience and good prospects. Freshwater is essential in civilization and development. Its demand is rapidly growing throughout the world and some regions are already being jeopardized with the shortage of fresh water. Seawater desalination is a process of separating dissolved saline components from seawater to obtain fresh water with low salinity, adequate for irrigation, drinking and industrial use.

Seawater desalination technologies¹⁰ have been well established in the middle of the 20th century, with still further improvement potential. The contracted capacity of desalination plants for desalinated water now exceeds 32 million m³/d worldwide [39].

Nuclear desalination is the production of potable water from seawater in an integrated facility in which a nuclear reactor is used as the source of energy (electrical and/or thermal) for the desalination process on the same site. The facility may be dedicated solely to the production of potable water, or may be used for the generation of electricity and the production of potable water, in which case only a portion of the total energy output of the reactor is used for water production.

The experience and future opportunities for nuclear desalination were reviewed at a Symposium on Nuclear Desalination of Seawater, [40] convened by the IAEA in May 1997. Reference [33] summarizes global experience in nuclear seawater desalination and provides a list of operating nuclear desalination plants as of mid-2000.

The technical feasibility of integrated nuclear desalination has been firmly established by successful operation at several plants. This successful operation has proved the compliance with safety requirements and the reliability of co-generation nuclear reactors. Operating experience exceeds 150 reactor-years (statistics updated [30]).

Many IAEA Member States are moving forward in preparing nuclear desalination projects [41] and [42]. Activities are currently ongoing in Argentina, Canada, China, Egypt, France, India, Indonesia, Pakistan, the Republic of Korea, Morocco, the Russian Federation, and Tunisia.

In 1996 the IAEA, in its Options Identification Programme (OIP) identified practical options [43] of technical configuration of nuclear and desalination coupling to build near term technical and economic confidence under specific conditions. They were: (1) desalination in combination with a nuclear power reactor being constructed or in an advanced design stage with construction expected in the near term; (2) desalination, as above, in combination with a currently operating reactor with some minor design modifications as required to the periphery of the existing nuclear system; and (3) desalination in combination with a small (heating) reactor.

In the Republic of Korea, the design of a nuclear desalination plant with the SMART reactor is developed to supply 40,000 m³/day of fresh water and 90 MW of electricity to an area with an approximate population of 100,000 or an industrialized complex. A detailed design and construction project of a one-fifth scale SMART Pilot plant for demonstration of the relevant technologies, is currently underway and will be completed by 2008. This is an example of option 1 identified in the OIP. Also in the Russian Federation efforts continue on a floating power unit based on a KLT-40 reactor for multipurpose use including desalination. A nuclear desalination project is foreseen in the Russian Arctic Sea coast area (Severodvinsk or Pevec) using an RO and/or MED process.

For option 2, three examples can be mentioned. A small RO facility set up at the KANUPP HWR unit in Pakistan has been in service since early 2000 producing 450 m³/day of fresh water, and work is

¹⁰ These technologies can be classified as:

Multi-Stage Flash (MSF): MSF is a distillation process by which feed saline water (usually seawater) is allowed to flash along the lower sections of flash chambers (or stages), after the feed water has been heated in a primary vessel called the brine heater to temperatures in the range of 90–110°C. Water vapor produced in the consecutive flashing stages is condensed in the upper sections on condensing tubes and collected on collection trays of the different stages as product distilled water. The concentrate brine reject is typically discharged to the sea.

Multi-Effect Distillation (MED): MED, similarly to MSF, takes place in a series of vessels (effects), where principles of condensation/evaporation and gradually reduced ambient pressure in down-stream effects permit the seawater feed to undergo boiling without the need to supply additional heat after the first effect.

Reverse Osmosis (RO): RO is a membrane process in which the water from pressurized saline water feed is separated from the solutes (the salts) while passing through a semi-permeable membrane. No heating or phase change is necessary in this process since most of the energy required is for pressurizing the feed saline water.

progressing on a Desalination Demonstration Plant, to be commissioned in 2005 at KANUPP. A 6300 m³/day Multi-Stage Flash-Reverse Osmosis hybrid desalination plant is in commissioning in India at the Kalpakkam nuclear power plant. The product water is both for process water for the nuclear power plant and for drinking water in the neighbouring community. The Reverse Osmosis plant segment at Kalpakkam has been operating since 2002.

In Europe, the European Commission's project EURODESAL, coordinated by the French CEA, with partners in Europe and Canada, has conducted feasibility studies for both option (1) and option (2) above.

In addition to these activities, preheat Reverse Osmosis desalination experimental facilities are being set up in Egypt and Canada. Other countries are assessing a possibility of nuclear desalination plant under different time frame. For example,

- Egypt is continuing its feasibility study for an electricity and desalination plant at El-Dabaa;
- Tunisia is about to collaborate with France on a feasibility study of nuclear desalination for a site (la Skhira) in the southern part of the country along the Mediterranean coast;
- Indonesia is starting a joint feasibility study with Republic of Korea of a nuclear desalination plant in its Madura Island;
- In China, a nuclear desalination plant, based on the 200 MW(th) nuclear heating reactor with a capacity of 150,000 m³/d is being studied for YanTai in Shandong province.

As any nuclear reactor can provide energy (low-grade heat and/or electricity), as required by desalination processes, in principle, a broad option of coupling configurations can be feasible for future deployment of nuclear desalination.

6.4. Heat for other industrial processes

Within the industrial sector, at temperatures higher than those needed for district heating and seawater desalination, process heat is used for a variety of applications. Heat applications at temperatures up to about 200 to 300°C include the pulp and paper industry and the textile industry. Chemical industries, oil refining, oil shale and oil-sand processing and coal gasification are examples of industries with temperature requirements up to the 500–600°C level. Refinement of coal and lignite, and hydrogen production by water splitting, are among applications that require temperatures of 600–1000°C and above. Unlike district heating, the load factors of industrial users of heat do not depend on climatic conditions. The demands of large industrial users usually have base load characteristics.

Experience with provision of process steam for industrial purposes with nuclear energy has been gained in Canada, Germany, Norway and Switzerland. In Canada, steam from the Bruce Nuclear Power Development (BNPD) was supplied until the mid-to-late 1990s to heavy water production plants and to an adjacent industrial park at the Bruce Energy Center.

In Germany, since December 1983, the Stade PWR, has supplied steam for a salt refinery that is located at a distance of 1.5 km. In Norway, the Halden Reactor has supplied steam to a nearby factory for many years. In Switzerland, since 1979, the Gösigen PWR has provided process steam for a nearby cardboard factory.

7. CONCLUSIONS

Clearly, nuclear power contributes significantly to the world's electricity supply and has great potential to contribute to emerging needs such as sea water desalination and hydrogen production. In the near term, nuclear power will expand, especially in Asia. Considerable development is on-going for new, advanced nuclear plant designs for all reactor lines with competitive economics and very high safety levels as common goals.

At the same time, nuclear power faces significant challenges, including: continuing to achieve a high level of safety at current plants; implementing high level waste disposal; achieving further advances in technology to assure economic competitiveness and very high levels of safety. Success in all of these areas will establish a sound basis for establishing nuclear power as a sustainable energy source.

REFERENCES

- [1] INTERNATIONAL ATOMIC ENERGY AGENCY, Energy, Electricity and Nuclear Power Estimates for the Period up to 2030, IAEA Reference Data Series No. 1, IAEA, Vienna (2004).
- [2] A. Voß, The Ability of the Various Types of Power Generation to Compete on the Liberalized Market; VGB Power Tech 4/2001.
- [3] EUROPEAN COMMISSION, “ExternE 1998, Externalities of Energy: New Results”, Directorate General XII, Science Research and Development, L-2920 Luxembourg.
- [4] INTERNATIONAL ATOMIC ENERGY AGENCY, The Safety of Nuclear Installations: Safety Fundamentals, Safety Series No. 110, IAEA, Vienna (1993).
- [5] INTERNATIONAL ATOMIC ENERGY AGENCY, Safety of Nuclear Power Plants: Design Requirements, Safety Standards Series No. NS-R-1, IAEA, Vienna (2000).
- [6] INTERNATIONAL ATOMIC ENERGY AGENCY, Safety Assessment and Verification for Nuclear Power Plants, Safety Standards Series No. NS-G-1.2, IAEA, Vienna (2001).
- [7] INTERNATIONAL ATOMIC ENERGY AGENCY, Safety Assessment and Verification for Nuclear Power Plants, Safety Standards Series No. NS-G-1.2, IAEA, Vienna (2001).
- [8] INTERNATIONAL NUCLEAR SAFETY ADVISORY GROUP, Basic Safety Principles for Nuclear Power Plants, Safety Series No. 75-INSAG-3 Rev. 1, INSAG-12, IAEA, Vienna (1999).
- [9] INTERNATIONAL NUCLEAR SAFETY ADVISORY GROUP, Basic Safety Principles for Nuclear Power Plants, Safety Series No. 75-INSAG-3, IAEA, Vienna (1988).
- [10] INTERNATIONAL NUCLEAR SAFETY ADVISORY GROUP, The Safety of Nuclear Power, Safety Series No. 75-INSAG-5, IAEA, Vienna (1992).
- [11] INTERNATIONAL NUCLEAR SAFETY ADVISORY GROUP, Defence in Depth in Nuclear Safety, INSAG-10, IAEA, Vienna (1996).
- [12] INTERNATIONAL NUCLEAR SAFETY ADVISORY GROUP, Basic Safety Principles for Nuclear Power Plants, Safety Series No. 75-INSAG-3 Rev. 1, INSAG-12, IAEA, Vienna (1999).
- [13] INTERNATIONAL ATOMIC ENERGY AGENCY, Design Measures to Facilitate Implementation of Safeguards at Future Water Cooled Nuclear Power Plants, Technical Reports Series No. 392, IAEA, Vienna (1998).
- [14] INTERNATIONAL ATOMIC ENERGY AGENCY, Methodology for the Assessment of Innovative Nuclear Reactors and Fuel Cycles: Report of Phase 1B of INPRO, IAEA-TECDOC-1434, Vienna (December 2004).
- [15] INTERNATIONAL ATOMIC ENERGY AGENCY, Improving Economics and Safety of Water Cooled Reactors: Proven Means and New Approaches, IAEA-TECDOC-1290, Vienna (2002).
- [16] ELECTRIC POWER RESEARCH INSTITUTE, Advanced Light Water Reactor Utility Requirements Document, Volume I, Rev. 1, December 1995; Vol. II and III, Rev. 8, (March 1999).
- [17] OECD/NEA, Reduction of Capital Costs of Nuclear Power Plants, OECD (2000).
- [18] INTERNATIONAL ATOMIC ENERGY AGENCY, Objectives for the Development of Advanced Nuclear Plants, IAEA-TECDOC-682, Vienna (1993).
- [19] INTERNATIONAL ATOMIC ENERGY AGENCY, Evolutionary Water Cooled Reactors: Strategic Issues, Technologies and Economic Viability, IAEA-TECDOC-1117, Vienna (1999).
- [20] INTERNATIONAL ATOMIC ENERGY AGENCY, HWRs: Status and Projected Development, Technical Reports Series, No. 407, IAEA, Vienna (2002).

- [21] INTERNATIONAL ATOMIC ENERGY AGENCY, Status of Advanced Light Water Cooled Reactor Designs: 2004, IAEA-TECDOC-1391, Vienna (2004).
- [22] INTERNATIONAL ATOMIC ENERGY AGENCY, Evolutionary Water Cooled Reactors: Strategic Issues, Technologies and Economic Viability, IAEA-TECDOC-1117, Vienna (1999).
- [23] INTERNATIONAL ATOMIC ENERGY AGENCY, Status of Liquid Metal Cooled Fast Reactor Technology, IAEA-TECDOC-1083, Vienna (1999).
- [24] INTERNATIONAL ATOMIC ENERGY AGENCY, Review of National Accelerator Driven System Programmes for Partitioning and Transmutation, IAEA-TECDOC-1365, Vienna (2003).
- [25] INTERNATIONAL ATOMIC ENERGY AGENCY, Current Status and Future Development of Modular High Temperature Gas Cooled Reactor Technology, IAEA-TECDOC-1198, Vienna (2001).
- [26] INTERNATIONAL ATOMIC ENERGY AGENCY, Terms for Describing New, Advanced Nuclear Power Plants, IAEA-TECDOC-936, Vienna (1997).
- [27] Charter of the Generation IV International Forum contained on the U.S. DOE website for the Generation-IV International Forum.
- [28] U.S. DEPARTMENT OF ENERGY, A Technology Roadmap for Generation IV Nuclear Energy Systems, issued by the U.S. DOE Nuclear Energy Research Advisory Committee and the Generation IV International Forum (GIF-002-00, December 2002).
- [29] T. KONISHI, J. KUPITZ and P.E. JUHN, "Experience and Prospects for Nuclear Heat Applications Other Than Power Generation", paper presented at GLOBAL 99 Conference.
- [30] INTERNATIONAL ATOMIC ENERGY AGENCY, Status of non-electric nuclear heat applications: Technology and safety, IAEA-TECDOC-1184, Vienna (2000).
- [31] B.J. CSIK and J. KUPITZ, "Nuclear power applications: Supplying heat for homes and industries," *IAEA Bulletin* **39**, 2, p. 21, IAEA, Vienna (1997).
- [32] INTERNATIONAL ATOMIC ENERGY AGENCY, Non-electrical Heat Applications of Nuclear Energy, IAEA TECDOC-923, Vienna (1995).
- [33] INTERNATIONAL ATOMIC ENERGY AGENCY, Nuclear Heat Applications: Design Aspects and Operating Experience, IAEA TECDOC-1056, Vienna (1998).
- [34] Overview of Generation IV Technology Roadmap; U.S.DOE Generation-IV website (18 Sept. 2002).
- [35] U.S. DEPARTMENT OF ENERGY, National Hydrogen Energy Roadmap: Production, Delivery, Storage, Conversion, Applications, Public Education and Outreach (November 2002).
- [36] EUROPEAN COMMISSION, Hydrogen Energy and Fuel Cells – A vision for your future" Summary Report of the High Level Group for Hydrogen and Fuel Cells (June 2003).
- [37] INTERNATIONAL ATOMIC ENERGY AGENCY, Design and Evaluation of Heat Utilization Systems for the High Temperature Engineering Test Reactor, IAEA-TECDOC-1236, Vienna (2001).
- [38] INTERNATIONAL ATOMIC ENERGY AGENCY, Current Status and Future Development of Modular High Temperature Gas Cooled Reactor Technology, IAEA-TECDOC-1198, Vienna (2001).
- [39] INTERNATIONAL DESALINATION ASSOCIATION, Worldwide Desalting Plants Inventory Report No. 17, Wangnick Consulting GmBh, Germany (2002).
- [40] INTERNATIONAL ATOMIC ENERGY AGENCY, Nuclear Desalination of Seawater, IAEA, Vienna (1997).
- [41] T. KONISHI, R.S. FAIBISH and M. GASPARINI, "Application of Nuclear Energy for Seawater Desalination: Design Concepts of Nuclear Desalination Plants", Proceedings of 10th International Conference on Nuclear Engineering, Apr. 14-18, 2002.
- [42] INTERNATIONAL ATOMIC ENERGY AGENCY, Design Concepts of Desalination Plants, IAEA-TECDOC-1326, Vienna (2002).
- [43] INTERNATIONAL ATOMIC ENERGY AGENCY, Options Identification Programme for Demonstration of Nuclear Desalination, IAEA-TECDOC-898, Vienna (1996).

Appendix 1

Table 1. Advanced light water reactor designs

A) Large size advanced LWR designs (700 MW(e) or larger)

Name	Type	MW(e) Gross	MW(e) Net	Design Organizations	Status
ABWR	BWR	1385	1300	General Electric, USA; Hitachi Ltd. and Toshiba Corp., Japan	Operating in Japan. Under construction in Japan and Taiwan, China Design certified by the U.S.NRC in USA
ABWR-II	BWR	1717	1638	Japanese utilities, General Electric, Hitachi Ltd. and Toshiba Corp.	In design phase – commercial introduction foreseen in latter half of 2010s
APWR	PWR	1538	-----	Mitsubishi, Japan/Westinghouse, USA	First units planned at the Japan Atomic Power Company's Tsuruga-3 and 4.
APWR ⁺	PWR	1750	-----	Mitsubishi, Japan	In design phase – target for starting construction of a first unit is the end of the 2010s.
BWR 90+	BWR	----	1575	Westinghouse Atom, Sweden	Plant design is essentially complete
EPR	PWR	1650	~1550	Framatome ANP France/Germany	Detailed design completed
ESBWR	BWR	1390	1333	General Electric, USA	The Design Certification Pre-application review by the U.S.NRC was initiated in 2002
KSNP ⁺	PWR	1050	1000	Korea Hydro and Nuclear Power Company, Republic of Korea	First units planned at KHNP's Shin-Kori-1 and 2
APR-1400	PWR	1450	1400	Korea Hydro and Nuclear Power Company etc., Republic of Korea	First units planned at KHNP's Shin-Kori-3 and 4
AP-1000	PWR	1200	1117	Westinghouse, USA	Under review by the U.S.NRC for Design Certification
EP-1000	PWR	(see values for AP-1000)		Westinghouse, USA/Genesi, Italy	Programme now merged with AP-1000 programme. Design and analyses are being conducted to document compliance with European Utility Requirements
SWR 1000	BWR	1290	1250	Framatome ANP, Germany	In the U.S., the Design Certification Pre-application review by the U.S.NRC was initiated in 2002
WWER-1000 (V-392)	PWR	1068	1000	Atomenergoproject/Gidropress, Russian Federation	Design is licensed for Novovoronezh Phase 2 (units 5 & 6) in Russia. The main design features were used for the two WWER units under construction at Kudankulam in India

Name	Type	MW(e) <u>Gross</u>	MW(e) <u>Net</u>	Design Organizations	Status
WWER-1000 (V-466)	PWR	---- ^{a)}	----	Gidropress, Russian Federation	Reactor plant design is developed for WWER-91/99, NPP92 and Balakovo-5 NPPs
WWER-1500 (V-448)	PWR	---- ^{b)}	----	Gidropress, Russian Federation	Detailed design of reactor plant is under development
CNP1000	PWR	1000	----	China National Nuclear Corporation, China	Engineering design
SCPR	SCWR	950	----	Toshiba, et al., Japan	Representative of Super-Critical Water-Cooled Reactor system selected by the Generation-IV International Forum
RMWR ^{c)}	BWR	1356	1300	JAERI, Japan	Design studies and experiments being performed. Small scale prototype possible by early 2010s; commercialization by 2020
RBWR	BWR	----	1356	Hitachi, Japan	Design studies

a) Thermal power is 3000 MW

b) Thermal power is 4250 MW

c) A small scale (300 MW(e) class) RMWR with passive safety features is also being developed by JAERI, JAPC, Hitachi and Tokyo Institute of Technology under the innovative and viable nuclear energy technology development program (IVNET) sponsored by the Ministry of Economy, Trade and Industries (METI) of Japan since FY2000

Table 1. Advanced light water reactor designs

B) Medium size advanced LWR designs (300–700 MW(e))

Name	Type	MW(e) Gross	MW(e) Net	Design Organizations	Status
AC-600	PWR	600	----	China National Nuclear Corporation, China	R&D results will be applied to development of large advanced PWR
AP-600	PWR	619	600	Westinghouse, USA	Design has been certified by the U.S. Nuclear Regulatory Commission
HSBWR	BWR	600	----	Hitachi, Japan	Conceptual design
HABWR	BWR	650	----	Hitachi, Japan	Conceptual design
WWER-640 (V-407)	PWR	640	----	Atomenergoprojekt, St. Petersburg / Hidropress, Russian Federation	Construction of pilot plant at Sosnovy Bor site is under consideration. This would be followed by units at the Kola nuclear power station and other sites.
VK-300	BWR	---	2x250 ^{d)}	RDIFE, Russian Federation	Design. Testing of key systems and components underway
IRIS	PWR	----	335	Westinghouse, USA	In Pre-application Review for Design Certification by the U.S.NRC. Westinghouse expects that IRIS will be submitted to the U.S. NRC for Design Certification in 2004/5, with Design Certification following in 2008/2009.
QS-600e/w Co-generation plant	PWR	644	610 ^{e)}	CNNC, China	Conceptual design
PAES-600 with twin VBER-300 units	PWR	---	2x295	OKBM, Russian Federation	Conceptual design
IMR	PWR	330	----	Mitsubishi, Japan	Conceptual design
NP-300	PWR	334	314	Technicatome, France	Basic design

d) A twin unit VK-300 electrical plant would produce 2×250 MW(e). The VK-300 may be used for co-generation of district heat and electricity (at a reduced electrical capacity rating).

e) This is the net electric rating for a plant that produces only electricity with no heat for desalination. A co-generation plant used for sea-water desalination and electric power production would have a lower net electric power capacity.

Table 1. Advanced light water reactor designs

C) Small size advanced LWR designs (below 300 MW(e))

Name	Type	MW(e) <u>Gross</u>	MW(e) <u>Net</u>	Design Organizations	Status
LSBWR	BWR	306	----	Toshiba, Japan	Conceptual design
CAREM	PWR	---- ^{f)}	27 ^{g)}	CNEA/INVAP, Argentina	Conceptual engineering for 27 MW(e) prototype, which is under consideration, has been completed
SMART	PWR	90	---- ^{h)}	KAERI, Republic of Korea	Design and construction project for a 1/5 th scale pilot plant is under way with completion planned by 2008
SSBWR	BWR	150	-----	Hitachi, Japan	Conceptual design
KLT-40	PWR	----	up to 70 ^{l)}	OKBM, Russian Federation	A first unit, an adaptation of a nuclear propulsion unit used for the ice-breaker fleet in Russia, is planned at Severodvinsk of the Arkhangelsk region in the Russian Federation.
PSRD-100	PWR	----	31 ^{j)}	JAERI, Japan	Conceptual design

f) CAREM concepts are in the small size range, utilizing natural circulation for plants below 150 MW(e), or forced flow for plants with larger ratings.

g) Rating of prototype.

h) The thermal power of the full sized unit is 330 MW, to be used in the co-generation mode for 90 MW(e) (gross) of electric power and for sea-water desalination to produce 40,000 m³ of fresh water per day.

i) Depending on amount of heat used in co-generating mode.

j) The concept reported here is rated 100 MWt. A 300 MWt concept is also being developed.

Appendix 2

INPRO BASIC PRINCIPLES AND USER REQUIREMENTS

Economics

Basic Principle 1. Energy and related products and services from Innovative Nuclear Energy Systems shall be affordable and available.

User Requirements:

- UR1.1 The cost of energy from innovative nuclear energy systems, taking all relevant costs and credits into account, C_N , should be competitive with that of alternative energy sources, C_A , that are available for a given application in the same time frame and geographic region.
- UR1.2 The total investment required to design, construct, and commission innovative nuclear energy systems, including interest during construction, should be such that the necessary investment funds can be raised.
- UR1.3 The risk of investment in innovative nuclear energy systems should be acceptable to investors taking into account the risk of investment in other energy projects.
- UR1.4 Innovative energy systems should be compatible with meeting the requirements of different markets.

Safety

Basic Principle 1. Installations of an Innovative Nuclear Energy System shall incorporate enhanced defence-in-depth as a part of their fundamental safety approach and ensure that the levels of protection in defence-in-depth shall be more independent from each other than in existing installations.

User Requirements:

- UR1.1 Installations of an INS should be more robust relative to existing designs regarding system and component failures as well as operation.
- UR1.2 Installations of an INS should detect and intercept deviations from normal operational states in order to prevent anticipated operational occurrences from escalating to accident conditions.
- UR1.3 The frequency of occurrence of accidents should be reduced, consistent with the overall safety objectives. If an accident occurs, engineered safety features should be able to restore an installation of an INS to a controlled state, and subsequently (where relevant) to a safe shutdown state, and ensure the confinement of radioactive material. Reliance on human intervention should be minimal, and should only be required after some grace period.
- UR1.4 The frequency of a major release of radioactivity into the containment / confinement of an INS due to internal events should be reduced. Should a release occur, the consequences should be mitigated.
- UR1.5 A major release of radioactivity from an installation of an INS should be prevented for all practical purposes, so that INS installations would not need relocation or evacuation measures outside the plant site, apart from those generic emergency measures developed for any industrial facility used for similar purpose.

- UR1.6 An assessment should be performed for an INS to demonstrate that the different levels of defence-in-depth are met and are more independent from each other than for existing systems.
- UR1.7 Safe operation of installations of an INS should be supported by an improved Human Machine Interface resulting from systematic application of human factors requirements to the design, construction, operation and decommissioning.

Basic Principle 2. Installations of an INS shall excel in safety and reliability by incorporating into their designs, when appropriate, increased emphasis on inherently safe characteristics and passive systems as a part of their fundamental safety approach.

User Requirements:

- UR2.1 INS should strive for elimination or minimization of some hazards relative to existing plants by incorporating inherently safe characteristics and/or passive systems, when appropriate.

Basic Principle 3. Installations of an INS shall ensure that the risk from radiation exposures to workers, the public and the environment during construction/commissioning, operation, and decommissioning, are comparable to the risk from other industrial facilities used for similar purposes.

User Requirements:

- UR3.1 INS installations should ensure an efficient implementation of the concept of optimization of radiation protection through the use of automation, remote maintenance and operational experience from existing designs.
- UR3.2 Dose to an individual member of the public from an individual INS installation during normal operation should reflect an efficient implementation of the concept of optimization, and for increased flexibility in siting may be reduced below levels from existing facilities.

Basic Principle 4. The development of INS shall include associated Research, Development and Demonstration work to bring the knowledge of plant characteristics and the capability of analytical methods used for design and safety assessment to at least the same confidence level as for existing plants.

User Requirements:

- UR4.1 The safety basis of INS installations should be confidently established prior to commercial deployment.
- UR4.2 Research, Development and Demonstration on the reliability of components and systems, including passive systems and inherent safety characteristics, should be performed to achieve a thorough understanding of all relevant physical and engineering phenomena required to support the safety assessment.
- UR4.3 A reduced-scale pilot plant or large-scale demonstration facility should be built for reactors and/or fuel cycle processes, which represent a major departure from existing operating experience.
- UR4.4 For the safety analysis, both deterministic and probabilistic methods should be used, where feasible, to ensure that a thorough and sufficient safety assessment is made. As the technology matures, "Best Estimate (plus Uncertainty Analysis)" approaches are useful to determine the real hazard, especially for limiting severe accidents.

Environment

Basic Principle 1. (Acceptability of Expected Adverse Environmental Effects) The expected (best estimate) adverse environmental effects of the innovative nuclear energy system shall be well within the performance envelope of current nuclear energy systems delivering similar energy products.

User Requirements:

UR1.1 The environmental stressors from each part of the INS over the complete life cycle should be controllable to levels meeting or superior to current standards.

UR1.2 The likely adverse environmental effects attributable to the INS should be as low as reasonably practicable, social and economic factors taken into account.

Basic Principle 2. (Fitness for Purpose) The INS shall be capable of contributing to the energy needs in the 21st century while making efficient use of non-renewable resources.

User Requirements:

UR2.1 (Consistency with Resource Availability) The INS should be able to contribute to the world's energy needs during the 21st century without running out of fissile/fertile material and other non-renewable materials, with account taken of reasonably expected uses of these materials external to the INS. In addition, the INS should make efficient use of non-renewable resources.

UR2.2 (Adequate Net Energy Output) The energy output of the INS should exceed the energy required to implement and operate the INS within an acceptably short period.

Waste Management

Basic Principle 1. (Waste minimization) Generation of radioactive waste in an INS shall be kept to the minimum practicable.

User Requirements:

UR1.1 (Reduction of waste at the source): The INS should be designed to minimize the generation of waste at all stages, with emphasis on waste containing long-lived toxic components that would be mobile in a repository environment.

Basic Principle 2. (Protection of human health and the environment) Radioactive waste in an INS shall be managed in such a way as to secure an acceptable level of protection for human health and the environment, regardless of the time or place at which impacts may occur.

User Requirements:

UR2.1 (Protection of Human Health) Exposure of humans to radiation and chemicals from INS waste management systems should be below currently accepted levels and protection of human health from exposure to radiation and chemically toxic substances should be optimised.

UR2.2 (Adequate Net Energy Output) The energy output of the INS should exceed the energy required to implement and operate the INS within an acceptably short period.

Basic Principle 3. (Burden on future generations) Radioactive waste in an INS shall be managed in such a way that it will not impose undue burdens on future generations.

User Requirements:

UR3.1 (End State): An achievable end state should be specified for each class of waste, which provides permanent safety without further modification. The planned energy system should be such that the waste is brought to this end state as soon as reasonably practicable. The end state should be such that any release of hazardous materials to the environment will be below that which is acceptable today.

UR3.2 (Attribution of Waste Management Costs): The costs of managing all waste in the life cycle should be included in the estimated cost of energy from the INS, in such a way as to cover the accumulated liability at any stage of the life cycle.

Basic Principle 4. (Waste optimization) Interactions and relationships among all waste generation and management steps shall be accounted for in the design of the INS, such that overall operational and long-term safety is optimized.

User Requirements:

UR4.1 (Waste Classification): The radioactive waste arising from the INS should be classified to facilitate waste management in all parts of the INS.

UR4.2 (Pre-disposal Waste Management): Intermediate steps between generation of the waste and the end state should be taken as early as reasonably practicable. The design of the steps should ensure that all-important technical issues (e.g., heat removal, criticality control, confinement of radioactive material) are addressed. The processes should not inhibit or complicate the achievement of the end state.

Proliferation resistance

Basic Principle 1. Proliferation resistance features and measures shall be implemented throughout the full life cycle for innovative nuclear energy systems to help ensure that INSs will continue to be an unattractive means to acquire fissile material for a nuclear weapons programme.

User Requirements:

UR1.1 States' commitments, obligations and policies regarding non-proliferation should be adequate.

UR1.2 The attractiveness of nuclear material in an INS for a nuclear weapons programme should be low. This includes the attractiveness of undeclared nuclear material that could credibly be produced or processed in the INS.

UR1.3 The diversion of nuclear material should be reasonably difficult and detectable. Diversion includes the use of an INS facility for the introduction, production or processing of undeclared nuclear material.

Basic Principle 2. Both intrinsic features and extrinsic measures are essential, and neither shall be considered sufficient by itself.

User Requirements:

- UR2.1 Innovative nuclear energy systems should incorporate multiple proliferation resistance features and measures.
- UR2.2 The combination of intrinsic features and extrinsic measures, compatible with other design considerations, should be optimized (in the design/engineering phase) to provide cost-efficient proliferation resistance.

Infrastructure

Basic Principle 1. Regional and international arrangements shall provide options that enable any country that so wishes to adopt INS for the supply of energy and related products without making an excessive investment in national infrastructure.

User Requirements:

- UR1.1 (Legal and institutional infrastructure): Prior to deployment of an INS installation, a national legal framework should be established covering the issues of nuclear liability, safety and radiation protection, control of operation and security, and proliferation resistance.
- UR1.2 (Economical and industrial infrastructure): The industrial and economic infrastructure of a country planning to install an INS installation should be adequate to support the project during construction and operation.
- UR1.3 (Socio-political infrastructure): The necessary human resources should be available to enable an operating organization to maintain a safety culture to achieve safe operation of the INS installation. The operating organization should have enough knowledge of the plant to be an intelligent customer and should keep a stable cadre of trained staff.
- UR1.4 (Socio-political infrastructure): The necessary human resources should be available to enable an operating organization to maintain a safety culture to achieve safe operation of the INS installation. The operating organization should have enough knowledge of the plant to be an intelligent customer and should keep a stable cadre of trained staff.

ANNEX 2

OVERVIEW ON SOME ASPECTS OF SAFETY REQUIREMENTS AND CONSIDERATIONS FOR FUTURE NUCLEAR REACTORS

N. Aksan

Paul Scherrer Institute, Switzerland

Abstract

In this paper, an overview of some aspects of the European Utility Requirements (EUR) and also for Generation IV initiative with the technology goals will be provided. The major objectives of the EUR document have been to develop requirements addressed to the LWR plant designers and vendors. It is a tool for promoting the harmonization of the most important plant features that were often too country specific. Generation IV is a new generation of nuclear energy systems that can be made available to the market by 2030 or earlier, and that offers significant advances toward challenging technological goals. These goals are defined in the broad areas of sustainability, safety and reliability, and economics. Use of EUR and Generation IV technology goals for safety aspects of future reactor designs is also discussed.

1. INTRODUCTION

The major European utilities decide to take a lead role in defining the main features of future plants and they initiated the development of a common requirements document, the European Utility Requirements (EUR). They agreed to propose a common set of safety requirements in an effort to harmonize the safety requirements between the different European countries. The EUR scope was to allow development of competitive, standardized designs that would match the conditions in Europe and be licensable in the respective countries. The utilities provided their practical experience in the preparation of the EUR document.

In the mean time with the turn of the millennium, the importance of nuclear energy as vital and strategic resource in the US and world's energy supply mix has also led to an initiative, termed Generation IV by the US Department of Energy (DOE), to develop and demonstrate new and improved reactor technologies. As a result of this initiative, Generation IV technology goals are set and defined.

The following sections provide overview both for European Utility Requirements and also for Generation IV initiative with the technology goals (sections 2 and 5, respectively). Section 3 presents in some detail some of the safety aspects of the EUR, including system and containment safety, and accident prevention. Use of the EUR and Generation IV technological goals for safety aspects of the advanced and future nuclear reactor designs are discussed in sections 4 and 6, respectively. The concluding remarks are presented in section 7.

2. A SHORT OVERVIEW ON EUROPEAN UTILITY REQUIREMENTS

The major European electricity producers have worked on a common requirement document for future LWR plants since 1992 to get specifications acceptable together by the owners, the public and the safety authorities. Thus the designers can develop standard LWR designs that could be acceptable across Europe and the utilities can open their consultations to vendors on a common basis. Public and regulatory authorities should be improved as well. The EUR promoters are a group of organizations that represent the major Western Europe electricity producers committed to keeping the nuclear option open in Europe. Started with five partners in 1992, the group now includes 10 utility organizations.

The major objectives of the EUR document have been to develop requirements addressed to the LWR plant designers and vendors. It is a tool for promoting the harmonization of the most important plant features that were often too country specific. The main items considered in this convergence process are the safety approaches, targets, criteria and assessment methods, the standardized environmental

design conditions and design methods, the performance targets, the design features of the main systems and equipment, and — at a lower level — the equipment specifications and standards. In the process of putting together the EUR document.

Significant benefits are expected in two fields:

- Better competitiveness vs. alternate electricity generation means;
- Improved public and authorities' acceptance, thus allowing an easier licensability of a design developed following the EUR.

The major objectives of the EUR organization are derived from these targets. These objectives are the foundation of the requirements developed in the EUR document: giving the producers means for controlling construction costs through standardization, signification, series ordering and consideration of maintenance at design stage. It also provides establishing a common specification valid in an area large enough so as to allow vendors to develop standard designs; establishing stable market conditions for a broader competition between suppliers; making sure that acceptable operation and fuel cycle costs can be achieved, even in an upset economic environment; prescribing ambitious — but achievable — availability and lifetime targets; harmonizing safety related requirements: common safety targets, common safety approaches and common technical solutions to safety problems; setting “good neighbour” requirements like low impact on the environment, reduction of emergency planning, consideration of decommissioning at the design stage, etc... On these bases, the main vendors are developing a number of standard designs that could be built in many countries with minimum adaptation, that show acceptable economic prospects and that actually meet the needs of the customer, including safety and licensing aspects.

EUR document is structured in 4 volumes [1], [2], and [3]. The whole document includes about forty chapters that deal with all topics a utility has to address to have a nuclear power plant developed and built.

- Volume 1 Main policies and top tier requirements: It is guidance on the safety policies and it defines the major design objectives that are implemented in the EUR document;
- Volume 2 Generic nuclear island detailed requirements: It contains all the generic requirements and preferences of the EUR utilities for the nuclear islands. It deals with matters applicable for all designs such as size, performance, safety approach and objectives, grid requirements, fuel cycle, component technology and functional requirements for systems. It also specifies the methodology to be used for safety and performance evaluation, and outline the information required by the utilities to carry out their own cost and performance assessment;
- Volume 3 Design specific nuclear island requirements: It contains a subset specific to each nuclear power plant design of interest to the participating utilities. Part 1 of this subset includes a plant description, Part 2 presents the results of the conformance assessment of the design versus the generic EUR requirements of Volume 2 and Part 3 contains the specific requirements, if any, that have been placed by EUR for the particular design. As of present five subsets have been released that are dedicated to BWR 90, EPR, EPP, ABWR and SWR 1000;
- Volume 4 Power generation plant requirements: It contains the generic detailed requirements for the Balance of Plant.

Altogether the EUR has some 150 requirements in Volume 1, 5,000 requirements in Volume 2 and 500 requirements in Volume 4. It is to be noted that the EUR promoters keep the final content of the document under close control and provide the contents of the different volumes in confidence and for limited use through the utilities, which are involved in the development of the EUR. Volumes 1, 2 and 4 have gone through number of revisions (presently, Volumes 1 and 2 have revision C, and Volume 4 has revision B [3]).

3. SOME OF THE EUROPEAN UTILITY REQUIREMENTS FOR SAFETY ASPECTS

Since the contents of the different volumes of the EUR was provided in confidence [2], only some of the requirements which are in open literature, e.g. [4] will be dealt in general terms. Additional chapters of EUR (e.g. 2.2, 2.4, 2.8, 2.9) are necessary to carry out specific application and compliance assessment. Some of these EUR safety requirements are:

- Application of “As low as reasonably achievable (ALARA)” principle;
- Forgiving design characterized by simplicity and passive safety features where appropriate;
- Safety classification based on: Design Basis Condition (DBC) and Design Extension Conditions (DEC);
- Redundancy and independence of safety systems performing DBC and some DEC functions to ensure prevention of common cause failure;
- For DBC’s reaching a safe shutdown state within 24 hours from the accident initiation and in any case within 72 hours. For DEC a safe shutdown state should be reached within one week as a goal and before 30 days in any case; The confinement of fission products and protection against external events in normal operation, DBC and DEC’s. The containment should not experience early failure under DEC conditions;
- The containment design has to exclude hydrogen detonation;
- If in-vessel coolability can not be demonstrated, then ex-vessel coolability and non-criticality features must be provided;
- The leakage rate from the containment should not exceed 0.5–1.0 V%/day for a pre-stressed concrete shell without a liner, 0.1–0.5 V%/day with a liner or for a metal shell;
- On-line monitoring of containment leak-tightness during operation;
- The containment should not remain at elevated pressure after the accident. The pressure should be reduced at least to 50% of its peak value in the worst DBC;
- Requirement for a secondary containment, for example by a partial solution of enclosing all penetrations;
- Secondary bypass leakage should not exceed 10% of the primary containment leakage;
- Next generation of NPPs will be safer by increasing design robustness, better operation and maintenance (preventive means) rather than through protective actions;
- If possible, public evacuation planning should not be necessary;
- For accident prevention- simplification of the safety systems, elimination of common mode failures by physical separation and diverse back-up systems, less sensitivity to human errors by designing components with larger inventories of water, optimized man-machine interface by digital instrumentation and control systems, use of probabilistic risk assessment to limit the residual risk due to total loss of safety grade systems.

These safety requirements for the system, EUR requirements for the containment and EUR top tier requirements including plant characteristics, operational targets, standardization, economic objectives, core damage prevention and mitigation, and release rates are itemized and given in tables 1 to 3.

4. USE OF EUROPEAN UTILITY REQUIREMENTS FOR SAFETY ASPECTS OF FUTURE NUCLEAR REACTOR DESIGNS

The EUR promoters are producing evaluations of selected LWR designs and they include the results of these applications in Vol. 3 of the EUR document. Five such subsets have been published between 1997 and 2002. Presently, five subsets dedicated to the ABWR, BWR90, EPR, EPP, and SWR1000 projects have been published and a sixth one dedicated to the Russian WWER AES92 is being drafted. The requirements are also being employed for the design of the ESBWR. Consequently, the EUR is being applied for the design of number of reactor systems.

All these EUR safety requirements have also been considered and taken into account during the evaluation of the merit and feasibility of the HPLWR concept and the results are provided in table

form for the primary system and the containment system in reference [5] and the general conclusions drawn are included in [6].

During applying the EUR to different types of reactor designs, the analyses of compliance, which is detailed process and application, have been carried to the elementary level. This process have requested and needed much resources and time both by the EUR utilities and by the interested vendors. These detailed assessment of compliance to EUR have resulted in a kind of qualification of the volumes 1 and 2 against actual reactor design projects.

It is to be noted that the EUR document is a reference user's document for LWR plants to be built in Europe beyond the turn of the century, but it is not a document for licensing the plants. The plant designs will always need to duly comply with the national licensing regulations and laws.

5. A SHORT OVERVIEW ON THE GENERATION IV INITIATIVE

The Generation IV project was initiated by the United States Department of Energy's (USDOE's) Office of Nuclear Energy, Science and Technology. Concerns over energy resource availability, climate change, air quality, and energy security suggest an important role for nuclear power in future energy supplies. While the current Generation II and III nuclear power plant designs provide an economically, technically, and publicly acceptable electricity supply in many markets, further advances in nuclear energy system design can broaden the opportunities for the use of nuclear energy. To explore these opportunities USDOE has engaged governments, industry, and the research community worldwide in a wide-ranging discussion on the development of next-generation nuclear energy systems known as "Generation IV". This has also resulted in the formation of the Generation IV International Forum (GIF), a group whose member countries are interested in jointly defining the future of nuclear energy research and development. The Generation IV project will be guided by a technology roadmap that will identify research and development pathways for the most promising technologies. The development of a technology roadmap is completed by the end of 2002.

Generation IV is a new generation of nuclear energy systems that can be made available to the market by 2030 or earlier, and that offers significant advances toward challenging goals. These goals are defined in the broad areas of sustainability, safety and reliability, and economics [7]. Sustainability goals focus on fuel utilization, waste management, and proliferation resistance. Safety and reliability goals focus on safe and reliable operation, investment protection, and essentially eliminating the need for emergency response. Economics goals focus on competitive life cycle and energy production costs and financial risk.

5.1. Generation IV technology goals

The goals have three purposes: *First*, they define and guide the development and design of Generation IV systems. *Second*, they are challenging and will stimulate the search for innovative nuclear energy systems—both fuel cycles and reactor technologies. *Third*, they serve as the basis for developing criteria to assess and compare the systems in a technology roadmap. Eight goals [7] for Generation IV nuclear energy systems are proposed in three areas: sustainability, safety and reliability, and economics. The goals are arranged to facilitate the flow of information rather than to recommend an order of importance. Each goal is stated concisely. Supporting each goal is a discussion that clarifies the intent of the specific wording and the background from which it evolved. The discussion cites illustrative examples and suggests potential approaches. It is not meant to direct or constrain creativity and innovation. Also, much of the discussion is purposely drawn from worldwide experience that is useful in guiding the development of goals.

- A set of guiding principles is used to derive the Generation IV technology goals;
- Technology goals for Generation IV systems must be challenging and stimulate innovation;
- Generation IV systems must be responsive to energy needs worldwide;
- Generation IV concepts must define complete nuclear energy systems, not simply reactor technologies.

- All candidates should be evaluated against the goals on the basis of their benefits, costs, risks, and uncertainties, with no technologies excluded at the outset;
- Since, the Generation IV technology goals are intended to stretch the envelope of current technologies, some word of caution for clarification need to be noted;
- The goals will guide the development of new nuclear energy systems. The objective of Generation IV systems is to meet as many goals as possible;
- The goals are not overly specific because the social, regulatory, economic, and technological conditions of 2030 and beyond are uncertain.

The goals must not be construed as regulatory requirements. The goals for Generation IV nuclear systems are:

Sustainability–1. Generation IV nuclear energy systems will provide sustainable energy generation that meets clean air objectives and promotes long-term availability of systems and effective fuel utilization for worldwide energy production.

Sustainability–2. Generation IV nuclear energy systems will minimize and manage their nuclear waste and notably reduce the long term stewardship burden, thereby improving protection for the public health and the environment.

Safety and Reliability –1. Generation IV nuclear energy systems operations will excel in safety and reliability.

Safety and Reliability–2. Generation IV nuclear energy systems will have a very low likelihood and degree of reactor core damage.

Safety and Reliability–3. Generation IV nuclear energy systems will eliminate the need for offsite emergency response.

Economics–1. Generation IV nuclear energy systems will have a clear life cycle cost advantage over other energy sources.

Economics–2. Generation IV nuclear energy systems will have a level of financial risk comparable to other energy projects.

Proliferation Resistance and Physical Protection-1. Generation IV nuclear energy systems will increase the assurance that they are a very unattractive and the least desirable route for diversion or theft of weapons-useable materials, and provide increased physical protection against acts of terrorism.

Detailed discussions of the goals are given in [7] and [8]. Only, the safety and reliability related aspects of the Generation IV technological goals are specifically provided in tables 4 to 5.

6. USE OF GENERATION IV TECHNOLOGY GOALS FOR SAFETY ASPECTS OF FUTURE NUCLEAR REACTOR DESIGNS

The GIF discussed the R&D necessary to support next-generation nuclear energy systems, from its beginning (January 2000). From those discussions a technology roadmap to guide the Generation IV effort began and was completed in two years with the participation of over 100 experts from the GIF countries. The effort ended in December 2002 with issue of the final Generation IV Technology Roadmap [8]. This Roadmap evaluated over 100 future systems proposed by researchers around the world.

The roadmap identified six most promising systems. Two employ a thermal neutron spectrum with coolants and temperatures that enable electricity production with high efficiency: The Supercritical Water Reactor (SCWR), and the Very High temperature Reactor (VHTR). Three employ a fast neutron spectrum to enable more effective management of nuclear materials through recycling of most components in the discharged fuel: The Gas-cooled Fast Reactor (GFR), the Lead-cooled Fast Reactor (LFR), and the Sodium-cooled Fast Reactor (SFR). The last one, the Molten Salt Reactor (MSR) employs a circulating liquid fuel mixture that offers considerable flexibility for recycling nuclear materials.

During the R&D phases of above mentioned reactor system designs, it is necessary to review the application of Generation IV Technology Goals at different stages of the development such that for the final design of the future reactor systems these goals are fulfilled and satisfied. As an example this process has already been applied to conceptual HPLWR design (it is European version of SCWR) and the results are for the preliminary design stage are reported in the literature [5] and [6]. Since many aspects of conceptual HPLWR design are not known in detail until the completion of the basic design and the related R&D efforts, the Generation IV technology goals in the safety and reliability area are applied to HPLWR design in general. This comparison indicates that the present preliminary design of the HPLWR has the potential to meet most of these goals.

7. CONCLUDING REMARKS

The European Utility Requirements (EUR), which are currently considered to be most advanced and most complete in Europe, have been applied in the design of advanced LWRs such as the EPR and the SWR 1000 (detailed designs of which are very advanced). As a general guide, the EUR can also be taken as basis for design of the future reactor systems. Additionally, the trends of future requirements, as expressed in the requirements known from the Generation IV initiative, can also be considered in order to include further advanced ideas.

It is also to be noted that, in general, the Generation IV requirements are generally compatible with the top tier EUR document [1], [2], and [3]. This is an important observation, since by using the EUR as a guide for the detailed design of the future reactor systems; it will also insure the conformity of these designs with Generation IV goals.

NOMENCLATURE

ABWR	Advanced Boiling Water Reactor
ALWR	Advanced Light Water Reactors
ADS	Automatic Depressurization System
ALARA	As Low As Reasonably Achievable
BWR	Boiling Water Reactor
DBC	Design Basis Condition
DEC	Design Extension Condition
EPP	European Passive Plant
EPR	European Pressurized Water Reactor
ESBWR	European Simplified BWR
EUR	European Utility Requirements
GIF	Generation IV International Forum
HP	High Pressure
HPLWR	High Performance Light Water Reactor
I&C	Instrumentation and Control
LOCA	Loss Of Coolant Accident
LP	Low Pressure
LPCI	Low Pressure Coolant Injection
R&D	Research and Development
SWR	Siede Wasser Reactor (Framatome ANP, Passive design BWR)

Table 1. Some EUR safety requirements

1.1	Application of "As Low As Reasonably Achievable (ALARA)" Principle
1.2	Design to be forgiving and characterized by simplicity and transparency with the use, where appropriate, of passive safety features
1.3	Safety classification based on: design basis conditions (DBC) and design extension conditions (DEC).
1.4	Safety systems performing DBC functions and certain DEC functions are required to have a degree of redundancy, diversity (e.g. passive versus active), independence, functional isolation and segregation to ensure prevention from common cause failure
1.5	Design shall ensure autonomy that for DBCs and Complex Sequences, a Safe Shutdown State can be reached, as a goal within 24 hours from accident start and anyway within 72 hours. For DEC a safe Shutdown State should be reached within 1 week as a goal and before 30 days anyway.
1.6	EUR requires in addition the consideration of other engineering criteria, such as prevention of Common Cause failures, diversity, independence and segregation
1.7	External hazards like earthquake, extreme weather, floods, aircraft crash, adjacent installations, electromagnetic interference, sabotage and internal hazards like fire, noxious substances, failure of pressure parts, disruption of rotary equipment, dropped loads and electromagnetic interference must be addressed
1.8	Requirements on the systems are set in terms of operational performance to ensure the reactivity control, heat removal and radioactivity confinement. Reactivity coefficients acceptable values, stable operation and reliability of the shutdown systems are all EUR requirements
1.9	For the core heat removal, temperature, pressure, flow and inventory control are required besides depressurization capability and pressure boundary integrity. For the latter, the use of the Leak Before Break (LBB) methodology is foreseen
1.10	In the very long term after an accident, provisions for the connection of mobile equipment are required
1.11	Important provisions required by EUR to demonstrate the in vessel corium cooling and avoidance of base mat perforation by the use of automatic depressurization system and the core spreading area that allows for solidification of the crust
1.12	Under DEC's, not a classical environmental qualification is required, rather the equipment survival has to be demonstrated

Table 2. EUR requirements for the containment system

EUR Requirements on the Containment System	
2.1	Aim mainly at strengthening the confinement of the fission products and protection against external events. The containment shall perform these functions in normal operation (including shutdown), DBC and DEC's
2.2	Under DEC's conditions early failure of the Containment system has to be ruled out by design (e.g. for PWR's adoption of a full primary circuit depressurization system). In vessel core debris interaction with water (steam explosion), high pressure ejection of molten core leading to direct containment heating; ex-vessel debris interaction with water (subcooled water, steam explosion) and reactivity accidents (including heterogeneous, boron dilution) have all to be prevented by design
2.3	The design of the Containment system has to exclude hydrogen concentrations that can lead to detonation. As a consequence the effectiveness of a hydrogen recombination system must be demonstrated. As an alternative inertization is required. The effect of other flammable gases e.g., CO must be accounted for
2.4	If in-vessel coolability cannot be demonstrated ex-vessel coolability and non-criticality features must be provided. A core catcher or corium spreading room must be provided to drive the corium into a stable situation
2.5	For the design of the Containment shell, particular attention has to be given in requiring that also severe accidents be taken into account, even if not necessarily directly determining the Containment design pressure. The Designer must demonstrate that, in case the pressure and temperature exceed the design values, the assumed leak rate is adequately supported. Also the local effects of hydrogen deflagration and sustained flames have to be considered
2.6	Credible Primary Containment leak rate values are provided by EUR: for a pre-stressed concrete shell without liner 0.5 to 1.0 V%/d; for a pre-stressed concrete with liner 0.1 to 0.5 V%/d; for a metal shell 0.1 to 0.5 V%/d
2.7	Means should be provided to ensure on-line monitoring of Containment leak-tightness during operation
2.8	Containment should not remain at elevated pressure for a long time after the accident. In 24 hours the pressure has to be reduced at least to 50% of its peak value in the worst DBC
2.9	In addition to the Primary Containment, the EUR requires also a Secondary Containment. Secondary Containment function can be demonstrated to meet also in the case that the Secondary Containment is not kept under a negative pressure, provided that the leak tightness is ensured. For the secondary containment a "partial" solution enclosing all the penetrations is acceptable.
2.10	The Secondary bypass leakage is required not to exceed 10% of the Primary Containment leakage
2.11	Through the combination of the different lines of defense the EUR Requirements aim at achieving a degree of protection of the population and the environment higher than the one achieved by previous generation of NPP and by the majority of other industrial hazards. This high degree of protection is aimed to be reached with very limited or no external mitigation. In the next generation of NPPs an improvement in safety will be reached through increasing the role of design robustness, better operation and maintenance (preventive means) rather than through protective actions.
2.12	Public evacuation planning should not be necessary. Eventually nuclear emergency situations should be managed with those protective measures normally planned in the industrialized countries for generic public protection

Table 3. EUR top tier requirements

European Utility Requirements (EUR)		
1. Plant Characteristics		
1.1	Maximum burnup 60 GWd/t for UO ₂ , 45GWd/t for MOX	
1.2	Refueling interval 12 to 24 months	
1.3	Design life 60 years	
1.4	Digital I&C technology	
1.5	Optimized role of operator	
1.6	High degree of automation for rapid, complex or frequently repeated actions	
1.7	Redundant operator workstations for main control room	
1.8	Diversified safety- classified actuators	
1.9	Extended autonomy with regard to operator actions (30 minutes) and water and power supply (24/72 hours)	
2. Operational Targets		
2.1	Plant availability greater than 87%	
2.2	Refueling and maintenance outage less than 25 days	
2.3	Refueling possible in less than 17 days	
2.4	Major 10 years outage less than 180 days	
2.5	Less than 1 unplanned scram per year	
2.6	Unplanned outage less than 5 days/year	
2.7	Specified maneuvering capabilities, e.g. 24 hours starting time from cold shutdown to full load; scheduled/unscheduled load variations- between 20% and 50% rated power: 2.5%/min; between 50% and 100% rated power: 5%/min	
2.8	Capability to withstand specified network faults	
3. Standardization		
3.1	Standard earthquake design acceleration level 0.25 g	
3.2	Seismic margin assessment for items critical for safety	
3.3	External explosion wave (100 mbar, 300 ms)	
3.4	Probabilistic approach for military aircraft crash, unless deterministic approach is required by authorities	

Table 3. (Continued)- EUR top tier requirements

4. Economic Objectives		
4.1	Competitive with coal fired or combined cycle plants (15% cheaper at base load operation, same generation costs at 4500 to 5500 full power hours/year) including capital, operation + maintenance, fuel cycle and decommissioning costs	
4.2	Overnight capital costs of 1100 ECU/KW (1995 value)	
4.2	60 months from first concrete to commercial operation	
5. Core damage prevention		
5.1	Core damage cumulative frequency less than 10^{-5} per year, considering both operation and shutdown states and including internal and external events	
6. Mitigation		
6.1	Cumulative frequency of exceeding the limiting release set for severe accident with core degradation shall be shown by a PSA to be less than 10^{-6} per reactor year	
6.2	Hydrogen control such that the H ₂ concentration in the containment will be less than 10% under dry conditions and considering the amount of H ₂ generated by 100% oxidation of the active fuel cladding	
6.3	Containment as a leak tight structure, and a secondary containment to collect any releases from the primary containment. Containment is designed for internal and external events and for severe accidents (including molten core materials)	
6.4	High pressure melt ejection during a severe accident is eliminated by RCS depressurization and the containment shall include measures to decrease pressure to 50% of peak value in 24 hours after the accident	
7. Release rates		
7.1	Release rates take into account national and international requirements and should implement the ALARA concept. Release targets for severe accidents are Limiting Release. The EUR anticipate that these targets will imply: minimal emergency protection beyond 800 m from the reactor during early releases from the containment; No delayed action (temporary transfer of people) at any time beyond about 3 km from the reactor; No long term actions involving permanent (longer than 1 year) resettlement of the public, at any distance beyond 800 m from the reactor; Restrictions on the consumption of food and crops shall be limited in terms of time scale and ground area. Target releases for 1500 MWe LWR are: Liquid discharge: GBq/a, Noble gases TBq/a, Halogen and aerosols GBq/a.	
7.2	Target for low activity solid radwaste: Total volume of the final solid radwaste produced by one plant should be less than 50 m ³ per 1000 MWe per year of normal operation	

Table 4. Safety and Reliability –1: Gen IV nuclear energy systems operations will excel in safety and reliability

Generation IV Safety and Reliability -1	
2.1.1	This goal aims at increasing operational safety by reducing: the number of events, equipment problems, human performance issues that can initiate accidents or cause them into more severe accident
2.1.2	It also aims at achieving increased nuclear energy systems reliability that will benefit their economics. Appropriate requirements and robust designs are needed to advance such operational objectives and to support the demonstration of safety that enhance public confidence
2.1.3	During the last two decades, operating nuclear power plants have improved their safety levels significantly. At the same time, design requirements have been developed to simplify their design, enhance their defense-in-depth in nuclear safety, and improve their constructability, operability, maintainability, and economics
2.1.4	Increased emphasis is being put on preventing abnormal events and on improving human performance by using advanced instrumentation and digital systems
2.1.5	Also, the demonstration of safety is being strengthened through prototype demonstration that is supported by validated analysis tools and testing, or by showing that the design relies on proven technology supported by ample analysis, testing, and research results
2.1.6	Radiation protection is being maintained over the total system lifetime by operating within the applicable standards and regulations. The concept of keeping radiation exposure as low as reasonably achievable (ALARA) is being successfully employed to lower radiation exposure
2.1.7	Gen IV nuclear energy systems must continue to promote the highest levels of safety and reliability by adopting established principles and best practices developed by the industry and regulators to enhance public confidence, and by employing future technological advances
2.1.8	The continued and judicious pursuit of excellence in safety and reliability is important to improving economics

Table 5. Safety and Reliability –2: Gen IV nuclear energy systems will have a very low likelihood and degree of reactor core damage

Generation IV Safety and Reliability -2	
2.2.1	This goal is vital to achieve investment protection for the owner/operators and to preserve the plant’s ability to return to power.
2.2.2	There has been a strong trend over the years to reduce the possibility of reactor core damage. Probabilistic Risk Assessment (PRA) identifies and helps prevent accident sequences that could result in core damage and off-site radiation releases and reduces the uncertainties associated with them. For example the US ALWR Utility Requirements Document requires the plant designer to demonstrate a core damage frequency of less than 10^{-5} per reactor year by PRA. This is a factor of about 10 lower in frequency by comparison to the previous generation of LWR energy systems.
2.2.3	Additional means, such as passive features to provide cooling of the fuel and reducing the need for uninterrupted electrical power, have been valuable factors in establishing this trend.
2.2.4	The evaluation of passive safety should be continued and passive safety features incorporated into Gen IV nuclear energy systems whenever appropriate.

Table 6. Safety and Reliability –3: Gen IV nuclear energy systems will eliminate the need for off-site emergency response

Generation IV Safety and Reliability -3	
2.3.1	The intent of this goal is, through design and application of advanced technology, to eliminate the need for off-site emergency response. Although its demonstration may eventually prove to be unachievable, this goal is intended to simulate innovation, leading to the development of designs that could meet it
2.3.2	The strategy is to identify severe accidents that lead to offsite radioactive releases, and to evaluate the effectiveness and impact on economics of design features that eliminate the need for offsite emergency response
2.3.4	Hence, for Gen IV systems a design effort focused on elimination of the need for offsite emergency response is warranted
2.3.5	This effort is in addition to actions, which will be taken to reduce the likelihood and degree of core damage required by the previous goal

REFERENCES

- [1] BERBEY, P., A fully updated version of the European Utility Requirement (EUR) document is available, *Proceedings of Ninth International Conference on Nuclear Engineering (ICONE-9), CD-ROM, Nice, France, (2001)*.
- [2] EUR, “Volume 2: Generic Requirements, Chapter 1: Safety Requirements (Parts 1 and 2)” *Revision C, CD-ROM (Proprietary), (2001)*.
- [3] BERBEY, P., European Utility Requirements: Actions in Progress and Next Steps, *2003 International Congress on Advances in Nuclear Power Plants, ICAPP'03 Proceedings CD-ROM, Cordoba, Spain, (2003)*
- [4] INTERNATIONAL ATOMIC ENERGY AGENCY, Status of Advanced Light Water Cooled Reactor Designs 1996, IAEA-TECDOC-968, Vienna (1997).
- [5] AKSAN, N., BITTERMANN, D., SQUARER, D., Potential Safety Features of the HPLWR and General Application of Some Safety Requirements,(Appendix 1: by V. H. Sanchez; Appendix 2: by O. Antoni, P. Dumaz, J. Grange) *European Commission Report, FIKI-CT-2000-00033, HPLWR-D06 (RE), (2002)*
- [6] AKSAN, N., SCHULENBERG, T., SQUARER, D., CHENG, X., STRUWE, D., SANCHEZ, V., DUMAZ, P., KYRKI-RAJAMAKI, R., BITTERMANN, D., SOUYRI, A., OKA, Y., KOSHIZUKA, S., Potential Safety Features and Safety Analysis Aspects for High Performance Light Water Reactor (HPLWR) *International Conference on Global Environment and Advanced Nuclear Power Plants, GENES4/ANP2003, Kyoto, Japan, Paper No. 1223, Sep. 15–19, 2003*.
- [7] “Technology goals for Generation IV nuclear energy systems” *Technology Goals GG01-07, Approved by Generation IV Roadmap NERAC Subcommittee (GRNS) on April 13, 2001, for presentation to NERAC on May 1, 2001*.
- [8] “A Technology Roadmap for Generation IV Nuclear Energy Systems”, *Generation IV International Forum report, GIF-002-00, December 2002*.

ANNEX 3

NATURAL CIRCULATION SYSTEMS: ADVANTAGES AND CHALLENGES

P.K. Vijayan, A.K. Nayak

Bhabha Atomic Research Centre, India

Abstract

Natural circulation loops transport heat from a source to a sink without the aid of fluid moving machineries. This lecture briefly explains the principle of working of a natural circulation system, its various advantages and applications in nuclear and other industries. The major challenges to be overcome before the wide acceptance of natural circulation as the normal mode of coolant circulation in nuclear power reactors are briefly described. Classification of NCSs and the terminologies commonly encountered in natural circulation systems are also briefly explained.

1. INTRODUCTION

In general, a heat source, a heat sink and the pipes connecting them form the essential hardware of a natural circulation system. The pipes are connected to the source and sink in such a way that it forms a continuous circulation path. When the flow path is filled with a working fluid, a natural circulation system is ready where fluid circulation can set in automatically following the activation of the heat source under the influence of a body force field like gravity. With both the source and sink conditions maintained constant, a steady circulation is expected to be achieved, which can continue indefinitely if, the integrity of the closed loop is maintained. The fluid circulation is the result of buoyancy forces, which in turn is the result of the density differences thermally induced by the transport of heat from the source to the sink. Usually, the heat sink is located above the source to promote natural circulation. Such loops in which the fluid circulation is caused by the thermally induced buoyancy force are also known as natural circulation loops, thermosyphon loops or natural convection loops.

The primary function of a natural circulation loop (NCL) is to transport heat from a source to a sink. The main advantage of the natural circulation system is that the heat transport function is achieved without the aid of any fluid moving machinery. The absence of moving/rotating parts to generate the motive force for flow makes it less prone to failures reducing the maintenance and operating costs. The motive force for the flow is generated within the loop simply because of the presence of the heat source and the heat sink. Due to this natural circulation loops find several engineering applications in conventional as well as nuclear industries. Notable among these are solar water heaters, transformer cooling, geothermal power extraction, cooling of internal combustion engines, gas turbine blades, and nuclear reactor cores. Other novel applications include low velocity corrosion studies where uninterrupted flow for long periods (of the order of years) is required and for heat dissipation by the so called 'liquid fins' [1]. Emerging new fields of application are computer cooling, and in the study of deterministic chaos.

2. BRIEF HISTORY OF NC

It is difficult to pinpoint when the commercial utilization of NCSs as heat transport devices began. First large-scale use of these systems appears to have been in the automobile industry to cool the engine block. With the advent of internal combustion engines of high compression ratio, their use in the automobile industry ceased practically in the 1940s. However, NCSs have found other applications in the chemical and power generation industries. Thermosyphon reboilers are extensively used in the chemical process industries. Many fossil-fuelled power plants of low and medium capacity use natural circulation boilers (NCB). To the author's knowledge NCBs up to 660 MW(e) rating are in operation today. An example is the Mount Piper plant in Central West Region of New South Wales in Australia. While deploying NCBs, no concession is given with regard to the thermal performance. At the same time NCBs have less maintenance and operating cost compared to assisted circulation (forced circulation) boilers. Due to this, it is not uncommon for plants with ratings greater than 900 MW(e) to go for 2 or 3 NCBs rather than assisted circulation boilers.

In the nuclear industry, NC based steam generators are extensively used in PWRs, PHWRs and VVERs. Natural circulation based steam generators of rating around 1000 MWt or more are in common use today. Natural circulation systems are also employed in nuclear industry for containment cooling, reactor building ventilation systems for cooling of HEPA filters for post accident scenarios (the source of heat is the decay of fission products retained in the filters during an accident) and for cooling of radioactive waste storage facilities.

Of particular concern to us is the application of NC systems in nuclear reactor core cooling. NC systems are extensively used in shutdown heat removal and post accident heat removal. Nuclear reactors continue to generate heat even after shutdown due to the decay of radioactive fission products and this heat has to be removed to maintain fuel temperatures within safe limits as was demonstrated by the TMI-2 accident. In view of this almost all designs of nuclear power reactors are designed to remove decay heat by natural circulation in the event of a complete loss of pumping power (CLOP). A few small sized nuclear power reactors like Humboldt Bay, Dodewaard and VK-50 demonstrated successfully the feasibility of operation with natural circulation as the normal mode of core cooling. Today natural circulation is beginning to be seriously considered for cooling of core under normal operating conditions. As a result, many innovative nuclear reactors are being designed with natural circulation as the normal mode of core cooling. Typical examples are the CAREM reactor, VK-300, AHWR and ESBWR. Even supercritical water cooled natural circulation reactors are being studied in several institutes (CANDU-X, etc.).

3. WORKING PRINCIPLE OF NATURAL CIRCULATION SYSTEMS

Before we move further, let us illustrate the working principle of natural circulation with reference to the simple uniform diameter rectangular loop with adiabatic pipes shown in Fig. 1. At the source, the fluid absorbs heat becomes lighter and rises. At the sink the fluid rejects heat becomes heavier and sinks thus establishing a circulation. If the source and sink conditions are maintained constant, a steady state is expected to be achieved when the heat absorbed at the source is equal to the heat rejected at the sink. Under steady conditions we assign a density of ρ_h to the vertical leg with upward flow and ρ_c to the other vertical leg with downward flow. Now we can obtain the hydrostatic pressure, p_a and p_b at the stations 'a' and 'b' located at the extremes of the bottom horizontal leg as:

$$p_a = \rho_c gH \quad (1)$$

$$p_b = \rho_h gH \quad (2)$$

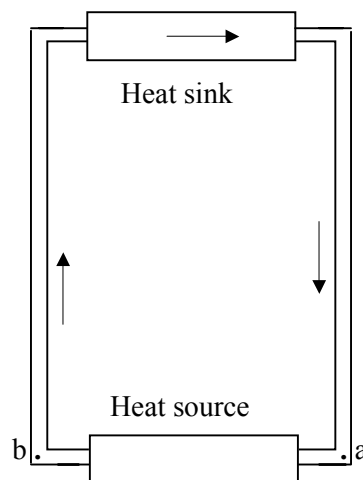


FIG. 1. A simple natural circulation system.

Where H is the loop height and g is the acceleration due to gravity. Clearly, since $\rho_c > \rho_h$, $p_a > p_b$ leading to a pressure difference between stations 'a' and 'b' which is the cause of the flow. At steady state, the driving pressure differential is balanced by the retarding frictional and accelerational forces, thus providing a basis for the estimation of the induced flow. What is more important to us is that this induced flow is unidirectional and while it passes through the source it absorbs heat and rejects it while flowing through the sink thus enabling transfer of heat from the source to the sink. In this function, it is indistinguishable from forced flow. It is easy to note that the induced pressure differential and hence the flow is enhanced by the loop height and the density difference between the two vertical legs.

4. ADVANTAGES OF NATURAL CIRCULATION

4.1. Elimination of pumps

The most apparent economic advantage of NCSs is the elimination of the circulating pumps. Elimination of the primary circulating pumps not only reduces capital, operating and maintenance costs but also eliminates all safety issues associated with the failure of the circulating pumps.

4.2. Better flow distribution

Commercial power plants, be it nuclear or fossil-fuelled, use a large number of parallel heated channels connected between an inlet and outlet header/plenum. All analyses are carried out assuming the pressure to be uniform in the inlet headers so that the pressure drop across the parallel channels is constant. However, use of pumps cause maldistribution of pressure in the headers leading to maldistribution of flow in the parallel channels. Operating experience with fossil-fuelled NCBs suggest that the problem is eliminated or an order of magnitude less.

4.3. Flow characteristics

In a NCS, the flow increases with power, whereas in a forced circulation two-phase system the flow decreases with increase in power. This has specific advantages in steam generating power plants. In fossil-fuelled power plants, this is cited as one important aspect for the preference of NCBs over the assisted (same as forced) circulation boilers. In forced circulation BWRs, the necessity of variable speed drives essentially arises from this fact. Although, the boiler tubes are designed for a specified power, the steam production rate of individual boiler tubes are far from uniform due to the maldistribution of power. In fossil fuelled power plants, the flow characteristic of NCBs also enables them to operate with nonuniform power distribution without causing CHF. Similar conditions in an assisted circulation boiler can cause CHF.

4.4. Safety aspects

Since NC is based on a natural physical law, it is not expected to fail like the fluid moving machineries such as pumps. This aspect of NC has enabled its application in many safety systems. In all current designs of nuclear power reactors, NC is a backup for the removal of decay heat in the event of a pumping power failure. Apart from this, the driving force for natural circulation systems is somewhat low compared to forced circulation systems. As a result, the power ratings of natural circulation systems are comparatively low. Consequently, systems of same power rating are larger in volume leading to a lower power density. Large volumes and low power densities make all transients sluggish.

4.5. Simplicity

Because of the necessity to minimize pressure losses to enhance flow rates, designers of NCSs tend to eliminate all unnecessary pipe bends, elbows, etc. The end result is a system with a simple piping layout which can be factory fabricated.

5. CHALLENGES OF NATURAL CIRCULATION

The first natural circulation based power reactor (63 MW(e)) Humboldt Bay 3 in California, USA, came into operation in 1963. The second NC based reactor is Dodewaard reactor in Netherlands which came into operation in 1969 and operated successfully upto 1997. The 50 MW(e) VK-50 reactor is operational in the Russian Federation since the past 31 years. All these reactors are of the same vintage. Subsequently, no new power reactor was operated with NC as the normal mode of coolant circulation although many concepts like the SBWR have been under active development for several years. In the mean time fossil fuelled power plants have demonstrated the feasibility of operating NCBs up to 660 MW(e), several units of which are in operation since 1980. In the recent past several innovative designs are being vigorously pursued the world over. In the backdrop of these activities it is relevant to examine the challenges being faced in the development of NCRs.

Large scale deployment of NC based reactors and safety systems depend on the successful resolution of the challenges specific to natural circulation which are described below.

5.1. Low driving force

One of the drawbacks of natural circulation systems is that their driving force is low. The most straightforward way to increase the driving force is to increase the loop height which may be uneconomic. In addition, use of tall risers can make natural circulation systems slender in structure and may raise seismic concerns. Due to these reasons, the incremental height of natural circulation systems compared to the corresponding forced circulation systems is often limited to a few metres (usually less than 10 m).

5.2. Low system pressure losses

With low driving force, the only way to obtain reasonably large flow rates is to design for low pressure losses. There are several measures to achieve low system pressure losses:

- a) Use of large diameter components/pipes
- b) Simplified system and
- c) Elimination of components

5.2.1. *Use of large diameter components/pipes*

The most straightforward way to reduce pressure losses is to use large diameter components. However, this also results in increased cost and enhanced system volume both of which have economic and safety implications. The large inventory of the passive systems is the direct result of the enhanced system volume. The advantage of large inventory is that it makes all transients sluggish. In case of accidents like LOCA, the large system inventory has a mixed effect. On the one hand it delays core uncover, but on the other hand it makes available large high enthalpy fluid for discharge into the containment resulting in increased peak containment pressure. Large inventory may also be an unwelcome outcome in case of costly coolants like heavy water.

5.2.2. *Simplified system*

Generally refers to the simplified piping and equipment layout of the NC system. Minimization of U-bends, elbows, loop seals etc. not only results in simplified system but also results in low pressure losses and prevents phase separation promoting natural circulation flow. However, from the viewpoint of piping flexibility the very same features are desirable necessitating a compromise between flexibility and simplicity.

5.2.3. Elimination of components

An example in this case is the possible elimination of mechanical separators. Elimination of mechanical separators can result in increased carryover and carryunder, both of which are undesirable. While the former directly affects the natural circulation flow, the latter is detrimental to the turbine operation. The alternative to mechanical separators is natural gravity separation. While gravity separation is adopted in several plants with horizontal drums its feasibility is not demonstrated well for vertical reactor vessels. Several studies carried out earlier found it feasible to eliminate the mechanical separators even for this case.

5.3. Low mass flux

Low driving force and the consequent use of large diameter components result in low mass flux in NC systems compared to the forced circulation systems. With low mass flux, the allowable maximum channel power is lower leading to a larger core volume compared to a forced circulation system of the same rating. For example, the Russian VK-300, a 250 MW(e) dual purpose NC based reactor uses the same reactor vessel as that of the 1000 MW(e) VVER [2] making it almost 3.3 times bigger in volume. In comparison, the 300 MW(e) Indian AHWR uses almost the same size of calandria vessel as that of the 600 MW(e) PHWR making it almost twice as big.

Large core volumes can result in zonal control problems and stability. Fortunately, these problems are rather well understood now. Size optimisation results in enhanced exit qualities.

5.4. Instability effects

While instability is common to both forced and natural circulation systems, the latter is inherently less stable than forced circulation systems. This is attributable to the nonlinear nature of the natural circulation phenomenon, where any change in the driving force affects the flow which in turn affects the driving force that may lead to an oscillatory behaviour. In addition, due to the low driving force, the stabilizing effect of inlet orificing is limited in NCRs. In forced circulation BWRs, a suitable pump can be selected to achieve stability with inlet orificing without affecting the flow rate. On the other hand, in NCRs, increasing the loss coefficient of the inlet orifice significantly reduces the flow rate and the pressure drop across the orifice reducing its effectiveness.

5.5. Low pressure low flow regime

In NCRs, the flow rate is a strong function of power and system pressure. Also, in NCRs the flow is stagnant when the reactor power is zero during the initial start up. Further, stage-wise power and pressure raising is relevant to the start up scenarios causing the reactor to operate anywhere between stagnant (zero power condition) and nominal flow (full power conditions). In other words, the operating conditions of NCRs can fall in the LPLF regime, where validated thermalhydraulic relationships are not readily available. Specific reactor designs might need an assessment of the applicability of the thermalhydraulic relationships in this regime.

5.6. Specification of a start-up and operating procedure

It is well known that most boiling systems exhibit instabilities at low pressure and low qualities. In many instances instability is observed right from boiling inception which may occur in the tall riser than in the core. Natural circulation reactors are to be started up from stagnant low pressure and low temperature condition. During the pressure and power raising process, passing through an unstable zone shall be avoided as instability can cause premature CHF occurrence. Under the circumstances, it is essential to specify a start-up procedure that avoids the instability. Selection of the pressure at which to initiate boiling and appropriate procedures for pressure and power raising is central to the specification of start-up procedure. In addition, it may become essential to control the inlet subcooling as a function of power. For a cold start-up (first start-up) an external source for pressurization may be required. Due to these reasons the selection of a start-up procedure for a NCR is not always an easy task.

In addition, the procedure for power step back from the normal full power condition also needs to be controlled to avoid landing in the unstable zone. In other words specification of the complete operating procedure is a challenging task for NCBWRs.

5.7. Low CHF

The basis for thermal margin could be the CHF, which depends on the geometric and operating parameters. The main operating parameters of concern are the pressure, flow, exit quality, inlet subcooling and heat flux distribution. There is practically no difference in the operating pressure of NCBWRs and FCBWRs. Since flow in natural circulation reactors is lower, they tend to use the maximum allowable exit quality to minimize their size. In the process, their CHF value tends to be significantly lower than that of FCBWRs. This calls for several measures to increase the CHF.

An acceptable design must satisfy both the thermal and stability margin requirements. For stability there is a lower (Type I instability threshold) and an upper threshold (Type II threshold) between which the system is stable. The lower threshold of instability is well below the CHF value and the upper threshold is much above the CHF value. The lower threshold is generally avoided by a validated start-up procedure and operational procedure. As a result even in the NCRs, the maximum power is limited by the CHF. Significant power uprating in these designs may require special fuel assembly design features to enhance CHF so as to obtain an optimum sized reactor. The problem is compounded by the fact that some of the parameters like inlet subcooling and strongly bottom peaked axial power profile have opposing effect on CHF and stability.

6. CLASSIFICATION OF NATURAL CIRCULATION SYSTEMS

Natural circulation systems can be classified depending on:

- 1) State of the working fluid,
- 2) Interaction with the surroundings
- 3) Shape of the loop,
- 4) Body force field
- 5) System inventory
- 6) Number of heated/cooled channels

6.1. State of the working fluid

Depending on the thermodynamic state of the working fluid, NCSs are classified as:

- a) Single-phase NCSs
- b) Two-phase NCSs and
- c) Supercritical NCSs

6.1.1. Single-phase NCS

In a single-phase NCS, the circulating fluid in the entire loop continues to remain in only one state. Under this category, liquid or gas filled NCSs are possible. However, liquid filled NCSs are more commonly used for nuclear reactor core cooling. For example, almost all PWRs, PHWRs, VVERs and FBRs are designed to remove the core decay heat by the single-phase NC in the event of Complete Loss of Pumping power (CLOP). Most district heating reactors use single-phase NC as the normal mode of coolant circulation. Typical examples are AST-500 [3] and NHR-200 [4]. An innovative power reactor design (27 MW(e) CAREM-X reactor being designed in Argentina) based on single-phase natural circulation as the normal mode of coolant circulation has been proposed.

Single-phase gas filled NC systems are used in the cooling of canisters containing radioactive waste in solid storage surveillance facilities. Following a LOCA, it is possible that the HEPA filters of the NPP ventilation system retain the suspended radioactive fission products discharged into the containment.

The ventilation systems of NPPs are so designed that NC can remove the heat generated by these fission products in the event of failure of the ventilation fans (Fig. 2).

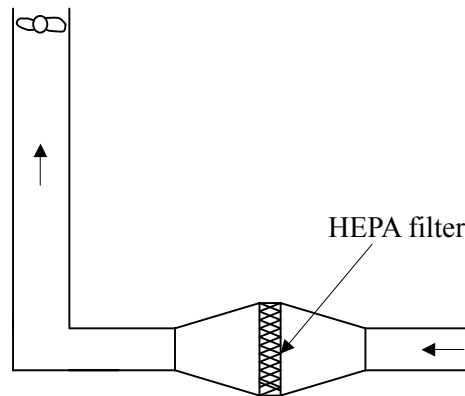


FIG. 2. Schematic of the ventilation system.

6.1.2. Two-phase NCS

If a part of the NC system experience two-phase flow conditions, then we refer to it as a two-phase NCS. Two-phase NCSs either with only boiling or with both boiling and condensation are relevant to NPPs. However, gas-liquid NCS (also known as adiabatic NCS) is also possible to be constructed and are used sometimes for experimentation [5]. In certain circumstances, adiabatic NCSs are preferable for phenomenological investigations due to their low operational cost.

Generally, two-phase NC occurs in a BWR following the failure of circulating pumps. In PWRs, PHWRs or VVERs it is possible to be observed following the partial loss of coolant inventory in case of a small break LOCA with pump failure. With two-phase systems, it is possible to obtain larger density differences and hence larger flow rates than in single-phase systems. Due to this, many innovative BWRs are being studied with two-phase NC as the normal mode of cooling. Typical examples are AHWR, ESBWR, VK-300, TOSBWR and HSBWR.

6.1.3. Supercritical NC system

These systems operate at or above the thermodynamic critical state. The main interest in supercritical systems stems from the fact that near the critical point there is a large change in the volumetric coefficient of thermal expansion, and hence they are capable of generating driving forces comparable to that of two-phase NCSs. Supercritical systems are more efficient than conventional LWRs. Besides since phase change is avoided separators and dryers can be eliminated along with the problems associated with the occurrence critical heat flux. Another advantage is that the heat transfer characteristics of supercritical water systems are excellent. Because of these, supercritical natural circulation systems are beginning to receive attention from nuclear as well as fossil-fuelled power plant designers. The first fossil fuelled power plant based on NC of supercritical water is operational in UK since 1999 [6]. Examples of reactor systems based on supercritical NC are B-500 SKDI [7] and CANDU-X [8].

6.2. Interaction with the surroundings

According to this NC loops can be classified as

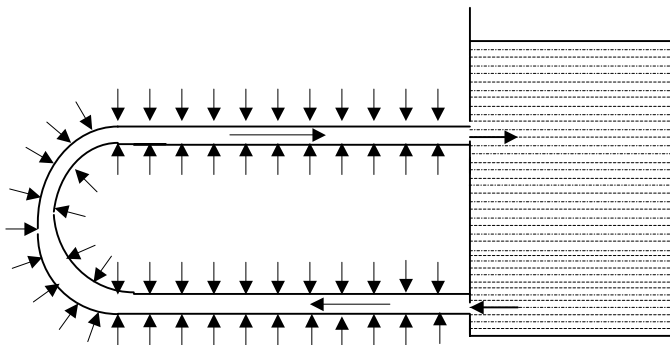
- a) Closed loop and
- b) Open loop systems

6.2.1. Closed loop NCS

Close loop NC systems exchange only energy with the surroundings. Fig. 1 is an example of a closed loop NC system. Most nuclear reactor loops relevant to PWRs, PHWRs and VVERs belong to this category.

6.2.2. Open loop NCS

Open loop NC systems exchange both mass and energy with the surroundings. Open-loop NCSs are used in ship based reactors (Fig.3), swimming pool type research reactors, both pressure tube type (Fig.4) and pressure vessel type BWRs, NCBs, NC based SGs in PWRs, thermosyphon reboilers, waste storage systems, geothermal heat extraction, etc. Most NCSs used in the ventilation (Fig.2) and waste storage surveillance facilities also belong to this category.



6.3. Shape of the loop

Based on the loop shape, NCSs are classified as toroidal, rectangular, square, figure-of-eight, etc. Such loops are studied mainly for improving our understanding of the natural circulation phenomenon. Toroidal loop (Fig. 5) has been extensively studied because of its simplicity. To the author's knowledge, this is the only loop where 1-D, 2-D and 3-D numerical simulations are reported in the literature. Rectangular loops have also been extensively studied for understanding of the steady state, transient and stability characteristics of NC. Stability characteristics of simple rectangular loops have been studied extensively theoretically [9], [10], [11], as well as experimentally [12], [13]. The loops relevant to PWRs and VVERs can be considered to be rectangular for the sake of analysis with different orientation of the heat sink. Figure-of-eight loop is relevant to pressure tube type heavy water reactors (PHWRs).

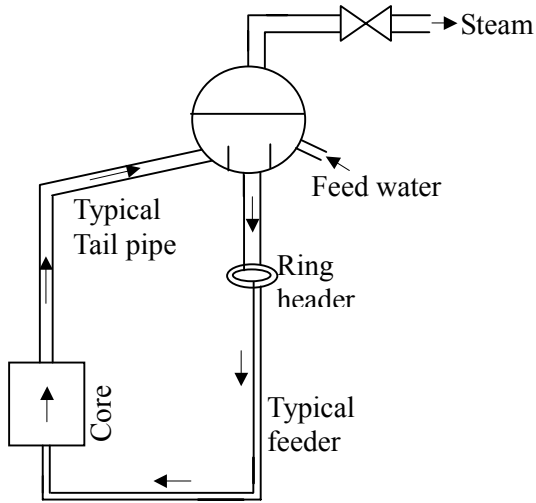


FIG. 4. A typical open-loop NCS relevant to a pressure tube type BWR.

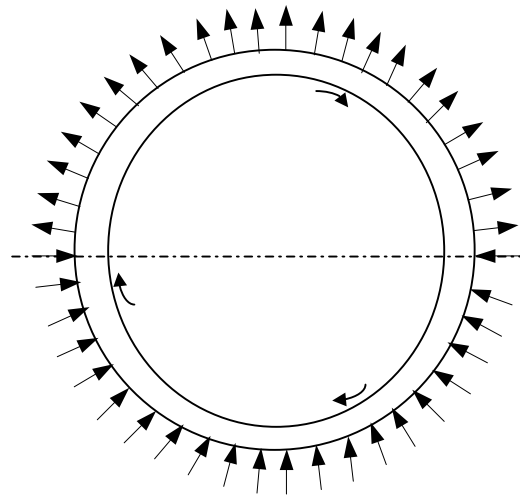


FIG. 5. Toroidal loop with bottom half heated and top half cooled.

6.4. Body force field

Natural circulation systems function only under the influence of a body force field. Two types of body force fields are relevant to NC systems. They are gravity and centrifugal force fields. Most loops in common use work in the gravity force field and are static. However, centrifugal force field can be advantageously employed in cooling of rotating machineries [14]. Such loops are referred to as rotating NCS (Fig. 6) to differentiate it from NCSs operating under the influence of gravity force field, which are stationary. In this case it is possible to have acceleration values several times as big as the gravity acceleration depending on the rotational speed.

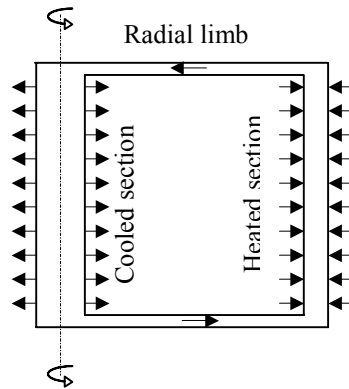


FIG. 6. A rotating closed loop NCS.

6.5. System inventory

Depending on the system inventory, one can obtain single-phase NC, two-phase NC or reflux condensation. Single-phase NC is the mode of circulation without inventory loss in nuclear reactors following pumping power failure. Two-phase NC is expected at inventory levels lower than that of single-phase NC. With significant reduction in inventory, the loop circulation breaks down and reflux condensation sets in. In this case, counter current flow in the U-tubes of the steam generator with the steam going up in the centre and condensate falling along tube wall is observed. Even this mode is capable of removing the decay heat although there is no loop circulation.

6.6. Number of heated or cooled channels

Depending on the number of heated or cooled channels, NCSs can be categorized as single channel or multi-channel systems. Multi-channel systems are often referred to as parallel channel systems or loops. Most industrial systems belong to the latter category. Typical examples are power reactor systems like BWR and PWR, NCBs, NC based SGs, etc. However, the average channel behaviour is often studied with single channel. Parallel channel systems can exhibit considerably different steady state and stability behaviour and are often referred to as parallel channel effects.

7. TERMINOLOGIES USED IN NCS

A brief understanding of the common terminologies used in natural circulation will be helpful to the understanding of natural circulation. Typical examples are: hot leg, cold leg, riser, downcomer, recirculation ratio, inlet subcooling, inlet orificing, decay ratio, etc. Some of these terms are described in Appendix-1.

8. CLOSURE

This lecture briefly explains the working principle of natural circulation systems which are mainly employed as heat transport devices in nuclear and other industries. The advantages and the challenges to be overcome for the adoption of natural circulation as the normal mode of coolant circulation in nuclear power reactors are briefly described. Commonly used terminologies in natural circulation systems and the various bases used to classify NCSs are also briefly described.

LIST OF ACRONYMS USED

AHWR	- advanced heavy water reactor
BWR	- boiling water reactor
CANDU	- Canadian deuterium reactor
CAREM	- NC based PWR being developed in Argentina
CLOP	- complete loss of pumping power
CHF	- critical heat flux
ESBWR	- European simplified boiling water reactor
FBR	- fast breeder reactor
FCBWR	- forced circulation boiling water reactor
HEPA	- high efficiency particulate filter
HSBWR	- Hitachi simplified boiling water reactor
LPLF	- low pressure low flow
LOCA	- loss of coolant accident
LWR	- light water reactor
MW(e)	- megawatt electric
MWt	- megawatt thermal
NC	- natural circulation
NCB	- natural circulation boiler
NCBWR	- natural circulation boiling water reactor
NCL	- natural circulation loop

NCR	- natural circulation reactor
NCS	- natural circulation system
NPP	- nuclear power plant
PHWR	- pressurized heavy water reactor
PWR	- pressurized water reactor
TMI	- Three Mile Island
TOSBWR	- Toshiba simplified boiling water reactor
SBWR	- simplified boiling water reactor
SG	- steam generator

REFERENCES

- [1] MADEJSKI, J., and MIKIELEWICZ, J., Liquid fin - a new device for heat transfer equipment, *Int. J. Heat Mass Transfer* 14 pp.354–363 (1971).
- [2] KUZNETSOV, YU.N., ROMENKOV, A.A., ALEKSEEV, A.I., LISITSA, F.D., TOKAREV, YU.I. and YARMOLENKO, O.A., NPP with VK-300 boiling water reactor for power and district heating grids, *Proceedings of International Seminar on Small and Medium Sized Reactors: Status and Prospects organised by IAEA, IAEA-SR-218/32, Cairo, Egypt, 27–31 May 2001* (2001).
- [3] SAMOILOV, O.B., KURACHENKOV A.V., Nuclear District heating plants AST-500: Present status and prospects for future in Russia, *Nuclear Engineering and Design* 173, pp.109–117 (1997).
- [4] DAZONG, W., ZUYING, G., and WENXIANG, Z., Technical design features and safety analysis of the 200 MWt Nuclear Heating Reactor, *Nuclear Engineering Design* 143, pp.1–7 (1993).
- [5] HIBIKI, T. and ISHII, M., Effect of inlet geometry on hot-leg U-bend two-phase natural circulation in a loop with a large diameter pipe, *Nuclear Engineering and Design*, 203, pp. 209–228 (2001).
- [6] FRANKE, J., The Benson boiler turns 75, *Siemens Power Journal online*, May 2002, pp.1–3 (2002).
- [7] SILIN, V. A., VOZNESENSKY, V. A. and AFROV, A.M., The light water integral reactor with natural circulation of the coolant at supercritical pressure B-500 SKDI, *Nuclear Engineering and Design*, 144, pp.327–336 (1993).
- [8] DIMMICK, G.R., CHATOORGOON, V., KHARTABIL, H.F., and DUFFEY, R.B., *Nuclear Engineering and Design*, 215 pp. 27–38 (2002).
- [9] KELLER, J.B., Periodic oscillations in a model of thermal convection, *J. Fluid Mech.* **26**, pp.599–606 (1966).
- [10] WELANDER, P., On the oscillatory instability of a differentially heated loop, *J. Fluid Mech.* 29, pp.17–30 (1967).
- [11] CHEN, K., On the Oscillatory Instability of Closed-Loop Thermosyphons, *Trans. ASME, J. Heat Transfer* 107, pp.826–832 (1985).
- [12] VIJAYAN, P.K, NAYAK, A.K, PILKHWAL, D.S, SAHA, D. and VENKAT RAJ, V, Effect of loop diameter on the stability of single-phase natural circulation in rectangular loops, *Proc. 5th Int. Topical Meet. on Reactor Thermalhydraulics, NURETH-5, Salt Lake City, UT, Vol.1*, pp.261–267 (1992).
- [13] MISALE, M., FROGHERI, M., and RUFFINO, P., Steady-state and stability behaviour of a single-phase natural circulation loop, *Heat Transfer 1998, Proceedings of 11th IHTC, vol. 3 August 23–28, Kyongju, Korea* (1998).
- [14] DAVIES, T.H. and MORRIS, W.D., Heat Transfer characteristics of a closed loop rotating thermosyphon, *Proceedings of the 3rd International Heat Transfer Conference, Chicago, USA, August 7-12, Vol. 2*, pp.172–181 (1966).

Appendix 1

SOME COMMON TERMINOLOGIES USED IN NCSS

Hot leg: Generally used for single phase NCSs and it refers to the pipe from the heat source to the heat sink in the direction of flow, so that it always contains the hot fluid.

Cold leg: Commonly used in single-phase NC systems to refer to the pipe carrying cold fluid from the heat sink to the heat source.

Riser: This is generally used in two-phase NC systems to refer to the vertical pipe carrying two-phase flow to the separator or the heat sink. Increasing riser height promotes natural circulation flow. An equivalent term used in vessel type BWRs is the chimney.

Downcomer: This is used to represent the pipe carrying the downward flow from the separator or the heat sink to the heat source in case of a two-phase NCS. Usually single-phase flow prevails in the downcomer.

Recirculation ratio: Some times referred to as only circulation ratio and is relevant to an open two-phase natural circulation system such as those relevant to NC based BWRs or steam generators or boilers. This is defined as

$$R = \frac{\text{Loop mass flowrate}}{\text{Mass flowrate of feed}}$$

Inlet subcooling: Normally used in the analysis of two-phase systems and is referred to the difference in the saturation temperature and the core inlet temperature. Inlet subcooling is sometimes expressed in terms of enthalpy. In this case, it is the difference between saturation enthalpy and the enthalpy at the core inlet.

Inlet orificing: In two-phase loops, the stability of the system can be enhanced if the single-phase pressure drop is a dominant part of the total system pressure drop. A simple way to achieve this is by incorporating an orifice of the required diameter in the inlet pipe where the flow is in single-phase condition.

Outlet orificing/Exit orificing: This is used sometimes to denote the pressure loss coefficient in the two-phase region, which has different influence on two-phase stability compared to inlet orificing.

Decay ratio, DR: This is defined as the amplitude of the succeeding oscillation to the amplitude of the preceding oscillation, the two oscillations being consecutive. In this way, $DR < 1$ indicates a stable system, $DR = 1$ refers to a neutrally stable system and $DR > 1$ refers to an unstable system.

ANNEX 4

APPLICATION OF NATURAL CIRCULATION SYSTEMS: ADVANTAGES AND CHALLENGES II

N. Aksan

Paul Scherrer Institute, Switzerland

Abstract

Applications of natural circulation systems are provided for advanced light water reactor designs. Design features proposed for the passive advanced light water reactors include the use of passive, gravity-fed water supplies for emergency core cooling and natural circulation decay heat removal from the primary system and the containment, and natural circulation cooling within the core for all conditions. Examples are given from different types of advanced reactor designs for the use of passive safety systems under the operational, transient, and accident conditions. Challenges encountered in the design of passive safety systems for HPLWR are discussed in short, as an example case.

1. INTRODUCTION

Advanced Light Water Reactor (ALWR) designs have been under development for the last fifteen years worldwide. Different aspects of these new plant designs are described fairly extensively and systematically in References [1] to [6]. Further information can be found in specialized international conferences [7] to [12].

New designs –designs that have not yet been built or operated- are generally, called advanced designs [3]. In general, an advanced plant design is a design of current interest for which improvement over its predecessors and/or existing designs is expected. Advanced designs can be categorized into two groups:

- Evolutionary design: An evolutionary design is an advanced design that achieves improvements over existing designs through small to moderate modifications, with a strong emphasis on maintaining proven design features to minimize technological risks. An evolutionary design requires at most engineering or confirmatory testing before commercial deployment. As examples for advanced LWRs are ABWR, EPR, etc. In this category, there are also designs, which are developed with a great emphasis on utilization of passive safety systems and inherent safety features. Typical examples are Advanced Passive PWR AP 600, AP1000, and the simplified BWR (SBWR), ESBWR, SWR 1000, etc.
- Innovative design: An innovative design is an advanced design, which incorporates radical conceptual changes in design approaches or system configuration with existing practice. This design category will most likely require a prototype or demonstration plant.

All ALWRs incorporate significant design simplifications, increased design margins, and various technical and operational procedure improvements, including better fuel performance and higher burnup, a better man-machine interface using computers and improved information displays, greater plant standardization, improved constructability and maintainability, and better operator qualification and simulator training.

The expanded considerations of severe accidents, increased safety requirements and the aim at introducing effective and transparent safety functions lead to growing consideration of passive safety systems for ALWRs. In the evolutionary designs, attempts have been made to reduce the complexity of the emergency core cooling and of the long-term decay heat removal systems by increased use of passive systems. Following the IAEA definitions [3], a passive component is a component which does not need any external input to operate and a passive system is either a system which is composed entirely of passive components or a system which uses active ones in a very limited way to initiate subsequent passive operation. Passive safety systems are characterized by their full reliance upon

natural forces, such as natural circulation, gravity, to accomplish their designated safety functions. They are also making safety functions less dependent on active systems and components, like pumps, diesel generators, electromotor-driven valves, etc. ALWR design incorporates passive safety features to perform safety-related functions.

Design features proposed for the passive ALWRs include the use of passive, gravity-fed water supplies for emergency core cooling and natural circulation decay heat removal, e.g. for AP600, AP1000, SBWR and ESBWR, and natural circulation cooling within the core for all conditions, e.g. SBWR and ESBWR. Both types of plants also employ automatic depressurization systems (ADSs), the operation of which are essential during a range of accidents to allow adequate emergency core coolant injection from the lower pressure passive safety systems. The low flow regimes associated with these designs will involve natural circulation flow paths not typical of current LWRs. These passive ALWR designs emphasize enhanced safety by means of improved safety system reliability and performance. These objectives are achieved by means of improved safety system simplification and reliance on immutable natural forces for system operation. Simulating the performance of these safety systems is central to analytical safety evaluation of advanced passive reactor designs.

Specially, the passive safety principles of the next generation ALWR designs include:

- Low volumetric heat generation rates;
- Reliance solely on natural forces, such as gravity and gas pressurization, for safety system operation;
- Dependence on natural phenomena, such as natural convection and condensation, for safety system performance.

The engineered safety features, which incorporate these passive safety principles, achieve increased reliability by means of system redundancy, minimization of system components, non-reliance on external power sources, and integral long-term decay heat removal and containment cooling systems. In the design of the current generation of operating reactors, redundancy and independence have been designed in the protection systems so that no single failure results in loss of the protection function. Since the new passive ALWR designs incorporate significant changes from the familiar current LWR designs and place higher reliance on individual systems, a thorough understanding of these designs is needed with respect to system interactions. These interactions may occur between the passive safety systems, e.g. the core make-up tanks and accumulators in the AP1000, and the ADS system and isolation condensers in the ESBWR. In addition, there is a close coupling in both plant designs between the reactor coolant system and the containment during an accident.

It can also be noted that in order fully profit from the safety benefits due to the introduction of the passive safety systems, the behavior of plants in which engineering safety features involving active components have been replaced with completely passive devices must be carefully studied to ensure the adequacy of the new design concepts for a wide spectrum of accident conditions. In fact, choice of passivity is an advantage in reducing the probability of the wrong operator interventions, especially in the short-term period after an accident, although passive systems require more sophisticated modelling techniques to ascertain that the natural driving forces that come into play can adequately accomplish the intended safety functions. Hence there is also the need for an in-depth study of the basic phenomena [1] concerning the design of ALWRs, which make use of passive safety features.

2. HEAT REMOVAL FROM INTACT PRIMARY SYSTEM

In the cases when the primary system is intact but the normal heat sink (e.g., secondary side of steam generator or turbine) has been lost, the decay heat is not transferred to the containment with the blowdown flow and must still be removed from either the reactor pressure vessel (for BWRs) or steam generator (for PWR). The solutions are proposed using the passive connection of the primary system to a heat exchanger (or condenser). Heat exchangers connected to the primary system and immersed in a water pool inside the containment are used. As one of the examples, the AP600/AP1000 designs ([6]

and [7]) where passive residual heat removal (PRHR) heat exchanger is immersed in the in-containment refueling water storage tank (IRWST) as shown in Figures 1 and 2.

The PRHR provides primary coolant heat removal via a natural circulation loop. Hot water rises through the PRHR inlet line attached to one of the hot legs. The hot water enters the tube sheet in the top header of the PRHR heat exchanger at full system pressure and temperature. The IRWST is filled with cold borated water and is open to containment. Heat removal from the PRHR heat exchanger occurs by boiling on the outside surface of the tubes. The cold primary coolant returns to the primary loop via the PRHR outlet line that is connected to the steam generator lower head.

Another example is the SWR-1000 ([5] and [6]), which has emergency condensers permanently connected to the core and located in the core reflooding pool, as in Figure 3. The emergency condensers are connected to the RPV without isolating elements, and thus actually form part of RPV. Each emergency condenser consists of a steam line leading from the RPV nozzle to a heat exchanger tube bundle. This tube bundle is located in the core flooding pool at a low elevation. The outlet on the heat exchanger primary side is the reflooding line with integrated anti-circulation loop. The working principle of the emergency condenser design is illustrated in figure 3. Given the normal water level inside the RPV, there prevails a stratified condition inside the emergency condenser. The upper part of the steam line is filled with steam while the lower part is filled with water. The water remains cold (except for a small layer below the RPV water level), as the anti-circulation loop prevents hot water from the RPV to enter the reflooding line from below. No convection occurs and thus thermal losses are negligible as long as the water level in the RPV remains normal. The water level in the steam line of the emergency condenser is several meters lower because the density of the water inside the RPV is lower than that of the water in the emergency condenser. This stratified condition changes to natural circulation if the water level inside the RPV drops by more than 0.7 m. Consequently, when the water level in the emergency condenser then drops by more than 0.5 m, steam enters the heat exchanger bundle. The steam then condenses inside the heat exchanger tubes and the resultant condensate flows via the reflooding line back into the RPV. If the water level inside the RPV is lower than the inlet nozzle of the reflooding line, the maximum driving pressure differential will be reached at a pressure of about 0.5 bar. This pressure differential is used to overcome the flow resistances in the steam line, heat exchanger tube bundle and reflooding line. The emergency condenser continues to function as long as the water level inside the RPV remains lower than 0.7 m below the normal RPV water level, as experimentally determined. On the secondary side, natural circulation also occurs once the emergency condenser begins to work. At low heat transfer rates, there is single-phase flow, while at higher rates two-phase flow occurs due to water evaporation. Normally, the water inventory of the flooding pool below the heat exchanger bundle could not be used as a heat sink due to stratification. To overcome this problem, the heat exchanger is enclosed in a chimney. Water enters the chimney at the bottom of the pool and exits at the top several meters above the heat exchanger.

Another solution is the use of isolation condensers connected to the reactor pressure vessel and immersed in external pools as in ESBWR design (Figure 4). The ESBWR uses isolation condensers for high-pressure inventory control and decay heat removal under isolated conditions ([8] and [9]). The isolation condenser system consists of four totally independent high-pressure loops, each containing a heat exchanger that condenses steam on the tube side and transfers the heat to water in large pool, outside the containment, which is vented to atmosphere. The isolation condenser (IC) is connected by piping to the RPV, and is placed at an elevation above the source of steam in the RPV and when steam is condensed, the condensate is returned to the vessel via a condensate return line. The steam line connected to the vessel is normally open and the condensate return line is normally closed. This allows the IC and drain piping to fill with condensate, which is maintained at a cooler temperature by the IC/PCC pool water during normal operation. The ICs are designed to handle the stored energy in the RPV and the core decay heat. In this way, there is no energy discharged to the suppression pool, there is no safety relief valve operation and there is no loss of reactor inventory. This makes a high-pressure make-up system unnecessary for ESBWR.

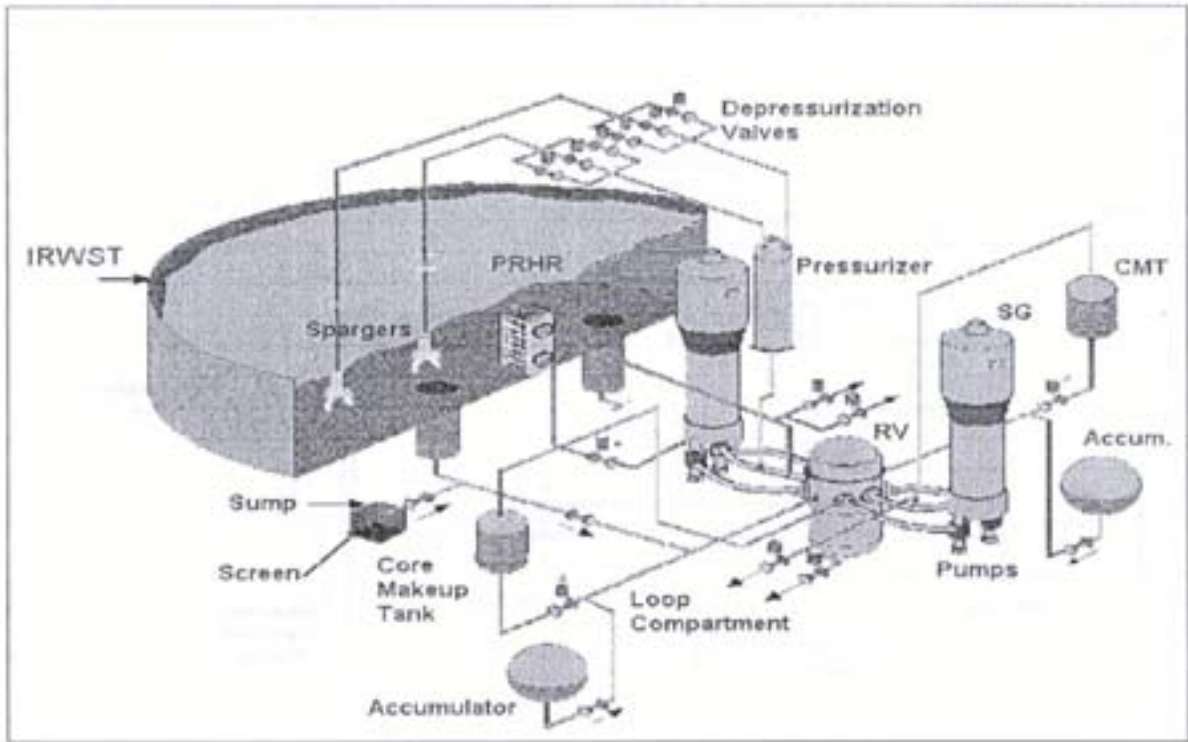


FIG. 1. Schematic of the passive safety systems used for the AP600/AP1000 designs.

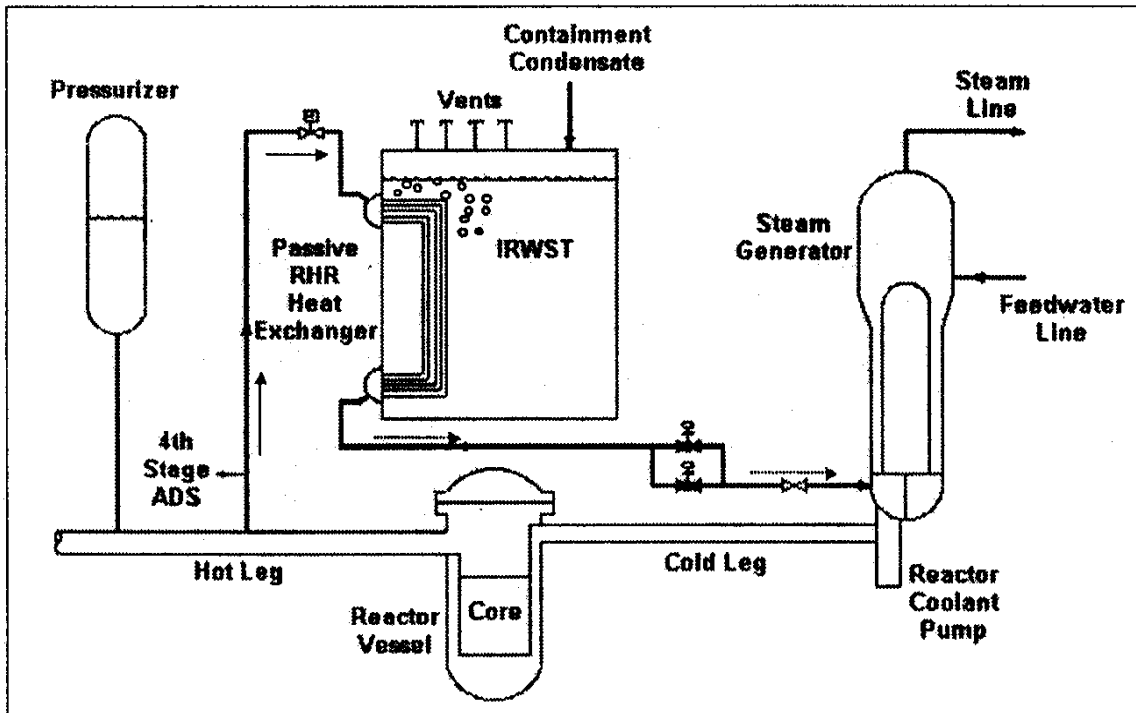


FIG. 2. The AP600/1000 Passive residual heat removal system (PRHR) using a heat exchanger connected to the primary system and immersed in the IRWST.

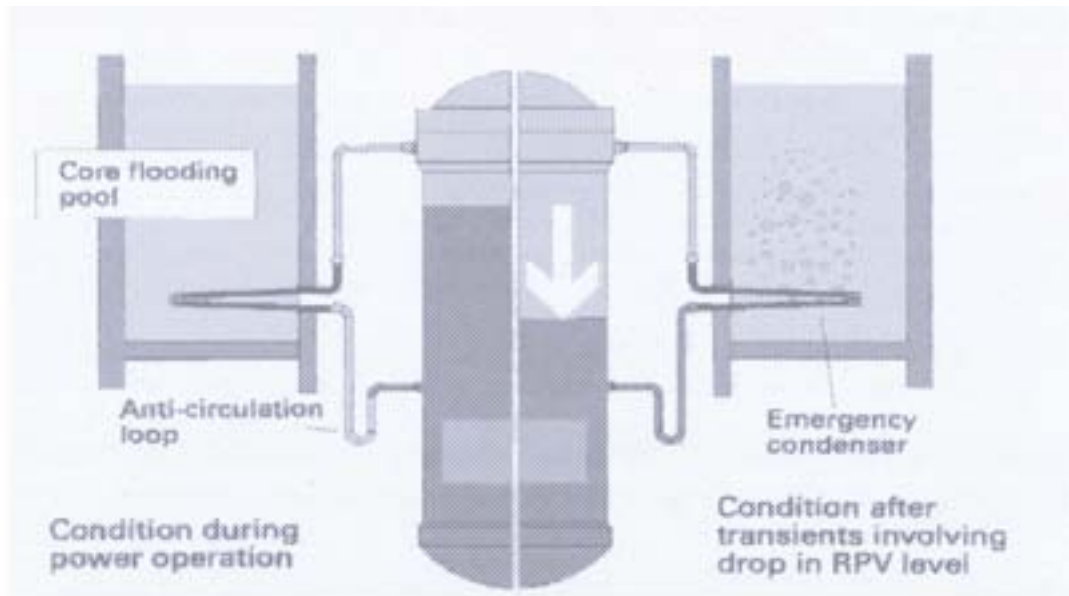


FIG. 3. The SWR1000 Emergency condenser for removing heat from the primary system by gravity flow.

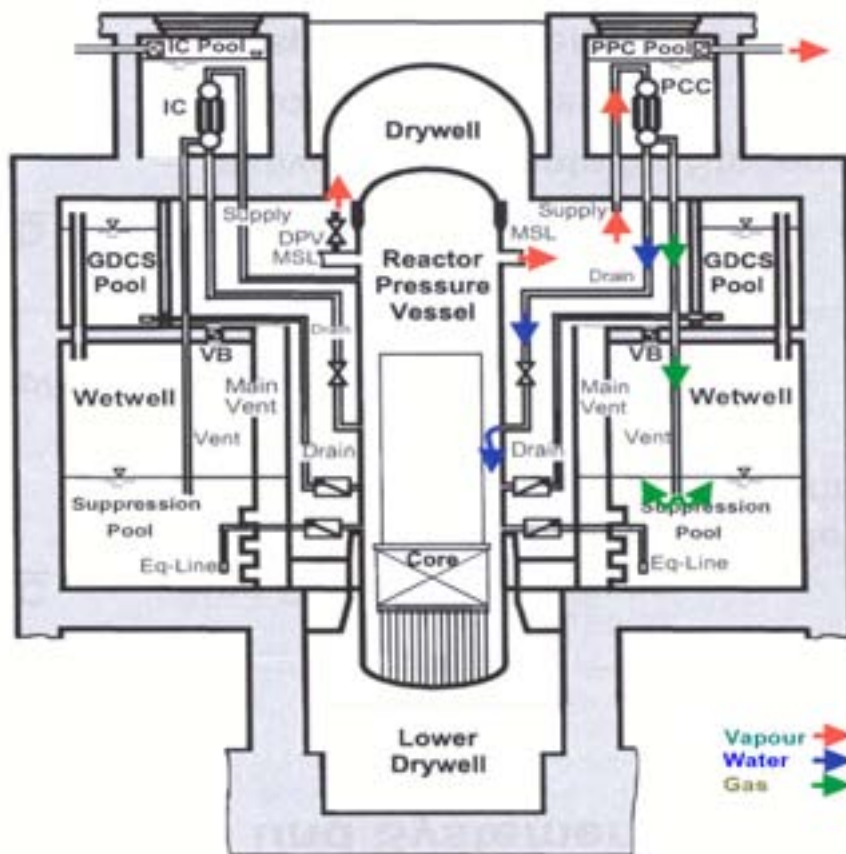


FIG. 4. The ESBWR design and passive safety systems.

3. HEAT REMOVAL FROM THE PRIMARY SYSTEM OF THE REACTOR IN CASE OF ACCIDENTS

In case of LOCA, passive solutions for decay heat removal from the core rely on:

- High-pressure gravity driven water tanks connected at their top to the primary system, e.g., Core Make-up Tanks (CMT) at any pressure, high-pressure accumulators at about 50 bar;
- Flooding of the core after depressurization of the primary system by ADS operation, e.g., lower-pressure Core Reflood Tanks (CRT) at about 15 bars, In-containment Refueling Water Storage Tank (IRWST), Gravity Driven Cooling System (GDSCS).

Several new designs have been improved by moving emergency cooling water sources inside the containment. As examples, the AP-600/AP-1000 have several water sources located inside the containment such as CMTs, high-pressure accumulators, lower pressure CRT and also IRWST (see figure 1); ESBWR have the GDSCS inside the containment (see figure 4). In case of the AP-600/AP-1000 using CMT, the pressure on top of this tank is equalized with primary system pressure. Thus the CMT can provide make-up water to the core by gravity at any pressure. For intermediate pressure levels in advanced PWRs, injection of water from accumulators (at about 50 bar) or core reflood tanks (at about 15 bar) is used.

The primary system of ALWRs is designed such that the core can be kept covered in spite of breaches in the primary system. In addition, elimination of primary system piping contributes, however, also to elimination of certain LOCA scenarios, e.g., elimination of large break LOCA as in PWRs and BWRs. Examples are the elimination of the recirculation piping in the ABWR by use of reactor internal pumps [6] and similar trend can be observed in the AP600/AP1000 where the primary system recirculation pumps are directly attached to the steam generators.

Two approaches have generally being used in order to better cope with the pressurized LOCA scenarios:

1. Intentional automatic depressurization of the primary system and subsequent use of low-pressure safety injection (LPCI) systems;
2. Increase of the capacity of the high-pressure coolant injection (HPCI) system.

In the passive plants, one relies on automatic depressurization of the primary system and, consequently, actuation of low-pressure gravity driven core make-up systems. This solution is chosen for the ESBWR and the SWR1000. Both of these passive BWRs provide gravity driven, low-pressure core flooding. It is the GDSCS pool that floods the ESBWR. The core reflooding pool provides the same function for the SWR1000 (see Figures 3 and 5). The ADS system is also incorporated in the AP-600/AP-1000. After depressurization, the AP-600/AP-1000 uses the IRWST inventory to reflood the RPV with gravity. On the other hand, the ABWR has a higher capacity HPCI relieving reliance on the ADS.

4. PASSIVE REMOVAL OF HEAT FROM CONTAINMENT

All containment systems profit from the passive heat sink provided by the structures inside the containment and the containment walls. The structures are usually needed to absorb the higher level of decay heat generation immediately after shutdown and limit the initial containment pressure. By the time these heat sinks get saturated (reach equilibrium temperatures with the containment atmosphere), the decay heat levels are lower and the containment systems can fully cope with the decay heat removal function. Thus, capacity needed for containment cooling is reduced.

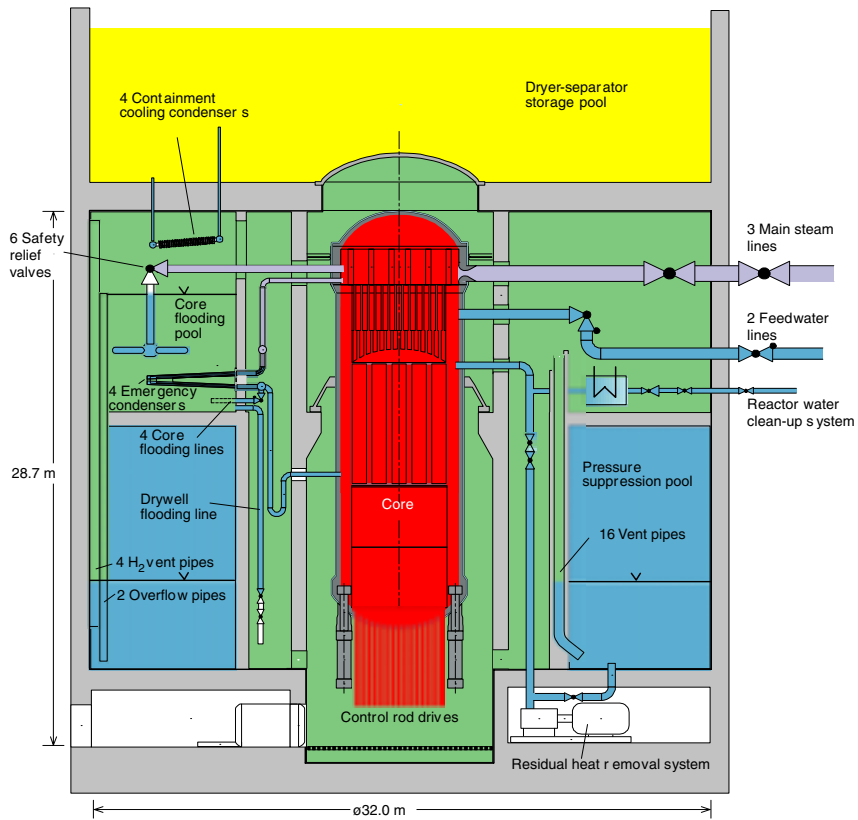


FIG. 5. Conceptual arrangement of the SWR1000 Containment and passive safety cooling systems.

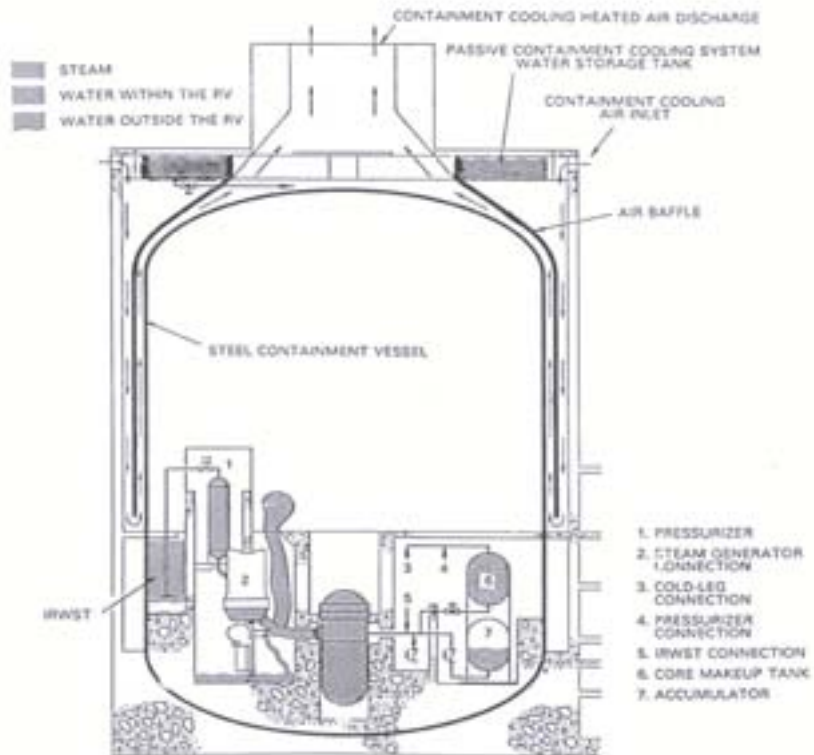


FIG. 6. Passive containment cooling for the AP600/AP1000 design.

A schematic of the AP600/AP1000 containment is presented in Figure 6, which shows the cooling of the containment building from the outside by natural draft enhanced by a water film on the thin metallic containment wall. It consists of a large steel vessel that houses the Nuclear Steam Supply System (NSSS) and all of the passive safety injection systems. The steel containment vessel resides inside of a concrete structure with ducts that allows cool outside air to come in contact with the outside surface of the containment vessel. The wetted surface of the containment shell is coated with a well-wetting paint to promote even distribution of water. When steam is vented into containment via a primary system break or ADS-4 valve actuation, it rises to the containment dome where it is condensed into liquid. The energy of the steam is transferred to the air on the outside of containment via conduction through the containment wall and natural convection to the air. As the air is heated, it rises through the ducts creating a natural circulation flow path that draws cool air in from the inlet duct and vents hot air out the top of the concrete structure. The condensate inside containment is directed back into the IRWST and the containment sump where it becomes a source of cool water in the sump recirculation process. Early in a LOCA transient, cold water is sprayed by gravity draining onto the containment vessel head to enhance containment cooling. A large tank of water, located at the top of the containment structure, serves as the source of water for this operation and is released in a programmed way producing a thin water film on the containment wall surface. By the time the water supply is exhausted, the decay heat removal needs are reduced and dry cooling of the wall suffices.

AP600/AP1000 containment cooling design is possible with metallic containment walls only. An alternative solution has been proposed for EP1000, which is a similar design to AP600 [10]. This design has two thick, concrete containment walls. It consists of finned condenser installed near the roof, inside the containment building, an intermediate sealed thermo-siphon loop penetrating through the double concrete containment walls, and an external hybrid (initially immersed, water-cooled and later air-cooled) heat exchanger, as in Figure 7. When the water inventory in the external pool is lowered, a passage for the air opens and the non-immersed part of the tubes acts as an air-cooled condenser.

The cooling of the containment atmosphere by containment condensers installed near the roof is also proposed for the SWR1000 reactor design. The SWR1000 has a containment-cooling condenser (CCC) with its secondary system connected to an external pool, as in Figure 5. In the event of failure of the active residual heat removal systems, four CCCs are designed to remove residual heat from the containment to the dryer-separator storage pool located above the containment. The CCCs are actuated by rising temperatures in the containment. They use natural circulation both on the primary and on the secondary sides. The working principle of the CCC is shown in Figure 8. It comprises a simple heat exchanger mounted about 1 m above the water level of the core reflooding pool. If the temperature in the drywell atmosphere increases over that in the dryer-separator storage pool, the water inside the heat exchanger tubes heats up. It flows to the outlet line due to the slope of the exchanger tubes. The outlet line ends at a higher elevation level than the inlet line; consequently the lifting forces are increased for the whole system. Depending on the heat transfer rate and cooling water temperature, secondary-side flow can be single-phase, intermittent, or two-phase. In the hypothetical case of a core melt accident, a hydrogen-steam mixture would also be possible. Given nitrogen, steam and mixture thereof, primary flow is downwards due to the densities of pure gases and a nitrogen-steam mixture increase with decreasing temperature. This results in the expected downward flow. Condensed steam drops into the core flooding pool. However, the opposite is true for a hydrogen-steam mixture, as the density of this mixture decreases with decreasing temperature, resulting in an upward flow through the heat exchanger tube bundle. But this does not pose any problem for the SWR1000 because both directions of flow on the primary side are equivalent.

The PCCS is the preferred means of decay heat removal following a LOCA for ESBWR (Figures 4 and 9). The system is a unique ESBWR engineered safety feature (similar to the SBWR PCCS). Containment heat removal is provided by the PCC system, consisting of four low-pressure loops, which is a safety related system ([8] and [9]). Each loop consists of a heat exchanger, which opens to the containment, a condensate drain line that returns the PCCS condensate to a PCCS condensate tank, which is connected to the RPV via its own nozzle, and a vent discharge line submerged in the suppression pool. The four heat exchangers, similar to the ICs, are located in cooling pools external to

the containment. Once PCCS operation is initiated following RPV depressurization, the condensate return line to the vessel is opened permanently. The PCCS uses natural convection to passively provide long-term containment cooling capability. The PCCS pool is sized to remove post-LOCA decay heat at least 72 hours without requiring the addition of pool inventory.

The PCCS heat exchangers are extensions of containment. The lines entering and leaving the PCCS from the drywell do not have containment isolation valves. No sensing, control, logic or power operated devices are required for the PCCS to initiate. Flow through the PCCS loop is driven by the pressure difference created between the containment drywell and the suppression pool that exists following a LOCA and the pressure drop through the PCCS tubes. The PCCS condensate is returned to the RPV under the force of gravity.

One key feature of the ESBWR allows an economical scale up of the reactor design. It effectively allows larger wetwell-to-drywell volume ratio, without significantly enlarging the containment. The GDCS pool region and the wetwell are connected by pressure equalization lines. As a result of this connection, the additional air space volume created by the GDCS pool draining, which is now available for the wetwell gases to expand keeping the containment pressure low, following an accident. This change improves the long-term containment pressure response.

5. AN EXAMPLE CASE: SAFETY FUNCTIONS, IN CASE OF TRANSIENTS AND IN THE EVENT OF ACCIDENTS FOR HPLWR DESIGN

It is the aim of the development of the High Performance Light Water Reactor (HPLWR) to use both passive and active safety systems ([11], and [12]) for performing safety-related functions in the event of transients or accidents (see Figure 10). The most frequent events requiring system function for prevention of intolerable fuel rod temperatures comprise anomalies in plant operation, or so-called transients. As a result of the specific properties of supercritical water, the water inventory within a HPLWR RPV is about 1/10th of that of a BWR or a PWR. This means that in case of incidents and accidents, the heat storage capacity of the existing water inventory in the primary circuit is low. Concerning the control of incidents and accidents this fact has to be considered appropriately. In general this means that as fast as possible, flow, which is able to cool the core has to be maintained. Later on the core has to be flooded with water from all sources, including water reservoirs external to the primary circuit.

From the comparison of analyses for a hot line break and a loss of feed-water flow accident, it is recognized that a reduction of temperature occurs in the first case, while in the second case under assumption of a fast HP water injection into the RPV a considerable larger temperature increase occurs [11]. As a consequence of these results, it is expected that the core cooling is more effective in case of loss of flow accidents, if the ADS is activated and followed by a low pressure water injection from the suppression pool, compared to an HP injection. Although this has to be substantiated by further analyses, this procedure seems to be the appropriate mode to control these kinds of accidents. Therefore in case of incidents with loss of feed-water flow it is proposed to apply the principle of ADS following by low-pressure coolant injection. Whether accumulators can be used in addition or even instead of the pumps need to be investigated in some detail. This mode should result in the lowest temperature loads of the fuel rods and in reliable systems for accident control. It should be pointed out that the same design philosophy has also been adopted in the design of Advanced Light Water Reactors (ALWR).

The HPLWR is being evaluated with particular emphasis on improved economics while maintaining the safety and reliability level achieved by advanced LWR. As mentioned above, it will rely on passive safety features to flood the core when necessary and to cool the containment. As the design of the HPLWR progresses and matures, additional evaluations will also be performed to assess the potential for new passive safety systems in the HPLWR design. In addition, the HPLWR design relies in part on existing proven technologies (e.g. supercritical fossil power plants).

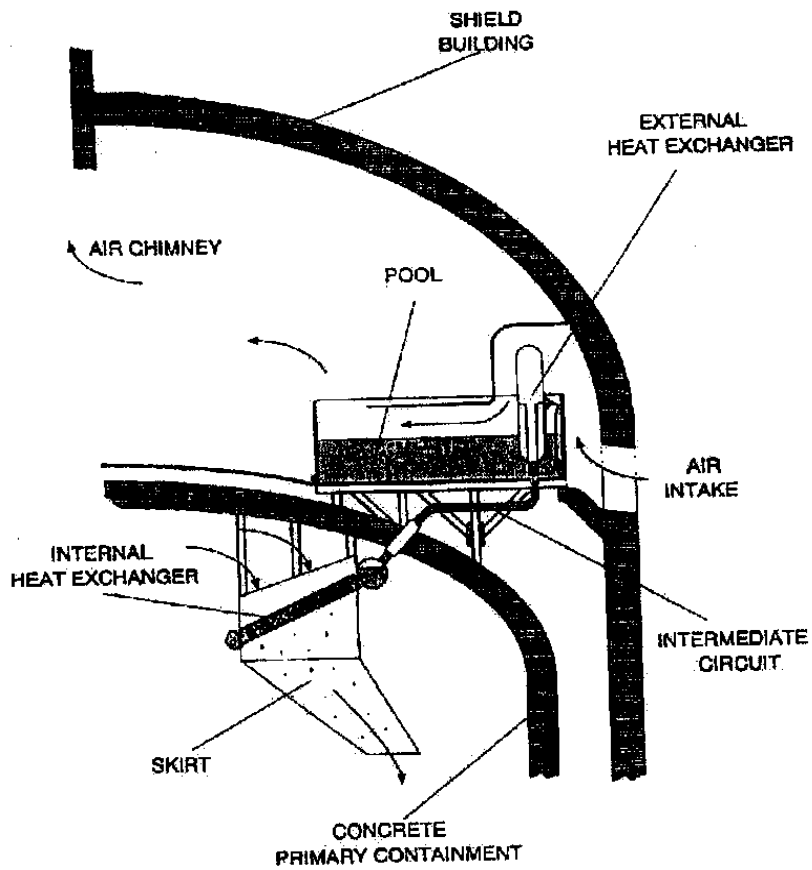


FIG. 7. Double concrete containment passive cooling system proposed as an alternative to the AP600 external wall-cooling concept.

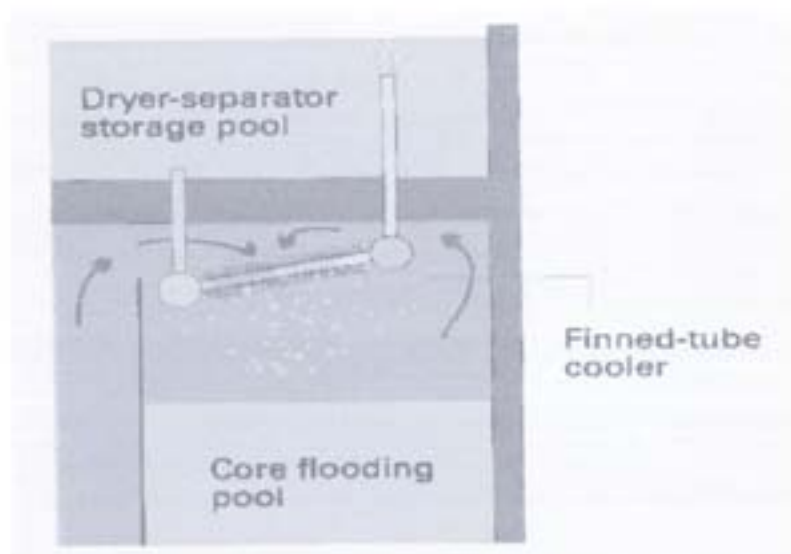


FIG. 8. Containment cooling condenser for SWR1000.

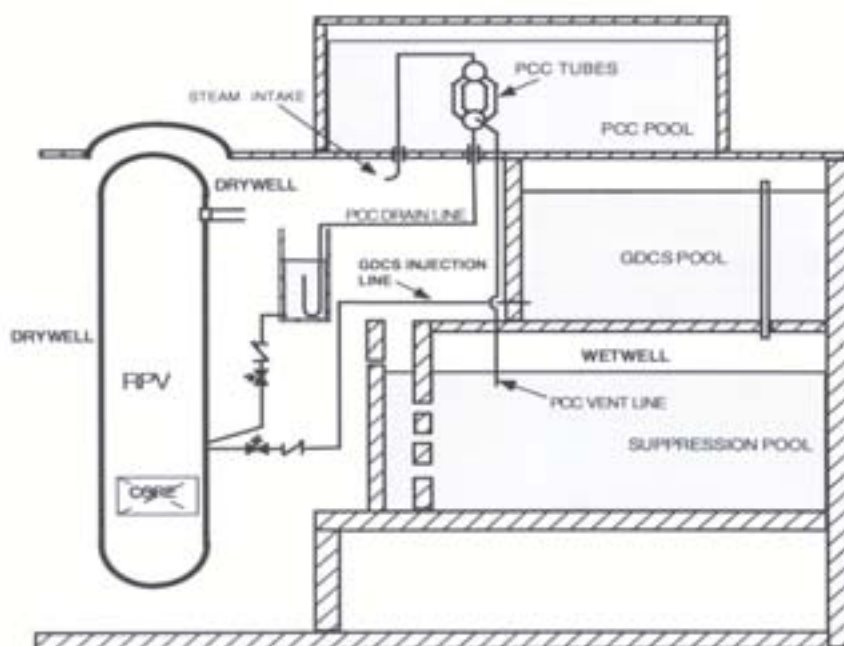


FIG. 9. The ESBWR passive containment cooling system condenses containment steam and vents the non-condensable to the suppression pool.

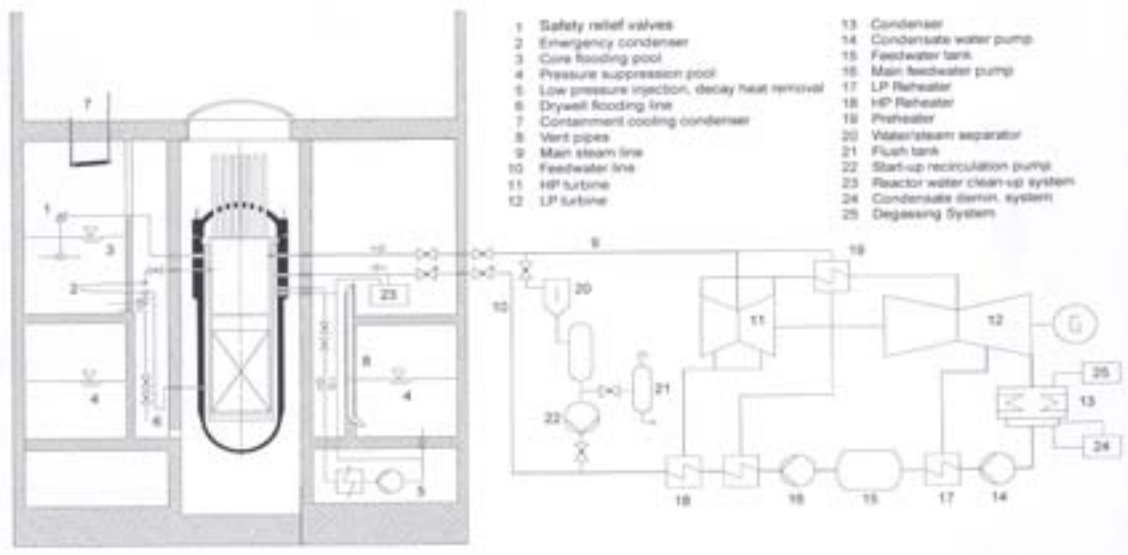


FIG. 10. Schematics of the HPLWR primary circuit, safety systems and containment concept.

6. CONCLUDING REMARKS

Passive ALWR designs emphasize enhanced safety by means of improved safety system reliability and performance. These objectives are achieved by means of improved safety system simplification and reliance on immutable natural forces for system operation. Most of the passive safety systems rely on boiling or condensation to obtain sufficiently high heat transfer rates under natural circulation conditions. Simulating the performance of these safety systems is central to analytical safety evaluation of advanced reactor designs.

For the intact primary system conditions, the decay heat can be removed by circulating the primary coolant in heat exchangers or condensers typically immersed in pools inside the containment. In case of LOCA, passive solutions for decay heat removal from the core rely either on high-pressure gravity driven core make-up tanks connected at their top to the primary system, or upon depressurization of the primary system followed by flooding of the core by gravity. Further, solutions for decay heat removal from the containment are based either on cooling of the metallic containment from the outside or on use of condensers. The condensers can be located either inside the containment, near the roof, or outside the containment, immersed in pools.

Since the new passive ALWR designs incorporate significant changes from the familiar current LWR designs and place higher reliance on individual systems, a thorough understanding of these designs is needed with respect to system interaction.

NOMENCLATURE

ABWR	Advanced Boiling Water Reactor
ADS	Automatic Depressurization System
ADS-4	Four stage ADS for AP600/AP1000
CMT	Core Make-up Tanks
CRT	Core Reflood Tanks
AP600	Advanced Pressurized Reactor, 600MWe
AP1000	Advanced Pressurized Reactor, 1000MWe
BWR	Boiling Water Reactor
CCC	Containment Cooling Condenser
ECCS	Emergency Core Cooling System
EP1000	European AP1000
EPR	European Pressurized Reactor
ESBWR	European Simplified Boiling Water Reactor
GDCS	Gravity Driven Cooling System
HP	High Pressure
HPIS	High Pressure Injection System
HPLWR	High Performance Light Water Reactor
IC	Isolation Condenser
IRIS	The International Reactor Innovative and Secure (Westinghouse with International co-operation)
IRWST	In-containment Refueling Water Storage Tank
LOCA	Loss Of Coolant Accident
LPIS	Low Pressure Injection System
LWR	Light Water Reactor
NSSS	Nuclear Steam Supply System
PCC	Passive Containment Cooling
PCCS	Passive Containment Cooling System
PIRUS	ABB Atom, Sweden, Passive Design Reactor
PRHR	Passive Residual Heat Removal
PWR	Pressurized Water Reactor
RPV	Reactor Pressure Vessel
SBWR	Simplified Boiling Water Reactor
SWR1000	Siedewasserreaktor, 1000MWe

REFERENCES

- [1] AKSAN, N., D'AURIA, F., Relevant thermal-hydraulic aspects of advanced reactor designs: Status report, OECD/NEA report, NEA/CSNI/R(96)2, OCDE/GD(97)8, November 1996.
- [2] INTERNATIONAL ATOMIC ENERGY AGENCY, Status of advanced light water cooled reactor designs: 2004, IAEA Report, IAEA-TECDOC-1391, May 2004.
- [3] INTERNATIONAL ATOMIC ENERGY AGENCY, Terms for describing new advanced nuclear power plants, IAEA Report, IAEA-TECDOC-936, April 1997.
- [4] INTERNATIONAL ATOMIC ENERGY AGENCY, Natural circulation data and methods for advanced water cooled nuclear power plant designs, Proceedings of a Technical Committee Meeting, Vienna, 18–21 July 2000, IAEA-TECDOC-1281, April 2002.
- [5] INTERNATIONAL ATOMIC ENERGY AGENCY, Experimental tests and qualification of analytical methods to address thermohydraulic phenomena in advanced water cooled reactors, Proceedings of a Technical Committee Meeting, Paul Scherrer Institut, Würenlingen and Villigen, Switzerland, 14–17 September 1998, IAEA-TECDOC-1149, May 2000.
- [6] INTERNATIONAL ATOMIC ENERGY AGENCY, Evolutionary water cooled reactors: Strategic issues, technologies, and economic viability, Proceedings of a Symposium, Seoul, Republic of Korea, 30 November–4 December 1998, IAEA-TECDOC-1117, December 1999.
- [7] YADIGAROGLU, G., Passive core and containment cooling systems: Characteristics and state of the art, Proceedings of the 9th International Topical Meeting on Nuclear Reactor Thermal Hydraulics (NURETH-9), San Francisco, California, October 3–8, 1999.
- [8] LUMINI, E., UPTON, H., MASONI, P., BILLIG, P., ESBWR Passive heat exchanger design and performance – Reducing plant development costs, Proceedings of the SFEN/ENS International Conference, TOPNUX 96 (1996).
- [9] CHALLBERG, R.C., CHEUNG, Y.K., KHORANA, S.S., UPTON, H.A., ESBWR Evolution of passive features, Proceedings of the 6th International Conference on Nuclear Engineering (ICONE-6), San Diego, California, USA, May 10–15, 1998.
- [10] CAVICCHIA, V., FIORINO, E., VANINI, P., Innovative containment cooling for a double concrete containment, Proceedings of the 1997 ANS International Meeting on Advanced Reactors Safety (ARS-97), Orlando, Florida, USA, 1–5 June 1997.
- [11] AKSAN, N., SCHULENBERG, T., SQUARER, D., CHENG, X., STRUWE, D., SANCHEZ, V., DUMAZ, P., KYRKI-RAJAMAKI, R., BITTERMANN, D., SOUYRI, A., OKA, Y., KOSHIZUKA, S., Potential safety features and safety analysis aspects for High Performance Light Water Reactor (HPLWR), Proceedings of International Conference on Global Environment and Advanced Nuclear Power Plants (GENES4/ANP2003), Kyoto, Japan, 15–19 September, 2003 (CD-ROM, Paper no. 1223).
- [12] BITTERMANN, D., SQUARER, D., SCHULENBERG, T., OKA, Y., DUMAZ, P., KYRKI-RAJAMAKI, R., AKSAN, N., MARACZY, C., SOUYRI, A., Potential Plant Characteristics of a High Performance Light Water Reactor (HPLWR), Proceedings of International Congress on Advances in Nuclear Power Plants, ICAPP'03, ANS, CD-ROM, Cordoba, Spain (2003).

ANNEX 5

LOCAL PHENOMENA ASSOCIATED WITH NATURAL CIRCULATION

D. Saha

Bhabha Atomic Research Centre, India

Abstract

This lecture describes the many types of phenomena encountered in the natural circulation systems of a nuclear reactor. All the components of the primary system of a nuclear reactor are described and phenomena occurring in each of them are explained. A comprehensive coverage of related thermohydraulic relationships is provided which will enable the participants to carryout the process design of a natural circulation system.

1. INTRODUCTION

Natural circulation in a closed loop is established by locating the heat sink at an elevation higher than the heat source. The circulating fluid removes heat from source and transports it to the sink. The flow can be single phase or two phase wherein vapor flows alongside the liquid. These loops are widely used in energy conversion systems. A rectangular closed loop is shown in Figure1. Important phenomena and parameters relevant to the natural circulation loop are discussed below.

1.1. Natural circulation flow rate

Natural circulation flow rate in the loop, under steady state condition is determined from the balance between the driving and the resisting forces. Driving force results from density difference between hot leg and cold leg of the loop. The resisting force is due to pressure losses in the system. The balance of forces can be expressed as:

$$\Delta P_d = \Delta P_f + \Delta P_l + \Delta P_a \quad (1)$$

$$\text{where } \Delta P_a = \oint \rho dz \quad (2)$$

The above expression indicates that the parameters of interest to determine flow rate are:

- a) Single phase and two phase **density**
- b) Single and two phase **pressure loss components**

It may be noted that since the driving force in a natural circulation loop is small, it is necessary to minimize and determine very accurately the pressure loss components.

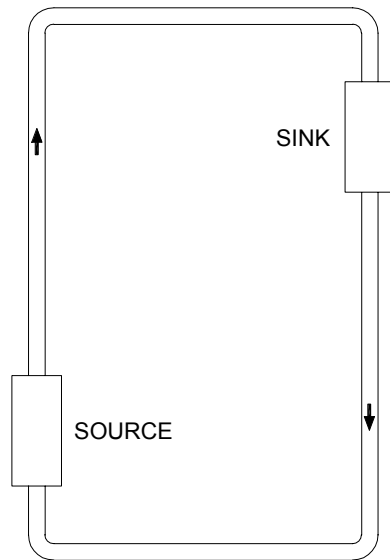


FIG. 1. A rectangular closed natural circulation loop.

1.2. Heat transfer in source

Figure 2 shows a simple configuration of a cylindrical fuel rod concentrically located inside a circular channel, heat being removed from the rod by coolant flowing through the annulus. Resistance to heat transfer from rod to coolant is mainly restricted to a thin layer of fluid adjacent to rod surface commonly called as film.

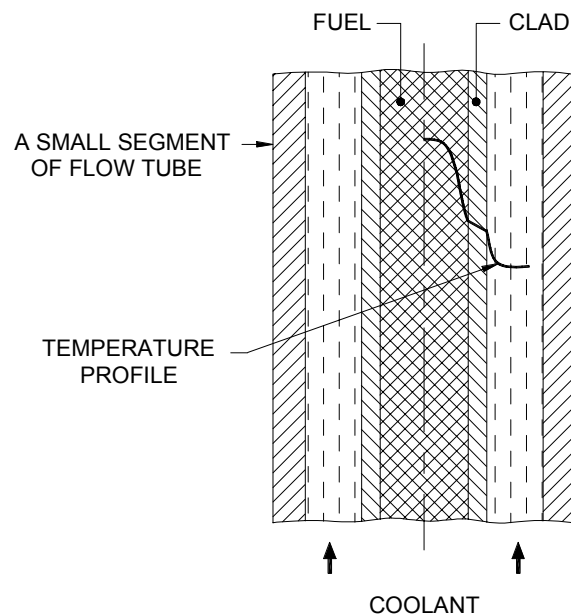


FIG. 2. Radial temperature distribution in fuel and coolant.

Heat transfer from rod to coolant is governed by the Newton's Law:

$$q = h (T_w - T_b) \quad (3)$$

This expression underscores the importance of the **film heat transfer coefficient**, h , in determining the fuel surface temperature and in turn the fuel center temperature.

The maximum heat flux achievable in fuel is mainly limited by **Critical Heat Flux (CHF)**. It is characterized by sudden rise in surface temperature at this flux level. At CHF, one of the following two phenomena are encountered:

- a) Departure from Nucleate Boiling (DNB)
- b) Dryout

1.3. Heat transfer in sink

In Pressurized Water Reactor (PWR) and Pressurized Heavy Water Reactor (PHWR), primary coolant that removes heat from fuel, transports it to steam generator. In steam generator, primary coolant transfers heat to secondary fluid, which starts **boiling**. Thus in the primary side of steam generator coolant temperature reduces without phase change whereas in the secondary side phase change takes place. Steam produced in the secondary side is ultimately condensed in the condenser. Fig. 3 depicts a simplified sketch of a steam generator.

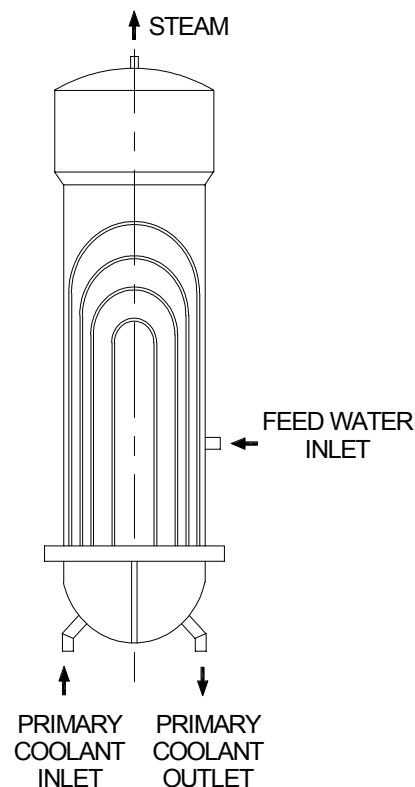


FIG. 3. Steam generator.

In Boiling Water Reactor (BWR), primary coolant itself boils in the core and the steam, after passing through turbine, is led to condenser where **condensation** of steam takes place. A simplified sketch of a condenser is shown in Fig. 4.

In new generation of reactors, a large water pool is being used as heat sink for core decay heat as well as heat released into containment (Fig. 5). **Thermal stratification** in the pool is an important phenomenon which influences heat transfer to the pool to a great extent.

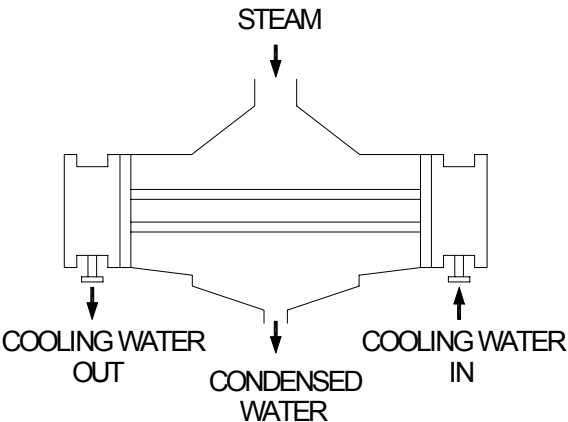


FIG. 4. Condenser.

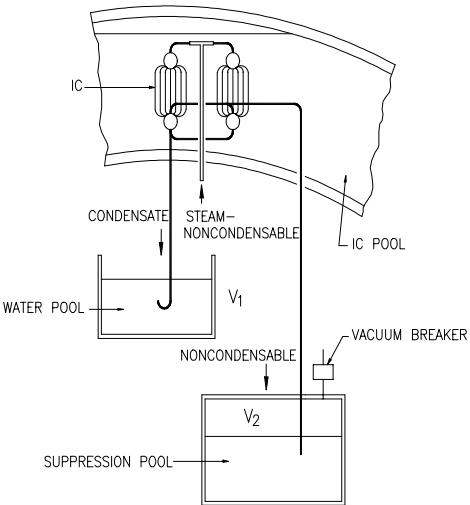


FIG. 5. Isolation condenser immersed in a large water pool.

Figure 6 depicts a block diagram of all the important phenomena / parameters related to natural circulation discussed so far. These parameters are further discussed in more details in the following sections. A number of correlations given in the following sections are derived based on experimental data generated with forced circulation. Though in most of the cases these correlations can be used for natural circulation, applicability of these correlations for natural circulation should be judiciously checked when secondary flows are present like natural circulation through large diameter pipe at low Reynolds number.

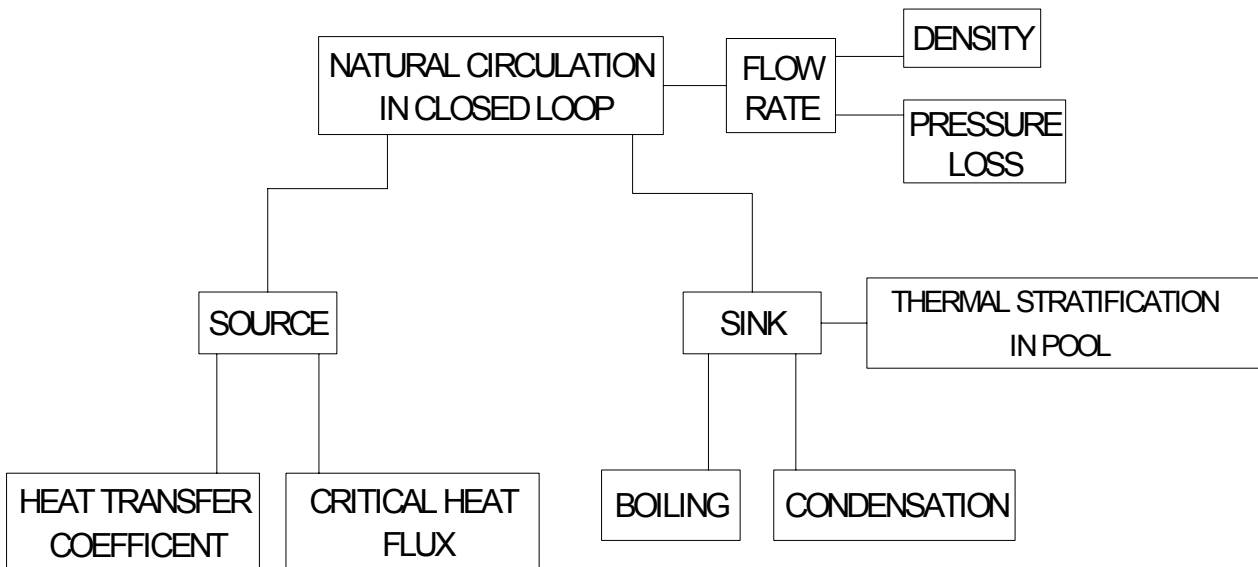


FIG. 6. Important phenomena/ parameters relevant to natural circulation in closed loop.

2. NATURAL CIRCULATION FLOW RATE

2.1. Density

For single phase flow, the density of fluid can be predicted reasonably well with established relationships for thermophysical properties of fluid [1]. For two phase flow the density of two phase mixture at any cross section in the flow path is given by the following equation:

$$\rho = \alpha \rho_G + (1 - \alpha) \rho_L \quad (4)$$

The above expression indicates that for two phase flow, it is necessary to predict void fraction accurately to determine density.

2.1.1. Void fraction

Figure 7a depicts upward two phase flow through a vertical channel. Figure 7b shows the flow pattern based on the assumption that the two phases are artificially segregated. Quality (x) at any cross section can be defined as

$$x = \frac{\text{Mass flow rate of vapor}}{\text{Mass flow rate of vapor} + \text{Mass flow rate of liquid}}$$

Void fraction at any cross section is defined as

$$\alpha = \frac{\text{Cross section area occupied by vapor}}{\text{Total channel cross section area}}$$

In general, the void fraction correlations can be classified into following categories:

- (a) slip ratio models,
- (b) $K\beta$ models and
- (c) correlations based on the drift flux model.

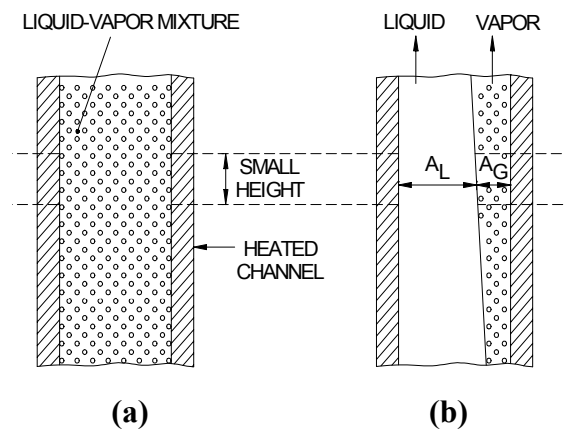


FIG. 7. Two phase flow in a vertical heated channel.

In addition, there are some empirical correlations, which do not fall in any of the three categories. Some of the commonly used correlations in all the above categories are described below.

a) Slip ratio models

These models essentially specify an empirical equation for the slip ratio, $S (=u_G/u_L)$. The void fraction can, then be calculated by the following equation:

$$\alpha = \frac{1}{1 + \left(\frac{1-x}{x}\right) S \frac{\rho_G}{\rho_L}} \quad (5)$$

For homogeneous flow, $u_G = u_L$ and $S = 1$. At high pressure and high mass flow rates the void fraction approaches that of homogeneous flow, and can be calculated by setting $S = 1$ in the above equation. But usually, the slip ratio is more than unity for both horizontal and vertical flows. A commonly used slip ratio model is given below as an example.

Modified Smith [2]

$$S = K + (1 - K) \left\{ \frac{\rho_L + K \left(\frac{1}{x} - 1 \right)}{\rho_G \left(1 + K \left(\frac{1}{x} - 1 \right) \right)} \right\}^{0.5} \quad (6)$$

where $K = 0.95 \tanh(5.0x) + 0.05$

b) $K\beta$ models

These models calculate α by multiplying the homogeneous void fraction, β , by a constant K .

Armand's model is given below as an example.

Armand [3]

$$K = 0.833 + 0.167x \quad (7)$$

c) Correlations based on the drift flux model

By far the largest number of correlations for void fraction reported in the literature are based on the drift flux model. The general drift flux formula for void fraction can be expressed as

$$\alpha = \frac{j_G}{C_0[j_G + j_L] + V_{Gj}} \quad (8)$$

where,

V_{Gj} is the drift velocity ($= u_G - j$, where j is the mixture velocity) and for homogeneous flow $C_0 = 1$ and $V_{Gj} = 0$. The various models (IAEA, 2001) [4] in this category differ only in the expressions used for C_0 and V_{Gj} which are empirical in nature.

The Chexal and Lellouche [5] correlation is applicable over a wide range of parameters and can tackle both co-current and counter-current steam-water, air-water and refrigerant two-phase flows. Details of this and some other commonly used correlations can be obtained from IAEA-TECDOC-1203 [4].

2.2. Components of pressure drop

As mentioned earlier in section 1.1, the total pressure loss, Δp comprises of three components, viz. ΔP_f , ΔP_l and ΔP_a which are components of pressure drop due to skin friction, form friction (also known as local friction) and acceleration respectively. The skin friction pressure drop is also known simply as friction pressure drop.

For the purpose of design of advanced reactors, the required correlations mainly cover the following configurations. For friction pressure loss, circular pipe, annulus and rod cluster and for local pressure loss, spacer, bottom and top tie plates, flow area changes like contraction, expansion, bends, tees, valves etc., are most common. In addition, in-core effects like radiation induced creep, blister formation, swelling, corrosion, etc. are also important factors affecting the pressure drop which are not dealt with here. A few pressure drop correlations for different components are given as examples in the following sections. These are described configuration-wise.

2.2.1. Friction pressure drop

This is the irreversible component of pressure drop caused by shear stress at the wall and can be expressed as:

$$\Delta p_f = \frac{fL}{D_h} \frac{W^2}{2\rho A^2} \quad (9)$$

where D_h is equal to 4 times flow area / wetted perimeter.

The pressure drop occurs all along the length and hence referred to as distributed pressure drop sometimes. This equation is applicable for single-phase and homogeneous two-phase flows, although, the method of calculation of the friction factor, f , and density, ρ , differ in the two cases. Pressure drop across tubes, rectangular channels, annuli, bare rod bundle (i.e. without spacers), etc., are examples of this component. Correlations commonly used to determine friction factor, f , is discussed below. The following pressure drop correlations are applicable to steady state fully developed flow.

Circular pipe

a) Adiabatic single-phase flow

For fully developed laminar flow, the friction factor is given by:

$$f = 64 / Re \quad (10)$$

which is valid for Reynolds number less than 2000. For turbulent flow in smooth pipes several friction factor correlations are proposed and in use. A few commonly used correlations for smooth pipe are given below.

Blasius [6] proposed the following equation:

$$f = 0.316 Re^{-0.25} \quad (11)$$

valid in the range $3000 \leq Re \leq 10^5$. The following equation valid in the range of $3000 \leq Re \leq 10^6$ is also often used for design.

$$f = 0.184 Re^{-0.2} \quad (12)$$

Colebrook [7] proposed the following equation:

$$\frac{1}{\sqrt{f}} = 0.86 \ln \left(\frac{e/D}{3.7} + \frac{2.51}{Re \sqrt{f}} \right) \quad (13)$$

valid for smooth and rough pipes for the whole range of Reynolds number above 3000. The following explicit equation proposed by Filonenko [8] is a good approximation of Colebrook equation for smooth tube in the range $4 \times 10^3 \leq Re \leq 10^{12}$.

$$f = [1.82 \log(Re) - 1.64]^{-2} \quad (14)$$

It may be noted from the above that well established correlations for friction factor do not exist in the transition region between $2000 \leq Re \leq 3000$. A simple way to overcome this problem is to use the following criterion for switch over from laminar to turbulent flow equation.

$$\text{If } f_t > f_l \text{ then } f = f_t \quad (15)$$

where f_t and f_l are friction factors calculated by turbulent and laminar flow equations respectively.

b) Diabatic single-phase flow

Generally isothermal friction factor correlations are used with properties evaluated at the film temperature $T_f = 0.4 (T_w - T_b) + T_b$, where T_w and T_b are the wall and bulk fluid temperatures [9]. Sometimes the friction factor for non-isothermal flow is obtained by multiplying the isothermal friction factor with a correction coefficient, F . The following empirical equation proposed by Leung and Groeneveld [10] is given as an example

$$F = (\mu_b/\mu_w)^{-0.28} \quad (16)$$

Where the subscripts b and w refer to the bulk fluid and wall respectively.

c) Adiabatic two-phase flow

A large number of two-phase flow pressure drop correlations can be found in literature. These correlations can be classified into the following four general categories.

- (1) Empirical correlations based on the homogeneous model,
- (2) Empirical correlations based on the two-phase friction multiplier concept,
- (3) Direct empirical models,
- (4) Flow pattern specific models.

Correlations in the first two categories are given below.

Homogeneous flow model

In the homogeneous flow model, the two-phase frictional pressure gradient is calculated in terms of a friction factor, as in single-phase flow. The friction factor is calculated using one of the equations given for single phase flow in Section 2.2.1(a), with the use of the two-phase viscosity in calculating the Reynolds number. A typical model for two-phase viscosity is given below.

Cicchitti [11]

$$\mu = x \mu_G + (1 - x) \mu_L \quad (17)$$

Correlations based on the multiplier concept

In this case, the two-phase pressure drop is calculated from the single-phase pressure drop by multiplying with a two-phase friction factor multiplier. The following definitions of two-phase friction multipliers are often used.

$$\phi_{LO}^2 = \frac{(dp/dz)_{TPF}}{(dp/dz)_{LO}}; \quad \phi_{GO}^2 = \frac{(dp/dz)_{TPF}}{(dp/dz)_{GO}},$$

$$\phi_L^2 = \frac{(dp/dz)_{TPF}}{(dp/dz)_L} \text{ and } \phi_G^2 = \frac{(dp/dz)_{TPF}}{(dp/dz)_G} \quad (18)$$

Where the denominators refer to the single-phase pressure gradient for flow in the same duct with mass flow rates corresponding to the mixture flow rate in case of ϕ_{LO}^2 and ϕ_{GO}^2 and individual phases

in case of ϕ_L^2 and ϕ_G^2 . Among these, ϕ_{LO}^2 is the most popular friction multiplier. An illustrative multiplier based correlation is given below.

Lottes-Flinn [12]

Correlation for annular upward flow through heated channels is

$$\phi_{LO}^2 = \left(\frac{1-x}{1-\alpha} \right)^2 \quad (19)$$

Martinelli – Nelson [13] is a commonly used correlation in this category.

d) Diabatic two-phase flow

The correlations discussed so far are applicable to adiabatic two-phase flow. The effect of heat flux on two phase pressure drop has been studied by Leung and Groeneveld [14], Tarasova [15] and Koehler and Kastner [16]. Tarasova observed that two phase friction pressure drop is higher in a heated channel compared to that in an unheated channel for same flow condition. However, Koehler and Kastner concluded that two phase pressure drops are same for heated and unheated channels. Studies conducted by Leung and Groeneveld indicate that the surface condition is significantly influenced by heat flux. Effective surface roughness increases due to the formation of bubbles at heated surface leading to larger pressure drop. They concluded that for the same flow conditions, the two phase multiplier is larger for low heat flux than high heat flux. The discussions indicate that there is not yet well established procedure to take the affect of heat flux into account. However some alternate approaches are suggested in IAEA-TECDOC-1203 [4].

Annulus

Correlations for circular pipe are normally used for the calculation of single phase pressure drop in annulus using the hydraulic diameter concept. For two-phase pressure drop, the same concept is expected to be applicable.

ROD BUNDLE

The rod bundle geometries used in advanced designs differ in several ways. In PWRs and BWRs, the fuel bundles are long (1.8 to 4.5 m approx.) whereas in PHWRs short fuel bundles of about 0.5 m are used. Generally grid spacers are used in PWRs and BWRs while split-wart spacers are used in PHWRs. In certain fast breeder reactors wire-wrapped bundles are still used. In PWRs and BWRs, the total pressure drop is obtained by summing up the pressure drop in bare rod bundle and the spacers. For wire-wrapped bundles empirical correlations for the pressure drop in the bundle considering the geometric details of the wire wraps are available. For PHWR type bundles, the total pressure drop is sometimes expressed in terms of an overall loss coefficient due to the closeness of the spacers and the complex geometry of the end plates [17] and alignment problem at the junction between two bundles [18].

Wire wrapped rod bundles

In the case of wire wrapped rod bundles, the geometry and shape of the system is quite rigid and the development of a general correlation for predicting the pressure drop is a reasonable task. Such a correlation proposed by Rehme [19], [20] is given below:

$$\Delta P = f_R \frac{L}{D_h} \frac{\rho u_R^2}{2} \frac{U_B}{U_G} \quad (20)$$

where

$U_B = U_S + U_D$ is the bundle perimeter

$U_G = U_S + U_D + U_K$ is the total perimeter

U_K , U_S and U_D are the shroud perimeter, pins perimeter and wire perimeter respectively. The reference velocity, u_R , is defined as:

$$u_R = u \sqrt{F}$$

where u is the average velocity in the rod bundle.

The geometrical factor F depends on the pitch to diameter ratio and on the ratio between the mean diameter and the wire pitch (H).

$$F = \left(\frac{p_t}{D}\right)^{0.5} + \left[7.6 \frac{d_m}{H} \left(\frac{p_t}{D}\right)^2\right]^{2.16} \quad (21)$$

where d_m is the mean diameter of wire wraps. The reference friction factor f_R is calculated by means of the following correlation based on Rehme's experimental data.

$$f_R = \frac{64}{Re_R} + \frac{0.0816}{Re_R^{0.133}} \quad \text{for } 2 \times 10^3 \leq Re_R \leq 5 \times 10^5 \quad (22)$$

where

$$Re_R = Re \sqrt{F} \text{ and } Re = (u_R D_h)/\nu \quad (23)$$

These are valid in the range $1.12 < p_t/D < 1.42$ and $6 < H/d_m < 45$.

Bare rod bundles

Single-phase

Correlations for circular pipes are commonly used to calculate pressure drop using hydraulic diameter of the rod bundle in the absence of experimental data. One of the commonly used correlation is:

Kays [21]

$$f = f_{cir} K_1 \quad (24)$$

where

K_1 - is provided as a function of p_t/D (pitch to diameter ratio) based on the work by Diessler and Taylor [22].

f_{cir} - can be calculated using correlations given for circular pipe.

Two-phase

CESNEF-2 [23] correlation is applicable for rod bundles. In addition, there are some empirical equations proposed for rod bundles one of which is given below.

CNEN [24] correlation

$$\Delta p_{\text{TPF}} = 1.7205 \times 10^{-6} (L M^{0.852}) / D_h^{1.242} \quad (25)$$

M is given by:

$$M = [xv_G + (1-x)v_L]G^2 \quad (26)$$

where M is in $[N/m^2]$, L & D_h are in metres.

Δp_{TPF} is obtained in metres of water at 25°C. This equation is applicable for square array fuel bundles with pitch to diameter ratio = 1.28, $D_h = 1.31$ cm, peripheral rod-channel gap = 0.55 x pitch, $8 < P < 70$ kg/cm² and $680 < G < 2700$ kg/m²s.

2.2.2. Local pressure drop

This is the localized irreversible pressure drop component caused by change in flow geometry and flow direction. Pressure drop across valves, elbows, tee, spacer, etc. are examples. The local pressure drop is given by

$$\Delta p_l = K \frac{W^2}{2\rho A^2} \quad (27)$$

where K is the local loss coefficient, the correlations for which differ for different geometries and for single-phase and two-phase flows.

GRID SPACERS

Because of variation and complexity of geometry, it is extremely difficult to establish a pressure loss coefficient correlation of general validity for grid spacers. But methods of calculation reasonably accurate for design purpose can be achieved. Some correlations used to determine pressure drop across grid spacers are discussed below.

Single-phase flow

Single-phase pressure drop is calculated using a spacer loss coefficient, K, as:

$$\Delta p = K \rho V_B^2 / 2 \quad (28)$$

In some cases, it may be possible to obtain a reasonable value of the spacer loss coefficient if its geometry can be approximated to one of those considered in [25]. For other cases, the different empirical models for K, one of which is described below may be used.

Rehme [26]

$$K = C_v \varepsilon^2 \quad (29)$$

where $\varepsilon = A_g/A_B$.

For $Re_B > 5 \times 10^4$, $C_v = 6$ to 7 and for $Re_B \leq 5 \times 10^4$ C_v values are given in graphical form as a function of Re_B . Subsequently Rehme [27] studied the effect of roughness of rod surface on the pressure drop across spacers. Cevolani [28] proposed $C_v = 5 + 6133 Re^{-0.789}$ for square bundles and $\ln(C_v) = 7.690 - 0.9421 \ln(Re) + 0.0379 \ln^2(Re)$ for triangular bundles with an upper limit of $K=2$ if the calculated value is greater than 2.

Two-phase flow

In general, the homogeneous model or the slip model is used for the estimation of the two-phase pressure drop across grid spacers.

a) Homogeneous model

$$\Delta p = K(\text{Re}_{\text{sat}}) v G^2/2 \quad (30)$$

where $K(\text{Re}_{\text{sat}})$ is the form loss coefficient for single phase flow estimated at the Reynolds number corresponding to the total flow in the form of saturated liquid and v is the specific volume given by

$$v = x v_G + (1-x) v_L \quad (31)$$

This model may be used when experimental data are not available.

b) Slip model

According to this model, the form loss coefficient for two phase flow can be obtained from

$$\Delta p_{\text{TPF}} = \frac{K_{\text{SPF}} G^2}{2\rho} = K_{\text{SPF}} \frac{\rho_L}{\rho} \frac{G^2}{2\rho_L} = K_{\text{TPF}} \frac{G^2}{2\rho_L} \quad (32)$$

where ρ is given by

$$\rho = \alpha \rho_G + (1-\alpha) \rho_L ; \quad \alpha = \frac{1}{1 + \left(\frac{1-x}{x}\right) S \frac{\rho_G}{\rho_L}}$$

It may be noted that this equation reduces to the homogeneous model if $S = 1$. Grillo and Marinelli [29] recommend a value of $S = 2$ for grid spacers.

Tie plate

Generally, tie plates are used at the ends of rod cluster fuel elements which structurally joins all the fuel pins. Unlike spacers, the flow areas at the downstream and upstream sides of the tie plates are different. Also, these are generally located in the unheated portion of the bundle. Reported studies on pressure drop for the tie plates are few in number. An approximate calculation for design purposes can be made using the contraction and expansion model for local pressure losses. In addition the friction losses in the thickness of the tie plates can be calculated using the hydraulic diameter concept. For two-phase pressure losses, the homogeneous or the slip model described above can be employed in the absence of experimental data.

AREA CHANGES

The single phase pressure losses due to area changes can be calculated by Eqn.(27) with loss coefficients calculated for the relevant geometry from Idelchik [25].

In general, for two phase flow the irreversible pressure drop due to area changes is estimated from the knowledge of single-phase loss coefficient using the homogeneous model. When details of the slip ratio are available, then the slip model given above can be used. Romey (see Ref. [30]) expresses the two-phase pressure drop across sudden expansion by the following equation:

$$\Delta p = G^2 A_r^2 \frac{(1 - A_r)}{\rho_L} \left\{ 1 + x \left(\frac{\rho_L}{\rho_G} - 1 \right) \right\} \quad (33)$$

Bends and fittings

The single-phase pressure drop due to bends and fittings can be calculated using the appropriate loss coefficients from Idelchik [25].

Chisholm and Sutherland [31] provide the following general equation for the calculation of two-phase pressure drop in bends and fittings.

$$\frac{\Delta p_{TP}}{\Delta p_L} = 1 + \left(\frac{\Delta P_G}{\Delta P_L} \right) + C \left(\frac{\Delta P_G}{\Delta P_L} \right)^{0.5} \quad (34)$$

$$C = \left\{ 1 + (C_2 - 1) \left(\frac{v_{fg}}{v_G} \right)^{0.5} \right\} \left\{ \left(\frac{v_G}{v_L} \right)^{0.5} \left(\frac{v_L}{v_G} \right)^{0.5} \right\} \quad (35)$$

where $v_{fg} = v_G - v_L$, and C_2 is a constant.

a) Bends

For bends C_2 is a function of R/D , where R is the radius of curvature of the bend and D is the pipe diameter.

R/D	1	3	5	7
C_2 for normal bend	4.35	3.40	2.20	1.00
C_2 for bend with upstream disturbance within 50 L/D	3.10	2.50	1.75	1.00

Chisholm provided the above values of C_2 by fitting Fitzsimmons [32] data.

Chisholm & Sutherland [31]

$$\text{For } 90^\circ \text{ bends: } C_2 = I + 35 N \quad (36)$$

$$\text{For } 180^\circ \text{ bends: } C_2 = I + 20 N \quad (37)$$

N is the number of equivalent lengths used for calculating single-phase pressure drop.

b) Tees

$$C_2 = 1.75$$

c) Valves

$$C_2 = 1.5 \text{ for gate valves}$$

$$= 2.3 \text{ for globe valves}$$

Alternatively the homogeneous model may be used.

2.2.3. Acceleration pressure drop

This reversible component of pressure drop is caused by a change in flow area or density. Expansion, contraction and fluid flowing through a heated section are the examples. The acceleration pressure drop due to area change for single-phase and two-phase flow can be expressed as

$$\Delta p_a = \frac{(1 - A_r^2) W^2 \phi}{2 A_0^2 \rho_L} \quad (38)$$

where A_0 = smaller flow area. $\phi = 1$ for single-phase flow and for two-phase flow ϕ is given by:

$$\phi = \left(\frac{x^3}{\rho_G^2 \alpha^2} + \frac{(1-x)^3}{\rho_L^2 (1-\alpha)^2} \right) \left(\frac{\rho_G \rho_L}{x \rho_L + (1-x) \rho_G} \right) \quad (39)$$

The acceleration pressure drop due to density change for single-phase and two-phase flows can be expressed as:

$$\Delta p_a = G^2 \left\{ \left(\frac{1}{(\rho_m)_o} \right) - \left(\frac{1}{(\rho_m)_i} \right) \right\} \quad (40)$$

For single-phase flows, this component is negligible, but can be significant in two-phase flows. For two-phase flow, the above equation can be used with ρ_m given by:

$$\frac{1}{\rho_m} = \left(\frac{x^2}{\rho_G \alpha} + \frac{(1-x)^2}{\rho_L (1-\alpha)} \right) \quad (41)$$

To evaluate the acceleration pressure drop due to density change, accurate prediction of the density of fluid is necessary.

3. HEAT TRANSFER IN SOURCE

3.1. Film heat transfer coefficient

Heat transfer coefficient, h , is normally expressed in terms of Nusselt Number (Nu), a dimensionless heat transfer parameter where $Nu = hd / k$. Relationships to determine h for flow through a pipe are discussed below.

3.1.1. Single phase laminar Flow

For constant wall temperature, the local Nusselt Number reaches a value of 3.65 asymptotically and for constant heat flux boundary condition, the local Nusselt number reaches a value of 4.36 asymptotically [33]. Hence, for developed flow through pipe, Nu of 3.65 for constant wall temperature and Nu of 4.36 for constant heat flux are recommended.

3.1.2. Single phase turbulent flow

The Dittus Boelter equation [34] given below is probably the most widely used correlation.

$$Nu = 0.023 Re^{0.8} Pr^{0.4} \quad (42)$$

Here the physical properties in the dimensionless numbers are evaluated at the bulk temperature of the fluid. For large temperature drop across the film the physical property most affected is the viscosity. The Sieder Tate equation [35] is frequently used in such cases.

$$Nu = 0.023 Re^{0.8} Pr^{0.4} (\mu_w / \mu_b)^{0.14} \quad (43)$$

Here the physical properties are evaluated at fluid bulk temperature except for μ_w , which is evaluated at wall temperature.

3.1.3. Two phase flow

In two phase flow the vapor formed due to boiling and the liquid move together in a channel. It can be classified into subcooled flow and saturated flow. This classification refers to the temperature of the bulk of the liquid. In saturated two phase flow, the bulk of the liquid is at saturation temperature whereas in subcooled two phase flow, the bulk of the liquid is at lower temperature. However, in either case, to generate bubble the heated surface and adjacent layer of fluid are always at higher temperature than the saturation temperature. Heat transfer regions and flow regimes in a vertical diabatic channel are shown in Fig. 8 [36]. Correlations used to determine heat transfer coefficients in two phase flow are described below.

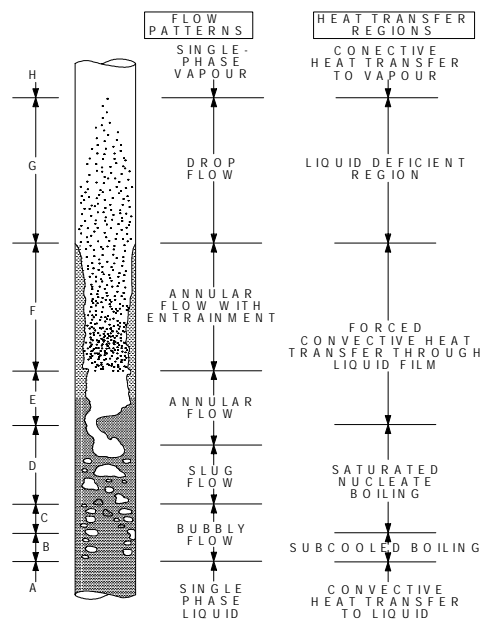


FIG.8. Regions of heat transfer in convective boiling.

Saturated Two Phase Flow Inside Horizontal and Vertical Tubes

Research in the flow boiling area has been directed towards gaining a fundamental understanding of the flow boiling phenomenon as well as towards obtaining experimental results that may be employed in equipment design. The fundamental studies clearly brought out the complexities of the flow boiling mechanisms (see Collier [36] for a comprehensive survey). Some of the major complexities involved are: bubble growth and departure behaviour in the flow field of a two-phase mixture, distribution of the two phases relative to each other and relative to the tube wall (flow pattern and entrainment effects), departure from thermodynamic equilibrium at local conditions, characteristics of the heat transfer surface, and the effect of fluid properties. There are a large number of saturated flow boiling correlations (well over 30) available in the literature. Two of them are described below.

a) Kandlikar's Correlation [37]

$$\frac{h_{TP}}{h_1} = C_1 Co^{C_2} (25Fr_{LO})^{C_3} + C_3 Bo^{C_4} F_{fl} \quad (44)$$

$$C_o = \left(\frac{1-x}{x} \right)^{0.8} \left(\frac{\rho_G}{\rho_L} \right)^{0.5} \quad (45)$$

The values of constants C_1 to C_5 are given in Table 1. Co is the convection number, Bo the boiling number and h_1 = single phase heat transfer coefficient with only the liquid fraction flowing in the tube. In the present work, the Dittus –Boelter equation is used to calculate h_1 . Table-2 gives the values of the fluid-dependent parameters F_{fl} .

Table 1. Constants in the proposed correlation equation (44)

Constant	Convective region	Nucleate boiling region
C_1	1.1360	0.6683
C_2	-0.9	-0.2
C_3	667.2	1058.0
C_4	0.7	0.7
C_5^*	0.3	0.3

* $C_5=0$ for vertical tubes, and for horizontal tubes with $Fr_{LO} > 0.04$

Table 2. Fluid dependent parameter F_{FL} in the proposed correlation, equation (44)

Fluid	F_{fl}
Water	1.00
R-11	1.30
R-12	1.50
R-1381	1.31
R-22	2.20
R-113	1.30
R-114	1.24
R-152a	1.10
Nitrogen	4.70
Neon	3.50

The two sets of values given in Table 1 correspond to the convective boiling and nucleate boiling regions, respectively. The heat transfer coefficient at any given condition is evaluated using the two

sets of constants for the two regions, and since the transition from one region to another occurs at the intersection of the respective correlations, the higher of the two heat transfer coefficient values represents the predicted value from the proposed correlation.

b) Chen's Correlation [38]

This correlation includes both the heat transfer coefficients due to nucleate boiling as well as forced convective mechanisms.

$$h_{TP} = h_{mic} + h_{mac} \quad (46)$$

where h_{mic} is the nucleate boiling part and h_{mac} is the convective part

$$h_{mic} = h_{Foster-Zuber} \cdot S \quad (47)$$

$$h_{mac} = h_{Dittus-Boelter} \cdot F \quad (48)$$

where S & F are functions of Re_L and χ_{tt}

S, suppression factor is the ratio of the effective superheat to wall superheat. It accounts for decreased boiling heat transfer because the effective superheat across the boundary layer is less than the super heat based on wall temperature.

$$S = \frac{1}{\left(1 + 2.53 \times 10^{-6} Re_L^{1.17}\right)} \quad (49)$$

F, the enhancement factor is a function of the Martinelli Parameter χ_{tt}

$$F = 1 \quad \text{for } \frac{1}{\chi_{tt}} \leq 0.1 \quad (50)$$

$$F = 2.35 \left(\frac{1}{\chi_{tt}} + 0.213 \right)^{0.736} \quad \text{for } \frac{1}{\chi_{tt}} > 0.1 \quad (51)$$

Forster – Zuber Correlation [39]

$$h = 0.0012 \left\{ \frac{k_L^{0.79} C_{pL}^{0.045} \rho_L^{0.49} g^{0.25}}{\sigma^{0.5} \mu_L^{0.29} h_{LG}^{0.24} \rho_G^{0.24}} \right\} \Delta T_w^{0.24} \Delta p^{0.75} \quad (52)$$

where $\Delta T = T_w - T_{sat}$

$\Delta p = P_{wall\ temperature} - P$

Subcooled flow

Chen's correlation [40] may be used for subcooled boiling.

$$h_{sub} = h_{mac} + h_{mic} \quad (53)$$

$$\text{where, } h_{mac} = h_{dittus-boelter} \quad (54)$$

$$h_{mic} = h_{forster-zuber} \cdot S \quad (55)$$

h_{mac} is calculated using equation 43.

S can be calculated by using single phase Reynolds number with $x=0$ (using eqn. 49). For calculating $h_{forster-zuber}$ equation 52 is used.

Another correlation by Jens and Lottes [41] is also used widely.

$$h = \left[\frac{1}{25} \exp^{P/62} \right] (\Delta T_{sat})^3$$

3.2. Critical heat flux (CHF)

Boiling crisis occurs when the heat flux is raised to such a high level that the heated surface can no longer support continuous liquid contact. This heat flux is usually referred to as the critical heat flux (CHF). It is characterized either by a sudden rise in surface temperature caused by blanketing of the heated surface by a stable vapour layer, or by small surface temperature spikes corresponding to the appearance and disappearance of dry patches. Failure of the heated surface may occur once the CHF is exceeded.

In flow boiling the CHF mechanisms depend on the flow regimes and phase distributions, which in turn are controlled by pressure, mass flux and quality. For reactor conditions of interest, the flow quality generally has the strongest effect on CHF: the CHF decreases rapidly with an increase in quality. The following sections describe some important CHF mechanisms encountered at different qualities and flow conditions [4].

3.2.1. DNB (departure from nucleate boiling)

In subcooled and saturated nucleate boiling (approximate quality range: from -5% to $+5\%$) the number of bubbles generated depends on the heat flux and bulk temperature. The bubble population density near the heated surface increases with increasing heat flux and a so-called bubble boundary layer often forms. If this layer is sufficiently thick it can impede the flow of coolant to the heated surface. This in turn leads to a further increase in bubble population until the wall becomes so hot that a vapour patch forms over the heated surface. This type of boiling crisis is also characterized by a fast rise of the heated surface temperature.

3.2.2. Dryout

In the annular dispersed flow regime (high void fraction) the liquid will be in the form of a liquid film covering the walls and entrained droplets moving at a higher velocity in the core. Continuous thinning of the liquid film will take place due to the combined effect of entrainment and evaporation. Near the dryout location the liquid film becomes very thin and due to the lack of roll waves (which normally occur at higher liquid film flow rates) entrainment is suppressed. If the net droplet deposition rate does not balance the evaporation rate the liquid film must break down. The temperature rise accompanying this film breakdown is usually moderate.

3.2.3. CHF Prediction Methodology

The complexity of predicting the CHF in a nuclear fuel bundle may be best understood by first considering the prediction of CHF of a simplest experimental setup; a uniformly heated tube cooled internally by a fluid flowing at a steady rate vertically upwards. Here the CHF is a function of the following independent variables:

$$CHF = f(De, G, \Delta H_{in}; P, E) \quad (57)$$

where E takes into account the effect of the heated surface, i.e. surface roughness, thermal conductivity and wall thickness.

Despite the simplicity of the experimental setup, over 400 correlations for CHF in tubes are currently in existence. The present proliferation of correlations illustrates the complex state-of-the-art in predicting the CHF phenomenon even for simple geometry at steady-state flow conditions.

Analytical models

Analytical CHF models are based on physical mechanisms. The most common models that have met with some success are

- a) Annular film dryout model [42]
- b) Bubbly layer model [43]
- c) Helmholtz instability model [44]

However, because of our limited understanding of the mechanisms involved, the models are still less accurate than empirical correlations.

Empirical methods

INLET-CONDITIONS-TYPE PREDICTION METHODS

For a given geometry and inlet conditions, the critical power N_{DO} i.e. power corresponding to the first occurrence of CHF for that geometry is expressed as

$$N_{DO} = f(P_{in}, G_{in}, T_{in}, c/s, L_H) \quad (58)$$

This method cannot be used for predicting the location and magnitude of CHF

LOCAL-CONDITIONS –TYPE PREDICTION METHODS

This type of prediction methods follow the local-conditions hypothesis which states that the local CHF is dependent only on the local conditions and not on upstream history.

$$CHF = f(P, G, X_{DO}, c/s) \quad (59)$$

The local conditions approach, is probably the most common method for predicting CHF. This form is more convenient since it depends on fewer parameters and permits the prediction of the location of CHF.

The large majority of the CHF prediction methods proposed are of this type. It is conservatively estimated that there are over 400 empirical correlations of this type proposed in the literature for directly heated tubes. Their main disadvantage is their limited range of application.

CHF LOOK-UP TABLE METHOD

The CHF look up table is basically a normalized data bank. The recently completed International CHF look up table [45] provides CHF values for water cooled tubes, at discrete values of pressure (P), mass flux (G), and quality (X), covering the ranges of 0.1–20 Mpa pressure, 0–7500 $\text{kg}\cdot\text{m}^{-2}\cdot\text{s}^{-1}$ (zero flow refers to pool-boiling conditions) mass flux and –50% to 100% vapour quality (negative qualities refer to subcooled conditions). Linear interpolation between table values is used for determining CHF. Extrapolation is usually not needed as the table covers a range of conditions much wider than any other prediction method. Groeneveld et al. [45] have presented a complete description of the Look up table for tubes. As an example, the 1995 CHF look up table for critical heat flux in 8mm tubes for 7.0 MPa is reproduced in Table 3.

The look up table needs to be converted into a prediction method for bundle geometries for nuclear reactor application. The CHF needs to be modified to account for bundle specific effects. The following correction factor methodology is adopted to evaluate the bundle CHF:

$$\text{CHF}_{\text{bundle}} = \text{CHF}_{\text{table}} \times K_1 \times K_2 \times K_3 \times K_4 \times K_5 \times K_6 \times K_7 \times K_8 \quad (60)$$

where $\text{CHF}_{\text{bundle}}$ is cross section average value of the heat flux at which the CHF first occurs at the cross-section, $\text{CHF}_{\text{table}}$ is the CHF value for a tube as found in the look up table for the same cross-sectional average values of P and G, and K_1 to K_8 are correction factors to account for specific bundle effects. A summary of correction factors is given in Table 4.

Table 3. The 1995 CHF look-up table for critical heat flux in 8 MM tubes (in kW/M²)

Pressure kPa	Mass Flux kg/m ² _s	Quality																						
		-5	-4	-3	-2	-1.5	-1	-0.5	0	0.05	0.1	0.15	0.2	0.25	0.3	0.35	0.4	0.45	0.5	0.6	0.7	0.8	0.9	1
7000	0	5361	5010	4651	4293	4118	3954	3762	3426	2692	2336	1918	1485	1212	996	834	723	641	575	466	369	357	339	0
7000	50	6002	5599	5236	4926	4778	4644	4483	4198	3498	3137	2769	2397	2165	1981	1826	1706	1604	1501	1200	984	940	774	0
7000	100	6539	6094	5738	5474	5355	5245	5105	4818	3957	3401	3239	3093	2941	2820	2707	2595	2489	2302	1710	1515	1479	1060	0
7000	300	6998	6441	6104	6015	6002	5947	5886	5865	5582	4834	4494	4247	4046	3862	3632	3430	3318	3065	2402	2144	1735	1179	0
7000	500	7264	6617	6233	6123	6088	5953	5940	5887	5690	5134	4682	4316	4157	3900	3634	3469	3366	3157	2596	2213	1587	1029	0
7000	1000	7798	6930	6386	6216	6135	5799	5604	5505	5318	5070	4472	3892	3626	3347	3136	3031	3028	2838	1774	1121	735	613	0
7000	1500	8557	7520	6715	6339	6253	5886	5603	5145	4673	4301	3874	3486	3189	2964	2735	2523	2250	1728	805	488	273	259	0
7000	2000	9793	8774	7597	6676	6480	6142	5684	4952	4275	3785	3407	3122	2890	2731	2451	2023	1445	844	432	322	196	190	0
7000	2500	10882	9986	8709	7496	7142	6690	5806	4876	4104	3537	3147	2922	2723	2445	1983	1367	789	424	261	204	99	51	0
7000	3000	11730	10850	9620	8170	7523	6953	5816	4724	3981	3369	2940	2714	2491	2133	1570	967	553	425	346	263	112	52	0
7000	3500	12535	11558	10344	8740	7757	7135	5848	4567	3834	3199	2786	2565	2294	1896	1323	782	519	490	409	317	135	57	0
7000	4000	13317	12216	10929	9320	8041	7398	5938	4372	3469	2928	2645	2490	2201	1730	1228	840	734	732	470	317	136	58	0
7000	4500	14070	12839	11469	9769	8188	7399	6061	4410	3347	2743	2515	2418	2139	1640	1200	930	872	854	492	317	137	59	0
7000	5000	14792	13465	11954	10124	8354	7427	6225	4552	3378	2696	2458	2380	2105	1591	1193	1010	949	888	521	326	138	63	0
7000	5500	15509	14000	12474	10713	9223	8025	6409	4682	3454	2710	2471	2382	2146	1673	1308	1154	1102	952	582	348	153	70	0
7000	6000	16208	14521	12931	11464	10460	9338	7226	4752	3483	2714	2470	2415	2213	1840	1539	1385	1228	1032	655	379	179	84	0
7000	6500	16875	15091	13336	12214	11432	10650	7804	4867	3535	2784	2519	2466	2330	2140	1879	1599	1311	1108	725	422	210	99	0
7000	7000	17529	15640	13763	12432	11718	11183	8065	5055	3745	3006	2708	2595	2464	2260	2014	1687	1401	1186	795	476	243	116	0
7000	7500	18170	16174	14182	12682	11740	11185	8202	5208	3974	3339	3032	2913	2779	2541	2199	1773	1489	1269	866	530	277	132	0
7000	8000	18806	16673	14610	12995	12067	11187	8424	5405	4172	3727	3483	3384	3259	2846	2288	1851	1576	1353	936	581	312	149	0

Table 4. Summary of correction factors applicable to the CHF look-up table [4]

FACTOR	FORM	COMMENTS
K ₁ Sub channel or Tube Diameter Cross- Section Geometry Factor	For $2 \leq D_{hy} \leq 25$ mm: $K_1 = (0.008/D_{hy})^{1/2}$ For $D_{hy} > 25$ mm $K_1 = 0.57$	Includes the observed diameter effect on CHF. This effect is slightly quality dependent.
K ₂ , Bundle-Geometry Factor	$K_2 = \min[1, (0.5 + 2\delta/d)\exp(-0.5x^{1/3})]$	This is a tentative expression, an empirically derived factor is preferred. K ₂ is also a weak function of P, G and X.
K ₃ , Mid-Plane Spacer Factor for a 37- element Bundle	$K_3 = 1 + A\exp(-BL_{sp}/D_{hy})$ $A = 1.5 K_L^{0.5} (G/1000)^{0.2}$ $B = 0.1$	This factor has been validated over a limited range of spacer geometries.
K ₄ , Heated - Length Factor	For $L/D_{hy} \geq 5$: $K_4 = \exp[(D_{hy}/L)\exp(2\alpha_h)]$ $\alpha_h = X\rho_L/[X\rho_L + (1-X)\rho_G]$	Inclusion of α_h correctly predicts the diminishing length effect at subcooled conditions.
K ₅ , Axial Flux Distribution Factor	For $X \leq 0$: $K_5 = 1.0$ For $X > 0$: $K_5 = q_{loc}/q_{BLA}$	Tong's F-factor method [46] May also be used within narrow ranges of conditions.
K ₆ , Radial or Circumferential Flux Distribution Factor	For $X > 0$: $K_6 = q(z)_{avg}/q(z)_{max}$ For $X \leq 0$: $K_6 = 1.0$	Tentative recommendation only and to be used with well-balanced bundle. May be used for estimating the effect of flux tilts across elements. Otherwise method of Yin (1991) [47] is recommended.
K ₇ , Flow- Orientation Factor	$K_7 = 1 - \exp(-(T_1/3)^{0.5})$ where $T_1 = \left(\frac{1-X}{1-\alpha}\right)^2 \frac{f_L G^2}{gD_{hy}\rho_L(\rho_L - \rho_G)\alpha^{0.5}}$ f_L is the friction factor of the channel.	This equation was developed by Wong and Groeneveld [48] based on the balance of turbulent and gravitational forces. The void fraction is evaluated with the correlation of Premoli et al. [49].
K ₈ , Vertical Low- Flow Factor	$G < -400$ kg m ² s ⁻¹ or $X \ll 0$: $K_8 = 1$ $-400 < G < 0$ kg m ² s ⁻¹ : Use linear interpolation between table value for upward flow and value predicted form $CHF = CHF_{G=0, X=0} (1 - \alpha_{hom}) C_1$	For $\alpha_h < 0.8$: $C_1 = 1.0$ For $\alpha_{hom} \geq 0.8$: $C_1 = \frac{0.8 + 0.2 \rho_L / \rho_G}{\alpha_{hom} + (1 - \alpha_{hom}) \rho_L / \rho_G}$ Minus sign refers to downward flow. $G=0$, $X=0$ refers to pool boiling.

4. HEAT TRANSFER IN SINK

4.1. Boiling

As stated earlier, boiling takes place on the secondary side of steam generators. To determine heat transfer coefficients on the secondary side of steam generators, the correlations given in section 3 can be used.

4.2. Condensation

Condensation occurs when the temperature of vapor is reduced below its saturation temperature T_{sat} . Vapor starts condensing on the surface when the surface is cooled below the saturation temperature of vapor. Two distinct forms of condensation on the surface are observed; Film condensation and Dropwise condensation as shown in Fig 9.

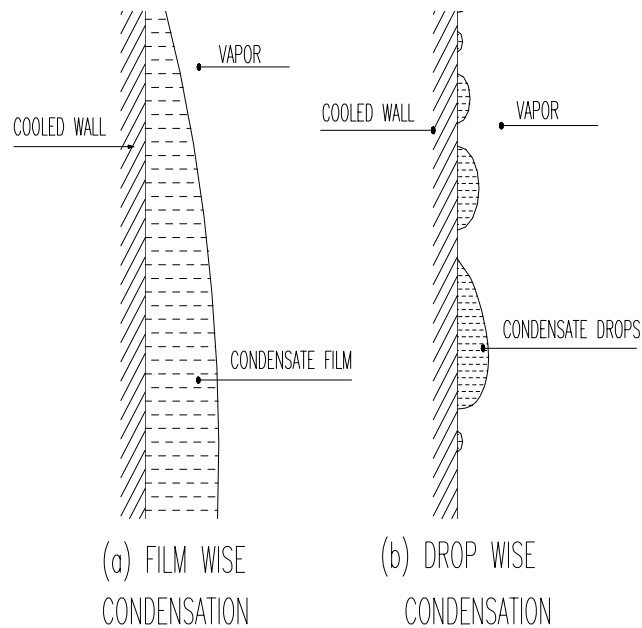


FIG. 9. Filmwise and dropwise condensation.

In film condensation the condensate wets the surface and forms a liquid film on the surface while in dropwise condensation the condensed vapor forms droplets on the surface instead of a continuous film and the surface is covered by countless droplets of varying diameters.

In film condensation the surface is blanketed by a liquid film of increasing thickness and this “liquid wall” between solid surface and the vapor serves as a resistance to heat transfer. The heat of vaporization h_{fg} released, as the vapor condenses, must pass through this resistance before it can reach the solid surface and be transferred to the medium on the other side. In dropwise condensation part of the surface is in contact with vapor leading to higher heat transfer rates.

Flow regimes in condensation heat transfer

The Reynolds number ($Re = \frac{4\dot{m}}{p\mu_L}$) for condensation on the outer surfaces of vertical tubes or plates

increases in the flow direction due to the increase of the liquid film thickness δ . The flow of liquid film exhibits different regimes depending on the value of the Reynolds number. It is observed that outer surface of the liquid film remains smooth and wave-free for about $Re < 30$ and thus the flow is clearly laminar. Ripples or waves appear on the free surface of the condensate flow as the Reynolds number increases, and the condensate flow becomes fully turbulent at about $Re \approx 1800$. The condensate flow is called wavy-laminar in the range $30 < Re < 1800$ and turbulent for $Re > 1800$. However some disagreement exists about the value of Re at which the flow becomes wavy-laminar or turbulent.

4.2.1. Vertical plates

Laminar Flow on a smooth vertical plate

The analytical relation for the heat transfer coefficient in the laminar film condensate on vertical plate was first developed by Nusselt [50]. The average heat transfer coefficient over the entire vertical plate is determined as follows

$$h = h_{ave} = \frac{1}{L} \int_0^L h_x dx = \frac{4}{3} h_{x=L} = 0.943 \left[\frac{g\rho_L(\rho_L - \rho_G)h_{fg}k_L^3}{\mu_L(T_{sat} - T_w)L} \right]^{\frac{1}{4}} \quad (61)$$

Where, x = distance from leading edge and L = length of the plate

This equation under predicts heat transfer because it does not take into account the effects of the nonlinear temperature profile in the liquid film and cooling of the liquid below the saturation temperature. Both of these effects can be accounted for by replacing h_{fg} with h_{fg}^* given by equation (62).

$$h_{fg}^* = h_{fg} + 0.68C_{pL}(T_{sat} - T_w) \quad (62)$$

The modified latent heat of vaporization h_{fg}^* is used to consider the extra heat that is released when the condensate in the actual condensation process is cooled further to some average temperature between T_{sat} and T_w . In equation (61) h_{fg} is substituted by h_{fg}^* .

Wavy Laminar Flow on Vertical Plates

At Reynolds numbers greater than about 30, it is observed that waves form at the liquid-vapor interface although the flow in liquid remains laminar. The flow in this case is said to be wavy laminar. The waves at the liquid-vapor interface tend to increase heat transfer. But the waves also complicate the analysis and make it very difficult to obtain analytical solutions. Therefore, we have to rely on the experimental studies. The increase in heat transfer due to wave effect is on the average about 20 percent but it can exceed 50 percent.

Kutateladze [51] recommended the following relation, based on his experimental studies, for the average heat transfer coefficient in wavy laminar condensate flow for $\rho_G \ll \rho_L$ and $30 < Re < 1800$,

$$h_{vert,wavy} = \frac{Re k_L}{1.08 Re^{1.22} - 5.2} \left(\frac{g}{v_L^2} \right)^{1/3} \quad (63)$$

A simpler alternative to the relation above proposed by Kutateladze [51] is

$$h_{\text{vert,wavy}} = 0.8\text{Re}^{0.11}h_{\text{vert(smooth)}} \quad (64)$$

Turbulent Flow on Vertical Plates

At a Reynolds number of about 1800, the condensate flow becomes turbulent. Several empirical relations of varying degrees of complexity are proposed for the heat transfer coefficient for turbulent flow. The Re relation in this case is given by

$$\text{Re} = \frac{4Q_{\text{conden}}}{\rho\mu_L h_{fg}^*} = \frac{4Ah(T_{\text{sat}} - T_w)}{\rho\mu_L h_{fg}^*} \quad (65)$$

Labuntsov [52] proposed the following relation for the turbulent flow of the condensate on vertical plates:

$$h_{\text{vert,turbulent}} = \left(\frac{\text{Re}k_L}{8750 + 58\text{Pr}^{-0.5}(\text{Re}^{0.75} - 253)} \left(\frac{g}{v_L^2} \right)^{\frac{1}{3}} \right), \quad \text{Re} > 1800, \rho_G \ll \rho_L \quad (66)$$

The physical properties of the condensate plate are to be evaluated at the film temperature $T_f = (T_{\text{sat}} + T_w)/2$.

For vertical tubes, the above equations for vertical plate can be used with height of tube as characteristic length.

4.2.2. Horizontal tubes and spheres

Nusselt's analysis of film condensation on the vertical plates can also be extended to horizontal tubes and spheres. The average heat transfer coefficient for film condensation on the outer surfaces of a horizontal tube is determined to be

$$h_{\text{horiz}} = 0.729 \left[\frac{g\rho_L(\rho_L - \rho_G)h_{fg}^*k_L^3}{\mu_L(T_{\text{sat}} - T_w)D} \right]^{1/4} \quad (67)$$

This relation can be modified for the sphere by replacing the constant 0.729 by 0.815.

A comparison of the heat transfer coefficient relations for a vertical tube of height L and a horizontal tube of diameter D yields

$$\frac{h_{\text{vert}}}{h_{\text{horiz}}} = 1.29 \left(\frac{D}{L} \right)^{1/4} \quad (68)$$

Setting $h_{\text{vert}} = h_{\text{horiz}}$ gives $L = 1.29^4 D = 2.77D$, which implies that for a tube whose length is 2.77 times its diameter, the average heat transfer coefficient for laminar film condensation will be the same whether the tube is positioned horizontally or vertically. For $L > 2.77D$, the heat transfer coefficient will be higher in a horizontal position. Considering that the length of a tube in any practical application is several times its diameter, it is common practice to place the tubes in a condenser horizontally to maximize the condensation heat transfer coefficient on the outer surfaces of the tubes.

4.2.3. Horizontal tube banks

Horizontal tubes stacked on top of each other are commonly used in condenser design. The average thickness of the liquid film at the lower tubes is much larger as a result of condensate falling on top of them from the tubes directly above. Hence the average heat transfer coefficient at the lower tubes in such arrangements is smaller. Assuming the condensate from the tubes drain smoothly to the tubes below it, the average film condensation heat transfer coefficient for all the tubes in a vertical tier can be expressed as [53]

$$h_{\text{horiz, Ntubes}} = 0.729 \left[\frac{g \rho_L (\rho_L - \rho_G) h_{fg}^* k_L^3}{\mu_L (T_{\text{sat}} - T_w) N D} \right]^{1/4} = \frac{1}{N^{1/4}} h_{\text{horiz, 1tube}} \quad (69)$$

where, N = No. of tubes

This relation doesn't take into account the increase in heat transfer due to the ripple formation and turbulence caused during drainage and thus generally yields conservative results.

4.2.4. Condensation inside horizontal tubes

So far we have discussed film condensation on the outer surfaces of tubes and other geometries which is characterized by negligible vapor velocity and unrestricted flow of the condensate. Heat transfer analysis of condensation inside tubes is complicated by the fact that it is strongly influenced by vapor velocity and the rate of liquid accumulation on the walls of the tubes.

For low vapor velocities Chato [54] recommends the following expression for condensation

$$h_{\text{internal}} = 0.555 \left[\frac{g \rho_L (\rho_L - \rho_G) k_L^3}{\mu_L (T_{\text{sat}} - T_w)} \left(h_{fg} + \frac{3}{8} C_{pL} (T_{\text{sat}} - T_w) \right) \right]^{1/4} \quad (70)$$

for

$$\text{Re}_G = \left(\frac{\rho_G V_G D}{\mu_G} \right)_{\text{inlet}} < 35,000 \quad (71)$$

where, Reynolds number for vapor is to be evaluated at the tube inlet conditions using the internal tube diameter as the characteristic length. T_L is the liquid temperature and is average of the wall and saturated steam temperatures.

4.2.5. Effect of the presence of noncondensable gases

In nuclear reactors, the condensation of steam in presence of noncondensable gas becomes an important phenomenon when steam released from the core mixes with the containment air following a Loss of Coolant Accident. Steam condenses in presence of noncondensable gas when flowing inside the vertical tubes of passive containment coolers. The drastic reduction in the condensation heat transfer coefficient in the presence of noncondensable gas can be explained as follows: When the vapor mixed with a noncondensable gas condenses, the noncondensable gas remains in the vicinity of the condensate layer. This gas acts as a barrier between the vapor and the condensate layer as shown in Fig. 10 and makes it difficult for the vapor to reach the surface. The vapor now must diffuse through the noncondensable gas first before reaching the surface and this reduces the effectiveness of the condensation process. Most condensers used in power plants operate at pressure below the atmospheric pressure and operation at such a low pressure raises the possibility of air leaking into the

condensers. Variation of heat transfer coefficient with non-condensable mass fraction is shown in Fig. 11 [55].

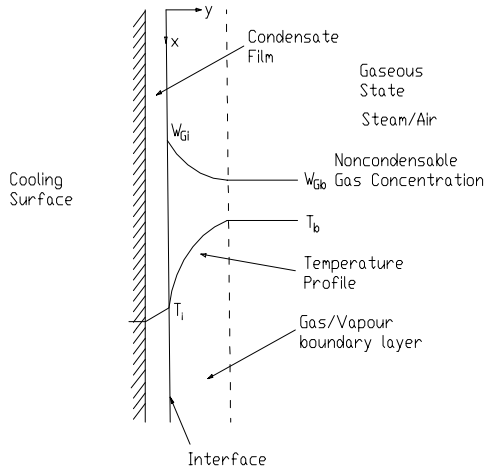


FIG. 10 Condensation in presence of non-condensables.

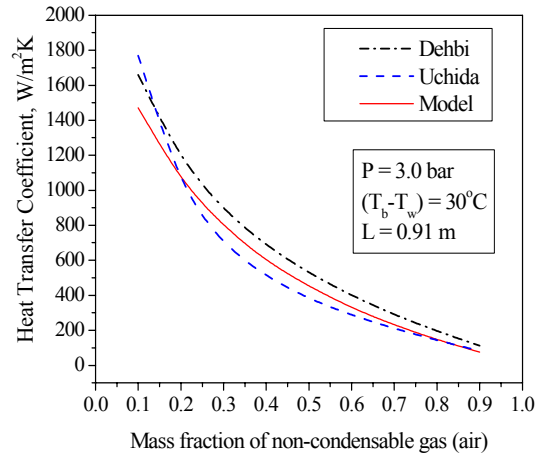


FIG. 11. Heat transfer coefficient vs. mass fraction (Maheshwari et al. (2004)).

Condensation when steam/noncondensable mixture is nonflowing

There are number of correlations available in the literature. Some of the correlations developed are given below.

The correlation developed by Uchida [56]

$$h_{\text{Uchida}} = 380 \left(\frac{W_{\text{nc}}}{1 - W_{\text{nc}}} \right)^{-0.7} \quad (72)$$

where, W_{nc} is the noncondensable mass fraction in the steam/noncondensable mixture. Experiments performed by Uchida were in fixed volumes with constant inventories of non-condensable gas (at atmospheric pressure). Wall temperature was held constant.

The Dehbi correlation [57]

$$h_{\text{Dehbi}} = \frac{L^{0.05} [(3.7 + 28.7P_{\text{tot}}) - (2438 + 458.3P_{\text{tot}})\log W_{\text{nc}}]}{(T_b - T_w)^{0.25}} \quad (73)$$

This correlation is applicable for the following conditions

$$\begin{aligned} 0.3 \text{ m} < L < 3.5 \text{ m} \\ 1.5 \text{ atm.} < P_{\text{tot}} < 4.5 \text{ atm.} \\ 10 \text{ }^\circ\text{C} < (T_b - T_w) < 50 \text{ }^\circ\text{C} \end{aligned}$$

Condensation when steam / noncondensable gas flowing inside vertical tube

For the calculation of condensation heat transfer coefficient, h_c , the correlation developed by Siddique [58] is given as

$$\text{Nu}(x) = 1.137\text{Re}_G^{0.404} W_a^{-1.105} \text{Ja}^{-0.741} \quad (74)$$

which applies in the following range of experiments

0.1	<	W_a	<	0.95
445	<	Re_G	<	22700
0.004	<	Ja	<	0.07

W_a is the air mass fraction in the steam/air mixture. The Jakob number, Ja , $C_{pG} (T_b - T_{wi})/h_{fg}$, is defined as the ratio of the sensible energy transfer in the vapor to phase change energy.

4.2.6. Thermal stratification

Thermal stratification as the name suggests, denotes formation of horizontal layers of fluid of varying temperature with the warmer layers of fluid placed above the cooler ones. Thermal stratification is encountered in large pool of water increasingly being used as heat sink in new generation of advanced reactors. In these reactors passive systems are being used to remove decay heat from primary system as well as heat energy released into the containment. In both the cases, a large pool of water acts as the heat sink. Stratification influences heat transfer to pool to a great extent and heat storage capacity of the pool in the form of sensible heat is significantly reduced.

When a heat source is placed vertically in a pool of water, the fluid adjacent to the source gets heated up. In the process, its density reduces and by virtue of the buoyancy force, the fluid in this region moves up. After reaching the top free surface, the heated water takes a turn, moves towards the wall of the pool along the surface. Since, density of this heated water is low, it does not flow downward. If a vertical sink is provided, downward flow takes place in a narrow region adjacent to the sink. Over a period of time, depending on the size and geometry of the pool and the source, the greater part of the pool gets thermally stratified except the regions close to the heat source and the heat sink. In the region of the thermal stratification fluid is almost static.

The forces involved in the flow field described above are buoyancy force, viscous force and inertia force. In many cases, one has to consider surface tension and turbulence. In case of free surface, mass transfer and heat transfer are to be considered at the free surface.

Towards the understanding of the complex flow pattern in a pool, one of the commonly studied approaches is the study of natural convection in heated enclosures. The enclosures are either differentially heated (with one wall heated and the other wall cooled) or symmetrically heated (both the walls equally heated while heat dissipation to atmosphere is allowed at the top). The bottom and top walls are kept adiabatic in the former case while only the bottom wall is maintained adiabatic in the latter case. The studies have indicated the importance of few parameters governing the flow phenomenon like Rayleigh number, Prandtl number and the aspect ratio of the enclosure (the ratio of height to the width of the enclosure). Depending on the magnitude of the Rayleigh number, the flow can be laminar or turbulent. Using finite volume techniques, transient CFD models are being developed for several of these cases for the prediction of flow patterns and temperature profiles. In particular, the stress is on developing better turbulence models, which require optimum computational effort and are satisfactorily accurate. For validation of theoretical results, experimental data are being generated.

A typical velocity profile in a side heated enclosure is shown in Fig. 12. From this figure, it may be noted that close to the top surface a narrow horizontal loop is formed. For the same case, the temperature profile obtained by Satish Kumar et al [59] is shown in Fig. 13. Similar observations are reported by Das and Dutta [60].

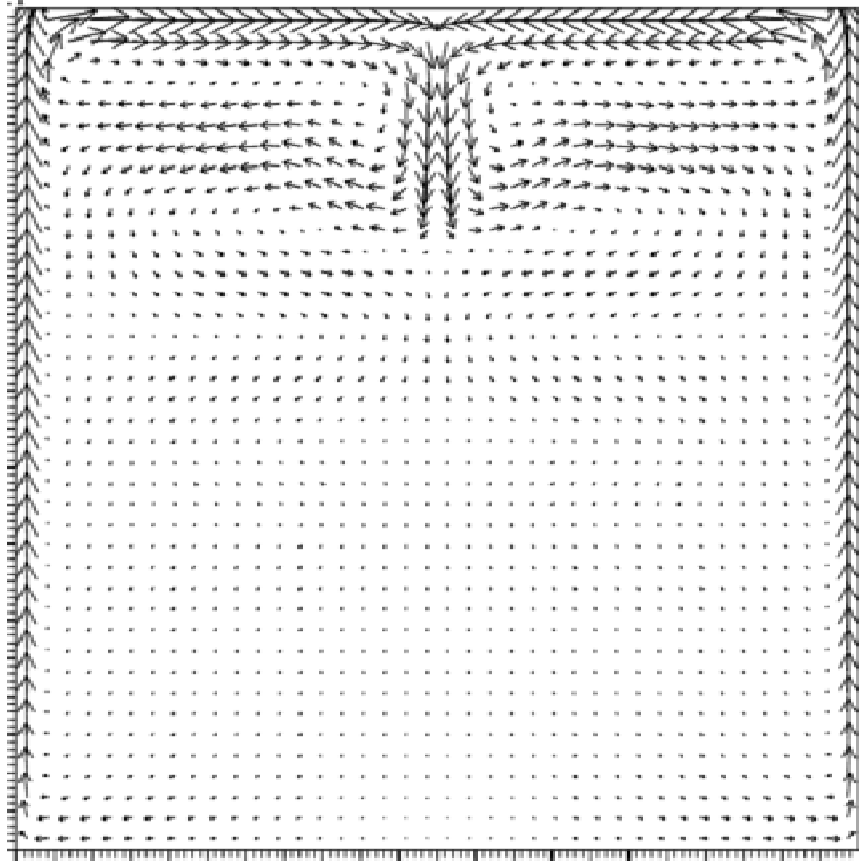


FIG. 12. Velocity plots.

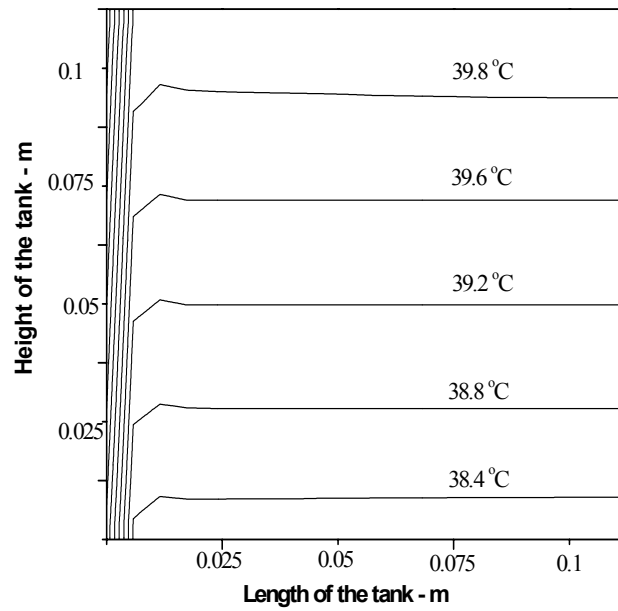


FIG. 13. Isotherms in the left half of tank after 15000 sec (case-1).

5. OTHER RELEVANT PHENOMENA

Aksan et. al. [61] have provided an extensive list of important thermal hydraulic phenomena for advanced reactor designs. Out of these, phenomena relevant for natural circulation are included in this section.

5.1. Carryover

Water in the form of droplets may get carried over with steam to the turbine, which can be detrimental to turbine because of erosion of turbine blades. Two-phase mixture leaving the core of the reactor enters the steam drum through risers (Fig. 14). Normally steam –water separation is effected in steam drum or steam generator using suitably designed mechanical separators. Since, pressure drop across mechanical separators is quite large, in natural circulation systems steam – water separation is effected by gravity without using mechanical separators. This may result in liquid carryover with the steam to the turbine. Carryover to the turbine is to be restricted to a permissible maximum of about 0.2%, by incorporating appropriate measures at the design stage, and hence, should be predicted accurately under different operating conditions.

Droplet carryover is a phenomenon associated with droplet entrainment, which is an outcome of dynamic interaction of two phases in relative motion. Various researchers have studied entrainment and two categories of entrainment are identified as film entrainment and pool entrainment. Film entrainment is entrainment of droplets from the liquid film by various mechanisms like roll wave shear-off and is typified by presence of a wavy interface of liquid film and vapor, broadly along the direction of flow. Dispersed annular flow is the typical flow regime exemplifying the film entrainment. On the other hand, pool entrainment is entrainment of droplets from the surface of pool due to bursting of bubbles and break-up of liquid jet. Pool entrainment is typified by the presence of liquid pool and turbulent liquid vapor flow. Modeling the entrainment requires the appropriate droplet formation mechanism, and prediction of average or maximum droplet size distribution function.

Film Entrainment Models and pool entrainment models are used to determine carryover. Zuber [62] studied entrainment associated with droplet formation due to bursting of bubbles on the surface of liquid pool and break-up of liquid jets. Ishii and Kataoka [63] have proposed the entrainment at the surface of pool as a function of physical properties. Entrainment is found to be a function of steam velocity and height from the free surface.

5.2. Carryunder

Carryunder is the entrainment of gas bubbles with the recirculating liquid (Fig. 14). Carryunder is particularly undesirable in a natural circulation system due to impaired thermal-margin, since the driving potential for the flow is density difference between hot and cold legs.

Carryunder depends on bubble dynamics as well as the geometrical configuration of flow path. Bubble dynamics is governed by various forces acting on the moving bubbles, of which the drag force is most significant and most uncertain to predict because of uncertainties in drag coefficient. Various researchers have empirically obtained the drag coefficient for various flow regimes. Geometrical parameters affecting the entrainment are the baffle spacing and liquid level with respect to baffle tip. Increasing the baffle spacing first increase the Carryunder due to large inter-baffle space available for entrainment and then decrease due to very low liquid velocity in the inter-baffle space. Thus with regard to baffle space, Carryunder may be attributed to area dominated regime and velocity dominated regime.

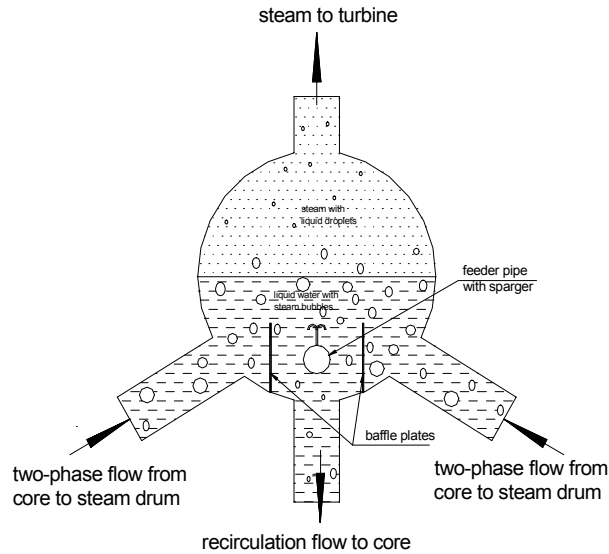


FIG. 14. Schematic of steam drum depicting carryover & carryunder.

5.3. Parallel channel effect

In respect of natural circulation, interaction between multiple parallel flow paths may become a critical phenomenon mainly in respect of instability. Presence of multiple parallel channels connected to two plenums and having different heat fluxes offer the possibility of number of flow configurations in which some channels may have flow direction opposite to others and some may even stagnate. Another important phenomena related to parallel channel instability is the oscillation in one group of channels 180° out of phase with oscillation in another group. This phenomenon is of special concern since this instability may not be detectable by monitoring total flow in the loop.

5.4. Effect of non-condensable gases

Containment:

Containment is the final physical barrier to prevent release of radioactivity to environment. To maintain structural integrity of the containment it is necessary to remove energy released into the containment under accidental condition. Passive containment coolers are commonly used for condensation of steam released into the containment. In some advanced designs, building condensers are provided at the top of the containment. The performance of these condensers are highly impaired by the presence of non-condensables. Besides air present in the containment, depending on the severity of accident, hydrogen may also get released into the containment. It is necessary to predict distribution of hydrogen, steam and air in the containment to assess the performance of the condensers. Potential stratification and separation of steam and non-condensables constitute an important factor for containment cooling. Many experiments have been conducted and various computer codes developed to predict the distribution of steam and non-condensables and the performance of condensers [64].

Primary Loop:

Non-condensables, if released into a loop may get accumulated at specific locations depending on the configuration and can inhibit natural circulation. For instance, in a PHWR non-condensables may

accumulate at the U-bend at the top of the inverted U tubes of steam generators since the driving head is low under accidental conditions. This may reduce or completely stop flow through the tube.

5.5. Vortex formation in pool

As stated earlier, in many advanced reactor design a large pool of water is provided which acts as a heat sink for many passive heat removal systems and/or source for low pressure injection of coolant into the core under accidental condition. Flow of water by gravity through small outlet pipes of these pools may lead to vortex formation [61]. Depending on the orientation of the outlet port and the depth of water above the port air or gas from top of pool may get entrained into the water. Presence of these non- condensables in cooling water will have adverse effect on core cooling.

5.6. Fluid mixing

Under accidental condition, coolant entering the pressure vessel of a PWR through inlet nozzle may have temperature and boron concentration different from the temperature and boron concentration of water present in downcomer. In absence of proper mixing, difference in temperature may lead to unacceptable thermal gradient affecting structural integrity. Difference in boron concentration may cause boron-diluted coolant to enter the core resulting in reactivity insertion. In recent years, renewed focus has been placed on the study of these accident scenarios. More emphasis is placed on fluid mixing phenomena taking place during boron dilution and thermal transients. Extensive experimental and theoretical studies have been conducted in this area [65].

5.7. Counter-current flow limitation (CCFL)

The onset of flooding or countercurrent flow limitation (CCFL) determines the maximum rate at which one phase can flow countercurrently to another phase. The thermal-hydraulic analysis of countercurrent two-phase flow has been of great importance in connection with the safety analysis of nuclear reactor systems. In the event of a loss of coolant accident (LOCA), steam is produced in the core of a pressurized water reactor (PWR). This steam flows upward through the hot leg, moving countercurrently to the flow of injected emergency core cooling water (Fig. 15). Steam condensed in the steam generator also flows back to the core. The cooling water should be able to flow, past the upcoming steam, into the core. However, this emergency core cooling (ECC) is limited by the flooding phenomenon that partly or totally inhibits the water flow into the core. To evaluate the effectiveness of ECC it is necessary to study countercurrent flow of the phases. Somchai Wangwises [66] has carried out extensive work on two-phase countercurrent flow in a model of PWR hot leg. The CCFL has been studied by a large number of researchers, both experimentally and analytically, mostly in vertical pipes. The CCFL in horizontal or nearly horizontal geometries has received comparatively little attention in the literature. H.T. Kim [67] has studied CCFL in horizontal-to-inclined pipes simulating a PWR hot leg. The study revealed the effect of L/D of pipes on CCFL phenomena.

6. CONCLUSIONS

An account of various phenomena encountered in the natural circulation systems of a nuclear reactor is provided. Thermohydraulic relationships related to these phenomena are given as examples. References are given that contain more relationships covering wider range of parameters to choose from. Some of the phenomena are briefly described. For these phenomena, references are given which will provide deeper insight into these phenomena.

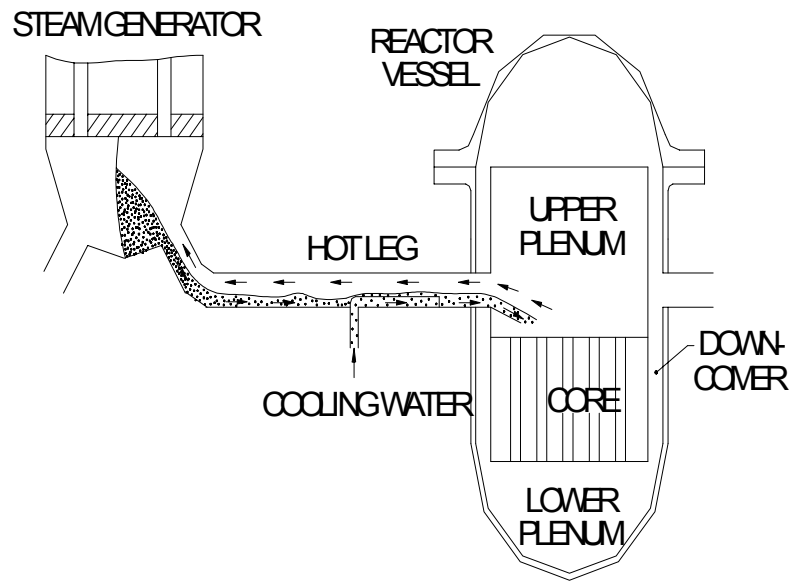


FIG. 15 Countercurrent flow of steam and cooling water in hot leg of PWR.

NOMENCLATURE

A	- flow area, heat transfer area
A_r	- flow area ratio (<1)
A_g	- projected grid cross section
Bo	- boiling number ($q/G h_{fg}$)
c/s	- cross section
Co	- convection number
C_f	- friction coefficient
C_d	- drag coefficient
C_p	- specific heat
C_v	- modified loss coefficient
C_0	- distribution coefficient
D, d	- diameter
D_e	- equivalent diameter
e	- absolute roughness
F	- correction coefficient, geometrical factor, enhancement factor
Fr	- Froude Number
f	- friction factor
f_l	- laminar friction factor
f_t	- turbulent friction factor
f_R	- reference friction factor
G	- mass flux
G_{SL}	- superficial liquid mass flux ($\rho_L j_L$)
g	- gravitational acceleration
H	- wire pitch
ΔH	- subcooling
h	- heat transfer coefficient, enthalpy
h_{fg}, h_{LG}	- latent heat
I	- specific enthalpy
j	- volumetric flux
Ja	- Jakob number
K	- loss coefficient
k	- thermal conductivity
L	- length
\dot{m}	- condensate mass flow rate
N	- power
Nu	- Nusselt Number
Pr	- Prandtl Number
p_t	- rod pitch
P, p	- pressure, perimeter
p	- wetted perimeter
q	- heat flux
Q	- heat flow rate
Re	- Reynolds Number
S	- slip ratio, suppression factor
T	- temperature
t	- thickness
u	- velocity
u_R	- reference velocity
U	- perimeter
V	- velocity
v	- specific volume
W	- mass flow rate, mass fraction
x	- mass quality, distance

Z - length, elevation

Greek Symbols

α - void fraction
 θ - angle of direction of flow with vertical
 β - homogeneous void fraction
 Δ - difference
 δ - thickness of film
 ϕ^2 - two phase friction multiplier
 μ - dynamic viscosity
 ρ - density
 σ - surface tension
 χ - Martinelli parameter
 ν - kinematic viscosity

Subscripts

a - acceleration, air
av, ave - average
B - bundle
b - bulk
cir - circular
crit - critical
conden- condensation
d - driving
DO - dryout
e - elevation
f - film, frictional
G - vapour
g - gas
GO - gas only
h - hydraulic
H - heated
horiz - horizontal
i - inlet, interface
L - liquid
LO - liquid only
l - local
m - mean
o - outlet
nc - noncondensable
R - relative
s - spacer
sat - saturated
SPF - single-phase flow
TP, TPF- two-phase flow
tot - total
vert - vertical
w - wall

ACKNOWLEDGEMENTS

The author wishes to thank IAEA and its consultants for the valuable suggestions provided. Thanks are also due to Mr. N.V. Satish Kumar and Mr. N.K. Maheshwari of RED, BARC for the help rendered in preparing this note.

REFERENCES

- [1] INTERNATIONAL ATOMIC ENERGY AGENCY, Thermophysical Properties of Materials for Water Cooled Reactors, IAEA-TECDOC-949, Vienna (1997).
- [2] MOCHIZUKI, Y., ISHII, Y., Study of thermohydraulics relevant to natural circulation in ATR, Proceedings of the fifth International Topical meeting on Reactor Thermal Hydraulics, vol. I, 127-134 NURETH-5, Salt Lake City, USA (1992).
- [3] ARMAND, A.A., TRESCHÉV, G.G., "Investigation of the Resistance During the Movement of Steam-Water mixtures in Heated Boiler Pipes at High Pressure", *Izv. Ves. Teplotekh. Inst.*; 4, 1–5 (1947).
- [4] INTERNATIONAL ATOMIC ENERGY AGENCY, Thermohydraulic Relationships for Advanced Water Cooled Reactors, IAEA-TECDOC-1203, Vienna (2001).
- [5] CHEXAL, B., MAULBETSCH, J., SANTUCCI, J., HARRISON, J., JENSEN, P., PETERSON, C., LELLOUCHE, G., HOROWITZ, J., "Understanding void fraction in steady and dynamic environments", TR-106326 / RP-8034-14, Electric Power Research Institute, 3412 Hillview Avenue, Palo Alto, California (1996).
- [6] BLASIUS, H., *Mitt. Forsch. Geb. Ing.-Wesen*, 131 (1913).
- [7] COLEBROOK, C.F., "Turbulent Flow in Pipes with Particular Reference to the Transition Region Between the Smooth and Rough Pipe Laws", *J. Inst. Civ. Eng. Lond.*; 133–156 (1938).
- [8] FILONENKO, G.K., On friction factor for a smooth tube, All Union Thermotechnical Institute (*Izvestija VTI*, No. 10), Russia (1948).
- [9] KNUDSEN, J.G., KATZ, D.L., *Fluid Dynamics and Heat Transfer*, p. 178, McGraw-Hill Book Company, Inc.; New York (1958).
- [10] LEUNG, L.K.H., GROENEVELD, D.C., AUBE, F., TAPUCU, A., New studies of the effect of surface heating on frictional pressure drop in single-phase and two-phase flow, NURETH-3, Grenoble, France (1993).
- [11] CICCHITTI, A., LOMBARDI, C., SILVESTRI, M., SOLDAINI, G., ZAVATTARELLI, R., "Two-phase cooling experiments: pressure drop, heat transfer and burnout experiments", *Energia Nucleare*, 7, 407–425 (1960).
- [12] LOTTES, P.A., FLINN, W.S., A Method of Analysis of Natural Circulation Boiling Systems, *Nuclear Science Eng.*; 19(2), 91-99 (1956).
- [13] MARTINELLI, R.C., NELSON, D.B., Prediction of pressure drop during forced-circulation boiling of water, *Trans. ASME*, 70, 695–702 (1948).
- [14] LEUNG, L.K.H., GROENEVELD, D.C., Frictional pressure gradient in the pre- and post-CHF heat-transfer regions, *Multiphase flows' 91*, Tsukuba, Sept. 24–27, 1991, Tsukuba, Japan (1991).
- [15] TARASOVA, N.V., et. al., Pressure drop of Boiling Subcooled Water and Steam Water Mixture Flowing in Heated Channels, Proceedings of 3rd Int. Heat Transfer Conf. 178, ASME (1966).
- [16] KOEHLER, W., KASTNER, W., Two phase pressure drop in boiler tubes, *Two-Phase Flow heat Exchangers: Thermohydraulic Fundamentals and Design*, Editors: S. Kakac, A.E. Bergles E.O. Fernandes, Kluwer Academic Publishers (1988).
- [17] VIJAYAN, P.K., SAHA, D., VENKAT RAJ, V., Measurement of pressure drop in PHWR fuel channel with 19 rod bundles (wire-wrap type) at low Reynolds numbers, BARC/I-811 (1984).
- [18] PILKHWAL, D.S., VIJAYAN, P.K., VENKAT RAJ, V., Measurement of pressure drop across the junction between two 37 rod fuel bundles for various alignments of the bundles, Proceedings of 19th National Conference on Fluid Mechanics and Fluid Power, IIT, Powai, Bombay, India (1992).
- [19] REHME, K., Systematische experimentelle Untersuchung der Abhängigkeit des Druckverlustes von der geometrischen Anordnung für längs durchströmte Stabbündel mit Spiraldraht-Abstandshaltern', *KfK*, Rep. 4/68-16 (1968).
- [20] REHME, K., Druckverlust in Stabbündeln mit Spiraldraht-Abstandshaltern", *Forsh. Ing.-Wes.* 35 Nr.4 (1969).
- [21] KAYS, W.M., *Convective Heat and Mass Transfer*, Tata-McGraw Hill Publishing Company Ltd.; New Delhi (1975).
- [22] DIESSLER, G., TAYLOR, M.F., Analysis of Axial Turbulent Flow Heat transfer Through Banks of rods or Tube, Reactor Heat Transfer Conference, TID-7529, Volume 2 (1956).

- [23] LOMBARDI, C., CARSANA, C.G., A dimensionless pressure drop correlation for two-phase mixtures flowing upflow in vertical ducts covering wide parameter ranges, *Heat and Technology*, 10, 125–141 (1992).
- [24] MARTINELLI, V., PASTORI, L., AMLETO - A Pressure drop computer code for LWR fuel bundles, RT/ING(73)11, Comitato Nazionale Energia Nucleare (CNEN) (1973).
- [25] IDELCHIK, I.E., *Hand Book of Hydraulic Resistances*, Hemisphere Publishing Company, New York (1986).
- [26] REHME K., Pressure Drop Correlations for Fuel Element Spacers, *Nuclear Technology*, 17, 15–23 (1973).
- [27] REHME, K., Pressure Drop of Spacer Grids in Smooth and Roughened Rod Bundles, *Nuclear Technology*, 33, 313–317 (1977).
- [28] CEVOLANI, S., “ENEA Thermohydraulic Data Base for the Advanced Water Cooled Reactor Analysis”, 1st Research Co-ordination Meeting of IAEA CRP on Thermohydraulic Relationships for Advanced Water Cooled Reactors, Vienna (1995).
- [29] GRILLO, P., MARINELLI, V., Single and Two-Phase Pressure Drops on a 16-ROD Bundle, *Nuclear Applications & Technology*, 9, 682–693 (1970).
- [30] LOTTES, P.A., Expansion losses in two-phase flow, *Nuclear Science Eng.*, 9, 26–31 (1961).
- [31] CHISHOLM, D., SUTHERLAND, L.A., “Prediction of Pressure Gradient in Systems During Two-phase Flow”, *Inst. of Mechanical Engineers, Symposium in Two-phase Flow Systems*, Univ. of Leeds (1969).
- [32] FITZSIMMONS, D.E., Two-phase pressure Drop in Piping Components, Hanford Laboratory Report”, HW-80970 (1964).
- [33] ECKERT, E.R.G. and DRAKE JR., R.M., *Analysis of Heat & Mass Transfer*, McGraw-Hill (1972).
- [34] DITTUS, F.W. and BOELTER, L.M.K., *University California Publs. Eng.*, Vol.2, p 443 (1930).
- [35] SIEDER, E.N. and TATE, G.E., Heat Transfer and Pressure Drop of Liquids in Tubes, *Industrial Engineering Chemistry*, 28, 1429–1435 (1936).
- [36] COLLIER, J.G., *Convective Boiling and Condensation*, McGraw-Hill, London (1981).
- [37] KANDLIKAR, S.G., A General Correlation for Saturated Two-Phase Flow Boiling Heat Transfer Inside Horizontal and Vertical Tubes, *Journal of Heat Transfer*, Vol. 112, 219–227 (1990).
- [38] CHEN, J.C., “A Correlation for Boiling Heat Transfer to Saturated Fluids in Convective Flow”, *Industrial and Engineering Chemistry, Process Design and Development*, Vol.5, No.3, 322–329 (1966).
- [39] FORSTER, H.K and ZUBER, N., Dynamics of Vapour Bubbles and Boiling Heat Transfer, *Journal of AIChE*, Vol.1, 531–535 (1955).
- [40] CHEN, J.C, “A Correlation for Boiling Heat Transfer to Saturated Fluid in Convective Flow”, *ASME Paper 63-HT-34* (1963).
- [41] JENS, W.H., LOTTES, P.A., Analysis of Heat Transfer, Burnout, Pressure Drop and Density Data for High Pressure Water, ANL-4627 (1951).
- [42] HEWITT, G.F.; HALL-TAYLOR, N.S., *Annular two-phase flow*, New York, NY, Pergamon Press (1970).
- [43] WEISMAN, J., PEI, B.S., Prediction of Critical Heat Flux in flow boiling at low quality conditions, *International Journal of Heat Mass Transfer* 26 (1463) (1983).
- [44] KUTATELADZE, S.S., Heat Transfer in Boiling and Condensation, USAEC Report AEC-Tr-3770 (1952).
- [45] GROENEVELD, D.C. et al., The 1996 Look-Up Table for Critical Heat Flux in Tubes, *Nuclear Engg. Design*, 163, 1–23 (1996).
- [46] TONG, L.S., Boiling crisis and critical heat flux, USAEC Rep. TID-25887 (1972).
- [47] YIN, S.T., GROENEVELD, D.C. and WAKAYAMA, M., The effect of radial flux distribution on critical heat flux in 37-rod bundles, *ANS Proceedings, 12th National Heat Transfer Conference*, Vol. 5, p.277–283 (Minneapolis, July 28–31) (1991).
- [48] WONG, Y.L., GROENEVELD, D.C., CHENG, S.C., CHF predictions in horizontal tubes, *International Journal of Multi-phase Flow* 16 (123) (1990).

- [49] PREMOLI, A., FRANCESCO, D., PRINA, A., An empirical correlation for evaluating two-phase mixture density under adiabatic conditions, European two-phase flow group meeting, Milan (1970).
- [50] NUSSELT, W., Die Oberflächenkondensation des Wasserdampfes, VDI Z. 60, 541-546, 569–575 (1916).
- [51] KUTATELADZE, S.S., Fundamentals of Heat Transfer, Academic Press, New York (1963).
- [52] LABUNTSOV, D.A., Heat Transfer in Film Condensation of Pure Steam on Vertical Surfaces and Horizontal tubes, Teploenergetika 4 (1957).
- [53] YUNUS, A., Heat transfer: A practical approach, McGraw-Hill, Boston (1998).
- [54] CHATO, J.C., “Laminar Condensation inside Horizontal and inclined Tubes.” ASHRAE Journal 4, p. 52 (1962).
- [55] MAHESHWARI, N.K., PATEL, A.G., VIJAYAN, P.K., SAHA, D. and ARITOMI, M., Evaluation of Free Convective Condensation Modeling in the Presence of Noncondensable Gas, Paper submitted at 5th International Conference on Multiphase Flow, Japan, May 30–June 4 (2004).
- [56] UCHIDA, H., OYAMA, A., TOGO, Y., Evaluation of Post-Incident Cooling Systems of Light-Water Power Reactors, Proc. Int. Conf. on peaceful Uses of Atomic Energy 13, 93–102 (1965).
- [57] DEHBI, A.A., “The Effect of Noncondensable Gases on Steam Condensation under Turbulent Natural Convection Conditions”, MIT Thesis, Dept. of Nucl. Engg., Massachusetts Institute of Technology (1991).
- [58] SIDDIQUE M., The Effects of Noncondensable Gases on Steam Condensation Under Forced Convection Conditions, PhD Thesis, Massachusetts Institute of Technology (1992).
- [59] SATISH KUMAR, N.V., MAHESHWARI, N.K., VIJAYAN, P.K., SAHA, D., SINHA, R.K., Studies on the Phenomenon of Thermal Stratification in a Side Heated Enclosures, 6th ISHMT-ASME Heat and Mass Transfer Conference and 17th National Heat and Mass Transfer Conference, IGCAR, Kalpakkam, India (2004).
- [60] DAS, S.P., DUTTA, P., Numerical and experimental study of thermal stratification in a side heated cavity, Proceedings of the fourth ISHMT-ASME Heat and Mass Transfer Conference, Pune, India (2000).
- [61] AKSAN, N., D’AURIA, F., “Status Report on Relevant Thermal hydraulic Aspects of Advanced Reactor Designs”, OCDE/GD(97)8 (1996).
- [62] ZUBER, N., YEHL, C.K. GORDAN, On the problem of liquid entrainment, ANL-6244 (1960).
- [63] ISHII, M., KATAOKA, I., Mechanistic modelling of pool entrainment phenomenon, International Journal of Heat Mass Transfer, Vol. 27, No.11, pp. 1999–2014 (1984).
- [64] MARTIN BERMEJO, J., VAN GOETHEM, G., Sponsored research activities on innovative passive safety systems, Nuclear Engineering and Design 201, 25–40 (2000).
- [65] KIGER, K.T., GAVELLI, F., Boron Mixing in Complex Geometries: Flow Structure Details, Nuclear Engineering and Design 208, 67–85 (2001).
- [66] SOMCHAI WONGWISES, Two-phase counter current flow in a model of a pressurized water reactor hot leg, Nuclear Engg. and Design, 166, 121–133 (1996).
- [67] KIM, HYOUNG TAE, NO, HEE CHEON, Assessment of RELAP5/MOD3.2.2 γ against flooding database in horizontal-to-inclined pipes, Annals of Nuclear Energy, 29, 835–850 (2002).

ANNEX 6

GOVERNING EQUATIONS IN TWO-PHASE FLUID NATURAL CIRCULATION FLOWS

J.N. Reyes, Jr.¹

International Atomic Energy Agency, Vienna

Abstract

This lecture presents the various models used to describe mass, momentum and energy transport processes in two-phase fluid flows related to natural circulation. By the conclusion of this lecture, the participant should have an understanding of the different types of thermal hydraulic transport models that have been implemented in nuclear reactor safety computer codes.

1. INTRODUCTION

The advent of high-speed computers has permitted analysts to develop computer models that can be applied to a wide range of complex thermal hydraulic studies. Certainly one of the more complex problems currently being studied involves the mass, momentum and energy transport in systems containing multiple phases (gas, liquid, and solids), multiple components (different chemical species) and multiple fields (continuous and dispersed geometries). This lecture provides an overview of the transport equations being applied in the study of two-phase transport behavior, particularly as related to nuclear reactor safety thermal hydraulics. Section 2 summarizes the one-dimensional differential conservation equations for two-phase flow and examines the models used in reactor safety analyses. However, before delving into the details of the various two-phase flow conservation equations, it would be useful to present a brief history of the development of nuclear reactor safety computer codes in the United States.

1.1. Brief history of U.S. nuclear reactor safety computer codes

The FLASH computer code, developed by Westinghouse-Bettis, is the earliest formally documented computer code used in nuclear reactor safety analysis in the United States of America [1]. As shown in Figure 1, this code used a very simple “node and branch” approach to modeling suitable for some studies of single-phase flow in PWRs. Each node consists of a control volume in which the time dependent mass and energy conservation equations are solved for a single-phase fluid. Each interconnecting line is modeled using the momentum conservation equation to take into account line resistance. Under steady-state conditions, the sum of the pressure drops around the loop would equal the sum of the buoyancy terms. The FLASH code served as the early basis for the RELAP series of computer codes.

From 1955 to 1975, numerous studies of boiling heat transfer and two-phase flow were conducted leading to significant breakthroughs in the modeling of two-phase flow. One of the pioneering efforts in the mid-1960s was Zuber’s development of the drift flux model. The success of his approach led to major advancements in code development.

¹ Henry and Janice Schuette Endowed Chair Professor of Nuclear Engineering, Department of Nuclear Engineering and Radiation Health Physics, Oregon State University, Corvallis, Oregon, USA, 97331. Funded by Oregon State University Sabbatical Leave, U.S. Department of Energy, and IAEA.

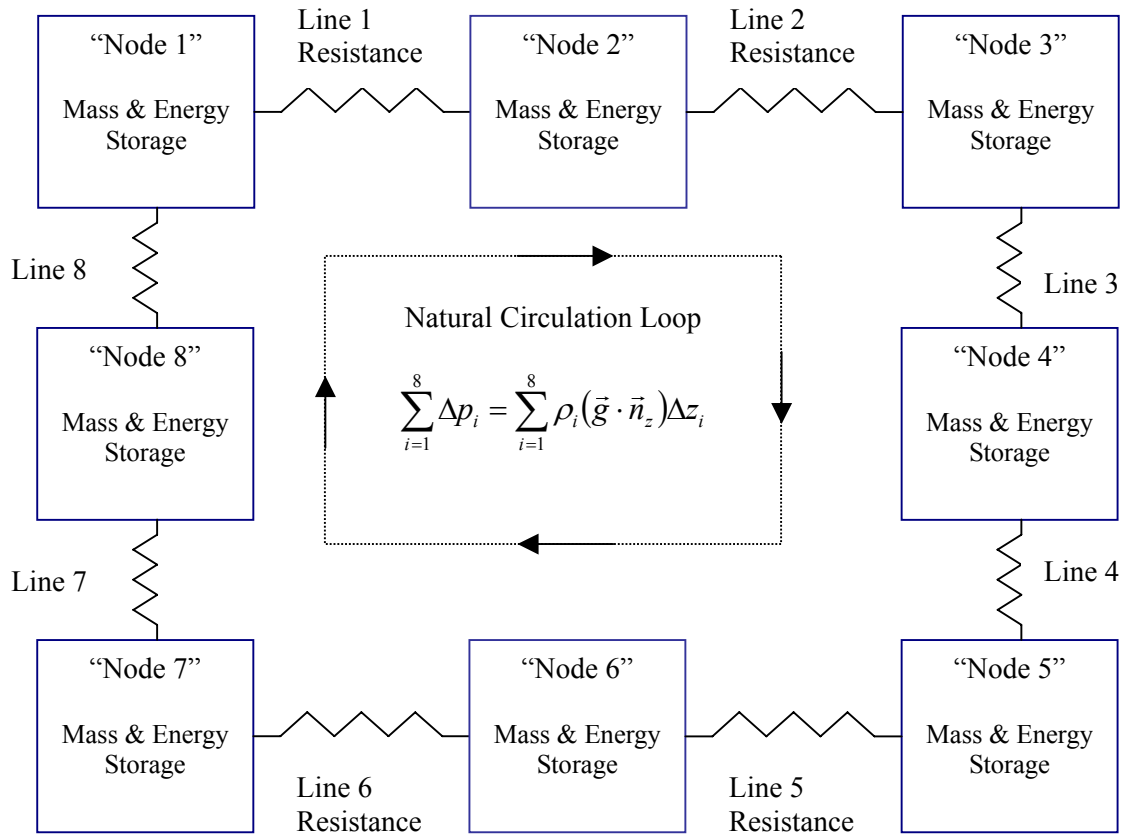


FIG. 1. Early computer modeling method used by westinghouse-bettis FLASH code to assess PWR safety.

From the early 1970s to the present, the U.S. Nuclear Regulatory Commission helped to support the development of a number of computer codes to predict loss of coolant accident (LOCA) phenomenon. These included RELAP2, RELAP3, RELAP3B (BNL), RELAP4, RELAP5, TRAC-PF1, TRAC-PD1, TRAC-BF1, RAMONA-3B, THOR, RAMONA-3B, RAMONA-4B, HIPA-PWR and HIPA-BWR. The Los Alamos National Laboratory held responsibility for the TRAC codes (with the exception of TRAC-BF1), the Idaho National Engineering Laboratory and Energy Incorporated (an Idaho-based consulting company) were responsible for the RELAP codes, and Brookhaven National Laboratory was responsible for THOR, RAMONA and HIPA codes.

TRAC, RELAP5 and RAMONA were recognized as the advanced simulation computer codes for PWR and BWR plants safety analysis and are currently being used for best-estimate calculations of plant behavior. In 1996, the NRC decided to produce an analysis package that combined the capabilities of RELAP5, TRAC-PWR, TRAC-BWR, and RAMONA. The software package, known as the TRAC/RELAP Advanced Computational Engine or TRACE, is currently under development by the NRC.

2. TWO-PHASE FLOW TRANSPORT EQUATIONS

Accurately describing the transport of mass, momentum and energy in a two-phase fluid flowing through a complex geometry, such as a nuclear reactor core, while undergoing phase change, is a formidable task. Nonetheless, this is only part of the challenge laid before the nuclear reactor safety analyst. Coupling the thermal hydraulic behavior to the core physics (which will not be discussed

here) further confounds the effort to obtain an accurate safety assessment tool. This chapter has the relatively straightforward goal of providing the reader with an overview of the different formulations of the two-phase flow transport equations as used in a variety of reactor analysis codes. The following section presents the one-dimensional two-fluid conservation equations that serve, either directly or through the development of the mixture equations, as the basis for the development of the remaining models.

2.1. One-dimensional two-fluid full non-equilibrium transport equations

This section presents the differential formulation of the one-dimensional, two-fluid, full non-equilibrium transport equations. The definition of each symbol is provided in the nomenclature. The formulation is similar to that of Todreas and Kazimi (1993) [2] with the exception of the fluid-structure transport terms.

The first transport equation considered is the conservation of mass for each phase. It is given by:

Mass Conservation Equation

$$\frac{\partial}{\partial t} \{ \rho_k \alpha_k \} + \frac{\partial}{\partial z} \{ \rho_k v_k \alpha_k \} = \Gamma_k \quad (1)$$

The subscript “k” indicates either liquid phase, when the subscript is set to “l”, or vapor phase, when the subscript is set to “v.” The first term on the left hand side of the equation represents the time rate of change of the “area averaged” mass for a given fluid phase. In this equation, and those that follow, the fluid phase parameters have been averaged over the cross-sectional flow area. That is, given a fluid phase parameter, ψ_k , area averaging is performed as follows:

$$\{ \psi_k \} \equiv \frac{1}{A} \iint_A \psi_k dA \quad (2)$$

The second term on the left hand side represents the change in mass along the flow axis. The Γ_k term represents the liquid or vapor mass generated as a result of phase change. It is the interfacial mass transfer rate per unit volume. For example, Γ_v , would represent the rate at which vapor mass is generated per unit volume as a result of liquid evaporation. Similarly, Γ_l , may represent the rate at which liquid mass is generated per unit volume as a result of vapor condensation.

The conservation of momentum for each phase is given by:

Momentum Conservation Equation

$$\frac{\partial}{\partial t} \{ \rho_k v_k \alpha_k \} + \frac{\partial}{\partial z} \{ \rho_k v_k^2 \alpha_k \} = \{ \Gamma_k \bar{v}_{ks} \cdot \bar{n}_z \} + \sum_{i=1}^N \{ \bar{F}_{wk} \cdot \bar{n}_z \}_i - \frac{\partial}{\partial z} \{ p_k \alpha_k \} + \{ \bar{F}_{sk} \cdot \bar{n}_z \} + \{ \rho_k \alpha_k \} \bar{g} \cdot \bar{n}_z \quad (3)$$

The first term on the left hand side of the equation represents the time rate of change of the area averaged momentum for a given fluid phase. The second term on the left hand side represents the change in the momentum along the flow axis. The first term on the right hand side represents the rate of momentum transfer due to phase change. The term, $\bar{v}_{ks} \cdot \bar{n}_z$, is the interface velocity of phase k along the z-coordinate. It is a scalar that can be either positive or negative. The second term on the right hand side represents the sum of the fluid phase drag forces on the structures in the flow. The third term on the right hand side represents the pressure gradient along the axis of the flow. It is typically assumed that the vapor and liquid phases have equal pressures. However, the stability studies of Ransom and Hicks (1984) [3], [4] indicate that this assumption results in an ill-posed set of equations that may result in numerical instabilities. The fourth term represents the drag forces acting on the fluid phase interface. The last term represents the gravity forces acting in the direction of the flow.

The conservation of energy for each phase is given by:

Energy Conservation Equation

$$\frac{\partial}{\partial t} \{ \rho_k u_k^o \alpha_k \} + \frac{\partial}{\partial z} \{ \rho_k h_k^o v_k \alpha_k \} = \Gamma_k h_{ks}^o - \left\{ p_k \frac{\partial \alpha_k}{\partial t} \right\} + \sum_{i=1}^N \left\{ q_k'' \alpha_k \frac{P}{A} \right\}_i - \{ \rho_k g v_k \alpha_k \} + \{ Q_{sk} \} \quad (4)$$

The energy conservation equation can be expressed in a various forms. This equation is an energy balance expressed in terms of the stagnation energy, u_k^o , and stagnation enthalpy, h_k^o , which are defined as follows:

$$u_k^o = u_k + \frac{v_k^2}{2} \quad (5)$$

$$h_k^o = u_k^o + \frac{p_k}{\rho_k} \quad (6)$$

The stagnation energy is defined as the sum of the thermodynamic internal energy and the kinetic energy of the fluid phase. The stagnation enthalpy has the usual definition, however, it is expressed in terms of the stagnation energy.

The first term on the left hand side of the energy conservation equation represents the time rate of change of the area averaged energy for a given fluid phase. The second term on the left hand side represents the change in the energy along the flow axis. The first term on the right hand side of the equation represents the rate of energy transfer due to phase change. The second term on the right represents the pressure work associated with changes in void fraction. The third term on the right represents the sum of the heat transfer between the fluid phase and structures in the flow. The fourth term on the right represent work due to gravity and the last term on the right hand side represents interfacial heat transfer.

For liquid and vapor systems, equations (1), (3) and (4) represent the six conservation equations that serve as a starting point for two-phase flow computer models. These equations are summarized in Table 1. The following section illustrates how these equations can be used to obtain a set of two-phase fluid mixture transport equations.

Table 1. One-dimensional transport equations for a two phase fluid
(Uniform Density within each Phase, Constant Axial Cross-Sectional Area)

<p>Conservation Equations for Each Phase “k”</p> <p><i>Mass:</i></p> $\frac{\partial}{\partial t} \{\rho_k \alpha_k\} + \frac{\partial}{\partial z} \{\rho_k v_k \alpha_k\} = \Gamma_k$ <p><i>Momentum:</i></p> $\frac{\partial}{\partial t} \{\rho_k v_k \alpha_k\} + \frac{\partial}{\partial z} \{\rho_k v_k^2 \alpha_k\} = \{\Gamma_k \bar{v}_{ks} \cdot \bar{n}_z\} + \sum_{i=1}^N \{\bar{F}_{wk} \cdot \bar{n}_z\}_i - \frac{\partial}{\partial z} \{p_k \alpha_k\} + \{\bar{F}_{sk} \cdot \bar{n}_z\} + \{\rho_k \alpha_k\} \bar{g} \cdot \bar{n}_z$ <p><i>Energy: (Neglecting axial heat conduction and axial shear effect)</i></p> $\frac{\partial}{\partial t} \{\rho_k u_k^o \alpha_k\} + \frac{\partial}{\partial z} \{\rho_k h_k^o v_k \alpha_k\} = \Gamma_k h_{ks}^o - \left\{ p_k \frac{\partial \alpha_k}{\partial t} \right\} + \sum_{i=1}^N \left\{ q_k'' \alpha_k \frac{P}{A} \right\}_i - \{\rho_k g v_k \alpha_k\} + \{Q_{sk}\}$
--

2.2. Two-phase mixture transport equations

A typical approach to the analysis of two-phase flows is to use mixture equations. That is, the individual fluid phases are assumed to behave as a flowing mixture described in terms of a mixture properties. To obtain the two-phase fluid mixture transport equations using the transport equations given in Table 1, one must first recognize that interfacial transfer inside the mixture would not impact the overall mixture behavior. This is best described in terms of the following interfacial jump conditions:

Interfacial Jump Conditions:

Mass

$$\sum_{k=1}^2 \Gamma_k = 0 \quad (7)$$

Momentum:

$$\sum_{k=1}^2 (\Gamma_k \bar{v}_{ks} \cdot \bar{n}_z + \bar{F}_{sk} \cdot \bar{n}_z) = 0 \quad (8)$$

Energy:

$$\sum_{k=1}^2 (\Gamma_k h_{ks}^o + Q_{sk}) = 0 \quad (9)$$

By summing the balance equations for each phase given in Table 1 and applying the interfacial jump conditions, the six equations are reduced to three as shown in Table 2. The mixture properties have also been defined in Table 2. These three mixture equations served as the basis for the two-phase flow mixture models developed in the following chapter.

Table 2. One-dimensional two-phase mixture transport equations
(Uniform Density within each Phase)

Conservation Equations	
<i>Mixture Mass:</i>	$\frac{\partial \rho_m}{\partial t} + \frac{\partial G_m}{\partial z} = 0 \quad (10)$
<i>Mixture Momentum:</i>	$\frac{\partial G_m}{\partial t} + \frac{\partial}{\partial z} \left(\frac{G_m^2}{\langle \rho_m \rangle} \right) = - \sum_{i=1}^N F_{wi} - \frac{\partial p_m}{\partial z} - \rho_m g \cos \theta \quad (11)$
<i>Mixture Enthalpy: (Approximate)</i>	$\frac{\partial}{\partial t} \{ \rho_m h_m - p_m \} + \frac{\partial}{\partial z} \{ G_m \langle h_m \rangle \} = \sum_{i=1}^N q_i'' \frac{P_i}{A_i} + \frac{G_m}{\rho_m} \left(\sum_{i=1}^N F_{wi} + \frac{\partial p_m}{\partial z} \right) \quad (12)$
Mixture Properties	
	$\rho_m = \{ \rho_v \alpha + \rho_l (1 - \alpha) \} \quad (13)$
	$\langle \rho_m \rangle = \frac{G_m^2}{\{ \rho_v v_v^2 \alpha + \rho_l v_l^2 (1 - \alpha) \}} \quad (14)$
	$G_m = \{ \rho_v v_v \alpha + \rho_l v_l (1 - \alpha) \} \quad (15)$
	$h_m = \frac{\{ \rho_v h_v \alpha + \rho_l h_l (1 - \alpha) \}}{\rho_m} \quad (16)$
	$\langle h_m \rangle = \frac{\{ \rho_v h_v v_v \alpha + \rho_l h_l v_l (1 - \alpha) \}}{G_m} \quad (17)$
	$\langle v^2 \rangle_m = \frac{\{ \rho_v \alpha v_v^2 + \rho_l (1 - \alpha) v_l^2 \}}{\rho_m} \quad (18)$
	$\langle v^2 \rangle_m = \frac{\{ \rho_v \alpha v_v^3 + \rho_l (1 - \alpha) v_l^3 \}}{G_m} \quad (19)$
	$p_m = \{ p_v \alpha + p_l (1 - \alpha) \} \quad (20)$

2.2.1. Homogeneous Equilibrium Mixture (HEM) Transport Equations

The homogeneous equilibrium mixture (HEM) model is the simplest of the two-phase fluid transport models. The HEM transport equations are derived from the two-phase mixture equations by assuming that the velocity of each fluid phase is equal (homogenous) and that both phases are at saturated conditions. The assumption of equilibrium means that the thermodynamic properties of each fluid phase can be expressed as a function of saturation pressure. Table 3 presents the HEM transport equations.

Table 3. Homogeneous equilibrium mixture (HEM) transport equations

<p>Restrictions Imposed on Two-Phase Mixture Equations</p> <ul style="list-style-type: none"> • Thermal Equilibrium ($T_l = T_v = T_{SAT}$) or Saturated Enthalpies ($h_l = h_f$ and $h_v = h_g$) • Equal Phase Pressures ($p_l = p_v = p$) • Equal Velocities ($v_l = v_v = v_m$) 	
<p>Conservation Equations</p> <p><i>Mixture Mass:</i></p> $\frac{\partial \rho_m}{\partial t} + \frac{\partial}{\partial z}(\rho_m v_m) = 0 \quad (21)$ <p><i>Mixture Momentum:</i></p> $\frac{\partial}{\partial t}(\rho_m v_m) + \frac{\partial}{\partial z}(\rho_m v_m^2) = -\sum_{i=1}^N F_{wi} - \frac{\partial p}{\partial z} - \rho_m g \cos \theta \quad (22)$ <p><i>Mixture Energy:</i></p> $\frac{\partial}{\partial t} \left\{ \rho_m \left[h_m + \frac{v_m^2}{2} \right] - p \right\} + \frac{\partial}{\partial z} \left\{ \rho_m v_m \left[h_m + \frac{v_m^2}{2} \right] \right\} = \sum_{i=1}^N \left(q_i'' \frac{P_i}{A_i} \right) - \rho_m v_m g \cos \theta \quad (23)$	
<p>Mixture Properties</p> $\rho_m = \{ \rho_v \alpha + \rho_l (1 - \alpha) \} \quad (24)$ $v_m = \frac{\{ \rho_v v_v \alpha + \rho_l v_l (1 - \alpha) \}}{\rho_m} \quad (25)$ $h_m = \frac{\{ \rho_v h_v \alpha + \rho_l h_l (1 - \alpha) \}}{\rho_m} \quad (26)$	

2.3. Two-phase drift flux transport equations

The Drift-Flux Model, developed by Zuber and Findlay [5] in 1965, provides a simple, yet reasonably accurate, method of introducing the relative velocity between fluid phases into the mixture equations. The basic premise is that the relative velocity between phases, (v_r), is related to a flow regime dependent drift velocity (V_{vj}) by the equation (27) presented in Table 4. Table 4 also presents several empirical correlations developed for the drift velocity.

Table 4. Drift velocity equations

Relationship Between Relative Velocity and Drift Velocity:	
$v_r = (v_v - v_l) = \frac{V_{vj}}{1 - \{\alpha\}} \quad (27)$	
Two-Phase Flow Regimes	Drift Velocity Equations
<i>Churn-Turbulent Flow</i>	$V_{vj} = 1.41 \left(\frac{\sigma g (\rho_l - \rho_g)}{\rho_l^2} \right)^{1/4} \quad (28)$
<i>Slug Flow</i>	$V_{vj} = 0.35 \left(\frac{g (\rho_l - \rho_g) D}{\rho_l} \right)^{1/2} \quad (29)$
<i>Annular Flow</i>	$V_{vj} = 23 \frac{\Delta \rho}{\rho_l} \left(\frac{\mu_l (1 - \{\alpha\}) v_l}{\rho_v D} \right)^{1/2} \quad (30)$

The two-phase fluid mixture transport equations shown in Table 2 can be written in terms of the relative velocities between phases. This requires a significant amount of algebra that is left to the astute reader. Having rearranged the mixture equations in terms the relative velocity, equation (27) is then substituted to obtain the final result shown in Table 5.

The following chapter describes how the transport equations presented in Sections 2.1, 2.2, and 2.3 have been used to build a variety of two-phase flow models for reactor analyses.

Table 5. One dimensional two-phase drift flux transport equations
(Uniform Density within each Phase)

Conservation Equations	
<i>Mixture Mass:</i>	
$\frac{\partial \rho_m}{\partial t} + \frac{\partial}{\partial z} (\rho_m v_m) = 0 \quad (31)$	
<i>Drift Flux Momentum:</i>	
$\rho_m \frac{\partial v_m}{\partial t} + \rho_m v_m \frac{\partial v_m}{\partial z} + \frac{\partial}{\partial z} \left(\frac{\rho_v \rho_l \{\alpha\} V_{vj}^2}{\rho_m (1 - \{\alpha\})} \right) = - \sum_{i=1}^N F_{wi} - \frac{\partial p_m}{\partial z} - \rho_m g \cos \theta \quad (32)$	
<i>Drift Flux Internal Energy:</i>	
$\begin{aligned} \frac{\partial}{\partial t} \{\rho_m u_m\} + \frac{\partial}{\partial z} \{\rho_m u_m v_m\} + \frac{\partial}{\partial z} \left[\frac{\{\alpha\} \rho_l \rho_v (u_v - u_l) V_{vj}}{\rho_m} \right] + \\ p_m \frac{\partial v_m}{\partial z} + p_m \frac{\partial}{\partial z} \left[\frac{\{\alpha\} (\rho_l - \rho_v) V_{vj}}{\rho_m} \right] = \sum_{i=1}^N q_i'' \frac{P_i}{A_i} + v_m \left(\sum_{i=1}^N F_{wi} \right) \end{aligned} \quad (33)$	

Mixture Properties

$$\rho_m = \{\rho_v \alpha + \rho_l (1 - \alpha)\} \quad (34)$$

$$v_m = \frac{\{\rho_v v_v \alpha + \rho_l v_l (1 - \alpha)\}}{\rho_m} \quad (35)$$

$$u_m = \frac{\{\rho_v u_v \alpha + \rho_l u_l (1 - \alpha)\}}{\rho_m} \quad (36)$$

$$p_m = \{p_v \alpha + p_l (1 - \alpha)\} \quad (37)$$

3. TWO-PHASE FLOW MODELS FOR REACTOR ANALYSES

This chapter provides an overview of the different types of two-phase flow models that have been developed and published in the literature. Figure 2 provides a simple overview of the components that comprise a two-phase flow model. A rigorous approach to modeling two-phase flow is to implement the two-fluid, full non-equilibrium, conservation equations. This includes a mass, momentum and energy conservation equation for each phase as presented in Section 2.1. Thus, it is typically referred to as the 6-equation model.

Because of the difficulty of working with a 6-equation model, a variety of simplified models have been developed. These models are derived by using mixture equations, or mixture equations in conjunction with individual phase equations, to obtain a reduced number of balance equations. Using this approach, it is possible to obtain 5-equation, 4-equation or 3-equation models for two-phase flow. Of course, the simpler models result in a reduced number of calculated parameters as dictated by the restrictions that have been imposed. One of the following three restrictions is typically imposed on the phase velocities.

1. *Homogeneous Flow.* This assumes that the velocity of both phases is equal. That is;

$$v_l = v_v = v_m \quad (38)$$

2. *Phase Slip.* This assumes that there is a relative velocity between the phases. The ratio of the vapor velocity to the liquid velocity is defined as the slip ratio, given a flow dependent correlation. Thus the slip ratio, S , equals:

$$S = \frac{v_v}{v_l} \quad (39)$$

3. *Drift Flux.* This assumes that there is a relative velocity between the phases. The relative velocity is determined from a known drift flux correlation, v_{vj} , that is flow regime dependent. That is,

$$\{v_v - v_l\} = \frac{v_{vj}}{\{1 - \alpha\}} \quad (40)$$

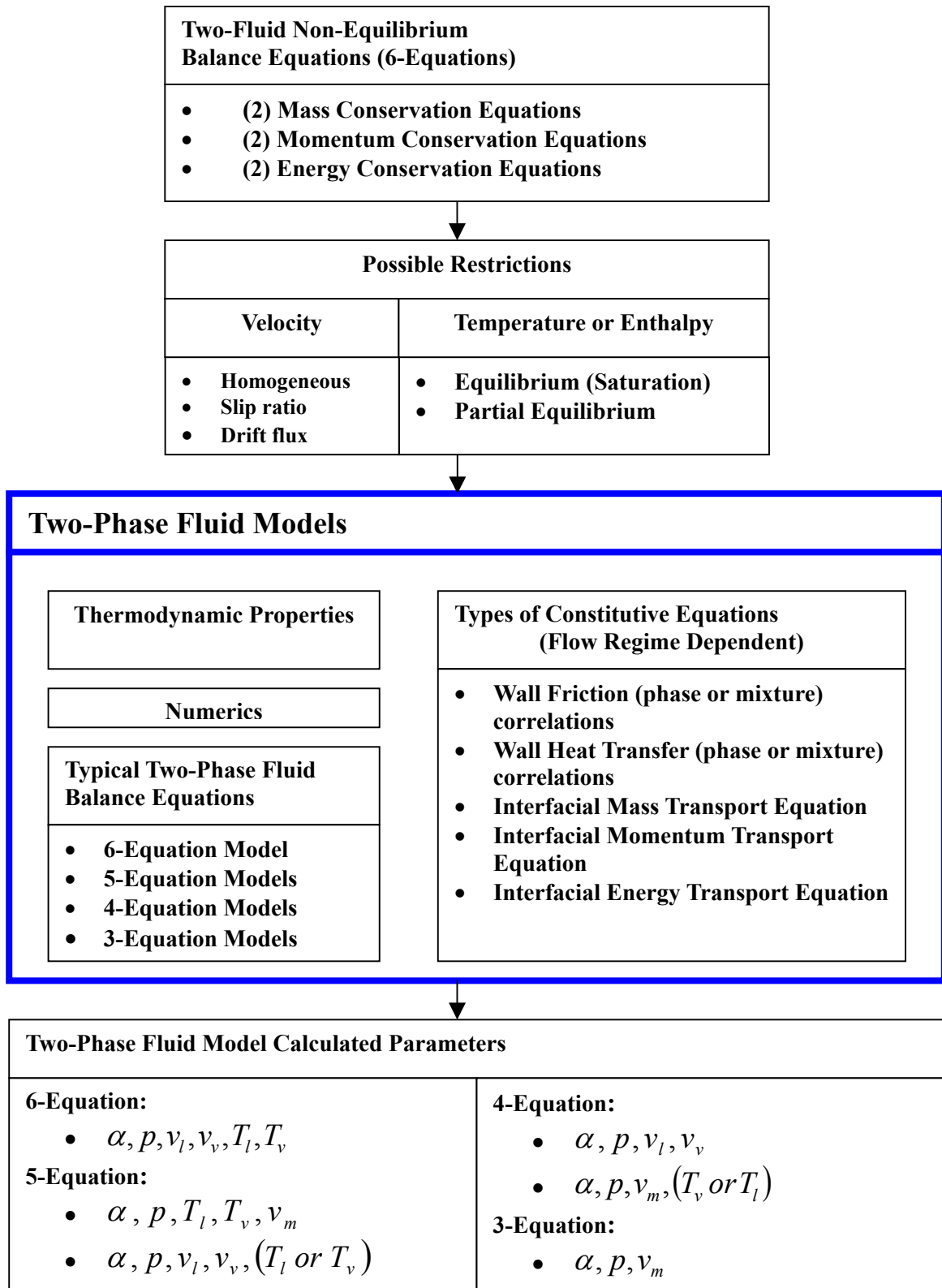


FIG. 2. Types of two-phase flow models used in nuclear reactor safety analyses.

One of the following two restrictions is typically applied to the phase temperatures or enthalpies.

4. *Full Thermal Equilibrium*. This refers to the assumption that both of the fluid temperatures are equal and at the saturation temperature corresponding to the local pressure. That is:

$$T_l = T_v = T_{SAT}(p) \tag{41}$$

5. *Partial Thermal Equilibrium*. This assumes that one of the two phases is at the saturation temperature corresponding to the local pressure. That is:

$$T_l \text{ or } T_v = T_{SAT}(p) \quad (42)$$

Figure 2 also shows that in addition to the balance equations, a two-phase flow model requires constitutive equations and thermodynamic property equations or tables to obtain a closed set of equations. The constitutive equations include fluid-structure and interfacial transport equations. These are as follows:

- A wall friction correlation for a mixture or for each of the phases. One such equation is needed for each momentum balance equation;
- A wall heat transfer correlation for a mixture or for each of the phases. One such equation is needed for each energy balance equation;
- An interfacial mass transport equation;
- An interfacial momentum transport equation;
- An interfacial energy transport equation.

Although not emphasized in Figure 2, nor expanded upon in this lecture, the numerical methods used to solve the equations play a major role in the accuracy and stability of the predictions. The topic can easily fill an entire course.

Lastly, the number of parameters calculated by each model depends on the number of balance equations. The 6-equation model can be used to calculate 6-unknowns; $\alpha, p, v_l, v_v, T_l, T_v$.

Table 6 provides the details of different types of two-phase flow models that have been used for nuclear reactor safety analyses. Eleven different models are presented, including their restrictions, types of constitutive equations and calculated parameters. It is important to recognize that, for any model formulation, a mixture conservation equation plus a phase conservation equation can be used in place of the two conservation equations for the phases. An example is provided in Figure 3.

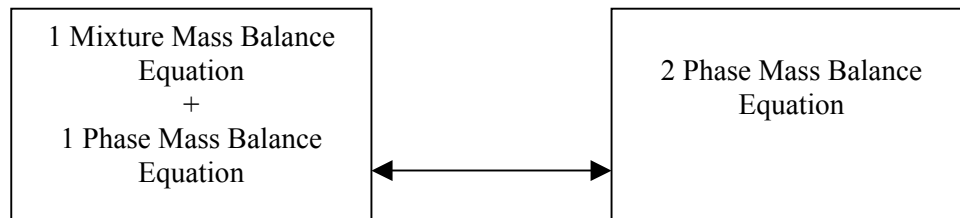


FIG. 3. Equivalent approaches to developing model mass balance equations.

Table 6. Two –phase flow models with equal phase pressures ($P_v = P_l = P$)

6-Equation Model			
governing Equations	Restrictions¹	Constitutive Laws²	Calculated Parameters
Two-Fluid Non-Equilibrium (2) Mass Phase Balance (2) Momentum Phase Balance (2) Energy Phase Balance		(2) Phase wall friction (2) Phase heat flux friction (1) Interfacial mass (1) Interfacial momentum (1) Interfacial energy	α, p, v_l v_v, T_l, T_v
5-Equation Models			
Two-Fluid Partial Non-Equilibrium (2) Mass Phase Balance (2) Momentum Phase Balance (1) Mixture Energy Balance	$T_l = T_{SAT}$ <i>or</i> $T_v = T_{SAT}$	(2) Phase wall friction (1) Mixture wall heat flux (1) Interfacial mass (1) Interfacial momentum	α, p, v_l, v_v $(T_l \text{ or } T_v)$
Two-Fluid Partial Non-Equilibrium (1) Mixture Mass Balance (2) Momentum Phase Balance (2) Energy Phase Balance	$T_l = T_{SAT}$ <i>or</i> $T_v = T_{SAT}$	(2) Phase wall friction (2) Phase heat flux friction (1) Interfacial mass ³ (1) Interfacial momentum (1) Interfacial energy	α, p, v_l, v_v $(T_l \text{ or } T_v)$
Slip or Drift Non-Equilibrium (2) Mass Phase Balance (1) Mixture Momentum Balance (2) Energy Phase Balance	Slip or Drift Velocity	(1) Mixture wall friction (2) Phase heat flux friction (1) Interfacial mass (1) Interfacial energy (1) Slip velocity or Drift flux	α, p, T_l T_v, v_m
Homogeneous Non-Equilibrium (2) Mass Phase Balance (1) Mixture Momentum Balance (2) Energy Phase Balance	Equal Velocity $v_l = v_v = v_m$	(1) Mixture wall friction (2) Phase heat flux friction (1) Interfacial mass ³ (1) Interfacial energy	α, p, T_l T_v, v_m

1. Restrictions imposed on fluid phase velocities or temperatures (or enthalpies in lieu of temperatures).
2. Minimum number of constitutive laws. For example, for N structures in the flow, N structure heat flux and N wall friction correlations may be required.
3. Interfacial mass transfer is required to determine interfacial momentum or interfacial energy transfer.

Table 6. (continued) Two-phase flow models with equal phase pressures ($P_V = P_L = P$)

4 -Equation Models			
Conservation Equations	Restrictions ¹	Constitutive Laws ²	Calculated Parameters
Two-Fluid Equilibrium Model (1) Mixture Mass Balance (2) Momentum Phase Balance (1) Mixture Energy Balance	$T_l = T_v = T_{SAT}$	(2) Phase wall friction (1) Mixture heat flux friction (1) Interfacial mass ³ (1) Interfacial momentum	α, p, v_l, v_v
Drift Partial Non-Equilibrium (2) Mass Phase Balance (1) Mixture Momentum Balance (1) Mixture Energy Balance	Drift Velocity $T_v \text{ or } T_l = T_{SAT}$	(1) Mixture wall friction (1) Mixture wall heat flux (1) Interfacial mass (1) Drift flux correlation	$\alpha, p, v_m,$ $T_v \text{ or } T_l$
Slip Partial Non-Equilibrium (1) Mixture Mass Balance (1) Mixture Momentum Balance (2) Phase Energy Balance	Slip Ratio $T_v \text{ or } T_l = T_{SAT}$	(1) Mixture wall friction (1) Mixture wall heat flux (1) Interfacial mass (1) Drift flux correlation	$\alpha, p, v_m,$ $T_v \text{ or } T_l$
Homogeneous, Partial Non-Equilibrium: (1) Mixture Mass Balance (1) Mixture Momentum Balance (2) Phase Energy Balance	$u_l = u_v = u_m$ $T_v \text{ or } T_l = T_{SAT}$	(1) Mixture wall friction (2) Phase wall heat flux (1) Interfacial mass ³ (1) Interfacial energy	$\alpha, p, v_m,$ $T_v \text{ or } T_l$
3-Equation Models			
Homogeneous Equilibrium (HEM): (1) Mixture Mass Balance (1) Mixture Momentum Balance (1) Mixture Energy Balance	$u_l = u_v = u_m$ $T_l = T_v = T_{SAT}$	(1) Mixture wall friction (1) Mixture wall heat flux	α, p, u_m
Slip or Drift Equilibrium: (1) Mixture Mass Balance (1) Mixture Momentum Balance (1) Mixture Energy Balance	Slip or Drift Velocity $T_l = T_v = T_{SAT}$	(1) Mixture wall friction (1) Mixture wall heat flux (1) Slip velocity or Drift flux	α, p, u_m

1. Restrictions imposed on fluid phase velocities or temperatures (or enthalpies in lieu of temperatures).
2. Minimum number of constitutive laws. For example, for N structures in the flow, N structure heat flux and N wall friction correlations may be required.
3. Interfacial mass transfer is required to determine interfacial momentum or interfacial energy transfer.

3.1. Advancements in two-phase flow modeling

This section touches briefly on some of the ongoing progress in the area of two-phase flow modeling in the United States. The first area discussed is the current effort to model the structure of two-phase flow regimes using an interfacial area concentration transport equation as opposed to a static flow regime map. The second area discussed is the U.S. Nuclear Regulatory Commission's effort to merge their current reactor analysis codes into a single multi-purpose code.

3.1.1. Interfacial Area Transport Model

The 6-equation, two-fluid model requires constitutive equations for the interfacial mass, momentum and energy transfer rates. These constitutive laws are quite important because the interfacial transfer rate govern the rate of phase change and the degree of mechanical and thermal non-equilibrium between phases. The interfacial transfer rate is related to the driving potential between the phases and the amount of interfacial area per unit volume of the mixture. This latter quantity is known as the interfacial area concentration.

Present day computer models for two-phase flows implement constitutive laws for interfacial transport that are based on *static flow regime maps*. That is, the computer codes include semi-empirical transition criteria to determine the two-phase flow regime present for a given combination of vapor and liquid flows and corresponding fluid properties. Having determined the two-phase flow regime, the code uses the criteria to select appropriate heat transfer and drag correlations. This approach has been relatively successful. However, efforts are underway to develop the tools for *dynamic flow regime modeling*.

Recent efforts by Kocamustafaogullari and Ishii (1995) [6], Wu, et al., (1998) [7], and Wu, Ishii and Uhle (1998) [8] have led to the development of the two-group interfacial area transport equations. The concept of two-group transport is, of course, not new. The application of multi-energy group models for neutron transport in reactors is well known. However its use in two-phase flows is relatively new. Reyes (1989) used a Boltzmann transport equation in his statistical derivation of the conservation equations for fluid particle flows. The novelty of this approach was the inclusion of breakage and coalescence "scattering integrals" that produce changes in the particle size distributions as the flow evolves. The interfacial area transport model extends that work by considering particle interfacial area as opposed to particle number density.

Two bubble groups are currently used. Group I consists of the spherical/distorted bubble group and Group II consists of the cap/slug bubble group. The two-group bubble number density transport equations can be derived from the Boltzmann transport equation to obtain:

Group I Number Density Transport:

$$\frac{\partial n_1}{\partial t} + \nabla \cdot n_1 \vec{v}_{pm,1} = \sum_j (S_{j,1} + S_{j,12}) + (S_{ph,1} + S_{ph,12}) \quad (43)$$

Group II Number Density Transport:

$$\frac{\partial n_2}{\partial t} + \nabla \cdot n_2 \vec{v}_{pm,2} = \sum_j (S_{j,2} + S_{j,21}) + (S_{ph,2} + S_{ph,21}) \quad (44)$$

where S_j is the net rate of change in the number density function due to the particle breakup and coalescence processes and S_{ph} is the net rate of change in the number density function due to phase change. Both terms have been integrated from the minimum to maximum particle volume. $S_{j,12}$ and $S_{j,21}$ are the inter-group particle exchange terms. The subscript "j" represents the different breakup and coalescence processes. The following expression is used to develop the interfacial area transport equations:

$$n_k = \psi_k \left(\frac{a_{i,k}^3}{\alpha_k^2} \right) \quad (45)$$

where, $a_{i,k}$ is the interfacial area concentration, α is the void fraction and ψ_k is the bubble shape factor. The subscript “k” represents the bubble group. Substituting equation (45) into (43) and (44) yields the following two-group interfacial area transport equations:

$$\frac{\partial a_{i,1}}{\partial t} + \nabla \cdot a_{i,1} \vec{v}_{i,1} = \frac{1}{3\psi_1} \left(\frac{\alpha_1}{a_{i,1}} \right)^2 \left[\sum_j (S_{j,1} + S_{j,12}) + (S_{ph,1} + S_{ph,12}) \right] + \left(\frac{2a_{i,1}}{3\alpha_1} \right) \left[\frac{\partial \alpha_1}{\partial t} + \nabla \cdot \alpha_1 \vec{v}_{i,1} \right] \quad (46)$$

$$\frac{\partial a_{i,2}}{\partial t} + \nabla \cdot a_{i,2} \vec{v}_{i,2} = \frac{1}{3\psi_2} \left(\frac{\alpha_2}{a_{i,2}} \right)^2 \left[\sum_j (S_{j,2} + S_{j,21}) + (S_{ph,2} + S_{ph,21}) \right] + \left(\frac{2a_{i,2}}{3\alpha_2} \right) \left[\frac{\partial \alpha_2}{\partial t} + \nabla \cdot \alpha_2 \vec{v}_{i,2} \right] \quad (47)$$

A significant effort is underway to develop the appropriate coalescence and breakage models for the two groups. Initial comparisons to data, including bubbly to slug flow transitions are very encouraging, Hibiki and Ishii (2000) [9].

3.1.2. TRACE reactor system analysis code [10]

The U.S. Nuclear Regulatory Commission (USNRC) is in the process of developing a modern code for reactor analysis. It is an evolutionary code that merges RAMONA, RELAP5, TRAC-PWR and TRAC-BWR into a single code. The reason for merging the codes, as opposed to starting new, is to maintain the sizable investment that exists in the development of input models for each of the codes. The consolidated code is called the TRAC/RELAP Advanced Computational Engine or TRACE.

TRACE is a component-oriented code designed to analyze reactor transients and accidents up to the point of fuel failure. It is a finite-volume, two-fluid, compressible flow code with 3-D capability. It can model heat structures and control systems that interact with the component models and the fluid solution. TRACE can be run in a coupled mode with the PARCS three dimensional reactor kinetics code. Typical TRACE reactor models range in size from a few hundred to a few thousand fluid volumes. TRACE can be run in parallel. TRACE has been coupled to CONTAIN through its exterior communications interface (ECI) and can be coupled to detailed fuel models or CFD codes in the future using the ECI. TRACE has been coupled to a user-friendly front end, SNAP, that supports input model development and accepts existing RELAP5 and TRAC-P input. Figure 4 illustrates the TRACE /SNAP environment architecture.

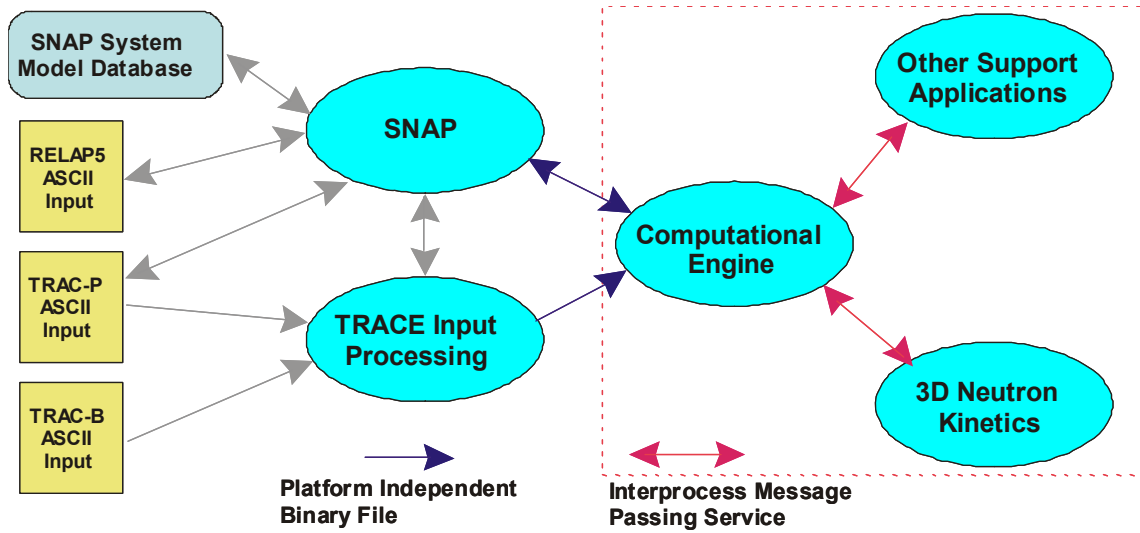


FIG. 4. TRACE /SNAP environment architecture [10].

Table 7 presents the conservation equations and constitutive equations for the TRACE computer code. It consists of a 3-D, 6-equation, non-equilibrium model that can be coupled to additional equations to solve for the non-condensable gas pressure, boron concentration and heat structure temperatures.

Table 7. Trace field equations [10]

<p>Conservation Equations</p> <p><i>Mixture Mass:</i></p> $\frac{\partial}{\partial t}(\rho_v \alpha + (1 - \alpha)\rho_l) + \nabla \cdot (\rho_v \bar{v}_v \alpha + \rho_l \bar{v}_l (1 - \alpha)) = 0$ <p><i>Vapor Mass:</i></p> $\frac{\partial}{\partial t}(\rho_v \alpha) + \nabla \cdot (\rho_v \bar{v}_v \alpha) = \Gamma_v$ <p><i>Liquid Momentum:</i></p> $\frac{\partial \bar{v}_l}{\partial t} + \bar{v}_l \cdot \nabla \bar{v}_l = -\frac{1}{\rho_l} \nabla p + \frac{c_i}{(1 - \alpha)\rho_l} (\bar{v}_v - \bar{v}_l) \bar{v}_v - \bar{v}_l - \frac{\Gamma_{Cond}}{(1 - \alpha)\rho_l} (\bar{v}_v - \bar{v}_l) + \frac{c_w}{(1 - \alpha)\rho_l} \bar{v}_l \bar{v}_l + \bar{g}$ <p><i>Gas Momentum:</i></p> $\frac{\partial \bar{v}_v}{\partial t} + \bar{v}_v \cdot \nabla \bar{v}_v = -\frac{1}{\rho_v} \nabla p + \frac{c_i}{\alpha \rho_v} (\bar{v}_v - \bar{v}_l) \bar{v}_v - \bar{v}_l - \frac{\Gamma_{Boiling}}{\alpha \rho_v} (\bar{v}_v - \bar{v}_l) + \frac{c_{wv}}{\alpha \rho_v} \bar{v}_v \bar{v}_v + \bar{g}$ <p><i>Mixture Energy:</i></p> $\frac{\partial}{\partial t}(\rho_v \alpha e_v + \rho_l (1 - \alpha) e_l) + \nabla \cdot (\rho_v \alpha e_v \bar{v}_v + \rho_l (1 - \alpha) e_l \bar{v}_l) = -p \nabla \cdot (\alpha \bar{v}_v + (1 - \alpha) \bar{v}_l) + q_{wl} + q_{dv}$ <p><i>Vapor Energy:</i></p> $\frac{\partial}{\partial t}(\rho_v \alpha e_v) + \nabla \cdot (\rho_v \alpha e_v \bar{v}_v) = -p \frac{\partial \alpha}{\partial t} - p \nabla \cdot (\alpha \bar{v}_v) + q_{wv} + q_{dv} + q_{iv} + \Gamma_v h_v$
--

<p>Constitutive Equations:</p> <ul style="list-style-type: none"> • Equations of State • Wall Drag • Interfacial Drag • Wall Heat Transfer • Interfacial Heat Transfer • Static Flow Regime Maps 	<p>Additional Equations:</p> <ul style="list-style-type: none"> • Non-condensable Gas • Dissolved Boron • Control Systems • Reactor <u>Power</u>
<p>Calculated Parameters:</p> <ul style="list-style-type: none"> • Vapor Void Fraction • Steam Pressure • Non-condensable Gas Pressure • Liquid Velocity and Temperature • Vapor Velocity and Temperature • Boron Concentration • Heat Structure Temperatures 	

NOMENCLATURE

a	interfacial area concentration
A	cross-sectional area
D	pipe diameter
e	total energy
F	force
g	gravitational constant
G	mass flux
h^0	stagnation enthalpy
\vec{n}	outward normal vector
p	pressure
q''	heat flux
Q_{sk}	interfacial heat transfer rate
S	velocity slip ratio
S_j	Interaction term for change in bubble number density due to bubble coalescence and breakage
S_{ph}	Interaction term for change in bubble number density due to phase change
T	temperature
u^0	stagnation energy
v_k	phase velocity
V_{vj}	drift velocity

Greek Symbols

α	vapor void fraction
Γ_k	mass generation rate per unit volume
ρ	density
σ	surface tension
ψ	bubble shape factor

ACKNOWLEDGEMENT

This work was supported through a U.S. Department of Energy Contract (DE- FC07-04ID14550) and the Oregon State University sabbatical program. This work was conducted through the IAEA Nuclear Power Technology Development Section.

REFERENCES

- [1] MARTIN, R., History of Nuclear Power Safety, <http://users.owt.com/smsrpm/nksafe/> , Public Information Committee of the American Nuclear Society (2000).
- [2] TODREAS, N. E., KAZIMI, M.S., Nuclear Systems I Thermal Hydraulic Fundamentals, Taylor and Francis (1993).
- [3] RANSOM, V.H., HICKS, D.L., Hyperbolic Two-Pressure Models for Two-Phase Flow, *Journal of Computational Physics*, 53, 124–151 (1984).
- [4] RANSOM, V.H., HICKS, D.L., Hyperbolic Two-Pressure Models for Two-Phase Flow Revisited, *Journal of Computational Physics*, 75, 498–504 (1988).
- [5] ZUBER, N., FINDLAY, J.A., Average volumetric concentration in two-phase flow systems, *Journal of Heat Transfer*, 87:453 (1965).
- [6] KOCAMUSTAFAOGULLARI, G., ISHII, M., Foundation of interfacial area transport equation and its closure relations, *International Journal of Heat and Mass Transfer* 38, 481–493 (1995).
- [7] WU, Q., KIM, S., ISHII, M., BEUS, S., One-group interfacial area transport in vertical bubbly flow, *International Journal of Heat and Mass Transfer* 41, 1103–1112 (1998).
- [8] WU, Q., ISHII, M., UHLE, J., Framework of two-group model for interfacial area transport I vertical two-phase flows, *Transactions of the American Nuclear Society* 79, 351–352 (1998).
- [9] HIBIKI, T., ISHII, M., Two-group interfacial area transport equations at bubbly-to-slug transition, *Nuclear Engineering and Design* 202, 39–76 (2000).
- [10] STAUDENMEIER, J., TRACE Reactor System Analysis Code, MIT Presentation, Safety Margins and Systems Analysis Branch, Office of Nuclear Regulatory Research, U.S. Nuclear Regulatory Commission (2004).

INTRODUCTION TO INSTABILITIES IN NATURAL CIRCULATION SYSTEMS

P.K. Vijayan, A.K. Nayak

Reactor Engineering Division,
Bhabha Atomic Research Centre, India

Abstract

This lecture reviews the various classifications of natural circulation instabilities that are in common use. The instabilities observed during various stages of natural circulation such as single-phase, boiling inception and fully developed two-phase flow are described. The mechanisms causing the instabilities are also briefly described.

1. INTRODUCTION

Natural circulation systems are susceptible to several kinds of instabilities. Although instabilities are common to both forced and natural circulation systems, the latter is more unstable than forced circulation systems due to a regenerative feedback inherent in the NC process and its low driving force. For example, any disturbance in the driving force of a NC system will affect the flow which in turn will influence the driving force leading to an oscillatory behaviour even in cases where eventually a steady state is expected. In other words, a regenerative feedback is inherent in the mechanism causing NC flow due to the strong coupling between the flow and the driving force. As a result, both single-phase and two-phase natural circulation systems exhibit instability whereas only forced circulation two-phase systems are known to exhibit instability. Even among two-phase systems, the NC systems are more unstable than forced circulation systems due to the above reasons.

Before we progress further, we need to define instability. Following a perturbation, if the system returns back to the original steady state, then the system is considered to be stable. If on the other hand the system continues to oscillate with the same amplitude, then the system is neutrally stable. If the system stabilizes to a new steady state or oscillates with increasing amplitude then the system is considered as unstable. It may be noted that the amplitude of oscillations cannot go on increasing indefinitely even for unstable flow. Instead for almost all cases of instability the amplitude is limited by nonlinearities of the system and limit cycle oscillations (which may be chaotic or periodic) are eventually established. The time series of the limit cycle oscillations may exhibit characteristics similar to the neutrally stable condition. Further, even in the steady state case, especially for two-phase systems with slug flow, small amplitude oscillations are visible. Thus, for identification purposes especially during experiments, often it becomes necessary to quantify the amplitude of oscillations as a certain percentage of the steady state value. Amplitudes more than $\pm 10\%$ of the mean value is often considered as an indication of instability. However, some authors even use $\pm 30\%$ of the mean as the cut-off value [1].

Instability is undesirable as sustained flow oscillations may cause forced mechanical vibration of components. Further, premature CHF (critical heat flux) occurrence can be induced by flow oscillations as well as other undesirable secondary effects like power oscillations in BWRs. Instability can also disturb control systems and cause operational problems in nuclear reactors. Over the years, several kinds of instabilities have been observed in natural circulation systems excited by different mechanisms. Differences also exist in the transport mechanism, oscillatory mode, the nature of the instability threshold and its prediction methods. In addition, effects of loop geometry and secondary phenomena also cause complications in the observed instabilities. Under the circumstances, it looks relevant to classify instabilities into various categories which will help in improving our understanding and hence control of these instabilities.

2. INSTABILITY CLASSIFICATION

Mathematically, the fundamental cause of all instabilities is due to the existence of competing multiple solutions so that the system is not able to settle down to any one of them permanently. Instead, the

system swings from one solution to the other. An essential characteristic of the unstable oscillating NC systems is that as it tries to settle down to one of the solutions a self-generated feedback appears making another solution more attractive causing the system to swing towards it. Again during the process of settling down on this solution, another feedback of opposite sign favoring the original solution is self-generated and the system swings back to it. The process repeats itself resulting in perpetual oscillatory behaviour if the operating conditions are maintained constant. Although this is a general characteristic it hardly distinguishes the different types of instabilities found to occur in various systems. In general, instabilities can be classified according to various bases as listed below:

- a) analysis method,
- b) propagation method,
- c) number of unstable zones,
- d) nature of the oscillations,
- e) loop geometry and
- f) disturbances or perturbations

2.1. Based on the analysis method (or governing equations used)

In some cases, the occurrence of multiple solutions and the instability threshold itself can be predicted from the steady state equations governing the process (pure or fundamental static instability). However, there are many situations with multiple steady state solutions where the threshold of instability cannot be predicted from the steady state laws alone (or the predicted threshold is modified by other effects). In this case, the cause of the instability lies in the steady state laws but feedback effects are important in predicting the threshold (compound static instability). Besides, many NCSs with only a unique steady state solution can also become unstable during the approach to the steady state due to the appearance of competing multiple solutions due to the inertia and feedback effects (pure dynamic instability). Neither the cause nor the threshold of instability of such systems can be predicted purely from the steady state equations alone. Instead, it requires the full transient governing equations to be considered for explaining the cause and predicting the threshold. In addition, in many oscillatory conditions, secondary phenomena gets excited and it modifies significantly the characteristics of the fundamental instability. In such cases, even the prediction of the instability threshold may require consideration of the secondary effect (compound dynamic instability). A typical case is the neutronics responding to the void fluctuations resulting in both flow and power oscillations in a BWR. In this case, in addition to the equations governing the thermalhydraulics, the equations for the neutron kinetics and fuel thermal response also need to be considered.

Thus we find that the analysis to arrive at the instability threshold can be based on different sets of governing equations for different instabilities. Based on the governing equations used to predict the threshold Boure, Bergles and Tong (1973) [2] classified instabilities into four basic types as:

- a) Pure static instability,
- b) Compound static instability¹,
- c) Pure dynamic instability, and
- d) Compound dynamic instability.

2.2. Based on the propagation method

This classification is actually restricted to only the dynamic instabilities. According to Boure et al. (1973) [2] the mechanism of dynamic instability involves the propagation or transport of disturbances. In two-phase flow, the disturbances can be transported by two different kinds of waves: pressure (acoustic waves) and void (or density) waves. In single-phase NCSs, however, only density wave instability is observed. In any two-phase system both types of waves are present, however, their velocities differ by one or two orders of magnitude allowing us to distinguish between the two.

¹ It may be noted that Boure, Bergles and Tong (1973) named this instability as compound relaxation instability.

2.2.1. Acoustic instability

Acoustic instability is considered to be caused by the resonance of pressure waves. Acoustic oscillations are also observed during blowdown experiments with pressurized hot water systems possibly due to multiple wave reflections. Acoustic oscillations are characterized by high frequencies of the order of 10–100 Hz related to the pressure wave propagation time [2]. Acoustic oscillations have been observed in subcooled boiling, bulk boiling, and film boiling. The thermal response of the vapor film to passing pressure wave is suggested as a mechanism for the oscillations during film boiling. For example, when a compression (pressure wave consists of compression and rarefaction) wave passes the vapor film is compressed enhancing its thermal conductance resulting in increased vapor generation. On the other hand when a rarefaction wave passes, the vapor film expands reducing its thermal conductance resulting in decreased vapor generation. The process repeats itself.

2.2.2. Density wave instability (DWI)

In a boiling system a temporary increase in the power causes a fluid packet of high void fraction and hence low density (i.e. a light fluid packet) to emerge from the heat source. As this light fluid packet moves up along the riser it increases the driving force and hence the flow. The increased flow reduces the exit enthalpy and the void fraction causing a fluid packet of high density (dense or heavy fluid packet) to emerge from the heat source. As the heavy fluid packet ascends along the riser, the driving force reduces causing the flow rate to decrease. This decrease in flow rate again increases the exit enthalpy and void fraction leading to the repetition of the process. It must be clearly understood that the above mechanism is at work in a NCS always. Instability, however, is observed only when the light and heavy fluid packets are formed with appropriate spacing (related to time delay) and magnitude, which are dependent on the operating conditions as well as the loop geometry. The instability is also observable in condensing as well as single-phase NCSs. In fact, DWI is the most commonly observed instability in natural circulation loops. The basic difference with acoustic instability is that the DWI is characterized by low frequency oscillations (of the order of 1 Hz).

Because of the importance of void fraction and its effect on the flow as explained above this instability is sometimes referred to as flow-void feedback instability in two-phase systems. Since transportation time delays (related to the spacing between the light and heavy packets of fluid as explained above) are crucial to this instability, it is also known as “time delay oscillations”. In single-phase, near critical and supercritical systems the instability is also known as thermally induced oscillations [3],[4]. However, Density Wave Instability (DWI) or density wave oscillations (DWO), first used by Stenning and Veziroglu (1965) [5], is the most common term used for the above described phenomenon as it appears that a density wave with light and heavy fluid packets is traveling through the loop.

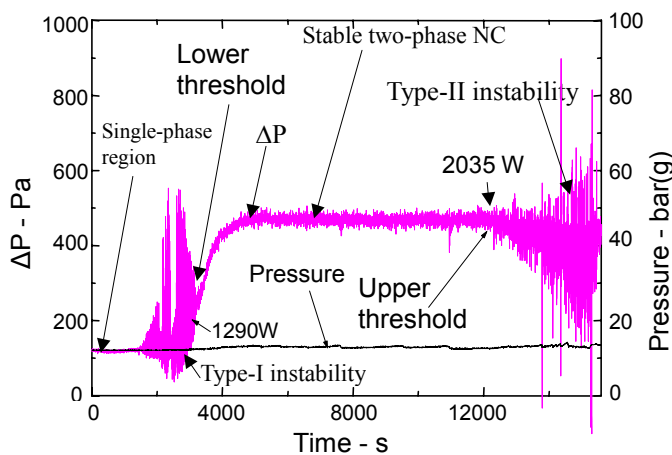


FIG. 1a. Typical low power and high power unstable zones for two-phase NC flow.

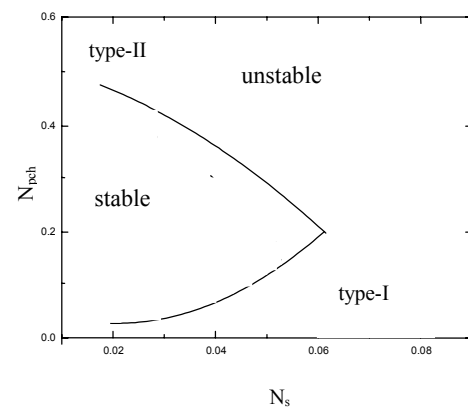


FIG. 1b. Typical stability map for two-phase density wave instability.

2.3. Based on the number of unstable zones

Fukuda and Kobori (1979) [6] gave a further classification of density wave instability based on the number of unstable zones. Usually, there exists a low power and a high power unstable zone for density wave instability in forced as well as NC two-phase flows (Fig. 1a). For the two-phase flow density wave instability, the unstable region below the lower threshold occurs at a low power and hence at low quality and is named as type I instability by Fukuda and Kobori (1979) [6]. Similarly, the unstable region beyond the upper threshold occurs at a high power and hence at high qualities and is named as type II instability. Theoretical analysis by the same authors has shown that the gravitational pressure drop in the unheated riser section plays a dominant role in type I instability where as frictional pressure drop is dominant in type II instability. Generally, if the stability map encloses the unstable region, then it has only one unstable zone (Fig. 2a and b). On the other hand if it encloses the stable zone, then it has two unstable zones (Fig. 1b). If the stability map is like that shown in Fig. 2c, then it is possible to get two unstable zones and three stable zones for certain operating conditions. Islands of instability have been observed to occur by Yadigaroglu and Bergles (1969) [7] within the stable operating region. Further recent theoretical investigations confirm the existence of islands of instability in stable zones [8] and islands of stability in unstable zones [9] in which case there are more than two zones of instability. Similarly Nayak et al. (2003) [10] has shown that more than two thresholds exist for flow pattern transition instability. Experiments by Vijayan et al. (2001) [11] have shown that even the lower instability threshold for density wave instability in single-phase NC flow can be different for different operating procedures due to the hysteresis phenomenon. Chen et al. (2001) [12] also observed hysteresis in a two-phase loop. As an unstable single-phase system progresses through single-phase NC to boiling inception to fully developed two-phase NC with power change, it can encounter several unstable zones. In view of the existence of more than two unstable zones, this method of classification could be confusing at times.

2.4. Based on the nature of the oscillations

All instabilities eventually lead to some kind of oscillations. The oscillations can be labeled as flow excursions or oscillations, pressure drop oscillations, power oscillations, temperature excursions or oscillations, etc. Besides, classifications based on the oscillatory characteristics are some times reported for dynamic instability. For example, based on the periodicity sometimes oscillations are characterized as periodic and chaotic. Based on the oscillatory mode, the oscillations are characterized as fundamental mode or higher harmonic modes. Depending on the phase lag we can classify oscillations as in-phase, out-of-phase or if both in-phase and out-of-phase modes are present it is referred to as dual oscillations. In natural circulation loops, flow direction can also change during oscillations. Based on the direction of flow, the oscillations can be characterized as unidirectional, bi-directional or it can switch between the two. Such switching is often accompanied by period doubling, tripling or n-tupling.

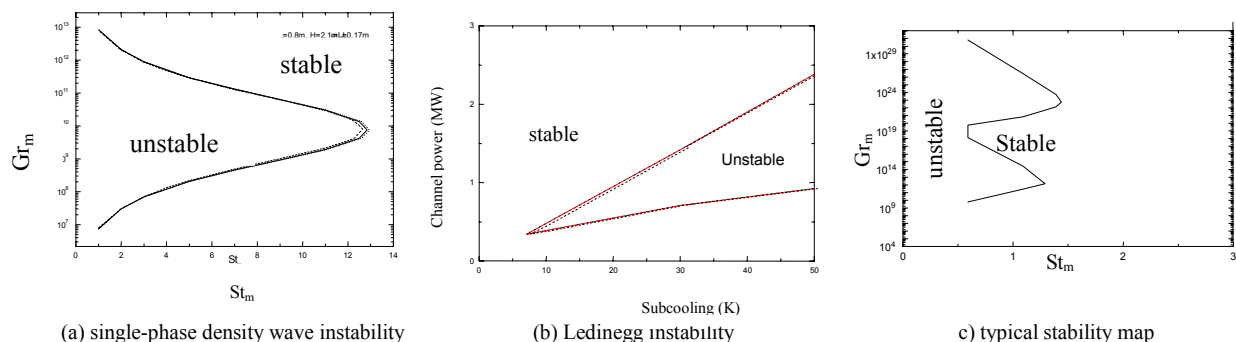


FIG. 2. Stability maps for various instabilities.

2.5. Based on the loop geometry

Certain instabilities are characteristic of the loop geometry. Examples are the instabilities observed in open U-loops, symmetric closed loops and asymmetric closed loops. In addition, pressure drop oscillations and the parallel channel instability are also characteristic of the loop geometry. Pressure drop oscillations normally occur in systems with a compressible volume (a pressurizer for example) at the inlet of the heated channel. Similarly, interaction among parallel channels can also lead to instability. Since both pressure drop and parallel channel oscillations are part of the compound dynamic instabilities, these will be discussed in detail later.

2.6. Based on the disturbances

Certain two-phase flow phenomena can cause a major disturbance and can lead to instability or modify the instability characteristics significantly. Typical examples are boiling inception, flashing, flow pattern transition or the occurrence of CHF. All these are static phenomena and are discussed either under static or compound static instability. Cold water injection can also cause a major disturbance and instability in natural circulation systems.

2.7. Closure

The classification based on the analysis methods is a very broad classification and all observed instabilities are found to belong to one or the other of the four classes, i.e. static, compound static, dynamic and compound dynamic instability. This is also the most widely accepted classification of instabilities. All other classifications are actually addressing only a subset of the instabilities considered in the above four main types. However, one of the major drawbacks is that it does not differentiate between natural and forced circulation systems. Today, we know that most known two-phase instabilities are observable in both forced and natural circulation systems. However, there are certain instabilities associated with natural circulation systems, which are not observable in forced circulation systems. For example, single-phase NC systems exhibit instability whereas single-phase forced circulation systems, generally, do not show instabilities. Besides, natural circulation systems exhibit an instability associated with flow direction whereas no such instability is reported for forced circulation systems with the exception of parallel channel systems.

All two-phase NCSs pass through the single-phase NC stage during the heat-up phase. In addition, boiling inception, which is an inevitable step for transition to two-phase flow, is a major disturbance for single-phase NCSs. As a result there are several instabilities associated with boiling inception. Therefore, while examining natural circulation instabilities it is convenient to consider the different stages of NC flow and categorize the instabilities into three separate classes as below:

- a) Single-phase NC instability,
- b) Instabilities associated with boiling inception, and
- c) Two-phase NC instability.

3. STABILITY OF SINGLE-PHASE NCS

Single-phase NC is the normal mode of coolant circulation in the district heating reactors and certain advanced reactors like CAREM-X. It is also relevant to the supercritical natural circulation boilers and reactors. It is the observed mode of circulation in most pressurized light and heavy water reactors in case of complete loss of pumping power. Further, all two-phase NCSs pass through the single-phase region during the heating up phase. Hence stability of single-phase natural circulation assumes importance during the start-up of natural circulation BWRs like AHWR and ESBWR.

Compared to two-phase flow instabilities, single-phase NC instability is not observed frequently in large industrial systems and the literature on it is much less. To the best of our knowledge, Keller (1966) [13] and Welander (1967) [14] carried out the early theoretical investigations on single-phase NC instability. The earliest reported experimental investigation is by Welander (1957) [3]. The first

systematic experimental investigation of single-phase instability is by Creveling et al. (1975) [15]. Single-phase instability serves as a platform for improving our understanding of the NC instability and is of interest in the study of deterministic chaos [16], [17]. Reviews on single-phase natural circulation instability are available in Zvirin (1981) [18] and Greif (1988) [19]. Single-phase instabilities are of four different types:

- a) Stability of the rest state,
- b) Static instabilities associated with multiple steady states,
- c) Dynamic instabilities, and
- d) Compound dynamic instabilities.

3.1. Stability of the rest state

Generally, in a NCL, the fluid is stagnant (i.e. rest state) in the absence of heating. Following the application of heating, if the fluid continues to remain stagnant then its rest state is stable. If it begins to flow then the rest state is considered as unstable. Welander (1967) [14] stated that the rest state of a loop with two vertical branches, a point heat source at the bottom and a point heat sink at the top, is always unstable. The stability of the rest state was also investigated by Bau and Torrance (1981) [20] in an open loop and reached the same conclusion as that of Welander. However, Zvirin's (1985) [21] analysis considering the effect of axial conduction in a vertical thermosyphon has shown that the rest state is unstable only if a suitably defined Rayleigh number exceeds a critical value. While Bau and Torrance employed a dynamic analysis, Zvirin has shown that the same result can be arrived at from the static as well as the dynamic analysis. Generally, the instability associated with the rest state is considered as a dynamic instability.

3.2. Static instabilities due to multiple steady states

Multiple steady states lead to two types of instabilities:

- a) Pure static instability and
- b) Compound static instability

3.2.1. *Pure static instability*

Two types of multiple steady states are possible, i.e. multiple steady states in the same flow direction and multiple steady states with differing flow direction. Traditionally pure static instability is associated with multiple steady states in the same flow direction. In closed loops, multiple steady states in the same flow direction have not been observed experimentally under single-phase natural circulation conditions. However, it may be mentioned that theoretically this possibility exists, as the momentum equation describing the steady state flow is a polynomial (see Appendix-1). Multiple steady states in the same flow direction have been found analytically for the toroidal loop with a throughflow [22] and such a system can, in principle, exhibit pure static instability.

3.2.2. *Compound static instability*

This instability is observed in systems with multiple steady states associated with different flow directions and for most cases, the threshold of instability cannot be predicted from the steady state laws alone. For single-phase forced circulation loops, usually multiple steady states with differing flow direction is not possible as the pump developed pressure has a unique direction. This is not so in natural circulation loops, where the flow direction is determined by the direction of the buoyancy force. There are several NCSs where steady state flow can prevail either in the clockwise or in the anticlockwise direction. Examples are symmetric loops with horizontal heaters, NCS with parallel channels, and simple loops with asymmetric heating or a throughflow. The instability manifests itself in the unpredictability of flow direction during flow initiation or a seemingly unexplained flow reversal following a transient. In certain instances an oscillation growth scenario terminated by a flow reversal is also observable. Following the flow reversal, steady state flow is observed. The instability can also be observed in large reactor systems or test facilities during natural circulation.

Symmetric loops

It is easy to see that steady NC flow in the loop shown in Fig. 3 can take place in the clockwise or anticlockwise direction depending on which vertical limb is the hot leg. For the loop shown in Fig. 3, irrespective of the flow direction, the flow rates will be of equal magnitude. For symmetric loops, the existence of the multiple steady states with differing direction manifests itself in the unpredictability of flow direction when heated during stagnant initial conditions. However, once the flow is initiated, it continues in the same direction even with increases in power if the loop is stable. It can also result in a flow reversal during transition from forced to natural circulation flow as follows:

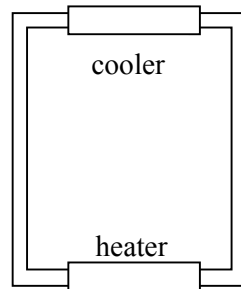


FIG. 3. A symmetric rectangular NCL..

During transition from forced to natural circulation, generally the flow continues in the same direction as that of the initial forced flow due to the 'memory effect' caused by the residual buoyancy force which is proportional to the temperature difference across the vertical legs during forced flow. However, the memory effect can be insignificant and the loop 'forgets' its initial flow direction if the initial forced flow is very large so that the temperature rise across the heater is too small. Tests indicated that the loop goes through a period of flow stagnation before the flow initiates again [23]. Flow, when it restarts can be opposite to the initial forced flow direction. Other symmetric loops like the toroidal or figure-of-eight loop can behave in this manner.

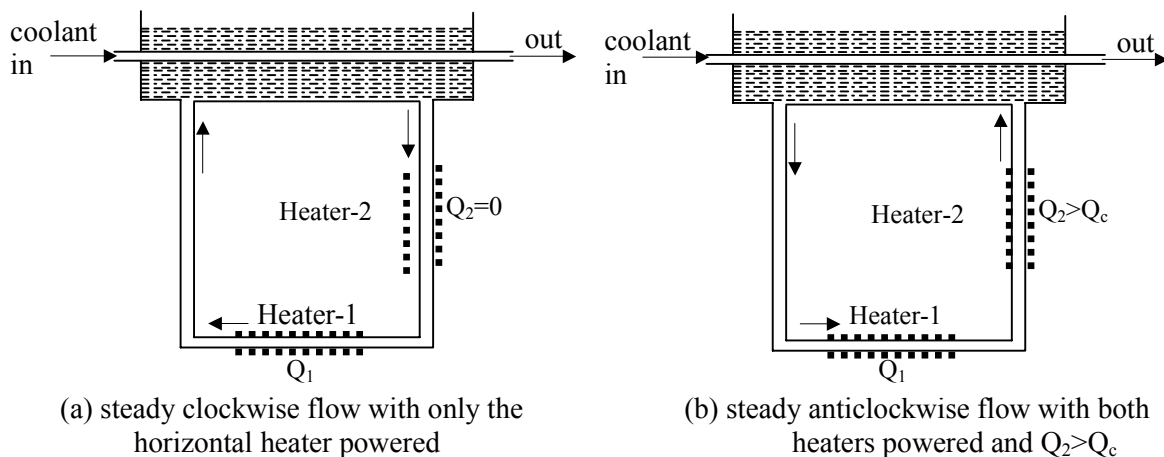


FIG. 4. Effect of flow direction on the instability.

Asymmetric loops

Bau and Torrance (1981a) [24] have shown that another kind of multiple steady states with differing flow directions can exist in simple loops with asymmetric heating. To understand this, consider the loop shown in Fig. 4a, where the flow is established in the clockwise direction with only the horizontal heater powered. Now keeping the power of the horizontal heater constant, if we begin to increase the power of the vertical heater beyond a critical value, then instability will set in. This instability will be terminated with the flow reversal and steady NC flow ensues subsequently in the anticlockwise direction (see Fig. 4b). Also, if we reduce the power of the vertical heater back to zero, the instability will not be found. The fundamental cause of the instability is the time delay associated with the travel of the hot fluid from the exit of the vertical heater through the horizontal heater to the other vertical limb.

Similar instability can also be found in loops with upward flow in vertical cooler (Fig. 5). In this case, also, flow can initiate in either directions due to the presence of the horizontal heater. Tests in a rectangular loop have shown that even if flow initiated in the anticlockwise direction, the flow can reverse automatically (Fig.5b) for certain loop geometries [11]. Stability analysis showed that no steady state with anticlockwise flow exists in the loop for the conditions of the experiment (Fig. 5c).

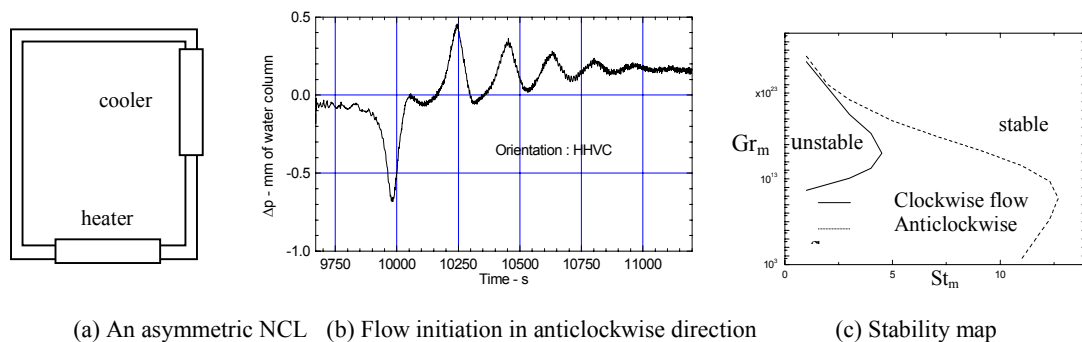


FIG. 5. Flow initiation in the anticlockwise direction in an asymmetric NC loop.

Simple loops with throughflow

In rectangular loops with vertical heaters (Fig. 6a), generally the flow direction is such that upward flow prevails always in the vertical heater during steady states without throughflow. Even in such cases, downward flow through the heater can be caused by cold water injection as shown in Fig. 6b. It has also been analytically found that multiple steady state solutions can be encountered when a throughflow (i.e. Feed mass flow equal to the bleed mass flow) is superimposed on the toroidal loop [22]. Experimentally, the instability associated with multiple steady states with different directions has been studied by Vijayan and Date [25], [26] in a figure-of-eight loop. Consider the figure-of-eight loop (relevant to PHWR) shown in Fig. 7 where a throughflow F is introduced into the loop while it was operating under steady state single-phase NC conditions. When the throughflow is small, it flows in the same direction as that of the NC flow (Fig. 7a). However, if the throughflow is above a critical value, then the loop flow begins to oscillate. One of the observed characteristics of this oscillation is that the amplitude in the low flow path is significantly higher and is 180° out-of-phase with that in the high flow path². With further increase in throughflow, the amplitude of oscillation increases eventually leading to a flow reversal in a part of the loop as shown in Fig. 7b. However, both experimental and numerical investigations showed that the threshold value of throughflow at which the flow reversal occurs is dependent on the operating procedure followed in the experiments. Similar instability can also occur in loops relevant to other reactor systems.

² The out-of-phase oscillations are typical of parallel channel systems and it can be easily seen from Fig. 7b that a closed loop is actually a parallel channel system with two channels when the throughflow rate is large.

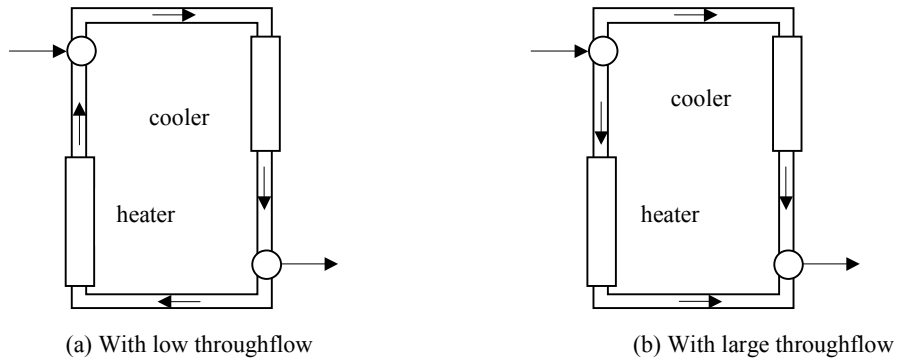


FIG. 6. Asymmetric loop with multiple steady states with throughflow.

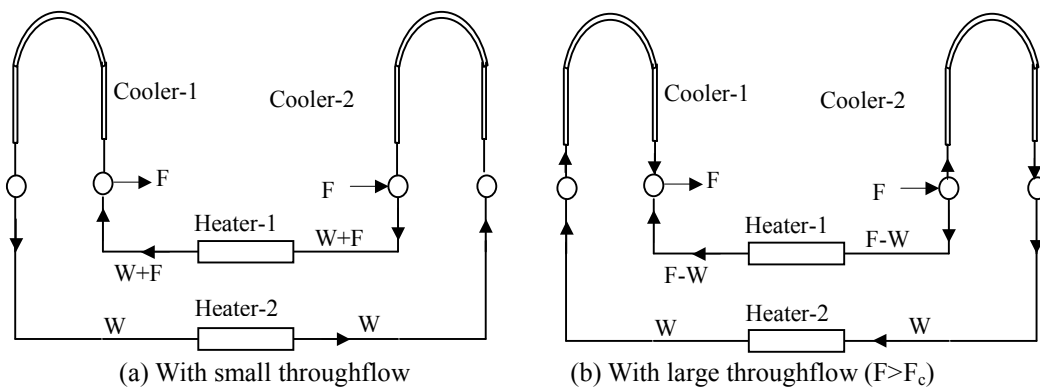


FIG. 7. Effect of throughflow on instability.

Parallel channel systems with mutually competing driving forces

Parallel channel systems occur in BWRs, PWRs, PHWRs, VVERs, and steam generators/boilers. In a natural circulation system, the heated or cooled parallel channels are loosely coupled hydraulically to the rest of the loop due to the presence of mutually competing driving forces. To understand the phenomenon let us consider a NCS with a large number of parallel vertical unequally heated channels (see Fig. 8) connected between a common inlet and an outlet header (or plenum) with an unheated downcomer connected between the two headers. There is a buoyancy force between the unheated downcomer and each individual heated channel favoring upward flow through the heated channel. In addition, there is a buoyancy force between any two channels (caused by the differences in densities resulting from the differences in the channel heating rates) favoring downward flow through the low power channel. The channel flow direction is decided by the greater of the two buoyancy forces. Hence, when conditions are ripe, the flow in a parallel channel can reverse. It can be shown that such a situation exists if any of the channels is brought to zero power. In fact upward flow is unstable for any unheated channel in a system of parallel vertical heated channels under natural circulation conditions (see Appendix-2). This is a fundamental difference when compared to forced circulation systems.

Chato (1963) [27] demonstrated that if the system in Fig. 9 is started up by heating only one channel ($Q_1 = 0$ and $Q_3 = 0$), then a steady state would be achieved with the heated channel flowing up and the unheated channels flowing down. Now, if we begin to increase power to the down flowing channel-1 keeping power of channel-2 constant, then it will start flowing upwards only after reaching a critical value of power, Q_c . On the other hand, if heating is started in both the channels 1 and 2 simultaneously, then upward flow would be observed in both the channels even if $Q < Q_c$. Between $0 < Q < Q_c$ channel-1 can flow up or down depending on the operating procedure and this region of power is called as metastable regime by Chato (1963) [27]. Fundamentally, this is the region where

steady states with different flow directions are possible. The instability manifests itself in the form of a seemingly unexplained flow reversal in one or more parallel channels during power changes. Near the flow reversal threshold, one could also get sustained oscillations as that observed in the figure-of-eight loop with throughflow.

With vertical parallel inverted U-tubes (such as that in the NC based steam generators of PWRs and PHWRs, Fig. 10a) Sanders (1988) [28] has shown that single-phase natural circulation can become unstable and stable flow can exist with flow in the reverse direction in some of the U-tubes. Experimentally, these were observed in integral test facilities simulating nuclear reactor systems. For example, Kukita et al. (1988) [29] observed reverse flows in some of the longest U-tubes during single-phase natural circulation tests in the ROSA-IV facility. Similar observations have been made in other integral test facilities simulating nuclear reactor systems.

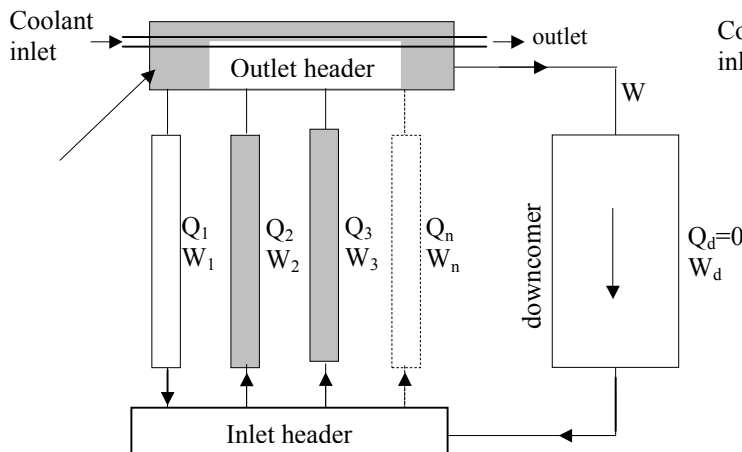


FIG. 8. A parallel channel natural circulation system.

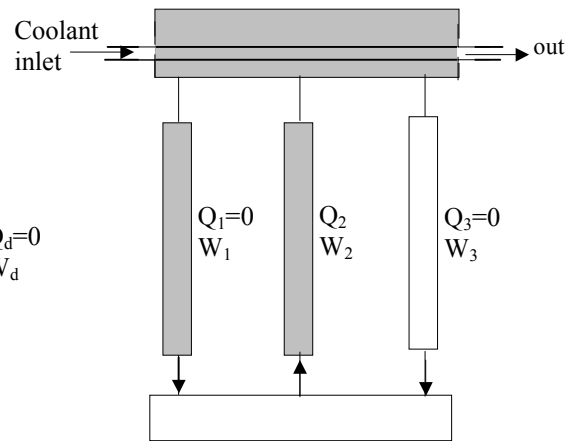


FIG. 9. Parallel channel system investigated by Chato (1963 [27]).

Thermosyphoning tests conducted in Narora Atomic Power Station unit-1, has shown flow reversals in two of the instrumented channels [30]. Flow in one of these channels continued in the reverse direction during the steady state condition. Channel flow reversals have also been reported by Caplan et al. (1983) [31] during transient thermosyphoning. All these evidences corroborate the existence of multiple steady states also in unequally heated parallel horizontal channels located at different elevations as in a PHWR (Fig. 10b).

3.3. Dynamic instabilities

Essentially the dynamic instability in single-phase systems is also density wave instability although it was referred to as DWI only recently [17]. The frequency of DWI in single-phase flow is very low (0.0015–0.005 Hz) compared to two-phase flow (1 to 10 Hz) as the velocity of flow in single-phase NC is significantly lower than that in two-phase systems. In general, single-phase natural circulation system can show two types of dynamic instabilities. They are system instabilities and parallel channel instabilities.

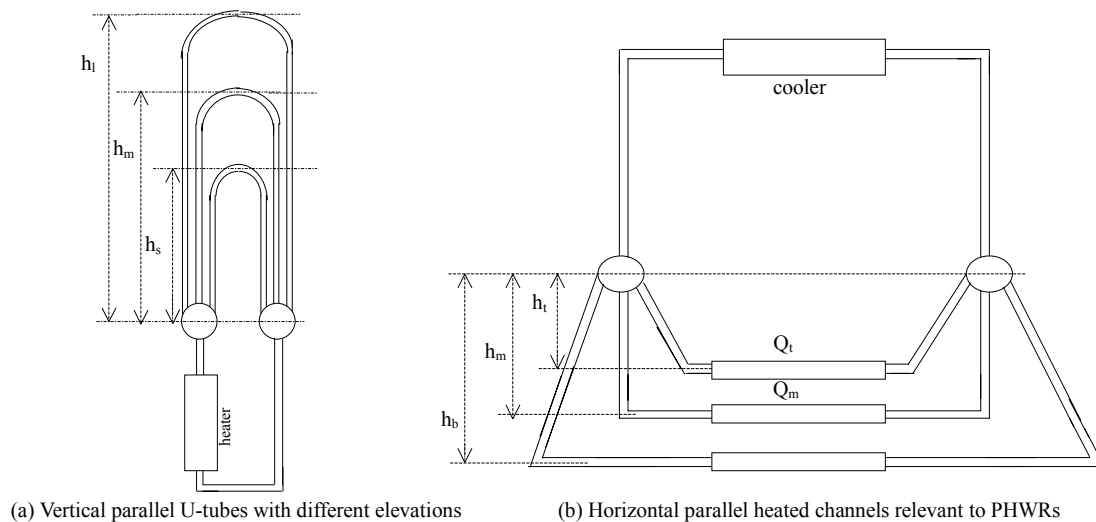


FIG. 10. Parallel channel systems.

3.3.1. System instabilities

Dynamic instabilities can develop in steady single-phase natural circulation systems through the oscillation growth mechanism. Compound static instabilities explained in the previous section also show oscillation growth mechanism near the threshold condition. The basic difference is that for the compound static instabilities, the oscillation growth and the instability can be terminated by a flow reversal. However, in case of pure dynamic instability, the oscillation growth is terminated by limit cycle oscillations, which can be periodic or chaotic. For example, Welander (1957) [3] observed periodic bi-directional oscillations in an open vertical U-loop with period ranging from 20 seconds to 4 hours (Fig. 11a). Keller (1966) [13] predicted unidirectional oscillations without flow reversal in a rectangular loop with a point heat source and a point heat sink located at the center of the bottom and top horizontal pipes respectively (Fig. 11b). Welander (1967) [14] predicted chaotic oscillations with flow reversal in a closed loop with two vertical branches and a point heat source and a point heat sink (Fig. 11c). All these oscillatory modes were experimentally observed by Vijayan et al. (2004) [32] in a rectangular loop with finite length of heater and cooler. They also identified the boundaries of each oscillatory regime in terms of the heater power for specified cooler conditions.

Welander (1967) [14] carried out both analytical and numerical investigations of the growth of small-amplitude oscillations in a loop with two vertical branches having a point heat source and a point heat sink located at the bottom and top respectively and came out with a physical explanation for the oscillation growth. According to him, the dynamics of the NCS is such that a temporary disturbance either in the heater or the cooler (like an increase in heater power or decrease in the cooling water flow) can cause a pocket of fluid to issue out from the heater (or cooler) which is hotter than normal. As this hot pocket ascends along the vertical branch, it increases the flow rate and hence reduces its residence time in the cooler with the result that the identity of the hot pocket is maintained when it enters the downward flowing vertical pipe. In this leg as the hot pocket descends it reduces the flow rate and the flow rate is the minimum when it enters the heater. The increased residence time in the heater causes the hot pocket to emerge from the heater hotter than in the previous cycle. Simultaneously a cold pocket is also formed in the cooler due to the larger residence time in the cooler. As this hot pocket ascends and the cold pocket descends induced flow rate is more than in the previous cycle. The oscillation growth can continue in this way until flow reversal. Subsequently, Welander (1967) [14] showed that the oscillation growth continues in the reverse direction leading to flow reversal and repetition of the process. Oscillation growth as a mechanism is found to be valid for the instability development from steady flow (Fig. 12). However, after the first flow reversal periodic bi-directional pulsing is observed in the experiments.

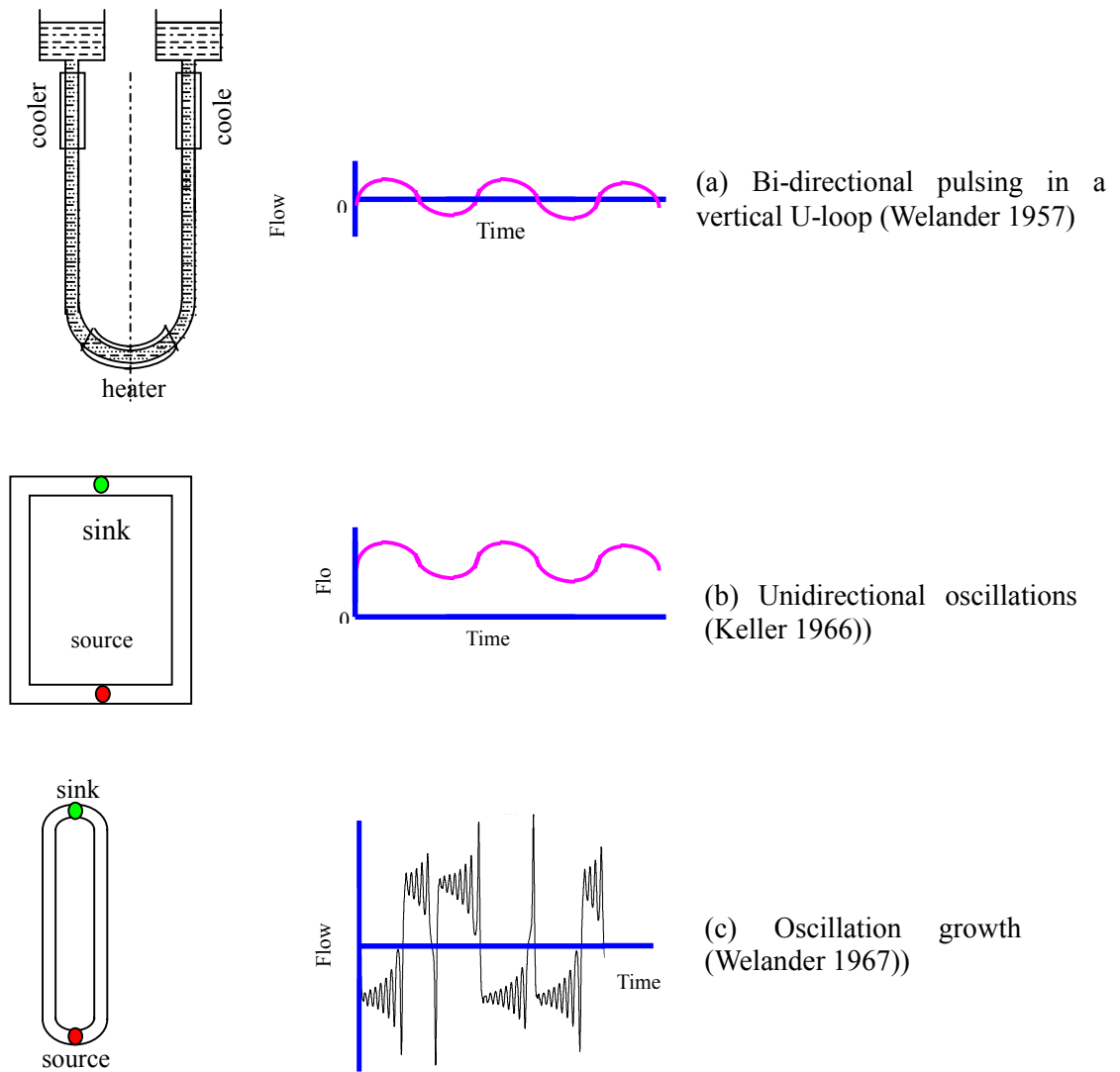


FIG. 11. Dynamic instability in single-phase NCSs.

Creveling et al. (1975) [15] experimentally investigated the stability characteristics of the toroidal loop, which showed oscillatory behaviour as predicted by Welander (1967) [14]. Unstable oscillatory behaviour was also observed in rectangular loops by Vijayan et al. (1992) [33], Misale et al. (1998 and 1999) [34], [35] and Nishihara (1997) [36]. Numerical simulation showed several oscillatory modes in the simple rectangular loop [37] other than those observed in the experiment. Recently Vijayan et al. (2004) [32] numerically simulated the entire unstable oscillatory regime in a rectangular loop from the lower threshold to the upper threshold which showed the rich variety of oscillatory modes possible. As we approach the instability threshold unidirectional oscillations are observed first followed by chaotic switching regime. With increase in power, periodic bi-directional flow is observed. With further increase in power, the periodic bi-directional oscillations become chaotic with the degree of chaos increasing with power.

3.3.2. Parallel channel instability

Apart from the static instability discussed earlier, parallel channel systems can have a dynamic instability mode, which is also related to the loose coupling of the parallel channels with the external circuit especially at low Δp across the parallel channels. A possible mechanism for this instability is as follows:

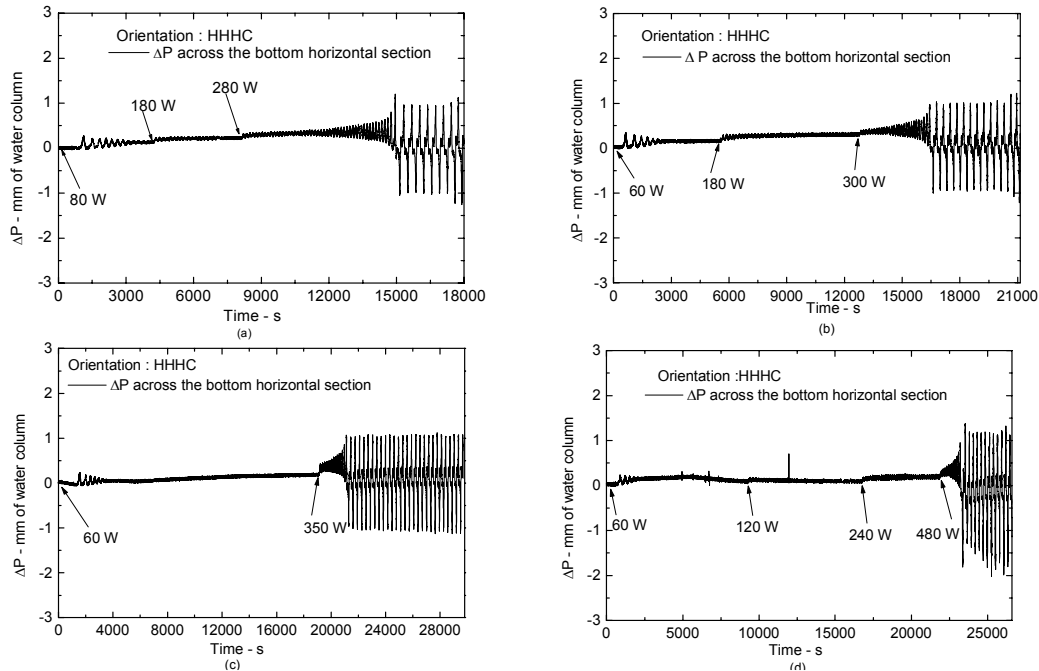


FIG. 12. Instability development by the oscillation growth mechanism.

Consider a system with a large number of parallel channels operating under steady single-phase NC condition. Let us consider a temporary disturbance in the form of an increase in the power of one of the channels (For convenience, we call it the disturbed channel). The increase in power will increase the exit temperature and reduce its density and hence the gravitational pressure drop causing the flow to accelerate (as the Δp across the parallel channels must be same). The neighbouring channel supplies the extra flow demanded by the disturbed channel as the increased buoyancy driving force (between the channels) retards the upward flow in the neighbouring channel. Because of the increased flow in the disturbed channel its exit temperature drops and its average density tends to increase. Simultaneously, the neighbouring channel that supplied the excess flow tends to experience an increase in exit temperature and a decrease in density and hence the pressure drop causing the flow to increase. This time the neighbour channel demands more flow from the disturbed channel which is decelerating and the process repeats itself if the conditions are right. It may be noted that the sum of the change in densities of the disturbed and the neighbour channel always add up to zero. As a result, the flow in the external circuit remains unaffected as it depends on the average density in the parallel channels, which does not change practically. The mechanism of parallel channel instability as explained above considered only two channels and out-of-phase oscillations with 180° phase shift is the expected mode. However, in a system with a large number of parallel channels, it is possible that several parallel channels can be involved, and the phase shift can obviously be different.

3.4. Compound dynamic instabilities

Compound dynamic instabilities with the system density wave oscillations superimposed on the parallel channel oscillations are possible with single-phase parallel channel natural circulation systems. Theoretical investigations in a two channel toroidal loop by Satoh et al (1998) [38] show an in-phase and an out-of-phase oscillation mode, but failed to cash in on the large literature available on

parallel channel instability. Experimental and theoretical study by Satou et al (2001) [39] shows that the parallel channel toroidal system becomes unstable at a higher power than single channel system.

4. INSTABILITIES ASSOCIATED WITH BOILING INCEPTION

Boiling inception is a large enough disturbance that can bring about significant change in the density and hence the buoyancy driving force in a NCS. A stable single-phase NCS can become unstable with the inception of boiling. Boiling inception also considerably affects pure single-phase instability. Boiling inception is a static phenomenon that can lead to instability in low pressure systems. However, prediction of the threshold of instability requires consideration of the feedback effects. Hence the instability belongs to the class of compound static instability. In this case, however, the instability continues with limit cycle oscillations. The oscillatory mode during boiling inception can also be significantly affected by the presence of parallel channels.

4.1. Effect of boiling inception on unstable single-phase NC

With increase in power, subcooled boiling begins in an unstable single-phase system leading to the switching of flow between single phase and two-phase regimes. Experiments in a rectangular loop showed that subcooled boiling occurs first during the low flow part of the oscillation cycle [11], [32]. The bubbles formed at the top horizontal heated wall flows along the wall into the vertical limb leading to an increase in flow rate. The increased flow suppresses boiling leading to single-phase flow. Several regimes of unstable flow with subcooled boiling can be observed depending on the test section power such as (a) instability with sporadic boiling (boiling does not occur in every cycle), (b) instability with subcooled boiling once in every cycle, (c) instability with subcooled boiling twice in every cycle and (d) instability with fully developed boiling. The change in power required from the first to the last stage is quite significant and it may not be reached in low power loops.

4.2. Effect of boiling inception on steady single-phase NC

A common characteristic of the instabilities associated with boiling inception is that single-phase conditions occur during part of the oscillation cycle. With the bubbles entering the vertical tubes, the buoyancy force is increased which increases the flow. As the flow is increased, the exit enthalpy is reduced leading to suppression of boiling. This reduces the buoyancy force and the flow, increasing the exit enthalpy resulting in boiling and leading to the repetition of the process. Krishnan and Gulshani (1987) [40] observed such instability in a figure-of-eight loop. They found that the single-phase circulation was stable. However, with power increase, the flow became unstable as soon as boiling was initiated in the heated section. It is known that the instability due to boiling inception disappears with increase in system pressure due to the strong influence of pressure on the void fraction and hence the density (Fig. 13). However, for a given system, it is not known at what pressure this instability disappears nor its dependence on the loop geometry. Knowledge of this pressure is essential for arriving at a rational start-up procedure for NCBWRs. Flashing and Geysering instability also belong to this category.

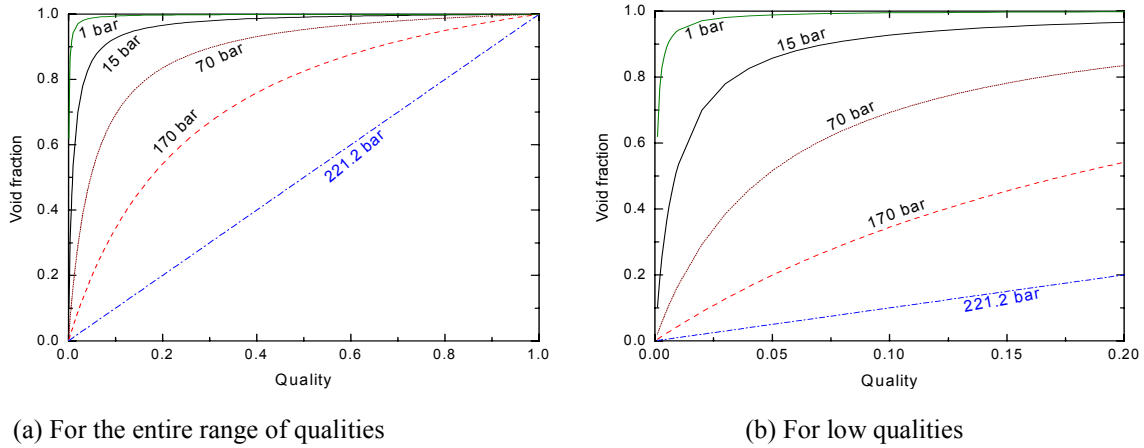


FIG. 13. Effect of pressure on the void fraction.

4.2.1. Flashing instability

Flashing instability is expected to occur in NCSs with tall, unheated risers. The fundamental cause of this instability is that the hot liquid from the heater outlet experiences static pressure decrease as it flows up and may reach its saturation value near the exit of the riser causing it to vaporize. The increased driving force generated by the vaporization, increases the flow rate leading to reduced exit temperature and suppression of flashing. This in turn reduces the driving force and flow causing the exit temperature to increase once again leading to the repetition of the process. The necessary condition for flashing is that the fluid temperature at the inlet of the riser is greater than the saturated one at the exit [41]. The instability is characterized by oscillatory behaviour and is observed only in low-pressure systems.

4.2.2. Geysering

Geysering was identified by both Boure et al. (1973) [2] and Aritomi et al. (1993) [42] as an oscillatory phenomenon which is not necessarily periodic. The proposed mechanism by both the investigators differ somewhat. However, a common requirement for geysering is again a tall riser at the exit of the heated section. When the heat flux is such that boiling is initiated at the heater exit and as the bubbles begin to move up the riser they experience sudden enlargement due to the decrease in static pressure and the accompanying vapor generation, eventually resulting in vapor expulsion from the channel. The liquid then returns, the subcooled nonboiling condition is restored and the cycle starts once again. The main difference with flashing instability is that the vapor is produced first in the heated section in case of geysering where as in flashing the vapor is formed by the decrease of the hydrostatic head as water flows up.

The mechanism as proposed by Aritomi et al. (1993) [42] also considers condensation effects in the riser. According to him, geysering is expected during subcooled boiling when the slug bubble detaches from the surface and enters the riser (where the water is subcooled) where bubble growth due to static pressure decrease and condensation can take place. The sudden condensation results in depressurization causing the liquid water to rush in and occupy the space vacated by the condensed bubble. The large increase in the flow rate causes the heated section to be filled with subcooled water suppressing the subcooled boiling and reducing the driving force. The reduced driving force reduces the flow rate increasing the exit enthalpy and eventually leading to subcooled boiling again and repetition of the process. Geysering involves bubble formation during subcooled conditions, bubble detachment, bubble growth and condensation. Geysering is a thermal nonequilibrium phenomenon. On the other hand, during flashing instability, the vapour is in thermal equilibrium with the surrounding

water and they do not condense during the process of oscillation. Both these instabilities are observed during low pressure conditions only.

5. TWO-PHASE NC INSTABILITY

Several reviews on two-phase instability are available [2], [43], [44]. None of these are specific to NCSs although most of the instabilities can be observed in forced and natural circulation systems.

5.1. Pure or fundamental static instability

The cause of the phenomenon lies in the steady state laws and hence the threshold of the instability can be predicted using the steady state governing equations. Static instability can lead either to a different steady state or to a periodic behavior. Commonly observed static instabilities are flow excursion and boiling crisis.

5.1.1. Flow excursion or excursive instability

It is also known as Ledinegg instability, after the scientist who discovered it for the first time [45]. It involves a sudden change in the flow rate to a lower value. The new flow rate may induce the occurrence of CHF. The occurrence of multiple steady state solutions is the fundamental cause of this instability (see Fig. 14a). While drawing the head versus flow characteristic of NCSs, it is customary to consider the driving pressure differential as that due to the liquid head in the downcomer (Fig. 14b) which is almost independent of the flow rate due to the negligible friction pressure loss [46]. The stability criterion for the Ledinegg type instability is given by $d(\Delta P)/dG < 0$ i.e. negative slope in static system characteristic. Point 'b' in Figure 14a satisfies this criterion and is therefore unstable.

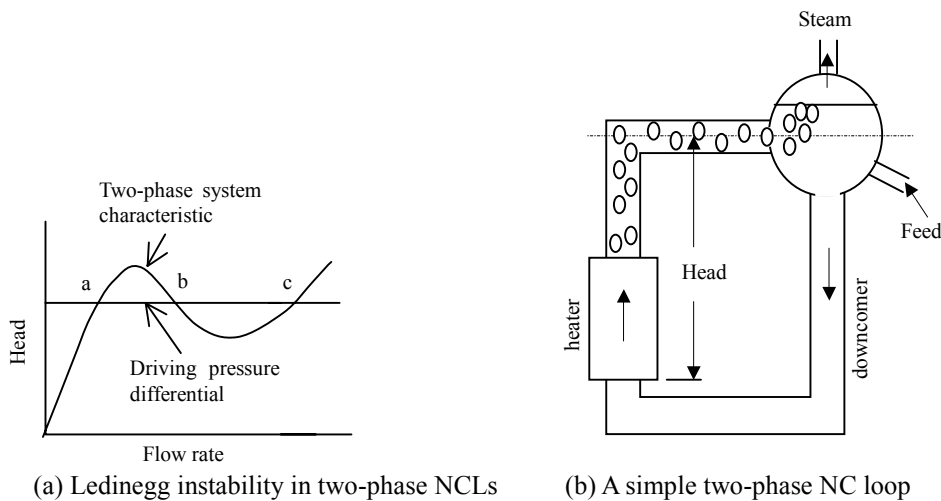


FIG. 14. Mechanism of excursive instability.

The instability can also be observed in forced flow systems. In forced circulation systems, the instability can be avoided by inlet throttling. However, this option may not work as effectively as in forced flow due to the reduction in the flow caused by the introduction of inlet throttling in NCSs.

5.1.2. Boiling crisis

Following the occurrence of the critical heat flux, a region of transition boiling may be observed in many situations as in pool boiling (see Fig. 15a). During transition boiling a film of vapour can prevent the liquid from coming in direct contact with the heating surface resulting in steep temperature rise and even failure. The film itself is not stable causing repetitive wetting and dewetting of the heating surface resulting in an oscillatory surface temperature. The instability is characterized by sudden rise

of wall temperature followed by an almost simultaneous occurrence of flow oscillations. This shall not be confused with the premature occurrence of CHF during an oscillating flow, in which case the oscillations occur first followed by CHF (see Fig. 15b).

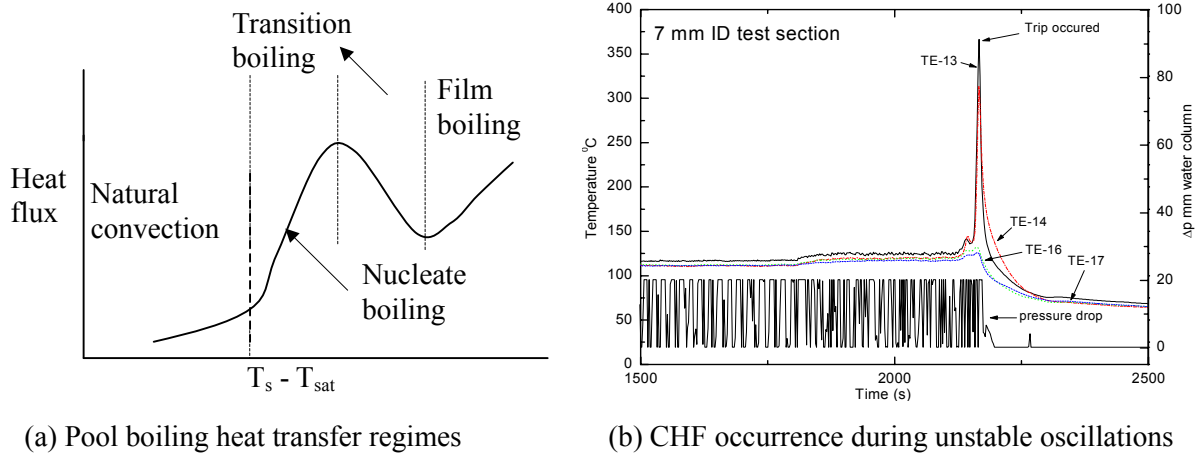


FIG. 15. Instability due to boiling crisis.

5.2. Compound static instability

Two-phase systems also exhibit the instabilities associated with multiple steady states in different flow directions as in single-phase flow and will not be discussed further here. All the instabilities associated with boiling inception such as flashing and geysering discussed earlier also belong to this category. Flow pattern transition instability also belongs to this category.

5.2.1. Flow pattern transition instability

Two-phase systems exhibit different flow patterns with differences in the pressure drop characteristics, which is the fundamental cause of this instability. For example, the bubbly-slug flow has a higher pressure drop compared to annular flow. Consider a two-phase NCS operating near the slug to annular flow transition boundary. A small temporary disturbance in power can slightly increase the vapour production rate causing the flow pattern to change to annular. Due to the low pressure drop in annular flow, the flow rate increases leading to lower exit enthalpy and reduction in steam quality. The reduced steaming rate cannot support annular flow and the flow pattern changes to slug. The increased pressure drop of slug flow pattern reduces the flow rate which in turn increases the exit enthalpy and steam production rate causing the flow to revert to annular and the cycle repeats itself. Theoretical analysis of the phenomena is hampered by the unavailability of validated flow pattern specific pressure drop correlations and flow pattern transition criteria. Recently Nayak et al. (2003) [10] proposed an analytical model for the flow pattern transition instability in a pressure tube type heavy water reactor. They found that the instability is similar to the Ledinegg type, but occurs at a higher power. The analysis neglected the transient effects.

5.2.2. Parallel channel systems

Two-phase parallel channel systems exhibit two types of multiple steady states: multiple steady states in the same flow direction (Ledinegg instability) as well as different flow direction (compound static instability). Linzer and Walter (2003) [47] studied the latter and derived a criterion for flow reversal in a parallel channel system with a common downcomer. For a system with two heated channels and a common downcomer, the critical power ratio at which the flow reversal occurs is found to be dependent on the power of the other heated channel. In fact the critical power ratio is found to increase with the power of the other heated channel.

5.3. Dynamic instability

Regenerative feedback and time delay effects are important for dynamic instability and hence analysis requires consideration of the unsteady governing equations. As already mentioned DWI is the most commonly observed instability in natural circulation loops. The mechanism causing this instability is already discussed in section 2.2.2. Tall risers and long horizontal or inclined pipes, can significantly influence the instability. Other geometric parameters that affect the instability are the orientation of the source and sink, inlet orificing, length and diameter of source, sink and connecting pipes, etc. The operating parameters that significantly affect the instability are the inlet subcooling, system pressure, power, power distribution and cooler (or SG) secondary conditions. A number of auxiliary parameters such as transient heat storage in the boundary walls, variable heat transfer coefficient and fluid friction influence the instability.

5.4. Compound dynamic instability

Instability is considered compound when more than one elementary mechanisms interact in the process and cannot be studied separately. If only one instability mechanism is at work, it is said to be fundamental or pure instability. Examples of compound instability are: (1) Thermal oscillations, (2) Parallel channel instability (PCI), (3) Pressure drop oscillations and (4) BWR (Boiling Water Reactor) instability.

5.4.1. Thermal oscillations

In this case, the variable heat transfer coefficient leads to a variable thermal response of the heated wall that gets coupled with the DWO. Thermal oscillations are considered as a regular feature of dryout of steam-water mixtures at high pressure [2]. The steep variation in heat transfer coefficient typical of transition boiling conditions in a post CHF scenario can get coupled with the DWO. During thermal oscillations, dryout or CHF point shift downstream or upstream depending on the flow oscillations. Hence thermal oscillations are characterized by large amplitude surface temperature oscillations (due to the large variation in the heat transfer coefficient). The large variations in the heat transfer coefficient and the surface temperature causes significant variation in the heat transfer rate to the fluid even if the wall heat generation rate is constant. This variable heat transfer rate modifies the pure DWO.

5.4.2. Parallel channel instability (PCI)

Interaction of parallel channels with DWO can give rise to interesting stability behaviours as in single-phase NC. Experimentally, both in-phase and out-of-phase oscillations are observed in parallel channels. However, in-phase oscillation is a system characteristic and parallel channels do not generally play a role in it. With in-phase oscillation, the amplitudes in different channels can be different due to the unequal heat inputs or flow rates. Occurrence of out-of-phase oscillations is characteristic of PCI. The phase shift of out-of-phase oscillations (OPO) is known to depend on the number of parallel channels. With two channels, a phase shift of 180° is observed. With three channels, it can be 120° and with five channels it can be 72° [48]. With n-channels, Aritomi et al. (1986) [49] reports that the phase shift can be $2\pi/n$. However, depending on the number of channels participating, the phase shift can vary anywhere between π and $2\pi/n$. For example, in a 3-channel system one can get phase shift of 180° or 120° depending on whether only two or all the three channels are participating. The mechanism of parallel channel instability is similar to that in single-phase systems. PCI is initiated by events within the parallel channels and is not observable in the common points of the system. The instability is also possible with the horizontal parallel channels used in pressure tube type PHWRs and with the vertical U-tube type parallel channels of SGs.

5.4.3. Pressure drop oscillations (PDO)

Pressure drop oscillations are associated with operation in the negative sloping portion of the pressure drop - flow curve of the system. It is caused by the interaction of a compressible volume (surge tank or

pressurizer) at the inlet of the heated section with the pump characteristics and is usually observed in forced circulation systems. DWO occurs at flow rates lower than the flow rate at which pressure drop oscillation is observed. Usually, the frequency of pressure drop oscillation is much smaller and hence it is easy to distinguish it from density wave oscillations. However, with a relatively stiff system, the frequency of PDO can be comparable to DWO making it difficult to distinguish between the two. Very long test sections may have sufficient internal compressibility to initiate pressure drop oscillations. Like Ledinegg instability, there is a danger of the occurrence of CHF during pressure drop oscillations. Also, inlet throttling (between the surge tank and the boiling channel) is found to stabilize PDO just as Ledinegg instability.

5.4.4. BWR instability

Here the void reactivity feedback gets coupled with the flow dynamics of the density wave instability. The system pressure, the fuel time constant and the void reactivity coefficient have a strong influence on the instability. It is also known as coupled neutronic-thermal hydraulic instability that manifests itself as induced power oscillations in the core through neutronic feedback. A schematic of the BWR dynamic feedback loop is given in Fig. 16. Feedback due to changes in coolant and moderator temperatures are not considered since their magnitudes are much smaller than the feedback due to void reactivity.

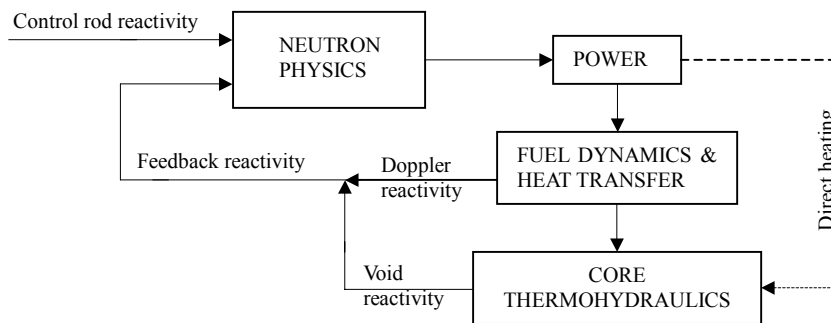


FIG. 16. The BWR feedback loop.

Normally, the BWRs have a negative void reactivity coefficient. That means, if the void increases due to reduction of flow during a thermal hydraulic oscillation event, the power will reduce by the negative void reactivity coefficient. However, the effect of negative void reactivity feedback coefficient on the thermal hydraulic stability depends on the fuel time constant. The fuel time constant is basically the delay time associated with the transfer of heat from the fuel to the coolant, which is dependent on the thermal conductivity of fuel, clad, the gap conductance across the fuel and clad, and the coolant side heat transfer coefficient. This also varies with operational conditions and burn-up. Mostly in commercial BWRs this value is of the order of 6 to 10 seconds. The thermal hydraulic oscillation frequency in BWRs is of the order of 0.3 to 0.5 Hz. Hence the fuel time constant can destabilize due to phase delay. But it can stabilize due to the inherent filtering of the oscillations having a frequency greater than 0.1 Hz as shown by March-Leuba and Ray (1993) [50]. It is seen from the work of Rao et al. (1995) [51] that a very small fuel time constant (less than 0.1 s) can stabilize the thermal hydraulic oscillations since there is no delay, and hence an increase in void fraction would reduce the power which will reduce the void fraction and hence stabilizes. Similar results are also observed for large fuel time constants when the negative void reactivity feedback stabilizes due to decrease in gain of void-power transfer function.

There are many incidents of instabilities in commercial BWRs. A review of the coupled neutronic-thermohydraulic instabilities is given by March-Leuba and Rey (1993) [50]. The BWR instability is a known phenomenon since the 1960s. The problem has been considered solved several times. For example, most reactors built during the 1960s and 1970s did not show instability. But instability events began to surface in the BWR designs of the 1980s (see Table-1). The knowledge gained from past instability events has helped to improve our understanding of BWR instabilities and to develop

techniques for avoiding it in future. Hence a brief review of the instabilities is given here. The reported BWR instabilities can be categorized into two: viz., instability events and instability tests. The instability events occurred inadvertently in the plant whereas instability was excited deliberately during tests. An overview of reported instability events including the date of occurrence, the plant involved, the country to which it belonged and the initiating event that caused the instability are given in Table-1.

Table 1: An overview of instability events

Date	Plant	Location	Remarks
30.06.82	Coarso	Italy	Core instability during start-up
13.01.84	Coarso	Italy	Instability after pump trip
17.10.84	S. maria	Spain	Power oscillations during operation
23.02.87	TVO	Finland	Power oscillations during power raising
09.03.88	La Salle2	USA	Core instability due to pump trip event
29.10.88	Vermont Yankee	USA	power oscillations
26.10.89	Ringhals	Sweden	Instability during power rise after refueling
08.01.89	Oskarshamn	Sweden	Power oscillations
29.01.91	Cofrentes	Spain	Power oscillations
03.07.91	Isar	Germany	Power oscillations following trip of 4 out of 8 pumps
15.08.92	WNP	USA	Power oscillations during start-up
09.07.93	Perry	USA	Entry into a region of core instability
01.1995	Laguna Verde	Spain	Power oscillations during start-up
17.07.96	Forsmark	Sweden	Local oscillations due to a bad seated fuel assembly
08.02.98	Oskarshamn-3	Sweden	Power oscillations during start-up
25.02.99	Oskarshamn-2	Sweden	Power oscillations after a turbine trip with pump run back
--.11.01	Philippsburg-1	Germany	In-phase power oscillations

These instability events helped to identify the initiating events that can lead to instability as listed below: (a) pump trip (partial or total), (b) start-up or power rise, (c) operator error, (d) loss of feed water heating, (e) power rise after refueling or improper fuel loading and (f) bad combination of core design and control rod pattern.

There are many cases of instability observed during stability tests. Typical examples are: Finnish BWRs (TVO-I and II), Swedish BWRs (Forsmark 1,2 &3, Ringhals, Oskarshamn & Barseback), US BWR (Peach Bottom), Italy (Coarso) and Switzerland (Leibstadt).

The instability events and tests show that current designs of BWRs are not completely stable for their entire flow-power map and core power oscillations is an inherent characteristic of the instability. Most of the plants showed limit cycle oscillations with decay ratio (DR) equal to 1. Oscillations started from one zone and propagated to the other zones. All instability events have occurred during low flow conditions (30 to 40%) with power in the range of 40 to 70% [52]. Both in-phase and out-of-phase oscillations were observed. The in-phase mode of oscillations could be deliberately transformed into out-of-phase oscillations by changing some control rod positions. Radial and axial power profile is found to affect the instability. A strongly bottom peaked axial power profile makes the core more unstable and a radially increasing power shape makes the core susceptible to excite out-of-phase oscillations.

Modern BWRs have a respectable size forbidden zone with clear operating procedures to avoid it. However, certain transients can cause entry into the forbidden zone. Instability events and tests have clearly established that three different types of oscillations can happen if we enter the forbidden zone. These are:

- (1) In-phase oscillations (IPO) (system instability, core-wide or global instability);
- (2) Out-of-phase oscillations (OPO) (parallel channel instability (PCI)); and
- (3) Dual Oscillations observed in the overlapping region of IPO and OPO.

The whole loop (in fact the entire plant) will take part in the in-phase instability (IPI). Usually it is initiated by events outside the core (i.e., parallel channels) like loss of feed water heaters, pumps (loss of pumps can excite PCI also), etc. It is easily detected and terminated by the scram system. During PCI, one half of the core oscillates azimuthally out-of-phase with the other half (commonly observed and also known as regional oscillations). During regional oscillations, average power level does not change as long as the sum of the positive and negative oscillations add up to zero and hence APRM (Average Power Range Monitor) cannot or timely detect OPO. Local oscillations in the core also is possible, but is rarely observed. Since the flow in the recirculation loop is in single-phase condition, the recirculation flow dynamics usually has a positive effect in reducing the thermal hydraulic feed back gain and hence stabilizes IPI. However, in case of an out-of-phase instability, the flow feed back has a very large gain since the flow in the channels are in two-phase condition and the recirculation loop friction does not come into play. But the neutronic feed back has higher gain for the core-wide instabilities (fundamental mode oscillation) and lower gain for the out-of-phase instabilities since they occur in damped subcritical modes.

5.4.5. *Instability in natural circulation BWRs*

The flow velocity in natural circulation BWRs is usually smaller than that of forced circulation BWR. Besides, due to the presence of tall risers in natural circulation BWRs, the frequency of density-wave oscillation can be much lower due to longer traveling period of the two-phase mixture in the risers. The effects of negative void reactivity feed back are found to stabilize the very low frequency Type I instabilities [53], [54]. But it may stabilize or destabilize the Type II instabilities depending on its time period.

In case of a natural circulation BWR, the existence of a tall riser or chimney over the core plays a different role in inducing the instability. Series of experiments carried out by Van der Hagen et al. (2000) [55] in the Dodewaard natural circulation BWR in The Netherlands showed that instabilities could occur at low as well as at high powers in this reactor. From measured decay ratio, it was evident that at very low power there is a trend of increase in decay ratio and similar results are seen at higher power also. The low power oscillations are induced by the Type I density-wave instabilities and high power oscillations are induced by the Type II density-wave instabilities. Type I and Type II instabilities have been predicted to occur in the Indian AHWR which is a natural circulation pressure tube type BWR, away from the nominal operating condition [54]. It may be noted that in case of forced circulation BWRs, instabilities observed under natural circulation conditions are due to pump trip transients when the core exit quality is high due to low flow and high power. Hence these are induced by the Type II density-wave instabilities only.

6. CONCLUDING REMARKS

Various bases used for classification of instabilities have been reviewed. The most widely accepted classification is based on the method of analysis used in identifying the stability threshold. This method of classification covers the entire spectrum of instabilities observed to date. Other classifications that are in common use today are in fact subcategories of a particular class of the instabilities covered under this classification. While classifying instabilities of NCSs, a need was felt to consider the instabilities associated with single-phase condition, boiling inception and two-phase condition separately as a natural circulation system progresses through all these stages before reaching the fully developed two-phase circulation. Most instabilities observed in forced circulation systems are observable in natural circulation systems. However, natural circulation systems are more unstable due to the regenerative feedback inherent in the mechanism causing the flow. Besides the instability in single-phase systems, natural circulation loops also exhibit an instability associated with flow reversal in contrast to forced circulation systems.

NOMENCLATURE

A	- flow area, m^2
b	- exponent in the friction factor correlation
C _p	- specific heat, J/kg K
D	- loop diameter, m
f	- Darcy friction factor
g	- acceleration due to gravity, m/s^2
H	- loop height, m
K	- local pressure loss coefficient
L _t	- total loop circulation length, m
p	- coefficient in the friction factor correlation
Δp	- pressure drop, Pa
Q	- total heating rate, W,
q	- heat flux, W/m^2
R	- total hydraulic resistance, m^{-4}
Re	- Reynolds number ($DW/A\mu$)
T	- temperature, K
t	- time, s
U	- overall heat transfer coefficient, W/m^2K
W	- mass flow rate, kg/s
x	- coordinate around the loop, m
z	- elevation, m

Greek Symbols

α	- thermal diffusivity, m^2/s
θ	- nondimensional temperature
μ	- dynamic viscosity, kg/ms
ρ	- density, kg/m^3
τ	- nondimensional time
ω	- nondimensional flow rate

Subscripts

1	- channel 1
2	- channel 2
c	- cooler
cl	- cold leg
d	- downcomer
e	- external circuit
f	- friction
i	- internal circuit
h	- heater
hl	- hot leg
s	- secondary

REFERENCES

- [1] MOCHIZUKI, H., Flow instabilities in boiling channels of pressure tube type reactor, *Nuclear Engineering Design*, 149, pp.269–277 (1994).
- [2] BOURE, J.A., BERGLES, A.E., and TONG, L.S., Review of two-phase flow instability, *Nuclear Engineering and Design* 25, pp.165–192 (1973).
- [3] WELANDER, P., Note on the self-sustained oscillations of a simple thermal system, *Tellus*, 9, pp.419–420 (1957).
- [4] ZUBER, N., An analysis of thermally induced flow oscillations in the near critical and supercritical thermodynamic region, NAS 8-11422, final rept. (1966).
- [5] STENNING, A.H., and VEZIROGLU, T.N., Flow oscillation modes in forced-convection boiling, *Proc. 1965 Heat Transfer and Fluid Mechanics Inst.*, pp. 301–316, Stanford University Press, Stanford, California (1965).
- [6] FUKUDA, K., and KOBORI, T., Classification of two-phase flow stability by density-wave oscillation model, *J. Nuclear Science and Technology*, 16, pp.95–108 (1979).
- [7] YADIGAROGU, G., and BERGLES, A.E., An experimental and theoretical study of density-wave oscillations in two-phase flow, MIT rept. DSR 74629-3 (HTL 74629-67) (1969).
- [8] ACHARD, J.L., DREW, D.A., LAHER JR, R.T., The analysis of nonlinear density wave oscillations in boiling channels, *Journal of Fluid Mechanics*, 155, pp.213–232 (1985).
- [9] AMBROSINI, W., FORGIONE, N., FERRERI, J.C., and BUCCI, M., The effect of wall friction in single-phase natural circulation stability at the transition between laminar and turbulent flow, to appear in *Annals of Nuclear Energy* (2004).
- [10] NAYAK, A.K., VIJAYAN, P.K., JAIN, V., SAHA, D., and SINHA, R.K., Study on the flow-pattern-transition instability in a natural circulation heavy water moderated boiling light water cooled reactor, *Nuclear Engineering Design*, 225, pp.159–172 (2003).
- [11] VIJAYAN, P.K., BHOJWANI, V.K., BADE, M.H., SHARMA, M., NAYAK, A.K., SAHA D., and SINHA, R.K., Investigations on the effect of heater and cooler orientation on the steady state, transient and stability behaviour of single-phase natural circulation in a rectangular loop, BARC/2001/E/034 (2001).
- [12] CHEN, W.L., WANG, S.B., TWU, S.S., CHUNG, C.R., and CHIN PAN, Hysteresis effect in a double channel natural circulation loop, *International Journal of Multiphase Flow*, 27, 171–187 (2001).
- [13] KELLER, J.B., Periodic oscillations in a model of thermal convection, *J. Fluid Mechanics* 26, pp. 599–606 (1966).
- [14] WELANDER, P., On the oscillatory instability of a differentially heated loop, *J. Fluid Mech.* 29, pp.17–30 (1967).
- [15] CREVELING, H.F., DE PAZ, J.F., BALADI, J.Y., and SCHOENHALS, R.J., Stability characteristics of a single-phase free convection loop, *J. Fluid Mechanics*. 67, pp.65–84 (1975).
- [16] BAU H.H., and WANG, Z.Y., Chaos: a heat transfer perspective, in C.L. Tien (ed.), *Annual Review of Heat Transfer*, Vol.4 (1992).
- [17] LAHEY JR., R.T., Engineering applications of fractal and chaos theory in Modern developments in multiphase flow & heat transfer, Center for Multiphase Research, Rensselaer Polytechnic Institute, Troy, NY - USA 12180–3590 (1992).
- [18] ZVIRIN, Y., A review of natural circulation loops in pressurised water reactors and other systems, *Nucl. Eng. Des.* 67, pp.203–225 (1981).
- [19] GREIF, R., Natural circulation loops, *J. Heat Transfer* 110, pp.1243–1258 (1988).
- [20] BAU, H.H., and TORRANCE, K.E., Transient and steady state behaviour of an open, symmetrically heated, free convection loop, *Int. J. Heat Mass Transfer* 24, pp.597–609 (1981).
- [21] ZVIRIN, Y., The instability associated with the onset of motion in a thermosyphon, *Int. J. Heat Mass Transfer*, 28, pp.2105–2111 (1985).
- [22] MERTOL, A., GREIF, R., and ZVIRIN, Y., The transient, steady state and stability behaviour of a thermosyphon with throughflow, *Int. J. Heat Mass Transfer*, 24, pp.621–633 (1981).
- [23] VIJAYAN, P.K., Investigations on the single-phase thermosyphon phenomenon in a figure-of-eight loop relevant to pressurised heavy water reactors, Ph. D. thesis, Indian Institute of Technology, Bombay (1988).

- [24] BAU, H.H., and TORRANCE, K.E., On the stability and flow reversal of an asymmetrically heated open convection loop, *J. Fluid Mech.* 106, pp.417–433 (1981a).
- [25] VIJAYAN, P.K., and DATE, A.W., Experimental and theoretical investigations on the steady-state and transient behaviour of a thermosyphon with throughflow in a figure-of-eight loop, *Int. J. Heat Mass Transfer*, 33, pp.2479–2489 (1990).
- [26] VIJAYAN, P.K., and DATE, A.W., The limits of conditional stability for single-phase natural circulation with throughflow in a figure-of-eight loop, *Nuclear Engineering and Design*, 136, pp.361–380 (1992).
- [27] CHATO, J.C., Natural convection flows in a parallel channel system, *J. Heat Transfer* **85**, pp.339–345 (1963).
- [28] SANDERS, J., Stability of single-phase natural circulation with inverted U-tube steam generators *J. Heat Transfer*, 110, pp.735–742 (1988).
- [29] KUKITA, Y., NAKAMURA, H., TASAKA, K., and CHAULIAC, C., *Nuclear Science and Engineering*, 99, pp.289–298 (1988).
- [30] VIJAYAN, P.K., VENKAT RAJ, V., NAGDAUNE, R.K., and PILKHWAL, D.S., Thermosyphon tests and comparison with code predictions for a PHWR', 3rd International Seminar on small and medium sized reactors, New Delhi, India, August 26–28 (1991).
- [31] CAPLAN, M.Z., GULSHANI, P., HOLMES, R.W., and WRIGHT, A.C.D., Experimental and modelling aspects of small break LOCA, Proceedings of specialists' meeting organized by the IAEA, Budapest, Hungary (1983).
- [32] VIJAYAN, P.K., SHARMA, M., PILKHWAL, D.S., SAHA, D., SINHA, R.K., BHOJWANI, V.K., and SANE, N. K., Experimental and numerical investigations on the nature of the unstable oscillatory flow in a single-phase natural circulation loop, HMT-2004-C100, 6th ISHMT/ASME Heat and Mass Transfer Conference, Kalpakkam, India, Jan. 5–7 (2004).
- [33] VIJAYAN, P.K., NAYAK, A.K., PILKHWAL, D.S., SAHA, D., and VENKAT RAJ, V., Effect of loop diameter on the stability of single-phase natural circulation in rectangular loops, Proc. 5th Int. Topical Meet. on Reactor Thermalhydraulics, NURETH-5, Salt Lake City, UT, Vol.1, pp.261–267 (1992).
- [34] MISALE, M., FROGHERI, M., and RUFFINO, P., Steady-state and stability behaviour of a single-phase natural circulation loop, *Heat Transfer 1998*, Proceedings of 11th IHTC, Kyongju, Korea, August 23–28, Vol. 3 (1998).
- [35] MISALE, M., FROGHERI, M., and D'AURIA, F., Experiments in natural circulation: Influence of scale factor on the stability behaviour, Misale, M., and Mayinger, F. (Eds.), 109–114, Proceedings of Eurotherm Seminar N^o 63 on Single and Two-phase Natural Circulation, Genoa, Italy, 6–8 September (1999).
- [36] NISHIHARA, T., Oscillatory instability of a single-phase natural circulation loop, Proceedings of NURETH-8, Kyoto, Sept. 30–Oct. 4, pp.839–847 (1997).
- [37] MANISH SHARMA, VIJAYAN, P.K., NAYAK, A.K., SAHA, D., and SINHA, R.K., Numerical study of stability behaviour of single-phase natural circulation in a rectangular loop, Proceedings of 5th ISHMT-ASME Heat and Mass Transfer Conference Kolkata, India, Jan. 3–5, pp.1204–1210 (2002).
- [38] SATOH, A., OKAMOTO, K., and MADARAME, H., Instability of single-phase natural circulation under double loop system, *Chaos, Solitons & Fractals* 9, pp.1575–1585 (1998).
- [39] SATOU, A., MADARAME, H., OKAMOTO, K., Unstable behaviour of single-phase natural circulation under closed loop with connecting tube, *Experimental Thermal and Fluid Science* 25, pp.429–435 (2001).
- [40] KRISHNAN, V.S., GULSHANI, P., Stability of natural-circulation flow in a Candu-type fuel channel. *Nuclear Engineering and Design* 99, pp.403–412 (1987).
- [41] JIANG, S.Y., YAO, M.S., BO, J.H., and WU, S.R., Experimental simulation study on the start-up of the 5 MW nuclear heating reactor, *Nuclear Engineering and Design* 158, pp.111–123 (1995).
- [42] ARITOMI, M., CHIANG, J.H., Geysing in parallel boiling channels, *Nuclear Engineering and Design*, 141, pp.111–121 (1993).
- [43] YADIGAROGLU, G., Two-phase flow instabilities and propagation phenomena, in *Thermohydraulics of two-phase systems for industrial design and nuclear engineering*, J.M.

- Delhaye, M. Giot and M.L. Reithmuller, A Von Karman Institute Book, Hemisphere Publishing Corporation, Washington (1978).
- [44] KAKAC, S., Review of two-phase flow instabilities, *J. Pure and Applied Sciences*, 18, pp.171–252 (1985).
- [45] LEDINEGG, M., 1938, Instability of flow during natural and forced circulation, *Die Wärme*, 61, pp.891–898, AEC-tr-1861, (1954).
- [46] TODREAS, N.E., and KAZIMI, M.S., *Nuclear Systems II, Elements of Thermal Hydraulic Design*, Hemisphere Publications, New York, USA (1990).
- [47] LINZER, W., WALTER, H., Flow reversal in natural circulation systems, *Applied Thermal Engineering*, 23, pp.2363–2372 (2003).
- [48] FUKUDA, K., and HASEGAWA, S., Analysis on two-phase flow instability in parallel multichannels, *J. Nuclear Science and Technology*, 16, pp.190–199 (1979).
- [49] ARITOMI, M., AOKI, S., INOUE, A., Thermo-hydraulic instabilities in parallel boiling channel systems, Part 1. A nonlinear and a linear analytical model, *Nuclear Engineering Design* 95, pp.105–116 (1986).
- [50] MARCH-LEUBA, J., REY, J.M., Coupled thermohydraulic-neutronic instabilities in boiling water reactors: a review of the state-of-the-art, *Nuclear Engineering and Design* 145, pp.97–111 (1993).
- [51] RAO, Y.F., FUKUDA, K., KANESHIMA, R., Analytical study of coupled neutronic and thermodynamic instabilities in a boiling channel, *Nuclear Engineering and Design*, 154, pp.133–144 (1995).
- [52] D’AURIA, F. et al., State of the Art Report on Boiling Water Reactor Stability, OCDE/GD(97)13, OECD-NEA (1997).
- [53] VAN BRAGT, D.D.B., VAN DER HAGEN, T.H.J.J., Stability of natural circulation boiling water reactors, Part II-Parametric study of coupled neutronic-thermohydraulic stability. *Nucl. Technology* 121, pp.52–62 (1998).
- [54] NAYAK, A.K., VIJAYAN, P.K., SAHA, D., VENKAT RAJ, V., and ARITOMI, M., Analytical study of nuclear-coupled density-wave instability in a natural circulation pressure tube type boiling water reactor, *Nuclear Engineering and Design*, 195, pp.27–44 (2000).
- [55] VAN DER HAGEN, T.H.J.J., STEKELENBURG, A.J.C., VAN BRAGT, D.D.B., Reactor experiments on type-I and type-II BWR stability, *Nuclear Engineering and Design*, 200, pp.177–185 (2000).

APPENDIX 1. Multiple Steady States in Single-phase NCLs

Consider a liquid filled uniform diameter loop as shown in Fig. A1.1. The 1-D governing equations for incompressible NC flow in the loop can be written as

$$\frac{\partial W}{\partial x} = 0$$

$$\frac{L_t}{A} \frac{dW}{dt} = g \oint \rho dz - \frac{fL_t W^2}{2D\rho A^2} + \frac{KW^2}{2\rho A^2}$$

$$\frac{\partial T}{\partial t} + \frac{W}{A\rho} \frac{\partial T}{\partial x} - \alpha \frac{\partial^2 T}{\partial x^2}$$

$$= \left\{ \begin{array}{l} \frac{4q}{D\rho C_p} \quad 0 < x < x_h \quad \text{heater} \\ 0 \quad x_h < x < x_{hl} \quad \text{and} \quad x_c < x < L_t \quad \text{pipes} \\ -\frac{4U}{D\rho C_p} (T - T_s) \quad x_{hl} < x < x_c \quad \text{cooler} \end{array} \right\}$$

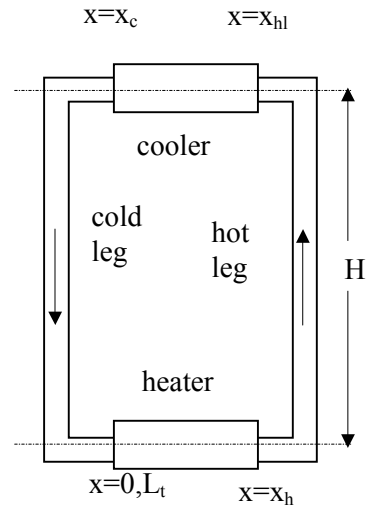


FIG. A1.1 : A uniform diameter rectangular loop

The integral momentum equation for the steady flow can be written as

$$(\rho_c - \rho_h)gH = \frac{\rho L_t \mu^b W^{2-b}}{2D^{1+b} \rho A^{2-b}} + \frac{KW^2}{2\rho A^2}$$

In writing the above equation, the form loss coefficient was considered to be constant and the friction coefficient was assumed to be given by the following equation:

$$f = \frac{p}{\text{Re}^b}$$

It may be noted that the LHS of the above equation is a constant for a specified power. Hence, the steady state flow equation is a polynomial and it can have as many roots as the order of the polynomial. Depending on the value of the exponent of the friction factor correlation, the above equation can have many roots. In the case of laminar flow with $b = 1$, it can be shown that there exists only one steady state solution with positive W . In case of transients, also, we cannot rule out the possibility of multiple steady state solutions.

APPENDIX 2. Flow behaviour in a parallel channel NC system

Unequally heated parallel channel systems can exhibit interesting flow behaviours during natural circulation. To understand the phenomenon, we consider a NCS with a large number of parallel vertical channels (see Fig. A2.1) connected between a common inlet and an outlet header (or plenum). It also has an unheated downcomer connected between the two headers. In such a parallel channel system, it must be recognized that there are two mutually competing driving forces, one between the downcomer and each channel and the other between two unequally heated channels. If the latter is dominant for any two channels, then the channel with low power will flow in the reverse direction.

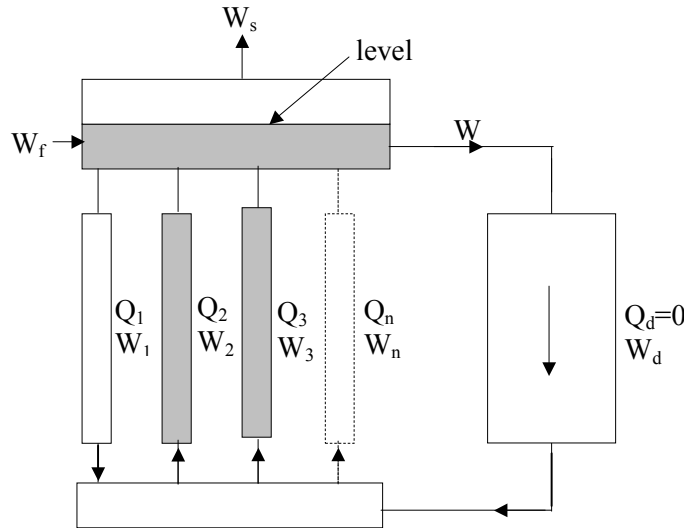


FIG. A2.1. A NCS with n parallel vertical unequally heated channels.

To simplify the analysis further, we replace the n -channel system with the schematic shown in Fig. A2.2 where the lumped channel represents all but two of the individual channels of the n -channel system. Rest of the loop remains same as in Fig. A2.1. When all the channels are equally heated, one would expect upward flow in all the vertical channels. However, since channel powers are different, the average density is different in individual channels and in such circumstances, it is possible to form a closed natural circulation loop between any two channels. To illustrate this further let us consider that the system shown in Fig. A2.2 was operating under steady state conditions with up flow in all heated channels. At this time, we have instantaneously brought down the channel-1 power to zero value and allow it to attain steady state. Now our task is to find out the steady flow direction in channel-1 for both single-phase and two-phase condition.

Single-phase PCS

Under steady state condition, the heat generated in the parallel channels is rejected to the cooling water through a coil inserted in the outlet plenum as shown in the figure A2.2. Let us focus our attention to the closed loop formed by the downcomer with channel-1. To conform to the downcomer flow direction, the flow must be upward in the unheated channel-1. Now, let us examine the pressure drops in the external circuit (from the outlet header/plenum through the downcomer to the inlet header/plenum) as well as the internal circuit (from the inlet header through the core to the outlet header/plenum). For convenience in calculation of the gravitational pressure drops, let H be the elevation difference between the lines BB and AA. The pressure drop Δp_e ($P_b - P_a$) for the external circuit through the downcomer can be written as

$$\Delta p_e = -\rho_d g H + (\Delta p_f)_e \quad (\text{A2.1})$$

Where Δp_f is the irreversible frictional pressure loss in the external circuit. Similarly, the total pressure drop, Δp_i ($P_a - P_b$) in the internal circuit through channel-1 is obtained as

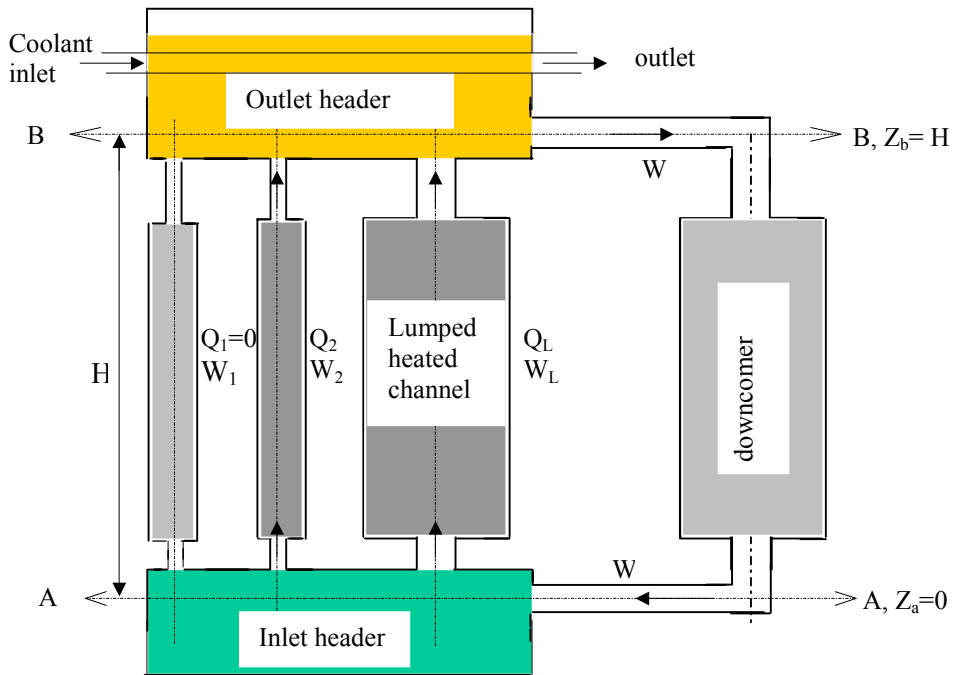


FIG. A2.2. Single-phase parallel channel system.

$$\Delta p_i = \rho_l g H + (\Delta p_f)_i \quad (\text{A2.2})$$

Since the external and the internal circuit form a closed loop, we obtain

$$\Delta p_e + \Delta p_i = 0 ; \text{ or } 0 = g H (\rho_l - \rho_d) + (\Delta p_f)_e + (\Delta p_f)_i \quad (\text{A2.3})$$

Since channel-1 is unheated, $\rho_l = \rho_d$ leading to

$$(\Delta p_f)_e + (\Delta p_f)_i = 0 \quad (\text{A2.4})$$

Note that there is a downward flow in the external circuit through the downcomer caused by the other heated channels. Hence $(\Delta p_f)_e$ is non-zero and therefore $(\Delta p_f)_i$ is also non-zero by the above equation. Considering that both $(\Delta p_f)_e$ and $(\Delta p_f)_i$ are irreversible pressure drops, the above result is possible only if the flow direction in the internal circuit is opposite to that in the external circuit. Considering clockwise flow as positive, we can rewrite Eq. (A2.4) as

$$\sum_{i=1}^N \left(\frac{fL}{DA^2} + \frac{K}{A^2} \right)_i \frac{W_d |W_d|}{2\rho_d} + \sum_{i=1}^N \left(\frac{fL}{DA^2} + \frac{K}{A^2} \right)_i \frac{-W_i |W_i|}{2\rho_d} = 0 \quad (\text{A2.5})$$

Thus, any unheated channel in a system of parallel channels under NC flow cannot have stable upflow. This is one of the fundamental differences between forced and natural circulation parallel channel systems.

Two-phase parallel channel system

The situation can be schematically represented as shown in Fig. A2.3. Normally in two-phase loops also, the downcomer will be in single-phase condition. As a result, the same derivation given above is also applicable for two-phase loops. The only difference is in calculating the frictional pressure loss in channel-2. Here we have to consider the two-phase multiplier and the accelerational pressure drop in the two-phase region of channel-2. However, the conclusions do not change. Linzer and Walter (2003) have presented a criterion for flow reversal.

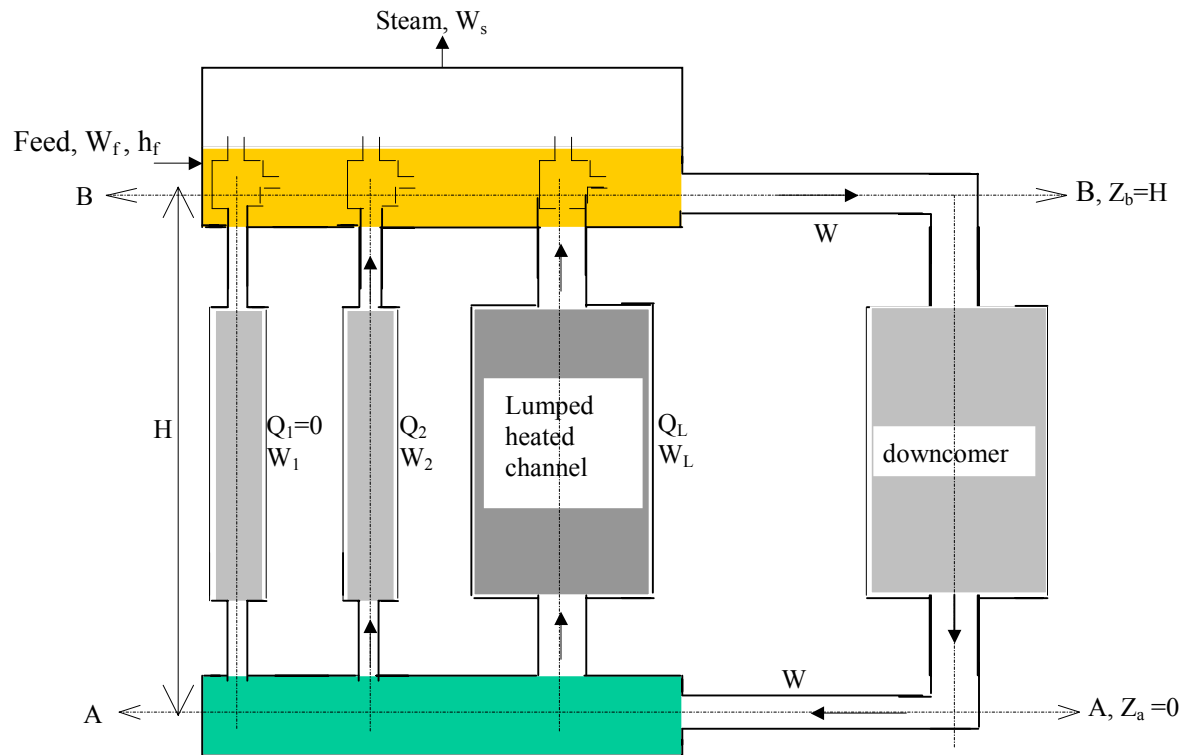


FIG. A2.3. Two-phase parallel channel system.

ANNEX 8

INSIGHTS INTO NATURAL CIRCULATION STABILITY

F.D'Auria¹, A. Del Nevo², N. Muellner³

^{1,2} University of Pisa, Italy

³ University of Vienna, Austria

Abstract

This lecture describes the meaning and importance of stability in fluid-dynamic systems, and mainly in natural circulation conditions. The student shall be able to perform the design of a natural circulation system accounting for stability, namely providing that the system is stable and, possibly, far from instability boundaries for the various operational conditions foreseen in the project.

1. INTRODUCTION

Stability of natural circulation flow is, apart from being very interesting, of utmost importance for industrial applications. What means stability in the content of natural circulation? One intuitive definition can be taken from [1]. If the flow of the system in question (simple loop, atmosphere, BWR, etc) is stationary with respect to the temperature and the velocity, it can be called "stable". If the flow and the temperature show some oscillations, but the amplitude of the oscillations and the sign of the velocity stay constant in time, the system can be called "neutral". If finally the system shows oscillations which grow in time and lead to flow reversal, the system can be called "unstable".

Why is it useful to still study instability? This question is best answered by pointing out the wide range of applications. Natural circulation phenomena are utilized in areas like solar heaters, geothermal energy production, space travel, cooling of engines, and of course for cooling nuclear reactors. Some reactors and reactor designs also utilize natural circulation primary source for the heat transfer during normal operation, like the Ringhals reactor in Sweden. It is obvious that for applications like this the engineer must have the theoretical tools available to study the regions of stability and instability and must know which parameters will influence the behavior of the system.

This lecture aims to provide an overview over stability in natural circulation. Important definitions will be introduced and explained, different kinds of instabilities and parameters which influence them will be introduced, and reference to new developments in the field will be made. The lecture follows a top-down approach, which means two examples for instabilities, one for one phase, one for two phase flow will be discussed in detail, and the theory will be introduced together with its application to the problems.

1.1. Lasalle Event

On March 9, 1988, LaSalle 2 underwent a dual recirculation pump trip following which the unit experienced excessive neutron flux oscillations while it was in natural circulation [2]. LaSalle 2 is a 930 MWe BWR designed by General Electric. The unit had been operating at 84% power with 76% flow when an instrument technician, performing surveillance on the initiation logic for the reactor core isolation cooling, opened a wrong valve. The resulting perturbation on the switches for anticipated transient without scram resulted in a trip of both recirculation pumps. This caused a reduction in flow to natural circulation, while the control rods remained in the 99% flow control line position. The resultant power-to-flow condition (about 40% power with natural circulation) after the pump trip was known to be a condition susceptible to instability. In addition, as a result of the rapid power reduction due to the loss of the recirculation pumps, there was a perturbation in the feedwater heaters causing a loss of various feedwater preheaters. This resulted in an insertion of positive reactivity as cooler feedwater was supplied to the reactor. The net effect was an increase in power that further reduced the margin to instability. Approximately 5 minutes after the recirculation pump trip,

the operators noted that the average power range monitor (APRM) indications were oscillating between 25 and 50% power every 2 to 3 seconds, and the local power range monitor (LPRM) alarms began to annunciate and clear. The operators unsuccessfully attempted to restart the recirculation pumps to re-establish the forced flow. Nearly 7 minutes after the pump trip, another attempt to restore the forced flow was unsuccessful and, while operators were preparing for a manual scram, the reactor automatically scrammed on high flux (118% trip). The plant was taken to cold shutdown. The oscillations were also in this case in-phase.

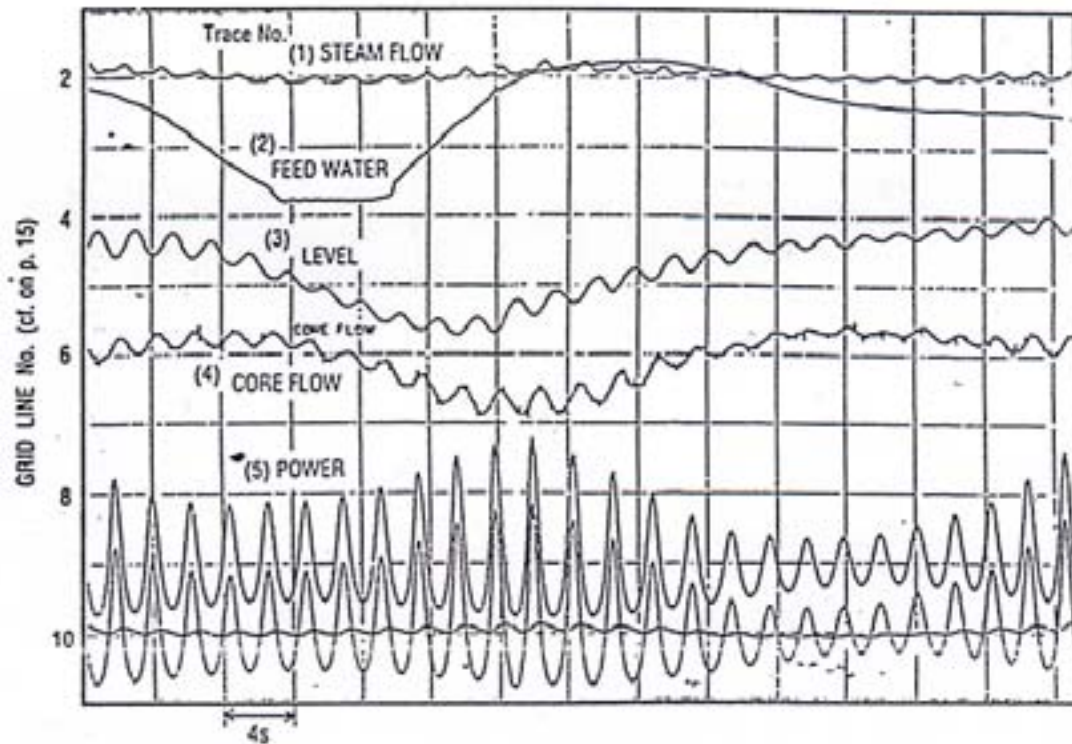


FIG. 1. Available plant measurements from STARTREC (STARTup Transient data RECorder system).

1.2. Reliability evaluation of a NC system

Jajil Jafari [3] investigated the reliability of a natural circulation system, namely the TTL-1 separate test facility. A structured approach was made: first the term reliability in the context of NC systems was defined — failure criteria were chosen; a number of parameters which could influence NC reliability were selected, finally 29 were chosen by expert judgment for an analysis with Relap5 on their influence on the reliability of the TTL-1 loop. The parameters were regrouped according to their importance, and finally some suggestions for design improvements were made.

The results showed that one of the most important issues for the reliability of the TTL-1 loop is the occurrence of instabilities and parameters which influence the stability of the loop respectively. This again shows the importance of stability in the context of natural circulation systems.

2. FUNDAMENTALS

2.1. Definition of stability in fluid dynamics

It appears worthwhile to introduce a series of definitions that are common in the stability analyses.

- Acoustic instability: this occurs when standing waves are excited in a single or two phase system with a frequency in the acoustic range (steam line resonance and acoustic instabilities in the steam dome and upper plenum regions of BWRs have been observed).
- Decay ratio: the DR is defined as the ratio of two consecutive maxima of the impulse response. Two methods for extracting the DR value from neutron noise signal are commonly in use: a) utilizing the autocorrelation function; b) from the impulse response which can be obtained by autoregressive modeling of the neutron noise. Either $A1/A2$ (ratio of two consecutive maxima related to the horizontal time axis) either $B1/B2$ (ratio of distances between two consecutive peaks and a line connecting the “opposite peaks”) can be taken to obtain the DR value.
- Density wave: a density wave is a perturbation in the density of the fluid mixture, which travels along the heated channel with a characteristic speed depending on local conditions. Density wave oscillations (DWOs) are the basic mechanism credited for triggering and sustaining the relevant oscillation phenomena in boiling water reactor cores. In other words, the observed instability phenomena have been explained making reference to the delays involved in density wave propagation.
- Dynamic instabilities: these terms characterize the wider class of instabilities that can be studied only through the use of time-dependent balance equations.
- Flow excursion (Ledinegg) instability: this is a type of static instability that is determined by the relationship between the pressure drop characteristic of a boiling channel and the pressure drop characteristic imposed by an external system.
- Flow regime induced instability: the periodicity of some flow regime (e.g. slug flow) excite this instability mode.
- Flow regime “relaxation” instability: this is a static instability due to flow regime changes.
- Limit cycle: limit cycle is a particular long term periodic solution of the differential equations describing a non-linear system, which is encountered studying the system behavior beyond the linear stability threshold. Limit cycles are named “stable”, if they attract system trajectories starting from nearby states, or “unstable”, if they repel them. Stable limit cycles have been observed in BWRs and other boiling systems during instabilities and are ideally characterized by a periodic oscillatory behavior with constant amplitude and frequency. As a matter of fact, limit cycles observed in BWRs during tests or inadvertent occurrences are not so ideal, showing gradual changes in amplitude and frequency of oscillations as a result of drift in system parameters.
- Pressure drop oscillations (PDO): in this case a Ledinegg type instability and a compressible volume in the boiling system interact. It might be noted that PDO is a dynamic type of oscillations and Ledinegg is a static one.
- Stability boundary: A stability boundary is represented by a relationship between the parameters describing a system status which defines the conditions in which the system shows marginal (or neutral) stability, i.e. in which perturbations are neither amplified nor damped. In a two-dimensional parameter space, this relationship can be represented as a curve separating

areas of stable and unstable behavior. Hyper-surfaces separating stable and unstable multidimensional domains are obtained in the case of systems described by several parameters.

- **Stability margin:** a stability margin is a properly defined measure of the distance of a system status from the stability boundary. For instance, control theory suggests the use of “gain” and “phase” margins as a measure of the stability of a linear system.
- **Static instability:** these terms identify a class of instabilities that can be theoretically explained without the use of time-dependent conservation equations.
- **Thermal-hydraulic instabilities:** These are identified by periodic time oscillations of various quantities in a boiling system (either single channel either parallel channels). Excursion of heated wall surface temperature may result from thermal-hydraulic instabilities. This includes the entire class of instabilities discussed.
- **Thermal oscillations:** Are oscillations heavily involving the heater dynamics in a boiling channel. Cyclic dry-out and rewet phenomena may be involved at a frequency lower than DWO.

2.2. Relevant stability related parameters

A classification of the thermal-hydraulic instabilities, summarized in Table 1, can be explained considering two main groups: the so-called ‘static’ instabilities, that are explainable in terms of steady state laws, and the ‘dynamic’ instabilities, that requires the use of the time dependent conservation equations and, in case, the adoption of concepts and techniques developed in the frame of control theory.

2.2.1. Parameters through which stability shows up (flow rate, pressure, density, temperature)

2.2.1.1. Ledinegg instabilities

Ledinegg instabilities are due to the particular S-shape that the flow rate versus pressure drop characteristic of a boiling channel often exhibits. The analyses performed in a simplified loop (representing an helical coil steam generator) has shown that the effect of the energy loss coefficient in the two-phase zone has a destabilizing effect, while the large inlet pressure drop due to orifice has a general stabilizing effect against the “Ledinegg” instability [4].

Table 1. Classification of thermal hydraulic instabilities

Class	Type	Mechanism	Characteristic
<i>Static instabilities</i>			
Fundamental (or pure) static instabilities	Flow excursion or Ledinegg instabilities	$\left. \frac{\partial \Delta p}{\partial G} \right _{\text{int}} \leq \left. \frac{\partial \Delta p}{\partial G} \right _{\text{ext}}$	Flow undergoes sudden, large amplitude excursion to a new, stable operating condition
	Boiling crisis	Ineffective removal of heat from heated surface	Wall temperature excursion and flow oscillation
Fundamental relaxation instability	Flow pattern transition instability	Bubbly flow has less void but higher ΔP than that of annular flow	Cyclic flow pattern transitions and flow rate variations
Compound relaxation instability	Bumping, geysering, or chugging	Periodic adjustment of metastable condition, usually due to lack of nucleation sites	Period process of super-heat and violent evaporation with possible expulsion and refilling
<i>Dynamic instabilities</i>			
Fundamental (or pure) dynamic instabilities	Acoustic oscillations	Resonance of pressure waves	High frequencies (10-100Hz) related to the time required for pressure wave propagation in system
	Density wave oscillations	Delay and feedback effects in relationship between flow rate, density, and pressure drop	Low frequencies (1Hz) related to transit time of a continuity wave
Compound dynamic instabilities	Thermal oscillations	Interaction of variable heat transfer coefficient with flow dynamics	Occurs in film boiling
	BWR instability	Interaction of void reactivity coupling with flow dynamics and heat transfer	Strong only for small fuel time constant and under low pressures
	Parallel channel instability	Interaction among small number of parallel channels	Various modes of flow redistribution
Compound dynamic instability as secondary phenomena	Pressure drop oscillations	Flow excursion initiates dynamic interaction between channel and compressible volume	Very low frequency periodic process (0.1Hz)

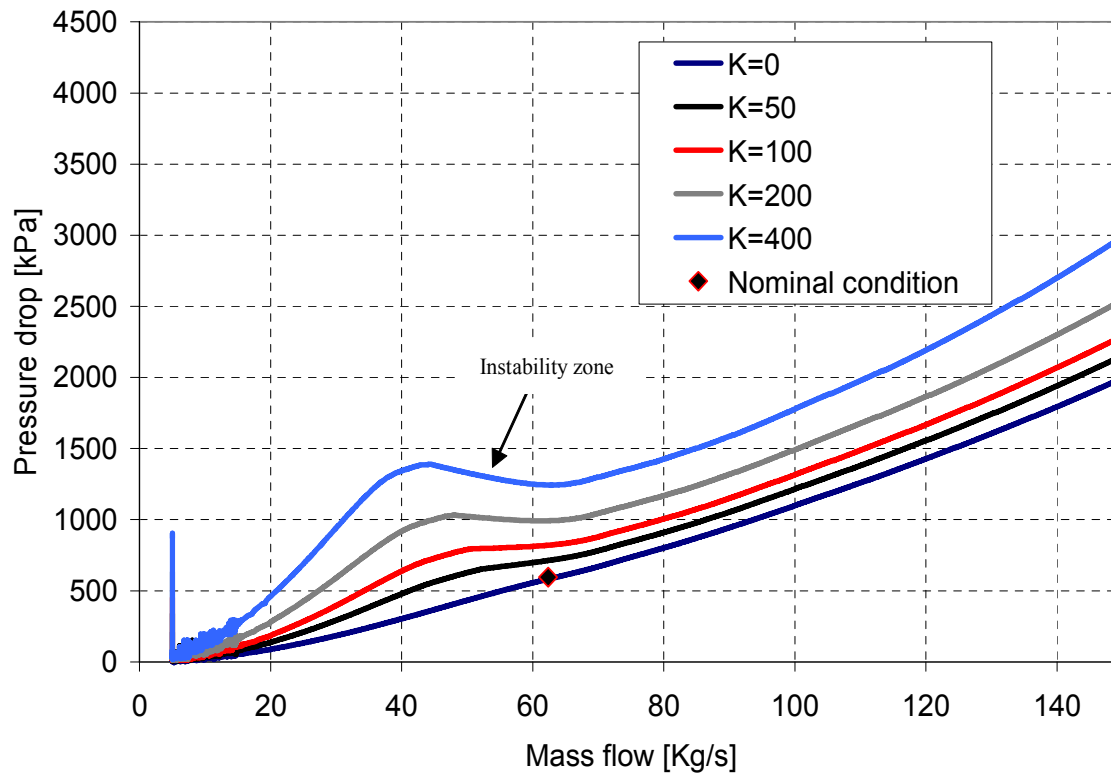


FIG. 2. Calculation of the static SG characteristics with Relap5 code; effect of the energy loss coefficient (in two phase zone) on the pressure drop characteristic.

2.2.1.2. Fundamental relaxation instability

Flow pattern transition instabilities have been postulated as occurring when the flow conditions are close to the point of transition between bubbly flow and annular flow. A temporary reduction in flow rate may cause the increase of the bubble population and the change of the flow pattern to annular flow (characterized by low pressure drop). The consequence is that with the flow rate increase, the vapor generated is not sufficient to maintain the annular flow and the flow pattern then reverts to that of the bubbly-slug flow. The cycle can be repeated. Length, inlet temperature, mass velocity, and pressure are related to the large scale fluctuations characteristic of the slug flow regime that can be viewed as a transition from bubbly to annular flow, in particular related to a low pressure diabatic flow [5].

2.2.1.3. Compound relaxation instability

Bumping, geysering and chugging involve static phenomena which are coupled so as to produce a repetitive behavior which is not necessarily periodic.

Bumping is exhibited in boiling of the alkali metals at low pressure. It has been postulated that it is due to the presence of gas in certain cavities.

Geysering has been observed in a variety of closed end, vertical columns of liquid which are heated at the base. In low pressure systems this is suddenly increased vapor generation due to reduction in hydrostatic head, and usually an expulsion of vapor from the channel. The liquid then returns, the sub-cooled non-boiling condition is restored, and the cycle starts over again.

The term chugging is usually reserved for the cycle phenomenon characterized by a periodic expulsion of coolant from the flow channel. The expulsion may range from simple transitory variations of the inlet and outlet flow rates to violent ejections of coolant, usually through both ends of the channel [5].

2.2.1.4. *Density wave oscillation*

Density-wave oscillations occur on the boiling positive slope branch of the pressure drop versus flow rate curve. Disturbances in gas-liquid two phase flows may be transported by different mechanisms among which are density wave resulting from fluctuations in void fraction (DWO) [6].

DWO are most often observed in flow boiling processes in which the flow enters as sub-cooled liquid. The time scale associated with DWO is about the time required for a fluid particle to travel through the channel. The relevance of this phenomenon is due to the possibility that it could affect the operation and the safety characteristics of the system. DWO may cause many undesired problems such as mechanical and thermal fatigue of the components though the mechanical vibration and thermal wave to require the system control considerations [7],[8].

The main parameters that influence the DWO are reported below [9],[10].

- Increase in mass flow rate increases stability,
- Increase in heater power decreases stability,
- Increase in overall density ratio decreases stability,
- Increase in power input to the channel increases frequency,
- Increase of inlet sub-cooling increases stability at high sub-cooling,
- Increase in system pressure for a given power input increases stability,
- Decrease of the heated length increases the flow stability in forced.

2.2.1.5. *Pressure drop oscillation*

Pressure-drop oscillations occur on the negative slope branch of the pressure drop versus flow rate curves. The name is referred to flow oscillations due to a multi-valued (S-shape) flow rate versus pressure drop characteristic. Flow oscillations, rather than one time excursion, can occur if there are a sufficient interaction and delay feedbacks between flow rate and mass accumulation (i.e. compressibility) in the heated section or in the system. The required compressible volume may be situated outside the heated section or can be provided by the internal compressibility of long heated sections [11].

- Increase in negative slope decreases stability;
- Increase in heater power decreases stability;
- Increase in exit pressure drop decreases stability;
- Increase in inlet pressure drop decreases stability;
- Period of pressure-drop oscillations increases with decrease in flow rate;
- Superimposed density-wave oscillations appear on low flow part of the pressure-drop type oscillation cycle;
- Boiling upward flows are more stable than horizontal flows.

2.2.1.6. *Thermal hydraulic oscillation*

- Thermal oscillations occur in a domain located within density-wave and pressure-drop oscillation regions where there is film boiling;
- During part of the cycle there are always superimposed density-wave oscillations;
- Both the period and the amplitude are nearly inversely proportional to inlet mass flow rate;
- The amplitude increases with heat input, and the period increases linearly with heat input;

- In certain operation regions, both the period and the amplitude increase with decreasing inlet liquid temperature;
- Increase in inlet pressure drop increases stability [12].

2.2.3. Parameters affecting stability - mechanical and heat transfer interactions

Parameters which affect stability in natural circulations and were not mentioned above are mainly mechanical interactions and heat transfer interactions. Mechanical interactions comprise for example the propagation of pressure waves through the piping caused by the rapid closure of a valve (water-hammer). Mechanical interactions which are affecting stability are beyond the scope of this introductory lecture and are only mentioned for completeness.

The influence of the thermal properties of the materials on the stability has been studied by M. Misale [1]. A rectangular natural circulation loop was considered (in principle the Welander - problem which will be discussed in detail later in section 3). A natural circulation loop is a simple rectangular loop of pipes, which is subjected to gravity, heated at the bottom and cooled at the top. The fluid in the loop will be heated at the bottom, expand, and due to the buoyancy rise to the top, where it will be cooled again and will sink to the bottom. By this, natural circulation is established. The first one who presented an analysis of this problem was Welander [13].

As will be shown later, even a simple system as just described can show regions of instability. And even more surprisingly, the regions of stability and behavior of the loop depend on the heat capacity of the piping, which was shown numerically by the cited paper [1] and experimentally by Vijayan et al. [14].

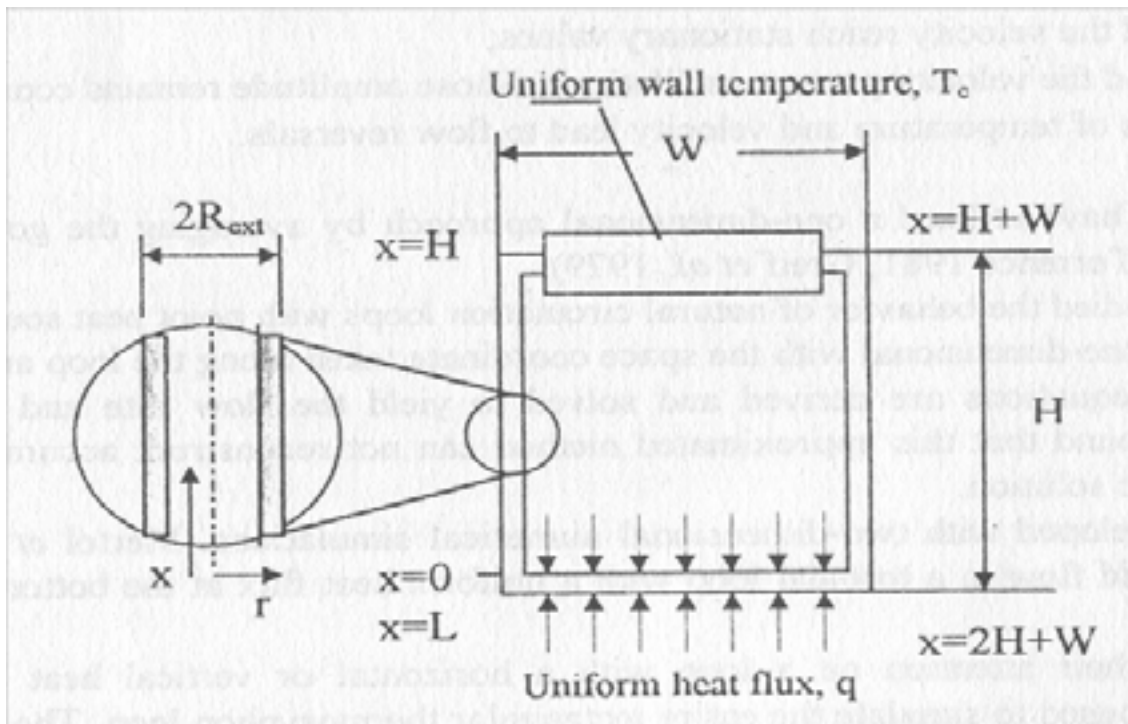


FIG. 3. The natural circulation loop investigated by [1]. Two spatial (x,r) and one time coordinate (t) were used. A uniform heat flux was imposed. The materials and therefore the heat capacities for the piping was varied. The results showed that the heat capacity of the piping has a considerable influence on the behavior of the system.

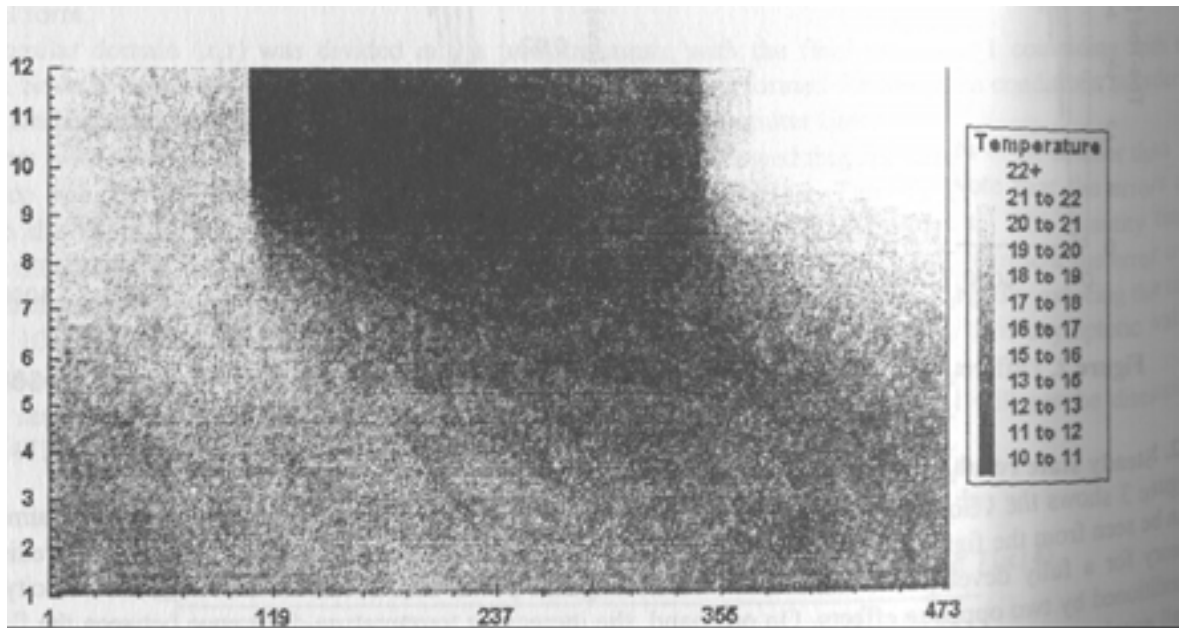


FIG. 4. The temperature distribution of the mesh for a steady-state solution. The horizontal axis indicates the x -coordinate, the vertical the r -coordinate. The radial mesh points 10, 11 and 12 are the wall of the pipe. The radial mesh point 1 designates the temperature of the fluid in the center of the pipe. The flow (as one can see) moves from the axial mesh point 1 to 473. The left and the right boundary are identified.

Table 2. The different behavior of the loop can be seen on some characteristic quantities like the Nusselt or Reynolds number. Although the heat flux is the same, the flow in the loop is different for different wall-materials. The main reason is the difference in the heat capacity.

	Heat flux	100	150	200	250
Copper	Nu	8.8	10.1	11.1	11.9
	Re	342	452	559	664
	Pr	8.2	7.9	7.7	7.5
	fRe	20.8	23.2	25.1	26.6
Steel	Nu	9.1	10.4	11.4	12.3
	Re	347	461	571	680
	Pr	8.2	7.9	7.6	7.4
	fRe	20.9	23.3	25.1	26.6
Plexiglass	Nu	13.2	15.4	16.9	18.1
	Re	563	865	1219	1622
	Pr	6.8	6.0	5.4	4.8
	fRe	24.6	28.1	30.9	33.1

3. ONE-PHASE STABILITY MECHANISM EXPLAINED ON AN EXAMPLE (WELANDER PROBLEM)

In 1967 Pierre Welander [13] published a paper in the Journal of Fluid Mechanics about a surprisingly simple problem, which still keeps the scientific community interested. Consider a closed loop, subjected to gravity, which is heated at the bottom and cooled at the top (Figure 5). The vertical tubes of the loop are insulated, the diameter of the loop stays the same over the whole loop. The fluid motion will be driven by the Boyancy force 1- the fluid will heat up at the bottom, expand with the expansion coefficient α and will be driven to the top due to gravity, where it will be cooled again. The motion will be retarded by frictional forces. Welander assumed that in first approximation frictional forces are linear proportional to the flow (2).

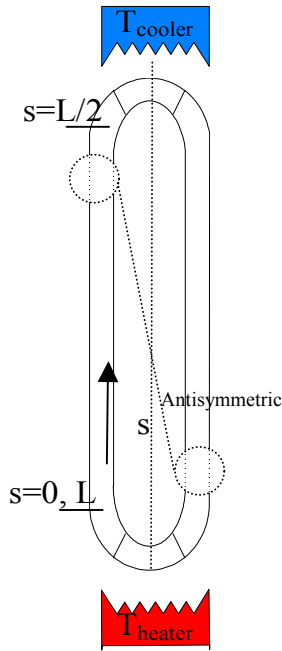


FIG. 5. A simple closed loop with a heater at the bottom and a heat sink at the top. It is filled with liquid in subcooled conditions.

$$\bar{B} = Ag\rho_0\alpha\oint Tdz \quad (1)$$

$$\bar{F} \propto q \quad (2)$$

If the equations (1) and (2) are used, the change of the flow (equation of motion) can be written as (3).

$$\dot{q} = \frac{A}{L} g\alpha\oint Tdz - Rq \quad (3)$$

For the heat transfer from the point source and sink to the fluid the ansatz shown in (4) was used. Welander assumes that the increase (decrease) in temperature of the fluid when the fluid passes the heat source (sink) is proportional to the difference between the heater temperature and the fluid upstream of the heater. The factor $(1-ek\Delta t)$ accounts for the time in which the fluid passes the heater. If the fluid velocity is high, the factor will be close to zero and TOUT will be almost equal to TIN. On the other hand, if the fluid velocity is small, the factor will be close to one and TOUT will be almost to THEATER.

$$T_{OUT} - T_{IN} = (T_{HEATER} - T_{IN}) \cdot (1 - e^{k\Delta s}) = (T_{HEATER} - T_{IN}) \cdot \left(1 - e^{\frac{kA\Delta s}{|q|}}\right) \quad (4)$$

Dimensionless coordinates were introduced (5).

$$s = \bar{s} \frac{L}{2}, \quad t = \bar{t} \frac{L}{2k\Delta s}, \quad q = \bar{q}kA\Delta s, \quad T = \bar{T}T_{HEATER} \quad (5)$$

The form of the differential equations is now

$$\dot{\bar{q}} + \varepsilon \cdot \bar{q} = a \int_0^1 \bar{T} d\bar{s} \quad (6)$$

$$\frac{\partial}{\partial \bar{t}} \bar{T} + \bar{q} \frac{\partial}{\partial \bar{s}} \bar{T} = 0 \quad (7)$$

$$\bar{T}_{\bar{s}=0} + \bar{T}_{\bar{s}=1} = (1 + \bar{T}_{\bar{s}=1}) \left(1 - e^{\frac{-1}{\bar{q}}}\right), \bar{q} > 0 \quad (8)$$

$$\bar{T}_{\bar{s}=0} + \bar{T}_{\bar{s}=1} = (-1 + \bar{T}_{\bar{s}=0}) \left(1 - e^{\frac{-1}{\bar{q}}}\right), \bar{q} < 0 \quad (9)$$

With the dimensionless parameters

$$a = \frac{g \cdot \alpha \cdot T_{HEATER} \cdot L}{2(k \cdot \Delta s)^2}$$

$$\varepsilon = \frac{RL}{2k\Delta s} \quad (10)$$

Some comments should be made on equation (8) and (9). $s=0$ denotes the bottom of the loop (heater) in the dimensionless coordinates, $s=1$ the top (sink). In left hand side of equation (4) in dimensionless coordinates for $q>0$ TOUT can be written as TOUT= $T_s=0+\Delta s$, while TIN= $T_s=0-\Delta s$. Using the antisymmetry of the problem $T_s=0-\Delta s = -T_s=1-\Delta s$. In the limit $\Delta s \rightarrow 0$ the left hand side of (4) becomes $T_s=0 + T_s=1$. Same considerations can be made for $q<0$.

3.1. Steady motion solutions

For simplicity coordinates without bars designate dimensionless coordinates from now on. If we assume the system is in steady state, we can consider that q and T are constant. For $q>0$, The equation (6) then takes the form

$$\varepsilon \cdot q_{ss} = a \cdot T_{ss} \quad (11)$$

Equation (8) takes the form

$$2T_{ss} = (1 + T_{ss}) \left(1 - e^{\frac{-1}{q_{ss}}}\right) \quad (12)$$

If TSS is eliminated equations (11) and (12) finally yield a solution

$$\frac{2q_{SS}}{\left(\frac{a}{\varepsilon}\right) + q_{SS}} = 1 - e^{-\frac{1}{q_{SS}}} \quad (13)$$

Equation (13) has one solution for a given (a/ε) . The solution for some ratios of (a/ε) is given in table. One can see that for a small (a/ε) q_{SS} is small, therefore TSS is near to one (this means the temperature of the upward flow has almost the temperature of the heater. For bigger values of (a/ε) increases, while TSS decreases.

3.2. Stability of the steady motion solutions

The concept which was used by Welander to analyse the stability of the solutions is referred to as linear stability analysis. Basically one considers small derivations to the solution and analyses how the derivations develop. Consider a system of differential equations (14) and its solution Y_{SOL} .

Consider also a small perturbation $\bar{\varepsilon}$ of the solution. The equation for the perturbation $Y_{SOL} + \bar{\varepsilon}$, (15) can be expanded (linearised) when only small perturbations are considered. One should notice that by doing so information is lost. The results of the analysis only indicate the qualitative behavior of the solution, stable or unstable; no remarks about the magnitude can be made. If more information is wanted a non linear stability analysis should be made (to see an example where a non linear stability analysis was applied, see e.g. [15], [16]).

$$\dot{Y}(t) = F(Y(t)) \quad (14)$$

$$\dot{Y}_{SOL} + \dot{\bar{\varepsilon}} = F(Y_{SOL} + \bar{\varepsilon}) \approx F(Y_{SOL}) + \left. \frac{\partial F}{\partial Y} \right|_{Y_{SOL}} \cdot \bar{\varepsilon} \quad (15)$$

By using the fact that Y_{SOL} is a solution of (14) the equation (15) can be simplified to (16). This equation can be solved using the ansatz (17). Substituting (17) in (16) leads to (18). If any eigenvalues $Re \lambda_i > 0$ exist the perturbation will grow in time and the solution is unstable.

$$\dot{\bar{\varepsilon}} = \left. \frac{\partial F}{\partial Y} \right|_{Y_{SOL}} \cdot \bar{\varepsilon} \quad (16)$$

$$\bar{\varepsilon} = \bar{\xi}_i e^{\lambda_i \cdot t} \quad (17)$$

$$\left(I \cdot \lambda_i - \left. \frac{\partial F}{\partial Y} \right|_{Y_{SOL}} \right) \bar{\xi}_i = 0 \quad (18)$$

Welander assumed the solution \bar{q}, \bar{T} with the derivations q', T' . Then the linearized form of the differential equation looks like (19), while the boundary conditions take the form (20).

$$\begin{aligned} \dot{q}' + \varepsilon \cdot q' &= a \int_0^l T' ds \\ \frac{\partial}{\partial t} T' + \bar{q} \frac{\partial}{\partial s} T' &= 0 \end{aligned} \quad (19)$$

$$\begin{aligned}
T'_{s=0} + mT'_{s=1} + nq' &= 0 \\
m &= e^{\frac{1}{\bar{q}}} = \frac{1 - \bar{T}}{1 + \bar{T}} \\
n &= \frac{1 + \bar{T}}{\bar{q}^2} e^{-\frac{1}{\bar{q}}} = \frac{1 - \bar{T}}{\bar{q}^2}
\end{aligned} \tag{20}$$

Exponential functions (21) were used to satisfy equation (20) and (19).

$$\begin{aligned}
q' &= \hat{q} \cdot e^{r \cdot t} \\
T' &= \hat{T}(s) \cdot e^{r \cdot t}
\end{aligned} \tag{21}$$

Substituting (21) in equation (19) and (20) leads to equations

$$\begin{aligned}
(r + \varepsilon)\hat{q} &= a \int_0^1 \hat{T} ds \\
r\hat{T} + \bar{q} \frac{d}{ds} \hat{T} &= 0 \\
\hat{T}(0) + m\hat{T}(1) + n\hat{q} &= 0
\end{aligned} \tag{22}$$

The solution $\hat{T} = C \exp(-rs/\bar{q})$ can be found from the second equation of (22), which can be used to find together with the first equation of (22) a solution for $\hat{q} = Ca\bar{q} \cdot (1 - \exp(-r/\bar{q})) / (r(r + \varepsilon))$. By inserting in the third equation of (22) finally the characteristic equation can be derived:

$$1 + m \cdot e^{-\frac{r}{\bar{q}}} + \frac{n \cdot a \cdot \bar{q}}{r(r + \varepsilon)} \left(1 - e^{-\frac{r}{\bar{q}}} \right) = 0 \tag{23}$$

By looking on the left hand side of equation (23) one can see that no real solutions with $r > 0$ exists, since for $r > 0$ every term on the LHS is positive. So Welander investigated weather oscillatory unstable solutions exist, which means r is complex and $\text{Re } r > 0$. For this investigation, the following new parameters (24) are introduced:

$$\begin{aligned}
r &= i\omega \\
\tilde{a} &= na/q \\
\tilde{\varepsilon} &= \varepsilon/q \\
\tilde{\omega} &= \omega/q
\end{aligned} \tag{24}$$

The characteristic equation then takes the form of (25)

$$\frac{e^{(i\tilde{\omega})} + m}{e^{(i\tilde{\omega})} - 1} + \frac{\tilde{a}}{i\tilde{\omega}(i\tilde{\omega} + \tilde{\varepsilon})} = 0 \tag{25}$$

Separating equation (25) in real and imaginary part and utilizing some relationships, which can be found in reference [13], the equation can be written in the form of (26).

$$\begin{aligned} \tilde{\omega}^2 + \left(\tilde{\varepsilon} - \frac{1}{2} A \right)^2 &= \left(\frac{1}{2} A \right)^2 \\ \tilde{\varepsilon} &= \left(\frac{1}{\bar{T}} \right) \tilde{\omega} \cot \left(\frac{1}{2} \tilde{\omega} \right) \\ A(\bar{T}) &= \frac{1 - \bar{T}^2}{\bar{T}^2} \ln \left(\frac{1 - \bar{T}}{1 + \bar{T}} \right) \end{aligned} \tag{26}$$

For a given \bar{T} the first equation of represents a circle with radius $\frac{1}{2} A$ in the $\tilde{\varepsilon} / \tilde{\omega}$ plane. The curves one and two of equation (26) are shown for two different values of \bar{T} in Figure 6.

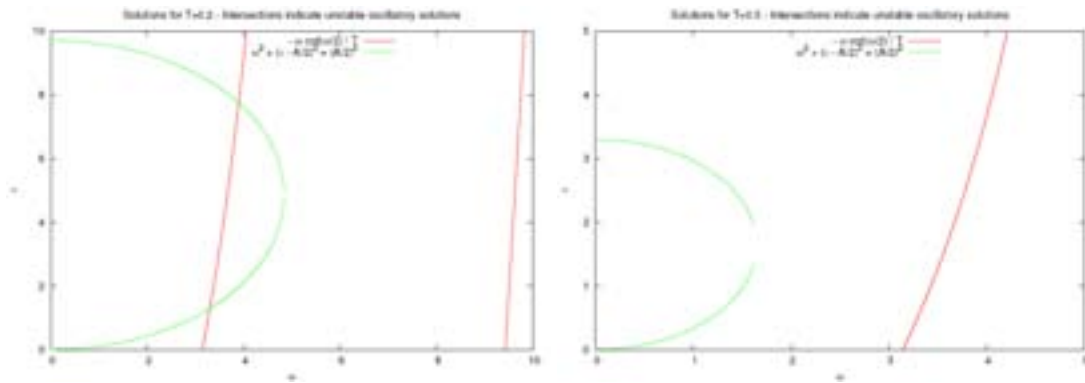


FIG. 6. Solutions to the characteristic equation for oscillatory instabilities. If the two curves intersect, the solution is oscillatory unstable. One can see that for $T=0.2$ the solution is oscillatory unstable, while this is not true for $T=0.5$.

By looking at the asymptotic behaviour it is possible to construct a region of stability/instability for the parameters ε and q . For large values of ε the region of stability and instability is separated by $\varepsilon \propto 4q^2$, while for large values of q the stability margin is proportional to $\varepsilon \propto \pi^2/4$. Welander numerically investigated the behaviour of the loop in several regions of stability. The results are shown in . For small values of ε the flow grows steadily to a steady state value. If the value of ε is increased a little bit, some instabilities begin to show up. With a further increase a “stable” oscillatory behaviour can be observed. Finally, growing oscillations in the flow rate show up, with a regularly occurring inversion of the flow.

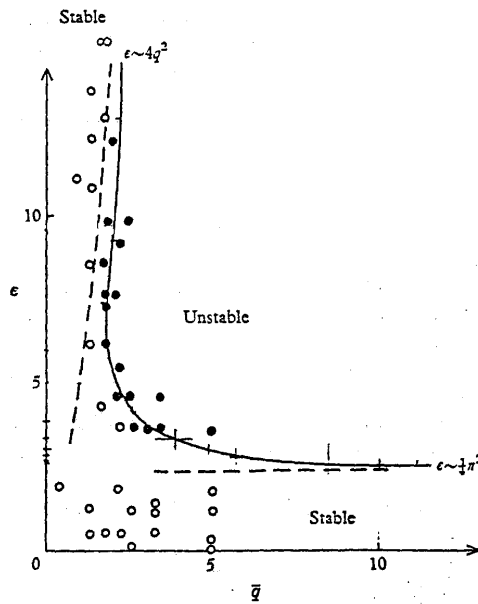


FIG. 7. The (pen and paper) curve which separates the stable from the unstable region. Remember that $\epsilon = RL/(2k\Delta s)$. So epsilon increases when the friction increases, and decreases when the quantity of heat transferred at the heat sink and source increases. \bar{q} indicates the flow rate of the steady state solution. The dots indicate numerical experiments. A solid dot means the numerical solution turned out to be unstable, an open circle indicates a stable solution..

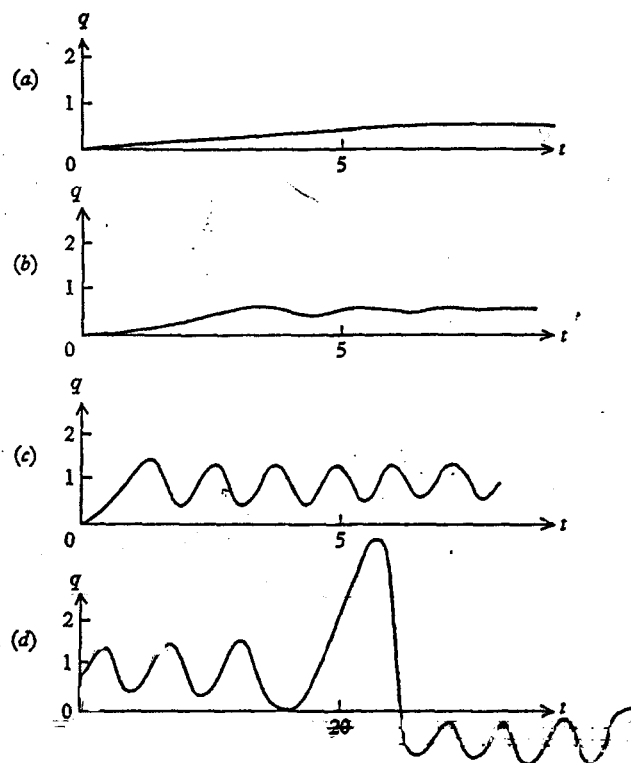


FIG. 8. Numerical solution for four cases: (a) $a = 0.4$, $\epsilon = 0.2$ (b) $a = 2.0$, $\epsilon = 2.0$, (c) $a = 20.0$, $\epsilon = 20.0$ (d) $a = 40.0$, $\epsilon = 6.0$.

3.3. Numerical aspects of the Welander Loop

W. Ambrosini et al. [17] investigated the effect of the truncation error on the stability of the numerical results for natural circulation of the Welander loop. The surprising result was that the region of stability changes dramatically with the length of the nodes which was chosen for the numerical calculation - if a very crude nodalization was chosen, instabilities would not show up at all. Since the numerical treatment is not a topic of this lecture, only one figure with the major results will be presented.

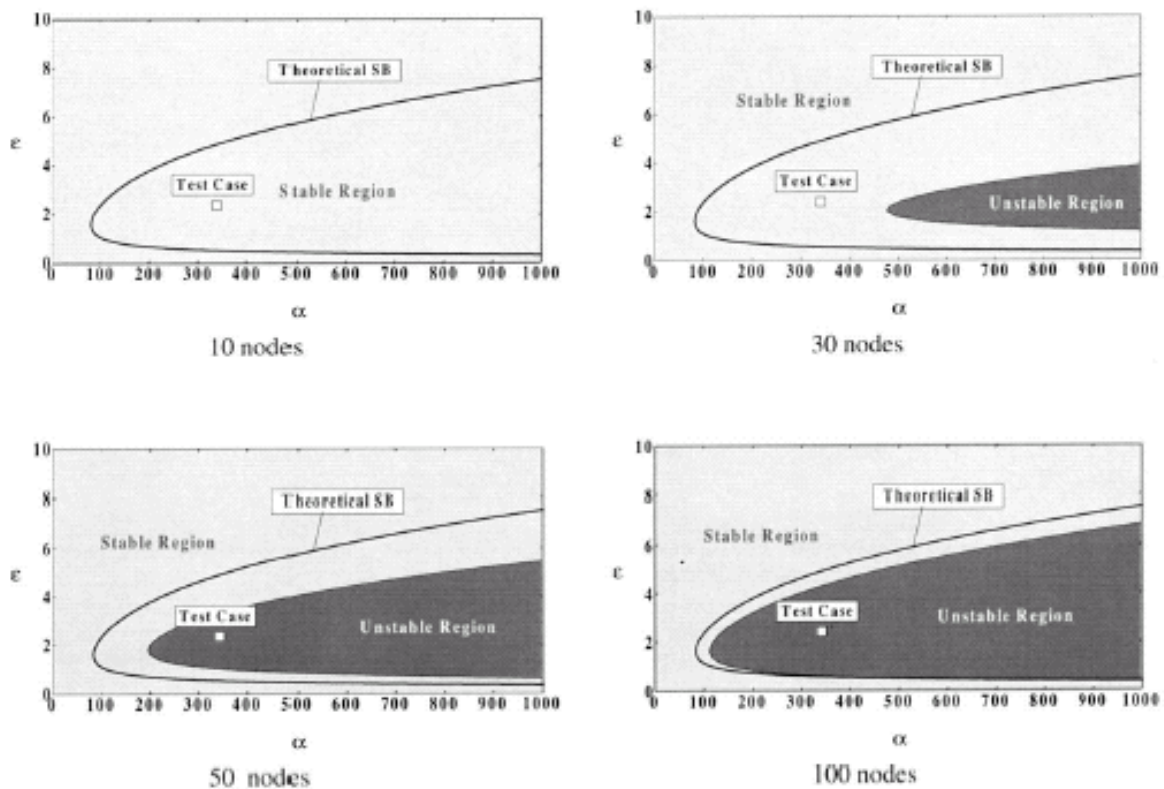


FIG. 9. Dependence of the stable and unstable region of the numerical results on the truncation error, compared to the theoretical boundary of stability (Theoretical SB). One can see the effect of the truncation error: at 10 nodes for the loop, the behavior seems stable for the whole epsilon/alpha plane. Only a nodalization with 100 nodes seems to adequately describe the problem. “Test case” refers to the selected case in the paper [17].

4. TWO PHASE STABILITY MECHANISM

Boiling natural circulation is a relevant cooling mechanism for the nuclear reactor system. This relevance increased with the 3rd generation and the studies of the 4th generation of the NPP (JPSR, AP600, SBWR, IRIS). In these reactors (i.e. AP600, IRIS, etc) the natural circulation is used for the emergency heat removal system (called “passive”), or is the major cooling mechanism (SBWR) [18].

Flow in natural circulation system is induced by the difference of fluid density, and in two phase flow the heat input and its removal induces a large volumetric change owing to phase changes (boiling and condensation), thus the system easily becomes unstable. Flow instabilities are undesirable in boiling, condensing, and other two phase flow processes for several reasons. Sustained flow may cause forced mechanical vibration of component or system control problems (see section 2.2.2). Flow oscillations affect

the local heat transfer characteristic and may induce boiling crisis (critical heat flux, DNB, burnout, dryout,...).

The mathematical model is based on the flow description and its boundary conditions. The flow description is based conservation equations (mass, momentum, energy), the constitutive laws (that define the properties of the system with a certain degree of idealization, simplification, or empiricism: equation of state, steam tables, friction correlation, heat transfer correlation, etc...).

A general the conservation principles yield three equations for each phase, plus three interface relationships. Using a six conservation equation model, such as the system codes (Relap5, Cathare2, etc...), it has been possible to take into account interfacial phenomena which result in slip and lack of thermal equilibrium [19]. A briefly summary of these equations is reported, for one-dimensional flow of constant cross section.

The conservation equations (mass, momentum, energy) are:

$$\frac{\partial(A_k \rho_k)}{\partial t} + \frac{\partial(A_k \rho_k j_k)}{\partial z} = M_k \quad (27)$$

$$\frac{\partial(A_k \rho_k j_k)}{\partial t} + \frac{\partial(A_k \rho_k j_k^2)}{\partial z} + A_k \frac{\partial p}{\partial z} = -A_k \rho_k g - F_{ki} - F_{kw} \quad (28)$$

$$\frac{\partial(A_k \rho_k H_k)}{\partial t} + \frac{\partial(A_k \rho_k j_k h_k)}{\partial z} = A_k \frac{\partial p}{\partial t} - A_k j_k \frac{\partial p}{\partial z} - Q_{ki} - Q_{kw} \quad (29)$$

while the interfacial relations are:

$$\sum_k M_k = 0 \quad (30)$$

$$\sum_k F_{ki} = 0 \quad (31)$$

$$\sum_k Q_{ki} = 0 \quad (32)$$

Considering the conservation equations of the mass and the momentum it is possible to derive the

SLIP equation for the two phases, by the elimination of the $\frac{\partial p}{\partial z}$ term. Considering the following hypothesis: $A_k = const$, $A_g = \alpha$ and $A_l = 1 - \alpha$.

$$A_k \frac{\partial p}{\partial z} + A_k \rho_k \frac{\partial j_k}{\partial t} + A_k j_k \left(\underbrace{\frac{\partial \rho_k}{\partial t} + \rho_k \frac{\partial j_k}{\partial z} + j_k \frac{\partial \rho_k}{\partial z} + \rho_k \frac{\partial j_k}{\partial z}}_{M_k} \right) = -A_k \rho_k g - F_{ki} - F_{kw} \quad (33)$$

Making the difference between the two equations for the liquid and the vapor phases, the result

$$\begin{aligned} & \rho_l \left(\frac{\partial j_l}{\partial t} + j_l \frac{\partial j_l}{\partial z} \right) - \rho_v \left(\frac{\partial j_v}{\partial t} + j_v \frac{\partial j_v}{\partial z} \right) = \\ & -(\rho_l - \rho_v)g - \left(\frac{F_{li} + j_l M}{1 - \alpha} \right) + \left(\frac{F_{vi} + j_v M}{\alpha} \right) - \left(\frac{F_{lw}}{1 - \alpha} - \frac{F_{vw}}{\alpha} \right) \end{aligned} \quad (34)$$

is the SLIP equation.

The equations 0, 0, 0, the interfacial relations 0, 0, 0 and the interfacial energy transfers, the interfacial momentum transfer, and the transport equation for non-condensable gas, not here reported, represent the equations of the basic module system codes [19] (i.e. Relap5, Cathare2, etc...) extensively used for the instability analyses [20],[21],[22].

Another approach consists by the utilization of the simplified models in order to gain some physical understanding of the phenomena.

This section is focused on the work performed by W. Ambrosini [23] related to the stability of the thermo-siphon loop and in particular on the linear analyses and non-linear analyses, discussing some of the basic mechanisms involved in density wave instabilities. The considered physical model is quite simple and involves a boiling channel with constant pressure drop and inlet sub-cooling boundary conditions. An arbitrary axial distribution of heat flux is allowed and both distributed and singular pressure drop are included. Heater dynamics is modeled making use of a radially lumped heat structure model, which is axially discretized coherently with the hydraulic channel.

The two phases are assumed in thermal and mechanical equilibrium according to the HEM. To analyze the flow in the system, the equations derive by the equations 0, 0, 0, written for each phase and summed, with the following hypotheses:

$$A_k = const, \quad A_g = \alpha \quad \text{and} \quad A_l = 1 - \alpha$$

$\frac{\partial p}{\partial t}$; $\frac{\partial p}{\partial z}$ are neglected in the energy equation in order to have the pressure only in momentum equation.

$$\sum_k Q_{kw} = \dot{q}''' \quad \text{where } \dot{q}''' \text{ is the heat input per unit of volume.}$$

$$\sum_k F_{kw} = F_{TP} \quad \text{where } F_{TP} \text{ is the two phase friction pressure drop.}$$

The equations are reduced to a set of three partial differential equations, where frictional dissipation and pressure energy are neglected.

$$\frac{\partial[\alpha\rho_v + (1-\alpha)\rho_l]}{\partial t} + \frac{\partial[\alpha\rho_v j_v + (1-\alpha)\rho_l j_l]}{\partial z} = 0 \quad (35)$$

$$\begin{aligned} & \frac{\partial[\rho_l(1-\alpha)j_l + \rho_v\alpha j_v]}{\partial t} + \frac{\partial[\rho_l(1-\alpha)j_l^2 + \rho_v\alpha j_v^2]}{\partial z} + \frac{\partial p}{\partial z} + F_{lw}(1-\alpha) + F_{vw}\alpha \\ & + [\rho_l(1-\alpha) + \rho_v\alpha]g = 0 \end{aligned} \quad (36)$$

$$\frac{\partial[\rho_l(1-\alpha)H_l + \rho_v\alpha H_v]}{\partial t} + \frac{\partial[\rho_l(1-\alpha)j_l H_l + \rho_v\alpha j_v H_v]}{\partial z} = q''' \quad (37)$$

The homogeneous equilibrium model (HEM) is characterized by the assumption that the two phase flow is an emulsion (i.e. a continuous fluid with small and evenly distributed bubbles or droplets) in thermal and mechanical equilibrium. Following this physical model the equations adopted in order to describe the boiling channel flow behavior are the equations 0, 0, 0.

$$\frac{\partial \rho}{\partial t} + \frac{\partial \rho j}{\partial z} = 0 \quad (38)$$

$$\frac{\partial \rho j}{\partial t} + \frac{\partial \rho j^2}{\partial z} + \frac{\partial p}{\partial z} = -\rho g - \left[\frac{f}{D_h} + 2K_{in}\delta_d(z) + 2K_{ex}\delta_d(z-L) \right] \frac{\rho j^2}{2} \quad (39)$$

$$\frac{\partial \rho h}{\partial t} + \frac{\partial \rho h j}{\partial z} = \begin{cases} q_0'' \frac{\Pi_h}{A} f_q(z) & \Rightarrow \text{no heater} \\ \frac{\Pi_h}{A} H[\mathcal{G}_H(z) - \mathcal{G}(z)] & \Rightarrow \text{with heater} \end{cases} \quad (40)$$

where δ_d is a dimensional Dirac's delta function [m-1].

The energy equations have been written for two different situations analyzed by Ambrosini: one consider only the heat flux imposed given to the fluid the second takes into account also the heat capacity of the heater.

The balance equation can be assumed in dimensionless form assuming a reference pressure to evaluate the saturated fluid properties, which are considered independent of the local value of the pressure. The main dimensionless groups useful for this analysis that are able to take into account the fluid proprieties, the gravity, the pressure, inlet velocity, inlet enthalpy, and heat flux are: N_{pch} , that is the phase change number involves the reciprocal flow rate versus heating power ratio and includes the specific volume ratio; N_{sub} , the subcooling number, that includes the specific volume ratio [24]; Fr , Froude number, that represents the ratio of inertia to buoyancy [25].

The resulting dimensionless equations are

$$\frac{\partial \rho^*}{\partial t^*} + \frac{\partial G^*}{\partial z^*} = 0 \quad (41)$$

$$\frac{\partial G^*}{\partial t^*} + \frac{\partial}{\partial z^*} \left(\frac{G^{*2}}{\rho^*} \right) + \frac{\partial \rho^*}{\partial z^*} = -\frac{\rho^*}{Fr} - [\Lambda + K_{in}\delta^*(z^*) + K_{ex}\delta^*(z^*-1)] \frac{G^{*2}}{\rho^*} \quad (42)$$

$$\frac{\partial \rho^* h^*}{\partial t^*} + \frac{\partial G^* h^*}{\partial z^*} = \begin{cases} N_{pch} f_q^*(z^*) & \Rightarrow \text{no heater} \\ K_H [\mathcal{G}_H^*(z^*) - \mathcal{G}^*(z^*)] & \Rightarrow \text{with heater} \end{cases} \quad (43)$$

where δ^* and f_q^* are respectively a dimensionless Dirac's delta function and the heat flux distribution function.

In the case of forward flow at both the inlet and the outlet sections, constant values of dimensionless pressure in the plena and $h^*_{in} = -N_{sub}$ and are assumed as boundary conditions for transient analysis.

Considering the boiling channel in Figure 10 divided in N_n nodes of equal size and connected by junctions.

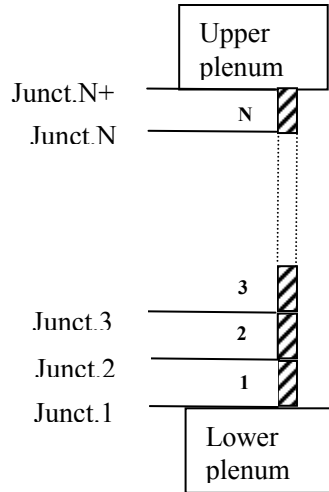


FIG. 10. Boiling channel discretization.

Mass and energy balance equations are solved within each node and momentum equations are solved at junctions, resulting in a classical staggered mesh scheme. Conservative and non-conservative forms of balance equations are adopted in order to impose basic conservation principles and obtain an implicit treatment of the coupling between pressure and flow.

Dimensionless mass and energy balances in conservative form turn out to be

$$\rho_i^{*n+1} = \rho_i^{*n} + \frac{G_i^{*n+1} - G_i^{*n}}{\Delta z^*} \Delta t^* \quad (i = 1, \dots, N_n) \quad (44)$$

$$(\rho_i^* h_i^*)^{n+1} = (\rho_i^* h_i^*)^n + \left[G_i^{*n+1} h_i^{*n} - G_{i+1}^{*n+1} h_{i+1}^{*n} \right] \frac{\Delta t^*}{\Delta z^*} + \begin{cases} N_{pch} \bar{f}_q^*(z_i^*) \Delta t^* & \Rightarrow \text{no heater} \\ K_{Hi} [\mathcal{G}_{Hi}^* - \mathcal{G}^*(h_i^*)] \Delta t^* & \Rightarrow \text{with heater} \end{cases} \quad (45)$$

where $\bar{f}_q^*(z_i^*)$ is an appropriate average over the i -th node of the flux distribution factor and quantities \bar{h}_i^{*n} and \bar{h}_{i+1}^{*n} are the “donored” junction enthalpies.

The momentum equation is discretized in space and time in the form:

$$G_i^{*n+1} = G_i^{*n} + \left[\frac{\overline{G}_{i-1}^{*n^2}}{\rho_{i-1}^{*n}} - \frac{\overline{G}_i^{*n^2}}{\rho_i^{*n}} \right] \frac{\Delta t^*}{\Delta z^*} - \frac{1}{2} [\rho_{i-1}^{*n} + \rho_i^{*n}] \frac{\Delta t^*}{Fr} - \left[\Lambda + K_{in} \hat{\delta}^*(z_i^*) + K_{ex} \hat{\delta}^*(z^* - 1) \right] \frac{2 |G_i^{*n}| G_i^{*n+1}}{\rho_{i-1}^{*n} \rho_i^{*n}} \Delta t^* + (p_{i-1}^{*n+1} - p_i^{*n+1}) \frac{\Delta t^*}{\Delta z^*} \quad (i = 1, \dots, N_n + 1) \quad (46)$$

where $\hat{\delta}^*$ is a Dirac's delta function operating over a discretized domain and \overline{G}_{i-1}^{*n} and \overline{G}_i^{*n} are node average mass fluxes. When the heater dynamics is consider, the following dimensionless equations are solved in closed form to provide the new time step values of heater temperature.

$$N_{MH} \frac{d\mathcal{G}_{Hi}^*}{dt^*} = N_{pch} \overline{f}_q(z_i^*) - K_{Hi} [\mathcal{G}_{Hi}^* - \mathcal{G}(h_i^*)] \quad (i = 1, \dots, N_n) \quad (47)$$

Once the heat input to the channel nodes is known (with or without heater dynamics), linearized (non-conservative) forms of mass and energy balance equations and the momentum balance equations and the momentum balance equation are combined resulting in a three point standard algorithm. Momentum equations is then used again to update dimensionless function mass fluxes on the basis of the new time step dimensionless nodal pressures; mass and energy balances in conservative form are then used to evaluate ρ_i^{*n+1} and h_i^{*n+1} .

To solve the ambiguity in the definition of nodal density as calculated by mass balance the state relationship, the value of nodal dimensionless density at the new time-step is assumed equal to the one corresponding to the new dimensionless enthalpy as it is justified by the fact that the mass error at each time step is very small.

For each assigned set of dimensionless parameters, steady-state conditions are calculated at constant dimensionless inlet mass flux, providing initialization of channel nodal variables and the value of the overall pressure drop across the channel to be imposed as a constant boundary condition during the analysis. An impulse perturbation in the outlet pressure is used to start system oscillation.

In order to provide information about the linear stability of the boiling channel, the obtained discretized equations are then linearized by perturbation. This approach adopted in the Ambrosini paper [26] is based on the simple matrix formulation that relates the vectors of the system state variables at two subsequent time step.

$$(\delta y)^{n+1} = -\left(J_{y^{n+1}}^s\right)^{-1} J_{y^n}^s (\delta y)^n = A(\delta y)^n \quad (48)$$

where $J_{y^{n+1}}^s$ and $J_{y^n}^s$ are the Jacobian matrices of the non-linear discretized equations with respect to y_n and y_{n+1} . Considering the eigenvalues ($\lambda_i \in C$) of the matrix A, the criterion $\rho(A) = |\lambda_{\max}| > 1$ is the condition for the asymptotic instability.

The quantities

$$z_R = \text{Re}(\lambda_{\max}) = \frac{\ln[\rho(A)]}{\Delta t^*} \quad z_I = \text{Im}(\lambda_{\max}) = \frac{1}{\Delta t^*} ar \cos \frac{\text{Re}(\lambda_{\max})}{\rho(A)} \quad (49)$$

are useful in studying stability of small perturbation. They represent respectively a measure of the amplification ($Z_R < 0$) or damping ($Z_R > 0$). The period (T) and the decay ratio (DR) of the oscillations are:

$$T_{fast} = \frac{2\pi}{z_I} \quad DR = e^{\frac{2\pi z_R}{z_I}} \quad (50)$$

The “stability plane” is the N_{sub} versus N_{pch} plane (see Figure 11) and the stability is studied in the regions in which $Z_R > 0$.

The figure concerns Ambrosini’s analyses, where two cases are analyzed. These differ for the Froude number and for the fiction parameters. In particular: the case (a) regards a vertical channel ($Fr = 0.033$) with $\frac{fl}{2D_h} = 2.85$ and the case (b) regards a nearly horizontal channel ($Fr = 105$) with $\frac{fl}{2D_h} = 0$.

These figures show the shape of the neutral stability, the expected separation between the density-wave and the Ledinegg (excursive) instability regions, and that for $N_{pch} > N_{sub}$, corresponding to positive exit thermodynamic quality, the system is ‘less stable’ the single phase region.

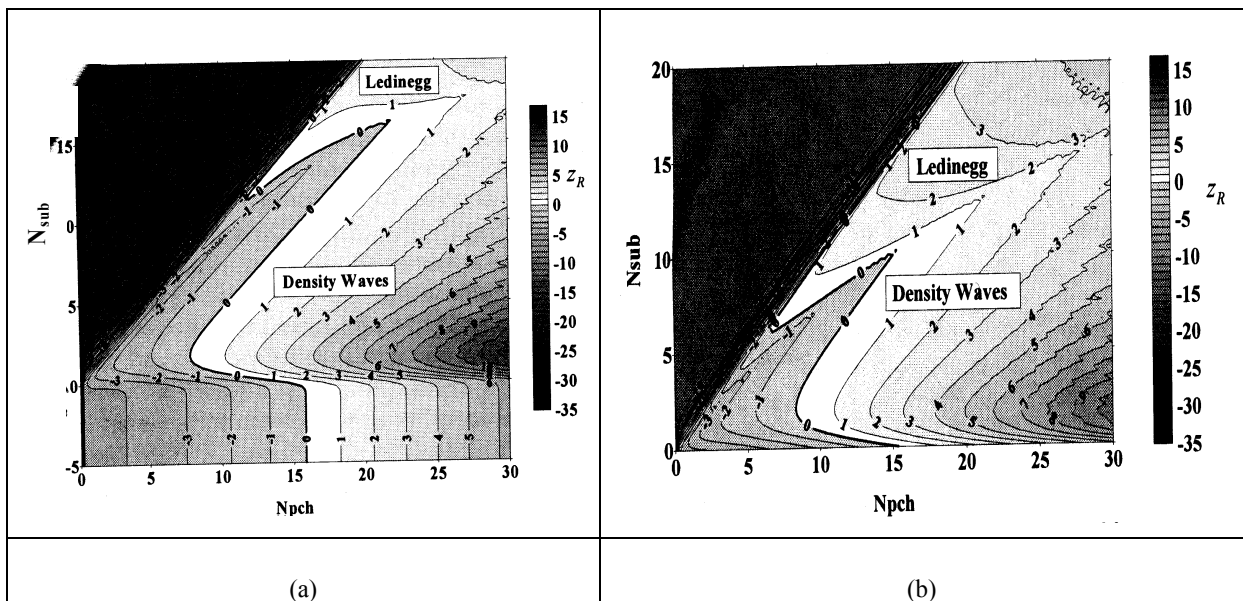


FIG. 11. Stability map.

4.1. Siphon condensation instability

D’Auria and Galassi [27] suggested that there is another relevant instability during two phase flow in PWRs, the siphon condensation.

RELAP5/Mod2 was used to analyse the test A2-77A at the LOBI facility. The LOBI facility is a 1:700 scaled model of the KWU PWR Biblis. The test A2-77A was planned as a characterisation test for the LOBI facility, but turned out to be the source of several interesting pieces of thermal hydraulics. In this test the facility was operated at nominal conditions (i.e. 14.0 MPa PS pressure, 8.6

MPa SS pressure, nominal PS coolant temperature, constant core power of 183kW, constant level of the SGs during all the test), but with the main circulation pumps switched off. A stable natural circulation was established. Then the PS inventory was drained discontinuously (in 17 steps) during the time of 8h. After several steps of draining a transition from single phase to two phase was observed (experimentally). Again after some steps of draining and several thousand seconds into the transient oscillation of a number of measured parameters were observed, and again after some steps of draining the “stable” region of reflux condensation was reached (see fig 12(a) and fig 12(b)).

D’Auria and Galassi investigated the region of 64% of the initial PS mass inventory, which is after the occurrence of the instabilities and before the reflux condensation.

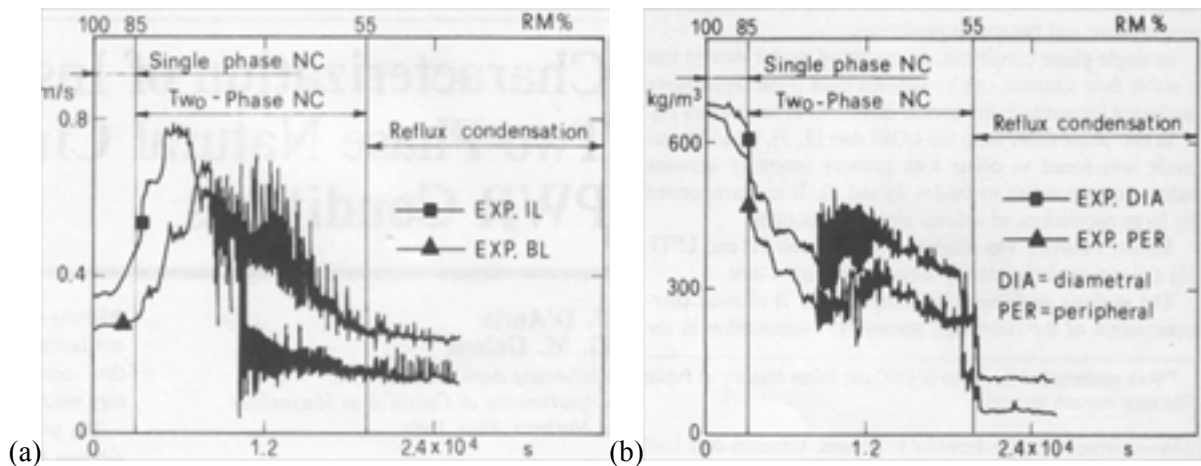


FIG. 12. Velocites (a) and density (b) in the two loops of the facility (IL - intact loop - designates a lumped loop, representing three loops of the plant, while BL - broken loop - represents a single loop).

Several interpretations for the instabilities were given in [28], but two of them lead to siphon condensation and were supported and predicted with Relap5 calculations:

1. A liquid level forms in the ascending leg of the U-tube due to the entrainment of droplets and flooding at the inlet, and draining occurs when the liquid level reaches the top of the U-tube,
2. A liquid level forms in the ascending leg because of condensation in the U-tubes, and again draining occurs when the liquid level reaches the top of the U-tubes.

In both cases the draining could occur due to the siphon effect, or due to CCFL from the bottom of the U-tubes to the top. The draining effect could be confirmed with the calculations. A detailed explanation of the mechanism can be seen from Figure 13.

NOMENCLATURE

Roman letter

A	Cross sectional area [m ²]
B	buoyancy force [N]
D_h	hydraulic diameter [m]
f	friction factor
f_q	power distribution factor
F	momentum losses and friction force [N]
$Fr = w_0^2 / gl$	Froud number
g	gravity [m/s ²]
G	mass flux [kg/(m ² s)]
$G^* = \rho^* j^*$	dimensionless mass flux
h	specific enthalpy [J/kg]
$h^* = \frac{h - h_f}{h_{fg}} \frac{v_{fg}}{v_f}$	dimensionless enthalpy
H	heat transfer coefficient [W/(m ² K)]
j	volumetric flux [m/s]
$j^* = j / w_0$	dimensionless volumetric flux
$K_{in,ex}$	singular pressure drop coefficient
$K_H = \frac{H \Pi_h L}{w_0 A c_{pf} \rho_f}$	dimensionless heat transfer coefficient
L	length [m]
$N_{MH} = \frac{M_h c_{pH}}{L A \rho_f c_{pf}}$	heater capacity number
$N_{pch} = \frac{q_0'' \Pi_h L}{\rho_f w_0 h_{fg} A} \frac{v_{fg}}{v_f}$	phase change number
$N_{sub} = \frac{h_f - h_{in}}{h_{fg}} \frac{v_{fg}}{v_f}$	subcooling number
N_n	number of nodes
p	pressure [kg/s ² m]
$p^* = p / \rho_f w_0^2$	dimensionless pressure
q	flow rate [kg/m ²]
q''	heat flux [W/m ³]
Q	heat transfer per unit time and volume
R	frictional coefficient [s ⁻¹]
t	time [s]
$t^* = t w_0 / L$	dimensionless time

v	specific volume [m ³ /kg]
z	axial coordinate [m]
$z^* = z/L$	dimensionless axial coordinate

Greek letter

α	thermal expansion coefficient [m]
Π_h	heated perimeter [m]
\mathcal{G}	temperature [K]
$\mathcal{G}^* = \begin{cases} h^* & \text{if } h < 0 \\ 0 & \text{if } h \geq 0 \end{cases}$	dimensionless fluid temperature
\mathcal{G}_h^*	dimensionless heater temperature
Λ	friction perimeter
ρ	density [kg/m ³]
$\rho^* = \rho / \rho_f$	dimensionless density

Subscripts

f	liquid phase
fg	difference between vapor and liquid
g	vapor phase
in	inlet
ex	exit
0	reference value

Superscripts

H	heater
i	i-th node or junction
n	n-th time level
n+1	(n+1)-th time level
•	dimensionless value
T	transposed

ACKNOWLEDGEMENT

The authors wish to acknowledge the support given by Boyan Neykov during the development of this work.

REFERENCES

- [1] MISALE, M., RUFFINO, P., FROGHERI, M., The Influence of the Wall Thermal Capacity and Axial Conduction Over a Single-Phase Natural Circulation Loop: 2-D Numerical Study, *Proceeding of Eurotherm Seminar N63, Genoa, Italy, 6-8 September*, Vol. , pp.177–187 (1999).
- [2] AMBROSINI, W., D'AURIA, F., GIGLIOLI, A., Coupled Thermal-Hydraulic and Neutronic Instabilities in the LaSalle-2 BWR Plant, *XIII Congresso Nazionale sulla Trasmissione del Calore dell'Unione Italiana di Termofluidodinamica - UIT*, Bologna, Italia (1995).
- [3] JAFARI, J., D'AURIA, F., KAZEMINEJAD, H., DAVILU, H., *Nuclear Engineering and Design*, Vol. 224, pp. 79–104 (2003).
- [4] AMBROSINI, W., DEL NEVO, A., ORIOLO, F., *Thermal-Hydraulic Stability Analyses in IRIS Helical Coil Steam Generators with the Relap5 Code*, DIMNP Internal Report, Pisa (2004).
- [5] BOURE, J.A., BERGLES, A.E., TONG, L.S., *Review of Two Phase Flow Instability*, Nuclear Engineering and Design, North-Holland Publishing Company (1973).
- [6] CAREY VAN, P., *Liquid-Vapor Phase Change Phenomena*, Taylor & Francis (1992).
- [7] SU GUANGHUI, et. al., Theoretical Study on Density Wave Oscillation of Two Phase Natural Circulation under Low Quality Conditions, *Journal of Nuclear Science and Technology* (2001).
- [8] KAKAC and LIU, H.T., Two-Phase Flow Dynamic Instabilities in Boiling Systems, *In Multiphase Flow and Heat Transfer - Second International Symposium*, Washington DC, Vol. 1, pp. 403–444 (1991).
- [9] CROWLEY, J.D., DEANNE, C., and GOUSE JR., S.W., Two Phase Oscillations in Vertical, Parallel, Heated Channels, *Proc. Symp. on Two Phase Flow Dynamics*, Commission of the European Communities, Brussels, pp. 1131–1172 (1969).
- [10] ISHII, M., *Study on Flow Instabilities in Two Phase Mixtures*, ANL-76-23 (1976).
- [11] YADIGAROGLU, G., CHAN, K.C., *Analysis of flow instabilities*, Departement of Nuclear Engineering, University of California, Berkeley, California).
- [12] NEA/CSNI/R(96), *State of the Art Report on Boiling Water Reactor Stability (SOAR on BWR)*, OECD/GD(97) (1997).
- [13] WELANDER, P., On the oscillatory instability of a differentially heated fluid loop, *Journal of Fluid Mechanics*, Vol. 29, part 1, pp. 17–30 (1967).
- [14] VIJAYAN, P.K., AUSTREGESILO, H., Scaling Laws for the Single Phase Natural Circulation Loops, *Nuclear Engineering and Design*, Vol. 152, 331–340 (1994).
- [15] SUSLOV, S.A., PAOLUCCI, S., Nonlinear stability of mixed convection flow under non-Boussinesq conditions. Analysis and bifurcations, *Journal of Fluid Mechanics*, Vol. 398, pp. 61–108 (1999).
- [16] SUSLOV, S.A., PAOLUCCI, S., Mean flow characteristics, *Journal of Fluid Mechanics*, Vol. 398, pp. 61–108 (1999).
- [17] AMBROSINI, W., FERRERI, J.C., The effect of truncation error on the numerical prediction of linear stability boundaries in a natural circulation single-phase loop, *Nuclear Engineering and design*, Vol. 183, pp. 53–76 (1997).
- [18] Technical Working Group1 – Advanced Water Cooled Reactors, 2001, Generation IV Water Cooled Reactor Concepts, Generation IV Roadmap Session, ANS Winter Meeting Reno, NV.
- [19] NUREG/CR-5535, *RELAP5/MOD3 – Volume I – Code Structure, System Models, and Solution Methods*, Thermal Hydraulics Group; Scientech, Inc.; Rockville, Maryland; Idaho Falls, Idaho, USA (1999).
- [20] D'AURIA, F., PELLICORO, V., *Local Instability in BWR Reactor Simulator* <http://virmap.unipi.it/cgi-bin/virmap/vmibo?doc_pubbl:10421868;main;proc>, Int. Conf. on Nuclear Engineering (ICONE-4), Vol. 3, pp. 157, New Orleans, USA (1996).
- [21] D'AURIA, F., PELLICORO, V., FELDMANN, O., *Use of Relap5 Code to evaluate the BoP influence following instability events in BWRs* <http://virmap.unipi.it/cgi-bin/virmap/vmibo?doc_pubbl:10431020;main;proc>, Int. Conf. on Nuclear Engineering (ICONE-4), Vol. 3, p. 71, New Orleans, USA (1996).

- [22] MISALE, M., FROGHERI, M., D'AURIA, F., Experiments in natural circulation: influence of scale factor on the stability behaviour, *Proceeding of Eurotherm Seminar N63, Genoa, Italy, 6–8 September*, Vol. 1, pp. 109, Genova, Italy (1999).
- [23] AMBROSINI, W., DI MARCO, P., SUSANEK, A., Prediction of Boiling Channel Stability by a Finite — Difference Numerical Method, *2nd International Symposium on Two Phase Flow Modelling and Experimentation*, Pisa, Italy (1999).
- [24] ISHII, M., ZUBER, N., Thermally Induced Flow Instabilities in Two Phase Mixtures, *4th Int. Heat Transfer Conference*, Paris, Italy (1970).
- [25] LATROFA, E., *Fisica Tecnica — Termodinamica*, A. Vallerini Editrice, Pisa, Italia (2000).
- [26] AMBROSINI, W., On Some Physical and Numerical Aspects in Computational Modelling of One-Dimensional Flow Dynamics, *7th International Seminar on Recent Advances in Fluid Mechanics*, Physics of Fluids and Associated Complex Systems, Buenos Aires, Argentina (2001).
- [27] D'AURIA, F., GALASSI, G.M., Flowrate and Density Oscillation during Two-Phase Natural Circulation in PWR Typical Conditions, *Nuclear Engineering and Design*, Vol. 122, pp. 209–218 (1990).
- [28] D'AURIA, F., GALASSI, G.M., Flowrate and Density Oscillation during Two-Phase Natural Circulation in PWR Typical Conditions, *Experimental Therapy and Fluid Science*, Vol. 3 N. 6, pp. 641–650 (1990).

ANNEX 9

STABILITY ANALYSIS OF NC BASED SYSTEMS: PRESSURE TUBE TYPE BWR AND STEAM GENERATORS

P.K. Vijayan, A.K. Nayak

Reactor Engineering Division,
Bhabha Atomic Research Centre, India

Abstract

This lecture reviews the methods used for the analysis of static, dynamic and compound dynamic instabilities in NCSs. The difference between the linear and nonlinear and the need to use both techniques in the stability analysis of NCRs is brought out. Effect of various geometric and operating parameters on the instability is presented taking a pressure tube type reactor as an example. The issues during the start-up of a natural circulation reactor is briefly described.

1. INTRODUCTION

Industrial natural circulation systems must operate stably and reliably over the entire range of power from start-up to full power. To ensure this, we must restrict operation of NCSs well within the stable zone. Thus, there is a need to establish the stable and unstable zones of operation of a NCS. The stable and unstable zones are usually identified by a linear stability (also known as frequency domain) analysis. To have flexibility in operation one also needs to know the effect of various operating parameters like power, pressure, inlet subcooling and design parameters like riser height, inlet orificing and loop geometry on the stability behaviour. Further, in many instances, there is a possibility that NCSs can land in an unstable zone of operation because of a system malfunction, an operator error, or an unanticipated transient. In such cases, the designer must be able to know what kind of oscillatory behaviour can be expected so that the plant operator can be forewarned. In addition, the operator must get an appropriate and useful signal so as to take timely corrective action. These requirements can be met by the nonlinear stability (time domain) analysis. Nonlinear analysis is also required to establish a stable start-up, power raising and setback procedures in NCSs. Further, it may be noted that the analysis methodologies are the same for different systems like the steam generators, pressure tube type heavy water reactors, BWRs, etc. Therefore, first the analysis methodologies will be presented followed by a parametric analysis and finally specific applications to the stability design of a pressure tube type reactor and the steam generator will be highlighted.

2. STABILITY ANALYSIS

Natural circulation systems can experience a large variety of instabilities as explained in the last chapter. Strictly speaking, NCS design must ensure stability for all possible types of instabilities. However, well-established analysis procedures do not exist for all observed instability phenomena.

Fortunately, all types of instabilities are not observed in every natural circulation system. Hence, design procedures usually address only the commonly observed static and dynamic instabilities. Ledinegg instability and density wave oscillations (DWO) are the commonly observed static and dynamic instabilities respectively. Most NC based systems, require some continuous feed and bleed like the feed water flow and steam flow in a BWR. Since the location of feed and bleed points in the system has an important bearing on the stability, it can be a design issue in some NCSs. In BWRs, neutronics plays a very important role in the thermalhydraulic instability. Hence BWRs require not only static and dynamic analysis but also coupled neutronic-thermalhydraulic analysis to arrive at the thresholds of instability. In short, we require analysis methods for

- a) Static instability,
- b) Dynamic instability, and
- c) Coupled neutronic thermal hydraulic instability.

3. STATIC INSTABILITY

3.1. Single-phase NCS

Most single-phase loops do not show pure static instability. The compound static instabilities associated with flow reversal in single-channel loops are analyzed in the same way as dynamic instabilities. Parallel channel systems also exhibit a static instability associated with flow reversal. 6 (1963) has developed a theoretical approach to calculate the critical power below which flow reversal is possible in a system of vertical unequally heated parallel channels. Similar approach can be used to develop a criterion for parallel horizontal channels or parallel vertical U-tubes. In case of parallel vertical channels, the flow reversal can be avoided if all the channels are equally powered. With horizontal heated channels (as in PHWRs) or vertical cooled U-tubes (as in SGs), unequal driving forces exist even if all the channels are equally powered due to the difference in elevation and hence flow reversal possibility cannot be eliminated.

3.2. Two-phase systems

Compound static instability associated with flow reversal in two-phase single channel systems can be analyzed by dynamic stability analysis.

3.2.1. Ledinegg type instability

The instability is observed in the negative slopping region of the pressure drop vs. flow curve and the criterion for this type of instability is given by

$$\frac{\partial \Delta p_f}{\partial W} - \frac{\partial \Delta p_d}{\partial W} \leq 0 \quad (1)$$

Where Δp_f is the total pressure losses in the system and Δp_d is the driving head due to buoyancy. Δp_f includes all losses in the inlet piping, heat source, outlet let piping and steam drum except the pressure drop due to gravity in the downcomer, ($\Delta p_d = \rho g H$) (Fig. 1). To check the occurrence of Ledinegg instability, the variation of Δp_f and Δp_d as a function of flow rate is required. Since the down comer is in the single-phase condition, Δp_d does not vary with flow rate for a fixed inlet subcooling. Hence an equivalent criterion to the above is sometimes used:

$$\frac{\partial \Delta p_f}{\partial W} \leq 0 \quad (2)$$

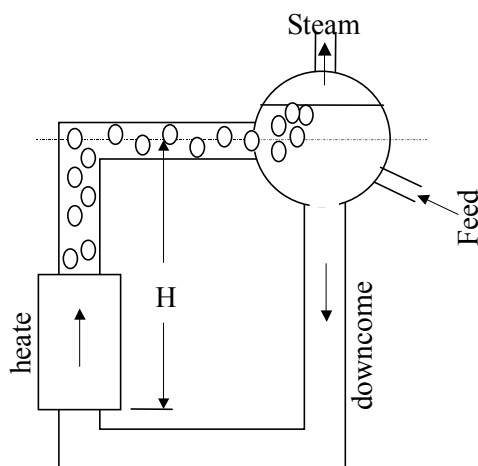


FIG. 1. Static instability in a two-phase NCS.

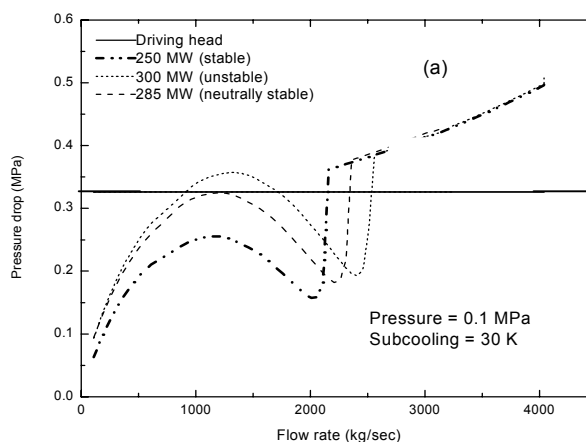


FIG.2. Identification of threshold values for Ledinegg type instability.

The pressure loss for the loop in Fig. 1 can be written as

$$\Delta p_f = \frac{W^2}{A^2} \oint \hat{\rho} v + g \int_{hi}^{SD} \rho dz + \frac{W^2}{2A^2 \rho_f} \left[K_i + \frac{f_f}{D} \left\{ L_{sp} + \left(\bar{\phi}_{Lo}^2 L_{tp} \right)_h + \left(\phi_{Lo}^2 L_{tp} \right)_p \right\} + K_o \phi_{Lo}^2 \right] \quad (3)$$

Where the subscript hi stands for the heater inlet. Fig. 2 illustrates the use of the above criterion to identify the lower threshold for Ledinegg type instability. The calculations were actually performed for the AHWR, which is a pressure tube type NC based BWR being designed in India (see Appendix-1). It shows that below a channel power of 0.285 MW, the system pressure loss characteristic intersects the driving buoyancy pressure differential only once indicating that only one operating point is possible. Above this power, the channel pressure loss characteristic intersects at three points indicating the existence of three operating points. In a similar way, the upper threshold can be identified. The lower and upper thresholds can be obtained similarly for other values of subcooling to generate the stability map as shown in Fig. 3. The instability is not observed below a certain subcooling for a given pressure. With increase in subcooling the unstable zone is found to increase and hence increasing the inlet subcooling has a destabilizing effect. It is found that as the pressure increases the unstable zone contracts as well as shifts up so that the easiest way to avoid this instability is to begin boiling at relatively higher pressures. In fact, it is found to shift beyond the operating envelope of power beyond a certain pressure.

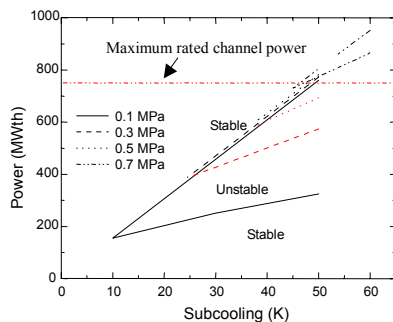


FIG..3. Effect of pressure on Ledinegg type instability.

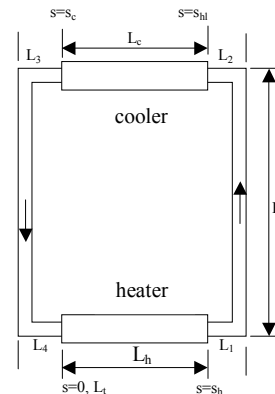


FIG..4. Geometry and coordinate system for a rectangular single-phase NCL.

In a loop optimized for NC, the pipe sizes are reasonably large and the mass flux is also correspondingly low making the friction pressure drop an insignificant part of the total loop pressure drop. Due to this, the different friction factor models do not make a significant impact on the stability map. The predictions reported here on two-phase instability are carried out with the Baroczy (1966) [1] model for two-phase friction multiplier. With increase of riser height, the unstable zone is found to enhance. Differences in power profiles do not make a major impact on the Ledinegg type instability in AHWR. A detailed parametric study of the instability can be found in Nayak et al (2000a) [2].

3.2.2. Static instability of parallel channel systems

Parallel channel systems under two-phase flow condition, exhibit both kinds of multiple steady states: i.e. multiple steady states in the same flow direction as well as opposite flow directions. Linzer and Walter (2003) have theoretically studied flow reversal in a two-phase natural circulation system with unequally heated parallel vertical channels and proposed a criterion for flow reversal. Flow reversal under two-phase NC can be expected in horizontal parallel channels of the type used in pressure tube type PHWRs and vertical parallel U-tubes in steam generators. A criterion for flow reversal can be derived based on the theoretical approach proposed by Linzer and Walter (2003) [3].

Several studies exist for the multiple steady states in the same flow direction (Ledinegg type instability). Rohatgi and Duffey (1998) [4] obtained a closed-form solution for the stability of uniformly heated parallel channels based on the homogeneous equilibrium model. Considering the

total pressure drop across a single channel as the sum of single-phase and two-phase region pressure drops, they obtained the following expression for the total pressure drop across a single channel:

$$\Delta p = \frac{fW^2}{2DA^2} \left\{ \frac{L_{sp}}{\rho_f} + \frac{L_h - L_{sp}}{\rho_m} \right\} + \frac{W^2}{2A^2} \left\{ \frac{K_i}{\rho_f} + \frac{K_o}{\rho_m} \right\} + g \left\{ L_{sp} \rho_f + (L_h - L_{sp}) \rho_m \right\} \quad (4)$$

Differentiating the above and using the condition of static instability as $\frac{\partial \Delta p}{\partial W} = 0$, they obtained the following nondimensional equation for the static instability of parallel channels.

$$N_p^2 N_{fr} (1 + \bar{K}_o) + 2 N_p N_{fr} [(1 - N_s)(2 + \bar{K}_o) + \bar{K}_i] + 3 N_{fr} N_s^2 + 2 N_{fr} (2 + N_s) = 0 \quad (5)$$

The instability region is bounded by the two roots of the above equation and hence provides a method for obtaining the region of instability. The stability map obtained from Eq. (5) is similar to that given in Fig. 3.

4. DYNAMIC INSTABILITY

Dynamic instability of the density wave type is the most commonly observed instability for both single-phase and two-phase natural circulation loops. In general, the dynamic stability analysis is performed either by the linear or the non-linear method.

4.1. Linear stability method

In the linear stability method, the time dependent governing equations are perturbed over the steady state. The perturbed equations are linearized and solved analytically to obtain the characteristic equation for the stability. The roots of the complex characteristic equation are then obtained numerically and the stability is judged by the Nyquist Stability Criterion. As per this criterion, if any of the roots of the characteristic equation has a positive real part, then the corresponding operating conditions are unstable. The marginal stability curves, which separate the stable and unstable zones, can be obtained in this way for both single-phase and two-phase loops. This method is also known as frequency domain analysis and is best suited for generating the stability map. The method is computationally less expensive and gives exact analytical solution of the linearized governing equations and is free from numerical stability problems. The mathematical derivation of the characteristic equation, however, is a tedious process. Even a small change in the geometry like changing the orientation of the heat source or the heat sink, pipe, etc. calls for re-derivation of the characteristic equation.

4.1.1. Linear analysis of single-phase NCSs

For a specified uniform diameter rectangular loop, the maximum steady state flow rate (for a given power and cooler secondary conditions) is achievable with horizontal heater and horizontal cooler (since it has the largest elevation difference) compared to any other orientation of heat source and heat sink. However, it does not tell us whether that particular steady state is stable. Experiments indicate that this is the least stable orientation of heater and cooler. Thus stability analysis is necessary to examine whether a particular steady state is stable or not. To illustrate the linear analysis technique, we consider the simple uniform diameter rectangular loop shown in Fig. 4. The integral momentum equation applicable to one-dimensional single-phase flow in nondimensional form is (see Appendix-2 for the derivation).

$$\frac{d\omega}{d\tau} = \frac{Gr_m}{Re_{ss}^3} \oint \theta dZ - \frac{pL_t \omega^{2-b}}{2D Re_{ss}^b} \quad (6)$$

Similarly, the nondimensional energy equation applicable for the various segments of the loop can be written as

$$\frac{\partial \theta}{\partial \tau} + \phi \omega \frac{\partial \theta}{\partial S} = \begin{cases} \frac{L_t}{L_h} & \text{heater} & (\text{for } 0 < S \leq S_h) \\ 0 & \text{pipes} & (\text{for } S_h < S \leq S_{hl} \text{ and } S_c < S \leq S_t) \\ -St_m \theta & \text{cooler} & (\text{for } S_{hl} < S \leq S_c) \end{cases} \quad (7)$$

During linear stability analysis, we slightly perturb the flow rate and temperature over the steady state as follows:

$$\omega = \omega_{ss} + \omega' \text{ and } \theta = \theta_{ss} + \theta' \quad \text{where } \omega' = \bar{\omega} \epsilon e^{n\tau} \text{ and } \theta' = \bar{\theta}(S) \epsilon e^{n\tau} \quad (8)$$

From the above, it is clear that knowledge of the exact steady state flow rate and temperatures are essential for performing the linear stability analysis. The steady state solutions of equations 6 and 7 for rectangular loops can be found in Appendix-2. The same can be extended to any single-phase loop as shown by Vijayan et al. (2004a) [5]. Substituting Eq. (8) into Eq. (6) and (7), the perturbed equations are obtained. Linearizing and solving the perturbed equations analytically, the characteristic equation for the stability parameter, n is given by (see appendix-3 for the derivation)

$$n - \frac{(p/2)^{1+m}}{(Gr_m I_{ss})^m (D/L_t)^{1+m}} \left[\left(\frac{\bar{I}/\bar{\omega}}{I_{ss}} \right) - (2-b) \right] = 0 \quad (9)$$

$$\text{Where } \frac{\bar{I}}{\bar{\omega}} = \frac{1}{\bar{\omega}} \oint \bar{\theta}(S) dZ \quad (10)$$

For the rectangular loop with horizontal heater and cooler, we obtain the following expression after integration (see Appendix-3)

$$\frac{\bar{I}}{\bar{\omega}} = \frac{\phi}{n} \left(1 - e^{-\frac{n}{\phi}} \right) \left\{ \frac{\bar{\theta}_h}{\bar{\omega}} e^{-\frac{nL_1}{L_t}} - \frac{\bar{\theta}_c}{\bar{\omega}} e^{-\frac{nL_3}{L_t}} \right\} \quad (11)$$

$$\text{If } L_1=L_3=L_x, \text{ then, } \frac{\bar{I}}{\bar{\omega}} = \frac{\phi}{n} \left(1 - e^{-\frac{n}{\phi}} \right) e^{-\frac{nL_x}{L_t}} \left\{ \frac{\bar{\theta}_h - \bar{\theta}_c}{\bar{\omega}} \right\} \quad (12)$$

Which is same as that in Vijayan (2002) [6]. The expression for $(\bar{\theta}_h - \bar{\theta}_c)/\bar{\omega}$ can be found in the Appendix-3. The characteristic equation is a complex transcendental equation in terms of the stability parameter n. To assess stability, either we search for the roots of this equation using a numerical technique or make Nyquist plots. The former method is more popular.

4.1.2. Linear analysis of two-phase NCSs

The principles of linear and nonlinear stability analyses are similar in single- and two- phase natural circulation systems. However, the governing equations are somewhat different for the two-phase regions of the system depending on the chosen equation system. For two-phase flow, one can make a wide choice starting from the homogeneous equilibrium model, which uses one equation each for the mass, momentum and energy conservation similar to single-phase flow. However, it is well known that there is a difference in the velocity between the vapour and liquid phases. The simplest model that takes care of this difference in velocity is the drift flux model (DFM). In many two-phase flow

situations, the temperature of the liquid and vapor phases can be different as in subcooled boiling and droplet flow. Considering both thermal and kinematic nonequilibrium require application of the conservation laws to each phase. Most two-fluid models are mathematically ill posed rendering them unsuitable for instability analysis. As a result linear stability analysis with the two-fluid model were not available till recently. Zhou and Podowski (2001) [7] have carried out a frequency domain analysis of the two-fluid equations for the first time. Recently Song and Ishii (2001) [8] proposed a well-posed two-fluid model (TFM) with certain restrictions on the liquid and gas momentum flux parameters. Thus, one can use the simple homogeneous model to a two-fluid model for analyzing two-phase flow instability. Table-1 demonstrates the equation system used in the various codes for stability analysis. Consideration of all these models is beyond the scope of this course. The linear analysis of two-phase flow instabilities is illustrated with the homogeneous equilibrium model (HEM) in Appendix-4.

Table 1. Commonly used linear stability analysis codes

Name of code	Thermalhydraulic model		Neutronics model	Reference
	Channels	TPFM (Eq)		
NUFREQ NP	A few	DFM (4)	Simplified 3-D	Peng (1985) [9]
LAPUR5	1-7	HEM (3)	P-K ¹ & M-P-K ²	Otaudy (1989) [10]
STAIF	10	DFM (5)	1-D	Zerreßen (1987) [11]
FABLE	24	HEM (3)	P-K ¹	Chan (1989) [12]
ODYSY	A few	DFM (5)	1-D	D'Auria (1997) [13]
MATSTAB	All	DFM (4)	3-D	Hänggi (1999) [14]

¹ P-K : point kinetics; ² M-P-K : modal point kinetics; TPFM: two-phase flow model

4.1.3. Parallel channel instability

The linear stability analysis described in Appendix-4 also includes the effect of parallel channels. For parallel channel instability, it is also of interest to know whether the oscillations are in-phase or out-of-phase. From the solution of the characteristic equation, we can estimate the ratio

$$\frac{(W'_{in})_i}{(W'_{in})_j} = \frac{G_j}{G_i} = M + jN \quad (13)$$

Where G_i is the sum of perturbed pressure drops in the i^{th} channel. The quantity $M+jN$ can be expressed as $Re^{j\theta}$ where the ratio of the amplitudes, R , is obtained as $R = \sqrt{M^2 + N^2}$ and the phase difference, θ , is obtained as $\theta = \tan^{-1}(N/M)$. Depending on the value of θ the oscillatory nature can be identified as in-phase or out-of-phase.

4.1.4. Coupled neutronic thermalhydraulic instability

In nuclear reactors, as the void fraction fluctuates, it also affects the neutronics via the void reactivity feedback resulting in power oscillations. It may be noted that if the void reactivity coefficient is zero, then the neutron kinetics and thermalhydraulics are decoupled and the instability threshold can be predicted from a pure thermalhydraulic model as in the case of a thermalhydraulic test facility. But in most BWRs, the void reactivity is significantly negative and a coupled stability analysis considering both neutronics and the thermalhydraulics are essential.

As we have seen in the last lecture, several modes of power oscillations such as global (in-phase), regional (out-of-phase) and local are possible in a nuclear reactor. It is easy to note that the analysis requirements are also different for the different oscillatory modes. For example, the in-phase mode can be easily analyzed with a point kinetics model. However, the point kinetics model can only give approximate results in case of axial power variation and 1-D kinetics model is better. The analysis of out-of-phase oscillations, in principle, requires a 3-D kinetics model. The major problem in linear

analysis of the 3-D kinetics equations is very complex mathematics with a lot of approximations. Non-linear codes such as TRAC which has 3-D neutronics has numerical problem for stability analysis. Hence, several simplified treatments relying on multi-point kinetics and modal kinetics are available for the analysis of out-of-phase instability. Linear stability analysis considering 3-D kinetics model is beyond the scope of the present course. Both multi-point kinetics and modal kinetics are briefly described in Nayak et al. (2000a and b) [2],[15].

4.2. Nonlinear stability analysis

Linear analysis tells us whether a particular steady state is stable or unstable and is well suited to generate a stability map. It does not tell us how the steady state can be approached. Stability thresholds of a NCS, depends on the way we approach the steady state due to the hysteresis effects [16] or conditional stability [17]. In other words, stability threshold depends on the operating procedure. Achard et al. (1985) [18] also show that finite amplitude perturbation can cause instability on the stable side of the linear stability boundary. Hence, nonlinear analysis is required to establish the stable operational domain and start-up procedure for NC based BWRs. This is carried out by the time domain codes based on direct numerical solution of the governing nonlinear partial differential equations. Usually such codes are based on the finite difference method and are not free from numerical instability problems. The stability analysis is carried out just like a normal transient analysis with the steady state conditions as the initial conditions. It is usual practice to perturb (but is not essential) one of the dependent variables like flow and track the behaviour of the disturbance. If the disturbance dies down with time, it is stable and if it oscillates with the same amplitude, it is neutrally stable and if it grows with time, then it is unstable. Nonlinear stability analysis is required to obtain the nature of the oscillatory behaviour like magnitude of the temperature and flow oscillations. They are capable of predicting the limit cycle oscillations and higher harmonic modes of oscillation. Generally both frequency domain and time domain codes are required for the complete stability analysis and establishing the operating and start-up procedure of NC BWRs.

Nonlinear analysis can, in principle, be carried out by codes used for the normal transient thermalhydraulic analysis of nuclear reactors (Table-2). For example, Vijayan et al. (1995) [19] used the ATHLET code to simulate the single-phase natural circulation instability in a rectangular loop. Ambrosini and Ferreri (1998) [20], Misale et al. (1999) [21] and Manish et al. (2002a) [22] and (2004) [23] used the RELAP5 code [24] for single-phase instability analysis of rectangular loops. Misale et al. (1999) have also used the CATHARE code for the same. There are also time domain codes dedicated to stability analysis like RAMONA-5.

Table 2. Commonly used codes for nonlinear stability analysis

Name of code	Thermalhydraulics model		Neutronics model	Reference
	Channels	TPFM (Eq)		
RAMONA-5	All	DFM (4 or 7)	3-D	RAMONA-5 catalogue
RELAP5/MOD 3.2	A few	TFM (6)	Point kinetics	RELAP5 (1995) [25]
RETRAN-3D	4	Slip Eq (5)	1-D	Paulsen (1991) [26]
TRACG	A few	TFM (6)	3-D	Takeuchi (1994) [27]
ATHLET	A few	TFM (6)	Point kinetics	Lerchl (2000) [28]
CATHARE	A few	TFM(6)	Point kinetics	Barre (1993) [29]
CATHENA	A few	TFM(6)	Point kinetics	Hanna (1998) [30]

4.2.1. Single-phase NCSs

While using large system codes for single-phase instability analysis, the reported experiences appear to vary significantly. With the ATHLET code Vijayan et al. (1995) [19] found that the adopted nodalization plays a very important role. Coarse nodalization led to stable steady flow always. With relatively finer nodalization, instability was observed and reasonable simulation of the essential

features of the single-phase instability was possible. While reproducing the results of Welander (1967) [31] using RELAP5, Ferreri and Ambrosini (2002) [32] found that depending on the node size used the code can predict stability or instability. Manish et al. (2002 & 2004) [22],[23] also reported similar dependency on nodalization while using RELAP5/MOD3.2 code. Manish et al. were able to reasonably reproduce the steady state flow rate and the instability threshold for a particular nodalization. However, if the nodalization is made finer then it is found that no steady state solutions exist. Ambrosini and Ferreri (1998) [20] studied the effect of various numerical schemes with different order of accuracy and found that second order schemes were better in reducing truncation error. Misale et al. (1999) [21] reported that the CATHARE code was able to predict the steady state quantities, but failed to show instability. On the other hand RELAP code is able to show instability but not at the same power levels as in the experiments. The main drawback of these codes is that they are somewhat unwieldy for the analysis of instability of single-phase natural circulation in simple loops. However, simpler codes for the same purpose can be easily developed, a theoretical formulation for which is given in Appendix-5. The nodalization related problem is found to exist even with such simple codes [17] and the predicted instability threshold was found to be much lower than the experimental values. However, the steady state flow rates could be predicted with reasonable accuracy. Even though the time series of the observed unstable flow regimes could be predicted, the shape of the limit cycles was significantly different. The deviations were attributed to the 3-D effects and the use of fully developed friction factor correlations for the unstable oscillatory flow where the flow is never fully developed.

4.2.2. Two-phase NCSs

Several formulations for the nonlinear stability analysis based on the homogeneous model are reported in the literature. Typical examples are those given by Chatoorgoon (1986) [33] and Chang and Lahey (1997) [34]. Again, codes used for the normal transient thermalhydraulic analysis are applicable for nonlinear stability analysis of two-phase NCSs. Most codes, however, use a point kinetics model which is sufficient for the analysis of in-phase instability but not good enough for the analysis of out-of-phase instability. There are time domain codes like RAMONA-5 with 3-D neutronics, which may be used for the analysis of out-of-phase instability.

5. PARAMETRIC EFFECTS ON THE DWI IN SINGLE-PHASE NCS

DWI is the most commonly observed instability in NCLs. Although there are a large number of identified mechanisms for instability, almost all of them ultimately lead to the occurrence of DWI in a single-phase loop. It may be noted that a generalized nondimensional correlation valid for steady state flow in uniform and nonuniform diameter single-phase natural circulation loops has been presented in Vijayan et al. (2004a) [5] However, even for uniform diameter single-phase loops, there does not exist a universal stability map. Instead it depends on a large number of parameters as listed below.

$$Stability = f(Gr_m, St_m, \frac{L_t}{D}, orientation, length\ scales, flow\ regime\ and\ direction) \quad (14)$$

The orientation includes, horizontal heater and horizontal cooler (HHHC), horizontal heater vertical cooler (HHVC), vertical heater horizontal cooler (VHHC) and vertical heater and vertical cooler (VHVC). The length scales include, L_t/H , L_t/L_h , L_c/L_t , L_h/L_t , L_c/L_t , L_1/L_t , L_2/L_t , L_3/L_t and L_4/L_t . The flow regime includes both laminar and turbulent and flow direction includes both clockwise and anticlockwise. A detailed study of all these parameter is available in Vijayan et al. (2001) [35].

5.1. Effect of orientation of source and sink

It may be noted that different reactor concepts use different orientations of the heat source (i.e. core) and sink (i.e. steam generator). The effect of the orientation of the source and sink is studied in a simple uniform diameter rectangular loop (Fig.5). With clockwise flow, the VHVC orientation is most stable and HHHC orientation is least stable (Fig. 6). For a given heater orientation, the horizontal

cooler orientation is less stable compared to the vertical cooler. Similarly, with fixed cooler orientation, the loop with vertical heater is more stable than that with horizontal heater. All these four orientations were experimented in a uniform diameter rectangular loop (Fig. 5) and instability could be observed only for the HHHC orientation.

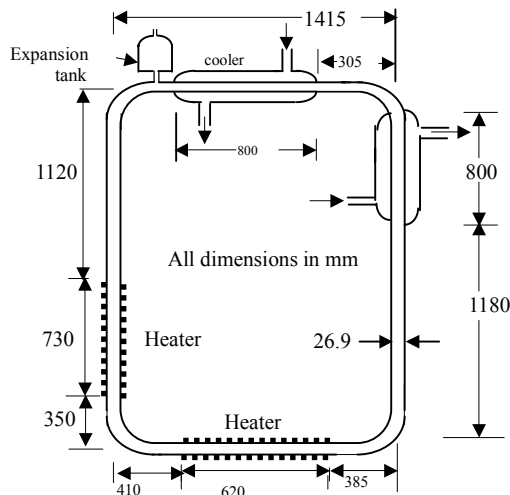


FIG. 5. Schematic of experimental loop.

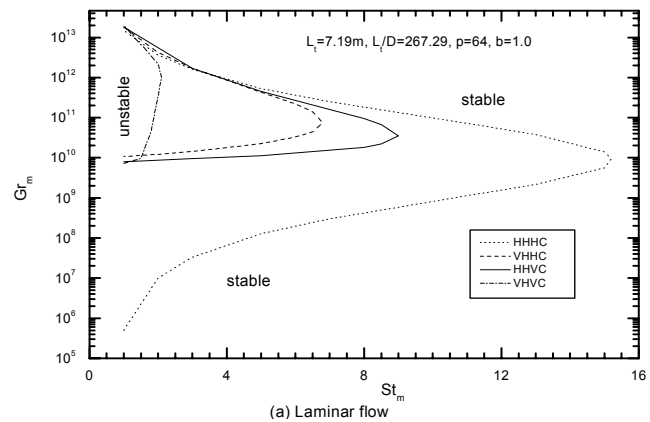
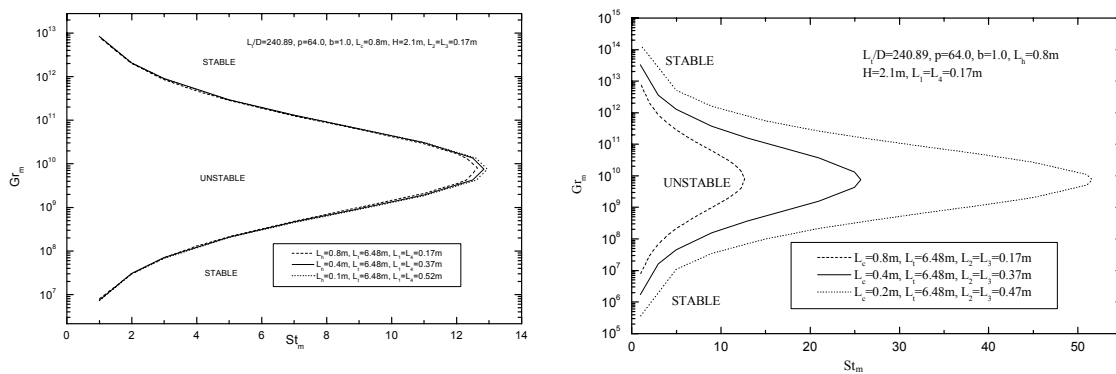


FIG. 6. Effect of heater and cooler orientation on the stability.

5.2. Effect of heater and cooler lengths

These studies were carried out for the HHHC orientation with clockwise flow for the loop in Fig. 5 by changing the heater or cooler lengths keeping the loop height and width the same. The results for varying the heater length alone and cooler length alone are given in figures 7a and b respectively. It is found that reducing the length of heater or cooler has a destabilizing effect. However, the heater length has only a marginal effect on the stability behaviour whereas the cooler length has a significant effect.



(a) Effect of heater length

(b) Effect of cooler length

FIG. 7. Effect of heater and cooler length on stability.

5.3. Effect of L_t/D

It may be noted that L_t/D is the contribution of the loop geometry to the friction number in a uniform diameter loop. Also, most techniques for stabilization results in enhanced L_t/D. A typical example is the introduction of orifices [36]. Increasing L_t/D stabilizes the loop flow [37]. Both the lower and upper thresholds are found to increase with L_t/D (Fig.8). It may be noted that single-phase NC instability has been observed in loops with low L_t/D (<500). Most reactor loops operate with L_t/D in the range of several thousands and that is the main reason why single-phase instability is not observed in reactors.

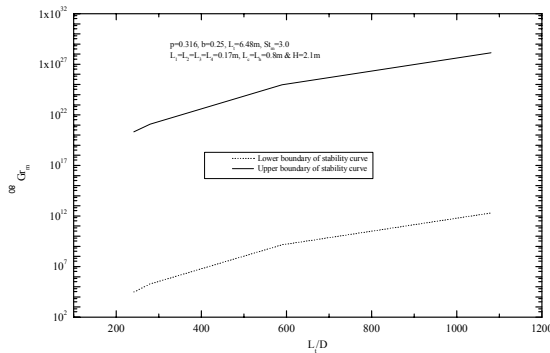


FIG. 8. Effect of L_v/D on the instability.

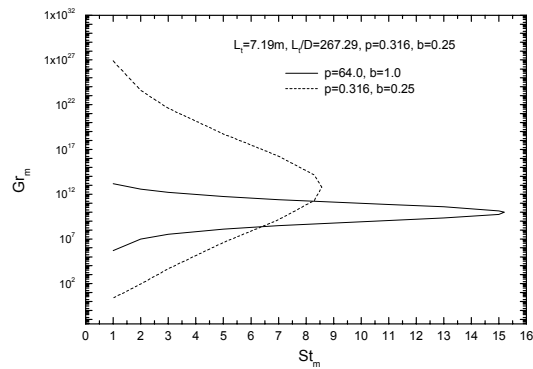


FIG. 9. Effect of flow regime.

5.4. Effect of flow regime

With the flow regime changing from laminar to turbulent, the constants p and b in the equation for friction factor changes and it has a significant influence on the stability behaviour (Fig.9). Good agreement with experimental data can be obtained with empirical friction factor correlation [37] and [38].

5.5. Effect of flow direction

In case of HHVC orientation, it appears possible from the steady state analysis to have flow in the clockwise or anticlockwise direction. However, from the stability analysis, it may turn out that no stable operation is possible with flow in the anticlockwise direction for certain loops. The derivation of the characteristic equation for the stability behaviour can be found in Appendix-3.

6. PARAMETRIC EFFECTS ON THE DWI IN TWO-PHASE NCSs

It may be noted that there does not exist a universal stability map valid for all loops. Under these conditions, it is only possible to examine the parametric effects to obtain general trends of the stability behaviour of NCSs. The parameters affecting two-phase flow instability can be classified into two: operating parameters and design parameters. The operating parameters include the inlet subcooling, pressure, heater power and its distribution. Design parameters include the loop geometry, the working fluid and the flow rate. Knowledge of the parametric dependence is useful in understanding the instability and to develop techniques for avoiding it. The parametric dependences of forced circulation BWRs are well known. In the following, parametric dependence of a pressure tube type reactor is illustrated with results from the AHWR.

6.1. Effect of inlet subcooling and pressure

As the inlet subcooling increases, the lower instability threshold is found to increase where as the upper threshold is found to decrease. The net effect is that the gap between the two thresholds decreases. Thus inlet subcooling has a destabilizing effect. The effect of pressure on the NC density wave instability is significant (see Fig. 10). Increase in system pressure enhances the area of the stable zone considerably. Hence pressure has a stabilizing effect on the two-phase density wave instability.

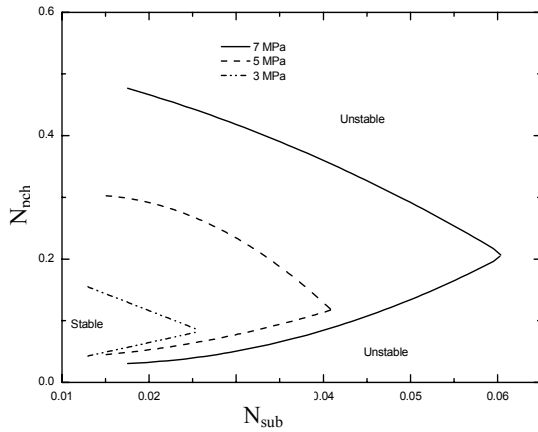


FIG. 10. Effect of pressure on DWI.

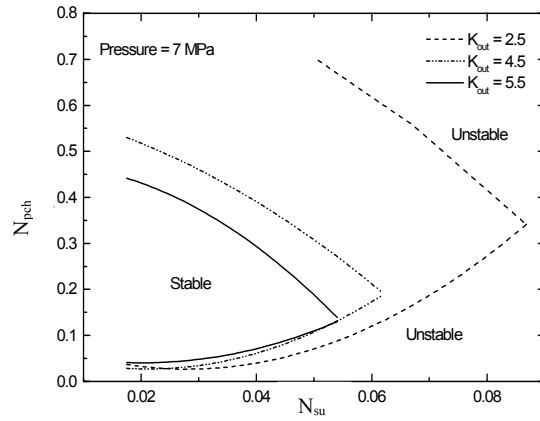


FIG. 11. Effect of outlet orificing on DWI.

6.2. Effect of riser height

It may be mentioned that the riser height has a significant influence on the steady state flow rate. Riser height is found to enhance the steady state flow rate. However, its effect on the stability is rather interesting. It has a stabilizing influence up to a certain value of the riser height. Beyond that it has a destabilizing influence due to its contribution to the two-phase pressure drop.

6.3. Effect of downcomer level

During a small break LOCA as the inventory loss continues the downcomer level decreases with time. Reducing the downcomer level has a significant destabilizing effect as it directly reduces the single-phase pressure drop.

6.4. Effect of outlet orificing

Enhancing the loss coefficients in the two-phase regions has a large destabilizing effect. Even for a pressure tube type reactor this is found to be true (see Fig. 11).

6.5. Effect of parallel channels

With the inclusion of parallel channels in the analysis, both in-phase and out-of-phase oscillation (OPO) modes are possible. The OPO is the unique characteristic of parallel channel instability. However, the effect of number of channels on the threshold of OPO needs to be established first as out-of-phase mode oscillations are possible with any number of parallel channels. Analysis was carried out for 2, 5, 8 and all parallel channels for AHWR by Nayak et al. [39],[2],[15],[40]. The results indicated that a conservative prediction of parallel channel instability could be made with the maximum rated twin channel system (Fig. 12). Hence all subsequent results presented here are for the twin channel system. It may also be noted that this result is of great significance even for experimental validation as all relevant stability data can be generated with a twin channel system.

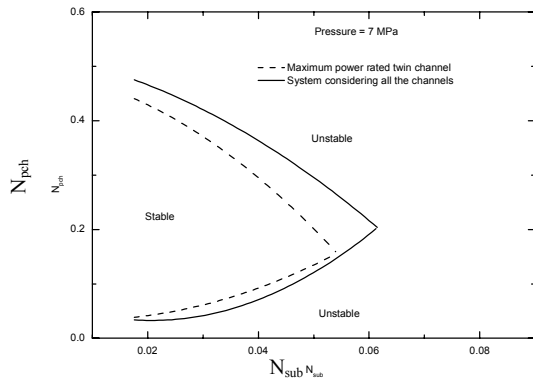


FIG. 12. Effect of number of channels on OPO.

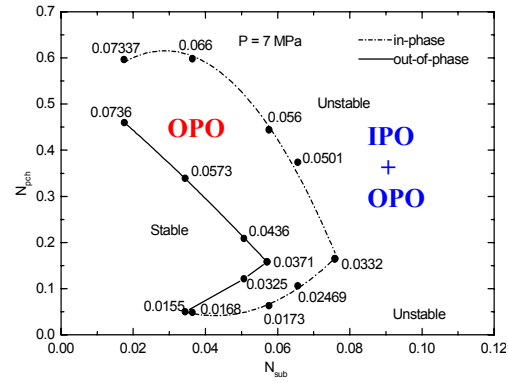


FIG. 13. Comparison of instability thresholds for IPO and OPO.

6.6. Unstable oscillatory regimes with parallel channels

A comparison of the in-phase and out-of-phase instability thresholds are shown in Fig. 13. With this plot, it is easy to identify the zone of OPO and dual oscillations as shown in the figure. In the dual oscillation regime, the natural circulation system is susceptible to both in-phase and out-of-phase oscillations. Van der Hagen et al. (1994) [41] and Pazsit (1995) [42] reported the occurrence of dual oscillations in BWRs. One characteristic feature of dual oscillations is that the decay ratio will show discontinuous behaviour, as both oscillation modes are dormant. Hence in the dual oscillation regime, use of decay ratio as stability margin is not recommended. It is found that the stable zone for the OPO is significantly lower than the stable zone of IPO. It follows that out-of-phase instability will be initiated at a higher power than in-phase instability for the NCRs. In other words, the out-of-phase instability is controlling. It may be recalled here that in forced circulation BWRs (e.g. Lasalle), out-of-phase instability was observed following the loss of all circulating pumps.

6.7. Effect of inlet orificing

Inlet orificing is always found to stabilize forced circulation BWRs. Even in AHWR, if all channels are uniformly orificed, then it is found to increase stability. However, in case of parallel channel systems, uniform orificing is rarely possible. In fact the high power channels are not orificed at all. The effect of increasing the inlet loss coefficient of one channel of a twin channel system is shown in Fig. 14. It is found that increasing the inlet loss coefficient beyond a certain value is destabilizing. This is again characteristic of natural circulation systems, as the driving force is limited.

6.8. Coupled neutronic thermalhydraulic instability

So far we have not considered the effect of neutronics on the stability behaviour. Its effect, however, is important in the design of both forced and natural circulation based BWRs.

6.8.1. Effect of void coefficient

It may be noted that if the void coefficient is zero, then there is no coupling between neutronics and thermalhydraulics and hence the stability map so obtained is identical to the pure thermalhydraulic stability map. Negative void coefficient stabilizes both in-phase and out-of-phase oscillations so that pure thermalhydraulic stability map is found to be conservative for AHWR (Fig. 15). It may be mentioned that the value of void coefficient is significantly higher at low pressures and hence with

neutronics, the influence of pressure on instability is amplified. Since the effect of neutronics on in-phase and out-of-phase instability show the same trend, henceforth we focus our attention to the out-of-phase instability only.

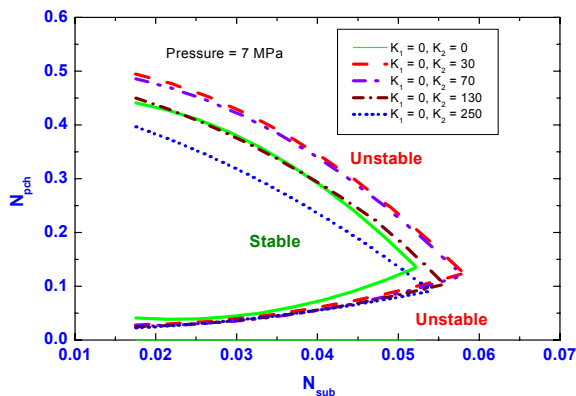


FIG. 14. Effect of inlet orificing on OPO.

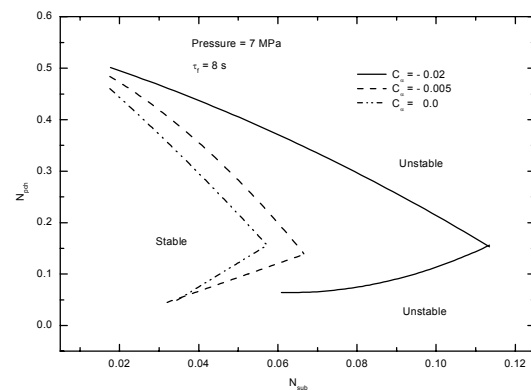


FIG. 15. Effect of void coefficient on OPO.

6.8.2. Effect of fuel time constant

Apart from fuel properties, the burnup also affects the fuel thermal time constant. Larger time constants have a destabilizing effect on the out-of-phase instability. The same trend is observed in forced circulation BWRs.

6.8.3. Effect of coupling coefficient

The above results have been obtained using a point kinetics model. As already explained, the point kinetics model is good enough only for the in-phase instability. During an out-of-phase instability interaction among the parallel channels may affect the stability thresholds. The simplest way to consider its effect is to assume that the core consists of two subcores. The degree of coupling between the subcores is defined in terms of the coupling coefficient. For use in coupled multi-point kinetics, the coupling coefficients are to be evaluated separately using more sophisticated codes. Results indicate that a large value of the coupling coefficient reduces stability.

6.8.4. Comparison of coupled multi-point and modal point kinetics models

The modal point kinetics model can also predict the out-of-phase instability. Based on the methodology of Turso et al. (1997) [43], the subcriticality can be calculated. Corresponding to this subcriticality, the coupling coefficient can be calculated from the theory of Nishina and Tokashiki (1996) [44]. A comparison of the stability maps so predicted by the multipoint and modal point kinetics models is given in Fig. 17.

7. NONLINEAR ANALYSIS

As already pointed out nonlinear or time domain analysis is required for obtaining the nature of the oscillatory behaviour such as the mode, periodicity, direction and amplitude of oscillations. It can also predict the time series and limit cycle of oscillations.

7.1. Single-phase natural circulation

Nonlinear analysis can be carried out with any initial condition. Using the steady state initial condition, the predicted stability map using the nonlinear method was essentially the same as that obtained using the linear stability method.

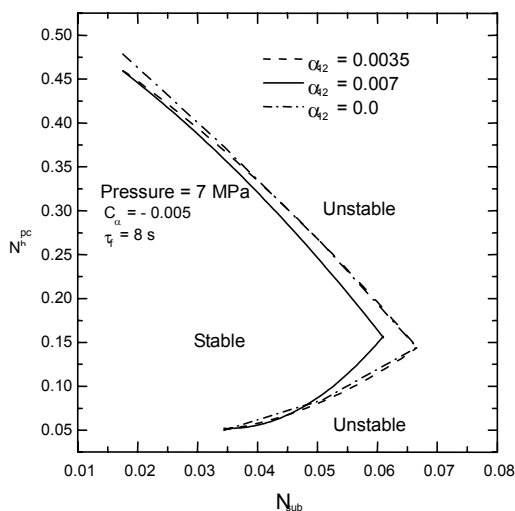


FIG. 16. Effect of coupling coefficient on OPO.

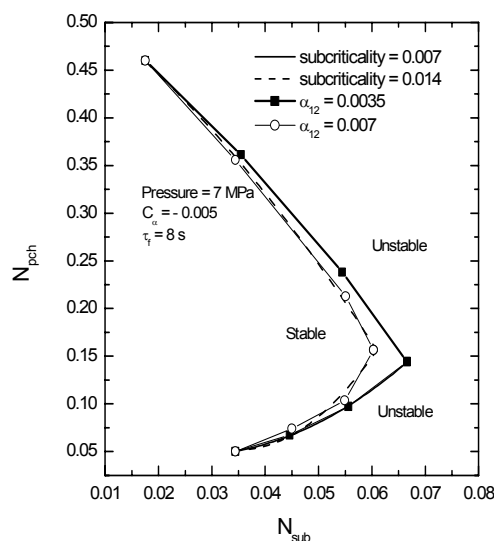


FIG. 17. Comparison of multi-point and modal point kinetics models.

7.1.1. Oscillatory modes

Nonlinear analysis can also be used to investigate the oscillation modes and the limit cycles. Experimentally only three oscillatory modes were observed for rectangular loops. They are periodic unidirectional pulsing, chaotic switching between unidirectional and bi-directional pulsing and periodic bi-directional pulsing. Using the nonlinear code, it was possible to obtain the three different oscillatory modes, albeit at somewhat different conditions [45]. Detailed study of the temperature profile showed that both unidirectional and bi-directional oscillations have 3 dense and light pockets each at any time and they differ only in their relative magnitudes.

In low pressure experimental loops, it is not possible to obtain the full spectrum of the oscillatory modes in the single-phase condition as it leads to boiling with increase in power. With the nonlinear code, however, it is possible to do so and it was found that even the simple rectangular loop exhibits a rich variety of oscillatory modes [45].

7.2. Two-phase flow

Nonlinear codes are extensively used to study the characteristics of in-phase and out-of-phase instability in BWRs [46]. It has also been used to analyze the chaotic behaviour in two-phase natural circulation loops [34], parallel channel behaviour [47]. Dimmick et al. (2002) [48] used the nonlinear code to obtain the stability boundaries of a supercritical reactor. For NC BWRs, due to the possibility of the hysteresis phenomenon, nonlinear analysis codes are used to establish stable operating procedures and start-up procedure. Nonlinear codes are used to study the effect of various initial conditions and operating procedures on the instability. Their use in establishing the start-up procedure of NC based reactors is discussed in the following section.

8. NC BASED PRESSURE TUBE TYPE REACTORS

Although, there are several NC based BWRs being pursued by many countries, most of them are vessel type BWRs. The Advanced Heavy Water Reactor (AHWR) is the only one using the pressure

tube concept. Other pressure tube type BWRs like the Fugen operate in the natural circulation mode only when the pumps fail. From the results of the parametric studies reported earlier, the stability behaviour in a pressure tube type BWR is found to be similar to that of vessel type BWRs. The issues during start-up and power raising are also expected to be similar. However, unlike vessel type BWRs the pressure losses in the inlet and outlet piping can have an influence on the steady state and stability behaviour. Hence size optimization of the inlet and outlet piping is an important design aspect of pressure-tube type reactor. In pressure tube type NC BWRs, the riser height is relatively large leading to much lower frequency of density wave oscillations. The stability issue significantly influences the start-up procedure for NC based BWRs. Detailed investigations were carried out for both the start-up and the power raising procedures for AHWR.

8.1. Design procedure

One of the considerations in a pressure tube type reactor at the design stage is the sizing of the inlet and outlet pipes. Larger pipe sizes decrease the frictional resistance and hence increase the flow rate. On the other hand large pipe sizes increases the capital cost. Often, pipe size has opposing influences on the CHF and stability of the system. For example, reducing the inlet pipe size can enhance stability but reduces the flow rate and hence increases the exit quality leading to a reduction in the CHF. An optimization of pipe sizes is therefore required for natural circulation systems.

8.2. The issues in start-up and power raising

The basic issues in the start-up of a natural circulation based BWR is the avoidance of flow reversal and overcoming the lower threshold of the density wave instability. Experience with natural circulation boilers suggests that flow reversal is a problem in case of hot start-up [3]. The problem with the down flowing heated channels is that they supply steam to the inlet header and the downcomer, which has a destabilizing effect on natural circulation. The studies by Chato (1963) [49] and Linzer and Walter [3] shows that flow reversal is expected to occur at very low powers. Above a critical power ratio the flow reversal phenomenon is not expected. This critical power ratio can be readily calculated using the maximum and minimum rated channels. The problems associated with flow reversal can be avoided by ensuring that boiling is initiated only above this power. Under single-phase conditions, even if flow reversal occurs, it is not expected to affect the subsequent two-phase NC process significantly.

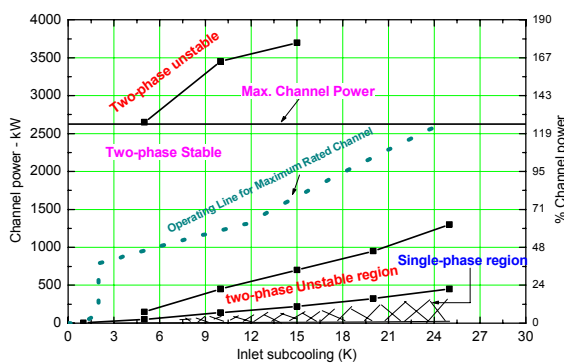


FIG. 18. Stability map for OPO in AHWR.

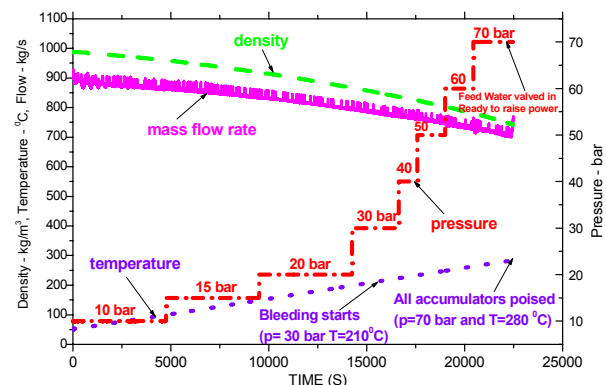


FIG. 19. Heat up procedure with stage-wise pressurization.

The lower threshold of stability occurs at relatively high power at the inlet subcooling corresponding to the full power condition. It happens at around 60 to 70 % FP in the currently operating BWRs if the flow comes down to about 40%. In AHWR, if the subcooling remains same as at full power condition, then the corresponding stability threshold is approximately 50% FP (Fig. 18). As the reactor is to be started up from cold condition (very high subcooling), the lower threshold has to be overcome without initiating instability. Fig. 18 shows that the lower threshold decreases with reduction in subcooling and below about 5°C the lower threshold occurs at very low power. Also, the lower threshold of instability does not exist for very low subcooling at the full pressure. Hence, there are several options for the start-up. Two options being pursued for AHWR are

a) Stage-wise pressurization using an external boiler and heat up with low reactor power. In this scheme, boiling is initiated at the full pressure and a very low subcooling at which the instability is not observed. Fig. 19 shows a simulation calculation for this scheme.

b) It is well known that the lower threshold is due to boiling inception and this instability disappears at relatively moderate pressures. Hence a start-up scheme involving a one-time pressurization to a moderate pressure followed by heat up with fission heat at low power is being investigated. Here boiling is initiated at the moderate pressure. Typical simulation of this procedure is shown in Fig. 20 at two different pressures. As expected at the higher power, the amplitude of oscillations observed at boiling inception is significantly low.

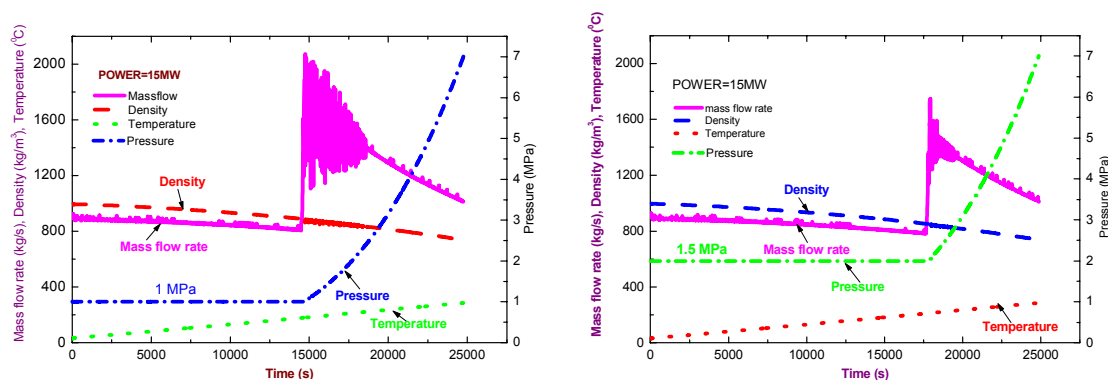


FIG. 20. Heat up procedure with one time pressurization.

8.3. Power raising procedure

It may be noted that the stability maps were generated with the linear stability method by assuming infinitesimal disturbances to the steady state condition. However, during actual operation of a NC reactor, the power raising is in finite small steps. Experimental evidence in natural circulation loops suggests that there is a hysteresis region where the stability threshold depends on the operating procedure. Hence the proposed procedure for power raising and setback needs to be validated experimentally. A simulation calculation for a typical power raising procedure where power is raised at the rate of 0.5% per second is given in Fig. 21. This shows that the standard power raising procedure followed in forced circulation BWRs can be adopted without causing instability. In addition simulation calculations are required to ensure that the adopted procedures for power step back, setback, etc. does not cause entry into the unstable zone.

8.4. Instability monitoring

In spite of specifying a start-up and operating procedure, it is possible to land in the unstable zone due to a malfunction or failure of equipments such as failure of feed water heaters or control rod drives. In such cases, incorporation of auto-detect and suppress systems can help in instability control. Generally such systems rely on the decay ratio calculated on the basis of the noise analysis of measured neutron flux signals. There are recent reports, questioning the adequacy of the decay ratio in BWR stability monitoring [50] especially in case dual oscillations.

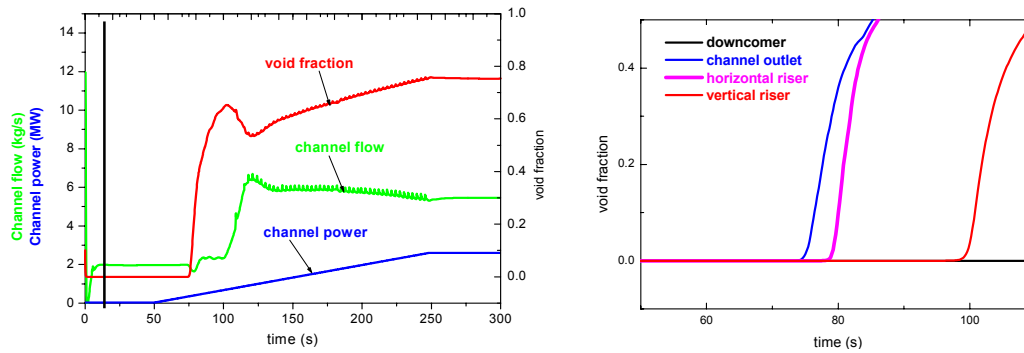


FIG.21. Simulation of power raising procedure from hot shutdown condition.

8.5. Closure

In most cases, the parametric effects are found to exhibit the same trend as in a forced circulation BWR. Differences exist in inlet orificing due to the low value of driving force. Since decay ratio is not an established indicator of stability margin especially during the dual oscillations, the operating and start-up procedures are to be extensively investigated to ensure adequate stability. The stability analysis carried out for AHWR has shown that the reactor power is not limited by stability just as in forced circulation boilers. Therefore, avoiding the stability only restricts the start-up procedure to some extent.

9. STABILITY CONSIDERATIONS IN NC BASED SGS

Steam generator is an important component of all PWRs, PHWRs and VVERs. Most PWRs and PHWRs use vertical natural circulation U-tube steam generators whereas VVERs use horizontal steam generators. Fig. 22 shows the schematic of a vertical natural circulation U-tube steam generator. It consists of a feed water system, downcomer section, heat exchange section, top plenum with separator assembly, dryer and a steam removal system. The feed water system essentially consists of a feed water nozzle and a ring header with J-tubes (not shown in Fig. 22). The subcooled feed water from the j-tubes mixes with the saturated water from the separator and flows down through the downcomer section. The heat exchange section is the tube bundle portion where the heat from the primary fluid is transferred across the tube wall to the secondary fluid causing steam generation. The steam-water separation takes place in the centrifugal separators and the separated water flows back to the downcomer whereas the steam goes through the dryer unit and exits from the SG dome. The NC flow on the secondary side takes place due to the density difference in the downcomer region and the heat exchange section. Generally, the recirculation ratio (downcomer flow/feed flow) is typically in the range of 3 to 5 at full power condition.

SGs are subject to static instability of the Ledinegg type and density wave dynamic instabilities. The stability behaviour of NC based SGs used in PWRs is rather well understood. Generally, the existing SG designs show instability only at significantly high power (> 1.5 times the nominal full power). Most of the recent studies pertain to liquid sodium cooled steam generators used in LMFBRs [51], Unal et al. (1977) [52]. Most of these SGs, however, are the forced circulation type. Often the SGs used in LMFBRs are stabilized by orificing at the inlet of the tubes at the expense of enhanced pumping power. Most SGs use very long U-tubes (typically 15 to 30 m) leading to very large transit times and hence very low frequency of oscillations. Analysis of SG instability is complicated because of the coupling with the primary fluid dynamics. Both linear (STEAMFREQ-X by Chan and Yadigaroglu (1986) [53]) and nonlinear codes [54] for stability analysis of steam generators are reported in literature. Again, nonlinear analysis can be carried out with system codes and codes developed for normal transient analysis of SGs. A computer code for normal transient analysis of NC based SGs is described by Hoeld (1978) [55].

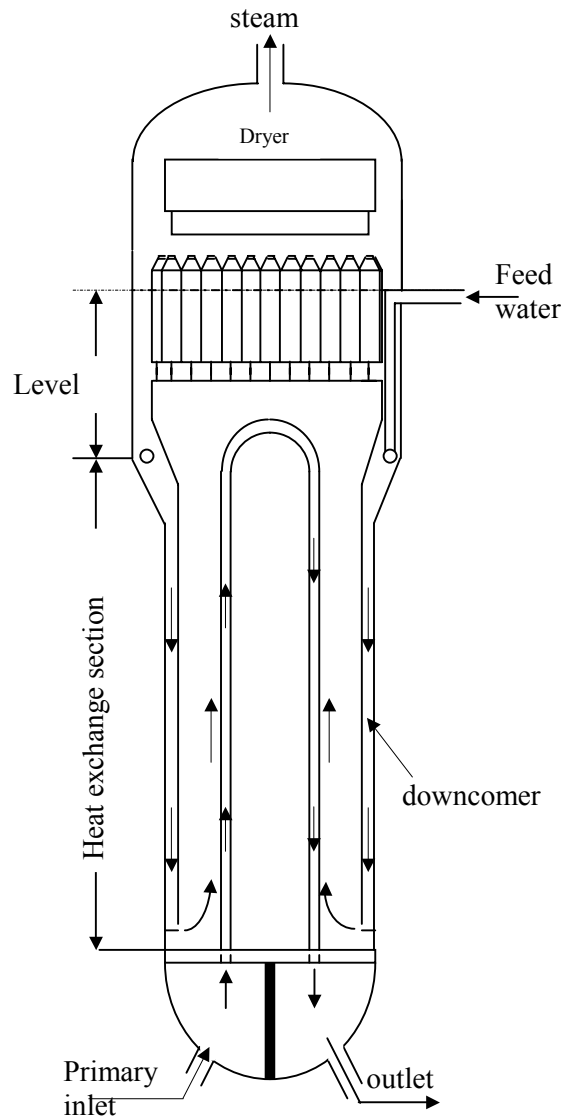


FIG. 22. NC based nuclear steam generator.

10. CLOSING REMARKS ON THE DESIGN PROCEDURE OF NC BWRs

Stability design of NC BWRs, where several different instability mechanisms can be simultaneously acting is somewhat involved and is not well documented. The same is the case with any two-phase NC loop with several parallel channels. Strictly speaking, natural circulation systems shall be analyzed for all known instabilities. However, well-established analysis procedures do not exist for all instabilities. Ledinegg instability, flashing instability and geysering are observed only at low pressures. Pressure drop oscillations may not be important for systems without compressible volumes at the inlet. Thermal oscillations are associated with systems after dryout which can be avoided by established design procedures. Both density wave and acoustic instabilities can occur at high pressures. But density wave instability is more common. Even so, DWI can be whole loop (system instability or in-phase instability) or parallel channel instability (out-of-phase instability) and both can be neutronically coupled. For design, the first issue is which of them is controlling (i.e. having the highest threshold)? Probing calculations may be necessary to identify this. For NC BWRs, the out-of-phase oscillations can be the controlling mode as was observed in AHWR. For AHWR, a conservative stability map could be generated with the maximum rated twin channel system. The effect of a negative void coefficient was to stabilize the pure thermalhydraulic instability. Usually, DWI has a

lower and an upper threshold of instability. For AHWR, the upper threshold is higher than the CHF threshold and is not expected to occur as CHF limits the power. The lower threshold can be encountered during start-up and power raising. To avoid this, a start-up procedure needs to be specified for avoiding the unstable zone. The start-up procedure also ensures that the boiling is initiated at powers above the flow reversal threshold. In spite of this, NC BWRs can land up in an unstable zone during an unanticipated operational transient. In such cases, incorporation of an auto-detect and suppress mechanism will be useful.

NOMENCLATURE

A - flow area, m^2
 a_i - dimensionless flow area, A_i/A_r
 b - constant in friction factor equation
 C_D - Doppler coefficient ($\Delta k/k/\Delta T$)
 $C_m(t)$ - delayed neutron precursor concentration of group m
 C_p - specific heat, J/kgK
 C_α - void reactivity coefficient ($\Delta k/k/\Delta \gamma$)
 D - hydraulic diameter, m
 d_i - dimensionless hydraulic diameter, D_i/D_r
 f - Darcy-Weisbach friction coefficient
 g - gravitational acceleration, m/s^2
 Gr_m - modified Grashof number, $D^3 \rho^2 \beta g \Delta T_r / \mu^2$
 h - enthalpy J/kg
 h_{fg} - latent heat of vaporization, J/kg
 H_f - heat transfer coefficient, W/m^2K
 H - loop height, m
 $k(t)$ - effective multiplication factor
 K - local pressure loss coefficient
 k - thermal conductivity, W/mK
 l - prompt neutron life time (s)
 l_i - dimensionless length, L_i/L_t
 L - length, m
 m_f - mass of fuel rods, kg
 $n(t)$ - neutron density
 N - total number of pipe segments
 N_f - Froude number, $gLA\rho_f^2 / W^2$
 N_{fr} - friction number, $fL/2D$
 N_p - phase change number, $Q_h \rho_f / (Wh_{fg} \rho_g)$
 N_{pch} - phase change number (Q_h / Wh_{fg})
 N_{sub} - subcooling number ($\Delta h_{sub} / h_{fg}$)
 N_s - subcooling number, $\Delta h_i \rho_f / h_{fg} \rho_g$
 Nu_m - modified Nusselt number, $U_i L_t / k$
 N_G - geometric contribution to the friction number
 p - pressure, N/m^2
 Pr - Prandtl number, $C_p \mu / k$
 p - constant in friction factor equation
 Q - total heat input rate, W
 q_h - volumetric heat generation, W/m^3
 Re - Reynolds number, $DW/A\mu$
 S - stability parameter
 S - dimensionless co-ordinate around the loop, s/H
 s - co-ordinate around the loop, m
 St_m - modified Stanton number, $4Nu_m / Re_{ss} Pr$
 t - time, s
 T - temperature, K

ΔT_r - reference temperature difference ($Q_h H / A \mu C_p$), K
 v - specific volume, m^3/kg
 $v_{fg} = v_g - v_f$, m^3/kg
 W - mass flow rate, kg/s
 Δz - centre line elevation difference between cooler and heater, m

Greek Symbols

α - coupling coefficient
 β - thermal expansion coefficient, K^{-1} and delayed neutron fraction
 γ - void fraction
 θ - dimensionless temperature
 λ - decay constant of delayed neutron group m
 μ - dynamic viscosity, Ns/m^2
 ρ_0 - reference density, kg/m^3
 σ - thermal expansion coefficient, K^{-1}
 τ - nondimensional time, and residence time, s
 τ_f - fuel time constant (s)
 ϕ - dimensionless circulation length, L_t/H
 ϕ_{LO}^2 - two-phase friction multiplier
 ω - dimensionless mass flow rate

Subscripts

av - average
 c - cooler, core
 ch - channel
 cl - cold leg
 d - downcomer
 e - equivalent
 eff - effective
 f - saturated liquid
 g - saturated vapour
 h - heater
 H - header
 hl - hot leg
 i - i^{th} segment
 in - inlet
 o - outlet
 r - reference value
 sat - saturation
 SD - steam drum
 sp - single-phase
 ss - steady state
 ss,av - average steady state
 sub - subcooling
 t - total
 tp - two-phase

Superscripts

$'$ - perturbed
 $-$ - average

REFERENCES

- [1] BAROCZY, C.J., A systematic correlation for two-phase flow pressure drop, *Chem. Eng. Progr. Symp. Ser.* 62, pp.232–249 (1966).
- [2] NAYAK, A.K., VIJAYAN, P.K., SAHA, D., VENKAT RAJ, V. and ARITOMI, M., Analytical study of nuclear-coupled density-wave instability in a natural circulation pressure tube type Boiling Water Reactor, *Nuclear Engineering and Design* 195, pp.27–44 (2000a).
- [3] LINZER, W. and WALTER, H., Flow reversal in natural circulation systems, *Applied Thermal Engineering*, 23, pp.2363–2372 (2003).
- [4] ROHATGI, U.S. and DUFFEY, R.B., Stability, DNB, and CHF in natural circulation two-phase flow, *Int. Comm. Heat Mass Transfer*, 25, pp.161–174 (1998).
- [5] VIJAYAN, P.K., BADE M.H, SAHA D., SINHA, R.K., and VENKAT RAJ, V., A generalized flow correlation for single-phase natural circulation loops, Proceedings of 6th ISHMT-ASME Heat and Mass Transfer Conference, Kalpakkam, Jan. 5–7, HMT-2004-C022 (2004a).
- [6] VIJAYAN, P.K., Experimental observations on the general trends of the steady state and stability behaviour of single-phase natural circulation loops, *Nuclear Engineering and Design* 215, pp.139–152 (2002).
- [7] ZHOU, J. and PODOWSKI, M.Z., Modeling and analysis of hydrodynamic instabilities in two-phase flow using two-fluid model, *Nuclear Engineering and Design* 204, pp.129–142 (2001).
- [8] SONG, J.H, and ISHII, M., On the stability of a one-dimensional two-fluid model, *Nuclear Engineering and Design*, 204, pp.101–115 (2001).
- [9] PENG, S.J., PODOWSKI, M.Z., and LAHEY, JR., R.T., NUFREQ-NP: A digital computer code for the linear stability analysis of boiling water nuclear reactors, NUREG/CR-4116 (1985).
- [10] OTAUDY, P. and MARCH-LEUBA, J., LAPUR User's Guide, NUREG/CR-5421 (1989).
- [11] ZERREBEN, K.W., KREUTER, D., Post-calculation of core instabilities measured in the German BWRs KRB-B/C Using the frequency domain code STAIF, International workshop on abnormal transients in nuclear *power plants*, Atlanta (1987).
- [12] CHAN, K.C., FABLE02V User's Manual, NEDE-31732P (1989).
- [13] D'AURIA, F. et al., State of the art report on boiling water reactor stability, OCDE/GD(97)13, OECD-NEA (1997).
- [14] HÄNGGI, PH., SMED, TH., LANSÄKER, P., MATSTAB, A fast frequency domain based code to predict boiling water reactor stability using a detailed three dimensional model, NURETH-9, San Francisco (1999).
- [15] NAYAK, A.K, VIJAYAN P.K., and SAHA, D., Analytical modelling and study of the stability characteristics of the advanced heavy water reactor, BARC/2000/E/011 (2000b).
- [16] CHEN, W.L., WANG, S.B., TWU, S.S., CHUNG, C.R. and CHIN PAN, Hysteresis effect in a double channel natural circulation loop, *International Journal of Multiphase Flow*, 27, pp.171–187 (2001).
- [17] VIJAYAN, P.K., MANISH SHARMA, PILKHWAL, D.S., SAHA, D., SINHA, R.K., BHOJWANI, V.K. and SANE, N. K., Experimental and numerical investigations on the nature of the unstable oscillatory flow in a single-phase natural circulation loop, Proceedings of 6th ISHMT-ASME Heat and Mass Transfer Conference, Kalpakkam, Jan. 5–7, 2004b, HMT-2004-C100 (2004b).
- [18] ACHARD, J.-L., DREW, D.A., LAHER JR, R.T., The analysis of nonlinear density wave oscillations in boiling channels, *Journal of Fluid Mechanics* 155, pp.213–232 (1985).
- [19] VIJAYAN, P.K., AUSTREGESILO, H. and TESCHENDORFF, V., Simulation of the unstable oscillatory behaviour of single-phase natural circulation with repetitive flow reversals in a rectangular loop using the computer code ATHLET, *Nuclear Engineering Design* 155, pp.623–641 (1995).
- [20] AMBROSINI, W. and FERRERI, J.C., The effect of truncation error on the numerical prediction of linear stability boundaries in a natural circulation single-phase loop, *Nuclear Engineering and Design* 181, pp.53–76 (1998).
- [21] MISALE, M., FROGHERI, M., D'AURIA, F., FONTANI, E. and GARCIA, A., Analysis of single-phase natural circulation experiments, *International Journal of Thermal Sciences*, 38, pp.977–983 (1999).

- [22] MANISH SHARMA, PILKHWAL, D.S., VIJAYAN, P.K., SAHA, D., and SINHA, R.K., Single-phase instability behaviour in a rectangular natural circulation loop using RELAP5/MOD3.2 computer code, BARC/2002/E/012 (2002a).
- [23] MANISH SHARMA, PILKHWAL, D.S., VIJAYAN, P.K., SAHA, D., and SINHA, R.K., Simulation of single-phase instability behaviour in a rectangular natural circulation loop, HMT-2004-C028, *Proceedings of 6th ISHMT-ASME Heat and Mass Transfer Conference*, Kalpakkam, India, Jan. 5–7 (2004).
- [24] FLETCHER, C.D. and SCHULTZ R.R., RELAP5/MOD3 Code Manual, NUREG/CR-5535, INEL, Idaho Falls, Idaho (1995).
- [25] RELAP5 development team, RELAP5/MOD3.2 Code Manual, Volume I: Code structure, system models, and solution methods, NUREG/CR-5535 or INEL-95/0174, Idaho National Engineering Laboratory, Lockheed Idaho Technologies Company, Idaho Falls, Idaho 83415 (1995).
- [26] PAULSEN, M.P., MCFADDEN, J.H., PETERSON, C.E., MCLURE, J.A., GOSE, G.C. and JENSEN, P.J., The RETRAN-03 Computer Code, *Nuclear Technology*, 95, pp.105–115 (1991).
- [27] TAKEUCHI, Y., UEMATSU, H., EBATA, S., SHAUG, J.C., SHIRALKAR, B.S., TRACG Transient Analysis Code, Three Dimensional Kinetics Model Implementation and Applicability or Space Dependent analysis, *Nucl. Technol.* 105 (1994).
- [28] LERCHL, G. and AUSTREGESILO, H., ATHLET Mod 1.2 Cycle C: User's Manual, Gesellschaft für Anlagen und Reaktorsicherheit (GRS) mbH, Nov. 2000.
- [29] BARRE, F., DOR, I., and BRUN, B., Advanced numerical methods for thermalhydraulics, *Nuclear Engineering Design*, 145, pp.147–158 (1993).
- [30] HANNA, B.N., CATHENA: A thermalhydraulic code for CANDU analysis, *Nuclear Engineering Design*, 180, pp.113-131 (1998).
- [31] WELANDER, P., On the oscillatory instability of a differentially heated loop, *J. Fluid Mech.* 29, pp.17–30 (1967).
- [32] FERRERI J.C., AMBROSINI, W., On the analysis of thermal-fluid-dynamic instabilities via numerical discretization of conservation equations, *Nuclear Engineering and Design*, 215, pp.153–170 (2002).
- [33] CHATOORGOON, V., SPORTS – a simple nonlinear thermal-hydraulic stability code, *Nuclear Engineering Design*, 93, pp.51–67 (1986).
- [34] CHANG CHIN-JANG and LAHEY JR. R.T., Analysis of chaotic instabilities in boiling systems, *Nuclear Engineering and Design* 167, pp.307–334 (1997).
- [35] VIJAYAN, P.K., BHOJWANI, V.K., BADE, M.H., SHARMA, M., NAYAK, A.K., SAHA, D. and SINHA, R.K., Investigations on the effect of heater and cooler orientation on the steady state, transient and stability behaviour of single-phase natural circulation in a rectangular loop, BARC/2001/E/034 (2001).
- [36] MISALE, M. and FROGHERI, M., Influence of pressure drops on the behaviour of a single-phase natural circulation loop: Preliminary results, *Int. Comm. Heat Mass Transfer* 26, pp.597–606 (1999).
- [37] VIJAYAN P.K. and AUSTREGESILO, H., Scaling laws for single-phase natural circulation loops, *Nuclear Engineering Design*, 152, pp.331-334 (1994).
- [38] VIJAYAN, P.K., VENKAT RAJ, V., NAGDAUNE, R.K and PILKHWAL, D.S., Thermosyphon tests and comparison with code predictions for a PHWR, *3rd International Seminar on small and medium sized reactors*, New Delhi, August 26–28 (1991).
- [39] NAYAK, A.K., VIJAYAN, P.K., SAHA, D., VENKAT RAJ, V. and ARITOMI, M., Linear analysis of thermo-hydraulic instabilities of the Advanced Heavy Water Reactor (AHWR), *Journal of Nuclear Science and Technology*, 35, pp.768–778 (1998).
- [40] NAYAK, A.K., VIJAYAN, P.K., SAHA, D., VENKAT RAJ, V. and ARITOMI, M., Study on the stability behaviour of a natural circulation pressure tube type boiling water reactor, *Nuclear Engineering and Design* 215, pp.127-137 (2002).
- [41] VAN DER HAGEN T.H.J.J., PAZSIT, I., THOMSON, O. and MELKERSON, B., *Nuclear Technology*, 107, pp.193–217 (1994).
- [42] PAZSIT, I., Determination of reactor stability in case of dual oscillations, *Ann. Nucl. Energy*, 22, pp.377–387 (1995).

- [43] TURSO, J.A., MARCH-LEUBA, J., EDWARDS, R.M., A modal reduced order model of BWR out-of-phase instabilities, *Ann. Nucl. Energy*, 24, pp.921–934 (1997).
- [44] NISHINA, K. and TOKASHIKI, M., Verification of more general correspondence between the eigenvalue separation and coupling coefficient, *Ann. Nucl. Energy*, 30, pp.277–286 (1996).
- [45] MANISH SHARMA, VIJAYAN, P.K., NAYAK, A.K., SAHA, D. and SINHA, R.K., Numerical study of stability behaviour of single-phase natural circulation in a rectangular loop, *Proceedings of 5th ISHMT-ASME Heat and Mass Transfer Conference*, Kolkata, India Jan. 3-5, pp. 1204–1210 (2002b).
- [46] MAQUA, M., KOTTHOFF, K. and POINTNER, W., Neutron flux oscillations at German PWRs, GRS Technical Report.
- [47] ARITOMI, M., AOKI, S. and INOUE, A., Thermo-hydraulic instabilities in parallel boiling channel systems Part 1. A non-linear and a linear analytical model, *Nuclear Engineering and Design* 95, pp.105–116 (1986).
- [48] DIMMICK, G.R., CHATOORGOON, V., KHARTABIL, H.F. and DUFFEY, R.B., Natural convection studies for advanced CANDU reactor concepts, *Nuclear Engineering and Design* 215, pp.27–38 (2002).
- [49] CHATO, J.C., Natural convection flows in a parallel channel system, *J. Heat Transfer* 85, pp.339–345 (1963).
- [50] VAN DER HAGEN, T.H.J.J., ZBORAY, R. and DE KRUIJF, W.J.M., Questioning the use of decay ratio in BWR stability monitoring, *Annals of Nuclear Energy* 27, pp.727–732 (2000).
- [51] LORENZINI, E., SPIGA, M., IADAROLA, G. and D'AURIA, F., Density wave instabilities in steam generators, *Annals of Nuclear Energy*, 18, pp.31–42 (1991).
- [52] ÜNAL, H.C., VAN GASSELT, M.L.G. and LUDWIG, P.W.P.H., Dynamic instabilities in tubes of a large capacity, straight-tube, once-through sodium heated steam generator, *International Journal of Heat and Mass Transfer*, 20, pp.1389–1399 (1977).
- [53] CHAN, K.C. and YADIGAROGLU, G., Analysis of density wave instability in counterflow steam generators using STEAMFREQ-X, *Nuclear Engineering and Design* 93, pp.15–24 (1986).
- [54] LECOQ, G., METAICH, M. and SLASSI-SENNOU, A simple model for the study of dynamic instabilities in steam generators, *Nuclear Engineering and Design*, 122, pp.41–52 (1990).
- [55] HOELD, A., A theoretical model for the calculation of large transients in nuclear natural circulation U-tube steam generators (Digital code UTSG), *Nuclear Engineering and Design* 47, pp.1–23 (1978).

APPENDIX 1. Brief description of AHWR

The Advanced Heavy Water Reactor being designed by India is a vertical pressure tube type heavy water moderated light water cooled BWR. It uses dual MOX fuel consisting of plutonium, thorium and U-233. Fig.A-1.1 shows a schematic of the AHWR primary circuit. Two-phase circulation is chosen as the mode of primary coolant circulation. To achieve the desired circulation rate, the steam drum is elevated. Total height of the loop is typically 40 m. The main components of the loop are the steam drum and the core. There are four steam drums (3.75 m inside diameter) connected to a common inlet header (600 mm NB) through 16 downcomers (300 mm NB and four from each steam drum). From the header 452 inlet feeders (100 mm NB) connect to an equal number of pressure tubes and joins the steam drum through an equal number of tail pipes (125 mm NB). The pressure tube inside diameter is 120 mm and it houses a 54-rod bundle with an active core height of 3.5 m. Under normal operation a level is maintained in the steam drum. The steam pressure is maintained at 7 MPa.

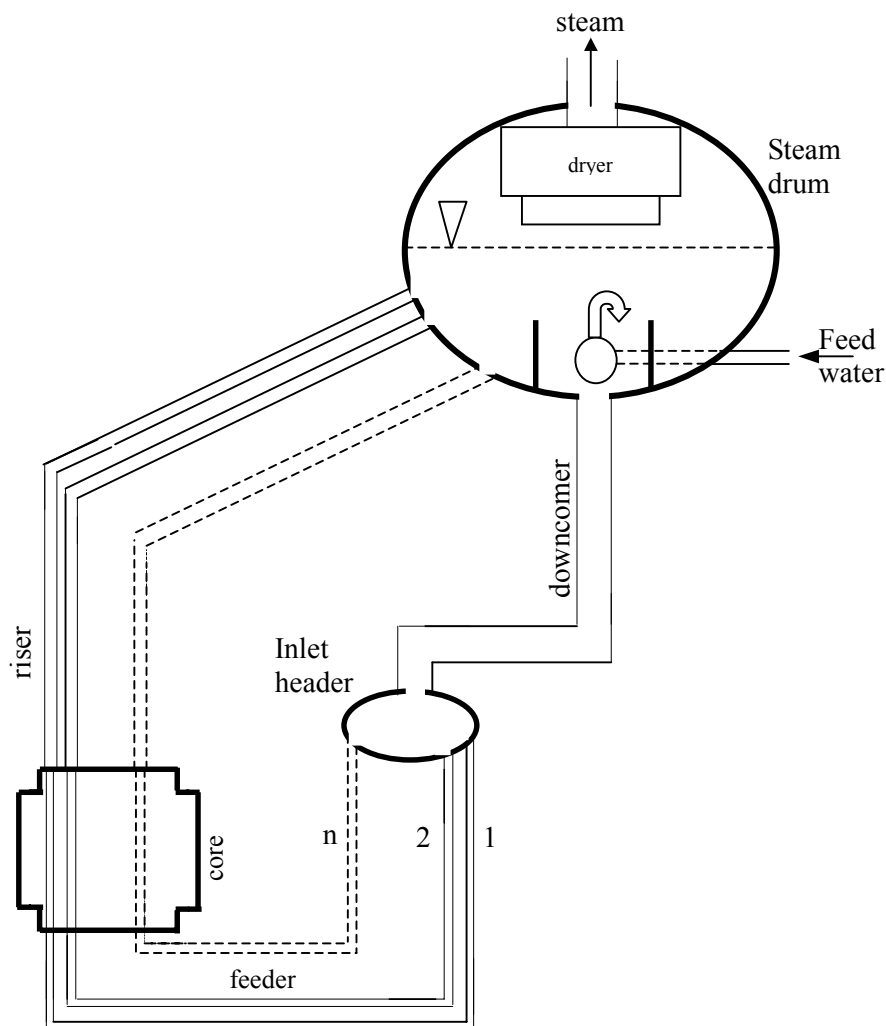


FIG. A-1.1: Schematic of AHWR system.

APPENDIX 2. STEADY STATE FLOW FOR SINGLE-PHASE NC

The governing equations in terms of the mass flow rate and cross-sectional average temperature for 1-dimensional incompressible single-phase natural circulation flow in a closed loop such as Fig. 4, can be written as

$$\frac{\partial W}{\partial s} = 0 \quad (\text{A-2.1})$$

$$\frac{L_t}{A} \frac{dW}{dt} = g \oint \rho dz - \frac{f(L_{\text{eff}})_t W^2}{2D\rho_0 A^2} \quad (\text{A-2.2})$$

where $(L_{\text{eff}})_t$ is the effective length taking into account the local losses. If the local losses are negligible, then $(L_{\text{eff}})_t$ is the loop circulation length, L

$$\frac{\partial T}{\partial t} + \frac{W}{A\rho_0} \frac{\partial T}{\partial s} = \left\{ \begin{array}{l} \frac{4q}{D\rho_0 C_p} \text{ heater (for } 0 < s \leq s_h) \\ 0 \text{ pipes (for } s_h < s \leq s_{hl} \text{ and } s_c < s \leq L_t) \\ -\frac{4U}{D\rho_0 C_p} (T - T_s) \text{ cooler (for } s_{hl} < s \leq s_c) \end{array} \right\} \quad (\text{A-2.3})$$

The energy equation neglects the effect of axial conduction and viscous dissipation. The above equations are nondimensionalized with the following substitutions:

$$\omega = \frac{W}{W_{ss}}; \theta = \frac{T - T_s}{(\Delta T_h)_{ss}}; \tau = \frac{t}{t_r}; S = \frac{s}{H} \text{ and } Z = \frac{z}{H} \quad (\text{A-2.4})$$

Where $t_r = V_t \rho_0 / W_{ss}$. Utilizing the Boussinesq approximation and nondimensionalizing the momentum and energy equations assuming negligible local pressure losses, we get

$$\frac{d\omega}{d\tau} = \frac{Gr_m}{\text{Re}_{ss}^3} \oint \theta dZ - \frac{pL_t \omega^{2-b}}{2D \text{Re}_{ss}^b} \quad (\text{A-2.5})$$

$$\frac{\partial \theta}{\partial \tau} + \phi \omega \frac{\partial \theta}{\partial S} = \left\{ \begin{array}{l} \frac{L_t}{L_h} \text{ for } 0 < S \leq S_h \text{ heater} \\ 0 \text{ for } S_h < S \leq S_{hl} \text{ and } S_c < S \leq S_t \text{ pipes} \\ -St_m \theta \text{ for } S_{hl} < S \leq S_c \text{ cooler} \end{array} \right\} \quad (\text{A-2.6})$$

Where ϕ is a non-dimensional parameter given by $\phi = L_t / H$. The steady state solution for the momentum and energy equations can be obtained by setting $\omega_{ss} = 1$ and $\partial \omega / \partial \tau = \partial \theta / \partial \tau = 0$. The solution of the energy equation for the various segments of the loop can be written as

$$\theta = \theta_{cl} + \frac{H}{L_h} S \quad \text{heater}(0 < S \leq S_h) \quad (\text{A-2.7a})$$

Where the boundary condition that at $S=0$, $\theta = \theta_{cl}$ has been used. Similarly for the hot leg (by setting $S=S_h$ in the above equation) we get

$$\theta = \theta_{cl} + 1 = \theta_{hl} \quad \text{hot leg } (S_h < S \leq S_{hl}) \quad (\text{A-2.7b})$$

For the cooler we get

$$\theta = \theta_{hl} e^{\frac{St_m(S_{hl}-S)}{\phi}} \quad \text{cooler } (S_{hl} < S \leq S_c) \quad (\text{A-2.7c})$$

Where the boundary condition that at $S=S_{hl}$, $\theta = \theta_{hl}$ has been used. For the cold leg using the boundary condition that at $S=S_c$, $\theta = \theta_{cl}$ we get

$$\theta = \theta_{hl} e^{\frac{-St_m L_c}{L_t}} = \theta_{cl} \quad \text{cold leg } (S_c < S \leq S_t) \quad (\text{A-2.7d})$$

From the above equations explicit expressions for the cold leg and hot leg temperatures can be obtained as

$$\theta_{cl} = \frac{1}{e^{\frac{St_m L_c}{L_t}} - 1} \quad (\text{A-2.8a})$$

$$\theta_{hl} = \frac{1}{1 - e^{\frac{-St_m L_c}{L_t}}} \quad (\text{A-2.8b})$$

The steady state solution of the momentum equation can be written as

$$\text{Re}_{ss} = \left[\frac{2}{p} Gr_m \frac{D}{L_t} I_{ss} \right]^{\frac{1}{3-b}} \quad (\text{A-2.9})$$

Where $I_{ss} = \oint \theta_{ss} dZ$. Using Eq. (A-2.7), expressions for I_{ss} for the different orientations of the heater and cooler can be derived. Even for the same orientation, the numerical value of the integral is different for the clockwise and anticlockwise flow. Steady flow in both the clockwise and anticlockwise directions is possible only with horizontal heaters. For the HHHC orientation, however, the integral is the same for both flow directions. Therefore, the integral is evaluated for both flow directions for the HHVC orientation only.

HHHC Orientation

The geometry and coordinate system adopted is shown in Fig. A-2.1. L_1, L_2, L_3 and L_4 are the lengths of the respective horizontal unheated sections in the figure. L_h, L_{hl}, L_c and L_{cl} are respectively the lengths of the heater, hot leg, cooler and cold leg. The pipe between end of the heated section and the beginning of the cooled section is the hot leg. Similarly, the pipe between the end of the cooler and the beginning of the heater is the cold leg. The nondimensional lengths S_h, S_{hl}, S_c and S_{cl} are the cumulative distances from the origin, which is taken as the beginning of the heated section. The nondimensional length S_1, S_2, S_3 and S_4 are the cumulative distances from the origin to the four corners of the rectangular loop.

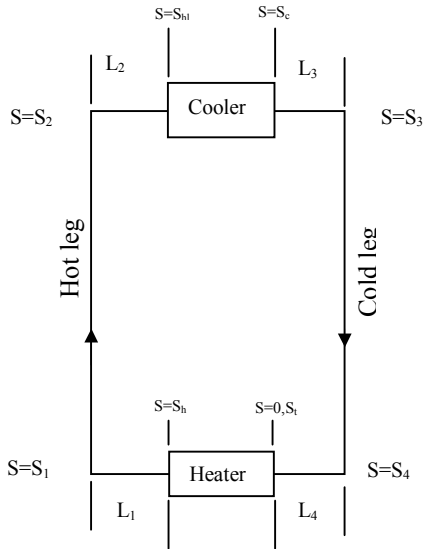


FIG. A-2.1. Loop Geometry and co-ordinates for the HHHC orientation.

Since $dZ=0$ for horizontal sections, the integral in the momentum equation can be written as

$$I_{ss} = \oint [\theta(S)]_{ss} dZ = \int_{S_1}^{S_2} (\theta_{hl})_{ss} dZ + \int_{S_3}^{S_4} (\theta_{cl})_{ss} dZ \quad (\text{A-2.10})$$

For the upleg $dZ=dS$ and for the downleg $dZ = -dS$. Also, $S_2 = S_1+1$ and $S_4=S_3+1$ since lengths are nondimensionalised using H (i.e. loop height). Hence

$$\oint [\theta(S)]_{ss} dZ = \int_{S_1}^{S_1+1} (\theta_{hl})_{ss} dS - \int_{S_3}^{S_3+1} (\theta_{cl})_{ss} dS \quad (\text{A-2.11})$$

Which can be written as

$$\oint [\theta(S)]_{ss} dZ = (\theta_{hl})_{ss} - (\theta_{cl})_{ss} \quad (\text{A-2.12})$$

From equation (A-2.7b) we obtain $(\theta_{hl})_{ss} - (\theta_{cl})_{ss} = 1$. Therefore, for the HHHC orientation we get

$$I_{ss} = \oint [\theta(S)]_{ss} dZ = 1 \quad (\text{A-2.13})$$

HHVC Orientation

The geometry and co-ordinate system adopted for the HHVC orientation is given in Fig. A-2.2. The integral can be evaluated as

$$I_{ss} = \int_{S_1}^{S_1+1} (\theta_{hl})_{ss} dS - \int_{S_3}^{S_{hl}} (\theta_{hl})_{ss} dS - \int_{S_{hl}}^{S_c} (\theta_{hl})_{ss} e^{\frac{St_m}{\phi}(S_{hl}-S)} dS - \int_{S_c}^{S_4} (\theta_{cl})_{ss} dS \quad (\text{A-2.14})$$

After integrating and substituting the limits we get

$$I_{ss} = (\theta_{hl})_{ss} - (\theta_{hl})_{ss} \frac{L_2}{H} + (\theta_{hl})_{ss} \frac{\phi}{St_m} \left[e^{\frac{-St_m L_c}{L_t}} - 1 \right] - (\theta_{cl})_{ss} \frac{L_3}{H} \quad (\text{A-2.15})$$

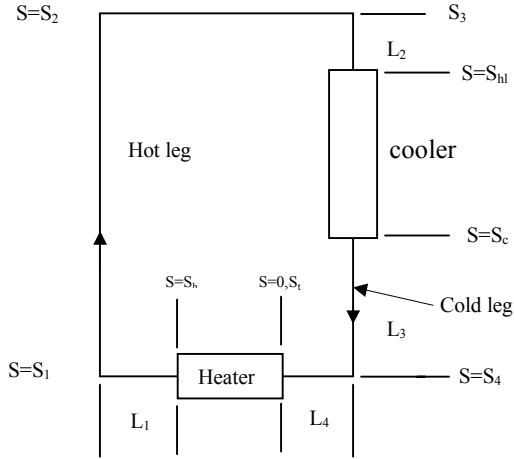


FIG. A-2.2. Loop Geometry and coordinates for the HHVC orientation.

Noting that $\theta_{hl} = \theta_{cl} + 1$ and using equations (A-2.8a) and (A-2.8b) we get

$$I_{ss} = \frac{H - L_2 - L_3}{H \left(e^{\frac{St_m L_c}{L_t}} - 1 \right)} + \left(1 - \frac{L_2}{H} \right) - \frac{L_t}{St_m H}$$

The integral can be evaluated as

$$I_{ss} = \int_{S_1}^{S_1+1} (\theta_{hl})_{ss} dS - \int_{S_3}^{S_{hl}} (\theta_{hl})_{ss} dS - \int_{S_{hl}}^{S_c} (\theta_{hl})_{ss} e^{\frac{St_m}{\phi}(S_{hl}-S)} dS - \int_{S_c}^{S_4} (\theta_{cl})_{ss} dS \quad (\text{A-2.14})$$

After integrating and substituting the limits we get

$$I_{ss} = (\theta_{hl})_{ss} - (\theta_{hl})_{ss} \frac{L_2}{H} + (\theta_{hl})_{ss} \frac{\phi}{St_m} \left[e^{\frac{-St_m L_c}{L_t}} - 1 \right] - (\theta_{cl})_{ss} \frac{L_3}{H} \quad (\text{A-2.15})$$

Noting that $\theta_{hl} = \theta_{cl} + 1$ and using equations (A-2.8a) and (A-2.8b) we get

$$I_{ss} = \frac{H - L_2 - L_3}{H \left(e^{\frac{St_m L_c}{L_t}} - 1 \right)} + \left(1 - \frac{L_2}{H} \right) - \frac{L_t}{St_m H} \quad (\text{A-2.16})$$

Since $L_c = (H - L_2 - L_3)$, we obtain

$$I_{ss} = \frac{L_c}{H} \left[1 + \frac{1}{e^{\frac{St_m L_c}{L_t}} - 1} \right] + \frac{L_3}{H} - \frac{L_t}{St_m H} = \frac{L_c}{H} \left[\frac{1}{1 - e^{-\frac{St_m L_c}{L_t}}} \right] + \frac{L_3}{H} - \frac{L_t}{St_m H} \quad (\text{A-2.17})$$

VHHC Orientation

The loop geometry and co-ordinate system for this case is shown in Fig. A-2.3. The integral in the momentum equation can be written as

$$I_{ss} = \int_0^{S_h} \left((\theta_{cl})_{ss} + \frac{H}{L_h} S \right) dS + \int_{S_h}^{S_2} (\theta_{hl})_{ss} dS - \int_{S_3}^{S_4} (\theta_{cl})_{ss} dS + \int_{S_1}^{S_i} (\theta_{cl})_{ss} dS \quad (\text{A-2.18})$$

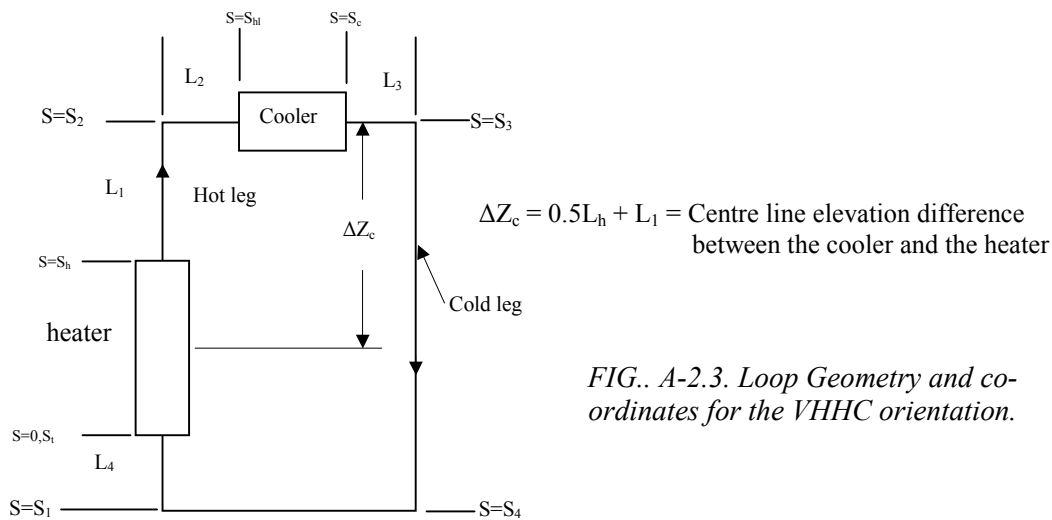


FIG. A-2.3. Loop Geometry and co-ordinates for the VHHC orientation.

Integration of Equation (A-2.18) and substituting the limits yields

$$I_{ss} = (\theta_{cl})_{ss} \left(\frac{L_h}{H} - 1 + \frac{L_4}{H} + \frac{L_1}{H} \right) + \frac{L_h}{2H} + \frac{L_1}{H} \quad (\text{A-2.19})$$

Where $(\theta_{hl})_{ss} = (\theta_{cl})_{ss} + 1$ has been used. Noting that $H = L_h + L_1 + L_4$ we obtain

$$I_{ss} = \frac{L_1 + 0.5L_h}{H} = \frac{\Delta Z_c}{H} \quad (\text{A-2.20})$$

VHVC Orientation

The loop geometry and co-ordinate system for this case is shown in Fig. A-2.4. The integral in the momentum equation can be written as

$$I_{ss} = \int_0^{S_h} \left((\theta_{cl})_{ss} + \frac{H}{L_h} S \right) dS + \int_{S_h}^{S_2} (\theta_{hl})_{ss} dS - \int_{S_3}^{S_{hl}} (\theta_{hl})_{ss} dS - \int_{S_{hl}}^{S_c} (\theta_{hl})_{ss} e^{\frac{St_m(S_{hl}-S)}{\phi}} dS - \int_{S_c}^{S_4} (\theta_{cl})_{ss} dS + \int_{S_1}^{S_t} (\theta_{cl})_{ss} dS \quad (\text{A-2.21})$$

Which on integration and substitution of the limits leads to

$$I_{ss} = (\theta_{cl})_{ss} \left(\frac{L_h}{H} - \frac{L_3}{H} + \frac{L_4}{H} \right) + \frac{L_h}{2H} + (\theta_{hl})_{ss} \left(\frac{L_1}{H} - \frac{L_2}{H} \right) + \frac{\phi}{St_m} \left(\frac{e^{\frac{-St_m L_c}{L_t}} - 1}{1 - e^{\frac{-St_m L_c}{L_t}}} \right) \quad (\text{A-2.22})$$

Where Eq. (A-2.8b) has been used. Noting that $\theta_{hl} = \theta_{cl} + 1$, we obtain

$$I_{ss} = (\theta_{cl})_{ss} \left[\frac{L_h + L_1 + L_4}{H} - \frac{L_3 + L_2}{H} \right] + \frac{0.5L_h + L_1 - L_2 - L_t / St_m}{H} \quad (\text{A-2.23})$$

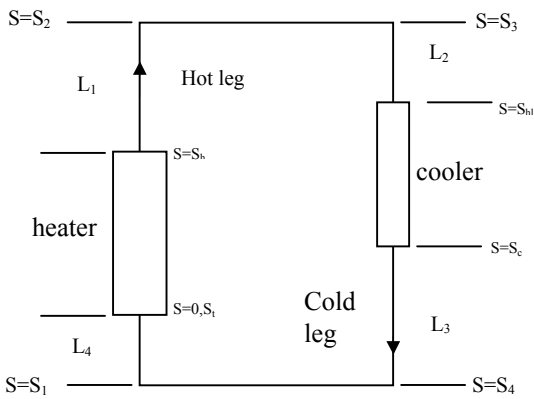


FIG.. A-2.4. Loop geometry and coordinates for VHVC orientation.

which can be rewritten as

$$I_{ss} = [\theta_{cl}]_{ss} \left[1 - \left(\frac{L_3 + L_2}{H} \right) \right] + \frac{0.5L_h + L_1 - L_2 - L_t / St_m}{H} \quad (\text{A-2.24})$$

Replacing $(\theta_{cl})_{ss}$ using (Eq. A-2.8a) and noting that $L_c = H - L_3 - L_2$ we get

$$I_{ss} = \frac{L_c}{H \left(e^{\frac{St_m L_c}{L_t}} - 1 \right)} + \frac{0.5L_h + L_1 - L_2 - L_t / St_m}{H} \quad (\text{A-2.25})$$

HHVC Orientation with anticlockwise flow

The geometry and coordinates with this flow direction are given in Fig. A-2.5.

$$I_{ss} = \oint [\theta(S)]_{ss} dZ = \int_{S_1}^{S_{hl}} (\theta_{hl})_{ss} dS + \int_{S_{hl}}^{S_2} (\theta_{hl})_{ss} e^{\frac{St_m(S_{hl}-S)}{\phi}} dS + \int_{S_c}^{S_2} (\theta_{cl})_{ss} dS - \int_{S_3}^{S_4} (\theta_{cl})_{ss} dS \quad (\text{A-2.26})$$

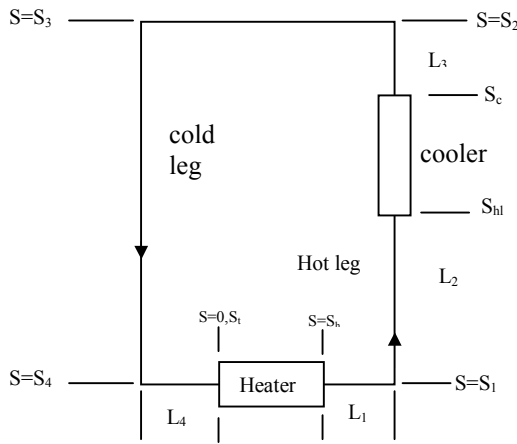


FIG.. A-2.5. Loop Geometry and co-ordinates for the HHVC orientation with flow in the anticlockwise direction.

Upon integration and substituting the limits we get

$$I_{ss} = (\theta_{hl})_{ss} \frac{L_2}{H} + \frac{\phi}{St_m} (\theta_{hl})_{ss} \left(1 - e^{\frac{-St_m L_c}{L_t}} \right) + (\theta_{cl})_{ss} \left(\frac{L_3}{H} - 1 \right) \quad (\text{A-2.27})$$

Noting that $H - (L_3 + L_2) = L_c$ and using equations (A-2.8b) and (A-2.7b) we get

$$I_{ss} = -(\theta_{cl})_{ss} \left(\frac{H - L_2 - L_3}{H} \right) + \frac{L_2}{H} + \frac{L_t}{HSt_m} \quad (\text{A-2.28})$$

which can be rearranged as

$$I_{ss} = \left(\frac{1}{1 - e^{\frac{St_m L_c}{L_t}}} \right) \left(\frac{L_c}{H} \right) + \frac{L_2}{H} + \frac{L_t}{HSt_m} \quad (\text{A-2.29})$$

APPENDIX 3. Linear Stability analysis of single-phase NC

For uniform diameter loops with negligible local pressure losses the governing momentum and energy conservation equations in nondimensional form can be expressed as

$$\frac{d\omega}{d\tau} = \frac{Gr_m}{Re_{ss}^3} \oint \theta dZ - \frac{pL_t \omega^{2-b}}{2D Re_{ss}^b} \quad (A-3.1)$$

$$\frac{\partial \theta}{\partial \tau} + \phi \omega \frac{\partial \theta}{\partial S} = \begin{cases} \frac{L_t}{L_h} \text{ heater} & (\text{for } 0 < S \leq S_h) \\ 0 \text{ pipes} & (\text{for } S_h < S \leq S_{hl} \text{ and } S_c < S \leq S_t) \\ -St_m \theta \text{ cooler} & (\text{for } S_{hl} < S \leq S_c) \end{cases} \quad (A-3.2)$$

Where ϕ is a non-dimensional parameter given by $\phi = L_t / H$. The steady state solution for the momentum and energy equations can be obtained by setting $\omega_{ss} = 1$ and $\partial \omega / \partial \tau = \partial \theta / \partial \tau = 0$. The steady state solutions for a rectangular uniform diameter loop are described in Appendix-2 for the various orientations of the heater and cooler. The stability analysis is performed by perturbing θ and ω as

$$\theta = \theta_{ss} + \theta' \text{ and } \omega = \omega_{ss} + \omega' \quad (A-3.3)$$

Where θ' and ω' are small perturbations over the steady state values. With these substitutions, the perturbed momentum equation can be written as

$$\frac{d\omega'}{d\tau} = \frac{Gr_m}{Re_{ss}^3} \oint \theta' dZ - \frac{pL_t(2-b)\omega'}{2D Re_{ss}^b} \quad (A-3.4)$$

Where $(\omega_{ss} + \omega')^{2-b} = (1 + \omega')^{2-b}$ and was replaced by $1 + (2-b)\omega'$ which is valid for small values of ω' (from binomial theorem neglecting the higher order terms). The perturbed energy equation for the various segments of the loop becomes

$$\frac{\partial \theta'}{\partial \tau} + \phi \frac{\partial \theta'}{\partial S} + \frac{L_t}{L_h} \omega' = 0 \quad \text{Heater } (0 < S \leq S_h) \quad (A-3.5a)$$

$$\frac{\partial \theta'}{\partial \tau} + \phi \frac{\partial \theta'}{\partial S} = 0 \quad \text{Pipes } (S_h < S \leq S_{hl} \text{ and } S_c < S \leq S_t) \quad (A-3.5b)$$

$$\frac{\partial \theta'}{\partial \tau} + \phi \frac{\partial \theta'}{\partial S} + St_m (\theta' - \omega' \theta_{ss}) = 0 \quad \text{Cooler } (S_{hl} < S \leq S_c) \quad (A-3.5c)$$

The small perturbations ω' and θ' can be expressed as

$$\omega' = \bar{\omega} \epsilon e^{n\tau} \text{ and } \theta' = \bar{\theta}(S) \epsilon e^{n\tau} \quad (A-3.6)$$

Where ε is a small quantity and n is the stability parameter so that $\partial\theta'/\partial\tau = \bar{\theta}(S)n\varepsilon e^{n\tau}$, $\partial\theta'/\partial S = \varepsilon e^{n\tau} \partial\bar{\theta}(S)/\partial S$ and $d\omega'/d\tau = \bar{\omega}n\varepsilon e^{n\tau}$. Using these in equation (A-3.4) and (A-3.5) we get

$$n\bar{\omega} - \frac{Gr_m}{Re_{ss}^3} \oint \bar{\theta}(S) dZ + \frac{pL_t(2-b)\bar{\omega}}{2D Re_{ss}^b} = 0 \quad (A-3.7a)$$

which can be rewritten as

$$n - \frac{Gr_m}{Re_{ss}^3} \frac{\bar{I}}{\bar{\omega}} + \frac{pL_t(2-b)}{2D Re_{ss}^b} = 0 \quad (A-3.7b)$$

Where $\bar{I} = \oint \bar{\theta}(S) dZ$.

$$\frac{d\bar{\theta}(S)}{dS} + \frac{n}{\phi} \bar{\theta}(S) + \frac{L_t \bar{\omega}}{\phi L_h} = 0 \quad \text{heater } (0 < S \leq S_h) \quad (A-3.8a)$$

$$\frac{d\bar{\theta}(S)}{dS} + \frac{n}{\phi} \bar{\theta}(S) = 0 \quad \text{pipes } (S_h < S \leq S_{hl} \text{ and } S_c < S \leq S_t) \quad (A-3.8b)$$

$$\frac{d\bar{\theta}(S)}{dS} + \left(\frac{n + St_m}{\phi} \right) \bar{\theta}(S) - \frac{St_m \theta_{ss} \bar{\omega}}{\phi} = 0 \quad \text{cooler } (S_{hl} < S \leq S_c) \quad (A-3.8c)$$

The above equations are of the form $dy/dx + py = Q$, whose solution can be expressed as $ye^{\int p dx} = \int Qe^{\int p dx} + C$. Hence, for each segment of the loop we obtain

$$\bar{\theta}(S) = \left[\bar{\theta}_{cl} + \frac{\bar{\omega} L_t}{n L_h} \right] e^{\frac{-nS}{\phi}} - \frac{L_t \bar{\omega}}{L_h n} \quad \text{heater } (0 < S \leq S_h) \quad (A-3.9)$$

Where the boundary condition that at $S=0$, $\bar{\theta}(S) = \bar{\theta}_{cl}$ has been used. Similarly we get the following equation for the hot leg

$$\bar{\theta}(S) = \bar{\theta}_h e^{\frac{n(S_h - S)}{\phi}} \quad (\text{for } S_h < S \leq S_{hl}) \quad (A-3.10)$$

Where the boundary condition that at $S=S_h$, $\bar{\theta}(S) = \bar{\theta}_h$ has been used. Similarly we get the following equation for the cold leg

$$\bar{\theta}(S) = \bar{\theta}_c e^{\frac{n(S_c - S)}{\phi}} \quad (\text{for } S_c < S \leq S_t) \quad (A-3.11)$$

Where the boundary condition that at $S=S_c$, $\bar{\theta}(S) = \bar{\theta}_c$ has been used. For the cooler the following equation can be obtained

$$\bar{\theta}(S) = \frac{\bar{\omega}}{n} St_m (\theta_{hl})_{ss} \left[e^{\frac{St_m(S_{hl}-S)}{\phi}} - e^{\frac{n+St_m(S_{hl}-S)}{\phi}} \right] + \bar{\theta}_{hl} e^{\frac{n+St_m(S_{hl}-S)}{\phi}} \quad (\text{for } S_{hl} < S \leq S_c) \quad (\text{A-3.12})$$

Where the boundary condition that at $S=S_{hl}$, $\bar{\theta}(S) = \bar{\theta}_{hl}$ has been used. The parameters $\bar{\theta}_{cl}$, $\bar{\theta}_h$, $\bar{\theta}_c$ and $\bar{\theta}_{hl}$ can be evaluated from the above equations by using appropriate boundary conditions. For example use of the boundary condition that at $S=S_h$, $\bar{\theta}(S) = \bar{\theta}_h$ in the equation for the heater gives

$$\bar{\theta}_h = \left[\bar{\theta}_{cl} + \frac{\bar{\omega} L_t}{n L_h} \right] e^{\frac{-nL_h}{L_t}} - \frac{L_t \bar{\omega}}{L_h n} \quad (\text{A-3.13a})$$

Substituting in (A-3.10) we get the following equation for the hot leg

$$\bar{\theta}(S) = \left[\bar{\theta}_{cl} + \frac{\bar{\omega} L_t}{n L_h} \right] e^{\frac{-nS}{\phi}} - \frac{L_t \bar{\omega}}{L_h n} e^{\frac{n(S_h-S)}{\phi}} \quad (\text{for } S_h < S \leq S_{hl}) \quad (\text{A-3.13b})$$

At $S = S_{hl}$, $\bar{\theta}(S) = \bar{\theta}_{hl}$. Hence

$$\bar{\theta}_{hl} = \left[\bar{\theta}_{cl} + \frac{\bar{\omega} L_t}{n L_h} \right] e^{\frac{-n(L_h+L_{hl})}{L_t}} - \frac{L_t \bar{\omega}}{L_h n} e^{\frac{-nL_{hl}}{L_t}} \quad (\text{A-3.13c})$$

Substituting this in the equation for the cooler, we get

$$\begin{aligned} \bar{\theta}(S) = \frac{\bar{\omega}}{n} St_m (\theta_{hl})_{ss} \left[e^{\frac{St_m(S_{hl}-S)}{\phi}} - e^{\frac{n+St_m(S_{hl}-S)}{\phi}} \right] + \left[\bar{\theta}_{cl} + \frac{\bar{\omega} L_t}{n L_h} \right] e^{\frac{-(n+St_m)S+St_mS_{hl}}{\phi}} \\ - \frac{L_t \bar{\omega}}{L_h n} e^{\frac{n(S_h-S)+St_m(S_{hl}-S)}{\phi}} \quad (\text{for } S_{hl} < S \leq S_c) \end{aligned} \quad (\text{A-3.13d})$$

From the above using the boundary condition that at $S=S_c$, $\bar{\theta}(S) = \bar{\theta}_c$ we get

$$\begin{aligned} \bar{\theta}_c = \frac{\bar{\omega}}{n} St_m (\theta_{hl})_{ss} \left(e^{\frac{-St_m L_c}{L_t}} - e^{\frac{-(n+St_m)L_c}{L_t}} \right) + \left(\bar{\theta}_{cl} + \frac{\bar{\omega} L_t}{n L_h} \right) e^{-\left\{ \frac{St_m L_c + n(L_h + L_{hl} + L_c)}{L_t} \right\}} \\ - \frac{L_t \bar{\omega}}{L_h n} e^{-\left\{ \frac{nL_{hl} + (n+St_m)L_c}{L_t} \right\}} \end{aligned} \quad (\text{A-3.13e})$$

Using this in Eq. (A-3.11) the cold leg equation can be written as

$$\begin{aligned} \bar{\theta}(S) = \frac{\bar{\omega}}{n} St_m(\theta_{hl})_{ss} \left[e^{\frac{St_m(S_{hl}-S_c)+n(S_c-S)}{\phi}} - e^{\frac{St_m(S_{hl}-S_c)+n(S_{hl}-S)}{\phi}} \right] + \left(\bar{\theta}_{cl} + \frac{\bar{\omega}}{n} \frac{L_t}{L_h} \right) e^{\frac{St_m(S_{hl}-S_c)-nS}{\phi}} \\ - \frac{L_t}{L_h} \frac{\bar{\omega}}{n} e^{\frac{n(S_h-S)+St_m(S_{hl}-S_c)}{\phi}} \quad (\text{for } S_c < S \leq S_t) \end{aligned} \quad (\text{A-3.13f})$$

Using the boundary condition that at $S=S_t$, $\bar{\theta}(S) = \bar{\theta}_{cl}$, we can get the following expression for $\bar{\theta}_{cl}$,

$$\bar{\theta}_{cl} = \frac{\bar{\omega}}{n} \left[\frac{St_m(\theta_{hl})_{ss} e^{\frac{n(L_t-L_{cl})}{L_t}} \left(1 - e^{-\frac{nL_c}{L_t}} \right) + \frac{L_t}{L_h} \left(1 - e^{-\frac{nL_h}{L_t}} \right)}{e^{\frac{St_m L_c + nL_t}{L_t}} - 1} \right] \quad (\text{A-3.14a})$$

From this, $\bar{\theta}_{cl} / \bar{\omega}$ can be written as

$$\frac{\bar{\theta}_{cl}}{\bar{\omega}} = \frac{St_m(\theta_{hl})_{ss} e^{\frac{n(L_t-L_{cl})}{L_t}} \left(1 - e^{-\frac{nL_c}{L_t}} \right) + \frac{L_t}{L_h} \left(1 - e^{-\frac{nL_h}{L_t}} \right)}{n \left(e^{\frac{St_m L_c + nL_t}{L_t}} - 1 \right)} \quad (\text{A-3.14b})$$

Expressions for $\bar{\theta}_h / \bar{\omega}$, $\bar{\theta}_{hl} / \bar{\omega}$ and $\bar{\theta}_c / \bar{\omega}$ can be obtained by using the above expression for $\bar{\theta}_{cl} / \bar{\omega}$ in equations (A-3.13a), (A-3.13c) and (A-3.13e) as follows:

$$\frac{\bar{\theta}_h}{\bar{\omega}} = \frac{St_m(\theta_{hl})_{ss} e^{\frac{nL_{hl}}{L_t}} \left(e^{\frac{nL_c}{L_t}} - 1 \right) + \frac{L_t}{L_h} \left(e^{-\frac{nL_h}{L_t}} - 1 \right) e^{\frac{(St_m L_c + nL_t)}{L_t}}}{n \left(e^{\frac{(St_m L_c + nL_t)}{L_t}} - 1 \right)} \quad (\text{A-3.14c})$$

$$\frac{\bar{\theta}_{hl}}{\bar{\omega}} = \frac{St_m(\theta_{hl})_{ss} \left(e^{\frac{nL_c}{L_t}} - 1 \right) + \frac{L_t}{L_h} e^{\frac{St_m L_c + n(L_t - L_{hl})}{L_t}} \left(e^{-\frac{nL_h}{L_t}} - 1 \right)}{n \left(e^{\frac{St_m L_c + nL_t}{L_t}} - 1 \right)} \quad (\text{A-3.14d})$$

$$\frac{\bar{\theta}_c}{\omega} = \frac{St_m(\theta_{hl})_{ss} e^n \left(1 - e^{-\frac{nL_c}{L_t}} \right) + \frac{L_t}{L_h} e^{\frac{nL_{cl}}{L_t}} \left(1 - e^{-\frac{nL_h}{L_t}} \right)}{n \left(e^{\frac{St_m L_c + nL_t}{L_t}} - 1 \right)} \quad (\text{A-3.14e})$$

Using the expressions (A-3.9) to (A-3.12), we can find the integral $\oint \bar{\theta}(S) dZ$. Substituting this in Eq. (A-3.7b) we obtain the characteristic equation for stability. However, the value of the integral is different for different orientations.

HHHC Orientation

For evaluating the integral consider the figure A-2.1 with the various distances marked as shown in the direction of flow. The relations between the various lengths are given below:

$$L_t = L_h + L_{hl} + L_c + L_{cl} = L_h + L_c + 2H + L_1 + L_2 + L_3 + L_4 \quad (\text{A-3.15})$$

$$L_{hl} = L_1 + H + L_2 \text{ and } L_{cl} = L_3 + H + L_4 \quad (\text{A-3.16})$$

The breadth of the loop, B, can be expressed as

$$B = L_1 + L_h + L_4 = L_2 + L_c + L_3 \quad (\text{A-3.17})$$

For generality, the lengths L_1, L_2, L_3 and L_4 are considered to be unequal. The cumulative lengths, s_1, s_2, s_3 and s_4 can be expressed as

$$s_1 = L_h + L_1 ; s_2 = s_1 + H ; s_3 = s_2 + B = s_c + L_3 = L_h + L_{hl} + L_c + L_3 \text{ \& } s_4 = s_3 + H \quad (\text{A-3.18})$$

The nondimensional lengths S_2 and S_4 can be expressed as

$$S_2 = S_1 + 1 \text{ and } S_4 = S_3 + 1 \quad (\text{A-3.19})$$

The integral $\oint \bar{\theta}(S) dZ$ can be expressed as

$$\oint \bar{\theta}(S) dZ = \int_{S_1}^{S_2} \left\{ \bar{\theta}(S) \right\}_{hot \ leg} dZ + \int_{S_3}^{S_4} \left\{ \bar{\theta}(S) \right\}_{cold \ leg} dZ \quad (\text{A-3.20})$$

For the hot leg $dZ=dS$ and for the cold leg $dZ= -dS$. Hence, using (A-3.10) and (A-3.11) we can obtain

$$\oint \bar{\theta}(S) dZ = \int_{S_1}^{S_1+1} \bar{\theta}_h e^{\frac{n(S_h-S)}{\phi}} dS - \int_{S_3}^{S_3+1} \bar{\theta}_c e^{\frac{n(S_c-S)}{\phi}} dS \quad (\text{A-3.21})$$

Integrating and substituting the limits yield

$$\oint \bar{\theta}(S) dZ = \frac{\phi}{n} \left(1 - e^{-\frac{n}{\phi}} \right) \left\{ \bar{\theta}_h e^{-\frac{nL_1}{L_t}} - \bar{\theta}_c e^{-\frac{nL_3}{L_t}} \right\} \quad (\text{A-3.22})$$

$$\frac{\bar{I}}{\bar{\omega}} = \frac{1}{\bar{\omega}} \oint \bar{\theta}(S) dZ = \frac{\phi}{n} \left(1 - e^{-\frac{n}{\phi}} \right) \left\{ \frac{\bar{\theta}_h}{\bar{\omega}} e^{-\frac{nL_1}{L_t}} - \frac{\bar{\theta}_c}{\bar{\omega}} e^{-\frac{nL_3}{L_t}} \right\} \quad (\text{A-3.23})$$

$\bar{\theta}_h / \bar{\omega}$ and $\bar{\theta}_c / \bar{\omega}$ are obtained from Eq. (A-3.14c) and (A-3.14e) respectively. If $L_1 = L_2 = L_x$, then this reduces to

$$\frac{\bar{I}}{\bar{\omega}} = \frac{1}{\bar{\omega}} \oint \bar{\theta}(S) dZ = \frac{\phi}{n} \left(1 - e^{-\frac{n}{\phi}} \right) \left(e^{-\frac{nL_x}{L_t}} \right) \left\{ \frac{\bar{\theta}_h - \bar{\theta}_c}{\bar{\omega}} \right\} \quad (\text{A-3.24})$$

Using Eqs. (A-3.14c) and (A-3.14e), the following expression for $(\bar{\theta}_h - \bar{\theta}_c) / \bar{\omega}$ can be obtained as

$$\frac{\bar{\theta}_h - \bar{\theta}_c}{\bar{\omega}} = \frac{St_m(\theta_{hl})_{ss} \left\{ e^{\frac{nL_{hl}}{L_t}} \left(e^{\frac{nL_c}{L_t}} - 1 \right) - e^n \left(1 - e^{-\frac{nL_c}{L_t}} \right) \right\} + \frac{L_t}{L_h} \left\{ e^{\frac{St_m L_c + nL_t}{L_t}} \left(e^{-\frac{nL_h}{L_t}} - 1 \right) - e^{\frac{nL_c}{L_t}} \left(1 - e^{-\frac{nL_h}{L_t}} \right) \right\}}{n \left(e^{\frac{St_m L_c + nL_t}{L_t}} - 1 \right)}$$

HHVC Orientation

Refer to Fig. A-2.2 for the geometry and co-ordinate system considered. For S_1 to S_2 $dZ = dS$, and for S_3 to S_4 , $dZ = -dS$. Hence

$$\begin{aligned} \oint \bar{\theta}(S) dZ &= \int_{S_1}^{S_1+1} \bar{\theta}_h e^{\frac{n(S_h-S)}{\phi}} dS - \int_{S_3}^{S_{hl}} \bar{\theta}_h e^{\frac{n(S_h-S)}{\phi}} dS - \int_{S_{hl}}^{S_c} \bar{\theta}_{hl} e^{\frac{n+St_m(S_{hl}-S)}{\phi}} dS - \\ &\quad - \frac{\bar{\omega}}{n} St_m(\theta_{hl})_{ss} \int_{S_{hl}}^{S_c} \left(e^{\frac{St_m(S_{hl}-S)}{\phi}} - e^{\frac{n+St_m(S_{hl}-S)}{\phi}} \right) dS - \int_{S_c}^{S_4} \bar{\theta}_c e^{\frac{n(S_c-S)}{\phi}} dS \end{aligned} \quad (\text{A-3.25})$$

On integration and substitution of limits yield the following equation for $\bar{I} / \bar{\omega}$.

$$\begin{aligned} \frac{\bar{I}}{\bar{\omega}} &= \frac{\bar{\theta}_h}{\bar{\omega}} \frac{\phi}{n} \left\{ e^{-\frac{nL_1}{L_t}} \left(1 - e^{-\frac{n}{\phi}} \right) + e^{-\frac{nL_{hl}}{L_t}} \left(1 - e^{-\frac{nL_2}{L_t}} \right) \right\} + \frac{\phi}{n} (\theta_{hl})_{ss} \left\{ e^{-\frac{St_m L_c}{L_t}} - 1 + \frac{St_m}{n + St_m} \left(1 - e^{-\left(\frac{n+St_m}{L_t} \right) L_c} \right) \right\} \\ &\quad + \frac{\bar{\theta}_{hl}}{\bar{\omega}} \left(\frac{\phi}{n + St_m} \right) \left[e^{-\frac{(n+St_m)L_c}{L_t}} - 1 \right] + \frac{\bar{\theta}_c}{\bar{\omega}} \frac{\phi}{n} \left[e^{-\frac{nL_3}{L_t}} - 1 \right] \end{aligned} \quad (\text{A-3.26})$$

The parameters $\bar{\theta}_h / \bar{\omega}$, $\bar{\theta}_{hl} / \bar{\omega}$, and $\bar{\theta}_c / \bar{\omega}$ are evaluated using equations (A-3.14c), (A-3.14d) and (A-3.14e) respectively.

VHHC Orientation

Refer to Fig. A-2.3 for the geometry and co-ordinate system considered. For S_1 to S_2 $dZ = dS$, and for S_3 to S_4 , $dZ = -dS$. Hence,

$$\oint \bar{\theta}(S) dZ = \int_0^{S_h} \left[\left(\bar{\theta}_{cl} + \frac{\bar{\omega} L_t}{n L_h} \right) e^{\frac{-nS}{\phi}} - \frac{\bar{\omega} L_t}{n L_h} \right] dS + \int_{S_h}^{S_2} \bar{\theta}_h e^{\frac{n(S_h-S)}{\phi}} dS - \int_{S_3}^{S_3+1} \bar{\theta}_c e^{\frac{n(S_c-S)}{\phi}} dS + \int_{S_1}^{S_1} \bar{\theta}_c e^{\frac{n(S_c-S)}{\phi}} dS \quad (\text{A-3.27})$$

$$\frac{\bar{I}}{\bar{\omega}} = \frac{\bar{\theta}_{cl}}{\bar{\omega}} \frac{\phi}{n} \left(1 - e^{\frac{-nL_h}{L_t}} \right) + \frac{L_t}{nL_h} \left\{ \frac{\phi}{n} \left(1 - e^{\frac{-nL_h}{L_t}} \right) - \frac{L_h}{H} \right\} + \frac{\bar{\theta}_h}{\bar{\omega}} \frac{\phi}{n} \left[1 - e^{\frac{-nL_1}{L_t}} \right] + \frac{\bar{\theta}_c}{\bar{\omega}} \frac{\phi}{n} \left[\frac{e^{\frac{-nH}{L_t}} - 1}{e^{\frac{nL_3}{L_t}}} + \frac{e^{\frac{nL_4}{L_t}} - 1}{e^{\frac{nL_t}{L_t}}} \right] \quad (\text{A-3.28})$$

The parameters $\bar{\theta}_{cl}/\bar{\omega}$, $\bar{\theta}_h/\bar{\omega}$ and $\bar{\theta}_c/\bar{\omega}$ are evaluated using equations (A-3.14b), (A-3.14c) and (A-3.14e) respectively.

VHVC Orientation

Refer to Fig. A-2.4 for the geometry and co-ordinate system considered. For S_1 to S_2 $dZ = dS$, and for S_3 to S_4 , $dZ = -dS$. Hence,

$$\bar{I} = \int_0^{S_h} \left\{ \left(\bar{\theta}_{cl} + \frac{\bar{\omega} L_t}{n L_h} \right) e^{\frac{-nS}{\phi}} - \frac{\bar{\omega} L_t}{n L_h} \right\} dS + \int_{S_h}^{S_2} \bar{\theta}_h e^{\frac{n(S_h-S)}{\phi}} dS - \int_{S_3}^{S_{hl}} \bar{\theta}_h e^{\frac{n(S_h-S)}{\phi}} dS - \int_{S_{hl}}^{S_c} \left\{ \frac{\bar{\omega}}{n} St_m (\theta_{hl})_{ss} \left(e^{\frac{St_m(S_{hl}-S)}{\phi}} - e^{\frac{n+St_m(S_{hl}-S)}{\phi}} \right) + \bar{\theta}_{hl} e^{\frac{(n+St_m)(S_{hl}-S)}{\phi}} \right\} dS - \int_{S_c}^{S_4} \bar{\theta}_c e^{\frac{n(S_c-S)}{\phi}} dS - \int_{S_1}^{S_1} \bar{\theta}_c e^{\frac{n(S_c-S)}{\phi}} dS \quad (\text{A-3.29})$$

After integration and substitution of limits we obtain

$$\frac{\bar{I}}{\bar{\omega}} = \frac{\bar{\theta}_{cl}}{\bar{\omega}} \frac{\phi}{n} \left(1 - e^{\frac{-nL_h}{L_t}} \right) + \frac{L_t^2}{n^2 L_h H} \left(1 - e^{\frac{-nL_h}{L_t}} - \frac{nL_h}{L_t} \right) + \frac{\bar{\theta}_h}{\bar{\omega}} \frac{\phi}{n} \left[1 - e^{\frac{-nL_1}{L_t}} + e^{\frac{-nL_{hl}}{L_t}} \left(1 - e^{\frac{-nL_2}{L_t}} \right) \right] + \frac{\phi (\theta_{hl})_{ss}}{n(n+St_m)} \left[n \left(e^{\frac{-St_m L_c}{L_t}} - 1 \right) + St_m e^{\frac{-St_m L_c}{L_t}} \left(1 - e^{\frac{-nL_c}{L_t}} \right) \right] + \frac{\bar{\theta}_{hl}}{\bar{\omega}} \frac{\phi}{n+St_m} \left[e^{\frac{-(n+St_m)L_c}{L_t}} - 1 \right] + \frac{\bar{\theta}_c}{\bar{\omega}} \frac{\phi}{n} \left\{ e^{\frac{-nL_3}{L_t}} - 1 + e^{\frac{-nL_{cl}}{L_t}} \left(e^{\frac{nL_4}{L_t}} - 1 \right) \right\} \quad (\text{A-3.30})$$

The parameters $\bar{\theta}_{cl}/\bar{\omega}$, $\bar{\theta}_h/\bar{\omega}$, $\bar{\theta}_{hl}/\bar{\omega}$ and $\bar{\theta}_c/\bar{\omega}$ are evaluated using equations (A-3.14b), (A-3.14c), (A-3.14d) and (A-3.14e) respectively.

HHVC Orientation with anticlockwise flow

Refer to Fig. A-2.5 for the geometry and co-ordinate system considered. For S_1 to S_2 $dZ = dS$, and for S_3 to S_4 , $dZ = -dS$. Hence,

$$\oint \bar{\theta}(S) dZ = \int_{S_1}^{S_{hl}} \bar{\theta}_h e^{\frac{n(S_h-S)}{\phi}} dS + \int_{S_{hl}}^{S_c} \left\{ \frac{\bar{\omega}}{n} St_m (\theta_{hl})_{ss} \left(e^{\frac{St_m(S_{hl}-S)}{\phi}} - e^{\frac{n+St_m(S_{hl}-S)}{\phi}} \right) + \bar{\theta}_{hl} e^{\frac{(n+St_m)(S_{hl}-S)}{\phi}} \right\} dS$$

$$+ \int_{S_c}^{S_2} \bar{\theta}_c e^{\frac{n(S_c-S)}{\phi}} dS - \int_{S_3}^{S_{3+1}} \bar{\theta}_c e^{\frac{n(S_c-S)}{\phi}} dS \quad (\text{A-3.31})$$

After integration and substitution of the limits and simplifying we obtain

$$\frac{\bar{I}}{\bar{\omega}} = \frac{\bar{\theta}_h}{\bar{\omega}} \frac{\phi}{n} e^{\frac{-nL_1}{L_i}} \left(1 - e^{\frac{-nL_2}{L_i}} \right) + \frac{\phi}{n} \frac{(\theta_{hl})_{ss}}{n + St_m} \left\{ n \left(1 - e^{\frac{-St_m L_c}{L_i}} \right) - St_m e^{\frac{-St_m L_c}{L_i}} \left(1 - e^{\frac{-nL_c}{L_i}} \right) \right\}$$

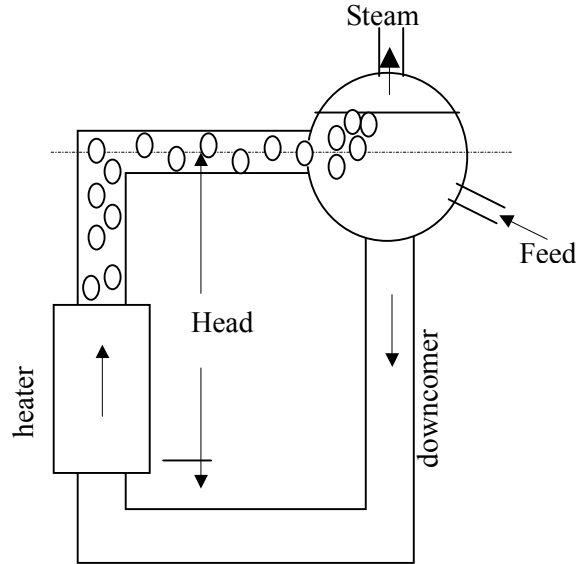
$$+ \frac{\bar{\theta}_c}{\bar{\omega}} \frac{\phi}{n} \left\{ 1 - e^{\frac{-nL_3}{L_i}} - \left(1 - e^{\frac{-n}{\phi}} \right) e^{\frac{-n(L_3+L_1+L_h+L_4)}{L_i}} \right\} + \frac{\bar{\theta}_{hl}}{\bar{\omega}} \frac{\phi}{n + St_m} \left(1 - e^{\frac{-(n+St_m)L_c}{L_i}} \right) \quad (\text{A-3.32})$$

The parameters $\bar{\theta}_h/\bar{\omega}$, $\bar{\theta}_{hl}/\bar{\omega}$ and $\bar{\theta}_c/\bar{\omega}$ are evaluated using equations (A-3.14c), (A-3.14d) and (A-3.14e) respectively.

APPENDIX 4. Linear Stability analysis of two-phase NCS

The analysis is carried out for a simple loop as shown in Fig. A-4.1 where complete separation of the steam-water mixture is assumed to take place in the steam drum. The separated water is assumed to completely mix with the feed water in the steam drum. For the sake of simplicity we use further simplifying assumptions like uniform axial heat flux in the heated section and insulated piping. In addition, the effect of $\partial p / \partial t$ is also neglected. With these assumptions, the governing equations can be rewritten as

FIG. A-4.1. A simple two-phase NC loop.



$$A \frac{\partial \rho}{\partial t} + \frac{\partial w}{\partial z} = 0 \quad (\text{A-4.1})$$

$$\frac{1}{A} \frac{\partial w}{\partial t} + \frac{1}{A^2} \frac{\partial}{\partial z} (w^2 / \rho) + \rho g \cos \phi + \frac{f}{2DA^2} (w^2 / \rho) + \frac{\partial p}{\partial z} = 0 \quad (\text{A-4.2})$$

The pressure drop due to bends, restrictions, spacers, etc. was estimated as

$$\Delta p_k = KW^2 / 2\rho A^2 \quad (\text{A-4.2a})$$

$$\rho A \frac{\partial h}{\partial t} + w \frac{\partial h}{\partial z} = \begin{cases} q_h'' A & \text{heated region,} \\ 0 & \text{adiabatic region.} \end{cases} \quad (\text{A-4.3})$$

In addition an equation of state is required for the density and is given by

$$\rho = f(p, h) \quad (\text{A-4.4})$$

The steady state solution, which is essential for performing the linear stability analysis, can be obtained by dropping the time derivatives from the above equations. These are

$$\frac{\partial w}{\partial z} = 0 \quad (\text{A-4.5})$$

$$\frac{1}{A^2} \frac{\partial}{\partial z} (w^2 / \rho) + \rho g \cos \phi + \frac{f}{2DA^2} (w^2 / \rho) + \frac{\partial p}{\partial z} = 0 \quad (\text{A-4.6})$$

$$w \frac{\partial h}{\partial z} = \begin{cases} \dot{q}_h A & \text{heated region,} \\ 0 & \text{adiabatic region.} \end{cases} \quad (\text{A-4.7})$$

Equations (5) to (7) are solved together to obtain the steady state flow rate for a given power and reactor inlet temperature or specific enthalpy conditions as follows.

- (i) Assume an initial flow rate
- (ii) With this flow rate, obtain the enthalpy in the heated region at any axial distance (z) as

$$h(z) = h_{in} + \frac{\dot{q}_h A z}{w} \quad (\text{A-4.8})$$

The specific enthalpy is constant in the adiabatic regions so that $h(z) = h_{in}$ for the downcomer to the heater inlet and $h(z) = h_o$ from heater outlet to the SD. The heater outlet enthalpy h_o can be calculated from Eq. (A-4.8) as

$$h_o = h_{in} + \frac{\dot{q}_h A L_h}{w} \quad (\text{A-4.9})$$

where L_h is the total length of the heated region. At steady state, the feed water flow rate is equal to the steam flow rate. Assuming complete mixing in the SD, the enthalpy h_{in} can be calculated as

$$h_{in} = (1 - x_e) h_f + x_e h_{FD} \quad (\text{A-4.10})$$

where x_e is the exit quality and h_{FD} is the feed water enthalpy. Noting that $h_o = x_e h_g + (1 - x_e) h_f$, the exit quality can be calculated from Eq. (A-4.9) as

$$x_e = \frac{h_{in} - h_f}{h_{fg}} + \frac{\dot{Q}_h A L_h}{w h_{fg}} \quad (\text{A-4.11})$$

- (iii) From the specific enthalpy, the length of the single-phase region, is determined as

$$L_{sp} = \frac{w(h_f - h_{in})}{\dot{q}_h A} \quad (\text{A-4.12})$$

In the single-phase heated region, the variation of density is obtained using the Boussinesq approximation as given by

$$\rho(z) = \rho_o [1 - \sigma(T(z) - T_{in})] \cong \rho_o \left(1 - \frac{\sigma(h(z) - h_{in})}{Cp} \right) \quad (\text{A-4.13})$$

where σ is the volumetric thermal expansion coefficient and Cp is the specific heat of the mixture. In the two-phase heated region, the variation of density is given by

$$\rho(z) = \alpha(z) \rho_g + (1 - \alpha(z)) \rho_f \quad (\text{A-4.14})$$

where $\alpha(z)$ is the void fraction at any axial location, which is calculated considering homogeneous two-phase mixture. The steady state mass flow rate is calculated by numerically integrating Eq. (A-4.6) along the loop. The integral momentum equation for the steady state case can be obtained as

$$\oint \frac{d(w^2v)}{A^2} + g \oint \rho dz + \frac{w^2}{2A^2\rho_f} \left[\frac{f_f L_{sp} \rho_f}{D\rho_{in}} + K_i \frac{\rho_f}{\rho_{in}} + \left(\frac{w^2}{\phi_{LO}^2 L_{tp}} \right)_h + \left(\phi_{LO}^2 L_{tp} \right)_p + K_o \frac{\rho_f}{\rho_{tp}} \right] = 0 \quad (\text{A-4.15})$$

While the density at any axial distance is known from equations (A-4.13) and (A-4.14), the friction factor in the single-phase region, is obtained from the local Reynolds number as follows.

$$f_{1\phi} = 64 / \text{Re} \quad \text{for laminar flow} \quad (\text{A-4.16a})$$

$$f_{1\phi} = 0.316 / \text{Re}^{0.25} \quad \text{for turbulent flow} \quad (\text{A-4.16b})$$

In the two-phase region, a two-phase friction factor multiplier (Φ_{lo}^2) was used to estimate the frictional pressure loss as given below.

$$\Phi_{lo}^2 = \frac{(dp/dz)_{2\phi}}{(dp/dz)_{1\phi}} \quad (\text{A-4.17})$$

In this work, the Baroczy (1966) model was used to evaluate the two-phase multiplier.

(vi) After calculating all the terms in the Eq. (A-4.15), check whether the equation is satisfied with the assumed flow rate. If not, then steps i) to vi) are iterated until Eq. (A-4.15) is satisfied within a chosen convergence criterion.

Flow distribution in the parallel channels

The gross flow obtained from Eq. (A-4.15) is divided into the channels of the reactor connected between the inlet header and the steam drum. The flow distribution in the channels is not uniform because of unequal heat generation in the channels. For obtaining the channel flow distribution, the pressure variation in the header and the steam drum is neglected. Since all parallel channels are connected between the inlet header and the steam drum, we have

$$\Delta p_{H-SD} = (\Delta p_{ch})_1 = (\Delta p_{ch})_2 = \dots = (\Delta p_{ch})_i \quad (\text{A-4.18})$$

To obtain $(\Delta p_{ch})_i$ Eq. (A-4.6) is integrated from the header to the SD. Similarly, the pressure drop between the steam drum and the inlet header is estimated as

$$\Delta p_{SD-H} = -\rho_{in} g \Delta Z + \frac{w_t^2}{2\rho_{in} A^2} \left(\frac{fL}{D} + K \right) \quad (\text{A-4.19})$$

where ΔZ is the elevation difference between the steam drum water level and the inlet header and w_t is the total loop flow rate and can be expressed as

$$w_t = \sum_{i=1}^N (w_{ch})_i \quad (\text{A-4.20})$$

The total flow rate w_t and individual channel flow rates $(w_{ch})_i$ are estimated by solving equations (A-4.18) to (A-4.20) iteratively with the condition that $\Delta p_{H-SD} + \Delta p_{SD-H} = 0$.

Linear Stability Analysis

The conservation equations (A-4.1) to (A-4.3) are perturbed by introducing small perturbations over the steady state as follows

$$w = w_{ss} + w'; h = h_{ss} + h'; p = p_{ss} + p'; v = v_{ss} + v'; q_h''' = q_{h,ss}''' + (q_h''')' \quad (A-4.21a)$$

$$\text{where } w' = \bar{w}(z)\varepsilon e^{st}; h' = \bar{h}(z)\varepsilon e^{st}; p' = \bar{p}(z)\varepsilon e^{st}; v' = \bar{v}(z)\varepsilon e^{st}; (q_h''')' = \bar{q}_h'''(z)\varepsilon e^{st} \quad (A-4.21b)$$

In Eq. (A-4.21) ε is a small quantity and $\bar{w}, \bar{h}, \bar{p}, \bar{v}$ and \bar{q}_h''' are the amplitudes of the perturbed flow rate, enthalpy, pressure, specific volume and heat added per unit volume of coolant respectively and s is the stability parameter. With these substitutions, the perturbed conservation equations after linearization can be written as follows for the single-phase region.

$$\frac{dw'}{dz} = 0 \quad (A-4.22)$$

$$\frac{dh'}{dz} + \frac{\rho_{in} A s h'}{w_{ss}} = \left\{ \begin{array}{l} -\frac{w' q_{h,ss}''' A}{w_{ss}^2} + \frac{(q_h''')' A}{w_{ss}} \text{ heated region} \\ 0 \text{ adiabatic region} \end{array} \right\} \quad (A-4.23)$$

$$\frac{dp'}{dz} + w' \left(\frac{s}{A} + \frac{f w_{ss}}{\rho_{in} D A^2} \right) - \frac{g \beta \rho_{in}}{C_p} = 0 \quad (A-4.24)$$

Similarly, the perturbed conservation equations for the two-phase region are

$$\frac{dw'}{dz} = \frac{A s v_{fg}}{v_{ss}^2 h_{fg}} h' \quad (A-4.25)$$

$$\frac{dh'}{dz} + \frac{s A}{v_{ss} w_{ss}} h' = \left\{ \begin{array}{l} -\frac{q_{h,ss}''' A w'}{w_{ss}^2} + \frac{(q_h''')' A}{w_{ss}} \text{ heated region} \\ 0 \text{ adiabatic region} \end{array} \right\} \quad (A-4.26)$$

$$\frac{dp'}{dz} + w' \left(\frac{s}{A} + \frac{f w_{ss} v_{ss}}{D A^2} \right) + h' \frac{v_{fg}}{h_{fg}} \frac{f w_{ss}^2}{2 D A^2} - \frac{g}{v_{ss}^2} + \frac{2 s w_{ss}}{A v_{ss}} + \frac{w_{ss}^2 v_{fg}}{A^2 h_{fg}} \frac{dh'}{dz} = 0 \quad (A-4.27)$$

Solutions of the perturbed differential equations for the heated single-phase region can be obtained as

$$w' = w'_{in} = \text{constant} \quad (A-4.28)$$

$$h' = \frac{1 - e^{-\tau_{sp} s}}{\rho_{ss,av} s} \left(-\frac{q_{h,ss}''' w'}{w_{ss}} + (q_h''')' \right) \quad (A-4.29)$$

where h'_{in} is the perturbed enthalpy at the inlet of core and $\tau_{sp} = (\rho_{ss,av} AL_{sp} / w_{ss})$ is the residence time of the fluid in the single-phase region of the heater.

$$-\Delta p'_{sp} = \left(\frac{s}{A} + \frac{fw_{ss}}{\rho_{ss,av} DA^2} \right) w' L_{sp} - \frac{g\sigma}{Cps} \left((q_h''') - \frac{q_{h,ss}'' w'}{w_{ss}} \right) \left(L_{sp} + \frac{w_{ss} (e^{-\tau_{sp}s} - 1)}{\rho_{ss,av} As} \right) \quad (A-4.30)$$

In the adiabatic single-phase region, the perturbed equations for flow rate, enthalpy and pressure drop were obtained from Eqs. (A-4.28) to (A-4.30) respectively, by setting Q_{ss} and Q' equal to zero. For the two-phase heated region

$$w' = w'_{sp} + \left(\frac{sA v_{fg}}{v_{ss}^2 h_{fg}} \right) \left[\frac{X}{r_1} (e^{r_1 L_c} - e^{r_1 L_{sp}}) + \frac{Y}{r_2} (e^{r_2 L_c} - e^{r_2 L_{sp}}) \right] \quad (A-4.31)$$

$$h' = X e^{r_1 L_c} + Y e^{r_2 L_c} \quad (A-4.32)$$

$$-\Delta p' = \left(\frac{s}{A} + \frac{fw_{ss} v_{ss,av}}{DA^2} \right) \left[w'_{sp} L_{tp} + \frac{Asv_{fg}}{v_{ss,av}^2 h_{fg}} \left\{ \frac{X}{r_1} \left[\frac{1}{r_1} (e^{r_1 L_c} - e^{r_1 L_{sp}}) - e^{r_1 L_{sp}} L_{tp} \right] + \frac{Y}{r_2} \left[\frac{1}{r_2} (e^{r_2 L_c} - e^{r_2 L_{sp}}) - e^{r_2 L_{sp}} L_{tp} \right] \right\} \right] + \frac{v_{fg}}{h_{fg}} \left[\frac{fw_{ss}^2}{2DA^2} - \frac{g}{v_{ss,av}^2} + \frac{2w_{ss}s}{Av_{ss,av}} \right] \left[\frac{X}{r_1} (e^{r_1 L_c} - e^{r_1 L_{sp}}) + \frac{Y}{r_2} (e^{r_2 L_c} - e^{r_2 L_{sp}}) \right] + \frac{w_{ss}^2}{A^2 h_{fg}} \left[X (e^{r_1 L_c} - e^{r_1 L_{sp}}) + Y (e^{r_2 L_c} - e^{r_2 L_{sp}}) \right] \quad (A-4.33)$$

$$\text{where } X = \left[-h'_{sp} (r_2 + As\rho_f / w_{ss}) - q_{h,ss}''' Aw'_{sp} / w_{ss}^2 + (q_h''') A / w_{ss} \right] / (r_1 - r_2) e^{r_1 L_{sp}} \quad (A-4.34)$$

$$Y = (h'_{sp} - X e^{r_1 L_{sp}}) / e^{r_2 L_{sp}} \quad (A-4.35)$$

$$r_{1,2} = \frac{1}{2} \left[-\frac{As}{v_{ss,av} w_{ss}} \pm \left(\left\{ \frac{As}{v_{ss,av} w_{ss}} \right\}^2 - \frac{4q_{h,ss}''' A^2 s v_{fg}}{v_{ss,av}^2 w_{ss}^2 h_{fg}} \right)^{1/2} \right] \quad (A-4.36)$$

where the positive sign applies for r_1 and negative sign applies for r_2 . h'_{sp} is the perturbed enthalpy at the inlet of boiling region of the channel. In the adiabatic two-phase region,

$$w' = w'_{in} + (w_{ss} / v_{ss}) (v_{fg} / h_{fg}) h'_{in} [1 - e^{-\tau L s}] \quad (A-4.37)$$

$$h' = h'_{in} e^{-\tau L s} \quad (A-4.38)$$

$$\begin{aligned}
-\Delta p' &= \left[\frac{s}{A} + \frac{fw_{ss}v_{ss}}{DA^2} \right] \left[w_{in}'L + \frac{w_{ss}v_{fg}}{v_{ss}h_{fg}} h_m' \left\{ L + \frac{w_{ss}v_{ss}}{As} (e^{-\tau_L s} - 1) \right\} \right] \\
&\quad - \frac{v_{fg}}{h_{fg}} \left[\frac{fw_{ss}^2}{2DA^2} - \frac{g}{v_{ss}^2} + \frac{2w_{ss}s}{Av_{ss}} \right] \left[(e^{-\tau_L s} - 1) h_{in}' \frac{w_{ss}v_{ss}}{As} \right] + \frac{w_{ss}^2 v_{fg}}{A^2 h_{fg}} (e^{-\tau_L s} - 1) h_{in}'
\end{aligned} \tag{A-4.39}$$

$$\text{where } \tau_L = (\rho_{in}AL / w_{ss}) \tag{A-4.40}$$

Similarly, the perturbed pressure drop due to bends, orifices and other restrictions in the single-phase region is given by

$$\Delta p'_{k,sp} = (K_{sp} / \rho A^2) w_{ss} w_{in}' \tag{A-4.41}$$

In the two-phase region,

$$\Delta p'_{k,tp} = (K_{tp} / 2A^2) \left[w_{ss}^2 h_{in}' (v_{fg} / h_{fg}) + 2w_{ss}v_{ss}w_{in}' \right] \tag{A-4.42}$$

The perturbed heat added/unit volume of coolant, (Q_h') , that appears in the above equations depends on the neutron kinetics and dynamics of heat transfer. This can be evaluated from the point kinetics model as follows:

$$\frac{dn}{dt} = \frac{k(1-\beta)-1}{l} n + \sum_{m=1}^6 \lambda_m C_m \tag{A-4.43}$$

$$\frac{dC_m}{dt} = \frac{k\beta n}{l} - \lambda_m C_m \tag{A-4.44}$$

where n is the neutron density, k is the effective multiplication factor, β is the delayed neutron fraction, λ_m and C_m are the decay constant and precursor concentration of delayed neutrons of group m respectively. Eqs. (A-4.43) and (A-4.44) are linearized by perturbing over the steady state as before to obtain

$$\frac{n'}{n_{ss}} = \frac{k'}{ls + \sum_{m=1}^6 \frac{s\beta_m}{s + \lambda_m}} \tag{A-4.45}$$

where n' is the perturbed neutron density and k' is the perturbed reactivity which is related to the void reactivity coefficient and Doppler coefficient as

$$k' = C_\alpha \gamma'_{av} + C_D T'_{f,av} \tag{A-4.46}$$

In the above equation, γ'_{av} and $T'_{f,av}$ are the perturbed void fraction and fuel temperature respectively averaged over the heated channel length. They can be estimated from the coolant density and the fuel heat transfer equations as discussed below.

Fuel heat transfer model

Assuming only radial heat transfer, the fuel heat transfer equation can be written as

$$m_f C_f \frac{dT_{f,av}}{dt} = Q_h(t) - H_f a_f (T_{f,av}(t) - T_{sat}) \quad (\text{A-4.47})$$

where m_f is the mass of fuel rods, C_f is the specific heat capacity of fuel, H_f is an effective heat transfer coefficient, $Q_h(t)$ is the heat generation rate in the fuel rods, $T_{f,av}(t)$ is the length average fuel temperature, a_f is the heat transfer area of fuel rods and T_{sat} is the coolant saturation temperature. Perturbing Eq. (A-4.47) over the steady state for $T_{f,av}(t)$ and $Q(t)$ and canceling the steady state terms, we get

$$T'_{f,av} (m_f C_f s + H_f a_f) = Q'_h, \quad (\text{A-4.48})$$

where Q'_h is the perturbed heat generation rate in the fuel rod. Applying the heat balance equation for the heat transfer from fuel to coolant

$$H_f a_f (T_{f,av} - T_{sat}) = q''_h A_c L_c. \quad (\text{A-4.49})$$

Perturbing Eq. (A-4.49) over the steady state and canceling the steady state terms we get

$$T'_{f,av} = (q''_h)' A_c L_c / H_f a_f. \quad (\text{A-4.50})$$

Substituting Eq. (A-4.50) into Eq. (A-4.48) and rearranging we get

$$(q''_h)' = q''_{h,ss} \frac{Q'_h}{Q_{h,ss}} \left[\frac{1}{1 + m_f C_f s / H_f a_f} \right] \quad (\text{A-4.51})$$

Since the heat generation rate in fuel is proportional to the neutron density, Eqs. (A-4.45) and (A-4.46) can be substituted into Eq. (A-4.51) to yield

$$(q''_h)' = G_f \gamma'_{av}, \quad (\text{A-4.52})$$

$$\text{where } G_f = \frac{C_\alpha / (1 + \tau_f s) (l s + \sum_{m=1}^6 \frac{s \beta_m}{s + \lambda_m})}{\frac{1}{q''_{h,ss}} - \frac{C_D A_c L_c}{H_f a_f (1 + \tau_f s) (l s + \sum_{m=1}^6 \frac{s \beta_m}{s + \lambda_m})}}, \quad (\text{A-4.53})$$

and $\tau_f = \frac{m_f C_f}{H_f a_f}$ is the fuel thermal time constant. The density of two-phase mixture is given by

$$\rho = \gamma \rho_g + (1 - \gamma) \rho_f. \quad (\text{A-4.54})$$

Perturbing Eq. (A-4.52) over the steady state and canceling for steady state condition, we get

$$\gamma' = -\rho' / \rho_{fg} = (\rho_{ss}^2 / \rho_{fg}) \frac{v_{fg}}{h_{fg}} h'. \quad (\text{A-4.55})$$

The channel average perturbed void fraction can be obtained by integration as

$$\gamma'_{av} = \frac{1}{L_c} \int_{z=L_{sp}}^{L_c} \frac{\rho_{ss}^2 v_{fg}}{\rho_{fg} h_{fg}} h' dz, \quad (\text{A-4.56})$$

which can be approximated after some algebraic simplification as

$$\gamma'_{av} = \psi_1 w'_{in} + \psi_2 q'_h, \quad (\text{A-4.57})$$

$$\text{where } \psi_1 = \frac{1}{L_c} \frac{v_{fg}}{h_{fg}} \frac{1}{v_{ss,av}^2} \frac{1}{h_{fg}} \left[\frac{X_1}{r_1} (e^{r_1 L_c} - e^{r_1 L_{sp}}) + \frac{X_2}{r_2} (e^{r_2 L_c} - e^{r_2 L_{sp}}) \right], \quad (\text{A-4.58})$$

$$\psi_2 = \frac{1}{L_c} \frac{v_{fg}}{h_{fg}} \frac{1}{v_{ss,av}^2} \frac{1}{h_{fg}} \left[\frac{Y_1}{r_1} (e^{r_1 L_c} - e^{r_1 L_{sp}}) + \frac{Y_2}{r_2} (e^{r_2 L_c} - e^{r_2 L_{sp}}) \right], \quad (\text{A-4.59})$$

$$X_1 = \frac{-q''_{h,ss} A}{w_{ss}^2} \left[1 + \left[(e^{-\tau_{sp} s} - 1) / \rho_{in} s \right] (w_{ss} / A) \left(r_2 + \frac{As \rho_{in}}{w_{ss}} \right) \right] / \left[(r_1 - r_2) e^{r_1 L_{sp}} \right], \quad (\text{A-4.60})$$

$$X_2 = \left\{ (q''_{h,ss} / w_{ss}) (e^{-\tau_{sp} s} - 1) / \rho_{in} s \right\} - X_1 e^{r_1 L_{sp}} / e^{r_2 L_{sp}}, \quad (\text{A-4.61})$$

$$Y_1 = \left[\left(\frac{e^{-\tau_{sp} s} - 1}{\rho_{in} s} \right) \left(r_2 + \frac{As \rho_{in}}{w_{ss}} \right) + \frac{A}{w_{ss}} \right] / (r_1 - r_2) e^{r_1 L_{sp}}, \quad (\text{A-4.62})$$

$$Y_2 = - \left[\frac{e^{-\tau_{sp} s} - 1}{\rho_{in} s} + Y_1 e^{r_1 L_{sp}} \right] / e^{r_2 L_{sp}}. \quad (\text{A-4.63})$$

Substituting Eq. (A-4.57) into Eq. (A-4.52) an expression for the perturbed heat added/unit volume of coolant (q'_h) to any channel i for a perturbation of channel inlet flow rate (w'_{in}) in the i_{th} channel can be easily obtained as given by

$$(q'_h)_i = \left(\frac{G_f \psi_1}{1 - G_f \psi_2} \right)_i (w'_{in})_i. \quad (\text{A-4.64})$$

Eq. (A-4.64) can be used to obtain the perturbed heat generation rates in the single-phase and two-phase regions of the heated channel. These can be further substituted into the perturbed pressure drop in single-phase and two-phase regions of the heated channel. Finally the characteristic equation changes accordingly.

Parallel Channel Stability:

In a multi-channel system in which the channels are connected between two plenums, out-of-phase instability can occur among the channels keeping the gross flow constant. So that

$$w'_{in} = \sum_{i=1}^N w'_{ch,i} \quad (\text{A-4.65})$$

The other boundary condition for analysing such a system is an equal pressure drop across the parallel channels, i.e.

$$\Delta p'_{H-SD} = (\Delta p'_{ch})_1 = (\Delta p'_{ch})_2 = \dots = (\Delta p'_{ch})_N \quad (\text{A-4.66})$$

$$\text{Since } \Delta p'_{c,i} = G_i (w'_{ch})_i \quad (\text{A-4.67})$$

$$\text{So } w'_{in} = \Delta p'_{ch} / \sum_{i=1}^N G_i = 0 \quad (\text{A-4.68})$$

$$\text{Or, the characteristic equation is } \sum_{j=1}^N \left(\prod_{k \neq j} G_k \right) = 0 \quad (\text{A-4.69})$$

APPENDIX 5. Nonlinear stability analysis for a single-phase NCL

The integral momentum equation applicable to one-dimensional single-phase flow in nondimensional form is (see Appendix-2 for the derivation).

$$\frac{d\omega}{d\tau} = \frac{Gr_m}{Re_{ss}^3} \oint \theta dZ - \frac{pL_t \omega^{2-b}}{2D Re_{ss}^b} \quad (A-5.1)$$

Similarly, the nondimensional energy equation applicable for the various segments of the loop can be written as

$$\frac{\partial \theta}{\partial \tau} + \phi \omega \frac{\partial \theta}{\partial S} = \begin{cases} \frac{L_t}{L_h} \text{ heater} & (\text{for } 0 < S \leq S_h) \\ 0 \text{ pipes} & (\text{for } S_h < S \leq S_{hl} \text{ and } S_c < S \leq S_t) \\ -St_m \theta \text{ cooler} & (\text{for } S_{hl} < S \leq S_c) \end{cases} \quad (A-5.2)$$

Nonlinear stability analysis is usually carried out by the direct numerical solution of the nonlinear governing equations (A-5.1) and (A-5.2) using the finite difference method. Before the calculations can commence the loop is divided into a number of small segments. A node separates two such segments (see Fig. A-5.1). Such nodes are the end nodes. Examples are N_h , N_1 , etc. in Fig. A-5.1. It may be mentioned here that there are several possibilities to solve these equations such as those listed below:

- 1) Explicit method for both energy and momentum equations,
- 2) Explicit method for one of the equation along with an implicit method for the other equation or
- 3) Implicit method for both the equations.

The method presented here solves the energy equation explicitly and the momentum equation implicitly. The energy equation for the various segments of the loop is discretised to obtain the following equations for the temperature of the i^{th} node at the new time step (i.e. $n+1$) as a function of the old (i.e. n^{th}) nodal temperatures at the i^{th} and $(i-1)^{\text{th}}$ nodes.

$$\theta_i^{n+1} = \theta_i^n \left[1 - \phi \omega_n \frac{\Delta \tau}{\Delta S} \right] + \theta_{i-1}^n \left[\phi \omega_n \frac{\Delta \tau}{\Delta S} \right] + \frac{L_t \Delta \tau}{L_h} \quad 1 < N \leq N_h \text{ (heater)} \quad (A-5.3)$$

$$\theta_i^{n+1} = \theta_i^n \left[1 - \phi \omega_n \frac{\Delta \tau}{\Delta S} \right] + \theta_{i-1}^n \left[\phi \omega_n \frac{\Delta \tau}{\Delta S} \right] \quad N_h+1 < N \leq N_{hl} \text{ and } N_c+1 < N \leq N_t \quad (A-5.4)$$

$$\theta_i^{n+1} = \theta_i^n \left[1 - \phi \omega_n \frac{\Delta \tau}{\Delta S} - St_m \Delta \tau \right] + \theta_{i-1}^n \left[\phi \omega_n \frac{\Delta \tau}{\Delta S} \right] \quad N_{hl}+1 < N \leq N_c \quad (A-5.5)$$

The explicit scheme has been used for the energy equation for which the stability criterion satisfying equations (A-5.3) to (A-5.5) is

$$\Delta \tau \leq \frac{1}{\frac{\phi \omega_n}{\Delta S} + St_m} \quad (\text{A-5.6})$$

To ensure stability, the calculated time step was multiplied with a number less than unity in the present calculations. The discretised momentum equation is

$$\omega_{n+1} + \frac{pL_i \Delta \tau}{2 \text{Re}_{ss}^b} |\omega_{n+1}| \omega_{n+1} = \omega_n + \frac{Gr_m \Delta \tau}{\text{Re}_{ss}^3} \theta_I \quad (\text{A-5.7})$$

$$\text{Where } \theta_I = \oint \theta_i^{n+1} dZ = \int_{Z_{N1}}^{Z_{N2}} \theta_i^{n+1} dZ - \int_{Z_{N3}}^{Z_{N4}} \theta_i^{n+1} dZ \quad (\text{A-5.8})$$

The limits Z_{N1} , Z_{N2} , Z_{N3} and Z_{N4} correspond to the elevation at nodes N_1 , N_2 , N_3 and N_4 (corner nodes) respectively (see Fig. A-5.1).

Calculation Procedure

The calculations can begin after selecting a node size. The marching calculations started with node 1 and (first node in the heater) equation (A-5.3) was used to calculate the nodal temperatures for $1 < N \leq N_h$. From $N_h + 1 < N \leq N_{hl}$ equation (A-5.4) was used. Similarly, equation (A-5.5) was used for $N_{hl} + 1 < N \leq N_c$. For the cold leg equation (A-5.4) was used for $N_c + 1 < N \leq N_t$. Once all the nodal temperatures are calculated the temperature integral, θ_I , is numerically evaluated using the Simpson's rule. Then ω_{n+1} is obtained by solving Eq. (A-5.7) numerically using the Newton-Raphson or the bisection method.

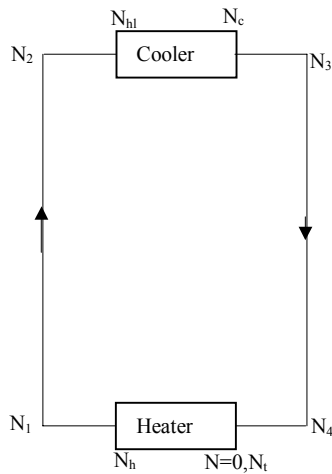


FIG. A-5.1. Nodalization for clockwise flow.

The adequacy of the nonlinear formulation can be checked by comparing with the analytical steady state equations. Also, the stability threshold predicted by the code can be compared with the corresponding threshold obtained by the linear method. For this comparison, the initial conditions corresponded to the steady state value for the orientation considered.

THE BOILING WATER REACTOR STABILITY

F.D'Auria, A.L. Costa, A. Bousbia-Salah

University of Pisa, Italy

Abstract

The purpose of this paper is to supply general information about Boiling Water Reactor (BWR) stability. The maintopics that will be approached are: phenomenological aspects, experimental database, modeling features and capabilities, numerical models, three-dimensional modeling, BWR system performance during stability, stability monitoring and licensing aspects.

1. INTRODUCTION

Currently, there are more than 80 BWRs operating as important contributors to electricity supply worldwide. But, in this type of reactor, safety margins obstruct the optimal exploitation of the plant because instability may occur under particular operating conditions. The stability of BWR reactor systems has been of a great concern from the safety and the design point of view.

Although events related to unstable behaviour occurred every now and then, stability was not a major issue for many years. Stability problems may only arise during start up or during transients which significantly shift the operating instructions for BWRs contain clear rules on how to avoid operating points (regions) that may produce power-void oscillations. Figure 1 shows an example of power-flow map for the Leibstadt NPP (Nuclear Power Plant) [1]. The lower right side of the plot marks the allowed operating region, the gray regime may only be entered if special measures are taken and finally, the black regime is forbidden due to stability concerns.

The current trend of increasing reactor powers and of applying natural circulation core cooling, however, has major consequences for the stability of new BWR designs. These modifications have allowed BWRs to work at high nominal power, but they have also favoured an increase in the reactivity feedback and a decrease in the response time, resulting in a lower stability margin when the reactor is operated at low mass flow and high nominal power. Also, the increase in core size has led to a weaker spatial coupling of neutronic processes, which result in a stronger susceptibility to so-called out-of-phase oscillations. In comparison to the situation in the seventies, the region of the power-flow map which has to be avoided grew to a respectable size. Instability events had been observed in commercial plants. Table 1 presents instability cases occurred in the last 20 years [2]. Some of the several instability events in BWR plants were inadvertent and other ones were induced intentionally as experiments. These instabilities were identified as periodic oscillations of the neutron flux via instrumentation readings. Essentially, neutronic power signals from Local Power Range Monitors (LPRM) and Average Power Range Monitors (APRM) have been used to detect and study the power oscillations.

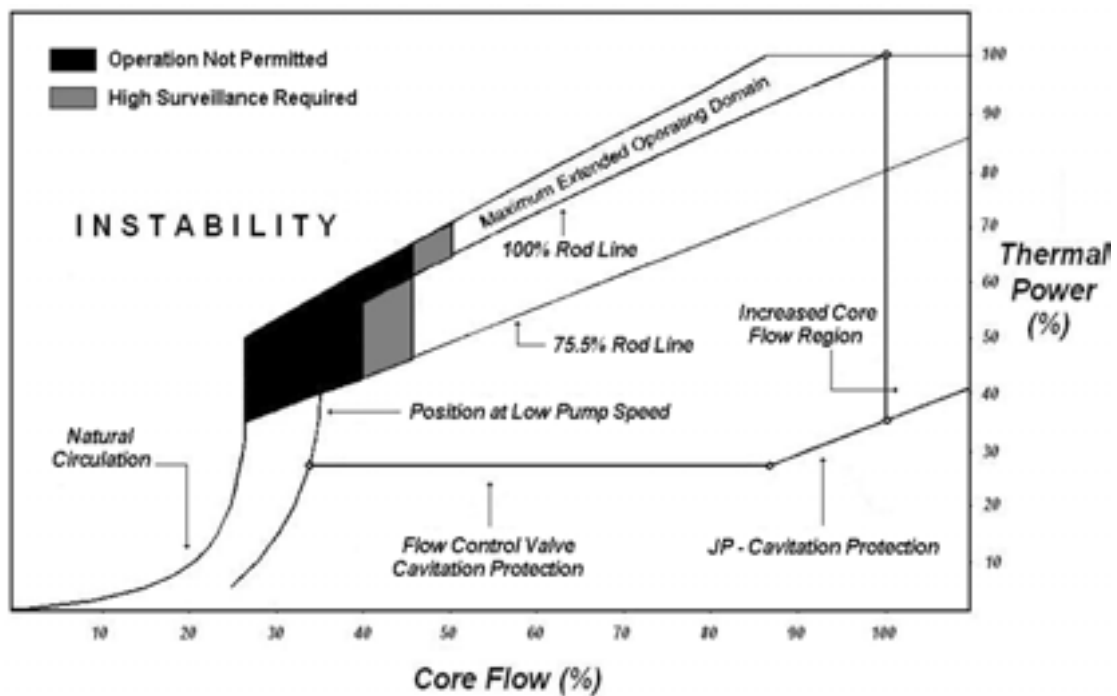


FIG. 1. Instability region in the power-flow map for the Leibstadt NPP.

After the first instability events, authorities in all countries required a review of the stability features of their BWRs. The authorities include analyses in the safety analysis reports and changes in the procedures and plant safety systems. The major safety concern associated with instability is the cooling of the fuel and cladding integrity. Consequently, the main objectives of BWR stability analyses could be summarized as follows:

- to assess the stability margins in reactor plant, including normal and off-normal conditions;
- to predict the transient behaviour of the reactor should an unstable condition occur;
- to help in designing and to assess the effectiveness of countermeasures adopted to prevent and mitigate the consequences of instabilities.

The purpose of this paper is to supply general information about BWR instability. The main topics that will be approached are: phenomenological aspects, experimental database, modeling features and capabilities, numerical models, three-dimensional modeling, BWR system performance during stability, stability monitoring and licensing aspects. Further information could be found with more details in the State of the Art Report on Boiling Water Reactor Stability (SOAR on BWR) [2].

Table 1. Summary of reported instability events

Date	NPP, Country, Manufacturer	Event
30.06.1982	Caorso, Italy, GE (General Electric)	It occurred during startup of the reactor. The reactor thermal power was 53.5% and the recirculation flow 38%. The operating point of the reactor entered the unstable region, the oscillations diverged and the reactor scrammed on high-high APRM signal (120% power).
13.01.1984	Caorso, Italy, GE	The second event occurred after trip of a recirculation pump and following loss of some preheater trains. The cold feed water and the strongly peaked axial power distribution led to neutron flux oscillations.
23.02.1987	TVO-I, Finland, ABB Atom	A power oscillation event took place when the plant was brought back to power after a short shutdown period. The reactor power was about 60% with a recirculation flow of 30% when increased APRM signal oscillations started to appear.
09.03.1988	LaSalle 2, USA, GE	Underwent a dual recirculation pump trip following which the unit experienced excessive neutron flux oscillations while it was in natural circulation. The resulting perturbation on the switches for anticipated transient without scram resulted in a trip of both recirculation pumps.
15.01.1989	Forsmark 1, Sweden, ABB Atom	After having carried out tests in several of the selected operating points, the stability boundary was very close. Moving from one point to another, the operator chose to switch from the pump speed control mode to the power control mode. This was done at 71% power and 4700 kg/s. A remaining control mismatch led to a small decrease in core flow. This, plus possibly an influence from the power control system, caused power oscillations with an amplitude that increased to about $\pm 20\%$ after 20 s, enough to initiate a pump run-down.
26.10.1989	Ringhals 1, Sweden, ABB Atom	In 1989 these NPP was starting up for a new cycle, power oscillations were observed in the core. During the oscillation, several LPRMs gave a high level alarm, indicating that the local power in those positions had exceeded 118 %. The core was stabilized about 30 seconds after the partial scram.
08.01.1990	Oskarshamn 2, Sweden, ABB Atom	A planned power reduction from 106% to 65% was performed. The power was reduced by reducing pump speed to minimum. After about 1 minute, power oscillations had developed, having peak-to-peak amplitudes of $\pm 10\%$. The APRM signals showed the oscillations to be in phase. A manual partial scram was performed which completely quenched the oscillations.
29.01.1991	Cofrentes, Spain, GE	Oscillations appeared after the operator withdraw control rods and reduced core flow in order to transfer the recirculation pumps from low to high speed.
03.07.1991	Isar 1, Germany, Siemens	The Isar 1 NPP had a trip of four internal recirculation pumps, due to a reduction in seal water flow to the 8 recirculation pumps. The power reduction due to the control rod insertion proved to be too slow to prevent the reactor from entering the unstable region of the power-flow map. Neutron flux oscillations with increasing amplitude appeared at about 50 % power and 30% core flow. When the oscillations reached peak-to-peak amplitude of 30 %, corresponding to a peak power of 67.5 % at 30 % flow, the reactor scrammed on the undelayed setpoint of neutron flux to core flow ratio. This occurred 44 seconds after the trip of the four recirculation pumps.

Date	NPP, Country, Manufacturer	Event
15.08.1992	WNP 2, USA, GE	The WNP 2 experienced power oscillations during startup. The event occurred early in cycle 8 operation. Upon recognizing the power oscillations, the operators manually initiated a reactor scram. Post event review indicated that the oscillations were in-phase and had grown to peak-to-peak amplitude of about 25 % of rated power.
09.07.1993	Perry, USA, GE	Entry into a region of core instability.
01.1995	Laguna Verde 1, Mexico, GE	During startup of the reactor, at 34% power, the operator was waiting to increase pump recirculation speed. Power was increased to 37% by control rod withdrawal and closure of the control valves of the pumps was initiated, thus leading to power reduction. During these operations the operator observed power oscillations with a tendency to diverge and he stopped the closure of the valves. At this time the peak-to-peak amplitude in the oscillations was 6%.
17.07.1996	Forsmark 1, Sweden, ABB Atom	Local oscillations due to a bad seated fuel assembly.
08.02.1998	Oskarshamn 3, Sweden, ABB Atom	Power oscillations due to a bad combination of core design and control-rod pattern during start up.
25.02.1999	Oskarshamn 2, Sweden, ABB Atom	Power oscillations after a turbine trip with pump runback.

2. PHENOMENOLOGICAL ASPECTS

Oscillations in two-phase systems may be originated or connected with different reasons ranging from delays between pressure and density waves propagation velocities, to change in the flow regime, to the interaction between conduction and convection heat transfer, to the feedback between thermal-hydraulic and neutronic parameters, to the presence of different parallel channels and of loops in parallel or in series with boiling channel. A number of modalities of oscillations, i.e. static, dynamic, with various frequencies, with constant or growing amplitudes, can be identified. The different causes and modalities of oscillations may co-exist and are at the origin of the complexity of some instability occurrences.

2.1. Classification

As a result some classifications of instabilities have been identified. These classifications can be based upon a) fundamental mechanisms, b) pattern of core oscillations, c) system interactions [2].

a) Classification based upon thermal-hydraulic fundamental mechanisms

The static instabilities are:

- Flow Excursion (Ledinegg type);
- Boiling Crisis;
- Relaxation types, including flow pattern transition, geysering and chugging.

The dynamic instabilities are:

- Density Wave oscillations;
- Pressure Drop oscillations;
- Acoustic oscillations;
- Thermal oscillations.

b) Classification based upon geometrical features of the oscillations

In this case the relationships between phases and amplitudes of the waves at different axial and azimuthal positions in the core of a reactor or of a reactor simulator are considered. Coupled neutronic-thermal-hydraulic and pure thermal-hydraulic oscillations can be distinguished, respectively. The following classification results:

- Core wide or in phase oscillations;
- regional or out-of-phase oscillations;
- single channel or local oscillations;
- punctual or not propagating oscillations (their existence can only be envisaged from the performed activity and considered documentation).

Most of the phenomena above can be explained making reference the concept of "harmonic modes" of the reactor diffusion equations.

c) Classification based upon system design

This classification is valid primarily for coupled nuclear-thermal-hydraulic systems (BWR plants), but may occur also in pure thermal-hydraulic systems. The overall system performance and the origin of oscillations are concerned. The following classification can be introduced:

- oscillations involving core-bypass;
- oscillations involving vessel downcomer;
- oscillations involving the entire primary loop (also referred as loop type oscillations);
- oscillations induced by the Balance of Plant, including the control systems.

This short outline demonstrates how the instability phenomena constitute a multidisciplinary subject, involving different technological areas like transient thermal-hydraulics, neutronics, fuel behavior and fuel cycle management, instrumentation, plant control and monitoring and detailed knowledge of plant features and operating conditions.

2.2. Definitions

It appears worthwhile to introduce a series of terms or expressions that are currently used in the stability analysis and in the present document giving them an agreed meaning or interpretation. Here are presented only some terms more used.

Acoustic instability: This occurs when standing waves are excited in a single or two-phase system with a frequency in the acoustic range: steam line resonance and acoustic instabilities in the steam dome and upper plenum regions of BWRs have been observed.

Balance of Plant (BoP): The Balance of Plant (BoP) in this report refers to components and systems, inside and outside the nuclear island, necessary to transform the thermal energy into electrical energy

with optimized overall efficiency and by hardware and software to control the entire plant performance.

Chimney: The chimney in a boiling water loop is intended as the zone of the riser comprised between the top of the core and the separators region.

Core Boiling Boundary Fraction: This is the ratio between the core power fraction up to the defined core average boiling boundary limit and the core power fraction required for coolant saturation.

Core or stability monitor: This is a sub-system specifically included in the monitoring system that accounts for core stability; the sub-system may only detect core stability or also take (automatically) effective countermeasures.

Coupled neutronic and thermal-hydraulic instabilities: They are the wide variety of oscillations occurring in BWRs which are the result of the interaction between thermal-hydraulic and neutronic phenomena. Core-wide, out-of-phase and local oscillations belong to this class.

Density wave: A density wave is a perturbation in the density of the fluid mixture, which travels along the heated channel with a characteristic speed depending on local conditions.

Dual oscillations: Simultaneous occurrence of in phase and out-of-phase oscillations.

Dynamic instabilities: These terms characterize the wider class of instabilities that can be studied only through the use of time-dependent balance equations.

Exclusion zone: In the BWR operating power/flow map, the exclusion zone is a region not allowed during the nominal operation of the reactor (see Fig. 1).

Flow biased APRM scram: The APRM signal is considered together with the core flow signal before taking control action in BWR plant.

Flow excursion (Ledinegg) instability: This is a type of static instability that is determined by the relationship between the pressure drop characteristic of a boiling channel and the pressure drop characteristic imposed by an external system.

Harmonic modes: Harmonic modes are represented by the eigenfunctions in which the general solution of the partial differential neutron diffusion equation, applied in a given domain (e.g., the reactor core) with appropriate boundary conditions (e.g., zero neutron flux at the extrapolated boundary), can be decomposed.

Kinematic wave: A wave that progresses with the speed of the fluid, either steam or liquid or two-phase mixture.

Monitoring system: Everything at hardware and software level that is used to detect reactor configuration (the core stability monitor is a part of this). For instance, the instrumentation used for measuring neutron flux, coolant flow, core inlet subcooling, pressure and Feed Water (FW) flow is part of the monitoring system.

Neutronic feedback: Thermal-hydraulic instabilities may occur even in out of core loops. Oscillation in thermal-hydraulic quantities may induce oscillations in neutronic related quantities (mostly, neutron flux), in in-core systems. Neutronic feedback identifies the physical variables carrying the (oscillatory) information from the neutron to the thermal-hydraulic domain and the resulting effects. The neutronic feedback occurs mostly (but not exclusively) through the average channel void fraction ("void coefficient") and the average fuel rod temperature ("Doppler coefficient").

Parallel channels: Different fuel elements up to including the entire core are reported as parallel channels. Parallel channel oscillations may be either "core wide" either "regional". These terms (i.e. parallel channel) are mostly appropriate for out of core test loops.

Phase delay: This is the phase shift between the phase of the oscillations of generic signal and the phase of a reference signal.

Pseudo Random Binary Sequence (PRBS): In the field of BWR stability, PRBS is a particular form of a perturbing signal adopted for checking stability in both reactor test conditions and calculations. It consists of alternate high and low values of a given parameter (e.g., a pressure setpoint) which are generally superimposed in a random like fashion to the nominal value with, eventually, some restriction on the mean value. When a PRBS is applied as an external forcing, the related system response can be used to characterize stability.

Single channel: This identifies a single fuel element of a BWR plant. Single unstable channel refers to a situation when only one of several parallel channels is oscillating in a stable system.

Stability boundary: A stability boundary is represented by a relationship between the parameters describing a system status which defines the conditions in which the system shows marginal (or neutral) stability, i.e. in which perturbations are neither amplified nor damped.

Stability margin: A stability margin is a properly defined measure of the distance of a system status from the stability boundary.

Static instability: These terms identify a class of instabilities that can be theoretically explained without the use of time-dependent conservation equations.

Thermal-hydraulic feedback: This includes all the thermal-hydraulic reaction mechanisms in a BWR plant that may intervene once an oscillatory condition arises in the core.

Thermal-hydraulic instabilities: These are identified by periodic time oscillations of various quantities in a boiling system (either single channel either parallel channels). Excursion of heated wall surface temperature may result from thermal-hydraulic instabilities.

Thermal Oscillations (THOs): Oscillations involving the heater dynamics in a boiling channel.

3. EXPERIMENTAL DATABASE

Loops offer many advantages for studies of two-phase flow thermal-hydraulics. An electrically heated mockup of a fuel assembly in a loop can be exposed to far more onerous operating situations (in terms of channel power and channel flow, for example) than could ever be permitted - for testing purposes - in the core of a reactor in commercial operation. Therefore, loop studies can be used to probe thermal-hydraulic operating limits of various fuel designs with respect to both dryout and flow stability (including the stabilizing influence of channel inlet orifices of various strengths), and also to study operating situations close to these limits. Moreover, loops can be used to investigate situations which differ significantly from those encountered during normal BWR operation (with regard to pressure, saturation temperature and inlet subcooling, for example). A fuel assembly mockup in a loop can be equipped with far more instrumentation than could be possibly introduced into the core coolant channels of operating BWRs. Notwithstanding the relevant importance of experimental data base, there are some drawbacks connected with loop or NPP experiments. For instance they are costly to build, and costly to run. This applies in particular to full-scale thermal-hydraulic testing of fuel assemblies at realistic BWR operating conditions, with respect to temperature and pressure. Cost reductions can be achieved via the use of scaled-down loops, but problems may then arise when it comes to extrapolating experience gained from such tests to the full-scale geometry. Further cost reductions may be gained by building low-pressure test loops that make use of alternative coolants with reduced boiling points, as compared to water.

3.1. Data from fundamental research

In modern BWRs, the number of parallel channels is so large (several hundreds) that the pressure head will remain essentially unaffected, even if one single channel were to experience undamped flow oscillations. On the other hand, when a heated channel in a loop experiment encounters undamped oscillations, the flow through the entire loop will oscillate - which normally influences the pressure drop over the channel. There are two ways of dealing with this problem:

- Introduce a bypass channel; this option demonstrates theoretically that if a test channel in a closed loop experiment is operated with a flow bypass in parallel, then this bypass will exercise a stabilizing influence on the pressure conditions at the inlet and outlet of the test channel - bringing the operating conditions of that channel closer to those representative of actual BWR cores. In this manner, improvements will be gained with respect to the applicability of the test results to realistic situations. However, reaching fully realistic BWR operating conditions in a test loop requires a very substantial bypass.
- Conduct the stability tests at natural circulation; the weight of the coolant in the downcomer of the loop then provides a constant pressure head. In this situation, all the single-phase pressure losses caused by friction in the downcomer and the piping leading to the inlet of the test section must be known accurately, since they all contribute to the flow-stabilizing pressure drop over the channel inlet orifice. Inertial effects in the flow through the same components must also be taken into account.

Unless either of these two measures are taken, flow stability experience obtained from loop experiments will not be directly representative of actual BWR core coolant channel operation. Nevertheless, results from such tests are still of great value for qualifying computer codes developed for numerical analysis of thermal-hydraulic stability. Such benchmarking exercises require that the modeling accounts for all the features of the entire loop which are of importance with respect to the flow dynamics.

3.2. Data from out-of-pile tests

In the late 1950's and the early 1960's, the first generation of modern BWRs were still in the stages of design and construction. Hence, any thermal-hydraulic issues of interest had to be investigated via either theory or loop experiments. A great number of such studies were made in those days, many of them addressing the topic of hydrodynamic stability of two-phase flows.

Up to the Eindhoven Symposium [3], the experimental studies largely addressed flow conditions up to the threshold of instability. Since then, considerable research effort has been directed towards investigations of what happens beyond that threshold. Among this studies, a more recent investigation, in the PIPER-ONE BWR simulator, installed at DCMN, led to characterize the "punctual" instability, or local instability, where is showed that in some situation, instability does not propagate along the channel axis. Amplitude of oscillations is close to zero at the channel inlet and outlet but it peaks around the zone of peak power [4]. Further experimental out-of-pile tests are described in the Appendix A1 as well as in the SOAR [2].

3.3. Data from in-core experiments

A limited number of experiments finalized to the study of stability, have been conducted in BWR NPPs. Some in-core experiments are described in the Appendix A2 and more details can be found in the reference [2].

4. MODELING FEATURES AND CAPABILITIES

A wide variety of codes and models exists that may be used to address the stability issues, ranging from sophisticated system codes, able to calculate an overall plant behaviour, to very simple models. All of them have the capability to deliver similar results to quantify stability, although reliability may be different. In fact, the objectives in the development and the level of approximation and of qualification, including the reliability of results, are different in the various cases. Multipurpose codes solving multi-dimensional equations both for neutronics and thermal-hydraulics are available. On the other hand, simplified codes based on Homogeneous Equilibrium Model (HEM) are still used in the same frame. Furthermore, in some cases qualification for BWR stability applications may include tens of applications to basic experiments, separate effect loop test and BWR plant occurrences; in other cases, it may be simply planned and just results, from predictions are presently available.

4.1. Numerical models

Various equation models are adopted for thermal-hydraulics and neutronics corresponding to different physical detail in the description. Space and time discretization of thermal-hydraulic balance equations is made by suitable numerical methods. Finite difference methods constitute a common choice, in which nodes representing the fluid contained in reactor components are connected each other through junctions, describing the related flow paths. The mass and energy balance equations are written in nodes, while momentum equations are written at junctions, making use of the staggered mesh technique which is acknowledged to improve numerical stability of the calculation. The donor cell principle is also used for calculating advection terms in mass and energy equations, assigning to the fluid at each junction the properties of the fluid in the upwind region; this principle has the fundamental role of assuring the transportive property of the numerical method, strongly affecting its numerical stability as well.

The type of time discretization adopted for thermal-hydraulic balance equations contributes to determine the effect of truncation errors on the calculated results. In particular, diffusion is responsible for smoothing out sharp propagation fronts in the calculated results, and for damping of free oscillations as a consequence of spurious energy dissipation. The latter phenomenon is particularly relevant for the simulation of thermal-hydraulic instabilities, and may lead to calculate stable conditions, whereas unstable ones would be expected on the basis of physical models.

In addition to the above described techniques, widely adopted in reactor thermal-hydraulics, time domain codes for the analysis of BWR stability adopt methods specially developed in the aim to improve computational efficiency or minimize truncation error effects. Integral formulations of momentum equations and higher order integration schemes are examples of these techniques.

A complementary effort has focused on the development of reduced order models, often consisting of a limited number of ordinary differential equation that represent the most important dynamical processes of a BWR. Muñoz-Cobo et al. [5] used DWOS_M_SU (Density Wave Oscillations with Modal Kinetics and Sub-cooled Boiling) to investigate the Cofrentes instability event (1991). The paper presents a study about the influence of the sub-cooled boiling on the feedback mechanisms that lead to the development of out-of-phase instabilities in boiling water reactors. In this sub-cooled boiling region the bubbles are formed in the walls (clad surface), and detach from the walls to travel to the sub-cooled region of the channel where they collapse. Because reactivity feedback is very sensitive to void variations and is axially weighted by a distribution factor that depends on the square of the power distribution. Then the void fraction variations in the sub-cooled boiling region will have a big contribution to the void feedback reactivity. In Figure 2 is displayed the power transferred to two opposite channels versus time. As can be observed, both powers are out-of-phase, i.e. while in one half of the reactor core the power attains its maximum value at the other half of the reactor core the power attains its minimum value.

4.2. System codes capable of simulating the BWR system

Computer programs are adopted to evaluate stability of BWRs and other boiling channel systems. In describing them, two classes are considered following a generally adopted classification:

- Frequency Domain Codes, whose purpose is the linear stability analysis of BWRs or other boiling systems. In the frequency domain, perturbing and Laplace transforming the neutron kinetics equations allow to easily include the fission power dynamics into the linear model for BWR stability. Examples of frequency domain codes can be seen in the Appendix B.1 (Tables B.1 to B.9).
- Time Domain Codes, which include analysis tools specifically developed to simulate the transient behaviour of plant systems; these codes have the capability to deal with the non-linear features of BWRs and are based in simulation techniques. Examples of time domain codes can be seen in the Appendix B.2 (Tables B.10 to B.26).

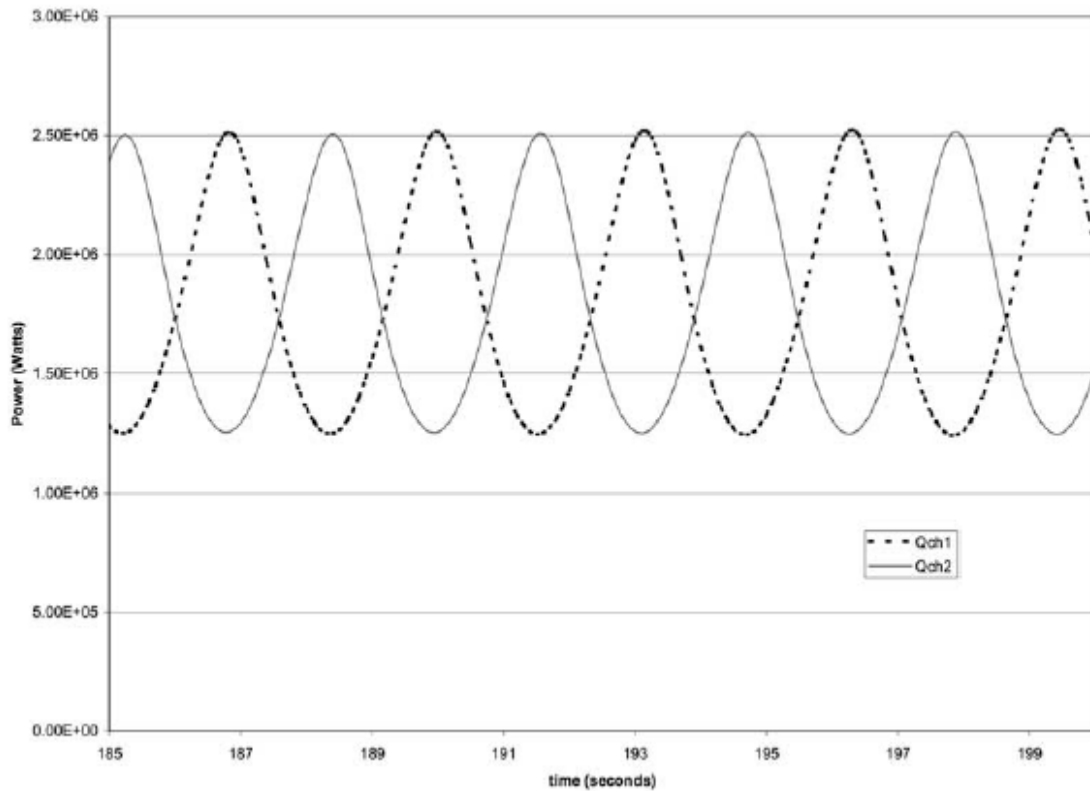


FIG. 2. Power transferred to two opposites channels versus time.

4.3. Current capabilities of system codes

Available models cover the whole range of phenomena observed in power reactors and experimental loops. This means that they are able to provide physical understanding of the evolution of meaningful quantities describing the transient behaviour of unstable boiling systems. It can be observed that the range of phenomena shown by models includes but it is even wider and denser than the one observed in experiments and reactor occurrences. In particular, the range of phenomena predicted by models is wider in connection with the extreme consequences of nonlinearities, e.g. the quasi-periodic or the non periodic behaviour.

The Appendix B presents information about codes whose application is most frequently reported in the literature concerning BWR stability. A more extended description can be found in the SOAR document [2] where is included also information about fuel dynamics and heat transfer, ex-core systems and assessment relevant to BWR stability.

4.4. Three-dimensional (3D) modeling

Nowadays, the coupled codes method, which consists in incorporating three-dimensional (3D) neutron modeling of the reactor core into system codes, is extensively used. It is particularly suited for simulating transients that involve core spatial asymmetric phenomena and strong feedback effects between core neutronics and reactor loop thermal-hydraulics. The recent 3D nodal neutron kinetic models usually employ planar meshes that are of the size of the fuel assemblies (or part of assemblies). In most of events, the complex three-dimensional nature of in-core coupled neutronic-thermal-hydraulic coupling processes will not play an important role in macroscopic plant behaviour. However, there exist those events in which the 3-D power distribution is strongly dependant on the plant dynamic [6]. Application of coupled code methods to the simulation of the stability events are reported in section 5.2.

Prediction by System Codes

The available literature on codes adopted for BWR stability reports many successful applications to out-of-pile and in-pile experiments, showing good agreement between observations and predictions. This supports the conclusion that presently available codes are capable to provide a detailed quantitative explanation of phenomena.

The coupled code RELAP5/PARCS was used by Costa et al. [7] to characterize the unstable behaviour of the Peach Bottom 2 Low-Flow Stability Test on the test point 3 [8]. This test was performed in the right boundary of the instability region of the power/flow map, i.e., in the area of low flow (around 38% core flow rate) and high power (59.2%). The Figure 4 shows the steady state mean axial power distribution. For the perturbation analysis, the reactor was disturbed with two peak pressure of 0.055 MPa. After the perturbation, the pressure oscillation turned to stable trend in few seconds. The same behavior was observed for the core power which exhibits damped oscillations ranging between 0.3 and 0.4 Hz (Figure 5). These values are typical frequency range of this kind of instability events.

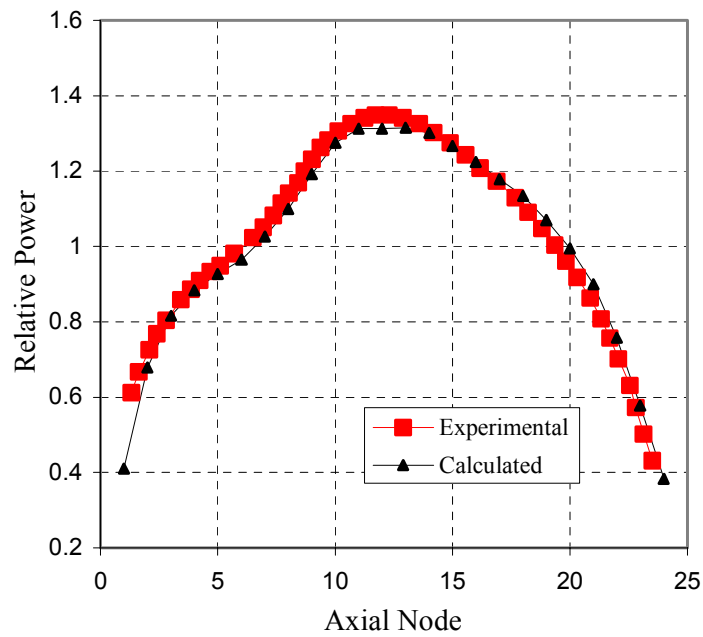


FIG. 4. Steady State mean power axial distribution.

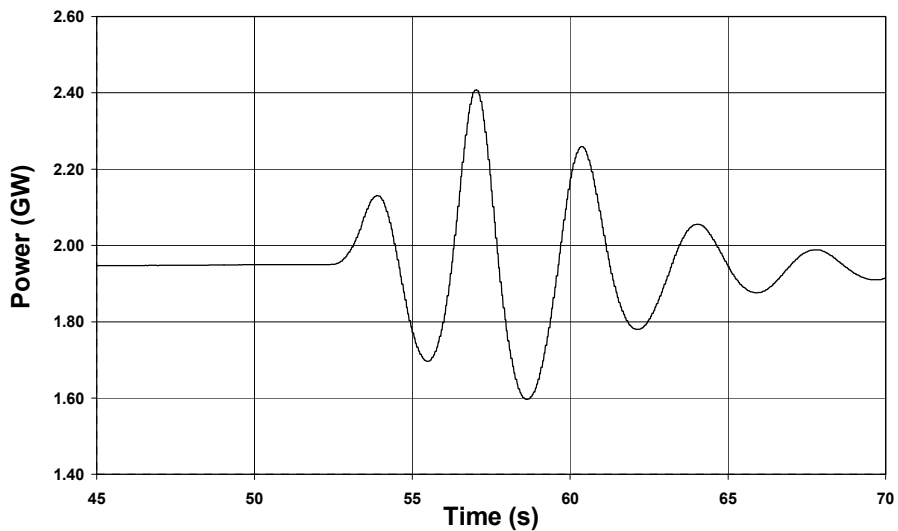


FIG. 5. Total reactor core power.

Solis et al. [9] developed a temporal adaptive algorithm to perform the synchronization and optimization of the performance of TRAC-BF1/NEM/COBRA-TF 3D neutron/thermal-hydraulics sub-channel analysis coupled system. The COBRA (Coolant Boiling in Rod Arrays) series of

programs was developed for the detailed analysis of boiling in rod bundles. The COBRA programs use a three-field representation of two-phase flow, modeling the liquid film and droplets separately. This code can only be used to analyze a portion of the reactor system and must be coupled to a system code, such as RELAP5-3D or TRAC-BF1, to perform an integrated analysis of the entire system [10].

To simulate the behaviour of a nuclear power reactor it is necessary to be able to integrate the time-dependent neutron diffusion equation inside the reactor core. In this way, it is interesting to develop fast and reliable methods to integrate this equation. Miró et al. [11] proposed a modal method to integrate the neutron diffusion equation in which the spatial part has been previously discretized using a nodal collocation method. The method has been implemented in a code called MODKIN. Five transients were studied; one of these was the behaviour of two operational points of the NPP Leibstadt (cycles 10 – in phase oscillation – and 7 – out-of-phase oscillation). With RAMONA code it is possible to obtain detailed information regarding the state of the reactor for each integration time step. To study the transients had used the nuclear cross-sections provided by RAMONA and had added the nuclear constants for the reflector nodes surrounding the reactor and the whole set is used as an input for the MODKIN 3D code. The power evolution for the in-phase case is represented in the Figure 6 where is observed the good agreement among the results calculated with both codes and shows the maintained limit cycle.

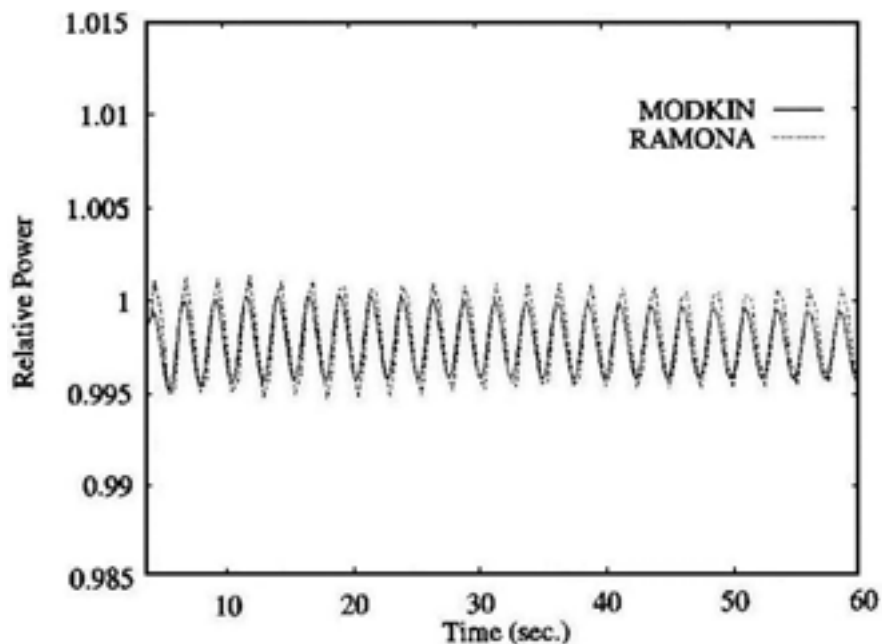


FIG. 6. Power evolution for Leibstadt in-phase case.

Hotta et al. [12] studied the applicability of TRAC/BF1-ENTRÉE to the regional instability. The fidelity of the numerical model was studied with regard to the thermal-hydraulic mechanism (density-wave oscillation) based on the FRIGG-4 loop test results. Electrically heated rods were arranged in three concentric circles. After measuring basic steady-state properties, such as pressure loss and void fraction, the stability limit power was measured at 11 natural circulation flow points by monitoring flow fluctuation with increasing power level. Among other conclusions, fidelity of the code was demonstrated in predicting the stability limit power and limit-cycle amplitude for a wide range of system pressures (based on the FRIGG-4 loop test). After, based on these results, Hotta and Ninokata [13] applied the system to the coupled neutronic-thermal hydraulic instability analysis and demonstrated that the system can predict the regional decay ratio under a wide range of operating conditions.

Hotta et al. [14], in a detailed work, also presented simulation results of a coupling system between the TRAC/BF1 and ENTRÉE codes based on the one-pump trip test performed in a Japanese BWR-5 plant. This reactor produces the rated heat output of 3293 MW (thermal), and the core was composed of 764 fuel assemblies. In the one-pump trip test, one of two recirculation pumps was intentionally tripped initiating a rapid decline in the core flow rate. The test was initiated at a relatively high-power (98%) and low-flow (86%) condition. In the Figures 7 (a) and 7 (b) are presented one of the various results obtained. The axial power profiles based on the bypass moderator density feedback were compared with the measured ones at two states. The inclusion of the moderator density feedback model improved the transient prediction since this would lead to less neutron slowing down in the upper region, and thus, the relative power level was suppressed in this part. At the initial state (see Fig. 7 (a)), a much better agreement was obtained. At the final state, the power skewed slightly upward due to the local control blade insertion, and the calculation slightly over-estimated this trend.

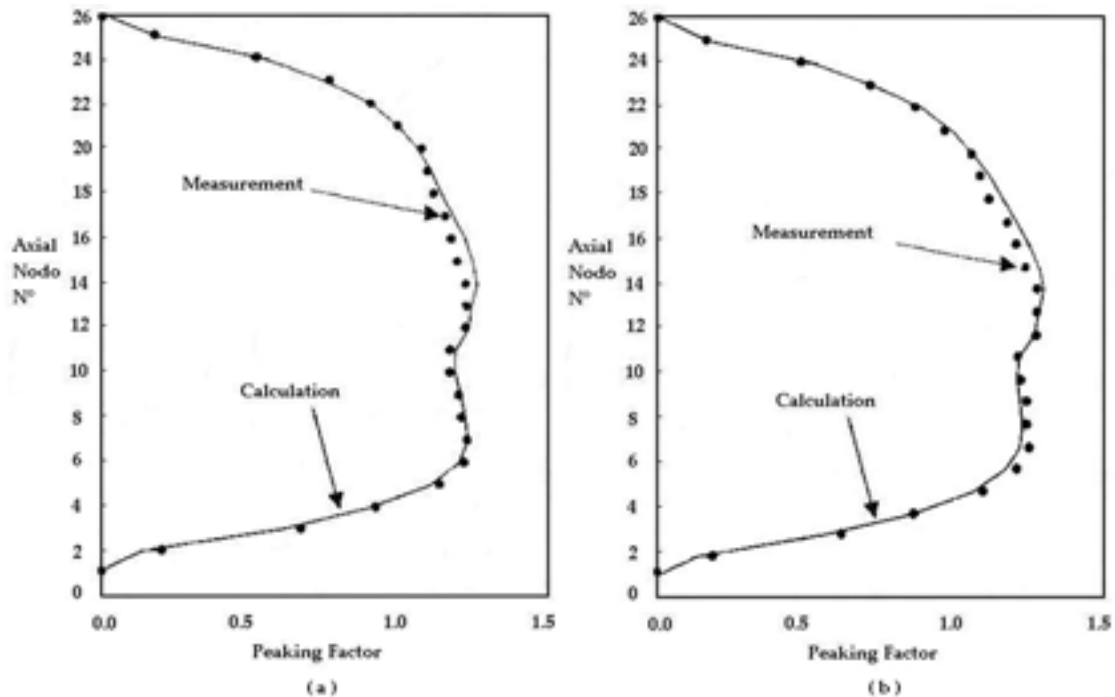


FIG. 7. Correlation between calculated and measured axial power profiles:

(a) initial state (0 s) and (b) final state (80 s).

5. THE BWR SYSTEM PERFORMANCE DURING STABILITY

5.1. NPP data (planned and un-planned events)

Some of the several instability events in BWR plants were inadvertent and other ones were induced intentionally as experiments. Several tens of stability tests have been performed in BWR plants. The following describes typical examples including sequences of events.

5.1.1. Planned Events

5.1.1.1. Peach bottom tests

One of the early stability tests was conducted at Peach Bottom-2 in April 1977 [8]. The reactor design was a 3293 MWt GE BWR-4 type and the stability tests were conducted along the low flow end of the rated power flow line, and along the power flow line corresponding to the minimum recirculation

pump speed. The reactor core stability margin was determined from an empirical model fitted to the experimentally derived transfer function between core pressure and the APRM signals.

Four test conditions for the low-stability tests were planned to be as close as possible to one of the following reactor operating conditions:

1. points along the rated power-flow control line (PT1 and PT2);
2. points along the natural circulation power-flow control line (PT2, PT3 and PT4);
3. extrapolated rod-block natural circulation power (test point PT3).

The main objective of these tests is to provide a data base for the qualification of transient design methods used for reactor analysis at operating conditions. The tests were performed in the right boundary of the instability region of the Power/Flow (Figure 3). During the stability testing was observed a strong effect of the xenon transient that carried to change lightly the planned tests.

5.1.1.2. TVO-2 tests

In November 1980, stability tests under natural circulation conditions were integrated into the normal start-up testing at TVO-2 [15]. It is an ABB ATOM internal pump type BWR with 2000 MWt rating. The reactor stability margin was evaluated by Fourier inversion of the transfer function from reactor pressure to APRM. This was obtained from measurements during sinusoidal perturbation of the turbine admission valve positions. Under natural circulation, established by tripping the pumps sequentially, four of the six pumps stopped and remained stationary while two pumps continued to rotate, driven by the flow and by inertia and connected with the respective engines. After the pump trip, reactor power was increased by control rod withdrawal. Self sustained neutron flux oscillations were recorded at 57.2% core power. The APRM signal oscillates almost purely sinusoidally at 0.34 Hz, with an amplitude of 5% of the rated power and in a global mode, i.e. the LPRM oscillated in phase at all radial locations.

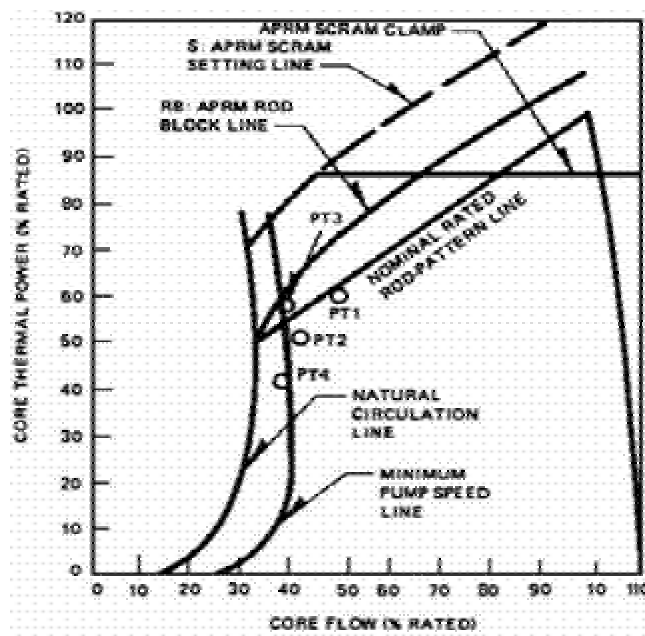


FIG.3 Peach Bottom-2 low-flow test conditions.

5.1.1.3. *Vermont Yankee tests*

The stability tests at Vermont Yankee in March 1981 [16], was one of the test during which oscillations were detected. The plant is equipped with a GE BWR-4 type reactor with 1593 MWt rated power. The tests were performed with recirculation pumps stopped (natural circulation) and with all pumps running at minimum speed. Control rod patterns were adjusted to achieve relatively high power levels. A limit cycle condition was achieved without perturbation at the highest power value under natural circulation. The limit cycle oscillation was suppressed when a few control rods were inserted slightly. Neither unusual behaviour nor equipment damage occurred.

5.1.1.4. *KRB-B and KRB-C tests*

The twin unit nuclear power plants KRB-B and KRB-C, each having a rated power of 3840 MWt, are BWR designed by KWU-Siemens. KRB-B and KRB-C stability tests were performed in April 1984 and November 1984, respectively [17]. The tests showed that both units were stable in normal operating range, and stable to the power level above the 100% control rod line at minimum recirculation pump speed. The limit cycles observed in neutron flux at slightly above the stability threshold power level, were characterized by out-of-phase oscillations: half of the core appeared to be out of phase with respect to the other half. The amplitude of APRM was only a fraction of the amplitude observed in LPRM. The out-of-phase oscillation mode developed from an initially more or less random situation and settled into a stable mode later on.

5.1.2. *Unplanned events*

Some of the inadvertent instability events in operating BWR plants are described below.

5.1.2.1. *Forsmark-1 event*

Forsmark-1 has been in operation since 1980. Originally, the core design output was 2711 MWt. This was referred as "100% power". In 1986, the core design output was raised to 2928 MWt, an up-rating of 8%. Forsmark-1 is a member of the ABB Atom supplied BWRs equipped with internal recirculation pumps. In each of the six ABB atom "internal pump plants", the coolant flow is measured via instrumentation that monitors the inlet flows to eight core coolant channels. When Forsmark-1 was in the power ascension phase, after the annual shutdown of 1987 for refuelling and maintenance, oscillations of unusually large amplitudes were observed in the APRM signal, shortly after reaching 65% power [18].

5.1.2.2. *LaSalle event*

LaSalle Unit 2 underwent a dual recirculation pump trip event [19], [20]. After the pump trip, the unit experienced an excessive neutron flux oscillation under natural circulation conditions. In addition, as a result of the rapid power decrease, the feedwater heater level control system was unable to control the level in the feedwater heaters and began isolating the extraction steam from the heaters. This resulted in a positive reactivity addition because cooler feedwater was being supplied to the reactor. This, in turn, caused a power increase further reducing the margins from instability. Approximately seven minutes after the recirculation pump trip, the reactor automatically scrammed on APRM neutron high flux (118% trip). Although the power oscillations were larger than expected, no fuel thermal or mechanical limits were exceeded during the event.

5.1.2.3. *WNP-2 event*

WNP-2 is a GE BWR-6 plant. The concerned reactor core consisted of two fuel types having slightly different pressure drops. On August 15 1992, WNP-2 experienced power oscillations during the start-up operation [21]. About 33 hours before the event, the operators commenced a controlled power reduction from full power to 5%; afterwards the power was increased again up to 34% and then held constant for 3 hours. The operators continued the power increase along the 30% flow line up to about

36% power. The operators then began closing one of the two flow control valves in preparation for shifting the associated recirculation pump to fast speed. During this period, when power and flow decreased along the 76% rod line to power and flow levels of about 34% and 27%, respectively, oscillations occurred. Manual scram followed-up. The post event review showed in-phase oscillations, core wide, with peak to peak amplitude of about 25% of the rated power. The primary cause of the oscillation was considered to be the very skewed radial and bottom peaked axial power distribution (1.92 and 1.62 radial and average axial peaking factor, respectively).

5.2. Consequences on fuel and clad integrity

Thermal-hydraulic flow instability may cause large fluctuations in the global or local neutron flux in BWR cores. The resulting power oscillations, at a frequency 0.4–0.5 Hz in the fuel rods will, however, produce fuel temperature and heat rate changes which are considerably damped and delayed (due to the thermal inertia), typically by a factor >10 and 85-90° out-of-phase relative to the imposed heat generation rate.

An extensive data base was collected and discussed in relation to fuel rod behaviour following cyclic thermal loads. This is mostly based upon recent findings obtained at the Halden reactor. As a main conclusion, it was found that there are large margins against cladding fatigue failure, partly due to the thermal damping by the fuel time constants. In addition, there is large margin to dryout as long as reverse flow is avoided following excessive amplitude oscillations; short dryout periods (cyclically followed by rewet) do not endanger the cladding integrity. The situation may be different under RIA (Reactivity Initiated Accident) conditions. Furthermore, recent experience shows that high burnup fuel may fail at energy releases as low as 30 Cal/g. This might have implications concerning the behaviour of high burnup fuel subjected to large amplitude oscillations.

The clad serves as a containment barrier to prevent radioactive fission products produced in the fuel from being released into the coolant. The cladding is subjected to rather severe stresses, both from the high-pressure coolant surrounding the fuel element, and by fission gas pressure and fuel swelling inside the fuel element. Above certain heat flux magnitudes, the heat transfer to the coolant will become unstable as a film of vapor forms to cover the fuel element surface. At this point the clad temperature will increase dramatically (several hundred degrees) leading to clad failure. This thermal limitation, known as the critical heat flux, is of primary concern in water-cooled reactor cores in which the coolant temperature is allowed to approach the boiling point.

6. STABILITY MONITORING AND LICENSING ASPECTS

As all areas in nuclear safety technology, there is a continuous feedback from operating experience, including stability events, to designers, to licensing authorities and vice versa (e.g. [22]). After investigation of the LaSalle 2 event by the licensee and further review by the NRC – Nuclear Regulatory Commission – (Bulletin N° 88-07) [23], the staff concluded that this event has significant generic safety implications.

6.1. Stability monitoring

Prevention, mitigation or suppression of the instabilities in a BWR plant constitute one of the safety operating requirement. So, instrumentation, mostly core related, plant control and protection systems, data interpretation and current strategies for prevention and mitigation, are considered. Among the implemented strategies, also as a follow up of specific requests by regulatory bodies, the “regional exclusion”, the “quadrant APRM”, the “power reduction”, and the extended use of the core monitors, can be mentioned. The regional exclusion implies the introduction of a forbidden region in the operational power-flow map; in a few cases, an expanded 'alarm' region is also introduced. The quadrant APRM consists in allowing the possibility of generating control signals, including scram, from regional APRM related signals. The power reduction is an event oriented strategy leading to automatic power reduction in the case of transients like pump trip and loss of feedwater pre-heaters.

Basically, a core (or stability) monitor consists or makes use of neutron detectors and signal preconditioning hardware, data sampling and recording, data analysis or process identification, estimation of the stability and data storing. An on-line feedback with the plant control system is avoided at the time being.

Examples are discussed, dealing with the use of stability monitors to detect sudden reductions of stability margins, to validate the exclusion region, to analyze stability test results, to follow the stability margins during an operational transient, to evaluate off-line stability, including the cases of core wide and regional oscillations, to predict stability boundaries (i.e. fixing the exclusion region) also as a function of fuel burn up.

Improvements in the performance of stability monitors can be envisaged in relation to the techniques for signal processing, i.e. noise analysis (limitations have been found in this area) and to the use as input signals of a larger number of plant signals including quantities like core flow and inlet subcooling, pump speed, feedwater flowrate and temperature.

As a general comment, it is noted that the number of LPRM is generally adequate for core stability monitoring. However, not all of these are directly and independently taken into account for deriving countermeasures. The recommendation is to give more emphasis to each LPRM, eventually improving the related reliability.

However, one of the several solutions designed is prevent operation in the region of the power-flow map most susceptible to oscillations using calculations to establish a region (the “exclusion region”) on the power-to-flow map in which instabilities are credible.

6.2. Regulatory issues and requirements

The stability issue deserved a strict and constant attention by the regulatory bodies throughout all the years since the BWR design, e.g. the item “Suppression of Reactor Power Oscillations” constitutes the General Design Criterion 12 of the US NRC, 10 CFR 50. Renewed attention was given to the problem after the Caorso event (owing to regional oscillations), the La Salle event (owing to the large recorded APRM power) and the WNP-2 (owing to the event occurrence notwithstanding the countermeasures taken following La Salle).

From the industry side, the two main options adopted so far to comply with the licensing requests can be summarized by “prevention” and “detect and suppress” solutions. A so called long term solution, implying modifications to the reactor protection system is under consideration.

Regulatory requirements and recommendations include areas like training of operators, procedures, changes in the protection systems, stability predictions for new core loadings, stability measurements and core monitors installation and qualification. In addition, reliability of methods used in the past to prove stability is considered questionable; in a few cases the amplitude of power oscillations revealed higher than expected, out-of-phase oscillations might grow without causing scram, fuel failures might be a consequence of dryout following oscillations.

Definitely, the review of the stability issue by the licensing authorities, led to an independent evaluation of the design basis and of the protection measures to guarantee the fuel failures limits during instability events.

6.3. The exclusion region in the BWR operational flow-map

The “interim corrective actions” establish three regions on the power to flow map that restrict plant operation. In the Figure 8, regions A and B require immediate actions to exit the regions, excluding restarting a recirculation pump [2]. Plants without adequate protection against regional mode instability must immediately trip the reactor upon entry into Region A. Operation in Region C is only allowed during reactor start-up. However common practise in all countries is to avoid operating

regions where power oscillations could occur. Because of the difference in the design of BWRs there is a variety of requirements and recommendations that have been issued by licensing authorities. Current regulatory requirements and recommendations include the following items:

- training of operators to handle instability;
- procedures to handle instability;
- changes in protection system;
- prediction of stability for new core loading;
- measurements of stability at start-up after refuelling;
- stability monitors.

Table 2 provides examples of requirements and recommendations that have been issued in different countries.

Percent of Rated Core Power

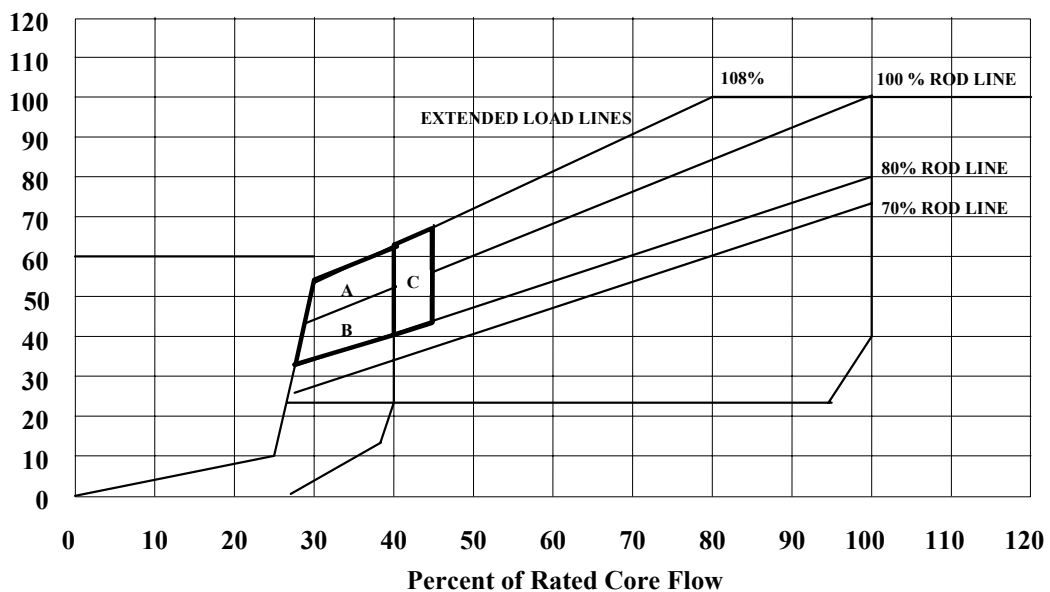


FIG. 8. Defined operating regions. Region A: reactor power greater than 100% rod line, core flow less than 40% of rated core flow; region B: reactor power between 80% and 100% rod lines, core flow less than 40% of rated core flow; region C: reactor power greater than 80% rod line, core flow between 40% and 45% of rated core flow.

Table 2. Requirements and recommendation to avoid regions of power oscillations

Country	Requirements and recommendation
Switzerland	<ul style="list-style-type: none"> operator training in handling power oscillations; restrictions in the operating region have been implemented; stability monitors are used because increased surveillance is requested near the exclusion region.
Sweden	<ul style="list-style-type: none"> have recommended that an overview of the operator training is to be made; measurements on core stability must be performed when new fuel types are introduced.
USA	<ul style="list-style-type: none"> procedural requirements must exist for initiating of manual scram under all operating conditions when all recirculation pumps trip or there are no pumps in operation.
Finland	<ul style="list-style-type: none"> improvements in the reactor protection system to detect oscillations, both global and regional, have been required.
Germany	<ul style="list-style-type: none"> automatic means of power limitation; precalculations or measurements are carried out after refuelling. That also includes regions outside the operating region where the reactor could end up after a transient.
Japan	<ul style="list-style-type: none"> all BWRs have implemented automatically selected rod insertion system and the operating region is defined to keep stable conditions; stability is checked by means of code calculations before each new fuel cycle.
Finland	<ul style="list-style-type: none"> the licensee is requested to define the limited stability values for power peaking factors and for control rod patterns; core supervision system will give an alarm if these limits are exceeded.
Netherlands	<ul style="list-style-type: none"> tests have been carried out to determine the stability of the Dodewaard reactor. The Dodewaard reactor is also equipped with an on-line monitor.
Spain	<ul style="list-style-type: none"> current technical specifications of the Spanish BWR plants consider the stability domain on the core flow-power map subdivided into three regions. For example, the Region I (Exclusion), characterized by core flow below 40 % and thermal power over the 100% load line, establishes that an immediate manual scram is required.

7. CONCLUSIONS

- Instabilities that may occur during the BWR operation constitute a widely known problem in the scientific community addressed for more than thirty years. A great deal of literature is available including data and models. The analysis of the phenomena involved requires a multidisciplinary approach comprising various areas like transient thermal-hydraulics, neutronics, fuel behaviour including in-core fuel management, instrumentation, plant control and monitoring, and detailed knowledge of plant features. The use of large thermal-hydraulic system codes should be promoted in this area, provided 3-D neutronics modeling and suitable numerics and specific user guidelines are implemented.

- All planned or unplanned instability events occurred in the region of low flow (around 30% core flowrate) and high power (around 50%). In a number of situations scram occurred, only in one case was the high neutron flux scram set point (118% nominal power) reached based on the APRM signal: the LaSalle 2 event. In all cases the oscillation frequency was around 0.5 Hz. Preventive and mitigative approaches have been used so far to deal with potential instability situations. Either systematic plant tests aiming at the identification of stability boundaries, or specifically developed monitoring techniques, or both of these, constituted the way to prevent undesired challenges to the scram system. In the area of monitoring, wide progresses have been observed as a consequence of the availability of powerful computers and of sophisticated techniques for noise analysis. An adequate number of LPRM transducers is available in each BWR plant.

Finally, the main conclusions and recommendations can be summarized below:

- Axial and radial power distributions have a strong influence on stability: the variation of these during the reactor life or during a transient may bring the core in a configuration prone to instability;
- Scram and coolant flowrate increase (when FW is available at nominal conditions), slight changes of control rod positions (including SRI) are typical countermeasures that can be taken, should an instability event originate;
- Reference experiments in qualified facilities and/or plant data should be used to develop a common understanding about suitability of predictive tools covering areas like user effect, uncertainties in boundary conditions, optimization of nodalization, capabilities of numerics;
- The sophistication and the qualification levels of core monitors could be largely improved and demonstrated, respectively;
- The execution of experiments in loops of different complexity allowed the identification and characterization of different types of instabilities;
- Experiments from out of pile facilities are necessary to qualify thermalhydraulic codes;
- The coupled codes method, which consists in incorporating three-dimensional (3D) neutron modeling of the reactor core into system codes, is particularly suited for simulating transients that involve core spatial asymmetric phenomena and strong feedback effects between core neutronics and reactor loop thermal-hydraulics;
- The use of calculations to establish a region (the "exclusion region") on the power-to-flow map in which instabilities are credible is essential to prevent operation in the region of the power-flow map most susceptible to oscillations;
- The review of the stability issue by the licensing authorities, led to an independent evaluation of the design basis and of the protection measures to guarantee the fuel failures limits during instability events;
- Current regulatory requirements and recommendations to avoid power oscillations regions include: training of operators to handle instability, procedures to handle instability, changes in protection system, prediction of stability for new core loading and measurements of stability at start-up after refuelling.

REFERENCES

- [1] HÄNGGI, P., Investigating BWR Stability with a New Frequency-Domain Method and Detailed 3D Neutronics, *Doctor Dissertation*, S. F. Institute of Technology Zurich, Switzerland (2001).
- [2] D'AURIA, F., AMBROSINI, W., ANEGAWA, T., BLOMSTRAND, J., IN DE BETOU, J., LANGENBUCH, S., LEFVERT, T., VALTONEN, K., State of the Art Report on Boiling Water Reactor Stability (SOAR on BWR), *OECD-CSNI report OECD/GD (97) 13*, Paris (1997).
- [3] EURATOM, Proceedings of "Symposium on Two-Phase Flow Dynamics" EURATOM, EUR 4288e, Vols. I and II, 4 - 9 September, Eindhoven, Holland (1967).
- [4] D'AURIA, F., PELLICORO, V., Local Instability in BWR Reactor Simulator, *ICONE-4 Conference*, New Orleans, USA (1996).
- [5] MUÑOZ-COBO, J.L., CHIVA, S., SEKHRI, A., A Reduced Order Model of BWR Dynamics with Subcooled Boiling and Modal Kinetics: Application to Out of Phase Oscillations, *Annals of Nuclear Energy*, 31, pp. 1135–1162 (2004).
- [6] BOUSBIA-SALAH, A., D'AURIA, F., BAMBARA, M., Sensitivity Analysis of the Peach Bottom Turbine Trip 2 Experiment, *Kerntechnik*, 69, pp. 7–14 (2004).
- [7] COSTA, A.L., MAGGINI, F., BOUSBIA-SALAH, A., D'AURIA, F., Peach Bottom Cycle 2 Stability Analysis Using RELAP5/PARCS, *UIT 2004*, Genova (2004).
- [8] CARMICHAEL, L.A. and NIEMI, R.O., Transient and Stability Tests at Peach Bottom Atomic Power Station Unit 2 at End of Cycle 2, EPRI Report NP-564 (1978).
- [9] SOLÍS, J., AVRAMOVA, M.N., IVANOV, K.N., Temporal Adaptive Algorithm for TRAC-BF1/NEM/COBRA-TF Coupled Calculations in BWR Safety Analysis, *Annals of Nuclear Energy*, 29, pp. 2127–2141 (2002).
- [10] WEAVER, W.L., TOMLINSON, E.T., AUMILLER, D.L., A generic semi-implicit coupling methodology for use in RELAP5-3D, *Nuclear Engineering and Design*, 211, pp. 13–26 (2002).
- [11] MIRÓ, R., GINESTAR, D., VERDÚ, G., HENNIG, D., A Nodal Modal Method for the Neutron Diffusion Equation. Application to BWR Instabilities Analysis, *Annals of Nuclear Energy*, 29, pp. 1171–1194 (2002).
- [12] HOTTA, A., HONMA, M., NINOKATA, H., MATSUI, Y., BWR Regional Instability Analysis by TRAC/BF1-ENTRÉE-I: Application to Density-Wave Oscillation, *Nuclear Technology*, 135, pp. 1–16 (2001).
- [13] HOTTA, A., NINOKATA, H., Numerical Study on Observed Decay Ratio of Coupled Neutronic-Thermal Hydraulic Instability in Ringhals Unit 1 under Random Noise Excitation, *Journal of Nuclear Science and Technology*, 39, pp. 138–149 (2002).
- [14] HOTTA, A., ANEGAWA, T., HARA, T., NINOKATA, H., Simulation of Boiling Water Reactor One-Pump Trip Transient by TRAC/BF1-ENTRÉE, *Nuclear Technology*, 142, pp. 205–229 (2003).
- [15] WAARANPERA, Y., ANDERSON, S., BWR Stability Testing: Reaching the Limit Cycle Threshold at Natural Circulation, *Trans. Am. Nucl. Soc.*, 39, pp. 868 (1981).
- [16] SANDOZ, A.A., CHEN, S.F., Vermont Yankee Stability Tests during Cycle 8, *Trans. Am. Nucl. Soc.*, 45, pp. 727 (1983).
- [17] DAYAL, D., PREUSCHE, G., BRANDES, L.P., FRANK, M., HECKERMANN, H., SEEPOLT, R., WACHTER, K.P., Stability Tests at KWU Nuclear Power Plants, *Proceedings of ANS Topical Meeting on Anticipated and Abnormal Transients in Nuclear Power Plants*, April 12–15, Atlanta, USA (1987).
- [18] BLOMSTRAND, J., SPENCER, A., GANEA, I., EKSTAM, L., REIBE, P., ADIELSSON, K., SCHWARTZ, F., KVARNSTRÖM, C., HÄLL, L.E., Noise Analysis of Core Coolant Channel Flow Signals, recorded in Swedish and Finnish BWRs, *Progress in Nuclear Energy*, 21, pp. 777–778 (1988).
- [19] US NRC, Augmented Inspection Team Report (AIT) Nos. 50-373/88008 and 50-374/880088 (1988).
- [20] WULFF, W., CHENG, H.S., MALLEEN, A.N., ROHATGI, U.S., BWR Stability Analysis with the BNL Engineering Plant Analyzer, *NUREG/CR-5816*, *BNL-NUREG-52312* (1992).
- [21] US NRC, Augmented Inspection Team (AIT) Report of WNP-2 No. 50-397/92-30 (1992).

- [22] LAURENCE, E., PHILLIPS, L., Resolution of US Regulatory Issues Involving Boiling Water Reactor Stability, *Proceedings of the OECD/CSNI International Workshop on Boiling Water Reactor Stability*, October 17–19, Brookhaven, Holtsville NY, CSNI Report 178 (1990).
- [23] US NRC, Power Oscillation in Boiling Water Reactors (BWRs), *NRC Bulletin No. 88-07*, Washington, USA (1988).

APPENDIX A1. OUT-OF-PILE TESTS

A.1.1. The FRIGG loop

The FRIGG loop was built by ASEA in the mid-1960's, and has been in operation since 1966. It is located in the ABB Atom Laboratories in Västerås, Sweden. Although its original design power was 8 MW, the loop was actually operated up to 9 MW occasionally during the late 1960's.

The test channels were equipped with an abundance of instrumentation, providing a wealth of detailed information. Three tests series were made for the 36-rod cluster geometry. Two of them are of interest, as regards flow stability:

- i) FRIGG-3 (channel FT 36 b). This test assembly combined a uniform axial power distribution with a non-uniform radial power distribution (which was varied to simulate the radial shape of the neutron flux depression in the fuel assemblies of the Marviken core). These measurements are of special interest in the context of flow stability, since a void impedance gauge had been installed at the exit of the test section which enhanced the two-phase pressure drop (detrimental to stability). Periodic flow oscillations were observed in several of the operating situations studied.
- ii) FRIGG-4 (channel FT 36 c). This test assembly made use of the same radial power distribution as in FRIGG-3, whereas the axial power distribution was of the "chopped cosine" type. This test series also made use of the above mentioned instrumentation at the channel exit. Although no periodic oscillations were encountered, the instability threshold was established via extrapolation of the flow noise.

The experience from the FRIGG-3 and FRIGG-4 tests has been used extensively for benchmarking of a variety of dynamic codes, for example various versions of RAMONA.

A.1.2. The Karlstein loop

This 15 MW loop has been designed and built by Siemens KWU. The facility, which has been operating since 1988, is located at the Siemens laboratories at Karlstein, in Germany. It is dedicated to the thermal-hydraulic development and testing of electrically heated mockups of fuel assemblies for both BWRs and PWRs. For BWR applications, the loop is fully qualified for testing of full-scale fuel assemblies.

The tests were conducted at natural circulation, in order to realise the "parallel channel boundary condition". The data recorded comprise: operating pressure, inlet subcooling, coolant mass flow at inlet and outlet of test section, surface temperatures of heater rods, differential pressures (downcomer, inlet, exit), etc.

The measurements were initiated at stable conditions, with fixed power and subcooling. For assessing the detailed stability characteristics, pseudo-random binary signals (PRBS) perturbations of the power input to the heated rods were imposed - for half an hour. Their amplitude was chosen so as to provide a significant signal response, while remaining within the linear domain. The decay ratio was then evaluated from the signal recordings.

This procedure was repeated as the bundle power was increased stepwise, in a gradual approach to the stability threshold. Further power increase was found to produce limit cycle oscillations. Their amplitudes turned out to depend on the power level. These power increases were allowed to continue, until periodic dryout and rewetting was observed. This procedure made it possible to establish the threshold power for boiling transition during flow oscillations. No data is available from this facility.

A.1.3. The ATLAS loop

This 17 MW full-scale thermal-hydraulic test facility for BWR fuel assemblies has been built by GE. It is located in San Jose, California.

ATLAS was built as a separate effects not as a system test facility. Thus, it was not configured for performing stability tests for single fuel bundles. Due to the complexity inherent in the BWR stability process (Parallel channel interactions, neutronic gain, excitation of higher harmonic modes, sensitivity to reactor operating state parameters such as core power distribution effects, etc.) GE's approach has been to perform stability testing of actual operating BWR's and to qualify computation models to the reactor test data which includes the coupled thermal hydraulics and neutronic phenomena. GE believes that the best approach for understanding and designing for BWR fuel stability is by reactor qualification of very sophisticated computer codes. Of course all the fuel component pressure drop loss coefficient data generated at ATLAS were a vital part of the stability assessment process.

A.1.4. The NFI loop

This 1.8 MW NFI loop was designed and built by NFI. The loop has been operating since 1993 and it is located at NFI Tokai-mura. The loop is designed for high temperature steam and water two-phase flow tests. The maximum working pressure and temperature are 9.8 MPa and 580 K, respectively. The large volume of the steam separator/condenser provides stable loop operation during the flow oscillating stability test. The total capacity of 1.8 MW dc electric power from the two rectifier units is shared by two test channels. The thermal-hydraulic testing that has been conducted so far includes single and two-phase pressure drop tests, flow-induced rod vibration tests, dry-out and post dry-out tests, and thermal-hydraulic stability tests in the parallel channel configuration.

The parallel channel test parameters included variations of flow rate, inlet, subcooling, inlet orifice, size, and axial power profile, i.e. uniform, chopped cosine and bottom peaked power distributions. The stability threshold was measured by increasing the test channel power until the amplitude of the inlet flow oscillation became larger than the noise level. Beyond the threshold, the inlet flow exhibited typical density wave oscillation with frequency of 0.2 to 0.6 Hz. This stationary limit cycle oscillation extended the flow amplitude to several tens of a percent at which periodic dry-out and rewetting were observed by the heater temperature measurements.

The test data were analyzed by the NFI stability analysis code STAIF-PK. The predicted threshold powers were always below the measured data. Agreement between data and predictions of the natural frequency was good. It was concluded that the conservative predictions by the STAIF-PK code imply a certain margin of the channel stability for the newly designed 9x9 fuel, since the stability performance of this fuel has been designed using the STAIF-PK code.

Among various results, it was found that a subcooling increase causes a decrease in the power threshold for oscillations, this effect is less pronounced when a high pressure drop inlet orifice is adopted.

A.1.5. The BEST loop

The acronym for BEST is BWR Experimental loop for Stability and Transients tests. This test facility was built by TOSHIBA in the early 1980's. The mechanism operating conditions for the loop are 10.3 MPa (fluid pressure), 538 K (fluid temperature), 6 MW (heated bundles power) and 17 kg/s (bundles flowrate). The facility can be used for investigating both steady-state and transient characteristics of various thermal-hydraulic conditions that may be encountered in BWR operation, for example: unusual combinations of high power and reduced coolant flow, thermal-hydraulic stability, exceptional transients, boiling transition, post-dryout, etc. Testing can be made of full-length bundles of BWR fuel assemblies, of reduced width.

In the early 1980's, stability tests were conducted which involved 2x2 lattice bundles: representing a reduced width version of an 8x8 lattice assembly. The stability tests which have been conducted in

recent years have involved a 3x3 lattice bundles, a reduced width version of an advanced High-Burnup 9x9 lattice assembly design (STEP-III type A). A substantial flow bypass was used in all these tests, to realise the “parallel channel condition”.

As regards the above mentioned advanced High Burnup fuel STEP III, there are two design versions: type A and type B. The thermal-hydraulic testing of the type A version of this fuel design was made in the BEST loop. The stability tests made use of a bypass section which was heated by an 8x8 lattice bundle. The actual tests addressed conditions up to the instability threshold, comprising investigations of the effects on stability of parametric changes in inlet mass flow, inlet subcooling and axial power profile, as well as the inclusion in the test bundle of part-length fuel rods.

A.1.6. The PIPER-ONE loop

Under the sponsorship of ENEA, the DCMN of the Pisa University (in Italy) commenced the design and construction of this loop in 1981. It is located at the Scalbatraio Laboratory, in the vicinity of Pisa. It was first operated in 1985.

The loop is an integral facility designed for reproducing the behaviour of BWR thermal-hydraulics in operating situations which are dominated by gravity forces. The main objective of the research is to provide experimental material that can be used to qualify computer codes for thermal-hydraulic analysis for simulating a variety of operating situations, for example flow stability.

The coolant channel was designed to permit testing of a full-length 4x4 lattice rod bundle also including the unheated length. The maximum power of the loop is slightly more than 300 kW, corresponding to about 30% of the nominal linear power of the reference BWR. The rods are indirectly heated with chopped cosine axial power distribution. The loop operates at natural circulation (which is convenient for flow stability testing) and can be used up to pressures of 10 MPa.

Instabilities have been analyzed by transforming into the frequency domain the time trends signals got from the experiments, the FFT (Fast Fourier Transform) was applied to the signals from pressure transducers (7 of these are installed throughout the core simulator).

A “quasi” stable limit cycle was observed by cross correlating DP signals along the core. The fundamental frequency of the oscillations was found at about 0.5 Hz. Unsteady dryout and rewet cycles were also observed.

A more recent investigation, led to characterize the “punctual” instability. Essentially, the use of the FFT technique showed that in some situation, instability does not propagate along the channel axis. Amplitude of oscillations is close to zero at the channel inlet and outlet but it peaks around the zone of peak power. Thermal-hydraulic mechanisms for rise and smoothing of instabilities appear to exist. 3D phenomena inside the bundle and friction could be important in this respect.

A.1.7. The FIST loop

In the early 1980's, a series of natural circulation tests was conducted in the FIST facility. They were done covering a wide range of powers, water levels and system pressures. This facility is a full height and full pressure BWR test loop. It was built in the late 1970's, and is located in San Jose, California. It was designed to investigate system responses to various transient events, including stability. In fact, FIST is an acronym for Full Integral Simulation Test. The facility is volume scaled by a ratio of 1/624 to a BWR/6 plant containing 624 fuel assemblies (such as Cofrentes, in Spain). The core is represented by an 8x8 electrically heated bundle.

In more detail, the facility embodied an accurate simulation of the complete BWR recirculation system, including two small functional jet pumps, full height test vessel and internals, and correctly scaled fluid volume distribution and flow resistances. The heated fuel bundle (including rod power distributions, spacers, zircaloy fuel channel, upper and lower tie plates) was faithfully simulated, and the same applied to the bypass region and the fuel leakage paths.

APPENDIX A2. IN-CORE EXPERIMENTS

A.2.1. The Halden Reactor

The OECD Halden Project operates a small (20 MW) natural circulation BHW, cooled and moderated by heavy water. It is located at Halden, in southern Norway, and was built in the late 1950's. The core is of the open-lattice type, containing about 100 fuel assemblies - all located within individual coolant channels which are rather widely spaced out. As regards stability, the following comments are pertinent:

- i) The coolant channels are free-standing without any supply tubes (where single-phase inertial effects might influence the stability characteristics).
- ii) Since the heavy water is close to saturation, there are virtually no effects from inlet subcooling on stability.
- iii) Almost all the moderation takes place in the heavy water located in between the channels. It follows that void variations which may occur within the coolant channels do not produce any significant reactivity feed-back via the fuel on the channel flow stability. Under these conditions, any periodic channel flow fluctuations which may appear are of purely thermal-hydraulic nature.

The issue of flow stability in the Halden Reactor was first investigated in 1964. These initial studies led to the design of an advanced test assembly to be used for more detailed investigations of the power removal capacity of a coolant channel in that reactor, as regards both dryout and stability. These test assemblies differed from the normal assemblies used in the reactor, as regards design, fuel weight and enrichment. The test channel was equipped with:

- i) an externally operated orifice at the channel inlet, making it possible to study the influence of the inlet throttling on flow stability over a very wide orificing range;
- ii) extra instrumentation at the channel exit. The corresponding pressure loss came to exercise a significant influence on the stability characteristics of the channel flows.

A.2.2. The Nordic BWRs of the design generation with internal pumps

Six of the Nordic BWRs are equipped with instrumentation for monitoring inlet flows to a number of core coolant channels. In these reactors, it is possible to make simultaneous observations of:

- i) channel flow fluctuations of purely thermal hydraulic nature (via the flow monitoring instrumentation);
- ii) coupled flow fluctuations which involve neutron feedback via the fuel.

Some experience from studies of these phenomena were conducted around the mid-1980's. They refer to conventional 8x8 lattice fuel, as well as the modified design of the same lattice fuel called SVEA-64 which was being introduced in some of these reactors at that time.

As regards the 8x8 lattice fuel, analyses of signal recordings that had been made in several of these plants showed that the two oscillatory phenomena mentioned above coexisted in the core, but appeared at different frequencies and had different damping characteristics. For example, at the minimum core coolant flow permitted at full power, the channel flows were found to fluctuate incoherently - and significantly faster (at about 1–1.1 Hz) than the neutron flux (at about 0.75 Hz), which indicates the frequency of the coherent components in the channel flow fluctuations. It was observed that the flow fluctuations through the individual channels were strongly coupled to the corresponding channel power, the flow noise levels depending almost linearly on the channel power.

During operation at stretch-out, the frequency of the flow fluctuations gradually increased up to about 1.4 Hz, which was reached at the upper end of the permitted core coolant flow range, at full power.

Conversely, when the core power was lowered via the core coolant flow along the flow control line (from full power and minimum permitted coolant flow), the frequency of the flow fluctuations was reduced. At 75 % power, for example, their frequency had fallen to 0.7 Hz — while the flow noise levels had increased.

In the operating situation studied, it was found that while the neutron flux had oscillated at 0.49 Hz with a decay ratio of 0.8, the four individual channel flows involved in the recordings had fluctuated at characteristic frequencies that ranged from 0.43 Hz up to 0.56 Hz, with decay ratios lower than 0.3. In this operating situation, the neutron flux and channel flows had reached frequencies that were at least of a similar order of magnitude, even though their damping properties differed significantly. Coherence studies showed that the channel flows had fluctuated independently of each other, and even of the neutron flux — despite the rather high decay ratio for the core.

APPENDIX B. CODES MORE FREQUENTLY REPORTED IN THE LITERATURE CONCERNING BWR STABILITY

B.1. Frequency-Domain Codes

Table B.1. Characteristics of FABLE/BYPASS code

Code	FABLE/BYPASS
Property/ Developer	<ul style="list-style-type: none"> • General Electric, USA
Capabilities	<ul style="list-style-type: none"> • 1D parallel channel (plus bypass) thermal-hydraulic simulation of the core • Point neutron kinetics • Calculation of the Decay Ratio • Simplified ex-core modeling • Adopted to confirm that new fuel design meet NRC acceptance criteria and define boundaries of exclusion region
Thermal- hydraulics	Multi-channel + bypass model; Mixture equations with subcooled boiling; Bankoff Slip correlation
Neutronics	Point neutron kinetics with void reactivity feedback; Void feedback based on flux squared weighting of nodal void reactivities from PANACEA 3D wrapup data; Axial variation in parameters such as control fraction not accounted for; Method of evaluating void coefficient tied to qualification basis and application procedure

Table B.2. Characteristics of HIBLE code

Code	HIBLE
Property/ Developer	<ul style="list-style-type: none"> • Hitachi, Japan
Capabilities	<ul style="list-style-type: none"> • 1D parallel channel thermal-hydraulic simulation of the core • Point neutron kinetics • Calculation of the Decay Ratio by linear Laplace transformed equations • Simulation of different BWR types: jet pumps and internal pumps • Simulation of pressure tube type reactors • Simulation of experimental test loops
Thermal- hydraulics	Three equation slip flow models; Options for two-phase flow correlations; Up to 20 channel groups
Neutronics	Point neutron kinetics with six delayed neutron groups; Coolant density and Doppler reactivity considered.

Table B.3. Characteristics of K2 code

Code	K2
Property/ Developer	<ul style="list-style-type: none"> • Toshiba, Japan
Capabilities	<ul style="list-style-type: none"> • 1D parallel channel thermal-hydraulic simulation of the core • Point neutron kinetics • Calculation of the Decay Ratio • Simulation of different BWR types: jet pumps and internal pumps • Simulation of experimental test loops • Licensing code for TOSHIBA BWR
Thermal- hydraulics	Three equation drift-flux model for parallel channels; Options for physical law from design correlations: void-quality, subcooled boiling, Δp ; Several channel groups; one group for bypass; Linearization of the equations and Laplace transformation
Neutronics	Point neutron kinetics with six delayed neutron groups; Laplace transformation of basic equations; Neutron flux transfer functions for fundamental and higher mode; Higher mode transfer function calculated from the higher mode subcriticality obtained by a 3D code; Transfer functions of fundamental and higher modes used for core-wide and regional oscillations respectively.

Table B.4. Characteristics of LAPUR 5 code

CODE	LAPUR-5
Property/ Developer	<ul style="list-style-type: none"> • Nuclear Regulatory Commission, USA • ORNL, USA
Capabilities	<ul style="list-style-type: none"> • Core-wide, out-of-phase, and channel decay ratios from calculated frequency-domain transfer functions • 1D parallel channel (maximum of 7) TH simulation of the core with dynamic flow redistribution • Full Laplace domain (i.e. not just along the imaginary axis) pole search for increased decay ratio estimate accuracy
Thermal- hydraulics	Two-fluid slip model in the core; Non-equilibrium (subcooled boiling) model; Integral formulation of ex-core vessel components (recirculation loop); Core pressure/flow boundary conditions are automatically selected to estimate the core-wide or out-of-phase oscillation modes.
Neutronics	Point kinetics for core-wide neutronics; Out-of-phase mode neutronics modelled using the point kinetics equivalent equations for the first subcritical mode; Reactivity feedback calculated as power-square average of "local" reactivity contributions; Density reactivity coefficient may be input as a polynomial of local density or it may be calculated by LAPUR-5 based on 2-group cross sections and control-rod positions.

TableB.5. Characteristics of NUFREQ code

Code	NUFREQ
Property/ Developer	<ul style="list-style-type: none"> R.T. Lahey, G. Yadigaroglu (General Electric)
Capabilities	<ul style="list-style-type: none"> Simulation of simple two-phase sections or loop Point neutron kinetics
Thermal- hydraulics	Homogeneous equilibrium flow for a single channel; ρ_p adjusted with correction factors; Linearization of the equations and Laplace transformation
Neutronics	Simple point neutron kinetics; Reactivity coefficients for void and Doppler; Linearization of the equations and Laplace transformation.

Table B.6. Characteristics of NUFREQ-NP code

Code	NUFREQ-NP
Property/ Developer	<ul style="list-style-type: none"> RPI, USA
Capabilities	<ul style="list-style-type: none"> 1D parallel channel TH simulation Coupling with point, 1D, 2D or 3D neutron kinetics models Ex-core recirculation dynamics
Thermal- hydraulics	Three balance equations in the liquid region of the channel; Four equations drift-flux model with thermal non-equilibrium in the subcooled boiling region; Thermal equilibrium drift-flux model in the bulk boiling region.
Neutronics	Coupling with models for point, 1D, 2D or 3D kinetics

Table B.7. Characteristics of ODYSY code

Code	ODYSY
Property/ Developer	<ul style="list-style-type: none"> General Electric, USA
Capabilities	<ul style="list-style-type: none"> 1D parallel channel thermal-hydraulic core simulation 1D neutron kinetics or point kinetics with higher harmonics Calculation of Decay Ratio Qualified for GE internal evaluation of new fuel design
Thermal- hydraulics	Multiple channel types; Five equation drift flux model (two mass and energy equations, plus a single momentum equations); In-channels and Bypass Regions; Transient redistribution of flows due to channel coupling; Direct moderator heating; Best estimate thermal-hydraulics correlations.
Neutronics	1-D kinetics with void and Doppler reactivity feedback; Kinetics parameters collapsed from 3D PANACEA wrapup at specific plant conditions; Flux squared weighting of kinetic parameters; Impact of axial and radial variations in control fraction and power shape accounted for; Sets of specific collapsed parameters for each fuel type, control and power distributions in axial nodes; Fitting of coefficients describing the effect of fuel temperature and moderator density considering the various channel groups.

Table B.8. Characteristics of STAIF code

Code	STAIF
Property/ Developer	<ul style="list-style-type: none"> • Siemens-KWU, Germany
Capabilities	<ul style="list-style-type: none"> • 1D parallel channel thermal-hydraulic core simulation • 1D neutron kinetics • Calculation of Decay Ratio for fundamental mode and the higher harmonics • Siemens design tool for linear stability
Thermal- hydraulics	Multiple channel types with independent geometry and axial power distributions; 2 mass (vapour, mixture), 2 energy (vapour, mixture) and one momentum (mixture) equations; Subcooled boiling consideration; In-channel and bypass flow simulation; Fraction of heat generated directly in the moderator including unheated parts; Up-to-date design basis thermal-hydraulic and pressure drop correlations.
Neutronics	1 group diffusion theory with 1D axial variation of neutron flux; 1D axial void and Doppler reactivity feedback; Influence of the control rod pattern by control rod dependent properties; 6 delayed neutron groups for Uranium and MOX Fuel; Data transfer from 3D core-simulator for accounting specific plant conditions; Determination of higher harmonics.

Table B.9. Characteristics of STAIF-PK code

Code	STAIF-PK
Property/ Developer	<ul style="list-style-type: none"> • Nuclear Fuel Industries Ltd., Japan
Capabilities	<ul style="list-style-type: none"> • One-dimensional parallel channel simulation of the BWR core • Point kinetics • Coupled thermal-hydraulic and neutronic core stability • Reactivity feedback associated with fundamental or higher harmonic modes • Calculation of decay ratio
Thermal- hydraulics	Multiple channel types with distinct geometry and power distributions; One dimensional two-phase drift-flux model; Five equations: 2 mass and 2 energy (vapour, mixture), 1 momentum; In-channel and bypass flow; Subcooled boiling model and direct moderator heating models.
Neutronics	Point kinetics for critical and subcritical mode; Six group delayed neutron equation; Void reactivity as a function of void fraction and control rod density for each node; Reactivity feedback with squared nodal power (or flux) weighting for the fundamental or higher harmonic mode.

B.2. Time Domain Codes

Table B.10. Characteristics of ATHLET code

Code	ATHLET
Property/ Developer	<ul style="list-style-type: none"> Gesellschaft für Anlagen- und Reaktorsicherheit (GRS) mbH, (Germany)
Capabilities	<ul style="list-style-type: none"> 1D parallel channel thermal-hydraulic simulation of the core Neutronic described by point or 1D kinetics Detailed description of the whole plant, including BoP
Thermal- hydraulics	1D flow models based on drift-flux and thermal non-equilibrium; six equation two-fluid model under development; Fully implicit time-integration with accuracy controlled time-step size
Neutronics	Point kinetics or 1D kinetics with six delayed neutron groups; Coupling with 3D neutronics model QUABOX/CUBBOX under development

Table B.11. Characteristics of DYNAS-2 code

Code	DYNAS-2
Property/ Developer	<ul style="list-style-type: none"> Nuclear Fuel Industries Ltd., Japan
Capabilities	<ul style="list-style-type: none"> One-dimensional parallel channel simulation of the BWR core Three-dimensional kinetics Coupled thermal-hydraulic and neutronic core stability Calculation of LPRM and APR signals Calculation of Critical Power Ratio
Thermal- hydraulics	Multiple channel types with distinct geometry; One-dimensional two-phase drift-flux model; Five equations: 2 mass and energy (vapour and mixture), 1 momentum (mixture); In-channel and bypass flow; Subcooled boiling and direct moderator heating models.
Neutronics	One-group diffusion model; One node for each bundle and 24 axial nodes; Six-group delayed neutron equation; Void reactivity and Doppler reactivity feedback as a function of void fraction and control rod density for each node

Table B.12. Characteristics of DYNOBOSS code

Code	DYNOBOSS
Property/Developer	<ul style="list-style-type: none"> Instituto de Estudos Avançados (Brazil), RPI (USA)
Capabilities	<ul style="list-style-type: none"> 1D parallel channel thermal-hydraulics Point neutron kinetics Vessel component modeling
Thermal-hydraulics	Four equation drift-flux model; Vapour phase always in saturated conditions; subcooled boiling models: mechanistic and profile fit; Zuber-Findlay drift-flux model; fluid thermophysical properties evaluated on the basis of an average system pressure; Liquid density taken at saturation; Semi-implicit numerical method, with capability to choose time discretization (explicit, Crank-Nicholson, implicit); Iterative procedure to attain steady-state conditions.
Neutronics	Point neutron kinetics; 2D one speed space dependent steady-state calculations; Either cylindrical or rectangular geometry; Reflection factors at the core top, bottom and lateral surfaces; Linear feedback for Doppler and void effect; Successive Line Overrelaxation (SLOR) method for matrix inversion.

Table B.13. Characteristics of EPA

Code	BWR-EPA (with HIPA-BWR Code)
Property/Developer	<ul style="list-style-type: none"> NRC and BNL, USA
Capabilities	<ul style="list-style-type: none"> 1D nonhomogeneous, nonequilibrium two-phase flow in vessel Point kinetics with approximation for 1D, time-dependent power shape Fixed nodal representation of vessel (55 nodes), 3 core channels Dynamic ex-vessel models for BoP, suppression pool, wetwell, drywell and control systems Interactive on-line graphics and acceptance of control and failure signals from keyboard via telephone line Four times faster than real-time simulation speed
Thermal-hydraulics	Four equations drift flux model with nonequilibrium phase change; Loop momentum balance and mixture volumetric flux divergence equations; Core-average, hot and bypass channels with 12 nodes each; Nonequilibrium boiling, flashing and condensing in the vessel, equilibrium phase change in containment for relative humidity; wall shear and form loss according to HTFS; Polytropic steam flow through turbines (power and FW pump drive, with speed-dependent isentropic turbine efficiency).
Neutronics	Point kinetics, six delayed neutron groups; Reactivity feedback for Doppler, moderator temperature, void, scram and boron; Decay heat mode with thirteen precursor groups; Direct gamma heating of liquid phase; Boron tracking in vessel

Table B.14. Characteristics of PANTHER code

Code	PANTHER
Property/Developer	<ul style="list-style-type: none"> • Nuclear Electric, United Kingdom
Capabilities	<ul style="list-style-type: none"> • 1D thermal-hydraulics • 3D neutronic representation of the core • Applicable also to PWR, VVER, RBMK, AGR and MAGNOX
Thermal-hydraulics	1D drift flux model with EPRI slip correlation; Subcooled boiling model; Tabular dependence of coolant thermophysical properties; Also coupled to VIPRE-01
Neutronics	Rectangular or hexagonal assemblies; Sector symmetries and range of boundary conditions; Simple mesh refinement consistent 3D to 1D condensation; Steady-state and transient analytic nodal solution of diffusion equations; Multigroup (up to 12 groups); Time differencing based on stiffness confinement; Nodal pin-power reconstruction; Extensive range of steady-state search options and transient drivers; Representation of within-node burn-up variation and rod tip treatment; Steady-state and transient thermal and poison feedback; Transient decay heat representation; Extensive tabular dependence of cross-sections on temporal and history parameters.

Table B.15. Characteristics of QUABBOX/CUBBOX-HYCA code

Code	QUABOX/CUBBOX-HYCA
Property/Developer	<ul style="list-style-type: none"> • Gesellschaft für Anlagen- und Reaktorsicherheit (GRS) mbH, (Germany)
Capabilities	<ul style="list-style-type: none"> • 3D neutronic representation of the core • 1D thermal-hydraulics
Thermal-hydraulics	1D-single and two-phase flow model using drift-flux correlations; Channel by channel representation; Core boundary conditions either specified at core inlet or pressure drop along the core
Neutronics	Full 3D two-group coarse mesh solution of neutron diffusion equations based on local polynomial flux expansion for steady-state and transient conditions; Time integration including frequency transformation; Flexible interface to cross-section library describing dependence on all relevant parameters.

Table B.16. Characteristics of RAMONA-3 code.

Code	RAMONA-3
Property/ Developer	<ul style="list-style-type: none"> ScandPower, Norway
Capabilities	<ul style="list-style-type: none"> 1D thermal-hydraulic simulation of vessel components with parallel channels in the core 3D neutronic representation of the core with 6x6 nodes Ex-core component modeling
Thermal-hydraulics	Four equation, drift-flux model in vessel; Two equations for acoustic effects in steam lines; Integral formulation of momentum equation; Boron mass conservation equation; Constitutive relationships for non-equilibrium vapour generation, heat transfer, two-phase pressure loss multipliers; Full core simulation with all fuel channels modelled as parallel channels; Conversion of PDEs into ODEs solved with Euler explicit numerical scheme in core; Runge-Kutta adopted in steam lines; Higher order explicit integration scheme.
Neutronics	3D neutron kinetics based on the PRESTO 11/2 group nodal method; Six delayed neutron groups; Implicit predictor-corrector time integration technique for neutronics and fuel thermodynamics; Full or reduced core symmetry; Nuclear cross-section data parametrized in history (burnup, void history, Xenon) and instantaneous parameters (density, fuel and coolant temperatures, control state, Boron); Boron tracking; Decay heat model ANS Standard 5.1.

Table B.17. Characteristics of RAMONA-4B code

Code	RAMONA-4B
Property/ Developer	<ul style="list-style-type: none"> NRC and BNL, USA
Capabilities	<ul style="list-style-type: none"> 1D nonhomogeneous, nonequilibrium two-phase flow in vessel 3D neutron kinetics for the core Fixed nodal representation of vessel, 200 core channels, 55 nodes in vessel Dynamic ex-vessel models for balance of plant, suppression pool, wetwell, drywell and control systems Dynamic models for SBWR-specific components Runs on workstations and PCs
Thermal-hydraulics	Four equations drift flux model with nonequilibrium phase change; Loop momentum balance and mixture volumetric flux divergence equations; Up to 200 hydraulic channels with 24 nodes; Nonequilibrium boiling, flashing and condensing in the vessel, equilibrium phase change in containment for relative humidity; Detailed boron transport model with boron mixing efficiency; Polytropic steam flow through turbines (power and FW pump drive, with speed-dependent isentropic turbine efficiency).
Neutronics	3D neutron kinetics based on 1½ group diffusion theory with six delayed neutron groups; Reactivity feedback for Doppler, moderator temperature, void, scram, control rod motion and boron; Decay heat mode consistent with ANS Standard 5.1; Direct gamma heating of liquid phase; Detailed boron tracking in core hydraulic channels.

Table B.18. Characteristics of RELAP5 code

Code	RELAP5/MOD2-RELAP5/MOD3
Property/ Developer	<ul style="list-style-type: none"> • Idaho National Engineering Laboratory, USA
Capabilities	<ul style="list-style-type: none"> • 1D parallel channel thermal-hydraulic simulation of the core • Point neutron kinetics • Detailed noding of the whole plant including BoP
Thermal-hydraulics	1D separated flow model (six equations; complete thermal and mechanical non-equilibrium between the phases); Physical laws selected on the basis of flow regime maps; Semi-implicit and nearly-implicit numerical methods
Neutronics	Point kinetics with six delayed neutron groups; Decay power model; Feedback mechanisms selected by input parameters

Table B.19. Characteristics of RETRAN-3D code

Code	RETRAN-3D
Property/ Developer	<ul style="list-style-type: none"> • EPRI, USA
Capabilities	<ul style="list-style-type: none"> • 3D, 1D parallel channel thermal-hydraulic simulation of the core • 3D, 1D and point neutron kinetics • Detailed noding of the whole plant
Thermal-hydraulics	1D nonequilibrium model with slip; 1D homogeneous equilibrium model with slip; Multi-dimensional vector momentum; Algebraic and dynamic slip correlations; Nodal discretization of the plant; Nondiffusive solution method; General purpose constitutive relationships.
Neutronics	3D, 1D, and point kinetics with six delayed neutron groups; Decay power model; Feedback mechanisms selected by input parameters; 3D and 1D kinetics void and Doppler feedback determined from cross sections.

Table B.20. Characteristics of SABRE code

Code	SABRE
Property/ Developer	<input type="checkbox"/> Pennsylvania Power & Light, USA
Capabilities	<input type="checkbox"/> 1D parallel channel thermal-hydraulic simulation of core <input type="checkbox"/> Point neutron kinetics <input type="checkbox"/> Boron transport <input type="checkbox"/> Reactor vessel, steam line, and primary containment modeling
Thermal-hydraulics	Three equation equilibrium model; Locally incompressible flow (no acoustic phenomena); Ohkawa-Lahey void model; Cocurrent and countercurrent flows; Conversion of PDEs into ODEs by control volume formulation; Mixture of implicit and explicit first-order temporal integration
Neutronics	Point neutron kinetics with six delayed neutron groups; Axial power shape varies with time; Reactivity coefficients vary with time and axial position; Nuclear kinetics library based on SIMULATE/SIMTRAN used to compute variations in axial power shape and reactivity coefficients.

Table B.21. Characteristics of SIMULATE-3K code

Code	SIMULATE-3K Code (Version 2.0)
Property/ Developer	<ul style="list-style-type: none"> • Studsvik, Sweden-USA
Capabilities	<ul style="list-style-type: none"> • 3D neutronic core representation • Channel-by-channel thermal-hydraulic representation of the core • Ex-core system simulation
Thermal- hydraulics	Three-equation thermal-hydraulic model using the SETS method with one hydraulic channel per fuel assembly; BWR channel pressure drop balancing; Water rod and bypass flow calculations; Boron advection and maps for modeling asymmetrical loop flows and temperatures (for PWR applications)
Neutronics	Full 3D two-group advanced nodal neutronics model with frequency transform time-integration for accuracy with large time steps, Full SIMULATE-3 cross section libraries (with dependencies on fuel and moderator temperatures, void, control rods, boron, exposure, enrichments, etc.); Neutronic feedback of intra-assembly burnup gradients and spectral histories; Axially zoned control rod models and control rod cusping model; Automatic geometry expansions to full or fractional cores; Automatic time step selection; Ex-core detector models (for prediction of SCRAM signals)

Table B.22. Characteristics of SPDA (NOW EUREKA-RELAP5) code

Code	SPDA (now EUREKA-RELAP5)
Property/ Developer	<ul style="list-style-type: none"> • Japan Institute of Nuclear Safety (JINS), Japan
Capabilities	<ul style="list-style-type: none"> • 1D parallel channel thermal-hydraulic simulation of the core • Multigroup 3D representation of the core • Detailed noding of the whole plant • Optional use of coupled of EUREKA/SPACE for neutronics and RELAP5/MOD1 for thermal-hydraulics, or of each code as a separate program
Thermal- hydraulics	1D, 2 phase flow model (five equations; partial thermal, full mechanical non-equilibrium) or 1D flow model (saturated vapour and drift flux); Maximum number of core nodes = (X x Y) 100; Physical laws selected on the basis of flow regime maps; Pre-CHF and post-CHF heat transfer coefficients; Semi-implicit and nearly-implicit numerical methods.
Neutronics	Multigroup time-dependent diffusion in 3D geometry combined with point kinetics; Six delayed neutron groups; Quasi-static solution method; Maximum 2000 material regions; Up to 50 x 50 x 50 space points.

Table B.23. Characteristics of STANDY code

Code	STANDY
Property/ Developer	<ul style="list-style-type: none"> • TEPCo, Toshiba Corp. and Hitachi Ltd., Japan, for the coupled multiregion version • TEPCo and Hitachi Ltd., Japan, for the full 3D version
Capabilities	<ul style="list-style-type: none"> • 1D parallel channel thermal-hydraulic simulation of the core • Element by element neutronic 3D representation of the core • Ex-core component modeling
Thermal-hydraulics	<p>1D separated flow model with 3 equations; Up to 26 axial nodes including 2 nodes for unheated region; Uniform core pressure assumed for property calculation; Compressibility of liquid and vapour neglected; Subcooled boiling considered according to Levy's profile fit; Drift flux according to Zuber-Findlay-Dix; Martinelli-Nelson multiplier for distributed losses and homogeneous flow multiplier for local losses; Iterative scheme comprising:</p> <ul style="list-style-type: none"> • solution of continuity and energy eqs. for given channel flow • solution of momentum equation for a given core Δp • use of the obtained results to modify core boundary conditions through ex-core models
Neutronics	<p><i>Coupled multiregion version:</i> Up to 20 radial regions composed of arbitrary numbers of fuel bundles (one to several fuel bundles may be included); Up to 24 axial regions; Neutronic coupling between nodes by effective transport kernels; Nuclear constants as a function of coolant density and fuel temperature supplied by a steady-state core simulator</p> <p><i>Fully 3D version:</i> Modified one-group time-dependent diffusion in 3D geometry; Six delayed neutron groups; Nuclear constants from a three group model as a function of coolant density and fuel temperature.</p>

Table B.24. Characteristics of TOSDYN-2 code

Code	TOSDYN-2
Property/ Developer	Toshiba Corp., Japan
Capabilities	<ul style="list-style-type: none"> • 1D parallel channel thermal-hydraulic simulation of the core • Element by element neutronic 3D representation of the core • Ex-core component modeling
Thermal-hydraulics	Thermal non-equilibrium, drift-flux model with five equations; 1D parallel channel core simulation; Optional design correlations for drift-flux, heat transfer, etc.; Predictor-corrector solution scheme for continuity and energy; Iterative procedure to achieve the same Δp across the channels, Subcooled boiling treatment.
Neutronics	Modified one-group time-dependent diffusion in 3D geometry; Six delayed neutron groups; Finite difference numerical discretization; One radial node and 24 axial nodes per fuel bundle; Coupling with few thermal-hydraulic channels and fuel structures; Consistency with 3D steady core simulator, used for initialization.

Table B.25. Characteristics of TRAB code

Code	TRAB
Property/ Developer	Valtion Teknillinen Tutkimuskeskus, Finland
Capabilities	<ul style="list-style-type: none"> • 1D thermal-hydraulic simulation (at most 3 parallel channels) • 1D neutronics simulation • Ex-core component modeling
Thermal- hydraulics	Four equation drift-flux model for parallel channels; Two equations for acoustic effects in steam lines; Boron mass conservation equation; Discretization in conservation form; space and time dependent discretization parameter to minimize truncation errors (diffusion).
Neutronics	Two-group diffusion in 1D geometry with radial shape function; Six delayed neutron groups; Two or three radial subregions; 21 to 41 axial nodes; Nuclear constants consistent with VTT nuclear data libraries; Boron tracking; Decay heat model ANS standard 5.1.

Table B.26. Characteristics of TRAC code

Code	TRAC-BF1 and TRACG
Property/ Developer	<ul style="list-style-type: none"> • Idaho National Engineering Laboratory, USA (TRAC-BF1) • General Electric, USA ; Toshiba, Japan (TRACG)
Capabilities	<ul style="list-style-type: none"> • 1D parallel channel thermal-hydraulic simulation of the core • 3D thermal-hydraulic simulation of the vessel • Element by element neutronic 3D representation of the core • Detailed description of reactor, piping and BOP • Used to determine the setpoints for scram of Oscillation Power Range Monitor (OPRM)
Thermal- hydraulics	Best Estimate thermal-hydraulics with 3D capabilities; Fully non equilibrium two-fluid model with six balance equations; Physical laws applied consistently with flow regime maps; Numerical Method: Stability Enhancing Two-Step (SETS); GE proprietary modifications included in TRACG.
Neutronics	<p><u>TRAC-BF1:</u> Point or 1D neutron kinetics; Six delayed neutron groups</p> <p><u>TRACG:</u> Modified one-group time-dependent diffusion in 3D geometry; Six delayed neutron groups; Equations derived from a three-group model; Quasi-static method for dynamic calculations; One radial node and 24-25 axial nodes per fuel bundle; Coupling with few thermal-hydraulic channels and fuel structures; Consistency with 3D steady core simulator, used for initialization.</p>

ANNEX 11

INTEGRAL SYSTEM EXPERIMENT SCALING METHODOLOGY

J.N. Reyes, Jr*

International Atomic Energy Agency, Vienna

Abstract

The objective of this lecture is to provide the participant with the methodology needed to design a single-phase or two-phase natural circulation Integral System Test Facility. By the conclusion of this lecture, the participant should be able to structure a Phenomena Identification Ranking Table (PIRT) for a Natural Circulation Based System and understand the method used to conduct a detailed scaling analysis to obtain the geometric dimensions and operating conditions for an integral system test facility.

1. INTRODUCTION

Integral system test (IST) facilities play a key role in the design, assessment and certification of innovative reactor designs. Data obtained using such facilities has been used to benchmark the best-estimate safety analysis computer codes used to evaluate nuclear plant safety. It has also been used to assess the effectiveness of safety system functions under simulated accident conditions. The purpose of this lecture is to describe a hierarchical scaling analysis method that can be used to design an integral system test facility in support of nuclear plant certification. This method has been successfully used to design the Advanced Plant Experiment at Oregon State University as part of the Westinghouse and US Department of Energy programs conducted in support of AP600 and AP1000 design certification. It has also been used to design the Multi-Application Small Light Water Reactor (MASLWR) test facility currently being evaluated at OSU. Where appropriate, examples will be drawn from the scaling analyses for these test facilities.

1.1. Qualified data for plant certification

It is important to note that testing done in support of the certification of a nuclear power plant requires strict adherence to a quality assurance (QA) plan that has been developed, approved and implemented prior to the start of testing. This plan remains in force throughout the testing program and can vary depending on how the data will be used. The QA plan should address the control of every aspect of testing that can affect the quality of the data. Generally speaking, for reduced scaled thermal hydraulic test facilities, the data is the product. Typically, the data's primary purpose will be to benchmark a computer code that will be used in safety analyses. Only *qualified data* is permitted in the certification process. Seek guidance from your laboratory or regulators regarding the QA program required for your specific test program.

The scaling analysis can be used to support the test program QA plan by identifying which features of the test facility (ie. geometric and operational features) must be controlled to assure that the important thermal hydraulic phenomena are accurately simulated in the facility. Examples of applicable QA criteria are found in Appendix B of Part 50 in Title 10 of the Code of Federal Regulations (10 CFR 50 Appendix B), and in NQA-1 issued by the American Society of Mechanical Engineers.

* Henry and Janice Schuette Endowed Chair Professor of Nuclear Engineering Department of Nuclear Engineering and Radiation Health Physics, Oregon State University, Corvallis, Oregon, USA, 97331. Funded by Oregon State University Sabbatical Leave, US Department of Energy, and IAEA.

1.2. Scaling analysis objectives

The general objective of a scaling analysis is to obtain the physical dimensions and operating conditions of a reduced scale test facility capable of simulating the important flow and heat transfer behavior of the system under investigation. To develop a properly scaled test facility, the following specific objectives must be met for each operational mode of interest.

- Identify the thermal hydraulic processes that should be modeled.
- Obtain the similarity criteria that should be preserved between the test facility and the full-scale prototype.
- Establish priorities for preserving the similarity criteria.
- Provide specifications for the test facility design
- Quantify biases due to scaling distortions.
- Identify the critical attributes of the test facility that must be preserved to meet Quality Assurance requirements.

Different similarity criteria are obtained for the different modes of system operation. These criteria depend on the geometry of the components, the scaling level required to address the transport phenomena of interest, and the initial and boundary conditions for each particular mode of operation. A method used to obtain similarity criteria for a test facility is presented in the following sections.

1.3. General scaling methodology

Meeting the scaling objectives of the previous section presents a formidable challenge. Therefore, to assure that these objectives are met in an organized and clearly traceable manner, a general scaling methodology (GSM) should be established. The model for this scaling methodology is largely drawn from the USNRC's Severe Accident Scaling Methodology presented in NUREG/CR-5809 [1]. A flow diagram for a GSM is presented in Figure 1-1.

The first task outlined by the GSM is to specify the experimental objectives. The experimental objectives define the types of tests that will be performed to address specific design or certification needs. These objectives determine the general modes of operation that should be simulated in the test facility. There are practical limits with regard to what can be studied in a single facility. The expectations for the facility and its limitations should be identified early.

The second task outlined by the GSM is the development of a Phenomena Identification and Ranking Table (PIRT) [3]. The nature of scaling forbids exact similitude between a reduced scale test facility and a full-scale prototype. As a result, the design and operation of the test facility is based on simulating the thermal hydraulic processes *most important* to the system operational modes that will be explored. One very valuable function of a PIRT is to identify the different phases of a scenario and the most important thermal hydraulic phenomena within those phases that should be simulated in the test facility. Many of the thermal hydraulic phenomena of importance to LWR behavior during a Loss-of-Coolant Accident (LOCA) have already been identified in existing PIRTs [2]. Therefore it is of significant value to conduct a literature review to determine if a PIRT already exists for similar designs and transient conditions. Note that full-scale plant information is needed to develop a well-informed PIRT. In addition, the scaling analysis results will naturally identify the dominant thermal hydraulic phenomena for a specific process. Their importance to plant safety or operation however is determined by the PIRT. A description of the PIRT development process is presented in Section 2.

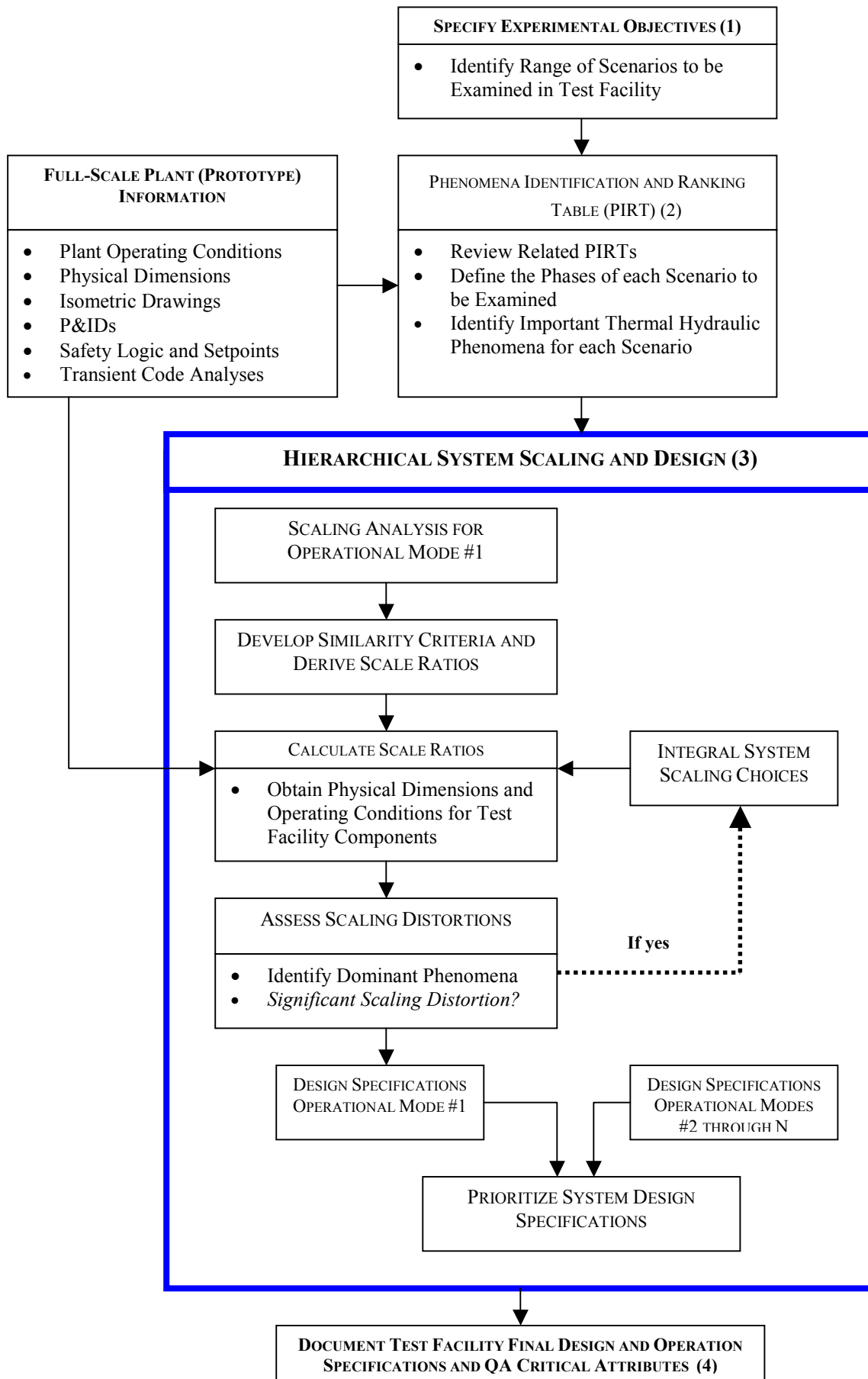


FIG. 1. General scaling methodology.

The third step in the GSM is to perform a scaling analysis for each of the modes of operation specified by the experimental objectives and further defined by the PIRT. The method to be used herein is based on the Hierarchical Two-Tiered Scaling (H2TS) Methodology [1]. This method is particularly well suited for complex systems having interconnected components.

The scaling methodology is used to develop a set of similarity criteria for each mode of operation. Because it is impossible to identically satisfy all of the similarity criteria simultaneously, the set will include only those criteria that must be satisfied to simulate the most important phenomena identified by the PIRT. Having obtained the pertinent set of similarity criteria, a set of scale ratios can be derived to specify the physical dimensions of the test facility, its initial conditions and boundary conditions. To provide closure to the set of equations that define scale ratios, the designer must define a length scale and flow area or volume scale. In addition, the designer has the flexibility to select the working fluid, the pressure range, and structural materials. Some examples of the rationale for these selections are provided in a later section.

The scaling analysis also requires a numerical evaluation of the similarity criteria to determine if the scale model geometry selected, its boundary conditions, and its operating conditions introduce significant scaling distortions. Distortions are also evaluated relative to the other modes of operation. If the distortions are significant, another iteration is required. Perhaps the length scale, volume scale, or the working fluid selections need to be revised. An important outcome of this assessment process is the identification of the dominant phenomena.

Having completed the scaling analysis for a specific operational mode, the same process is repeated for all of the operational modes for the system. One may find that the scaling ratio requirements for one operational mode may partially conflict with the scaling ratio requirements of another operational mode. Therefore, the final step in the scaling analysis is to prioritize the system design specifications. A description of the Hierarchical Scaling Analysis Method is described in Section 3.

The fourth and final step of the GSM is to document all of the test facility design and operation specifications. All of the essential geometric features and operating parameters that must be controlled to assure an accurate simulation of the important thermal hydraulic phenomena are identified and designated as critical attributes for use in the quality assurance plan.

Figure 2 presents the general scaling methodology implemented for the MASLWR test facility. The scaling analysis was divided into four modes of operation:

- Natural Circulation Scaling Analysis
- Sump Recirculation Scaling Analysis
- Reactor Coolant System Depressurization Scaling Analysis
- Containment Pressurization Scaling Analysis

Other nuclear power plant designs undergo different operating modes during transients. Therefore familiarity with plant operations is essential to obtaining a properly scaled test facility. The Phenomena Identification and Ranking Table (PIRT) helps the designer define the operating modes for a particular reactor type and transient.

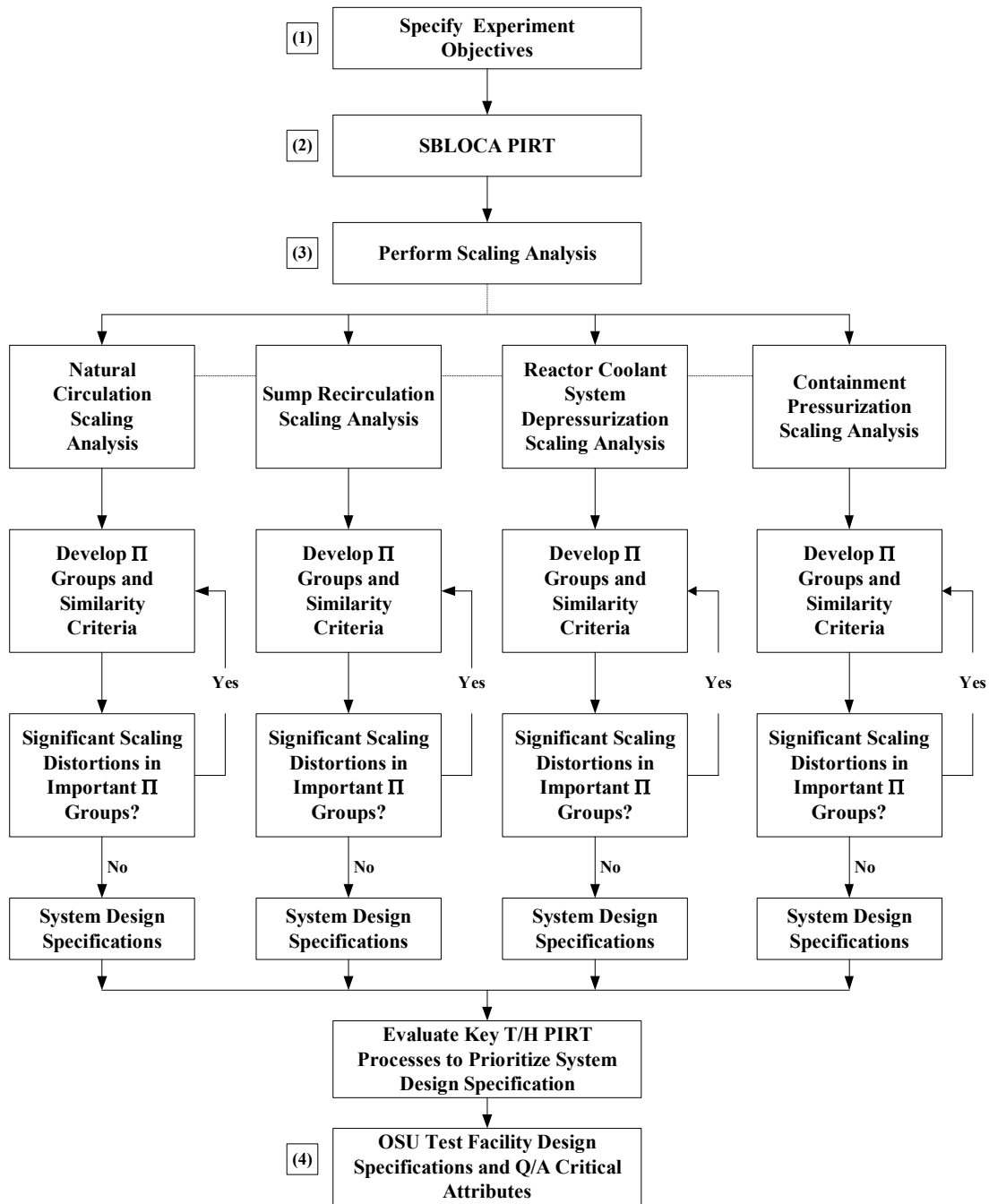


FIG. 2. General scaling methodology for the MASLWR test facility.

2. PHENOMENA IDENTIFICATION AND RANKING TABLES (PIRT)

The primary function of a Phenomena Identification and Ranking Table (PIRT) is to rank, relative to a well-defined figure of merit, the importance of systems, components, processes and phenomena in driving a particular plant response. An detailed description of this technique is described in Wilson and Boyack, 1998 [3]. A PIRT can be used to provide guidance in establishing the requirements in:

- Separate effects and integral effects test (SET, IET) programs, where the objective is to insure that the important phenomena are considered in the scaling, design, instrumentation layout and operation of a test facility.
- Code development and improvement programs, where the objective is to insure that the code adequately predicts the important phenomena; and
- Code uncertainty quantification programs, where the objective is to identify and determine the importance of the various sources of code uncertainty.

The role of the PIRT in guiding an integral system scaling analysis is the focus of this section. In this regard, the goal of the PIRT is to identify the most important thermal hydraulic phenomena for a specific scenario (e.g. Single-Phase Natural Circulation Flow, SBLOCA, etc) for the full-scale plant being investigated. Figure 3 briefly outlines the method used to develop a PIRT for a specific plant and scenario.

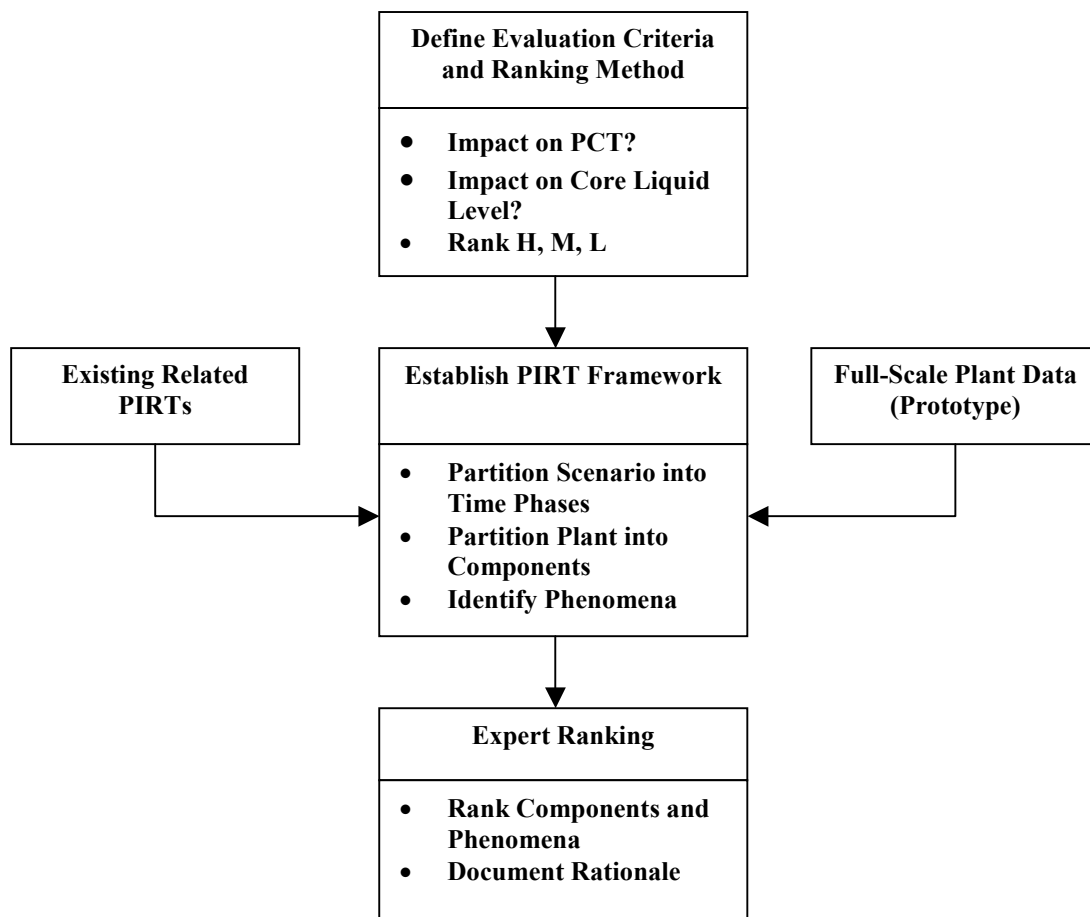


FIG. 3. Process used to develop a “Phenomena Identification and Ranking Table” (PIRT).

As shown in the GSM outlined in Figure 1, the development of a PIRT requires having already identified the types of scenarios to be investigated in an experimental facility and having obtained a significant amount of data on the full-scale plant. Typically, the PIRT developers consist of an expert

panel capable of deducing how the full-scale plant might behave for the scenario being considered. They must have access to the plant operating conditions, drawings, physical dimensions, safety logic and setpoints. Quite often code calculations are used to gain insights into plant behavior during a scenario of interest.

2.1. Evaluation criteria and ranking scale

Having established an expert team with adequate knowledge of the full-scale plant, the first step is to define the basis and method for determining the importance of a phenomenon or component. This requires establishing both a set of evaluation criteria, usually related to the safety of the plant, and a ranking system. An evaluation criterion defines the area of impact the phenomenon has relative to the plant operation and the ranking system defines the extent of impact. The following is an example of the evaluation criterion and ranking method used for the MASLWR SBLOCA PIRT.

Evaluation Criterion: How does this particular phenomenon in this particular component impact the fuel's Peak Cladding Temperature (PCT) during this phase of the scenario?

Ranking Scale: High (H), Medium (M), Low (L), Plausible (P), Inactive or Not Applicable (I)

- A High Ranking means that the phenomenon significantly impacts the PCT during a specific phase of the scenario.
- A Medium Ranking means the phenomenon has a moderate impact on the PCT during a specific phase of the scenario.
- A Low Ranking means that the phenomenon has little impact on the PCT during a specific phase of the scenario.
- A Plausible Ranking means that the phenomenon has not been previously assessed in other designs or its impact on PCT is not well understood or modeled by computer codes. For purposes of test facility scaling, these phenomena were considered highly ranked.
- An Inactive or Not Applicable Ranking means that the phenomenon cannot physically impact the PCT during a specific phase of the scenario.

The evaluation is quite specific so as to limit the response to a relatively narrow window. The high, medium low scale is easiest to apply, however, a scale of 1–5 is often used because it permits a greater differentiation in ranking. The value of (1) assigned to the lowest of the low in importance, (2) low importance, (3) Moderate importance (4) high importance and (5) the highest of the high in importance.

2.2. PIRT framework

The layout of the PIRT, that is the structure of the table itself, is essential to the ranking process. First the scenario of interest must be divided into well-defined logical phases. Next the plant must be divided into the key systems of the plant. These key systems are further subdivided into components. All of the phenomena that could occur within a component during a phase of the transient are then listed. This process of dividing the scenario into phases and the plant into systems, components and identifying plausible phenomena requires significant effort and lays the framework for the PIRT. In addition to having access to full-scale plant data and analyses for the scenario in question, the use of existing PIRTs developed for similar scenarios in similar plants would be of some assistance.

Three phases of a SBLOCA in MASLWR were identified and defined as follows:

- Phase 1 - *Blowdown* begins with the opening of the break and ends with the ADS initiation.
- Phase 2 - *ADS Operation* begins with the opening of the ADS valve and ends when the containment and reactor system pressures are equalized.
- Phase 3 - *Long Term Cooling* begins with the equalization of the containment and reactor system pressures and ends when stable cooling is established.

The breakdown of the MASLWR design into systems, components and phenomena within components is shown in Table 1.

2.3. Expert ranking methods and PIRT results

There are various techniques used by expert panels to come to consensus regarding the rank for a specific phenomenon. A formal ranking technique, known as the Analytical Hierarchy Process (AHP), is described in Saaty, 1982 [4]. The method requires a pair-wise comparison of phenomena. That is, the expert only considers two phenomena at a time to determine which one is more important. After this information is gathered, the AHP method is applied to obtain the relative importance of each phenomenon. The simplest ranking method is a group discussion on each phenomenon followed by a vote of the experts. If the vote is not unanimous with regard to a rank, additional discussion may be encouraged to resolve the difference, the chairman may offer a compromise rank, or the default may be to apply the highest rank. It is very important that the basis for an assigned rank be justified and documented. The use of a tape recorder is recommended during the deliberation process. It will prove very valuable when developing the ranking rationale document. Table 1 presents the SBLOCA PIRT for the MASLWR design.

2.4. High-ranked phenomena

For the test facility designer, the ultimate result of a PIRT is to obtain a list and ranking of all of the thermal hydraulic phenomena pertinent to the full-scale plant for the specific scenarios that will be examined in the test facility. As a minimum, it is desired that all of the phenomena that have been highly ranked (i.e. ranked “H” or “4-5” on their respective scales) be properly simulated in the test facility. The method for doing so is addressed in Chapter 3.

Table 1. Small break loca PIRT for the MASLWR design

System	Period			Component	Period			Process/Phenomenon	Period		
	1	2	3		1	2	3		1	2	3
Vent Valves	H	H	H	Valves	H	H	H	Mass Flow (Choked/Nonchoked)	H	H	H
				Piping	M	M	H	Line Flow Resistance	M	M	H
ADS	I	H	H	Valves	I	H	H	Mass Flow (Choked/Nonchoked)	I	H	H
				Piping	I	M	H	Line Flow Resistance	I	M	H
				Sparger	I	H	M	Condensation	I	H	M
								Energy Release	I	H	M
								Mass Release	I	H	M
Passive Cont. Cooling Sys.	P	P	H	External Cont. Cooling Pool	I	I	H	Natural Convection Heat Transfer	I	I	H
								Thermal Stratification	I	I	L
				Containment Shell	P	P	H	Internal			
								Pressure	L	M	H
								Buoyancy Driven Flow	P	P	P
								Heat Transfer	L	L	H
								Wall - condensation rate	L	L	H
								Noncondensable Gas Mass Fraction	L	L	H
								Wall			
								Thermal Capacitance	L	L	H
								Thermal Conduction	L	L	H
Passive Safety Recirculation	L	L	H	Sump	L	L	H	ADS Heat-up of Sump	I	L	M
								Condensation (Surface of Pool)	L	I	I
								Thermal Stratification	L	L	L
								Recirculation (Flow Resistance)	I	I	H
								Resupply from Containment	L	L	H
NOTES											
<i>Phase 1 - Blowdown</i>				<i>H - Significantly Impacts PCT</i>				<i>I - Inactive during the transient Phase</i>			
<i>Phase 2 - ADS Operation</i>				<i>M - Moderately Impacts PCT</i>				<i>P - Plausible</i>			
<i>Phase 3 - Long Term Cooling</i>				<i>L - Little Impact on PCT</i>							

Table 1. Small break loca PIRT for the MASLWR design (continued)

System	Period			Component	Period			Process/Phenomenon	Period		
	1	2	3		1	2	3		1	2	3
Primary Coolant System	H	H	H	Hot Leg Riser	H	H	H	Flashing	M	H	L
								Flow Resistance (wall/control rod tubes)	M	M	M
								Riser Inventory/Circulation/Level	H	H	H
				SG Tube Annulus	H	H	H	SG Tube Condensation	H	H	H
								Flow			
								Entrainment/De-entrainment	L	L	I
								CCF	I	I	I
								Flow Resistance	H	L	L
								Multidimensional Flow	L	L	L
								Level	L	L	H
							Flashing	H	H	L	
							Stored Energy Release- Hot wall effect	M	M	H	
Reactor System	H	H	H	Vessel - Control Rods	H	L	L	Reactivity Change	H	L	L
				Vessel - Core Subchannels	H	H	H	Flow			
								Interfacial Drag	L	H	L
								Mass Flow	H	H	H
								Flow Resistance	H	H	H
								Two-Phase Mixture Level	H	H	H
								Flashing	M	H	L
				Vessel - Downcomer	H	H	H	Flow			
								Entrainment/De-entrainment	L	L	I
								CCF	L	L	L
								Flow Resistance	H	M	H
								Multidimensional Flow	L	L	L
								Level	L	L	H
								Flashing	M	H	L
								Stored Energy Release- Hot wall effect	M	M	H
NOTES											
<i>Phase 1 - Blowdown</i>		<i>H - Significantly Impacts PCT</i>				<i>I - Inactive during the transient Phase</i>					
<i>Phase 2 - ADS Operation</i>		<i>M - Moderately Impacts PCT</i>				<i>P - Plausible</i>					
<i>Phase 3 - Long Term Cooling</i>		<i>L - Little Impact on PCT</i>									

3. HIERARCHICAL TWO-TIERED SCALING (H2TS) METHODOLOGY

This section describes the Hierarchical Two-Tiered Scaling (H2TS) method. This method has been successfully used to develop the similarity criteria necessary to scale the APEX-600 and APEX-1000 systems for LOCA transients. The H2TS method was developed by the USNRC and is fully described in Appendix D of NUREG/CR-5809 [1].

Figure 4 is taken from NUREG/CR-5809. It presents the four basic elements of the H2TS analysis method. The first element consists of subdividing the plant into a hierarchy of systems. Each system is subdivided into interacting subsystems which are further subdivided into interacting modules which are further subdivided into interacting constituents (materials) which are further subdivided into interacting phases (liquid, vapor or solid). Each phase can be characterized by one or more geometrical configurations and each geometrical configuration can be described by three field equations (mass, energy and momentum conservation equations). Each field equation can incorporate several processes. Figure 5 shows the general approach used for a system breakdown and Figure 6 presents an example based on the MASLWR design.

After identifying and subdividing the system of interest, the next step is to identify the scaling level at which the similarity criteria should be developed. This is determined by examining the phenomena being considered. For example, if the phenomenon being considered involves mass, momentum or energy transport between materials such as water and solid particles, then the scaling analysis would be performed at the constituent level. If the phenomenon of interest involves mass, momentum or energy transport between vapor and liquid, then the scaling analysis would be performed at the phase level. Therefore identifying the scaling level depends on the phenomenon being addressed.

Table 1. Small break loca PIRT for the MASLWR design (continued)

System	Period			Component	Period			Process/Phenomenon	Period		
	1	2	3		1	2	3		1	2	3
Reactor System (continued)	H	H	H	Vessel - Fuel Rods	H	H	H	Fuel Heat Transfer			
								Conduction	H	H	H
								Gap Conductance	H	H	H
								Stored Energy Release	H	H	L
								Cladding Convective Heat Transfer			
								Subcooled Liquid	H	L	L
								Subcooled Boiling	H	L	L
								Nucleate Boiling	L	L	H
								CHF by DNB	L	L	H
								Film Boiling	L	L	H
								Forced Convection to vapor	L	L	H
								Reactivity			
								Void	H	I	I
								Moderator temperature	H	I	I
								Fuel Temperature (Doppler)	H	I	I
								Decay Heat	H	H	H
				Vessel - Guide Tubes	L	L	L	Film Draining	L	L	I
								Stored Energy Release	L	L	L
				Vessel - Lower Plenum	H	H	H	Flow transient			
								Flow Resistance	H	L	H
								Flashing	M	H	L
								Stored Energy Release	M	M	H
				Vessel - Structures	L	L	L	Stored Energy Release	L	L	L
				Vessel - Upper Head	H	H	L	Flow Transient			
								Entrainment/De-entrainment	L	L	L
								Stored Energy Release	H	H	L
								Flashing	M	H	L
Steam Generator/Heat Exchanger	L	L	H	Tubes	L	L	H	Heat Transfer with FW Available	H	H	H
NOTES											
<i>Phase 1 - Blowdown</i>			<i>H - Significantly Impacts PCT</i>			<i>I - Inactive during the transient Phase</i>					
<i>Phase 2 - ADS Operation</i>			<i>M - Moderately Impacts PCT</i>			<i>P - Plausible</i>					
<i>Phase 3 - Long Term Cooling</i>			<i>L - Little Impact on PCT</i>								

Thermal hydraulic phenomena involving integral reactor coolant system interactions, such as primary system depressurization or loop natural circulation, would be examined at the “system” level. Thermal hydraulic phenomena, such as steam generator heat transfer, would be examined at the “subsystem” level. Specific interactions between the steam-liquid mixture and the stainless steel structure would be examined at the “constituent” level.

The H2TS method requires performing a “Top-Down” (system) scaling analysis. The top-down scaling analysis examines the synergistic effects on the system caused by complex interactions between the constituents deemed important by the PIRT. Its purpose is to use the conservation equations at a given scaling level to obtain characteristic time ratios and similarity criteria. It also identified the important processes to be addressed in the bottom-up scaling analysis.

The H2TS method also required performing a “Bottom-Up” (process) scaling analysis. This analysis provides similarity criteria for specific processes such as flow pattern transitions and flow dependent heat transfer. The focus of the bottom-up scaling analysis is to develop similarity criteria to scale individual processes of importance to system behavior as identified by the PIRT.

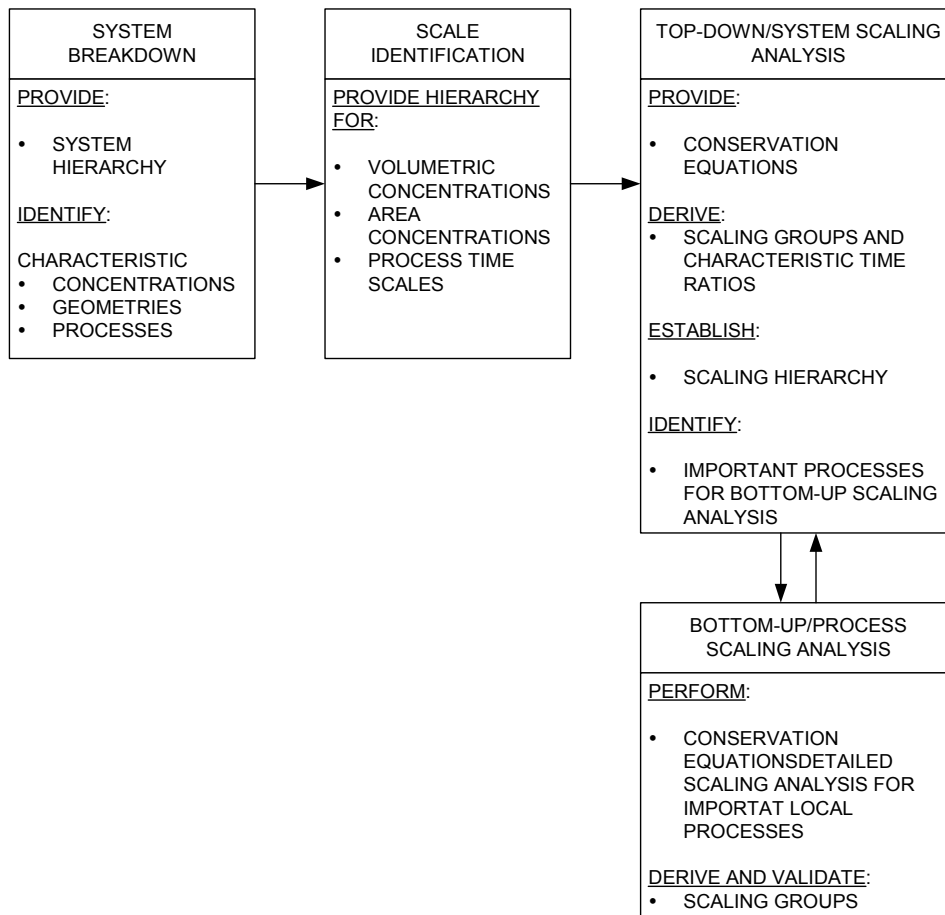


FIG. 4. Flow diagram for the hierarchical, two-tiered scaling analysis. [1].

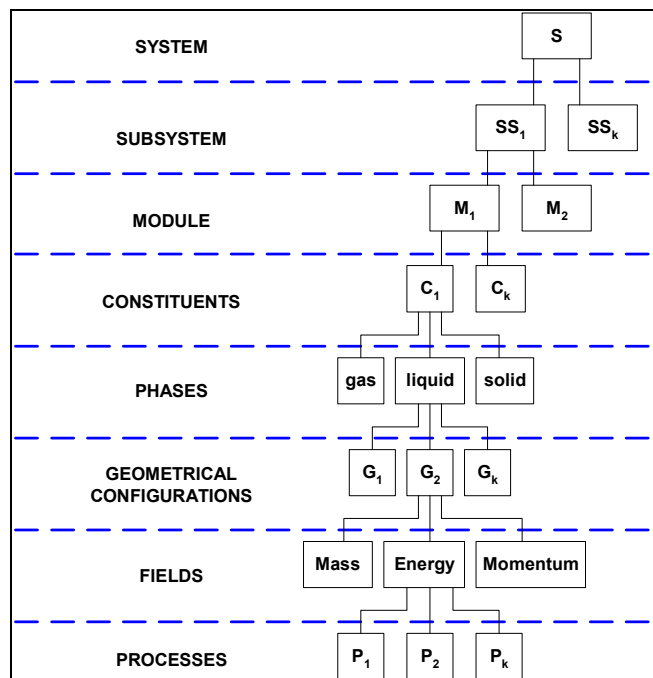


FIG. 5. System breakdown into components, geometries, fields and processes.

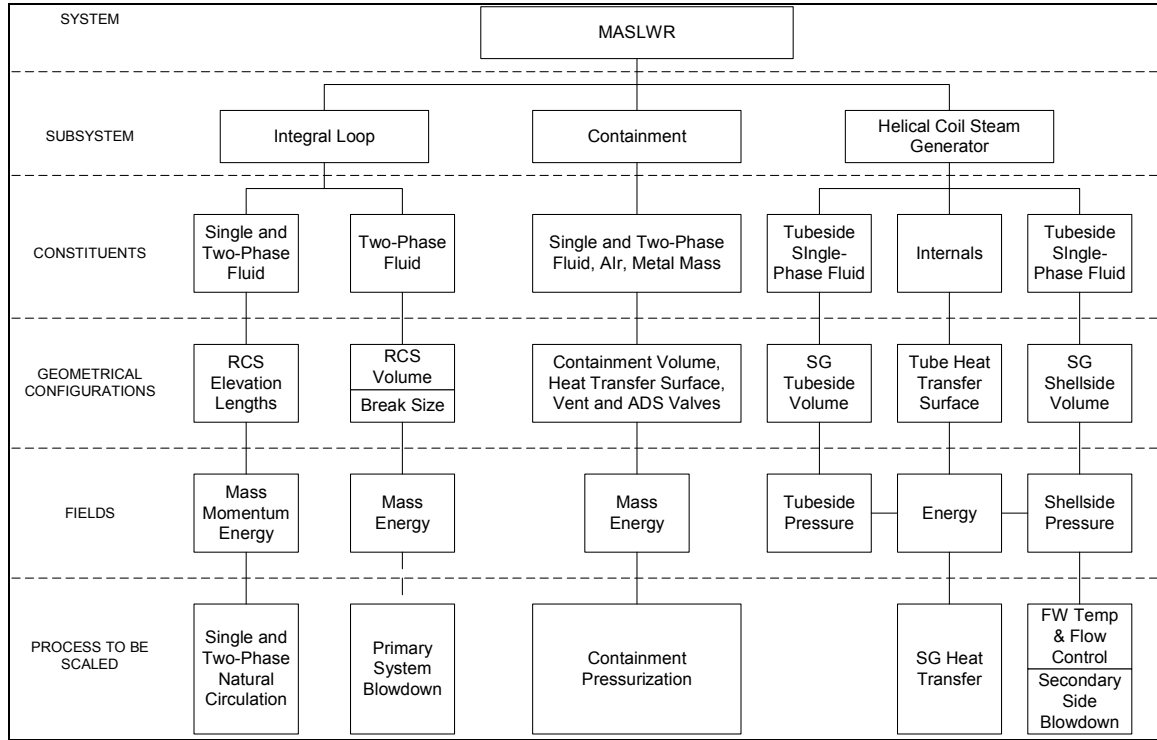


FIG. 6. MASLWR system breakdown into components, geometries, fields and processes.

3.1. Time ratios

The basic objective of the H2TS method is to develop sets of characteristic time ratios for the transfer processes of interest. This is done by writing the control volume balance equations for each constituent “k” as follows:

$$\frac{dV_k \psi_k}{dt} = \Delta[Q_k \psi_k] \pm \Sigma (j_{kn} A_{kn}) + S_k \quad (1)$$

where

$$\Delta[Q_k \psi_k] = [Q_k \psi_k]_{in} - [Q_k \psi_k]_{out} \quad (2)$$

In equation (1) the ψ_k term represents the conserved property; $\psi_k = \rho, \rho u$ or ρe (mass, momentum or energy per unit volume), V_k is the control volume, Q_k is the volumetric flow rate, j_{kn} is the flux of property ψ_k transferred from constituent “k” to “n” across the transfer area A_{kn} . Hence, $\Delta[Q_k \psi_k]$ represents the usual mass, momentum, or energy convection terms, and $\Sigma j_{kn} A_{kn}$ represents transport process terms such as condensation and S_k represents the distributed sources, such as decay power or body forces acting internal to the control volume. Equation (1) can be put in dimensionless form by specifying the following dimensionless groups in terms of the constant initial and boundary conditions:

$$V_k^+ = \frac{V_k}{V_{k,0}}, \psi_k^+ = \frac{\psi_k}{\psi_{k,0}}, Q_k^+ = \frac{Q_k}{Q_{k,0}}, j_{kn}^+ = \frac{j_{kn}}{j_{kn,0}}, A_{kn}^+ = \frac{A_{kn}}{A_{kn,0}}, S_k^+ = \frac{S_k}{S_{k,0}} \quad (3)$$

Substituting these groups into equation (1) yields:

$$V_{k,0} \psi_{k,0} \frac{dV_k^+ \psi_k^+}{dt} = Q_{k,0} \psi_{k,0} \Delta[Q_k^+ \psi_k^+] \pm \Sigma (j_{kn,0}^+ A_{kn,0}^+) j_{kn}^+ A_{kn}^+ + S_{k,0} S_k^+ \quad (4)$$

Dividing both sides of this equation by $Q_{k,0} \psi_{k,0}$ yields:

$$\tau_k \frac{dV_k^+ \psi_k^+}{dt} = \Delta [Q_k^+ \psi_k^+] \pm \Sigma \Pi_{kn} J_{kn}^+ A_{kn}^+ + \Pi_{sk} S_k^+ \quad (5)$$

where the *residence time* of constituent “k” is

$$\tau_k = \frac{V_{k,0}}{Q_{k,0}} \quad (6)$$

and the *characteristic time ratio* for a transfer process between constituents “k” and “n” is given by:

$$\Pi_{kn} = \frac{J_{kn,0} A_{kn,0}}{Q_{k,0} \psi_{k,0}} \quad (7)$$

The characteristic time ratio for the distributed source term within the control volume is given by:

$$\Pi_{sk} = \frac{S_{k,0}}{Q_{k,0} \psi_{k,0}} \quad (8)$$

Because each transfer process has a characteristic time ratio, it is possible to rank the importance of each process by comparing the time ratios. If a specific transfer process is to have the same effect in the prototype and the model, then the characteristic time ratios must be preserved.

3.2. Similarity of trajectories in dimensionless phase space

One of the goals of a test program is to operate the test facility such that the various trends that evolve in the facility for a given scenario would be the same for a similar scenario in the full-scale prototype when the results are plotted in *dimensionless phase space*. For example, given a dimensionless depressurization rate equation of the form:

$$\frac{dP^+}{dt^+} = - \sum \Pi_i S_i^+ \quad (9)$$

plotting a scenario’s pressure history as $P^+ = P/P_o$ versus $t^+ = t/\tau_{RCS}$ would yield overlaying curves for the two facilities. This condition can be achieved by satisfying the following requirements:

1. The scenarios are initiated from the same initial condition in dimensionless phase space. In this case P^+ at $t^+=0$, is 1.
2. The rate of change, (i.e. slope), is preserved in dimensionless phase space. This imposes the following scaling criterion:

$$\left(\frac{dP^+}{dt^+} \right)_R = 1 \quad (10)$$

Satisfying the requirement given by equation (10) implies preserving all of the dimensionless Π groups on the right hand side of the balance equation. If the two requirements listed above are satisfied, then the following is true:

$$\left(\frac{P}{P_o} \right)_m = \left(\frac{P}{P_o} \right)_p \quad (11)$$

This means that the dimensionless pressure at any point along the scenario trajectory will be the same in model and in the prototype.

3.3. Process ranking using characteristic time ratios (Π Groups)

Let us define $M[(\Pi_{i,j}), (\Pi_{i+1,j}), \dots, (\Pi_{N_i, N_j})]$ as the set of time ratios that characterize all of the individual processes that occur during the evolution of a transient. The subscripts i, j, N_i, N_j identify the specific process, the hierarchical level, the total number of specific processes and the total number of hierarchical levels respectively. Because of differences in geometrical scale and fluid properties, it is impossible to exactly duplicate the “time ratio set” for the full-scale prototype, M_p , in a reduced scale model. That is, exact similitude for all processes cannot be preserved; therefore:

$$M_p \neq M_m \quad (12)$$

The subscript, p , refers to the full-scale prototype and the subscript, m , refers to the reduced scale model. It is possible to design a reduced scale test facility that preserves the similitude of a subset of time ratios $T[\Pi_{i,j}]$, that characterize the processes of greatest importance to the transient. This optimizes the model design to investigate the important processes while distorting the less important processes. To determine which processes govern the overall evolution of a transient, numerical estimates of the characteristic time ratios for the prototype and the model must be obtained for each hierarchical level of interest. Physically, each characteristic time ratio, Π_i , is composed of a specific frequency, ω_i , which is an attribute of the specific process, and the residence time constant, τ_{cv} , for the control volume. That is:

$$\Pi_i = \omega_i \tau_{cv} \quad (13)$$

The specific frequency defines the mass, momentum or energy transfer rate for a particular process. The residence time defines the total time available for the transfer process to occur within the control volume. A numerical value of:

$$\Pi_i < 1 \quad (14)$$

means that only a small amount of the conserved property would be transferred in the limited time available for the specific process to evolve. As a result, the specific process would not be important to the overall transient. Numerical values of:

$$\Pi_i \geq 1 \quad (15)$$

means that the specific process evolves at a high enough rate to permit significant amounts of the conserved property to be transferred during the time period, τ_{cv} . Such processes would be important to the overall transient behavior.

3.4. Similarity criteria and scaling ratio development

The scaling analysis results in a set of characteristic time ratios (dimensionless Π groups) that characterize the various processes in the mode of operation being examined. Because it is impossible to identically satisfy all of the similarity criteria simultaneously, the set only includes those criteria that must be satisfied to scale the most important phenomena identified by the PIRT. *Similarity Criteria* are developed by requiring that the characteristic time ratios for a subset of specific processes in the prototype (usually those of greatest importance) match in the model at each hierarchical level. That is,

$$T\{\Pi_i\}_m = T\{\Pi_i\}_p \quad (16)$$

Specifically, for each process, there will be a similarity criterion given by:

$$\frac{\Pi_m}{\Pi_p} = 1 \quad (17)$$

Each similarity criterion can be satisfied by adjusting the physical geometry, fluid properties, and operating conditions of the model; thus optimizing the model design for the specific process of interest. In the process of satisfying the similarity criteria, the scale ratios for the components and operating conditions are obtained.

3.5. Evaluation of scale distortion

The scaling criteria were evaluated to determine if the scale model geometry, boundary conditions or operating conditions would introduce significant scaling distortions. Distortions were also evaluated relative to other modes of operation.

The effect of a distortion in the model for a specific process can be quantified as follows:

$$DF = \frac{[\Pi_i]_p - [\Pi_i]_m}{[\Pi_i]_p} \quad (18)$$

The distortion factor, DF, physically represents the fractional difference in the amount of conserved property transferred through the evolution of a specific process in the prototype to the amount of conserved property transferred through the same process in the model during their respective residence times. A distortion factor of zero would indicate that the model ideally simulates the specific process. A distortion factor of +0.05 would indicate that the specific process in the model transfers 5 percent less of the conserved property (on a scaled basis) than the same process in the prototype. The distortion factor can also be written as:

$$DF = 1 - [\omega_i]_R [\tau_{cv}]_R \quad (19)$$

or

$$DF = 1 - [\Pi_i]_R \quad (20)$$

The degree to which a specific transfer process could impact a particular transient can be determined by comparing the *maximum* characteristic time ratio for each of the transfer processes that arise during the transient. The following section provides some examples for the MASLWR design.

4. SINGLE-PHASE NATURAL CIRCULATION SCALING ANALYSIS

This section briefly outlines the results of the H2TS single-phase natural circulation scaling analysis method as applied to the MASLWR test facility. Figure 7 provides a flow diagram that describes the scaling analysis process for this operational mode. First, a top-down scaling analysis was performed. This included an analysis at the system level (integrated loop behavior) for normal operating conditions. The objective of the top-down scaling analysis was to scale the primary loop mass flow rates and core and steam generator heat exchange rates. Following the top-down scaling analysis, a bottom-up/process scaling analysis was performed to develop similarity criteria to scale specific thermal hydraulic phenomena such as the hydraulic resistance and the core decay power.

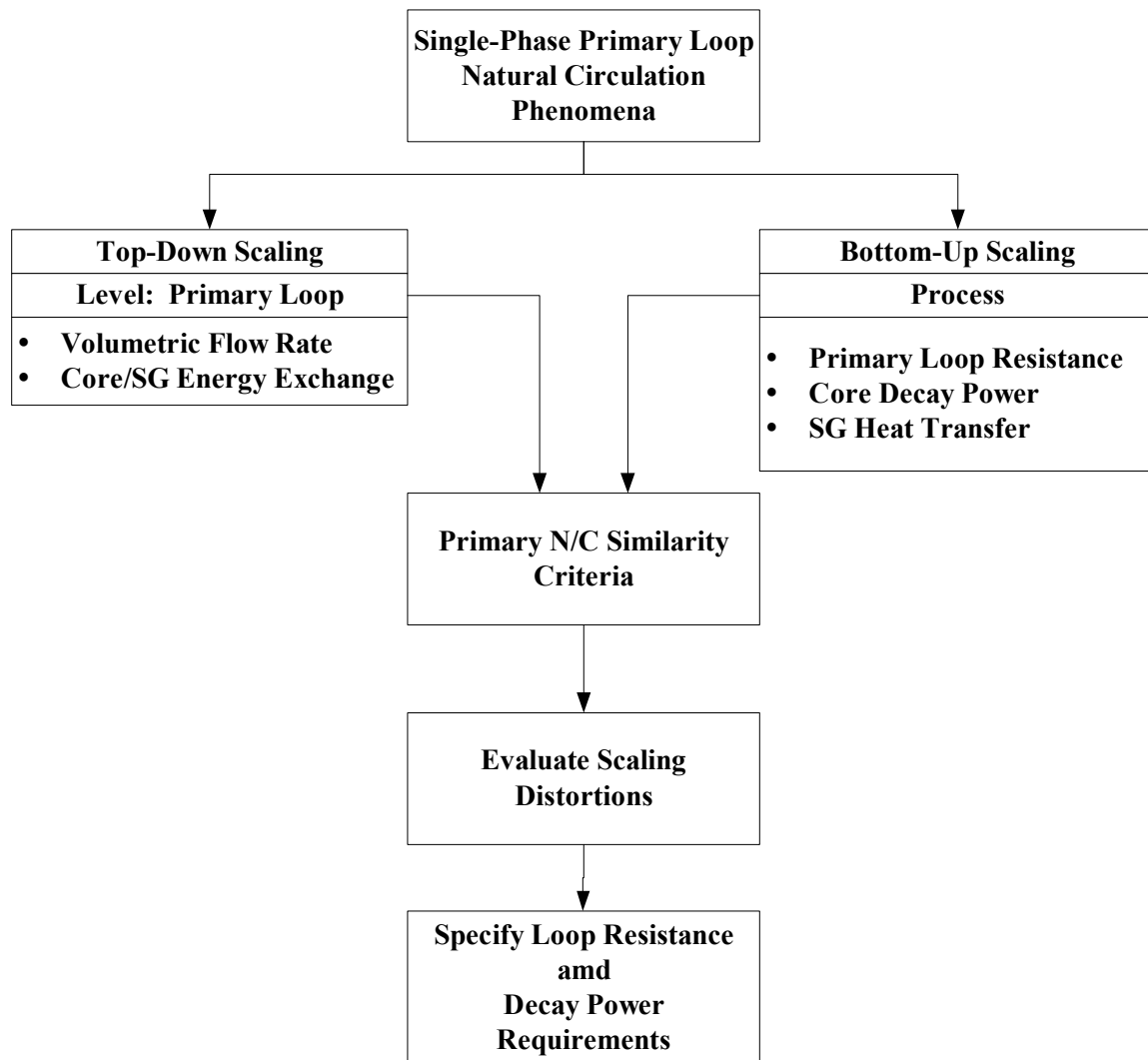


FIG. 7. Scaling analysis flow diagram for single-phase natural circulation.

4.1. Top-down scaling analysis for single-phase natural circulation

The loop being considered consists of the core, which serves as a heat source, the riser, the annular downcomer region between the riser and the reactor vessel, and the helical steam generator coil that serves as the heat sink. A simple sketch is presented in Figure 8. As shown in this figure, the primary loop is divided into a hot fluid side having an average temperature T_H and a cold fluid side having an average temperature T_C .

Mass, momentum and energy control volume balance equations can be written for each component. For purposes of the single-phase natural circulation scaling analysis, the following assumptions were made:

1. The flow was one-dimensional along the loop axis, therefore fluid properties were uniform at every cross-section.
2. The Boussinesq approximation was applicable.
3. The fluid was incompressible.
4. T_C is constant
5. Form losses, primarily in the core and steam generator regions, dominate the loop resistance.

By implementing the Boussinesq approximation, all of the fluid densities in the loop were assumed equal to an average fluid density except for those that comprise the buoyancy term. T_M is a mixed mean temperature for the system

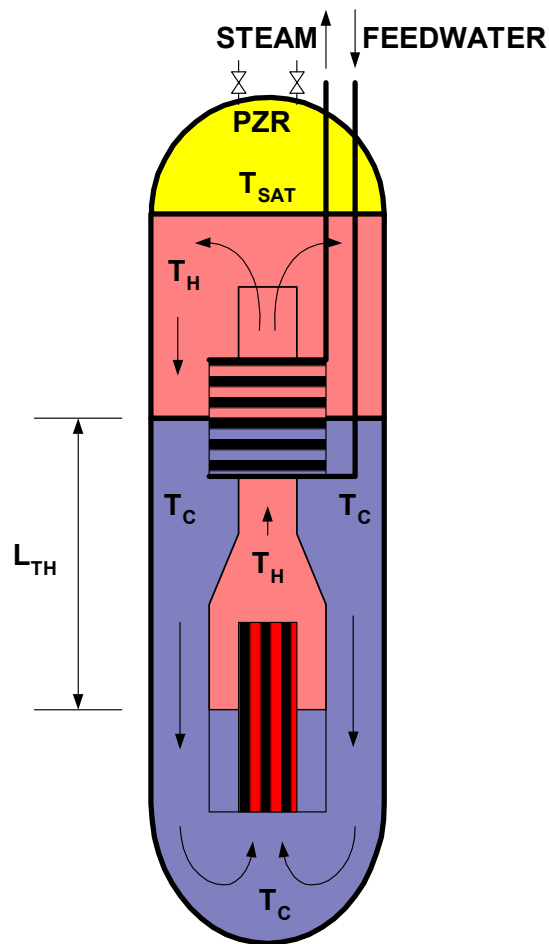


FIG. 8. Hot and cold regions of single-phase natural circulation flow within MASLWR.

The fact that the components of the loop remain liquid filled during the natural circulation mode of operation coupled with the third assumption eliminates the time dependence in the component mass conservation equation. Applying these assumptions to the component balance equations and integrating the momentum and energy equations over the entire loop, yielded the momentum and energy balance equations for fluid transport around the loop as shown in Table 2.

The loop momentum and energy balance equations were made dimensionless by normalizing each term relative to its steady-state initial or boundary condition. These terms are also shown in Table 2.

Table 3 presents the dimensionless momentum and energy balance equations for the loop. The characteristic time constant and the characteristic ratios (Π groups) arising in the equations are also defined in the table. Lastly, the steady-state solution for the governing equation is presented. The steady-state solution is obtained by setting the time dependent term to zero and setting all of the “+” superscripted terms to unity. This results in a very simple equation. That is, the Richardson Number, Π_{Ri} equals the Loop Resistance Number Π_{Fl} . Thus, substituting equation (35) into (40) yields the well-known equation for the for the fluid velocity at the inlet to the core.

4.2. Bottom-up scaling analysis for single-phase natural circulation

The bottom-up scaling analysis provides the information required to evaluate the dimensionless groups obtained in the Top-Down Scaling Analysis. These are local transport models and correlations. For a single-phase natural circulation loop, models are needed for:

- Core Decay Power,
- Friction and Form Loss Coefficient Models
- Core Heat Transfer Models

For the MASLWR test facility design, core decay power was modeled using ANSI/ANS-5.1.24, 1979 with a G-Factor included. Friction and form losses were modeled using the Moody Friction factor correlations and standard tables for loss coefficients for fittings, elbows and valves. Orifices were used to obtain the desired pressure drop around the loop.

4.3. Similarity criteria and scale ratios for a single-phase fluid natural circulation loop

The similarity criteria for a single-phase fluid natural circulation loop is obtained by setting the model to prototype ratios of each dimensionless group in Table 3 to unity. Expressions for the time, length, and velocity scale ratios are obtained using the ratio of the characteristic time constant and the steady state solution for the fluid velocity at the core inlet. The results are presented in Table 3.

The flow area scale ratio shown in equation (45) was set to unity to preserve the kinematic behavior within the loop components. To obtain a closed set of design parameters, the designer must “select” values for the time, length, flow area and the loop resistance scale ratios. In addition, the designer must also select the working fluid. Hence the designer has significant flexibility for the loop design.

Exercise: Assuming fluid property similitude (i.e., same working fluid), find the core power scale ratio given, $\tau_R = 0.5$, (i.e., isochronicity); $l_R = 0.25$; $a_R = 1:50$; $(II_{FI})_R = 1$

Table 2. Governing equations and normalizing ratios for single-phase natural circulation

<i>Governing Balance Equations</i>	
<i>Loop Momentum Balance Equation:</i>	
$\sum_{i=1}^N \left(\frac{l_i}{a_i} \right) \cdot \frac{d\dot{m}}{dt} = \beta g \rho (T_H - T_C) L_{th} - \frac{\dot{m}^2}{\rho_l a_c^2} \sum_{i=1}^N \left[\frac{1}{2} \left(\frac{fl}{d_h} + K \right)_i \left(\frac{a_c}{a_i} \right)^2 \right] \quad (21)$	
<i>Loop Energy Balance Equation:</i>	
$C_{vl} M_{sys} \frac{d(T_M - T_C)}{dt} = \dot{m} C_{pl} (T_H - T_C) - \dot{q}_{SG} - \dot{q}_{loss} \quad (22)$	
<i>Initial and Boundary Conditions</i>	
$t^+ = \frac{t}{\tau_{loop}} \quad (23)$	
$\dot{m}^+ = \frac{\dot{m}}{\dot{m}_o} \quad (24)$	
$\left\{ \sum_{i=1}^N \left[\frac{1}{2} \left(\frac{fl}{d_h} + K \right)_i \left(\frac{a_c}{a_i} \right)^2 \right] \right\}^+ = \frac{\sum_{i=1}^N \left[\frac{1}{2} \left(\frac{fl}{d_h} + K \right)_i \left(\frac{a_c}{a_i} \right)^2 \right]}{\sum_{i=1}^N \left[\frac{1}{2} \left(\frac{fl}{d_h} + K \right)_i \left(\frac{a_c}{a_i} \right)^2 \right]_o} \quad (25)$	
$(T_M - T_C)^+ = \frac{(T_M - T_C)}{(T_M - T_C)_o} \quad (26)$	
$(T_H - T_C)^+ = \frac{(T_H - T_C)}{(T_H - T_C)_o} \quad (27)$	
$\dot{q}_{SG}^+ = \frac{\dot{q}_{SG}}{\dot{q}_{SG_o}} \quad (28)$	
$\dot{q}_{loss}^+ = \frac{\dot{q}_{loss}}{\dot{q}_{loss_o}} \quad (29)$	

Table 3. Dimensionless equations and Π groups for single-phase natural circulation

<p><i>Dimensionless Balance Equations</i></p> <p><i>Loop Momentum Balance Equation:</i></p> $\Pi_L \frac{d\dot{m}^+}{dt^+} = \Pi_{Ri} (T_H - T_C)^+ - \Pi_{Fl} (\dot{m}^+)^2 \left\{ \sum_{i=1}^N \left[\frac{1}{2} \left(\frac{fl}{d_h} + K \right)_i \left(\frac{a_c}{a_i} \right)^2 \right] \right\}^+ \quad (30)$ <p><i>Loop Energy Balance Equation:</i></p> $\frac{1}{\gamma} \frac{d(T_M - T_C)^+}{dt^+} = \Pi_T \dot{m}^+ (T_H - T_C)^+ - \Pi_{SG} \dot{q}_{SG}^+ - \Pi_{loss} \dot{q}_{loss}^+ \quad (31)$	
<p><i>Characteristic Time Constant</i></p> $\tau_{loop} = \sum_{i=1}^N \frac{l_i}{u_i} = \sum_{i=1}^N \tau_i = \frac{M_{sys}}{\dot{m}_o} = \frac{M_{sys}}{\rho_l u_{co} a_c} \quad (32)$	
<p><i>Dimensionless Groups</i></p> <p><i>Loop Reference Length Number:</i></p> $\Pi_L = \sum_{i=1}^N \frac{l_i}{l_{ref}} \frac{a_c}{a_i} \quad (33)$ <p>where: $l_{ref} = \frac{M_{sys}}{\rho_l a_c}$</p> <p><i>Loop Richardson Number:</i></p> $\Pi_{Ri} = \frac{\beta g (T_H - T_C)_o L_{th}}{u_{co}^2} \quad (34)$ <p>or</p> $\Pi_{Ri} = \frac{\beta g \dot{q}_{co} L_{th}}{\rho_l a_c C_{pl} u_{co}^3} \quad (35)$ <p><i>Loop Resistance Number:</i></p> $\Pi_{Fl} = \sum_{i=1}^N \left\{ \frac{1}{2} \left(\frac{fl}{d_h} + K \right)_i \left(\frac{a_c}{a_i} \right)^2 \right\} \quad (32)$	<p><i>Ratio of Specific Heats:</i></p> $\gamma = \frac{C_{pl}}{C_{vl}} \quad (36)$ <p><i>Loop Energy Ratio:</i></p> $\Pi_T = \frac{(T_H - T_C)_o}{(T_M - T_C)_o} \quad (37)$ <p><i>Steam Generator Heat Transport Number:</i></p> $\Pi_{SG} = \frac{\dot{q}_{SGo}}{\rho_l u_{co} a_c C_{pl} (T_M - T_C)_o} \quad (38)$ <p><i>Loop Heat Loss Number:</i></p> $\Pi_{Loss} = \frac{\dot{q}_{loss,o}}{\rho_l u_{co} a_c C_{pl} (T_M - T_C)_o} \quad (39)$
<p><i>Steady-State Solution</i></p> $\Pi_{Ri} = \Pi_{Fl} \quad (40)$ <p><i>Core Inlet Velocity:</i></p> $u_{co} = \left(\frac{\beta \dot{q}_{co} L_{th} g}{\rho_l a_c C_{pl} \Pi_{Fl}} \right)^{1/3} \quad (41)$	

Table 4. Scale ratios for a single-phase natural circulation loop

Time Scale Ratio:

$$\tau_{loop,R} = \left(\frac{\rho_l C_{pl}}{\beta} \right)_R \left(\frac{a_c \Pi_{Fl} l^2}{\dot{q}_{co}} \right)_R^{1/3} \quad (42)$$

Fluid Velocity Scale Ratio:

$$u_R = \left(\frac{\beta}{\rho_l C_{pl}} \right)_R \left(\frac{\dot{q}_{co} l}{a_c \Pi_{Fl}} \right)_R^{1/3} \quad (43)$$

Loop Length Scale Ratio:

$$l_R = (L_{th})_R \quad (44)$$

Flow Area Scale Ratio (Kinematic Similarity):

$$\left(\frac{a_i}{a_c} \right)_R = 1 \quad (45)$$

Loop Energy Scale Ratio:

$$\left[\frac{(T_H - T_C)_o}{(T_M - T_C)_o} \right]_R = 1 \quad (46)$$

Steam Generator Power Scale Ratio:

$$\left(\frac{\dot{q}_{SGo}}{\dot{q}_{co}} \right)_R = 1 \quad (47)$$

Heat Loss Scale Ratio:

$$\left(\frac{\dot{q}_{loss,o}}{\dot{q}_{co}} \right)_R = 1 \quad (48)$$

5. TWO-PHASE NATURAL CIRCULATION SCALING ANALYSIS

This section presents a scaling analysis for two-phase natural circulation. Figure 9 provides a flow diagram which describes the scaling analysis process for this operational mode. First a top-down integral system scaling analysis was performed. The primary objective of the top-down scaling analysis was to scale the primary loop mass flow rates. Following the top-down scaling analysis, a bottom-up scaling analysis was performed to scale the loop resistance for two-phase flow conditions and to assess the degree of similarity between flow pattern transitions in the model and prototype.

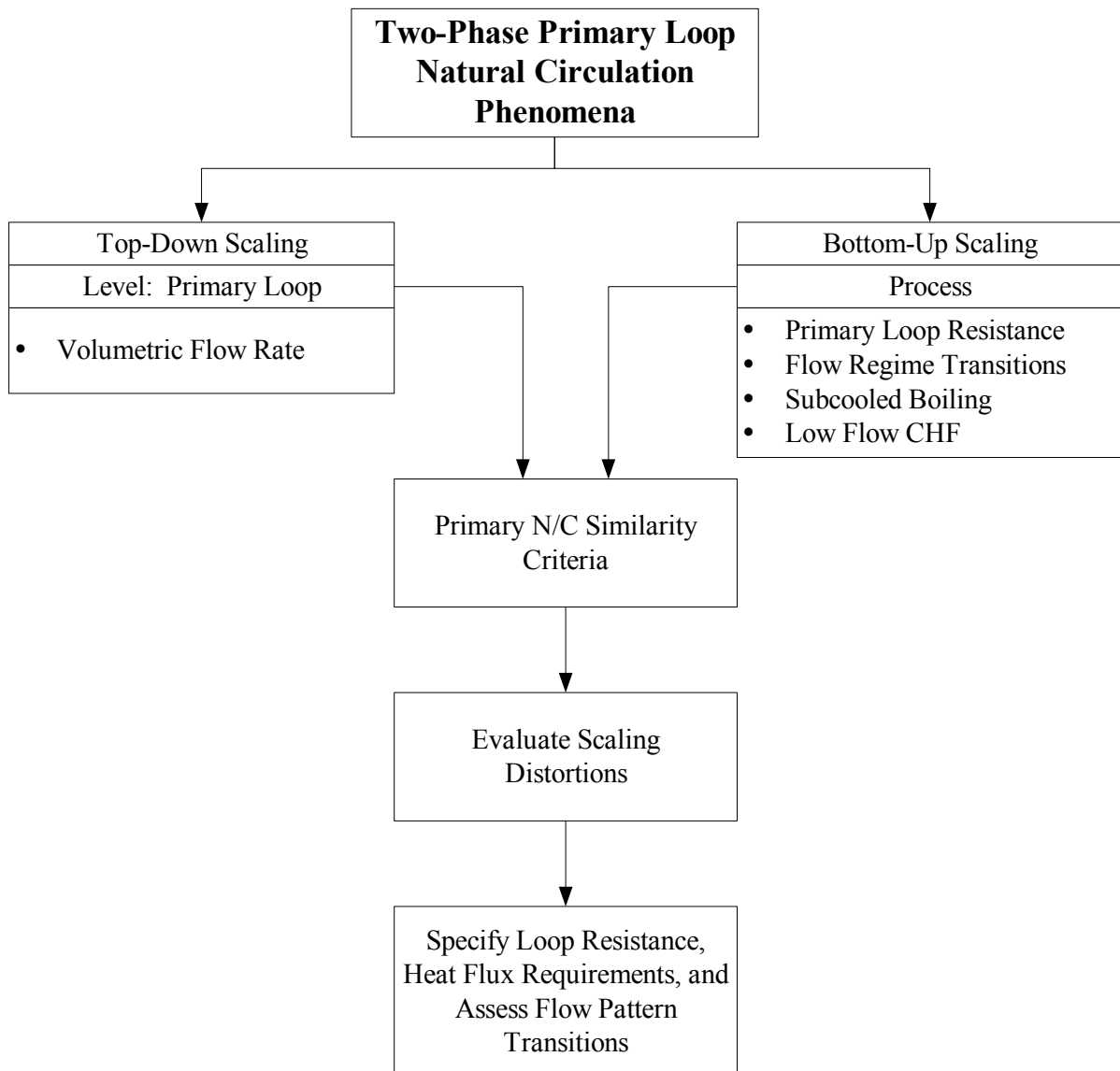


FIG. 9. Scaling analysis flow diagram for two-phase natural circulation.

5.1. Top-down scaling analysis for two-phase natural circulation

Figure 10 depicts the loop geometry considered for this analysis. The loop is divided into two regions; a two-phase region with a fluid density ρ_{TP} and a single-phase region with a fluid density ρ_l . The simplifying assumptions are as follows:

Integral Analysis Assumption:

- Constant core inlet enthalpy
- Uniform fluid properties at every cross-section,
- Homogeneous flow in the two phase region,
- Chemical Equilibrium – no chemical reactions,
- Thermal Equilibrium – both phases at the same temperature,
- The sum of convective accelerations due to vaporization and condensation are negligible,
- Viscous effects included in determination of form losses only.
- Form losses, primarily in the core and steam generator regions, dominate the loop resistance.

The assumptions listed above were applied to the mass, momentum, and energy equations for each component in the loop to obtain the conservation equations. The equations were then integrated over their respective single-phase and two-phase regions to obtain the loop balance equations. These equations are listed in Table 5. Also listed in Table 5 are the normalized initial conditions that were substituted into the balance equations to make them dimensionless. The set of dimensionless balance equations is presented in Table 6. It includes the set of dimensionless groups (i.e., characteristic time ratios) that characterize two-phase natural circulation in the loop. The ratio of each group was used to form the similarity criteria needed for test facility scaling.

Unlike single-phase natural circulation, a simple analytical expression for the velocity at the core inlet cannot be readily obtained from the steady-state solution. This is due to the fact that the two-phase mixture density is dependent on core flow rate. The resulting steady-state expression for the velocity is a cubic equation as described in Table 7. The coefficients for this equation include the terms for the subcooled liquid phase.

The problem becomes much more manageable when considering saturated conditions at the core inlet. Examining this special case (i.e. zero subcooling) results in the simpler dimensionless equation (78) presented in Table 7. It is a cubic equation expressed in terms of the Zuber Number and dimensionless coefficients. This equation can be used to obtain the desired scale ratios for two-phase natural circulation as shown in the next section.

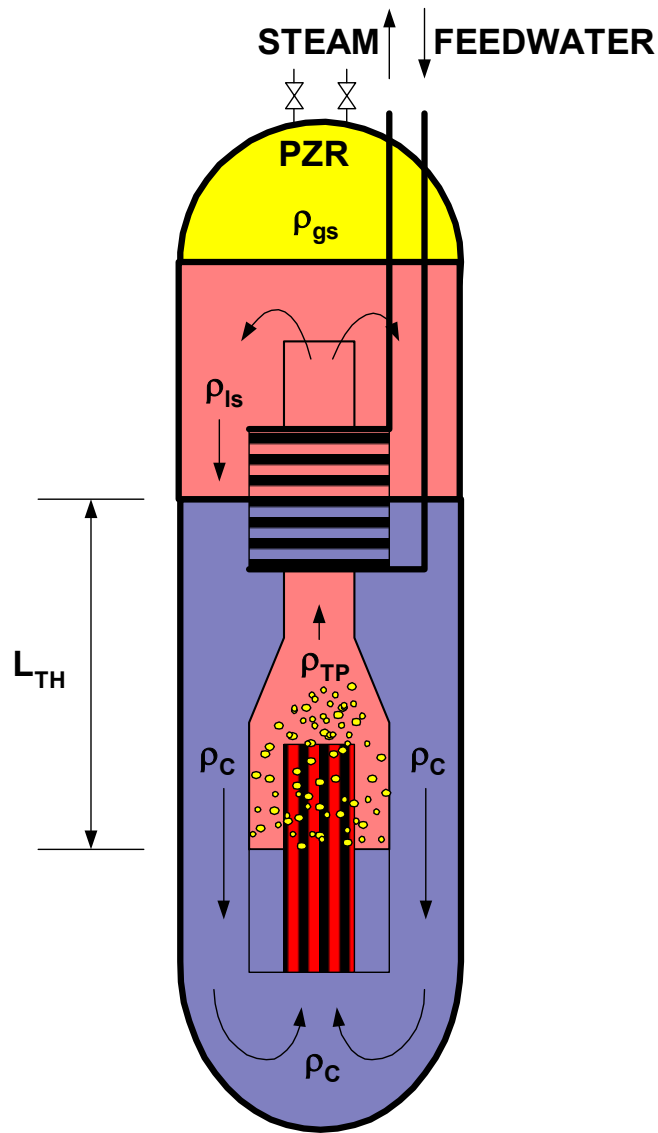


FIG. 10. Regions of single-phase and two-phase natural circulation within MASLWR.

Table 5. Governing equations and normalizing ratios for two-phase natural circulation

<p><i>Governing Balance Equations</i></p> <p><i>Loop Momentum Balance Equation:</i></p> $\sum_{i=1}^N \left(\frac{l_i}{a_i} \right) \cdot \frac{d\dot{m}}{dt} = g(\rho_l - \rho_{TP})L_{th}$ $-\frac{\dot{m}^2}{\rho_l a_c^2} \left\{ \sum_{SP} \left[\frac{1}{2} \left(\frac{fl}{d_h} + K \right)_i \left(\frac{a_c}{a_i} \right)^2 \right] + \frac{\rho_l}{\rho_{TP}} \sum_{TP} \left[\frac{1}{2} \left(\frac{fl}{d_h} + K \right)_i \left(\frac{a_c}{a_i} \right)^2 \right] \right\} \quad (49)$	
<p><i>Loop Energy Balance Equation:</i></p> $M_{sys} \frac{d(e_M - e_l)}{dt} = \dot{m}(h_{TP} - h_l) - \dot{q}_{SG} - \dot{q}_{loss} \quad (50)$	
<p><i>Equilibrium Vapor Quality at Core Exit:</i></p> $x_e = \frac{h_{TP} - h_f}{h_{fg}} \quad (51)$	
<p><i>Homogeneous Two-Phase Fluid Mixture Density:</i></p> $\rho_{TP} = \frac{\rho_f}{1 + x_e \left(\frac{\rho_f - \rho_g}{\rho_g} \right)} \quad (52)$	
<p><i>Initial and Boundary Conditions</i></p> $t^+ = \frac{t}{\tau_{loop}} \quad (53)$	$(h_{TP} - h_l)^+ = \frac{(h_{TP} - h_l)}{(h_{TP} - h_l)_o} \quad (57)$
$\dot{m}^+ = \frac{\dot{m}}{\dot{m}_o} \quad (54)$	$\dot{q}_{SG}^+ = \frac{\dot{q}_{SG}}{\dot{q}_{SG,o}} \quad (58)$
$(\rho_l - \rho_{TP})^+ = \frac{(\rho_l - \rho_{TP})}{(\rho_l - \rho_{TP})_o} \quad (55)$	$\dot{q}_{loss}^+ = \frac{\dot{q}_{loss}}{\dot{q}_{loss,o}} \quad (59)$
$(e_M - e_l)^+ = \frac{(e_M - e_l)}{(e_M - e_l)_o} \quad (56)$	$\left(\frac{\rho_l}{\rho_{TP}} \right)^+ = \frac{(\rho_l / \rho_{TP})}{(\rho_l / \rho_{TP})_o} \quad (60)$
$\left\{ \sum_{SP} \left[\frac{1}{2} \left(\frac{fl}{d_h} + K \right)_i \left(\frac{a_c}{a_i} \right)^2 \right] \right\}^+ = \frac{\sum_{SP} \left[\frac{1}{2} \left(\frac{fl}{d_h} + K \right)_i \left(\frac{a_c}{a_i} \right)^2 \right]}{\sum_{SP} \left[\frac{1}{2} \left(\frac{fl}{d_h} + K \right)_i \left(\frac{a_c}{a_i} \right)^2 \right]_o} \quad (61)$	
$\left\{ \sum_{TP} \left[\frac{1}{2} \left(\frac{fl}{d_h} + K \right)_i \left(\frac{a_c}{a_i} \right)^2 \right] \right\}^+ = \frac{\sum_{TP} \left[\frac{1}{2} \left(\frac{fl}{d_h} + K \right)_i \left(\frac{a_c}{a_i} \right)^2 \right]}{\sum_{TP} \left[\frac{1}{2} \left(\frac{fl}{d_h} + K \right)_i \left(\frac{a_c}{a_i} \right)^2 \right]_o} \quad (62)$	

Table 6. Dimensionless equations and Π groups for two-phase natural circulation

<i>Dimensionless Balance Equations</i>	
<i>Loop Momentum Balance Equation:</i>	
$\Pi_L \frac{d\dot{m}^+}{dt^+} = \Pi_{Ri,\rho} (\rho_l - \rho_{TP})^+ - (\dot{m}^+)^2 \left[\Pi_{F1} \left\{ \sum_{SP} \left[\frac{1}{2} \left(\frac{fl}{d_h} + K \right)_i \left(\frac{a_c}{a_i} \right)^2 \right] \right\}^+ + \Pi_{F2} \Pi_\rho \left(\frac{\rho_l}{\rho_{TP}} \right)^+ \left\{ \sum_{TP} \left[\frac{1}{2} \left(\frac{fl}{d_h} + K \right)_i \left(\frac{a_c}{a_i} \right)^2 \right] \right\}^+ \right] \quad (62)$	
<i>Loop Energy Balance Equation:</i>	
$\frac{d(e_M - e_l)^+}{dt^+} = \Pi_e \dot{m}^+ (h_{TP} - h_l)^+ - \Pi_{SG} \dot{q}_{SG}^+ - \Pi_{loss} \dot{q}_{loss}^+ \quad (63)$	
<i>Characteristic Time Constant</i>	
$\tau_{loop} = \sum_{i=1}^N \frac{l_i}{u_i} = \sum_{i=1}^N \tau_i = \frac{M_{sys}}{\dot{m}_o} = \frac{M_{sys}}{\rho_l u_{co} a_c} \quad (64)$	
<i>Dimensionless Groups</i>	<i>Loop Two-Phase Resistance Number:</i>
<i>Loop Reference Length Number:</i>	$\Pi_{F2} = \sum_{TP} \left\{ \frac{1}{2} \left(\frac{fl}{d_h} + K \right)_i \left(\frac{a_c}{a_i} \right)^2 \right\} \quad (68)$
$\Pi_L = \sum_{i=1}^N \frac{l_i}{l_{ref}} \frac{a_c}{a_i} \quad (65)$	<i>Loop Energy Ratio:</i>
<i>where:</i>	$\Pi_e = \frac{\dot{q}_{co}}{\dot{m}_o (e_M - e_l)_o} \quad (69)$
$l_{ref} = \frac{M_{sys}}{\rho_l a_c}$	<i>Steam Generator Heat Transport Number:</i>
<i>Loop Richardson Number:</i>	$\Pi_{SG} = \frac{\dot{q}_{SGo}}{\dot{m}_o (e_M - e_l)_o} \quad (70)$
$\Pi_{Ri,\rho} = \frac{g(\rho_l - \rho_{TP})_o L_{th}}{\rho_l u_{co}^2} \quad (66)$	<i>Heat Loss Number:</i>
<i>Loop Liquid-Phase Resistance Number:</i>	$\Pi_{Loss} = \frac{\dot{q}_{loss,o}}{\dot{m}_o (e_M - e_l)_o} \quad (71)$
$\Pi_{F1} = \sum_{SP} \left\{ \frac{1}{2} \left(\frac{fl}{d_h} + K \right)_i \left(\frac{a_c}{a_i} \right)^2 \right\}_o \quad (67)$	<i>Density Ratio:</i>
	$\Pi_\rho = \left(\frac{\rho_l}{\rho_{TP}} \right) \quad (72)$

Table 7. Steady state solution for two-phase natural circulation flow rate

<i>Governing Equation:</i>	
	$\Pi_{Ri,\rho} = \Pi_{F1} + \Pi_{F2}\Pi_{\rho}$ (73)
<i>Liquid Velocity at Core Entrance::</i>	
	$u_{co}^3 + \phi_a u_{co}^2 + \phi_b u_{co} - \phi_c = 0$ (74)
<i>where:</i>	
	$\phi_a = \frac{\dot{q}_{co}\Delta\rho}{\rho_f a_c} \left(\frac{(\Pi_F + \Pi_{F2})\rho_g h_{fg} - \Delta\rho\Pi_{F2}h_{sub}}{\Pi_F\rho_g^2 h_{fg}^2 - (\Pi_F + \Pi_{F2})\rho_g h_{fg}\Delta\rho + \Pi_{F2}(\Delta\rho)^2 h_{sub}^2} \right)$ (75)
	$\phi_b = \frac{\Delta\rho}{(\rho_f a_c)^2} \left(\frac{\Delta\rho\Pi_{F2}\dot{q}_{co}^2 + L_{th}g(\rho_f a_c)^2 h_{sub}\rho_g h_{fg}}{\Pi_F\rho_g^2 h_{fg}^2 - (\Pi_F + \Pi_{F2})\rho_g h_{fg}\Delta\rho + \Pi_{F2}(\Delta\rho)^2 h_{sub}^2} \right)$ (76)
	$\phi_c = \frac{1}{\rho_f a_c} \left(\frac{L_{th}g\dot{q}_{co}\Delta\rho\rho_g h_{fg}}{\Pi_F\rho_g^2 h_{fg}^2 - (\Pi_F + \Pi_{F2})\rho_g h_{fg}\Delta\rho + \Pi_{F2}(\Delta\rho)^2 h_{sub}^2} \right)$ (77)
<i>where:</i>	$\left\{ \begin{array}{l} \Delta\rho = (\rho_f - \rho_g) \\ h_{sub} = (h_f - h_l) \\ \Pi_F = \Pi_{F1} + \Pi_{F2} \end{array} \right\}$
<i>Saturated Conditions at Inlet:</i>	
	$\Pi_z^3 + \psi_a \Pi_z^2 + \psi_b \Pi_z - \psi_c = 0$ (78)
<i>where:</i>	
	$\Pi_z = \frac{1}{N_{Zuber}} = \frac{\rho_g \dot{m}_o h_{fg}}{\rho_f \dot{q}_{co}}$ (79)
	$\psi_a = \left(\frac{\Delta\rho}{\rho_f} \right) \left(\frac{\Pi_F + \Pi_{F2}}{\Pi_F} \right)$ (80)
	$\psi_b = \left(\frac{\Delta\rho}{\rho_f} \right)^2 \left(\frac{\Pi_{F2}}{\Pi_F} \right)$ (81)
	$\psi_c = \left(\frac{\Delta\rho}{\rho_f} \right) \left(\frac{gL_{th}\rho_g^2 h_{fg}^2 a_c^2}{\dot{q}_{co}^2} \right) \left(\frac{1}{\Pi_F} \right)$ (82)

5.1.1. Scale Ratios for Saturated Two-Phase Natural Circulation

To simulate the same fluid velocity behavior in the model as in the full-scale prototype, the coefficients of equation (78) must be scaled properly. It is noted that the form of equation (78) is a special class of catastrophe function known as a constraint catastrophe. A general method of scaling single-state variable catastrophe functions was developed by Reyes [5]. That is, it is required that the following condition be satisfied:

$$\beta^3(\Pi_{zp}^3 + \psi_{ap}\Pi_{zp}^2 + \psi_{bp}\Pi_{zp} - \psi_{cp}) = \Pi_{zm}^3 + \psi_{am}\Pi_{zm}^2 + \psi_{bm}\Pi_{zm} - \psi_{cm} \quad (83)$$

This condition is satisfied by scaling each of the coefficients as follows:

$$\beta = (\Pi_z)_R \quad (84)$$

$$\beta = (\psi_a)_R \quad (85)$$

$$\beta^2 = (\psi_b)_R \quad (86)$$

$$\beta^3 = (\psi_c)_R \quad (87)$$

Evaluating each of the ratios results in the scale ratios presented in Table 8.

Table 8. Scale ratios for a saturated two-phase natural circulation loop

<p><i>Time Scale Ratio:</i></p> $\tau_{loop,R} = \frac{l_R}{(L_{th})_R^{1/2}} \quad (88)$	
<p><i>Fluid Velocity Scale Ratio:</i></p> $u_R = (L_{th})_R^{1/2} \quad (89)$	
<p><i>Power Scale Ratio:</i></p> $(\dot{q}_{co})_R = a_{c,R} (L_{th})_R^{1/2} \left(\frac{\rho_f \rho_g h_{fg}}{\Delta\rho} \right) \quad (90)$	
<p>Assuming:</p>	
<p><i>Flow Area Scale Ratio (Kinematic Similarity):</i></p> $\left(\frac{a_i}{a_c} \right)_R = 1 \quad (91)$	<p><i>Heat Loss Scale Ratio:</i></p> $\left(\frac{\dot{q}_{loss,o}}{\dot{q}_{co}} \right)_R = 1 \quad (93)$
<p><i>Steam Generator Power Scale Ratio:</i></p> $\left(\frac{\dot{q}_{SGo}}{\dot{q}_{co}} \right)_R = 1 \quad (92)$	<p><i>Loop Resistance Scale Ratios:</i></p> $\begin{aligned} (\Pi_{F1})_R &= 1 \\ (\Pi_{F2})_R &= 1 \end{aligned} \quad (94)$

5.2. Bottom-up scaling analysis for two-phase natural circulation flow

Several important local phenomena need to be scaled to evaluate the scale ratios given in Table 8. The two-phase friction and form loss coefficients are needed to evaluate equation (94). Heat transfer models for the steam generator and interconnecting piping heat loss are needed to evaluate equations (92) and (93). Core heat transfer may be of interest for some studies. Local transport models are provided as part of the lectures in this series given by Saha, et al. (2004).

Transitions in two-phase flow patterns may impact integral system behavior. Therefore an assessment must be made for each component in the system to determine which two-phase flow patterns may be delayed or entirely missed in a reduced scale test facility. In their paper, Schwartzbeck and Kocamustafaogullari [6] catalogued the applicable flow pattern transition criteria for horizontal and vertical flows. These have been summarized in Table 9.

Table 9. Scale ratios for a saturated two-phase flow pattern transitions

Horizontal Pipe Flow	
Stratified-Smooth to Stratified-Wavy:	
	$(l_R)^{3/4} = \alpha_R \left(\frac{1-\alpha}{1-x} \right)_R^{1/2} \left(\frac{\Delta\rho^3 v_f}{\rho_f^2 \rho_g} \right)_R^{1/2} \quad (95)$
Stratified to Intermittent or Annular-Dispersed Liquid:	
	$u_R = D_R^{1/2} \left(\frac{\Delta\rho}{\rho_f} \right)_R^{1/2} \quad (96)$
Intermittent or Dispersed Bubbly to Annular-Dispersed:	
	$\alpha_R = \left(\frac{\rho_f}{\Delta\rho} \right)_R \quad (97)$
Vertical Pipe Flow	
Bubbly to Slug Flow:	
	$\alpha_R = \left(\frac{\rho_f}{\Delta\rho} \right)_R \quad (98)$
Slug/Churn to Annular Flow:	
	$u_R = \left(\frac{\sigma\Delta\rho}{\rho_g^2} \right)_R^{1/4} \quad (99)$

ACKNOWLEDGEMENT

This work was supported through a U.S. Department of Energy Contract (DE- FC07-04ID14550) and the Oregon State University sabbatical program. This work was conducted through the IAEA Nuclear Power Technology Development Section.

NOMENCLATURE

Acronyms

ADS – Automatic Depressurization System
AP600 – Advanced Passive 600 MW(e)
H2TS – Hierarchical Two-Tiered Scaling
MASLWR – Multi-Application Small Light Water Reactor
PIRT – Phenomena Identification and Ranking Table
PCT – Peak Cladding Temperature
SBLOCA- Small Break Loss-of-Coolant-Accident

Symbols

a – flow area
 d_h – hydraulic diameter
e – specific internal energy
f – friction factor
g – gravity constant
h – enthalpy
j – flux term
K- Loss Coefficient
 L_{th} – Distance between heat source and heat sink thermal centers
 \dot{q} - power or heat transport rate
Q – Volumetric flow rate
S –Source term
T – Temperature
u – velocity
V – Volume
x – vapor quality

Greek Symbols

Π - Characteristic Time Ratio (Dimensionless Parameter)
 ρ - density
 τ - residence time constant
 $\Psi_k = \rho, \rho u$ or $\rho \epsilon$ (mass, momentum or energy per unit volume)

REFERENCES

- [1] ZUBER, N., Appendix D: Hierarchical, Two-Tiered Scaling Analysis, *An Integrated Structure and Scaling Methodology for Severe Accident Technical Issue Resolution*, U.S Nuclear Regulatory Commission, Washington, D.C. 20555, NUREG/CR-5809, November 1991.
- [2] SHAW, R.A. et al., Development of a Phenomena Identification and Ranking Table (PIRT) for Thermal Hydraulic Phenomena during a PWR Large Break LOCA, U.S Nuclear Regulatory Commission, Washington, D.C. 20555, NUREG/CR-5074, November 1985.
- [3] WILSON G.E. and BOYACK, B.E., The role of the PIRT process in experiments, code development and code applications associated with reactor safety analysis. *Nuclear Engineering and Design*, 186, pp. 23-37 (1998).

- [4] SAATY, T., Decision-Making for Leaders. Belmont, California Lifetime Learning Publications, Wadsworth, Inc. (1982).
- [5] REYES, J.N., Scaling Single State Variable Catastrophe Functions: An Application to Two-Phase Natural Circulation, *Nuclear Engineering and Design* 151, pp. 41-48 (1994).
- [6] SCHWARTZBECK, R.K. and KOCAMUSTAFAOGULLARI, G., Similarity Requirements for Two-Phase Flow Patter Transitions, *Nuclear Engineering and Design* 116, pp135-147 (1989).

Appendix A

DESCRIPTION OF THE MASLWR DESIGN

The Multi-Application Small Light Water Reactor (MASLWR) is a 150 MW(t) modular nuclear reactor that uses natural circulation for primary loop cooling. Figure A.1 shows a single power generation module for the MASLWR design. MASLWR implements an integrated reactor vessel with an internal helical coil steam generator. The reactor vessel is enclosed in a high-pressure steel containment vessel that is partially filled with water to serve as a suppression pool. The containment vessel in turn resides in a large exterior cooling pool that acts as the ultimate heat sink.

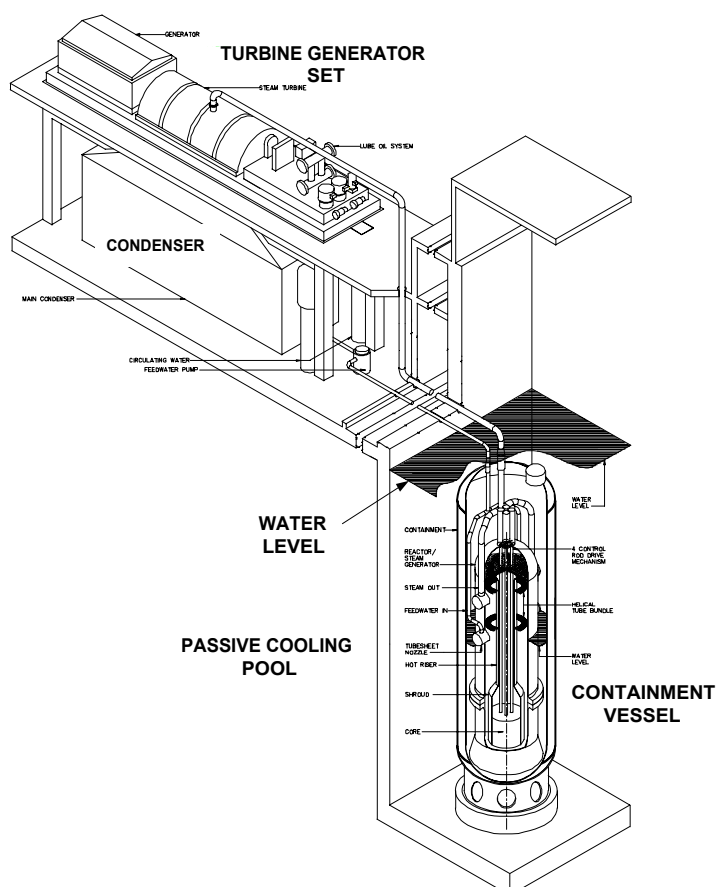


FIG. A.1. Schematic of the MASLWR exterior cooling pool and turbine-generator set.

A.1 MASLWR primary loop design

Because MASLWR uses natural circulation for primary loop flow, reactor coolant pumps are not needed. In this regard, its primary flow loop is quite simple as shown in Figure A.2. The long vertical tube in the center of the reactor vessel is called the riser and functions like a chimney to enhance the driving head of the natural circulation flow. Starting from the bottom of the riser, fluid enters the core which is located in a shroud connected to the riser entrance. Upon traveling through the core, the fluid is heated and thus ascends through the riser due to its buoyancy. Hot fluid in the surrounding annulus, outside the riser is cooled by convective heat transfer to a helical coil steam generator. The fluid inside the tubes is at a lower pressure, hence boiling occurs inside the tubes to generate superheated steam. The steam produced within the tube side of this coil travels on to the turbine generator set where it is used to produce electrical power. The cooled primary fluid in the annulus is negatively buoyant and descends to the bottom of the vessel and the inlet of the core thereby completing its loop.

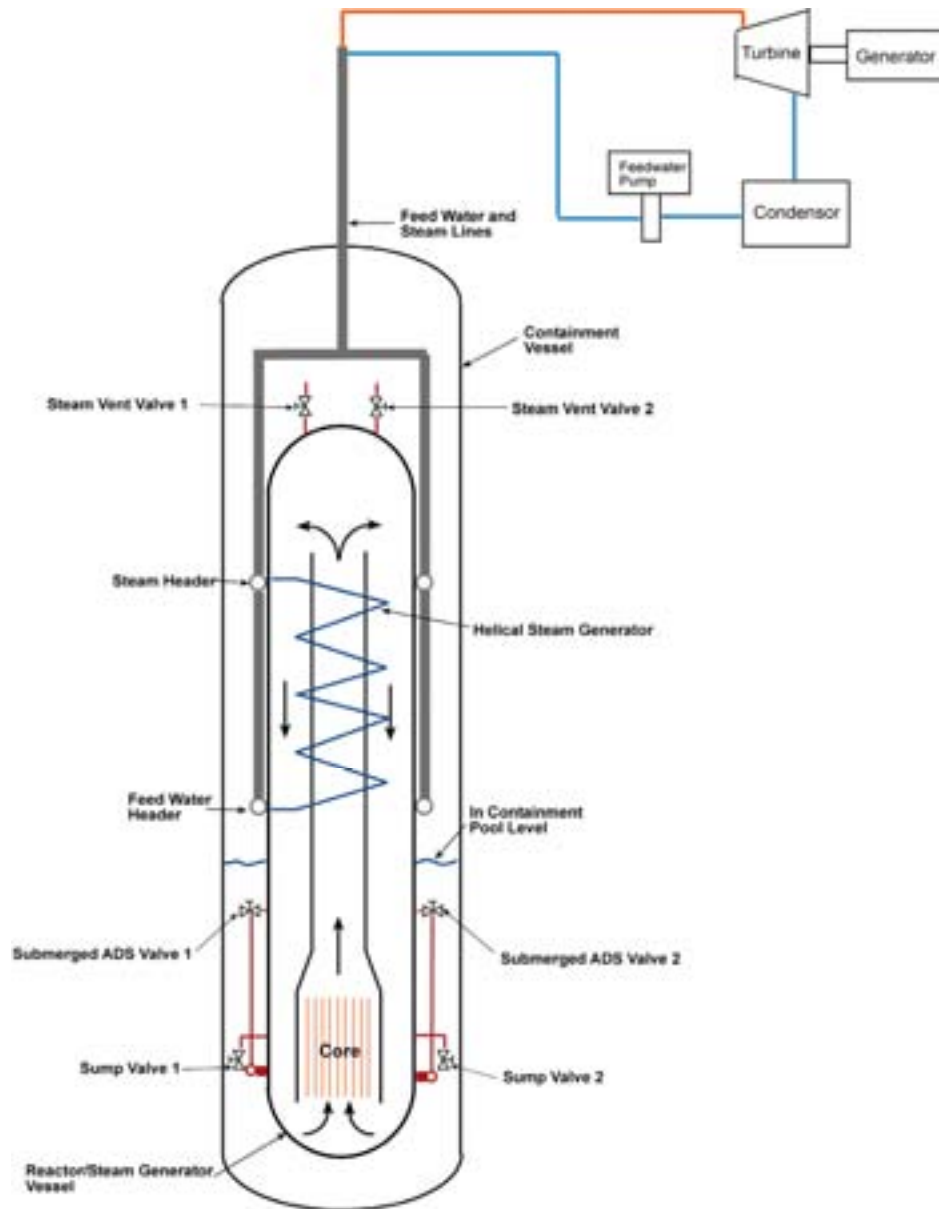


FIG. A.2. Schematic of the MASLWR reactor cooling system and containment.

Table A.1 lists the steady-state operating conditions for MASLWR. The design provides a 53°K temperature rise from the core inlet to the core outlet. In addition, it is designed to provide superheated steam at the helical coil outlet to eliminate the need for separators and driers. The secondary side pressure was selected so that off-the-shelf low pressure steam turbines could be implemented.

Table A.1 MASLWR steady-state operating conditions

Primary Side	
Reactor Power (MW)	150.00
Primary Pressure (MPa)	7.60
Primary Mass Flow Rate (kg/s)	597.00
Reactor Inlet Temperature (K)	491.80
Reactor Outlet Temperature (K)	544.30
Saturation Temperature (K)	565.00
Reactor Outlet Void Fraction	0.00%
Secondary Side	
Steam Pressure (MPa)	1.50
Steam Outlet Quality	1.00
Steam Temperature (K)	481.40
Saturation Temperature (K)	471.60
Feedwater Temperature (K)	310.00
Feedwater Flowrate (kg/s)	56.10

A.2 MASLWR passive safety system SBLOCA operations

This section briefly describes the evolution of a Small Break Loss-of-Coolant Accident in MASLWR. Because MASLWR is an integrated reactor system, there are very few plausible primary break scenarios. In the event of a small break, the MASLWR passive safety systems would respond to the accident. The passive safety systems consist of the following components:

- Two, independent, small diameter, steam vent valves (SVV)
- Two, independent, small diameter, Automatic Depressurization System (ADS) valves
- Two, independent, small diameter, Sump Recirculation Valves (SV)
- A high-pressure containment vessel with an internal pressure suppression pool, and
- An external cooling pool that serves as the ultimate heat sink for the high-pressure containment and reactor decay heat.

Let us postulate the inadvertent opening of an ADS valve. Figure A.3 provides a schematic of the postulated pressure trend for illustration purposes. As shown in the figure, the transient begins with a relatively short blowdown period that consists of a subcooled blowdown into the suppression pool within the stainless steel containment. The suppression pool consists of the annular space bounded by the exterior surface of the reactor vessel and inner surface of the containment walls. It is partially filled with water. This water region is integral to the long term removal of decay heat following system depressurization (blowdown). The rapid rise in containment pressure results in a Safety Injection signal which automatically opens the steam vent valves, the ADS valves and the sump recirculation valves. The ADS blowdown period serves to further reduce the reactor vessel pressure well below the saturation pressure corresponding to the hot leg temperature. A major advantage to the small volume, high-pressure containment is that the blowdown quickly results in equalizing the containment and reactor vessel pressures, effectively terminating the blowdown. As the pressures become equalized, a natural circulation flow path is established in which the sump fluid enters through the sump recirculation valves, descends through the downcomer region in the lower portion of the reactor vessel, rises through the core and riser, and finally exits through the upper vent valve into the containment as a saturated vapor. From the vent valve, the fluid returns to the sump via condensation on the containment walls and/or water surface, thus completing its circuit.

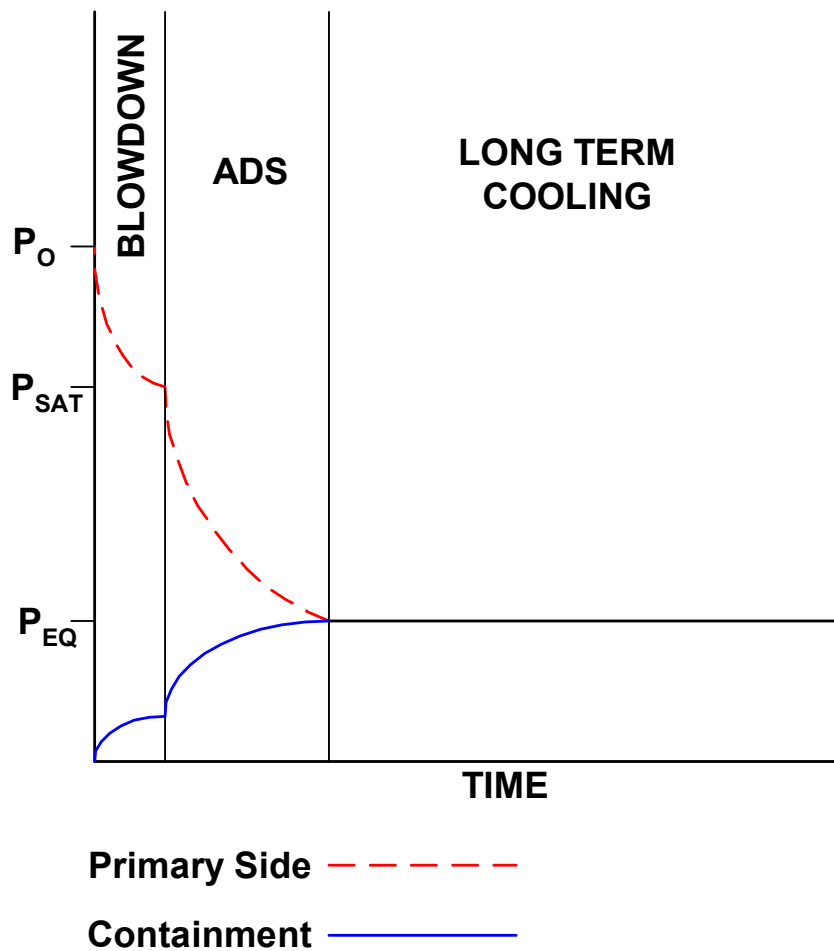


FIG. A.3. Illustration of transient phases for a MASLWR SBLOCA.

Finally, to ensure the long term removal of heat from the containment and thus to moderate the containment pressure, the containment itself is submerged in an outer pool of water which is open to the atmosphere. Within this pool, thermal energy is transferred from the outer containment wall to the atmosphere via natural convection and circulation of the water. The pool is formed in the space between the outer containment wall and the inner wall of the concrete structure in which the containment is placed.

In conclusion, a SBLOCA in MASLWR can be divided into three phase, or modes of operation, a blowdown phase, an ADS operation phase and a long term cooling phase. A more detailed description of the MASLWR design will be made available as part of the documentation for the IAEA Small to Medium Reactor (SMR) program.

ANNEX 12

AP600 AND AP1000 PASSIVE SAFETY SYSTEM DESIGN AND TESTING IN APEX

J.N. Reyes, Jr*

International Atomic Energy Agency, Vienna

Abstract

This lecture describes the integral operation of the AP600/AP1000 passive safety systems. It presents methods to calculate and scale injection flow rates for gravity drain tanks and pressurized tanks and a method to estimate depressurization flow rates for an ADS system.

1. INTRODUCTION

The application of passive safety systems in new nuclear power plants is a potential means of achieving simplification and improving economics. The use of passive systems is not entirely new, and is not unique to any particular line of new reactor designs. But an increased reliance on this approach, making safety functions less dependent on active components like pumps and diesel generators, is potentially an important means to achieve reduced costs for future nuclear power plants. Many new reactor designs that are under development incorporate passive systems based on natural circulation.

The purpose of this lecture is to introduce the passive safety systems used in the Westinghouse *Advanced Passive 600* MWe (AP600) and *Advanced Passive 1000* MWe (AP1000) nuclear plant designs and to provide some simple modeling and scaling techniques for these systems.

1.1. Definition of passive safety systems

What is meant by a passive safety system? A passive safety system provides cooling to the nuclear core using processes such as, natural convection heat transfer, vapor condensation, liquid evaporation, pressure driven coolant injection, or gravity driven coolant injection. It does not rely on external mechanical and/or electrical power, signals or forces such as electric pumps. A useful list of terminology related to passive safety is found in IAEA-TECDOC-626 [1] It is important to note that passive safety systems can provide an equal or greater degree of safety as active safety systems used in conventional plants. For example, to obtain final design approval in the U.S., a passively safe nuclear plant must demonstrate that under worst-case accident conditions the plant can be passively cooled without external power or operator actions for a minimum of 3 days [2].

2. DESCRIPTION OF AP600/AP1000 DESIGN AND PASSIVE SAFETY SYSTEMS

The AP600 and AP1000 are pressurized light water nuclear reactors designed to produce thermal powers of 1933 MW and 3400 MW, respectively [3]. Figure 1 shows the overall layout of the plant. Figure 2 is a schematic that illustrates the primary system components. The primary loop consists of the reactor vessel, which contains the nuclear fuel assemblies; two hot legs, which connect the reactor vessel to the steam generators; two steam generators; a pressurizer; four canned motor pumps; and four cold legs.

Normal full power operation is straightforward. Heat is generated in the reactor fuel. This heat is transported by forced convection to the water. Since the entire system operates at 15.5 MPa (2250 psia), bulk boiling of the water does not occur. The heated water is transported through the hot legs to the U-tubes inside the steam generators. The energy of the primary coolant inside the tubes is

* Henry and Janice Schuette Endowed Chair Professor of Nuclear Engineering Department of Nuclear Engineering and Radiation Health Physics, Oregon State University, Corvallis, Oregon, USA, 97331. Funded by Oregon State University Sabbatical Leave, U.S. Department of Energy, and IAEA.

transferred to the water on the secondary side by forced convection inside the tubes, conduction through the tube walls and boiling on the outside surface of the U-tubes. The cooled water leaving the steam generator is pumped by four canned motor pumps, through four cold legs, back into the reactor vessel where the heating cycle is repeated. Primary system pressure is maintained constant by the pressurizer.

2.1. AP600/AP1000 passive safety systems

With respect to thermal hydraulic phenomena, normal full-power operation is typical of most pressurized water reactor (PWR) systems. A key feature of the AP600 and AP1000 designs is that it uses core decay heat to drive the core cooling process. In fact, the AP600/AP1000 designs use core decay heat to drive the following six natural circulation processes:

- Primary System Natural Circulation (2x4 Loop),
- PRHR Loop Circulation (1 Loop),
- CMT Loop Circulation (2 loops),
- Lower Containment Sump Recirculation (2 loops),
- Containment Internal Circulation (Steam),
- Containment External Circulation (Air).

Figure 3 presents a simple schematic that describes the connections of the primary system passive safety systems.

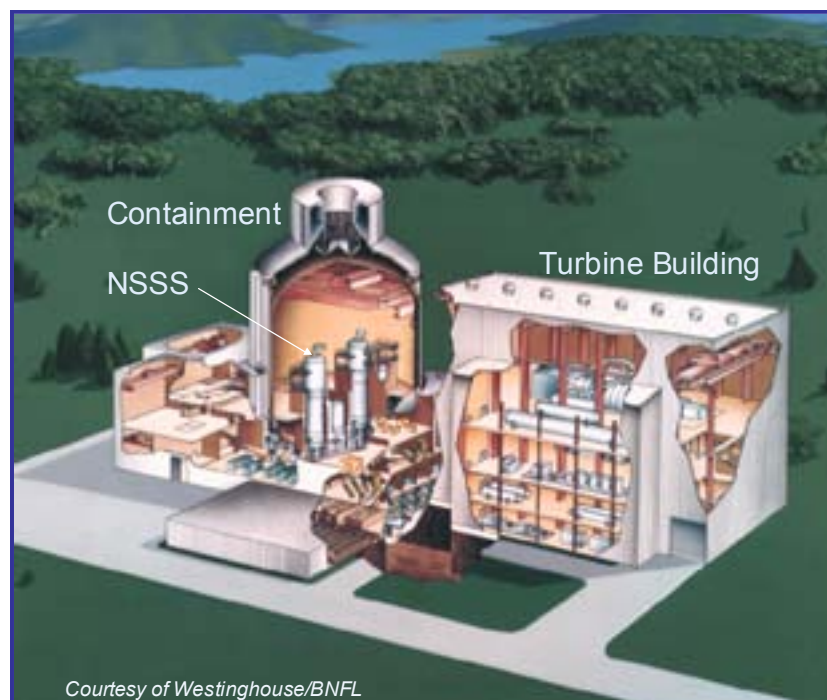


FIG. 1. General layout of the AP600 and AP1000 plants.

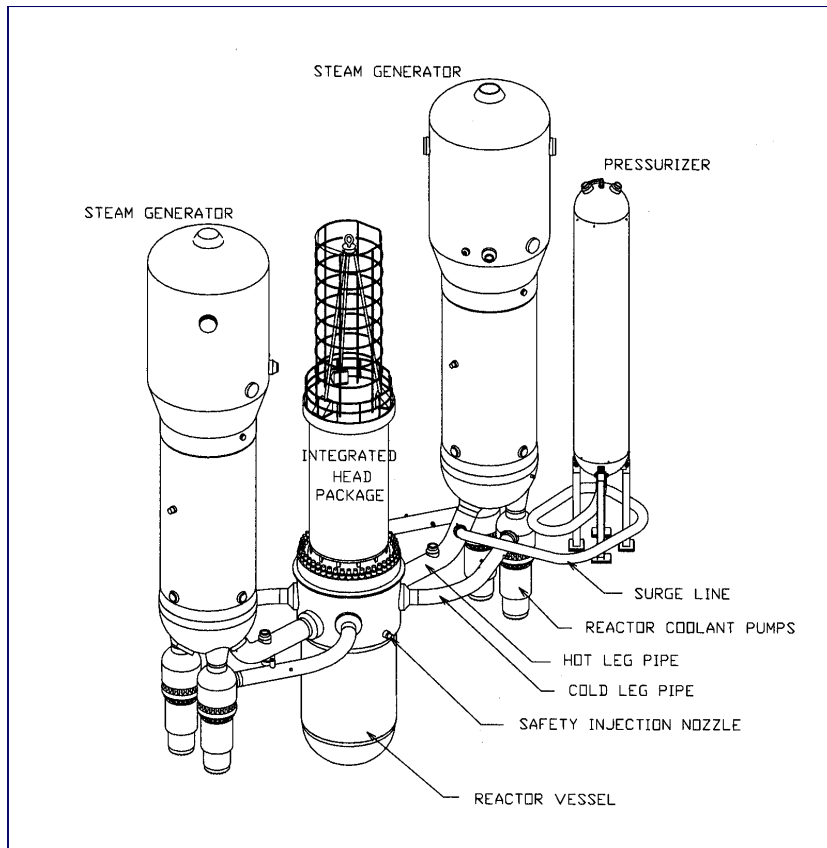


FIG. 2. Schematic of primary loop of the AP600 and AP1000 plants.

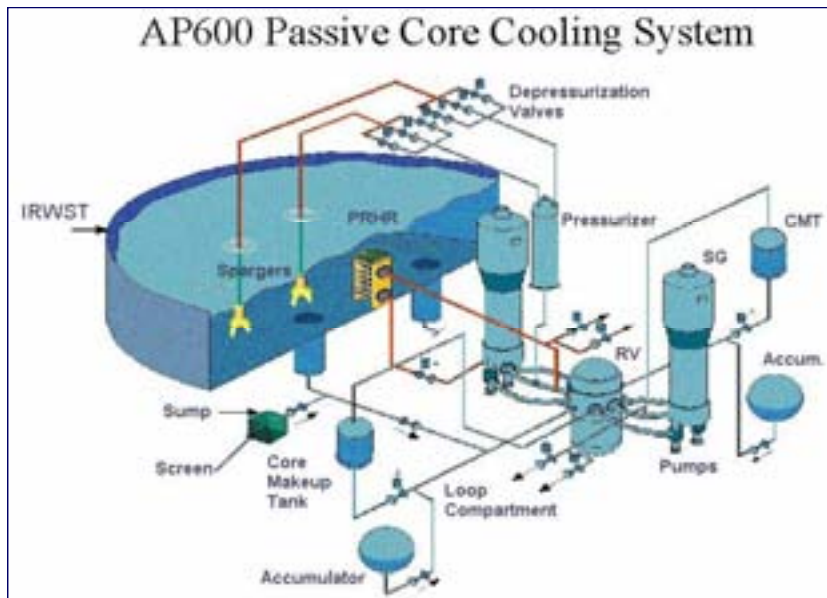


FIG. 3. Passive safety systems used in the AP600/AP1000 designs.

The AP600/AP1000 passive safety systems consist of:

- A Passive Residual Heat Removal (PRHR) System
- Two Core Make-up Tanks (CMTs)
- A Four Stage Automatic Depressurization System (ADS)
- Two Accumulator Tanks (ACC)
- An In-containment Refueling Water Storage Tank, (IRWST)
- A Lower Containment Sump (CS)
- Passive Containment Cooling System (PCCS)

Passive Residual Heat Removal (PRHR) System: The passive residual heat removal (PRHR) consists of a C-Tube type heat exchanger that resides in the water-filled In-containment Refueling Water Storage Tank (IRWST) as shown in the schematic given in Figure 4. The PRHR provides primary coolant heat removal via a natural circulation loop. Hot water rises through the PRHR inlet line attached to one of the hot legs. The hot water enters the tubesheet in the top header of the PRHR heat exchanger at full system pressure and temperature. The IRWST is filled with cold borated water and is open to containment. Heat removal from the PRHR heat exchanger occurs by boiling on the outside surface of the tubes. The cold primary coolant returns to the primary loop via the PRHR outlet line that is connected to the steam generator lower head.

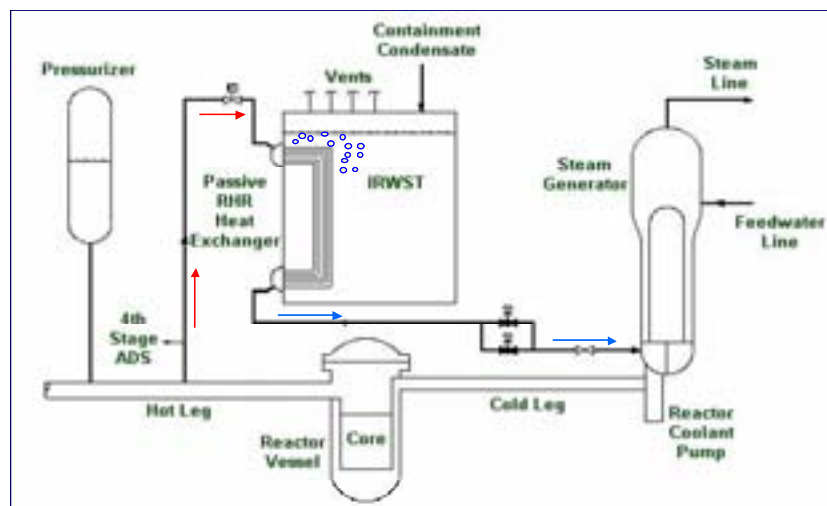


FIG. 4. Passive residual heat removal (PRHR) system.

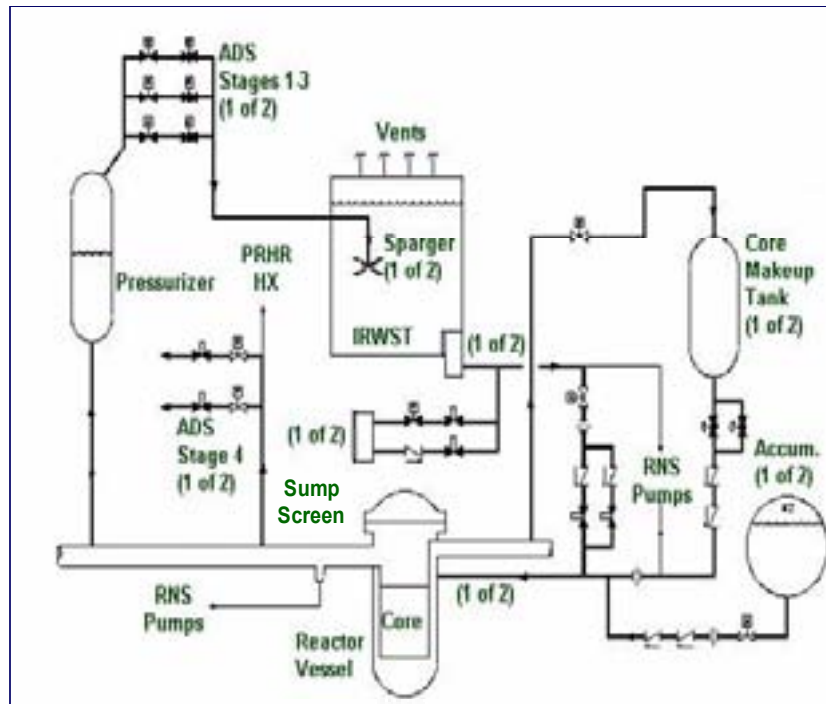


FIG. 5. Passive safety injection and sump recirculation.

Core Make-up Tank (CMT): The Core Make-up Tanks effectively replace the high-pressure safety injection systems in conventional PWRs. Each CMT consists of a large volume stainless steel tank with an inlet line that connects one of the cold legs to the top of the CMT and an outlet line that connects the bottom of the CMT to the Direct Vessel Injection (DVI) line. The DVI line is connected to the reactor vessel downcomer. Each CMT is filled with cold borated water. The CMT inlet valve is normally open and hence the CMT is normally at primary system pressure. The CMT outlet valve is normally closed, preventing natural circulation during normal operation. When the outlet valve is open, a natural circulation path is established. Cold borated water flows to the reactor vessel and hot primary fluid flows upward into the top of the CMT.

Automatic Depressurization System (ADS): The Automatic Depressurization System consists of four stages of valves that provide for the controlled reduction of primary system pressure. The first three stages consist of two trains of valves connected to the top of the pressurizer. The first stage opens on CMT liquid level. ADS stages two and three open shortly thereafter on timers. The ADS 1-3 valves discharge primary system steam into a sparger line that vents into the IRWST. The steam is condensed by direct contact with the highly subcooled water in the IRWST. The fourth stage of the ADS consists of two large valves attached to ADS lines on each hot leg. The ADS-4 valves open on low CMT liquid level and effectively bring primary side pressure down to containment conditions. The ADS-4 valves vent directly into the containment building.

Accumulators (ACC): The accumulators are similar to those found in conventional PWRs. They are large spherical tanks approximately three-quarters filled with cold borated water and pre-pressurized with nitrogen. The accumulator outlet line is connected to the DVI line. A pair of check valves prevents injection flow during normal operating conditions. When system pressure drops below the accumulator pressure (plus the check valve cracking pressure), the check valves open allowing coolant injection to the reactor downcomer via the DVI line.

In-containment Refuelling Water Storage Tank (IRWST): The In-containment Refuelling Water Storage Tank is a very large concrete pool filled with cold borated water. It serves as the heat sink for the PRHR heat exchanger and a source of water for IRWST injection. The IRWST has two injection lines connected to the reactor vessel DVI lines. These flow paths are normally isolated by two check valves in series. When the primary pressure drops below the head pressure of the water in the IRWST,

the flow path is established through the DVI into the reactor vessel downcomer. The IRWST water is sufficient to flood the lower containment compartments to a level above the reactor vessel head and below the outlet of the ADS-4 lines.

Containment Sump Recirculation: After the lower containment sump and the IRWST liquid levels are equalized, the sump valves are opened to establish a natural circulation path. Primary coolant is boiled in the reactor core by decay heat. This low-density mixture flows upward through the core and steam and liquid is vented out of the ADS-4 lines into containment. Cooler water from the containment sump is drawn in through the sump screens into the sump lines that connect to the DVI lines.

Containment and Passive Containment Cooling System (PCCS): Figure 6 presents a schematic of the AP600/AP1000 containment. It consists of a large steel vessel that houses the Nuclear Steam Supply System (NSSS) and all of the passive safety injection systems. The steel containment vessel resides inside of a concrete structure with ducts that allows cool outside air to come in contact with the outside surface of the containment vessel. When steam is vented into containment via a primary system break or ADS-4 valve actuation, it rises to the containment dome where it is condensed into liquid. The energy of the steam is transferred to the air on the outside of containment via conduction through the containment wall and natural convection to the air. As the air is heated, it rises through the ducts creating a natural circulation flow path that draws cool air in from the inlet duct and vents hot air out the top of the concrete structure. The condensate inside containment is directed back into the IRWST and the containment sump where it becomes a source of cool water in the sump recirculation process. Early in a LOCA transient, cold water is sprayed by gravity draining onto the containment vessel head to enhance containment cooling. A large tank of water, located at the top of the containment structure, serves as the source of water for this operation.

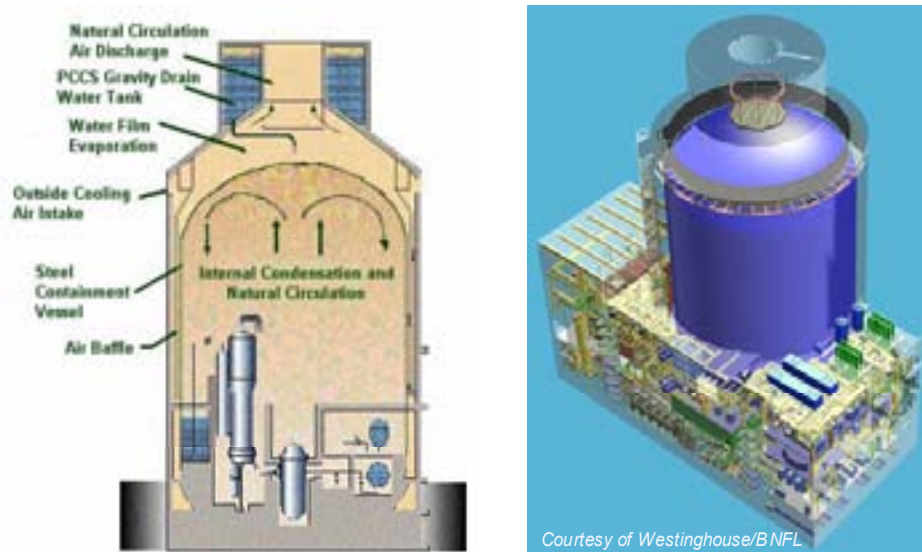


FIG. 6. Containment and passive containment cooling system (PCCS).

2.1.1. Integrated passive safety system response during a SBLOCA

The most effective means of describing the function of each of these passive safety systems is to relate their operation in response to a Small Break Loss-of-Coolant-Accident (SBLOCA). The first phase of a SBLOCA is the subcooled blowdown phase. During this phase, high-pressure subcooled liquid is venting from the break under choked flow conditions. The primary system pressure and primary liquid inventory will be decreasing. When low pressure or low liquid level is sensed in the pressurizer, a safety signal is issued that results in the following automatic actions:

- Scram reactor,
- Open the PRHR inlet and outlet valves,
- Open the CMT outlet valves,
- Isolate Steam Generators (Feedwater and Main Steam),
- Trip Reactor Coolant Pumps (Coastdown).

Natural circulation is established in the PRHR loop and the CMT loops. Boiling occurs on the PRHR tubes and hot water begins to fill the top of the CMTs. If the plant continues to depressurize, eventually the primary system reaches the saturation pressure corresponding to the hot leg temperature. Depending on the break size, the system pressure will reach a plateau during which the loop will experience a period of two-phase natural circulation.

If primary coolant inventory continues to decrease, eventually the CMTs will begin to drain. At a predetermined CMT level, the ADS-1 valves will open followed by the ADS 2-3 valves. System pressure will drop very quickly as a result of the ADS 1-3 venting steam into the IRWST. The primary system pressure soon drops below the accumulator tank pressure significant quantities of cold borated water are injected into the reactor vessel.

If the CMT liquid level continues to decrease, the ADS-4 actuation setpoint will be reached. The ADS-4 valves open, dropping primary system pressure below the head pressure of the IRWST liquid. The IRWST drains by gravity into the reactor vessel, out the break and ADS 4 valves into the containment sump. Eventually the IRWST and containment sump liquid levels equalize and long term sump recirculation cooling is established by opening the sump valves.

Steam vented through the ADS-4 valves is condensed on the inside surfaces of the containment vessel and the containment vessel is externally cooled by air and water as needed. The condensate inside containment is returned to the containment sump and IRWST where it is available to sump recirculation cooling.

3. PASSIVE SAFETY INJECTION SYSTEMS

This chapter provides some simple models for passive safety injection systems of the type used in the AP600 and AP1000 designs. It includes a description of the governing equations for pressurized and gravity drain tanks. These are applicable to the accumulators, CMTs, and IRWST. Scaling relations are also provided for passive safety injection experiment design.

3.1. Governing equations

Figure 7 shows the simple passive safety system tank considered in this section. The pressure at the liquid free surface is denoted by P_{FS} . The pressure at the injection line exit is denoted by P_E . Most passive safety tanks are filled with cold borated water. Hence, it is reasonable to assume that the working fluid is incompressible. The cross-sectional area of the tank, A_{Tank} , is assumed constant for this analysis. The injection flow area is denoted by A_E . The injection lines usually include multiple check valves, isolation valves and bends. As a result, the form loss coefficient, K , typically dominates the pressure drop in the line.

The injection mass flow rate is denoted by \dot{m}_{inj} and the time dependent liquid level by $L(t)$.

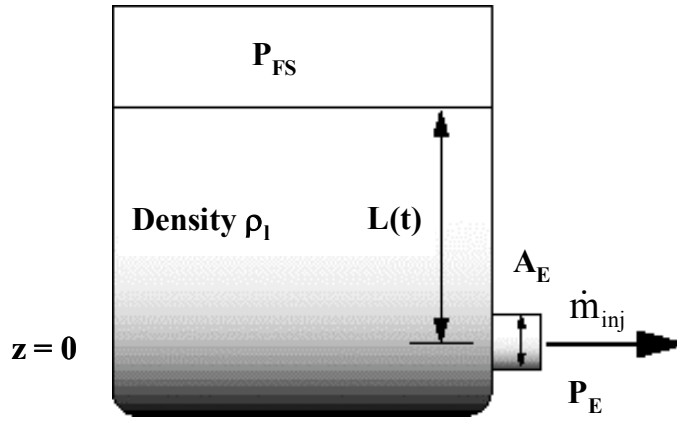


FIG. 7. Schematic for a passive safety system tank.

The governing equations for a passive safety injection tank are provided in Table 1. These equations will be examined for two types of passive safety systems. The first passive safety system implements tanks that drain under the influence of gravity, such as the CMT or the IRWST. The second passive system uses a pressurized tank to inject coolant, such as an accumulator.

Table 1. Governing equations for a passive safety system injection tank

Governing Equations	
<i>Mass Conservation:</i>	
$\rho_1 A_{Tank} \frac{dL}{dt} = -\dot{m}_{inj} \quad (1)$	
<i>Bernoulli Equation:</i>	
$\frac{P_{FS}}{\rho_1 g} + z_{FS} + \frac{v_{FS}^2}{2g} = \frac{P_E}{\rho_1 g} + z_E + \frac{v_E^2}{2g} + h_l \quad (2)$	
<i>Darcy Formula:</i>	
$h_l = \frac{v_E^2}{2g} \left(\frac{fl}{d} + K \right)_E = \frac{v_E^2}{2g} \Pi_{FE} \quad (3)$	
Governing Differential Equation	
$\rho_1 A_{Tank} \frac{dL}{dt} = -\dot{m}_o \left[\frac{\Delta P + \rho_1 g L}{\Delta P_o + \rho_1 g L_o} \right]^{1/2} \quad (4)$	
where:	
$\dot{m}_o = A_E \left\{ \frac{2\rho_1(\Delta P_o + \rho_1 g L_o)}{1 + \Pi_{FE}} \right\}^{1/2} \quad (5)$	

3.2. Gravity draining tanks (CMT and IRWST)

For tanks that drain by gravity, it is assumed that the static pressure at the free surface equals that at the injection line exit. Thus the governing differential equation is given by equation (6) in Table 2. Using the initial conditions described by equations (7) and (8), the governing differential equation can be written in dimensionless form as given by equation (9). Equation (11) defines a characteristic residence time, τ , as the ratio of the initial liquid mass in the tank and the initial injection flow rate. Equation (9) can be integrated to obtain a very simple expression for the liquid level as a function of time.

Table 2. Governing equations and analytical solution for a gravity drain tank

Governing Differential Equation	
	$\rho_l A_{Tank} \frac{dL}{dt} = -\rho_l A_E \left\{ \frac{2gL}{1 + \Pi_{FE}} \right\}^{1/2} \quad (6)$
Initial Conditions	
	$M_o = \rho_l A_{Tank} L_o \quad (7)$
	$\dot{m}_o = \rho_l A_E \left\{ \frac{2gL_o}{1 + \Pi_{FE}} \right\}^{1/2} \quad (8)$
Dimensionless Equation	
	$\frac{dL^+}{dt^+} = -(L^+)^{1/2} \quad (9)$
<i>where</i>	$L^+ = \frac{L}{L_o} \quad (10)$
	$\dot{m}^+ = \frac{\dot{m}}{\dot{m}_o} \quad (11)$
	$t^+ = \frac{t}{\tau} = \frac{t}{(M_o/\dot{m}_o)} \quad (12)$
Analytical Solutions	
	$L^+ = \left(1 - \frac{t^+}{2} \right)^2 \quad (13)$
	$\dot{m}^+ = \left(1 - \frac{t^+}{2} \right) \quad (14)$
<i>Ranges:</i>	$0 \leq L^+ \leq 1$
	$0 \leq t^+ \leq 2$
	$0 \leq \dot{m}^+ \leq 1$

Figure 8 presents a universal curve for gravity draining for the case of a tank with constant cross-sectional area with an incompressible working fluid and an exit line pressure drop that is dominated by form losses.

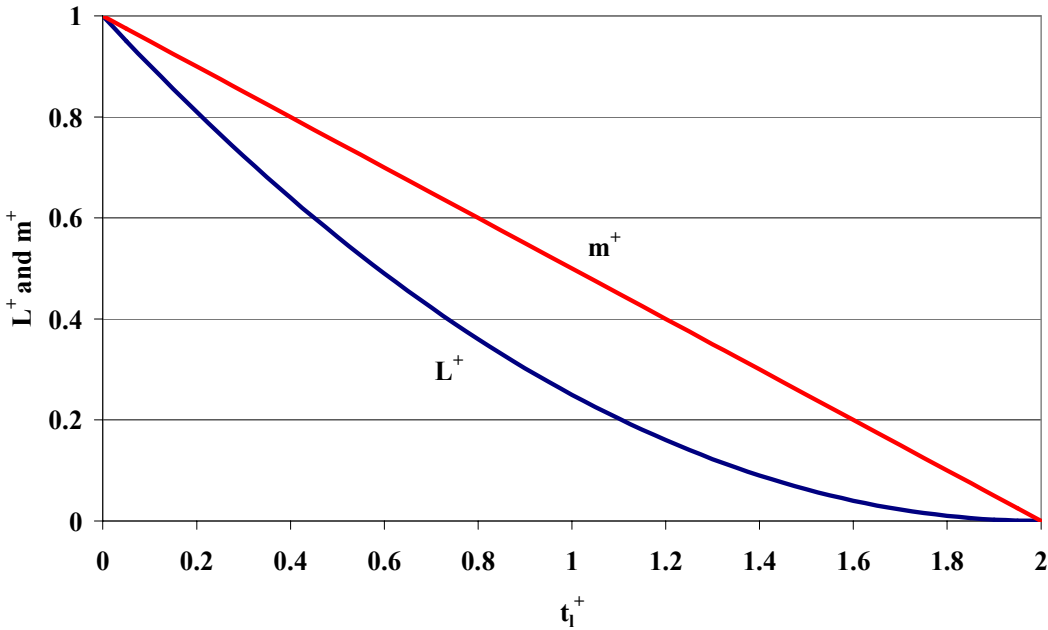


FIG. 8. Gravity draining curve of dimensionless liquid level and injection mass flow rate versus dimensionless time. (Constant tank cross-sectional area, incompressible fluid, form loss dominated at exit).

Table 3 illustrates how one can use the dimensionless groups presented above to develop similarity criteria for the design of a passive safety system experiment. It is important to note that the designer has many choices in the process. For example, the tank length scale ratio and cross-sectional area ratio can be selected based on commercial availability and cost. However, if the tank is connected to an integral system, such flexibility might be lost because other factors may be fixed, such as the injection mass flow rate scale ratio. Using the same working fluid usually simplifies the problem. The example provided is illustrative of the process.

Table 3. Similarity criteria for the design of a passive safety system gravity drain tank

<p>Similarity Criteria</p> $L_R^+ = \frac{\left(\frac{L}{L_o}\right)_m}{\left(\frac{L}{L_o}\right)_p} = 1 \quad (15)$	$t_R^+ = \frac{\left(\frac{t}{\tau}\right)_m}{\left(\frac{t}{\tau}\right)_p} = 1 \quad (16)$
<p>Scaling Example</p>	
<p><i>Scale Model Requirements</i></p> <ul style="list-style-type: none"> • Time Scale Ratio = 1:2 • Length Scale Ratio = 1:4 • Tank Area Ratio = 1:50 • Fluid Property Similitude (i.e., same working fluid) 	
<p><i>Scale Ratios</i></p> $t_R = \tau_R = \frac{(M_o)_R}{(\dot{m}_o)_R} = \frac{1}{2} \quad (17)$ <p>Hence:</p> $(M_o)_R = (A_{Tank})_R (L_o)_R = \frac{1}{200} \quad (18)$ <p>Substituting into (15) yields:</p> $(\dot{m}_o)_R = \frac{1}{100} \quad (19)$ <p>Preserving the 1/2 time scale in a 1/4 length scale injection line requires the fluid to travel at a 1/2 velocity ($L_R/t_R = 1/2$). This yields the design requirement:</p> $(A_E)_R = \frac{1}{50} \quad (20)$ <p>Lastly, equation (8) is used to obtain the following, scale ratio:</p> $(\dot{m}_o)_R = \frac{(A_E)_R (L_o)_R^{1/2}}{(\Pi_{FE})_R^{1/2}} = \frac{(A_E)_R}{2(\Pi_{FE})_R^{1/2}} \quad (21)$ <p>Substituting the length scale ratio and the injection line flow area ratio yields the last design requirement needed to</p> $(\Pi_{FE})_R = 1 \quad (22)$	

3.3. Pressurized coolant injection tanks (accumulators)

This section presents an analysis for the liquid discharge of a pressurized tank into a reservoir having a fixed backpressure. In actual practice, the backpressure would be decreasing at a rate dictated by the overall system transient.

For pressurized coolant injection tanks, the difference between the charging pressure in the tank and the system pressure is typically much greater than the gravity head of the liquid in the tank. Hence the gravity term can be neglected. It has been assumed that the liquid is incompressible. Because the tanks are normally quite large, the expansion of the gas can be relatively slow, particularly during a SBLOCA. Thus, the assumption that the gas expands isothermally is reasonable. However, this assumption becomes less applicable to the LBLOCA. Therefore a second analysis was conducted assuming an isentropic expansion of the gas. The similarity criteria will remain the same for both bases. Table 4 lists the governing equations for the pressurized injection tank.

Table 4. Governing equations for a passive safety system pressurized injection tank

Governing Equations	
<i>Mass Conservation (Liquid):</i>	
	$\rho_l \frac{dV_l}{dt} = -\dot{m}_o \left(\frac{P - P_E}{P_o - P_E} \right)^{1/2} \quad (23)$
<i>Bernoulli Equation (Liquid):</i>	
	$\frac{P}{\rho_l g} + z_{FS} + \frac{v_{FS}^2}{2g} = \frac{P_E}{\rho_l g} + z_E + \frac{v_E^2}{2g} + h_l \quad (24)$
<i>Darcy Formula (Liquid Injection Line):</i>	
	$h_l = \frac{v_E^2}{2g} \left(\frac{fl}{d} + K \right)_E = \frac{v_E^2}{2g} \Pi_{FE} \quad (25)$
<i>Component Volumes:</i>	
	$V_g = V_{Tank} - V_l \quad (26)$
<i>Isothermal Expansion (Gas):</i>	
	$P_o V_{go} = P V_g \quad (27)$
<i>Isentropic Expansion (Gas):</i>	
	$\frac{P}{P_o} = \left(\frac{V_{go}}{V_g} \right)^{\gamma} \quad (28)$

Table 5 presents the depressurization rate equations for the case of isothermal expansion and isentropic expansion of the charging gas. The governing differential equations are very similar. The solution to the isentropic case is an approximate integral, nonetheless the two results are similar as shown in Figures 9 and 10.

Table 5. Governing differential equation and analytical solutions

Dimensionless Terms:	
$P^+ = \frac{P}{P_o}$ $P_E^+ = \frac{P_E}{P_o}$ $\Delta P_E^+ = 1 - P_E^+$ $\Delta P^+ = P^+ - P_E^+$ $t_g^+ = \frac{t}{\tau_g} = \frac{t}{(\rho_l V_{go} / \dot{m}_o)}$	
<p>Isothermal Expansion:</p> $\frac{dP^+}{dt^+} = -(P^+)^2 \left[\frac{\Delta P^+}{\Delta P_E^+} \right]^{1/2} \quad (29)$ <p>Analytical Solution: (31)</p> $\frac{(\Delta P^+)^{1/2}}{P^+} + \frac{1}{(P_E^+)^{1/2}} \tan^{-1} \left(\frac{\Delta P^+}{P_E^+} \right)^{1/2} = \phi - \frac{P_E^+ t_g^+}{(\Delta P_E^+)^{1/2}}$ <p>where:</p> $\phi = (\Delta P_E^+)^{1/2} + \frac{1}{(P_E^+)^{1/2}} \tan^{-1} \left(\frac{\Delta P_E^+}{P_E^+} \right)^{1/2}$	<p>Isentropic Expansion:</p> $\frac{dP^+}{dt^+} = -\gamma (P^+)^{\gamma+1} \left[\frac{\Delta P^+}{\Delta P_E^+} \right]^{1/2} \quad (32)$ <p>Analytical Solution: (33)</p> $P^+ \approx \frac{4P_E^+ \Delta P_E^+}{4\Delta P_E^+ - (2\Delta P_E^+ - \gamma P_E^+ t_g^+)^2}$

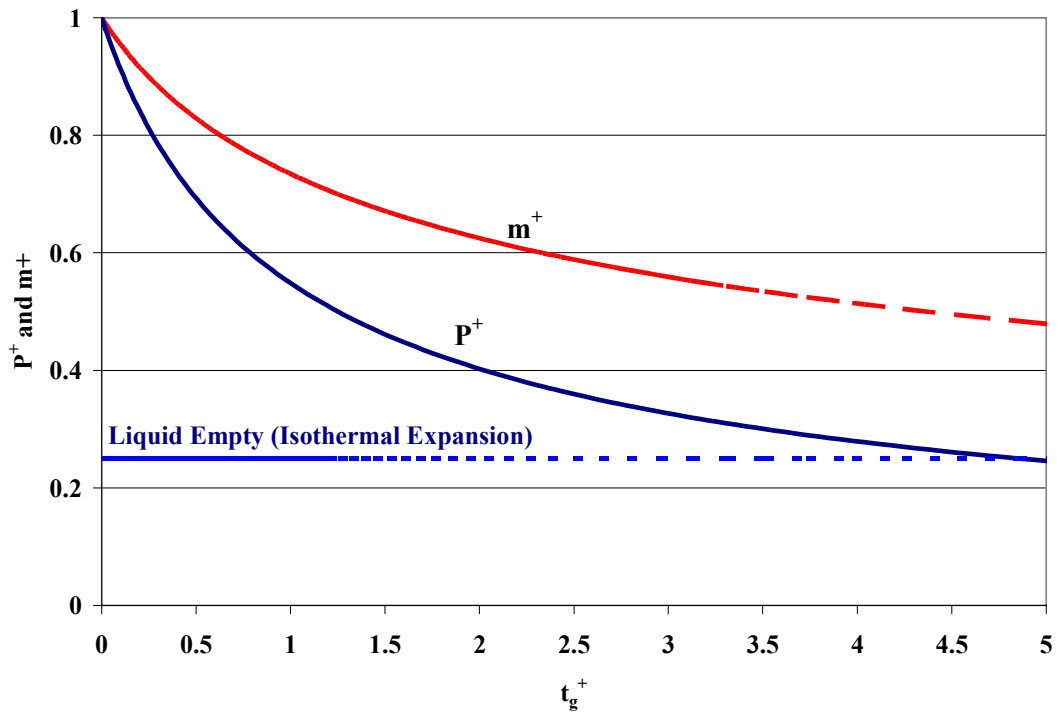


FIG. 9. Accumulator depressurization and liquid injection versus time in dimensionless coordinates (isothermal gas expansion).

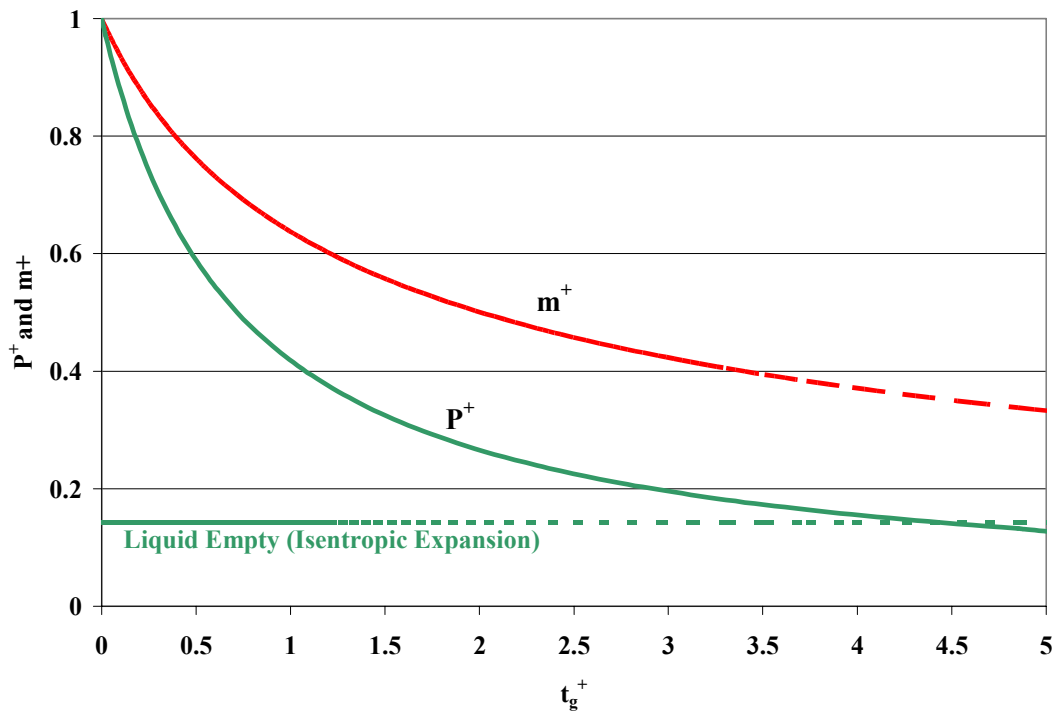


FIG. 10. Accumulator depressurization and liquid injection versus time in dimensionless coordinates (isentropic gas expansion).

4. AUTOMATIC DEPRESSURIZATION SYSTEMS (ADS)

The AP600 and AP1000 implements an Automatic Depressurization System to reduce primary side pressure to containment pressure in a controlled manner. This section presents a Reactor Coolant System (RCS) depressurization rate equation and similarity criteria for the ADS valve flow areas.

4.1. Governing equations for RCS two-phase fluid depressurization

The mass conservation equation for a RCS control volume undergoing a depressurization event is given by:

$$\frac{dM}{dt} = \sum \dot{m}_{inj} - \sum \dot{m}_{ADS} \quad (34)$$

where M is the fluid mass within the RCS and \dot{m} represents the mass flow rate entering or leaving the reactor coolant system. The energy conservation equation for the RCS fluid is expressed as follows:

$$\frac{dU}{dt} = \sum (\dot{m}h)_{inj} - \sum (\dot{m}h)_{ADS} + \dot{q}_{SG} + \dot{q}_{core} + \dot{q}_{loss} - P \frac{dV}{dt} \quad (35)$$

where U is the bulk internal energy of the fluid within the RCS, h is the enthalpy of the fluid entering or leaving the RCS, \dot{q}_{SG} , \dot{q}_{core} and \dot{q}_{loss} are the steam generator energy transfer rate, the core power and the heat loss respectively. P is the RCS pressure and V is the RCS volume. The specific internal energy and the specific volume are defined respectively as follows:

$$e = \frac{U}{M} \quad (36)$$

$$v = \frac{V}{M} \quad (37)$$

The total change in specific internal energy is written in terms of partial differentials with respect to pressure and specific volume as follows:

$$de = \left(\frac{\partial e}{\partial p} \right)_v dP + \left(\frac{\partial e}{\partial v} \right)_p dv \quad (38)$$

Substituting equation (39) into (38) yields:

$$\frac{dMe}{dt} = \sum (\dot{m}h)_{inj} - \sum (\dot{m}h)_{ADS} + \dot{q}_{SG} + \dot{q}_{core} + \dot{q}_{loss} - P \frac{dV}{dt} \quad (39)$$

Expanding the term on the LHS of equation (39), substituting equation (34) and rearranging yields:

$$M \frac{de}{dt} = (\sum \dot{m}_{inj}) (h_{inj} - e) - (\sum \dot{m}_{ADS}) (h_{ADS} - e) + \dot{q}_{SG} + \dot{q}_{core} + \dot{q}_{loss} - P \frac{dV}{dt} \quad (40)$$

In equation (40), it has been assumed that h_{in} is the same for all the injection locations and h_{out} is the same for all the vent paths. Substituting equation (38) into (40), and rearranging yields

$$M \left(\frac{\partial e}{\partial P} \right)_v \frac{dP}{dt} = (\sum \dot{m}_{inj}) (h_{inj} - e) - (\sum \dot{m}_{ADS}) (h_{ADS} - e) + \dot{q}_{SG} + \dot{q}_{core} + \dot{q}_{loss} - P \frac{dV}{dt} - M \left(\frac{\partial e}{\partial v} \right)_p \frac{dv}{dt} \quad (41)$$

Using equation (37), and the mass conservation equation, the last term on the RHS of equation (41) is written as:

$$M \left(\frac{\partial e}{\partial v} \right)_p \frac{dv}{dt} = \left(\frac{\partial e}{\partial v} \right)_p \frac{dV}{dt} - v \left(\frac{\partial e}{\partial v} \right)_p (\sum \dot{m}_{inj} - \sum \dot{m}_{ADS}) \quad (42)$$

Substituting back into equation (41) yields:

$$M \left(\frac{\partial e}{\partial P} \right)_v \frac{dP}{dt} = (\sum \dot{m}_{inj}) \left[h_{inj} - e + v \left(\frac{\partial e}{\partial v} \right)_p \right] - (\sum \dot{m}_{ADS}) \left[h_{ADS} - e + v \left(\frac{\partial e}{\partial v} \right)_p \right] + \dot{q}_{SG} + \dot{q}_{core} + \dot{q}_{loss} - \left[P + \left(\frac{\partial e}{\partial v} \right)_p \right] \frac{dV}{dt} \quad (43)$$

which is the ‘‘depressurization rate equation.’’ For the RCS control volume, which has rigid boundaries, equation (43) becomes:

$$M \left(\frac{\partial e}{\partial P} \right)_v \frac{dP}{dt} = (\sum \dot{m}_{inj}) \left[h_{inj} - e + v \left(\frac{\partial e}{\partial v} \right)_p \right] - (\sum \dot{m}_{ADS}) \left[h_{brk} - e + v \left(\frac{\partial e}{\partial v} \right)_p \right] + \dot{q}_{SG} + \dot{q}_{core} + \dot{q}_{loss} \quad (44)$$

The net energy transfer rate is given as:

$$\dot{q}_{net} = \dot{q}_{SG} + \dot{q}_{core} + \dot{q}_{loss} \quad (45)$$

Equation (44) is the governing equation for depressurization behavior in the RCS. Table 6 summarizes the governing equations and normalizing ratios for RCS depressurization. Table 7 presents the

dimensionless balance equations and the dimensionless groups that should be preserved in a scaled test facility [4],[5].

Table 6. Governing equations and normalizing ratios for RCS depressurization

<p>Governing Balance Equations</p> <p><i>Mass Balance Equation:</i></p> $\frac{dM}{dt} = \sum \dot{m}_{inj} - \sum \dot{m}_{ADS} \quad (46)$ <p><i>Depressurization Rate Equation:</i></p> $M \left(\frac{\partial e}{\partial P} \right)_v \frac{dP}{dt} = (\sum \dot{m}_{inj}) \left[h_{inj} - e + v \left(\frac{\partial e}{\partial v} \right)_p \right] - (\sum \dot{m}_{ADS}) \left[h_{ADS} - e + v \left(\frac{\partial e}{\partial v} \right)_p \right] + \dot{q}_{SG} + \dot{q}_{core} + \dot{q}_{loss} \quad (47)$	
<p>Normalized Initial and Boundary Conditions</p> $t^+ = \frac{t}{\tau_{RCS}} \quad (48)$ $M^+ = \frac{M}{M_o} \quad (49)$ $P^+ = \frac{P}{P_o} \quad (50)$ $\dot{q}_{net}^+ = \frac{\dot{q}_{net}}{\dot{q}_{net,o}} \quad (51)$ $\sum \dot{m}_{inj}^+ = \frac{\sum \dot{m}_{inj}}{\sum \dot{m}_{inj,o}} \quad (52)$	$\sum \dot{m}_{ADS}^+ = \frac{\sum \dot{m}_{ADS}}{\sum \dot{m}_{ADS,o}} \quad (53)$ $\left[h_{inj} - e + v \left(\frac{\partial e}{\partial v} \right)_p \right]^+ = \frac{\left[h_{inj} - e + v \left(\frac{\partial e}{\partial v} \right)_p \right]}{\left[h_{inj} - e + v \left(\frac{\partial e}{\partial v} \right)_p \right]_o} \quad (54)$ $\left[h_{ADS} - e + v \left(\frac{\partial e}{\partial v} \right)_p \right]^+ = \frac{\left[h_{ADS} - e + v \left(\frac{\partial e}{\partial v} \right)_p \right]}{\left[h_{ADS} - e + v \left(\frac{\partial e}{\partial v} \right)_p \right]_o} \quad (55)$

Table 7. Dimensionless equations and Π groups for RCS depressurization

<p>Dimensionless Balance Equations</p> <p><i>RCS Mass Balance Equation:</i></p> $\tau_{RCS} \frac{dM^+}{dt} = \Pi_m \Sigma \dot{m}_{inj}^+ - \Sigma \dot{m}_{ADS}^+ \quad (56)$ <p><i>RCS Depressurization Rate Equation:</i></p> $M^+ \left(\frac{\partial e}{\partial P} \right)_v^+ \tau_{RCS} \frac{dP^+}{dt} = \frac{\Pi_h}{\Pi_\varepsilon} \Sigma \dot{m}_{inj}^+ \left[h_{inj} - e + v \left(\frac{\partial e}{\partial v} \right)_p^+ \right] - \frac{\Sigma \dot{m}_{ADS}^+}{\Pi_\varepsilon} \left[h_{ADS} - e + v \left(\frac{\partial e}{\partial v} \right)_p^+ \right] + \frac{\Pi_\Gamma}{\Pi_\varepsilon} \dot{q}_{net}^+ \quad (57)$	
<p>Characteristic Time Constant</p> $\tau_{rcs} = \frac{M_o}{\Sigma \dot{m}_{ADS,o}} \quad (58)$	
<p>Dimensionless Groups</p> <p><i>Mass Balance Number:</i></p> $\Pi_m = \frac{\Sigma \dot{m}_{inj,o}}{\Sigma \dot{m}_{ADS,o}} \quad (59)$ <p><i>Enthalpy Balance Number:</i></p> $\Pi_h = \frac{\Sigma \dot{m}_{inj,o} \cdot \left[h_{inj} - e + v \left(\frac{\partial e}{\partial v} \right)_p \right]_o}{\Sigma \dot{m}_{ADS,o} \cdot \left[h_{Brk} - e + v \left(\frac{\partial e}{\partial v} \right)_p \right]_o} \quad (60)$	<p><i>Heat Source Number:</i></p> $\Pi_\Gamma = \frac{\dot{q}_{net,o}}{\Sigma \dot{m}_{ADS} \cdot \left[h_{brk} - e + v \left(\frac{\partial e}{\partial v} \right)_p \right]_o} \quad (61)$ <p><i>Fluid Mixture Dilation Number:</i></p> $\Pi_\varepsilon = \varepsilon_o = \frac{P_o \left(\frac{\partial e}{\partial P} \right)_{v,o}}{\left[h_{ADS} - e + v \left(\frac{\partial e}{\partial v} \right)_p \right]_o} \quad (62)$

The dimensionless group, Π_h , is the energy flow rate ratio. It represents the ratio of the total energy change due to fluid injection to the energy change caused by the break flow. Π_Γ is the power ratio. It represents the ratio of the net heat into the system to the rate of fluid energy transport through the break. Π_ϵ is the fluid mixture dilation property group. Equation (62) reveals that the fluid dilation property group couples the system intensive energy change to the intensive energy at the break. For high pressure systems venting to the ambient, the fluid properties at the break are determined at critical flow conditions. Evaluating the RCS time constant, τ_{RCS} , and the dimensionless groups Π_m , Π_h , Π_r , Π_ϵ requires knowledge of the pressure dependent fluid properties and the critical mass flux.

For the case of fluid property similitude, all of the dimensionless groups simplify to produce the simple set of scale ratios presented in Table 8. For fluid property similitude, the critical mass flux in the model, $(G_{ADS})_m$, would be identical to that in the prototype and the ratio of Π_ϵ would be unity.

Table 8. RCS depressurization scale ratios assuming for isochronicity and fluid property similitude

Fluid Property Similitude Yields:	
	$\begin{aligned} (G_{ADS,o})_R &= 1 \\ (M_o)_R &= (V_o)_R \\ (\dot{m}_{ADS,o})_R &= (A_{ADS,o})_R \end{aligned}$
Scale Ratios	
	$(\tau_{RCS})_R = \left(\frac{M_o}{\dot{m}_{ADS,o}} \right)_R = \left(\frac{V_o}{A_{ADS,o}} \right)_R = 1 \quad (63)$
Flow Area Scaled to Volume :	
	$(A_{ADS})_R = (V_o)_R \quad (64)$
Injection Flow Rates Scaled to Volume:	
	$(\dot{m}_{inj,o})_R = (A_{ADS})_R = (V_o)_R \quad (65)$
Power Scaled to Volume:	
	$(\dot{q}_{net,o})_R = (A_{ADS})_R = (V_o)_R \quad (66)$

5. COMPARISON OF APEX-600 AND SPES PASSIVE SAFETY SYSTEM RESPONSES

The AP600 design has undergone extensive testing for plant certification. Three scaled integral system test facilities were operated to assess passive safety system performance; ROSA-AP600, SPES-2 and APEX-600. This section presents a brief comparison of a two-inch break simulation conducted in the Full Height-Full Pressure SPES-2 and in the Quarter Height Reduced Pressure OSU APEX. Table 9 presents the scale ratios for each of the facilities.

Table 9. Scale ratios for SPES-2 and APEX-600 relative to AP600

Scaling Ratios	APEX	SPES-2
Lengths	1:4	1:1
Relative elevations	1:4	1:1
Flow Areas	1:48	1:395
Volumes	1:192	1:395
Decay Power	1:96	1:395
Fluid Velocity	1:2	1:1
Fluid Transient Time	1:2	1:1
Mass Flow Rate	1:96	1:395

Figure 11 outlines a typical SBLOCA scenario. Initially there is a sharp decrease in system pressure due to the subcooled blowdown of fluid from the break. Being a reduced pressure test facility, the APEX-600 test facility did not model this portion of the transient. It begins the simulation when the system has reached saturated conditions. Subsequent to that point, all of the safety system actions were simulated by both facilities. Figures 12 through 16 compare the dimensionless depressurization histories, the CMT draining and flow behavior, and the Accumulator draining and flow behavior. The plots show excellent agreement between the two facilities and support the scaling methods used to design the facilities.

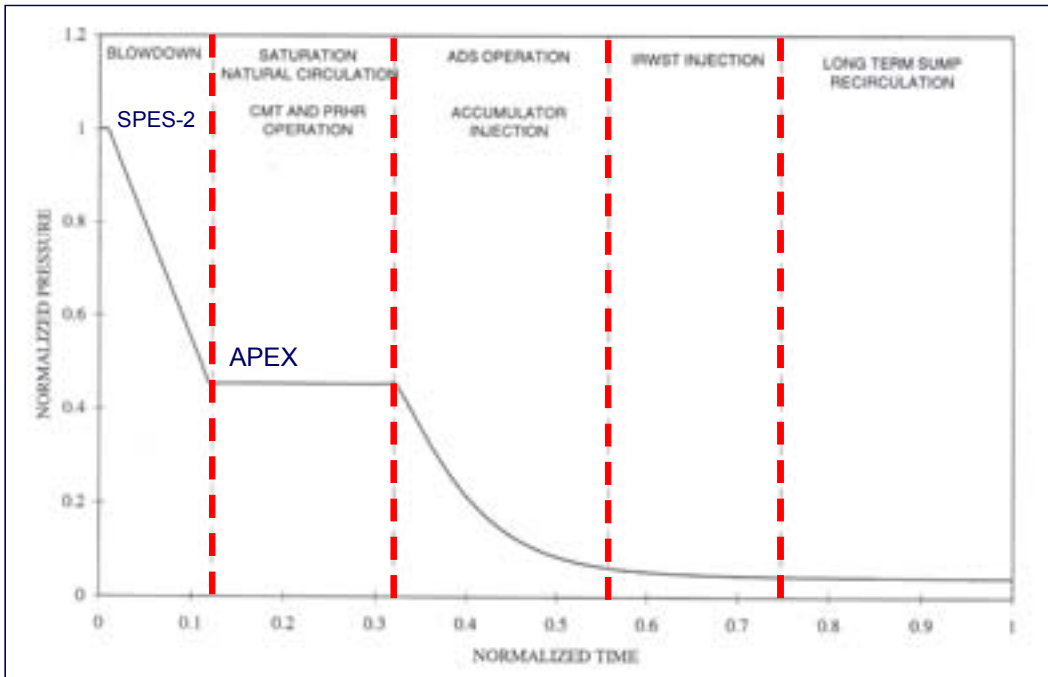


FIG. 11. Typical phases of an AP600/AP1000 SBLOCA pressure history.

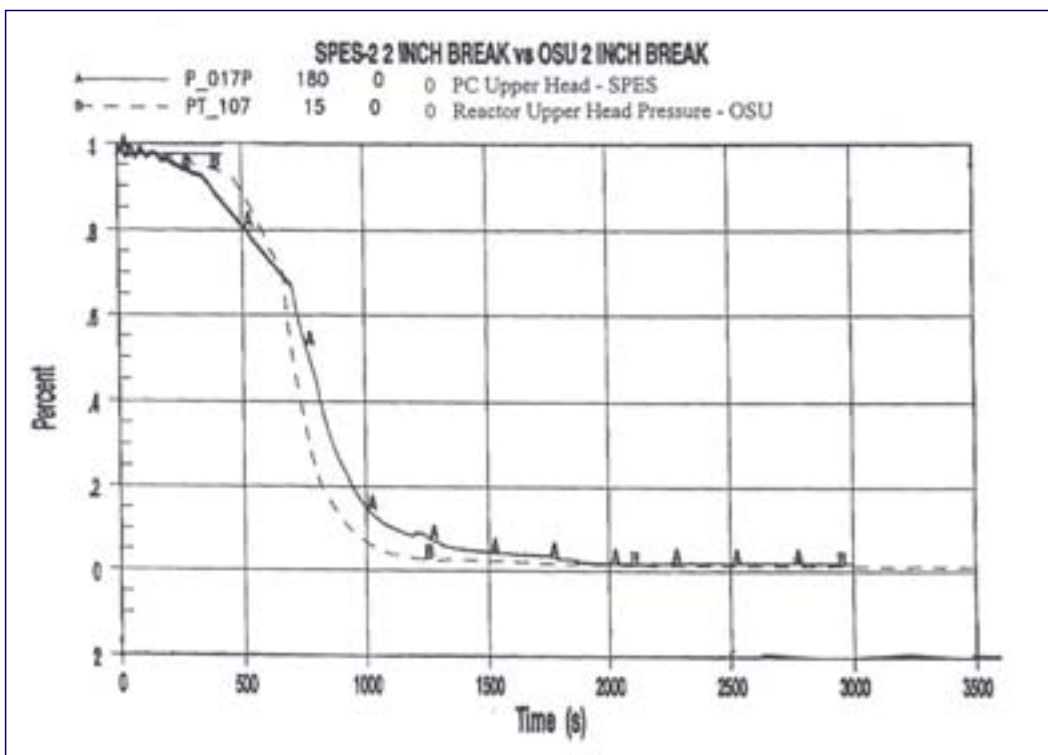


FIG. 12. Comparison of SPES-2 and APEX-600 two-inch SBLOCA pressure histories.

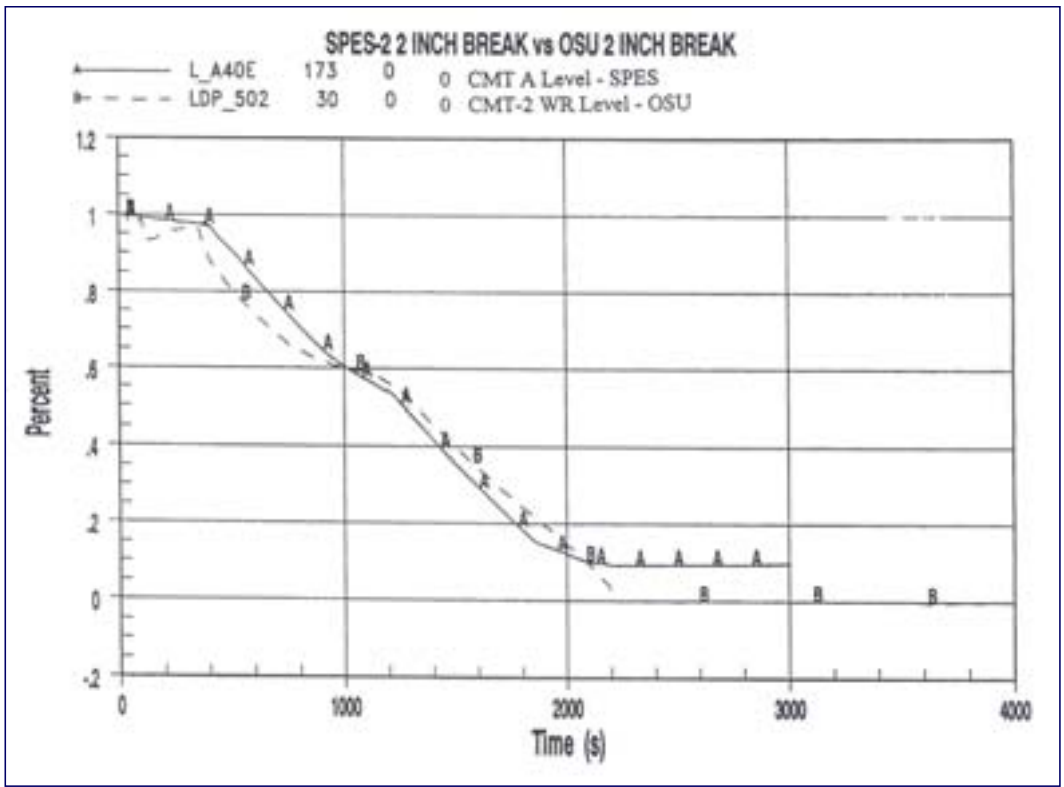


FIG. 13. Comparison of SPES-2 and APEX-600 two-inch SBLOCA CMT level histories.

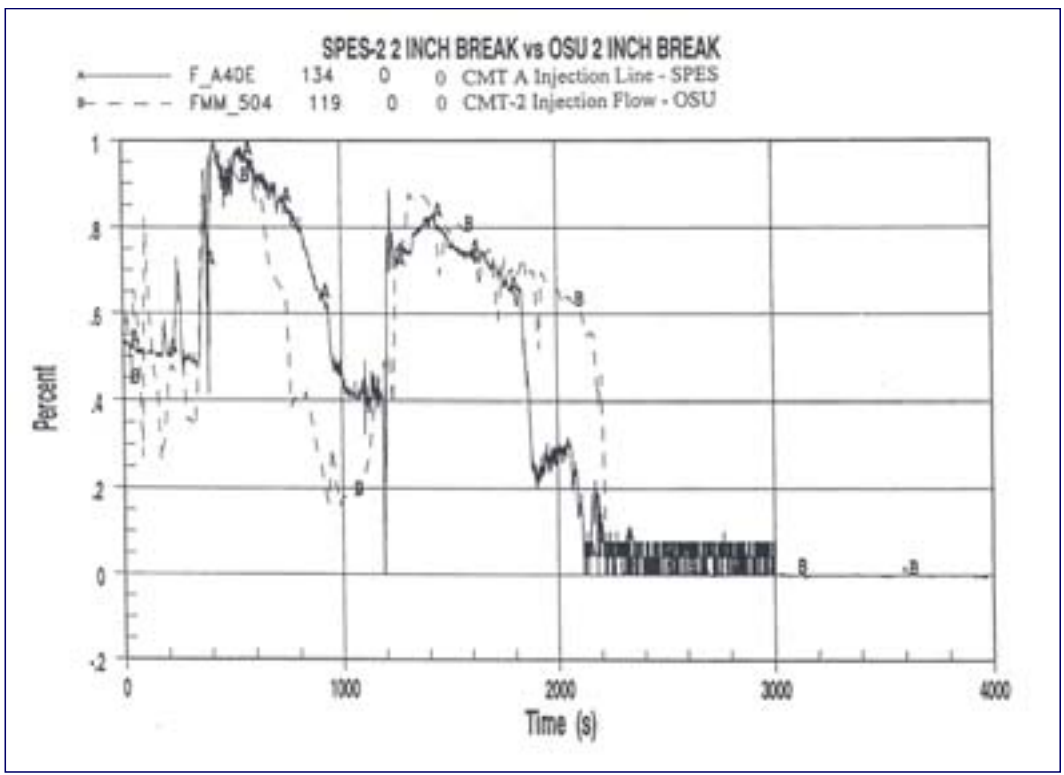


FIG. 14. Comparison of SPES-2 and APEX-600 two-inch SBLOCA CMT flow histories.

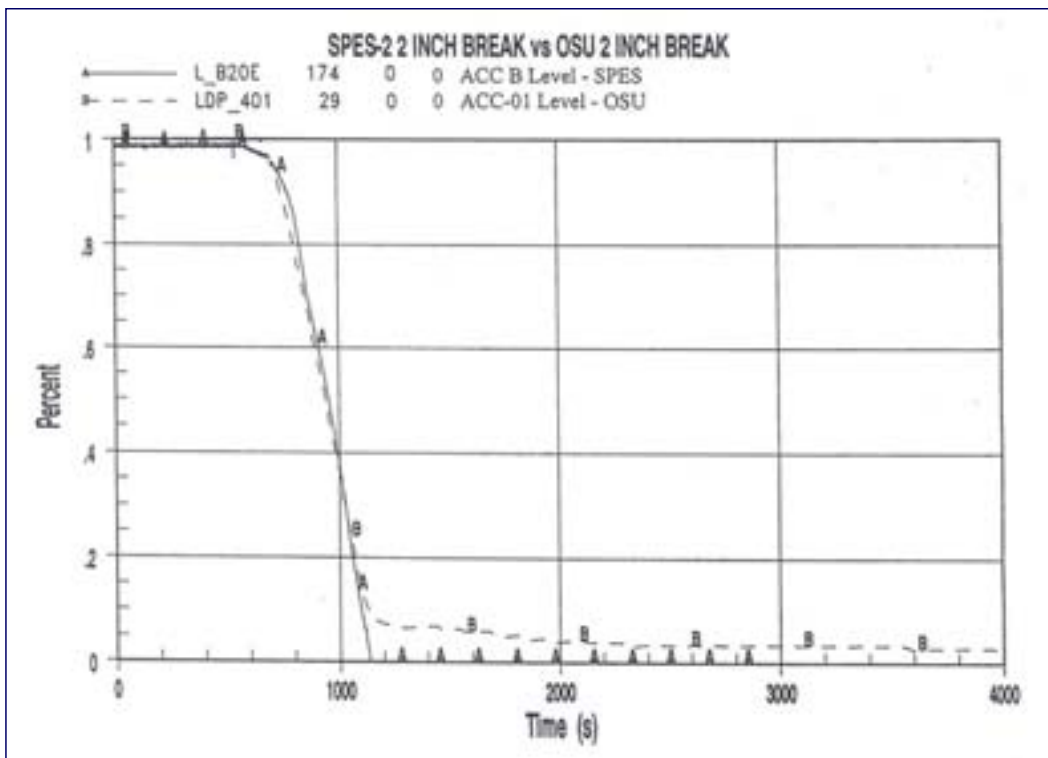


FIG. 15. Comparison of SPES-2 and APEX-600 two-inch SBLOCA accumulator liquid level histories.

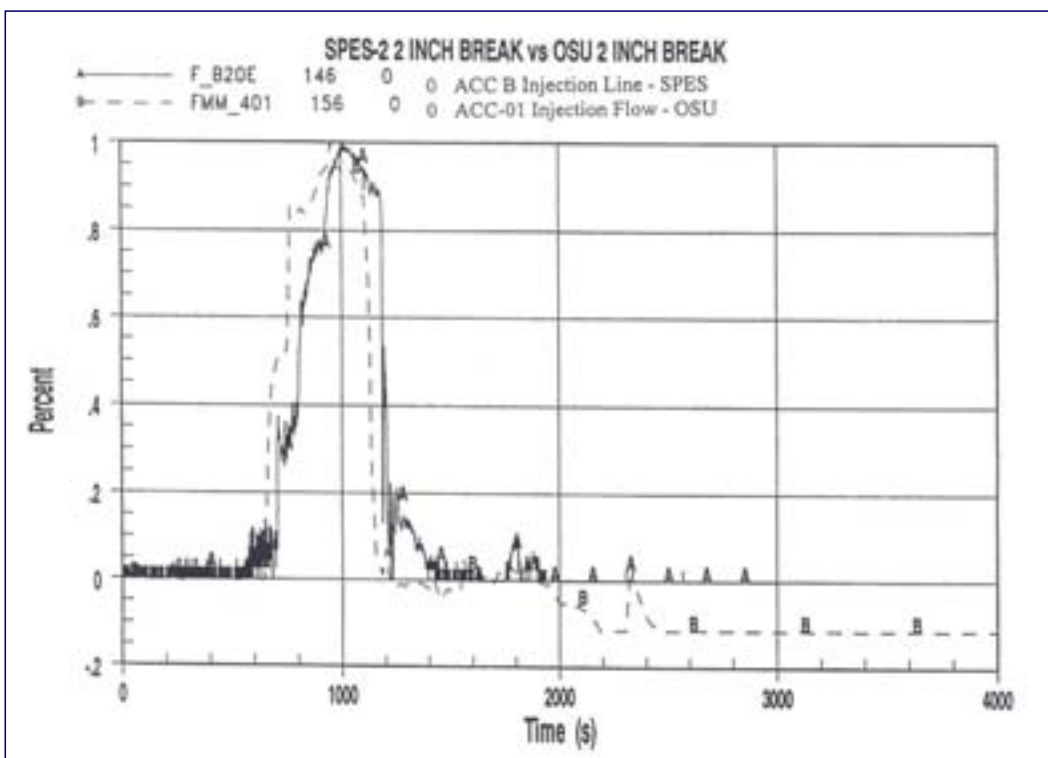


FIG. 16. Comparison of SPES-2 and APEX-600 two-inch accumulator flow histories.

NOMENCLATURE

Acronyms

ACC	Accumulator Tank
ADS	Automatic Depressurization System
CMT	Core Make-up Tanks
CS	Containment Sump
IRWST	In-containment Refueling Water Storage Tank
PCCS	Passive Containment Cooling System
PRHR	Passive Residual Heat Removal System

Symbols

A	cross-sectional area
d	line diameter
e	specific internal energy
f	friction factor
g	gravitational constant
G	mass flux
h_l	head loss
h_{inj}	enthalpy of injected liquid
h_{ADS}	enthalpy of ADS vapor
K	loss coefficient
l	line length
L	level
\dot{m}	mass flow rate
M	Mass
P	static pressure
\dot{q}	heat loss or power
t	time
v_E	liquid velocity at exit
v	specific volume
V	volume
Z	elevation

Greek Symbols

γ	ratio of specific heats
$\Pi_{FE} = \left(\frac{fl}{d} + K \right)_E$	
ρ	density

ACKNOWLEDGEMENT

This work was supported through a U.S. Department of Energy Contract (DE- FC07-04ID14550) and the Oregon State University sabbatical program. This work was conducted through the IAEA Nuclear Power Technology Development Section.

REFERENCES

- [1] INTERNATIONAL ATOMIC ENERGY AGENCY, Safety Related terms for Advanced Nuclear Plants, IAEA-TECDOC-626, Vienna (1991).
- [2] Title 10, Energy, Code of Federal Regulations, Part 50, Office of Federal Register, National Archives and Records Administration, Available through Superintendent of Documents, U.S. Government Printing Office, Washington, D.C. 20402 (2004).
- [3] VERTES, C.M., Passive safeguards design optimization studies for the Westinghouse AP600, Fifth Proceedings of the Nuclear Thermal Hydraulics, 1989 Winter Meeting of the ANS, San Francisco, California, November 26–30 (1989).
- [4] REYES, J.N., JR., RUSHER, C., Analytical models for pressure vessel blowdowns of saturated fluid mixtures, Proceeding of the 1999 NURETH-9 Conference, October 3–8, 1999, San Francisco, CA.
- [5] REYES, J.N., JR., Scaling the depressurization behavior of fluids in phase equilibria, Proceedings of the Japan-U.S. Seminar on Two Phase Flow Dynamics, Kyushu University, Fukuoka, Japan, July 15–20 (1996).

ANNEX 13

EXPERIMENTAL VALIDATION AND DATA BASE OF SIMPLE LOOP FACILITIES

P.K. Vijayan, A.K. Nayak

Reactor Engineering Division,
Bhabha Atomic Research Centre, India

Abstract

Industrial NCSs are quite complex in geometry and as such the phenomena taking place is not easy to understand and hence simple loop facilities are found to be useful in phenomena tracking. This lecture will highlight the contribution of simple loop facilities in improving our understanding of the steady state, transient and stability behaviour of NCSs.

1. INTRODUCTION

Simple loops are easier to construct and operate, require a minimum of instrumentation and large amount of easily reproducible data can be generated in less time at a very low cost. The greatest advantage of simple loop facilities is that the phenomena taking place is easily traceable and hence they are well suited for phenomenological investigations. Above all, theoretical and computational modelling of simple loops is far easier and less time consuming. Consequently, experiments in simple loop facilities have contributed greatly to improve our understanding of the natural circulation process. Besides, the experimental data from simple loop facilities have been useful in theoretical model development, computer code development as well as validation and phenomena identification. Both single-phase and two-phase natural circulation have been studied extensively in simple loop facilities, and the topics of investigation included steady state, transient and stability behaviour, development and testing of scaling laws, effect of operating procedures on the stability threshold, etc. Other favourite topics with experimentalists include parametric study of the effect of loop geometry, inventory variation, cold-water injection, start-up of NCSs, inception of boiling, parallel channel effects, effect of noncondensables, transition from forced to natural circulation, etc. Some notable contributions from simple loop experiments in the field of single-phase and two-phase NC are reviewed below.

2. STEADY STATE BEHAVIOUR OF SINGLE-PHASE LOOPS

Steady state flow prevails in a natural circulation loop when the driving buoyancy force is balanced by the retarding frictional force. The situation can be mathematically expressed as

$$-g \oint \rho dz = \frac{RW^2}{2\rho} \quad (1)$$

Where R is the total hydraulic resistance of the loop and is given by

$$R = \sum_{i=1}^N \left(\frac{fL}{D} + K \right)_i \frac{1}{A_i^2} \quad (2)$$

If we assume the Bossinesq approximation to be valid, then the density in the buoyancy force term can be expressed as

$$\rho = \rho_0 [1 - \beta(T - T_0)] \quad (3)$$

Where ρ_0 is a reference density corresponding to the reference temperature T_0 . Using this in Eq. (1), the steady state equation can be rewritten as

$$g\rho_0\beta\oint Tdz = \frac{RW^2}{2\rho_0} \quad (4)$$

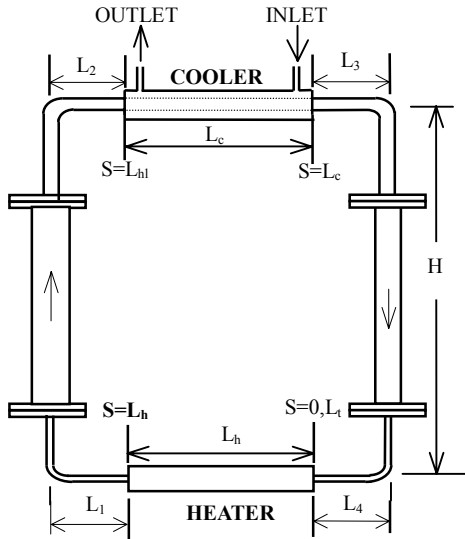


FIG. 1. NCL with horizontal heater and cooler.

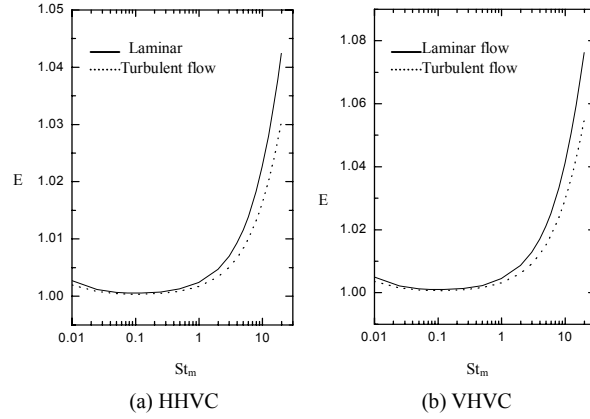


FIG. 2. Error of approximation.

Where the same reference density has been used to evaluate the loop hydraulic resistance. For a rectangular loop of height H with both cooler and the heater horizontal (Fig. 1), we obtain

$$g\rho_0\beta(T_{hl} - T_{cl})H = \frac{RW^2}{2\rho} \quad (5)$$

The steady state temperature rise across the heater, ΔT_h can be expressed as

$$\Delta T_h = \frac{Q_h}{WCp} \quad (6)$$

Since $\Delta T_h = (T_{hl} - T_{cl})$, the steady state flow rate from Eq. (5) is obtained as

$$W = \left[\frac{2\rho_0^2\beta g Q_h H}{RCp} \right]^{\frac{1}{3}} \quad (7)$$

Thus, we find that the steady state mass flow rate is proportional to the one-third power of the heater power. Many experimentalists used this equation to predict the natural circulation flow rate and compared with the measured flow [1]. As the natural circulation flow rate in simple loops is too low to be accurately measured, it is usual to use the measured ΔT_h for comparison with data [1]. By substituting the flow rate from Eq. (7) into Eq. (6), the ΔT_h at steady state can be estimated as

$$\Delta T_h = \left[\frac{RQ_h^2}{2\rho_0^2\beta g HCp^2} \right]^{\frac{1}{3}} \quad (8)$$

Thus the steady state temperature rise across the heater is found to be proportional to the two-third power of the heater power. It may be noted that both equations (7) and (8) are strictly valid for a rectangular loop with both the heater and cooler horizontal. However, other orientations of the heater and cooler are important to nuclear reactors. For example, in PWRs both the core and the steam generator (SG) are vertical whereas PHWRs have horizontal core and vertical SG and in VVERs,

vertical core and horizontal SG is found. To account for the differences in orientation, often an additional assumption that the variation of temperature is linear in both the heater and cooler is used. With this assumption, the flow rate for any single-phase natural circulation loop can be obtained [2,3] as

$$W = \left[\frac{2\rho_0^2 \beta g Q_h \Delta Z_c}{RCp} \right]^{\frac{1}{3}} \quad (9)$$

Where ΔZ_c is the centre line elevation difference between the cooler and the heater. The above correlation was used to predict the flow rate in integral test loops for comparison with the measured values [4]. It may be noted that the problem with this approach is that the above equations are dimensional and it is not often possible to compare the performance of different natural circulation loops. For example, it is possible to obtain a larger flow rate in a loop with smaller height if its resistance is small. Therefore, search for a nondimensional equation for the steady state flow rate in natural circulation loops began. Today, it is possible to express the flow rate in a natural circulation loop in terms of generalized dimensionless groups [5,6] if the local loss coefficient is replaced by an equivalent length, Le , such that

$$Le_i = \frac{K_i D_i}{f_i} \quad (10)$$

Thus, the effective length of the i^{th} segment can be expressed as

$$(L_{eff})_i = L_i + Le_i \quad (11)$$

where the actual physical length is L_i . Using this, Eq. (4) can be recast as

$$g\rho_0\beta \oint Tdz = \frac{W^2}{2\rho_0} \left(\frac{fL_{eff}}{DA^2} \right)_i \quad (12)$$

Noting that the friction factor can be expressed by a correlation of the form

$$f_i = \frac{p}{Re^b} \quad (13)$$

where p and b depend on the nature of the flow. For example, $p=64$ and $b=1$ for laminar flow and assuming the Blassius correlation to be valid for turbulent flow p and b are respectively 0.316 and 0.25. In a nonuniform diameter loop, it is possible that some pipe sections are in laminar flow, and some in turbulent flow and still others in transition flow. Even in uniform diameter loops, due to the differences in properties, the hot leg can be in the transition/turbulent region with the cold leg in the laminar region. However, if the entire loop is assumed to be either in laminar or in turbulent flow, then we obtain

$$\frac{2\rho_0^2 \beta g Q_h H}{Cp} = p\mu^b W^{3-b} \sum_{i=1}^N \left(\frac{L_{eff}}{D^{1+b} A^{2-b}} \right)_i \quad (14)$$

For nonuniform diameter loops, we define a reference diameter and reference area as

$$D_r = \frac{1}{L_t} \sum_{i=1}^N D_i L_i \quad \text{and} \quad A_r = \frac{1}{L_t} \sum_{i=1}^N A_i L_i = \frac{V_t}{L_t} \quad (15)$$

where L_t is the total physical circulation length and V_t is the total loop volume. Using D_r , A_r and L_t to nondimensionalise the quantities in the bracket we obtain

$$\text{Re} = \left[\frac{2}{p} \frac{Gr_m}{N_G} \right]^{\frac{1}{3-b}} = C \left(\frac{Gr_m}{N_G} \right)^r \quad (16)$$

$$\text{Where } N_G = \frac{L_t}{D_r} \sum_{i=1}^N \left(\frac{l_{eff}}{d^{1+b} a^{2-b}} \right)_i; C = \left(\frac{2}{p} \right)^r \text{ and } r = \left(\frac{1}{3-b} \right) \quad (17)$$

Thus, knowing the values of p and b the constants C and r can be evaluated. Eq. (16) is valid only for the case where both the heater and cooler are horizontal. With uniform heat flux, the actual temperature profile over the heater is linear. Similarly, the actual temperature profile in the primary side of the cooler is exponential. However, if we approximate it by a linear profile, then the generalized correlation valid for all orientations of the source and sink is given by

$$\text{Re} = C \left[\frac{(Gr_m)_{\Delta z_c}}{N_G} \frac{H}{\Delta z_c} I_{ss} \right]^r \quad (18)$$

For the orientation with both the heater and cooler horizontal, we obtain $I_{ss}=1$, and $H=\Delta z_c$ leading to

$$\text{Re} = C \left[\frac{(Gr_m)_{\Delta z_c}}{N_G} \right]^r \quad (19)$$

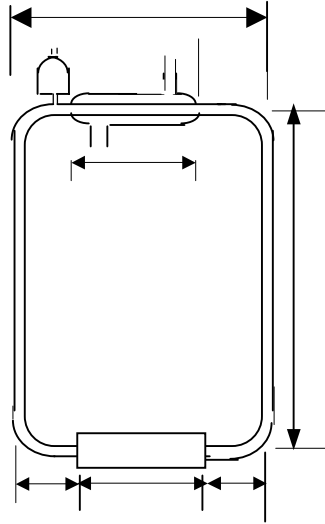
For other orientations of the source and sink, the same equation can be used if the error, E ($E=(H/\Delta z_c)I_{ss}$), is small. For the case with uniform heat generation in the source, it is found that $I_{ss}=\Delta z_c/H$ for the VHHC orientation leading to the same result as Eq. (19). For the HHVC and VHVC orientations, the calculations reported in Vijayan et al. (2004) [6] shows that the error in using Eq. (19) is negligible (less than 1% if St_m is less than unity which is normally the case, see also Fig. 2). Hence, the respective equations for a fully laminar and a fully turbulent loop can be obtained as

$$\text{Re} = 0.1768 \left[\frac{(Gr_m)_{\Delta z_c}}{N_G} \right]^{0.5} \quad \text{Laminar loop} \quad (20)$$

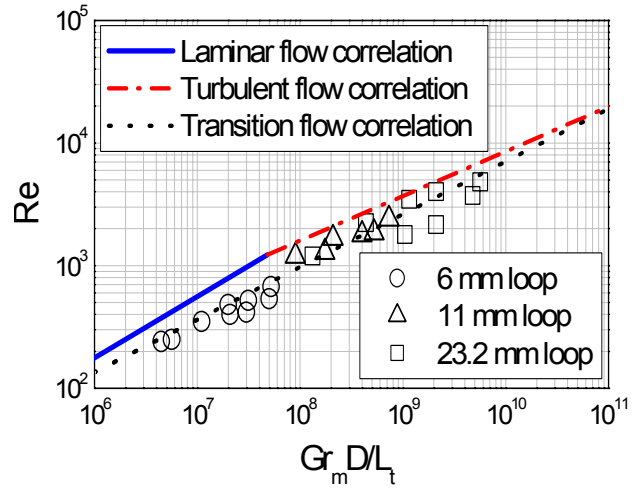
$$\text{Re} = 1.96 \left[\frac{(Gr_m)_{\Delta z_c}}{N_G} \right]^{\frac{1}{2.75}} \quad \text{Turbulent loop} \quad (21)$$

If part of the loop is in laminar or turbulent condition, then the above equations are not applicable. It may be possible to generate a correlation for part of the loop in laminar and part in turbulent flow. But if part of the loop is in laminar/turbulent flow with the rest in transition flow, then theoretical correlation is not possible due to the unavailability of friction factor correlation for the transition regime. However, it is possible to generate empirical correlations. One such correlation valid in the range $2 \times 10^8 < Gr_m < 10^{10}$ is given below [7].

$$Re = 0.3548 \left[\frac{(Gr_m)_{\Delta z_c}}{N_G} \right]^{0.43} \quad (22)$$



(a) The experimental loop



(b) Comparison of data with correlations

FIG.3. Effect of loop diameter on steady state NC [7].

For the special case of uniform diameter loops, $D_r=D$, $A_r=A$ so that $d_r=a_r=1$ leading to the following equation for N_G

$$N_G = \frac{L_t}{D} \sum_{i=1}^N (l_{eff})_i = \frac{(L_{eff})_t}{D}, \quad (23)$$

$$\text{so that } Re = C \left[(Gr_m)_{\Delta z_c} \frac{D}{(L_{eff})_t} \right]^r. \quad (24)$$

If the local losses are also negligible, then $N_G = L_t / D$ so that

$$Re = C \left[(Gr_m)_{\Delta z_c} \frac{D}{L_t} \right]^r. \quad (25)$$

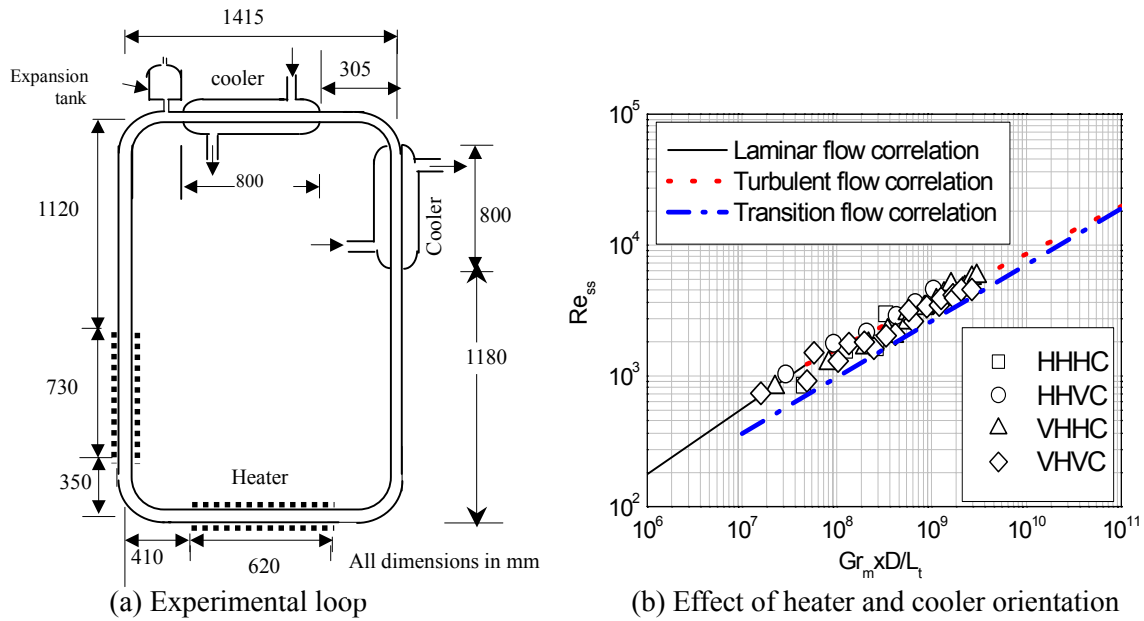


FIG.4. Effect of heater and cooler orientation on steady state NC [8].

2.1. Database for uniform diameter loops (UDL)

The above correlations were extensively tested with data from simple loops. The loops considered included both uniform diameter loops (UDL) as well as nonuniform diameter loops (NDL). Among the simple uniform diameter loops, rectangular loops are experimentally studied most. Typical examples are the investigations by Holman and Boggs (1960) [9], Huang and Zelaya (1988) [10], Misale et al. (1991) [11], Bernier and Baliga (1992) [12], Vijayan et al. (1992) [7], Ho et al. (1997) [13], Nishihara (1997) [14] and Vijayan et al. (2001) [8]. Uniform diameter open loops were investigated by Bau-Torrance (1981) [15] and Haware et al. (1983) [16]. Creveling et al. (1975) [17] experimented with a uniform diameter toroidal loop. For all the UDL data covered in the present database, the loop diameter was in the range of 6 to 40 mm and the loop height varied from 0.38 to 2.3 m. The total circulation length varied from 1.2 to 7.2 m and the L_t/D ratio varied from 75 to 1100. The working fluid was mostly water and in one case Freon. The loop pressure was mostly near atmospheric except for the data of Holman and Boggs [9] which was for near critical pressure. Database for all the four orientations of heater and cooler are included.

It was found that UDL data from rectangular loops of different diameter could be reasonably represented by the above correlation (Fig. 3). Even better comparison is obtained with data having different orientations of heater and cooler (Fig. 4). The data from all uniform diameter loops neglecting the effect of local losses are plotted in Fig. 5a. Effect of local losses was found to improve the agreement with the data in the turbulent regime (Fig. 5b). However, it has no significant influence in the laminar regime data since fL_t/D is much greater than sum of all loss coefficients.

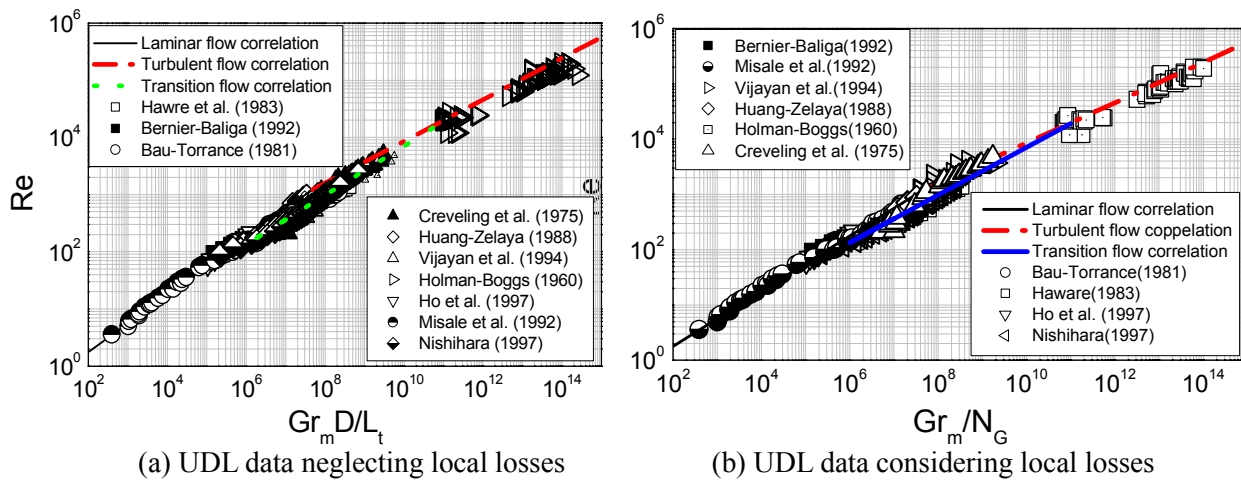


FIG. 5. Data from all uniform diameter loops

2.2. Database for nonuniform diameter loops (NDLs)

Most practical applications of natural circulation employ non-uniform diameter loops. Common examples are the nuclear reactor loop, solar water heater, etc. Most test facilities simulating nuclear reactor loops also use non-uniform diameter loops. The non-uniform diameter loops experimentally studied can be categorized into two groups depending on the operating pressure as (1) High pressure loops and (2) Low pressure loops. Most studies are conducted in the high-pressure test facilities simulating nuclear reactor loops. Typical examples of such facilities are the SEMISCALE, LOBI, PKL, BETHSY, ROSA, RD-14 and FISBE. Some studies, however, are carried out in low pressure facilities. Examples are the experiments carried out by Zvirin et al. (1981) [1], Jeuck et al. (1981) [18], Hallinan-Viskanta (1986) [19], Vijayan (1988) [20], and John et al. (1991) [21]. Most of the available experimental data in a useable form (i.e. full geometrical details are known) are from the low-pressure test facilities. High-pressure test data in a useable form was available only from FISBE. The nonuniform loops considered had pipe segments with diameter varying from 3.6 mm to 97 mm and loop height varying from 1 to 26 m with pressure ranging from near atmospheric to 90 bar. The total circulation length of the loops considered varied from about 10 to 125 m. All these loops used water as the working fluid.

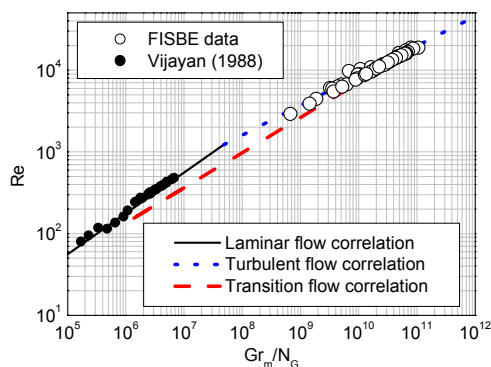


FIG. 6. In-house data on figure-of-eight loops.

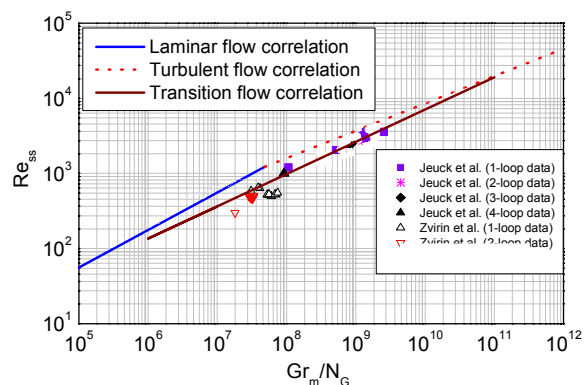


FIG. 7. Parallel loops data neglecting local losses.

In-house data on nonuniform diameter figure-of-eight loops are tested with the correlations in Fig. 6. The parallel loop data of Jeuck et al. (1981) [18] and Zvirin et al. (1981) [1] are found to be in reasonable agreement with the empirical correlation (Fig.7). The data from all NDLs are plotted in Fig. 8 neglecting the local losses. Both uniform diameter and nonuniform diameter loop data neglecting the local losses are plotted together in Fig. 9. In general, the low Reynolds number laminar ($Re < 350$) and high Reynolds number turbulent ($Re > 10000$) flow data show very good agreement with the respective theoretical correlations. For specific loops, good agreement with laminar flow correlation is observed even up to Re of 1200 and similarly turbulent flow correlation is found to give good results for $Re > 2000$. For the intermediate values of Gr_m/N_G ($2 \times 10^6 < Gr_m/N_G < 10^{11}$) significant deviation is observed where the flow is neither fully laminar nor fully turbulent. Thus, it becomes clear that normal fully developed flow friction factor correlations are valid if the entire loop is either in laminar or turbulent flow irrespective of whether it is a UDL or NDL.

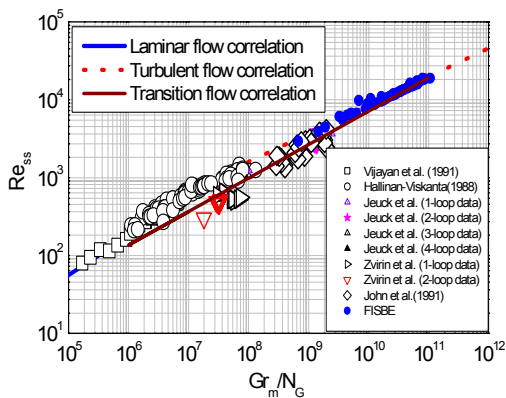


FIG. .8. NDL data neglecting local losses.

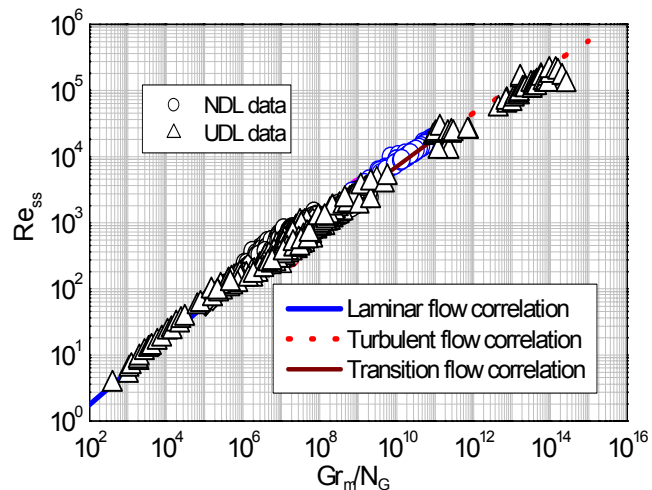


FIG. .9. All single-phase NC data neglecting local losses.

3. STEADY STATE BEHAVIOUR OF TWO-PHASE LOOPS

Two types of closed loops are relevant to nuclear industry as shown in Fig. 10. One is a closed loop with a SG (or condenser) relevant to PWRs, PHWRs and VVERs and the other is an open loop without SG relevant to BWRs. Under two-phase flow conditions, the steam generator functions as a condenser as far as the primary fluid is concerned. One of the problems of two-phase natural circulation is that explicit equation for flow rate like Eq. (9) is not readily available even with homogeneous equilibrium model. However, it is possible to get approximate dimensional equation for flow rate [22,23].

$$W \approx \left\{ \frac{2A^2 \rho_f \rho_{fg} \beta g Q_h \Delta Z}{h_{fg} K} \right\}^{1/3} \quad (26)$$

Todreas and Kazimi (1990) [3] presents an equation for the steady state flow rate in a two-phase natural circulation loop relevant to a PWR. However, unlike single-phase NC, for two-phase loops, a well-tested generalized relation for the steady flow in terms of a single dimensionless group does not exist. Relatively untested correlations for special cases have been proposed [24]. For example, for a uniform diameter loop with horizontal heater and cooler, explicit dimensionless equations for flow rate can be obtained as

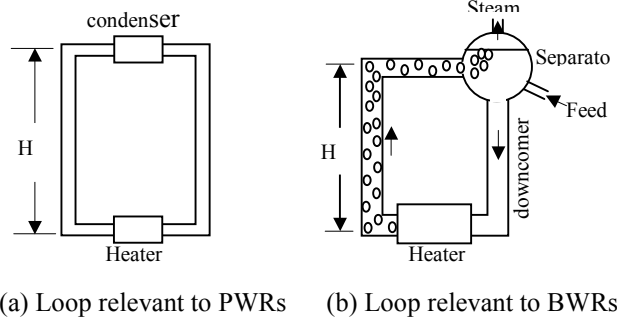


FIG. 10. Two-phase NCLs relevant to nuclear industry.

$$\text{Re}_{ss} = C \left[\frac{Gr_m^*}{pN_G} \right]^r \quad (27)$$

$$\text{Where } N_G = \frac{L_t}{D} \left[l_{sp} + (\phi_{LO}^2 l_{tp})_h + (\phi_{LO}^2 l_{tp})_p + (\phi_{LO}^2 l_{tp})_c \right] = \frac{L_t}{D} \sum_{i=1}^N (\phi_{LO}^2 l)_i \quad (28)$$

with $\phi_{LO}^2=1$ for the single-phase region and i refers to the regions in the loop. The equation is strictly valid only for the case without inlet subcooling.

$$C = \left(\frac{2}{p} \right)^r \text{ and } r = \frac{1}{2-b}$$

For laminar flow ($b=1, p=64$), $C=0.03125$ and $r=1$ and for turbulent flow ($b=0.25, p=0.316$), $C=2.87$ and $r=0.5714$. The same relationship can be obtained for loops with other orientations of heater and cooler if we use the elevation difference between the thermal centres of the cooler and heater in place of the loop height in Gr_m^* . In cases where the acceleration pressure drop is significant an explicit equation for the steady state Reynolds number as above cannot be obtained. Instead a polynomial in Re_{ss} can be obtained as

$$\text{Re}_{ss}^{2-b} = \frac{2Gr_m^*}{pN_G^*} - \frac{2\text{Re}_{ss}^2}{pN_G^*} \left\{ 1 - \frac{A_h^2}{A_{sep}^2} \right\} \rho_L v_{fg} x_e \quad (29)$$

where x_e is the exit quality, which for saturated feed water flow can be expressed as $x_e = Q_h/W_{ss}h_{fg}$. With this substitution, the flow rate equation can be rewritten as

$$\text{Re}_{ss}^{2-b} = \frac{2Gr_m^*}{pN_G^*} - \frac{2\text{Re}_{ss}^2}{pN_G^*} \left\{ 1 - \frac{A_h^2}{A_{sep}^2} \right\} \frac{\rho_f v_{fg} Q_h D}{A \mu_f h_{fg}} \quad (30)$$

Rohatgi and Duffey (1998) [25] obtained the following dimensionless equation for the steady state condition neglecting the acceleration pressure drop

$$N_p^2 (1 + \bar{K}_o) + N_p \left[(1 - N_s)(2 + \bar{K}_o) + \bar{K}_i + \frac{N_f}{N_{fr}} \left(1 - \frac{2}{L^*} \right) \right] + N_s^2 + \frac{N_f N_s}{N_{fr}} = 0 \quad (31)$$

Knowing the loop geometry, inlet subcooling and the power, the steady state flow rate can be easily estimated from Eq. (31).

Extensive database exists for the steady state flow in two-phase natural circulation loops. But unlike single-phase NC, a single dimensionless group cannot represent steady state flow in a two-phase NCS. Due to this it was not possible to compare the performance of various loops in terms of dimensionless quantities. Therefore, in most cases, the steady state flow rate in two-phase natural circulation loops are still compared using dimensional quantities. A typical case is shown in Fig. 11, which shows that the steady state flow rate is a strong function of the system pressure. For a specified pressure, Fig. 12a shows the effect of power on the steady state natural circulation flow rate. The steady state flow rate is found to saturate beyond a certain power. Apparently, this is due to the saturation of the average void fraction with increase in power. However, the power at which the flow rate saturates is different for different pressures (Fig. 12b). Increasing the power beyond this value does not affect the driving force much, but increases the frictional force causing the flow to decrease. Again, the power at which this happens also depends on the pressure and loop geometry.

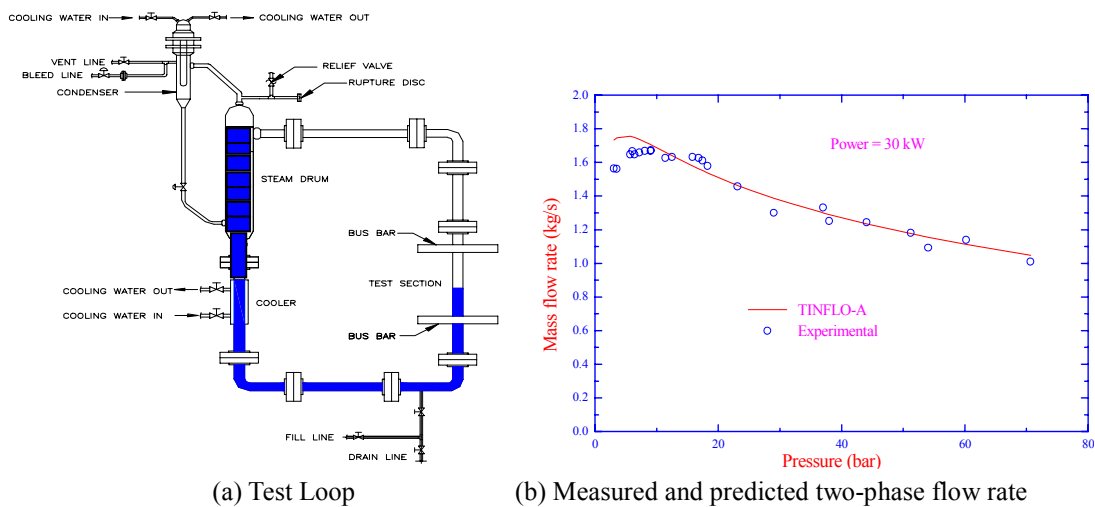


FIG. 11. Effect of pressure on two-phase NC flow rate.

Similar behaviour of the natural circulation flow rate with power was found for the HTL (High Temperature Loop) facility which simulates the prototype ATR [26]. In addition, they found that with decrease in downcomer level, the natural circulation flow rate is found to decrease since the driving head is reduced. They also compared the predictions of the homogeneous equilibrium model (HEM) and the slip model with the test data. The HEM was always found to predict larger flow rate than the slip model since it predicts larger void fraction and hence larger driving force.

In general, most of the previous experiments have shown that the natural circulation mass flow rate increases with increasing heating power in a low power region and then decreases with increasing power in a high power region for low pressure systems [27,28,29,30]. As well known, at lower powers, the gravitational pressure drop dominates the loop pressure drop, and the gravitational pressure drop decreases with an increasing void fraction in the heated region and riser. Hence, the loop mass flow rate increases with an increase in heating power. On the other hand, in the high power region, the frictional pressure drop becomes dominant and it increases with an increase in the void fraction; consequently, the loop mass flow rate decreases with an increase in heating power.

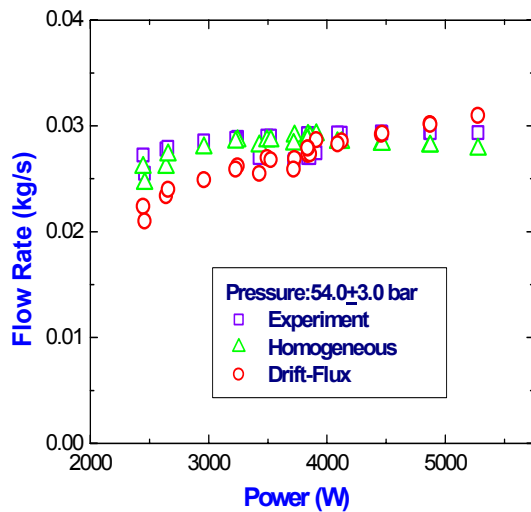


FIG. 12a. Measured and predicted flow rates showing the effect of power.

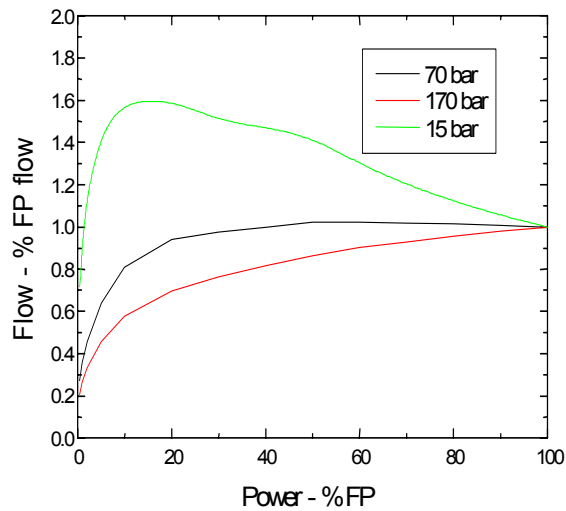


FIG. 12b. Effect of pressure and power on NC flow.

One of the major observation from these test data and predictions have shown that it is possible to predict the natural circulation flow behaviour at a given power, inlet subcooling and operating pressure using simple models with empirical relations for void fraction and friction factor. However, under very low power conditions, most of the models still overpredict the flow rate. One of the reasons could be the applicability of conventional friction factor relationships at such low flow conditions, and the possible existence of multi-dimensional flow in large diameter pipes such as in risers or chimney or across bends, etc. Even though, there are several two-fluid codes such as RELAP5, TRAC and RAMONA5, etc. extensive validation of these codes with the test data from simple loops are not reported.

4. STABILITY BEHAVIOUR OF SINGLE-PHASE LOOPS

Several investigators have carried out experimental investigations on the single-phase natural circulation instability. Examples are those by Creveling et al. (1975) [17], Gorman et al. (1986) [31], Widmann et al. (1989) [32], Vijayan et al (1992) [7], Nishihara (1997) [14], Misale et al. [33,34], Satoh et al. (1998) [35], Vijayan et al. (2001) [8], Satou et al. (2001) [36], Jiang et al. (2002) [37] and Vijayan et al. (2004) [6]. A few general characteristics of the oscillatory behaviour are brought out below.

4.1. Conditionally stable (Metastable or Hysteresis) regime

Linear stability analysis tells us that the threshold of instability is a unique value for specified operating and geometric conditions. However, an important characteristic of the natural circulation instability is that the threshold of instability is not a unique value, but depends on the path followed in the experiment. For example, experiments in the rectangular loop of Fig. 4a [8] showed that the instability thresholds are different for start-up from rest (Fig. 13), power raising from a stable steady state (Fig. 14) and power reduction from an unstable steady state (Fig. 15). The region in which the instability threshold shows path dependence is referred to as the conditionally stable or hysteresis regime ($65 < Q_h < 270$ W for the loop in Fig. 4a). The region above the conditionally stable region is unconditionally unstable as it is always unstable independent of the heat addition path. Similarly the region below the lower limit of the conditionally stable region is unconditionally stable. Conditional stability (metastable or hysteresis region) is also found in systems with parallel channels [38] and in simple loops with a throughflow [7]. The hysteresis phenomenon is also observed in two-phase loops [39].

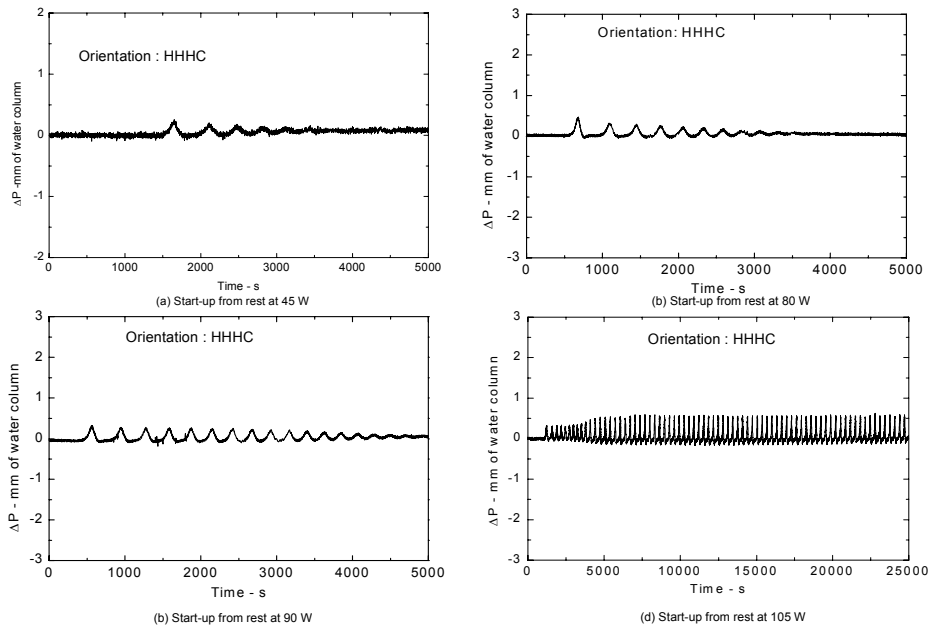


FIG. 13. Instability threshold for start-up from rest.

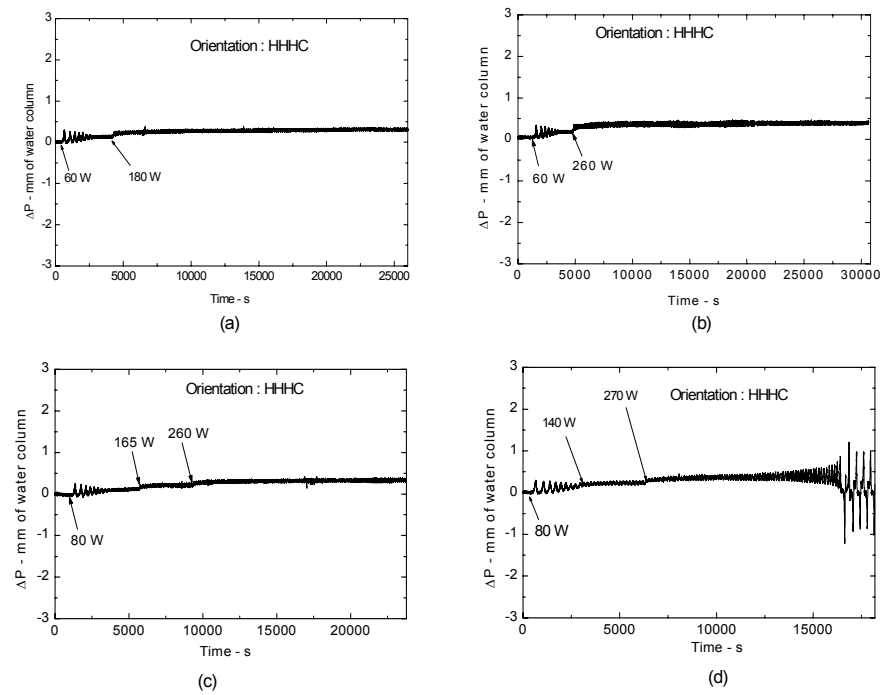


FIG. 14. Instability threshold for power raising from stable steady state.

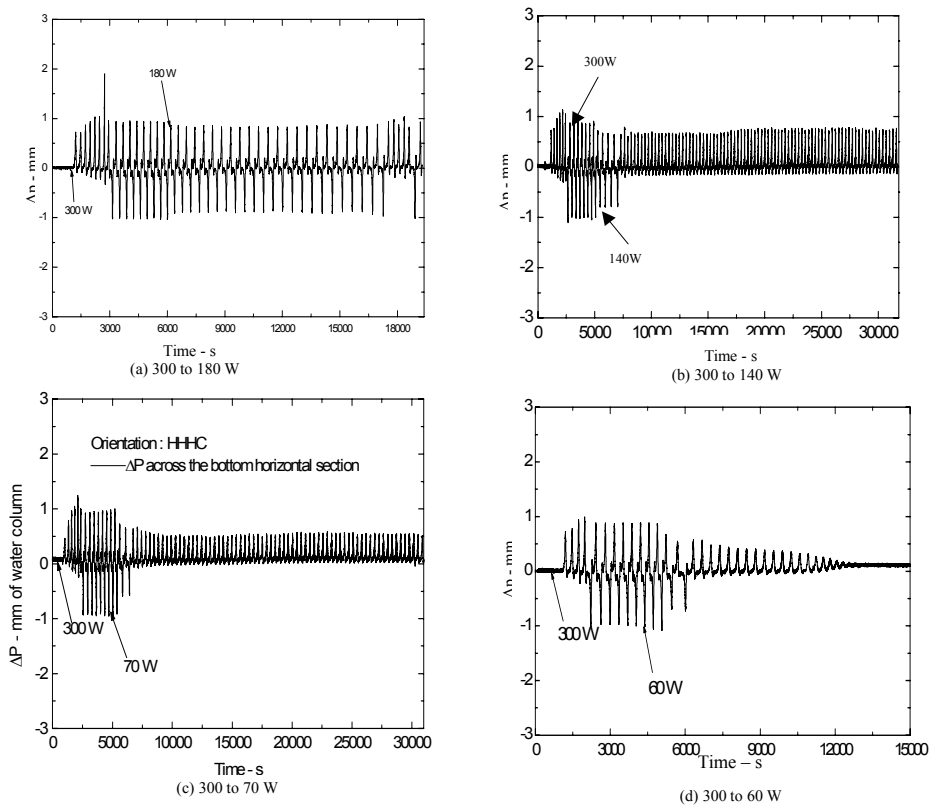
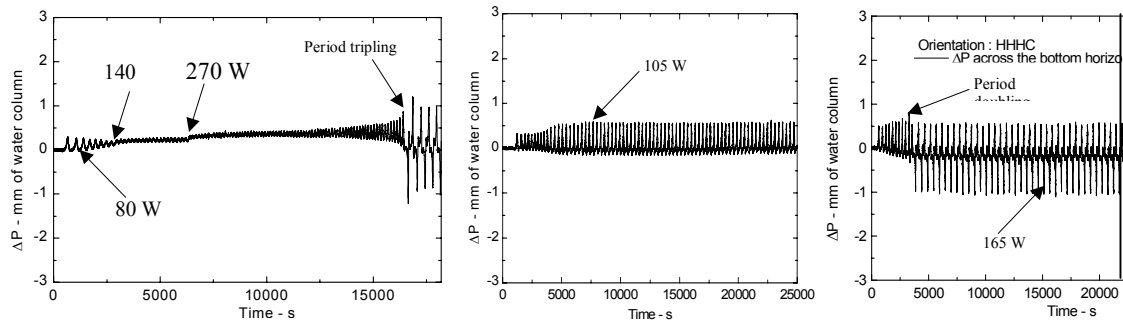


FIG. 15. Stability threshold for power reduction from an unstable state.

4.2. Mechanism causing instability and the unstable flow regimes

Based on numerical investigations in a rectangular loop with a point heat source at the bottom and a point heat sink at the top, Welander (1967) [40] proposed that oscillation growth is the mechanism causing the instability. Available experimental data suggests that oscillation growth is indeed the mechanism causing instability (Fig. 16). However, subtle differences in oscillation growth can be seen from Fig. 16. Oscillation growth as proposed by Welander is always observed for the development of instability from the steady state case (Fig. 16a). For the case of start-up from rest, the oscillations are observed right from flow initiation (Fig. 16b & c) although an initial oscillation growth is visible. In all the three cases, the oscillation growth is terminated by the system nonlinearities leading to limit cycle oscillations with constant amplitude. In this particular case, the condition that the cooler outlet temperature on the primary side cannot be less than the secondary side coolant inlet temperature limits the minimum temperature. This together with the corresponding flow fixes the upper limit on heater outlet temperature as the heater power is fixed. However, the characteristics of the limit cycle oscillations achieved are different as explained below.



(a) Oscillation growth from steady state (b) Start-up from rest at low power (c) Start-up from rest at high power

FIG. 16. Development of instability through the oscillation growth mechanism.

A qualitative difference in the limit cycle oscillations was observed at low and high powers. In the low power region ($0 < Q_h < 140 \text{ W}$ for the loop in Fig. 4a), periodic unidirectional pulsing (UDP) as predicted by Keller (1966) [41] was observed. Unidirectional pulsing portrays a bean shaped limit cycle in phase space (Fig. 17b). At high power ($> 196 \text{ W}$ for the loop in Fig 4a), periodic bi-directional pulsing (BDP) characterized by alternate forward and reverse flow is observed. Bi-directional pulsing portrays a double dumbbell shaped limit cycle in phase space (Fig. 17d). Between these two, a regime where the oscillatory behavior switches from unidirectional to bi-directional pulsing in a chaotic manner is observed (Fig. 17e). Chaotic switching results in the spread around the dumbbell shaped phase trajectory in Fig. 17f. With increase in power, the bi-directional pulsing regime continues but it becomes chaotic with each oscillation cycle depicting a distinct line resulting in the thick dumbbell shaped trajectory given in Fig. 17h. Long-term time series of unidirectional pulsing shows a characteristic comb like structure (Fig. 16b) whereas bi-directional pulsing shows a snake bone structure (Fig. 16c). In the short term, unidirectional pulsing appears to be repetitive flow initiations in the same direction whereas bi-directional pulsing is repetitive flow initiations in the opposite directions.

An interesting observation is that bi-directional pulsing flow regime alone is observed if power is raised from a stable steady state to an unstable value (Fig.18). Both the other flow regimes occur below the threshold power for this heat addition path. Unidirectional pulsing and chaotic switching, however, are observable both for start-up from rest (Fig. 13) and power step back from an initially unstable state. Even Keller (1966) had discussed the effect of initial conditions on unidirectional oscillations in his paper. Even though he had shown that the unidirectional oscillations in the loop with point heat source and point heat sink is not due to the initial conditions considered, it is not observable for all initial conditions in the present loop with finite length of heater and cooler.

Flow regimes observed in toroidal loops are much different from that observed in rectangular loops. For example, Gorman et al. (1986) [31] observed three different chaotic regimes: a globally chaotic regime whose essential features can be described by a one-dimensional cusp-shaped map, a subcritical regime in which the flow can be either chaotic or steady, and a transient regime in which the flow remains chaotic for a time and then decays into a steady flow: The description of the subcritical regime appears to fit the conditionally stable regime observed in rectangular loops. However, periodic unidirectional oscillations were not observed in the toroidal loop [17,36] report unidirectional oscillations, albeit in an inclined toroidal loop with a connecting tube.

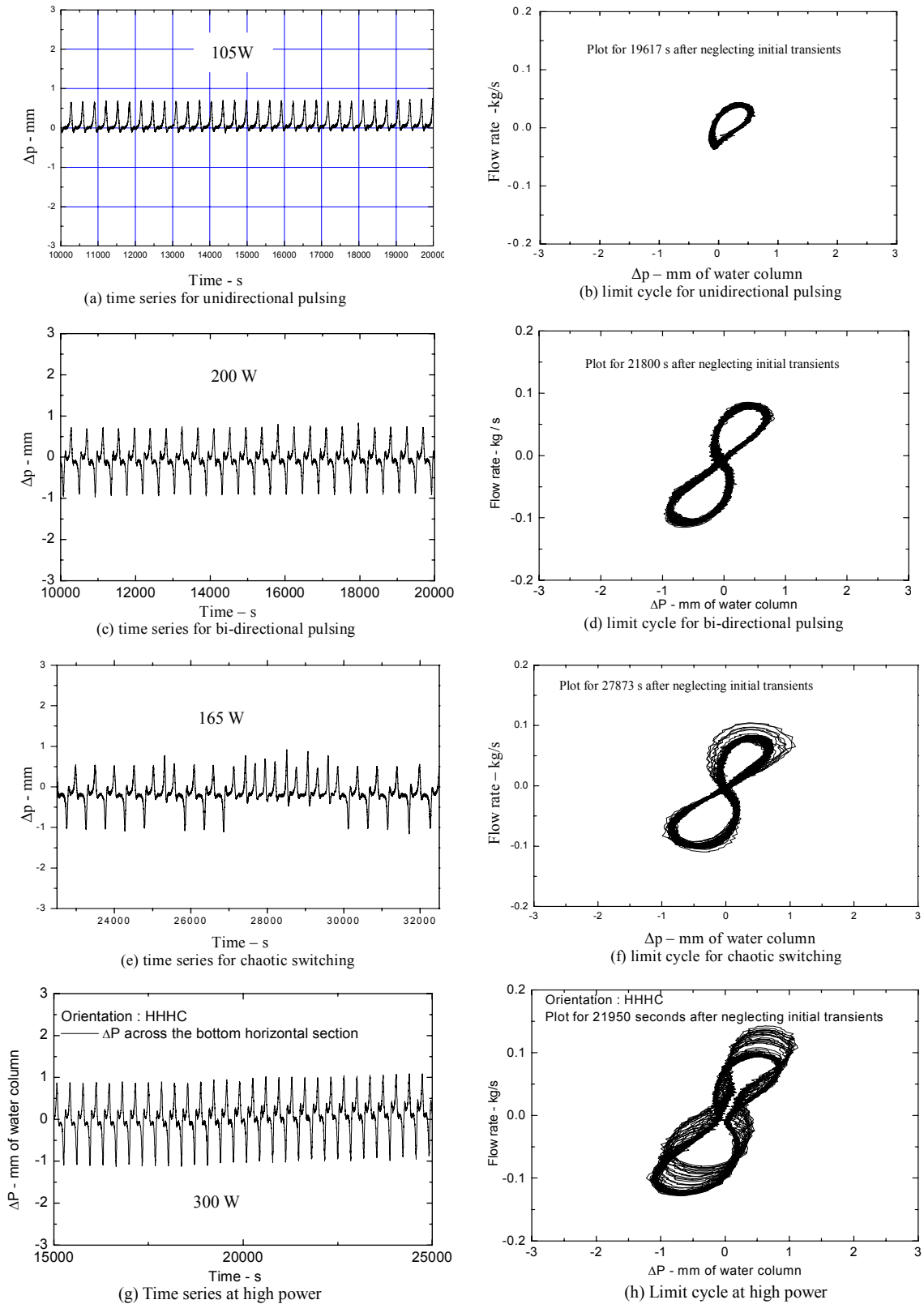


FIG. 17. Time series and limit cycles of unstable flow regimes in single-phase NC.

4.3. Flow regime switching and oscillation period

Whenever the flow regime switches from unidirectional to bi-directional pulsing, the oscillation period enhances (Fig. 16c). On the other hand, when the flow regime switches from bi-directional to unidirectional pulsing, the oscillation period reduces (Fig 17e). Period doubling is a usual step for transition to chaos [42]. Incidentally, the range of power where period doubling is observed is closely matching the observed chaotic switching regime. Beyond a critical value of power, chaotic switching is not observed. However, for start-up from rest flow initiates with unidirectional pulsing and then switches to bi-directional pulsing once (Fig. 15a and 16c). The period ratio for this first switching is found to be less than 2 and is found to decrease with increase in power. Tests carried out to check the repeatability of period ratio during flow regime switching, showed that the period ratio is reproducible within $\pm 8\%$. For switching from UDP to BDP following the small amplitude oscillation growth from an initial steady state, the period ratio can be significantly more than two (16a). However, there is no regular pattern in the observed period ratio and its value can be anywhere between 2 and 3.

4.4. Shape of the limit cycle

The shape of the limit cycle depends on the chosen parameter space. Depending on the chosen parameter space, unidirectional pulsing can portray the jaws of a shark, the hood of a cobra, the sole of a shoe or a bean shaped limit cycle (Fig. 19). Similarly, bi-directional pulsing can portray a squirrel, a butterfly, a duck or a dumbbell (Fig. 20). Still, more shapes are possible with other parameter spaces.

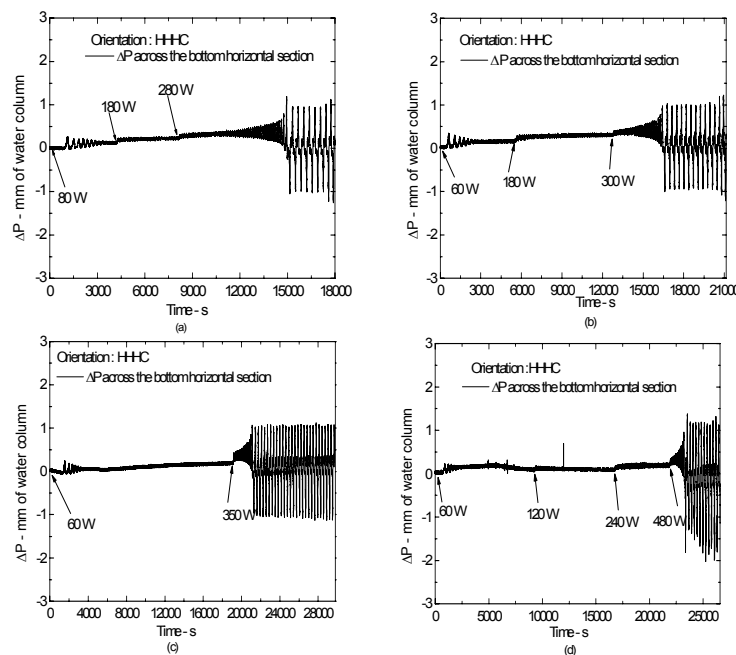


FIG. 18. Development of instability through the oscillation growth mechanism.

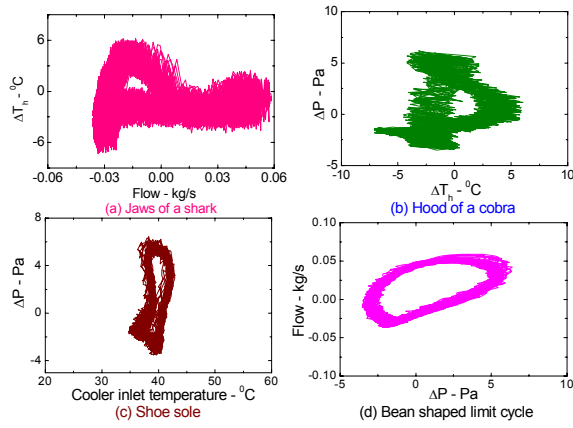


FIG. 19. Parametric effect on the phase plots for UDP at 140 W.

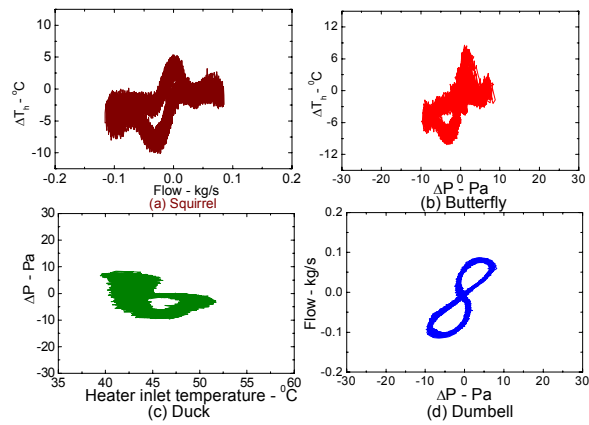


FIG. 20. Parametric effects on the limit cycle for BDP.

4.5. Effect of power

The effect of power is to enhance the amplitude and frequency of the oscillations. Bi-directional pulsing is found to have considerably large period than unidirectional pulsing (Fig. 21). For unidirectional pulsing, the period decreases linearly with power whereas an exponential decrease is observed for bi-directional pulsing. As the power increases, the phase plots deform due to the occurrence of the higher oscillatory modes. At low power, the dumbbell just touches in the middle (Fig. 22) whereas it separates out at higher powers. Fig. 22 also shows that the bi-directional pulsing is somewhat aperiodic and the aperiodicity increases with power as is observed from the increased thickness of the phase plot. A 3-D phase plot showing the effect of power on the unstable flow regimes is shown in Fig. 23. The increase in amplitude with power results in the enhancement of the space enclosed by the limit cycles as seen in Fig. 23. The observed unstable flow regimes are also marked in this figure. A point in the phase space represents the stable steady state.

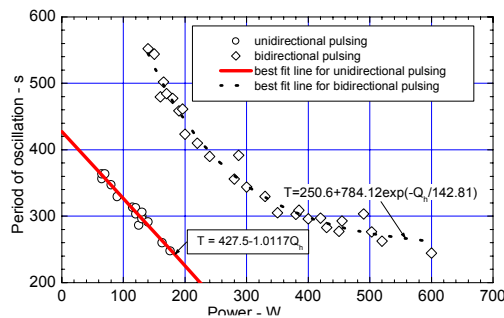


FIG. 21. Variation of oscillation period with power.

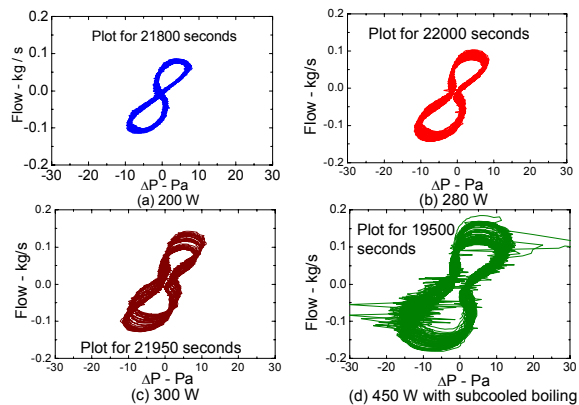


FIG. 22. Effect of power on BDP (plots neglect the initial transients).

4.6. Prediction of the stability map

The stability map for single-phase NCSs is usually generated with the 1-D model neglecting the boundary wall effect. 1-D models show a very strong influence of the friction factor correlation on the stability threshold. Good comparison with experimental data can be obtained with a loop specific empirical correlation even though the theoretical model neglects the wall thermal capacitance, heat losses and 3-D effects [17, 7]. The same empirical correlation, when applied for other loops can show significantly different results. For example, Eq. (22) was found to predict the instability threshold of a 23.2 mm inside diameter rectangular loop of Fig. 3a reasonably well [7]. However, when the same correlation is used for the 26.9 mm inside diameter loop of Fig. 4a, the results are significantly different (Fig. 24). However, considering the heat losses and the thermal capacitance of the boundary walls, good prediction of the stability threshold can be expected for the fully laminar and fully turbulent loops. For certain geometric configurations such as that of the toroidal loop, the adequacy of the 1-D theory is questionable as the gravitational acceleration changes continuously over the loop.

4.7. Prediction of limit cycles

One dimensional theory using the fully developed friction factor and heat transfer correlations are found to be adequate for predicting the steady state behaviour of single-phase fully laminar and fully turbulent loops if the local pressure losses are also accounted. Good prediction of the stability map using the 1-D theory is expected for the fully laminar and fully turbulent loops if the thermal processes at the wall and the heat losses are accounted. However, predicting the limit cycle oscillations in natural circulation loops with repetitive flow reversals is a bigger challenge as all three (i.e. laminar, transition and turbulent) flow regimes can be encountered in the clockwise and anticlockwise directions in rapid succession in every oscillation cycle. In such cases, a criterion for laminar to turbulent flow transition is essential to be incorporated in the nonlinear codes. The transition criteria used are different in different codes [43, 44]. Ambrosini et al. (2004) [44] have shown that the use of an ad hoc friction correlation can lead to very interesting results like the appearance or disappearance of islands of stability. Prediction using the 1-D theory and the transition criterion described in Vijayan et al. (1995) [43], the limit cycles predicted (Fig. 25) for the loop in Fig. 4a is found to be significantly different from the experimentally observed limit cycles [6].

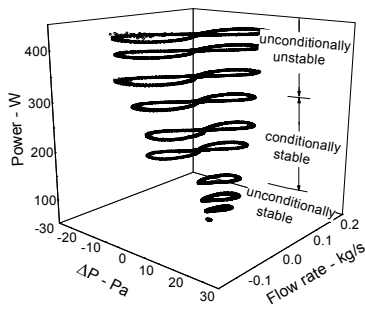


FIG. 23. 3-D phase space of instability (plot for 2500 seconds for each power neglecting the initial transients).

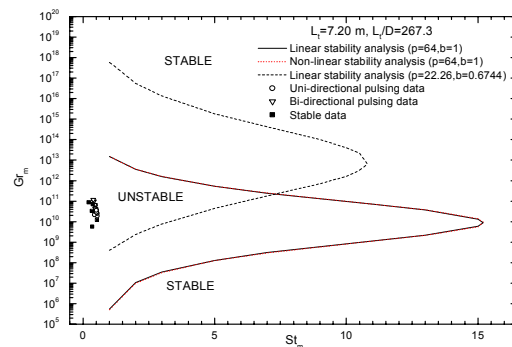


FIG. 24. Effect of friction correlations on the predicted stability map.

Due to the occurrence of laminar, transition and turbulent regimes with forward and reverse flow in every oscillation cycle (e.g. during oscillations with periodic flow reversals) the flow is never fully developed and the use of fully developed friction factor correlations and even the validity of the 1-D approximation itself is questionable for prediction of unstable flows. Use of 3-D computer codes is appropriate for prediction of the limit cycles as it can eliminate the uncertainty associated with the friction factor correlations.

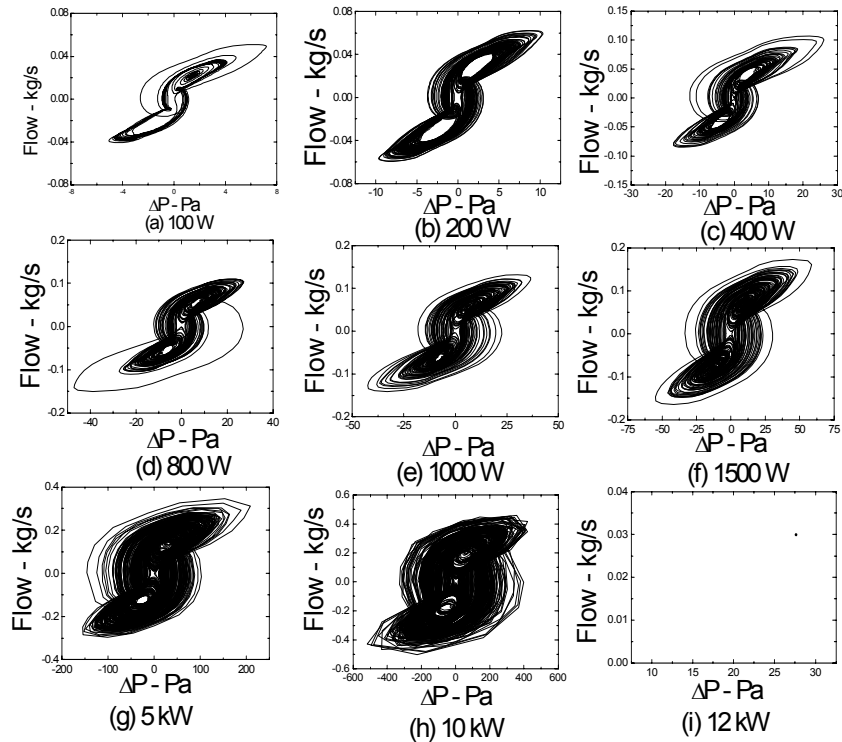


FIG. 25. Predicted limit cycles for different powers.

4.8. Techniques for stabilizing

Knowledge of parametric effects helps us in avoiding instabilities. For example, vertical heater and vertical cooler is found to be the most stable orientation of the source and sink in a rectangular loop. Hence, selection of this orientation is better for improving stability. The analysis results show that increasing the St_m and the L_t/D are ways of stabilizing. The latter option is more commonly used in natural circulation systems. In fact, single-phase instability is observed only for systems with $L_t/D < 300$. Increasing the length or decreasing the diameter will stabilise the loop. Misale et al. (1999) [34] has used an orifice to stabilise single-phase NC flow. In single-phase flow, the location of the orifice does not play a significant role. However, one of the basic problems of orificing is that it reduces the flow rate significantly. Reduction in the flow rate results in the reduction of the heat transport capability of NC loops. However, there are several ways to stabilize NCS without significantly reducing the flow rates. One of them is to use highly conducting or thick walled pipes for construction of the loop. Thick-walled tubes can diffuse the hot and cold pockets leading to stability [45, 37]. In addition, process control techniques can be used to stabilize the NC flow. These are beginning to be used in single-phase flow. For example, Fichera, and Pagano (2003) [46] demonstrated the use of a proportional derivative control to stabilize single-phase NC instability.

5. EXPERIMENTAL DATABASE FOR INSTABILITY OF TWO-PHASE NC LOOPS

Extensive experimental database exist in literature for different kinds of flow instabilities which can occur in boiling two-phase natural circulation systems. Jain et al. (1966) [27] conducted systematic investigations to find out the effects of various operating conditions such as heating power, subcooling, pressure, etc. on instability. Mostly, they observed the Type II density-wave instability in their experiments. Such behaviour was also observed in parallel heated channels of a two-phase natural circulation loop by Mathisen (1967) [47]. They observed density-wave instability in their experiments, which was found to increase with increase in channel exit restriction, inlet subcooling, and decrease in channel inlet restriction and downcomer level. Chexal and Bergles (1973) [48] observed seven flow regimes when their loop was heated from cold condition, out of which three were steady and four were unstable. These regimes are (i) surface evaporation; (ii) a static instability characterized by periodic exit large bubble formation; (iii) a steady flow with continuous exit of small bubbles; (iv) a static instability characterized by periodic exit of small bubbles; (v) another static instability characterized by periodic extensive small bubble formation; (vi) a steady natural circulation; and (vii) the density-wave oscillation (dynamic instability). The static instabilities observed in their loop are due to the high heat flux and subcooled boiling occurring in the heated section, which are ideal for the chugging-type instability. Fukuda and Kobori (1979) [49] observed two modes of oscillations in a natural circulation loop with parallel heated channels. One was the U-tube oscillation characterized by channel flows oscillating with 180° phase difference, and the other was the in-phase mode oscillations in which the channel flow oscillated along with the whole loop without any phase lag among them.

There are several recent studies on the flow instability under low power conditions. Lee and Ishii (1990) [50] found that non-equilibrium conditions existed between the phases and flashing created flow instability in the loop under low power conditions. Aritomi et al. (1992) [51] observed three kinds of instabilities during the power raising process of a two-phase natural circulation loop with twin boiling channels, such as geysering, in-phase oscillation and out-of-phase density-wave oscillations. Kyung and Lee (1994) [30] investigated the flow characteristics in an open two-phase natural circulation loop using Freon-113 as test fluid. They observed three different modes of oscillation with increase in heat flux such as

- (i) periodic oscillation characterized by flow oscillations with an incubation period,
- (ii) continuous circulation which is maintained with the churn/wispy-annular flow pattern. This was found to be a stable operation mode in which the flow was found to increase with increase in heat flux first and then decrease with further increase in heat flux, and
- (iii) periodic circulation characterized by flow oscillations with continuous boiling inside the heater section (i.e. there is no incubation period) and void fraction fluctuates from 0.6 to 1.0 repeatedly. In this mode, mean circulation rate was found to decrease with increase in heat flux although the mean void fraction kept on increasing.

Jiang et al. (1995) [52] observed three different kinds of flow instability such as geysering, flashing and Type I density-wave oscillations during start-up of the natural circulation loop. Wu et al. (1996) [53] observed that the flow oscillatory behaviour was dependent on the heating power and inlet subcooling. Depending on the operating conditions, the oscillations can be periodic or chaotic.

Moreover, it is evident from these studies that a lot of experimental data exist for various types of flow instabilities in simple two-phase natural circulation systems. Most instabilities such as flashing, geysering, Type I density-wave instability, Ledinegg type instability, etc. in natural circulation systems are found to occur during initiation of boiling and under low quality conditions. For model validation, it is important to know how to separate them from each other based on their mechanisms and characteristics.

6. STATIC INSTABILITY OF TWO-PHASE NC LOOPS

Extensive comparison of the characteristic equation for static instability (Eq. 5 in lecture T#8) with experimental data has been carried out by Rohatgi and Duffey (1998) [25]. Stability maps for natural circulation flow are presented in the phase change number and subcooling number plane (i.e. N_p - N_s plane). The characteristic equation predicts two roots corresponding to the instability at low and high quality. According to them, the boundary of the unstable region closer to the zero-quality line is the precursor of static instability, and represents the transition from the single-phase region to the two-phase region. Based on thermal equilibrium, the limiting solution for the first unstable line is $N_p/N_s = 1$. However, if we include subcooled boiling, the first unstable line will be predicted for $N_p/N_s < 1$. Using the Saha-Zuber model [54], the limiting stability line for Peclet number greater 70,000 is given by

$$\frac{N_p}{N_s} = \frac{1}{1 + 38.4/(L/D)} \quad (32)$$

The above equation was found to match well with data for $N_p < 150$ [25]. Based on extensive data, they suggest the first unstable line can be represented by

$$\frac{N_p}{N_s} = 0.7 \quad (33)$$

The second boundary represents the transition from two-phase region to very-high void region. Rohatgi and Duffey also found that the high void stability boundary matches fairly well with that predicted by the detailed perturbation analysis. Based on the available experimental data on density wave instability, Rohatgi and Duffey obtained a best fit line given by

$$\frac{N_p}{N_s} = 3 \quad (34)$$

Thus the unstable region is given by $0.7 < N^* < 3$ where $N^* = N_p/N_s$. It is also found that stable natural circulation flow can be maintained below a critical subcooling number. The same equations are also valid for the static instability of parallel channels.

7. DYNAMIC STABILITY OF TWO-PHASE NC LOOPS

In general, two-phase natural circulation loops exhibit two unstable zones as the power is increased. One of these occurs at a low power just at the boiling inception point (and hence at low quality) and the other at a high power (and hence at high quality). Corresponding to these, there are two stability thresholds; the lower stability threshold is sometimes referred to as the threshold of type-I instability and upper one is referred to as threshold of type-II instability [49]. However, due to the hysteresis effects, the stability thresholds are not unique. Chen et al. (2001) [40] provided some experimental evidence for the hysteresis effect on the threshold of instability. Theoretically Achard et al. (1985) [55] established that islands of instability could occur in the stable zone. Although, the first experimental evidence on the existence of islands of instability was provided by Yadigaroglu and Bergles (1969) [56], to our knowledge, experimental data is lacking.

7.1. Instability due to boiling inception (Type-I instability)

Boiling inception has a significant effect on the loop density and hence the gravitational pressure drop. Fukuda and Kobori (1979) [49] have shown that the gravitational pressure drop in the unheated riser plays a dominant role in Type I instability. The mechanism for this instability has already been explained in the second lecture. The homogeneous equilibrium model can predict the instability as has

been shown in case of start-up of AHWR in the last lecture. Boiling inception influences both unstable and stable single-phase natural circulation loops.

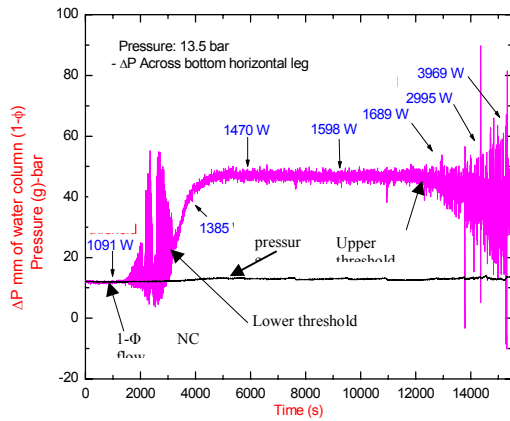


FIG. 26. Typical experimental stability map at 13.7 bar.

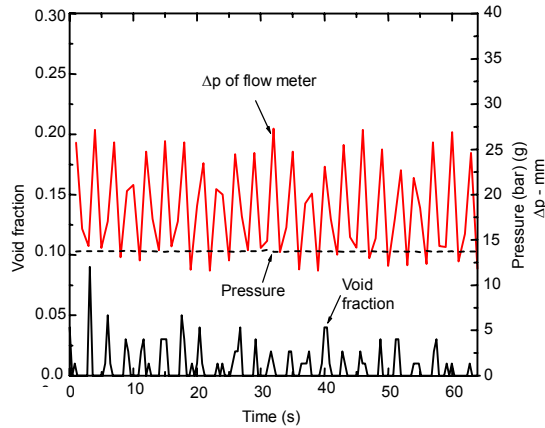


FIG. 27. Instability due to boiling inception.

7.1.1. Boiling inception in an unstable single-phase loop

In this case, the instability continues with part of the oscillation cycle in single-phase flow. Various flow regimes observed with the inception of boiling in an unstable loop were briefly described in the second lecture. Subcooled boiling leads to the formation of the cusps in the phase trajectory (compare Fig. 22a and d). The main reason for the instability is the jump in flow rate occurring during phase change and the accompanying reduction in the exit enthalpy that cannot support two-phase flow.

7.1.2. Boiling inception in a stable single-phase loop

A stable single-phase system can become unstable due to the inception of boiling as shown in Fig. 26. This instability is important for natural circulation BWRs. A basic characteristic of this instability is that single-phase conditions occur in the loop during a part of the oscillation cycle as shown in Fig. 27. Flashing induced instability and geysering also belong to this category. A general characteristic of all instabilities associated with boiling inception is that these are not observed beyond a critical value of the system pressure (Fig.28). The critical pressure beyond which the instability disappears is found to be a function of loop diameter (Compare Figs. 28 and 29).

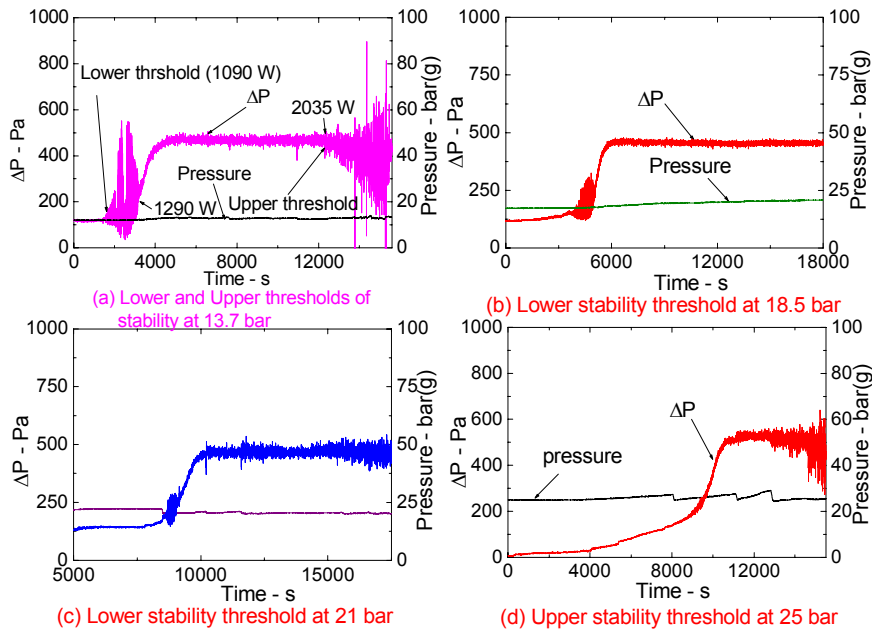


FIG. 28. Effect of pressure on the instability due to boiling inception in 9.6 mm loop.

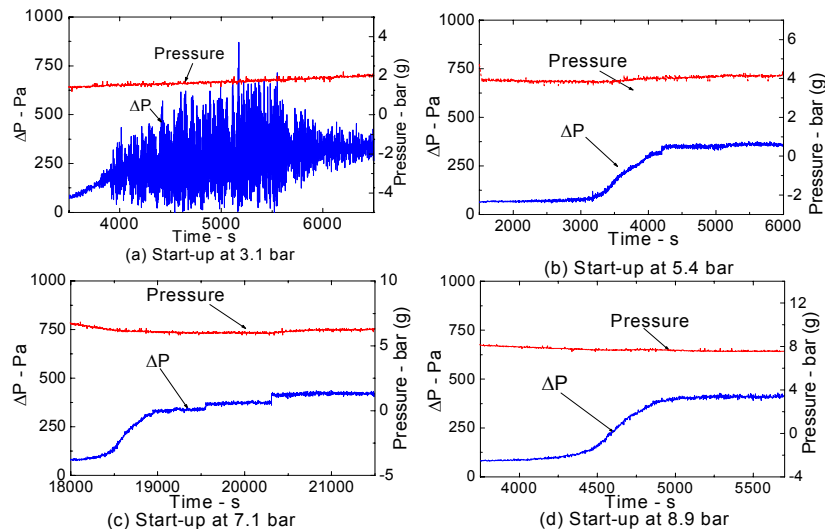


FIG. 29. Effect of pressure on the instability due to boiling inception in 19.2 mm i.d. loop.

7.2. Limit cycles

Unidirectional oscillations are more often observed in two-phase loops with vertical heaters. However, bi-directional pulsing and chaotic switching could be observed in loops with horizontal heaters. A typical limit cycle observed for unidirectional oscillations in the loop of Fig.11 is given in Fig.30. It is found to be similar to that observed in single-phase loops (Fig 17b) except that it is more chaotic.

Non-linear analyses can be used to generate limit cycles of density-wave oscillations [57,58,59]. Nigamutlin et al. [59] found that the heat transfer coefficient does not affect the threshold of stability while the thermal wall inertia has a strong stabilising effect. Non-linear analyses also revealed the presence of chaotic oscillations in two-phase flow systems [55,60,61]. However, there are very few studies on validation of numerical codes for limit cycle oscillations.

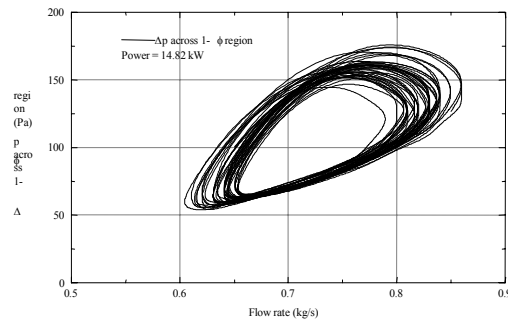
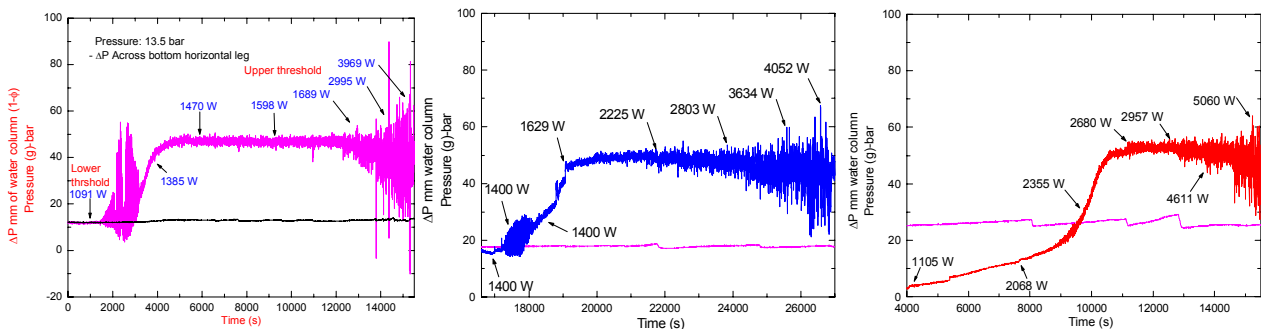


FIG. 30. Typical limit cycle at 2.2 bar.

7.3. Type II instability

Two-phase systems are observed to be stable between a lower and an upper threshold as already explained. The unstable region beyond the upper threshold is known as type II instability. Calculations by Fukuda and Kobori (1979) [49] showed that the frictional pressure drop is dominant in type II instability. The upper instability threshold (type-II instability) occurs at high quality and can be predicted by the homogeneous equilibrium model. Experimental data on the occurrence of the upper threshold is shown in Figure 31 at different pressures. In general, type II instability is observed when the system flow rate begins to reduce with increase in power (Fig. 31).



(a) 13.7 bar

FIG.31. The upper threshold of instability at different pressures.

7.4. Prediction of stability map

Several studies based on linear and non-linear analyses have already been carried out in the past to validate the two-phase flow models for prediction of the threshold of instability. Ishii and Zuber (1970) [62] developed a linear analytical model based on a drift flux model for a two-phase natural circulation loop and plotted the stability maps on non-dimensional parameters. Saha and Zuber (1978) [54] modified Ishii and Zuber's model by taking into account the thermal non-equilibrium effect between the phases. They found that the thermal non-equilibrium effect predicts a more stable system at low subcooling when compared with the thermal equilibrium model. However, their predictions when compared with experiments for the threshold of stability showed poor agreement for high subcooling conditions. Furutera (1986) [63] was probably the first to report the dependence of the threshold of instability on the two-phase friction factor multiplier model and the heat capacity in the subcooled boiling region. Moreover, they showed that the threshold of instability could be predicted with reasonable accuracy using the homogeneous model. Since that many others [64, 65, 66, 67] showed that it is possible to predict the threshold of instability for density-wave instabilities in two-phase natural circulation systems using the HEM.

However, the applicability of the HEM for prediction of stability threshold still is debatable. Strictly speaking, two fluid model is the ideal one to take care of kinematic and thermodynamic nonequilibrium. However, solution of these balance equations require the models of constitutive relations for interfacial and wall transfer laws which are not well established and are being continuously upgraded. Further, solution of so many equations which are highly non-linear in nature is extremely difficult by the linearised analytical model. An alternative to the two-fluid approach is the drift flux model which replaces the two momentum equations for the liquid and vapour by one momentum equation for the mixture plus a non-differential constitutive law for the relative velocity. So far as the phasic temperature is concerned, one can assume either the thermal equilibrium or thermal nonequilibrium between the phases. Employment of a drift flux model is more realistic than the pure homogenous model. But this needs well assessed models for the drift velocity which is mostly dependent on the flow patterns. It is well known that an increase in drift velocity which is an indication of the slip between the phases, reduces the void fraction and hence the mixture density. This can increase the gravitational and reduce the frictional component of two-phase pressure drop. At the same time, an increase in drift velocity also reduces the transportation time lag for the fluid to pass through the system. Hence, they can significantly affect the stability.

Aritomi et al. (1983) [68] found that the effect of slip between the phases is to stabilize the flow, since the fluctuation of density reduces with increase in slip for low quality conditions. Fukuda and Hasegawa [69] analysed the effect of slip on Type I and Type II density-wave instabilities. They found that the Type I instability stabilizes but the Type II instability destabilizes with inclusion of slip in the model. Since the Type I instability occurs under low quality conditions, the fluctuation of gravitational component of pressure loss can be reduced by slip between the phases which stabilizes the flow. But Ishii and Zuber found an opposite effect to the above for Type II instability. They found that with inclusion of slip, the Type II instability stabilizes due to decrease of pressure drop with increase in slip. A similar result was found by Peng et al. (1984) [70] and Rizwaan-Uddin and Dorning (1986) [71] who found that with increase in slip the flow stabilizes.

Moreover from these studies it can be understood that the slip has a tremendous effect on flow stability. A systematic research must be carried out to understand their effects on the Type I and Type II instabilities. However, mostly the homogenous model is found to be conservative in estimating the stability boundaries, which are good approximations for design purposes of natural circulation systems (Fig. 32).

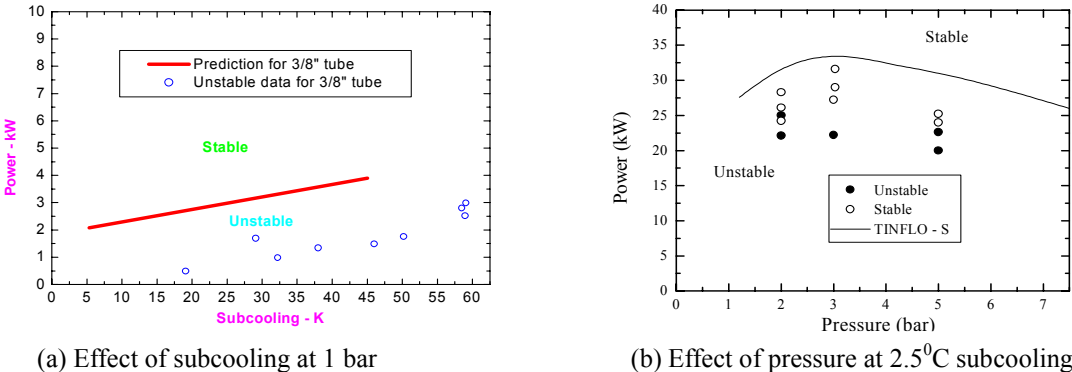


FIG. 32. Comparison of measured and predicted stability maps.

8. CONCLUDING REMARKS

A brief review of the steady state and stability data obtained from simple loop facilities have been carried out. Data from simple loops were useful to develop the scaling relationships for single-phase flow. Although, large database exists for two-phase flow, due to the lack of generalized dimensionless groups, it is not possible to compare the performance of different loops. It is possible to express the steady state two-phase NC flow in terms of a single dimensionless group for special cases. Phenomenological studies indicate that several unstable flow regimes are possible for both single-phase and two-phase NCSs. Hysteresis phenomenon also exists in both single-phase and two-phase loops. Comparison of stability data shows that the friction pressure drop correlation plays a significant role in case of single-phase loops. Neglecting the heat losses and wall effects, even the same friction factor correlation that gives good steady state results is found to perform poorly while predicting the stability data. For predicting the stability thresholds, it is required to consider the heat transfer to the wall and the heat losses. Although, a pathological friction factor correlation, can give good prediction of the stability threshold, it is not expected to give good prediction of the limit cycles while simulating the unstable flows. For single-phase unstable flows, although, the predicted time series appears similar, the frequency and the shape of the limit cycle are found to be significantly different from the experimental value. Simulation of unstable flows with repetitive flow reversals is a complex problem, since the flow can experience laminar, transition and turbulent regimes repetitively. Besides the flow is never fully developed and 3-D effects are significant. For this case unsteady 3-D nonlinear analysis may be the right choice.

Although, extensive database exists for instability of two-phase loops, often it is not possible to identify the instability type from the data. Both the steady state and the stability threshold of two-phase NCSs can be predicted with reasonable accuracy using the HEM with selected two-phase friction factor multiplier correlations. Extensive validation of the nonlinear codes for the prediction of limit cycle oscillations does not exist. Complete understanding of the occurrence of hysteresis phenomena and islands of stability (or instability) in two-phase NCSs are lacking. Without this, the computer codes for nonlinear analysis cannot be fully validated.

NOMENCLATURE

- A - flow area, m^2
- a_i - dimensionless flow area, A_i/A_r
- b - constant in friction factor equation
- C_p - specific heat, J/kgK
- D - hydraulic diameter, m
- d_i - dimensionless hydraulic diameter, D_i/D_r
- f - Darcy-Weisbach friction coefficient
- g - gravitational acceleration, m/s^2
- Gr_m - modified Grashof number, $D^3\rho^2\beta g\Delta T_r/\mu^2$
- h - enthalpy J/kg
- h_{fg} - latent heat of vaporization, J/kg
- H - loop height, m
- K - local pressure loss coefficient
- k - thermal conductivity, W/mK
- l_i - dimensionless length, L_i/L_t
- L - length, m
- N - total number of pipe segments
- N_f - Froude number, $gLA\rho_f^2/W^2$
- N_{fr} - friction number, $fL/2D$
- N_p - phase change number, $Q_h\rho_f/(Wh_{fg}\rho_g)$
- N_{pch} - phase change number (Q_h/Wh_{fg})

N_{sub} - subcooling number ($\Delta h_{\text{sub}}/h_{\text{fg}}$)
 N_s - subcooling number, $\Delta h_i \rho_l / h_{\text{fg}} \rho_g$
 Nu_m - modified Nusselt number, $U_i L_t / k$
 N_G - geometric contribution to the friction number
 p - constant in the friction factor equation
 Pr - Prandtl number, $C_p \mu / k$
 Q_h - total heat input rate, W
 Re - Reynolds number, $DW / A \mu$
 S - dimensionless co-ordinate around the loop, s/H
 s - co-ordinate around the loop, m
 St_m - modified Stanton number, $4Nu_m / Re_{ss} Pr$
 t - time, s
 T - temperature, K
 ΔT_r - reference temperature difference ($Q_h H / A \mu C_p$), K
 v - specific volume, m^3/kg
 v_{fg} - $v_g - v_f$, m^3/kg
 W - mass flow rate, kg/s
 Δz - centre line elevation difference between cooler and heater, m

Greek Symbols

β - thermal expansion coefficient, K^{-1}
 μ - dynamic viscosity, Ns/m^2
 ρ_0 - reference density, kg/m^3
 τ - nondimensional time, and residence time, s
 ϕ - dimensionless circulation length, L_t/H
 ϕ_{LO}^2 - two-phase friction multiplier
 ω - dimensionless mass flow rate

Subscripts

c - cooler,
 cl - cold leg
 d - downcomer
 e - equivalent
 eff - effective
 f - saturated liquid
 g - saturated vapour
 h - heater
 hl - hot leg
 i - i^{th} segment
 in - inlet
 r - reference value
 sp - single-phase
 ss - steady state
 sub - subcooling
 t - total
 tp - two-phase

Superscripts

$-$ - average

REFERENCES

- [1] ZVIRIN, Y. JEUCK III P., SULLIVAN, C.W., DUFFEY, R.B., Experimental and analytical investigation of a natural circulation system with parallel loops, *J. Heat Transfer* 103, pp.645–652 (1981).
- [2] LEWIS E.E., *Nuclear Power Reactor Safety*, John Wiley and Sons, New York (1977).
- [3] TODREAS, N.E. and KAZIMI, M.S., *Nuclear Systems II, Elements of Thermal Hydraulic Design*, Hemisphere Publications, New York, USA (1990).
- [4] LOOMIS, G.G. and SODA, K., Results of the Semiscale Mod-2A natural-circulation experiments, NUREG/CR-2335, EGG-2200, Idaho National Engineering Lab., Idaho Falls (USA) (1982).
- [5] VIJAYAN, P.K., Experimental observations on the general trends of the steady state and stability behaviour of single-phase natural circulation loops, *Nuclear Engineering and Design*, 215, pp.139–152 (2002).
- [6] VIJAYAN, P.K., BADE¹, M.H. SAHA, D., SINHA, R.K. and VENKAT RAJ V., A Generalized Flow Correlation For Single-Phase Natural Circulation Loops, HMT-2004-C022, Proceedings of 6th ISHMT-ASME Heat and Mass Transfer Conference, Kalpakkam, India, Jan. 5–7 (2004).
- [7] VIJAYAN, P.K., NAYAK, A.K., PILKHWAL, D.S., SAHA, D. and VENKAT RAJ, V., Effect of loop diameter on the stability of single-phase natural circulation in rectangular loops, Proc. 5th Int. Topical Meet. on Reactor Thermalhydraulics, NURETH-5, Salt Lake City, Vol.1, pp.261–267 (1992).
- [8] VIJAYAN, P.K., BHOJWANI, V.K., BADE, M.H., SHARMA, M., NAYAK, A.K., SAHA, D. and SINHA, R.K., Investigations on the effect of heater and cooler orientation on the steady state, transient and stability behaviour of single-phase natural circulation in a rectangular loop, BARC/2001/E/034, BARC, Mumbai (2001).
- [9] HOLMAN, J.P. and BOGGS, J.H., Heat transfer to freon 12 near the critical state in a natural circulation loop, *J. Heat Transfer*, 82, pp.221–226 (1960).
- [10] HUANG, B.J. and ZELAYA, R., Heat transfer behaviour of a rectangular thermosyphon loop, *J. Heat Transfer* 110, pp.487–493 (1988).
- [11] MISALE, M., TAGLIAFICO, L. and TANDA, G., Experiments in a free convection rectangular loop, Proceedings of the fourth International Symposium on Transport phenomena in heat and mass transfer, Sydney (Australia), 14-19 July, pp.203–211 (1991).
- [12] BERNIER, M.A. and BALIGA, B.R., A 1-D/2-D model and experimental results for a closed-loop thermosyphon with vertical heat transfer sections, *Int. J. Heat Mass Transfer* 35, pp.2969–2982 (1992).
- [13] HO, C.J., CHIOU, S.P. and HU, C.S., Heat transfer characteristics of a rectangular natural circulation loop containing water near its density extreme, *Int. J. Heat Mass Transfer*, 40, pp.3553–3558 (1997).
- [14] NISHIHARA, T., Oscillatory instability of a single-phase natural circulation loop, NURETH-8, Kyoto, Sept. 30–Oct. 4, pp.839-847 (1997).
- [15] BAU, H.H. and TORRANCE, K.E., Transient and steady state behaviour of an open, symmetrically heated, free convection loop, *Int. J. Heat Mass Transfer*, 24, pp.597–609 (1981).
- [16] HAWARE, S.K., GROVER, R.B. and VENKAT RAJ, V., Experimental investigation into natural convection heat transfer in an open-loop thermosyphon with horizontal tubes, HMT-D2-83, Proc. VIIth National Heat and Mass Transfer Conference, Kharagpur, India (1983).
- [17] CREVELING, H.F., DE PAZ, J.F., BALADI, J.Y. and SCHOENHALS, R.J., Stability characteristics of a single-phase free convection loop, *J. Fluid Mech.* 67, 65–84 (1975).
- [18] JEUCK III, P., LENNERT and KIANG, R.L., Single-phase natural circulation experiments on small-break accident heat removal, EPRI-NP-2006 (1981).
- [19] HALLINAN, K.P. and VISKANTA, R. Heat Transfer from a rod bundle under natural circulation conditions, NUREG/CR-4556 (1986).
- [20] VIJAYAN, P.K., Investigations on the single-phase thermosyphon phenomenon in a figure-of-eight loop relevant to pressurized heavy water reactors, Ph. D. thesis, Indian Institute of Technology, Bombay (1988).

- [21] JOHN, B. and KANNAN IYER, Proceedings of 24th National Fluid Mechanics Conference, 1991 (1991).
- [22] DIMMICK, G.R., CHATOORGOON, V., KHARTABIL, H.F. and DUFFEY, R.B., Natural convection studies for advanced CANDU reactor concepts, Nuclear Engineering and Design, 215, pp.27–38 (2002).
- [23] DUFFEY, R.B., Natural convection and natural circulation flow and limits in advanced reactor concepts, IAEA-TECDOC-1281, pp.49–65 (2000).
- [24] VIJAYAN P.K., et al., Scaling of the steady state and stability behaviour of single and two-phase natural circulation systems, in IAEA-TECDOC-1281, pp.139–156 (2002).
- [25] ROHATGI, U.S. and DUFFEY, R.B., Stability, DNB, and CHF in natural circulation two-phase flow, Int. Comm. Heat Mass Transfer, 25, pp.161–174 (1998).
- [26] NAYAK, A.K., VIJAYAN P.K., and SAHA, D., Analytical modelling and study of the stability characteristics of the Advanced Heavy Water Reactor, BARC/2000/E/011 (2000).
- [27] JAIN, K.C., PETRIC, M., MILLER, D., BANKOFF, S.G., Self-sustained hydrodynamic oscillations in a natural-circulation boiling water loop. Nuclear Engineering and Design, 4, pp.233–252 (1966).
- [28] CHEN, K.S., CHANG, Y.R., Steady-state analysis of two-phase natural circulation loop. Int. J. Heat and Mass Transfer, 31, pp.931 (1988).
- [29] IMURA, H., SAITO, Y., In: Xin, M (Ed.), Advances in Phase Change Heat Transfer, Pergamon Press, p. 579 (1988).
- [30] KYUNG, I.S., LEE, S.Y., Experimental observations on flow characteristics in an open two-phase natural circulation loop, Nucl. Eng. Des., 150, pp.163–176 (1994).
- [31] GORMAN, M., WIDMANN P.J. and ROBBINS, K.A., Nonlinear dynamics of a convection loop: a quantitative comparison of experiment with theory, Physica D 19, pp.255–267 (1986).
- [32] WIDMANN, P.J., GORMAN M. and ROBBINS K.A, Nonlinear Dynamics of a convection loop II. Chaos in laminar and turbulent flows, Physica D 36, pp.157–166 (1989).
- [33] MISALE, M., FROGHERI, M. and RUFFINO, P., Steady-state and stability behaviour of a single-phase natural circulation loop, Heat Transfer 1998, Proceedings of 11th IHTC, Kyongju, Korea, August 23–28, Vol. 3 (1998).
- [34] MISALE, M., and FROGHERI, M., Influence of pressure drops on the behaviour of a single-phase natural circulation loop: Preliminary results, Int. Comm. Heat Transfer, 26, pp.597–606 (1999).
- [35] SATOH, A., OKAMOTO, K. and MADARAME, H., Instability of single-phase natural circulation under double loop system, Chaos, Solitons & Fractals, 9, 1575–1585 (1998).
- [36] SATOU, A., MADARAME, H., OKAMOTO, K., Unstable behaviour of single-phase natural circulation under closed loop with connecting tube, Experimental Thermal and Fluid Science 25, pp.429–435 (2001).
- [37] JIANG, Y.Y. SHOJI, M. and NARUSE, M., Boundary condition effects on the flow stability in a toroidal thermosyphon, International Journal of Heat and fluid flow, 23 pp.81–91 (2002).
- [38] CHATO, J.C., Natural convection flows in a parallel channel system, J. Heat Transfer, 85, pp.339–345 (1963).
- [39] CHEN, W.L., WANG, S.B., TWU, S.S., CHUNG, C.R. and CHIN PAN, Hysteresis effect in a double channel natural circulation loop, International Journal of Multiphase Flow, 27, 171–187 (2001).
- [40] WELANDER, P., On the oscillatory instability of a differentially heated loop, J. Fluid Mech. 29, pp.17–30 (1967).
- [41] KELLER, J.B., Periodic oscillations in a model of thermal convection, J. Fluid Mech. 26, pp.599–606 (1966).
- [42] KAPITANIAK, T., Chaos for engineers, theory, applications and control, p 69–86, 2nd revised edition, Springer - Verlag, Berlin (2000).
- [43] VIJAYAN, P.K., AUSTREGESILO, H. and TESCHENDORFF, V., 'Simulation of the unstable oscillatory behaviour of single-phase natural circulation with repetitive flow reversals in a rectangular loop using the computer code ATHLET', Nuclear Engineering Design 155, pp.623–641 (1995).

- [44] AMBROSINI, W., FORGIONE, N., FERRERI, J.C., and BUCCI, M., The effect of wall friction in single-phase natural circulation stability at the transition between laminar and turbulent flow, to appear in *Annals of Nuclear Energy*, (2004).
- [45] MISALE, M., RUFFINO, P., FROGHERI, M., The influence of the wall thermal capacity and axial conduction over a single-phase natural circulation loop: 2-D numerical study, *Heat and Mass Transfer*, 36, pp.533–539 (2000).
- [46] FICHERA, A. and PAGANO A., Modelling and control of rectangular natural circulation loops, *International Journal of Heat and Mass Transfer* 46, pp.2425–2444 (2003).
- [47] MATHISEN, R.P., Out of pile instability in the loop Skalvan, *Symp. on Two-phase Flow Dynamics*, EURATOM, EUR 4288e, vol. 1, 19–64 (1967).
- [48] CHEXAL, V.K., BERGLES, A.E., Two-phase flow instabilities in a low pressure natural circulation loop, *AICHE Symposium Series*, 69, pp.37–45 (1973).
- [49] FUKUDA, K., KOBORI, T., Classification of two-phase flow stability by density-wave oscillation model, *J. Nucl. Sci. Technol.*, 16, pp.95–103 (1979).
- [50] LEE, S.Y., ISHII, M., Characteristics of two-phase natural circulation in Freon-113 boiling loop, *Nucl. Eng. Des.*, 121, pp.69–81 (1990).
- [51] ARITOMI, M., CHIANG, J.H., NAKAHASHI, T.M., WATARU, M., MORI, M., Fundamental study on thermohydraulics during start-up in a natural circulation Boiling Water Reactor (I), *Thermohydraulic Instabilities*, *J. Nucl. Sci. Technol.*, 29, pp.631–640 (1992).
- [52] JIANG S.Y., YAO, M.S., BO, J.H., WU, S.R., Experimental simulation study on start-up of the 5 MW nuclear heating reactor, *Nucl. Eng. Des.*, 158, pp.111–123 (1995).
- [53] WU, C.Y., WANG, S.B., CHIN-PAN, Chaotic oscillations in a low pressure two-phase natural circulation loop, *Nucl. Eng. Des.*, vol. 162, pp.223–232 (1996).
- [54] SAHA, P., ZUBER, N., An analytical study of the thermally induced two-phase flow instabilities including the effects of thermal non-equilibrium, *Int. J. Heat Mass Transfer*, vol. 21, pp.415–426 (1978).
- [55] ACHARD, J-L, DREW, D.A, LAHER JR, R.T, The analysis of nonlinear density wave oscillations in boiling channels, *Journal of Fluid Mechanics*, 155, pp.213–232 (1985).
- [56] YADIGAROGLU, G. and BERGLES, A.E., An experimental and theoretical study of density-wave oscillations in two-phase flow, MIT rept. DSR 74629-3 (HTL 74629-67) (1969).
- [57] GURUGENCI, H., VEZIROGLU, T.N., KAKAC, S., simplified non-linear descriptions of two-phase flow instabilities in vertical boiling channel, *Int. J. Heat Mass Transfer*, 26, pp.671–679 (1983).
- [58] CHATOORGOON, V., SPORTS - A simple non-linear thermal hydraulic stability code, *Nucl. Eng. Des.*, vol. 93, pp.51–67 (1986).
- [59] NIGAMUTLIN, B.I., MELIKOV, O.I., BLINKOV, V.N., GAKAL, P.G., The numerical analysis of boiling flow instabilities in parallel heated channels, *Nucl. Eng. Des.*, 139, pp.235–243 (1993).
- [60] RIZWAN-UDDIN, DORNING, J.J., Some non-linear dynamics of a heated channel, *Nucl. Sci. Eng.*, 93, pp.1–14 (1986).
- [61] LIN, Y.N., PAN CHIN, Non-linear analysis for a natural circulation boiling channel, *Nucl. Eng. Des.*, 152, pp.349–360 (1994).
- [62] ISHII, M., ZUBER, N., Thermally induced flow instabilities in two-phase mixtures, 4th *International Heat Transfer Conference*, Paris (1970).
- [63] FURUTERA, M., Validity of homogeneous flow model for instability analysis”, *Nucl. Eng. Des.*, 95, pp.65–74 (1986).
- [64] LEE, S.Y., LEE, D.W., Linear analysis of flow instabilities in an open two-phase natural circulation loop, *Nucl. Eng. Des.*, 128, pp.317–330 (1991).
- [65] WANG, F.S., HU, L.W., PAN, C., Thermal and stability analysis of a two-phase natural circulation loop, *Nuclear Science and Engineering*, 117, pp.33–46 (1994).
- [66] NAYAK, A.K, VIJAYAN, P.K, SAHA, D., VENKAT RAJ, V. and ARITOMI, M., Linear analysis of thermo-hydraulic instabilities of the Advanced Heavy Water Reactor (AHWR), *Journal of Nuclear Science and Technology*, 35, pp.7687–78 (1998).
- [67] VAN BRAGT, D.D.B., VAN DER HAGEN, T.H.J.J., Stability of natural circulation Boiling Water Reactors: part I - description stability model and theoretical analysis in terms of dimensionless groups, *Nucl. Technol*, 121, pp.40–51 (1998).

- [68] ARITOMI, M., AOKI, S., INOUE, A., Instabilities in parallel channels of forced convection boiling upflow system, *J. Nucl. Sci. Technol.*, 20, pp.286–301 (1983).
- [69] FUKUDA, K., RAO, Y.F., HASEGAWA, S., NAKAGAWA, K., KAGE, K., Study on two-phase flow instability in parallel multi channels, *Heat Transfer, Japanese Research*, 23, pp.693–709 (1994).
- [70] PENG, S.J., PODOWSKI, M.Z., LAHEY, R.T., BECKER, M., A computer code for the stability analysis of Boiling Water reactors, *Nucl. Sci. Eng.*, 88, pp.404–411 (1984).
- [71] RIZWAN-UDDIN, DORNING, J.J., Chaotic dynamics of a triply forced two-phase flow system, *Nucl. Sci. Eng.*, 105, pp.123 (1990).

ANNEX 14

OVERVIEW ON PANDA TEST FACILITY AND ISP-42 PANDA TESTS DATA BASE

N. Aksan

Paul Scherrer Institute, Switzerland

Abstract

As an example of test facilities in which passive decay heat removal systems are tested, the PANDA test facility and the ISP-42-PANDA tests will provide an overview on experimental validation and database. A short overview on the test programs performed in this facility is also given.

1. INTRODUCTION

PANDA is a large-scale facility, which has been constructed at the Paul Scherrer Institute (PSI) for the investigation of both overall dynamic response and the key phenomena of passive containment systems during the long-term heat removal phase for Advanced Light Water Reactors (ALWRs). Using a modular concept with a basic set of cylindrical vessels (typical diameter 4m), which are interconnected by piping, the facility can be adapted to simulate different passive containment designs (Fig. 1).

Since early 1990's there has been number of projects related to the use of PANDA test facility for various evolutionary reactor designs, e.g., SBWR, ESBWR, SWR-1000, etc. Different PCCS concepts were experimentally investigated in the PANDA test facility with some minor modifications in the facility for each program. This is being a confirmation of its flexibility, due to the modular construction, in use of various applications. The earlier investigations in the PANDA test facility, in addition to the current and future investigations, will be briefly provided in coming sections.

In PANDA test facility some tests were also performed for use as the basis of International Standard Problem number 42 (ISP-42). The OECD/NEA Committee on the Safety of Nuclear Installations (CSNI) approved, at its meeting on December 3-5, 1997, an International Standard Problem (ISP) involving a test in the PANDA facility, based on a recommendation from the Principal Working Group 2 (PWG2) on System Behaviour. The main interest for this ISP is code validation in relation to a range of LWR and advanced LWR (ALWR) (mainly) containment issues that have been designated as important and involving thermalhydraulic phenomena. The ISP-42 test was subdivided in six well-defined sequential phases, restricting the phenomena, which are taking place in each test phase, to a reasonable number and separating them as much as possible. This gives the ISP-42 participants the choice to calculate one, several, or all of the six test phases, depending on the type of transient and the phenomena that they are interested in. For each test phase, the initial and boundary conditions are defined separately so that if there are code model deficiencies in the preceding test phase the calculations for the next phase can be started and performed independently. Overview on the ISP-42 PANDA test with a sample result obtained from Phase-A and summary of the major conclusions from the ISP-42 exercise are also presented in this paper.

2. SUMMARY OF PANDA FACILITY DESCRIPTION

PANDA is a large-scale facility, which has been constructed at the Paul Scherrer Institute (PSI) for the investigation of both overall dynamic response and the key phenomena of passive containment systems during the long term heat removal phase for Advanced Light Water Reactors (ALWRs). The facility has been configured to simulate the containment of a passive BWR, but the phenomena, which are taking place, are of a more generic character and of interest to LWR containment's in general. Using a modular concept with a basic set of cylindrical vessels (typical diameter 4m) which are interconnected by piping, the facility can be adapted to simulate different passive containment designs. The facility configuration used for ISP-42 tests is a scaled down model of European Simplified BWR containment and safety systems. After a detailed scaling analysis, power and volumes are scaled 1:40, and pressure, relevant heights and pressure drops are 1:1.

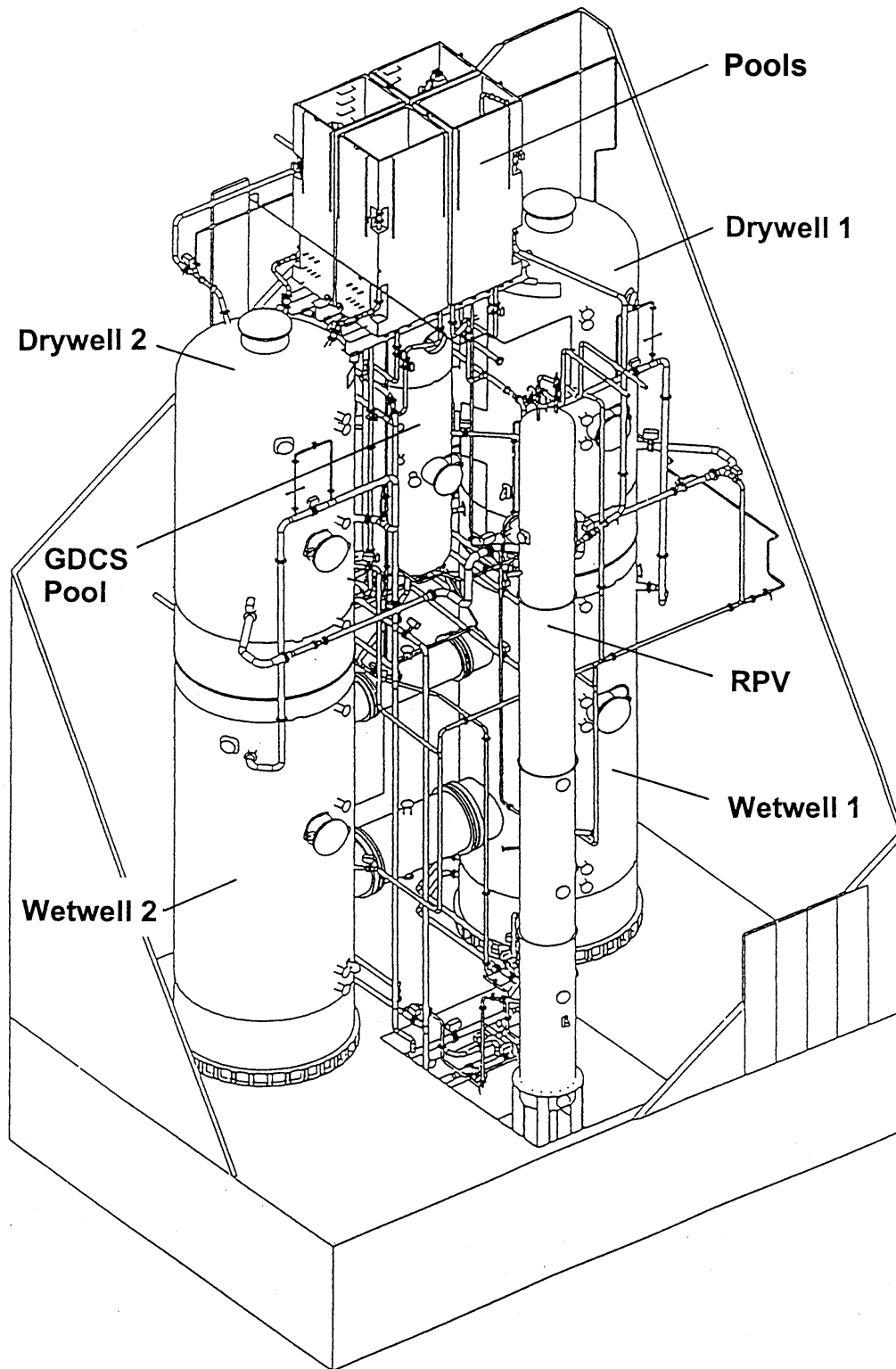


FIG. 1. 3-D View of the PANDA test facility.

As can be seen from the 3-dimensional drawing of Figure 1 and it is illustrated in the schematic sketch of Figure 2, the PANDA facility mainly consists of six large pressure vessels, simulating the various containment volumes. One of these vessels represents the Reactor Pressure Vessel (RPV), which acts as the steam source during a transient. RPV contains at its bottom a core simulator consisting of 115 electrically heated heater elements, which are located in a shroud acting as a riser/down-comer configuration and thus enabling natural circulation in the lower two thirds of the RPV. Electrical heater rods simulate the history of core decay heat generation with programmable power generation, maximum being 1.5 MW. The RPV is connected to the PANDA facility via the two Main Steam Lines (steam supply to the system), the PCC drain line (liquid return of the condensed steam in the PCCs) and the GDCS drain line. At the top of the RPV, an additional flange may be used for helium injection.

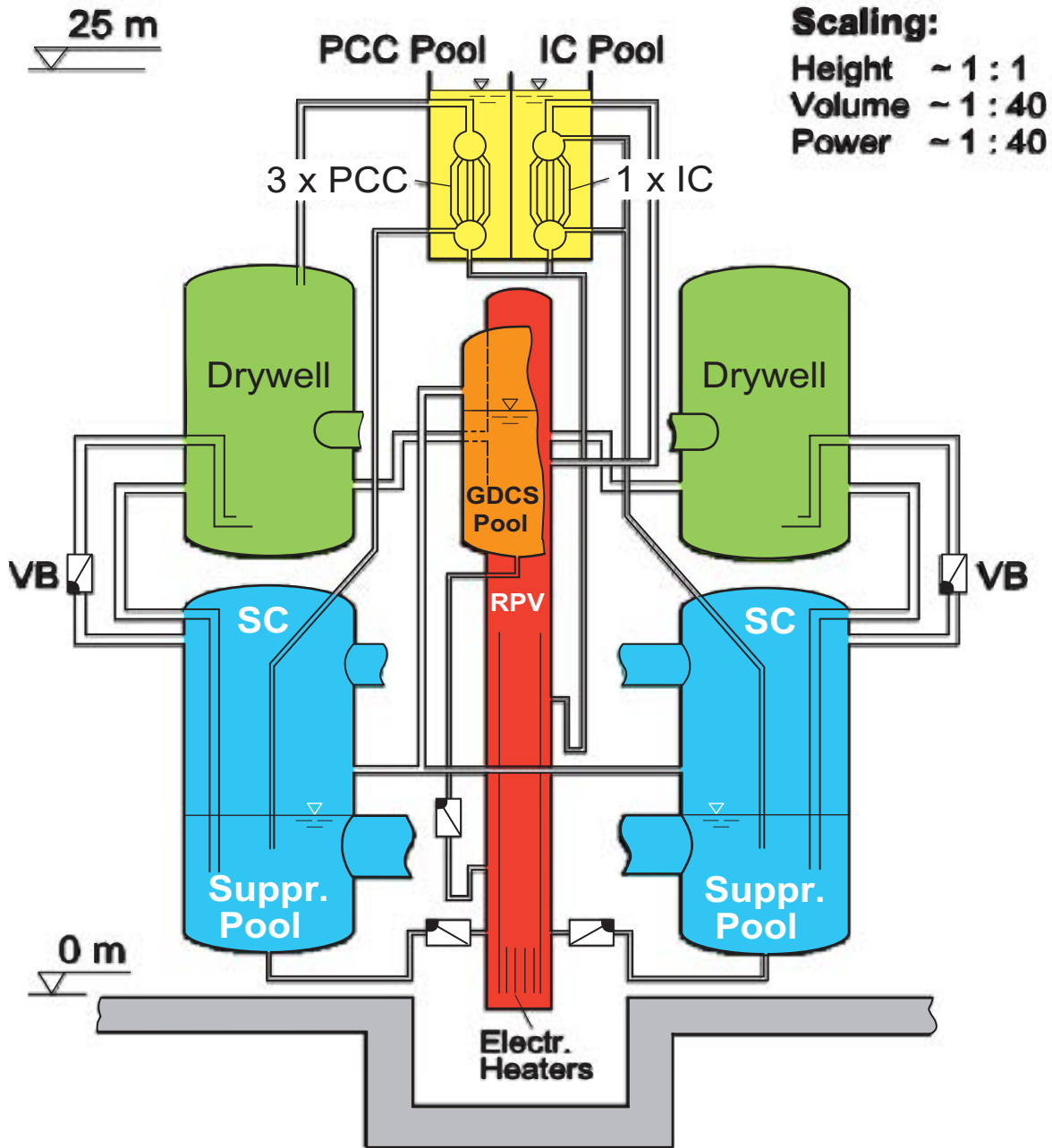
Two other large cylindrical vessels of an inner height 8.0 m and an inner volume of 89.9 m³ each, represent the Drywell (DW), connected each other with a large diameter dry-well connection pipe (outer diameter of 1.0 m). The dry-well as a whole is connected to the rest of the system via the two Main Steam Lines (steam supply to the system and input from RPV), the PCC feed lines (output of dry-well), the Main Vent Lines (output of dry-well) and the Vacuum Breaker Lines (input to dry-well, in case the wet-well pressure exceeds the dry-well pressure). At the top of the dry-well-1, air may be injected to simulate a sudden release of trapped air into the system. The two DW vessels are filled with gas. Except under start-up conditions, this is more or less pure steam (air fraction is quite small).

The other two large cylindrical vessels, of inner volume of 115.9 m³ each and an inner height of 10.11 m, filled with water at a level of approximately 4m, represent the Wetwell (WW, also called suppression chamber). The two WW vessels are connected each other by two large diameter pipes of 4m length each, one in the liquid section of the wetwell (1.5 m diameter), and the other one in the gas space of the wetwell (1.0 m diameter). The wetwell as a whole is connected to the PANDA facility via the two Main Vent Lines (input), the three PCC vent lines (input), the two pressure equalization lines and the Vacuum Breaker Lines (output, in case the wetwell pressure exceeds the dry-well pressure significantly).

The last vessel primarily represents a Gravity Driven Cooling System (GDCS) pool with a volume of 17.6 m³ and inner height of 6.06m, and it can function as additional containment volume for wetwell gas space. The GDCS tank is connected to the rest of the facility via the GDCS drain line to RPV (output) and the pressure equalization line to the wetwell vessels. GDCS drain line connects the inside bottom of the GDCS tank with the lower part of the downcomer of the RPV. A check valve allows only one directional flow from the tank to the RPV. To establish similar pressure in the gas spaces of GDCS tank and wetwell, the pressure equalization line connects GDCS tank with the gas space of the two wetwells.

In addition, four rectangular pools open to the atmosphere are located on top of the facility. These pools may be equipped with immersed heat exchangers and used as heat sinks outside the containment, or as cooling storage pools in other configuration. As mentioned earlier, the modular facility arrangement provides the flexibility needed to investigate a variety of containment design. For the ISP-42 tests, these pools contain three Passive Containment Coolers (PCCs) connected to dry-well. Each of the three PCCs consists of a PCC unit, which is submerged in a separate water pool, where the bottom of the pool is located 19.8 m above the ground floor. The PCC unit is a heat exchanger and is made of an upper drum, a tube bundle (20 tubes, diameter of 0.0508 m and length of between 1.778 m and 2.066 m), and a lower collector drum. Each PCC unit is submerged into the secondary side water inside the PCC pool tank and is connected to the drywell and the rest of the system via the PCC feed line (input) at the top of the upper drum, whereas the PCC lower drum has two connections, one of them is the PCC vent line (non-condensable output) on the right side of the lower drum and the other one is the PCC drain line (output) at the bottom of the lower drum. Steam/air mixture enters from the top of the PCC unit, and then the steam part is condensed in the tube bundle and drained out of the PCCs via the drain line to the RPV, whereas non-condensable may be vented via the vent line to the wetwell. The two PCC units are connected to one of the drywell, the third unit is connected to the

other drywell. The fact that the three PCC units are connected to two drywell vessels allows asymmetric behaviour and creates flows between these vessels. Such an asymmetric flow also occurs with equal flow resistance from the RPV to two of the drywell vessels when all three PCCs are in operation.



PANDA Test Facility ESBWR Configuration

FIG. 2. Schematic of the PANDA test facility for the ESBWR configuration.

The different vessels and the primary side of the PCCs are connected to each other by means of different pipes. The major system lines are: Main Steam Lines (MSLs), which connect the upper part of the RPV with dry-well-1 and dry-well-2, respectively; Main Vent Lines (MVLs) connect the lower part of the dry-well with the wetwell pool, approximately 1.6m below the surface of the pool. Each MVL enters its respective wetwell vessel nearly at the top and is then led inside the vessel to the pool. The exit of the MVL pipe is submerged in the pool water.

In general, BWR containment concepts rely on Vacuum Breaker (VB) installed between the drywell and wetwell. Their function is not to allow the wetwell pressure to exceed drywell pressure by a certain margin. There are two vacuum breakers connecting the upper part of the two wetwells to the lower part of the two dry-wells by VB lines (VBLs) in the PANDA facility. The operation of the actual vacuum breaker is simulated in PANDA by control valves. These are opened and closed by the facility control system when the measured differential pressure between the wetwell and the dry-well exceeds an upper and a lower limit, respectively. Therefore, under normal conditions, the lines are closed by the VB valves. Additional auxiliary lines are available to establish the desired stationary conditions at the beginning of each of the sequences of the experiment. These lines are not shown in Figures 1 and 2.

The system line pressure losses were carefully scaled using orifices and the theoretical line resistances were measured and verified by system characterization tests. In addition all vessels and system lines were carefully insulated using rock-wool and the heat losses were determined and provided, separately. The facility is instrumented with over 500 sensors and axial distributions of temperatures and non-condensable concentrations in the vessels can be obtained from thermocouple, pressure and (a limited number) of oxygen (air) probe measurements. Further detailed description of the PANDA test facility for ISP-42 test series can be found in reference [1], and the boundary and initial conditions with the list of measurement locations for each phases of the ISP-42 are provided in reference [2].

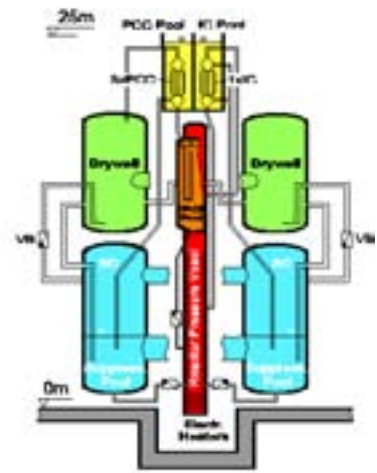
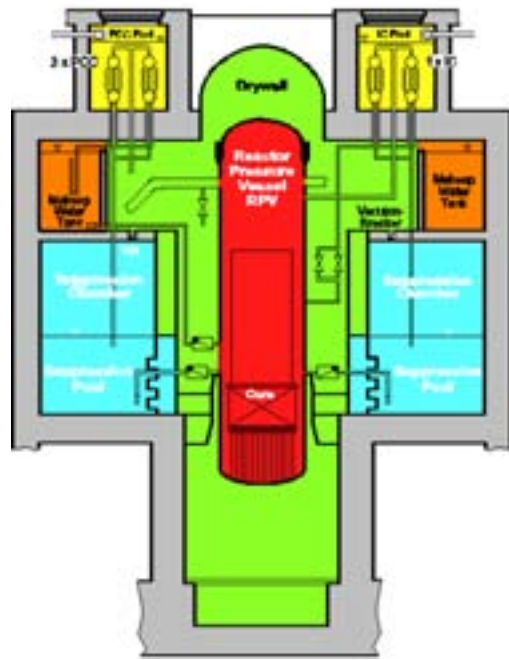
3. EARLIER INVESTIGATIONS IN PANDA TEST FACILITY

In early 1990's, the Simplified Boiling Water Reactor (SBWR) design was used as reference design for the PANDA test facility (Figure 3), and the main goal of the project were the experimental and analytical investigation of the start-up and long-term operation of the passive containment cooling system of the SBWR and related aspects [3] and [4]. In a first test series, the steady-state characteristics of the PCCS condenser units were investigated. In addition, ten integral system tests were performed addressing specific topics of concept demonstration, asymmetric steam injection, reduced condenser capacity, isolation condenser and PCC system interaction, and vacuum breaker leakage.

European SBWR (ESBWR) was also simulated in PANDA test facility using different scaling as in SBWR simulation and some component modifications were done (Figure 2). Series of transient system tests were carried out in the PANDA facility to investigate the performance of the passive containment cooling system of the ESBWR [5]. Eight system tests in PANDA with challenging conditions were performed to explore the real PCCS limitations, e.g., low water level in PCC pool, deferred release of "trapped air" in drywell. During one of the tests, helium was injected (as simulation of hydrogen) to simulate beyond design basis accident conditions.

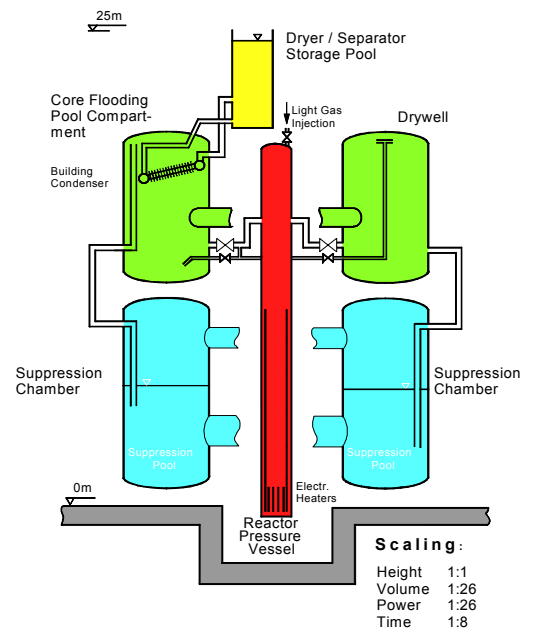
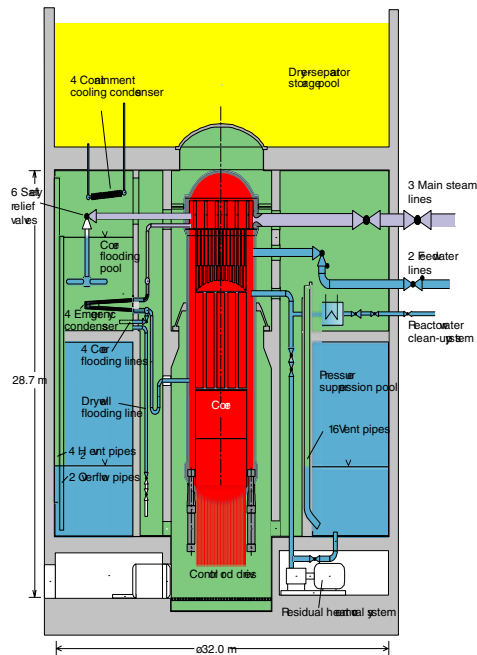
Further, different PCCS concepts were experimentally investigated in the existing PANDA test facility (Figure 4). In this specific case SWR-1000 Building condenser was simulated and tested by using different scaling and also some specific limited modifications in the facility (confirming the flexibility of the modular construction of the PANDA test facility) [6].

On the basis of the ESBWR configuration for the PANDA test facility, ISP-42 tests were performed. Further details on ISP-42 exercise are provided in the next sections.



Scaling:
 Height 1:1
 Volume 1:25
 Power 1:25

FIG. 3. SBWR versus PANDA test facility.



Scaling:
 Height 1:1
 Volume 1:26
 Power 1:26
 Time 1:8

FIG. 4. SWR 1000 versus PANDA test facility.

4. ISP-42 PANDA TEST OUTLINE AND OVERVIEW

Following a proposal, the OECD/NEA Committee on the Safety of Nuclear Installations approved, at its meeting on December 3-5, 1997, a new International Standard Problem (ISP) involving a test in the PANDA facility, based on a recommendation from the Principal Working Group 2 (PWG2) on System Behaviour. The main interest for this ISP is code validation in relation to a range of LWR and advanced LWR (ALWR) (mainly) containment issues that have been designated as important and involving thermohydraulic phenomena. This ISP on PANDA test is also financially supported by the research foundation of the Swiss Utilities (Project- und Studienfonds der Elektrizitätswirtschaft, PSEL).

A preparatory meeting in March 1998 was called to discuss the scenario of the proposed ISP with some representatives from the OECD member countries. The ISP-test scenario has been defined taking into account the recommendations received from the representatives who attended this meeting and also comments received from other organizations. The ISP-PANDA test was performed on 21/22 April 1998, taking about 14 hours. Since the first phase of ISP-42 was going to be conducted as a “double-blind” or “blind” exercise, the experimental data was locked. In the second phase, the “open” exercise has been conducted by providing the ISP-42 PANDA test data to the participants and by performing post-test analysis.

ISP-42 PANDA test scenario was established to cover many typical LWR and ALWR containment and primary system phenomena. The test was subdivided in six well-defined sequential phases, restricting the phenomena, which are taking place in each test phase, to a reasonable number and separating them as much as possible. This gives the ISP-42 participants the choice to calculate one, several, or all of the six test phases, depending on the type of transient and the phenomena that they are interested in. For each test phase, the initial and boundary conditions are defined separately so that if there are code model deficiencies in the preceding test phase the calculations for the next phase can be started and performed independently.

The main issues and phenomena covered in the ISP-42 PANDA test are the following:

- Transient and quasi steady-state operation of a passive containment cooling system (condenser immersed in pool),
- Coupled primary system and containment behavior and phenomena,
- Reactor Pressure Vessel (RPV) operation at low power and low pressure under natural circulation conditions,
- Gravity driven ECCS injection in an initially saturated RPV,
- Venting of a steam/non-condensable gas mixture (through an immersed vent pipe into a wetwell compartment),
- Steam condensation in the presence of non-condensable gases in tubes,
- Mixing and stratification of light (helium) and/or heavy (air) gases with steam in large volumes (3D effects, steam jets, air or helium release),
- Mixing and stratification in large water pools.

The ISP-42 PANDA departs to some degree from the traditional procedures in that it has to some extent an exploratory character: it is partly designed to answer certain interesting questions with respect to how far can system or containment codes go in addressing the classes of phenomena investigated and what could be expected either from available “commercial” CFD codes or “large mesh” codes suitable for containment analysis. Thus one of the outcomes of the ISP could be the clarification of certain development needs in relation to the calculational precision needed and the safety relevance of considering in detail certain particular phenomena.

The first part of the ISP-42 was “blind” or “double blind” for the organizations that have no previous familiarity with the facility, as noted above. Only the system description and the phase initial and boundary conditions were given to the participants for the blind part of the ISP. After completing the

“blind” part, an open part was initiated by providing all the ISP-PANDA test data to the interested organizations. It should be emphasized again that the various phases of the test are clearly defined by providing simple initial and boundary conditions; thus participants were not forced to do the entire ISP but were able to choose the phases of interest to their organizations. Different sets of codes were also used for the various phases, as appropriate.

The configuration used for ISP-42 was corresponding to the European Simplified Boiling Water Reactor (ESBWR) containment and passive decay heat removal system at about 1:40 volumetric and power scale, and full scale for time and thermodynamic state (Figure 2). The actual test took over ten hours, including all conditioning and test phases. The ISP-42 PANDA test consists of six phases, A through F. These phases represent a sequence of concatenated operating modes or processes as used for the simulation and study of the behaviour of ALWR containment’s with passive safety systems. Each of these phases in fact a separate experiment, with its own initial and boundary conditions The six different test phases are listed as below:

- Phase A: Passive Containment Cooling System Start-up
- Phase B: Gravity-Driven Cooling System Discharge
- Phase C: Long-Term Passive Decay Heat Removal
- Phase D: Overload at Pure-Steam Conditions
- Phase E: Release of Hidden Air
- Phase F: Release of Light Gas in Reactor Pressure Vessel

The ISP-42 participants in the exercise chose the number of test phases they wished to calculate. Ten organisations from nine countries did participate in the “blind” phase pre-test calculations. 49 submitted calculational results are included in the “blind” phase comparisons report [7]. A large number of physical parameters were selected for comparison. In general, most of the predicted results were in quite good agreement with the test results; however, some prediction cases differed significantly and the reasons for these differences were in detail discussed.

The experimental data was distributed to all ISP-42 participants for their post-test calculations by June 2000. There were 27 new submissions for different phases of “open” phase analyses of ISP-42 by some of the participants, 8 organizations from 8 countries. “Open” phase submissions, comparisons, and analyses for ISP-42 are based on the outcome of the results presented in the “blind” phase report of ISP-42 [7]. It is to be noted that as outcome of the good results obtained in the “blind” phase comparisons, some ISP-42 participants decided not to submit “open” phase calculations. Consequently, the number of submissions for “open” phase was less than “blind” phase and they were mostly dealing with improvements of system modelling (re-nodalization) or the modifications of the code physical models. One of the submissions using GOTHIC code, in relation to test phase E, was a new submission. The detailed comparisons and analyses of the “open” phase of the ISP-42 were issued as a separate report [8]. Improvements on the cases submitted were observed with the recent versions of the codes, use of some other physical models and re-nodalization of the system depending on the specific phenomenon observed in the six phases of the ISP-42. In addition to the good results obtained in the “blind” phase, these improvements also provided additional good agreements with the test results. Some of the prediction cases still differed significantly, for these cases the reasons of differences were identified to some limited degree.

5. SHORT DESCRIPTION OF ISP-42 PHASE-A TEST AND SOME RESULTS AS EXAMPLE CASE

The objective of the first test phase (Phase A) of ISP-42 was to investigate the startup of a passive cooling system when steam is injected into a cold vessel filled with air and to observe the resulting gas mixing and system behaviour.

A sketch of the setup used for this phase is shown in Figure 5. Here, the parts of the system filled with water are slightly darker than those filled with steam, air, or a steam/air mixture. As it can be seen from Figure 5, all three PCCs are operational, and there is no interconnection between the different

PCC pools. The GDCS is filled with water whereas the water level in the RPV is much below the downcomer entrance/ riser exit. The main vent lines and the vacuum breaker lines are not operational for this test and therefore are not depicted in this scheme.

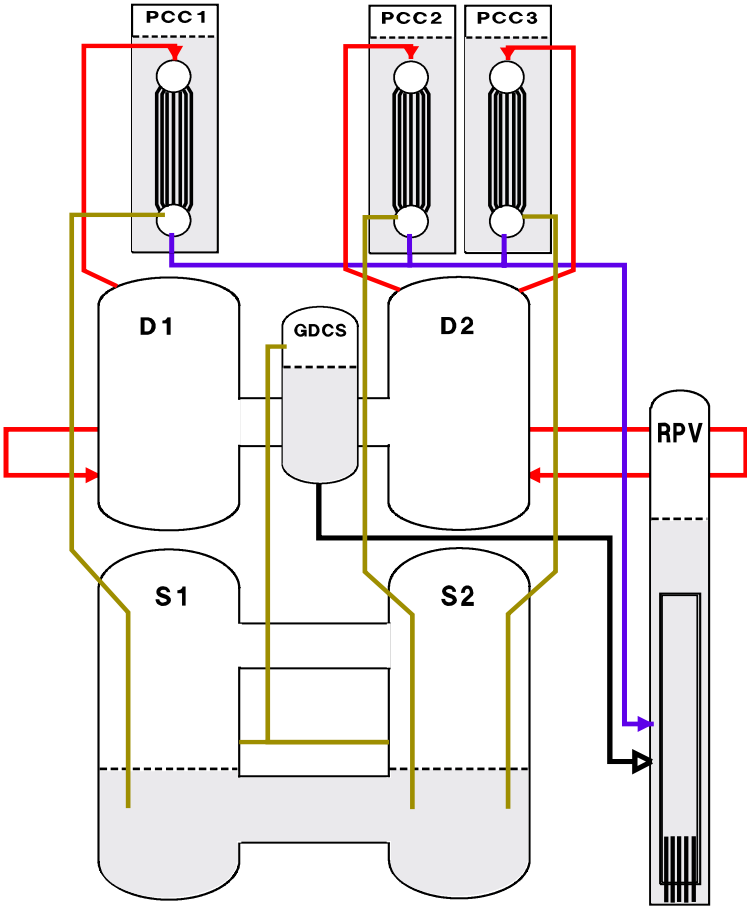


FIG. 5. ISP-42 Phase A: Passive containment cooling system start-up.

At zero seconds, RPV power has been switched on thus allowing steam to flow into the two drywell vessels. There, the steam slowly diluted the gas content of the drywell, which initially consisted of pure cold air and was also partially condensed at the cold vessel walls. Due to the inflow of additional gas (steam) into the drywell, pressure in the drywell as well as in the PCCs increased until it exceeded wetwell pressure approximately 10 kPa, the hydrostatic head at the outlet of the PCC vent lines. Then, drywell content partially was pushed through the PCC primary sides into the two wetwell pools via the PCC vent lines; the rest of the steam was stored in the drywells or has been condensed on the drywell walls. As long as the feed flow is small (due to a high condensation rate at the drywell walls) or/and the steam content of the flow mixture is low, no condensation has taken place in the PCCs. Instead, the mixture has been vented into the wetwells where the steam content has been condensed and the air content was separated into the gas space. Here, the separated air increased the amount of gas in the gas space thus increasing the system pressure. After some time into the transient, the dilution of the initial air content by the steam has been progressed and steam condensation started in the PCC tubes removing significant amounts of steam out of the vent flow, thus decreasing the inflow of air into the wetwell gas space, which resulted in a decrease of the pressure increase. The condensed steam has flown through the drain lines back into the RPV whereas a reduced gas flow is vented into the wetwells. During the final almost stationary part of the experiment, nearly the whole gas flow consisted of steam, which was condensed in the PCC tubes removing steam in the same order of magnitude than produced in the RPV, which resulted in ceasing the inflow of air into the wetwell gas space and consequently the pressure increase in the primary system. Further details on the description of phase -A- can be obtained from refs. .

The phenomena, which may be expected during this test, are:

- System pressurization due to a delayed startup of the passive containment coolers (PCCs);
- Injection of a hot steam jet into the cold air atmosphere of both drywell vessels. This includes:
 - Gas mixing and/or stratification in the drywell vessels and in the gas spaces of the two wetwell vessels,
 - Steam condensation on walls for a wide range of gas flow rates and non-condensable gas (air) fractions;
- PCC performance. This includes:
 - Steam condensation in tubes for a wide range of gas flow rates and non-condensable gas (air) fractions,
 - Air/steam venting from drywell to wetwell pools, gas plumes in the wetwell pools.

The time behaviour of the pressures defines the response of the whole system to the specific transient and it is the first item of the phenomena to be investigated as well as the main parameter with respect to safety issues. As may be seen in Figure 6, all ISP-42 phase-A test participants except one predicted the right time behaviour for the system pressure (i.e. a steady increase followed by a turn into a approximately stationary phase when the energy balance has become close to zero). The decrease of the liquid mass inventory in the RPV determines the production of steam, which is injected into the two drywells. The injected steam partly condenses in the drywells (at least at the beginning of the transient) and afterwards mostly condenses on the primary sides of the PCCs. Figure 7 shows the comparison of the liquid mass inventory predictions in the RPV to the experimental data. The three Passive Containment Coolers (PCCs) on top of the PANDA building remove the heat out of the primary system by condensing the steam on the primary side and evaporating the water on the secondary side water pools. The amount of steam removed out of the gas space of the primary system (which includes wetwell, drywell and GDCS gas spaces) either by condensing in the PCCs or in the wetwell pools, which controls the final system pressure. Therefore, correctly predicting the performance of the three PCCs was one of the key issues for the correct simulation of the whole system, assuming that the influence of air transport to the wetwell gas space was correctly modelled and the effect of stratification/mixing in the wetwell pool was negligible which is shown as comparison of calculated to experimental data in Figures 9 and 10 as axial temperature distribution at 500 s and 4000s of the transient. In addition, Figure 8 for the drywell pressure provides some indication of the “User Effect”. The same code used by different organizations, in this case RELAP5

and CATHARE codes, produced quite different results as seen in this figure. For further detailed analysis of the comparisons of the calculated and experimental data for ISP-42 Phase-A, interested reader can refer to the references [7] and [8].

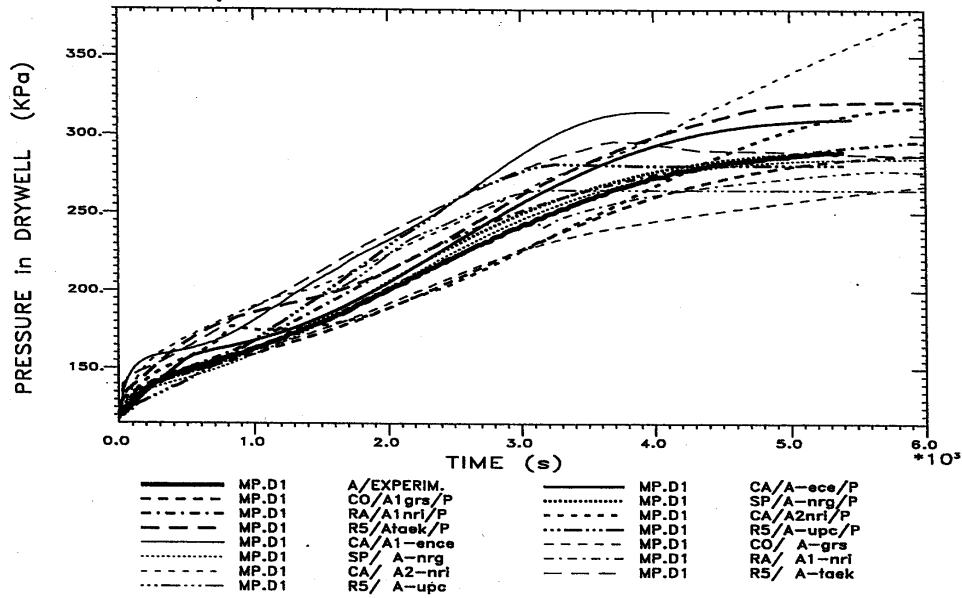


FIG. 6. Comparison of drywell pressure calculations (blind and open phases) with experimental data for Phase A of ISP-42.

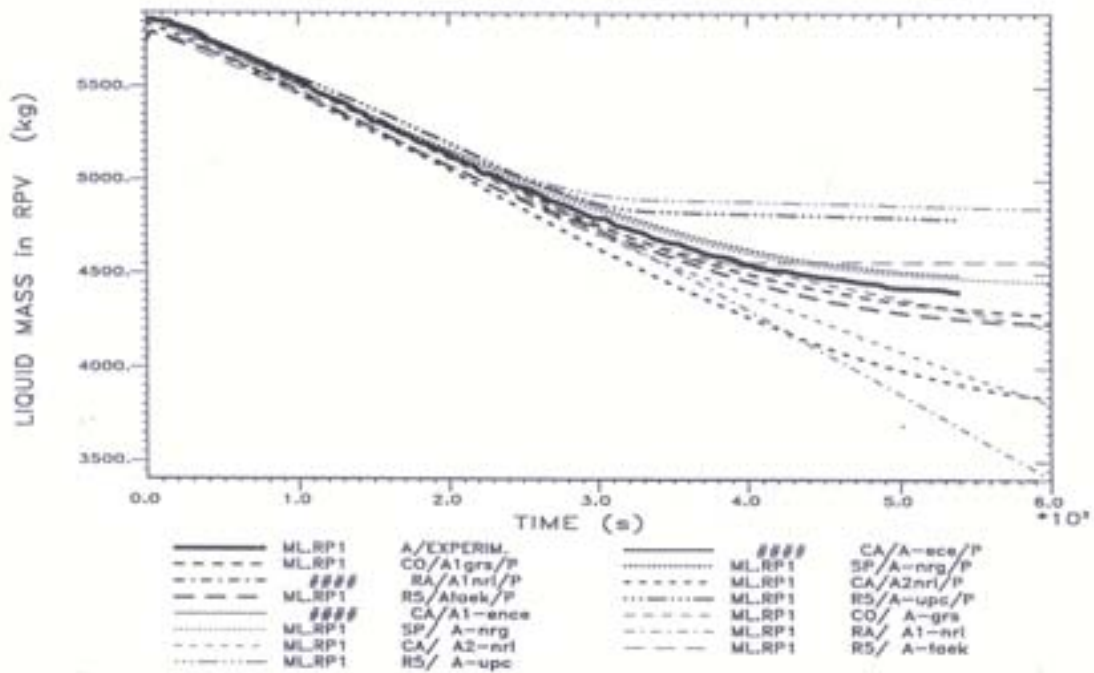


FIG. 7. Comparison of liquid mass inventory predictions (blind and open phases) with experimental data (Reactor Pressure Vessel) for Phase A of ISP-42.

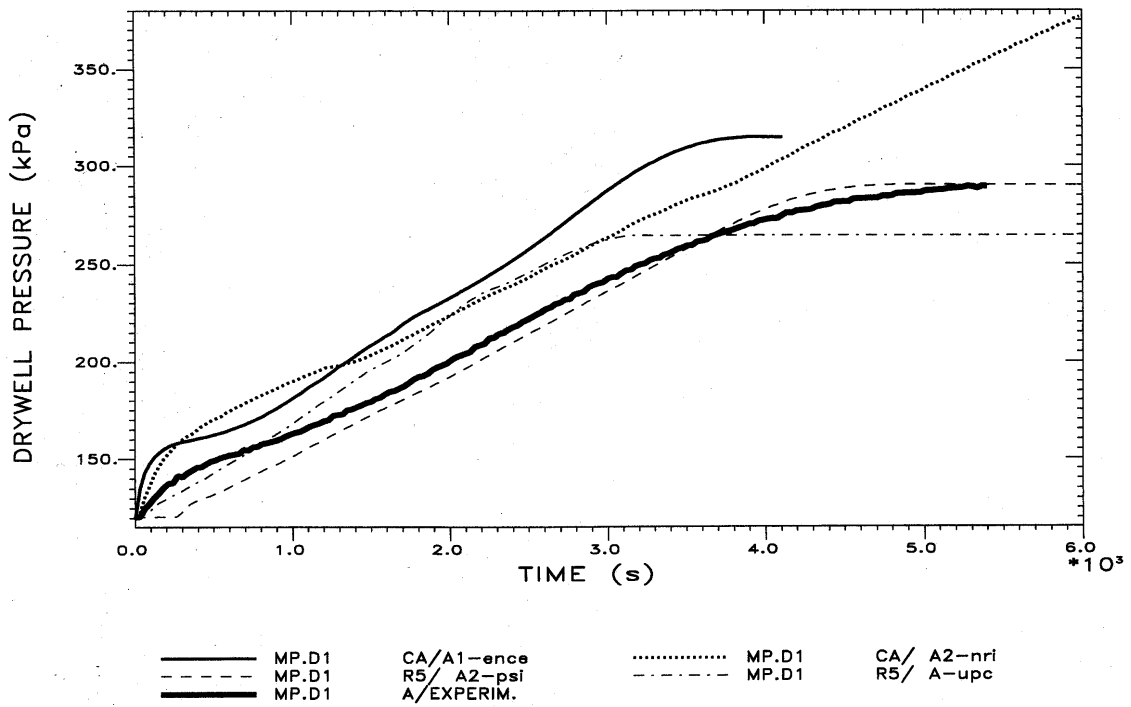


FIG. 8. Drywell pressure RELAP5/Mod3 and CATHARE code calculations compared to experimental data for Phase A of ISP-42.

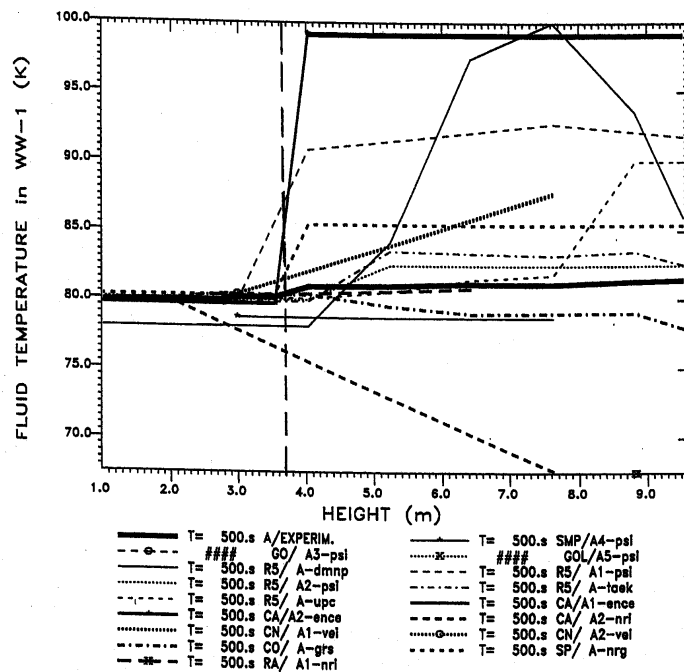


FIG. 9. Measured and predicted axial temperature distribution in wetwell-1 at 500s for Phase A of ISP-42.

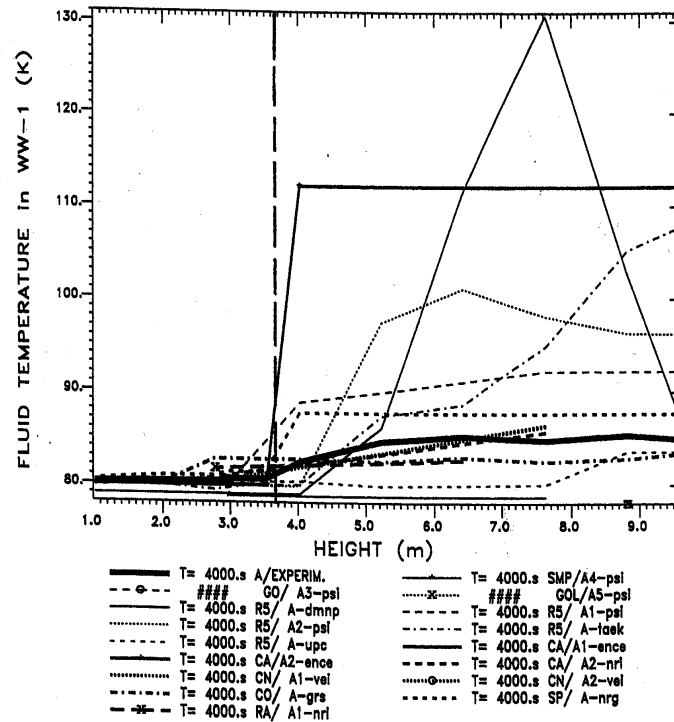


FIG. 10. Measured and predicted axial temperature distribution in wetwell-1 at 4000s for Phase A of ISP-42.

6. SUMMARY OF THE MAJOR CONCLUSIONS FROM ISP-42 PANDA TEST

Some of the major conclusions drawn on the basis of the six phases of the ISP-42 post test cases and also covering the “blind” phase results can be summarized as follows (Interested readers should refer to References [7] and [8] for more detailed information):

- Objectives set at the beginning of this ISP-42 activity have been achieved, even though very demanding efforts needed for such multiple exercises with six different phases.
- Most important parameter in relation to reactor safety, the containment pressure history has been calculated sufficiently correct for most of the ISP-42 participants for all six phases of ISP-42.
- The overall best results were obtained by the lumped parameter code SPECTRA
- Although system codes like CATHARE or RELAP5 were not designed to calculate typical containment problems in low pressure environments in the presence of large amounts of noncondensibles, they produced acceptable results. Containment code COCOSYS also produced globally acceptable results.
- Some codes (like GOTHIC) had problems to model specific equipment (e.g. PCCs) properly, some tuning of physical models, which needed some knowledge of the facility behaviour, were introduced. The RELAP5 or CATHARE codes were superior with respect to the higher flexibility to simulate special components and, in this case, specifically the modelling of the PCCs.
- Most of the major deviations could be attributed to problems with the nodalization or simply input errors rather than deficiencies of the specific codes. For example, in the case of RELAP5 and CATHARE, the same code used by different organizations produced quite different results (“user effect” and also different level of experience of the code users).
- It was observed that major attention should be given to provide the appropriate input parameters, which are used in the analysis. As an example, use of loss coefficients and their

distribution, especially for low power, low pressure transients as in ISP-42, is a very important factor. Even though experimentally measured data are provided to the code users, due to modelling necessities specific to the computer code used, there could be substantial deviations in the input data. In order to ensure the appropriateness of these types of parameters, every input model could be reviewed as carefully as possible. An important factor is the computer code user's discipline. This discipline cannot be forced, or substituted by Quality Assurance (QA) procedures. But it may help to reduce inappropriate use of some input parameters.

- For simple physical situations (e.g., well-mixed conditions in phase A), choice of a lumped parameter approach is permitted. In such cases, little gain in predictive capability is achieved at the cost of very large computation time for 3-D simulation and detailed nodalizations. Sensitivity studies can help to select the appropriate detailed nodalization and needed sophistication of physical models, and determine criteria for reasonable compromises between accuracy and computing time or costs.
- 3-D models such as in GOTHIC code include right physical representation of phenomena but number of difficulties currently prevents to take full advantage of these capabilities, e.g., accurate calculation of stratified conditions and its effect on system pressure (global parameter). Consequently, further assessment of 3-D models and advanced modelling features (e.g., turbulence) are necessary using well defined separate effects experiments for specific phenomena related to containment multi-compartment geometries.
- The use of CFD codes still exploratory, as they usually lack built-in physical models, interfaces (boundary conditions) with other components are difficult to set, and they occasionally show problems with respect to convergence. Consequently, there was no submission with CFD codes.
- The knowledge gained in ISP-42 and other PANDA tests indicated the need to improve and upgrade some of the instrumentation, e.g. improved measurement of injected medium, improved measurement of local concentration of air, helium and steam in the gas spaces of the different PANDA compartments.
- The data set produced for the six phases of the ISP-42 PANDA tests will be used as the basis of assessment of computer codes in relation to the passive containment cooling systems in the next future, at least next ten years. These data will be available to the requesting organizations through NEA-Data Bank and European Community Project CERTA.

7. CURRENT AND FUTURE INVESTIGATIONS IN PANDA TEST FACILITY

In this section, the test programs, which are performed in the recent years together with the investigations planned for the future, are provided in brief form. These programs are being TEMPEST, NACUSP, and SETH/PANDA. TEMPEST and NACUSP are performed within the 5th Frame Work Program of EU and SETH/PANDA is performed within a cooperative program of OECD/NEA.

The primary objective of TEMPEST (Testing and Enhanced Modelling of Passive Evolutionary Systems Technology for Containment Cooling) was to validate and improve advanced modelling methods, with emphasis on CFD and other tools with 3-D capabilities [9]. It included experimental investigations of the effect of light gases on containment behaviour and of new design features for accident mitigation, as well as evaluation of the performance of CFD codes and containment codes. The objectives of the PANDA tests in the TEMPEST project were:

- To assess effects of light gases on PCCs and containment performance,
- To investigate new accident mitigating design feature (Drywell Gas Recirculation System, DGRS),
- To provide a database for assessing the capabilities of CFD and other 3-D codes. For this purpose, improved instrumentation (including concentration measurements by means of a mass spectrometer) was installed in the PANDA test facility.

The configuration of the system was similar to that used for the ESBWR tests (Figure 2). The DGRS consisted of a fan blower, sucking gas from the vent lines of the PCCs and re-injecting the gas into the

Drywell. Total of five tests were performed (including symmetric and asymmetric injection conditions).

The NACUSP project offers the opportunity to validate the codes in relation to the capability to simulate natural circulation behaviour at low pressure [10]. In the PANDA test facility, 25 tests have been carried out in order to investigate natural circulation and stability, at low pressure and low power conditions. The test configuration (Figure 11) includes the Reactor Pressure Vessel (RPV) with core simulator, riser and down-comer (DC) and a condenser submerged in a pool, which is used as a heat sink. The configuration used for the NACUSP tests (not using any of the large vessels used for containment tests) demonstrates again the flexibility of the facility, and its multi-purpose feature. The tests were performed at a constant power, balanced by a specific condenser heat removal capacity (which was kept constant all over the test period). The test matrix allowed for varying the RPV power and pressure, and also other parameters influencing the natural circulation such as water level in the RPV and the core inlet hydraulic resistance.

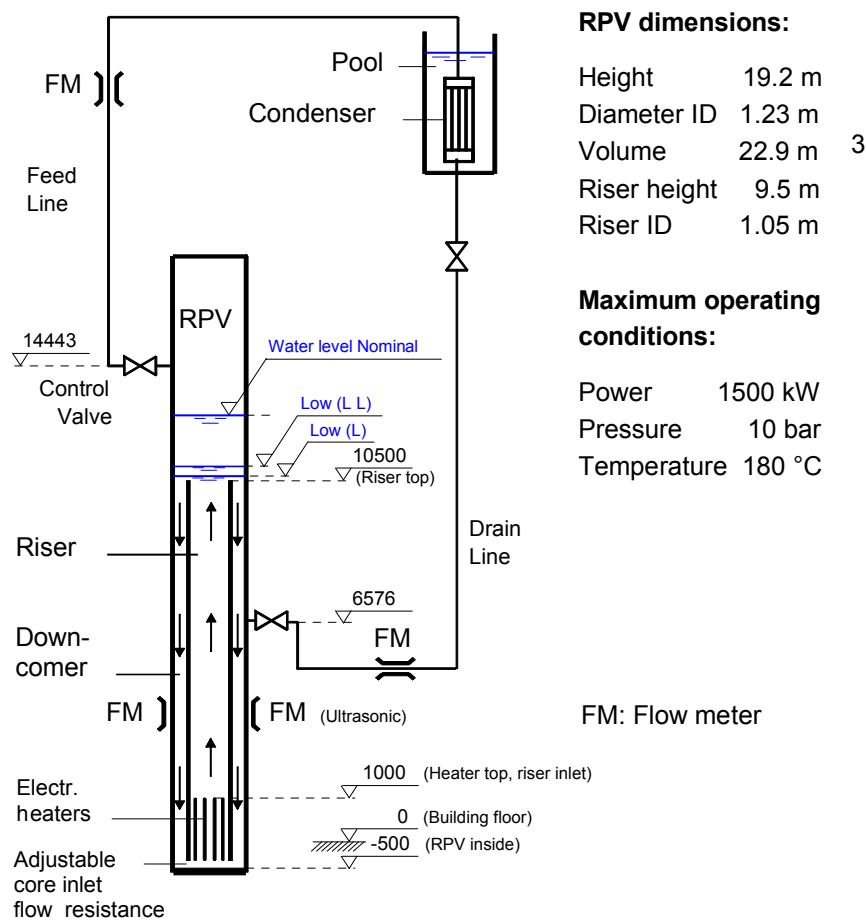


FIG. 11. PANDA experimental facility, natural-circulation loop and condensation/cooling loop (NACUSP) configuration.

OECD/NEA SETH project is an international cooperation project. It has also a component SETH/PANDA and it utilizes the PANDA test facility. The program addresses relevant safety issues in both PWR and BWR containment gas spaces with steam and air (or helium to simulate hydrogen) as working fluids. The PANDA facility can be used for this purpose with relatively minor hardware changes and several instrumentation improvements. The objective of SETH/PANDA is to provide a better understanding of 3D phenomena and the database needed for the validation of advanced codes through a set of experiments. The experiments aim to study the mixing and distribution of steam and non-condensable gas (air or helium) in multidimensional, well-defined geometry configurations, at scales approaching those of actual containment buildings or compartments, under a variety of well-established initial and boundary conditions. The tests will reveal the nature of mixing and stratification phenomena under accident conditions of interest to current and advanced power reactors and will produce data for field code development and validation.

8. CONCLUDING REMARKS

The extensive database established using the PANDA test facility will contribute to further improve containment cooling systems and containment design of passive plants; and allow for system code, containment code and CFD code assessment in a wide parameter range.

NOMENCLATURE

ABWR	Advanced Boiling Water Reactor
ALWR	Advanced Light Water Reactor
CSNI	Committee on the Safety of Nuclear Installations
AP600	Advanced Pressurized Reactor, 600MWe
BWR	Boiling Water Reactor
CFD	Computational Fluid Dynamics
DC	Down-comer
DW	Drywell
ESBWR	European Simplified Boiling Water Reactor
EU	European Union
GDSC	Gravity Driven Cooling System
IC	Isolation Condenser
ISP	International Standard Problem
LOCA	Loss Of Coolant Accident
LWR	Light Water Reactor
MVL	Main vent line
NEA	Nuclear Energy Agency
OECD	Organization for Economic Cooperation and Development
PANDA	<u>P</u> assive <u>N</u> achwärmeabfuhr- und <u>D</u> ruckabbau- Testanlage (Passive Decay Heat Removal and Depressurization Test Facility)
PCC	Passive Containment Cooling
PCCS	Passive Containment Cooling System
PWG2	Principal Working Group no.2 on System Behaviour
PWR	Pressurized Water Reactor
RPV	Reactor Pressure Vessel
SBWR	Simplified Boiling Water Reactor
SETH	SESAR (Senior Group of experts of CSNI) Thermal Hydraulics
SWR1000	Siede Wasser Reaktor, 1000Mwe
VB	Vacuum Breaker
WW	Wetwell

REFERENCES

- [1] LUEBBESMEYER, D., AKSAN, N., AUBERT, C., DREIER, J., HUGGENBERGER, M., FISCHER, O., ISP-42 Description of the PANDA-Facility, PSI Internal Report, TM-42-98-41, January, 1999.
- [2] AUBERT, C., DREIER, J., ISP-42 PANDA Test Phases: History of Events, Boundary and Initial Conditions, Calculational Parameters, PSI Internal Report, TM-42-98-40, January, 1999.
- [3] DREIER, J., HUGGENBERGER, M., AUBERT, C., BANDURSKI, T., FISCHER, O., HEALZER, J., LOMPERSKI, S., STRASSBERGER, H.J., VARADI, G., YADIGAROGLU, G., The PANDA Facility and First Test Results, *Kerntechnik* 61, pp.214–222 (1996).
- [4] DREIER, J., AKSAN, N., AUBERT, C., FISCHER, O., LOMPERSKI, S., HUGGENBERGER, M., STRASSBERGER, H.J., FALUOMI, V., YADIGAROGLU, G., PANDA Test Results and Code Assessment for Investigation of Passive Decay Heat Removal from the Core of a BWR, Proceedings of The 6th International Conference on Nuclear Engineering (ICONE-6), Paper no. ICONE-6463, 10–14 May, 1998.
- [5] HUGGENBERGER, M., AUBERT, C., BANDURSKI, T., DREIER, J., FISCHER, O., STRASSBERGER, H.J., YADIGAROGLU, G., TEPSS Related PANDA Tests (ESBWR)", Proceedings of a IAEA Technical Committee Meeting On Experimental Tests and Qualification of Analytical Methods to Address Thermohydraulic Phenomena in Advanced Water Cooled Reactors, 14–17 September 1998, Villigen, Switzerland, IAEA-TECDOC-1149, 267–276 (2000).
- [6] DREIER, J., AUBERT, C., HUGGENBERGER, M., STRASSBERGER, H.J., YADIGAROGLU, G., SWR 100 Related Containment Cooling System Tests in PANDA, Proceedings of a IAEA Technical Committee Meeting On Experimental Tests and Qualification of Analytical Methods to Address Thermohydraulic Phenomena in Advanced Water Cooled Reactors, 14–17 September 1998, Villigen, Switzerland, IAEA-TECDOC-1149, 277–286 (2000).
- [7] LUEBBESMEYER, D., AKSAN, N., ISP-42 PANDA Tests: Behaviour of Passive Containment Systems During the Long-Term Heat Removal Phase In Advanced Light Water Reactors; Blind Phase Comparison Report" OECD/NEA Report, NEA/CSNI/R(2003)6, May 2003, CD-ROM.
- [8] LUEBBESMEYER, D., AKSAN, N., ISP-42 PANDA Tests: Behaviour of Passive Containment Systems During the Long-Term Heat Removal Phase In Advanced Light Water Reactors; Open Phase Comparison Report, OECD/NEA Report, NEA/CSNI/R(2003)7, May 2003, CD-ROM.
- [9] WICHERS, V.A., MALO, J.Y., STARFLINGER, J., HEITCH, M., PREUSSER, G., TUOMAINEN, M., HUGGENBERGER, M., Testing and Enhanced Modelling of Passive Evolutionary Systems Technology for Containment Cooling (TEMPEST), FISA 2001, EU Research in Reactor Safety, Luxembourg, November 2001, p. 514–526.
- [10] KETELAAR, K.C.J., DE KRUIJF, W.J.M., AVAKIAN, G., GUBERNATIS, P., CARUGE, D., MANERA, A., VAN DER HAGEN, T.H.J.J., YADIGAROGLU, G., DOMINICUS, G., ROHDE, U., PRASSER, H.-M., CASTRILLO, F., HUGGENBERGER, M., HENNIG, D., MUNOZ-COBO, J.L., AGUIRRE, C., Natural Circulation and Stability Performance of BWRs (NACUSP), FISA 2001, EU Research in Reactor Safety, Luxembourg, November 2001, p. 535–546.

ANNEX 15

FLOW STAGNATION AND THERMAL STRATIFICATION IN SINGLE AND TWO-PHASE NATURAL CIRCULATION LOOPS

J.N. Reyes, Jr*

International Atomic Energy Agency, Vienna

Abstract

The objectives of this lecture are to describe the mechanisms by which natural circulation flow is interrupted in single-phase and two-phase loops and to identify the impact of loop stagnation on thermal stratification within the loop components. By the conclusion of this lecture, the participant should be able to identify the operating conditions that lead to the onset of loop stagnation and the methods that can be used to calculate fluid mixing and plume behavior in the system.

1. INTRODUCTION

This lecture describes the mechanisms that can interrupt natural circulation in loops transporting single and two-phase fluids and the subsequent impact of this stagnation on fluid mixing in the primary loop. The investigation of these mechanisms was conducted in the APEX-CE test facility, at Oregon State University. A schematic of the test facility is shown in Figure 1. APEX-CE was configured to model a 2x4 loop Combustion Engineering PWR. It included the reactor vessel with an electrically heated rod bundle, a pressurizer, two inverted U-tube steam generators, four cold legs and reactor coolant pumps, two hot legs and a safety injection system. The facility had a length scale ratio of approximately 1:4 and a volume ratio of 1:274. It was operated at decay powers ranging down from 6%. Therefore, the tests were conducted after reactor scram with the reactor coolant pumps tripped in a natural circulation mode of operation.

The motivation for the studies in APEX-CE was an issue known as Pressurized Thermal Shock (PTS). In the event of an emergency that results in a significant loss in system pressure or fluid inventory, cold borated water is typically injected into the primary system via the cold legs. If the flow rate in the primary loop is significant, the cold injected fluid will thoroughly mix with the hot water in the primary loop. However, at very low flow rates, the cold injected fluid will stratify in the loops and form cold plumes in the downcomer. Should a pre-existing flaw in the vessel wall or welds exist at a location experiencing prolonged contact with a cold plume, while at high pressure, there is a potential for the flaw to grow into a “through-wall” crack. Sections 2 and 3 describe mechanisms leading to a loss of primary loop flow and Section 4 describes the fundamentals of thermal fluid stratification and plume formation.

* Henry and Janice Schuette Endowed Chair Professor of Nuclear Engineering, Department of Nuclear Engineering and Radiation Health Physics, Oregon State University, Corvallis, Oregon, USA, 97331. Funded by Oregon State University Sabbatical Leave, U.S. Department of Energy, and IAEA.

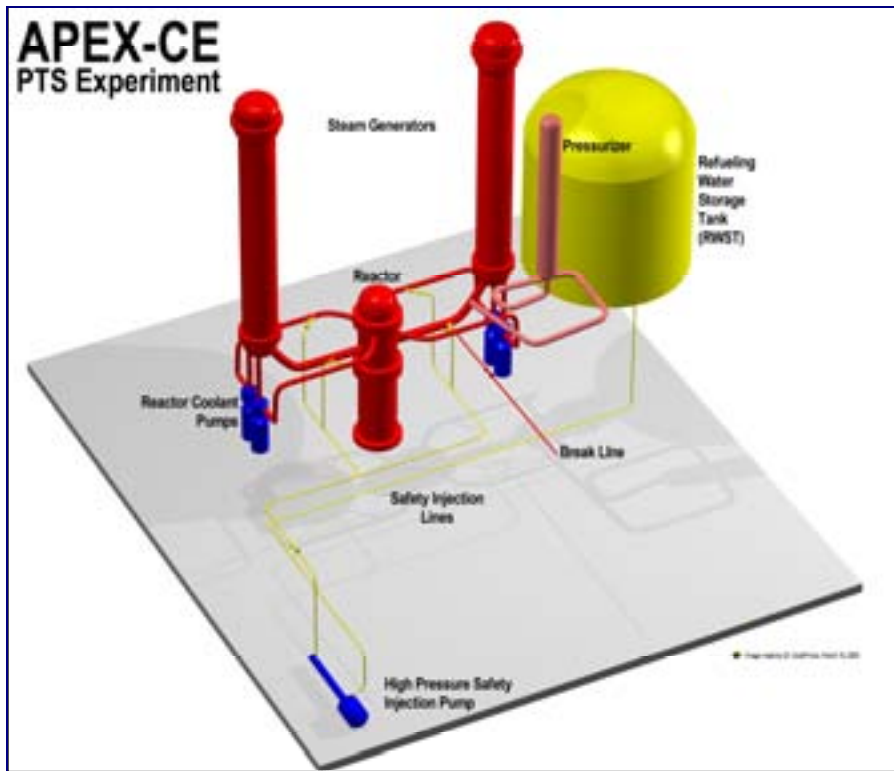


FIG. 1. Schematic of the APEX-CE test facility.

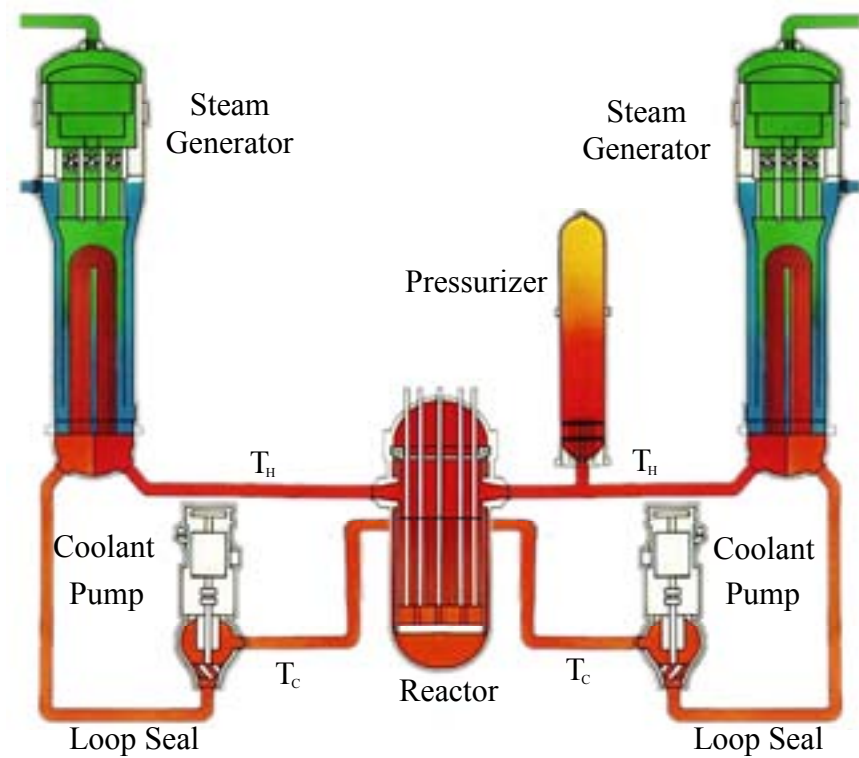


FIG. 2. Control volume for single-phase natural circulation in a two-loop PWR.

2.1. Loss of heat sink (Steam generator reverse heat transfer)

One mechanism for losing single-phase natural circulation flow is a loss of heat sink. This can occur as a result of a loss of main and auxiliary feedwater supplies. This could also occur as a result of a Main Steam Line Break (MSLB) in a single steam generator in a multi-loop plant. In the event of a MSLB, the operators isolate the feedwater to the steam generators and close the main steam isolation valves. This affected steam generator, however, will continue vent steam and depressurize. The blowdown of a steam generator may result in a rapid cooling of the primary system fluid. As a result, the primary loop fluid temperatures may drop below the secondary side temperatures of the “unaffected” steam generators. The result is a loss of heat sink in the loops not experiencing the steam line break. Figure 3 shows that stagnation occurs in cold legs #1 and #3, connected to the unaffected Steam Generator #1 for this test. Figure 4 shows the flow rates for cold leg #1 and #3. When primary side temperature exceeds the secondary side temperature, natural circulation flow is restored.

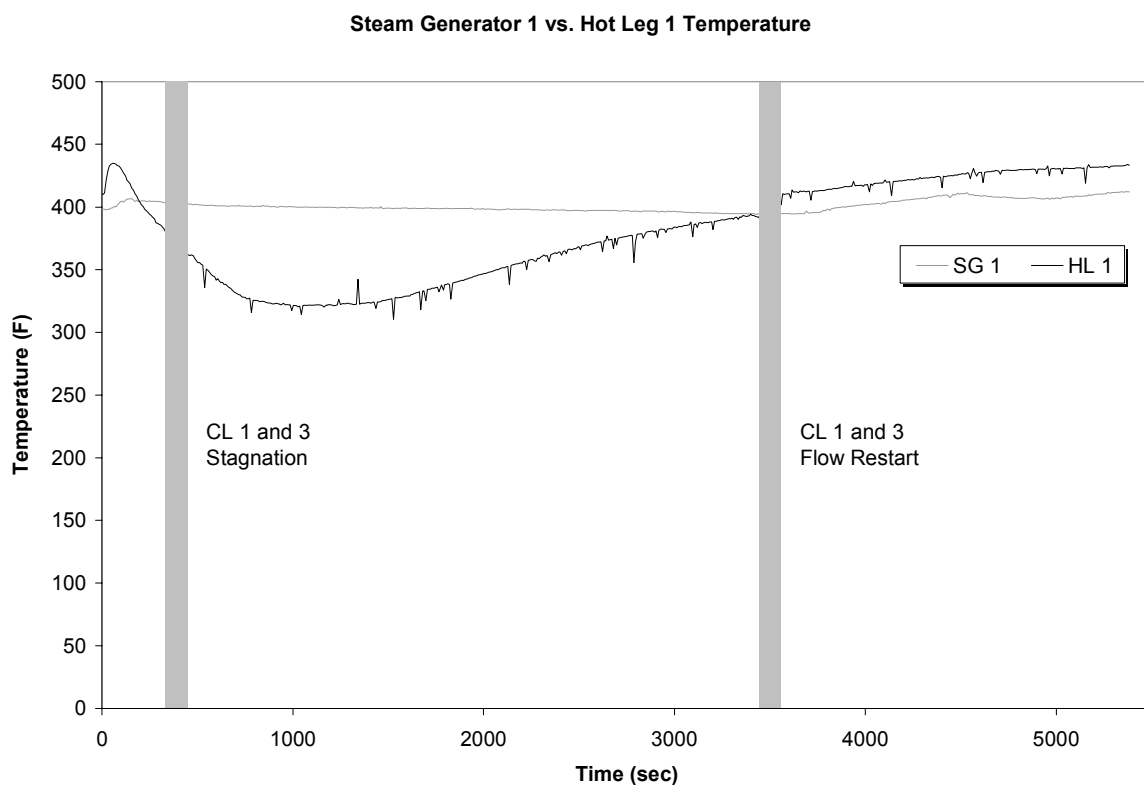


FIG. 3. Illustration of steam generator reverse heat transfer during a main steam line break simulation and recovery (OSU-CE-0012).

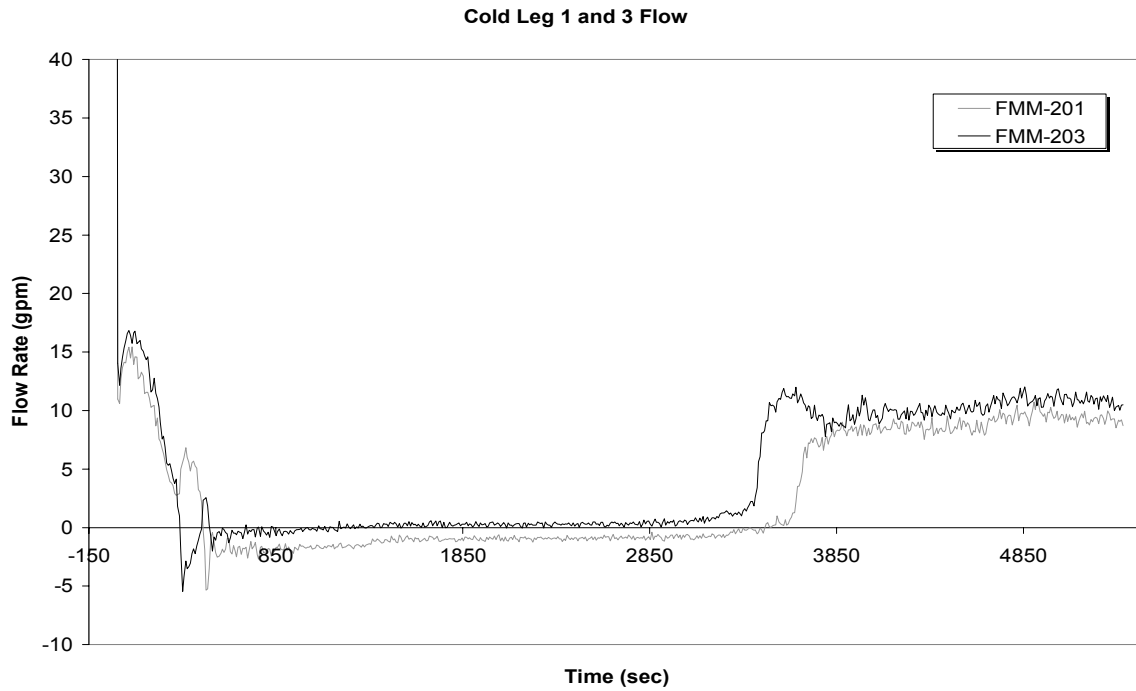


FIG. 4. Illustration of loss of natural circulation flow during a main steam line break simulation and recovery (OSU-CE-0012).

2.2. Negatively buoyant regions in loop (Loop seal cooling)

Another mechanism that can interrupt single-phase natural circulation flow is loop seal cooling. The piping that connects the steam generator lower channel head to the reactor coolant pump is known as the cross-over leg or the reactor pump loop seal as shown in Figure 2. Overcooling transients, such as main steam line breaks, result in a primary side cooldown. If the primary side pressure drops below the safety injection actuation setpoint, cold boric water will be injected into the loop. This water is typically injected into the cold legs of a PWR between the reactor coolant pump and the reactor vessel. Figure 5 is a picture of the transparent Separate Effects Test Loop at Oregon State University used to visualize fluid mixing in a side-injection cold leg.



FIG. 5. Flow visualization of injected coolant mixing with fluid in a transparent loop seal.

The dense injected fluid, simulated using fluorescent salt-water, falls to the bottom of the cold leg where it spreads out towards the vessel and the reactor coolant pump loop seal. Countercurrent flow is established with hot water at the top of the cold leg pipe flowing towards the injection point. The dense injected water mixes with the less dense water in the loop seal creating a negatively buoyant region in the loop, effectively increasing the resistance to flow in that loop. For multi-loop plants, the flow is preferentially diverted to the adjacent cold leg through the SG lower provided the same condition does not also exist there. Figure 6 shows the asymmetric cooling of two loop seals attached to a single steam generator in APEX-CE. Loop seal #4 cools faster than loop seal #2 because the dense fluid back flows over the lip of RCP #4 earlier during this particular transient. Figure 7 shows that loop flow in cold leg #4 stagnates earlier than the flow in cold leg #2.

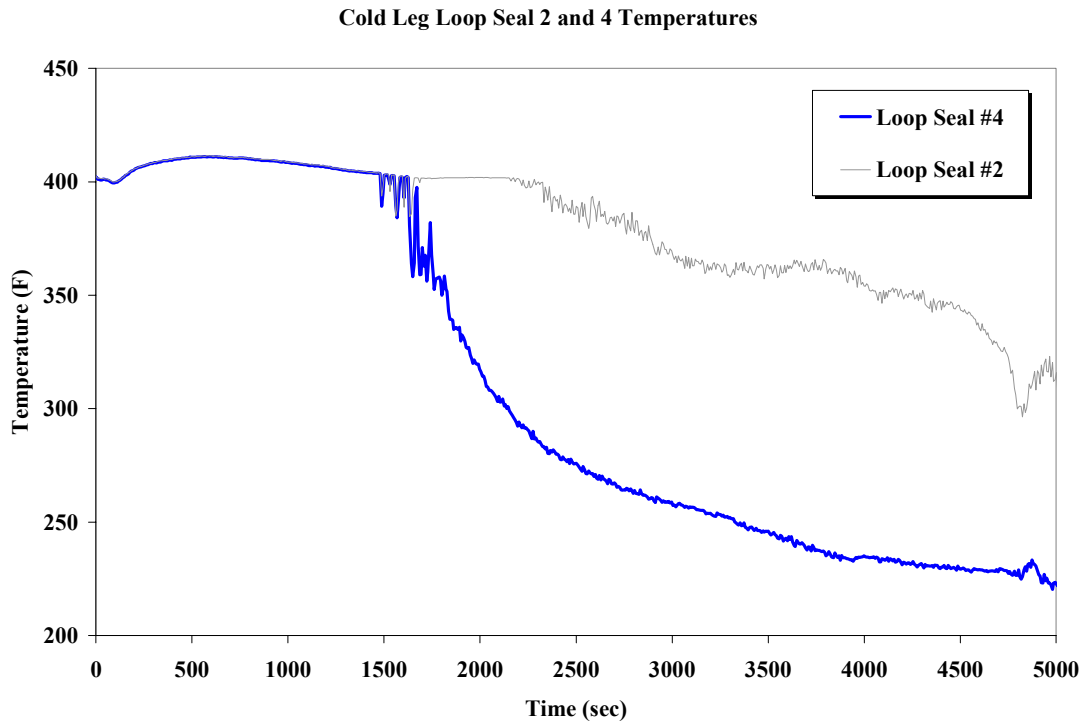


FIG. 6. Asymmetric loop seal cooling (OSU-CE-0008).

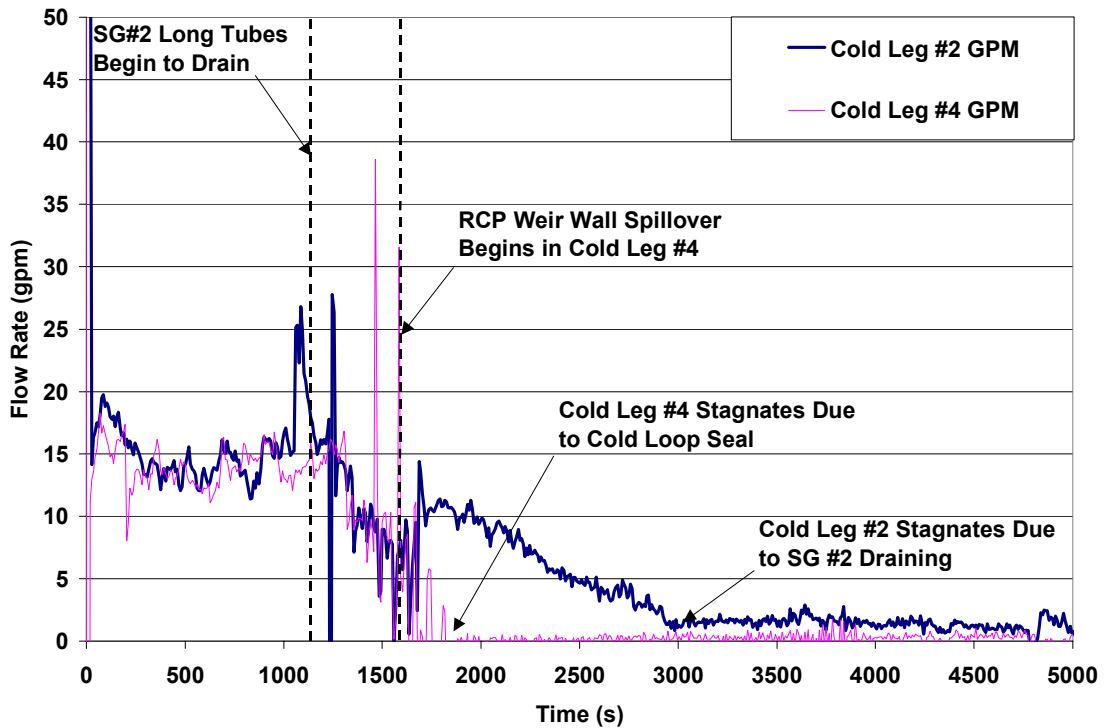


FIG. 7. Stagnation of a primary loop due to loop seal cooling (OSU-CE-0008).

3. TWO-PHASE NATURAL CIRCULATION STAGNATION MECHANISMS

During a Small Break Loss of Coolant Accident (SBLOCA) in a PWR, steam generator tube draining will result in a gradual decrease in primary side natural circulation flow until it transitions to a boiling-condensing mode of operation. Figure 8 shows the results of a test conducted at OSU to investigate this phenomenon. The test, OSU-CE-0002, was a stepped reduction in inventory test. In essence, it is a quasi-steady SBLOCA. It was conducted at a constant core power of 275 kW and initiated from steady-state single-phase natural circulation conditions. A break valve on the reactor vessel was opened to remove primary fluid in stepped intervals. After a short period, the break valve was closed and the loop was allowed to reach a new quasi-steady state flow rate. The cold leg flow rates were measured at each interval. These tests were similar to tests performed at the Semiscale test facility at the Idaho National Engineering Laboratory as shown in Figure 9 [2].

As liquid mass is removed from the system, the loop void fraction increases. This resulted in a rise in the loop flow rates above those observed for single-phase natural circulation as shown in Figure 8. At approximately 70% inventory in APEX-CE, the flow reaches a maximum value. This corresponds to the maximum two-phase buoyancy driving head for the test. Eventually the steam generator tubes begin to drain causing a decrease in flow rate because the distance between the core and steam generator thermal centers has decreased and interruption of flow in the longest tubes.

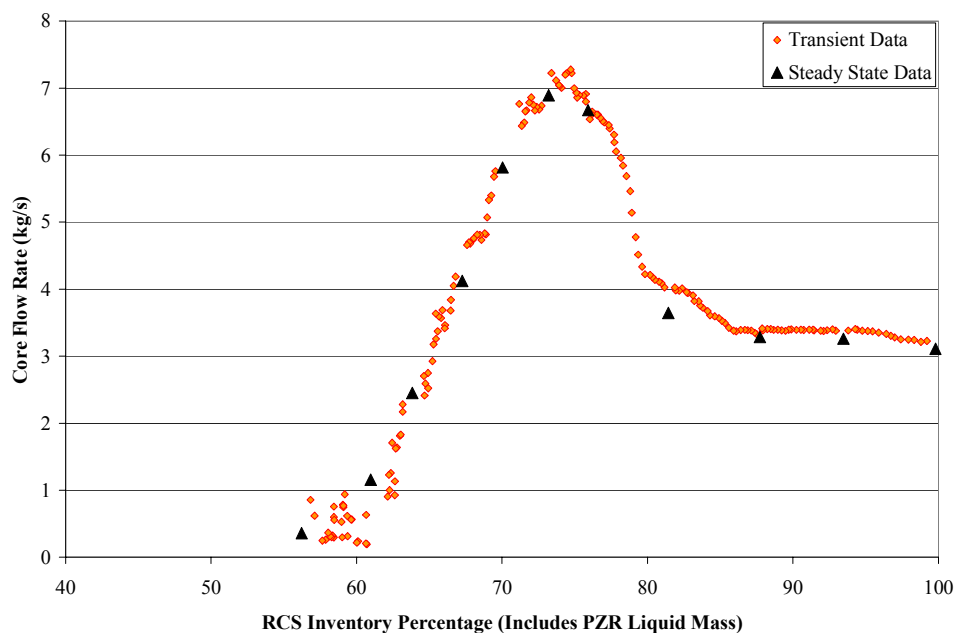


FIG. 8. Cold leg flow rates as a function of primary side inventory during a stepped-inventory reduction test (OSU-CE-0002).

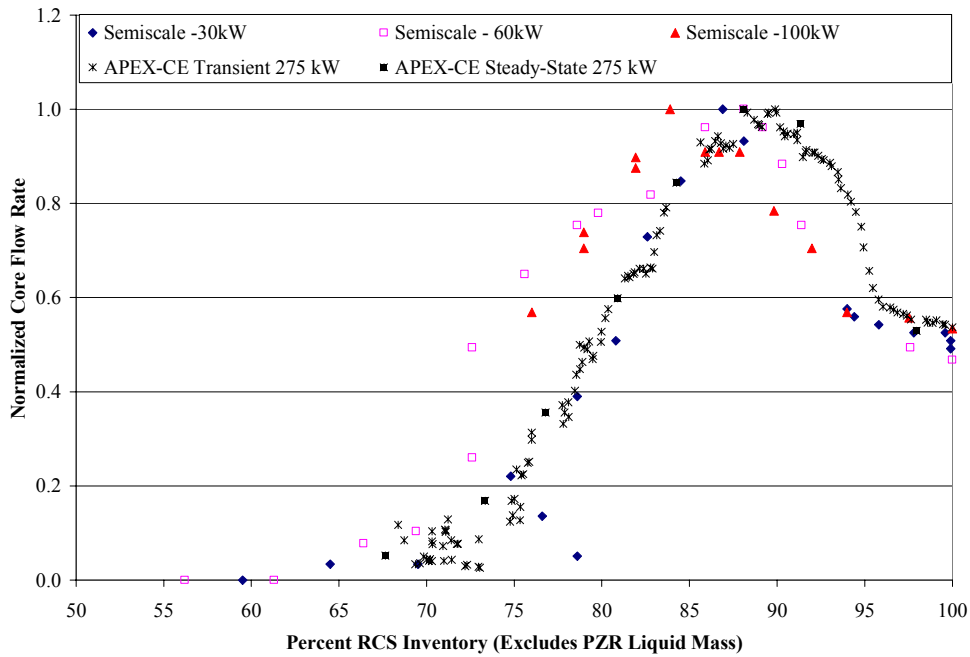


FIG. 9. Cold leg flow rates as a function of primary side inventory during a stepped-inventory reduction test (OSU-CE-0002) and semiscale Mod 2A data.

Figure 10 illustrates the significant difference in draining time for the longest U-tubes at the top of the bundle and the shortest U-tubes at the bottom of the bundle. The long tubes drained much earlier than short tubes. However some primary loop natural circulation continued until the short tubes drained. It is interesting to note that many computer codes typically use one tube to simulate an entire steam generator bundle.

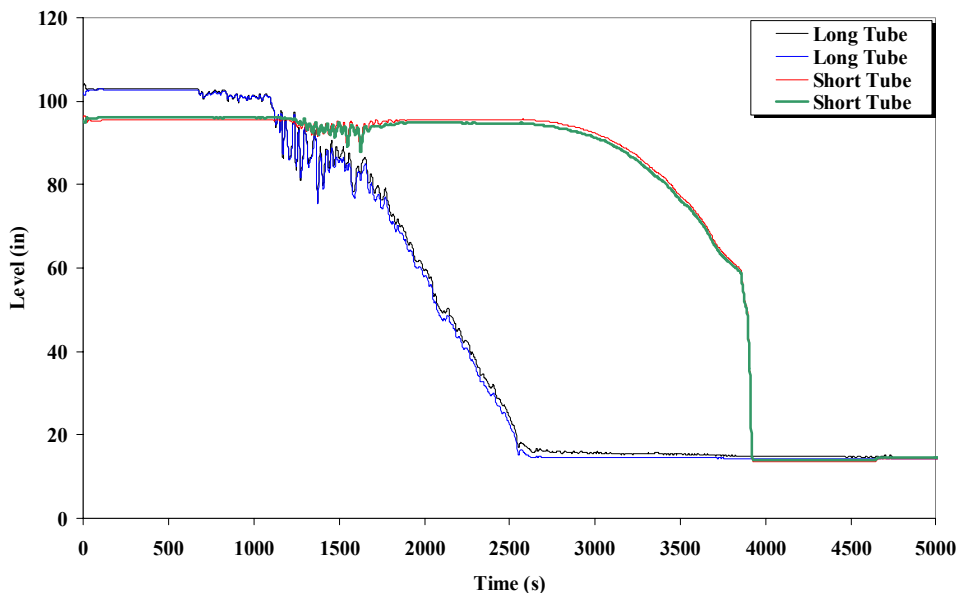


FIG. 10. Liquid levels in the longest and shortest tubes of steam generator #2 during SLOCA test (OSU-CE-0008).

4. THERMAL FLUID STRATIFICATION AND PLUME FORMATION

The loss of natural circulation flow during safety system operation is of particular interest because the flow tends to keep the fluid relatively well mixed in the primary loop. Figure 11 illustrates various regions where thermal stratification can occur.

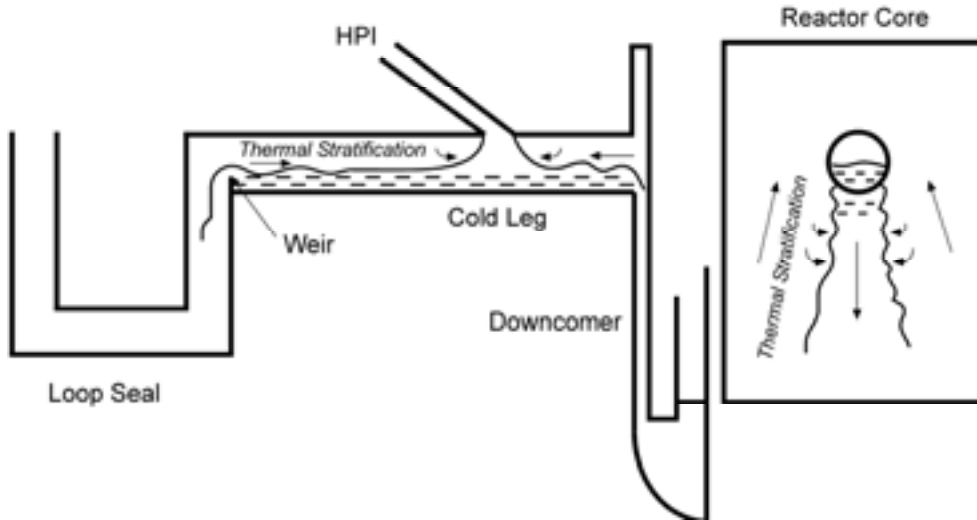


FIG. 11. Regions of thermal stratification in the primary loop of a PWR..

This section presents criteria to predict the onset of thermal stratification in the cold leg and the fundamentals of plume formation in the cold leg and downcomer regions of a reactor vessel.

4.1. Onset of thermal stratification in a horizontal cold leg

Theofanous, et al. (1984) [2], successfully correlated the onset of cold leg thermal stratification for the geometry shown in Figure 11 using the following criterion:

$$Fr_{HPI/CL} = \left[1 + \frac{Q_L}{Q_{HPI}} \right]^{-7/5} \quad (1)$$

where Q_L is the volumetric flow rate through a cold leg, Q_{HPI} is the volumetric flow rate through a single injection nozzle and $Fr_{HPI/CL}$ is a modified Froude number defined as:

$$Fr_{HPI/CL} = \frac{Q_{HPI}}{a_{CL} \left[g D_{CL} \frac{\rho_{HPI} - \rho_{CL}}{\rho_{HPI}} \right]^{1/2}} \quad (2)$$

Reyes (2001) [3] developed a criterion similar to that of equation (1) using a hydraulic jump analysis. The criterion is as follows:

$$Fr_{HPI/CL} = \left[1 + \frac{\rho_L Q_{HPI}}{\rho_{HPI} Q_L} \right]^{-1/2} \left[1 + \frac{Q_L}{Q_{HPI}} \right]^{-3/2} \quad (3)$$

As shown in Figure 12, the two criteria given by equations (1) and (3) are similar at the high loop flow to injection flow ratios (i.e., $Q_L/Q_{HPI} \gg 1$). The two criteria diverge significantly as Q_L/Q_{HPI} approaches 1.

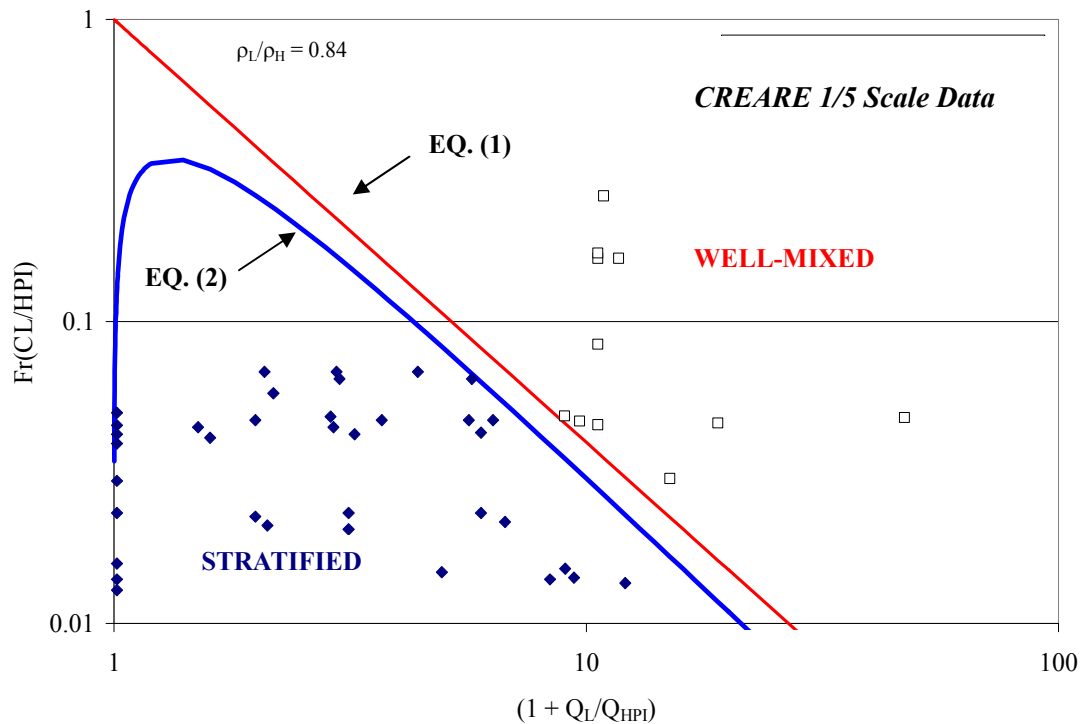


FIG. 12. Comparison of thermal stratification criteria in a horizontal cold leg.

4.2. Governing equations for axisymmetric forced plumes

The criteria of the previous section indicates that upon a loss of natural circulation flow in the loop, (i.e., $Q_L = 0$), the fluid in the cold leg becomes thermally stratified. As illustrated in Figure 13, the cold (approximately 5°C to 20°C) HPI fluid enters the top of the cold leg, creating an axisymmetric plume that falls to the bottom of the pipe. Mixing occurs at the boundary of the HPI plume and at the free shear layers as illustrated in Figure 13. The falling plume produces a head wave that spreads the cold HPI fluid in both directions. After the initial transient, a stagnant pool of HPI fluid forms on the RCP side of the cold leg and all of the HPI flow is directed towards the reactor vessel downcomer. As depicted in this figure, hot water from the loop and downcomer is entrained into the falling plume. This is shown as Region 1 of the figure.

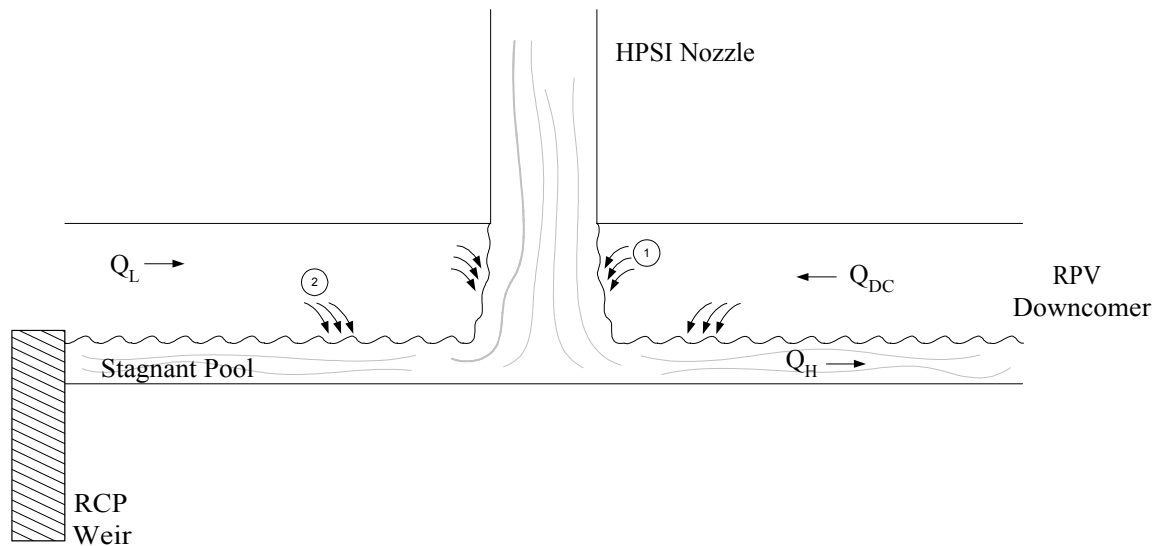


FIG. 13. Thermally stratified conditions for the top-entry HPI..

Mixing also occurs at the free shear layers identified as Region 2 on the figure. Experimental evidence from the CREARE 1/5 [4], CREARE 1/2 [5] and Purdue 1/2 [6] scale test facilities indicate that mixing at the free shear layers is negligible compared to plume entrainment mixing. This may not be true for side injection. The focus of this section will be to describe the governing equations for the HPI mixing in Region 1. That is, entrainment mixing of the vertical forced plume and the resulting plume temperature decay.

A. Fundamental Assumptions

Early studies of the behavior of forced plumes relied on similarity solutions derived from the governing conservation equations. Particularly notable in this regard are the works of Rouse, Yih and Humphreys (1952) [7], Batchelor (1954) [8], Morton (1958) [9], and Turner (1979) [10].

Based on Batchelor's work, vorticity, or shearing motion, is generated inside a falling plume as a result of friction at its outer surface. This shearing motion is distributed through the plume by the downward motion along the vertical axis of the plume. The fluid outside the plume will be free from vorticity except in the thin boundary layer near the interface. The turbulent motion inside the plume will produce velocity fluctuations near the interface that will penetrate into the ambient fluid. The plume will break-up only if the inertia of the fluid within the plume is not small compared with the inertia of the fluid surrounding the plume. Therefore, turbulent entrainment of the ambient fluid into the plume, dilution (thermal or solute concentrations) of the density difference and the rate at which the plume falls depends greatly on the ambient fluid density. Further studies by Turner revealed that entrainment takes place in two stages, the engulfing of external fluid by larger eddies at the boundary, followed by rapid, smaller scale, mixing across the central core.

In Morton's analysis of forced plumes, he made three key assumptions that enabled him to obtain solutions to the governing conservation equations. These assumptions are described in the following paragraphs.

i Taylor's Entrainment Assumption

G.I. Taylor [11] was the first to recognize that the linear spread of the plume radius with axial position implies that the mean inflow velocity across the edge of the plume is proportional to the local mean downward velocity of the plume. That is,

$$-v_E = \alpha_E u_p \tag{1}$$

Where the ratio of the mean speed of inflow v_E at the edge of the forced plume to the mean vertical speed on the plume axis, u_p is equal to an entrainment constant, α_E , which is a value between zero and one. Taylor's assumption of a constant value of α_E is known to be true for pure plumes or pure jets. Other correlations for α_E have been developed for forced plumes in which both the momentum flux and buoyancy flux are important.

ii Similarity of Velocity and Buoyancy Profiles

Morton assumed that the profiles of mean vertical velocity and buoyancy are each of similar form at all axial elevations. The experimental data strongly supports this assumption as shown in Figure 14, which is a plot of the local velocity inside a planar plume. Figure 15 demonstrates that all of the data collapses to a single curve when plotted in dimensionless coordinates.

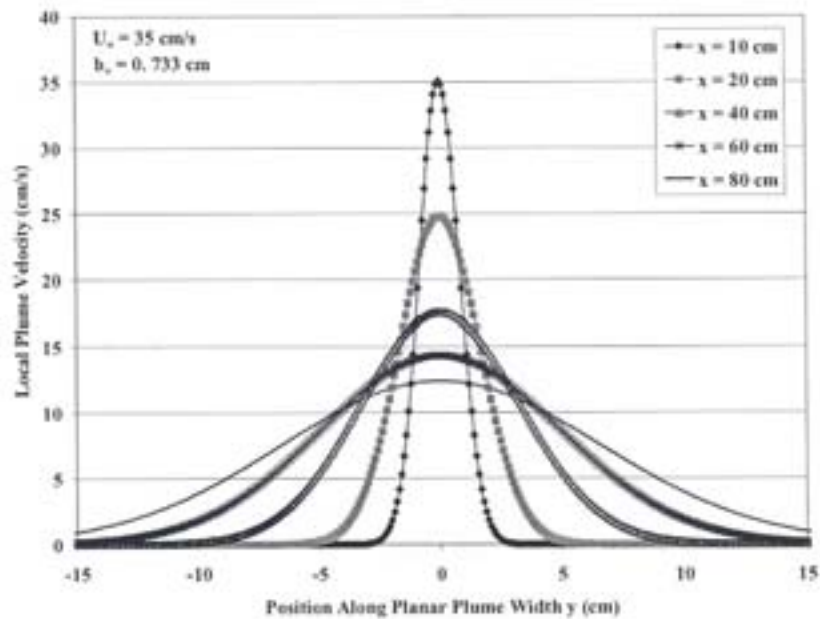


FIG. 14. Correlation of velocity distributions measured in a planar jet (1934) [12].

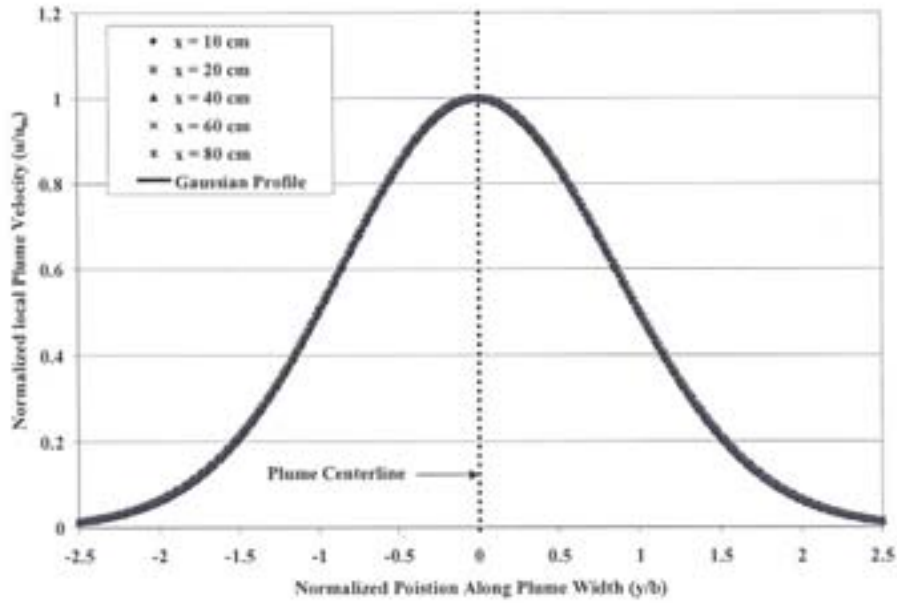


FIG. 15. Velocity distributions in a planar jet plotted in dimensionless Coordinates [12] and compared to a gaussian profile (1934).

By assuming a particular profile shape, typically a Gaussian profile as shown in Figure 15, the mass and momentum fluxes can be replaced by mean value defined by integrals across the plume width. The assumption of similarity implies that the rate of spread of the plume, which is governed by the turbulence generated by its own motion, must have the same relation to the mean flow whatever the scale of motion.

i Gaussian Profile

The following Gaussian profiles are typically assumed for the mean vertical velocity and mean buoyancy respectively.

$$u(r, z) = u_p(z) \exp\left(-\frac{r^2}{b_u^2}\right) \quad (2)$$

and

$$g\Delta\rho(r, z) = g\Delta\rho_p(z) \exp\left(-\frac{r^2}{b_u^2}\right) \quad (3)$$

where

$$\Delta\rho = (\rho - \rho_m) \quad (4)$$

In these profiles, u_p and $g\Delta\rho_p$ are the mean axial velocity and buoyancy of the forced plume. These mean values are functions of the axial position (z). The ambient fluid density is denoted by ρ_m . The profile dependence on the radial position is given by the r -coordinate found in the exponent. The length b_u characterizes the radial spread of the velocity profiles whereas the length b_g characterizes the radial spread of the buoyancy profile. Both are functions of axial position. The values of b_u and b_g are empirically determined. Figure 16 illustrates the profile nomenclature that has been implemented in this analysis.

The following equation of state for the fluid:

$$(T - T_m) = \frac{(\rho - \rho_m)}{\beta_o \rho_o} \quad (5)$$

where β_o is the reference thermal expansion coefficient and ρ_o is a reference density, can be applied to the buoyancy profile to obtain the following fluid temperature profile:

$$(T - T_m) = (T - T_m)_p \exp\left(-\frac{r^2}{b_g^2}\right) \quad (6)$$

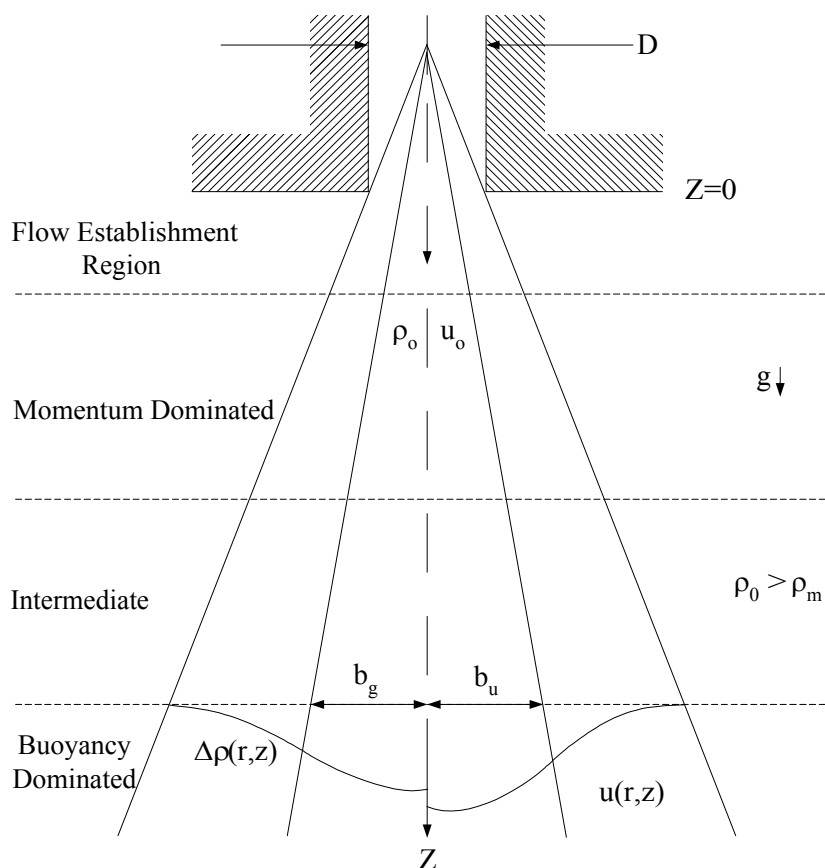


FIG. 16. Gaussian profiles in forced plumes.

B. Governing Equations for Axisymmetric Forced Plumes

The governing equations for the flow quantities in an axisymmetric vertical buoyant jet, where gravity acts along the z-coordinate, are as follows (Chen and Rodi) [13]:

Mass Conservation:

$$\frac{\partial}{\partial z}(\rho ur) + \frac{\partial}{\partial r}(\rho vr) = 0 \quad (7)$$

Momentum Conservation:

$$\frac{\partial}{\partial z}(\rho u^2 r) + \frac{\partial}{\partial r}(\rho uvr) = g(\rho - \rho_m)r - \frac{\partial}{\partial r}(r\rho u'v') \quad (8)$$

Thermal Energy Conservation:

$$\frac{\partial}{\partial z}(\rho uTr) + \frac{\partial}{\partial r}(\rho vTr) = -\frac{\partial}{\partial r}(r\rho v'T) \quad (9)$$

The equations listed above were obtained by Chen and Rodi using the boundary-layer assumptions and the Boussinesq approximation under steady-flow conditions. The $\rho u'v'$ term represents the turbulent shear stress. The thermal energy equation can also be written in terms of a stratified ambient temperature, $T_m(z)$ as follows:

$$\frac{\partial}{\partial z}[\rho ur(T - T_m)] + \frac{\partial}{\partial r}[\rho vr(T - T_m)] = -\rho ur \frac{\partial T_m}{\partial z} - \frac{\partial}{\partial r}(\rho v'rT') \quad (10)$$

Integrating the mass conservation equation yields the following balance equation for the plume volume flux:

$$\frac{d}{dz} \int_0^R ur dr = -v_E R \quad (11)$$

Where 2π and ρ (Boussinesq approximation) were canceled from both sides of the equation. In this equation, v_E is the entrainment velocity at the plume boundary.

Integrating the momentum conservation equation yields the following balance equation for the momentum flux:

$$\frac{d}{dz} \int_0^R \rho u^2 dr = g \int_0^R (\rho - \rho_m) r dr \quad (12)$$

A value of 2π was canceled from both sides of the equation. In arriving at this equation, it was assumed that the terms u and $\rho u'v'$ are close to zero at r equal to R .

Integrating the energy conservation equation yields the following balance equation for the thermal energy flux:

$$\frac{d}{dz} \int_0^R u(T - T_m) r dr = - \frac{dT_m}{dz} \int_0^R u r dr \quad (13)$$

The terms 2π and ρ (Boussinesq approximation) were canceled from both sides of the equation. Use has also been made of the approximation that u , $(T - T_m)$, and $\rho v' T'$ are zero at r equal to R .

The integral volume flux, momentum flux, and thermal energy flux equations can be evaluated by substituting the Gaussian profiles presented earlier. This will yield a set of ordinary differential equations which can be made dimensionless to obtain the desired scaling groups. Substituting equation (2) into (11) and performing the integration yields the balance equation for the volume flux:

$$\frac{d}{dz} (b_u^2 u_p) = -2Rv_E \quad (14)$$

Use has been made of the fact that $\exp(-R/b_u^2)$ is approximately zero. Substituting equation (3) into (10) and performing the integration yields the balance equation for the momentum flux:

$$\frac{d}{dz} (\rho b_u^2 u_p^2) = 2g(\rho - \rho_L)_p b_g^2 \quad (15)$$

Substituting equation (6) into (13) and integrating yields the thermal energy flux balance equation:

$$\frac{d}{dz} \left(\frac{b_g^2 b_u^2 u_p \Delta T_p}{b_g^2 + b_u^2} \right) = -b_u^2 u_p \frac{dT_m}{dz} \quad (16)$$

Equations (14) through (16) are similar to those obtained by Rodi [14]. The integrated balance equations given by (14) through (16) can also be written in terms of volumetric flow rates, Q . The volumetric flow rate of the plume, Q_p is given by:

$$Q_p = 2\pi \int_0^R u r dr \quad (17)$$

Substituting the Gaussian velocity profile, equation (2) and integrating yields:

$$Q_p = \pi b_u^2 u_m \quad (18)$$

The entrainment volumetric flow rate can be related to the entrainment velocity by:

$$\frac{dQ_p}{dz} = 2\pi R v_E \quad (19)$$

Substituting equations (18) and (19) into (14) through (16) yields the governing equations for a forced axisymmetric plume as shown in Table 1. At $z = 0$, Q_{HPI} is approximately equal to Q_p , D_{HPI} is approximately $2R$ and ΔT_p is approximately $(T_{HPI} - T_m)$. Substituting the dimensionless boundary conditions into the balance equations in Table 1 yields the dimensionless balance equations in Table 2.

The dimensionless group Π_{QE} represents the ratio of the entrainment volumetric flux to the plume volumetric flux at the entrance. The dimensionless group, Fr_{HPI} , is the ratio of inertia to buoyancy and represents a modified Froude number. Here a_{HPI} is the cross-sectional flow area of the HPI nozzle. The dimensionless group, $\Pi_{\Delta T}$, characterizes the degree of ambient thermal stratification. In conclusion, the dimensionless groups that govern the behavior of axisymmetric forced plumes in vertical flows are (D_{HPI}/z) , Π_{QE} , Fr_{HPI} , and Π_{DT} .

Theofanous [15] and Rodi [14] have used a $k-\gamma-\theta N$ turbulence model to predict the plume volumetric flow and temperature decay. Theofanous correlated the results of the more detailed analysis using the plume decay equations shown in Table 2. It is noted that these same dimensionless groups used in his correlation were also obtained in the present scaling analysis.

Table 1. Governing equations for a forced axisymmetric plume

Governing Balance Equations	
<i>Volume Balance:</i>	
	$\frac{dQ_p}{dz} = -\frac{dQ_E}{dz} \quad (20)$
<i>Momentum Balance:</i>	
	$\frac{d}{dz} \left(\frac{\rho Q_p^2}{b_u^2} \right) = 2\pi^2 g b_g^2 (\rho - \rho_L)_p \quad (21)$
<i>Energy Balance:</i>	
	$\frac{d}{dz} \left(\frac{Q_p \Delta T_p}{1 + \lambda^2} \right) = -Q_p \frac{dT_m}{dz} \quad (22)$
where λ is equal to b_u/b_g .	
Initial and Boundary Conditions:	
	$z^+ = \frac{2z}{D_{HPI}} \quad (23)$
	$Q_p^+ = \frac{Q_p}{Q_{HPI}} \quad (24)$
	$Q_E^+ = \frac{Q_E}{Q_{E,o}} \quad (25)$
	$b_u^+ = \frac{2b_u}{D_{HPI}} \quad (26)$
	$b_g^+ = \frac{2b_g}{D_{HPI}} \quad (27)$
	$\Delta T_p^+ = \frac{\Delta T_p}{(T_{HPI} - T_m)} \quad (28)$
	$\left(\frac{dT_m}{dz} \right)^+ = \left(\frac{dT_m}{dz} \right) / \left(\frac{dT_m}{dz} \right)_o \quad (29)$
	$\Delta \rho_p^+ = \frac{\Delta \rho_p}{(\rho_{HPI} - \rho_m)} \quad (30)$

Table 2. Dimensionless balance equations and Plume Decay Correlations

DIMENSIONLESS BALANCE EQUATIONS	
<i>Volume Balance:</i>	$\frac{dQ_p^+}{dz^+} = -\Pi_{QE} \frac{dQ_E^+}{dz^+} \quad (31)$
<i>Momentum Balance:</i>	$(Fr_{HPI})^2 \frac{d}{dz^+} \left(\frac{\rho Q_p}{b_u^2} \right)^+ = 2(b_g^2 \Delta \rho_p)^+ \quad (32)$
<i>Energy Balance:</i>	$\frac{d}{dz^+} \left(\frac{Q_p \Delta T_p}{1 + \lambda^2} \right)^+ = -\frac{\Pi_{\Delta T}}{2} Q_p^+ \left(\frac{dT_m}{dz} \right)^+ \quad (33)$
DIMENSIONLESS GROUPS	
	$\Pi_{QE} = \left(\frac{Q_E}{Q_{HPI}} \right)_o \quad (34)$
	$Fr_{HPI} = \frac{Q_{HPI}}{a_{HPI} \left(\frac{g \Delta \rho_p D_{HPI}}{\rho_{HPI}} \right)_o^{1/2}} \quad (35)$
	$\Pi_{\Delta T} = \frac{D_{HPI}}{(T_{HPI} - T_m)_o} \left(\frac{dT_m}{dz} \right)_o \quad (36)$
PLUME DECAY CORRELATIONS (THEOFANOUS)	
<i>Entrainment Correlation:</i>	$\Pi_{QE} = 0.5176 \left(\frac{z}{D_{HPI}} \right)^{1.236} (Fr_{HPI})^{-0.414} \quad (37)$
<i>Temperature Decay Correlation:</i>	$\Delta T^+ = 1 - 0.326 \left(\frac{z}{D_{HPI}} \right)^{0.65} (Fr_{HPI})^{-0.274} \quad (38)$

4.3. Governing equations for planar plumes

Chen and Rodi (1980) [13] have provided a valuable treatise which includes detailed discussions on planar plumes. The analysis for the planar plume follows that presented in Section 4.2 for the axisymmetric forced plume. The three fundamental assumptions, Taylor's entrainment assumption, the similarity of velocity and buoyancy profiles in the plume, and the Gaussian profile assumption remain applicable. Figure 17 illustrates the planar plume geometry.

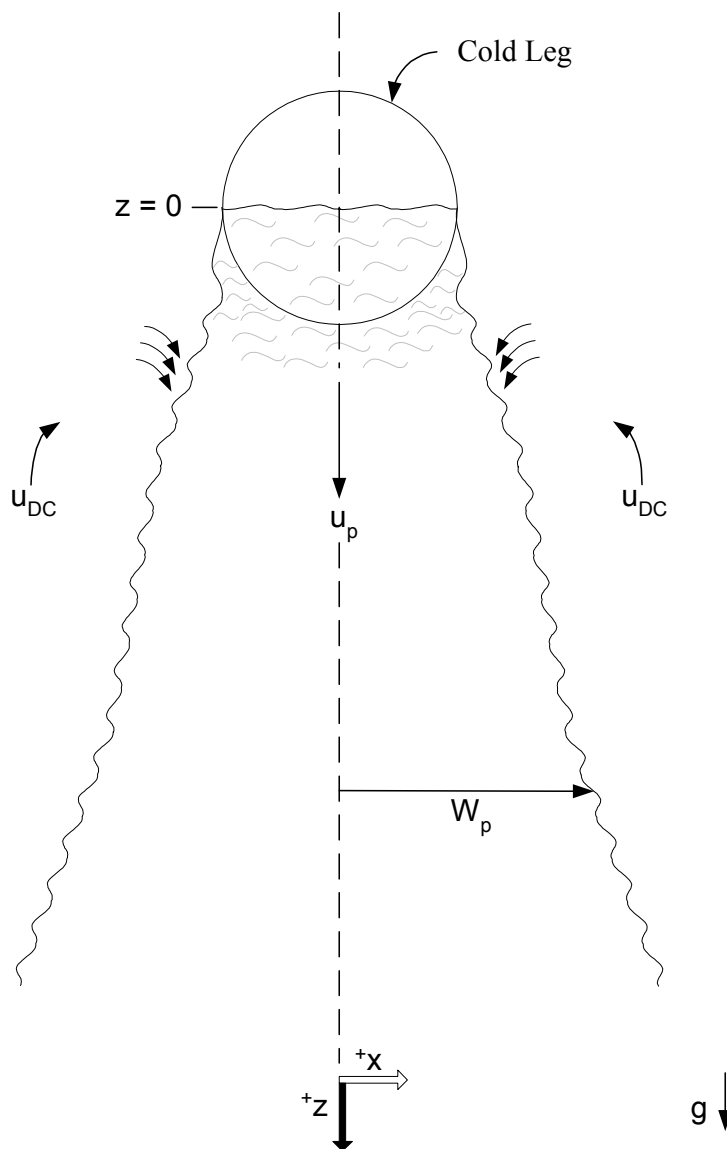


FIG. 17. Schematic of a single planar plume in the RPV downcomer.

The Gaussian profiles for the plume velocity, buoyancy and temperature are expressed as follows:

$$u(x, z) = u_p(z) \exp\left(-\frac{x^2}{b_u^2}\right) \quad (39)$$

$$g\Delta\rho(x, z) = g\Delta\rho_p(z) \exp\left(-\frac{x^2}{b_g^2}\right) \quad (40)$$

$$(T - T_m) = (T - T_m)_p \exp\left(-\frac{x^2}{b_g^2}\right) \quad (41)$$

The governing equations for the planar plume where gravity acts along the z-coordinate are (Chen and Rodi) [13]:

Mass Conservation:

$$\frac{\partial}{\partial z}(\rho u) + \frac{\partial}{\partial x}(\rho v) = 0 \quad (42)$$

Momentum Conservation:

$$\frac{\partial}{\partial z}(\rho u^2) + \frac{\partial}{\partial x}(\rho uv) = g(\rho - \rho_m) - \frac{\partial}{\partial x}(\rho u'v') \quad (43)$$

Thermal Energy:

$$\frac{\partial}{\partial z}[\rho u(T - T_m)] + \frac{\partial}{\partial x}[\rho v(T - T_m)] = -\rho u \frac{\partial T_m}{\partial x} - \frac{\partial}{\partial x}(\rho v'T') \quad (44)$$

where the definitions of the terms are the same as given in Section 4.2, and the thermal energy equation has been written in terms of the stratified ambient temperature, T_m . Integrating the equations over the cross-sectional area of the plume yields:

Volume Flux:

$$\frac{d}{dz} \int_0^{w_p} u dx = -v_E W_p \quad (45)$$

Momentum Flux:

$$\frac{d}{dz} \int_0^{w_p} \rho u^2 dx = g \int_0^{w_p} (\rho - \rho_m) dx \quad (46)$$

Thermal Energy Flux:

$$\frac{d}{dz} \int_0^{W_p} u(T - T_m) dx = -\frac{dT_m}{dz} \int_0^{W_p} u dx \quad (47)$$

where ρ (Boussinesq approximation) and a factor of $2s$ were canceled from both sides of each equation and the plume boundary assumptions of Section 4.2 were applied. The downcomer gap width is denoted by “ s .”

Substituting the Gaussian profiles given by equations (39) through (41) into (45) through (47) respectively, yield the integral equations for the mean flow properties of the planar plume.

Volume Flux:

$$\frac{d}{dz} (b_u u_p) = -\frac{2}{\sqrt{\pi}} v_E \quad (48)$$

Momentum Flux:

$$\frac{d}{dz} (\rho b_u u_p^2) = 2g\Delta\rho_p b_g \quad (49)$$

Thermal Energy Flux:

$$\frac{d}{dz} \left[b_u u_p \Delta T_p \left(\frac{\lambda^2}{1 + \lambda^2} \right)^{1/2} \right] = -b_u u_p \frac{dT_m}{dz} \quad (50)$$

The integral balance equations can be expressed in terms of volumetric flow rates as was done in Section 4.2. The volumetric flow rate of the plume, Q_p , is given by:

$$Q_p = 2s \int_0^{W_p} u dx \quad (51)$$

Substituting the Gaussian profile and integrating yields:

$$Q_p = \sqrt{\pi} b_u u_p s \quad (52)$$

The entrainment volumetric flow rate can be related to the entrainment velocity by:

$$\frac{dQ_E}{dz} = s W_p v_E \quad (53)$$

Substituting equations (52) and (53) into the integrated balance equation yields the governing balance equations for a planar plume. These equations are summarized in Table 3.

Table 3. Governing equations for planar plumes

Governing Balance Equations	
<i>Volume Balance:</i>	$\frac{dQ_p}{dz} = -\frac{dQ_E}{dz} \quad (20)$
<i>Momentum Balance:</i>	$\frac{d}{dz} \left(\frac{\rho Q_p^2}{b_u^2} \right) = 2\pi^2 s^2 g \Delta \rho_p b_g \quad (21)$
<i>Energy Balance:</i>	$\frac{d}{dz} \left(\frac{Q_p \Delta T_p \lambda}{\sqrt{1 + \lambda^2}} \right) = -Q_p \frac{dT_m}{dz} \quad (22)$
where λ is equal to b_u/b_g .	
Initial and Boundary Conditions:	
	$z^+ = \frac{2z}{D_{CL}} \quad (23)$
	$Q_p^+ = \frac{Q_p}{Q_{po}} \quad (24)$
	$Q_E^+ = \frac{Q_E}{Q_{E,o}} \quad (25)$
	$b_u^+ = \frac{2b_u}{D_{CL}} \quad (26)$
	$b_g^+ = \frac{2b_g}{D_{CL}} \quad (27)$
	$\Delta T_p^+ = \frac{\Delta T_p}{(T_{po} - T_m)} \quad (28)$
	$\left(\frac{dT_m}{dz} \right)^+ = \left(\frac{dT_m}{dz} \right) / \left(\frac{dT_m}{dz} \right)_o \quad (29)$
	$\Delta \rho_p^+ = \frac{\Delta \rho_p}{(\rho_{po} - \rho_m)} \quad (30)$

The initial half plume width, W_{po} , is assumed to be one half the cold leg diameter, D_{CL} . Substituting the dimensionless parameters into the integrated balance equations yields the dimensionless balance equations presented in Table 4. For uniform ambient fluid conditions in the downcomer, the fluid temperature gradient, dT_m/dz , would be zero.

Summarizing, the dimensionless groups that govern the behavior of the planar plume in the downcomer are (D_{CL}/z) , Π_{QE} , Fr_{DC} , and Π_{AT} .

Table 4. Dimensionless balance equations for planar plumes

DIMENSIONLESS BALANCE EQUATIONS		
<i>Volume Balance:</i>		
	$\frac{dQ_p^+}{dz^+} = -\Pi_{QE} \frac{dQ_E^+}{dz^+}$	(31)
<i>Momentum Balance:</i>		
	$(Fr_{DC})^2 \frac{d}{dz^+} \left(\frac{\rho Q_p}{b_u^2} \right)^+ = \frac{\pi}{2} \Delta \rho_p^+ b_g^+$	(32)
<i>Energy Balance:</i>		
	$\frac{d}{dz^+} \left(\frac{Q_p \Delta T_p \lambda}{\sqrt{1 + \lambda^2}} \right)^+ = -\frac{\Pi_{\Delta T}}{2} Q_p^+ \left(\frac{dT_m}{dz} \right)^+$	(33)
DIMENSIONLESS GROUPS		
	$\Pi_{QE} = \left(\frac{Q_E}{Q_p} \right)_o$	(34)
	$Fr_{DC} = \frac{Q_{p,o}}{s D_{CL} \left(\frac{g \Delta \rho_p D_{CL}}{\rho_p} \right)_o^{1/2}}$	(35)
	$\Pi_{\Delta T} = \frac{D_{CL}}{(T_p - T_m)_o} \left(\frac{dT_m}{dz} \right)_o$	(36)
PLANAR PLUME VELOCITY AND HEAT TRANSFER		
<i>Plume Velocity Correlation (Kotsovinos):</i>		
	$u_p = 1.66 \left(\frac{Q_{p,o} g (\rho_{HPI} - \rho_m)}{s \rho_m} \right)^{1/3}$	(37)
<i>Dimensionless Plume Velocity:</i>		
	$u_p^+ = \frac{u_p s D_{CL}}{Q_{p,o}} = 1.66 \left(\frac{\rho_p}{\rho_m} \right)^{1/3} (Fr_{DC})^{-2/3}$	(38)
	$Nu_p = C \cdot Re_p^{0.8} Pr^{0.4}$	(39)
$Nu_p = \frac{2sh_p}{k_f} \quad (40)$	$Re_p = \frac{2u_p s}{\nu_f} \quad (41)$	$Pr = \frac{c_p \mu_f}{k_f} \quad (42)$

Table 4 also includes correlations for the mean planar plume velocity and planar plume convective heat transfer. The correlation presented in Table 4 was adapted from the work of Kotsovinos [16] to predict the mean fluid velocity at the axis of a plume.

Valenzuela and Dolan used the well-known Dittus-Boelter correlation for turbulent flow to predict the plume heat transfer coefficients in the CREARE 1/2-Scale test facility [5]. However, the Reynolds number and Prandtl Number have been expressed in terms of the plume velocity, u_p . Figure 18 shows the comparison of this equation to the CREARE 1/2- scale data. The data collapse quite neatly to a single line.

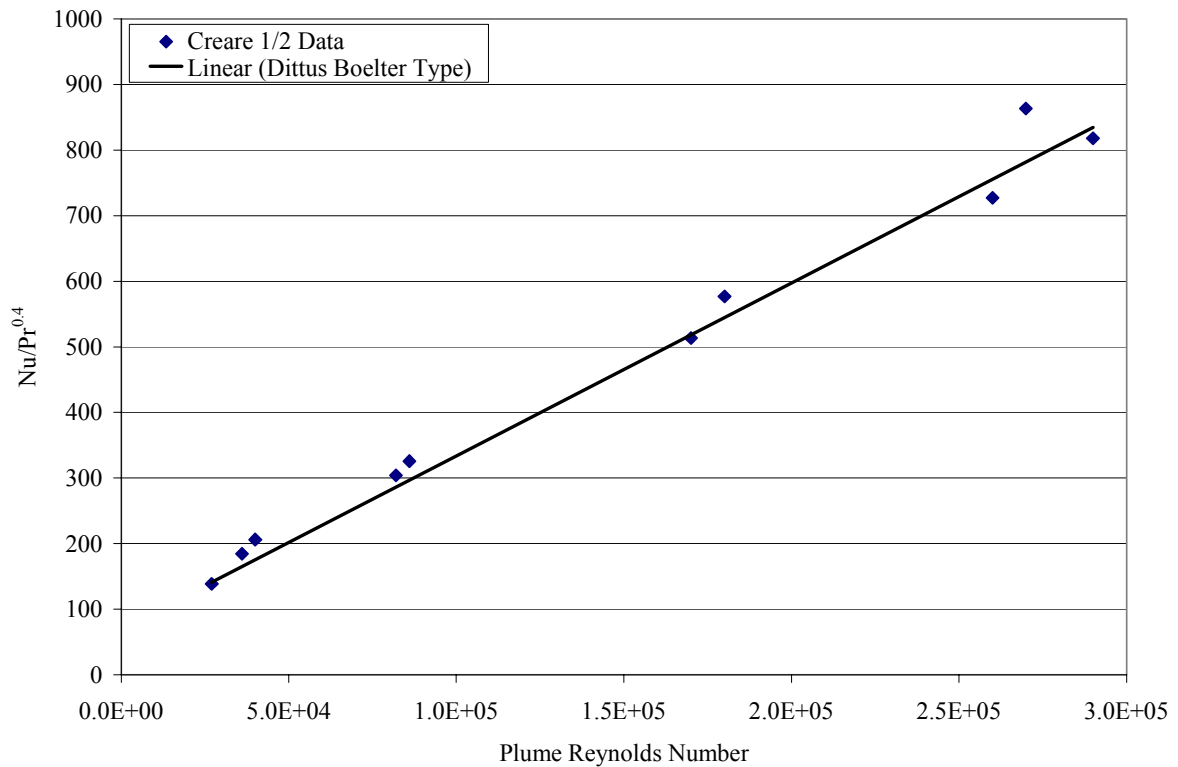


FIG. 18. Comparison of plume heat transfer correlation predictions to the Creare 1/2-Scale Downcomer Heat Transfer Data.

4.4. Downcomer plume behavior

Flow visualization tests examining downcomer plume behavior were obtained from the 2/5 scale, multi-loop, transparent test facility at Imatran Voima Oy (IVO) in Helsinki, Finland [17]. Figure 19 presents two snapshots of IVO Test #102 showing plume penetration into the downcomer and the resulting thermal stratification that arises. Dense HPI fluid flows through Cold Leg B as indicated by the dye, while a loop flow rate 10 times greater flows through Cold Leg C.



FIG. 19. Photographs of the IVO transparent test loop. Cold Leg C flow rate = 66 gpm (4.2 liters/s) and HPI flow in Cold Leg B = 6.6 gpm (0.42 liters/s).

Plume interactions, similar to those observed in the IVO test loop were also measured in the APEX-CE tests. Figure 20 is a schematic of planar plumes generated by two cold legs merging to form a stronger central plume. The complexity of the behavior, in particular the interactions between plumes, does not lend itself to simple analysis.

Researchers at Purdue and University of California, Santa Barbara developed a regional mixing model called REMIX [18] to assess thermal fluid mixing behavior in the HPI line, cold leg and downcomer or a PWR. Assessments of REMIX using APEX-CE thermal data indicate that the model typically predicts lower temperatures than measured. The code is limited however, in that it cannot model multiple plume interactions.

A variety of Computational Fluid Dynamics (CFD) codes have been used to examine fluid mixing in reactor vessels. STAR-CD, CFX, and FLUENT are examples of commercially available codes that offer promising methods for analyzing the complex mixing behavior produced by nuclear reactor safety injection systems. This topic will be discussed in a separate lecture.

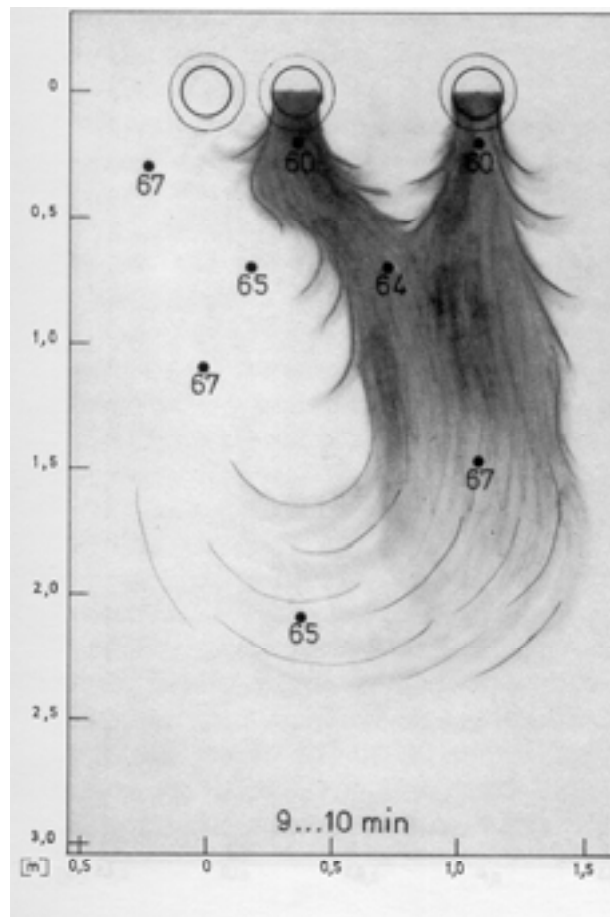


FIG. 20. Downcomer plume interactions as observed in IVO 2/5 scale transparent test loop (IVO Mixing Test #115).

NOMENCLATURE

- Fr_x – Froude Number Modified (HPI or HPI/CL)
- Q – Volumetric flow rate
- g - gravitational constant
- a – cross-sectional flow area
- D – Diameter
- ρ - density
- v_E – Entrainment velocity
- α_E – Entrainment constant
- u – velocity
- T – Temperature
- R – Radial coordinate
- b_u – Empirically determined constant for radial spread of velocity profile
- b_g - Empirically determined constant for radial spread of buoyancy profile
- β_o - Reference thermal expansion coefficient
- z – Axial Coordinate
- R – Plume radius
- W – Plume Half-width
- s – Downcomer gap size

ACKNOWLEDGEMENT

This work was supported through a U.S. Department of Energy Contract (DE- FC07-04ID14550) and the Oregon State University sabbatical program. This work was conducted through the IAEA Nuclear Power Technology Development Section.

REFERENCES

- [1] LOOMIS, G.G, SODA, K., Results of the Semiscale MOD-2A Natural Circulation Experiments, U. S. Nuclear Regulatory Commission, NUREG/CR-2335 (1982).
- [2] THEOFANOUS, T.G, NOURBAKHSH, H.P., GHERSON, P., IYER, K., Decay of Buoyancy Driven Stratified Layers with Applications to Pressurized Thermal Shock (PTS), U.S. Nuclear Regulatory Commission, NUREG/CR-3700, May 1984.
- [3] REYES, J.N., JR., A transition criterion for the onset of slugging or mixing in horizontal conduits, experimental heat transfer, fluid mechanics, and thermodynamics 2001, Eddizioni ETS Pisa Italy, Volume II-1477 (2001).
- [4] FANNING, M.W. and ROTHE, P.H., *Transient Cooldown in Model Cold Leg and Downcomer; Electric Power Research Institute*, Interim Report EPRI NP-3118, May 1983.
- [5] VALENZUELA, J.A., DOLAN, F.X., Thermal and Fluid Mixing in a 1/2 –Scale Test Facility, U.S. Nuclear Regulatory Commission, NUREG/CR-3426, September 1985.
- [6] THEOFANOUS, T.G, IYER, K., NOURBAKHSH, H.P., GHERSON, P., Buoyancy effects of overcooling transients calculated for the NRC pressurized thermal shock study, driven stratified layers with applications to pressurized thermal shock (PTS), U.S. Nuclear Regulatory Commission, NUREG/CR-3702, May 1986.
- [7] ROUSE, H., YIH, C.S. and HUMPHREYS, H.W., Gravitational convection from a boundary source, *Tellus*, Vol. 4, pp. 201–210 (1952).
- [8] BATCHELOR, G.K., Heat convection and buoyancy effects in fluids, *Quarterly Journal of the Royal Meteorological Society*, Vol. 80, pp. 339–358 (1954).
- [9] MORTON, B.R., Forced plumes, *Journal of Fluid Mechanics*, Vol. 5, pp. 151–163 (1959).
- [10] TURNER, J.S., Buoyancy effects in fluids, Cambridge University Press, Cambridge (1979).
- [11] MORTON, B.R., TAYLOR SIR G. and TURNER, J.S., Turbulent gravitational convection from maintained and instantaneous sources, *Proceedings of the Royal Society*, A 234, pp. 1–23 (1956).
- [12] FOERTHAMANN, E., Turbulent jet expansion, English Translation, A.C.A. TM-789, (Original paper in German, 1934, Ing. Archiv., 5) 1934. (Reproduced by N.P. Cheremisinoff, Editor, Dynamics of Single-Fluid Flows and Mixing, *Encyclopedia of Fluid Mechanics*, Vol. 2, Gulf Publishing Company, Houston (1986).
- [13] CHEN, C.J., and RODI, W., *Vertical Turbulent Buoyant Jets- A Review of Experimental Data*, *HMT*, Vol. 4, Pergamon Press, New York (1980).
- [14] RODI, W., *Turbulent Buoyant Jets and Plumes*, *HMT*, Vol. 6, Pergamon Press, New York (1982).
- [15] THEOPANOUS, T.G., ANGELINI, S, and YAN, H., Universal Treatment of Plumes and Stresses for Pressurized Thermal Shock Evaluations, U.S. Nuclear Regulatory Commission, NUREG/CR-5854, June 1982.
- [16] KOTSOVINOS, N.E., Plane turbulent buoyant jets, Ph.D. Thesis, California Institute of Technology (1975).
- [17] TUOMISTO, H., and P. MUSTONEN. Thermal Mixing Tests in a Semiannular Downcomer with Interacting Flows from Cold Legs, U.S. Nuclear Regulatory Commission, NUREG/IA-0004, October 1986.
- [18] IYER, K. NOURBAKHSH, H.P. and THEOFANOUS, T.G., REMIX: A computer program for temperature transients due to high pressure injection after interruption of natural circulation, Purdue University, U.S. Nuclear Regulatory Commission, NUREG/CR-3701, May 1986.

ANNEX 16

EXAMPLES OF NATURAL CIRCULATION IN PHWR

D. Saha

Reactor Engineering Division,
Bhabha Atomic Research Centre, India

Abstract

The main objective of this lecture is to provide deep insight into the complex natural circulation phenomena in the core of a Pressurised Heavy Water Reactor. A detailed account of natural circulation tests conducted in an Indian PHWR is given in this lecture. This will enable the participants to appreciate the importance of natural circulation in a nuclear reactor to a greater extent.

1. INTRODUCTION

Natural circulation can take place in a nuclear reactor under following circumstances:

- a) As design intent
- b) Under accidental condition
- c) Under planned experimental programme

Experiments have been conducted in very few nuclear power reactors; NAPS-1, the Indian Pressurised Heavy Water Reactor (PHWR), and Dodewaard, the Boiling Water Reactor of Holland, now decommissioned, are among them. Rated power of Narora Atomic Power Station (NAPS-1) is 235 MWe and for Dodewaard it was 50 MWe.

In the following sections experiments on natural circulation conducted in NAPS-1 are described. Natural circulation phenomenon is quite complex in a PHWR because of following features.

- 1) In PHWR core is horizontal leading to horizontal flow path in core. In this case, it is difficult to predict direction of flow when started from stationary condition.
- 2) Different rows of channels are at different elevations leading to difference in driving force.
- 3) Hydraulic resistance of flow path is large because of the presence of long inlet and outlet feeder pipes and long fuel channels.

2. DESCRIPTION OF THE REACTOR

The Indian Pressurised Heavy Water Reactors (PHWRs) are dependent on thermosyphon in the primary coolant loop for decay heat removal from core following power failure and reactor trip. Figure 1 shows a simplified flow diagram of the Primary Heat Transport System (PHTS) of a PHWR. It comprises of two passes of the coolant past the fuel. Flow direction in one pass is just opposite the flow direction in other pass. The coolant passes through coolant channels in half-core 1, steam generator 1, pump 1, coolant channel in half-core 2, steam generator 2, pump 2, and back to coolant channels in half core 1. This path of the coolant shown by arrows in Fig. 1 is known as a figure-of-eight loop. In a 235 MWe PHWR, in each core pass there are 153 horizontal fuel channels located at different elevations inside the calandria vessel. Each channel is connected by an inlet and an outlet feeder pipes to large diameter inlet and outlet headers. Large diameter piping connects the headers to the steam generators (SGs) and pumps. Two SGs and two pumps are connected in parallel between a Reactor Outlet Header (ROH) and a Reactor Inlet header (RIH). The SGs comprise of large number of vertical inverted U-tubes through which the hot heavy water flows. The SG is of the natural circulation type with light water as the secondary coolant. The top of the SG U-tubes are located at about 16 m above the headers and the headers are located about 7 m above the core centre line. The total difference between the top of the U tube and the centre of the core is 23 m. The density difference between hot and cold legs in this height provides the buoyancy force for natural circulation. Figure 2 shows core configuration.

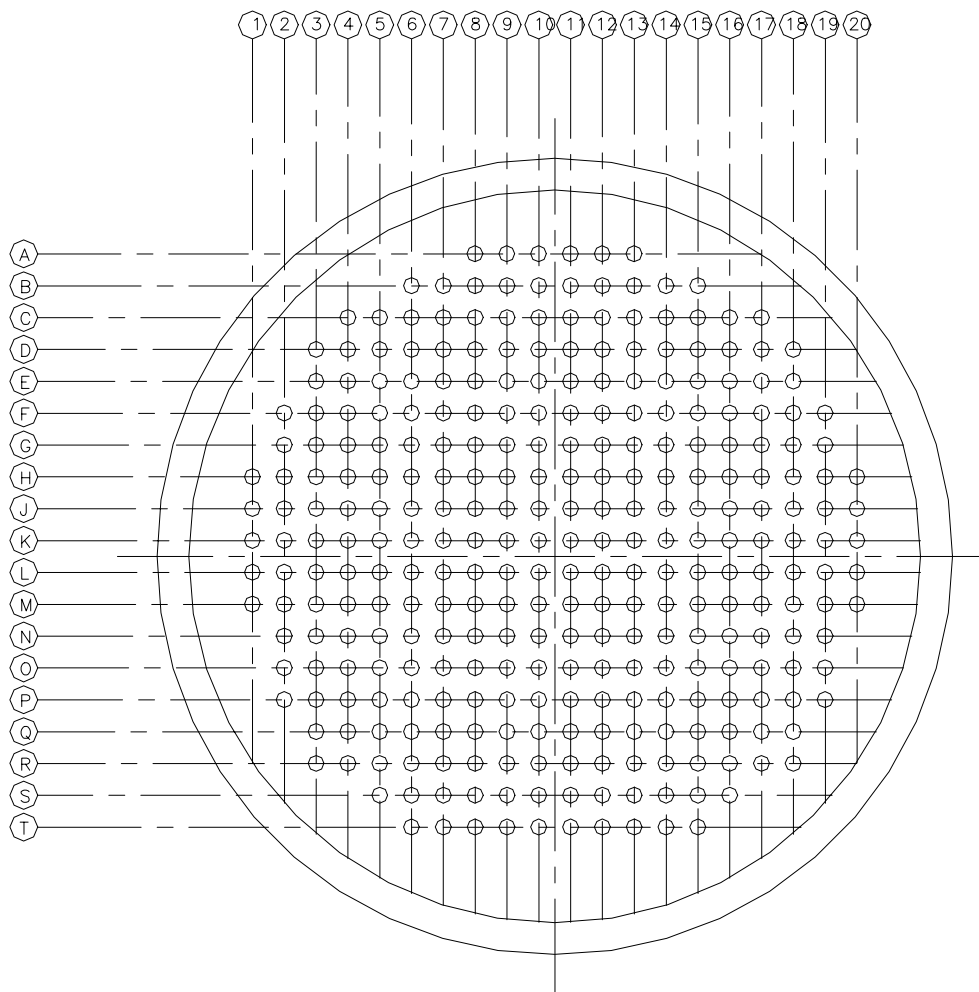


FIG. 2. Core configuration.

4.1. Initial conditions

For all the tests, the secondary side of the SGs was maintained at about 14.6 bar with the help of the Atmospheric Steam Discharge Valves (ASDV). The SG level was maintained at around 12.9 m with the help of the Auxiliary Boiler Feed Pump (ABFP). On the primary side, the pressure was maintained at about 86 bar. The initial conditions of flow and temperature on the primary side were somewhat different for the three tests. For the 0.956% FP and 1.991% FP tests, two primary heat transport system (PHTS) pumps were running (1-1 mode of pump operation). Since the boiler branches with the idle pumps were isolated, the heat removal was accomplished by only two SGs in the 0.956% FP tests. For the 1.991% FP tests, the boiler branches having idle pumps were not isolated and heat removal was by all the four SGs. The flow in the SGs on the idle pump branches was in the reverse direction to start with. For the tests at 3.249% FP, the initial PHTS flow rate, pressure and temperature corresponded to those of steady state thermosyphon at 1.991% FP.

5. TEST PROCEDURES

Tests at 0.956% and 1.991% FP were initiated by switching off the PHTS pumps. The test at 3.249% FP was initiated by increasing the power from 1.991% FP to 3.249% FP when the reactor was thermosyphoning at 1.991% FP. During the tests, the PHTS pressure was maintained with the help of the fuelling machine supply pump.

5.1. Measurements made

The important parameters recorded during the tests are:

1. Channel flows and differential temperatures for 16 channels
2. SG differential temperatures, pressure and level for all the four SGs
3. Differential pressure across each RIH and the corresponding ROH
4. PHTS pressure
5. Neutron power and
6. Channel outlet temperature for all the channels

During the tests, the transient variation of channel flows, outlet temperatures and SG were monitored till the steady state was achieved.

6. RESULTS AND DISCUSSIONS

A complete description of the test results is given in Ref. [3]. The channel delta-T transients are plotted in Fig. 3. Typical transient behaviour, representative of most of the channels is shown by channel S-8 (Fig. 3). The delta-T reaches a peak value before a steady state with minor oscillations is reached. The peak and the steady state values of most of the channels are quite close to each other. The time of occurrence of the peak varies from 250 to 380 seconds for the different channels.

The delta-T behaviour of channels N-13 and Q-16, shown in Fig. 3, need special mention. In channel N-13, the delta-T increased as expected upto a time of about 265 seconds and then suddenly started reducing at a very fast rate and went out of the chart range of the visicorder at about 325 seconds. Just before going out of the range of the chart the delta T indication was about -16.1°C . i.e., 16.1°C delta-T with flow reversal. The delta-T variation of channel Q-16, on the other hand, shows a peak (approx. 54.7°C) at about 340 seconds and then suddenly reduces to about -25.7°C with flow reversal at about 480 seconds. Subsequently, the delta -T decreases and flow direction changes again to the original and the delta-T stabilizes at about 21.4°C . Thus flow reversal has taken place twice in this channel and hence the initial and final steady directions in the channel are the same leading to positive delta-T before and after the flow reversals. Channel flow reversals, during transient thermosyphoning, have been reported for CANDU systems [4]. However, instances of a majority of the channels in one half-core flowing in the forward direction with a few flowing in the reverse direction under steady state conditions are not reported for these systems. None of the monitored channel delta-Ts showed negative values for the 1.991% and 3.249% FP tests indicating the absence of flow reversal.

From the measurements obtained from the channel temperature monitoring system, the individual channel outlet temperatures of rows having the same flow direction are plotted in Fig. 4. Since the channels at the bottom of the calandria have a larger elevation difference compared to the top channels, the flows in lower channels are expected to be more than those in the top channels. This would indicate lower outlet temperatures for the bottom channels as compared to the corresponding top channels generating the same power. This trend is generally observed for the tests at 1.991% and 3.249% FP (see Fig. 4). This is all the more significant since the bottom channels generate more power (approx. 10% for fresh core) than the corresponding top channels in the same column.

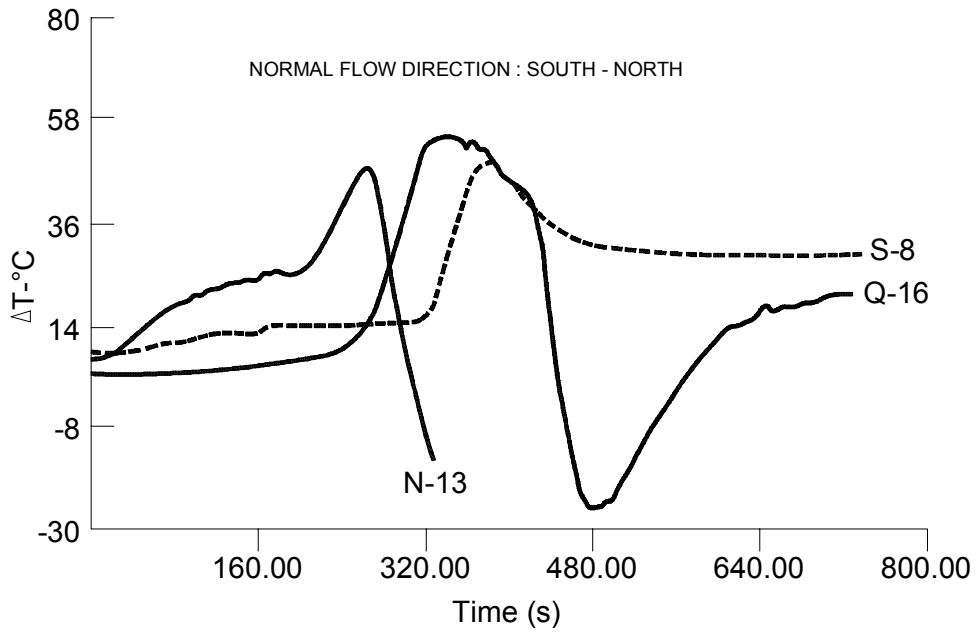


FIG. 3. Channel ΔT variation at 0.956%FP.

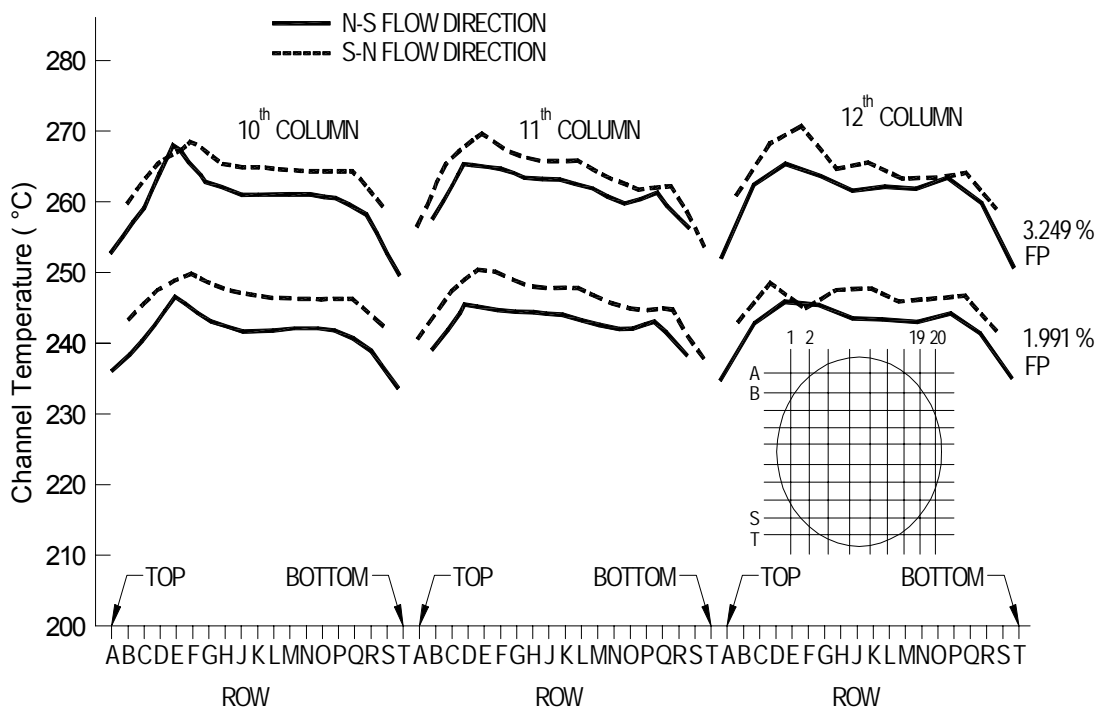


FIG. 4. Channel outlet temperature variation across different vertical columns for tests at 1.991 and 3.249% FP.

7. METHOD OF ANALYSIS

Analysis for test conditions was carried out using the computer code TINFLO-III, which solves the one-dimensional momentum and energy equations using the finite difference method. Flow coastdown phase is modeled based on the test data on pump speed vs. time. Steam Generator secondary side is modeled by a single volume. Initial temperature of the SG secondary is specified as input and the primary temperatures are calculated by the code.

The code lumps all parallel flow paths in the half-core into one equivalent flow path. Therefore the code can predict only the average core behaviour and not the individual channel behaviour. Further details of the code and the solution procedure are given in Vijayan et al (1988) [2].

8. COMPARISON OF EXPERIMENTAL AND ANALYTICAL RESULTS

The observed and predicted transient and steady state behaviour are described and discussed below.

8.1. Channel flows

Figures 5 and 6 show the predicted and measured variation of normalized flow, with time, for the tests at 0.956% FP and 1.991%FP respectively. The normalization of flow is with respect to the flow corresponding to 2-2 operation mode. In both the tests, a very good match is obtained between the predicted and measured flows during the initial coastdown phase (upto 60 seconds). Beyond this, the prediction and the test value, though showing somewhat similar trends, differ widely in magnitude. This difference is attributed to the large measurement inaccuracy of the normal plant instrumentation at these low flows (less than 10% of the full flow). The steady state core flow rates estimated based on heat balance from the measured SG delta-T and reactor power are also plotted in these figures. It may be noted that these are very close to those predicted by the code.

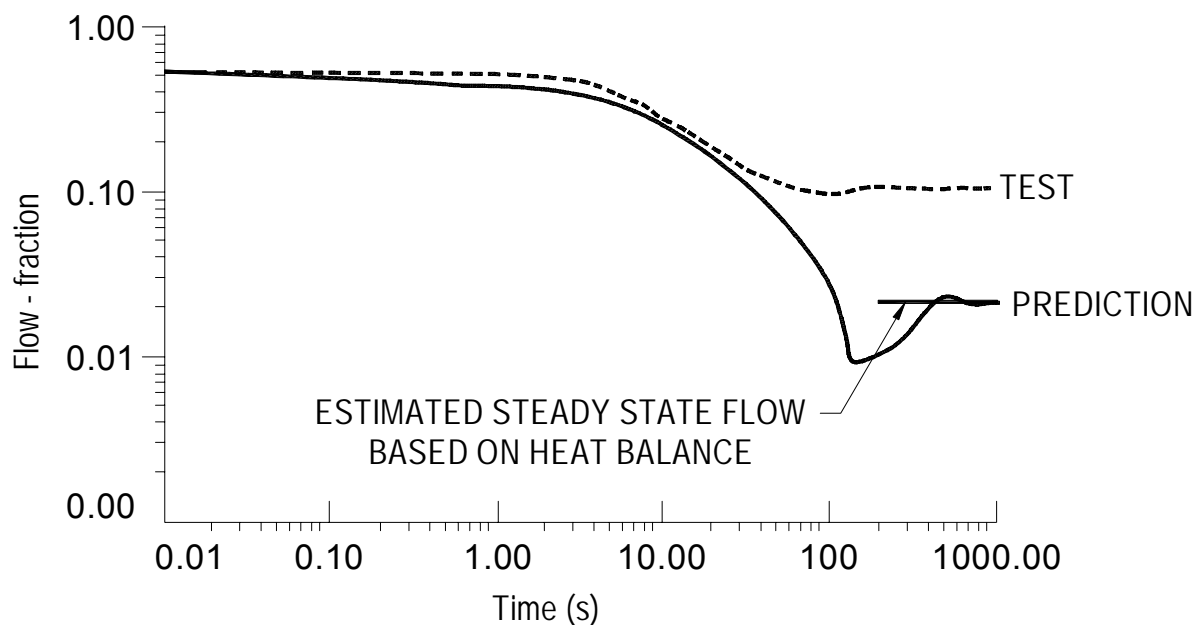


FIG. 5. Variation of flow with time for test at 0.956%FP.

8.2. Header to header pressure drop

Figure 7 shows the measured and predicted variation of header-to-header pressure drop from tests at 1.991% FP. The prediction and the measurements show the same trend. However, there is a time lag between the predicted and measured minimum and peak pressure drops.

At time $t=0$ the delta-P indications are off-scale since these delta-P indicators have a range of only -50 cm to $+250$ cm and the delta-P is much higher than this (13000 cm) when the primary pumps are operating. The first indication of header delta-P is obtained at about 30 to 40 seconds after the pumps are switched off.

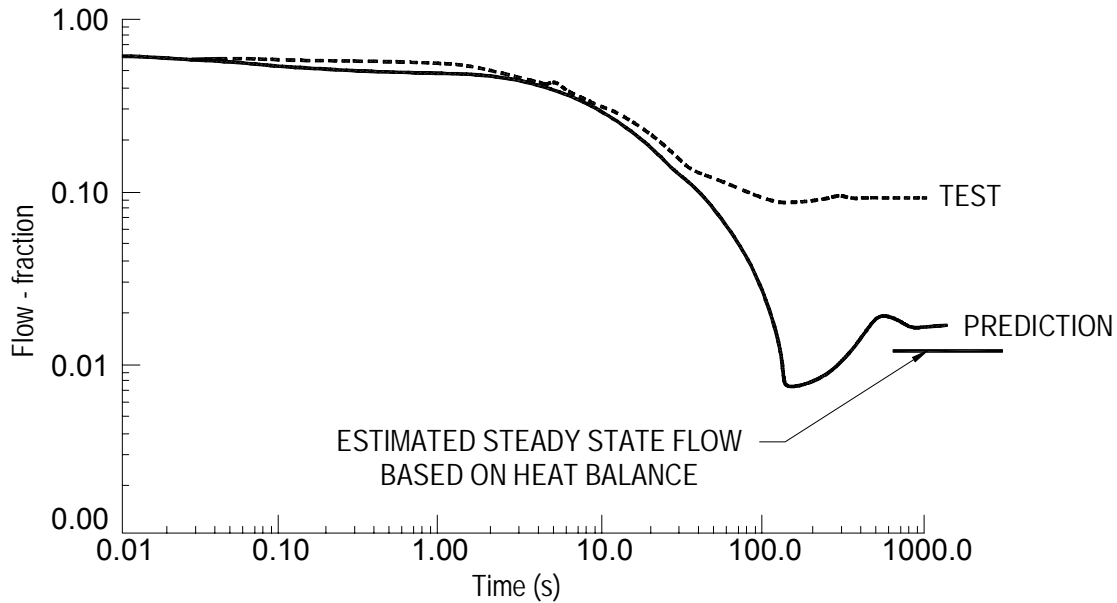


FIG. 6. Variation of flow rate for test at 1.991%FP.

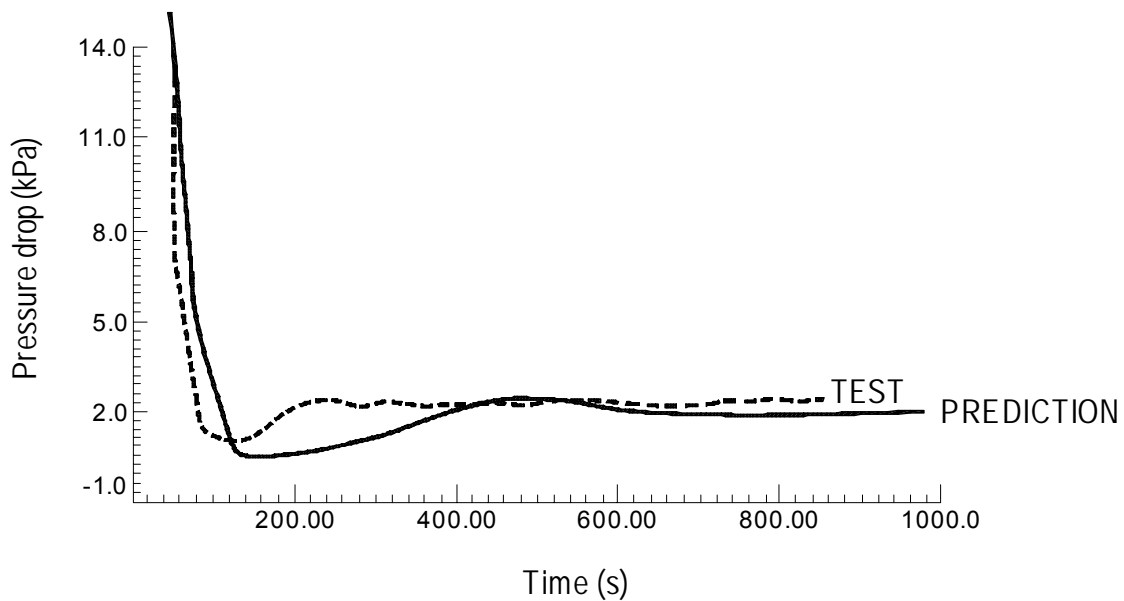


FIG. 7. Variation of header to header delta-P for test at 1.991%FP.

8.3. Channel delta-T variation

Figures 8 and 9 show the measured and predicted channel delta-T variations for the tests at 0.956% and 1.991% FP respectively. The experimental curve is the mean of the seven channel delta-Ts. The measured and predicted delta-Ts show the same trend. Although the agreement between the measured and predicted steady state values is quite good, the predicted peak value is much larger (about 30%) than that measured. The experimental peak value is observed to be lower than the predicted peak due to following reasons. The different channels have different feeder lengths and are located at different elevations and therefore individual peaks having different values occur at different times. On averaging these delta-Ts, a smaller peak value is obtained. However, in the analysis all the channels in one half core are lumped into one equivalent channel having one length and one elevation. There is a time lag between the peak values predicted and obtained during these tests. This is again attributed to the difference in the lengths of various feeder pipes in the reactor, whereas the prediction is based on an equivalent feeder of average length. Improvement of prediction with regard to this aspect can be obtained by avoiding the lumping of all the parallel channels in a half core. However, this will involve increase in computational effort.

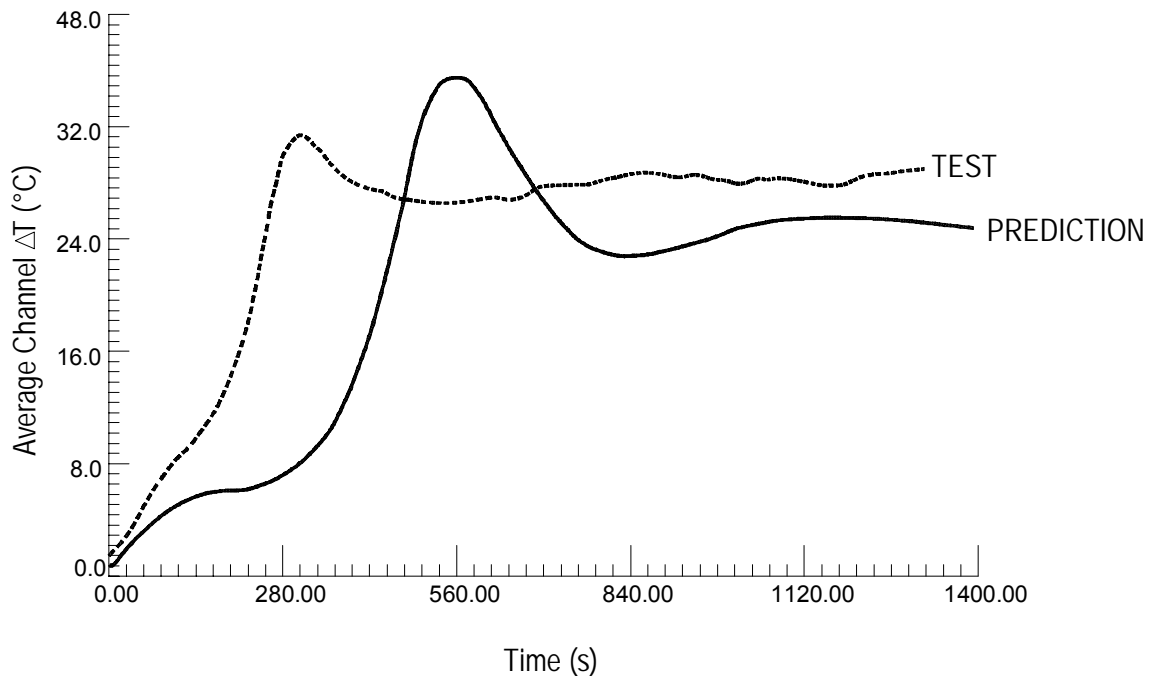


FIG. 8. Variation of average channel delta-T for test at 0.956%FP.

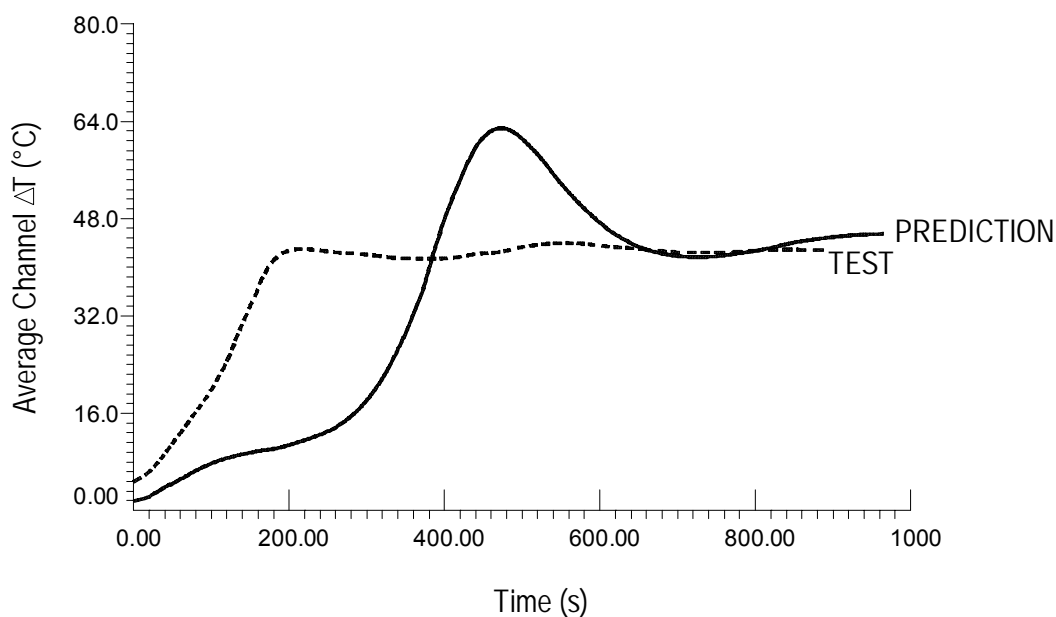


FIG. 9. Variation of average channel delta-T for test at 1.991%FP.

9. CONCLUSIONS

1. The tests conducted in unit-1 of NAPS have confirmed the efficacy of natural circulation core cooling at decay power levels following failure of forced circulation of the primary coolant.
2. An interesting observation from the tests is that flow reversal occurred in some channels during the test at 0.956% FP, with only two steam generators valved in.
3. The channel elevation plays a significant role in determining the flow rate through the different channels.
4. The most interesting aspect of the NAPS-1 experimental programme is the fact that the same unit of the same power station could be saved because of natural circulation core cooling in the face of an accident. A few years after the experiments, the unit faced a prolonged station blackout. Even class-1 power supply was not available. Fire fighting water was injected by diesel pumps into the secondary side of steam generator. Steam pressure was maintained in the secondary side using the ASDVs. The main function of removal and transportation of heat from core to SG was achieved by natural circulation very efficiently and the unit could be saved.

ACKNOWLEDGEMENTS

The author wishes to thank IAEA and its consultants for the valuable suggestions provided. Thanks are also due to Mr. D.S.Pilkhwal and Mr. Vikas Jain of RED, BARC for the help rendered in preparing this note.

REFERENCES

- [1] VIJAYAN, P.K., DATE, A.W., Experimental and theoretical investigations on the steady state and transient behaviour of a thermosyphon with through flow in a figure-of eight loop, *Int. J. Heat Mass Transfer*, Vol.33.pp.2479–2489 (1990).
- [2] VIJAYAN, P.K., NAGDAUNE, R.K., VENKAT RAJ, V., Analysis of Flow Coast Down and transition to thermosyphon Cooling in the PHT system of a PHWR following Power Failure, *Proceedings of the Indo-Polish Seminar on Development of Advanced Codes and Methods for Transient and Accident Analysis of Nuclear Power plants*, pp 10.1–10.26, B.A.R.C. Bombay (1988).
- [3] VIJAYAN, P.K., VENKAT RAJ, V., PILKHWAL, D.S., Thermosyphon Tests conducted on Unit – 1 of Narora Atomic Power Station, BARC Internal Report (1991).
- [4] CAPLAN, M.Z., GULSHANI, P., HOLMES, R.W., WRIGHT, A.C.D., Flow behaviour in a CANDU Horizontal Fuel Channel from stagnant subcooled initial conditions, *Experimental and Modeling Aspects of Small break LOCA*, *Proceedings of Specialists' meeting organized by the IAEA, Budapest, Hungary* (1983).

ANNEX 17

SELECTED EXAMPLES OF NATURAL CIRCULATION FOR SMALL BREAK LOCA AND SOME SEVERE ACCIDENTS

N. Aksan

Paul Scherrer Institute, Switzerland

Abstract

In all Light Water Reactors (LWRs), natural circulation is an important passive heat removal system. The March 1979 accident at TMI-2 brought into question the capability of natural circulation cooling to remove core decay heat, especially during accident situations. Because natural circulation is expected to be an essential core heat rejection mechanism during certain kinds of accidents or transients in a PWR (e.g., small break LOCAs or operational transients involving loss of pumped circulation), a thorough understanding of natural circulation processes and factors that influence the natural circulation response of the reactor system is necessary. In this paper, natural circulation and related major phenomena are discussed with examples for small break LOCA and severe accident cases, e.g., TMLB station black-out. Descriptions of three modes of natural circulation are provided: Single-phase natural circulation, two-phase natural circulation, and reflux condensation/boiling condensation. The basic phenomena associated with the three types of natural circulation being considered for severe accidents are also addressed: In-vessel natural circulation, hot leg countercurrent flow, coolant loop flows.

1. INTRODUCTION

The natural circulation cooling is an essential means of removing shutdown decay heat in PWRs following the loss of forced circulation by the reactor coolant pumps (RCPs) during operational transients or following accidents. The loss of forced circulation may result from the loss of offsite power, pump failure, or operator action based on operating procedures for abnormal conditions. Natural circulation in PWRs refers to primary coolant flow within the loops of a closed primary system. Natural circulation flow is driven by differences in the average coolant density within the primary system. These density differences result from the heating of the reactor coolant in the core and the subsequent cooling of the reactor coolant in the steam generators, which are elevated relative to the core, resulting in a loop gravitational driving force. This paper will concentrate on PWRs having plant designs utilizing U-tube steam generators and it will provide overview on the importance of natural circulation for small break LOCA and severe accident cases with emphasize on natural circulation phenomena.

The paper provides a short overview on small break LOCA issue (section 2) as well as looking at the small break LOCA scenario and related main phenomena (section 3). Natural circulation and its importance are addressed in section 4. Severe accident scenario in PWRs leading to natural circulation is described in section 5. Section 6 describes and shows the importance of natural circulation during severe accidents. The final section includes concluding remarks. A list of references is given for further reading and information basis.

2. ORIGIN OF SMALL BREAK LOCA ISSUE (SYSTEM THERMAL HYDRAULICS BEFORE AND AFTER TMI-2)

In early 1970's, former U.S. Atomic Energy Commission convened a public hearing to explore the safety question in relation to the effectiveness of systems to mitigate the consequences of a loss of coolant accident in a nuclear reactor, in case it happens. Ultimately, after extensive public hearings, in 1974, the interim regulations were modified to provide a set of specific requirements for computer codes for ECCS analyses in Appendix K and a new section, 10 CFR 50.46 [1], requiring ECCS meet established standards. This included a definition that LOCAs are hypothetical accidents that would result from the loss of reactor coolant, at a rate in excess of the capability of the reactor coolant makeup system, from breaks in pipes in the reactor coolant pressure boundary up to and including break equivalent in size to the double-ended rupture of the largest pipe in the reactor coolant system. The safety criteria prescribed in 10 CFR 50.46 are applicable to both large and small break LOCAs.

That is to say the limits on peak cladding temperature, cladding oxidation and hydrogen generation must not be exceeded in a design basis accident. Calculations of ECCS performance using the conservative prescriptions of Appendix K resulted in the large break LOCA generally being the most limiting accident. At the time, there was a major safety research program to support code development for large break LOCA and also some limited work on small break LOCA.

The March 1979 accident at the Three Mile Island Unit 2 (TMI-2) reactor led to an extensive reorientation of light water reactor safety research programs and also regulatory changes. The TMI-2 accident was a small break LOCA, an event given significantly less attention because of the major emphasis on the large break LOCA at the time. Consequent to TMI-2, small break LOCA and plant operational transients received major attention. The experimental simulation of the natural circulation phenomena in the primary loops, including those in the two-phase stratified and counter-current flow regimes, is of primary importance to the thermalhydraulic response of a nuclear power plant during such transients. Since these phenomena are significantly dependent on facility scale, and geometry, large-scale tests for a primary system geometry representative of operational nuclear power plants are required. Either operational facilities were modified to carry out small break LOCA experiments or there were new facilities designed and constructed. It is to be noted that unlike the large break LOCA, the sequence of events following a small break LOCA can evolve in a variety of ways. Operator actions, reactor design, ECCS set points, break size and location will have a bearing how the small break LOCA scenario unfolds. Therefore in order to predict the integral system behaviour during a small break LOCA, a best estimate code must have sufficient modelling capabilities to take these factors into account. These codes are also needed to be assessed against integral system tests. After having been successfully assessed against data from a large number of scaled test facilities, best estimate codes become the ultimate repository of all previous thermal hydraulic safety research.

3. SMALL BREAK LOCA SCENARIO IN A PWR WITH RELEVANCE TO NUCLEAR REACTOR SAFETY AND MAIN PHENOMENA

The major characteristic difference between a small break and a large break LOCA are in the rates of coolant discharge and pressure variations with time. A typical PWR system and elevations are illustrated schematically in Figure 1. In general, small break LOCA's are characterized by an extended period (this can be tens of minutes to several hours at the lower end of the break spectrum) after the occurrence of the break, during which the primary system remains at a relatively high pressure and the core remains covered (Figure 2). As soon as the pumps are tripped, either automatically or manually, gravity controlled phase separation occurs and gravitational forces dominate the flow and distribution of coolant inside the primary system (Figure 3). The subsequent sequence of events, whether or not the core uncovers and is recovered or reflooded, depends not only on the location, shape and size of the break, but also on the over-all behaviour of the primary and secondary systems. This behaviour is strongly influenced by both automatic and operator initiated mitigation measures. In general, the reactor system response to a small break is slower compared to events after a large break. This allows more time, and different possibilities, for operator interventions. Another principal difference is the domination of gravity effects in small breaks versus inertial effects in the large breaks.

Breaks can occur in a number of ways, i.e., pump seal failure, steam generator tube failure, power-operated relief valve (PORV), automatic depressurisation system (ADS), or safety valves sticking open, and instrument-tube failure, in addition to simple pipe break or leaks. The PORV and ADS may be activated intentionally to reduce pressure and/or remove energy. The location of the break may be such as to enhance or reduce the loop flow rate due to natural circulation alone.

It is to be noted that there is no unique path of development of events following a small break LOCA in PWRs. The scenarios may change drastically by many factors such as the reactor design (e.g. U-tube or once-through steam generators, such as TMI-2), the break size, the size core bypass (allowing some fraction of the inlet cold leg flow directly into the core upper structure without passing through the core), and most importantly, by different operator interactions. As an example, the primary circulation pumps may be shut down early in a small break LOCA transient or they may be allowed to run and circulate the coolant through the core for a long time. These alternative actions can make a

large difference in the nature of discharge flow, early heat removal from the core, and the liquid inventory in the system after one hour or so in the transient.

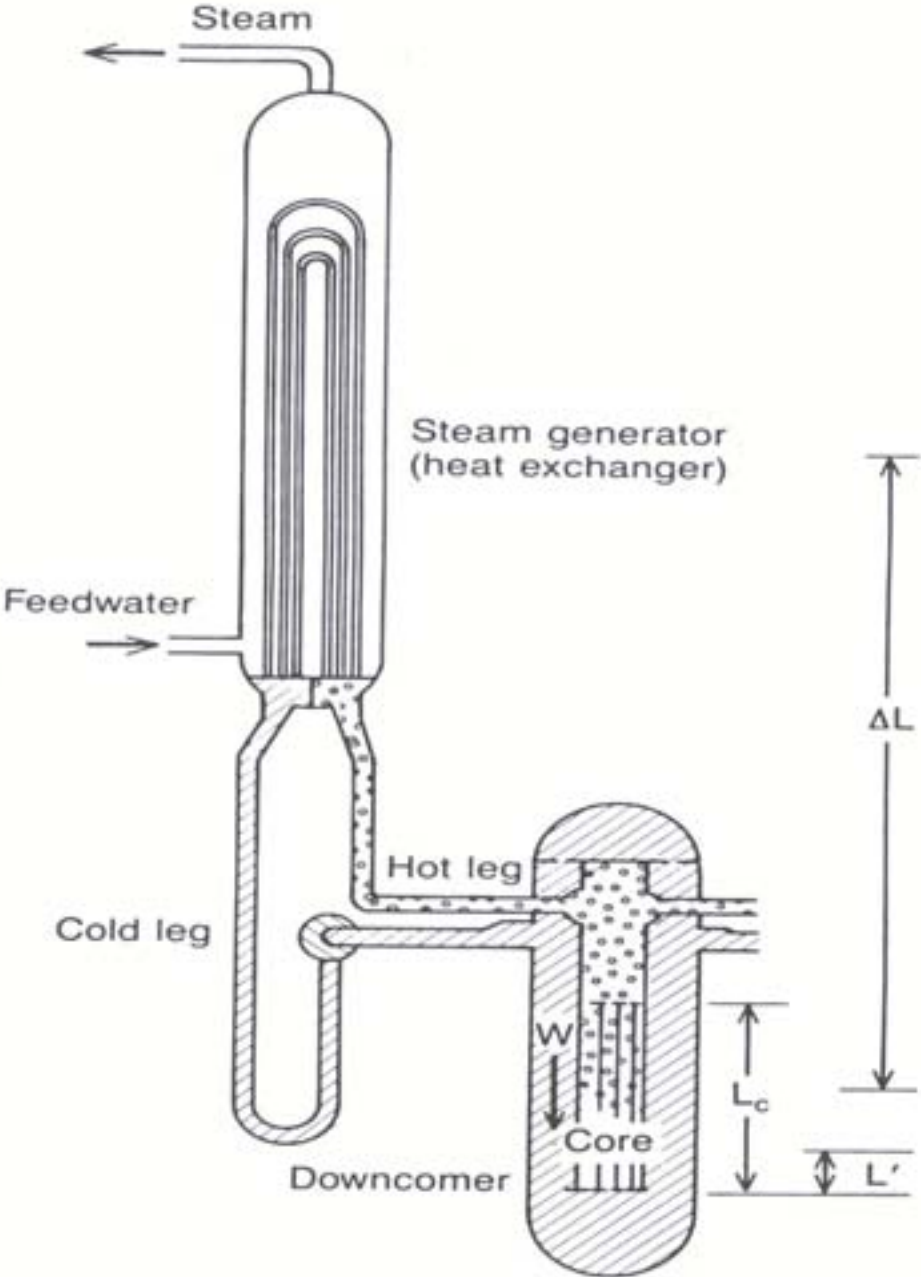


FIG.1. Schematic of a typical PWR system and elevations.

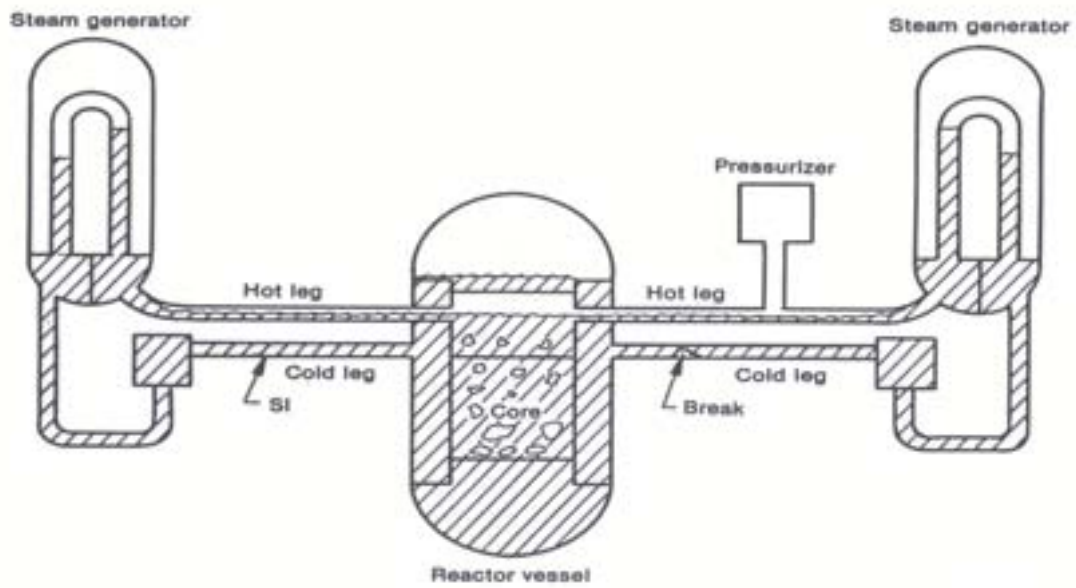


FIG. 2. Formation of a continuous vapor phase at the top of the steam generator U-tube and vessel during a small break LOCA in PWR..

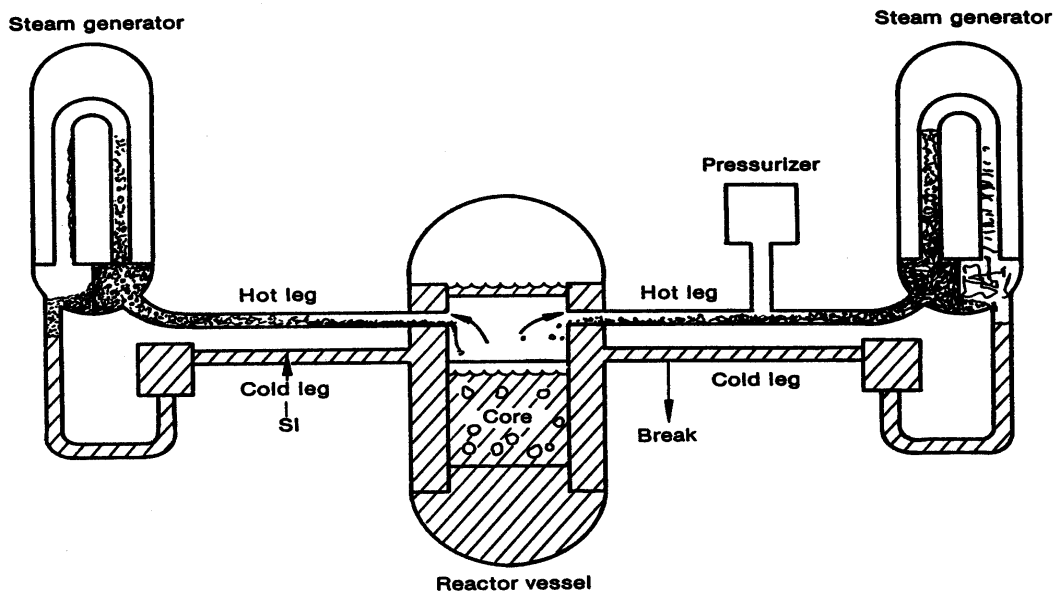


FIG. 3. Initiation of core uncover during a small break LOCA in PWR..

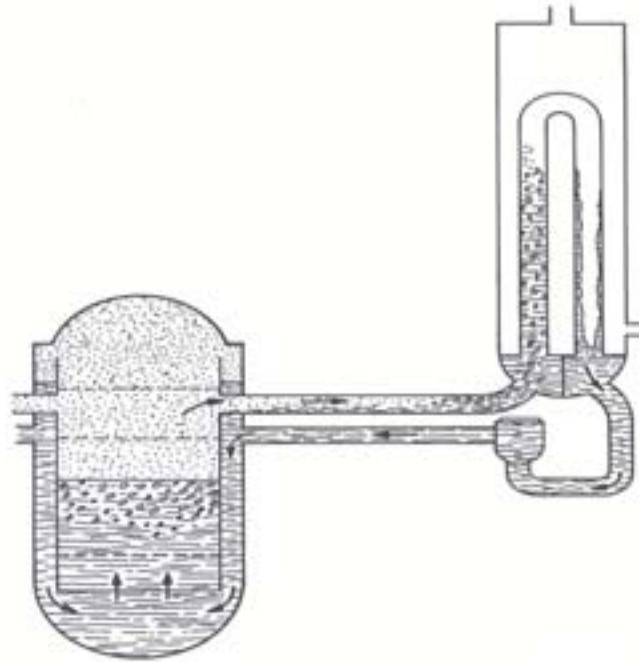


FIG. 4. Liquid inventory trapped outside of the reactor vessel due to a loop seal.

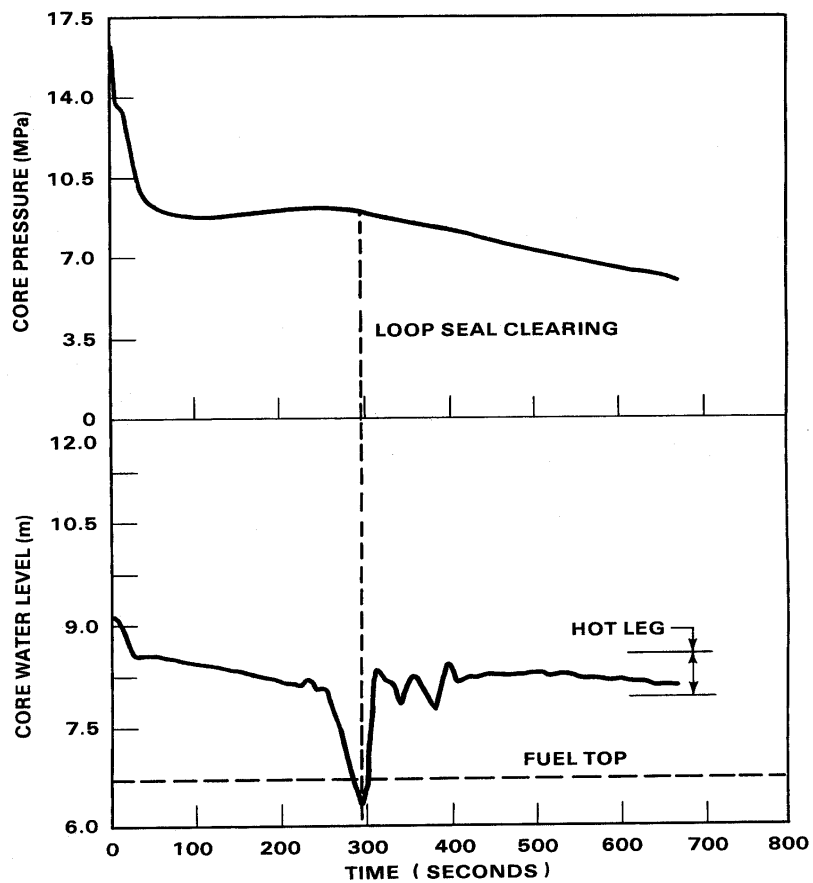


FIG. 5. Typical transients of the primary system pressure and reactor vessel water level following a small break LOCA at the cold leg in a PWR.

Another important possibility of different interactions is through the steam generators. The secondary side of steam generators can be isolated (no feed water flow) or they can be used for a controlled heat removal. It is also possible to cool the reactor through the so-called “feed-and-bleed” process (on the primary side). Either of these actions will have a major effect on the course of the transient. It is not the intent in this section to provide a catalogue of all possible scenarios following small break LOCA accidents. But it is important to note that an adequate set of modelling capabilities for any of the plausible scenarios will be equally adequate for all other scenarios. This is because the phenomena and processes are the same but their interactions and timing of various developments changes in different operations. Therefore in order to predict the integral system behaviour during a small break LOCA, a best-estimate code must have sufficient modelling capabilities to take these factors into account.

During a PWR small break LOCA, there is the potential for three distinct core heat ups. A typical transient history for primary system pressure and reactor vessel water level following a small break LOCA at the cold leg in a PWR is shown in Figure 5. The first heat up is caused by loop seal formation and the manometric core liquid level depression (Figure 4). Naturally occurring events including loop seal clearing and break uncovering mitigate this heat up. The second heat up occurs following the core quench caused by loop seal clearing and is caused by a simple core boil-off. During this period the primary pressure is decreasing to the accumulator set point and the steam produced by the core boil-off leaves the system via the break. Any heat ups that occur during this period are mitigated by the reflood from the accumulator water. The third possible heat up can occur following depletion of the accumulator tanks and before LPIS injection begins. One drawback to the reflood process accompanying the accumulator injection is a decrease in the ongoing depressurisation process such that another possible heat up occurs before the LPIS primary pressure set points are reached and long-term cooling is provided. Various factors affect the magnitudes of the three potential core heat ups. Some examples are break size, break direction and location, availability of HPIS, and the degree of upper head to downcomer bypass flow. Although the magnitudes of the core heat ups may vary, ECCS performance must be such that the criteria, e.g., 10. CFR 50.46 [1] is not exceeded. The interested readers can obtain further details on small break LOCA in reference [2].

4. NATURAL CIRCULATION AND ITS IMPORTANCE DURING SB LOCA

The March 1979 accident at TMI-2 brought into question the capability of natural circulation cooling to remove core decay heat, especially during accident situations. Because natural circulation is expected to be an essential core heat rejection mechanism during certain kinds of accidents or transients in a PWR (e.g., small break LOCAs or operational transients involving loss of pumped circulation), a thorough understanding of natural circulation processes and factors that influence the natural circulation response of the reactor system is necessary. Characterization of the natural circulation cooling processes requires:

- Identifying conditions under which natural circulation will occur,
- Determining the effectiveness of natural circulation in removing core decay heat and recovering the plant (i.e., what are natural circulation cooling limitations)
- Identifying how changing plant conditions affect natural circulation cooling.

Natural circulation will occur in a PWR primary loop (in the absence of pumped flow) whenever buoyant forces caused by differences in loop fluid densities are sufficient to overcome the flow resistance of loop components (steam generators, primary coolant pumps, etc.). The fluid density differences occur as a result of heating fluid in the core region (causing the liquid become less dense) and cooling fluid in the steam generators (causing the fluid to become more dense).

The buoyant forces resulting from those density differences cause fluid to circulate through the primary loops, providing a means of removing the core decay heat. Depending on the primary loop fluid inventory, natural circulation consists of three distinct modes of cooling [3]:

- Single-phase
- Two-phase (liquid continuous)
- Reflux condensation (or boiler-condenser mode for once-through steam generators)

Progression from the single-phase mode through the two-phase and reflux condensation modes occurs as primary system liquid inventory decreases (Figure 6). Natural circulation flow in PWRs is driven by temperature induced density gradients, enhanced by a thermal center elevation difference between the hot (core) and cold (steam generator) regions in the primary loop. This density gradient produces a buoyancy effect that drives the natural circulation flow. Thus, single-phase natural circulation is the flow of an essentially subcooled primary liquid driven by liquid density differences within the primary loop. Two-phase natural circulation is normally defined as the continuous flow of fluid and vapor. In this mode of natural circulation, vapor generated in the core enters the hot leg and flows along with the saturated liquid to the steam generator, where at least some of the vapor is condensed. Hence, density gradients are affected in two-phase mode not only by temperature differences, but also mainly by the voids in the primary loop. In both single-phase and two-phase natural circulation, the mass flow rate is the most important heat removal parameter. In contrary, during reflux condensation, the loop mass flow rate has a negligible effect because the primary mechanism of heat removal is vapor condensation. In the reflux condensation mode, single-phase vapor generated in the core flows through the hot leg piping, is condensed in the steam generator, and flows back to the core as a liquid. In summary, the three modes of natural circulation are distinguishable based upon characteristic mass flow rates, loop temperature difference behavior, and basic phenomenological differences.

The dominant heat transfer mechanism in single-phase natural circulation cooling is convection, making the loop flow rate the most important parameter governing heat removal. Heat generated by the core is convected away from the reactor vessel through the hot leg to steam generators (heat sink) via the subcooled primary liquid. Heat is transferred from the primary side to the secondary side in the steam generator. The cooling cycle is completed when the cooled primary fluid flows back to the reactor vessel. The amount of heat removed from the core through single-phase natural circulation cooling is normally the amount produced by decay heat power levels (about 5% core power).

Since the study of natural circulation cooling in PWR systems became of interest, work on the characterization of natural circulation has been focused in several areas, including effects of both primary and secondary liquid inventory and distribution on natural circulation effectiveness, the stability of the various natural circulation modes and transitions between modes as well as the possibilities of natural circulation flow interruption due to instabilities, countercurrent-flow limiting in the hot leg [4] and steam generator tubes, and the effects of noncondensables on natural circulation process. With respect to the primary side liquid inventory issue, natural circulation will provide decay heat removal at significantly reduced primary side inventory. The concern here is identifying the minimum primary side liquid inventory at which natural circulation will continue to provide adequate cooling of the core. Similarly, the steam generator secondary will continue to be a heat sink for the primary a significantly reduced secondary liquid inventories. Again, the concern is identifying the minimum secondary inventory that will ensure continued natural circulation flow in the primary loop. An additional concern with respect to the secondary inventory is the instabilities in primary side natural circulation flow caused by severely reduced secondary side liquid levels. These secondary side induced flow instabilities could reduce the effectiveness of natural circulation cooling.

Generally, the stability of the different modes of natural circulation cooling, as well as the stability of transients between the modes, is of concern because natural circulation will be the primary mechanism for core decay heat rejection for certain kinds of PWR accidents or transients [5], and instabilities in natural circulation process could lead to an interruption of natural circulation flow with a corresponding reduction in the removal of core decay heat. Thus an understanding of factors that influence the onset of flow instabilities as well as the effects of the instabilities on decay heat removal is necessary.

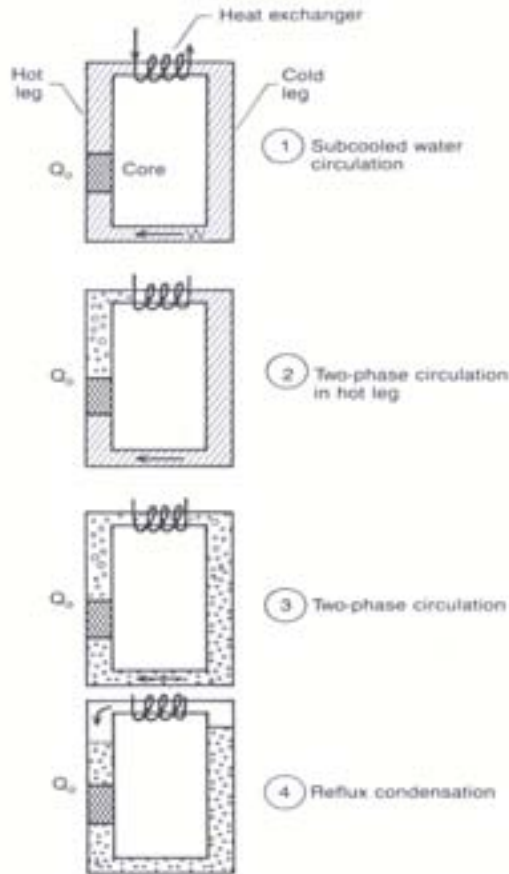


FIG. 6. Different modes of natural circulation cooling in a PWR..

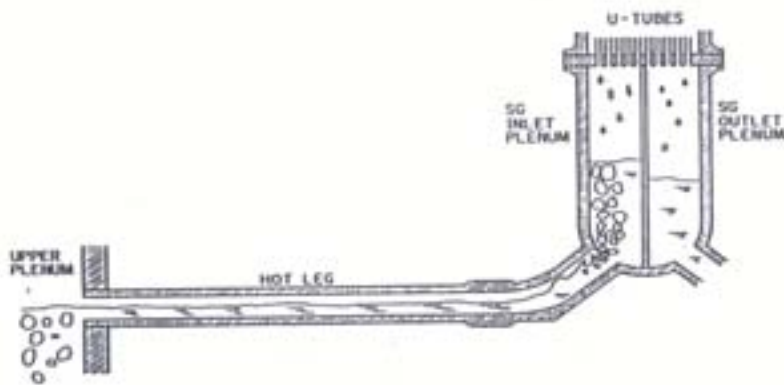


FIG. 7. Schematic of liquid distribution during reflux condensation in PWRs.

The presence of noncondensable gas in the primary side of a steam generator operating in the two-phase or reflux condensation mode of natural circulation is of concern because the gas may have a large effect on the condensation process occurring in the steam generator. The noncondensable gas in the steam generator tubes can cause a redistribution of the condensation locations as well as influence the amount of liquid being carried to the down side of the U-tubes. Thus the potential exists for the noncondensable gas to have a considerable influence on the natural circulation process. The presence of noncondensables in the primary loop may impede or even stagnate the natural circulation flow,

thereby significantly reducing or terminating the heat removal capability of the steam generators both for single-phase and two-phase natural circulation cooling. Noncondensable gases can be introduced into the primary system through safety injection and by fuel degradation. As examples, hydrogen from the pressurizer vapor space, air dissolved in the refueling water, and nitrogen from accumulators (once they are depleted of water), are several sources of noncondensable gases. In addition, helium may enter the primary flow system if breaching of cladding occurs. Research has concentrated on determining whether noncondensables will migrate to and collect in the upper elevations of the primary loop. There, they may interrupt the natural circulation flow and jeopardize the effectiveness of single-phase and two-phase natural circulation cooling.

In PWRs with U-tube SGs, reflux condensation occurs when single-phase vapor generated in the core flows through the hot leg piping to the SGs, and is condensed in both the upflow and downflow sides of the steam generator U-tubes. Condensate in the upflow sides of the steam generator U-tubes drains back to the hot leg and eventually back to the vessel along the bottom of the hot leg. A countercurrent flow of liquid and vapor exists in the upflow sides of the steam generator U-tubes and in the hot leg. Condensate in the downflow sides flows into the cold leg pump suction piping cocurrently with any uncondensed steam. The reflux condensation process is shown in Figure 7. During reflux condensation, primary to secondary heat transfer is accomplished through vapor condensation in SGs. This heat transfer is very effective due to the high latent heat associated with condensation. Consequently, removal of decay heat from the core during reflux condensation does not require large mass flow rates or large primary to secondary temperature differences. Small mass flow rates and primary to secondary temperature differences are characteristic of the reflux condensation mode of natural circulation. The experiments carried in the PKL test facility [6], which simulates PWR plant with U-tube steam generators, shows the major modes of energy transport observed in this facility for natural circulation cooling, as already discussed above (Figure 8).

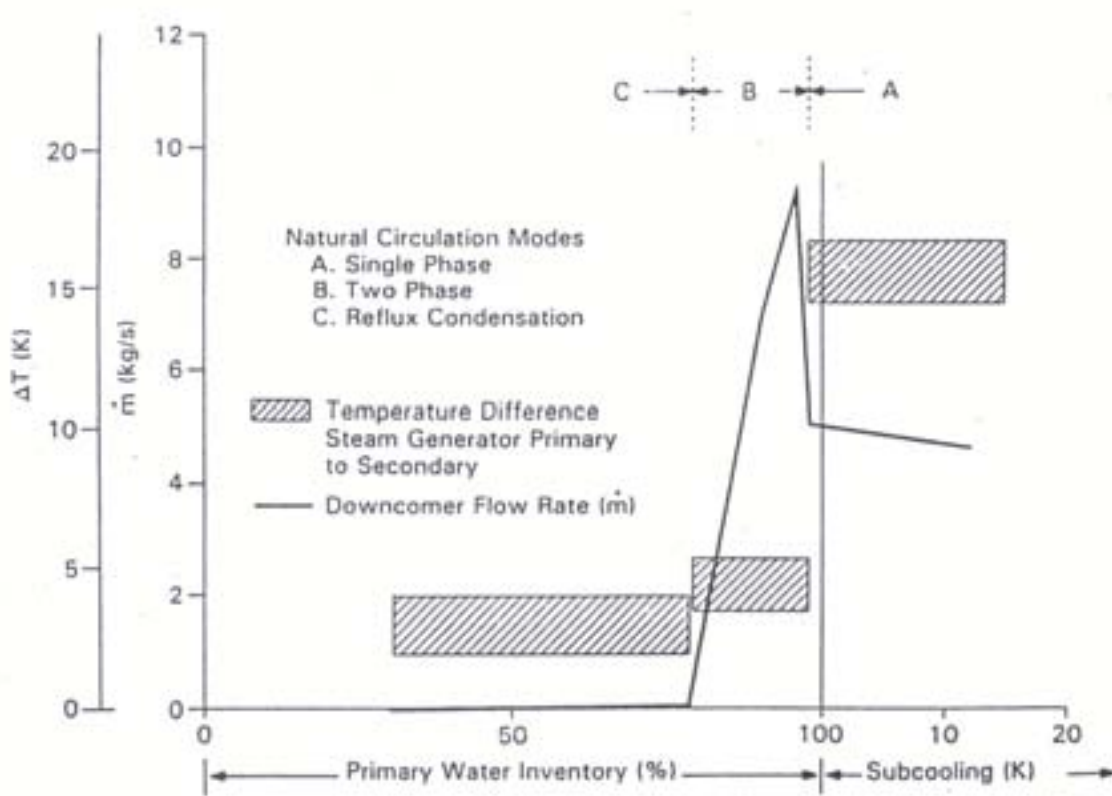


FIG. 8. Mass flow rates and primary to secondary temperature differences as functions of primary mass inventory for PKL test facility.

5. SHORT DESCRIPTION OF SEVERE ACCIDENT SCENARIO IN PWR LEADING TO NATURAL CIRCULATION

There are innumerable accident sequences that lead to core damage, but not all of them can or will result in natural circulation playing an important role in the accident progression [7]. Those, in which natural circulation will be significant, do have several characteristics in common.

The reactor coolant pumps can not be running, because forced flow through the reactor coolant system (RCS) will preclude the existence of natural circulation flows. Along a similar line of thought, there should be no pumped emergency core coolant injection. While the initial injection of liquid may increase the natural circulation flow because there is now more steam being generated in the core, the temperature of the steam exiting the core will decrease as the core continues to be cooled. The decreasing temperature will result in a reduced temperature difference between hot and cooler vapor, thereby reducing the driving potential for natural circulation flows. Heat transfer from the now hotter structures in the RCS to the cooler steam leaving the core will also tend to reduce the natural circulation flow. Additionally, the presence of pumped injection flow likely means that the accident is being terminated, so that further core damage will not occur.

There should be no large breaks in the system. For example, opening of the safety relief valves (SRV) or PORVs on the pressurizer draws enough flow through the surge line that hot leg countercurrent flow disrupted, although in vessel circulation is not. Small enough breaks will still allow natural circulation flows to exist in the reactor vessel and the hot legs. For example, pump seal leaks are not large enough to preclude hot leg natural circulation flows.

As examples, two transients that would result in significant natural circulation flows are designated the TMLB and S₂D sequences. The TMLB sequence refers to a transient in which all AC power is lost and no steam-driven auxiliary feedwater is supplied to the steam generators. The TMLB' station blackout sequence has traditionally been used in severe accident natural circulation studies. The steam generators receive no feedwater, there is no AC power available for the duration of the accident, and the core undergoes a high-pressure boil-off with relief valves cycling. If reactor coolant pump seal leaks are considered, the RCS pressure will depend on the size of the leaks. The pressure may still be controlled by the relief valves, or it may approach and fall below the accumulator pressure. As the core uncovered, heat is transferred from the fuel to the metal mass of the primary coolant system through a process of natural circulation. Superheated steam and hydrogen carries heat to structures, including the upper reactor vessel, the hot leg, inlet plenum of the SGs, and the SG tubes. In this specific scenario, the loop seals remain filled with water and full loop circulation blocked. A countercurrent natural circulation is expected during this phase of accident (Figure 7). The S₂D sequence is a small break LOCA with no high-pressure coolant injection. This transient will result in a core boil-off somewhere above the accumulator pressure, with the RCS pressure depending on the size of the break.

6. DESCRIPTION AND IMPORTANCE OF NATURAL CIRCULATION DURING SEVERE ACCIDENTS

Three natural circulation flows can be important during severe accidents:

- In-vessel natural circulation,
- Hot leg countercurrent flow,
- Flow through the coolant loops.

Figure 9 illustrates these flows. Each of these flows may be present during high-pressure boil-off transients such as the TMLB sequence mentioned in above section 5.

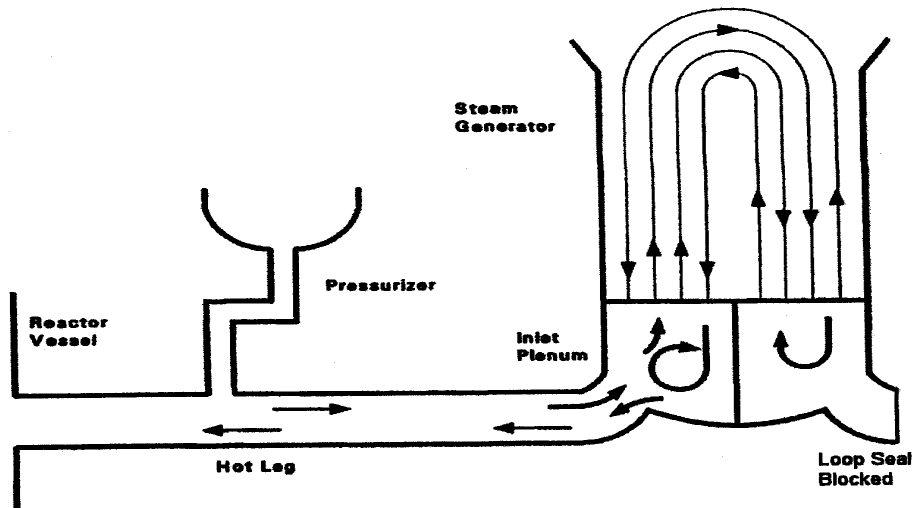


FIG. 9. Overview of natural circulation flow pattern in a hot leg of a PWR during severe accident conditions.

The primary effect of the natural circulation flows is to redistribute the energy being generated in the core. This energy redistribution will slow the heat-up of the core, which in turn may affect the damage progression or the extent of the core damage. Slowing the core damage would allow more time for systems to be recovered to mitigate or terminate the accident. However, the energy removed from the core will affect the structures in which it is deposited, in both the upper plenum and the coolant loops. The discussions below address the basic phenomena associated with the three types of natural circulation being considered, together with how the transient progression may be affected by the coolant flow. In addition, the importance of natural circulation flows will also be addressed in summary form.

6.1. In-vessel natural circulation

In-vessel natural circulation begins when the core heat-up begins. Because the center part of the core is at a higher power than the periphery, the super-heated steam there is hotter and less dense, and a radial density gradient is established. The denser vapour in the outer part of the core tends to flow toward the centre, replacing the hot vapor that rises into the upper plenum. This vapor plume rises to the top of the upper plenum, where it is turned radially outward to the core barrel, and then flows back down toward the top of the core. Heat transfer to the structures in the upper plenum cools the vapor, reinforcing the density gradient between the center of the vessel and periphery. The cooler steam reenters the core through the top of the peripheral fuel assemblies. As core uncovering continues and the liquid level drops, the recirculating flow extends farther down into the core. Depending on the axial power profile, the flow may eventually extend to the bottom of the core. The density gradient in the upper plenum also establishes a recirculating flow within the upper plenum. In reality, many natural circulation cells will probably be established in the core, especially during the core damage portion of the transient. These cells will exist between fuel assemblies, between parts of fuel assemblies, and even between subchannels. Wherever a radial temperature gradient exists, a natural convection flow may be established. The rapid increases in local temperature associated with the accelerated oxidation of zircaloy fuel rod cladding, at a temperature about 1850 K, will in particular result in the establishment of these relatively small natural circulation cells. These smaller flow cells are assumed to exist within larger overall natural convection cells involving the entire core. It is these core-wide patterns that are being investigated, because it is the global core behavior that is of interest, not the individual fuel rods or assemblies.

The in-vessel natural circulation flow may affect the cladding oxidation. Because steam is being recirculated from the upper plenum back into the core, it is less likely that the oxidation reaction will become steam-starved. The slower cladding heat-up caused by the removal of some of the core energy to the upper plenum structures, combined with steam reach environment, may result in more extensive oxidation of the cladding at lower temperatures. This in turn may lead to smaller amounts of unoxidized zircaloy melting as the temperature increases, which could delay relocation of molten material and cause less dissolution of the fuel pellets.

Increased heating of the upper plenum structures resulting from the natural circulation flow could also lead to their oxidation or melting. This could add to the hydrogen generated in the RCS before vessel failure, and could add more material to the melt that flows from the vessel at the time of lower head failure. Higher vapor temperatures in the upper plenum will also make hotter vapor available to the hot legs. Flow through the hot leg and surge line to the pressurizer PORVs will heat the piping. If the pipe temperatures are high enough, creep rupture failure of these pipes may become a concern. Failure of the RCS piping before the vessel fails could allow the system to depressurize, initiating accumulator injection. If the depressurization continues far and fast enough, the RCS pressure at the time of vessel failure can be low enough to preclude direct containment heating.

6.2. Hot leg countercurrent flow

Single-phase countercurrent flow in the hot leg is significant in PWRs with U-tube steam generators, because these participate in the natural circulation flow and heat transfer. Natural circulation flow pattern in a hot leg of a PWR during severe accident conditions is shown in Figure 9. Superheated vapor enters the top of the hot leg, displacing saturated vapor, which then flows back to the reactor vessel along the bottom of the hot leg. When the hotter vapor enters the steam generator inlet plenum, it will rise toward the steam generator tubes. Vapor enters some of the tubes, displacing the cooler steam that was in the tubes. The displaced vapor enters the outlet plenum, then reenters other steam generator tubes, forcing vapor into the inlet plenum. A density gradient is thus established between tubes. This density gradient then pulls hotter vapor into the tubes, displacing additional cooler steam. The process continues until a steady flow is established, with hot vapor flowing from the inlet plenum to the outlet plenum through some of the steam generator tubes, and cooler vapor returning to the inlet plenum through the remaining tubes.

Mixing in the steam generator plenum is a controlling phenomenon for the hot leg natural circulation flow. It limits the mass flow in the hot leg by increasing the temperature (and lowering the density) of the vapor returning from the steam generator along the bottom of the hot leg. It limits the heat transfer in the steam generator by reducing the temperature of the hot vapor entering the tubes. While accurate modelling of the mixing is important in providing realistic simulation of the hot leg flow behavior, neglecting the mixing in the steam generator inlet plenum in the analyses will yield steam temperature tube temperatures and hot leg mass flow rates that are higher than would be expected.

Hot leg countercurrent flow can affect the structural integrity of the RCS piping. Heating of the pipes and steam generator tubes may lead to melting and creep rupture failure of those components. Steam generator tubes are very thin compared to the loop or surge line piping, and can be quickly heated if exposed to high temperature vapor. Should the tubes fail, a direct path outside of containment (through the steam line relief valves) becomes available to any fission products carried in the coolant. While flow through pressurizer relief valves in some transients will draw hot vapor into the hot leg and surge line, the countercurrent flow may accelerate the heating and possible failure of these pipes. For lower pressure transients in which relief valves are not open, the hot leg countercurrent flow may result in hot leg piping failures that would not otherwise be expected to occur.

Fission product behavior may also be affected by the flow to the steam generators. An extremely large surface area is available on the steam generator tubes for deposition of fission products. If the tubes remain cool, deposited species may remain there and not be released from the RCS. If the tubes continue heat-up so that revolatilization occurs, the flow may simply carry the resuspended fission products to cooler parts of the tubes, where they would again be deposited. The mixing in the steam

generator inlet plenum may also play a part in the fission product behavior. The countercurrent flow in the hot leg itself may also affect the fission product transport. If gravitational settling is an important mechanism for fission product deposition in the hot leg, fission products falling from the flow that is heading toward the steam generators would enter the return vapor stream, where they would be carried back toward the reactor vessel, rather than away from it.

6.3. Coolant loop flow

If the loop seals clear of liquid during a transient with the reactor coolant pumps off and the steam generators removing heat from the RCS, loop natural circulation would be reestablished. In contrast to the natural circulation that occurs following the reactor coolant pump coast down early in a transient, the fluid flowing through the coolant loops would now be superheated vapor. Loop natural circulation flow is a buoyancy-driven one-dimensional flow with heat addition in the core and heat rejection primarily in the steam generators. However, in this situation heat would be transferred to the piping through out the coolant loops. Because of the resulting large vapor density differences and the height of the steam generator, this flow is generally large enough that it disrupts any multidimensional natural circulation flows that might exist in the hot leg or reactor vessel.

The high flow rate and large amount of metal structures available as heat sinks result in a much slower core heat up. The slower heat up rate could result in complete oxidation of the cladding before any of the zircaloy melts. Fuel rod relocation would be delayed for several hours. Failure of the piping anywhere in the RCS is possible, although the steam generator tubes would be particularly susceptible because they are much thinner than the hot or cold legs, as already mentioned in section 6.2. Heating of all the piping will also tend to reduce the extent of fission product retention in the RCS.

6.4. Importance of natural circulation flows

The significance of natural circulation flow in severe accidents is that it transfers energy from the core to the other regions of RCS. This energy transfer both slows the core heat-up, delaying fuel damage, and increases the temperature of structures elsewhere in the RCS (upper plenum, hot leg and surge line piping, SG tubes, etc.) so they may get hot enough to melt or fail.

Slowing the core heat-up provides additional time for system recovery or operator actions, either of which could terminate the transient by returning the core to a covered, cooled state. The core heat-up rate also affects the composition of the molten core. A slower core heat-up allows more complete oxidation of the fuel rod cladding in place, so that the melt contains mostly ceramic materials. A thick oxide shell builds up in the cladding, preventing relocation until ceramic melting temperatures are reached. A rapid core heat-up allows cladding melt and relocation much earlier, as molten zircaloy dissolves the thinner oxide shell. The relocation material in this case contains more metallic cladding, which can still be oxidized in either the molten pool or in containment through core/concrete interaction.

If the upper plenum structures melt, their mass is added to the core debris that may eventually reach the lower head. If the RCS piping gets hot enough to fail, either through melting or creep rupture, a breach of the RCS pressure boundary results that would allow the system to blow down to the containment. This could significantly alter the containment response at the time of vessel melt-through, in that the dispersion of molten core material is minimized if there is no pressure difference between the RCS and the containment (no DCH). Natural circulation flows may result in unintentional depressurization of the RCS by causing failures of the surge line or hot leg. If the failure location is the steam generator tubes, a containment bypass is established. Fission products released from the fuel can flow through the failed tubes to the secondary side of the SG, and from there through atmospheric dump valves or safety relief valves to the environment, bypassing the containment.

7. CONCLUDING REMARKS

Natural circulation plays an important role in the accident progression during small break LOCA. Single-phase natural circulation is generally an effective and dependable means for removing decay heat in PWRs. Nonuniform flow, noncondensable gases, and secondary side conditions can significantly influence the single-phase mode of natural circulation. Although it can be much more complex than single-phase natural circulation, the two-phase natural circulation can provide an adequate method for removing decay heat from the core. Two-phase flow is more tolerant for noncondensable gases than is single-phase natural circulation. But the effects of noncondensable gases can still significantly influence two-phase natural circulation cooling effectiveness. The reflux condensation is also very efficient way of heat removal mechanism.

In all modes of natural circulation, the heat sink must remain active. The effects of noncondensable gases, secondary side conditions, and nonuniform flow behavior do affect, to a certain degree, the different modes of natural circulation.

Natural circulation in severe accidents redistributes energy from the core to structures in the upper plenum and coolant loops. This energy transfer not only slows the heat-up of the core, it also contributes to potential failure of the RCS piping. Such a failure, if it happens early enough in the transient, may allow the RCS sufficient time to depressurize before lower head failure that high-pressure melt ejection will not occur, minimizing the effects of direct containment heating (DCH).

Information from separate effects tests and integral test facilities [8], operating plant data and analysis have made significant contributions to the knowledge base concerning natural circulation cooling in PWRs. Many important natural circulation phenomena have been identified through these studies. It is extremely important that the commonly used thermal-hydraulic system codes together with the CFD computer codes (used for detailed specific phenomena, e.g., mixing and natural circulation at the inlet and outlet of U-tube steam generators, etc.) are able to simulate natural circulation during transients and accidents, because they will be relied upon to predict full-scale plant behavior.

NOMENCLATURE

AC	Alternate Current
ADS	Automatic Depressurization System
CFD	Computational Fluid Dynamics
DCH	Direct Containment Heating
ECCS	Emergency Core Cooling System
HPIS	High Pressure Injection System
LOCA	Loss Of Coolant Accident
LPIS	Low Pressure Injection System
LWR	Light Water Reactor
PORV	Power Operated Relief Valve
PWR	Pressurized Water Reactor
RCP	Reactor Coolant Pump
RCS	Reactor Coolant System
S ₂ D	Small Break LOCA with no HPIS
SG	Steam Generator
TMI-2	Three Mile Island Unit 2
TMLB	Station Blackout Sequence

REFERENCES

- [1] 10 CFR 50.46, Acceptance Criteria for Emergency Core Cooling Systems for Light Water Cooled Nuclear Power Reactors, and Appendix K, (ECCS Evaluation Models”, to 10 CFR Part 50, U.S. Code of Federal Register, Vol. 39, No.3, January 4, 1974.
- [2] OECD/NEA, Thermal-hydraulic of Emergency Core Cooling in Light Water Reactors, A State-of-the-Art Report by a Group of Experts of the NEA Committee on the Safety of Nuclear Installations, CSNI Report no. 161, Paris (F), October 1989.
- [3] DUFFEY, R.B., and SURSOCK, J.P., Natural Circulation Phenomena Relevant to Small Breaks and Transients, Proceedings of Specialists Meeting on Small Break LOCA Analysis in LWRs, Vol. 1, Pisa, Italy, 23–27 June 1985.
- [4] NAGUAB LEE “Limiting Countercurrent Flow Phenomenon in Small Break LOCA Transients”, Proceedings of Specialists Meeting on Small Break LOCA Analysis in LWRs, Vol. 1, Pisa, Italy, 23–27 June 1985.
- [5] ZVIRIN, Y., A Review of Natural Circulation Loops in Pressurized Water Reactors and Other Systems, Nuclear Engineering and Design 67, pp. 203–225 (1981).
- [6] WEISSHAUPL, H. and BRAND, B., “PKL Small Break Tests and Energy Transport Mechanisms”, Proceedings of the ANS Specialists Meeting on Small Break Loss-of-Coolant Accident Analyses in LWRs, Monterey, California; August 25–27, 1981.
- [7] BAYLESS, P.D. et.al., Severe Accident Natural Circulation Studies at the INEL, NUREG/CR-6285, February 1995.
- [8] AKSAN, N., The CSNI Separate Effects Test and Integral Test Facility Matrices for Validation of Best-estimate Thermal-hydraulic computer codes, Lecture to be presented at the IAEA Course on Natural Circulation in Water Cooled Nuclear Power Plants (Paper ID. T16), International Centre for Theoretical Physics (ICTP), Trieste, Italy, 28 June–2 July, 2004.

ANNEX 18

USE OF NATURAL CIRCULATION FLOW MAP

F. D'Auria, D. Araneo, B. Neykov
University of Pisa, Italy

Abstract

This lecture describes the different loop flow regimes encountered in single-phase and two-phase natural circulation. The database gathered from ten integral system experiments has been used to establish a Natural Circulation Flow Map that can be used to characterize the effectiveness of a natural circulation system.

1. INTRODUCTION

Natural Circulation (NC) is an important mechanism in several industrial systems and the knowledge of its behaviour is of interest to nuclear reactor design, operation and safety. In the nuclear technology, this is especially true for new concepts that largely exploit the gravity forces for the heat removal capability. Natural circulation in a PWR occurs due to the presence of the heat source (core) and the heat sink constituted by the steam generators. In a gravity environment, with core located at a lower elevation than steam generators, driving forces occur that generate flowrate suitable for removing nuclear fission power. At present, the NC core power removal capability is only exploited for accident situations, basically to demonstrate the inherent safety features of the plants.

The NC scenarios occurring at different values of the primary system mass inventories were considered. Data have been gathered and analyzed coming from the PWR simulators Semiscale, Spes, Lobi, Bethsy, Pkl and Lstf [1].

Reference is made to both single phase and two-phase natural circulation. In order to evaluate the NCP of the mentioned facilities, significant information comes from the analysis of the trend of the core inlet mass flowrate and the primary loop mass inventory. The flowrate and the residual masses have been normalised taking into account of the volume of each facility and of the power level (typically n times 1% of the nominal core power, where n ranges between 1 and 5) utilized in the selected experiment. Four main flow patterns were characterized depending upon the value of the mass inventory of the primary loop.

1.1. Single-phase NC (SPNC)

SPNC regime implies no void occurrence in the upper plenum of the system. Therefore, coolant at the core outlet shall be subcooled up to nearly saturated. Core flowrate derives from the balance between driving and resistant forces. Driving forces are the result of fluid density differences occurring between [descending side of U-Tubes & vessel downcomer] and [core & ascending side of U-Tubes]. Resistant forces are due to irreversible friction pressure drops along the entire loop. Resulting fluid velocities are sufficient for removing core power in (subcooled) nucleate boiling or forced convection heat transfer regimes: no film boiling condition is experienced in the core. It may be noted that the secondary side of SG is also a natural circulation system working in two-phase conditions.

SPNC may occur at any primary system pressure, consistently with SG pressure. However, typical primary system pressures range between 8 and 16 MPa with secondary pressure close to the nominal operating condition. It is expected from the NPP design that SPNC, provided the availability of SG cooling, is capable to remove the nuclear heat decay from the core. Experimental database, including NPP tests, confirms this capability.

1.2. Stable two-phase NC (TPNC)

TPNC regime occurs as a consequence of coolant loss from the primary system. Owing to this, both driving and resistant forces increase when decreasing mass inventory of primary system. Assigned the

typical geometrical layout of PWR, the former effect, i.e. increase of driving forces, is prevalent at small decreases of mass inventories. The opposite occurs for larger decreases of mass inventories. The net result is a 'peak' in core mass flowrate versus primary system inventory (when primary mass flowrate decreases), as can be observed in Fig. 1. Forced convection, subcooled and saturated heat transfer regimes occur in the core. Condensation occurs inside the U-Tubes of SG. The average core void fraction is typically less than 30%, whereas at the outlet values around 50% can be reached without occurrence of thermal crisis in the considered pressure range.

1.3. Siphon condensation NC (SCNC)

The decreasing of NC driving forces, the small temperature difference across U-Tubes of steam generators, and the occurrence of the CounterCurrent Flow Limiting Phenomenon (CCFL) at the entrance of U-tubes (e.g. see Ref. [2]), are at the origin of wide system oscillations of core inlet flowrate. The phenomenon has been investigated in [3] and [4], based on a natural circulation experiment performed in Lobi facility [5]. Evidence of the phenomenon has been found also in other facilities.

At mass inventories of the primary system around 70% of the nominal value, the efficiency of the condensation heat transfer across U-Tubes causes the release of almost all core thermal power in the ascending side of U-Tubes. Liquid level builds up and is prevented to drain down by the steam-liquid mixture velocity at the tube entrance, i.e. the CCFL condition occurs. Therefore, liquid level rises in the U-Tubes till reaching the top. During this period, typical duration of the order of 10 s, flowrate at core inlet is close to zero and core boil-off occurs. Once the liquid level reaches the upper bend of U-Tubes, the siphon effect occurs and causes the emptying of the ascending side of U-Tubes and the re-establishment of core inlet flowrate. A new cycle starts. The phenomenon is made more complex by the interaction of the several thousands of U-Tubes that constitute a SG tube bundle. Different groups of tubes may stay at a different stage of the oscillation at the same time, also causing flow reversal in the tube bundle. Suitable core cooling still can be achieved in these conditions.

1.4. Reflux condensation (RCNC)

At 'low' mass inventories of primary coolant and/or at low core power, steam velocities in the upper part of the system including hot legs and steam generator entrance are low. Weak interactions occur at the steam-liquid interface that are not enough to cause CCFL. In these conditions, the liquid that is condensed or entrained in the ascending side of the U-Tubes may flow back to the hot leg and to the core. Stratified countercurrent steam and liquid flow simultaneously in the hot legs. Mass flowrate at core inlet is close to zero, although a 'minor' natural circulation path may establish between core and downcomer inside the vessel. However, upward two-phase mixture and downward liquid flows occur at the core outlet. Core thermal power can be removed by boil-off in the saturated nucleate boiling heat transfer regime.

1.5. Dryout occurrence

The terms 'dryout occurrence' appear in the right part of Fig. 1, when primary system mass inventory is roughly lower than 40% of the nominal value. Dryout is caused by the combination of low flow and high void fraction. As a consequence, film boiling heat transfer regime is experienced with low coefficient for heat transfer. Rod surface temperature increases in various zones of the core and the overall process of thermal power transfer from fuel rods to the fluid may become unstable. The system operation in these conditions is not acceptable from a technological point of view. It may be noted that the temperature excursion is strongly affected by primary system pressure and thermal power levels: the linear rod power plays a role in these conditions. At primary system pressure around 15 MPa (nominal operation for PWR), 'post-dryout' surface temperature jumps may be as low as a few tens of Kelvin, tolerable for the mechanical resistance of the rod-clad material.

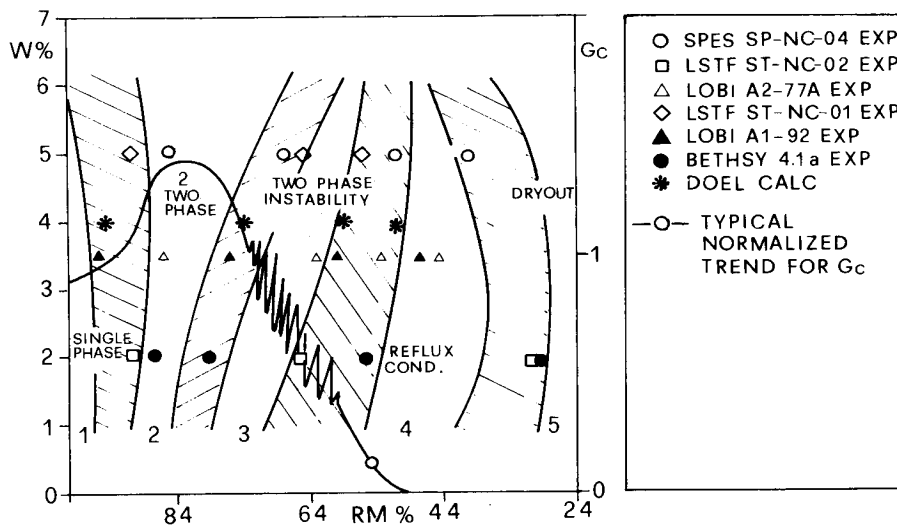


FIG. 1. Characterization of natural circulation flow regimes based on experimental data and system codes calculations.

On the vertical axis we have the n times 1% of the nominal core power, where n ranges between 1 and 5. On the horizontal axis we have the residual mass inventory in the primary circuit

2. THE NATURAL CIRCULATION FLOW MAP

The database gathered from ten experiments performed in the six ITF listed in Tab. 1 has been used in [6] and [7], to establish a Natural Circulation Flow Map.

In all the considered ITF, NC experiments with similar modalities have been performed and the NC regimes discussed in the previous chapter are experienced. The linear power of fuel rod simulators, the fraction of nominal core power and the primary system pressure constitute the main differences for the boundary conditions of the considered experiments. In relation to pressure, PKL experiments have been performed at a pressure value roughly one half the value adopted in the other facilities. The range of design and operational parameters of the ITF (e.g. pipe diameter, system volume, number of steam generators, heat losses to the environment), not explicitly discussed here, and the identified differences are assumed to produce an envelope for any expected NC situation in a typical PWR when decay heat removal is concerned.

Measured values of core inlet flowrate (G , Kg/s), core power (P , MW), primary system fluid mass inventory (RM , Kg) and net volume of the primary system ($V = \text{const.}$, m³), have been used for setting up the NCFM. The diagram G/P versus RM/V has been preferred for the NCFM over other possible choices including non-dimensional quantities.

The experimental database from ITF (six ITF, ten experiments) and the envelope of curves are given in Figs. 2 and 3, respectively. The envelope in Fig. 3 is assumed to constitute the NCFM of PWR at decay core power.

Seven commercial NPP systems and three ITF, not used for setting up the database presented in Fig. 2, for demonstrating the use of the NCFM [7], [8]. Main characteristics of the NPP and of the ITF can be drawn from Tables 2 and 3, respectively.

The geometric layout of primary systems for reactors 1, 2, 5, 6 and 7 is similar to the geometric layout of ITF originating the database for the NCFM. However, differences are present in the relative

elevations between core and SG. Reactors 3 and 4 are equipped with OTSG and HTSG, respectively. So the geometric layout of the primary system is different from the geometric layout of ITF originating the database for NCFM [9].

Table 1. Nominal parameters of the plant

CNA-I Overall Plant Data	
Reactor type	PHWR
Net power station output	~ 345 MWe
Reactor Coolant System and Moderator System	
Total thermal power	1179 MW
Number of fuel channels	253
Active core length	5300 mm
Shape of fuel assembly	37-rod cluster
Reactor Coolant System and Moderator System	
Coolant and moderator	D ₂ O
Total thermal power transferred to the feed water/main steam cycle	1186 MW
Total thermal power transferred to steam generators	1076 MW
Total thermal power transferred to moderator coolers	110 MW
Number of coolant circuits	2
Number of moderator circuits	2
Total coolant circulation flow	6000 kg/s
Total moderator circulation flow	440 kg/s
Pressure at reactor vessel outlet	114 bar
Coolant temperature at reactor pressure vessel	573 K
Average moderator temperature normal/maximum	443 K/ 493 K
Steam pressure at steam generator outlet	4.4 MPa
Total steam flow	510 kg/s

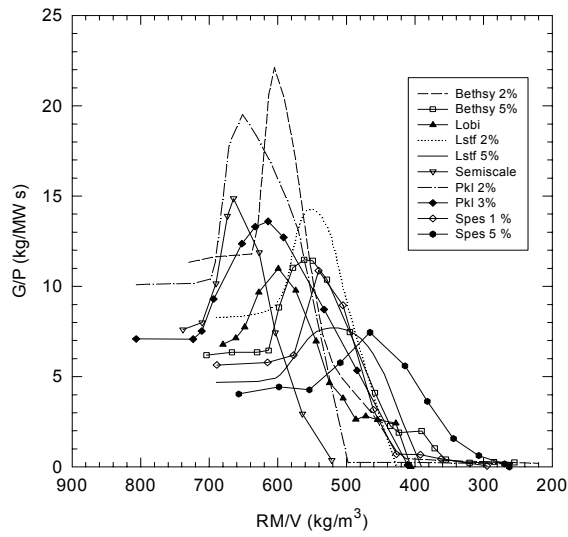


FIG. 2. Natural circulation system behavior measured in ten experiments performed in six PWR simulators.

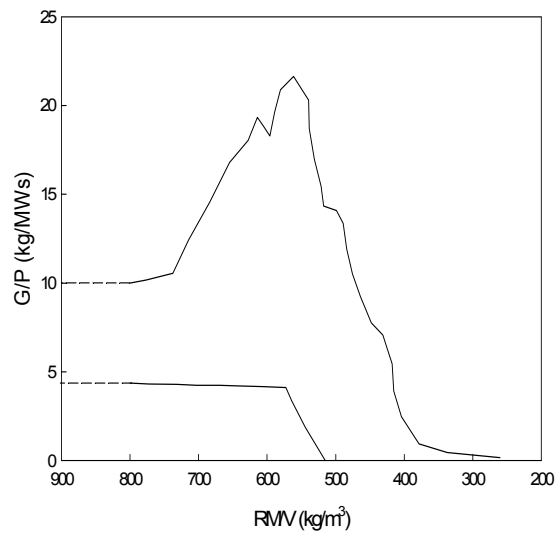


FIG. 3. Natural circulation flow map achieved from the envelope of measured curves in PWR simulator.

Table 2. Relevant characteristics of NPP considered for the application of the NCFM

	1 PWR	2 PWR	3 PWR	4 WWER- 1000	5 EPR	6 AP- 600	7 EP-1000
Nominal Power (MW)	1877	870	2733	3000	4250	1972	2958
Primary System volume (m ³)	167	150	330	359	459	211	339
SG type	U-Tubes	U-Tubes	Once-Through	Horizontal	U-Tubes	U-Tubes	U-Tubes
No. of loops	2	4	2	4	4	2	3
No. of pumps	2	4	4	4	4	4	6
Nominal mass inventory (Mg)	108	108	224	240	307	145	227
Nominal Core Flow (Kg/s)	9037	3150	17138	15281	20713	8264	14507
Pressurizer and SG pressure (MPa)	15.6 6.	14.0 3.1	15.0 6.4	15.7 6.3	15.5 7.2	15.5 5.5	15.8 6.4

Pactel and RD14M (Tab. 3) are experimental simulators of WWER-440 and CANDU NPP, respectively. Their geometric layout is different from those of a PWR. In the case of WWER-440, six loops equipped with HTSG are connected to the vessel, though only three are simulated in Pactel. Horizontal core configuration characterizes the CANDU design, that otherwise is equipped with UTSG.

Table 3. PACTEL and RD14M

	Pactel (original)	Pactel (with CMT) °	RD14M
Reference reactor and power (MW)	WWER-440 1375	WWER-440 1375	CANDU 1800
No. of rods	144	144	70
No. of SG	3	3	2
SG type	Horizontal	Horizontal	U-Tubes
Actual Kv +	1/433	1/462	1/378

° CMT = Core Make-up Tank

+ Definition introduced for database in Table 1.

An evaluation of the NC Performance (NCP) of the reported NPP and ITF has been conducted by the use of the NCFM. A comparison has been made between measured (case of ITF) and calculated (case of NPP) system behaviours during NC and the data that characterize the NCFM. NCP is used as synonymous of NC system behaviour. To this aim, code calculations assuming stepwise draining of primary system fluid mass inventory have been performed (case of NPP) and relevant NC experimental data are utilized (case of ITF).

The generic objective of the activity is to gather an estimation of the maximum thermal power removable by NC in PWR systems. This may be relevant for the existing reactor technology in the extremely unlikely event of main circulation pump trip and simultaneous failure of scram and in the design of new reactors fully based upon natural circulation. As already mentioned, no care is given to the thermohydraulic neutronic interaction and, therefore to the actual possibility of generating the considered fission power [10].

The analysis is carried out into two parts the former related to ITF, to give more realism to the calculated results, the latter related to a PWR. (see Tab. 4) [11].

In all cases, the primary system pressure and the SG conditions (pressure, level and feedwater temperature) are kept constant at the nominal values if not differently specified. The main circulation pumps are at zero speed and the locked rotor hydraulic resistance of the impeller is taken into account. The core power and the feedwater flowrate levels are consistently varied.

Table 4. Removable power by natural circulation in ITF

ITF	Core power when void achieves 0.1 at the upper core level (°)	Core power when dryout occurs (°)	Void at the upper core level when dryout occurs	Primary system mass inventory at dryout (°)	G/P at dryout (Kg/MWs)	RM/V at dryout (Kg/m ³)
Bethsy	15	70	0.8	69	1.12	475
Lobi	20	70	0.7	80	1.23	570
Lstf	10	30	0.9	62	1.87	480
Spes	15	50	0.6	75	1.29	528

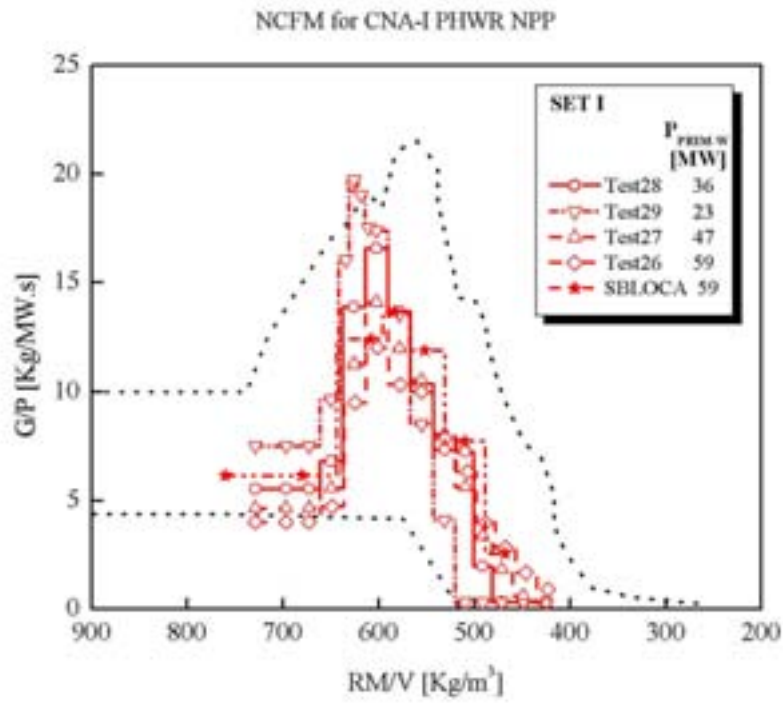
(°) % of the nominal operational value

The main results of the study can be summarized as follows [12]:

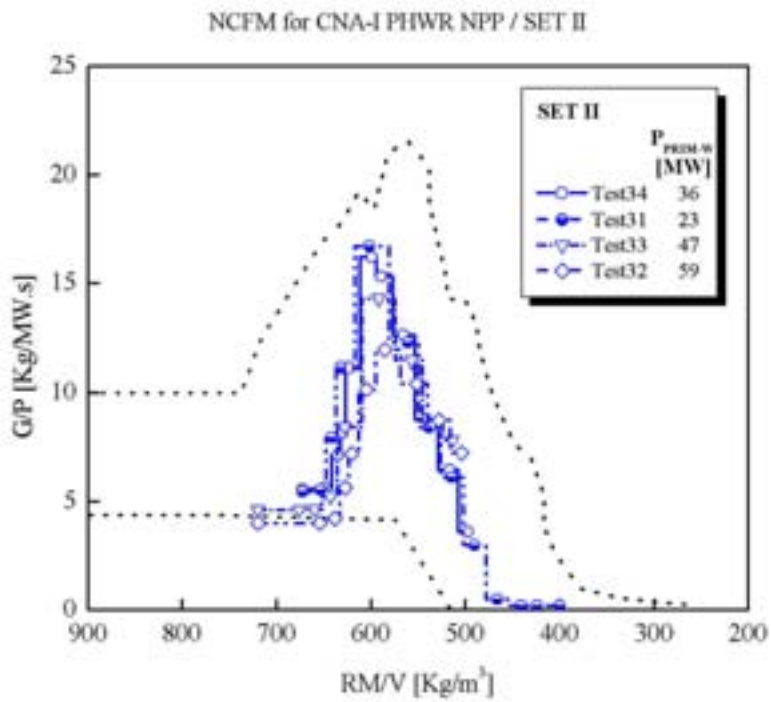
- A uniform NC flowrate increase occurs with core power, until core power achieves values around 40% of the nominal value. Further increases of core power do not cause proportional increases in core flow;
- Oscillatory flows are calculated for core power larger than 40% in Bethsy and Lobi;
- The primary mass inventory decrease occurs via the pressurizer relief valve that is assumed to open and close to keep constant the system pressure;
- PWR cores, in the actual configuration can operate in NC conditions with power up to about 15% the nominal value;
- The largest facilities are designed to operate at low core power (ITF design finalized to the simulation of small break LOCA): this may explain the small value of % core power at which dryout occurs in Lstf. Neglecting the Lstf case, up to 70% core power can be removed by NC before experiencing dryout. This can be assumed as the thermohydraulic limit for system (not any more PWR) operation in NC.

The NCFM was used to characterize the behaviour of the CNA-I PHWR NPP in NC flow conditions, in a reduced primary mass inventory scenario. The simulations have been performed using three different nodalizations of increasing detail. The coarser one (SET I) was used as a basic set, just to represent a plant layout similar to a PWR. This permitted to verify that the trends known for most ITFs working in similar situations give an envelope to the CNA-I behaviour, considering appropriate trips of some of its safety systems. On the other side, the results of the rest of the calculations SET II and SET III, more representative of the plant, may be considered almost parametric deviations from the previously stated behaviour. The results have been verified considering a plant transient, which gave results quite similar to the ones obtained by simulation. Dispersion of results of the different simulations is systematic, showing that they may be further adjusted to get closer agreement. However, this objective was not pursued. The results have been correlated using simple expressions in the limited scope of power fractions studied and for a representative set of SGs secondary side BCs. In so doing, two coefficients have been obtained to calculate core flowrate as a function of power delivered to primary water. Summarizing, it may be stated that the analyses provide new data on the behaviour of an existing NPP working in a NC scenario. A parametric analysis on the effects of system's working BCs is presently under way.

[a]



[b]



[c]

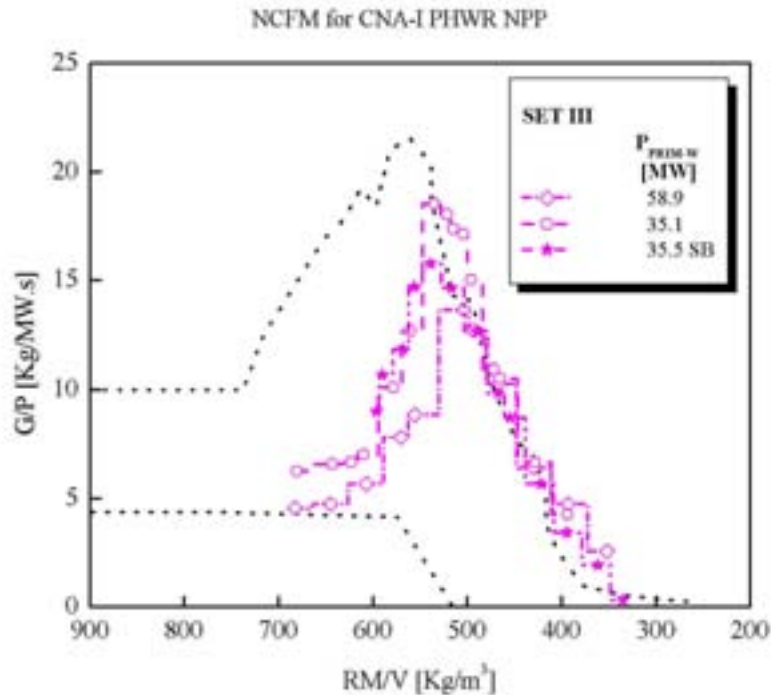


FIG. 4. Natural circulation maps for (a) SET I, (b) SET II and (c) SET III.

On the vertical axis we have the core inlet flowrate (G, Kg/s) toward core power (P, MW).

On the horizontal axis we have primary system fluid mass inventory (RM, Kg) toward the net volume of the primary system ($V=\text{const.}$, m³),

Similar results are received with the natural circulation analyzes on the PSB facility. PSB facility is an experimental facility of reactors type WWER 1000 in Russia. Below is presented an experimental and imulation results compared with PWR NC Flow limits in a Natural Circulation Flow Map.

3. CONCLUSIONS

The same experimental data base has been utilized to set up a reference natural circulation flow map. This allowed the judgement of performance in natural circulation of pressurised water reactors not necessarily of the same type as those used for deriving the map. It was found that the PWR equipped with Once-Through steam generators have a poor natural circulation performance when primary mass inventory is decreased. Otherwise, reasonable natural circulation performances of Russian designed reactors WWER were characterized. This is mainly true for the WWER-1000. Passive systems in the AP-600 innovative reactor are effective in keeping the primary system under single-phase natural circulation notwithstanding removal of coolant mass.

Power removal by natural circulation strongly depends upon primary and secondary system boundary condition. Two thermohydraulic thresholds are considered in the present framework. These are the void formation in the core that prevents a PWR from being 'pressurised' and the technological limit constituted by the overpassing the critical heat flux. When primary and secondary system boundary conditions are kept close to their nominal values, with main reference to pressure, it is found that:

- Single phase natural circulation is effective for removing up to around 20% of core nominal power,
- Two phase natural circulation, with the primary system in a boiling condition, is effective for removing up to about 70% of core nominal power avoiding the occurrence of the dryout crisis.

A deeper investigation shows that the 100% core power can be removed in two-phase natural circulation, provided the steam generator pressure and the feedwater temperature are lowered to values of the order of 3 MPa and 100 °C, respectively. An increase of primary pressure also brings to increase the power removal capability by natural circulation.

Core flowrates that brings to dryout conditions when core power is about 100% are five-six times less than the nominal value. This confirms the wide safety margins that characterize the nominal operation of a PWR. Furthermore, dryout occurrence at high pressure is self limiting. Rod surface temperatures, following the overpassing of the critical heat flux limit, jump up for a few tens of Kelvin and remain at these levels in steady state conditions.

The following comments may be considered for possible follow-up analyses aiming at the design of a natural circulation PWR:

- The removal of the pumps and minor changes in the primary and secondary circuits hardware, in the direction of reducing pressure losses, may improve the natural circulation performance of the system;
- A systematic nodalisation study must be completed to improve the qualification level of the achieved results;
- Thermal efficiency of the entire thermodynamic cycle must be considered;

REFERENCES

- [1] D'AURIA, F., GALASSI, G.M., VIGNI, P., CALASTRI, A., Scaling of Natural Circulation in PWR Systems, *J. Nuclear Engineering and Design*, col 132, pp 187–205 (1991).
- [2] D'AURIA, F., GALASSI, G.M., INGEGNERI, M., Evaluation of the data base from high power and low power small break LOCA counterpart tests performed in LOBI, SPES, BETHSY and LSTF facilities, University of Pisa Report, DCMN - NT 237(94), Pisa (I), Nov (1994).
- [3] KUKITA, Y., TASAKA, K., Single Phase Natural Circulation in Pressurized Water Reactors under degraded Secondary Cooling Conditions, *ASME Winter Meeting* (1989).
- [4] AKSAN, N., D'AURIA, F., GLAESER, H., POCHARD, R., RICHARDS, C., SJOBERG, A., Separate Effects Test Matrix for Thermal-Hydraulic Codes Validation: Phenomena Characterisation and selection of Facilities and Tests, OECD/CSNI Report OCDE/GD (94) 82, Paris (F), Jan (1995).
- [5] D'AURIA, F., GALASSI, G.M., Relevant results obtained from the analysis of LOBI/MOD2 natural circulation experiment A2-USNRC NUREG/IA-0084, Washington (US), April (1992).
- [6] J.C. FERRERI, MAZZANTINI, O., VENTURA, M.M., ROSSO, R.D., D'AURIA F., Natural Circulation in the CNA-I PHWR NPP, October 5–9, 2003, Seoul, Korea.
- [7] D'AURIA F., FROGHERI, M., LEONARDI, M., Natural Circulation Performance in Western type and Eastern type PWR, *Simulator Multiconference*, San Diego (CA), April 11–13 (1994).
- [8] D'AURIA, F., GALASSI, G.M., FROGHERI, M., Natural Circulation Performance in Nuclear Power Plants, *2nd Conf. of the Croatian Nuclear Society, Dubrovnik (HR)*, June 17-19 (1998).
- [9] ANNUNZIATO, A., GLAESER, H., LILLINGTON, J.L., MARSILI, P., RENAULT, C., SJOBERG, CSNI Code Validation Matrix of Thermalhydraulic Codes for LWR LOCA and Transients, OECD/CSNI Report No. 132-Rev. 1, Paris (F), July (1996).
- [10] D'AURIA, F., GALASSI, G.M., Characterisation of Instabilities during Two-Phase Natural Circulation in PWR typical conditions, *J. Experimental Thermal and Fluid Science*, Vol. 3 (1990).
- [11] D'AURIA, F., GALASSI, G.M., Flowrate and Density Oscillations during Two-Phase Natural Circulation in PWR typical Conditions, *J. Nuclear Engineering and Design*, Vol 122 (1990).
- [12] D'AURIA, F., FROGHERI, M., MONASTEROLO, U., Removable Power by Natural Circulation in PWR Systems *ICONE-5*, Nice (F) May 26–30 (1997).

ANNEX 19

COUPLED 3D NEUTRON KINETICS AND THERMAL-HYDRAULICS TECHNIQUES AND RELEVANCE FOR THE DESIGN OF NATURAL CIRCULATION SYSTEMS

F. D'Auria, A. Bousbia-Salah

University of Pisa, Italy

Abstract

This lecture describes the use of coupled 3D neutron kinetics and thermal hydraulics computer codes for various natural circulation systems. Examples of coupled calculations are provided for a Main Steam Line Break (MSLB) in a PWR, for a BWR turbine trip, and for a VVER-1000 commissioning test. Each of the transient models, including their nodalisation, is described.

1. INTRODUCTION

The availability of advanced-coupled neutronics/thermalhydraulics computer tools and of powerful computers enlarged the possibility to perform realistic best estimate analyses of 'very' complex transients and, possibly, achieve optimization of EOPs (Emergency Operating Procedures) for the existing NPPs. These capabilities have not yet been fully exploited due to lack of funding. They may allow the solution of 'old-fashioned' problems (critical issues) in nuclear reactor technology. Issues connected with the interaction between thermalhydraulics and neutronics that still challenge the design and the operation of light water reactors, with main reference to RIA (Reactivity Initiated Accidents) constitute the subject of the project. Additional motivations for the activity are:

- Spread of results calculated in the last few years. Nowadays, there is not any more a clear-agreed-common view within the technical community about the safety relevance of issues like those considered herein.
- There are many initiatives in progress, not only within the EU, to produce State-of-the-Art-Reports or Status-Reports concerning a number of topics. However, owing to lack of funding, these are not based upon a deep analysis of existing information. As a consequence, related planning is not very clear.
- The wide interest within the technical community toward two Benchmarks proposed by the OECD/NEA/NSC, i.e. the PWR MSLB (TMI-1 NPP) and the BWRTT (Peach Bottom NPP). The former scenario is originated by the Main Steam Line Break in one of the two steam generators of the TMI-1 NPP: asymmetric core cooling gives rise to a fission power peak localized in one part of the core. The latter is the BWR Turbine Trip: closure of the turbine inlet valve causes a pressure wave propagation into the vessel that leads to void collapse and, again, to fission power peak. Both of these involve tight neutronics/thermalhydraulic interaction and require for obtaining adequate simulation 3-D neutron kinetics tools coupled with thermalhydraulic codes.

The first seven institutions provided under the list of authors are 'official' partners of the project. The institutions from 'eight' to 'twelve' have signed Memorandum of understanding with the other partners and contributed to the activities. In this paper typical application of coupled system Thermal-hydraulic 3D Neutron kinetic code for simulating the complex transients in PWR and BWR and VVER NPPs is presented.

2. MSLB PWR SYSTEM DESCRIPTION AND BOUNDARY CONDITIONS

A sketch of the TMI-1 reactor including design data adopted in the MSLB benchmark calculation is given in Fig. 1. The two Cold Legs (CL) in each loop and the OTSG layout can be observed. The nominal working condition for the plant can be derived from Tab. 1. Superheating at the outlet (i.e. in

the steam lines) and ‘bypass recirculation’ occurring through holes between riser and downcomer (DC) below the feed-water entrance nozzle, characterize the OTSG.

The list of imposed sequences of main events during MSLB accident can be drawn from Tab. 2. The plant status relates to hot full power at the end of the cycle. The main assumptions or relevant information for the transient calculation are as follows:

1. The assembly relative radial power distribution is given with quarter symmetry;
2. The axial power is assigned in twenty-four nodes not uniformly spaced;
3. The break is assumed to be double ended in one of the two 24” Steam Lines (SL) departing from each OTSG, at the location upstream of the MSIV (Main Steam Isolation Valves), and one additional 8” break occurs in the cross connection pipe;
4. The PRZ (Pressurizer) is connected to the Hot Leg (HL) of the loop with broken SG;
5. The four reactor Main Coolant Pumps (MCP) are assumed to not trip in order to maximize the potential for reactivity excursion following the MSLB;
6. Laws for HPIS (High Pressure Injection System) flow versus pressure (two pumps inject cold water in two cold legs, one per each loop), of FW (Feed-Water) flow rate and of scram reactivity worth versus time, are assigned;
7. No credit is given to the operation of the PRZ heaters and to the CVCS (Chemical and Volume Control System);
8. Boron concentration is assumed constant (i.e. notwithstanding the HPIS actuation) and its reactivity coefficient is included in the overall moderator coefficient;
9. The containment is assumed as an infinite volume at 0.103 MPa.

Additional details about the plant, the initial conditions and the imposed sequence of main events can be found in Refs. [1] and [2].

Table 1. Relevant initial conditions for nominal operation of the TMI-1 plant

Quantity	Design Value
Core power [MW(thermal)]	2772
Cold leg temperature and subcooling (K/K)	563.76/51.30
Hot leg temperature and subcooling (K/K)	591.43/23.63
Lower plenum pressure (Mpa)	15.36
Outlet plenum pressure (Mpa)	15.17
Reactor coolant system pressure (Mpa)	14.96
Total reactor coolant system flow rate (kg/s)	17602.2
Core flow rate (kg/s)	16052.4
Bypass flow rate (total) (kg/s)	1549.8
PZR level (m)	5.588
Feedwater flow per OTSG (Kg/s)	761.59
OTSG outlet pressure (Mpa)	6.41
OTSG outlet temperature (K)	572.63
OTSG superheat (K)	19.67
Feedwater temperature and subcooling (K/K)	510.93/42.12
MCP velocity (rad/s)	124
Core pressure drops (kPa)	129 irreversible 200 total
Primary system mass (kg)	—
Initial SG mass inventory (kg)	28 395
Reactor coolant system pressure drop (kPa)	738

Table 2. Imposed sequence of main events for the OECD/CSNI/NSC TMI-1 benchmark

Event Description	Time (s)
Breaks open	0.0
Reactor trip	6.9
MCP trip	Not occurring
Turbine valve closure (start-end)	7.9 to 11.9
High-pressure injection start	46.4
Transient end	100.0

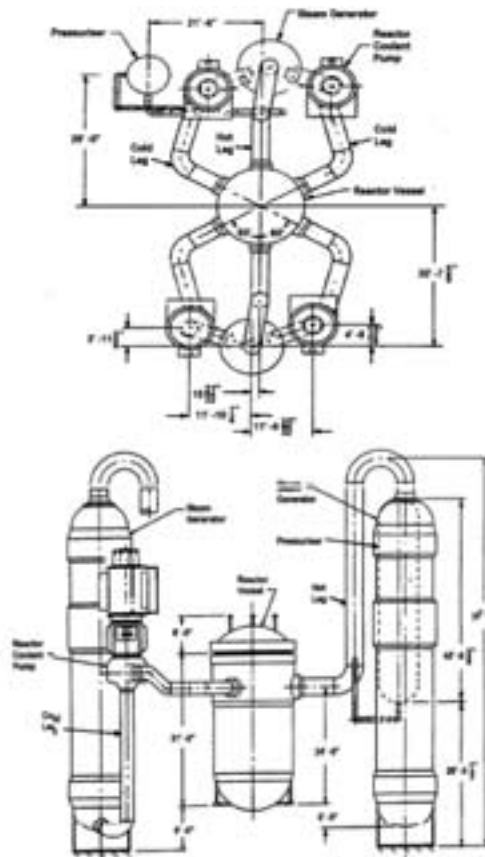


FIG. 1. Sketch and layout of the TMI-1 plant.

Physical phenomena of interest

The steam line break occurrence causes, at first, fast depressurization of the concerned steam generator. Critical flow establishes at each of the two sides of the two broken pipes. The turbine side break flowrate is 'early' (i.e. in a time less than a few seconds from the break occurrence event) terminated by the turbine system side depressurization and isolation of turbine valves.

The SG system side depressurization implies increase in feed-water flowrate toward the affected SG. The FW flow-rate increase, in conjunction with the depressurization itself, causes a positive peak in the thermal power removal capability from the affected SG. The consequence of this is a 'plug' of 'colder' water exiting from the outlet of the primary side SG, i.e. bottom of the steam generator, toward the main coolant pump.

The 'plug' of cold water reaches the reactor pressure vessel and the core a few seconds after the break occurrence. This is also possible owing to the continuous operation of the MCP that are not tripped for the entire duration of the predicted transient (i.e. 100 s after the break occurrence).

The 'cold' water into the core is the source of a positive reactivity insertion that causes fission power peak. This is terminated at a time less than 10 s (always since the break occurrence) owing to the occurrence of the scram signal from high power.

Scram control rod insertion is assumed to be 'incomplete' owing to one stuck withdrawal rod, but is enough to shut-down the core in a couple of seconds. However, the scram itself and the MCP operation, cause further cooling of the moderator temperature and a total reactivity insertion, that, from a 'large' negative value connected with the scram rod insertion, achieves values close to zero. The thermal power exchange across both steam generators achieves negligible values (compared with core power) at about 30 s into the transient.

At about 60 s from the break occurrence, with the contribution of the ‘peak’ of delayed neutrons produced during the first fission power peak above mentioned, a return-to-power is predicted. This shows-up as the ‘second power peak’. Termination of the peak in delayed neutrons and the dryout of the steam generators that bring to zero the thermal power exchange across the ‘once-through’ tubes, cause the final power reduction and brings to the end of the calculated transient that was fixed at 100 s after the break occurrence, as already mentioned.

2.1. Adopted codes and nodalizations

Codes

Four thermal-hydraulic codes and three neutronics codes have been adopted for calculating the OECD/NEA/NSC/CSNI MSLB Benchmark based on a TMI-1 transient. The system thermalhydraulic codes are the US NRC and the INEEL current versions of the Relap5. These are identified as the Relap5/mod3.2 beta and gamma and the Relap5-3D, respectively, Refs. [3] and [4]. The (thermalhydraulics) sub-channel code is the Cobra, Ref [5].

The 3-D neutron kinetics codes are Quabbox, Parcs and Nestle, Refs. [6] to [9]. Quabbox and Parcs are coupled to the Relap5/mod3.2 gamma and beta. Nestle is coupled with Relap5-3D. Coupling of the involved thermalhydraulics and neutronics software has been done by (or under the control of) the thermalhydraulic code developers in the case of Parcs coupled with the Relap5/mod3.2 beta and Nestle. Direct coupling between Quabbox or Parcs and Relap5/mod3.2 gamma has been completed at University of Zagreb. In all cases ‘officially’ released code versions are adopted.

Code Coupling

A technology has recently been developed in relation to code coupling. This is especially true in relation to system thermal-hydraulics and 3-D neutron kinetics codes.

System thermalhydraulics codes have the capability to model the heat transfer and the hydraulic phenomena occurring in the core during by adopting a level of detail that corresponds to one thousand nodes, roughly. However, the neutronics model embedded into these codes is the punctual kinetics model that solves the diffusion equation and makes use of input quantities such as void and Doppler (or fuel) reactivity coefficients. Hence the recent availability of powerful computer made it possible the coupling with 3-D neutron kinetics codes that have been developed in parallel, so far.

It is well beyond the purpose of the present article to discuss with some level of detail the various steps of the coupling and the possibilities that exist in this area. Here we only mention that ‘full dynamic’ coupling was adopted in all cases. This implies that results at an assigned time step (of the order of 10^{-3} in the performed analyses) from one code are supplied to the other code and achieved results affect the calculation of the first code in the next time step. When Cobra is used (a thermalhydraulic code, suitable for predicting core sub-channel performance) in combination with Relap, this last code is needed at an assigned time step to fix the thermalhydraulic conditions at the core boundaries. Cobra performs sub-channel analysis and supplies relevant conditions to the 3-D neutronics code at the next time step.

Among the other things, not documented in the present article, extensive “qualification” of the code-coupling was performed. This also involved verification of the influence of the time step and search for the optimum time step for this transient with the selected code coupling strategy.

Nodalizations

Thermalhydraulics

A reference thermalhydraulic-system nodalisation for the TMI-1 NPP has been developed and qualified (as far as possible) at the University of Pisa. Starting from the reference one a number of different nodalisations have been developed to address different objectives of the activity, including:

- evaluating the influence of hydraulic splitting of the core,
- evaluating the influence of fluid mixing in the lower plenum and upper plenum.

The various nodalisations, the objectives of their use and the obtained results are described in Ref. [10]. In the present context (code comparison) only one nodalisation is used. In the nodalisation adopted in this study, the liquid mixing in upper and lower plenum is minimized, thus creating the largest potential for neutron power excursion.

The thermalhydraulic nodalisation of the entire system is given in Fig. 2 and the vessel nodalisation including the core region is shown in Fig. 3.

Subdivision of the core in eighteen core channels can be seen in Fig. 4. The host Organization of the Benchmark proposes the regions 1 to 18 of the core. Two bypass channels are shown in Fig. 3. Limitations in the maximum number of junctions belonging to a single BRANCH (Relap5 code component) imposed the need to split the lower (LP) and upper (UP) plena into four parts, at least in the zones of connection between LP and UP with the core itself. The DC has been split into four parts, corresponding to the four cold legs of the system. The coolant flowing in each part does not mix with the fluid flowing in the other parts. The UP has been subdivided into two parts because only two hot legs are present in the reactor system. The relative azimuthal positions of the hot and cold legs have been preserved. The passive structures, as well as the core active structures, have been split consistently with the hydraulic nodes. The 'N 12' stuck control rod, Ref. [1], is in the vessel quarter pertaining to the broken loop cold leg No. 1.

Main characteristics of the nodalisation can be derived from Tab. 3 where the number of neutronics nodes is given too.

Table 3. Computational resources in the coupled RELAP5/MOD3.2-PARCS input deck developed for the TMI-1 nuclear power plant

Number	Quantity	Value
1	Total number of hydraulic nodes	1499
2	Total number of mesh points for conduction heat transfer	15700
3	Total number of slabs	1032
4	Total number of neutron kinetics nodes	4602
5	Number of parallel hydraulic stacks in the core region	18
6	Number of parallel core bypass regions	2
7	Number of elements in each core stack (hydraulics, heat conduction, and neutronics)	26

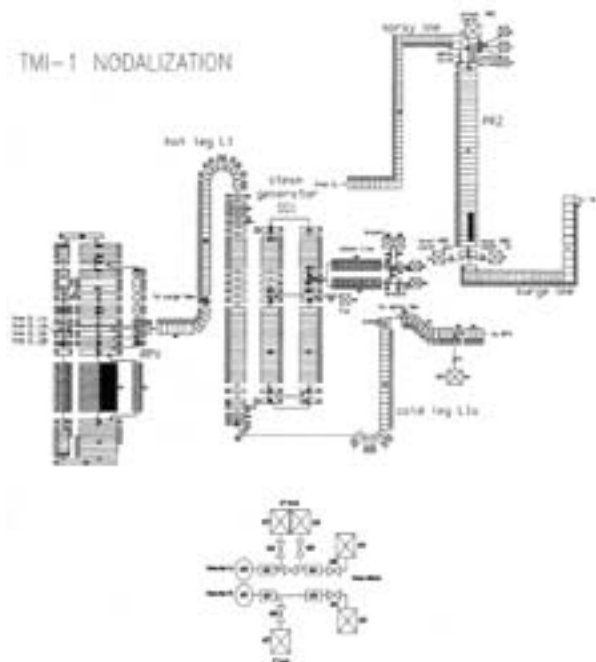


FIG. 2. Sketch of the nodalisation for the TMI-1 MSLB benchmark (entire system).

3-D Neutronics

The layout of the Fuel Assemblies (FA, 177) and of the Reflector Assemblies (RA, dashed zones, 64) is shown in Fig. 4. One 'neutronics node' is used per assembly in radial direction and up to 26 layers in axial direction. The stuck withdrawn rod can be identified in Fig. 4: shadowed fuel element on the right side.

Twenty-nine different FA types are selected for cross-section generation assuming a 1/8 core symmetry. Fifteen axial layers are used to simulate burn-up distribution. Separate material composition is used to model influence of top, bottom and radial reflectors. Total number of un-rodged cross-section compositions is 438. For fuel assemblies where control rods can be inserted additional 195 rodged compositions are needed. Cross section sets have been derived, outside from the present activity, by the Casmo code in each FA and RA type. The cross-section library includes dependence of group constants on moderator density and Doppler temperature. Two-dimensional linear interpolation scheme was provided together with cross-section data. An effort was needed to modify the format of the cross section values to make these consistent with the requirements of the

adopted 3-D neutronics codes. The digits 1 to 18 (Fig. 4) relate to groups of ‘homogeneous FA’ from the thermalhydraulics point of view. All the RA constitute one group, again from the thermalhydraulic point of view.

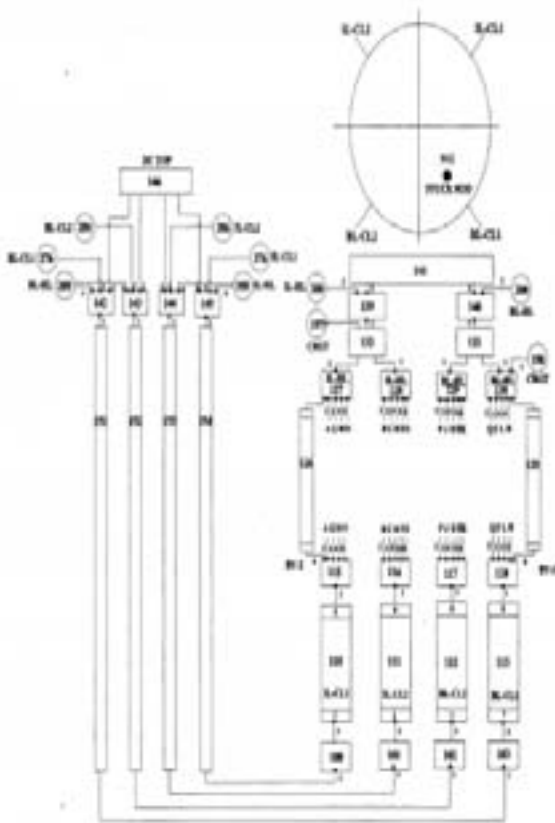


FIG. 3. Outline of the relap5 noding scheme for the vessel downcomer, the upper and the lower plenum adopted in the present work.

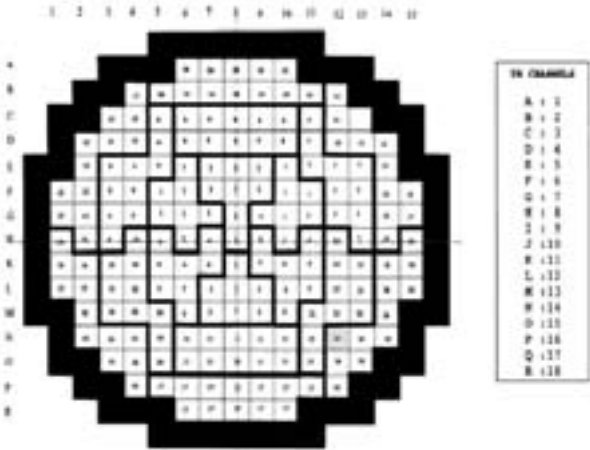


FIG. 4. Identification of fuel and reflector assemblies on a radial plane and subdivision in thermalhydraulic zones (Ref. [1]).

2.2. Considered calculations

A wide range research has been performed to get the 3-D core behavior during a complex transient. In order to achieve confidence in the results, ‘preparatory activities’ have been planned. The lack of a reference or physical solution should be mentioned, too. An idea of these activities is given below, including a procedure for the system analysis and the 3-D neutronics evaluation of the core performance.

Preparatory Activities

Procedure for the System Analysis

A detailed, step-by-step procedure has been adopted in order ‘to keep under control’ the achieved results, as documented in Ref. [10]. The starting point for the step-by-step procedure is the Relap5 calculation adopted for the Phase 1 of the TMI-1 MSLB Benchmark. This is the standard thermalhydraulic code calculation where 1-D thermohydraulics is coupled with the 0-D neutron kinetics. Three main steps constitute the procedure adopted for a ‘consistent’ use of the 3-D neutron kinetics:

- I 1-D thermohydraulics of the core and 3-D neutronics (to check consistency among results obtained from the application of 0-D and 3-D neutron kinetics).
- II ‘Fictitious’ 2-D core thermohydraulics and 3-D neutronics (perfect mixing in lower plenum).
- III ‘Fictitious’ 2-D core and vessel thermohydraulics and 3-D neutronics (no mixing in the vessel).

Twenty calculations are discussed in Ref. [10]. The obtained results are used to check the influence of the changes during conversion of the Phase 1 nodalisation to the nodalisation required for completing the Phase 3 calculations. The influence of the changes in boundary and initial conditions (as a result of changes in benchmark specification), changes in cross section data and interpolation scheme and changes in steam generator and reactor vessel nodalisations have been studied into detail. Different reactor core and vessel nodalisations have been prepared: the nodalisation with perfect mixing and the nodalisation with the core and related parts of the vessel subdivided into four completely separated parts (no mixing in the vessel) have been developed. The influence of the four cold legs over the fuel assemblies situated in the same core quadrant has been considered.

One nodalisation was prepared with the core sub-divided into two parts and with the inlet and outlet mixing as prescribed by the benchmark specifications, but most of the calculations were performed using nodalisation with four core parts without mixing.

3-D neutronics Evaluation of the Core Performance

The direct mutual influence of thermalhydraulics and neutronics coupling in the core was analyzed in frame of Phase 2 of the MSLB benchmark. Special versions of the Relap5/mod 3.2 gamma coupled with Quabbox and Parcs were developed and applied. Nineteen thermalhydraulic channels constitute the core (Relap5 pipe components) of the base nodalisation: eighteen of these are distributed (in spatial terms) as proposed in the MSLB Benchmark specification and one channel is used to model the bypass flow.

In order to assess the influence of the number of the thermalhydraulic channels and corresponding heat structures in the model, in one Relap5/Quabbox calculation 177 channels were used. In addition, in one case the Cobra sub-channel thermalhydraulic model (again with 177 channels) was added to the already coupled Relap5 and Quabbox. In the case of the use of the Cobra sub-channel code, the thermalhydraulic coupling in the central row of fuel assemblies was based upon “weighted” influence of neighboring thermalhydraulic channels. In all cases, axial node subdivision and radial meshes for conduction heat transfer were the same as in the original nodalisation. Both Quabbox and Parcs used

cross section libraries with the same bilinear table interpolation scheme. The benchmark boundary conditions are applied using Relap5 time dependent volume components for specifying inlet temperature and outlet pressure for each channel, and time dependent junctions for specifying channel inlet mass flows.

The analysis of the influence of number of thermalhydraulic channels on global and local parameters was the main goal of these calculations. Calculated total core power is shown in Fig. 5. The physical scenario that causes the time trend for power depicted in Fig. 5 is described in section 2, above.

Four calculations are identified with labels: r5qc (Relap5/Quabbox), r5qcx (Relap5/Quabbox 177 channels), r5qcv (Relap5/Quabbox/Cobra), and r5pa (Relap5/Parcs). Both qualitative and quantitative agreement is rather good and influence of increased number of thermalhydraulic channels is limited to local effects. In the case of Parcs calculation, reactor trip was predicted slightly earlier than in case of Quabbox based calculations and power calculated during the second peak was higher when Cobra was used (small differences in fuel rod heat conduction model). The second power peak calculated in this case is lower than in Phase 3 calculations, that will be shown later, due to mixing built in inlet thermalhydraulic boundary conditions. Some oscillations in reactor power calculated in Phase 3 (these have no role within the framework of the present article and are just mentioned to give an idea about the complexity of the performed analysis) before reactor scram are not present here, what means that the reason for the oscillations can be searched in the model or phenomenology outside the reactor core.

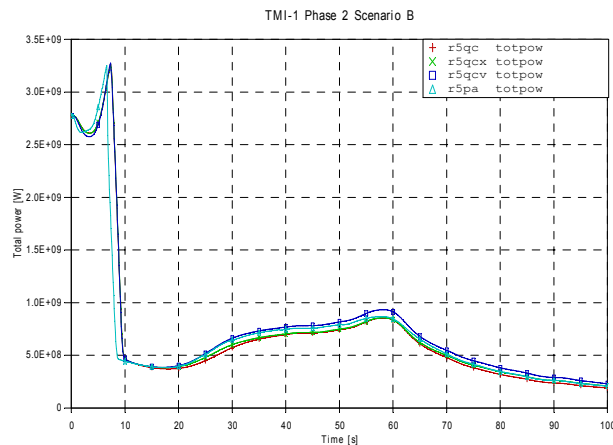


FIG. 5. Core power in Phase2 scenario B calculation.

The ability of different models to predict local core conditions can be derived from Fig. 6. Due to significant local thermalhydraulic feedback the values of power peaking factor (f_{nq} , i.e. ratio between local power and average core power) are lower in cases when detailed thermalhydraulic feedback is modeled.

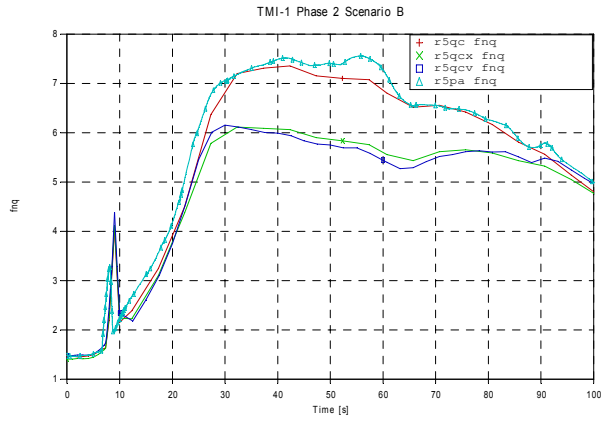


FIG. 6. Power peaking factor in Phase2 scenario B calculation.

The influence of the thermohydraulic averaging in the case of the eighteen core channels can be seen in Figs. 7a and 7b. Radial distributions of coolant temperatures at core outlet at the time of the second power peak, as predicted by r5qc with eighteen core channels and by r5qcv with 177 core channels, are reported. Related to both r5qc and r5qcv calculations, fluid temperature is higher in the side of the core corresponding to the intact steam generator and opposite to the side where the stuck control rod is located. The increase in the calculation detail going from calculation r5qc to calculation r5qcv brings to higher values for fluid temperature around the stuck withdrawn rod (comparison between Figs. 7a and 7b). Local fluid temperature increases and coolant density decreases close to the stuck rod position limit the local power increase also causing lower power peaking factors in the calculation with 177 core channels compared with the calculation with eighteen core channels.

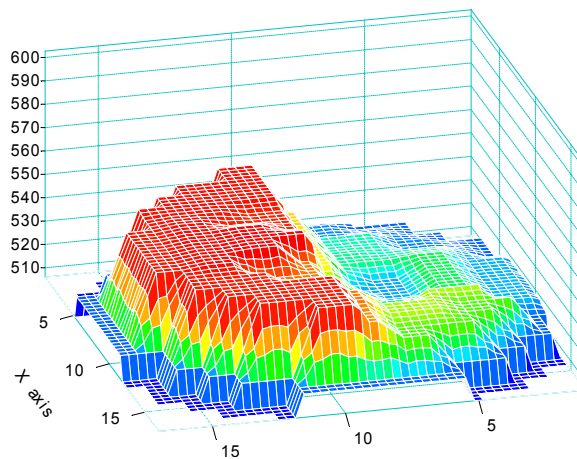


FIG. 7a. Core outlet coolant temperature in Phase 2 scenario B r5qc calculation.

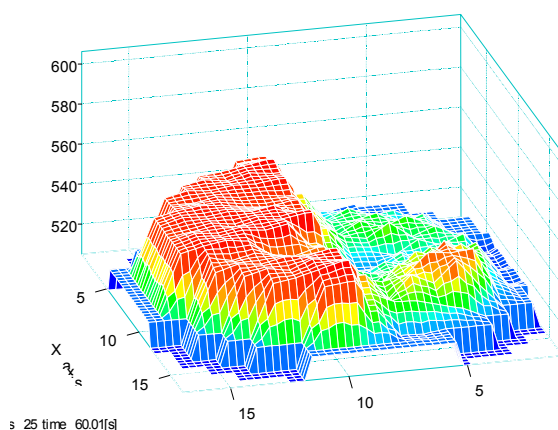


FIG. 7b. Core outlet coolant temperature in Phase 2 scenario B r5qcv calculation.

Comparison Calculations

The Phase 3 coupled code calculations, in relation to which input decks have been discussed in the previous section, have been carried out by the coupled Relap5/mod3.2 beta and Parcs codes. The run 10b, including ‘fictitious’ 2-D core and vessel thermohydraulics (i.e. no mixing in the vessel) and the cross section set ‘return-to-power’ (also reported below as ‘scenario B’) is taken as reference for the present comparison calculations.

Table 4. Coupled code runs considered in the present comparison

Run Number	Thermal-Hydraulic Code	Neutron Kinetics Code	Plots
10b*	Relap5/mod3.2 beta ^b	Parcs	10bp
11	Relap5/mod3.2 gamma ^c	Quabbox	10bq
12	Relap5-3D	Nestle	10b3D

*Run 10b in Table 4 of Ref. 14.

^bPVM coupling.

^cDirect coupling.

The list of calculations and the codes considered in the present comparison is given in Tab. 4. The following should be noted:

- Complex nodalisations must be developed to run 3-D neutron kinetics code coupled to thermalhydraulic code. These may consist of up to seventy thousands ‘lines’;
- Several error sources occur during the process of nodalisation development and steady-state running;
- Huge resources are needed for the development of each nodalisation and for a suitable evaluation of results (long lasting activity). Consideration of Quality Assurance in the process may reveal non-feasible;
- Feedback (automatic, unavoidable), as expected, occurs between neutronics and thermalhydraulics. The problem derives from achieving steady-state conditions before transient initiation. For instance, differences in predicting entrainment in secondary side (affected by the interfacial drag, a model ‘easily’ changed in different code versions) causes differences in steam generator removed power, therefore differences in primary system temperatures. Definitely differences in core fission power result. These differences can be set to zero by proper procedures for achieving steady state. Initial mass in steam generators is also affected by the interfacial drag: different transient behavior of the entire system can be predicted;

- Averaging processes and lumping hydraulic and thermal nodes to neutronics nodes depend upon user choices and partly upon the features of the interface between the thermohydraulic and the 3-D neutronics code.

As a consequence of the above, the processing of the same input information within each of the code runs listed in Tab. 4, may give (slightly) different steady state results. Limited attempts were made to achieve a ‘converged’ set of boundary and initial conditions before the transient start (additional discussion on this topic can be found below).

2.3. Discussion of achieved results

In order to present and document the results of coupled thermohydraulic 3-D neutron kinetics calculation, both global and local (spatial) parameters must be considered for steady state and transient periods. Usual approach is to show:

1. Tables of conditions reached at the end of steady state and tables of calculated sequences of events during transient;
2. Relevant (global and characteristic local values) time trends (quantity reported as a function of time);
3. Spatial distributions taken at selected times during the transient (1D axial and/or 2D radial distributions);
4. 3-D graphical representations;
5. Animated spatial distributions to facilitate the interpretation of the overall system behavior (e.g. evolution of core power distribution during transient).

The calculation 10b in Ref. [10] is discussed hereafter.

Steady state conditions

The demonstration of a thermohydraulics and neutronics stable steady state before the initiation of the transient calculation ($t = 0$ s in the following) is a necessary condition to achieve reliable results. Differences in thermohydraulic code versions models affected the steady state results. The reasons already mentioned in the previous section prevented the achievement of a unique set of initial conditions, though the same thermohydraulic input deck was adopted.

The data in Tab. 5 have been taken at the beginning of the MSLB transient, after 200 s of steady-state/transient run and are related to the calculations identified in Tab. 4. Ranges of values resulting from the calculations discussed in Ref. [10] are also reported in the first row of Tab. 4. It is assumed that main thermohydraulic values reached during steady state calculations are close enough to guarantee proper transient behavior and to enable comparison of the transient results.

Table 5. Main results obtained from the application of coupled thermohydraulics 3-D neutron kinetics code to the OECD/CSNI/NSC TMI-1 MSLB benchmark (end of steady state)

Run Number	PRZ Pressure (MPa)	SG1 Pressure (MPa)	Core Power (MW)	SG1 Mass (kg)	SG1 Superheat (K) ^a
1 to 10b ^b	14.9 to 15.0	6.38 to 6.46	2606 to 2772	25 536 to 29 052	3.6 to 22.0
10b ^c	15.0	6.38	2772	25 536	19.4
11 ^c	14.89	6.36	2772	25 231	19.9
12 ^c	14.96	6.36	2772	27 799	23.4

^aTaken at the entrance of the SL1.

^bCode runs identified in Table 4 of Ref. 14.

^cCode runs identified in Table IV of the present paper.

Relative axial and radial power distributions are checked against run 10b results at the end of steady state. The satisfactory agreement was achieved from the various coupled codes predictions. The axial distribution proposed by the Organizers of the MSLB is very close to the distribution predicted by the Relap5-Parcs coupled code. Relative radial power distribution at the end of the steady state, obtained from code run 10b is shown in Fig. 8.

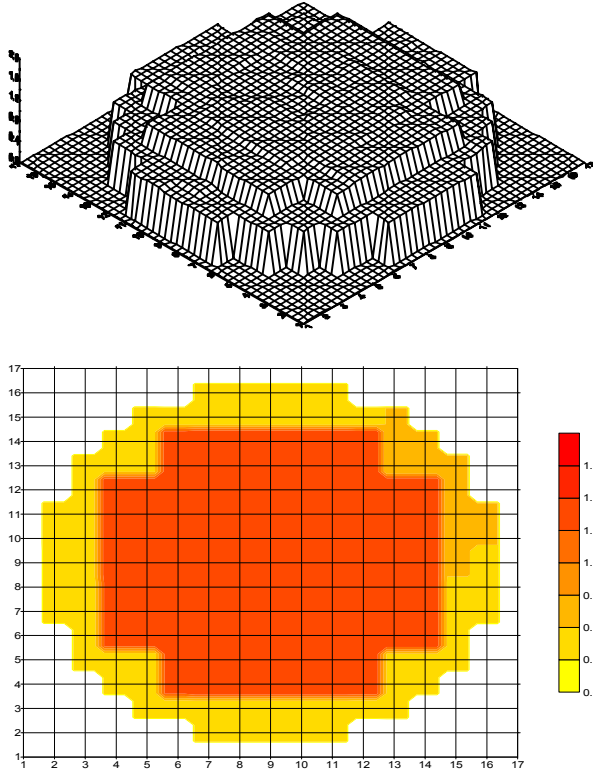


FIG. 8. Relative radial power distribution for the TMI-1 MSLB at SS, code run 10b (Relap5/Parcs code).

Transient scenario

The overall system response during TMI-1 MSLB Phase 3 scenario with return to power and quality of the different coupled codes predictions can be derived from the set of Figs. 9 to 13. The results are related to the code runs 10b, 11 and 12 of Tab. 4. The additional close comparison of the global and local thermalhydraulic values, as well as of the characteristic spatial distributions are provided for directly coupled Relap5/mod 3.2 gamma with Quabbox and Parcs (Figs. 14 to 21).

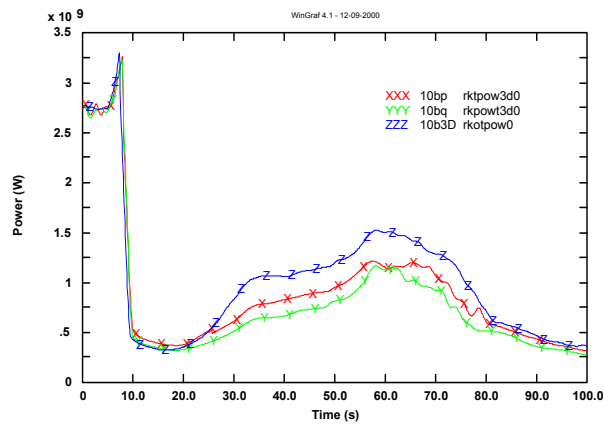


FIG. 9. Application of coupled thermalhydraulics/3-D neutronics codes to the TMI-1 MSLB: core power.

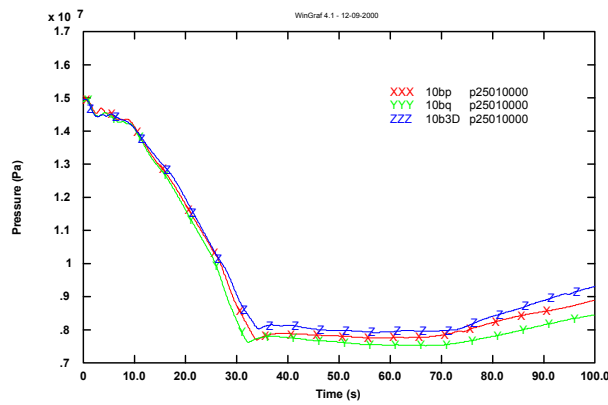


FIG. 10. Application of coupled thermalhydraulics/3-D neutronics codes (Tab. 4) to the TMI-1 MSLB: primary system pressure.

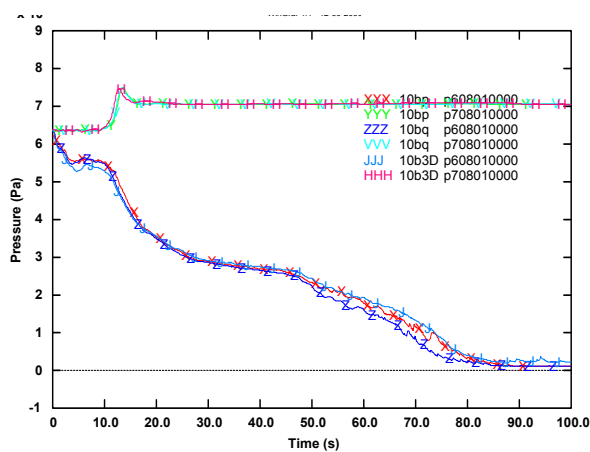


FIG. 11. Application of coupled thermalhydraulics/3-D neutronics codes (Tab. 4) to the TMI-1 MSLB: steam generator pressure.

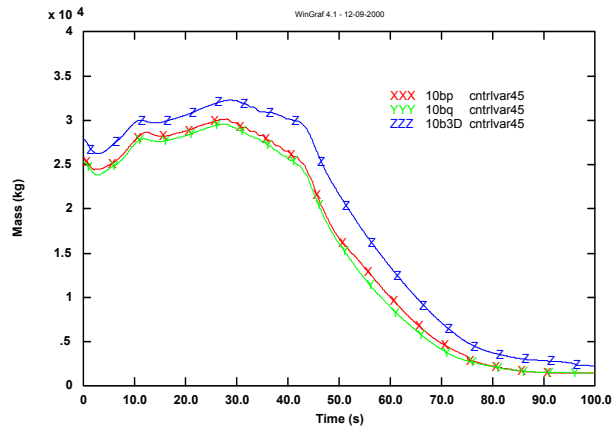


FIG. 12. Application of coupled thermalhydraulics/3-D neutronics codes (Tab. 4) to the TMI-1 MSLB: mass inventory in broken steam generator (Steam Generator No. 1).

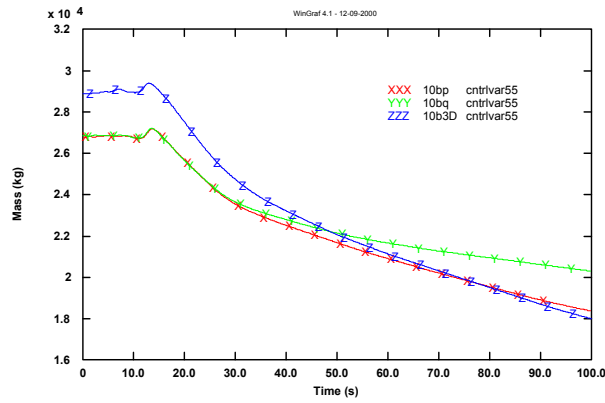


FIG. 13. Application of coupled thermalhydraulics/3-D neutronics codes (Tab. 4) to the TMI-1 MSLB: Mass inventory in intact steam generator (Steam Generator No. 2).

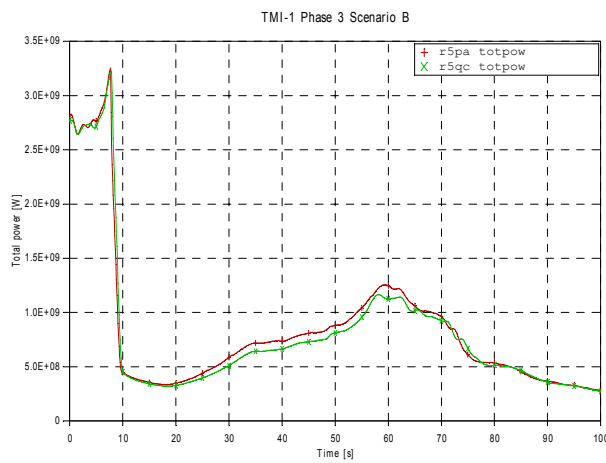


FIG. 14. Core Power calculated by Parcs and Quabbox based coupled codes (direct coupling).

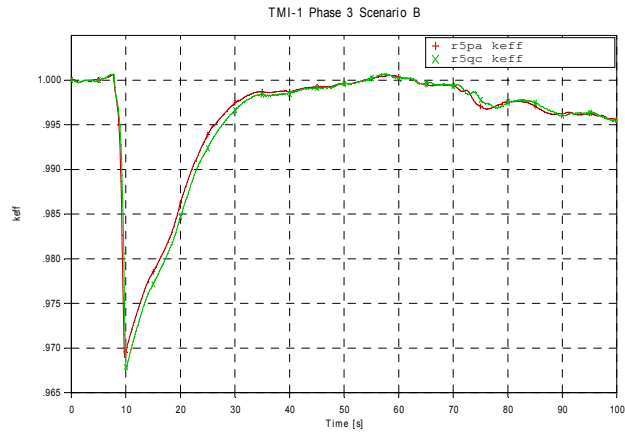


FIG. 15. Effective multiplication factor calculated by *Parcs* and *Quabbox* based coupled codes.

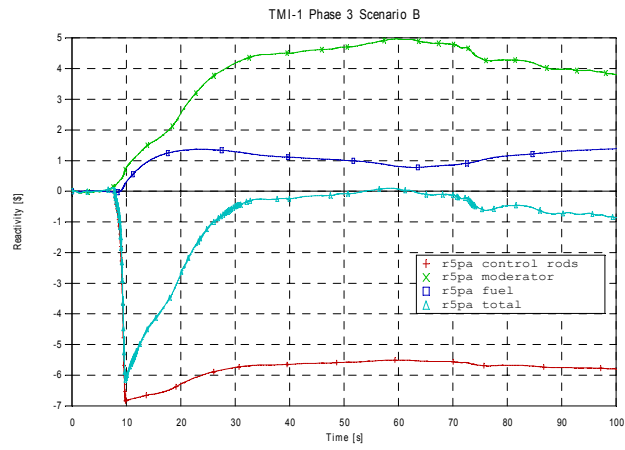


FIG. 16. Reactivity components calculated by *Relap5/mod3.2 gamma* / *Parcs* coupled codes.

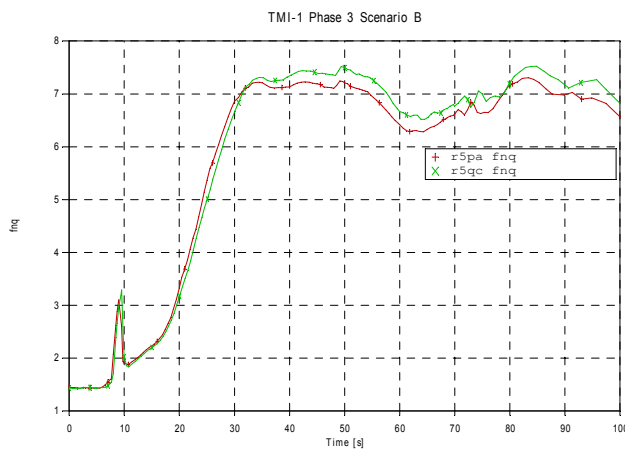


FIG. 17. Power peaking factor calculated by *Parcs* and *Quabbox* based coupled codes.

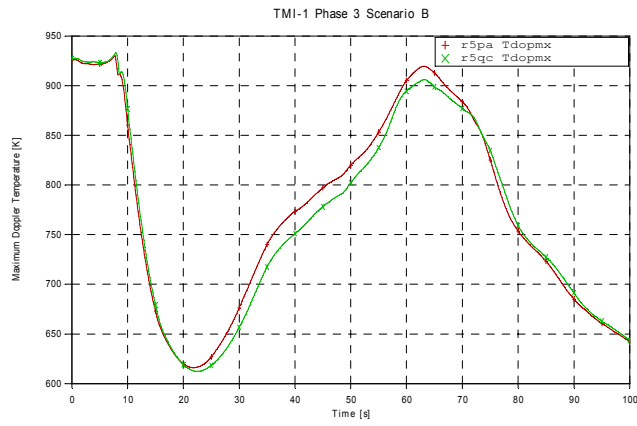


FIG. 18. Maximum Doppler temperature calculated by Parcs and Quabbox based coupled codes (direct coupling).

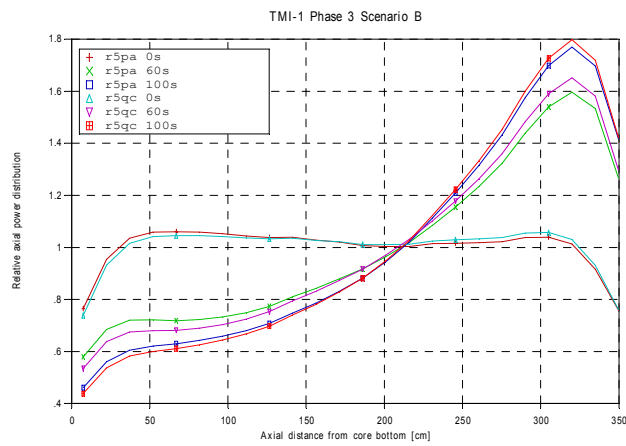


FIG. 19. Relative axial power distributions calculated by Parcs and Quabbox based coupled codes (direct coupling).

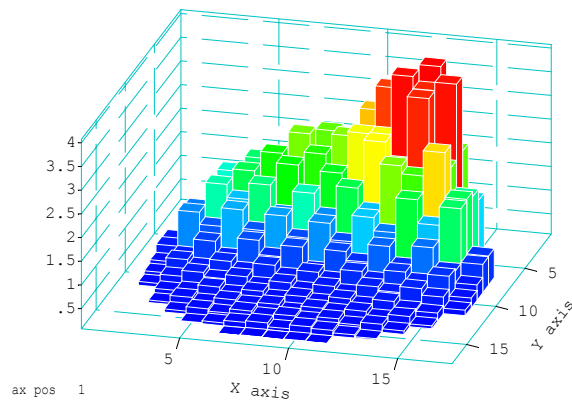


FIG. 20. Relative radial power distribution at $t = 60$ s calculated by Relap5/mod3.2 gamma /Parcs based coupled code (direct coupling).

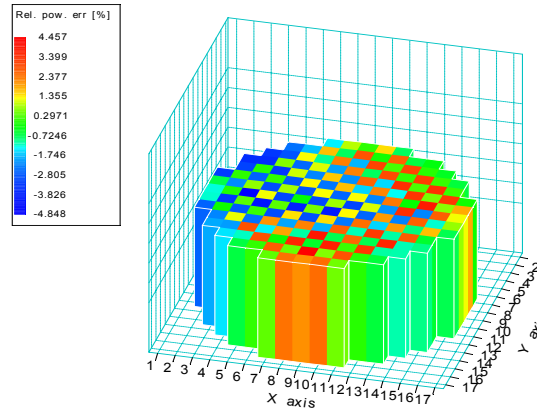


FIG. 21. Relative error in f_{xy} power peaking factor at $t = 60$ s calculated by *Parcs* and *Quabbox* based coupled codes (direct coupling).

Phenomenology predicted by the three coupled codes runs (overall system behavior)

The most relevant outcome from the study is constituted by the prediction of the core power and of the primary system pressure, Figs. 9 and 10, respectively. The core power excursion is controlled by the assumed scram logic; the power does not overpass 120% of the initial value. The primary system pressure decreases to a value that allows the actuation of the HPIS.

The fast depressurization of the broken steam generator (loop 1) can be observed in Fig. 11. The fluid mass in the broken SG does not decrease in the early phase of the transient (Fig. 12) due to assumption of increased FW flowrate before MFW isolation that compensates break flows. Only limited number of thermohydraulic parameters of primary importance for codes comparison is shown here. Rest of the system behavior is as expected for this type of overcooling transient.

Core mass flowrate slightly increases during the transient, owing to improved Main Coolant Pumps (MCP) efficiency caused by increased density of the cooler liquid. In the intact loop cold leg fluid temperature becomes higher than in the hot leg of the same loop due to the heat transfer reversal in the intact steam generator.

The present results are basically within the dispersion bands obtained from the envelope of results predicted by other participants to the Benchmark, Ref. [11]. In this connection it should be noted that we did not consider the recommendation, coming from the Benchmark proponents, to neglect passive structure masses in the secondary side of SG in order to overestimate the cooling potential of the MSLB event. This actually causes a delay of a few seconds in the power excursion compared to the case when passive structures are not modeled.

Comparison among results obtained by different coupled codes

The system performance including the 3-D core behavior is similarly predicted from a qualitative viewpoint by the three calculations that are considered in the present work. However, noticeable differences in the results related to total core power can be seen (Fig. 9), and that has corresponding influence on rest of the system variables.

Differences are mostly connected with the return-to-power phenomenon, while the first power peak has similar features for the three code runs (slightly earlier scram predicted by *Relap-3D*). In relation to the second power peak the run 10b (*Relap5/mod3.2* beta coupled with *Parcs*, Tab. 4) was used as a reference (predicted power in case 10b is bounded by case 11 and case 12 values).

The power ‘underestimation’ resulting from the Relap5/mod3.2 gamma coupled with Quabbox appears mostly to be due to the different neutron kinetics code and to the coupling options, because steam generator mass inventories and pressures are similarly predicted in code runs 10b and 11 (Figs. 11 and 12). Primary system pressure is also underestimated in code run 11 compared with code run 10b (Fig. 10), but this is a consequence of the underestimation of core power.

The power ‘overestimation’ resulting from the Relap5-3D coupled with Nestle appears mostly to be due to the different values of initial conditions predicted at the end of the steady-state and to the thermalhydraulic prediction. In particular, larger initial fluid mass in the broken steam generator gives rise to a larger potential for primary system cooling, that is a prerequisite for wider return-to-power.

Additional notes from the analysis are:

- Core power, following the second peak, converges to a similar value at a similar time in the three calculations (Fig. 9);
- Core power (slightly) oscillates in the period 0-6 s in calculations 10b and 11, but it is stable in calculation 12.

The timing of important values, peak power values just before scram and at return to power, as well as power integral up to the scram and for the first 100 s of the transient, for three calculations, are given in Tab. 6.

Table 6. Main TMI-1 MSLB benchmark transient results obtained from different coupled codes

Run Number	Break Open/ Calculation End (s)	Peak Power Time (s)	Shutdown Initiation (s)	SP2 Start (s)	Power at t=2 (W)	Peak Power (W)	Power Integral 0 to 20 s (MJ)	Power at 70 s (W)	Power Integral 0 to 100 s (MJ)
1 to 10b*	0/100	1.2 to 29.7	11.6 to 10.1	44.8 to 49.4	94 to 100	114.0 to 116.0	2.4 to 2.9 MJ*	4.3 to 39.5	2.5 to 24.7 MJ*
10b	0/100	7.9	12.4	46.4	100	117.4	2.504	36.9	9.004
11	0/100	7.65	12.2	46.2	100	116.6	2.504	21.03	9.1204
12	0/100	7.1	11.9	47.1	100	119.1	2.464	25.6	10.204

*Code runs identified in Table 4 of Ref. 14.

†Based on 2.4×10^7 .

*Code runs identified in Table IV of the present paper.

Additional comparison for Parcs and Quabbox based coupled codes

In order to take closer look on possible causes of differences in coupled codes predictions additional calculations are performed taking nodalisation used in run 10b as a reference for both Parcs and Quabbox coupled codes. The idea was to eliminate all differences originated from the coupling procedure (as far as practicable).

The standard Parcs is coupled to Relap5 mod3.2 beta (different default break flow models compared with the gamma version) using PVM for ‘external’ coupling and specific steady state to transient transition sequence, with thermalhydraulics feedback realized through functional dependence of cross section data. The new Parcs based coupled code was prepared using direct coupling to the Relap5/mod 3.2 gamma (the same coupling structure adopted for Quabbox). Steady state is achieved using repeated calls to Parcs in steady state mode during Relap5 steady state calculation, and cross section thermalhydraulic feedback part was realized using original cross section libraries and PSU interpolation scheme.

The new Phase 3 Scenario B (or return-to-power cross sections) calculation was performed using the new Parcs (directly coupled, label r5pa) and the old Quabbox (directly coupled, label r5qc) coupled codes. The agreement in calculated reactor power is better than before, but Parcs calculated power is still slightly higher during the time period between 20 and 70 s from the start of the transient (Fig. 14). The second power peak is reached at around 60 s.

Graphical representations of core related parameters are limited to additional calculations performed with Parcs and Quabbox coupled codes. The effective multiplication factor for both calculations is shown in Fig. 15. Except slightly higher inserted negative reactivity in Parcs case, k_{eff} is very similar in both calculations. The discrepancies appear to be related to the way the control rods are treated by the two codes.

A useful insight in the MSLB neutronics behavior is possible by inspecting reactivity components shown in Fig. 16 (Parcs calculation). After initial reactivity and power decrease due to control rod insertion, the reactivity increases due to negative moderator and fuel temperature coefficients (the influence of moderator is more significant). A similar dependence of reactivity components can be seen even in the point kinetic case. What can not be seen in point kinetic case is the decrease in reactivity worth of inserted control rods due to shift of axial power distribution toward the upper part of the core during the transient. The reactor experiences a slight re-criticality just before 60 s after transient initiation. All up to now mentioned reactor parameters are global values available from the point kinetics calculation, too.

The comparison among the characteristic (in relation to 3-D neutron kinetics) point values and spatial distributions shows the actual advantage of the coupled code prediction. In Fig. 17 the comparison of power peaking factor is shown. The agreement is complete in the beginning (up to 30 s) and very good in the second part of the accident. The power factor values predicted by the Parcs are always slightly below the values predicted by Quabbox. The maximum calculated f_{pq} value is between 7.2 and 7.5. Another important local parameter is the maximum “fuel Doppler” temperatures (proper weighting was prescribed in the benchmark and was used to relate fuel center and surface temperatures) is shown. The agreement between the time trends predicted by the coupled codes is again very good. However, the value calculated by Parcs is higher than the value calculated by Quabbox up to the time of the second power peak.

This may imply that local feedback is responsible for corresponding lower f_{pq} in Parcs case. Relative axial power distributions calculated by Parcs and Quabbox at the end of steady state ($t = 0$ s), at time of second power peak ($t = 60$ s) and at the end of calculation ($t = 100$ s) are shown in Fig. 19. The prediction of both codes is very close at the beginning and at the end of the transient, with slightly higher differences at time of return to power. Relative radial power distribution (power of the fuel assembly divided by power produced in average fuel assembly) at $t = 60$ s as calculated by Parcs is shown in Fig. 20. Namely, the f_{xy} quantity is reported in the vertical axis: this quantity represents the power produced within the fuel element identified by ‘x’ and ‘y’ and the average core power. It can be seen that most of the power is produced in the “affected” half of the core with power of the assembly in the vicinity of the stuck control rod being almost four times larger than the average assembly power.

In the similar representation of Fig. 21 the relative error in f_{xy} values calculated by Parcs and by Quabbox is shown. The relative error is defined by $100 \cdot (f_{\text{xyQC}} - f_{\text{xyPA}}) / f_{\text{xyPA}}$, where the pedices QC and PA refer to Quabbox and Parcs codes calculations, respectively. The maximum relative difference between the results is bounded by $\pm 5\%$, which appears acceptable for this type of calculation. A minor power tilt across the reactor core can be seen in the adopted representation of power distribution. The position of the stuck rod is in the North-East corner of the graphs.

3. BWRTT TEST DESCRIPTION

The experiment was carried out by manually (tripping the turbine) closing the Turbine Stop Valve (TSV) at an operating prescribed power level equal to 61.65% of its nominal value [12], [14]. As a result, a pressure wave is generated in the main steam piping and propagates at sound velocity with relatively little attenuation into the reactor core. The pressure wave reaches the core zone following two different paths; through the steam separator filled with a mixture of water and steam and through the vessel downcomer filled with water. This double unsynchronized effect, results in dramatic

changes of the core void inventory. The inherent feedback of the core makes the reactor power to exhibit a rapid exponential rise. Few milliseconds after the TSV closure, the Bypass Valve (BPV) is opened automatically to reduce the pressure rise in the steam line. The TSV signal that activates the reactor scram initiation was intentionally delayed to allow a relative neutron flux effect to take place in the core. When the scram setting point is exceeded (95% of the nominal power), the control rods are inserted after a delay time of 0.12 s.

3.1. Calculation model

In the current framework a parallel processing for coupling 3-D kinetics PARCS code with RELAP5 system code is adopted. This allows the codes to be run separately and exchange data during the calculation. The coupling process consists in performing calculations to evaluate the thermal-hydraulic parameters evolution using the RELAP5 modules and the kinetic solution is obtained using the PARCS solver. The PARCS reads the fuel and coolant temperature, coolant density from the RELAP5 interface to estimate the feedbacks that affect the instantaneous neutron flux value. In the same way the RELAP5 performs its calculations using as input the time-space dependent core power from the PARCS interface.

Neutron kinetic model

The PARCS/2.3 code is used to evaluate 3D space-time core power history and group fluxes. It uses a non-linear nodal method to solve two energy groups' diffusion equations. The PB core is modeled neutronicly by considering 18 fuel assembly types and one reflector element. Each composition is defined by the material properties and its burn up (exposure, spectral history and control rod history). All these data are readily available from a two-energy group cross-section library. The library has two independent variables: the fuel temperature and the coolant density as shown in Table 7. For six fixed values of fuel temperature and six fixed values of moderator density, a series of cross section data are specified in a lookup table format.

These include the diffusion coefficients, the macroscopic cross sections for scattering, absorption and fission, the assembly discontinuity factors, the xenon absorption cross sections, and the detector cross section. A linear surface interpolation is straightforwardly performed to derive intermediate cross section values.

According to Ref. [15] four fundamental pre-conditions shall be fulfilled for the correct application of a complex thermal-hydraulics system code to the prediction of transient in NPP:

- The code should be frozen,
- The code should be properly qualified through wide, international, assessment program,
- The developer of the nodalisation should be a qualified code user for the selected code,
- The nodalisation (of the plant) once developed should be properly qualified.

Table 7. Macroscopic cross section lookup tables format

T_f fuel temperature (°K)	400	800	1200	1600	2000	2400
ρ_m moderator density (kg/m ³)	141.59	226.15	299.64	435.04	599.17	779.4
Macroscopic cross sections (cm ⁻¹)	Σ_1	Σ_2	...			
			...	Σ_{34}	Σ_{35}	Σ_{36}

Thermal-hydraulic model

A plant nodalisation was performed for the system code RELAP5 Mod3.3 as shown in Fig. 22. This later has been previously qualified through a series of sensitivity analyses [16]. It includes various vessel components, coolant and steam and recirculation loops. In the current model, the four steam lines are lumped into one, and each of the two pumps of the recirculation loop drives one jet pump that represent ten jet pump in the real plant. The core region is modeled by 33 heated channels with 24 axial active nodes. Each channel lumps a specified number of fuel assembly. These fuel assemblies were grouped together according to their thermal-hydraulic and kinetic properties which take into account the lattice type, the relative power, the inlet flow area, and the relative position within the core.

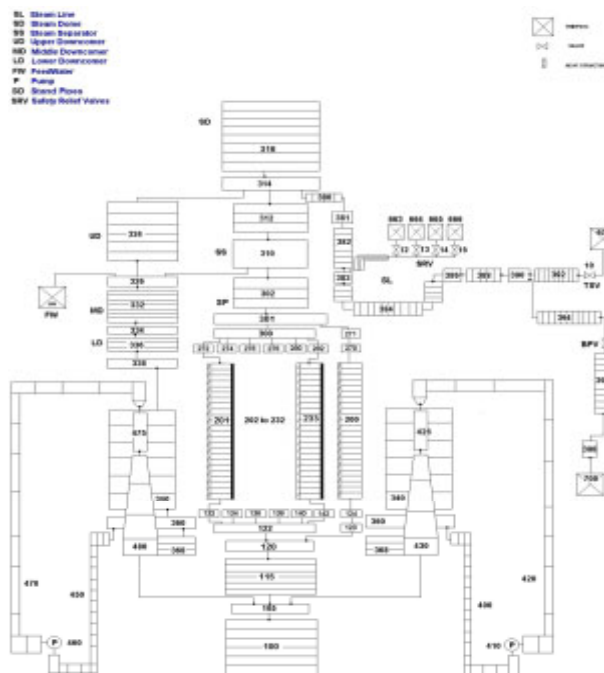


FIG. 22. Adopted nodalisation schema for the peach bottom.

3.2. Main initial and boundary conditions

The PB-TT2 experiment was carried out under the operating conditions summarized in Table 8. For the TSV closure mode, as pointed out in [17], the initial part of the TSV closure causes small amount of flow reduction. Hence in the present work it is assumed a non-linear TSV closure in order to better reproduce the measured pressure wave amplitude in the core zone. On the other hand, a linear steam Bypass valve opening is considered. On the other hand, it is assumed that 2% of the reactor power is released as gamma heating in the in channel coolant and 1.7% in the core coolant bypass; the rest is generated in the fuel.

Table 8. Main PB2 TT2 initial conditions

Item	Value
Core thermal power, MW	2 030.0
Feedwater flow, kg/s	980.26
Reactor pressure, MPa	6.79847
Total core flow, kg/s	10 445.0
Core inlet subcooling, J/kg	48 005.3
Feedwater temperature, K	442.31

3.3. Results

Steady state calculations

The main coupled achievements for the steady state are compared with some available reference and experimental data as outlined in Table 9. A two dimensional flux map is sketched in Fig. 23, the power peak is located in a peripheral zone. This spatial flux asymmetry justify the use of the coupled code technique. The trends of relevant parameters such as the average axial void and power profile are plotted in Fig. 24 and Fig. 25, respectively. Discrepancies between the measured and calculated axial power shape could be related to the resolution of the lookup table (Table 7) used to derive the cross sections or the accuracy of the system code constitutive relations in estimating the void distribution in sub cooled and saturated nucleate boiling zone.

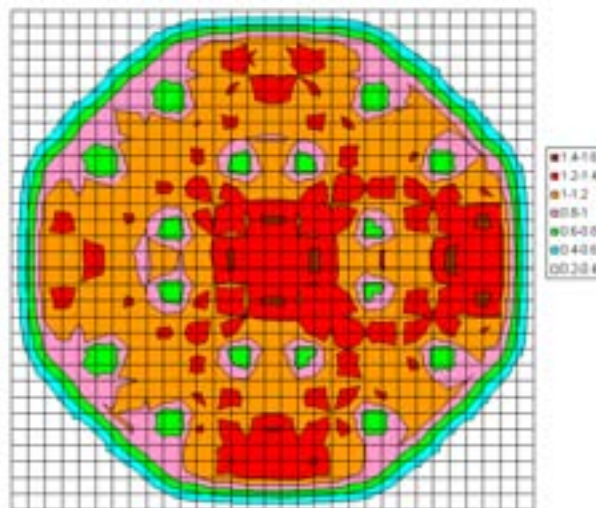


FIG. 23. Steady state 2D flux core distribution.

Table 9. Main steady state achievement compared with experimental data

Parameter	Calculated	Specifications
Core exit Pressure, MPa.	6.82430	6.83412
Vessel Dome Pressure, MPa.	6.80130	–
Core Pressure drop, MPa.	0.0989 ^{**}	0.113561
Total Jet pump flow, Kg/s.	10418.5	10445.0
Core inlet flow, Kg/s.	9639.71	9600.0
Core Bypass flow, Kg/s.	779.62	–
Inlet core Temperature, K.	547.73	547.67
Inlet core Enthalpy, KJ/Kg	1208.2	1209.055
Core average Void Fraction	0.316	0.304
Core average Exit quality	0.0967	0.0970
K-eff	1.004856	
Position of Maximal value, Radial Peaking factor	(x = 27, y = 19, z = 16) (2.38)	
Maximum Mean axial position, Axial Peaking factor	15 (1.446)	13 (1.413)

(**) Pressure (vol_301)-Pressure (vol_120) see also Fig. 1.

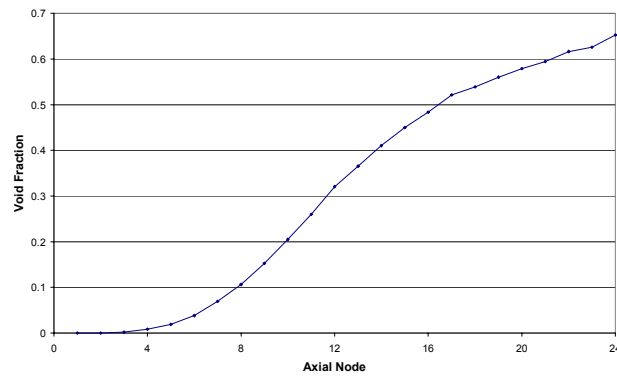


FIG. 24. Mean axial void profile.

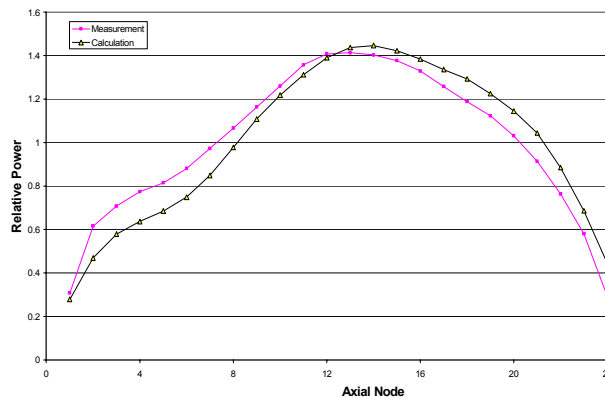


FIG. 25. Steady state mean power axial distribution.

Transient calculations

During the Turbine Trip transient complex kinetic and thermal-hydraulic feedback mechanisms are involved. These interactions could be classified, as summarized in Table 10, according to their nature; prompt and delayed feedback, and to their time of occurrence.

Table 10. Main sequences and events occurred during the TT transient

	Leading Events	Resulted Events	Reactivity Response	Power Course According to the experimental results
Phase-1 0.0-0.3 s	TSV Closure – First core pressure response	Pressure wave propagation along the steam lines.	No reactivity is induced	Power at its steady state level
Phase-2 0.3-0.8 s	Pressurization of the core.	Reduction of the core Void inventory.	Positive reactivity insertion due to void collapsing	Power rises exponentially with decreasing period.
Phase-3 0.3-0.8 s	Pressurization of the core.	Reduction of the core Void inventory. Increase of inlet mass flow rate	Prompt feedback effects. Small Negative reactivity is induced due principally to Doppler effects and secondary to gamma heating in the coolant.	Power excursion slowed down and initiates its self-limiting behavior followed by its peak value.
Phase-4 0.8 – 5 s	Release of the power excursion Energy into the coolant. Control rods insertion	Increase of voids in the core.	Delayed feedback. Large negative reactivity is introduced due to void regeneration followed by the shut down reactivity of the control rods	Power course exhibits a self shut down trend followed by a sharp decrease after the scram.

Transient coupled code results are outlined in Table 11. The key parameter of the Turbine Trip test i.e. the amplitude of the pressure wave in the core zone is sketched in comparison with the experimental one in Fig. 26. The calculated trend matches with good agreement the measured pressure wave even though little differences exist in the time response prediction. The calculated response is anticipated by approximately 0.1 s. This difference seems to be related to the adopted dimension of the plant, which does not reproduce exactly the real coolant flow path lengths.

Table 11. Main transient achievements compared with experimental data

Parameter	Calculated	Experimental/or Specifications
Amplitude of Pressure Wave MPa Occurrence time (s).	0.3007 (0.82)	0.3025 (0.975)
Maximum core Power, %. Time occurrence (s).	279.97 (0.745)	279.09 (0.726)
Maximum steam flow through the bypass valve, Kg/s. Time occurrence (s).	665.86 (0.87)	647.25 (0.87)
Vessel dome pressure initial response, s.	0.28	0.38
Core exit pressure initial response, s.	0.32	0.42
Core exit Pressure (after 5s of transient), MPa.	7.1409	7.14621
Steam Bypass flow (after 5s of transient), Kg/s.	537.87	507.9
Maximum inserted reactivity, \$ Time occurrence (s).	0.79721 (0.74)	0.76 (0.69)

Owing to the inherent feedback effects, the rapid core pressurization leads to a partial void collapse, this in turns results in a positive reactivity insertion within the core. The power response is an exponential rise with decreasing period [18] (as it can be seen in Fig. 27 where the calculated trend is fitted against the measured one). Both curves display more or less the same global trend but the phenomena involved during the transient are different. In fact, the coupled code calculations predict slower power exponential rise at the beginning of the excursion phase, and the power runaway is stopped by control rods insertion. While the experiment shows prompt exponential excursion with faster decreasing reactor period.

Furthermore, as it is pointed out in Ref. [17] the power course after a rapid runaway exhibits a typical self-limiting behavior slightly before the reactor scram.

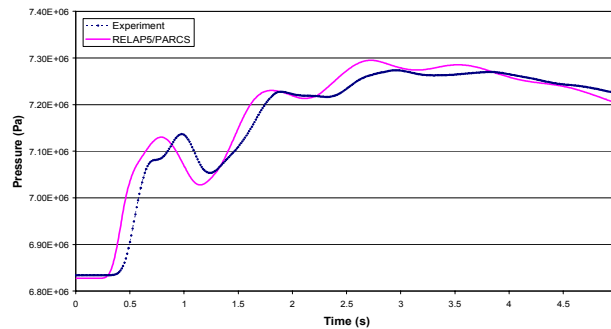


FIG. 26. Core pressure wave evolution.

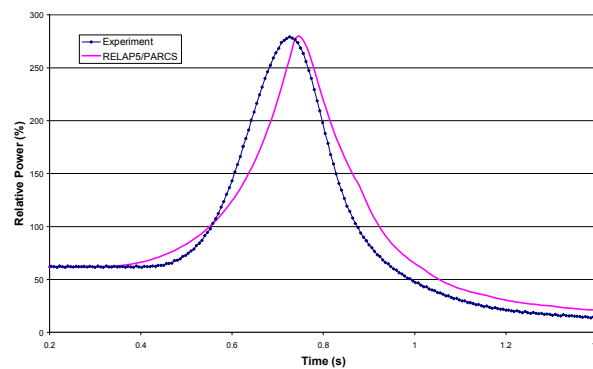


FIG. 27. Reactor power response during the TT transient.

Since the feedback expression could be put represented by the following relationship:

$$\text{Feedback} = f(\alpha_K) \cdot g(\Delta X_{TH})$$

Where:

α_K is a Kinetic coefficient depending on the cross section derived from bilinear interpolation of the values specified in the lookup table (Table 7).

ΔX_{TH} is variation of a thermal-hydraulic parameter such as fuel temperature, coolant density or void fraction.

Discrepancies between the calculated and measured data could likely be explained by either uncertainties related to the estimation of the thermal-hydraulic parameters or uncertainties related to calculations of the feedback coefficients [19].

Sensitivity analyses

In order to identify the degree of dependence between feedback mechanisms and the power course, a series of sensitivity analyses were performed. Through the considered cases (see Table 13), the positive and negative prompt and delayed feedback responses [20] are assessed.

Table 12. Sensitive cases and their relative investigated feedback

Case Number	Description
Case-1 Case-2	Gap Conductance +20 % Gap Conductance -20 %
Case-3 Case-4	Fuel heat capacity +20 % Fuel heat capacity -20 %
Case-5 Case-6	4 % of direct gamma heating 0 % of direct gamma heating
Case-7 Case-8	77 core channels Single core channel
Case-9 Case-10	Point kinetic (0D): Low void Feedback coefficient Point kinetic (0D): High void Feedback coefficient

The positive void feedback is a result of the first pressure wave amplitude which collapses a certain amount of the core void. In absence of the possibility of investigating the slip model closures relationships the dynamic of void collapsing can be considered by varying the number of heated channels of the model (cases 7 and 8). In these cases the dynamic of different void distribution profiles during steady state and transients are investigated.

The negative prompt feedback response is a combination of the Doppler and the direct gamma heating void reformation effect. This feedback governs the self-limiting power peak amplitude and time occurrence. It is assessed by varying the gap conductivity or the fraction of gamma heating in the coolant (cases 1, 2, 5, 6).

The negative delayed feedback response could be assessed by changing the fuel heat capacity which is the main predominant effect of the core thermal resistance (cases 3 and 4).

The base case for this series of sensitivity analysis is a Turbine Trip without Scram since that the main difference between the experiment and the coupled code calculations is about the self-limiting power behavior prediction. The main results of the sensitivity study are summarized in Table 13, and the power evolutions are shown in Fig. 28 and Fig. 29 for 3D and 0D calculations, respectively. Steady state power distribution for cases 7 and 8 are sketched in Fig. 30 and 31, respectively. It is interesting to notice that more is the number of heated channel less is the core power distribution asymmetry.

Table 13. Considered cases for the sensitivity analyses

Case Number	Amplitude of Pressure wave MPa	Relative Peak Power (%)	Maximal inserted Reactivity (β)
Base Case	0.298 (0.785)	392.8 (0.830)	0.824 (0.785)
Case-1	0.299 (0.79)	370.2 (0.825)	0.814 (0.780)
Case-2	0.276 (0.77)	330.0 (0.830)	0.788 (0.785)
Case-3	0.297 (0.785)	444.4 (0.835)	0.843 (0.785)
Case-4	0.277 (0.775)	270.36 (0.810)	0.747 (0.770)
Case-5	0.298 (0.785)	393.1 (0.830)	0.824 (0.785)
Case-6	0.293 (0.785)	372.6 (0.835)	0.814 (0.79)
Case-7	0.301 (0.785)	403.6 (0.835)	0.828 (0.790)
Case-8	0.298 (0.785)	365.83 (0.835)	0.812 (0.795)
Case-9	0.284 (0.783)	238.02 (0.867)	0.709 (0.831)
Case-10	0.312 (0.867)	736.0 (0.795)	0.922 (0.747)

* Quantities between brackets indicate the time occurrence of the relative event.

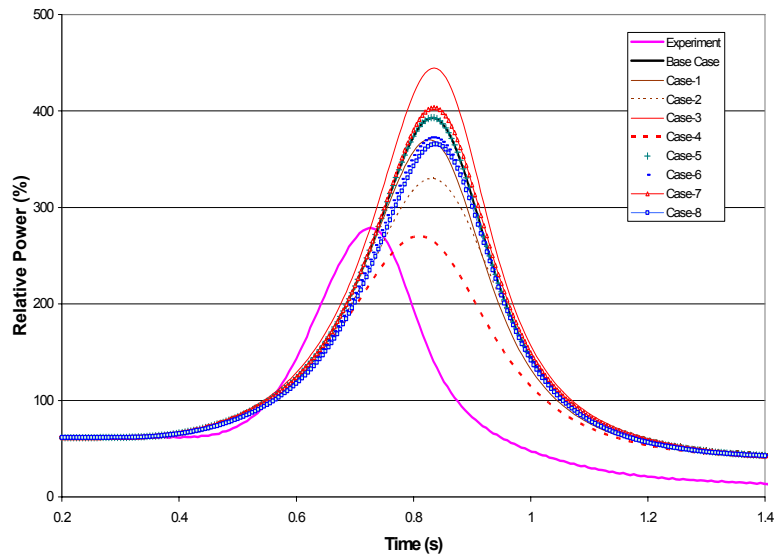


FIG. 28. Sensitive 3D calculations power response.

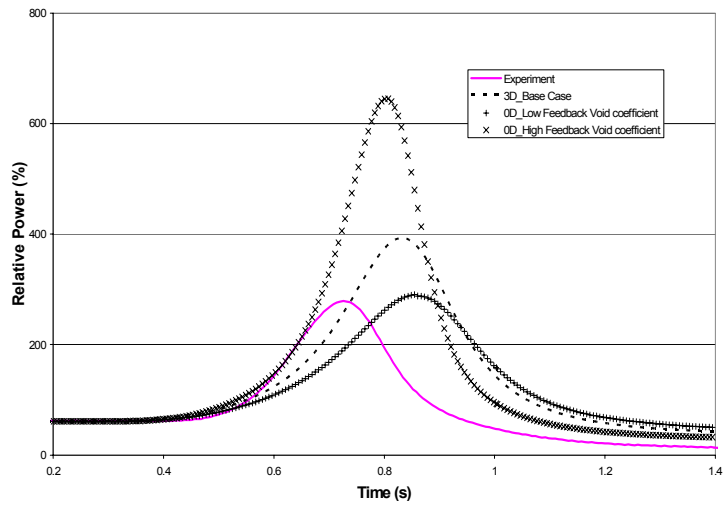


FIG. 29. Sensitive power responses.

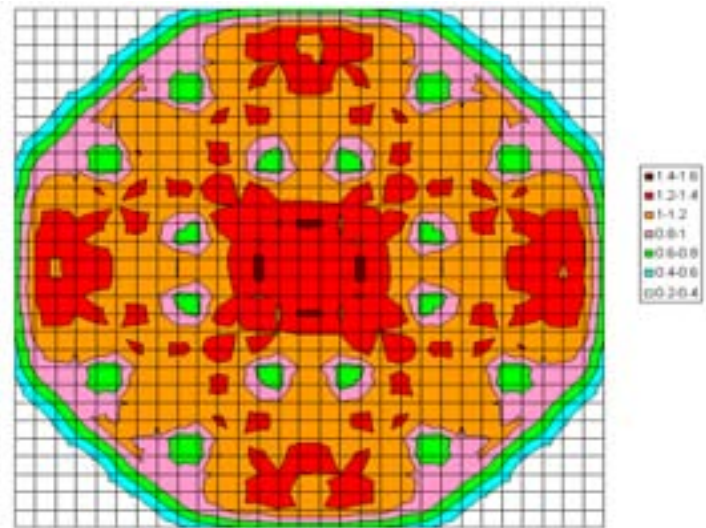


FIG. 30. Steady state mean 2D core power distribution for 77 channels nodalisation.

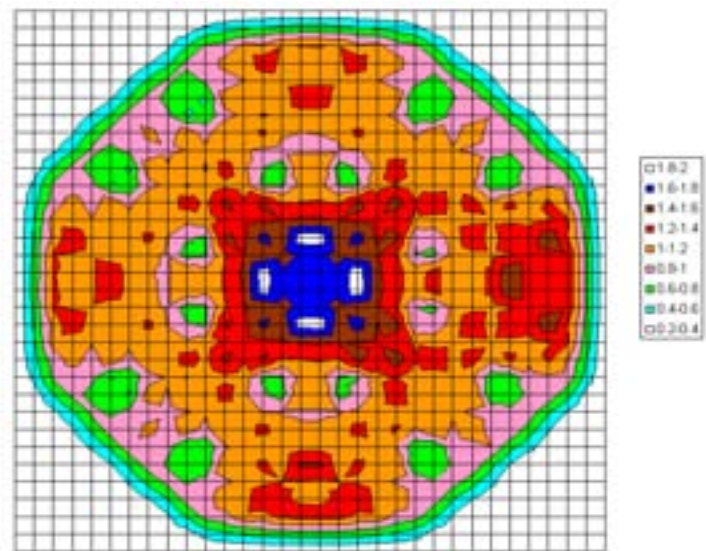


FIG. 31. Steady state mean 2D core power distribution for single channel model.

On the whole, according to the results outlined in Table 13 the following conclusion can be derived:

- The 3D calculations (cases 1 to 8) show that the self-limiting power behavior occurs at almost the same time even though slight differences are observed for the power peak value. This means that the effect of the prompt feedback did not influence significantly the power course. Then it is concluded that unlike the experiment where the power excursion and quenching is governed by the prompt void feedback response, the coupled code calculation predicts a power self-limiting behavior due mainly to delayed moderator feedback contribution (after the release of the excursion energy into the coolant). On the other hand the effect of the gamma heating which should be the predominant effect on the power self-limiting behavior [21] is overshadowed by the coupled code calculations since no significant effect is observed when varying this parameter.

The experimental self-limiting behavior occurs during the distortion (inflection) of the pressure wave amplitude following the bypass valve opening. During this lap of time (See Fig.32) the pressure rise stops momentary and consequently the void collapsing is relaxed. This phenomenon is not observed by the coupled code calculations since it is governed by roughly fast prompt feedback phenomena.

- The 0D calculations (case 9 to 10) were performed in order to investigate the power course behavior considering other feedback coefficient rather than those estimated through the lookup table. For this purpose and since the transient is governed by the void dynamics, two extremes values of the void feedback coefficient are chosen. Fig.28 shows that the power self-limiting behavior time occurrence, as well as the power peak variations, are too much pronounced than the results of the 3D calculations. It is interesting to notice that the experimental power trend is located between the two extremes 0D power curves. This confirms the fact that the coupled codes models did not estimate accurately the feedback involved during the TT transient.

4. VVER1000 CT DESCRIPTION

During the plant-commissioning phase at the Kozloduy VVER 1000 NPP Unit #6 a number of experiments were performed. One of them is the investigation of the behaviour of the nuclear power reactor parameters in case of switching on one main coolant pump (MCP) when the other three main coolant pumps are in operation [22]. The non-symmetric cooling of the reactor core results in non-symmetric reactivity feedback and subsequently non-symmetric radial power distribution

Before the experiment the reactor power level was reduced from 75% (2250 MW) to approximately 21% by consecutive switching off of MCP#2 and MCP#3. A few hours before the experiment MCP #2 was switched on, and the power was stabilised at 30% following the Technical specification requirements. According to the Technical specification for safety operation of the Units 5 and 6, switching on one main coolant pump in operation is performed when the reactor power is at 30% of the nominal level.

Depending on the initiating event, the reactor power is lowered to and then kept at specified set-points by RPLC as follows:

- 1) 1 out of 4 MCP trip; to 67%.
- 2) 2 out of 4 diametrically placed MCP trip; to 50%.
- 3) 2 out of 4 (neighbouring) MCP trip; to 40%.

During the experiment of switching on the MCP #3 the system and equipment of the Unit 6 performed according to design requirements for the corresponding level of the reactor power. Registrations of the parameters when there is a transient event are recorded by the design equipment, which includes the universal electronic system (UES), and NFMS (in-core reactor control system).

The initial power level is about 29.45% of the nominal with control rod group #10 inserted into the core at about 36% of the reactor core height. Control rod group #10 is not changing its position during the transient. Analysis of the initial 3-D relative power distribution showed that this insertion introduced axial neutronics asymmetry in the core. At the beginning of the transient there is also a thermal-hydraulic asymmetry coming from the colder water introduced in $\frac{1}{4}$ of the core when MCP #3 is switched on. This causes a spatial asymmetry in the reactivity feedback, which has been propagated through the transient and combined with insertion of positive reactivity.

4.1. Transient modeling

In the current framework a parallel processing for coupling 3-D kinetics PARCS code with RELAP5 system code is adopted. e.

Neutron kinetic model

The PARCS/2.3 code is used to evaluate 3D space-time core power history and group fluxes. It uses a non-linear nodal method to solve two energy groups' diffusion equations. The core region is subdivided considering 9 Hexagonal radial rings x 22 core axial planes taking into account peripheral, upper and bottom reflector. In total 283 rodDED and 110 UnrodDED compositions are considered. The cross sections related to these compositions are read according to five specified fuel temperatures and four coolant densities.

Thermal-hydraulic model

A plant nodalisation was performed for the system code RELAP5 Mod3.3. It includes various primary and secondary loop components. In the current model the following items are considered;

- the core fuel assemblies are lumped in 29 channels as shown in Fig.32.
- 4 Loops with 4 Horizontal Steam Generators.
- 20 axial levels for the core and 48 axial levels for the vessel
- ECCS Modeling.
- Make-up and Let-down systems modeled
- 2 different radial core mapping have been developed:
 - 28 T-H channels for the core (+ 1 bypass) based on the 28 different FA type (BU, enrichment) present into the core (see fig.33)
 - 27 T-H channels for the core (+ 1 bypass) based on the geometry of the core and on the position of the loops.

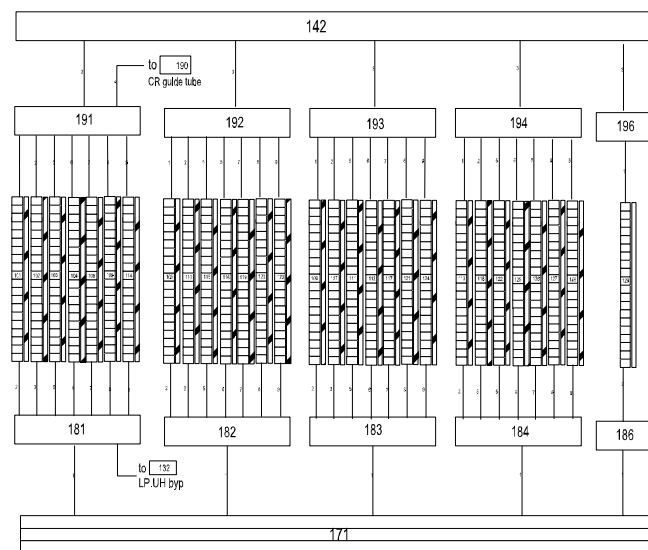


FIG. 32. RELAP5 core nodalization.

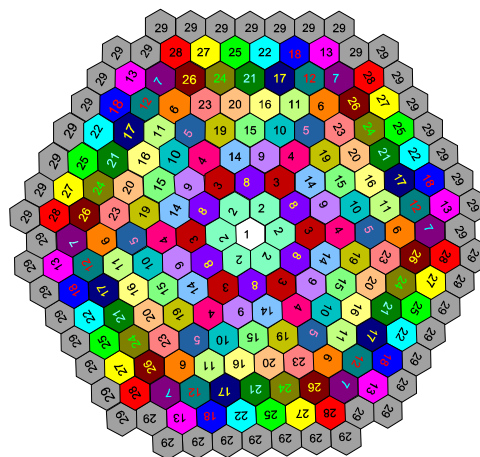


FIG. 33. Schema of the Adopted core channel configuration.

The Used Boundary Conditions are :

- SG Feedwater
- MSH secondary side pressure
- MCP #3 rotor speed.

4.2. VVER-1000 CT results

Steady state calculations

The main coupled achievements for the steady state are compared with some available code results. The Hot Zero Power calculation results are sketched in Fig.33. Good agreement is obtained with the reference results obtained by NEM code.

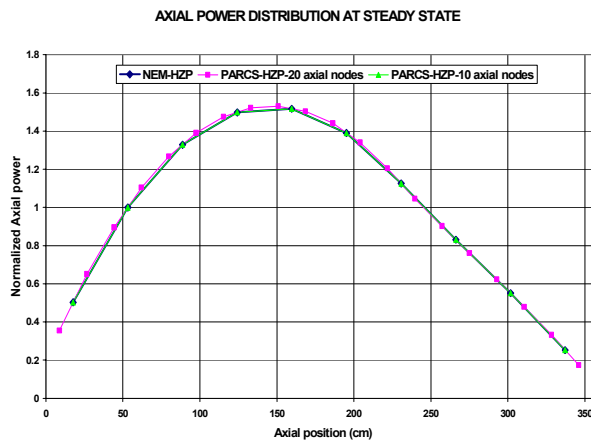


FIG.33. HZP calculation results.

For the steady state conditions, the calculated power profile is sketched against the TRAC/NEM results in Fig.34. Good agreement is obtained also for the SS axial power profile. RELAP5/PARCS results show that the number of axial nodes used to model the core has an impact of 2-3% on the maximum axial peaking factor (APF). The number of axial nodes modeled should then be considered in comparing APF distribution among participants (and, of course, also for the axial offset). The error in radial power distributions between RELAP5/PARCS and TRAC/NEM shows the same trend both for HZP and HP conditions. The distribution is that symmetric that it looks like the error is due to a systematic issue.

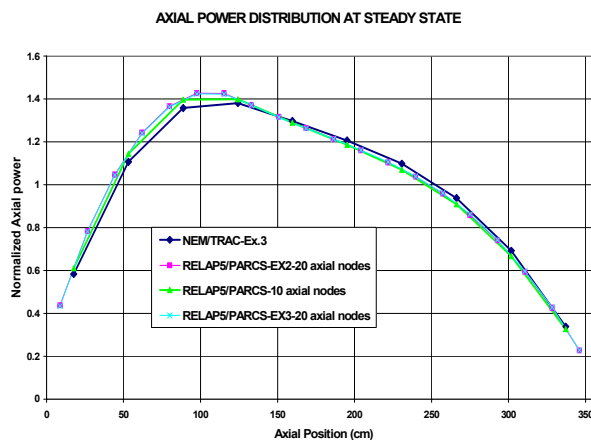


FIG.34. Steady _state mean axial power profile.

A two dimensional flux map is also sketched in Fig. 35. It is interesting to notice that the power peak is located in the peripheral zone with relatively symmetrical distribution.

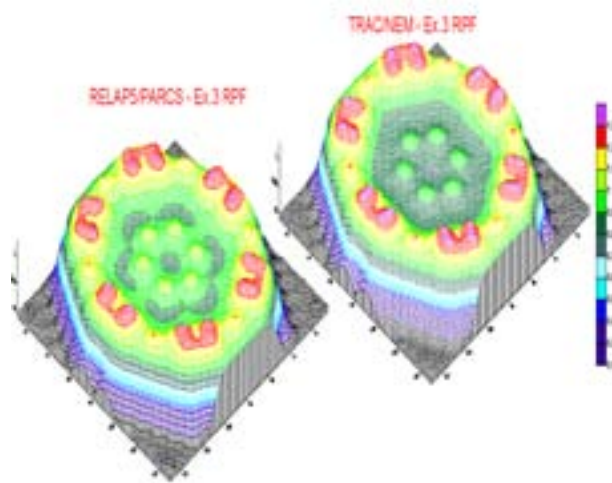


FIG. 34. Steady state 2D flux core distribution.

Transient calculations

During the Complex kinetic and thermal-hydraulic feedback mechanisms are involved due to the asymmetrical phenomena involved by the pump switching event. The main coupled code results are shown in comparison with experimental data in Fig.36 to 40 [23]. The agreement for almost all of the considered parameters is good with respect to the measurements. However, further work will be performed to investigate the mapping effects as well as the extreme scenario, which concerns rod ejection of the rod of group 10 inserted in the sector of switching the MCP.

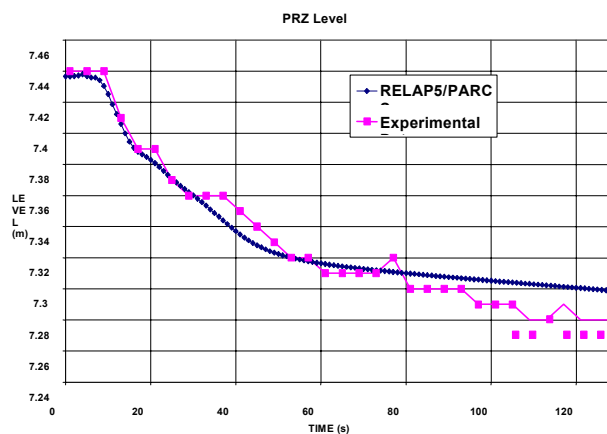


FIG. 36 Transient pressurizer level.

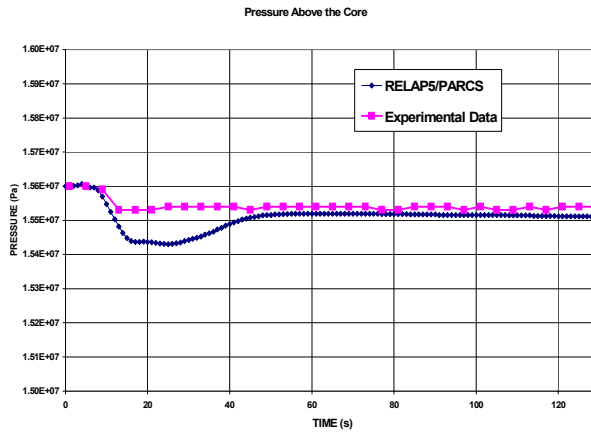


FIG. 37. Upper core zone pressure.

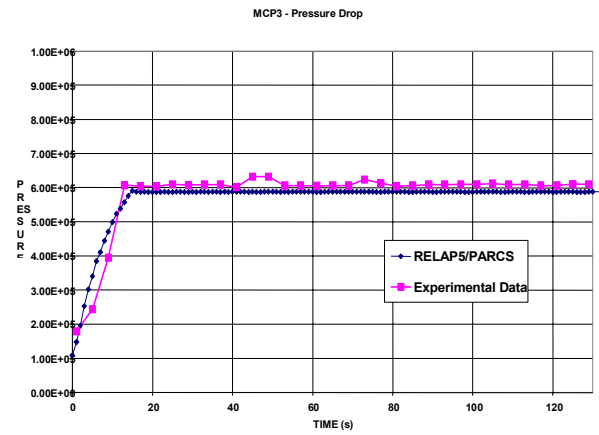


FIG. 38. Pressure drop in the MCP#3 zone.

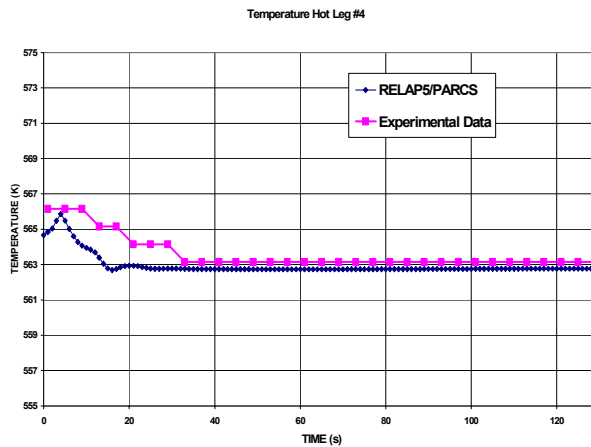


FIG. 39. Hot Leg#4 temperature.

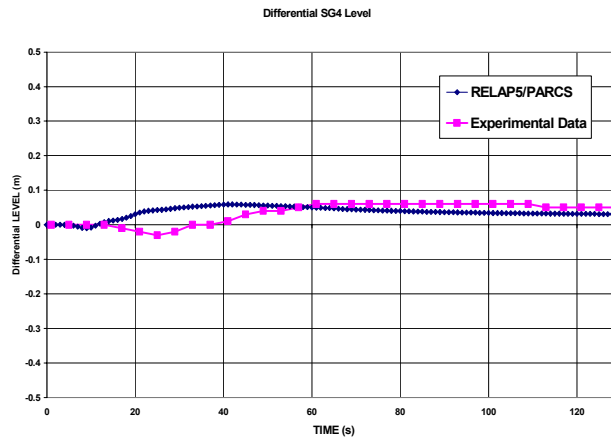


FIG. 40. Differential SG4 level.

5. RELEVANCE TO NATURAL CIRCULATION

Working conditions for nuclear power plants imply the existence of neutron kinetics feedback and, with very few exceptions, operation of main circulation pumps (MCP). In case of accidents or, more in general, off-normal operation, scram occurs and, MCP are switched off. This implies that, steady-state nominal conditions are characterized by neutron kinetics feedback and off-normal conditions are characterized by decay power and natural circulation. Therefore, in the majority of conditions or scenarios (accident or nominal) expected during the life of NPP, natural circulation and neutron kinetic feedback do not co-exist. However, this is not strictly true for existing NPP and the design of innovative reactors, based on natural circulation may completely change this picture. Situations, for existing NPP where natural circulation and neutron kinetics feedback co-exist can be summarized as:

- a. Anticipated Transient Without Scram including a number of RIA (Reactivity Initiated Accident);
- b. BWR instabilities.

In the former case, the methods used and qualified for coupled 3D neutron kinetics thermal-hydraulic calculations (status described above) are applicable. In the latter case the same statement is valid, however the predictive capabilities of coupled models may not be the same as in standard applications. This concept can be better understood from the lecture (in this Workshop) dealing with stability in BWR conditions.

6. CONCLUSION

Evaluation of the nuclear power plant performances during transient conditions has been the main issue of safety researches since the beginning of the exploitation of nuclear energy. Until recent years most of the safety analyses were successfully performed using thermal-hydraulics system codes. However, these codes cannot afford situations where complex feedback exists between core neutronics and thermal-hydraulics or when asymmetric phenomena are involved. Nowadays, significant increase of computer technology made possible the switch to new generation of computer codes. The accuracy of the simulations is now significantly improved by modeling directly the interaction between the neutron kinetics and the fluid-dynamics using the coupled codes calculation method. This technique consists in incorporating three-dimensional kinetic modeling of reactor core into thermal-hydraulic system codes. Benefits of such technology are expected for the industry, regulatory and licensing bodies, and more particularly relaxation of some safety margins, without compromising the NPP safety, allowing higher operating power and extended fuel cycles.

The present work constitutes a contribution to wider international activities, including the OECD/NEA benchmarks, the EC-CRISSES and VALCO projects, as well as the IAEA program aiming at characterizing the capabilities, validation, and use of coupled codes techniques in simulating realistically complex transients in NPPs. Three examples of application are considered, including various transients in PWR, BWR, and VVER NPPs. BE calculations of these transients were performed using the coupled RELAP5/PARCS code. In the current case the diffusion neutron kinetics equations were solved using the nodal method with two neutron energy groups and specified cross sections depending upon the fuel and coolant temperature. On the other hand the thermal-hydraulic evolution is derived through the governing two-fluid equations of mass momentum and energy and appropriate closure relationships. A coupling between the two BE codes was performed taking into account some additional procedures. On the whole, good general agreement between the calculation and the experimental trends is obtained notwithstanding some disagreements.

In fact, computer code calculations, as any simulation tools, are affected by errors arising from the unavoidable approximations connected with modeling requirements and limitations. Therefore, uncertainty and sensitivity analyses should be performed in order to quantify the error margins as well as to identify the origin of the observed discrepancies. This could be done by considering the CIAU method, which appear to have achieved a reasonable maturity level especially for deriving error bands related to BE codes simulations [24].

The main findings of the current study could be summarized as follows:

- The two energy group diffusion equations accuracy is quite good for common transients. However, better solutions should be obtained with more sophisticated techniques, including Monte Carlo and detailed neutron transport or multigroup diffusion equations and multidimensional cross section tables to get more realistic flux distribution.
- Constitutive models used to determine the evolution of the two-phase mixture, being mostly developed under steady state conditions, should be made more adapted to transient situation especially empirical correlation connected with the feedback between thermal-hydraulic and kinetic.
- 3-D nodalizations for the core or the vessel regions as needed for Best Estimate simulation of some phenomena as pressure wave propagation and flow redistribution in the core lower plenum zone.
- The importance and the need of uncertainty evaluations for coupled codes predictions is imperative owing to a large number of reasons discussed in this work. Therefore, uncertainty must be connected with any prediction.
- Also it is, till this date, not feasible to use too many radial nodes in the kinetic and thermal-hydraulic simulations despite the current availability of powerful computers. Nevertheless the ideal situation should be possible in the near future where the coupling will be performed considering each fuel assembly without any need to the lumping process.
- Careful considerations have to be taken in specifying spatial mapping between thermal-hydraulic and kinetic nodes of the core models, especially, when asymmetric or local core behavior is expected.
- Finally, the industry and the regulatory bodies should become fully aware about the capabilities and the limitations of the coupled code techniques.

Nevertheless, further and continuous assessment studies and investigations should be performed to enhance the degree of the Best Estimate simulations and consequently to improve the common understanding of safety issues, the design/operating conditions of nuclear reactors and, definitely, putting the basis for advancing the nuclear technology.

REFERENCES

- [1] IVANOV, K.I. BEAM, T.M., BARATTA, A.J., IRANI, A., TRIKOUROS, N., PWR Main Steam Line Break (MSLB) Benchmark – Volume I: Final Specifications, NEA/NSC/DOC(99)8 – (1999).

- [2] CAPPARIELLO, A., D'AURIA, F., GALASSI, G.M., BAJIS, T., Participation in the OECD/NEA/NSC TMI-1 MSLB Benchmark — Phase 1 0-D Neutronics, University of Pisa Report, DCMN - NT 328(98), Pisa (I), Jan. 1998.
- [3] USNRC "RELAP5/MOD3.2 Code Manual", NUREG/CR-5535. INEL-95/0174. August 1995.
- [4] The RELAP5-3D© Code Development Team "RELAP5-3D© Code Manual", INEEL-EXT-98-0083 – Rev. 1.2 May 2000.
- [5] THURGOOD, M. J., et al., Cobra/TRAC: A Thermohydraulic Code for Transient Analysis of Nuclear Reactor Vessel and Primary Coolant System“, NUREG/CR 2046, PNL 4385 (Pacific Northwest Laboratory), March 1983.
- [6] LANGENBUCH, S., QUABBOX/CUBBOX-HYCA, Ein Dreidimensionales Kernmodell mit parallelen Kuhlkanalen für Leichtwasserreaktoren“, GRS-A-926, Garching (G), (1984).
- [7] JOO, H.G., BARBER, D. A., JIANG, G., DOWNAR, T.J., PARCS: A Multidimensional two-group reactor kinetic code based on the non linear analytical nodal method, University of Purdue Report PU/NE-98-26, (1998).
- [8] BARBER, D.A., DOWNAR, T.J., WANG, W., Final completion report for the coupled Relap5/parcs Code, University of Purdue Report PU/NE-98-31, (1998).
- [9] TURINSKY, P.J., et al., NESTLE: A few-Group Neutron diffusion Equation Solver utilizing the Nodal Expansion Method for Eigenvalue, Adjoint, Fixed-Source Steady State and Transient Problems, EGG-NRE-11406, Idaho National Engineering Laboratory, June 1994.
- [10] D'AURIA, F., GAGO, J.L., GALASSI, G.M., TMI-1 MSLB coupled 3D Neutronics/Thermohydraulics analysis: planning and results, University of Pisa Report, DCMN NT 398(00)-rev.1, Pisa (I), Feb. 2000.
- [11] D'AURIA, F., GALASSI, G.M., Code Validation and Uncertainties in System Thermohydraulics, J. Progress in Nuclear Energy, vol 33 n° ½, pp. 175-216, (1998).
- [12] BEAM, T.M., IVANOV, K.N., BARATTA, A.J., Preliminary Report on First Phase of OECD PWR MSLB Benchmark, 2nd Benchmark Workshop, May 22-23, Madrid (E), (1998).
- [13] SOLIS, J., IVANOV, K., SARIKAYA, B., OLSON, A., and HUNT, K.W., Boiling Water Reactor Turbine Trip (TT) Benchmark, Volume 1: Final specifications. NEA/NSC/DOC (2001).
- [14] CARMICHAEL, L.A., NIEMI, R.O., Transient and Stability Tests at Peach Bottom Atomic Power Station Unit2 at end of cycle 2, EPRI NP-564, June 1978.
- [15] D'AURIA F., GALASSI G.M., Code Validation and Uncertainties in System Thermohydraulics. J. Progress in Nuclear Energy. 33, (1998).
- [16] BOUSBIA SALAH, A., D'AURIA, F., Analysis of the Peach Bottom 2 BWR Turbine Trip Experiment by RELAP5/Mod3.2. Nuclear Technology & Radiation Protection, XVII, pp. 44 (2002).
- [17] HORNYIK, K., NASER, J.A., RETRAN Analysis of the Turbine Trip Tests at Peach Bottom Atomic Power Station Unit 2 at the End of Cycle 2, EPRI-NP-1076-SR, (1979).
- [18] SPANO, A. H., BARRY, J.E., STEPHAN, L.A., and YOUNG, J.C., Self-Limiting Power Excursion Tests of a Water Moderated Low-Enrichment UO₂ Core in SPERT-1. IDO-16751, (1962).
- [19] WATSON, J.K., IVANOV, K. N.: Improved Cross-section Modeling Methodology for Coupled Three-dimensional Transient Simulations. Annals of Nuclear Energy, 29, pp. 937 (2002).
- [20] LEWIS, E.E., Nuclear Power Reactor Safety. John Wiley & Sons, (1977).
- [21] FRISCH, W., LANGENBUCH, S., and PETERNELL, P., The significance of Fast Moderator Feedback Effects in a Boiling Water Reactor During Severe Pressure Transients. Nuclear Science and Engineering. 64, pp. 843 (1977).
- [22] IVANOV, B., IVANOV, K., VVER-1000 Coolant Transient Benchmark: Phase-1 (V1000CT-1), Volume I: Final Specifications, OECD Paris, NEA/NSC/DOC2002/6, (2002).
- [23] VEDOVI, J., D'AURIA, F., IVANOV, K., 3D Neutron-Kinetics/Thermal-Hydraulics Coupled Analysis with RELAP5/PARCS of the OECD/DOE/CEA, VVER-1000 CT-1 Benchmark, Seminar and Training on Transfer of Competence Knowledge and Experience on Scaling, Uncertainty And 3d Coupled Calculations, University Park, Pa (USA), May 24–27, 2004.
- [24] PETRUZZI, A., D'AURIA, F., IVANOV, K., A novel methodology of Internal Assessment of Uncertainty for coupled 3D neutronics/thermal-hydraulics system codes, NURETH-10 Int. Conf., Seoul (S. Korea), Oct. 5–11, 2003.

COMPUTATIONAL FLUID DYNAMICS FOR NATURAL CIRCULATION FLOWS

B.L. Smith

Paul Scherrer Institute, Villigen, Switzerland

Abstract

This paper presents an overview of current methods employed in computational fluid dynamics (CFD). A description of the Navier-Stokes equations, and their extension to turbulent and multi-phase fluid flows, is presented; aspects of grid generation and numerical methods are also discussed. Lastly, to further elucidate some of the concepts presented, some sample applications are provided.

1. ORIGINS OF COMPUTATIONAL FLUID DYNAMICS (CFD)

Professor D. B. Spalding of Imperial College, London is known as the “Father of CFD”, and is also founder of the CHAM (Concentration, Heat And Momentum) organisation. With the advent of fast, digital computers in the 1960s, it became possible to attempt the numerical solution of the Navier-Stokes equations. In the early days, the general policy was to write specific codes for specific tasks, and universities, research laboratories and industry followed this trend. The result was a myriad of special-purpose codes, with each code almost exclusively operated by the person, or group, who wrote it. Documentation was usually poor, and often non-existent. There was almost always one key, central code developer, without whose presence the code would “die”. It would then be up to the new person coming along to write a new code, and himself/herself become the one central source of knowledge for the new software. In the 1970s, CHAM followed this general trend, but in 1980 adopted a single-code policy, with a central, robust solver, and then concentrated on model development. This new code system, PHOENICS, could be regarded as the first, genuinely multi-purpose CFD code, and a model for those that followed.

The exploitation of the commercial potential of this concept also began with PHOENICS. Its modular design, including a central solver, a pre-processor (mesh generator), a post-processor (graphical display of results) and modules to link in, as needed for the application, is now followed by all the main commercial CFD vendors. Currently the “Big 3” are FLUENT, ANSYS (CFX) and STAR-CD.



FIG. 1. The new era of CFD led by the modular design of PHOENICS.

2. THE BASIC EQUATION SET (NAVIER-STOKES EQUATIONS)

There are many ways of writing the governing equations, at different levels of complexity. As a starting point, those reproduced here are the basic set for single-phase, laminar flow. Later, we will discuss turbulence and multi-phase effects.

Mass continuity:

$$\frac{\partial \rho}{\partial t} + \frac{\partial}{\partial x_j} (\rho u_j) = 0 \quad (1)$$

Momentum transfer:

$$\frac{\partial (\rho u_i)}{\partial t} + \frac{\partial}{\partial x_j} (\rho u_i u_j) = B_i - \frac{\partial p}{\partial x_i} + \frac{\partial}{\partial x_j} \sigma_{ij} \quad (2)$$

Energy transfer:

$$\frac{\partial (\rho H)}{\partial t} + \frac{\partial}{\partial x_j} (\rho u_j H) - \frac{\partial}{\partial x_j} \left(\lambda \frac{\partial T}{\partial x_j} \right) = \frac{\partial p}{\partial t} \quad (3)$$

Here, σ is the viscous stress tensor and B_i is a body force. The Einstein summation convention, (i.e. summation over repeated indices) has been employed, and will be used throughout the paper. For a Newtonian fluid, the stress tensor is linearly related to the rate of strain tensor according to:

$$\sigma_{ij} = \mu D_{ij} + \left(\zeta - \frac{2}{3} \mu \right) \frac{\partial u_k}{\partial x_k} \delta_{ij} \quad (4)$$

$$D_{ij} = \frac{1}{2} \left(\frac{\partial u_i}{\partial x_j} + \frac{\partial u_j}{\partial x_i} \right) \quad (5)$$

where μ and ζ are the shear and bulk viscosity coefficients. H is the total enthalpy, given by:

$$H = h + \frac{1}{2} \mathbf{u} \cdot \mathbf{u} \quad (6)$$

All the other symbols have their usual meanings.

3. EXTENSION TO TURBULENT FLOWS

The equations written here are in conservative form, since this is the form that lends itself most readily to discretisation by the finite-volume method (as currently employed by the major CFD vendors). The equations refer to laminar flow situations only.

Turbulent flows are characterised by rapid fluctuations, and are extremely complex. Though the laminar equation set still applies to such situations, it is impractical to attempt a solution, except in a few low-Reynolds-number cases: this is the domain of Direct Numerical Simulation (of turbulence), or simply DNS. In all other situations, some form of turbulence model needs to be employed. The development of such models remains an active research area. No universal model is known, and existing models give only approximate solutions. However, a large body of knowledge on the use of specific turbulence models to particular flow situations has been accumulated, and guidelines do exist on which model should be used for a given application. We shall concentrate here on two approaches:

- Reynolds-Averaged Navier-Stokes (RANS)
- Large Eddy Simulation (LES)

The most popular model, and the one considered the “standard” for industrial applications, is based on the RANS approach, and is called the k-ε model.

3.1. RANS turbulence models: eddy viscosity concept

The derivation of the turbulence flow equations starts with a decomposition of all instantaneous flow quantities into their mean and fluctuating parts, as shown in equation (7), and averaging the basic conservation equations:

$$u_i = \bar{u}_i + u'_i \quad H = \bar{H} + H' \quad p = \bar{p} + p' \quad (7)$$

This process results in a set of equations similar to those for laminar flow. However, the non-linear terms in these equations give rise to products of fluctuating quantities, the most important of which are the Reynolds stress $-\overline{\rho u'_i u'_j}$ and Reynolds flux $-\overline{\rho u'_i H'}$. These quantities cannot formally be expressed in terms of the mean quantities, and require modelling assumptions. Analogous to the reasoning for Newtonian fluids in laminar flow, the most popular assumption is to express the Reynolds stress tensor as a linear function of the rate of deformation tensor (this now expressed in terms of mean velocities):

$$-\overline{\rho u'_i u'_j} = -\frac{2}{3} \rho k - \frac{2}{3} \mu_t \frac{\partial \bar{u}_k}{\partial x_k} + \mu_t \left(\frac{\partial \bar{u}_i}{\partial x_j} + \frac{\partial \bar{u}_j}{\partial x_i} \right) \quad (8)$$

Here, $k = \frac{1}{2} \overline{u'_k u'_k}$ is the mean turbulent kinetic energy, and μ_t the (yet unknown) turbulent (or eddy) viscosity.

Likewise, the Reynolds flux is assumed to be linearly related to the mean total enthalpy gradient as follows:

$$-\overline{\rho u'_i H'} = \Gamma_t \frac{\partial \bar{H}}{\partial x_i} \quad (9)$$

Here, Γ_t is the turbulent heat diffusivity, and is usually related to the turbulent eddy viscosity according to:

$$\Gamma_t = \mu_t / \sigma_t \quad (10)$$

where σ_t is the turbulent Prandtl number, which needs to be supplied empirically.

In summary, conservation equations for mean-flow quantities can be assembled for turbulent flows, using analogies with those that can be derived much more rigorously for laminar flows. It should be emphasised that the equations are only approximate. In particular, the averaging process cannot be legitimised, since it is carried out over all turbulence scales. In addition, the model contains empirical parameters: namely, μ_t and σ_t . In contrast to the situation for molecular viscosity, the turbulent viscosity is not a material property, but is a function of the flow field. However, the assumption $\sigma_t = 0.9$ is often adequate for many applications.

3.1.1. The k-ε turbulence model

This model in its original form provides an expression for the turbulent viscosity in the form:

$$\mu_t = C_\mu \rho \frac{k^2}{\varepsilon} \quad (11)$$

In this equation, $C_\mu = 0.9$ is an empirical constant, k is the mean turbulent kinetic energy (already introduced), and ε is the rate of dissipation of this quantity. It is possible to formally derive transport equations for k and ε directly from the Navier–Stokes equations, but these contain triple products of fluctuating quantities, and modelling assumptions have to be made to express them in terms of mean quantities to close the equation set. For reference purposes, we list the final equations here, which are transport equations for k and ε :

$$\frac{\partial(\rho k)}{\partial t} + \frac{\partial}{\partial x_j}(\rho \bar{u}_j k) - \frac{\partial}{\partial x_j} \left(\left(\mu + \frac{\mu_t}{\sigma_k} \right) \frac{\partial k}{\partial x_j} \right) = P + G - \rho \varepsilon \quad (12)$$

$$\frac{\partial(\rho \varepsilon)}{\partial t} + \frac{\partial}{\partial x_j}(\rho \bar{u}_j \varepsilon) - \frac{\partial}{\partial x_j} \left(\left(\mu + \frac{\mu_t}{\sigma_\varepsilon} \right) \frac{\partial \varepsilon}{\partial x_j} \right) = C_1 \frac{\varepsilon}{k} (P + C_3 \max[G, 0]) - C_2 \rho \frac{\varepsilon^2}{k} \quad (13)$$

Here, P and G are the rates of energy production due to shear and buoyancy, respectively, and $\sigma_k, \sigma_\varepsilon, C_1, C_2, C_3$ are empirical constants. The model, though often criticised, has a large validation database.

For completeness, we list here the equations governing turbulent flows in the framework of the RANS approach, without further comment:

Mass continuity:

$$\frac{\partial \rho}{\partial t} + \frac{\partial}{\partial x_j}(\rho \bar{u}_j) = 0 \quad (14)$$

Momentum transfer:

$$\frac{\partial(\rho \bar{u}_i)}{\partial t} + \frac{\partial}{\partial x_j}(\rho \bar{u}_i \bar{u}_j) = \bar{B}_i - \frac{\partial \bar{P}}{\partial x_i} + \frac{\partial}{\partial x_j} \left((\mu + \mu_t) \frac{\partial \bar{u}_i}{\partial x_j} \right) \quad (15)$$

Energy transfer:

$$\frac{\partial(\rho \bar{H})}{\partial t} + \frac{\partial}{\partial x_j}(\rho \bar{u}_j \bar{H}) - \frac{\partial}{\partial x_j} \left(\left[\frac{\lambda}{c_p} + \frac{\mu_t}{\sigma_t} \right] \frac{\partial \bar{H}}{\partial x_j} \right) = \frac{\partial \bar{p}}{\partial t} \quad (16)$$

where

$$\bar{P} = \bar{p} + \frac{2}{3} \rho k - \left(\zeta - \frac{2}{3} [\mu + \mu_t] \right) \frac{\partial u_k}{\partial x_k} \quad (17)$$

These equations, when combined with the transport equations for k and ε (12, 13), form a closed set. If the fluid is a compressible gas, the approach is only slightly modified. The procedure is then often referred to *Favre averaging* rather than *Reynolds averaging*, and an equation of state linking the thermodynamic quantities needs also to be specified. In comparison to the laminar situation, for turbulent flows, two extra transport equations need to be solved, and there is increased non-linearity due to the expression for μ_t .

3.2. LES turbulence models

In turbulent flow, the fluctuations occur over a wide range of scales. The averaging procedure employed in the RANS approach is carried out over all scales. Therefore, certain characteristics of the turbulent flow field, often important ones, are lost, or at least smeared out.

In LES, the larger scales of turbulence are computed explicitly, though modelling assumptions are still required for the small-scale motions. The expectation is that, since these smaller scales are more localised, isotropic and homogeneous, there is a better chance of finding a universal model for them.

The principle of the LES formulation is to decompose instantaneous quantities into resolved-scale and subgrid-scale components via a filtering operation as follows:

$$u_i = \langle u_i \rangle + u'_i \quad p = \langle p \rangle + p' \quad H = \langle H \rangle + H' \quad (18)$$

Applying the filtering process to the Navier-Stokes equations produces the set of governing equations for LES. These have much the same form as those derived in the RANS approach, except that extra terms appear, because the non-linear advection terms do not commute with the filtering operation. For example, the stress term is:

$$\sigma_{ij} = -\langle \rho u_i u_j \rangle + \rho \langle u_i \rangle \langle u_j \rangle \quad (19)$$

The computational overhead of LES calculations (time-dependent and 3-D) is very high.

4. EXTENSION TO MULTI-PHASE FLOWS

The most general formulation is the multi-fluid model, in which there is an equation set for each phase. The derivation of the governing equations involves additional averaging: over the phases (and thereby additional restrictions and uncertainties). Basically, the different phases are assumed to form interpenetrating continua, the presence of each phase p being measured by the volume fraction α^p such that

$$\sum_{p=1}^{p=N} \alpha^p = 1 \quad (20)$$

The governing equations resemble those for single-phase flow, but with additional source terms to represent inter-phase transfer of mass (e.g. evaporation and condensation), momentum (phase drag) and energy (phasic heat transfer). For illustration purposes only, we reproduce the conservation of phasic mass:

$$\frac{\partial(\alpha^p \rho^p)}{\partial t} + \frac{\partial}{\partial x_j} (\alpha^p \rho^p u^p_j) = \sum (\dot{m}_{ab} - \dot{m}_{ba}) \quad (21)$$

Note the presence of α^p in the differential terms. By convention, \dot{m}_{ab} is the mass flow rate per unit volume into phase a from phase b . It should be emphasised that specification of the inter-phase transfer terms is a major problem in multi-phase CFD modelling, and requires considerable further research investment.

5. MESH GENERATION

These days, all major CFD solvers require separate software to generate the computational mesh. The following diagrams illustrate more graphically than can be expressed in words how quickly the size of a problem increases with the dimensions.

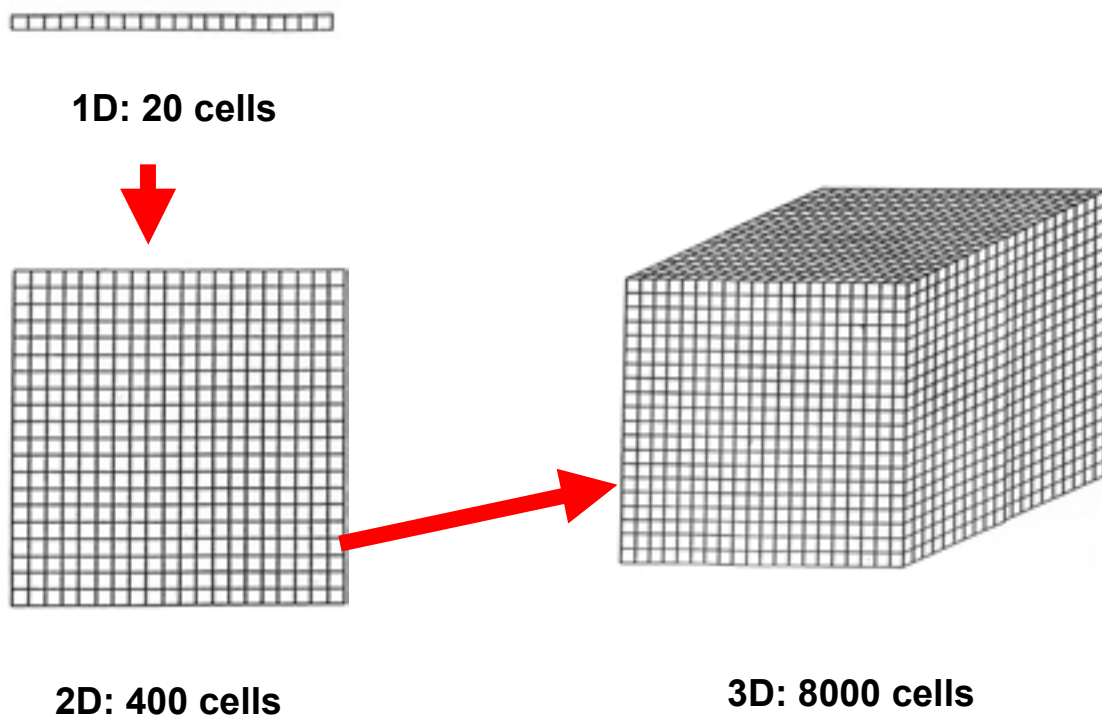


FIG. 2. The rapid growth in the number of mesh cells in going from 1-D to 3-D problems.

In 1-D, 20 mesh points would often be considered a very crude level of discretisation. In 3-D, 8000 mesh cells is considered likewise! The data structures are very large in 3-D. Today, the number of meshes used in CFD simulations often exceeds 10 million.

5.1. Multi-block strategy (hexahedral cells)

The problem geometry may be built up using blocks. The joining of the E and W faces of adjacent blocks is accomplished using the concept of shared nodes; i.e. nodes which have the same number in the global node numbering system. The blocks can have curved edges, to fit the problem geometry, but still remain topologically equivalent to a rectangular block. Blocks are subdivided into as many computational cells as needed to resolve the flow. In this way, the exact problem geometry may be accurately represented, however complex.

5.2. Examples of mesh construction

CFD is widely used in the aerospace and automotive industries. The concept of moving meshes, for example to represent the motion of engine exhaust valves, has been introduced. As the valve moves, the meshes in the vicinity are adapted to the new flow geometry. Traditionally, the major CFD vendors offered custom-built mesh generators with their CFD solvers. More recently, stand-alone mesh generators, with built-in interfaces to different commercial CFD packages, have become popular.

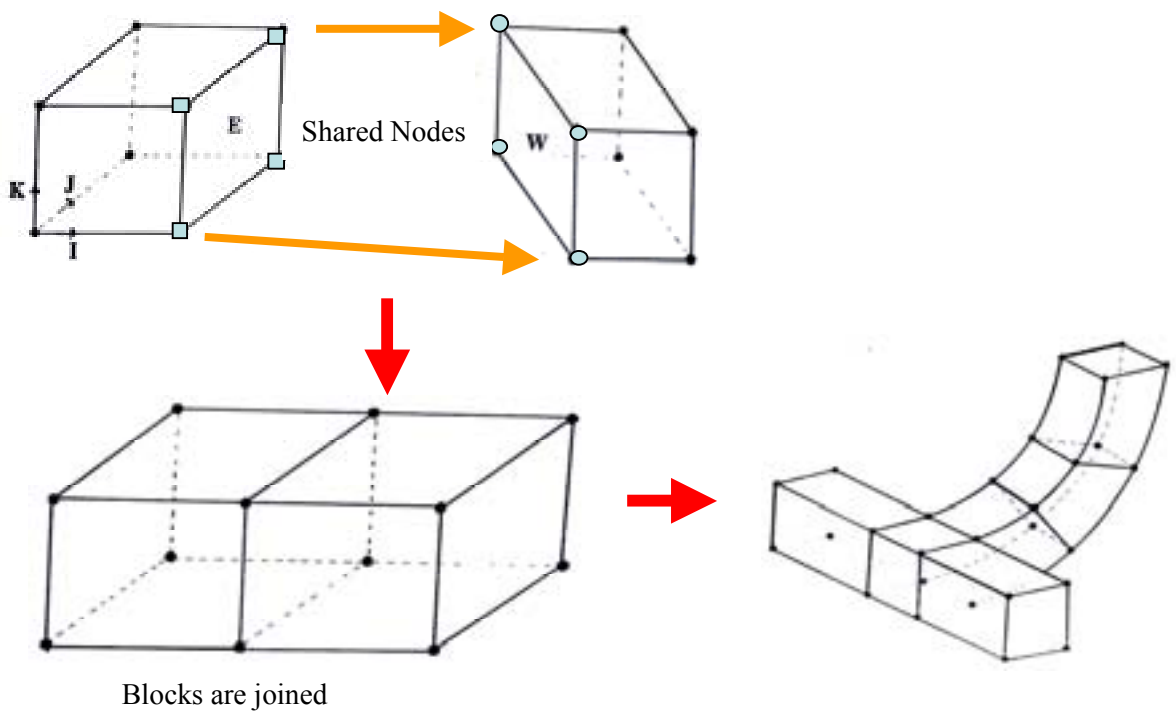


FIG. 3. Hexahedral cells used to build the problem geometry.



FIG. 4. Examples of mesh construction for various shaped volumes and surfaces.

6. NUMERICAL SOLUTION OF THE EQUATIONS

It is only possible to give the briefest of sketches of the numerical techniques employed to solve the fluid flow and heat transfer equations. We will restrict ourselves to pressure-velocity coupling algorithms, since these are the most popular for the major commercial CFD codes, and in particular to the SIMPLE algorithm.

Modern mesh generators produce grids that are body-fitted to the problem geometry, so that mesh edges follow the boundaries of the fluid domain. This simplifies the application of the boundary conditions (BCs). However, most numerical algorithms have been developed for rectangular meshes. The two mesh systems are linked via a coordinate transformation. This itself can be a source of error or approximation. Figure 5 illustrates the concept of the coordinate transformation process required to move from a body-fitted grid to rectangular computational grid. The general algorithms are very well described in Numerical *Heat Transfer and Fluid Flow*, S. U. Patankar, Hemisphere (1983).

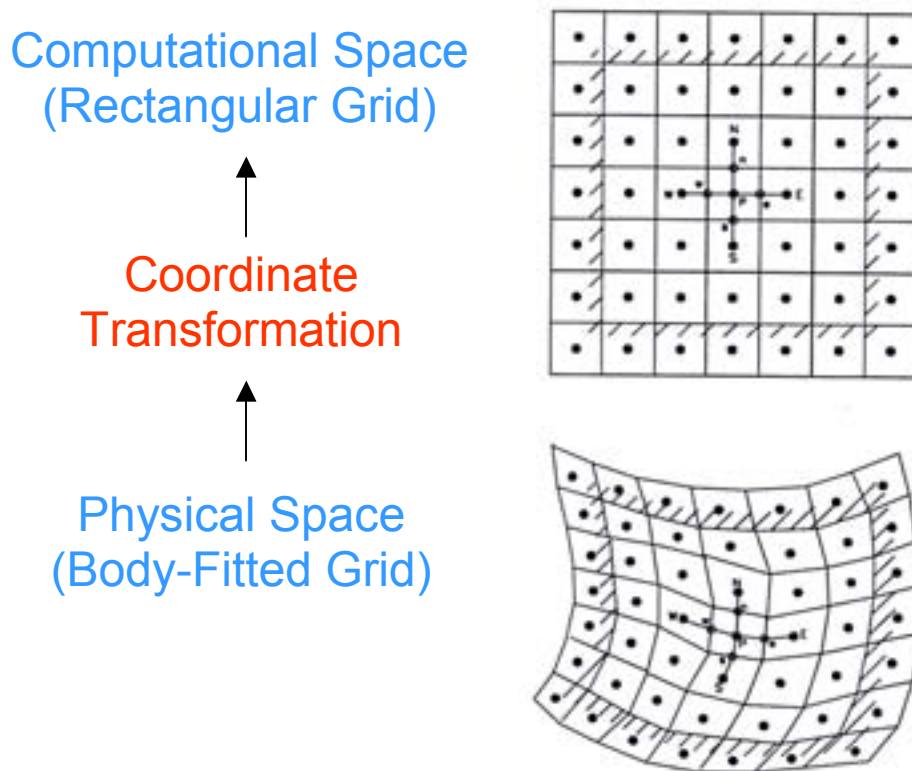


FIG. 5. Example of coordinate transformation process.

6.1. Discretisation: control-volume method

There are many ways of deriving a discrete set of equations from the differential equation set, in preparation for the computational solution: e.g. finite difference, finite volume, finite element, spectral methods, as well as some specialist techniques for certain classes of problems. We follow the control-volume method here, and for simplicity consider the equations only for 2-D rectangular grids. However, the concepts are more general, and may be extended to 3-D body-fitted meshes and other shapes.

The momentum and heat equations are each of the same general form as follows:

$$\frac{\partial(\rho\Phi)}{\partial t} + \frac{\partial}{\partial x_j}(\rho u_j \Phi) - \frac{\partial}{\partial x_j} \left(\Gamma \frac{\partial \Phi}{\partial x_j} \right) = S \quad (22)$$

Here Φ is the conserved quantity. The left side represents the local rate of change, advection and diffusion of the quantity Φ . The source terms appear on the right side of the equations.

The equations are integrated over a control volume, as shown in Figure 6. The control volume may be a mesh cell (as shown here) or staggered over the cell faces.

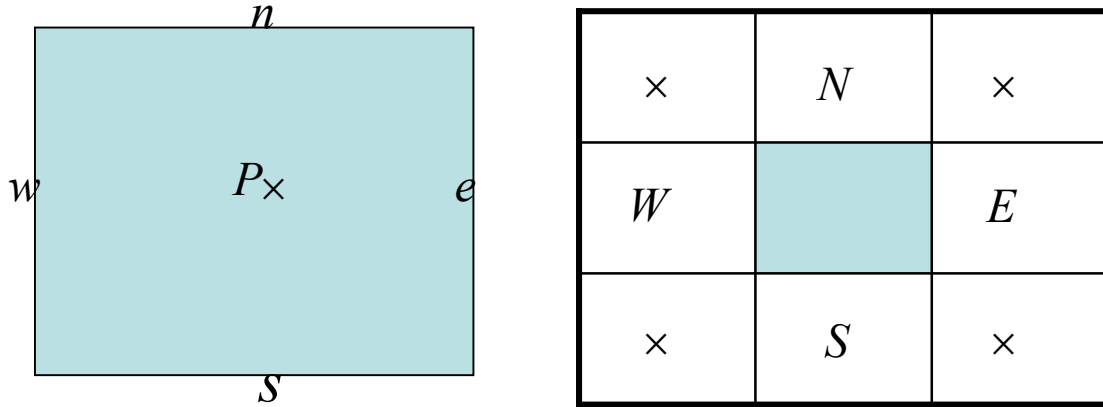


FIG. 6. Integration over control volume.

6.2. Discretised equation set (fully-implicit scheme)

With the face and cell-centre convention introduced in Figure 6, we can write the mass continuity ($\Phi=1$) and one momentum equation ($\Phi = u$) in the following forms:

$$(\rho_p - \rho_p^0) \frac{\Delta x \Delta y}{\Delta t} + F_e - F_w + F_n - F_s = 0 \quad (23)$$

$$(\rho_p u_p - \rho_p^0 u_p^0) \frac{\Delta x \Delta y}{\Delta t} + J_e - J_w + J_n - J_s = - \left(\frac{\partial p}{\partial x} \right)_p + (S_C^u + S_U^u u_p) \Delta x \Delta y \quad (24)$$

where the superscript ⁰ refers to values at previous time-step, and, for example, F_e is the mass flux over the *east* face, and J_e the total (advective plus diffusive) momentum flux over the same face. The flux terms are given as follows:

$$F_e = (\rho u)_e \Delta y \quad F_n = (\rho v)_n \Delta x \quad J_e = \left(\rho u u - \Gamma \frac{\partial u}{\partial x} \right)_e \Delta y \quad J_n = \left(\rho v u - \Gamma \frac{\partial u}{\partial y} \right)_e \Delta x \quad (25)$$

with analogous expressions for the other faces. The other momentum equation and the energy equation (in terms of the heat flux), are developed similarly. The source terms for the u equation are often split into those dependent on u_p and those not. Provided the coefficient S_U^u is non-positive, this arrangement can aid convergence.

The fluxes now need to be expressed in terms of neighbouring cell-centred quantities, and there are many ways of doing this (e.g. central/upwind differencing, QUICK, etc.), the choice being governed by the trade-off between ease of convergence and accuracy.

6.3. Pressure-velocity coupling: SIMPLE scheme

After this substitution, and one also to relate the pressure gradient to neighbouring values, each momentum equation may be written in the following general form:

$$A_p^u u_p - \sum_{nb} A_{nb}^u u_{nb} = S_U^u - \sum_{nb} B_{nb}^u p_{nb} \quad (26)$$

$$A_p^v v_p - \sum_{nb} A_{nb}^v v_{nb} = S_U^v - \sum_{nb} B_{nb}^v p_{nb} \quad (27)$$

The energy equation may be expressed in a similar manner. The point to note here is that, if the pressure field were known, the velocity field could be determined by solving the linear equations above. However, in general, the resulting velocities would not then satisfy the mass continuity condition. Instead,

$$\left(\rho_p - \rho_p^0\right) \frac{\Delta x \Delta y}{\Delta t} + F_e - F_w + F_n - F_s = b, \quad (28)$$

where b is the mass residual. However, the procedure can be used as the basis of an iterative scheme in which pressure corrections are made, starting from an initial guess, to successively reduce the mass residual. This approach is known as SIMPLE: Semi-Implicit Method for Pressure-Linked Equations. Some details are given in the next section.

The idea now is to find a procedure to improve the initial guessed pressure p^* so that the resulting velocity field is closer to satisfying the mass continuity equation. This is done by expanding in terms of perturbations, or corrections. Thus:

$$p = p^* + p' \quad u = u^* + u' \quad v = v^* + v' \quad (29)$$

Here p^* is the initial guess at the pressure field, and u^* , v^* are the velocities derived from the momentum equations (26) and (27) using this pressure. As is standard in perturbation approaches, the above expansions are introduced into the discretised momentum equations, subtracting out the starred variables, to obtain a linear equation relating the pressure and velocity corrections. For example:

$$A_p^u u_p' - \sum_{nb} A_{nb}^u u_{nb}' = S_U^u - \sum_{nb} B_{nb}^u p_{nb}' \quad (30)$$

In the basic SIMPLE scheme, the second term is simply ignored! This leaves a trivial assignment of the velocity correction in every cell in terms of nearby pressures:

$$A_p^u u_p' = S_U^u - \sum_{nb} B_{nb}^u p_{nb}' \quad (31)$$

Substituting into the mass conservation equation gives a linear matrix equation to be solved for the pressure correction, which is then used to update the original guess at the pressure field. The whole

process is repeated until the mass residual is reduced to a specified tolerance. The scheme works! But, the iterations do need under-relaxation.

7. THE ROLE OF CFD IN NUCLEAR REACTOR TECHNOLOGY

The needs of the nuclear industry did not originally provide the primary driving force for the development of CFD codes. Consequently, the models incorporated in these codes are not purpose-built for the nuclear reactor community. Nonetheless, CFD is a proven and validated technology, and can be used with advantage. For example, to achieve better efficiency and safety of nuclear installations, more accurate estimation of safety margins (e.g. for plant life extension) are required.

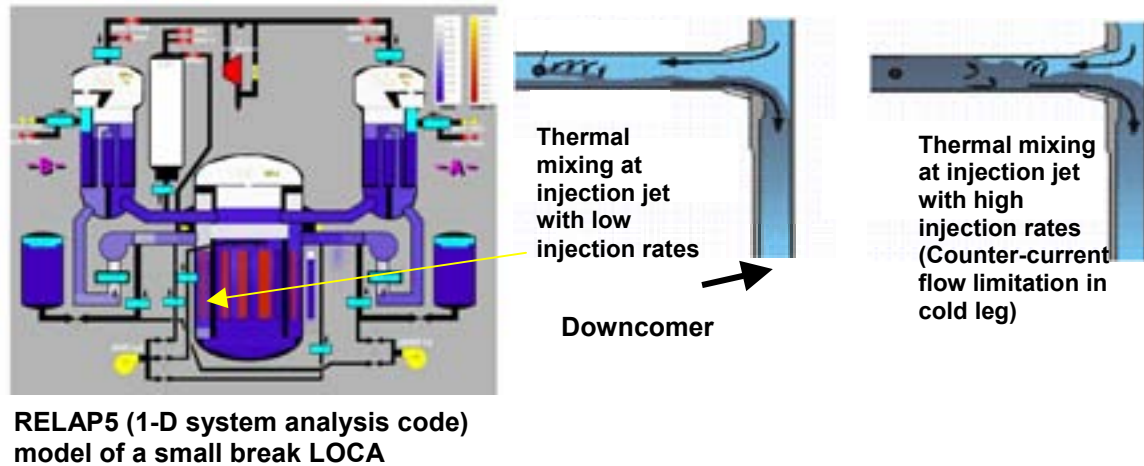


FIG. 7. Thermal fluid mixing applications in NPP.

Figure 7 shows an important example of CFD use in the nuclear industry. For ageing plants, the intervention of the Emergency Core Cooling (ECC) system, with injection of cold water, may lead to unsustainable thermal loads to the reactor vessel and barrel. A local, detailed CFD analysis can help to quantitatively assess the risk potential.

7.1. Boron dilution and in-vessel mixing

Fuel performance in PWRs depends on efficient mixing of incoming streams from the cold-legs in the downcomer and lower plenum. In addition, there is a safety issue associated with the injection of a slug of unborated water during pump start-up, which could lead to a local power excursion. Figure 8 shows a 3-D CFD model of the reactor vessel of a 3-loop plant. The inset shows that hotter (or unborated) water injected into one loop is not thoroughly mixed with the water from the other loops at the entrance to the core.

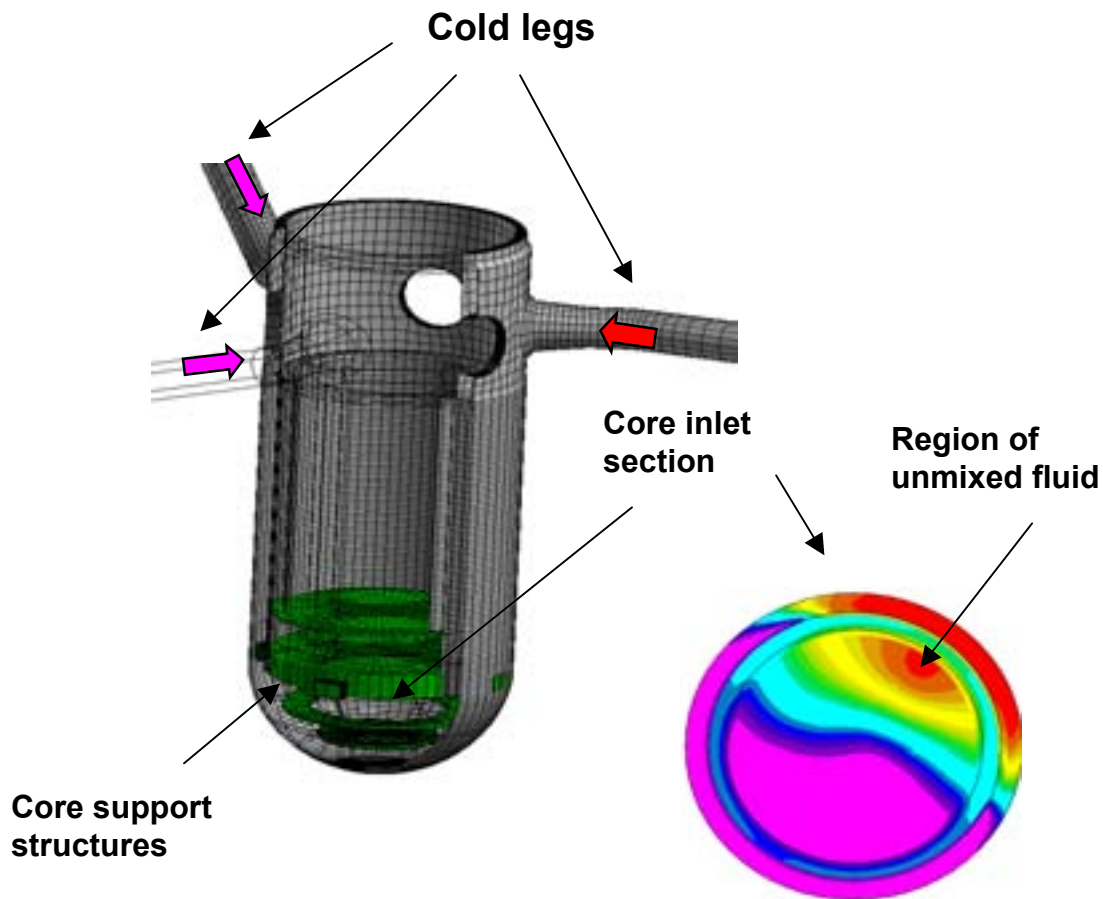


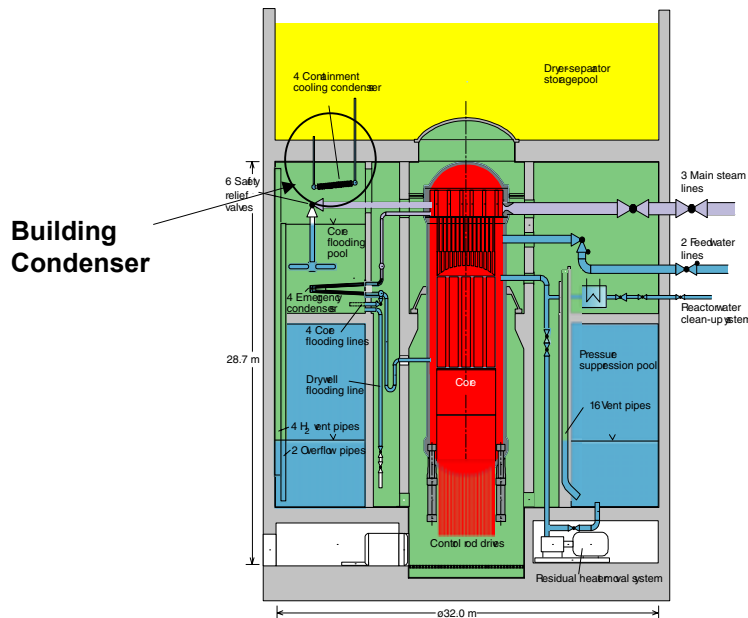
FIG. 8. 3-D CFD model used to analyse boron mixing in a reactor vessel.

7.2. Passive decay-heat removal

Future, innovative reactor designs are likely to incorporate passive safety systems for long-term decay-heat removal. Passive cooling relies on the efficient energy transfer of the steam produced by decay heat in the core of the reactor to a number of large heat sinks (i.e. large water pools) utilising inherent mechanisms such as buoyancy, gravity-driven flow, evaporation and condensation.

Two examples from the Generation III series are the Simplified Boiling Water Reactor (SBWR, and its European equivalent, the ESBWR) and the SWR-1000 concept from Framatome-Siemens. Some details are given in the following paragraphs. Figure 9 presents a schematic of the SWR-1000 building condenser concept. Figure 12 presents a similar schematic for the ESBWR.

Both reactors are designed to operate at full power in a natural-circulation mode. With the primary circuit intact, operational and accident transients, as well as passive decay-heat removal, may be adequately described using 1-D system codes, such as RELAP5. However, if there is a break in the main steam line, steam will enter the containment atmosphere. For each design concept, engineered devices are in place to prevent over-pressurisation, and to maintain heat removal by passive means. Driving forces for such mechanisms tend to be small, and careful analysis has to be undertaken to ensure that cooling proceeds within the design specifications (for the ESBWR, up to 72 hours without operator intervention). Given the complexity of the containment geometry, the circulation patterns will be 3-D, and CFD will be required for the analysis.



PANDA Facility (PSI)

FIG. 9. Building condenser concept of the SWR-1000.

As shown in Figure 9, the building condensers are located near the roof of the containment. The condensers, which operate in natural circulation mode, transfer heat to a large water pool situated above the containment building.

The PANDA facility, also shown in Figure 9, is a near full height model of the reactor, and is used to examine the viability of the passive-cooling concept. For this application, a building condenser had been installed in the PANDA facility, as shown in Figure 10. For the simulation, the condenser tubes were modelled as a porous volume, with anisotropic resistance factors, and the drain plate underneath as a thin shell. The presence of the plate had an important influence on the natural circulation flow pattern in the vessel. In Figure 10, steam injected near the bottom of the vessel, is seen to rise as a plume along the opposite side wall. The model produced good predictions of the condenser efficiency when compared to the PANDA experimental data.

Another aspect of the PANDA experiments was also modelled using CFD. Figure 11 shows the CFD simulation of a plate condenser. The conditions for this simulation correspond to a phase in the PANDA experiment in which pure steam is injected into a steam/air environment, at low injection velocity. For this concept, the circulation pattern is almost completely buoyancy-driven (the buoyancy is due to concentration differences, not thermal). Comparisons were made with results obtained using the GOTHIC containment code, with coarse nodalisation.

Aspects of the ESBWR safety operation were also modelled with CFD, as shown in Figure 12. During a Main Steam Line Break in the containment building, as pressure builds in the Drywell, a steam/N₂ mixture is discharged to the suppression pool. Condensation (in the presence of the non-condensable N₂) occurs on walls.

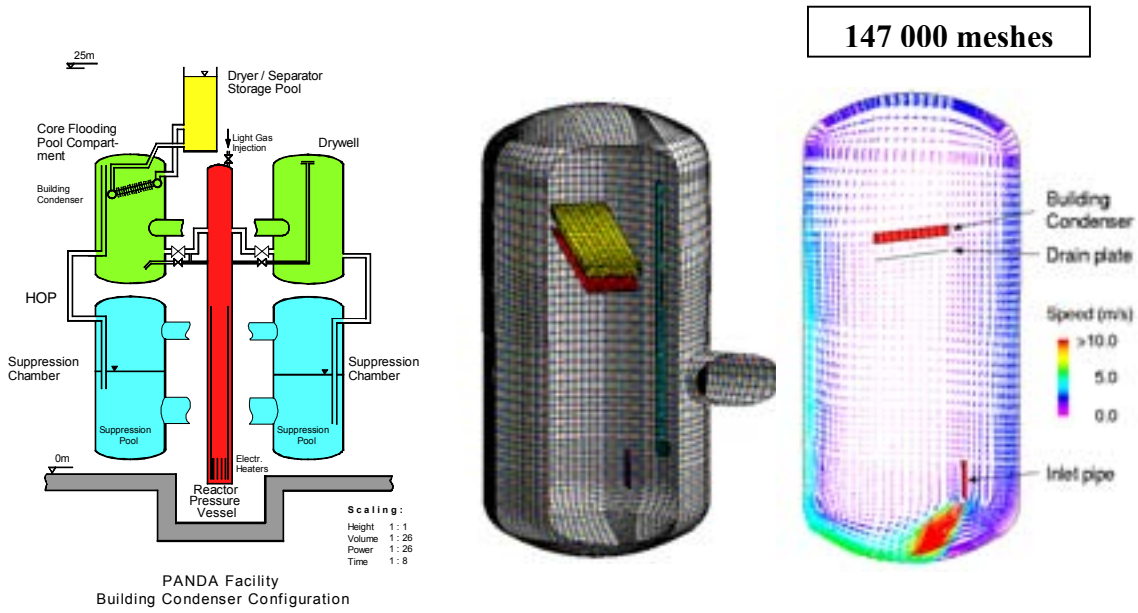


FIG. 10. CFD simulation of building condenser.

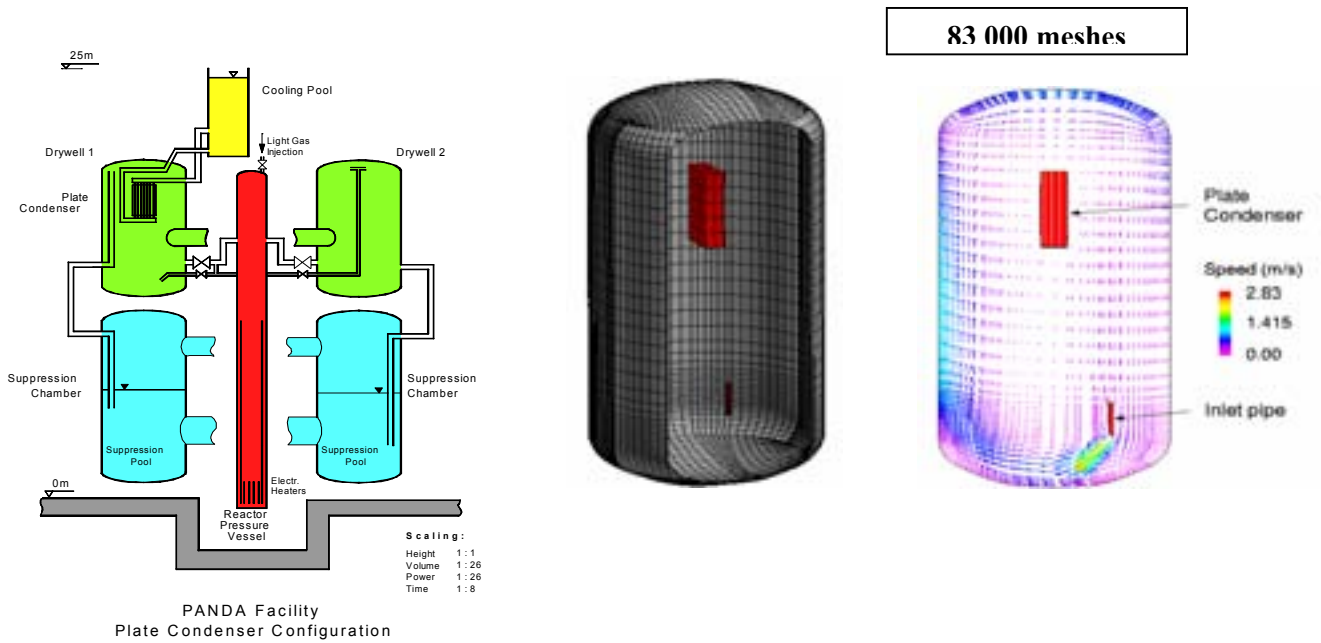


FIG. 11. CFD simulation of plate condenser.

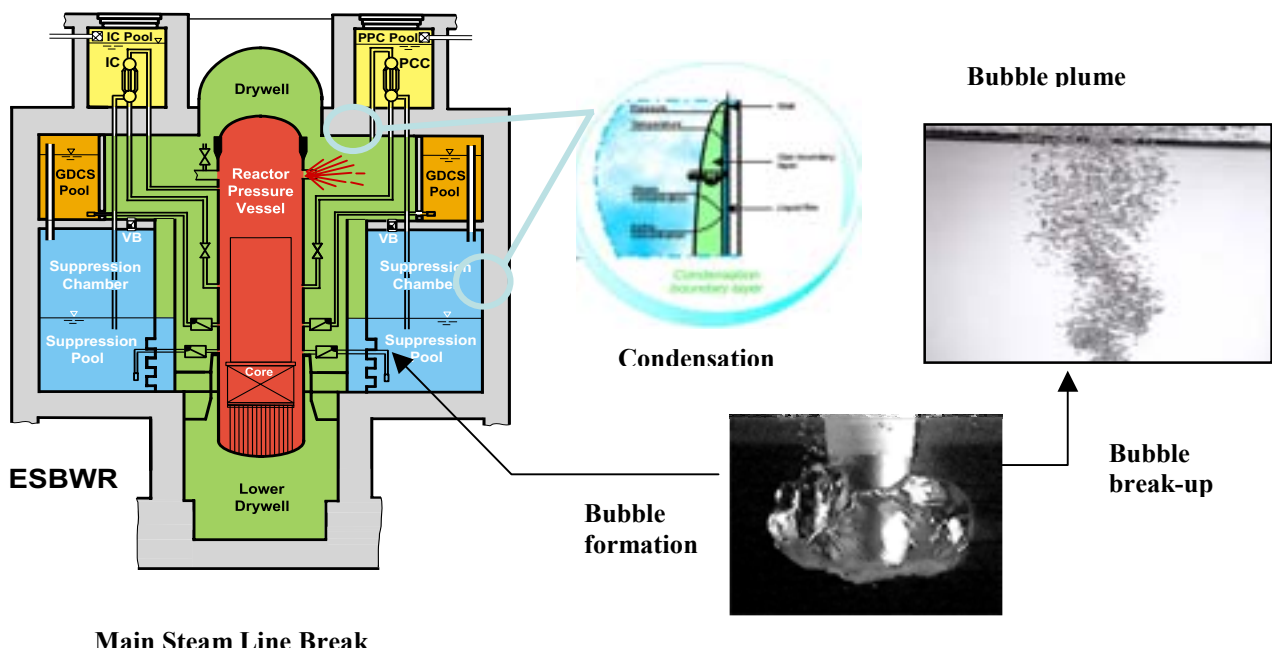


FIG. 12. Some CFD modelling aspects for the ESBWR.

Many containment phenomena require gas/liquid interface modelling. An important example, gas discharge into a suppression pool, is shown in Figure 13. Figure 14 shows the subsequent formation of bubble plumes that can occur after break-up of the primordial bubble in the suppression pool. Complete condensation now occurs, and this induces mixing in the pool, the process being determined by two-phase natural circulation. It is important to understand the break-up and plume-stirring mechanisms, because the system pressure is ultimately controlled by the pressure in the vapour space above the water surface in the suppression chamber. This pressure is the sum of the partial pressures of steam and N₂, the former controlled by the temperature at the pool surface. The pool surface temperature, in turn, depends on the efficiency of steam condensation in the pool (no “blow-by”), and the degree of mixing in the pool (no stratification). Over-conservatism in the estimates will result in over-design of the containment, and this is VERY expensive.

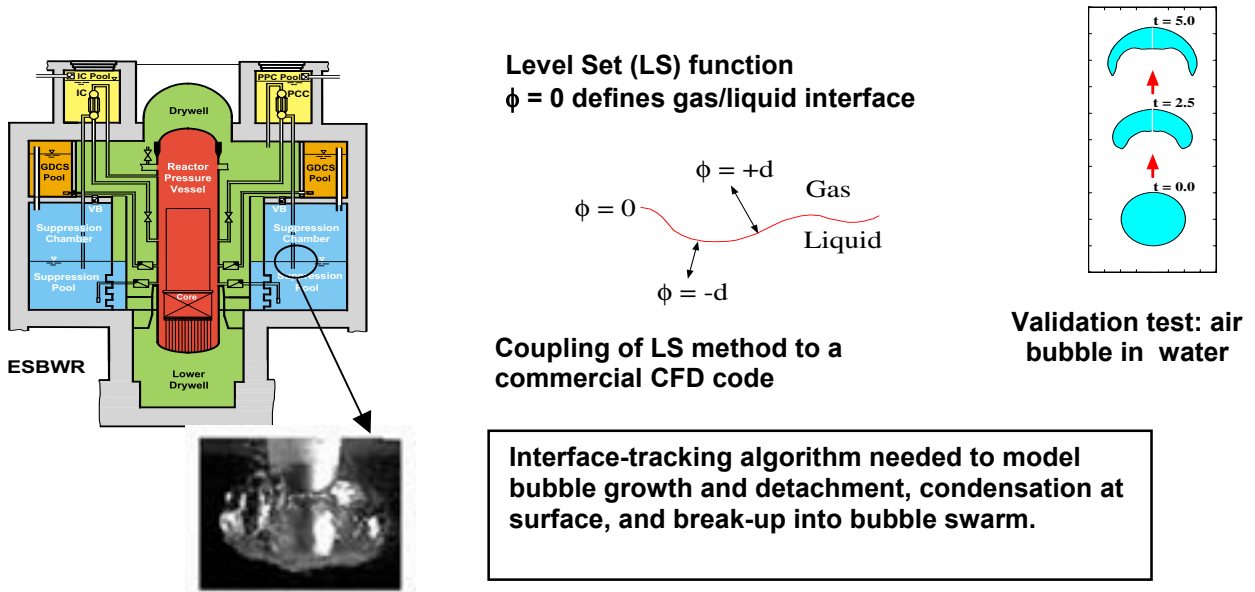


FIG. 13. CFD modelling of gas/liquid interfaces.



FIG. 14. Sequence of photos taken from a scale test (Meier, 1999).

CFD modelling of bubble plumes is shown in Figure 15. The CFD modelling of gas/liquid interfaces requires an interface-tracking algorithm to model bubble growth and detachment, condensation at the surface, and break-up into a bubble swarm. Interface-tracking is not a standard model in most commercial CFD codes, and illustrates the “model-development” aspect of a modular code system.

RANS approaches to modelling bubble plumes are largely unsuccessful, since extensions of existing turbulence models (usually k-ε) do not properly account for bubble-induced turbulence. The results shown in Figure 15 were derived using LES.

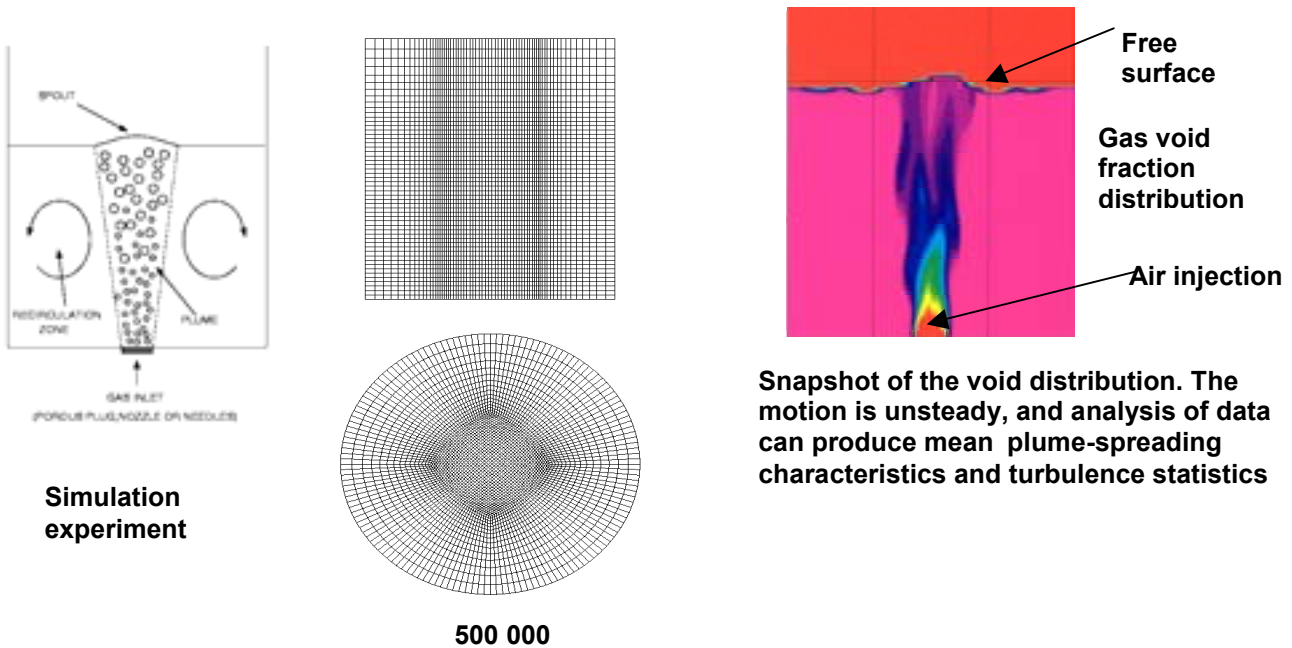


FIG. 15. Modelling of bubble plumes.

8. FINAL SUMMARY

Current system analysis codes (mainly 1-D, and using empirical, scale-dependent correlations) provide fairly reliable simulations for natural circulation phenomena in the primary loop, and often too in the containment. However, these codes cannot take into account those local effects which could influence overall system behaviour: for example, the thermal shock associated with ECC injection, 3-D in-vessel mixing (incl. boron dilution), and bubble dynamics in suppression pools. This translates into large uncertainties, which leads to large safety margins and to large expense.

CFD is a powerful engineering tool. The technology is thoroughly mature in many other disciplines, and can be used to provide detailed information in the nuclear technology area. However, CPU overheads are large for CFD, so the approach cannot be considered a total replacement for existing methods. Additionally, there remains considerable effort required to provide an adequate database for inter-phase transfer models. While we wait for more powerful computers/models, a multi-scale strategy, as shown in Figure 16, can be used. For the large length scales encountered in analysing NPPs, systems codes can be used. For smaller length scales encountered when analysing plant components, component codes and models can be used with an increasing number of calculation cells. For the fine scales encountered in 3-D flows, turbulence and mixing, CFD provides a powerful analysis tool.

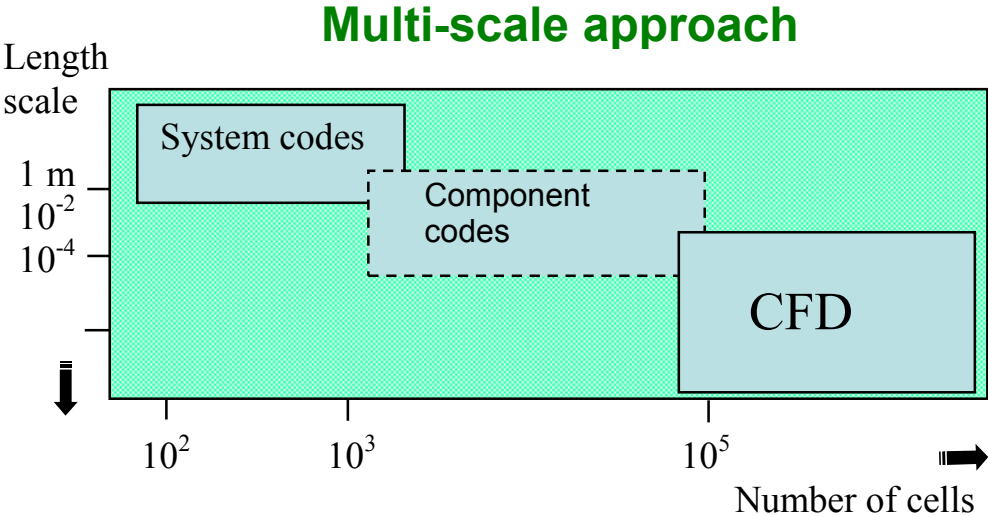


FIG. 16. Multi-scale approach to NPP computation.

ANNEX 21

THE CSNI SEPARATE EFFECTS TEST AND INTEGRAL TEST FACILITY MATRICES FOR VALIDATION OF BEST-ESTIMATE THERMAL-HYDRAULIC COMPUTER CODES

N. Aksan

Paul Scherrer Institute, Switzerland,

Abstract

This paper provides an overview of the test MATRICES developed by CSNI for the validation of best-estimate thermal hydraulic computer codes.

1. INTRODUCTION

For the analyses of transients and loss-of-coolant accidents (LOCAs) in Light Water Reactors (LWRs) thermal-hydraulic computer codes have been developed over the last thirty years.

Starting with relative simple computer codes in the early 1970's, a continuous development of the codes has been performed with respect to a more realistic description of thermal hydraulic phenomena and a more detailed system representation.

At the beginning of the 1970's, codes for the analysis of large break LOCAs had been requested. The codes were based on the homogeneous equilibrium model, assuming equal velocities and temperatures of vapour and liquid phases. The next effort in code development was directed by the demand for the simulation of transients and small break accidents. The implementation of new models allowed for the separation of vapour and liquid by gravity. The representation of primary and secondary side with control systems and balance of plant models were extended.

In the middle of the 1970's the development of a new generation of thermal-hydraulic codes were initiated to provide analytical tools for a more realistic simulation of LWR behaviour under transient and accident conditions. Thermal and mechanical non-equilibrium phenomena have been taken into account. The effects of non-condensables and boron tracking have been considered. These codes allow the simulation of transients, the entire range of break sizes as well as beyond design basis accidents including accident management procedures with operator interventions.

Parallel to the development of the analytical tools a large variety of experimental programmes have been executed to improve the understanding of thermal-hydraulic phenomena, to study system behaviour, and to provide the required data base for code development and code validation.

A very high number of separate effects tests have been performed for the development and validation of code models. Separate effects tests investigate individual phenomena under clear boundary conditions. While in the 1970's the experiments were conducted mainly on small scale test facilities, in the 1980's more attention has been directed to scaling. For example, in 1986, the first tests at the test facility UPTF, a representation of a four loop 1300 MWe PWR with upper plenum, downcomer and the main coolant pipes in full scale reactor geometry, were performed.

The overall results of the code calculations are validated mainly by data from integral test facilities representing the primary and secondary coolant systems. While in the early 1970's the experiments were focused on large break issues, in the following, up to now, parallel to the advancement in code development, integral tests have been carried out to investigate LWR system behaviour during transients, small breaks, transients under shutdown conditions, and beyond design basis accidents. In addition to the results of integral tests LWR plant data of transients or accidents are being used to validate the predictive capability of the codes.

Construction of validation matrices is an attempt to collect together the best sets of test data for code validation and improvement from the wide range of experiments that have been carried out worldwide in the field of thermal-hydraulics. The first formulation of a validation matrix was proposed by

Wolfert and Frisch from GRS [1]. This activity was taken by a CSNI sub-group to establish matrices for PWR and BWR.

In addition, to set-up validation matrices for Russian Pressurized Water-cooled and Water-moderated Energy Reactor (WWER) analyses, an international Working Group was formed on the initiative of the Federal Ministry for Research and Technology (BMFT) of the Federal Republic of Germany. A further evaluation of the WWER matrices was performed by a CSNI Support Group. Based on these CSNI matrices the lists of phenomena have been reviewed and adopted to the characteristics of WWER-440 and WWER-1000 systems respectively, and the lists of test facilities suitable for code assessment have been completed.

2. DEFINITIONS

Computer codes simulate the system behaviour of nuclear power plant as realistic as possible („best estimate“). These computer codes are used to investigate:

- Incidents and accidents of different scenarios and their consequences,
- the effectiveness of emergency procedures.

The process carried out by comparing code predictions with experimental measurements or measurements in a reactor plant (if available) are called validation. A code or code model is considered validated when sufficient testing has been performed to ensure an acceptable level of predictive accuracy over the range of conditions over which the code may be applied. Accuracy is a measure of the difference between measured and calculated quantities taking into account uncertainties and biases in both. Bias is a measure, usually expressed statistically, of the systematic difference between a true mean value and a predicted or measured mean. Uncertainty is a measure of the scatter in experimental or predicted data [2]. The acceptable level of accuracy is judgmental and will vary depending on the specific problem or question to be addressed by the code. The procedure for specifying, qualitatively or quantitatively, the accuracy of code predictions is also called code assessment.

The international literature often distinguishes between the terms validation and verification. A mathematical model, or the corresponding computer code, is verified when it is shown that the code behaves as intended, i.e., it is a proper mathematical representation of the conceptual model and that the equations are correctly encoded and solved. In this context, the comparison with measured values is not part of the verification process. The term verification, however, is often used synonymously with validation and qualification [2]. Therefore, the term verification has also been used in the code validation work, including comparisons between calculations and measurements.

3. SEPARATE EFFECTS TEST VALIDATION MATRIX

In March 1987, the OECD/NEA Committee on the Safety of Nuclear Installations (CSNI) published a document that identified a set of tests which were considered to provide the best basis for the assessment of the performance of thermohydraulic codes, "CSNI Code Validation Matrix of Thermohydraulic Codes for LWR LOCA and Transients", [3], [4], and [5]. The set of tests was chosen to include examples of all phenomena expected to occur in plant transients and LOCA analyses. Tests were selected on the basis of the quality of the data, variety of scaling and geometry, and appropriateness of the range of conditions covered. A decision was made to bias the validation matrix towards integral tests in order that code models were exercised, and interacted, in situations as similar as possible to those of interest in LWR plant. This decision was taken on the assumption that sufficient comparison with separate effects tests data would be performed, and documented, by code development, that only very limited further assessment against separate effects test data would be necessary. This last expectation has proved unrealistic; it is now recognized that continued comparison of calculations with separate effects test data is necessary to underwrite particular applications of codes, especially where a quantitative assessment of prediction accuracy is required, as well as for code model improvement.

It has been decided to develop a distinct Separate Effects Test Matrix rather than extend the original CSNI Code Validation Matrix (CCVM), which consisted almost entirely of integral tests. Only in some specific cases where integral test facility data were not available, were separate effects tests used in the CCVM. The development of the separate effects test matrix was found to require an extension of the methodology employed for the CCVM both in the scope and definition of the thermal hydraulic phenomena and in the categorization and description of facilities.

There are several reasons for the increased importance now placed on the comparison of codes with separate effects test data. Firstly, it has been recognized that the development of individual code models often requires some iteration, and that a model, however well conceived, may need refinement as the range of applications is widened. To establish a firm need for the modification or further development of a model it is usually necessary to compare predictions with separate effects data rather than rely on inferences from integral test comparisons.

Secondly, there is the question of uncertainties in predictions of plant behaviour. A key issue concerning the application of best estimate codes to LOCA and transient calculations is quantitative code assessment. Quantitative code assessment is intended to allow predictions of nuclear power plant behaviour to be made with a well defined uncertainty. Most schemes for achieving this quantification of uncertainty rely on assigning uncertainties to the modelling by the code of individual phenomena, for instance by the determination of reasonable ranges which key model parameters can cover and still produce results consistent with data. This interest has placed a new emphasis on separate effects tests over and above that originally envisaged for model development.

In the thermohydraulic codes, the physical processes are simulated by mechanistic models and by correlations. The prediction of particular phenomena, such as level swell or counter-current flow limitation, by a code are usually dominated by one, or perhaps a few, code models. Comparison of code predictions of basic phenomena with events observed in the relatively simple situations contrived in separate effects test facilities, often allows a better assessment of the accuracy of code models than it is possible to make with data from integral tests. This may be, for instance, because steady state rather than transient observations are possible in the separate effects tests; or because in a separate effects test facility dedicated to the study of one particular phenomenon, the measurement instrumentation can be chosen more appropriately, with less need to compromise. The more highly controlled environment of the SET is likely to lead to a more systematic evaluation of the accuracy of a model across a wide range of conditions.

A further incentive to conduct separate effects tests, in addition to those carried out in integral facilities, is the difficulty encountered in scaling predictions of phenomena from integral test facilities (which of necessity are in some sense small scale) to plant applications. Where a phenomenon is known to be highly scale dependent and difficult to model mechanistically, there is a strong case for conducting separate effects tests at full scale. In general, it is desirable to have a considerable overlap of data from different facilities; successfully predicting data from different facilities provides some confirmation that a phenomenon is well understood. The main objective in producing the SET cross reference matrix is to identify the best available sets of data for the assessment, validation and, finally, the improvement of code predictions of the individual physical phenomena. While both integral test data and SET data are appropriate for code validation and assessment, for model development and improvement there should be a strong preference for SET data.

3.1. The methodology developed

In the process of establishing the SET validation matrix, a methodology has been developed. This methodology helps to collect and present the data and information collected in a comprehensive and systematic manner. It is a general methodology and therefore, in principal, also applicable to the other type of validation matrices (e.g. on severe accidents). The methodology can be summarized as follows:

1. Identification of phenomena relevant to two-phase flow in relation to LOCAs and thermal-hydraulic transients in light water reactors (LWRs).
2. Characterisation of phenomena, in terms of a short description of each phenomenon, its relevance to nuclear reactor safety, information on measurement ability instrumentation and data base. In addition to these points, the present state of knowledge and the predictive capability of the codes is included in the characterisation of each phenomenon.
3. Setting up a catalogue of information sheets on the experimental facilities, as a basis for the selection of the facilities and specific tests [6b].
4. Forming a separate effects test facility cross-reference matrix by the classification of the facilities in terms of the phenomena they address.
5. Identification of the relevant experimental parameter ranges in relation to each facility that addresses a phenomenon and selection of relevant facilities related to each phenomenon.
6. Establishing a matrix of experiments (the SET matrix) suitable for the developmental assessment of thermal-hydraulics transient system computer codes, by selecting individual tests from the selected facilities, relevant to each phenomenon.

3.2. Forming a set cross-reference matrix

The main objective in producing the Separate Effects Test Facility Cross Reference Matrix (SET CRM) is to identify the best available sets of data for the assessment, validation and, finally, the improvement of code predictions of the individual physical phenomena. While both integral test data and SET data are appropriate for code validation and assessment, for model development and improvement there should be a strong preference for SET data.

The thermohydraulic phenomena of interest in LWR LOCA and transients are listed in Table 1. A set of basic two-phase flow and heat transfer processes which are important for the thermohydraulic codes in the form of basic constitutive relations have been added explicitly to the list under the heading "Basic Phenomena". The scope of the SET Facility CRM has been restricted to those phenomena directly affecting the thermohydraulic behaviour in a transient or LOCA.

The resulting list of 67 thermohydraulic phenomena forms one axis of the SET Facility CRM. The second axis of the Matrix consists of the 187 facilities identified as potential sources of separate effects data. The test facilities in 12 OECD member countries are compiled (Table 2) according to the country in which they operate: Canada, Finland, France, Germany, Italy, Japan, Netherlands, Sweden, Switzerland, United Kingdom, USA, Norway. An example for SET facility CRM is shown in Table 3. The SET facility CRM tables for each country can be seen in [6a]. For each test facility the phenomena addressed by the corresponding experimental research programme have been indicated in these Matrix tables, yielding the SET CRM for test facilities and thermohydraulic phenomena.

The correlation between phenomena and SET Facility is assigned to one of three levels:

- suitable for model validation, which means that a facility is designed in such a way as to simulate the phenomenon assumed to occur in a plant and is sufficiently instrumented (x);
- limited suitability for model validation: the same as above with problems due to imperfect scaling, different test fluids (e.g. Freon instead of water) or insufficient instrumentation (o);
- not suitable for model validation: obvious meaning, taking into account the two previous items (-).

This Matrix shows both the number of different phenomena covered by the experimental investigation with one test facility, and the number of different facilities in which an individual phenomenon has been investigated. The test facilities differ from each other in geometrical dimensions, geometrical configuration and operating capabilities or conditions. Therefore, the number of facilities relevant to an individual phenomenon provides some indication of the range of parameters within which a

phenomenon has been investigated and experimental data generated. For instance, it is obvious from the SET CRM presented in [6a] that heat transfer phenomena, especially post critical heat flux, departure from nucleate boiling/dryout and quench front propagation/rewet, were investigated in many SET facilities.

For the systematic evaluation of the capabilities of a thermohydraulic code, appropriate experiments have to be identified which provide data over the range of conditions of interest (as far as such data is available), for each phenomenon listed.

3.3. Establishing the separate effects tests (SET) matrix

For each of the 67 phenomena, a table presents the tests, which have been identified as suitable for code validation with respect to that phenomenon, from the test facilities selected. An example for a phenomena and related tests are given in Table 4. The arguments for the selection of the facilities for a given phenomenon are already identified with the previous step of the methodology.

In order to try to be practical, the number of facilities has been limited to 3 on the average, though in some special cases up to 5 are used. For heat transfer, a larger number was used, because of the large number of parameters affecting heat transfer and its high degree of importance. The total maximum number of tests has been fixed at up to 20 per phenomenon. Here a test is considered to be a set of data points involving one key parameter variation (e.g. a flooding curve at a single pressure and tube geometry). These numbers indicate the large amount of work, which is necessary to assess a code.

It must be emphasized that tests have been chosen on the basis of available information: It is not always possible to determine how satisfactory data is for code validation until it is actually used (completeness of boundary condition information; measurement accuracy, internal consistency etc.) The situation of the various experimental programs and chosen tests varies greatly in this respect.

The tests have been selected in order to cover the experimental data range as defined, knowing that the plant range is not always covered. Particular attention has been given to the geometric scaling problem and small, medium and large scale separate effect facilities have been integrated whenever possible.

As some facilities are useful with respect to several separate effects phenomena, a cross check and a tentative harmonization of the selected tests have been made when possible, in order to try to minimize the number of input data needed for code validation.

In this matrix the selected tests are ordered following one arbitrary chosen main parameter (for example system pressure) with, optionally, additional parameters (for example, representative diameter). This will give the user an indication of the available range of data for code validation, and the possible need for additional tests.

At the bottom of the table the main references, if identified, are given for the chosen tests. The reader is supposed to have enough information in these references to be able to compute the test. Some examples of the SET matrix for selected number of phenomena are given in Table 5. Further tables for each of the 67 phenomena are given in detail in [6a].

Additional information related to the type of tests, or parameter ranges for instance are also provided in the listed references. This matrix has been published as a first attempt. It may be updated by new and additional input from the owners and by remarks from the users. Nevertheless, as it is, this separate effect test matrix covers a large number of phenomena within a large range of selected parameters. If a thermal-hydraulic code is to be used to cover a certain number of phenomena then calculation of the relevant identified tests in the matrix is considered to be a basic step toward the achievement of code qualification.

4. INTEGRAL TEST FACILITY VALIDATION MATRICES

The validation of codes is mainly based on pre-test and post-test calculations of separate effect tests, integral system tests, and transients in commercial plants. An enormous amount of test data, available for code validation, has been accumulated. In the year 1987 the Committee on the Safety of Nuclear Installations (CSNI) of the Nuclear Energy Agency (NEA) in the Organisation for Economic Co-Operation and Development (OECD) issued a report compiled by the Task Group on the Status and Assessment of Codes for Transients and ECC [3, 4, 5]. It contains proposed validation matrices for LOCA and transients, consisting of the dominating phenomena and the available test facilities, and the selected experiments.

Since the issue of the Validation Matrix Report in 1987, new tests have been performed and an update of the validation matrix was published in the year 1996 [7]. In this report a revision and update of the matrices, including experimental facilities and identified experiments was performed. Two new matrices were included, those for „accident management for a non degraded core in PWRs“ and „transients at shutdown in PWRs“. Additional phenomena and test types were identified for these new matrices. A special chapter on counter-part tests, similar tests and International Standard Problem tests was introduced in this revision of the report. Counter-part tests and similar tests in differently scaled facilities are considered highly important for code validation. International Standard Problem experiments are carefully controlled, documented and evaluated. Therefore, these experiments are a good basis for code validation, and they were included in the tables of selected experiments. Additional work was performed to describe the content of the validation matrices, i.e. the test types, the phenomena, and most of the selected tests. A brief description of thermal-hydraulic aspects of severe accidents was included. The thermal-hydraulic codes are being extended to the thermal-hydraulics prevailing under severe accident conditions. They cannot be considered validated at the present time. Experimental data are limited. The important phenomena for severe accident conditions, with particular emphasis on the thermal-hydraulic phenomena were summarized in the report [7].

It is to be noted that the methodology established for the SET validation matrix (as described in section 3, above) has been applied during the establishment of the Integral Test Facility validation matrices.

4.1. Integral test cross reference matrices

To systematize the selection of tests for code validation, so called „cross reference matrices“ have been established for the first step. Based on these matrices, phenomenologically well founded sets of experiments, for which comparison of measured and calculated parameters form a basis for establishing the accuracy of test calculation results, have been defined in a second step.

In the cross reference matrices the important physical phenomena which are believed to occur during the transient or LOCA, the experimental facilities suitable for reproducing these effects, and the test types of interest are listed. The relationships:

- phenomenon versus test type indicate which phenomena are occurring in which test types,
- test facility versus phenomenon indicate the suitability of the test facilities for code validation of the different phenomena, and
- test type versus test facility indicates which test types are performed in which test facilities.

For PWR facilities six individual matrices were prepared, differentiating between:

- large breaks,
- small and intermediate breaks for PWR with U-tube steam generators,
- small and intermediate breaks for PWR with once-through steam generators (OTSG),
- transients,
- transients at shut-down conditions,
- accident management for a non-degraded core.

The matrix for small and intermediate breaks in PWRs with once-through steam generators have been prepared to address in particular phenomena which are unique to this reactor type.

For BWR facilities two individual matrices have been prepared, differentiating between:

- loss of coolant accidents (LOCA),
- transients.

In Tables 6 to 10 cross reference matrices for PWR facilities with U-tube steam generators are shown. Among the integral system test facilities the category „PWR“ is included under „test facilities“. The analysis of accidents in actual nuclear power plants is potentially valuable with reference to scaling and simulation problems. Descriptions of phenomena and test types can be found in reference [7].

The relationship phenomenon versus test type is rated at one of three levels:

- occurring: which means that the particular phenomenon is occurring in that kind of test (plus sign in the matrix);
- partially occurring: only some aspects of the phenomenon are occurring (open circle in the matrix);
- not occurring (dash in the matrix).

The relationship test facility versus phenomenon is rated at one of three levels:

- suitable for code assessment: a facility is designed in such a way as to simulate the phenomenon assumed to occur in the plant and it is sufficiently instrumented to reveal the phenomenon (plus sign in the matrix);
- limited suitability: the same as above with problems due to imperfect scaling or insufficient instrumentation (open circle in the matrix);
- not suitable: obvious meaning, taking into account the two previous items (dash in the matrix).

The relationship test type versus facility is rated at one of three levels:

- performed: the test type is useful for code assessment purposes (plus sign in the matrix);
- performed but of limited use: this kind of test has been performed in the facility, but has limited usefulness for code assessment purposes, due to poor scaling or lack of instrumentation (open circle in the matrix);
- not performed (blank).

Based on these cross reference matrices, phenomenologically well founded sets of experiments have been defined in a second step. Criteria for the selection of these tests are listed in the following Section. These selected tests form a basis for establishing the accuracy of test calculation results comparing measured and calculated values. A total number of 177 PWR and BWR-specific integral tests have been selected as potential source for thermal hydraulic code validation.

4.2. Selection of individual tests

A number of specific experiments were selected from those facilities, which are included in the cross reference matrices described before. These selected tests versus phenomena establish the individual code validation matrices. During the selection process a number of factors were considered, including:

- typicality of facility and experiment to expected reactor conditions,
- quality and completeness of experimental data (measurement and documentation),
- relevance to safety issues,
- test selected must clearly exhibit phenomena,
- each phenomenon should be addressed by tests of different scaling (at least one test if possible)
- high priority to International Standard Problems (ISP), counterpart and similar tests (for more explanations see [7]),
- challenge to system codes.

Where counterpart tests or similar tests were identified between two or more facilities, they were included in order to address questions relating to scaling and facility design compromises. For the accident management matrix, priority was given on how realistically the test represented typical accident management procedures [8].

5. CROSS REFERENCE MATRICES FOR WWER ANALYSIS (INTEGRAL AND SEPARATE EFFECTS TESTS)

A multi-national Working Group consisting of experts from Czech Republic, Finland, France, Germany, Hungary, Russia, Slovak Republic, Poland and Ukraine has been formed on the initiative of the Federal Minister for Research and Technology (BMFT) of the Federal Republic of Germany, giving the task to GRS in close co-operation with the Nuclear Protection and Safety Institute (IPSN) of France in May 1993 to elaborate the topic "Verification Matrix for Thermal-hydraulic System Codes Applied for WWER Analysis".

The topic was combined with the objective of a co-operation to formulate an internationally agreed WWER-specific validation matrix as a supplement to the existing CSNI matrix for PWRs with U-tube steam generators.

Based on the CSNI cross reference matrices the lists of phenomena have been reviewed and adopted to the characteristics of WWER-440 and WWER-1000 systems respectively, and the lists of test facilities suitable for code assessment have been completed.

The above tasks have been performed successfully by the Working Group under the leadership of GRS in close co-operation with IPSN during 1993-1995, and the results were published by Liesch and Réocreux [9].

The selection of tests from the large number of experiments proposed has to be continued, in order to get the ones which are the most suitable for code assessment with respect to a given phenomenon or test type. In order to support the selection, detailed explanations of the choices for the selected data have to be given.

As a consequence these activities will continue under the auspices of the OECD/NEA. Therefore, in June 1995 a new Support Group has been installed to continue with the further evaluation of the matrices, concentrating on three tasks:

- description of WWER-specific phenomena and safety relevance,
- optimization of the WWER-specific code validation matrices,
- development of criteria for the data bank storage of experimental data valid for the matrices.

As a result of this work, WWER validation matrix has been completed and published in 2001 [10].

6. CONCLUSIONS

A systematic study has been carried out to select experiments for thermal-hydraulic system code validation. The main experimental facilities for SETs, PWRs, BWRs and WWERs have been identified.

Matrices have been established to identify, firstly, phenomena assumed to occur in LWR plants during accident conditions and secondly, facilities and tests suitable for code validation. The matrices also permit identification of areas where further research may be justified [11], and [12]. While the activities for code validation matrices for SETs, PWRs, BWRs and WWERs are completed and the validation matrices, which are established, are ready for use by the research community [13].

A periodic updating of the matrices will be necessary to include new relevant experimental facilities and tests (e. g. investigating boron dilution or behaviour of advanced reactors) and to include improved understanding of existing data as a result of further validation.

The first volume of the SET matrix report [6a] provides cross references between test facilities and thermal-hydraulic phenomena, and lists tests classified by phenomena. As a preliminary to the classification of facilities and test data, it was necessary to identify a sufficiently complete list of relevant phenomena for LOCA and non-LOCA transient applications of PWRs and BWRs. The majority of these phenomena are also relevant to Advanced Water Cooled Reactors and to WWERs. To this end, 67 phenomena were identified for inclusion in the SET matrix. Phenomena characterization and the selection of facilities and tests for the SET matrix are included in volume I of the report [6a]. In all, about 2094 tests are included in the SET matrix.

To validate a code for a particular LWR plant application, it is recommended that the list of tests in the relevant matrix be viewed as the phenomenologically well founded set of experiments to be used for an adequate validation of a thermal hydraulic computer code. This set of data could serve as a basis for the estimation of code accuracy and quantification of code uncertainty.

The development and application of methods to quantify uncertainties in plant calculations is a major task for the future. This requires a determination of code uncertainties, which is based on a systematic code validation. The validation matrices are a necessary prerequisite to achieve such a systematic validation.

ACKNOWLEDGEMENT

The author is grateful to F. D'Auria (University of Pisa, Italy), H. Glaeser (GRS Garching, Germany), C. Richards (AEA Technology, Winfrith, UK), J. Lillington (AEA Technology, UK), R. Pochard (IPSN:DPEI-CEA/FAR, Fontenay-Aux-Roses, France) and A. Sjöberg (Studsvik Eco & Safety AB, Nyköping, Sweden), who are also contributors and authors of the OECD separate effects tests (SET) validation matrix.

This paper also summarizes the work performed by A. Annunziato (JRC, Ispra, Italy), J. N. Lillington (AEA Technology, Winfrith, UK), P. Marsili (ENEA, Rome, Italy), C. Renault (CEA, Cadarache, France), A. Sjöberg (Studsvik Eco & Safety AB, Nyköping, Sweden), and H. Glaeser (GRS Garching, Germany). Their contributions to the results presented in this paper are gratefully acknowledged.

NOMENCLATURE

BWR	Boiling Water Reactor
CCVM	CSNI Code Validation Matrix
CRM	Cross Reference Matrix
CSNI	Committee on Safety of Nuclear Installations
ECC	Emergency Core Cooling
ISP	International Standard Problem
ITF	Integral Test Facility
LOCA	Loss Of Coolant Accident
LWR	Light Water Reactor
NEA	Nuclear Energy Agency
OECD	Organization for Economic Co-operation and Development
OTSG	Once-through Steam Generator
PWR	Pressurized Water Reactor
SET	Separate Effects Test
UPTF	Upper Plenum Test Facility
WWER (VVER)	Water-cooled and Water-moderated Energy Reactor

REFERENCES

- [1] WOLFERT, K., FRISCH, W., "Proposal for the Formulation of a Validation Matrix", CSNI-SINDOC (83) 117 (1983).
- [2] OECD/NEA, Thermohydraulics of emergency core cooling in light water reactors; a state-of-the-art report (SOAR), by a group of experts of the NEA Committee on the Safety of Nuclear Installations, CSNI Report No. 161, October 1989.
- [3] OECD/NEA, CSNI code validation matrix of thermal-hydraulic codes for LWR LOCA and transients, OECD/NEA-CSNI Report 132, March 1987.
- [4] WOLFERT, K. and BRITTAIN, I., CSNI Validation Matrix for PWR and BWR Thermal-Hydraulic System Codes, *Nuclear Engineering and Design*, Vol., pp 108 107–199 North-Holland, Amsterdam (1988).
- [5] WOLFERT, K., GLAESER, H., AKSAN, N., CSNI validation matrix for PWR and BWR codes, Proceedings of the CSNI-Specialist Meeting on Transient Two-Phase Flow Aix-en-Provence, France, edited by M. Reocreux and M.C. Rubinstein, NEA/CSNI/RL(92)/12 (1992).
- [6] AKSAN, N., D'AURIA, F., GLAESER, H., POCHARD, R., RICHARDS, C., SJÖBERG, A., Separate Effects Test Matrix for Thermal-Hydraulic Code Validation,
 - a) Volume I: Phenomena Characterisation and Selection of Facilities and Tests,
 - b) Volume II: Facility and Experiment Characteristics.NEA/CSNI/R(93)14/Part 1 and Part 2, Paris (1994).
- [7] ANNUNZIATO, A., GLAESER, H., LILLINGTON, J., MARSILI, P., RENAULT, C., SJÖBERG, A., CSNI integral test facility validation matrix for the assessment of thermal-hydraulic codes for LWR LOCA and transients", NEA/CSNI/R(96)17, July 1996.
- [8] AKSAN, N., and GLAESER, H., Overview on the CSNI separate effects test and integral test facility matrices for validation of best-estimate thermal-hydraulic computer", Proceedings of OECD/CSNI Seminar on "Best Estimate Methods in Thermal-Hydraulic Safety Analysis", Ankara, Turkey, 29 June–1 July 1998, NEA/CSNI/R(99)10, February 2000.
- [9] LIESCH, K., RÉOCREUX, M., Concerted actions on safety research for WWER reactors. verification matrix for thermalhydraulic system codes applied for WWER analysis, Common Report IPSN/GRS No. 25, July 1995.
- [10] OECD/NEA, Validation matrix for the assessment of thermal-hydraulic codes for VVER LOCA and transients; by a group of experts of the NEA Committee on the Safety of Nuclear Installations, NEA/CSNI/R(2001)4, June 2001.
- [11] D'AURIA, F., AKSAN, N., GLAESER, H., SJÖBERG, A., POCHARD, R., LILLINGTON, J., Further evaluation of the CSNI separate effect test activity, Proceedings of the 7th International Meeting on Nuclear Reactor Thermal-Hydraulics NURETH-7, Saratoga Springs, NY (USA), September 10–15, 1995.
- [12] AKSAN, N., D'AURIA, F., GLAESER, H., LILLINGTON, J., POCHARD, R., SJÖBERG, A., Evaluation of the separate effects tests (SET) validation matrix", NEA/CSNI/R(96)16, November 1996.
- [13] AKSAN, N., Overview on CSNI separate effects test facility matrices for validation of best estimate thermal-hydraulic computer codes, presented at the OECD/NEA Seminar on Transfer of Competence, Knowledge and Experience Gained Through CSNI Activities in the Field of Thermal-Hydraulics, INSTN, Saclay, France, June 7–11, 2004.

Table 1. List of phenomena

0	BASIC PHENOMENA	1	Evaporation due to Depressurisation
		2	Evaporation due to Heat Input
		3	Condensation due to Pressurisation
		4	Condensation due to Heat Removal
		5	Interfacial Friction in Vertical Flow
		6	Interfacial Friction in Horizontal Flow
		7	Wall to Fluid Friction
		8	Pressure Drops at Geometric Discontinuities
		9	Pressure Wave Propagation
1	CRITICAL FLOW	1	Breaks
		2	Valves
		3	Pipes
2	PHASE SEPARATION/VERTICAL FLOW WITH AND WITHOUT MIXTURE LEVEL	1	Pipes/Plena
		2	Core
		3	Downcomer
3	STRATIFICATION IN HORIZONTAL FLOW	1	Pipes
4	PHASE SEPARATION AT BRANCHES	1	Branches
5	ENTRAINMENT/DEENTRAINMENT	1	Core
		2	Upper Plenum
		3	Downcomer
		4	Steam Generator Tube
		5	Steam Generator Mixing Chamber (PWR)
		6	Hot Leg with ECCI (PWR)
6	LIQUID-VAPOUR MIXING WITH CONDENSATION	1	Core
		2	Downcomer
		3	Upper Plenum
		4	Lower Plenum
		5	Steam Generator Mixing Chamber (PWR)
		6	ECCI in Hot and Cold Leg (PWR)
7	CONDENSATION IN STRATIFIED CONDITIONS	1	Pressuriser (PWR)
		2	Steam Generator Primary Side (PWR)
		3	Steam Generator Secondary Side (PWR)
		4	Horizontal Pipes
8	SPRAY EFFECTS	1	Core (BWR)
		2	Pressuriser (PWR)
		3	Once-Through Steam Generator Secondary Side (PWR)
9	COUNTERCURRENT FLOW / COUNTERCURRENT FLOW LIMITATION	1	Upper Tie Plate

	COUNTERCURRENT FLOW LIMITATION	2	Channel Inlet Orifices (BWR)
		3	Hot and Cold Leg
		4	Steam Generator Tube (PWR)
		5	Downcomer
		6	Surge line (PWR)
10	GLOBAL MULTIDIMENSIONAL FLUID TEMPERATURE, VOID AND FLOW DISTRIBUTION	1	Upper Plenum
		2	Core
		3	Downcomer
		4	Steam Generator Secondary Side
11	HEAT TRANSFER: NATURAL OR FORCED CONVECTION	1	Core, Steam Generator, Structures
	SUBCOOLED/NUCLEATE BOILING	2	Core, Steam Generator, Structures
	DNB/DRYOUT	3	Core, Steam Generator, Structures
	POST CRITICAL HEAT FLUX	4	Core, Steam Generator, Structures
	RADIATION	5	Core
	CONDENSATION	6	Steam Generator, Structures
12	QUENCH FRONT PROPAGATION/REWET	1	Fuel Rods
		2	Channel Walls and Water Rods (BWR)
13	LOWER PLENUM FLASHING		
14	GUIDE TUBE FLASHING (BWR)		
15	ONE AND TWO PHASE IMPELLER-PUMP BEHAVIOUR		
16	ONE AND TWO PHASE JET-PUMP BEHAVIOUR (BWR)		
17	SEPARATOR BEHAVIOUR		
18	STEAM DRYER BEHAVIOUR		
19	ACCUMULATOR BEHAVIOUR		
20	LOOP SEAL FILLING AND CLEARANCE (PWR)		
21	ECC BYPASS/DOWNCOMER PENETRATION		
22	PARALLEL CHANNEL INSTABILITIES (BWR)		
23	BORON MIXING AND TRANSPORT		
24	NONCONDENSABLE GAS EFFECT (PWR)		
25	LOWER PLENUM ENTRAINMENT		

Table 2.: List of facilities

		Info sheet	Selected in the CCVM			Info sheet	Selected in the CCVM
1	CANADA			5.14	FOB Blowdown, ANSALDO		
				5.15	GEST-SEP, SIET	a	x
1.1	Elbow Flooding Rig	a		5.16	GET-GEN (20 M W SG), SIET		
1.2	CWIT (CANDU reactors)	a		5.17	PIPER (Blowdown), PISA	a	x
1.3	Pumps			5.18	JF Blowdown, ENEA		
1.4	Header Test Facility (CANDU reactors)	a					
				6	JAPAN		
2	FINLAND						
				6.1	TPTF, JAERI	a	x
2.1	REWET-I	a		6.2	Air/Water Horiz. Flow Loop JAERI	a	
2.2	REWET-II	a	x	6.3	T-Break TF (Air/Water), JAERI	a	
2.3				6.4	Air/Water Rod Bundle TF, JAERI		
2.4	VEERA	a		6.5	SG U-Tube TF, JAERI		
2.5				6.6	Single Pin Heat Transf. TF, Jaeri	a	
2.6	IVO-CCFL (air.water)	a	x	6.7	SRTF (Reflood), Toshiba	a	
2.7	IVO-Thermal Mixing	a	x	6.8	ESTA (18 Degree Sector), Toshiba		
2.8	IVO-Loop Seal Facility (Air/Water)	a	x	6.9	ESTA-KP (KWU-PWR), Toshiba		
				6.10	RRTF (Refill/Reflood), Toshiba		
3	FRANCE			6.11	SHTF (Spray Heat Transf.) Toshiba		
				6.12	Guide Tube CFL TF, Toshiba		
3.1	MOBY-DICK	a	x	6.13	Swell Level Tests, Toshiba		
3.2	SUPER MOBY-DICK	a	x	6.14	SCTF, JAERI	a	x
3.3	CANON and SUPER CANON (Horiz)	a	x	6.15	CCTF, JAERI	a	
3.4	VERTICAL CANON	a		6.16	HICOF (Hitachi Core and Fuel Tests		
3.5				6.17			
3.6	TAPIOCA (Vertical)	a	x	6.18	Hot Leg CCFL Rig, JAERI	a	
3.7	Dadine (Vertical Tube, Inside)	a	x				
3.8	PERICLES Rectangular	a	x	7	NETHERLANDS		
3.9	PERICLES Cylindrical	a	x	7.1	Bcn Boiloff/Reflood Tests (36 rods)	a	
3.10	PATRICIA GV 1	a	X	7.2			
3.11	PATRICIA gv 2	a	X	7.3	NEPTUNUS	a	x

3.12	ERSEC Tube (Inside)	a	x				
3.13	ERSEC Rod Bundle	a	x	8	SWEDEN		
3.14	OMEGA Tube (Inside)	a	x				
3.15	OMEGA Rod Bundle	a	x	8.1	GÖTA BWR ECC Tests	a	x
3.16	ECTHOR Loop Seal (Air/Water)	a	x	8.2	MARVIKEN	a	x
3.17	COSI	a	x	8.3	FRIGG/FRÖA	a	x
3.18	SUPER MOBY-DICK TEE	a	x	8.4	120 bar Loop		
3.19	PIERO (Air/Water)	a	x	8.5	SIV		
3.20	EPOPEE			8.6	SEPA		
3.21	EVA	a	x				
3.22	SEROPS			9	SWITZERLAND		
3.23	BETHSY Pressuriser						
3.24	SUPER MOBY-DICK Horizontal	a	x	9.1	NEPTUN-I (Boiloff)	a	x
3.25	REBECA	a	x	9.2	NEPTUN-I and II (Reflood)	a	x
3.26	ECOTRA			9.3	PEANUT (Reflood Inside Tube)	a	
4	GERMANY			10	UNITED KINGDOM		
4.1	UPTF	a	x	10.1	ACHILLES Reflood Loop	a	x
4.2	HDR Vessel	a	x	10.2	THETIS Bundle	a	x
4.3	BATTELLE PWR RS 16	a	x	10.3	REFLEX Tube Reflood		
4.4	BATTELLE BWR 150396	a	x	10.4	Post Dryout Ins. Tube (HP, Winfrith)	a	x
4.5	Blowdown Heat Transfer RS 37			10.5	TITAN/9 MW Rigs	a	
4.6	Het Transfer Refill/Reflod RS 36			10.6	High Pressure Rig	a	
4.7	Steady state DNB Exp. RS 164			10.7	Post Dryout Ins. Tube (LP, Harwell)	a	x
4.8	Trans. Boil. Inst. Tube (Freon) RS 370	a		10.8	Air/Water Pipeline Fac. (Large Sc.)		
4.9	Rewet RS 62/184	a		10.9	Hot Leg (Air/Water, Offt., Large Sc.)	a	
4.10	Thermodyn. Nonequilibrium RS 77	a	x	10.10			
4.11	LOCA Pump Behaviour RS 92	a		10.11	Horiz. CCFL Rig (Air/Water, Small Sc.)	a	
4.12	Thermalhyd. UP-BBR 373			10.12	Air/Water Rigs (Small Scale)		
4.13	Pressuriser-Valve RS 240, 347 636			10.13	LOTUS (Air/Water Ann. Flow in Tube)	a	x
4.14	Steam/Water Disch. Flow RS 93, 397	a		10.14	Single Tube Level Swell (Harwell)	a	x
4.15				10.15	Single Tube Reflood (Harwell)	a	
4.16	T-Junction Test Facility (KfK)	a	x	10.16	Crossflow Two-Phase Wind Tunnel	a	
				10.17	Loop Seal Air/Water Rig		

5	ITALY			10.18	Hot Leg Co and CCF Rig		
				10.19	Single tube Reflood (Leatherhead)	a	
5.1	Pressuriser (Vapore Plant) ENEA	a	x	10.20	Boiler Dynamics Rig	a	
5.2	Pressuriser Spray, TURIN	a	x	10.21	Valve Blowdown Test Facility	a	x
5.3	Pressuriser Flooding, CISE			10.22	Single Pin Reflood		
5.4	JETI-4 Fuel Channel SIET	a	x	10.23	Multipin Cluster Rig		
5.5	Safety VALVE SIET	a	x	10.24	Blowdown Rig		
5.6	Gen 3x3 (Steam Generator), SIET	a	x	10.25	ECCS Condensation Rig		
5.7	8x8 Bundle, CISE			10.26	1/6 th Sc. Broken Cold Leg Nozzle Rig	a	
5.8	FREGENE (Steam Generator) ENEA			10.27	1/10 th Scale PWR Refill Strath Clyde		
5.9	ARAMIS (Separator) ENEA			10.28	R113 Vertical Forced Circul. Loop		
5.10	Jet Condensation, TURIN			10.29	R113 Horiz. Forced Circul. Loop		
5.11	Jet Condensation, ENEA			10.30	Vertical Flow Rigs		
5.12	CHF, ENEA			10.31	High Press. Steam/Water Forced Circ.		
5.13	CCF, ENEA			10.32	Low Pressure Boiling Fac. (Harwell)	a	

Table 2 (cont.). List of facilities

		Info sheet	Selected in the CCVM
11	USA		
11.1	LTSF 1/6 Scale Jet Pump	a	x
11.2	Univ. California SB. LP BWR	a	x
11.3	THEF Post CHF Ins.Tube	a	x
11.4	Battle Columbus Laboratory		
11.5	Wyle Lab. Marshall Steam Station TF		
11.6	Micellaneous Sources		
11.7	Univ. California SB. Vert. Tube		
11.8	Univ. California B. Tube Reflood	a	x
11.9	Univ. California Berkeley		
11.10	Columbia rod Bundle	a	x
11.11	State Univ. New York at Buffalo		
11.12	State Univ. New York at Buffalo		
11.13	1/30, 1/5 + 1/5 VESSEL CREARE	a	x
11.14	1/5 DC + CL CREARE	a	
11.15	CDN DART Bubbly Flow Nozzles	a	
11.16	VERT TUBE PL/DART Annular CCF	a	x
11.17	TUBE + CHANNEL DART Air/Water		
11.18	SNTF DART BWR Spray Nozzle		
11.19	CE + MIT		
11.20	J-Loop Test Fac. Westinghouse		
11.21	HCNTL Univ. of Cincinnati		
11.22	Heat Transf. Loop Baboock and Wilcox		
11.23	FLECHT SEASET Westinghouse	a	x
11.24	Univ. California Los Angeles		
11.25	SCTF Univ. California LA	a	x
11.26	Univ. California Santa Barbara		
11.27	Univ. California Berkeley		
11.28	HST, SSTF, VSF/GE Spray Tests	a	x
11.29	Four Loop Natural Circulation/SRI		

11.30	U-Tube SG Two-Loop Test Fac/SRI	a	
11.31	1/5 EPRI-CREARE Mixing Facility		
11.32	EPRI-SAI Thermal Mixing Test Fac.	a	
11.33	1/8 Scale Test Facility/CREARE	a	x
11.34	EPRI-Wyle Pipe Rupture Test Fac.		
11.35	TPFL/INEL Tee Critical Flow	a	x
11.36	EPRI-SAI Carryover Large Dim.		
11.37	PHSE/PURDUE 1/8 Scale Facility		
11.38	Thermal Hydr. Test Fac/ORNL		
11.39	INEL Pump Characterisation	a	x
11.40	Semiscale/INEL		
11.41	BWR-FLECHT/GE	a	x
11.42	LEHIGH Post CHF Heat Tr. Bundle	a	x
11.43	MIT Pressuriser	a	x
11.44	LS/GE Level Swell in Blowdown	a	
11.45	HOUSTON		
11.46	Cocurrent Hor, Flow/Northwest	a	x
11.47	ANL Power-Void Transf. Funct. BWR	a	x
11.48	Natural Circulation Boiling/ANL	a	
11.49	G2 Loop/Westinghouse		
11.50	Air/Water TF/B. Willamette Pump		
11.51	Univ. California Berkley		
11.52	MB-2 SG Transient/Westinghouse	a	x
11.53	Strat. Condens. Flow/Northwest	a	
11.54	Critical Flow Rig/GE	a	x
11.55	Reflux Rig/Univ. Cal. St. Barbara	a	x
11.56	LTSF Blowdown Quench/INEL	a	x
11.57	LEHIGH Post CHF Vertical Tube	a	x
12	NORWAY		
12.1	Halden Reactor, Reflood Tests	a	x

Table 4. Phenomenon no. 11.4 – heat transfer post-CHF in the core, in the steam generator and at structures (PART A)

FACILITY IDENTIFICATION			KEYWORDS	RELEVANT PARAMETERS RANGES			REASONS FOR SELECTION OR NOTES
No.	Status in the matrix	Name		Pressure (MPa)	Inlet mass flow (kg/m ² /s)	Heat flux (W/cm ²)	
3.7	a x	DADINE (VERTICAL TUBE INSIDE)	Vertical tube, Steady-state, Boil-off	0.1-0.6	20-150	1-3	
3.12	a x	ERSEC TUBE (INSIDE)	Tube, reflooding	0.1-0.6	10-120	1-7	1 5 6
3.14	a x	OMEGA TUBE (INSIDE)	Blowdown	16	–	60-125	5 6 7
3.15	a x	OMEGA ROD BUNDLE	Blowdown	13-15	–	44-60	5 6 7
4.5	a x	BLOWDOWN HEAT TRANSFER RS 37	Blowdown Rod bundle	15-1.3	3828-3300	163-74	5 6 7
4.9	a x	REWET (RS 62/184)	Reflooding, tube, single rod	0.1-0.45	2-10 cm/s	2-6	5 6
5.6	a x	GEN 3x3 (STEAM GENERATOR) ENEA	SG Secondary, Steady-state, transient	3.5-8	200-600	–	
5.7	a x	8x8 BUNDLE CISE	BWR-6 Bundle, Steady state	7.1	125-1600	–	6 7
5.12	x	CHF ENEA					
6.1	a x	TPTF JAERI	Core heat transfer, Boil-off, Reflooding, BWR and PWR bundle	0.5-12	20-410	3-25	2 3 5 6
6.16	x	HICOF (HITACHI CORE AND FUEL TESTS)					
8.4	x	120 BAR LOOP					
9.1	a x	NEPTUN-I (BOIL-OFF)	Bundle	0.15	–	25-75 kW	2 3 5 6
10.3	x	REFLEX TUBE REFLOOD					
10.4	a x	POST DRYOUT INST. TUBE (HP, WINFRITH)	Hot patch	0.2-7	50-2000	1-30	2 3 5 6
10.7	a x	POST DRYOUT INST. TUBE (LP, HARWELL)		0.2-0.4	25-200		2 3 5 6
10.20	a x	BOILER DYNAMICS RIG	SG, transient boundary conditions	28	12 kg/s	12 MW	6 7
10.23	x	MULTIPIN CLUSTER RIG					
11.3	a x	THEF POST CHF INS. TUBE	Steady state, quasi-steady state	0.2-7	12-70	0.8-22.5	2 3 4 5 6
11.7	x	UNIV. CALIFORNIA B. TUBE REFLOOD					
11.8	a x	UNIV. CALIFORNIA B. TUBE REFLOOD	Reflooding	0.1-0.3	2.5-18 cm/s		1 5 6

Table 5. Heat transfer post-CHF in the core, in the steam generator and at structures (7/7)

FACILITIES IDENTIFIER		11.56	11.57	12.1		
Main parameters						
P (MPa)	Inlet fluid velocity (m/s)					
6.86	3.7	12				
6.92	0.4	7				
	Mass Flux (kg/m ² s)					
0.378	14.8		100			
0.255	14.9		105			
0.409	20.7		112			
0.396	42.7		124			
0.39	29.5		130			
0.272	42.9		158			
0.302	60		174			
0.395	29.9		191			
	Reflood rate (cm/s)					
0.2-0.4	9.6			IFA-511-2		
	5.6			5236		
	7.4			5239		
				5247		
	9.6			IFA-511-3		
	5.6			5258		
	7.4			5261		
	2.1			5265		
				5266		
SELECTED TESTS						
<u>References:</u>						
11.56	N. Aksan: "Evaluation of Analytical Capability to predict cladding Quench" EGG-LOFT 5555, August 1982.					
11.57	D.G. Evans, et al. "Measurement of Axially Varying Nonequilibrium in Post-Critical Heat-Flux Boiling in a Vertical Tube" NUREG/CR-3363, Vols. 1 and 2, June 1983.					
12.1	C. Vitanza et al.: "Blowdown/reflood tests with Nuclear Heated Rods (IFA-511.2)" OECD Halden Reactor Project, HPR-248, May 1980.					
	T. Johnsen, C. Vitanza: "Blowdown/Reflood Tests with Semiscale Heaters (IFA-511.3)" OECD Halden Reactor Project HWR-17, May 1981.					

Table 6. Cross reference matrix for large breaks in PWRs

Matrix I CROSS REFERENCE MATRIX FOR LARGE BREAKS IN PWRs		Test Type			Test Facility and Volumetric						
		Blowdown	Refill	Reflood	CCTF 1:25	LOFT 1 : 50	BETHSY 1 : 100	PKL 1 : 145	LOBI 1 : 712	SEMISCALE 1 : 1600	UPTF 1 : 1 (a)
Phenomena versus test type + occurring o partially occurring - not occurring - test facility versus phenomenon + suitable for code assessment o limited suitability - not suitable - test type versus test facility + performed o performed but of limited use - not performed or planned											
Phenomena	Break flow	+	+	+	o	o	o	o	o	o	o
	Phase separation (condition or transition)	o	+	+	+	+	+	+	+	+	+
	Mixing and condensation during injection	o	+	+	o	o	o	o	o	o	+
	Core wide void + flow distribution	o	+	+	o	o	o	o	o	-	O
	ECC bypass and penetration	o	+	o	+	+	-	o	o	-	+
	CCFL (UCSP)	o	+	+	o	o	o	o	o	-	+
	Steam binding (liquid carry over, ect.)	-	o	+	o	o	-	o	o	o	O
	Pool formation in UP	-	+	+	o	o	o	o	o	o	+
	Core heat transfer incl. DNB, dryout, RNB	+	+	+	o	+	+	+	o	o	-
	Quench front propagation	o	o	+	+	+	+	+	-	+	-
	Entrainment (Core, UP)	o	o	+	o	o	+	o	o	o	+
	Deentrainment (Core, UP)	o	o	+	o	o	o	o	o	o	+
	1 - and 2-phase pump behaviour	+	o	o	-	o	-	o	+	+	-
	Noncondensable gas effects	-	o	o	-	-	o	-	-	-	O
Test Facility	CCTF	-	o	+	important test parameter - break location/break size - pumps off/pumps on - cold leg injection/combined injection (a) UPTF integral tests						
	LOFT	+	+	+							
	BETHSY	-	-	+							
	PKL	o	+	+							
	LOBI	+	+	-							
	SEMISCALE	+	+	+							
	UPTF	o	+	+							

Table 7. Cross reference matrix for small and intermediate breaks in PWRs

Matrix II CROSS REFERENCE MATRIX FOR SMALL AND INTERMEDIATE BREAKS		Test Type								Test Facility and Volumetric Scaling							
		Stationary test addressing energy transport on primary side	Stationary test addressing energy transport on secondary side	Small leak overfeed by HPIS, secondary side necessary	Small leak without HPIS overfeeding, secondary side	Intermediate leak, secondary side not necessary	Pressurizer leak	U-tube rupture									
Phenomena versus test type + occurring o partially occurring - not occurring - Test facility versus phenomenon + suitable for code assessment o limited suitability - not suitable - Test type versus test facility + performed o performed but of limited use - not performed or planned	Natural circulation in 1-phase flow, primary side	+	+	+	o	-	+	+	+	+	+	+	+	+	+	+	-
	Natural circulation in 2-phase flow, primary side	+	-	o	+	+	o	-	-	+	+	+	+	+	+	+	o
	Reflux condenser mode and CCFL	+	-	-	+	+	-	-	-	o	+	+	o	o	o	o	+
	Asymmetric loop behaviour	-	-	+	+	-	o	+	-	-	o	+	+	+	o	o	+
	Break flow	-	-	+	+	+	+	+	-	+	+	+	+	+	+	+	o
	Phase separation without mixture level formation	+	-	o	+	+	+	o	-	o	+	+	+	+	+	o	+
	Mixture level and entrainment in SG second side	-	+	+	+	+	+	+	-	-	+	+	+	o	o	-	-
	Mixture level and entrainment in the core	+	-	-	+	+	+	-	-	o	+	+	+	o	o	o	o
	Stratification in horizontal pipes	+	-	-	+	+	-	-	-	+		o	o	+	o	o	+
	Phase separation in T-junct. and effect on breakflow	-	-	-	+	+	-	-	-	o	o	o	o	o	o	-	+
	ECC-mixing and condensation	-	-	o	+	+	+	+	-	o	o	o	o	o	o	o	+
	Loop seal clearing	-	-	-	+	+	o	-	-	+	+	+	+	+	+	+	+
	Pool formation in UP/CCFL (UCSP)	+	-	-	o	+	+	-	-	o	o	o	o	o	-	o	+
	Core wide void and flow distribution	+	-	-	o	+	+	-	-	o	o	o	o	-	-	-	o
	Heat transfer in covered core	+	+	+	+	+	+	+	o	+	+	+	+	+	+	+	-
	Heat transfer in partly uncovered core	+	-	-	o	+	-	-	-	+	+	+	+	o	o	o	-
	Heat transfer in SG primary side	+	o	o	+	+	o	o	-	o	+	+	+	+	+	o	-
	Heat transfer in SG secondary side	o	+	+	+	+	+	+	-	o	+	+	+	o	+	o	-
	Pressurizer thermohydraulics	o	-	o	o	+	+	+	o	o	o	o	o	o	o	o	+
	Surgeline hydraulics	o	-	-	o	+	+	o	-	o	o	o	o	o	o	o	+
1- and 2-phase pump behaviour	-	-	-	o	+	-	-	o	o	o	o	o	o	+	+	-	
Structural heat and heat losses (1)	+	-	o	+	+	o	o	-	o	o	o	o	o	o	o	o	
Noncondensable gas effects	+	-	-	-	-	-	-	-	-	o	o	o	-	-	o	+	
Boron mixing and transport	+	-	+	+	+	+	+	+	-	-	-	-	-	-	-	o	
Test Facility	PWR	-	-	o	-	-	+	+	(1) problem for scaled test facilities								
	LOFT	-	-	+	+	+	+	-	(2) UPTF integral tests								
	LSTF	+	+	+	+	+	+	+	(3) for intermediate breaks phenomena included in large break reference matrix may be also important								
	BETHSY	+	+	+	+	+	+	+									
	PKL-III	+	+	+	+	+	+	+									
	SPES	+	+	+	+	-	-	-									
	LOBI-II	+	+	+	+	+	+	+									
	SEMISCALE	o	o	+	+	+	+	+									
UPTF, TRAM	-	-	-	-	+	+	-										

Table 8. Cross reference matrix for transients in PWRS

Phenomenon versus test type + occurring o partially occurring - test facility versus Phenomenon + suitable for code assessment o limited suitability - not suitable - test type versus test facility + performed o performed but of limited use - not performed or planned		ATWS	Loss of feedwater, non ATWS	Loss of heat sink, non ATWS (c)	Station blackout	Steam line break	Feed line break	Reactivity disturbance	Over-cooling	PWR 1 : 1	LOFT 1 : 50	LSTF 1 : 50	BETHSY 1 : 100	PKL-III 1 : 134	SPES 1 : 430	LOBI-II 1 : 712	SEMISCALE 1 : 1000
		Phenomena															
Phenomena	Natural circulation in 1-phase flow	+	+	+	+	+	+	o	o	+	o	+	+	+	+	+	+
	Natural circulation in 2-phase flow	+	+	+	+	-	-	o	-	-	o	+	+	+	+	+	+
	Core thermohydraulics	+	+	+	+	o	o	+	o	o	+	+	+	+	+	+	+
	Thermohydraulics on primary side of SG	+	o	o	+	o	o	o	+	o	o	+	+	+	+	+	o
	Thermohydraulics on secondary side of SG	+	+	+	+	+	+	o	+	o	o	+	+	+	+	o	+
	Pressurizer thermohydraulics	+	+	+	+	o	o	o	+	o	o	o	o	o	o	o	o
	Surgeline hydraulics (CCFL, choking)	+	+	+	+	o	o	o	o	o	o	o	o	o	o	o	o
	Valve leak flow (a)	+	+	+	+	+	+	+	+	-	o	o	o	o	o	o	o
	1- and 2-phase pump behaviour	+	+	+	+	o	o	o	+	o	o	+	o	o	o	+	+
	Thermohydraulic-nuclear feedback	+	-	-	-	-	-	+	-	+	+	-	-	-	-	-	-
	Structural heat and heat losses (b)	o	o	o	o	o	o	o	o	-	o	o	o	o	o	o	o
	Boron mixing and transport	-	-	-	-	o	-	-	o	-	-	-	-	-	-	-	-
	Separator behaviour	o	-	-	-	+	-	-	-	-	-	-	-	-	-	o	o
	Test Facility	PWR	-	-	-	-	-	-	o	(a) valve flow behaviour will be strongly design-dependent, specific experimental data should be used if possible (b) problem for scaled test facilities (b) problem for scaled test facilities							
LOFT		+	+	+	o	-	-	+	+								
LSTF		-	+	-	+	+	+	-	+								
BETHSY		-	+	+	-	+	+	-	-								
PKL-III		-	+	+	+	+	+	-	+								
SPES		-	+	-	+	-	-	-	-								
LOBI-II		+	+	+	+	+	+	-	-								
SEMISCALE	-	+	+	+	+	+	-	+									

Table 9. Cross reference matrix for transients at shut down conditions in PWRS

Matrix V CROSS REFERENCE MATRIX FOR TRANSIENTS AT SHUT-DOWN CONDITIONS IN PWRS		Test Type				Test Facility and Volumetric Scaling		
		Loss of RHR with no openings	Loss of RHR with openings	Loss of RHR with dam in HL	Boron dilution at shut-down	LSTF	BETHSY	PKL III
Phenomenon versus test type + occurring o partially occurring - not occurring - Test facility versus phenomenon + suitable for code assessment o limited suitability - not suitable - Test type versus test facility + performed o performed but of limited use - not performed or planned								
Phenomena	Pressurization due to boiling	+	+	+	-	+	+	+
	Reflux condenser mode and CCFL	+	+	o	-	+	+	O
	Asymmetric loop behaviour	-	o	+	-	+	+	+
	Flow through openings (manways, vents)	-	+	+	-	+	+	-
	Mixture level formation in upper plenum and hot legs	+	+	+	-	+	+	+
	Mixture level and entrainment in the core	+	+	+	-	+	+	+
	SG syphon draining	-	-	+	-	+	-	-
	Asymmetry due to the presence of a dam	-	-	+	-	+	-	-
	Stratification in horizontal pipes	+	+	+	-	+	o	+
	Phase separation in T-junctions and effect on flow	-	+	+	-	o	o	O
	ECC mixing and condensation	+	+	+	-	o	o	O
	Loop seal clearing and filling	+	+	+	-	+	+	-
	Pool formation in UP/CCFL (UCSP)	-	-	-	-	-	-	-
	Core 3D thermalhydraulics	+	+	+	+	o	o	O
	Heat transfer in covered core	+	+	+	-	+	+	+
	Heat transfer in partially uncovered core	+	+	+	-	o	o	-
	Heat transfer in SG primary side	+	+	+	-	+	+	+
	Heat transfer in SG secondary side	+	+	+	-	+	+	+
	Pressurizer thermalhydraulics a)	-	x	x	-	o	o	O
	Surge line thermalhydraulics a)	-	x	x	-	o	o	O
	Structural heat and heat losses	-	-	-	-	-	-	O
	Non-condensable gas effects	+	+	+	-	+	+	+
Boron mixing and transport	-	-	-	+	-	-	-	
Thermalhydraulics-nuclear feedback	-	-	-	+	-	-	-	
Test Facility	LSTF	+	+	+	-			
	BETHSY	-	+	-	-			
	PKL III	+	-	-	-			

- a) x is dependent on opening location
 + pressuriser manway open
 - pressuriser manway shut

Table 10. Cross reference matrix for accident management for non-degraded core in PWRs

Matrix VI CROSS REFERENCE MATRIX FOR ACCIDENT MANAGEMENT FOR A NON DEGRADED CORE IN PWRs		Test Type					Test Facility and Volumetric Scaling						
		High pressure primary side feed and bleed	Low pressure, primary side feed and bleed	Secondary side, feed and bleed	RCP-Restart in a highly, voided PCS	Primary to secondary break with multiple failures	LOFT 1 : 50	LSTF 1 : 50	BETHSY 1 : 100	PKL-III 1 : 1 : 145	SPES 1 : 430	LOBI-II 1 : 712	UPTF, TRAM 1 : 1 (2)
Phenomena	Natural circulation in 1-phase flow, primary side	+	-	+	-	+	+	+	+	+	+	+	+
	Natural circulation in 2-phase flow, primary side	+	+	+	-	+	+	+	+	+	+	+	o
	Reflux condenser mode and CCFL	-	-	+	-	+	o	+	o	o	o	o	+
	Asymmetric loop behaviour	+	+	+	+	+	-	o	+	+	+	o	+
	Break flow	+	+	o	+	+	+	+	+	+	o	+	o
	Phase separation without mixture level formation	+	+	+	+	+	o	+	+	+	+	+	+
	Mixture level and entrainment in SG secondary side	-	-	+	-	+	-	+	+	+	o	o	-
	Mixture level and entrainment in the core	+	+	+	o	+	o	+	+	+	o	o	o
	Stratification in horizontal pipes	+	+	+	o	+	+	+	o	o	o	o	+
	Phase separation in T-junct. and effect on breakflow	+	+	o	-	+	o	o	o	o	o	o	+
	ECC-mixing and condensation	+	+	+	-	+	o	o	o	o	o	o	+
	Loop seal clearing (3)	o	o	+	o	+	+	+	o	o	+	+	+
	Pool formation in UP/CCFL (UCSP)	+	+	+	-	+	o	o	o	o	o	-	+
	Core wide void and flow distribution	+	+	+	+	+	o	o	o	o	-	-	o
	Heat transfer in covered core	o	o	+	-	+	+	+	+	+	+	+	-
	Heat transfer in partly uncovered core	+	+	+	+	+	+	+	+	+	o	o	-
	Heat transfer in SG primary side	-	-	+	o	+	o	+	+	+	+	+	-
	Heat transfer in SG secondary side	-	-	+	o	+	o	+	+	+	o	+	-
	Pressurizer thermohydraulics	+	+	o	o	+	o	o	o	o	o	o	+
	Surgeline hydraulics	+	+	o	o	+	o	o	o	o	o	o	+
	1- and 2-phase pump behaviour	o	o	+	+	+	o	o	o	o	o	+	-
	Structural heat and heat losses (1)	+	+	+	+	+	o	o	o	o	o	o	o
	Noncondensable gas effects	o	+	+	+	+	-	o	o	+	-	-	+
	Accumulator behaviour	-	+	+	-	o	o	+	+	+	+	+	+
	Boron mixing and transport	+	+	+	+	+	-	-	-	-	-	-	o
	Thermohydraulic-nuclear feed back	-	-	-	+	-	-	-	-	-	-	-	-
	Separator behaviour	-	-	-	-	-	-	-	-	-	-	-	-
	Test Facility	LOFT	-	-	+	-	-	(1) problem for scaled test facilities (2) UPTF integral tests (3) long term cooling not included					
LSTF		+	+	+	-	o							
BETHSY		+	+	+	-	+							
PKL-III		o	+	+	+	-							
SPES		+	+	+	-	+							
LOBI-II		+	+	+	-	+							
UPTF, TRAM		o	+	-	-	-							

Table 11. Cross reference matrix for loca in BWRs

Matrix VII CROSS REFERENCE MATRIX FOR LOCA IN BWRs		Test Type							Test Facility and Volumetric Scaling						
		Large Steam Line Break with Fast Depressurization	Large Break Below Water Level with Fast Depress.	Small Break without Depress. before ADS Actuation	Intermediate Break with Slow Depress.	Spray Line Break	Refill - Reflood	BWR 1 : 1 (a)	TBL, 1 : 382, 2 Chan., Full Pow., Full Height	ROSA III, 1 : 424, 4 Channels	TLTA, 1 : 624, 1 Chan., Full Power	FIST, 1 : 624, 1 Chan., Full Pow., Full Height	FIX 2, 1 : 777, 1 Chan., Full Pow., Full Height	PIPER 1, 1 : 2200, 1 Chan., Full Height	
Phenomena	Break flow	+	+	+	+	+	o	-	o	o	o	o	o	+	
	Channel and Bypass Axial Flow and Void Distribution	+	+	+	+	+	+	o	+	o	+	+	+	+	
	Corewide Radial Void Distribution	o	o	+	+	+	+	o	o	+	o	o	o	-	
	Parallel Channel Effects-Instabilities	-	-	+	+	+	+	-	o	+	-	-	-	o	
	ECC Bypass	-	-	o	o	o	+	-	o	o	o	o	-	+	
	CCFL at UCSP and Channel Inlet Orifice	o	+	-	+	+	+	-	o	o	-	o	o	o	
	Core Heat Transf. incl. DNB, Dryout, RNB. Surf. to Surf Radiation	+	+	o	+	o	+	-	+	+	+	+	+	+	
	Quench Front Propagation for both Fuel Rods and Channel Walls	-	-	-	-	-	+	-	+	+	+	+	-	+	
	Entrainment and Deentrainment in Core and Upper Plenum	+	+	o	o	o	+	-	-	o	o	o	-	o	
	Separator Behavior incl. Flooding, Steam Penetration and Carryover	+	+	o	o	o	-	o	+	o	o	+	o	o	
	Spray Cooling	-	-	o	o	o	+	-	o	o	o	o	-	+	
	Spray Distribution	-	-	o	o	o	+	-	-	o	-	-	-	-	
	Steam Dryer - Hydraulic Behavior	+	-	o	o	-	-	o	o	o	o	o	-	o	
	One and Two Phase Pump Recirc. Behavior incl. Jet Pumps	o	o	+	+	+	o	o	o	o	o	o	o	-	
	Phase Separation and Mixture Level Behavior	+	+	+	+	+	+	-	o	+	o	+	+	o	
	Guide Tube and Lower Plenum Flashing	+	+	-	o	o	-	-	+	+	+	+	+	+	
	Natural Circulation- Core and Downcomer	-	-	+	o	o	+	+	+	o	o	+	+	+	
	Natural Circulation Core Bypass, Hot and Cold Bundles	-	-	+	o	o	+	-	o	o	o	o	o	o	
	Mixture Level in Core	-	-	+	o	o	+	-	+	+	+	+	+	o	
	Mixture Level in Downcomer	+	+	+	+	+	+	-	+	o	o	+	+	o	
	ECC Mixing and Condensation	-	-	+	o	+	+	-	o	o	o	o	-	o	
	Pool Formation in Upper Plenum	o	o	-	o	o	+	-	o	o	o	o	o	o	
	Structural Heat and Heat Losses	o	o	o	+	+	+	-	+	o	o	o	o	o	
Phase Separ. in T - Junction and Effect on Break Flow	-	-	+	o	+	-	-	-	-	-	-	-	+		
Test Facility	BWR	-	-	-	-	-	-	(a) These are non-LOCA data but may be used for assessment							
	TBL	+	+	+	+	-	+								
	ROSA III	+	+	+	+	-	+								
	TLTA	+	+	-	+	-	+								
	FIST	+	+	+	+	-	+								
	FIX 2	-	+	-	+	-	-								
PIPER 1	-	+	+	+	-	+									

Table 12. Cross reference matrix for transients in BWRs

Matrix VIII CROSS REFERENCE MATRIX FOR TRANSIENTS IN BWRs		Test Type									Test Facility and Volumetric Scaling			
		Stationary Test Measuring Power Flow Map	Recirculation Pump Trip	Core Stability	Loss of Main Heat Sink	Feedwater Flow or Temperature Disturbance e. g. LOFW	Loss of Feedwater (LOFW) up to time of Const. Pressure	Inadvertent Increase in Steam Flow	ATWS	Station Blackout (Loss-of-Offsite Power)	BWR 1 : 1	ROSA III, 1 : 424, 4 Channels	FIST, 1 : 642, 1 Channel, Full Power, Full Height	FIX 2, 1 : 777, 1 Channel, Full Power, Full Height
Phenomenon versus test type + occurring o partially occurring - not occurring Test facility versus phenomenon + suitable for code assessment o limited suitability - not suitable Test type versus test facility + performed o performed but of limited use - not performed or planned														
Phenomena	Natural Circulation in One- and Two-Phase Flow	+	+	+	+	-	-	-	+	+	+	o	+	o
	Collapsed Level Behaviour in Downcomer	-	+	o	+	+	+	+	+	+	+	o	+	+
	Core Thermal Hydraulics	o	+	+	+	o	o	o	+	+	o	+	+	+
	Valve Leak Flow	-	-	-	+	-	-	-	+	+	o	o	o	-
	Single Phase Pump Behaviour (a)	o	+	o	+	o	o	+	+	+	o	o	o	o
	Parallel Channel Effects and Instabilities	-	+	+	o	-	-	-	+	+	o	+	-	-
	Nuclear Thermalhydraulic Feedback Including Spatial Effects	o	o	+	-	o	o	o	+	-	+	-	-	-
	Nuclear Thermalhydraulic Instabilities	-	o	+	-	-	-	o	+	-	+	-	-	-
	Downcomer Mixing	-	-	-	-	+	+	-	+	+	o	o	-	-
	Boron Mixing and Distribution	-	-	-	-	-	-	-	+	-	-	-	-	-
	Steam Line Dynamics	-	-	-	+	-	-	+	+	+	o	-	o	-
	Void Collapse and Temp. Distribution During Pressurization	-	-	-	+	-	-	-	+	+	o	+	+	+
	Critical Power Ratio	-	+	+	+	+	+	+	+	+	o	+	+	+
	Rewet after DNB at High Press. and High Power Incl. High Core Flow	-	+	-	+	-	-	o	+	o	-	o	+	+
	Structural Heat and Heat Losses	-	o	-	o	-	o	o	o	o	-	o	o	o
Test Facility	BWR	+	+	+	+	+	+	+	-	o				
	ROSA III	-	+	+	+	-	+	-	-	+				
	FIST	-	o	-	+	-	+	+	o	+				
	FIX 2	-	+	-	+	-	-	-	-	-				

(a) Two-phase pump behaviour is of interest for certain special ATWS and inadvertent increase of steam flow transients

RELIABILITY OF PASSIVE SYSTEMS THAT UTILIZE NATURAL CIRCULATION

M. Marquès

CEA/DEN, Cadarache, France

Abstract

The objective of this lecture is to make the students sensitive to the problem of the failure risk of passive systems that utilize natural circulation and to propose to them a methodology to evaluate the reliability of these systems and to carry out sensitivity analyses. An example of passive system will be used in the lecture to illustrate the methodology.

1. INTRODUCTION

The expanded consideration of severe accidents, the increased safety requirements, and the aim of introducing effective — yet transparent — safety functions lead to growing consideration of passive safety systems for future nuclear reactors.

Innovative reactor concepts make use of passive safety features to a large extent in combination with active safety or operational systems. Following the IAEA definitions (IAEA, 1991), a passive system does not need external input (especially energy) to operate. This is why it is expected that passive systems combine among others the advantages of simplicity, reduction of the need for human interaction, reduction or avoidance of external electrical power or signals.

Besides the open feedback on economic competitiveness, special aspects like lack of data on some phenomena, missing operating experience over the wide range of conditions, and the smaller driving forces as - in most cases - compared to active safety systems must be taken into account.

This remark is especially applicable to the passive systems B or C (i.e. implementing moving working fluid, following IAEA classification¹ (IAEA, 1991)) and in particular to the passive systems that utilize Natural Circulation (NC). These passive safety systems in these designs rely on natural forces (i.e. natural convection), to perform their accident prevention and mitigation functions once actuated and started. These driving forces are not generated by external power sources (e.g., pumped systems), as is the case in operating and evolutionary reactor designs. Because the magnitude of the natural forces, which drive the operation of passive systems, is relatively small, counter-forces (e.g. friction) can be of comparable magnitude and cannot be ignored as in usually done with pumped systems. Moreover, there are considerable uncertainties associated with factors on which the magnitude of these forces and counter forces depends (e.g. values of heat transfer coefficients and pressure losses). In addition, the magnitude of such natural driving forces depends on the specific plant conditions and configurations which could be existing at the time a system is called upon to perform its safety function. All these uncertainties affect the passive system thermal-hydraulic performances. For this reason, the reliability of the systems that utilize NC must be assessed.

Up to now the codes used in T-H analysis, like RELAP, ATHLET and CATHARE, are best estimate codes, which don't account for the uncertainties in their input variables and in their inner correlation. But the value of the physical response predicted by a T-H computer code can significantly differ from its actual value because of:

- a) uncertainties in the value of code input variables;
- b) approximations and uncertainties in modelling the physics of the process;
- c) approximations in modelling the system geometry.

To assess the impact of uncertainties on the predicted response of the code, a large number of calculations is needed and if we consider all the sequences where the passive system studied is implied, this number of calculations can be prohibitive.

¹ See Annex 1 for these classification.

For all these reasons, it appeared necessary to create a specific methodology to assess the reliability of passive systems B or C.

The methodology has been developed in the framework of a Project called Reliability Methods for Passive Safety Functions (RMPS), performed under the auspices of the European 5th Framework Programme. The methodology deals with following problems:

- Identification and quantification of the sources of uncertainties and determination of the important variables;
- Propagation of the uncertainties through T-H models and assessment of T-H passive system unreliability;
- Introduction of passive system unreliability in the accident sequence analysis.

Each step of the methodology is described and commented and a diagram of the methodology is presented. An example of passive system is presented with the aim to illustrate the possibilities of the methodology. This example is the Residual Passive heat Removal system on the Primary circuit (RP2), an innovating system supposed to be implemented on a 900 MWe Pressurized Water Reactor.

2. EXAMPLE OF A NC SYSTEM: THE RP2 SYSTEM

The Residual Passive heat Removal system on the Primary circuit (RP2) system is composed of three circuits dedicated to the heat removal, each one being connected on a loop of the primary circuit (Fig. 2.1) (Gautier, 1999). Each circuit includes an exchanger immersed in a cooling pool located inside the containment, and a valve to allow its starting. For the study in progress, this valve was put on the cold leg of the system, downstream the exchanger. The exchanger is located higher than the main piping of the primary circuit to allow a natural convection between the core and the exchanger. On criterion of emergency shutdown of the reactor, the valve opens and the natural convection starts. The residual power produced by the fuel is transferred to the cooling pool via the RP2 exchanger.

This system is quite similar to the PHRS from AP600, but its missions are different. AP600 only rely upon passive systems for Design Basis Accidents. RP2 has been designed within the framework of a new management principle, termed “Base Operation Passive Heat Removal” (BOPHR), where the residual power is removed jointly by active and passive systems, immediately after emergency shutdown.

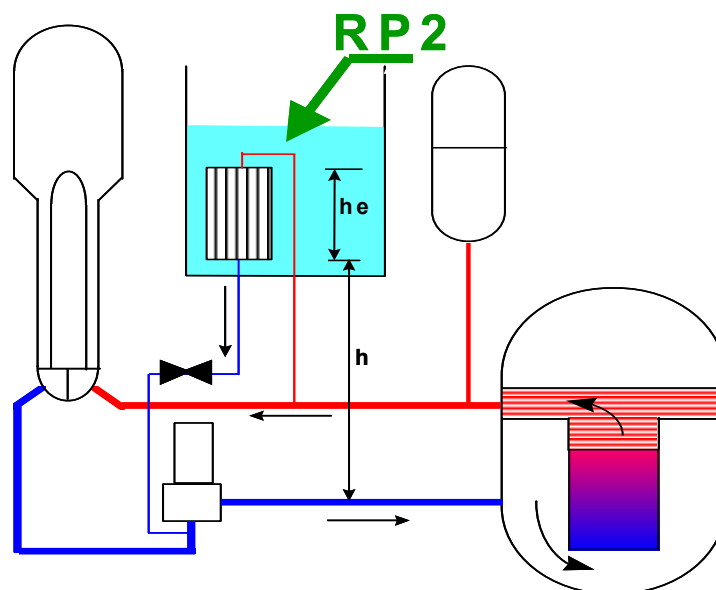


FIG. 2.1. BOPHR/RP2 system.

3. CHARACTERISATION OF THE NC SYSTEM, IDENTIFICATION AND QUANTIFICATION OF THE SOURCES OF UNCERTAINTIES, SENSITIVITY ANALYSIS

3.1. Characterisation of the system

The goal of this analysis is to obtain information about the behavior of a passive system that utilize NC, in an accident occurring during the life of the nuclear reactor and to identify the failure zones and conditions, if they exist. For that, we have to define the missions of the system, its failure modes and the failure criteria.

3.1.1. *Definition of the accidental scenario*

The first step of the analysis is the definition of the accidental scenario in which the system will operate. The knowledge of this scenario will allow the specific definition of failure criteria and relevant parameters and the specific quantification of the uncertainties. On the other hand the results obtained in the reliability and sensitivity analyses of the system will be specific to this scenario. A global evaluation of the system, could be obtained by the integration of the system reliability in a Probabilistic Safety Assessment in which all the sequences involving the passive system will be considered (see chapter 5). Another possibility can be the evaluation of the system reliability for the worse scenario considered or to take large ranges of variation of the uncertain parameters in order to take into account the larger variability covering all the scenarios involving the system.

3.1.2. *Mission of the system*

The missions of the system are the goals for which the Passive System has been designed and located within the complete system. For instance, the mission of the passive system can be the decay heat removal, the cooling of the vessel, the pressure decrease of the primary circuit... In some case, the passive system can be designed to fulfil several missions in the same time or different missions depending on the considered scenario.

3.1.3. *Failure mode*

Due to the complexity of thermal-hydraulic phenomena and to the interaction between the passive system and the complete system, it is not always obvious to associate a failure mode to a mission of the system.

A qualitative analysis is often necessary in order to identify potential failure modes and their consequences associated with the passive system operation. The aim of this analysis is to identify the parameters judged critical for the passive system performance allowing the association between failure modes and corresponding indicators of the failure cause. The methodology can be combined with a hazard identification qualitative method as FMEA (Failure Mode and Effect Analysis).

The FMEA approach implies the introduction, in addition to mechanical components of the system (piping, drain valve, etc.), of a “virtual” component identified as Natural Circulation and its evaluation in terms of potential “phenomenological” factors (the list of these includes e.g. non-condensable gas build-up, thermal stratification, surface oxidation, cracking, etc.), the consequences of which can affect the passive system performance.

During the process of characterisation, modelling and evaluation of the passive system, new failure modes can be identified (such as flow oscillations, plugs phenomena due to non-condensable gazes...) which have also been taken into account.

3.1.4. *Success/failure criteria*

The knowledge of the system missions and failure modes allows the evaluation of the failure criteria. The failure criteria can be established as single-targets (e.g. the system must deliver a specific quantity of liquid within a fixed time) or as a function of time targets or integral values over a mission

time (e.g. the system must reject at least a mean value of thermal power all along the system intervention).

In some cases, it can be better to define a global failure criterion of the complete system instead of a specific criterion concerning the passive system. For instance the failure criterion can be based on the maximal clad temperature during a specified period. In this case, it is necessary to have modelled the complete system and not only the passive system.

3.1.5. Modelling of the system

Due to the lack of suitable experimental databases for passive systems in operation, the evaluation should rely on numerical modelling, e.g. by means of simulation via best-estimate codes. The system analysis should be carried out with a qualified thermal-hydraulic system code and performing best estimate calculations.

Indeed there is an increasing interest in computational reactor safety analysis to replace the conservative evaluation model calculations by best estimate calculations supplemented by a quantitative uncertainty analysis. Specially in the present methodology where the objective is the evaluation of the reliability of the passive system, it is important to calculate the passive system performance in a realistic and not in a conservative way.

3.2. Identification of the sources of uncertainties

3.2.1. Overview on uncertainties related to Passive Systems that utilize NC

The overall uncertainty relating the thermal hydraulic analysis of passive systems that utilize NC consists of two kinds of uncertainties:

- Uncertainties related to thermal hydraulic code
- Uncertainties related to natural circulation performance.

Uncertainties may have different origins ranging from the approximation of the models characterizing any physical phenomena, to the approximation of the numerical solutions, to the lack of precision of the values adopted for boundary and initial conditions, and to the parameters that are the input to the phenomenological models. The amount of uncertainty that affects a calculation strongly depends upon the involved area in the technology and upon the sophistication of the adopted models and modeling techniques. This is even more relevant as far as natural circulation is concerned, due to the small engaged driving forces and the thermal hydraulic phenomena affecting the system performance that may induce large uncertainties.

The potentially important contributors to uncertainty of the code results can be classified as:

- Approximations in modelling the physical process : for instance the treatment of a liquid steam mixture as an homogeneous fluid, the use of empirical correlation.
- Approximations in modelling the system geometry : simplification of complex geometry features and approximation of a three-dimensional system.
- The input variables: initial and boundary conditions, such as plant temperatures, pressures, water levels and reactor power, dimensions, physical properties, such as densities, conductivities, specific heats, and thermal-hydraulic parameters, such as heat transfer coefficients or friction factors.

Various methodologies have been developed in order to evaluate the overall uncertainty in the physical model predictions and some efforts have been made aimed at the internal assessment of uncertainty capability for thermal hydraulic codes (Kwang-II, 2000), (D'Auria, 2000).

This identification of the relevant parameters must be based on the Expert Opinion of the physical process and of the thermal hydraulic codes.

3.2.2. Identification of the relevant parameters

Among all the sources of uncertainties, the evaluation of the reliability of a passive system requires the identification of the relevant parameters which really affect the accomplishment of the target of the system. The **Analytic Hierarchy Process** (Saaty, 1980), (Zio, 2003), which provides a qualitative and schematic, but rigorous and transparent, method to model the process under investigation. This method is composed of three major steps: the building of a hierarchy to decompose the problem at hand, the input of pairwise comparison judgments regarding the relevance of the considered parameters and the computation of priority vectors to obtain their ranking.

The method is intended, in our case, to provide a transparent method to model the thermal-hydraulic process of the passive system under investigation, so as to allow selecting the important parameters related to the target of the system design.

The building of the hierarchy is performed in three steps:

- i. Define precisely the top goal of the hierarchy and place it at the top level;
- ii. Build downward the hierarchy in different levels by putting in each level those factors directly influencing the elements of the level just above and directly influenced by the elements of the level just below. Directed arrows are placed to specify the interconnections between the elements;
- iii. At the bottom of the hierarchy place the basic parameters.

In this way, decomposition of the problem (top goal) is provided, interactions are represented and one can describe how elements belonging to a level affect elements of the level just above.

The successive phase of the analysis is that of collecting pairwise importance judgments, through the following steps:

- i. For each element of each level build a pairwise comparison matrix to assess the importance of the influence of the relevant entries of the level below in relation to the element under analysis. In other words, given an element k in level s , all entries of the level below, $s-1$, which affect k are compared in a pairwise fashion in terms of their relevance to k . The proper question in the pairwise comparison is of the form: 'Considering entries X and Y of level $s-1$, how much more important is entry X compared to entry Y with respect to their influence on element k of level s ?'

The pairwise comparisons can be performed directly into a certain numerical scale or on a qualitative fashion and then translated into a numerical scale. Typically, the scale of integer numbers from 1 to 9 is used and the values a_{ij} obtained from the comparisons are organized in a square matrix. For example, performing qualitatively the comparison of element A with element B , the scale is the following:

- 1 = A and B equally important,
- 3 = A slightly more important than B ,
- 5 = A strongly more important than B ,
- 7 = A very strongly more important than B ,
- 9 = A absolutely more important than B .

By definition an element is equally important when compared to itself so the principal diagonal of the matrix is filled with ones. The appropriate reciprocals, $1/3, 1/5, \dots, 1/9$ are inserted where the reverse comparison, B vs. A , is required. The numbers 2, 4, 6, 8 and their reciprocals can be used to facilitate expressing judgments for intermediate situations. In other words, the expert is allowed to resort to the use of a measure of 4, for example, when making a comparison of A and B which he believes cannot exactly be expressed by 3 nor 5;

- ii. For each element k in level s , determine the *potency (strength, priority, weight)* $w_{i(s-1),k(s)}$ with which each element i in level $s-1$ affects element k . The priorities $\{w_{i(s-1),k(s)}\}$ of the entries i in level $(s-1)$, relative to their importance for an element k in the next level (s) can be determined by solving an eigenvector problem. More precisely, it can be shown that given the matrix of pairwise comparisons for the element of interest, the principal eigenvector provides the vector of priorities, when normalized, and the maximum eigenvalue is a measure of consistency of the comparisons entered in the matrix. For complete consistency, the maximum eigenvalue, λ_{max} should be equal to the order of the matrix, n .

The level of consistency of a given pairwise comparison matrix can be measured by a parameter called consistency ratio, CR, defined as the ratio of the consistency index $CI = (\lambda_{max} - n)/(n-1)$ and the random index RI, which is the statistically averaged consistency index of randomly generated matrices of order n with entries artificially forced to be consistent. A consistency ratio of 0.10 or less is considered acceptable. Further clarification regarding the meaning of consistency in this case can be obtained with the aid of a simple example. Suppose that in doing pairwise comparisons of three elements A, B, C , the following relations are obtained: A is 4 times more important than B ; A is 8 times more important than C . Then, in order for our matrix of comparisons to be consistent we expect that the judgment relating B and C will state that B is twice as important as C .

Although this matter might seem trivial, in practice it is quite common to encounter inconsistencies particularly when the order of the matrix is large;

- iii. In case of large inconsistencies in a matrix, revise its entries by redoing the judgments on the individual pairwise comparisons or by forcing the values a_{ij} to be mathematically consistent by setting them equal to w_i / w_j , where $w_i = w_{i(s-1),k(s)}$, $w_j = w_{j(s-1),k(s)}$ are the priority values of elements i and j of level $s-1$ in regards to their relevance to element k of level s immediately above. Indeed, in the ideal case of the comparisons being the results of exact physical measurements w_i , $i = 1, 2, \dots, n$, the relation between the matrix entries and the weights is simply $a_{ij} = w_i / w_j$, for $i, j = 1, 2, \dots, n$. Note that usually it is sufficient to revise the values for those entries a_{ij} for which $|a_{ij} - w_i/w_j|$ is maximum or for all the entries of the row for which the root mean square deviation of a_{ij} and w_i / w_j is maximum.

At this point, we can compute the priority ranking of each parameter. Once all the priority vectors are available, multiply them appropriately through the branches of the hierarchy (just like in a probability tree) to determine the overall weights of the bottom-level alternatives with regards to the previously defined top goal. For example, referring to a simple example of a three-level hierarchy with three alternatives at the bottom, as shown in Figure 3.1, if $w_{AY} = \{w_{AY1}, w_{AY2}, w_{AY3}, \dots\}$ is the vector $(1 \times n)$ of strengths of alternative A at the bottom level of the hierarchy and $w_Y = \{w_{Y1}, w_{Y2}, w_{Y3}, \dots\}^T$ is the vector $(n \times 1)$ of priorities for the elements at the second level, then we multiply $w_A = w_{AY} \cdot w_Y$ to get the weight of alternative A measuring its relative importance with regards to the top goal.

The major advantage of the pairwise comparison approach to quantification is the simple and intuitive way of expressing judgments on the relative importance of the different constituents of the hierarchy, and the possibility of checking for consistency in the judgment entries.

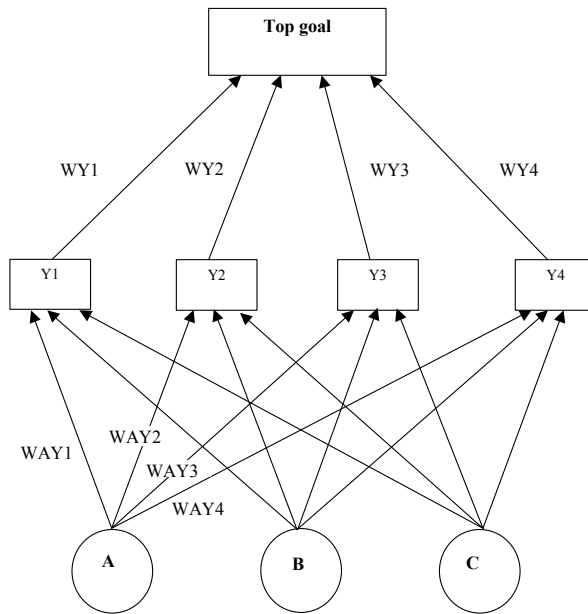


FIG. 3.1. A simple three-levels hierarchy.

3.3. Quantification of the uncertainties

A key issue in this process is the selection of the distributions for the input parameters. This is based on the experience from validation of the computer code by comparison between model predictions and test data of integral tests and separate effects tests for the model parameters as well as on known measurement uncertainties. The main objective is that the selected distribution for each input parameter must quantify the analyst's state of knowledge for that parameter and express the reliable and available information about the parameter. The choice of distribution may highly affect the passive system reliability evaluations.

Different points of view have to be considered for this quantification:

- The amount of data:

When the data on a parameter are abundant, we can use statistical methods such as maximum likelihood method or method of moments to adjust analytical Density Functions and we can use different goodness-of-fit tests (Chi square, Kolmogorov...) to find the best analytical fit to the data.

When the data are sparse or non-existent and this is generally the case when we consider the uncertainties affecting the passive system performance, the evaluation of the probability functions of the uncertain parameters must be based on the expert judgments. The classical interpretation of probability as the limit of a relative frequency, expressing the uncertainty due to stochastic variability, is not applicable here. Thus a subjective approach is used here where the uncertainty is characterised as a probability density function that shows the range of values where the actual value of the parameter may be and what parts of the range the analyst considers more likely than others. In the case where no preferences can be justified, uniform distribution will be specified, i.e. each value between minimum and maximum is equally likely the appropriate parameter value. These distributions are quantitative expressions of the state of knowledge and can be modified if there is new evidence. If suitable observations become available, they can be used consistently to update the distributions. As the consequence of probability distributions of input parameters, the computer code results also have a subjective probability distribution, from which uncertainty limits or intervals are derived.

- The dependence between the parameters:

If parameters have contributors to their uncertainty in common, the respective states of knowledge are dependent. As a consequence of this dependence parameter values can not be combined freely and independently. Instances of such limitations need to be identified and the dependencies need to be quantified, if judged to be potentially important. If the analyst knows of dependencies between parameters explicitly, multivariate distributions or conditional subjective probability distribution function (pdf) may be used. The dependence between the parameters can be also introduced by covariance matrices or by functional relations between the parameters.

3.4. Sensitivity analysis

3.4.1. Objectives

An important feature of the methodology is to evaluate sensitivity measures of the importance of parameter uncertainties on the uncertainty of the passive system performance. These sensitivity measures give a ranking of input parameters. This information provides guidance as to where to improve the state of knowledge in order to reduce the output uncertainties most effectively. If experimental results are available to compare with calculations, sensitivity measures provide guidance where to improve the models of the computer code.

Different sensitivity indices exist (Saltelli, 2000); their use depends on the nature of the model representing the passive system operation and giving its performances.

3.4.2. Qualitative methods for sensitivity analysis

Sometimes the lack of operational experience and significant data concerning the passive system performance forces the analysis to be performed in a **qualitative** way aimed at identifying for each failure mode, both the level of uncertainty associated with the phenomenon and the sensitivity of failure probability to that phenomenon (Burgazzi, 2000).

For example, even if a phenomenon is highly uncertain (because of deficiencies in the physical modelling) this may not be important for the overall failure probability. Conversely a phenomenon may be well understood (therefore the uncertainty is small) but the failure probability may be sensitive to small variation in this parameter. The grading scheme is given in Table 3.1.

Table 3.1. Grade rank for uncertainty and sensitivity

	Grade	Definition
Uncertainty	H	The phenomenon is not represented in the computer modelling or the model is too complex or inappropriate which indicates that the calculation results will have a high degree of uncertainty.
	M	The phenomenon is represented by simple modelling based on experimental observations or results.
	L	The phenomenon is modelled in a detailed way with adequate validation.
Sensitivity	H	The phenomenon is expected to have a significant impact on the system failure
	M	The phenomenon is expected to have a moderate impact on the system failure
	L	The phenomenon is expected to have only a small impact on the system failure

An example of qualitative point of view analysis as outcome of expert judgment assessment is given in Table 3.2, regarding the failure modes of the natural circulation.

Table 3.2. Failure modes related uncertainty and sensitivity

TOPIC	UNCERTAINTY	SENSITIVITY
Envelope failure	L	H
Cracking	L	L
Non-condensable gas	H	H
Thermal stratification	H	H
Surface characteristics modification (e.g. oxidation)	M	L

From the above qualitative table it seems that only for the structural failure modes there is a deep knowledge of the relative phenomenology. In the other cases the level of uncertainties is high or medium and in every case an effort must be devoted for their quantification. The sensitivity grades are the results of only a qualitative analysis: the natural circulation failure is very sensitive either to the loss of primary boundary or to the thermalhydraulic phenomena arising during the system performance.

It's clear that the worst case is characterized by "high" rankings relative to either sensitivity or uncertainty (see e.g. non-condensable gas and thermal stratification), making the corresponding phenomena evaluation a critical challenge.

3.4.3. *Quantitative methods for sensitivity analysis*

The **quantitative** sensitivity analysis is performed by T-H calculations. It consists in ranking the parameters according to their relative contribution on the whole code response uncertainty and quantifying this contribution for each parameter.

The sensitivity analysis can be performed by the following steps:

- Design the experiment and determine which of its input factors should concern the analysis;
- Assign probability density functions or ranges of variation to each input factor;
- Generate an input vector/matrix through an appropriate design;
- Evaluate the model, thus creating an output distribution for the response of interest;
- Assess the influences or relative importance of each input factor on the output variables.

To apportion the variation in the output to the different parameters, many techniques could be used (Saltelli, 2000), each yielding different measures of sensitivity.

An usual approach is to base the sensitivity analysis on a linear regression method, which is based on the hypothesis of a **linear** relation between response and input parameters. This, in case of passive systems is often restrictive. However, the method is simple and quick, and provides useful insights in case of a restricted number of sampling, as will be our case. Three different sensitivity coefficients have been considered, each one providing a slightly different information on the relevance of a parameter: Standardized Regression Coefficients (SRC), Partial Correlation Coefficients (PCC) and Correlation Coefficients (CC).

Standardized Regression Coefficients (SRC)

These coefficients suppose that the response Y is a linear function of the random input variables X_i :

$$Y = \beta_0 + \sum_{i=1}^p \beta_i X_i$$

The SRC are given by:

$$\text{SRC}(Y, X_i) = \beta_i \sqrt{\frac{\text{Var}(X_i)}{\text{Var}(Y)}}$$

The SRCs quantify the effect of varying each input variable away from its average by a fixed fraction of its variance. The sign of SR coefficient indicates if the response increases (+) or decreases (-) when the variable increases.

Partial correlation coefficients (PCC)

The partial correlation coefficient between the output variable Y and the input variable X_j is defined as the correlation coefficient between $Y - \hat{Y}$ and $X_j - \hat{X}_j$:

$$\hat{Y} = b_0 + \sum_{h \neq j} b_h x_h, \quad \hat{X}_j = c_0 + \sum_{h \neq j} c_h x_h$$

The PCCs provide a measure of variable importance that tends to exclude the effects of other variables.

Small differences between the different coefficients may be due to a certain degree of correlation between the inputs and to the system non-linearity. These occurrences should be analysed, the first one possibly through the examination of the correlation matrix and the second one calculating the model coefficient of determination R^2 for example.

These results on SR and PC coefficients are based on the hypothesis that the model is linear. To validate this hypothesis, it is important to calculate the determination coefficients of the linear model:

$$R^2 = \frac{\sum_{i=1}^N (\hat{y}_i - \bar{y})^2}{\sum_{i=1}^N (y_i - \bar{y})^2}$$

Where \hat{y}_i denotes the estimate of y_i obtained from the regression model. R^2 provides a measurement of how well the linear regression model can reproduce the actual output y . The closer R^2 to unity; the better the model performance.

Depending on the nature of the model representing the passive system operation and giving its performances, it can be more accurate to use sensitivity methods developed for non-monotonous or non linear models. In case of **non-linear but monotonous models**, we can perform rank transformations and calculate associated indices: standardized rank regression coefficients (SRRCs) and partial rank correlation coefficients (PRCCs). The rank transform is a simple procedure, which involves replacing the data with their corresponding ranks. We can also calculate a coefficient of determination based on the rank R^{2*} . The R^{2*} will be higher than the R^2 in case of non-linear models. The difference between R^2 and R^{2*} is a useful indicator of nonlinearity of the model.

For **non linear and non monotonous models**, two methods exist: the Fourier Amplitude Sensitivity Test (FAST) and the Sobol method. The general idea of these methods is to decompose the total variance of the response, in terms corresponding to part of the variance coming from the uncertainty

on the input parameters taken independently, in terms corresponding to the interaction between two parameters, in terms corresponding to the interaction between three parameters, etc.

The general idea of these methods is to decompose the total variance of the response, noted D into $2^p - 1$ terms (p is the number of random variables).

For instance, if there are 3 random variables, we obtain:

$$D = D_1 + D_2 + D_3 + D_{12} + D_{13} + D_{23} + D_{123}$$

The generalization to a model with p inputs:

$$D = \sum_{i=1}^p D_i + \sum_{1 \leq i < j \leq p} D_{i,j} + \dots + D_{1,2,\dots,p} \quad (3.1)$$

The first order terms D_i gather the effect of the uncertainty on the input parameter x_i (taken independently) on the response variance. The terms $D_{i,j}$, $i \neq j$ gather the effect of the interaction between the parameters x_i and x_j . And so on.

In dividing the equation (3.1) by D , we obtain:

$$1 = \sum_{i=1}^p S_i + \sum_{1 \leq i < j \leq p} S_{i,j} + \dots + S_{1,2,\dots,p}$$

where the terms S are called the sensitivity indices.

The S_i terms evaluate the contribution of the parameter x_i taken independently, the $S_{i,j}$ terms evaluate the contribution of the interaction between parameters x_i and x_j, \dots

In order to rank the random variables according to their influence on the response, we need to evaluate the total contribution of each parameter. The following indices were introduced:

$$S_{T_i} = 1 - S_{\sim i}$$

where $S_{\sim i}$ is the sum of S_{i_1, \dots, i_s} for which the index i is not present. Or

$$S_{T_i} = 1 - \frac{D_{\sim i}}{D}$$

Thus S_{T_i} is the total contribution of the variable x_i on the response. For example, for a 3 parameter model:

$$S_{T1} = S_1 + S_{12} + S_{13} + S_{123}$$

$$S_{T2} = S_2 + S_{12} + S_{23} + S_{123}$$

$$S_{T3} = S_3 + S_{13} + S_{23} + S_{123}$$

The Sobol indices are calculated by Monte-Carlo simulation. The Fast indices are calculated by Fast Fourier Transformation.

The problem of these methods, and specially Sobol method (Archer, 1997), is that a good estimation of these indices requires a great number of calculations. (i.e. 10000 simulations). Thus it is necessary first to calculate a response surface validated in the domain of variation of the random variables.

If the model is not linear, nor monotonous, we propose:

- adjust non linear models on the data,
- test the validity of the model (R^2 , residue, predictive robustness),
- use the model as a response surface in order to evaluate the SOBOL or FAST indices.

The Sobol indices are calculated by Monte-Carlo simulation. The problem of these methods, and specially Sobol method, is that a good estimation of these indices requires a great number of calculations. (i.e. 10000 simulations). Thus it is often necessary first to calculate a response surface validated in the domain of variation of the random variables. Thus, if the model is really not linear, nor monotonous, we propose to:

- adjust non linear models on the data,
- test the validity of the model (R^2 , residue, predictive robustness),
- use the model as a response surface in order to evaluate the SOBOL or FAST indices.

3.5. Application to the RP2 system (Marquès, 2004)

3.5.1. Characterisation of the RP2 system

The transient of Total Loss of the Power Supplies (or Blackout) was selected as reference accident for the reliability evaluation of the system.

The objective of the safety systems is to avoid the core fusion in pressure. Thus the mission of the RP2 system is double, on the one hand to depressurise the primary circuit, and on the other hand to avoid the fusion of the core.

For the exercise, the duration of accidental calculation was fixed arbitrarily at 12 hours, relatively long time where no human intervention is simulated. The failure of the system is obtained if the maximum temperature of the clad or the temperature of the fluid at the core output go beyond respectively the values of 500°C and 450°C, in less than 12 hours.

3.5.2. Modelling of the RP2 system

A modelling with CATHARE (1.5a Mod 3.1) (Barre, 1990) of a complete pressurized water reactor PWR 900 MWe with the 3 independently simulated primary/secondary loops has been carried out. Each loop is equipped with the RP2 system with its exchanger immersed in a pool. The 3 cooling pools are modelled independently. Each system RP2 is connected to a primary loop between the hot and cold legs. Steady state calculation consists in carrying out the regulations of the characteristic parameters retained in the study with their target values. Once the regulations finish (primary circuit flow rate in the loops, Steam Generator levels, pools levels and feedwater flow rate of the Steam Generators) and all the values of the uncertain parameters imposed, the transient can start with all the physical parameters with the desired values. The following assumptions are taken into account for the Blackout reference calculation:

- Shutdown of the pumps of the primary circuit;
- Curve ANS 100% NP (2775 MW) for the decay of residual power;
- Loss of the Feedwater Flow Control System and the Auxiliary Feedwater System;
- Core Power at 100% NP: 2775 MW;
- Primary pressure: 15.5 MPa;
- Level of the pressurizer: 7.3 m;
- Initial level of fluid in the Steam Generators: 12.78 m;
- Secondary pressure: 5.8 Mpa;
- 3 RP2 available;
- Initial temperature of the water of the pool: 30°C.

With an aim of differentiating the various effects, the accumulators were not modelled.

3.5.3. Identification of the sources of uncertainties of the RP2 System

A set of 24 parameters likely to be more or less uncertain at the time of the RP2 passive system start-up and influencing significantly the performances of the system was identified by expert judgment. These parameters are called hereafter the characteristic parameters and are listed below.

For each of the three BOPHR/RP2 systems ($i = 1,3$):

- I_i : instant of opening of the isolation valve of the RP2;
- X_i : rate of incondensable at the inlet of the RP2 exchanger;
- L_i : initial pool level;
- T_i : initial temperature of the water of the pool;
- C_i : fouling of the tubes of RP2 exchanger;
- R_i : number of broken tubes of RP2 exchanger.

For the primary circuit:

- PUI: percentage of the nominal power of the core;
- PP: pressure in the pressurizer;
- ANS: decay of residual power according to the ANS law.

For the secondary circuit ($i = 1,3$):

- NGVi: real secondary level in the three steam generators.

3.5.4. Quantification of the sources of uncertainties of the RP2 System

The chosen probabilistic model is presented in Table 3.3. The choice of the ranges of variation and *pdf* of the parameters was based on expert judgment. We detailed these choices for two parameters: the instant of opening of the RP2 valve and for the non-condensable fraction at the inlet of the RP2 exchanger.

Instant of opening of the RP2 Valve (minutes): I_1, I_2, I_3

The RP2 is started by opening a valve placed on the cold leg of the system, downstream the exchanger. This valve is supposed to be a pneumatic valve opened by default of power supply (a default of power supply implies the closure of the valve of compressed air supply which causes the opening of the pneumatic valve). We suppose that the failure of opening of the pneumatic valve is due to the failure of closure of the valve of compressed air supply. After half an hour, we suppose that the action of an operator is possible in case of non-opening of the valve. We have considered only two states for the valve, completely open or completely close.

The state of the valve (open/close) is then modeled by :

- a discrete variable with two values, giving the state of the valve at the initial time just after the black-out :

$$O_{t=0} : P(O_{t=0}) = 0.95$$

$$F_{t=0} : P(F_{t=0}) = 0.05$$

- a continuous variable giving the instant of opening of the valve after the time $t = 30$ mn , in the case the valve fails to open at the initial time:

$$P(O_{t>30}/F_0) = \text{Log}(1.0607t + 0.809) \text{ (--> } P=1 \text{ à } t = 5\text{heures)}$$

Non-condensable fraction at the inlet of the RP2 exchanger: X_1, X_2, X_3

(In the exchanger tubes and in the inlet pipes from a level corresponding to the lower part of the exchanger)

The presence of non-condensables could be caused e.g. by an incorrect maintenance of the passive system piping or by gas accumulation during the nominal operational life of the system.

Table 3.3. Probabilistic model of the input characteristic parameters

Variable	Distribution	Average	Standard deviation	X_{\min}	X_{\max}	λ	μ
I_1, I_2, I_3	Composed						
X_1, X_2, X_3	Exponential					182	0
L_1, L_2, L_3	Truncated normal	4.5	0.6	2	5		
T_1, T_2, T_3	Truncated normal	303	20	280	368		
C_1, C_2, C_3	Truncated normal	15	5	0	30		
R_1, R_2, R_3	Exponential					7	0
PUI	Truncated normal	100	1	98	102		
PP	Truncated normal	155	4	153	166		
ANS	Truncated normal	10	5	0	20		
NGV_1, NGV_2, NGV_3	Truncated normal	12.78	0.30	12.08	13.91		

3.5.5. Sensitivity analysis of the RP2 system

88 samples of the 24 random variables have been generated and for each sample a CATHARE calculations have been performed.

Among these 88 calculations, we have obtained 7 failures of the system considering the failure criterion: fluid temperature at core output greater than 450 °C in less than 12 hours. All these 7 failure cases correspond to cases with one tube rupture in one of the RP2's. Depending on the cases, the limit core output temperature is reached between 4100s and 7100s. All the other calculations are a success for the system mission.

In a second step, we have decided to suppress the possibility of tube rupture at the RP2 startup. We can imagine that probability of tube rupture could be included in the failure of mechanical components of the system in a Probability Safety Analysis (See chapter 5.3.3). In this case, we have 21 random variables.

85 samples of the 21 random variables have been generated and for each sample a CATHARE calculations have been performed. All these cases lead to a success of the system mission considering the failure criterion (fluid temperature at core output greater then 450 °C in less than 12 hours).

Criterion of performance of the system

In order to analyse the performance of the system, we have considered the following performance criterion:

$$\text{Ratio} = \frac{\text{Sum of the energy extracted by each RP2 during the transient (42000s)}}{\text{Energy of the core during the transient}}$$

Sensitivity analysis

In order to perform sensitivity analysis on the performance of the system, we have try to fit different types of mathematical model between the 21 input parameters X_i and the output value Y (ratio) calculated by CATHARE.

We have first fitted polynomial response surface of the form:

$$Y = a + \sum_{i=1}^{21} b_i X_i + \sum_{i=1}^{21} c_i X_i^2 + \sum_{i=1}^{21} d_i X_i^3$$

Table 3.4 gives for each types of polynomial, the coefficient of determination obtained.

Table 3.4. R2 Obtained for each polynomial fitted

Polynomial	R ²
1 st degree	0.77
2 nd degree	0.90
3 rd degree	0.93

Figure 3.2 compares the values of the ratio obtained by CATHARE and predicted by the 3rd degree polynomial. We have also tried responses surfaces obtained by Neural Network. Among different NN tested, the network 21_30_1 gives the best result with a R² equal to 0.90. The Figure 3.3 compares the values of the ratio obtained by CATHARE and predicted by the NN 21_30_1.

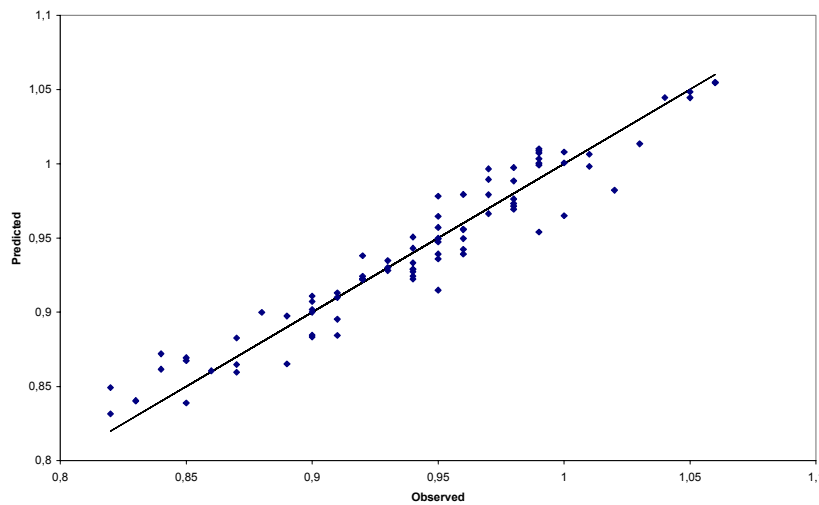


FIG. 3.2. Comparison the values of the ratio obtained by CATHARE and predicted by the 3rd degree polynomial.

We have performed two types of sensitivity analysis: a) a sensitivity analysis with linear coefficients (Standardized Regression Coefficients) even if the model is not fully linear ($R^2 = 0.77$) and b) with SOBOL indices calculated in using the response surface (Neural Network 21-30-1) and in performing 10000 simulations. The results of the calculation of the Standardised Regression Coefficients are presented in the Figure 3.4 and the results of the calculation of the SOBOL indices in the Figure 3.5. They give both the same indications: the most important variables are *ANS*, the residual power decay which is mainly due to the state of the fuel in the core when the transient occurs and I_1, I_2, I_3 , the instants of opening of the RP2 valves which govern directly the duration of the heat exchange time in the RP2's.

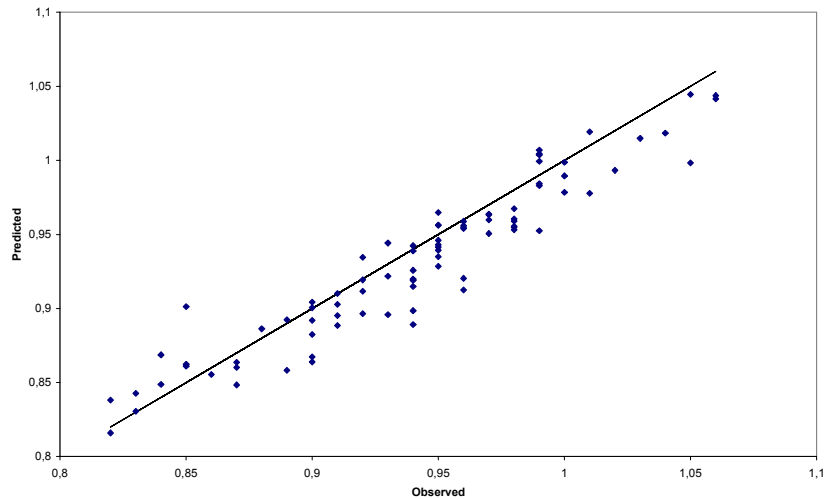


FIG. 3.3. Comparison the values of the ratio obtained by CATHARE and predicted by the response surface model (Neural Network 21_30_1).

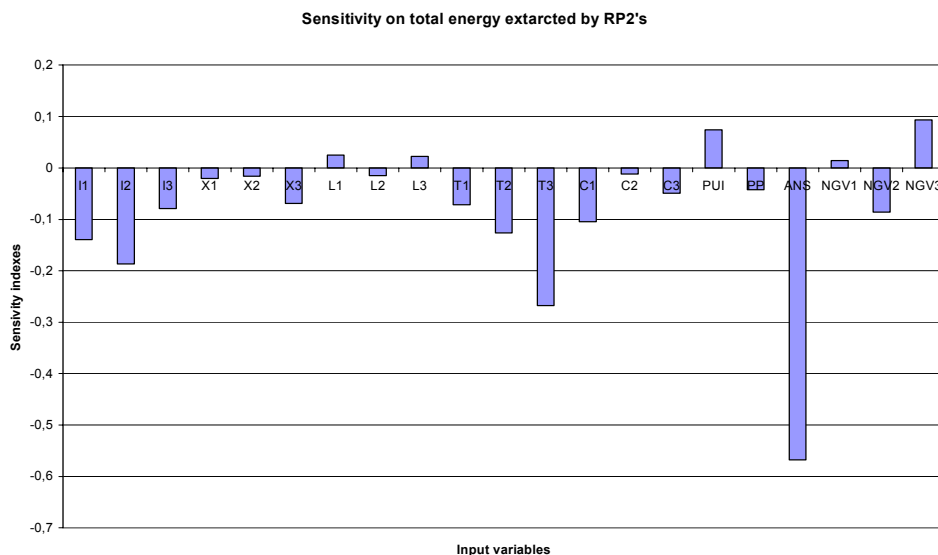


FIG. 3.4. Standardised regression coefficients (SRC).

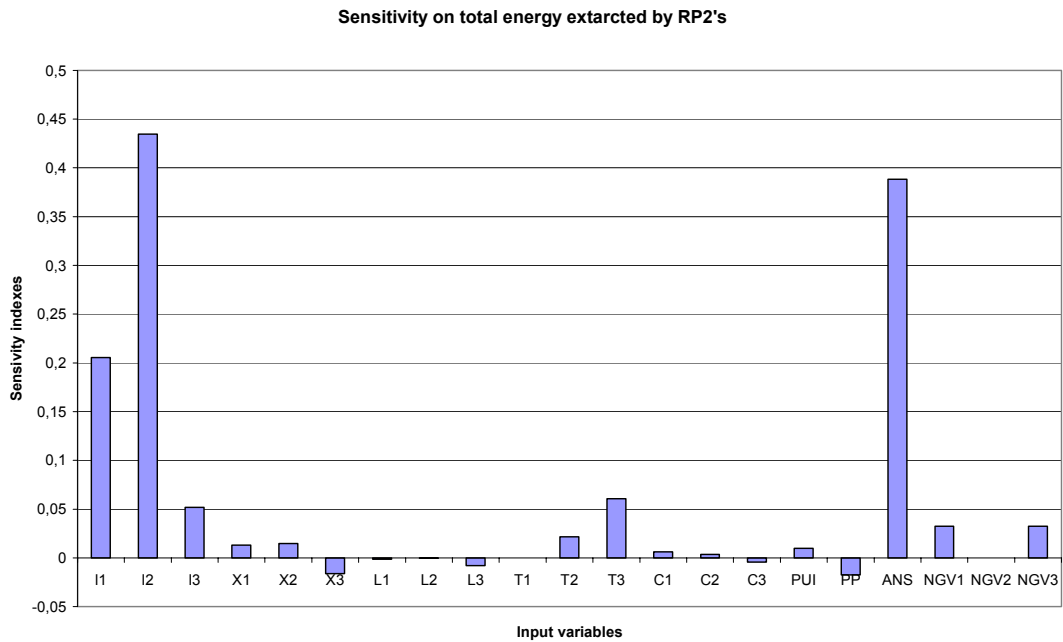


FIG. 3.5. SOBOL indices.

3.6. Summary of chapter 3

The first step of the analysis is the definition of the accidental scenario in which the system will operate. Then the system can be characterized. The goal of this analysis is to obtain information about the passive system behaviour, in an accident occurring during the life of the complete system and to identify the failure zones and conditions, if they exist. For that, the missions of the system, its failure modes and the failure criteria are defined. Due to the lack of suitable experimental databases for passive systems in operation, the evaluation rely on qualified thermal-hydraulic system code performing best estimate calculations.

The method requires the identification of the potentially important contributors to uncertainty of the code results. In the present study the uncertainties pertaining to the code itself are not accounted for, focusing the attention on the uncertainties relative to the input parameters of the code, characteristic of the passive system or of the complete system.

Among all the sources of uncertainties, the evaluation of the reliability of a passive system requires the identification of the relevant parameters which really affect the accomplishment of the target of the system. The tool here chosen for this task is the Analytic Hierarchy Process.

An important feature of the methodology are the sensitivity measures of the importance of parameter uncertainties for the uncertainty of the passive system performance. These sensitivity measures give a ranking of input parameters and provides guidance as to where to improve the state of knowledge in order to reduce the output uncertainties most effectively. In the methodology, the use of linear and non linear sensitivity indices are proposed.

4. RELIABILITY EVALUATIONS OF PASSIVE SYSTEMS THAT UTILIZE NC

Once the different sources of uncertainties have been identified and modelled, the problem is how to propagate these uncertainties through the thermal-hydraulic (T-H) code and how to assess the system reliability. It is beyond the purpose of the course the full integration between uncertainty methods

(adopted for best-estimate T-H code predictions) and reliability methods (object of the present research activity). Nevertheless, starting from the consideration of some methods used for assessing the uncertainty of T-H system code predictions, an attempt is made hereafter to present ‘support methods’ that can be helpful for the evaluation of the reliability of passive systems.

In the studies of uncertainty propagation, we are interested with the uncertainty evaluation of a response Y according to uncertainties on the input data $X = (X_i, i=1, \dots, p)$ and on the functional relation g connecting Y to X . In chapter 4.1, the statistical bases of some methods where the uncertainty on the response are evaluated either in the form of an uncertainty range, or in the form of a probability distribution function (*pdf*) are outlined.

The reliability of the system is often defined as the probability that an output parameter $Y(X)$ exceeds a threshold or a critical value Y_c . In the chapter 4.2, we will describe the methods used to evaluate the reliability of the system: the simulation methods and the approximate methods FORM/SORM.

4.1 Propagating the uncertainties

Different methods are used for the propagation of uncertainty or for determining the uncertainty that characterises the results of T-H system code calculations (D’Auria, 2002). Hereafter reference is made to some of these methods that are based on the use of statistics.

In a passive system that utilizes NC, a large number of variables influences the performance of the system, e.g. temperatures, pressures, water levels, non-condensable fraction... The performance of the system is evaluated by a *best-estimate* code. Suppose performance criterion Y of the system depends on the inputs variables X_1, X_2, \dots, X_n . Although the actual response Y is a function of the input variables, i.e., $Y=g(X_1, \dots, X_n)$, this function is generally unavailable in closed form. In order to get information about the uncertainty of Y , a number of code runs have to be performed. For each of these calculation runs, all identified uncertain parameters are varied simultaneously.

According to the exploitation of the result of these studies, the uncertainty on the response can be evaluated either in the form of an uncertainty range, or in the form of a probability distribution function (*pdf*).

4.1.1 Uncertainty range (Glaeser, 2000), (Wilks, 1941)

A two-sided tolerance interval $[m, M]$ of a response Y , for a fractile α and a confidence level β is given by:

$$P\{P(m \leq Y \leq M) \geq \alpha\} \geq \beta$$

Such a relation means that one can affirm, with at the most $(1-\beta)$ percent of chances of error, that at least α percents values of the response Y lie between the values m and M .

To calculate the limits m and M , the technique usually used is a method of simulation combined with the formula of Wilks. The formula of Wilks determines the minimal size N of a sample to be generated randomly according to the values of α and β .

For two-sided statistical tolerance intervals the formula is:

$$1 - \alpha^N - N(1 - \alpha)\alpha^{N-1} \geq \beta$$

The minimum number of calculations can be found in Table 4.1.

Table 4.1. Minimum number of calculations N for one sided and two for one-sided and two-sided statistical tolerance limits

β/α	One-sided statistical tolerance limit			Two-sided statistical tolerance limit		
	0.90	0.95	0.99	0.90	0.95	0.99
0.90	22	45	230	38	77	388
0.95	29	59	299	46	93	473
0.99	44	90	459	64	130	662

The bounds m and M of the confidence interval of Y are obtained by retaining the minimal and maximal values of the sample $\{Y_j, j = 1, \dots, N\}$.

This method supposes that the function g is continuous and that all uncertainties on the input data X_i are distributed according to continuous laws.

The advantage of using this technique is that the number of code calculation needed is independent of the number of uncertain parameters.

However for reliability evaluation, this method is not very useful because it is difficult, indeed impossible to interpret the two levels of probability (α and β) in term of reliability value for the system.

4.1.2 Density of probability

The uncertainty evaluation in the form of a *pdf* gives richer information than a confidence interval. Once the *pdf* of the system performance is determined, the reliability of the system can be directly obtained if a failure criterion is given. But the determination of this distribution can be expensive in computing times. The following paragraphs describe the various methods available for this evaluation.

Method of Monte-Carlo (Rubinstein, 1981), (Devictor, 1996)

The method of Monte-Carlo is used to build *pdf*, but also to assess the reliability of components or structures or to evaluate the sensitivity of parameters. Monte Carlo simulation consists of drawing samples of the basic variables according to their probabilistic characteristics and then feeding them into the performance function. In this way, a sample of response $\{Y_j, j = 1, \dots, N\}$ is obtained.

The *pdf* is obtained by fitting a law on the sample $\{Y_j, j = 1, \dots, N\}$. This fitting is a problem well known and many tests exist and are adapted to the law tested (Chi-square, Kolmogorov-Smirnov, Anderson-Darling...). Degrees of confidence can be associated to the fitting.

It is obvious that the quality of the fitting depends on the number of simulations carried out and on the good repartition of these simulations in the random space, especially if the tails of distributions are one of the interests of the study. It is necessary to notice that no rule exists, when there is no a priori knowledge on the type of *pdf*, to determine the number of simulations necessary to obtain this distribution with confidence.

It is necessary to select the points, which bring the maximal information, but the determination of these points remains an open question.

The main advantage of the Monte-Carlo method, is that this method is valid for static, but also for dynamic models and for probabilistic model with continuous or discrete variables. The main drawback of this method is that it requires often a large number of calculations and can be prohibitive when each calculation involves a long and onerous computer time.

Response Surface Methods (Rajashekhar, 1993)

To avoid the problem of long computer time in the method of Monte-Carlo, it can be interesting to build an approximate mathematical model called response surface.

Experiments are conducted with design variables X_1, X_2, \dots, X_n a sufficient number of times to define the response surface to the level of accuracy desired. Each experiment can be represented by a point with coordinates $x_{1j}, x_{2j}, \dots, x_{nj}$ in an n-dimensional space. At each point, a value of y_i is calculated. The basic response procedure is to approximate $g(X)$ by a simple mathematical model, such as an n^{th} order polynomial $\tilde{g}(X)$ with undetermined coefficients. Thermal-hydraulic analysis is performed at various points x_i , in order to determine the unknown coefficients in the polynomial $\tilde{g}(X)$ so as to minimise the error in the domain of interest.

When a response surface has been determined, the passive system reliability can be easily assessed with Monte Carlo simulation, in using the approximate mathematical model.

Such a response surface can be useful not only for uncertainty propagation but also for reliability evaluation and sensitivity studies.

Different types of response surface can be used: polynomial, thin plate splines, neural networks, generalised linear model (GLM), PLS (Partial Least Squares) regression...

For polynomial surfaces, the fitting is obtained by minimisation of the sum (weighted or not) of the squares of the error.

Before any use of response surface, it is necessary to qualify it for a foreseen utilisation. This qualification keeps a part of subjectivity. For example for reliability studies, a good representation of the domain of maximum of failure probability is often sufficient and it is not necessary to seek a good quality of approximation in all the field of variation of the input parameters. If the response surface is used in a problem where uncertainties are not very well known, it is not judicious to seek response surfaces explaining 99% of the variability.

In general, we expect from a response surface qualities of approximation and prediction:

- (1) The quality of approximation is given by statistical analyses carried out on the base of points used to build the surface. A "good approximation" means that the value obtained by the model of response surface is close to the value obtained by the code in any point of the studied field.
- (2) The quality of prediction is obtained by statistical analyses carried out on points not belonging to the building base (this set of points is called the "test base").

A simple method to qualify a response surface is to compare indicators obtained from the response surface with those obtained directly with the code, if it is possible to calculate it. These indicators can be: average, standard deviation, number of values in an interval, or results of uncertainty or sensitivity analyses. It is necessary to check the coherence and the consistency of the results and that the same hierarchy is obtained for the most influential parameters.

Different statistical tools can also be applied on the building base and on the test base: variance analysis, coefficients of correlation, and Bootstrap method.

The practical problems encountered by the use of the response surface method are in:

- the analysis of strongly non-linear phenomena where it is not obvious to find a family of adequate functions (multi-layer neural networks can bring a solution);
- the analysis of discontinuous phenomena: a solution is to build a preliminary function of classification and to calculate response surfaces for each branch of the bifurcation.

In these two cases, the number of calculations to be performed can become relatively significant.

Experimental design (Sacks, 1989), (Morris, 1991)

The selection of points in the space of the random variables (or design space) where the response must be evaluated is commonly called design of experiments. The choice of the experimental design can have a large influence on the accuracy of the approximation and the cost of constructing the response surface.

A commonly used experimental design is the factorial design, which in its simplest form, is a hypercube in the design space. A total of 2^n experimental points must therefore be examined, where n is the number of random variables. The 2^n design only estimates the first-order and interaction terms of the approximating function g . In the absence of prior information, the experiments initially can be centred on the mean of the variables. Points are located along the axes and elsewhere. The axial points define the effect of each variable and are needed to determine coefficients for the terms involving only that variables i.e., $x_i, x_i^2 \dots$. The points in the plane $x_i x_j$ define the interaction effects of variables x_i and x_j and are needed to determine coefficients for the cross terms i.e., $x_i x_j$ in polynomial.

For a quadratic approximation three levels of the design variables must be considered, giving 3^n factorial experimental design. Factorial design is useful when the number of variables is large and the number of experiments (calculations) that can be conducted is less than the number of combinations in the full factorial set.

But before to make calculations for each point points, it must be checked that the information brought by the set of point is sufficient for the postulated model. A high value of the number of candidate points is not a sufficient guarantee. This coherence between the postulated model and information contained in the set of candidate points is checked by the help of indicators of quality (D-optimality criterion...) of the experiment matrix for a postulated model.

Method of moments (Baldeweck, 1999)

Another method to obtain the density of probability of the response is to calculate the first four moments by using the Gauss integration method and then to fit a distribution of probability to these moments by using the Pearson or Johnson methods.

The first objective is to evaluate the first moments of the random response Y . The expectation of Y can be calculated by:

$$E(Y) = E(g(X)) = \int \dots \int g(x) f_X(x) dx_1 \dots dx_p$$

where f_x is the joint density distribution of X .

This equation can be evaluated by a squaring method of Gauss.

This method allows the integration of a continuous function with the desired precision. It consists in the discretisation of the interval of integration in a number of X -coordinates x_i to which a weight w_i is associated. The number of X -coordinates is a function of the desired precision. For an integrable continuous function $g(x)$, we obtain:

$$\int_a^b W(x)g(x)dx \approx \sum_{i=1}^N \omega_i g(x_i)$$

Practically, a set of order j orthogonal polynomial $\{p_j(x)\}_{j=0,1,2,\dots}$ are associated to the weight function $W(x)$. These polynomials verify the following relations:

$$\int_a^b W(x)p_i(x)p_j(x)dx = 0 \text{ si } i \neq j$$

$$\int_a^b W(x)p_i(x)^2 dx = 1$$

The N X-coordinates of a squaring formula with a weight function $W(x)$ are the zeros of the polynomial $p_N(x)$, which has exactly N zeros in the interval $[a, b]$. These polynomials are generally defined by relations of recurrence. The weights are calculated by solving the system of linear equations:

$$\sum_{j=1}^N p_i(x_j)\omega_j = \int_a^b W(x)p_i(x) dx \quad i = 1 \dots N$$

Then the average is evaluated from:

$$E(Y) = E(g(X)) \approx \sum_{i=1}^N \omega_i \times g(u_i)$$

and the moment of order k from.

$$M_Y(k) = \int [g(x) - \mu_Y]^k f_X(x) dx \approx \sum_{i=1}^N \omega_{i,X} \times [g(u_{i,X}) - \mu_Y]^k$$

From the first four moments knowledge, it is possible to determine the associated distribution of Pearson.

Pearson et al. show that one can define in an approximate way a density of probability from the average, the standard deviation and two additional coefficients called coefficients of Fisher:

1. The coefficient of symmetry: $\gamma_1 = \sqrt{\beta_1} = \frac{|\mu_3|}{\sigma^3}$
2. The coefficient of flatness: $\gamma_2 = \beta_2 = \frac{\mu_4}{\sigma^4}$

Where β_1 is the Skweness and β_2 the Kurtosis.

A great number of continuous distributions can be written in the following form:

$$f(x) = f(x_0)(x - a_1)^{p_1} (a_2 - x)^{p_2}$$

where the parameters a_1, a_2, p_1 and p_2 can be real or imaginary and $f(x_0)$ is defined by the condition $\int_{\mathbb{R}} f(x) dx = 1$.

The distribution law, which depends on 4 parameters, can be expressed according to $m, \sigma, \beta_1, \beta_2$. The set of these distribution laws is called the family of Pearson. The curves can have several shapes (bell-shaped curve, curved in J, curved in U).

4.1.3 Conclusion on the methods for propagating uncertainties

We have presented some of the methods used to propagate the uncertainty through a T-H code and usable for the reliability assessment of a passive system. These methods are based on the estimation of the *pdf* of the system performance. Once the *pdf* of the system performance is determined, the reliability of the system can be directly obtained if a failure criterion is given.

The method of Monte-Carlo is used to build the *pdf*. The main advantage of the method of Monte-Carlo, is that this method is valid for static, but also for dynamic models and for probabilistic model with continuous or discrete variables. The main drawback of this method is that it requires often a large number of calculations. To avoid this problem, it can be interesting to build a response surface, which approximates the complex physical phenomena. But this response surface must be qualified. The practical problems encountered by the use of the response surface method are in the analysis of strongly non-linear phenomena where it is not obvious to find a family of adequate functions and in the analysis of discontinuous phenomena.

Another approach consists in calculating the first four moments of the system performance and then to fit a *pdf* to these moments. However this approach can be also very time consuming.

4.2. Evaluating the reliability

Different methods can be used to quantify the reliability of a passive systems that utilizes NC once given a best estimate T-H code and a model of the system. We present now specific methods usable for a direct evaluation of the passive system reliability, without the need of defining the *pdf* of the system performance.

The performance function of a passive system according to a specified mission is given by:

$$M = \text{performance criterion} - \text{limit} = g(X_1, X_2, \dots, X_n)$$

in which the X_i ($i=1, \dots, n$) are the n basic random variables (input parameters), and $g(\cdot)$ is the functional relationship between the random variables and the failure of the system. The performance function can be defined such that the limit state, or failure surface, is given by $M = 0$. The failure event is defined as the space where $M < 0$, and the success event is defined as the space where $M > 0$. Thus a probability of failure can be evaluated by the following integral:

$$P_f = \int \int \dots \int f_X(x_1, x_2, \dots, x_n) dx_1, dx_2, \dots, dx_n \quad (4.1)$$

where f_X is the joint density function of X_1, X_2, \dots, X_n , and the integration is performed over the region where $M < 0$. Because each of the basic random variables has a unique distribution and they interact, the integral (4.1) cannot be easily evaluated. Two types of methods can be used to estimate the probability of failure: the Monte Carlo simulation with or without variance reduction techniques and the approximated methods (FORM/SORM).

4.2.1 Reliability evaluations using Monte-Carlo simulation

Direct Monte-Carlo simulation techniques (Rubinstein, 1981), (Sundarajan 95)

Direct Monte Carlo simulation techniques can be used to estimate the probability of failure defined in Eqs. (4.1) (or its complement to 1, the reliability). Monte Carlo simulation (Figure 4.1) consists of drawing samples of the basic variables according to their probabilistic characteristics and then feeding them into the performance function. An estimate of the probability of failure P_f can be found by:

$$\overline{P}_f = \frac{N_f}{N}$$

where N_f is the number of simulation cycles in which $g(.) < 0$, and N the total number of simulation cycles. As N approaches infinity, \overline{P}_f approaches the true probability of failure.

The accuracy of the estimation can be evaluated in terms of its variance computed approximately as

$$Var(\overline{P}_f) \cong \frac{(1 - \overline{P}_f)\overline{P}_f}{N} \quad (4.2)$$

It is recommended to measure the statistical accuracy of the estimated probability of failure by computing its coefficient of variation as

$$COV(\overline{P}_f) \cong \frac{\sqrt{\frac{(1 - \overline{P}_f)\overline{P}_f}{N}}}{\overline{P}_f} \quad (4.3)$$

The smaller the coefficient of variation, the better the accuracy of the estimated probability of failure. It is evident from (4.2) and (4.3) that as N approaches infinity, $Var(\overline{P}_f)$ and $COV(\overline{P}_f)$ approach zero.

For a small probability of failure and a small number of simulation cycles, the variance of \overline{P}_f can be quite large. Consequently, it may take a large number of simulation cycles to achieve a specific accuracy.

The amount of computer time needed for the direct Monte Carlo method is large, specially in our case where each simulation cycle involves a long calculation performed by a thermal-hydraulic code.

Characteristics of the direct Monte Carlo simulation (Bjerager, 1989)

The direct Monte Carlo simulation is completely general, and applies to any distribution of the basic random variables, including discrete random variables. Furthermore, there is no requirement on the failure functions – only the sign of the failure function is being used.

Accuracy: For samples size $N \rightarrow \infty$, the estimated probability converges to the exact probability which accuracy is driven only by deterministic model and code used. For finite sample sizes, uncertainty estimates on the results are provided.

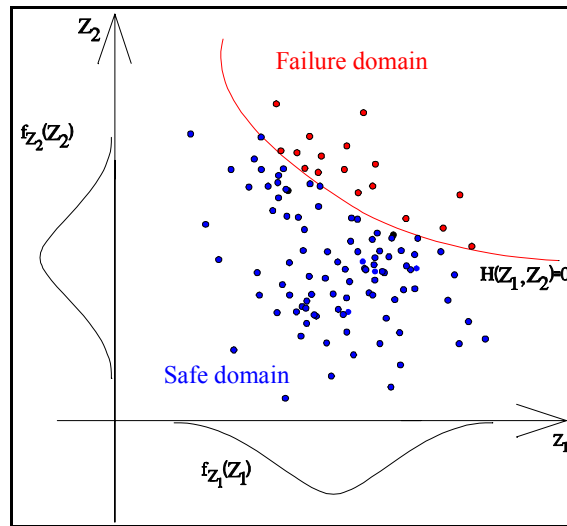


FIG. 4.1. Reliability assessment by Monte-Carlo simulation.

Efficiency: As a general rule, the calculation time grows approximately linearly with $1/P_f$ for a given coefficient of variation on the estimator. The absolute computation time depends on the time necessary to evaluate the failure function. For small range of probabilities, the method is generally very expensive in CPU-time. As a rule of thumb, the necessary sample size to get a probability estimate with good confidence is around $100/P_f$.

Variance reduction techniques (Rubinstein, 1981), (Madsen, 1986)

Variance reduction techniques offer an increase in the efficiency and accuracy of the simulation-based assessment of the system reliability for a relatively small number of simulation cycles. Several variance reduction techniques exist: Importance sampling, Stratified sampling, Latin hypercube sampling, Adaptive sampling, Conditional expectation, Directional simulation, Antithetic variates...

We present in the following some of these techniques.

Importance sampling

Importance sampling consists in biasing the simulation by the use of another distribution so that the part of the integrand in Eq. (4.1) that makes the highest contribution to the integrand is emphasized in the sampling. To avoid that a bias is introduced in the final result, corrections are made at the end.

The failure probability is then expressed as:

$$P_f = \frac{1}{N} \sum_{i=1}^N I_f \frac{f_X(x_{1i}, \dots, x_{ni})}{h_X(x_{1i}, \dots, x_{ni})}$$

where N is the number of simulations, $f_X(x_{1i}, \dots, x_{ni})$ is the original joint density function and $h_X(x_{1i}, \dots, x_{ni})$ is the importance density function and I_f is the failure indicator function that takes values of 0 for failure or 1 for survival.

Efficiency of this method depends on the choice of the sampling density function. A number of procedures for selecting the sampling density functions have been suggested.

Stratified sampling

The stratified sampling method (Fig. 4.2) is based on the theorem of total probability. The integration domain of the integral (4.1) is divided into several (k) regions (R_1, R_2, \dots, R_k). The probability of failure is then estimated as:

$$P_f = \sum_{j=1}^k \left[P(R_j) \frac{1}{N_j} \sum_{i=1}^{N_j} I_{f_i} \right]$$

where $P(R_j)$ is the probability of region R_j , N_j is the number of simulations performed in region R_j , and I_{f_i} is the failure indicator function that takes the value 0 for failure or 1 for survival, evaluated at the i^{th} simulation. This method allows the analyst to concentrate the simulation effort (i.e. perform more simulations) in important region, for example, the failure regions, or to concentrate the effort on important basic random variables. The failure region may not be known in advance; only a “guess” can be made.

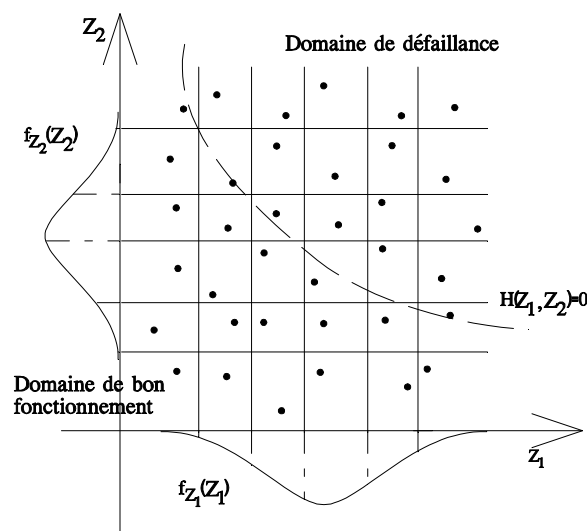


FIG. 4.2. Stratified sampling.

Latin Hypercube sampling method

The importance sampling method, or the stratified sampling method, requires the analyst to know in advance the important variables of the problem. In many practical problems, this requirement cannot be met. The Latin Hypercube sampling (LHS) method offers an advantage for these problems, as well as for problems in which the important regions or variables are time variant. The LHS method provides a constraint sampling scheme instead of random sampling as in direct simulation. Traditionally, random numbers are randomly generated between 0 and 1. They are used to generate the input random variables according to their prescribed probability distribution. In the LHS method, the region between 0 and 1 is uniformly divided into N non-overlapping equal intervals for each random variable, where N is the number of random numbers that need to be generated for each random variable, that is, number of simulation. The N non-overlapping intervals for each random variable have the same probability of occurrence. Then, N different values are randomly selected from the N intervals, one value per interval. A generated random value in the i^{th} interval can be computed as:

$$u_i = \frac{u}{N} + \frac{i-1}{N}$$

where u is a random number in the range $[0, 1]$, and u_i ($i = 1, 2, \dots, N$) is the random value for the i^{th} interval. Once the u_i ($i = 1, 2, \dots, N$) values are obtained, then inverse transformation can be used to generate values for the input random variables. Thus a set of N random values is generated for each input random variable. One value from each is picked randomly and substituted into the performance function to decide whether the system fails ($G(X) < 0$) or not ($G(X) \geq 0$).

Directional simulation

If the density f_X is continuous, then there is a bijective transformation $T : X \rightarrow U$, where U is a random vector of p independent random variables distributed according to a standard normal law. The space of the vectors U is called Gaussian space. As the transformation is bijective, the value of G at the point U is equal to the value of the function of failure g as in point $x=T^{-1}(u)$. Thus the surface of failure in the Gaussian space is defined by $G(u) = g(T^{-1}(u))$.

The probability of failure P_f is expressed by:

$$P_f = P[G(\bar{U}) \leq 0] = \int_{g(\bar{x}) \leq 0} f_{\bar{x}}(\bar{x}) d\bar{x} = \int_{G(\bar{u}) \leq 0} \varphi_N(\bar{u}) d\bar{u}$$

where φ_N is the function standard normal density with N dimensions.

The idea of the method of directional simulation is to generate directions resulting from the origin of standard space and to calculate P_f conditionally with these directions. The Gaussian vector U is expressed in the form $U = R A$ ($R \geq 0$) where R^2 follows a Chi-square law χ_p^2 with p degrees of freedom independently of the random vector A uniformly distributed on the sphere unit. An estimator of P_f is obtained starting from N simulations a_i of the vector A . If R_i is solution of $G(R_i \times a_i) = 0$ and by noting $p_i = P(G(R_i \times a_i) \leq 0)$, an un-biased estimator is obtained by a Monte Carlo simulation:

$$\hat{E}[P_f] = \frac{1}{N} \sum_{i=1}^N p_i$$

$$\hat{D}[P_f]^2 = \frac{1}{N(N-1)} \sum_{i=1}^N (p_i - \hat{E}[P_f])^2$$

The selection of the directions of research influences the efficiency of this technique. It is sometimes interesting to combine this technique with a method of importance sampling. To concentrate the directions drawn towards the area from the field of failure nearest to the origin allows the acceleration of the convergence. To determine this area is not obvious; methods FORM/SORM (see § 4.2.2) make possible to determine this area.

The principal advantage of the method of Monte-Carlo, but also of the majority of the methods of reduction of the variance, is that they are valid for static, but also for dynamic models and for probabilistic model with continuous or discrete variables. In case of large computing times, it can be interesting to build an approximate mathematical model called response surface (see § 4.1.2).

4.2.2 Approximated methods (FORM/SORM) (Rackwitz, 1979), (Madsen, 1986), (Melcher, 1999)

The first- and second-order reliability methods (FORM/SORM) consist of 4 steps (Fig. 4.3):

1. the transformation of the space of the basic random variables X_1, X_2, \dots, X_n into a space of standard normal variables,
2. the research, in this transformed space, of the point of minimum distance from the origin on the limit state surface (this point is called the design point),

3. an approximation of the failure surface near the design point,
4. a computation of the failure probability corresponding to the approximating failure surface.

FORM and SORM apply to problems where the set of basic variables are continuous.

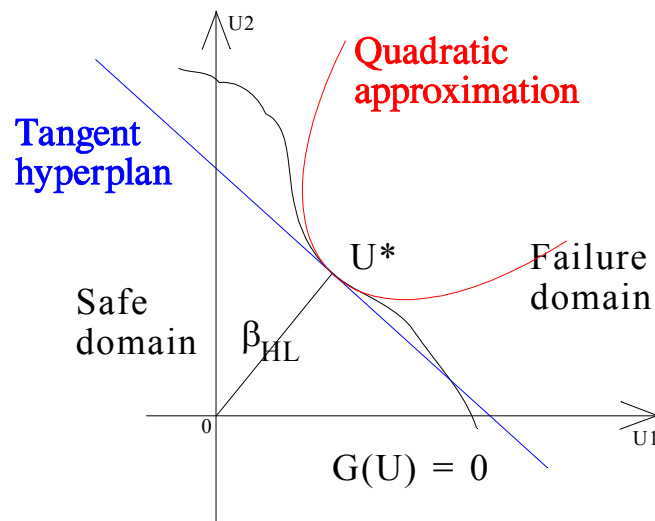


FIG. 4.3. Reliability assessment with FORM/SORM methods.

Transformation of space

The choice of the transformation to be used depends on the characteristics of the joint density of vector X the most current transformations are:

- the transformation of Rosenblatt when the joint density is known,
- the transformation of Nataf, when the probabilistic model is only made up of the marginal densities and of the matrix of covariance.

In the Gaussian space, the surface of failure is defined by $G(u) = g[T^{-1}(u)]$.

Design point research

The indice of Hasofer-Lind is defined as the minimal distance between the failure surface and the origin of the Gaussian Space. The calculation of β_{HL} consists in solving the following problem of optimisation under constraint:

$$\min_{G(u)=0} \sqrt{u^t u}$$

The point associated with this minimal distance is often called the design point. It corresponds to the point of maximum of probability of failure and is noted u^* . Indeed, in the Gaussian space, the joint density of the vector U is symmetrical in rotation with respect to the origin and thus involves that the point of design coincides with the most probable point of the failure.

The probability of failure can be calculated by:

$$P_f = P[G(\bar{U}) \leq 0] = \int_{g(\bar{x}) \leq 0} f_{\bar{x}}(\bar{x}) d\bar{x} = \int_{G(\bar{u}) \leq 0} \varphi_N(\bar{u}) d\bar{u}$$

where φ_N is the multi-normal standard distribution of dimension N .

FORM method

Approximate method FORM (First Order Reliability Method) consists in approaching the surface of failure by a hyper plane tangent to the surface of failure at the design point. Then an estimate of the probability of failure is obtained by:

$$P_f = \Phi(-\beta_{HL})$$

where Φ is related to cumulative distribution of the standard normal law. The precision of this approximation depends on the non-linearity of the failure surface.

The knowledge of this design point makes it possible to determine the most influential variables on reliability. By supposing that there is a single design point and that the index of reliability defined by Hasofer and Lind β_{HL} is positive, the vector directional cosine unit α is defined by $\alpha = u^*/\beta_{HL}$.

The components α_i are also called factors of sensitivity and the factors α_i^2 are interpreted like factors of importance associated to the variables U_i . A variable associated with one significant α_i is regarded as having a significant influence on the probability of failure.

Note: the area of maximum of probability of failure is often different from the area around the average. Consequently the most influential variables are often different for these two domains. In consequence, the factors of importance have a different interpretation than the sensitivity indices (Standardized regression Coefficients, Partial Correlation Coefficients...) calculated in global sensitivity analyses (See § 3.4.3).

SORM method and variants (Melchers, 1999), (Devictor, 1996)

If the linear approximation is not satisfactory, more precise evaluations can be obtained from approximations to higher orders of the failure surface at the design point. The approximation by a quadratic surface at the design point is called the SORM method (Second Order Reliability Method). The corresponding formula uses the knowledge of the (q-1) principal curvatures κ_i of the failure surface at the design point:

$$P_f \approx \Phi(-\beta_{HL}) \prod_{i=1}^{N-1} \frac{1}{\sqrt{1 + \beta_{HL} \kappa_i}}$$

This result is known as asymptotically exact, in the sense that the approximation of the probability of failure obtained is better for large indices of reliability. The computing time is influenced by the calculation of the matrix of the second-order derivative, or Hessian matrix. Another idea to contribute to the validation of a result FORM or to improve the precision of the result is to use a method of simulation in the vicinity of the design point u^* . The methods of importance sampling and directional simulation are the most used. For an importance sampling (Fig. 4.4) around the design point, the probability of failure is estimated by:

$$P_f = \int_F \frac{\phi_n(\mathbf{u})}{h(\mathbf{u})} h(\mathbf{u}) d\mathbf{u} \approx \frac{1}{n} \sum_{i=1}^n 1_{H(\mathbf{u}) \leq 0}(\mathbf{u}_i) \frac{\phi_n(\mathbf{u}_i)}{h(\mathbf{u}_i)}$$

where $h(u)$ is the density of importance defined by a multinormal distribution centred on the point of design.

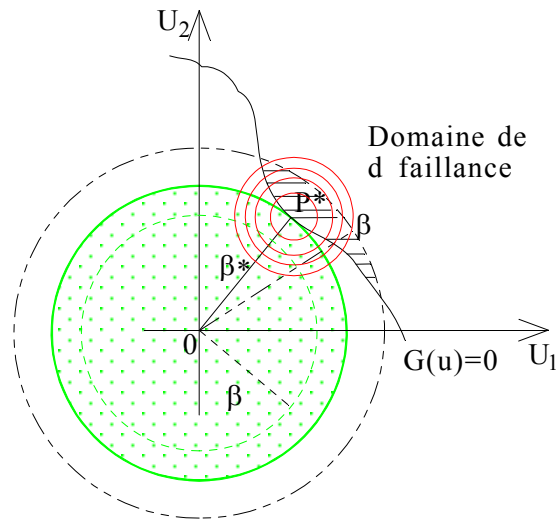


FIG. 4.4. Conditional importance sampling.

If several local minima exist, the field of failure can be approached, for example, by the union of subfields of failure obtained by the linearization of the function of failure at each minimum. The methods multi-FORM and multi-SORM allow estimating the probability of failure.

Coupling by response surface (Bucher, 1990), (Devictor, 1997).

FORM/SORM methods are often efficient to compute the reliability of a component or a system. But if the model is complex, the evaluation of the failure function can lead to expensive computation costs and the direct coupling (Fig. 4.5) can be inadequate.

In order to solve the reliability problem, efficient coupling techniques (Fig. 4.6) between complex codes and reliability codes using response surfaces have already been proposed. In practice, this coupling consists in determining a response surface locally and then performing a reliability study in replacing the failure function by this response surface.

The validation of these reliability results requires, that the response surface is a good approximation of the failure surface in the region of maximum probability. The approximation quality depends on the choice of the points in the experimental design and must be verified by statistic criteria.

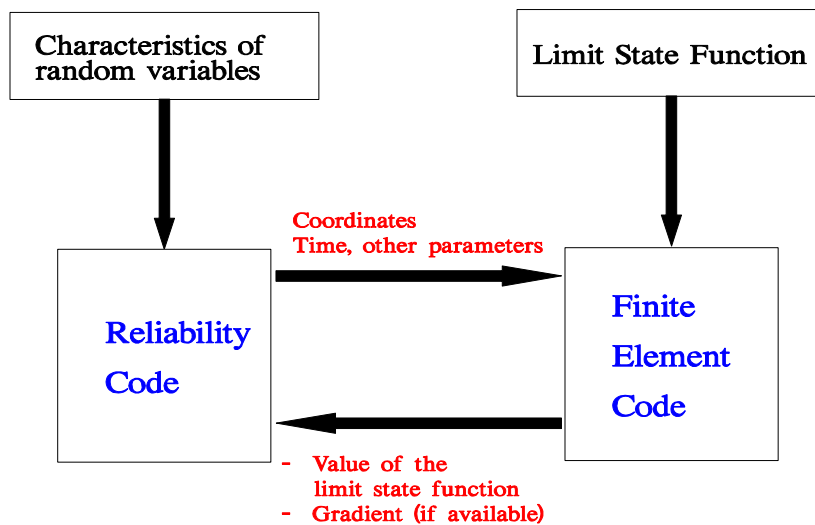


FIG. 4.5. Direct coupling between reliability code and T-H code.

It can be interesting to couple methods FORM/SORM with quadratic response surfaces. Indeed methods FORM/SORM aim to determine the area of maximum of probability of failure and then to estimate the probability of failure in this area. For many problems, a quadratic response surface is sufficient to represent the continuous function in the vicinity of the design point. Thus if such a response surface is validated in the vicinity of the point of maximum of probability of failure, then it is possible to validate a calculation FORM or a calculation SORM with the hypothesis that the surface of failure is either an hyper plan or a quadratic surface in the vicinity of this point. (Devictor, 1996) proposed an iterative method called RSAED (Response Surface with Adaptive Experimental Design) coupling FORM/SORM and quadratic response surfaces.

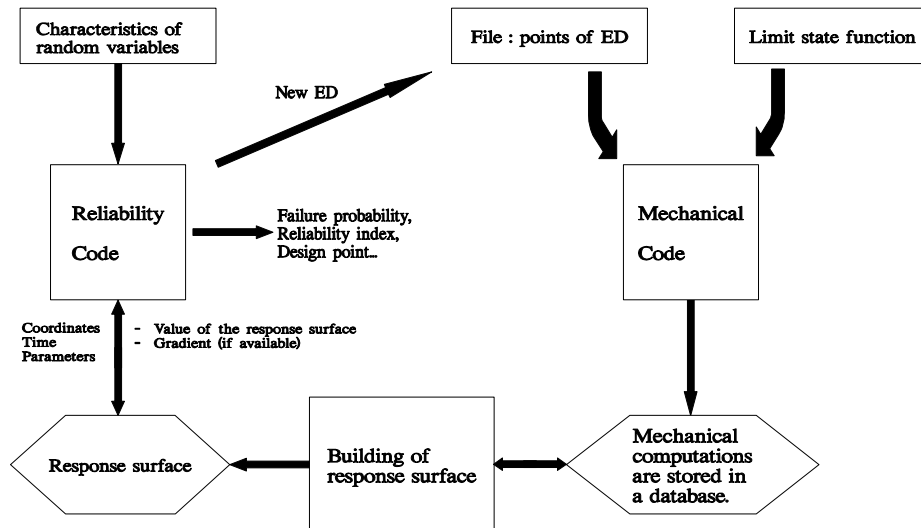


FIG. 4.6. Coupling by use of response surface.

Characteristic of FORM/SORM methods (Bjerager, 1989)

FORM and SORM are approximate methods, and their accuracy is generally good for small probabilities. The analytical properties enable the methods to yield relatively inexpensive sensitivity factors. The basic random variables must be continuous, and the failure function must be continuous. With the optimisation procedures presently used in most cases, the failure functions should be smooth.

Accuracy: The methods are approximate, but yield generally accurate results for practical purposes, in particular for small range probabilities (10^{-3} – 10^{-8}).

Efficiency: For small order probabilities FORM/SORM are extremely efficient as compared to simulation methods. The CPU-time is for FORM approximately linear in the number of basic variables n , and the additional CPU-time for a SORM computation grows approximately with n^2 . The absolute computation time depends on the time necessary to evaluate the failure function. This time may in fact depend on the actual values of the basic variables. Extreme values may take longer due to increased non-linearities in the problem. The CPU-time is independent of the probability level, assuming a constant time for evaluation of the failure function.

Restrictions and further developments: When the failure surface is not sufficiently smooth, the most likely failure point cannot be identified by efficient mathematical programming methods applying the gradient of the function. In this case it would be advantageous to fit the exact failure function by a differentiable function. If the function is extremely CPU-time costly to evaluate, a simpler function may be used. It was suggested to use response surface methods. In particular, linear and quadratic response surfaces are well suited in combination with FORM/SORM, since the exact result with respect to the response surface is extremely efficiently computed.

4.2.3 Conclusion on the methods for evaluating the reliability

The following table summarizes the advantages and drawbacks of Monte-Carlo simulation and FORM/SORM methods.

Simulations	FORM/SORM
<p><u>RESULTS</u></p> <p>FAILURE PROBABILITY</p> <p>ERROR ON THE ESTIMATION</p> <p>PROBABILITY DISTRIBUTION OF THE RESPONSE</p> <p><u>ASSUMPTIONS</u></p> <p>NO ASSUMPTION ON THE RANDOM VARIABLES (DISCRETE, CONTINUOUS, DEPENDANCY...)</p> <p>NO ASSUMPTION ON THE LIMIT STATE FUNCTION</p> <p><u>DRAWBACKS</u></p> <p>COMPUTATION COSTS (depends on the probability level)</p>	<p><u>RESULTS</u></p> <p>FAILURE PROBABILITY</p> <p>MOST INFLUENTIAL VARIABLES (PROBABILITY)</p> <p>EFFICIENCY (depends on the number of random variables)</p> <p><u>ASSUMPTIONS</u></p> <p>CONTINUOUS RANDOM VARIABLES</p> <p>CONTINUOUS LIMIT STATE FUNCTION</p> <p><u>DRAWBACKS</u></p> <p>NO ERROR ON THE ESTIMATION</p> <p>GLOBAL MINIMUM</p>

4.3. Influence of Choices of the Input Distribution on the Output (Bolado, 2003)

The codes used to calculate the performance of the passive systems that utilize NC may require several hours for each run. The evaluation of the reliability of the passive system may require hundreds of calculation. This fact makes almost impossible to run again the code hundreds of time to estimate the effect of changes in the probabilistic distributions of the input parameters on the system reliability.

Let us consider a k components vector of input parameters \mathbf{X} . Let us assume that two different distribution functions $f_1(\mathbf{x})$ and $f_2(\mathbf{x})$ may be assigned to that input parameter vector. Let us also assume that the first one is the reference one and the second one is the one we are addressing for sensitivity. For simplicity, let us consider only one output variable Y . This variable is the transformation of \mathbf{X} through the system model H (computer code), so that we can write $Y=H(\mathbf{X})$. Since \mathbf{X} is a random vector, Y will also be random and its distribution function will depend on the distribution function of \mathbf{X} . Let us call $F_1(y)$ and $F_2(y)$ to the distribution functions of Y when \mathbf{X} follows the distributions $f_1(\mathbf{x})$ and $f_2(\mathbf{x})$ respectively.

Let $\mathbf{X}_1, \mathbf{X}_2, \dots, \mathbf{X}_n$ be a random sample of \mathbf{X} obtained under the reference distribution. After running the code with those input vectors we get a random sample Y_1, Y_2, \dots, Y_n . Once we have this sample we may estimate $F_1(y)$ though the empirical distribution function and any other usual statistic like the sample mean or the sample variance, or any order statistic. It is almost impossible to run again the code n or n' additional times to estimate $F_2(y)$.

Beckman and McKay (Beckman, 1987) proposed the weighting and the rejection methods to estimate the effect of such change in the input distributions on the output mean and the output cumulative distribution function. We present here only the rejection method.

4.3.1 *The rejection method (Johnson, 1987), (Fishman, 1996).*

The rejection method is based on the acceptance/rejection sampling method for random variables with cumulative distribution function with no analytical inverse function.

There are two conditions for the application of this method: First, as in the previous method, the support of $f_2(\mathbf{x})$, R_2 , must be contained in the support of $f_1(\mathbf{x})$, R_1 ; and second, the quotient $f_2(\mathbf{x})/f_1(\mathbf{x})$ must be bounded. Let us assume that the bound is M ; in other words, $(f_2(\mathbf{x})/f_1(\mathbf{x})) \leq M \quad \forall \mathbf{x} \in R_2$. In the following lines there is the procedure to be followed:

- **Step 1** \Rightarrow Obtain a sample of size n of the input random vector under the reference distribution: X_1, X_2, \dots, X_n . Their actual values will be x_1, x_2, \dots, x_n .
- **Step 2** \Rightarrow Run the code for those n sets of inputs in order to get the corresponding sample of the output variable: Y_1, Y_2, \dots, Y_n . Their actual values will be y_1, y_2, \dots, y_n .
- **Step 3** \Rightarrow For each sample x_i , take a sample of the uniform distribution V_i between 0 and $Mf_1(x_i)$.
- **Step 4** \Rightarrow Retain in the sample the corresponding output value $Y_i=y_i$ if the realisation v_i of V_i is less or equal to $f_2(x_i)$, otherwise reject that value from the sample.
- **Step 5** \Rightarrow Consider the values of Y remaining in the sample as a random sample of Y under $f_2(\mathbf{x})$, and use this sample of size $k \leq n$ to build up an empirical distribution function that estimates the actual distribution function of Y under $f_2(\mathbf{x})$. Each step in that empirical distribution function will have a height $1/k$.

The objective of sampling Y under $f_1(\mathbf{x})$ and under $f_2(\mathbf{x})$ is to get an estimate of the probability of failure of the system under those different circumstances. If we assume that the system fails when the variable Y exceeds the value y_0 , our estimate of the probability of failure will be the number of observations of Y that exceed such a value divided by n for the reference case and divided by k in the sensitivity case.

This procedure for estimating the distribution function of Y under $f_2(\mathbf{x})$ produces an unbiased estimator for that function since we are applying strictly the acceptance/rejection method for sampling X under $f_2(\mathbf{x})$ using as an ancillary function $f_1(\mathbf{x})$. The acceptance/rejection method provides a random sample of X under $f_2(\mathbf{x})$. This fact guaranties that the transformation of this sample through the model provides a random sample of Y under $f_2(\mathbf{x})$. This sample may be used in the usual way to provide any unbiased estimator related to Y , in particular the empirical distribution function.

4.3.2 *Conclusions on the methods for testing the influence of the input distribution on the output*

The two methods proposed provide unbiased estimates for the mean of the output variable (weighting method) and its distribution function (rejection method). The most important one of these two methods, under the perspective of estimating the reliability of a passive system, is the second one since it allows getting estimates of the change in the probability of failure of the system. Nevertheless, the weighting method provides valuable information about the average shift of the output variable values. That average shift is measured through the shift in the mean. Additionally, both methods are suitable for measuring the sensitivity to the change in one, several or all the input parameters, though with some restrictions (if a set of the input parameters are mutually dependent, the sensitivity to a change in one subset may not be addressed separately).

In some way we may consider the results provided by these two methods as ‘qualitative’ since, though we get numeric estimates, no test is provided to test the significance of the differences obtained. That is a problem not addressed yet.

In many cases, the experts will provide marginal distributions for the input parameters and the multivariate input distribution will be computed as the product of those marginal distributions (independence). If alternative distributions are provided for each marginal, the efficiency of the rejection method will be the product of the quotients of the alternative and the reference distribution in each input. This product may become really low, what will provide a low efficiency for the estimate if we try to address the sensitivity to the whole multivariate distribution change.

4.4 Application to the RP2 system

The RP2 example consists of a 21 dimension input space, which, after executing CATHARE code, generates as output the ratio between the amount of energy extracted by the three RP2 systems in the reactor protection system and the amount of energy generated at the core during a certain transient. The parameters considered in that study and their respective distributions are shown in Table 4.2. An 85 run random sample was obtained. That random sample was used to perform the sensitivity analysis.

The first task developed was to check the quality of the input sample used to perform the analysis. Each input parameter is assumed to follow a given distribution (those available in Table 1). The first check consists in performing Kolmogorov goodness of fit test to see if the samples of each parameter fit adequately the postulated distribution. The last column of Table 4.2 shows the p-values of those Kolmogorov tests. Only in one case (L_1 , p-value = 0.028) the null hypothesis (adequate sampling) is rejected with a significance level of 0.05 ($\alpha = 0.05$). The probability rejecting the null hypothesis at least one time out of 18 is equal to the probability of getting one or more failures in a binomial distribution with 18 trials and probability of failure 0.05, which is quite a likely event (probability close to 0.60). So, the sample is acceptable from the point of view of the fits to the theoretical distributions. Variables I_1, I_2 and I_3 were not tested due to their unusual shape.

Table 4.2. Probability distribution functions for the parameters in the RP2 bases case and KOLMOGOROV'S tests results

Variable	Distribution	Average	Standard deviation	X_{min}	X_{max}	λ	μ	Kolmogorov test p-values
I_1, I_2, I_3	Composed							
X_1, X_2, X_3	Exponential					182	0	0.080; 0.188; 0.792
L_1, L_2, L_3	Truncated normal	4.5	0.6	2	5			0.028; 0.636; 0.789
T_1, T_2, T_3	Truncated normal	303	20	280	368			0.561; 0.884; 0.701
C_1, C_2, C_3	Truncated normal	15	5	0	30			0.722; 0.592; 0.769
PUI	Truncated normal	100	1	98	102			0.135
PP	Truncated normal	155	4	153	166			0.998
ANS	Truncated normal	10	5	0	20			0.803
NGV_1, NGV_2, NGV_3	Truncated normal	12.78	0.30	12.08	13.91			0.110; 0.740; 0.370

Distribution sensitivity analysis for the RP2 base case

Parameter ANS

This variable has turned out to be, as observed in the sensitivity analysis (§ 3.5.5), the most important variable. ANS follows a truncated normal distribution with mean 10, standard deviation 5, and with lower and upper bounds of 0 and 20. The purpose of this sensitivity analysis is to study the effect of changing the mean up to 0.25 times the standard deviation, and altering the standard deviation in a 10%, as shown in Figure 4.7. Figure 4.8 shows the results provided by the extended rejection method.

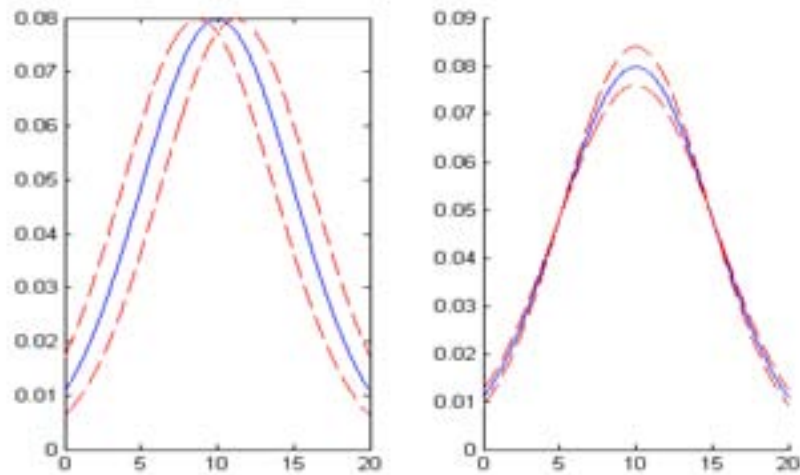


FIG. 4.7. Real distribution and hypothetical extreme alternative distributions for parameter ANS.

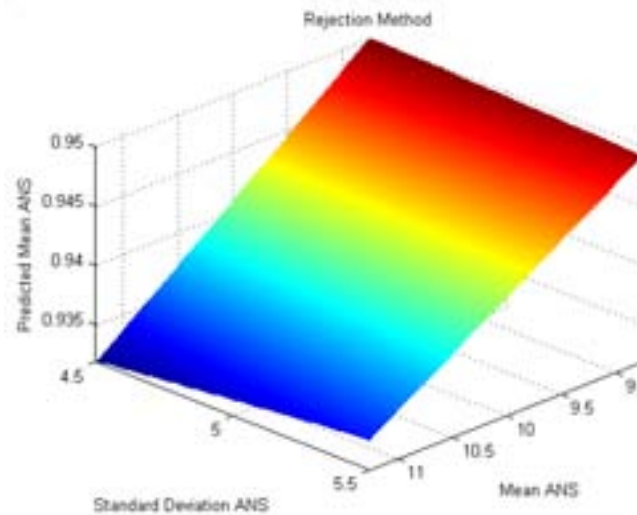


FIG. 4.8. Predicted Means for different alternative input distribution functions for ANS using the extended rejection method.

As mentioned above, the extended rejection method also provides empirical CDF's under different alternative input distributions f_2 . Figure 4.9 shows the evolution of the output variable Ratio CDF as the mean of ANS increases.

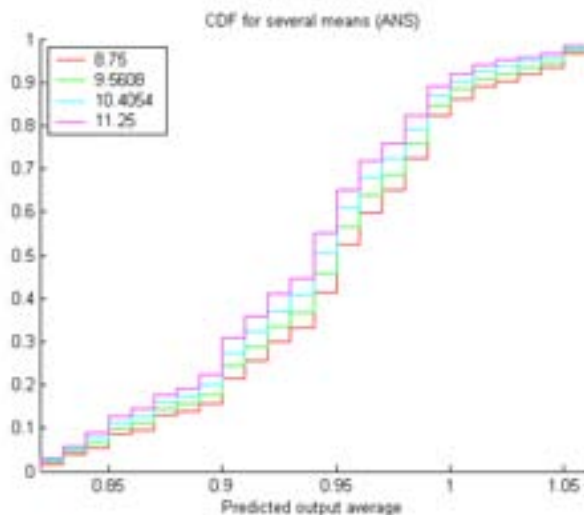


FIG. 4.9. Evolution of Ratio CDF for increasing ANS means.

Figure 4.9 shows a clear tendency of the ratio CDF to move towards lower values as ANS distribution moves towards higher values. This fact is in agreement with the negative value for the regression coefficient estimate for ANS in the regression analysis. The advantage of the CDF is that it provides all the statistical information contained in the sample: mean, standard deviation, percentiles, etc.

4.5 Summary of chapter 4

The reliability of a passive system that utilize NC can be assessed in introducing uncertainties in a T-H code reputed to give a best estimation of the system performances. Then, once the different source of uncertainties have been identified and modelled, the problem is how to propagate these uncertainties through the T-H code and how to evaluate the reliability of the passive system.

The uncertainty in the physical response of the T-H code can be evaluated by a confidence interval or by a probability density function (*pdf*). Methods giving an uncertainty range of the system performance are not very useful for reliability estimation. On the other hand, the *pdf* of the system performance can be directly used for reliability estimation once a failure criterion is given.

For the evaluation of the *pdf*, the existing methods are generally based on Monte-Carlo simulations. These methods require a large number of calculations and can be often prohibitive when each calculation involves a long and onerous computer time. To avoid this problem, two approaches are possible: the variance reduction techniques in Monte-Carlo methods or the use of response surfaces where a simpler mathematical model no leading to expensive computation costs replaces the physical model. In order to estimate the reliability of a system, it is also possible to use approximate methods such as First and Second Order Reliability Methods (FORM/SORM).

It is also important to assess the influence of input distribution changes in the mean and in the distribution functions of the output variables, without running again the T-H code, in using the weighting and the rejections methods.

5. INTEGRATION OF NC SYSTEM RELIABILITY IN PROBABILISTIC SAFETY ANALYSIS

The treatment of passive systems that utilize NC in the Probabilistic Safety Assessment (PSA) models is a difficult and challenging task. No commonly accepted practices exist so far on how to estimate reliability of passive systems. The main challenge arises from the nature of passive systems which main operating principles are based not on active components, but on physical phenomena.

This chapter provides different approaches how to integrate reliability evaluation of the passive systems into PSA models of accident sequences.

The chapter is divided into three sections. Section 5.1 provides general information on PSA and its structure. Section 5.2 discusses a number of possibilities to develop interface between PSA model and passive systems reliability methodology and specifies the requirements for output of reliability calculations. The section 5.3 presents the example of the integration of RP2 passive system in a PSA.

5.1. Overview of PSA (Kopustinskas, 2003)

The first comprehensive application of the PSA dates back to 1975, to the United States Nuclear Regulatory Commission's (U.S. NRC) Reactor Safety Study (WASH-1400, 1975). Since that pioneering study, there has been substantial methodological development, and PSA techniques have become a standard tool in the safety evaluation of the nuclear power plants (NPPs) and industrial installations in general. Due to historical reasons, the PSA sometimes is called PRA.

5.1.1. Levels of PSA.

As the most important area of PSA projects remains nuclear power plants, mainly due to the specific features of the nuclear installations, three levels of PSA have evolved:

Level 1: The assessment of plant failures leading to core damage and the estimation of core damage frequency. A Level 1 PSA provides insights into design weaknesses and ways of preventing core damage. In the case of other industrial assessments, Level 1 PSA provides estimates of the accidents frequency and the main contributors.

Level 2: As possible releases are additionally protected by containment in most NPPs, PSA at this level provides estimates of off-site release frequencies, based on the containment response and severe accident management possibilities. The results obtained in Level 1 are the basis for Level 2 quantification. In the case of other industrial assessments, Level 2 PSA might be fully covered by Level 1, as containment function is rather unique feature and is not common in other industries.

Level 3: The assessment of off-site consequences leading to estimates of risks to the public. Level 3 incorporates results from both previous levels.

5.1.2 PSA structure

Level 1 PSA is the most important level and creates the background for further risk assessment, therefore it will be presented in detail. The structure of the other levels is much more application-specific, and will be discussed only in general.

The typical phases of a PSA project are shown in Figure 5.1.

During the planning phase, scope of the study, as well as assumptions, limitations, level of detail and other boundary conditions have to be defined. Physical boundaries of the system have to be determined, which parts are to be included in the analysis and which are not? Operational state of the system have to be fixed, at which capacity the system is analyzed (full or reduced), what are the equipment states (valves open or closed etc.)? What external factors are to be analyzed (e.g. earthquake, extreme wind etc.)? The level of detail is also an important issue, e.g. is it enough to identify the reason as a "pump failure" or the detailed classification is required as pump failure at start, while running, due to cooling failure or oil leak and so forth. The level of detail is often restricted by the amount of information available.

The model construction consists of selection of initiating events (IE), modeling of accident sequences by FT/ET and quantification of the model components (initiating events, basic events, success criteria).

The calculations is a broad area of PSA work. It includes calculations of top event probabilities, minimal cut sets, importance, sensitivity and uncertainty analysis, quantification of sequences and consequences.

The last phase is to draw conclusions, provide recommendations and support for safety improvement decisions.

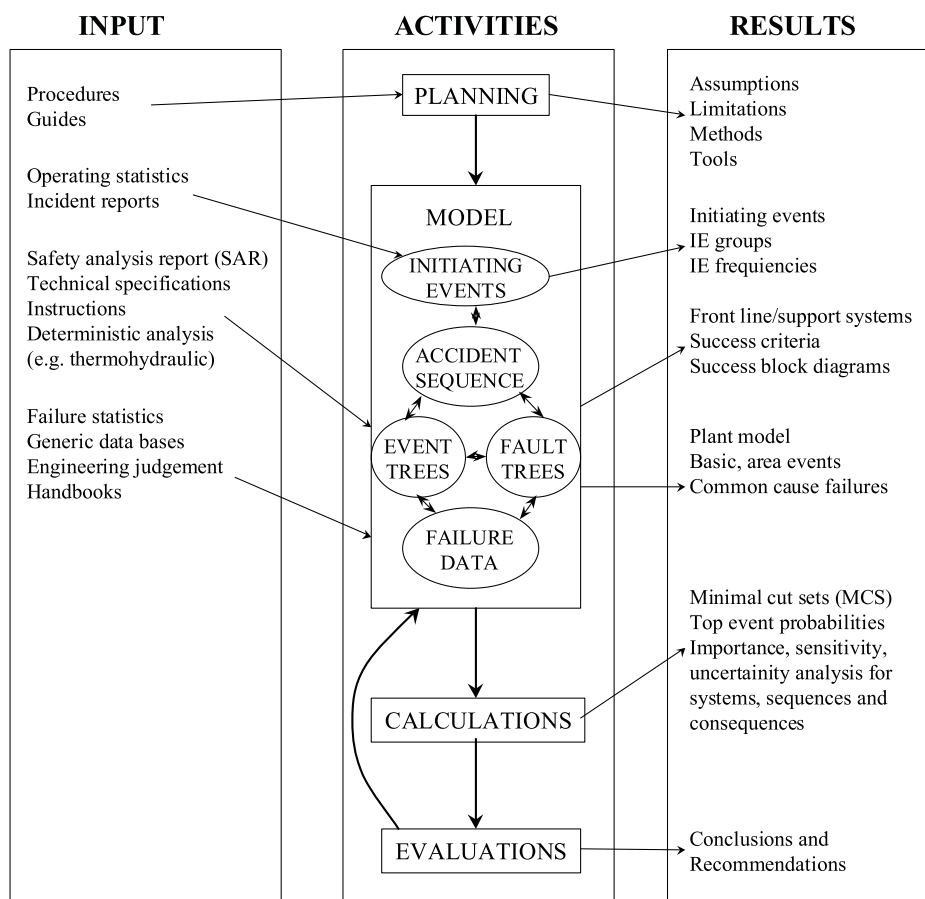


FIG. 5.1. PSA structure and phases.

The model

The initial step in the construction of the model is to select initiating events. The initiating event is an event (e.g. equipment failure, transient) that can lead to the accident if no protective actions are taken. The protective actions can be either automatic (most safety systems are actuated in this way) or manual (operator intervention is required). Identification of the IE is usually performed by combination of several approaches, like failure mode and effect analysis (FMEA), operation experience, incidents reports.

For each selected IE, detailed examination of the accident progression has to be made and accident sequences as logical combinations of success/failure conditions of functions or systems are identified. Each accident sequence ends with certain consequence, which also have to be defined. Consequences in the case of Level 1 PSA of NPPs are usually defined as degrees of reactor core damage, including 'safe' state and 'severe' accident state.

Event trees are used for the graphical and logical presentation of the accident sequences. An example of an event tree is shown in Figure 5.2. The logical combinations of success/failure conditions of functions or systems (usually safety systems, also called front-line systems) in the event tree are modeled by the fault trees.

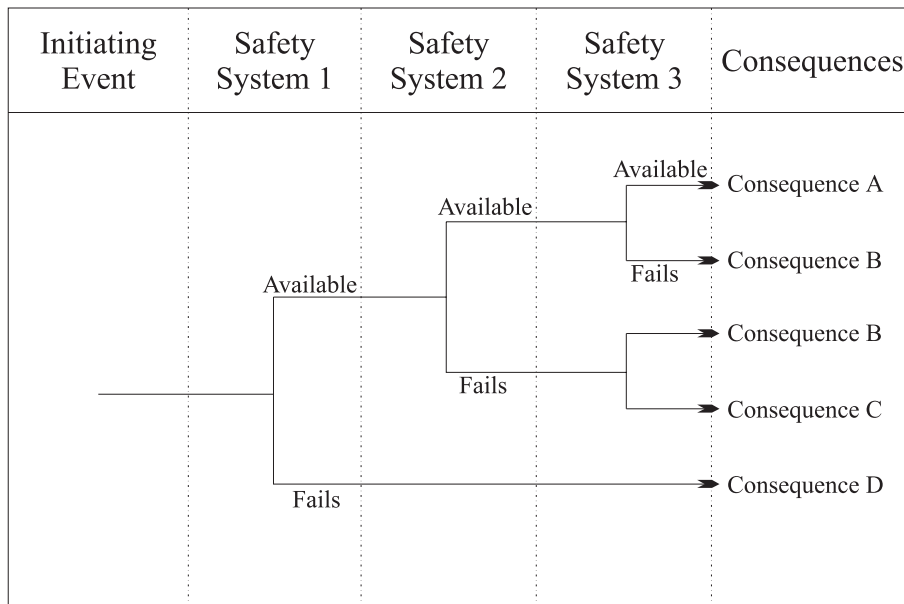


FIG. 5.2. Example of an event tree.

A fault tree logically combines the top event (e.g. complete failure of a support system) and the causes for that event (e.g. equipment failure, operator error etc.). An example of the fault tree is shown in Figure 5.3. The fault tree mainly consists of the basic events (all possible causes of the top event that are consistent with the level of detail of the study) and logical gates (OR, AND, M out of N and other logical operations). Other modeling tools, like common cause failures, house or area events are also used in the fault trees. All front-line and support systems are modeled by the fault trees and then combined in the event trees depending on the initiating event.

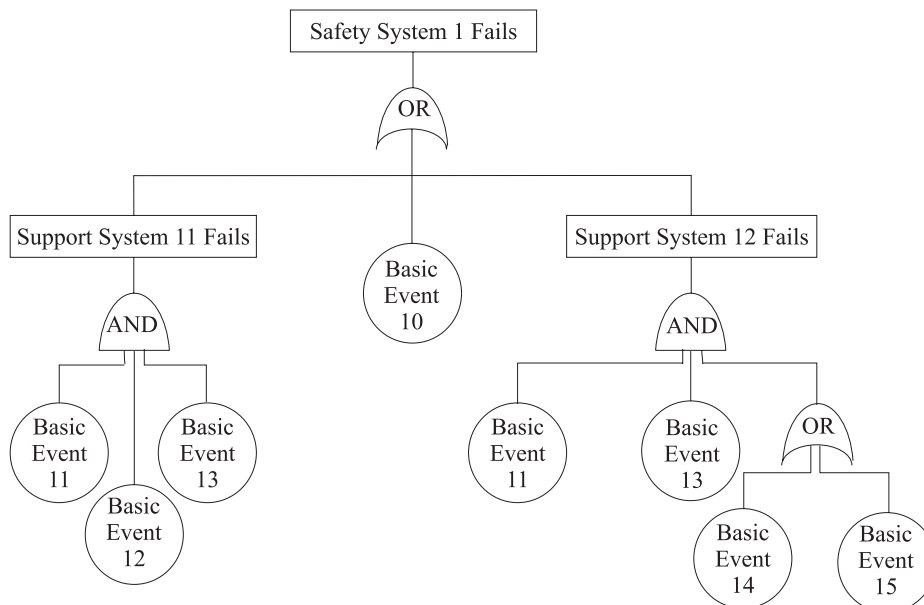


FIG. 5.3. An example of a fault tree.

A fault tree is capable to include rather special cases, usually identified in complex systems. This include system and components dependencies, called common cause failures (simultaneous failures of several components due to the same reason), area events (usually fire, flood etc., which damages groups of components in certain rooms), human actions (operator errors or mitigation actions).

Data in PSA

Quantification of the model involves data analysis of the generic and plant-specific failure data. Data analysis should produce the following input to the model:

- Initiating event frequencies,
- Basic event failure parameters (failure probability per demand, failure rate, repair rate, test intervals, mission time),
- Human error probabilities,
- Data for common cause failures,
- Uncertainty data.

Calculations in PSA

A number of computer codes were developed to visualize PSA model construction and perform various calculations. The most popular of them are Risk Spectrum PSA (Sweden), IRRAS, CAFTA (USA), CAFTAN (Norway) and others.

Many kinds of different calculations can be performed with the model depending on the purpose. The most important of them are the following:

- Minimal cut sets,
- Probabilities of top events, sequences and consequences,
- Importance analysis,
- Uncertainty analysis,
- Sensitivity analysis.

A fault tree contains valuable information about possible combinations of faults that can result in a critical failure defined by the top event. Such a combination is called a *cut set*, which in fault tree terminology is defined as a set of basic events whose (simultaneous) occurrence ensures that the top event occurs. We are most interested in *minimal cut sets* which are cut sets that can not be reduced without losing their status as cut sets. Several algorithms are available to determine minimal cut sets in large FT, e.g. MOCUS. Minimal cut set analysis highlights the main contributors to the top event, which can be ranked on a quantitative basis. Quantitative as well as qualitative analysis of the cut sets provide insights of the system weaknesses and dominating sequences.

Top event probability shows unreliability of the system or function for which the top event is constructed. Probabilities of the accident sequences and consequences provide likelihood estimates of certain scenarios. As the logical structure of the fault and event tree is known, there should not be any problems to calculate top event or consequence probability using simple operations of Boolean algebra. However, even for simple systems, exact computational methods such as inclusion-exclusion, pivotal decomposition or ERAC may be cumbersome and time-consuming. Realistic applications may however contain thousands of basic events and hundreds of fault and event trees. Therefore, a number of approximate methods were developed for mathematical treatment of large FTs, many of them are based on the inclusion-exclusion principle.

The importance analysis is aimed at identification of the components that, by being improved, would increase the reliability of the system the most. It is obvious that reliability importance of a component in a system depends on two factors:

- The location of the component in the system,
- The reliability of the component in question.

A number of different reliability importance measures are proposed: Birnbaum's, Vesely-Fussell's, critical importance, improvement potential, risk achievement worth, risk reduction worth and others. However, different measures lead to different rankings, since the measures are defined differently. To

identify the component that should be improved to increase system reliability, Birnbaum's and improvement potential are the most appropriate. To identify the component that has the largest probability of being the cause of system failure, the critical importance and Vesely- Fussell's measures are used.

The uncertainty analysis is an important task of a PSA. Any model of a large scale facility inevitably contains uncertainties, usually grouped into three categories:

Completeness. This part of uncertainty reflects the lack of confidence in completeness of accident sequences and initiating events analysed in the study. There is no guarantee that other scenarios are impossible. This is the most difficult kind of uncertainty for assessment and quantification.

Modelling adequacy. Even those scenarios and sequences that have been identified do not precisely represent reality because of simplifying assumptions, idealizations, mathematical models, numerical approximations or computational limits. Sensitivity studies are usually performed to assess importance of the key assumptions.

Input parameters uncertainties. The parameters of various failure models are not exactly known because of lack of data, variability within the samples or assumptions. This category of uncertainties is quantified assuming that PSA result as well as input parameters (e.g. failure rates) are random variables. The probability distribution functions are assumed for each parameter and then by propagation through the model the uncertainty of the results is obtained. The most widely used technique for propagating uncertainties is a Monte-Carlo simulation.

The uncertainty analysis is still considered by many scientists and many scientific papers show increased interest in this field. The most recent area of uncertainty analysis is to assess uncertainties of the deterministic calculations, which play also essential role in the determination of success criteria in a PSA.

The purpose of sensitivity analysis is twofold: (1) to determine the sensitivity of the system failure frequency to possible dependencies among basic events and (2) to analyze those modeling assumptions suspected to have a potentially significant impact on the results. The general practice of the realistic models shows that results should not be too sensitive to any of the model parameters.

5.1.3. Benefits of PSA

The PSA is a powerful tool that can be used in many different ways to assess, understand and manage risk. Its primary objectives are the following:

- estimate risk level of the facility,
- identify dominant event sequences affecting safety of the facility,
- identify systems, components and human actions important for safety,
- assess important dependencies (among systems or man-machine interactions),
- provide decision support in various application areas.

The growing area of PSA use is extensive support of probabilistic results in risk management and decision-making processes. The main areas of the PSA applications are assessment of design modifications and back-fitting, risk informed optimization of the Technical Specifications, accident management, emergency planning and others. Several modern tools of risk management are also based on the PSA model, such as risk monitoring, precursor analysis and others.

5.1.4 Limitations and drawbacks of PSA

Despite its popularity among the risk assessment tools, the PSA has a number of imitations and drawbacks. The main limitations of the PSA model are the following:

Binary representation of the component state. Only two states are analyzed: failed state or fully functioning state. However, this is not always realistic, as intermediate states are also possible. The same limitation exists for the redundant systems with certain success criteria - system is in failed state (success criteria is not satisfied) or in full power. The intermediate states for redundant systems are even more important.

Independence. In most cases, the components are assumed to be independent (except modelled by CCF), however there are many sources of dependencies, not treated by the model.

Aging effect. The aging effect is ignored because of the constant failure rate assumption. The only conservative possibility to treat the aging impact is to perform sensitivity study.

Time treatment. The FT/ET model is not capable to treat time explicitly during the accident progression. This is one of the major drawbacks of the methodology. In realistic systems, many parameters and functions depend on time and this is not encountered in the model and only approximate chronological order is assumed.

Uncertainty of the calculations. Uncertainties are inevitable in the PSA results and calculations and therefore direct treatment of the quantitative PSA estimates might be misleading. Due to the fact of uncertainties, the qualitative PSA results (identification of dominant accident sequences, comparison of different safety modifications) are of greater importance than quantitative.

5.2. Interface between PSA and passive system reliability model

There is a number of different ways how to integrate passive system reliability model into the whole plant PSA model. It could be done directly in the event tree of relevant accident sequence as a single basic event, or a separate fault tree could be developed. The most commonly used approach is to develop a fault tree for each safety system. The system fault tree in a case of passive systems would be very simple, consisting of several basic events, representing failure of physical phenomena (natural circulation) and failure of activating valve or other means of initial system activation, connected together by “OR” gate, as shown in Figure 5.4.

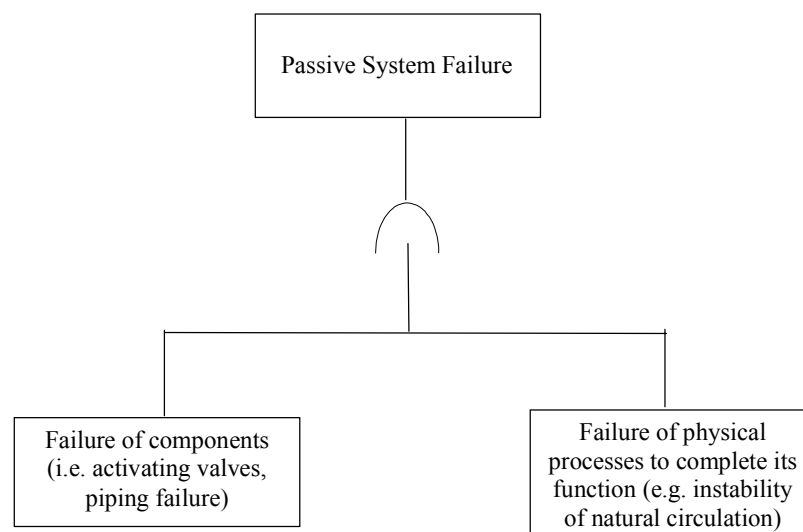


FIG. 5.4. Frame of a passive system fault tree.

The component part of a fault tree should model reliability of active or passive components of a passive system. This part of a fault tree is strongly related to specific design of a system, but the usual

design includes some active components responsible mostly only for actuation of the system – e.g. valves, including actuation signals or manual actuation. The modeling should include different failure modes of the components during start-up and during operation of a system. The examples of failure modes could be failure to open or inadvertent closure of a valve, plugged heat-exchanger or others.

Reliability of passive components (e.g. piping) could also be modeled in this part of a fault tree, but usually omitted due to high reliability of these components. In general, the component part of a fault tree is modeled by conventional methods, applied also to other systems.

Another part of a passive system fault tree deals with modeling of physical phenomena reliability. There is no common approach so far how to model this type of failures. The RMPS project proposes to derive reliability estimate of physical phenomena from thermal hydraulic modeling calculation. In this approach, the fault tree would contain a single basic event, showing unavailability of the process to complete its function when demanded.

Integrating such passive system into the PSA model requires the determination of plant demands for the specific passive system given specific initiating events and then to develop relevant accident sequences. Depending on the particular initiating event, demand for the system could be different and this usually impacts on the reliability of the system. The accident sequence modeling techniques by event trees are not different for active or passive systems and are well known to PSA practitioners.

The new element in the probabilistic modeling of the passive system is the methodology to quantify reliability of the physical process, represented as a single basic event. It is important that the results of quantification procedure are compatible with the probabilistic data format used in the PSA calculations. It is common practice to base the main calculations on the mean reliability parameter values and then to provide boundaries by performing uncertainty analysis. Ideally, for each basic event reliability parameter its distribution type and parameters are estimated. If this procedure is numerically too costly, only the most important percentiles are used in the uncertainty analysis: 5%, 50%, 95% and mean value.

5.3 Application to the RP2 system (Marques, 2004 B)

5.3.1 Approach used

In a first approach, applied to a simplified PSA carried out on a fictive reactor equipped with two types of safety passive systems, we have chosen an Event Tree (ET) representation of the accidental scenario. ET techniques allows identifying all the different chains of accident sequences deriving from the initiating events. ET development implies each sequence represents a certain combination of events, corresponding to failed or operating safety or front-line systems: thus ETs, starting from the initiators, branch down following success or failure of the mitigating features, that match the ET headings, providing therefore a set of alternative consequences.

The failures analyses performed on this reactor have allowed the characterisation of the technical failures (on valves, tubes in exchanger and safety injection check valves) and the ranges of variation of uncertain parameters which influence the physical process.

The majority of the sequences of this event tree have been analysed by deterministic evaluations with envelope values of the uncertain parameters. For some sequences where the definition of envelope cases was impossible, basic events corresponding to the failure of the physical process have been added and uncertainty analyses have been performed.

For this purpose the thermal-hydraulic code has been coupled to a Monte-Carlo simulation modulus. The failure probabilities obtained by these reliability analyses have been integrated in the corresponding sequences. This methodology allows the probabilistic evaluation of the influence of the passive system on an accidental scenario and could be used to test the interest to replace an active system by a passive system on specific situations.

5.3.2 Specific reliability analyses for the PSA integration

In the framework of the integration of the system reliability in a PSA in order to test the influence of the passive system on different accidental situations, specific ranges of variation and specific probabilistic density functions of the characteristic parameters have been identified for the studied sequences. Specific reliability and sensitivity analyses have been carried out for these sequences. For two sequences where the definition of envelope cases was impossible, uncertainty analyses have been performed to evaluate the corresponding probability of failure. These sequences were: the sequence with 2 RP2 available and no broken tube and the sequence with 2 RP2 available and one broken tube.

We present here the example of the sequence with two RP2 available and no broken tube in the RP2 exchanger. In this case, the number of characteristic parameters was reduced to 14 (there is only two RP2 systems and the number of broken tubes and the valve failure are no more considered in the uncertainty analysis, but taken into account in the event tree of the PSA). In addition, a monitoring system was supposed to be implemented on the RP2 system, in order to verify continuously that the RP2 loops are available when they are solicited. This led to narrower ranges of variation for the levels and the temperatures of the two pools. The choice of the probabilistic model presented in Table 5.1 was based on engineer judgment.

The results of the sensitivity analysis performed in calculating the Standardized Regression Coefficient and the Partial Correlation Coefficient show that the more influential parameters on the performance ratio are L_1 and L_2 the initial pool levels and the *ANS* curve.

Table 5.1. Probabilistic model of the 14 parameters

Variable	Distribution	Par 1	Par 2	X_{\min}	X_{\max}
X_1, X_2	Truncated log-normal	0.12	0.43	0	1
L_1, L_2	Truncated normal	4.5	0.5	4	5
T_1, T_2	Truncated normal	30	20	10	50
C_1, C_2	Truncated log-normal	12	0.4	0	30
PUI	Truncated normal	100	2	98	102
PP	Truncated normal	155	2	153	157
ANS	Truncated log-normal	6	0.4	0	20
NGV_1, NGV_2, NGV_3	Truncated normal	12.78	0.70	12.08	13.91

The objective of the uncertainty calculations was to evaluate the probability p_1 corresponding to the failure of the physical process, considered as a basic event in the event tree, when only two RP2 are available. We have carried out 76 calculations with CATHARE with values of the input variables randomly generated in considering this probabilistic model.

Among these 76 calculations, we obtained 18 cases of failure, leading to a rough estimation of the failure probability p_1 to 0.24. This failure probability is conditional with respect to the sequence considered and has to be multiplied by the probabilities of all the basic events involved in the sequence in order to determine the failure probability of the sequence.

In the same way, we determine a failure probability p_2 equal to 0.04 for the RP2 passive system in the sequence with 2 RP2 available and one broken tube.

5.3.3 *Integration of the reliability of the RP2 passive system in PSA*

This study consisted in:

- carrying out a global quantitative evaluation of the reliability of the RP2 passive system,
- including this evaluation in a simplified PSA of PWR reactor,
- carrying out calculations of a set of CATHARE transients,
- including the CATHARE results in the PSA,
- evaluating the yearly occurrence frequency of core damage for the reactor equipped with safety passive systems, in case of transient of Total Loss of the Power Supplies (or Blackout),
- identifying complementary CATHARE calculations to test and validate the methodology.

The reliability analysis of the RP2 passive system underlines the existence of two types of failures which could affect the system:

- Failures on passive system components, which lead, directly or indirectly, to the loss of the system,
- The occurrence of an initial configuration of the passive system, which is not standard and leads to the loss of the system, mainly because of thermal-hydraulic reasons. The not standard configuration of the passive system does not allow to guarantee the good working of the system in case of demand.

For this second type of failures, we can consider two possibilities:

- A monitoring system can detect, before the occurrence of the blackout, the existence of the not standard configuration of the passive system. It is also considered that, as soon as the not standard configuration is detected, the automatic safety systems or the operators shutdown the reactor in safety state (shutdown of the reactor by instruction). The occurrence of this type of configuration lies in the failure of monitoring systems. For the reliability analyses, the initial configuration of the passive system to be considered is the one corresponding to the limit conditions generating the shutdown of the reactor in safety state (shutdown of the reactor by instruction).
- No monitoring system can detect, before the occurrence of the blackout, the existence of a not standard configuration of the passive system. It is not considered that operators shutdown the reactor in safety state. The occurrence of this type of configuration lies in the existence of a set of characteristic parameters, corresponding to an initial not standard configuration of the passive system.

Table 5.2 gives the failure probabilities obtained, for each of the 3 types of failures previously identified. Concerning the first and the second types of failures, the analysis consists in taking into account the failure in form of a probability of occurrence. The probability of failure per demand for each RP2 loop is estimated through a failure analysis. The values adopted for the failure probabilities leading to the failure of the RP2 system are evaluated by analogy with similar components existing on PWR reactors.

Table 5.2. Failure probabilities

FAILURE TYPE	FAILURE PROBABILITY (/demand)
Non opening per demand of the RP2 valve (defined for each RP2 loop)	3.10^{-3}
Broken tubes in the RP2 exchanger (for at least 1 of the 3 RP2 loop)	3.10^{-3} / hypothesis : 10^{-3} per RP2 loop
Failure of the pool level measure (captor, calculator)	3.10^{-3}
Failure of the pool water temperature measure (captor, calculator)	3.10^{-3}
Failure of the steam generator level measure (captor, calculator)	Negligible (reactor safety system)
Failure of the primary pressure measure	
T-H process failure (p1) with 1 RP2 loop not available and no broken tubes	0.24
T-H process failure (p2) with 1 RP2 loop not available and broken tubes	0.04
Failure of safety injection by accumulators	10^{-3}

The accidental transient of Total Loss of the Power supplies (reactor in full power) has been chosen, as it was the reference transient having been used for the dimensioning of the safety systems dedicated to residual power removal. The probability of occurrence of this initiating event is 10^{-5} /year. The analysis is carried out through the method of event tree, integrating the RP2 loops and the safety injection by accumulators. The event tree is presented on Figure 5.5. In order to simplify the event tree representation, the different numbers of RP2 loops available are presented in the same event tree.

The core damage frequency, after a blackout, is estimated at 7.5×10^{-8} /year. This frequency corresponds to the sum of the probabilities of each accident sequence leading to the core melt in pressure for the transient of blackout. The main accident sequence (sequence 5) represents 96% of the core damage frequency. This sequence corresponds to a T-H process failure when 1 RP2 loop has failed. This frequency is at the limit of the acceptability, as it does not respect the probabilistic objectives 10^{-7} /year for all the transient families, which corresponds for a transient family to 10^{-8} /year. This result does not affect the conception of the RP2 system which is efficient to avoid the high pressure core melt.

As result of this exercise, we concluded that it would be desirable to re-examine the dimensioning of the RP2 system, in order to obtain a well-running process, when 1 RP2 loop is in failure. The probabilistic objective to reach is 0.03 for the T-H process failure in case of 2 RP2 loops available. This value would allow to reach a yearly core damage frequency of 10^{-8} regarding the high pressure core damage for the studied transient family (blackout). The RP2 passive system, dimensioned in this way should allow to reach the probabilistic safety objectives for a reactor integrating passive safety systems. These results underline the importance to take into account the T-H process failure probability to evaluate the reliability of a safety passive system.

The current analysis was an illustrating exercise, dedicated to the test and the validation of the reliability method applied to the passive system. This exercise implies some specific limits in the analysis. In any case, these limits should be analysed in a PSA. These specific limits are:

- The analysis concerns only one initiating event, the Total Loss of Power supplies, even if this transient is the transient of reference having been used for the dimensioning of the safety systems dedicated to the residual power removal; other initiating events have to be analysed;
- The consequences of a system failure, when it is not in demand (valve opening, valve leak, rupture of a primary nozzle) are not considered (i.e. the initiating events created by a failure of the RP2 are not taken into account), even if this failure could have a potential effect on the safety;
- No aggravating event is considered, relative to the initiating event of Total Loss of Power supplies, else than the RP2 passive system failures (component failures or T-H process failure) and the safety injection;
- Human factor (operator errors) are not explicitly taken into account (the presence of a crisis team allows limited error possibilities);
- No “mechanical” common cause failure between the 3 RP2 loops have been considered. Only the “thermal-hydraulic” common cause failure has been taken into account through the global CATHARE modelling of the 3 RP2 loops. Thus, the mechanical failure of 1 RP2 loop has no consequence on the operation of the others;
- The common cause failure between the monitoring systems of the RP2 loop are considered as negligible;
- No common cause failure is considered between the RP2 passive system and the safety injection;
- Only 1 failure is considered for each RP2 loop.

Loss of electrical supply $10^{-5}/\text{year}$	Number of RP2 available Failure on solicitation $10^{-2}/\text{demand}/\text{RP2 loop}$	Broken tubes in, at least, one of 3 RP2 loops $3.10^{-3}/\text{for 3 RP2}$	Failure of the T-H Process	Safety injection $10^{-3}/\text{demand}$	Number of the sequence	Final situation of the reactor	Occurrence yearly frequency	
ϵ	3 RP2 loops $P = 1 - 3.10^{-2}$				1	Safe situation	$3.10^{-11}/\text{year}$	
					2	Safe situation		
					3	Core fusion		
	2 RP2 loops $P = 3.10^{-2}$			p_1	4	Safe situation		
					5	Core fusion		$p_1 * 3.10^{-7}/\text{year}$
					6	Safe situation		
	1 RP2 loop $P = 3.10^{-4}$			p_2	7	Core fusion		$9.10^{-13}/\text{year}$
					8	Core fusion		$p_2 * 9.10^{-10}/\text{year}$
					9	Core fusion		
	0 RP2 loop $P = 10^{-6}$				10	Core fusion (envelop effect)		$10^{-12}/\text{year}$
					11	Core fusion		$9.10^{-15}/\text{year}$
					12	Core fusion		$10^{-11}/\text{year}$

FIG. 5.5. Simplified even tree of loss of electrical supply including passive systems.

5.4 Summary of chapter 5

The objective of this part of the methodology is the development of a consistent approach for introducing passive system reliability in an accident sequence of Probabilistic Safety Assessments (PSA).

There is a number of different ways how to integrate passive system reliability model into the whole plant PSA model. It could be done directly in the event tree of relevant accident sequence as a single basic event, or a separate fault tree could be developed. The new element in the probabilistic modeling of the passive system is the methodology to quantify reliability of the physical process, represented as a single basic event, from thermal-hydraulic modeling calculations.

In a first approach, applied to a simplified PSA carried out on a fictive reactor equipped with two types of safety passive systems, we have chosen an Event Tree (ET) representation of the accidental scenario. ET techniques allows identifying all the different chains of accident sequences deriving from the initiating events. ET development implies each sequence represents a certain combination of events, corresponding to failed or operating safety or front-line systems: thus ETs, starting from the initiators, branch down following success or failure of the mitigating features, that match the ET headings, providing therefore a set of alternative consequences.

The failures analyses performed on this reactor have allowed the characterisation of the technical failures (on valves, tubes in exchanger and safety injection check valves) and the ranges of variation of uncertain parameters which influence the physical process. The majority of the sequences of this event tree have been analysed by deterministic evaluations with envelope values of the uncertain parameters. For some sequences where the definition of envelope cases was impossible, basic events corresponding to the failure of the physical process have been added and uncertainty analyses have been performed to evaluate the corresponding probability of failure. For this purpose the thermal-hydraulic code has been coupled to a Monte-Carlo simulation modulus. The failure probabilities obtained by these reliability analyses have been integrated in the corresponding sequences.

This methodology allows the probabilistic evaluation of the influence of the passive system on an accidental scenario and could be used to test the interest to replace an active system by a passive system on specific situations.

6. CONCLUSION

The RMPS project has allowed the development of a specific methodology for the evaluation of the reliability of passive system and its integration into the probabilistic analyses of accidental sequences. The methodology obtained deals with the following problems:

- Identification and quantification of the sources of uncertainties and determination of the important variables.
- Propagation of the uncertainties through Thermal-Hydraulic (T-H) models and assessment of T-H passive system unreliability.
- Introduction of passive system unreliability in the accident sequence analysis.

Each step of the methodology has been described and commented and a diagram of the methodology is presented in Figure 6.1.

These methodology has been tested on three examples of passive systems: the Residual Passive heat Removal system on the Primary circuit (RP2) of Pressurized Water Reactor which is presented in this course, the Isolation Condenser System (ICS) of Boiling Water Reactor, the Residual Passive heat Removal system on the Primary circuit (RP2) of Pressurized Water Reactor and the Hydro-Accumulator (HA) of VVER 1000 reactors.

Thermal-hydraulic calculations have been carried out with different codes (RELAP, ATHLET and CATHARE), and various methods of sensitivity analysis and reliability evaluation have been tested.

The Analytical Hierarchy Process has been chosen for the identification of the relevant parameters which really affect the accomplishment of the system mission.

The results obtained on the examples have shown the interest of sensitivity analysis for the determination, among the uncertain parameters, of the main contributors to the risk of failure of the passive system. They have shown also that it is possible to evaluate the reliability of the systems for specific situations, once the probability density functions of the input parameters is defined, in using Monte-Carlo or FORM method. The use of response surface methods where the physical model is approximated by a simpler mathematical model is often necessary in order to reduce the number of calculations with the physical model.

The possibilities to integrate passive system reliability in a PSA sequence have been tested on an example. In a first approach, applied to a simplified PSA carried out on a fictive reactor equipped with two types of safety passive systems, we have chosen an Event Tree (ET) representation of the accidental scenario. This methodology allows the probabilistic evaluation of the influence of the passive system on an accidental scenario and could be used to test the interest to replace an active system by a passive system on specific situations.

The developed methodology participates to the safety assessment of reactors equipped with passive systems.

The development and the validation of a methodology of reliability analysis relative to the safety passive systems are a precondition to the implementation of such systems on a nuclear reactor. This methodology is required to gain the necessary confidence of:

- The designers who define the architecture of reactors and safety systems. Indeed, the designers will accept new safety systems only if these systems remain at reasonable costs and with same efficiencies in comparison with the existing safety systems,
- Regulatory authorities who will have to accept the implementation of such systems on a nuclear reactor.

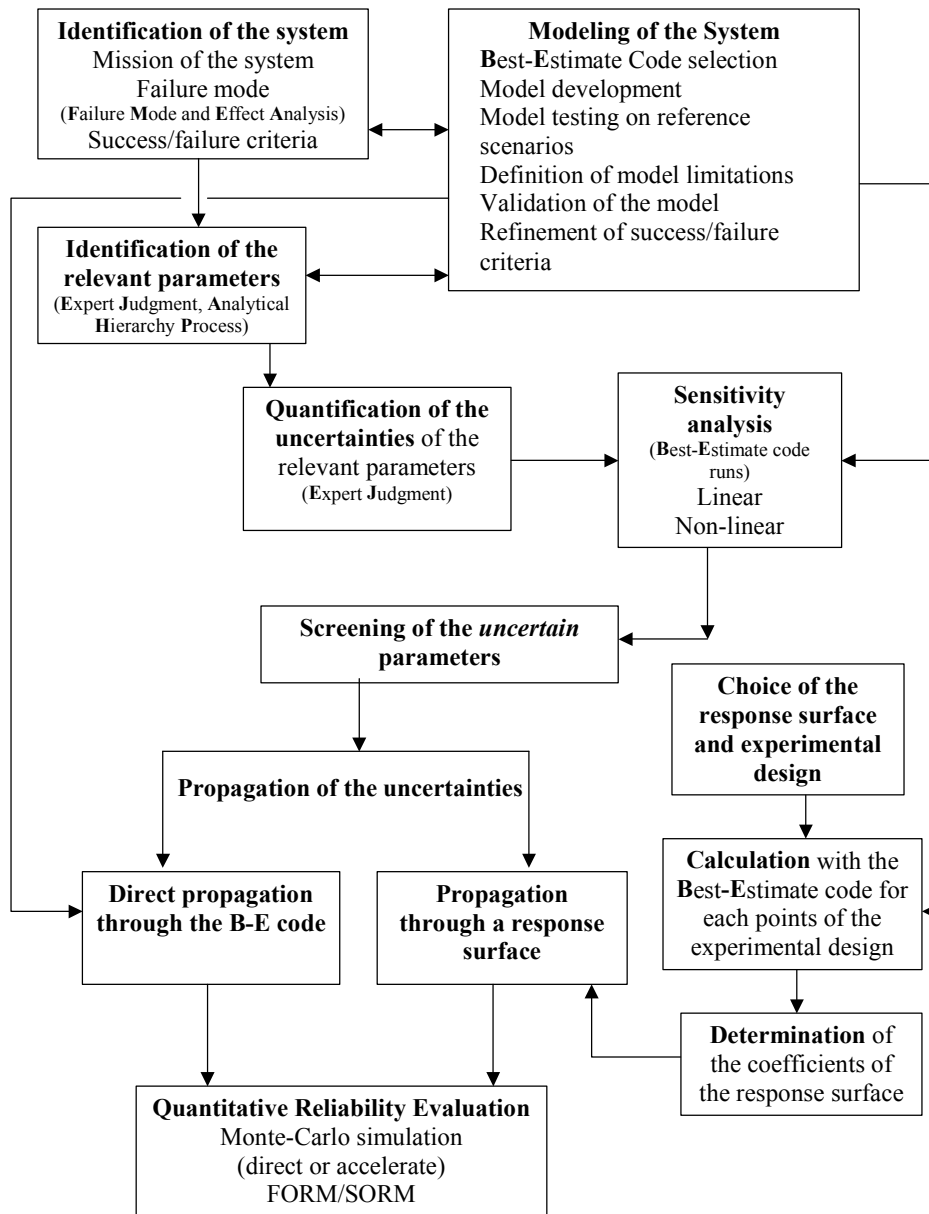


FIG. 6.1. RMPS methodology roadmap.

Annex 1: Passive system classification

Following the IAEA definition (IAEA, 1991), a passive system is either a system which is composed of passive components and structures or a system which uses active components in a very limited way to initiate subsequent passive operation.

Some broad categories of passivity can be drawn for qualitative evaluation and classification. The following categories can be considered as passive:

Category A

This category is characterized by :

- no signal inputs of “intelligence”, no external power sources or forces,
- no moving mechanical parts,
- no moving working fluid.

Examples of safety features included in this category are:

- physical barriers against the release of fission products, such as nuclear fuel cladding and pressure boundary systems;
- hardened building structures for the protection of a plant against seismic and other external events;
- core cooling systems relying only on heat radiation and/or conduction;
- static components of safety related passive systems (e.g. , tubes, pressurizers, accumulators) as well as structural parts (e.g., supports, shields).

Category B

This category is characterized by :

- no signal inputs of “intelligence”, no external power sources or forces,
- no moving mechanical parts, but
- moving working fluids.

The fluid movement is only due to thermal-hydraulic conditions occurring when the safety function is activated.

Examples of safety features included in this category are:

- reactor shutdown/emergency cooling systems based on injection of borated water from an external water pool,
- reactor emergency cooling systems based on air or water natural circulation in heat exchangers immersed in water pools (inside the containment),
- containment cooling systems based on natural circulation of air flowing around the containment walls.

Category C

This category is characterized by :

- no signal inputs of “intelligence”, no external power sources or forces,
- moving mechanical parts, whether or not moving working fluids are also present.

The fluid motion is characterized as in category B; mechanical movements are due to imbalances within the system (e.g., static pressure in check and relief valves, hydrostatic pressure in accumulators) and forces directly exerted by the process.

Examples of safety features included in this category are:

- emergency injection systems consisting of accumulators or storage tanks and discharge lines equipped with check valves;
- mechanical actuator, such as check valves and spring-loaded relief valves.

Category D

This category addresses the intermediary zone between active and passive where the execution of the safety function is made through passive methods as described in the previous categories except that internal intelligence is not available to initiate the process. In these cases an external signal is permitted to trigger the passive process.

Examples of safety features included in this category are:

- emergency core cooling systems, based on gravity-driven flow of water, activated by valves which break open on demand.

Annex 2: Nomenclature

A nomenclature of the terms adopted in the project has been defined. This task was mandatory in order to clarify the methodology and allow a better comprehension of it. As much as possible, terms coming from Reliability and Sensitivity Analyses and Probabilistic Safety Assessment have been adopted, or at least a certain parallelism in meaning has been pursued. Table A.1 presents both the terms and the meanings proposed.

Table A.1. Terminology used in the RMPS methodology

Term	Meaning (within the methodology)
Accuracy	A measure of agreement between measured and predicted quantity. An “accurate” model should be precise and unbiased.
Availability	The state of an item of being able to perform its required function, under given conditions and at a given time.
Availability (Measure of)	Probability ($A(t)$) of an item of being able to perform its required function, under given conditions and at a given time.
Bias	Systematic difference between a true mean value and a predicted or measured mean.
Boundary Condition	Functional relationship between parameters at the boundary of the system.
Code Assessment	Procedure for specifying, qualitatively or quantitatively, the accuracy of code predictions.
Code Deficiency	Shortcoming in a code model, correlation or numerical solution scheme resulting in a bias in the calculated parameter(s).
Code Uncertainty	Uncertainty on code physical models, correlations and numerical solution scheme.
Code Validation	A process carried out by comparison of model predictions with experimental measurements that are independent of those used to develop the model. A model cannot be considered validated until sufficient testing has been performed to ensure an acceptable level of predictive accuracy over the range of conditions over which the model may be applied. (Note that the acceptable level of accuracy is judgemental and will vary depending on the specific problem or question to be addressed by the model).
Code Verification	A mathematical model, or the corresponding computer code, is verified when it is shown that the code behaves as intended, i.e. that it is a proper mathematical representation of the conceptual model and that the equations are correctly encoded and solved.
Confidence Interval (two sided Confidence Interval)	Interval limited by two values (confidence limits) such as the probability, that a parameter to be estimated belongs to this interval, is equal to a given value $1 - \alpha$ (confidence level).
Cumulative Distribution Function	Function giving, for all value x , the probability that the random variable X will be less than or equal to x . Noted: $F(x) = P [X \leq x]$

Failure	The termination of the ability of an item to perform a required function. Note: After failure the item has a fault. “Failure“ is an event, as distinguished from “fault“, which is a state. (This concept as defined does not apply to items consisting of software only).
Failure Mode	Effect by which a failure is observed.
Failure Criteria	Logical and/or numerical relationships which define the failure condition for the Passive System.
Initial Condition	The steady state value of a plant parameter at the initiation of a postulated transient.
Probability density function	Derivative, if exists, of the cumulative distribution function of a random variable. Noted: $f(x)$; $f(x) = \frac{dF}{dx}(x)$
Random variable	Variable taking any value of a set of determined numerical values and at which is associated either a probability density function (continuous random variable) or a probability mass function (discrete random variable). A random variable which can take only isolated values is “discrete”. A random variable which can take all the values of an interval is “continue”.
Reliability	The probability that a system or service will perform its intended function in a satisfactory manner for a given period of time, $[0,t]$, when used under specified operating conditions. Noted: $R(t)$
System Mission	Goal(s) for which the Passive System has been designed and located within the Complete System.
Unreliability	The probability that a system or service will not perform its intended function in a satisfactory manner for a given period of time, $[0,t]$, when used under specified operating conditions. Equivalent to failure probability. Noted : $F(t) = 1 - R(t)$
Unavailability	The state of an item of being unable to perform its required function, under given conditions and at a given time. Measure of unavailability : probability of an item of being unable to perform its required function, under given conditions and at a given time. Unavailability factor: the ratio of the down duration to the period of time under consideration. Instantaneous unavailability: the probability that an item is in a down-state at a given instant time. Noted: $U(t) = 1 - A(t)$
Uncertainty interval	Interval around the true value of a parameter resulting from the inability to either measure or calculate it accurately.
Virtual Component	Characteristic phenomenology for the Passive System, that are unidentifiable as a classic component in the Fault-Tree analysis.

ACKNOWLEDGMENTS

This course is based on the results of the methodology developed within the framework of a Project called Reliability Methods for Passive Safety Functions (RMPS), performed under the auspices of the European 5th Framework Programme.

The author thanks all the participants in the RMPS project. The cost sharing from the European Commission under the Nuclear Fission Program is kindly acknowledged.

REFERENCES

- [1] ARCHER, et al., Sensitivity measures, anova-like techniques and the use of bootstrap. *Journal of statistical Computation and Simulation*, vol. 58, pp 99,120 (1997).
- [2] BALDEWECKH, Méthodes des éléments finis stochastiques – Applications à la géotechnique et à la mécanique de la rupture. Thèse Université d'Evry Val d'Essonne (1999).
- [3] BARRE, et al., The CATHARE code strategy and assessment. *Nuclear Engineering and Design* 124, p257-284 (1990).
- [4] BECKMAN, R.J. and MCKAY, M.D., Monte Carlo Estimation under Different Distributions., *Technometrics*, Vol. 29, No. 2, pp. 153-160 (1987).
- [5] BJERAGER, P., Methods for structural reliability computations. Lecture notes. *Structural Reliability: Methods and applications*. University of California, Berkeley, April 27-29 (1989).
- [6] BOLADO, R., Notes on two Monte Carlo Methods for Estimating the Influence of Different Input Distributions on the Output Distribution from a Computer Code Simulation, European Commission technical note TN.P.03.84 (2003).
- [7] BUCHER, C.G., A fast and efficient response surface approach for structural reliability problems, *Structural safety*, 7 pp 57-66 (1990).
- [8] BURGAZZI, Passive System Reliability Analysis: a Study on Decay Heat Removal Passive Systems, Topical Meeting on Advanced Nuclear Installation Safety”, San Diego (USA), June 4-8 (2000).
- [9] D'AURIA, F., and GIANNOTTI, W., University of Pisa, “Development of a Code with Internal Assessment of Uncertainty”, *Nuclear Technology* Vol.131 (2000).
- [10] D'AURIA, F., State of the art on uncertainty evaluation. Eurofastnet. W3 T3.3. Final draft (2002).
- [11] DEVICTOR, N., Fiabilité et mécanique : méthodes FORM/SORM et couplages avec des codes d'éléments finis par surfaces de réponse adaptative. Thèse, Université Blaise Pascal, Clermont-Ferrand (1996).
- [12] DEVICTOR N. et al., Adaptive use of response surfaces in the reliability computations of mechanical components. *ESREL 97* (1997).
- [13] FISHMAN, G.S., Monte Carlo. Concepts, algorithms and applications, Springer Series in Operations Research. Springer Verlag (1996).
- [14] GAUTIER, et al., Passive heat removal system with the « Base Operation Passive Heat Removal » strategy. Application with Primary Heat Exchangers – ICONE 7 – April 20-23 (1999).
- [15] GLAESER, H., Uncertainty evaluation of thermal-hydraulic code results. International meeting on “Best-Estimate” Methods in Nuclear Installation Safety Analysis (BE-2000). Washington, DC (2000).
- [16] INTERNATIONAL ATOMIC ENERGY AGENCY, Safety Related Terms for Advanced Nuclear Plant, IAEA-TECDOC-626 (1991).
- [17] JOHNSON, M.E., Multivariate Statistical Simulation, Wiley Series in Probability and Mathematical Statistics. Wiley (1987).
- [18] KOPUSTINSKAS, V., Approaches for introducing passive system unreliability in accident sequence. Deliverable 7 of RMPS project. EVOL-RMPS-D07 (2003).
- [19] KWANG-IL AHN and HEE-DONG KIM, Korean Atomic Energy Research Institute, A Formal Procedure for Probabilistic Quantification of Modeling Uncertainties Employed in Phenomenological transient Models, *Nuclear Technology* Vol.130 (2000).
- [20] MADSEN, H., et al., Methods of structural safety, Prentice Hall (1986).

- [21] MARQUÈS, M., et al., Reliability Methods for Passive Systems. Proceedings of ICAPP'04. Pittsburgh, PA USA, June 13-17 (2004).
- [22] MARQUÈS, M., et al., Integration of the reliability of passive system in probabilistic safety assessment. Proceedings of ICAPP'04. Pittsburgh, Pa USA, June 13-17 (2004).
- [23] MELCHERS, R.E., Structural reliability analysis and prediction, J.Wiley & Sons (1999).
- [24] MORRIS, M., Factorial Sampling Plans for preliminary computational experiments. Technometrics, vol. 33, no 2 (1991).
- [25] RACKWITZ, R., et al., Structural reliability under combined random load sequences. Computers and structures, vol.9, pp 489-494 (1979).
- [26] RAJASHEKHAR et al., A new look at the response surface approach for reliability analysis. Structural Safety, 12, pp 205-220 (1993).
- [27] RUBINSTEIN, R.Y., Simulations and Monte-Carlo Method. Wiley Series in Probability and Mathematical Statistics, J. Wiley & Sons (1981).
- [28] SAATY, The Analytical Hierachy Process, McGraw-Hill International, New York (1980).
- [29] SACKS, J., et al., Design and analysis of computer experiments. Structural Science, Vol. 4 , No 4, 409-435.
- [30] SALTELLI et al., Sensitivity Analysis. John Wiley & Sons (2000).
- [31] SUNDARAJAN, Probabilistic Structural Mechanics Handbook. Chapman & Hall (1995).
- [32] Wash-1400, Reactor Safety Study, U.S. Nuclear Regulatory Commission, NUREG-75/014 (1975).
- [33] WILKS, S.S., Determination of sample sizes for setting tolerance limits; Ann. Math. Statist., 12 , pp. 91-96, (1941).
- [34] ZIO, E., CANTARELLA, M., CAMMI, A., The analytic hierarchy process as a systematic approach to the identification of important parameters for the reliability assessment of passive systems, Nuclear Engineering and Design, 226, pp. 311-336 (2003).

CONTRIBUTORS TO DRAFTING AND REVIEW

Aksan, N.	Paul Scherrer Institute, Switzerland
Araneo, D.	University of Pisa, Dipartimento di Ingegneria Meccanica, Nucleare e della Produzione (DIMNP), Italy
Bousbia-Salah, A.	University of Pisa, Dipartimento di Ingegneria Meccanica, Nucleare e della Produzione (DIMNP), Italy
Bovalini, R.	University of Pisa, Dipartimento di Ingegneria Meccanica, Nucleare e della Produzione (DIMNP), Italy
Burgazzi, L.	Advanced Physics Technology Division, ENEA, Italy
Cleveland, J.	International Atomic Energy Agency
Costa, A.L.	University of Pisa, Dipartimento di Ingegneria Meccanica, Nucleare e della Produzione (DIMNP), Italy
D'Auria, F.	University of Pisa, Dipartimento di Ingegneria Meccanica, Nucleare e della Produzione (DIMNP), Italy
Del Nevo, A.	University of Pisa, Dipartimento di Ingegneria Meccanica, Nucleare e della Produzione (DIMNP), Italy
Gimenez, M.O.	Comisión Nacional de Energía Atómica (CNEA), Centro Atómico Bariloche, Argentina
Hwang, D.H.	Korea Atomic Energy Research Institute, Republic of Korea
Ishii, M.	School of Nuclear Engineering, Purdue University, United States of America
Kirchsteiger, C.	European Commission Joint Research Center, Institute of Energy, Netherlands
Korotaev, K.	Experimental Design Organization "Gidropress", Russian Federation
Krepper, E.	Forschungszentrum Rossendorf, Germany
Macek, J.	Nuclear Research Institute Rež, Czech Republic
Marques, M.	Commissariat à l'énergie atomique, (CEA/DEN), France
Mateiovic, P.	IVS Trnava, Slovakia
Muellner, N.	University of Vienna, Institute for Risk Research, Austria
Muñoz-Cobo, J.L.	Universidad Politécnica de Valencia, Spain
Nayak, A.K.	Bhabha Atomic Research Centre, India
Reyes, Jr., J.N.	International Atomic Energy Agency
Saha, D.	Bhabha Atomic Research Centre, India
Smith, B.L.	Paul Scherrer Institute, Switzerland
Vijayan, P.K.	Bhabha Atomic Research Centre, India
Wu, Q.	Oregon State University, United States of America
Yonomoto, T.	Japan Atomic Energy Research Institute, Japan

WHERE TO ORDER IAEA PUBLICATIONS

In the following countries IAEA publications may be purchased from the sources listed below, or from major local booksellers. Payment may be made in local currency or with UNESCO coupons.

- BELGIUM** Jean de Lannoy, avenue du Roi 202, B-1190 Brussels • Telephone: +32 2 538 43 08 • Fax: +32 2 538 08 41
E-mail: jean.de.lannoy@infoboard.be • Web site: http://www.jean-de-lannoy.be
- CANADA** Renouf Publishing Company Ltd., 1-5369 Canotek Rd., Ottawa, Ontario, K1J 9J3
Telephone: +613 745 2665 • Fax: +613 745 7660
E-mail: order.dept@renoufbooks.com • Web site: http://www.renoufbooks.com
- CHINA** IAEA Publications in Chinese: China Nuclear Energy Industry Corporation, Translation Section, P.O. Box 2103, Beijing
- FINLAND** Akateeminen Kirjakauppa, PL 128 (Keskuskatu 1), FIN-00101 Helsinki
Telephone: +358 9 121 4418 • Fax: +358 9 121 4435
E-mail: sps@akateeminen.com • Web site: http://www.akateeminen.com
- FRANCE** Nucléon Editions, 20, rue Rosenwald, F-75015 Paris
Telephone: +33 1 42 50 15 50 • +33 6 86 92 69 39 • Fax +33 1 53 68 14 93 • *E-mail: nucleon@nucleon.fr*
Form-Edit, 5, rue Janssen, P.O. Box 25, F-75921 Paris Cedex 19
Telephone: +33 1 42 01 49 49 • Fax: +33 1 42 01 90 90 • *E-mail: formedit@formedit.fr*
- GERMANY** UNO-Verlag, Vertriebs- und Verlags GmbH, Am Hofgarten 10, D-53113 Bonn
Telephone: +49 228 94 90 20 • Fax: +49 228 94 90 222
E-mail: bestellung@uno-verlag.de • Web site: http://www.uno-verlag.de
- HUNGARY** Librotrade Ltd., Book Import, P.O. Box 126, H-1656 Budapest
Telephone: +36 1 257 7777 • Fax: +36 1 257 7472 • *E-mail: books@librotrade.hu*
- INDIA** Allied Publishers Limited, 1-13/14, Asaf Ali Road, New Delhi 110002
Telephone: +91 11 3233002, 004 • Fax: +91 11 3235967
E-mail: aplnd@del2.vsnl.net.in • Web site: http://www.alliedpublishers.com
- ITALY** Libreria Scientifica Dott. Lucio di Biasio "AEIOU", Via Coronelli 6, I-20146 Milan
Telephone: +39 02 48 95 45 52 or 48 95 45 62 • Fax: +39 02 48 95 45 48
- JAPAN** Maruzen Company, Ltd., 13-6 Nihonbashi, 3 chome, Chuo-ku, Tokyo 103-0027
Telephone: +81 3 3275 8582 • Fax: +81 3 3275 9072
E-mail: journal@maruzen.co.jp • Web site: http://www.maruzen.co.jp
- NETHERLANDS** Martinus Nijhoff International, Koraalrood 50, P.O. Box 1853, 2700 CZ Zoetermeer
Telephone: +31 793 684 400 • Fax: +31 793 615 698 • *E-mail: info@nijhoff.nl • Web site: http://www.nijhoff.nl*
Swets and Zeitlinger b.v., P.O. Box 830, 2160 SZ Lisse
Telephone: +31 252 435 111 • Fax: +31 252 415 888 • *E-mail: infoho@swets.nl • Web site: http://www.swets.nl*
- SLOVAKIA** Alfa Press, s.r.o., Račianska 20, SQ-832 10 Bratislava • Telephone/Fax: +421 7 566 0489
- SLOVENIA** Cankarjeva Založba d.d., Kopitarjeva 2, SI-1512 Ljubljana
Telephone: +386 1 432 31 44 • Fax: +386 1 230 14 35
E-mail: import.books@cankarjeva-z.si • Web site: http://www.cankarjeva-z.si/uvoz
- SPAIN** Díaz de Santos, S.A., c/ Juan Bravo, 3A, E-28006 Madrid
Telephone: +34 91 781 94 80 • Fax: +34 91 575 55 63 • *E-mail: compras@diazdesantos.es • carmela@diazdesantos.es
barcelona@diazdesantos.es • julio@diazdesantos.es • Web site: http://www.diazdesantos.es*
- UNITED KINGDOM** The Stationery Office Ltd, International Sales Agency, 51 Nine Elms Lane, London SW8 5DR
Telephone: +44 870 600 552 • Fax: +44 207 873 8416
*E-mail: Orders to: book.orders@theso.co.uk • Enquiries to: ipa.enquiries@theso.co.uk
Web site: http://www.the-stationery-office.co.uk*
- On-line orders**
DELTA Int. Book Wholesalers Ltd., 39 Alexandra Road, Addlestone, Surrey, KT15 2PQ
E-mail: info@profbooks.com • Web site: http://www.profbooks.com
Books on the Environment
SMI (Distribution Services) Limited, P.O. Box 119, Stevenage SG1 4TP, Hertfordshire
E-mail: customerservices@earthprint.co.uk • Web site: http://www.earthprint.co.uk
- UNITED STATES OF AMERICA** Bernan Associates, 4611-F Assembly Drive, Lanham, MD 20706-4391
Telephone: 1-800-274-4447 (toll-free) • Fax: (301) 459-0056/1-800-865-3450 (toll-free)
E-mail: query@bernan.com • Web site: http://www.bernan.com
Renouf Publishing Company Ltd., 812 Proctor Ave., Ogdensburg, NY, 13669
Telephone: +888 551 7470 (toll-free) • Fax: +888 568 8546 (toll-free)
E-mail: order.dept@renoufbooks.com • Web site: http://www.renoufbooks.com

Orders and requests for information may also be addressed directly to:



Sales and Promotion Unit, International Atomic Energy Agency
Wagramer Strasse 5, P.O. Box 100, A-1400 Vienna, Austria
Telephone: +43 1 2600 22529 (or 22530) • Fax: +43 1 2600 29302
E-mail: sales.publications@iaea.org • Web site: http://www.iaea.org/worldatom/Books

